UNIVERSITÀ DELLA CALABRIA

DIPARTIMENTO DI FISICA

DOTTORATO DI RICERCA IN

SCIENZE E TECNOLOGIE FISICHE, CHIMICHE E DEI MATERIALI

CICLO XXXI

Measurement of single and double differential cross-section of top-quark pair production using data collected by the ATLAS detector in pp collisions at $\sqrt{s} = 13$ TeV

SETTORE SCIENTIFICO DISCIPLINARE FIS/01

Presentata da:
Francesco LA RUFFA

Coordinatore Dottorato:
Prof. Vincenzo CARBONE

Supervisore:
Prof. Enrico TASSI

Alla mia famiglia,
A Giusi

UNIVERSITA' DELLA CALABRIA

Abstract

Dipartimento di Fisica

Doctor of Philosophy

Measurement of single and double differential cross-section of top-quark pair production using data collected by the ATLAS detector in pp collisions at $\sqrt{s} = 13$ TeV

by Francesco LA RUFFA

In this thesis, measurements of the differential cross-section for top-quark pair production in proton-proton collisions at a centre-of-mass energy of $\sqrt{s} = 13\,\text{TeV}$ are presented. The measurements are performed using data collected by the ATLAS detector at the Large Hadron Collider at CERN during 2015 and 2016, corresponding to an integrated luminosity of $36.1\,\text{fb}^{-1}$. The top-quark pair events are selected in the lepton (electron or muon) plus jets channel and the analysis employs two separate selections and top-quark reconstruction strategies according to the value of the transverse momentum of the top quark. The single and double differential distributions are measured as a function of several kinematic variables of the top quark and the $t\bar{t}$ system in a fiducial phase-space and extrapolated to the full phase-space. Given the large $t\bar{t}$ production cross-section at the LHC, the measured spectra provide stringent tests of perturbative QCD and are relevant for the tuning of Monte Carlo simulations of the top-quark modelling. For this reason, the differential cross-section distributions are compared to several theoretical Monte Carlo predictions and state-of-the-art fixed-order QCD predictions.

UNIVERSITA' DELLA CALABRIA

Abstract

Dipartimento di Fisica

Doctor of Philosophy

Measurement of single and double differential cross-section of top-quark pair production using data collected by the ATLAS detector in pp collisions at $\sqrt{s} = 13$ TeV

by Francesco LA RUFFA

In questa tesi sono presentate le misure di sezione d'urto differenziale di produzione di coppie di quark top in collisioni protone-protone ad un'energia del centro di massa di $\sqrt{s} = 13\,\text{TeV}$. Le misure sono state fatte utilizzando i dati raccolti con il rivelatore ATLAS al Large Hadron Collider del CERN durante il 2015 ed il 2016, per una luminosità integrata corrispondente di $36.1\,\text{fb}^{-1}$. Gli eventi di coppie di quark top sono selezionati nel canale leptone (elettrone o muone) più getti e l'analisi ha impiegato due selezioni e due strategie di ricostruzione del quark top a seconda del valore dell'impulso trasverso del quark top. Le distribuzioni singolo e doppio differenziali sono misurate in funzione di diverse variabili cinematiche del quark top e del sistema $t\bar{t}$ in uno spazio delle fasi fiduciale ed estrapolate al completo spazio delle fasi. Data l'alta sezione d'urto di produzione di coppie di top quark ad LHC, le distribuzioni misurate offrono la possibilità di effettuare test molto stringenti della QCD perturbativa e sono importanti per il tuning delle simulazioni Monte Carlo che modellano il quark top. Perciò, le distribuzioni di sezioni d'urto differenziali sono confrontate con diverse predizioni Monte Carlo e predizioni ad un ordine fissato dello sviluppo perturbativo in QCD che rappresentano lo stato dell'arte dei calcoli teorici a riguardo della produzione di coppie di top quark.

Contents

List of Figures

List of Tables

Introduction

Testing the validity of the Standard Model (SM) in the high-energy regime at the Large Hadron Collider (LHC) is one of the main purposes of the ATLAS experiment. The top quark plays a crucial role in the SM, and so in the ATLAS physics programme, due to its peculiar properties: it is the most massive fundamental particle currently known and it is the only quark which can be studied before hadronisation. The top-quark pair is produced mainly by gluon fusion at LHC and its cross-section ($\sim$ 800 pb at a center-of-mass energy $\sqrt{s}$ = 13 TeV) is one of the largest among the SM processes investigated by the ATLAS experiment. Given the large value of the integrated luminosity of the 2015 and 2016 data taking periods collected by the ATLAS experiment, as well as the availability of recent calculations at the next-to-next-to-leading order (NNLO) in perturbative QCD of the top-quark pair production, very stringent tests of the QCD predictions can be performed by using the $t\bar{t}$ differential cross-section measurements.

In this thesis, the measurements of single and double differential cross-sections for top-quark pair production in the lepton plus jets channel are presented. The measurements are performed both in resolved and boosted regime using the data sample collected in 2015 and 2016. The cross-sections are measured as a function of the main kinematic variables of the top quark and the $t\bar{t}$ system that are well suited to study the different aspects of the $t\bar{t}$ production at the LHC. The combination of the resolved and boosted regimes covers the full kinematic region characterized by the transverse momentum p_{T} of the top quark.

The differential cross-section measurements are compared with several Monte Carlo (MC) predictions as well as fixed-order QCD calculations in order to asses the level of accuracy of the theoretical description of top-quark pair production. Moreover, the measured spectra are particularly useful for the tuning of MC simulations which is relevant in the process of improving the understanding of $t\bar{t}$ production and, as a consequence, for the reduction of the uncertainties related to top-quark modeling. In addition, the results can be used as inputs for detailed phenomenological studies such as NNLO QCD DGLAP analysis for the determination of the proton's PDFs, the mass of the top quark and the strong coupling constant α_s, even simultaneously.

The structure of the thesis is as follows. In Chapter 1 a general overview of the SM and the theoretical framework for top-quark pair production is presented. In addition, a summary

of the current status of both theoretical and experimental results is presented. The experimental apparatus of the ATLAS detector is described in Chapter 2. Chapter 3 is focused on the description of the Monte Carlo simulation of the physics processes and of the detector. The objects used in the analysis are defined in Chapter 4 where a particular emphasis is given to the b-tagging algorithms and a recently published calibration analysis performed on semileptonic $t\bar{t}$ events. The event selections as well as the techniques employed to reconstruct the top quark are presented in Chapter 5. The unfolding procedure used to correct for detector effects on the measurement is described in Chapter 6. The sources of systematic uncertainties affecting the measurements are presented in Chapter 7. Finally, in Chapter 8 the results of the measurement of the single and double differential cross-sections are presented, together with a comparison with theoretical predictions.

Chapter 1

The Standard Model and the Top quark

During the last century, the number of discoveries of fundamental particles had undergone a rapid increase and it led physicists to face an apparently disordered collection of elementary constituents of matter, the so-called *particle zoo*. The introduction of new ideas in the context fo quantum field theory helped to describe these observations in a coherent framework, together with the interactions occuring between the known fundamental particles. In the 1960s, the Standard Model (SM) fundations were set by Sheldon Glashow, Steven Weinberg and Abdus Salam [1, 2]. The SM is the currently accepted and experimentally well-tested theory that descibes the all known fundamental particles and the interactions between them. The SM is a gauge quantum field theory, in which all particles are represented as quanta of an associated field and the interactions between them are descibed in terms of exchange of a mediator. The quantum field theory extends the classic quantum mechanical description of the state of a system from a wave function ψ to excitations of a local field $\phi(x)$. In classical Lagrangian formalism, the Lagrangian density $\mathcal{L}$ describes the state of system as a fuction of the field $\phi(x)$ and its space-time derivatives

$$\mathcal{L}(x) = \mathcal{L}(\phi, \partial_\mu \phi) \tag{1.1}$$

The evolution of a system is described by the Euler-Lagrange equation of motion

$$\partial_\mu \left[\frac{\partial \mathcal{L}}{\partial(\partial_\mu \phi)} \right] - \frac{\partial \mathcal{L}}{\partial \phi} = 0. \tag{1.2}$$

According to Noether's theorem, every symmetry produces a conservation law and viceversa. All the fundamental interactions of the SM are based on lagrangians which are gauge invariant and they are represented by the exchange of gauge mediators.

1.1 The fundamental particles

The fundamental particles of the SM are shown in the schematic overview in Figure 1.1 and they are divided into two categories:

- **fermions**, particles with half-integer spin which follow the Fermi-Dirac statistics and the Pauli exclusion principle. The fermions are described by the Dirac equation, which provides both positive and negative energy solutions. The negative solutions are interpreted as anti-particles. Each anti-particle owns the same mass and spin value of the corresponding particles, but it has the opposite charge. The SM fermions are the leptons and the quarks.
- **bosons**, particles with integer spin which follow the Bose-Einstein statistics. In the SM, the bosons act as gauge mediators of the fundamental interactions between the particles. The SM fundamental bosons are the photon, the gluon, the $W^{\pm}$, Z and Higgs (H) bosons.

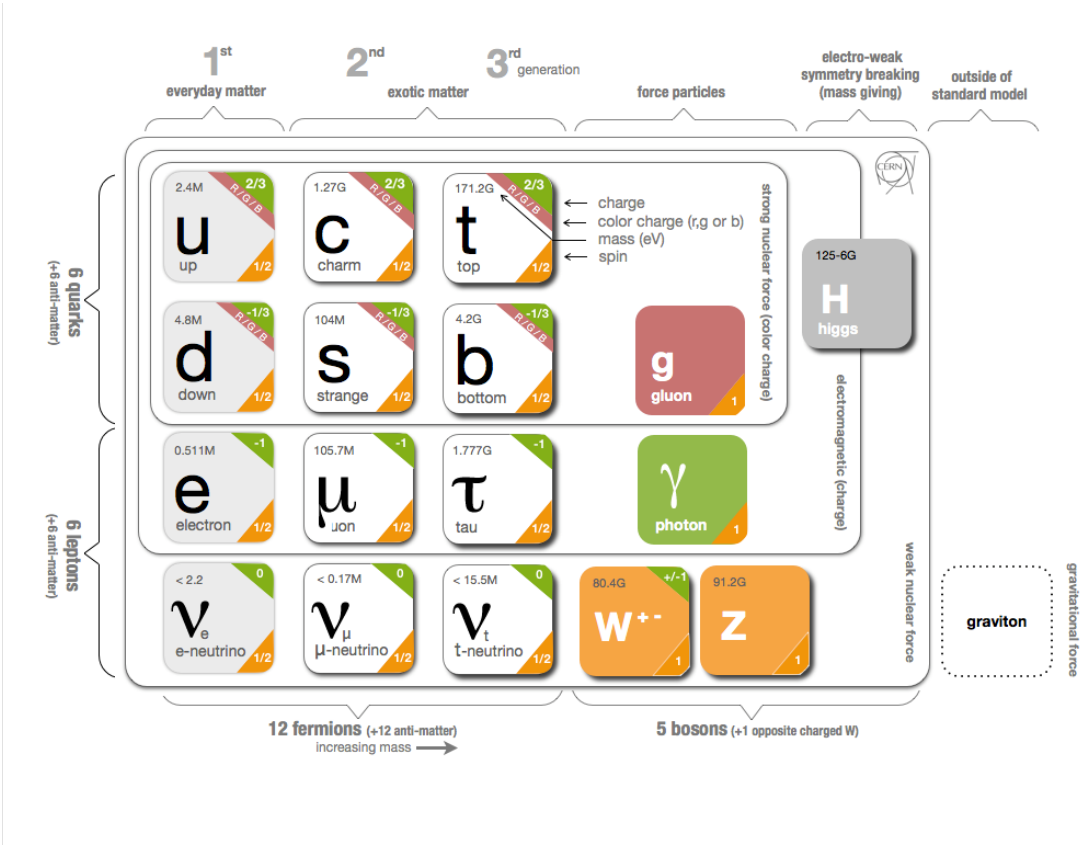

FIGURE 1.1: The Standard Model of Particle Physics: fundamental constituents of matter and gauge bosons.

The leptons are divided into three generations:

$$\begin{pmatrix} e \\ \nu_e \end{pmatrix} \begin{pmatrix} \mu \\ \nu_\mu \end{pmatrix} \begin{pmatrix} \tau \\ \nu_\tau \end{pmatrix} \tag{1.3}$$

The leptons e, μ and τ have equal electric charge value ($-1 \cdot e$), while their masses vary within a wide range of energies (0.5 MeV of the electron and 1.7 GeV of the tau). They can interact both electromagnetically and via the weak force. All the leptonic generations have an internal charge, called leptonic number, with value $1(-1)$ for leptons (anti-leptons) and it is conserved in all the interactions, with the exception of the experimentally-evident phenomenon of neutrino oscillation. In the SM, neutrinos are electrically neutral particles, can interact only via the weak force and they are supposed to be massless. This last assumption is in contrast with the experimental evidence of their oscillation, i.e. the possibility for a neutrino of one of the three generations to transform into a different one. In fact, this phenomenon implies that neutrinos are not massless.

The quarks are the second category in which the fundamental fermions are divided. The quarks are also divided into three generations as the leptons:

$$\begin{pmatrix} u \\ d \end{pmatrix} \begin{pmatrix} c \\ s \end{pmatrix} \begin{pmatrix} t \\ b \end{pmatrix} \tag{1.4}$$

and have fractional electric charge, in particular $2/3 \cdot e$ for the quarks in the first row of (1.4), called u-type, and $-1/3 \cdot e$ for the ones belonging to the second row, called d-type. The quarks own an internal charge called *flavour* (up, down, charm, strange, top, bottom) and different quantum numbers:

- **colour** (red, blue and green for particles and anti-red, anti-green and anti-blue for anti-particles) which is the charge of the strong force and the choice of this name is for analogy with the properties of primary colours. The only states that can be observed in nature are colourless combinations. This property of the colour charge is called confinement. Given the fermionic nature of the quarks, they combine to produce bound states (hadrons) in two ways: a quark/anti-quark pair with the same colour/anti-colour charge (mesons) or three quarks/anti-quarks with all the three different colours mixed together (baryons).
- **baryon number**, which is 1/3 (−1/3) for the quarks (anti-quarks), is a strictly conserved additive quantum number.
- **flavour number** which is preserved under strong and electromagnetic interactions, but not under weak interactions.

1.2 Interactions

The fundamental interactions included in the SM are the electromagnetic interaction, described by the Quantum Electrodynamics (QED), the weak interaction, modelled by the ElectroWeak (EW) theory together with the electromagnetic force, and the strong interaction, described in the context of the Quantum Chromodynamics (QCD). The gravitational interaction is not included in the SM framework as it is not coherently described by a gauge quantum field theory. Due to its negligible contribution (by about a factor of 10^{-36} with respect to the electromagnetic interaction at the GeV scale), there is no need for modification of the SM predictions to take into account also the gravitational interaction. In general, in a quantum field theory the interaction can be studied by the probability of transition between two different states. A convenient way to visualize this transition and to calculate the matrix element of the transition is a Feynman diagram, in which the particles and the mediators are schematized according to general conventions: the solid straight lines represent the fermions, the curved or dashed lines describe the gauge bosons. In this framework, time goes from the left to the right and the particles have an associated arrow which indicates whether it is a particle (anti-particle) in case it is pointing to the positive (negative) time direction. The interaction is represented by the vertex of a Feyman diagram and its contribution to the calculation is proportional to the typical coupling of the interaction involved in the process under study. In perturbation theory, the transition probability can be expanse in series in terms of the coupling α and the number of vertices gives the order of precision of the perturbative calculation. Finite order calculations can lead to infrared and ultraviolet divergencies which need to be compensated by the *renormalization* [3] procedure and it introduces a dependency in the theory on arbitrary scales which represent the cut-offs needed to deal with these divergences. The dependence on these arbitrary scales tend to decrease as higher orders are included in the perturbative calculation. The gauge symmetry and the coupling costants characterize each fundamental interation and further details will be discussed in the following sections.

1.2.1 Quantum Electrodynamics

QED was the first relativistic quantum field theory to be formulated. It describes the electromagnetic interaction that is mediated by the photon, a massless and chargeless gauge boson. Except for neutrinos, all known elementary fermions interact via the electromagnetic force.

The QED Lagrangian is

$$\mathcal{L}_{\text{QED}} = \bar{\psi}(i\gamma^\mu D_\mu - m)\psi - \frac{1}{4}F_{\mu\nu}F^{\mu\nu}, \tag{1.5}$$

where ψ is the fermion field with mass m, γ^μ are the Dirac matrices, D_μ is the covariant derivative defined as

$$D_\mu = \partial_\mu + ieA_\mu(x) \tag{1.6}$$

and

$$F_{\mu\nu} = \partial_\mu A_\nu - \partial_\nu A_\mu. \tag{1.7}$$

In (1.6) and (1.7), e is the elementary charge unit and A_μ is the electromagnetic 4-vector potential. The Lagrangian in (1.5) is invariant under local $U(1)$ phase transformations

$$\psi = e^{i\alpha(x)}\psi \tag{1.8}$$

and under the gauge trasformation

$$A_\mu \rightarrow A_\mu - \frac{1}{e}\partial_\mu \alpha(x) \tag{1.9}$$

where $\alpha(x)$ is an arbitrary scalar function. The $U(1)$ symmetry leads to the conservation of electromagnetic charge. In the Lagrangian (1.5), the addition of a mass term as

$$\frac{1}{2}m_\gamma A^\mu A_\mu \tag{1.10}$$

would violate gauge invariance and would contradict massless photon observations. The QED Lagrangian (1.5) can be written as

$$\mathcal{L}_{\text{QED}} = -\frac{1}{4}F_{\mu\nu}F^{\mu\nu} + \bar{\psi}(i\gamma^\mu\partial_\mu - m)\psi - eA_\mu\bar{\psi}\gamma^\mu\psi, \tag{1.11}$$

where the first and the second terms describes the free propagation of the photons and the charged particles, respectively, and the third term describes the elementary interaction between photons and charged particles. The strength of the electromagnetic interaction is proportional to the inverse of the square of the distance between the particles involved and to the coupling costant [4]

$$\alpha_{\text{EM}} = \frac{e^2}{4\pi} = \frac{1}{137.036}. \tag{1.12}$$

The fact that the photon does not carry the electromagnetic charge implies that self-interaction vertices are not possible for the photon. QED has been stringently verified by experiments and the most accurate experimental confirmation is the measurement of the anomalous magnetic moment of the electron [5].

1.2.2 Weak interaction

All fermions interact via the weak force, it is responsible for different decay processes (e.g. the neutron β-decay) and the mediators of this force are the W^+, W^- and Z bosons. Following predictions of Yang and Lee [6] in late 1950s, Wu observed that the weak decays violate parity [7]. Therefore, the weak interaction has a $V-A$ (vector - axial vector) structure, i.e. the weak field ψ can be decomposed into a left-handed ψ_L and a right-handed ψ_R component,

by applying the projection operators:

$$P_L = \frac{1-\gamma^5}{2}, \qquad P_R = \frac{1+\gamma^5}{2} \tag{1.13}$$

where γ^5 is the chirality operator ($\gamma^5 = i\gamma^0\gamma^1\gamma^2\gamma^4$). The symmetry group for the weak interactions is $SU(2)$ and its generators are the Pauli matrices $\tau_i (i = 1,2,3)$, or $T = \tau/2$. Since generators do not commute, the weak interaction gauge group is non-Abelian. The weak force only applies to left-handed particles, so particles are arranged in weak isospin doublets ($T = 1/2$) and singlets ($T = 0$)

$$\begin{pmatrix} u \\ d \end{pmatrix}_L \begin{pmatrix} c \\ s \end{pmatrix}_L \begin{pmatrix} t \\ b \end{pmatrix}_L \qquad u_R \quad c_R \quad t_R \quad d_R \quad s_R \quad b_R$$

$$\begin{pmatrix} \nu_e \\ e \end{pmatrix}_L \begin{pmatrix} \nu_\mu \\ \mu \end{pmatrix}_L \begin{pmatrix} \nu_\tau \\ \tau \end{pmatrix}_L \qquad e_R \quad \mu_R \quad \tau_R$$

The invariance under $SU(2)_L$ transformations introduces three massless vector fields, $W_\mu^{1,2,3}$, but the presence of massive gauge bosons suggests that there must be a mechanism which assigns the corresponding masses to these particles.

1.2.3 The Electroweak Theory

The EW theory is the unification of Quantum Electrodynamics (QED) and the weak force into a common description, introduced by Glashow, Weinberg and Salam in the late 1960s. The basic idea to achieve this unification is the introduction of a new quantum number, the hyper-charge Y, defined by:

$$Q = T_3 + \frac{Y}{2} \tag{1.14}$$

where Q is the electromagnetic charge, Y is the hyper-charge and T_3 is the third component of the weak isospin. The EW symmetry group is $SU(2)_L \otimes U(1)_Y$, where $SU(2)_L$ is related to the weak isospin and $U(1)$ to the hyper-charge. The theory foresees the existence of four massless bosons, a weak isospin triplet $\mathbf{W}_\mu = (W_\mu^1, W_\mu^2, W_\mu^3)$ and a weak hypercharge singlet B_μ and so, the Lagrangian density of the EW theory is

$$\begin{aligned} \mathcal{L} =& \bar{\psi}_L \gamma^\mu \left(i\partial_\mu - g\mathbf{T}\cdot\mathbf{W}_\mu - g'\frac{Y}{2}B_\mu \right)\psi_L + \bar{\psi}_R\gamma^\mu\left(i\partial_\mu - g'\frac{Y}{2}B_\mu \right)\psi_R \\ & - \frac{1}{4}\mathbf{W}_{\mu\nu}\mathbf{W}^{\mu\nu} - \frac{1}{4}B_{\mu\nu}B^{\mu\nu} \end{aligned} \tag{1.15}$$

where

$$\mathbf{W}_{\mu\nu} = \partial_\mu \mathbf{W}_\nu - \partial_\nu \mathbf{W}_\mu - g\mathbf{W}_\mu \times \mathbf{W}_\nu \tag{1.16}$$

and

$$B_{\mu\nu} = \partial_\mu B_\nu - \partial_\nu B_\mu \tag{1.17}$$

Since the electroweak theory combines two symmetry groups, two different couplings constants g and g' are needed. The electroweak theory is not a complete description because two points are not solved. Firstly, the four gauge bosons are all massless, while experimental observations confirm that only the photon is massless and the three gauge bosons of the weak interaction are heavily massive. Then, the global $SU(2)$ invariance forbids mass terms for the fermions. These two points are explained by the spontaneus symmetry breaking and the Higgs mechanism, discussed in the next session.

1.2.4 The Higgs Mechanism

The Higgs mechanism predicts the existence of a field, the *Higgs field*, which permeates the universe and the interaction with this field provides the mass to the fundamental fermions and the gauge vector bosons of the SM. The Higgs mechanism is responsible for the Spontaneous Symmetry Breaking (SSB) of the EW theory. In order to achieve the SSB, an isospin doublet of complex scalar fields containing four real fields ϕ_i ($i = 1, \ldots, 4$)

$$\phi = \begin{pmatrix} \phi^+ \\ \phi^0 \end{pmatrix} = \frac{1}{\sqrt{2}} \begin{pmatrix} \phi_1 + i\phi_2 \\ \phi_3 + i\phi_4 \end{pmatrix} \tag{1.18}$$

is introduced into the theory and the corresponding potential, the so-called Higgs potential, has the form

$$V(\phi) = -\mu^2 \phi^\dagger \phi + \lambda (\phi^\dagger \phi)^2 = \mu^2 \phi^2 + \lambda \phi^4, \tag{1.19}$$

where the first term of (1.19) is related to the mass of the field and the second term represents the self-interaction of the field. The potential is then minimised in order to determine the ground state, ϕ_0, and the vacuum expectation value, v, of the Higgs field as a consequence. The parameter λ of the potential is assumed to be positive since negative values of λ are unphysical. For $\mu^2 > 0$, the potential V has an unique minimum at $\phi_0 = 0$ and it is symmetric under $SU(2)$. Selecting $\mu^2 < 0$, the minimum of the potential is not at $\phi_0 = 0$, but at $\phi_0^2 = -\frac{\mu^2}{2\lambda} = \frac{v^2}{2}$, so the vacuum expectation value is non-zero and it corresponds to a circumference with radius $\phi_0^2 = v^2/2$ in the complex plane. A graphical representation of the typical shape of the Higgs potential is shown in Figure 1.2. A choice of the physical vacuum state among the infinte possible ground states spontaneously breaks the symmetry[1]. According to the Nambu-Goldstone theorem [8], Goldstone bosons appear in theories that exhibit spontaneous breakdown of continuous symmetries and they correspond to the generators of the internal symmetry spontaneously broken. In the case of the Higgs mechanism, the Goldstone bosons are massless scalars which are absorbed by the gauge fields as a longitudinal polarization component. This additional polarization component allows the gauge fields to acquire mass. A minimum for the local gauge transformation can be

[1]The spontaneous symmetry breaking of a system is defined as a process by which the Lagrangian of a system has a particular symmetry but its physical vacuum state does not exhibit the same symmetry.

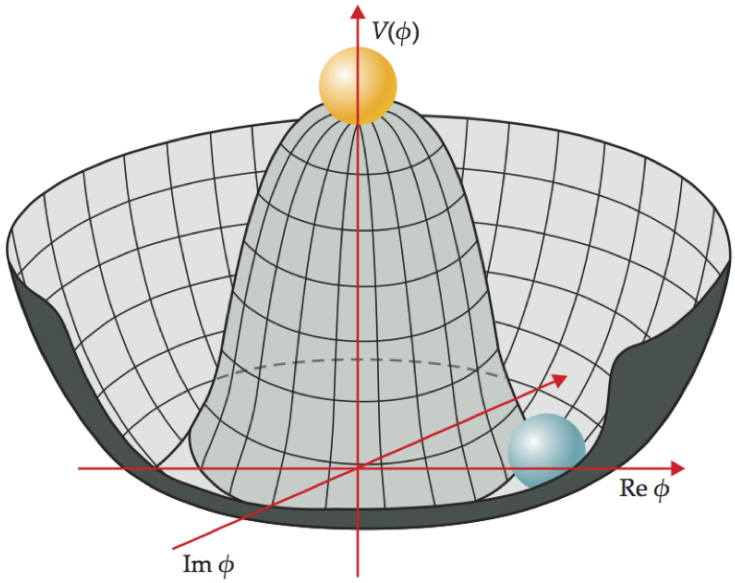

FIGURE 1.2: The peculiar shape of the Higgs potential.

choosen as reference without loosing any generality

$$\phi_0 = \frac{1}{\sqrt{2}}\begin{pmatrix}0\\v\end{pmatrix}. \tag{1.20}$$

The complex scalar field ϕ is now expanded around the minimum, so

$$\phi(x) = \frac{e^{i\boldsymbol{\tau}\cdot\boldsymbol{\theta}(x)/v}}{\sqrt{2}}\begin{pmatrix}0\\v+H(x)\end{pmatrix}, \tag{1.21}$$

where $H(x)$ is the physical scalar Higgs field and $\boldsymbol{\theta}$ represent the three Goldstone boson fields which will be absorbed by the gauge fields. By including the kinematic term, the Lagrangian of the Higgs field can be written as

$$\mathcal{L}_{\text{Higgs}} = (D_\mu H)^\dagger (D^\mu H) - \frac{1}{2}(-2\mu^2)H^2 - \lambda v H^3 - \frac{1}{4}\lambda H^4, \tag{1.22}$$

in which self-interaction terms (cubic and quadratic) and the mass term (the second) are presented and from which the tree-level mass of the Higgs field can be computed as

$$m_H = \sqrt{-2\mu^2} = \sqrt{2\lambda v^2}. \tag{1.23}$$

Since the value of λ is not predicted, the Higgs boson mass is a free parameter in the SM. On July 2012, the ATLAS and CMS experiments announced the discovery of a new boson [9, 10] compatible with the predicted SM Higgs boson. The Higgs boson mass combining

measurements from ATLAS and CMS [11] is

$$m_H = 125.09 \pm 0.21 \text{ (stat.)} \pm 0.11 \text{ (syst.)} \text{ GeV} \tag{1.24}$$

So far, the measured properties of this boson are consistent with SM Higgs boson. On October 2013 François Englert and Peter Higgs were awarded the 2013 Nobel Prize in Physics for the theoretical formulation of the Higgs mechanims in 1964 [12, 13]. From (1.22) and explicitly expressing the covariant derivative as

$$D^\mu = \partial^\mu + ig\vec{T} \cdot \vec{W}^\mu + i\frac{g'}{2} Y B^\mu, \tag{1.25}$$

the charged fields can be defined as

$$W^+_\mu = \frac{W^1_\mu - iW^2_\mu}{\sqrt{2}} \tag{1.26}$$

$$W^-_\mu = \frac{W^1_\mu + iW^1_\mu}{\sqrt{2}} \tag{1.27}$$

and the neutral physical fields are expressed in terms of W^3_μ and B_μ

$$\begin{pmatrix} Z_\mu \\ A_\mu \end{pmatrix} = \begin{pmatrix} \cos\theta_W & -\sin\theta_W \\ \sin\theta_W & \cos\theta_W \end{pmatrix} \begin{pmatrix} W^3_\mu \\ B_\mu \end{pmatrix} \tag{1.28}$$

where θ_W is Weinberg or weak mixing angle, defined in terms of the EW coupling constants g and g' as

$$\cos\theta_W = \frac{g'}{\sqrt{g'^2 + g^2}}, \qquad \sin\theta_W = \frac{g}{\sqrt{g'^2 + g^2}}. \tag{1.29}$$

Finally, the $W^\pm$ and Z masses are related by the Weinberg angle

$$M_Z = \frac{M_W}{\cos\theta_W}. \tag{1.30}$$

The SSB of the $SU(2)_L \otimes U(1)_Y$ gauge symmetry is expolited also to generate the fermion masses. By introducing a Yukawa interaction between the Higgs and the fermion fields,

$$\mathcal{L}_{\text{Yukawa}} = \sum_{f=l,q} y_f \left[\bar{\psi}_L \phi \psi_R + \bar{\psi}_R \bar{\phi} \psi_L\right], \tag{1.31}$$

fermions acquire masses

$$m_f = y_f \frac{v}{\sqrt{2}} \tag{1.32}$$

and the combinations $\bar{\psi}_L \phi \psi_R$ and $\bar{\psi}_R \bar{\phi} \psi_L$ leave the Langrangian gauge invariant as they represent $SU(2)_L$ singlets. The y_f denote the Yukawa coupling between the fermions and the Higgs boson. In order to evaluate the eigenvalues of the Yukawa couplings, unitary transformations can be applied to the fermion fiels and so diagonalize the y_f matrices. Given

the absence of right-handed neutrinos, this unitary transformation does not redefine the leptonic sector. On the other hand, in the quark sector, there is a mismatch between the weak and the mass eigenstates since the W boson couples $u \leftrightarrow d'$, $c \leftrightarrow s'$ and $t \leftrightarrow b'$ where d', s' and b' denote left-handed eigenstates of quarks. As the quark eigenstates are mixing states of mass eigenstates, quarks can decay directly into lower generation quarks and the mixing probability is described by the Cabibbo-Kobayashi-Maskawa (CKM) matrix [14, 15]

$$\begin{pmatrix} d'_L \\ s'_L \\ b'_L \end{pmatrix} = V_{CKM} \begin{pmatrix} d_L \\ s_L \\ b_L \end{pmatrix}, \tag{1.33}$$

with

$$V_{CKM} = \begin{pmatrix} V_{ud} & V_{us} & V_{ub} \\ V_{cd} & V_{cs} & V_{cb} \\ V_{td} & V_{ts} & V_{tb} \end{pmatrix} \tag{1.34}$$

Currently, the best determination of the CKM matrix element is [4]

$$= \begin{pmatrix} 0.97446 \pm 0.00010 & 0.22452 \pm 0.00044 & 0.00365 \pm 0.00012 \\ 0.22438 \pm 0.00044 & 0.97359^{+0.00010}_{-0.00011} & 0.04214 \pm 0.00076 \\ 0.00896^{+0.00024}_{-0.00023} & 0.04133 \pm 0.00074 & 0.999105 \pm 0.000032 \end{pmatrix}. \tag{1.35}$$

The choice of using d-type quarks in (1.33) is purely arbitrary and does not represent any sort of deep physical asymmetry between u-type and d-type quarks. Since the CKM matrix is unitary (i.e. its inverse is equal to its conjugate transpose), defining the weak interaction partners of mass eigenstates with the u-type quarks leads to the same results. According to (1.35), favourite couplings are those internal to a quark family as the diagonal elements are close to 1.

1.2.5 Quantum Chromodynamics

Quantum Chromodynamics (QCD) is a non-Abelian gauge theory that describes the strong interactions of quarks and gluons mediated by the gluon, a massless gauge boson. The QCD symmetry group is $SU(3)$ and its Lagrangian density is

$$\mathcal{L}_{QCD} = \sum_q \bar{\psi}_{q,a}(i\gamma^\mu \partial_\mu \delta_{ab} - g_s \gamma^\mu t^C_{ab} \mathcal{A}^C_\mu - m_q \delta_{ab})\psi_{q,b} - \frac{1}{4} F^A_{\mu\nu} F^{A\mu\nu} \tag{1.36}$$

where

$$F^A_{\mu\nu} = \partial_\mu \mathcal{A}^A_\nu - \partial_\nu \mathcal{A}^A_\mu - g_s f_{ABC} \mathcal{A}^B_\mu \mathcal{A}^C_\nu, \tag{1.37}$$

ψ is the quark field, $\mathcal{A}^B_\mu$ are the gluon fields, t^A are the generators of $SU(3)$ and f_{ABC} are the group structure constants. As already briefly discussed in Section 1.1, colour is the strong interaction charge and there are three different types of colours: red green and blue. Given

that the gluons are also coloured, the QCD Lagrangian includes quark-gluon and gluon-gluon interaction terms.

The strong coupling constant, defined as

$$\alpha_s = \frac{g_s^2}{4\pi} \tag{1.38}$$

represents the fundamental parameter of QCD, together with the quark masses m_q present in (1.36). The renormalization procedure used to absorb the divergencies that arise from pQCD calculations redefines the parameters and the fields of the Lagrangian. In particular, this leads to the renormalized or so-called *running* coupling costant $\alpha_s(\mu_R^2)$ expressed as a function of the unphysical renormalization scale μ_R. The choice of the arbitrary scale μ_R is often taken by considering the scale of the momentum transfer Q in the particular process under study, in order to evaluate the effective strenght of the strong coupling in that process. The exact value of $\alpha_s(\mu_R^2)$ at a fixed scale μ_R can not be analitically predicted, but the dependence of the strong coupling constant on μ_R is determined by the renormalization group equation

$$\mu^2 \frac{d\alpha_s}{d\mu_R^2} = \beta(\alpha_s) = -b_0\alpha_s^2 + b_1\alpha_s^3 + O(\alpha_s^4), \tag{1.39}$$

where β is the so-called β-function of QCD and $b_0 = (33 - 2n_f)/(12\pi)$ and $b_1 = (153 - 19n_f)/(24\pi^2)$ are the first two coefficients of the perturbative expansion of this function. The parameter n_f present in the coefficients is the number of the "light" quark flavours ($m_q \ll \mu_R$). The property of QCD interaction called confinement, briefly introduced in Section 1.1, is related to the behaviour of α_s at large distances (or low exchanged momentum); for $Q^2 \to 0$, α_s diverges and, as a consequence, it is not possible to observe free coloured state. Considering only the first term of the expansion in (1.39), it is possible to express the solution as

$$\alpha_s(\mu_R^2) = \frac{1}{b_0 \ln(\mu_R^2/\Lambda_{\text{QCD}}^2)} \tag{1.40}$$

where $\Lambda_{\text{QCD}}^2 \sim 200\,\text{MeV}$ defines the scale of the formal divergence of α_s. Confinement leads to a process called *hadronization*, discussed in more details in Section 3.6, where quarks and gluons radiated by coloured particles are bound in color singlet hadrons. The experimental signature of this process is a jet, which will be discuss in detail in Section 4.4.

At large Q^2, the behaviour of α is the opposite and tends to zero. This property is called *asymptotic freedom* and it was originally predicted by Politzer [16], Gross and Wilczek [17] who were awarded the Nobel Prize in Physics in 2004. This property allows to apply a perturbative approach to QCD scattering processes as α_s becomes small. A summary of the measurements of α_s as a function of the scale Q is shown in Figure 1.3.

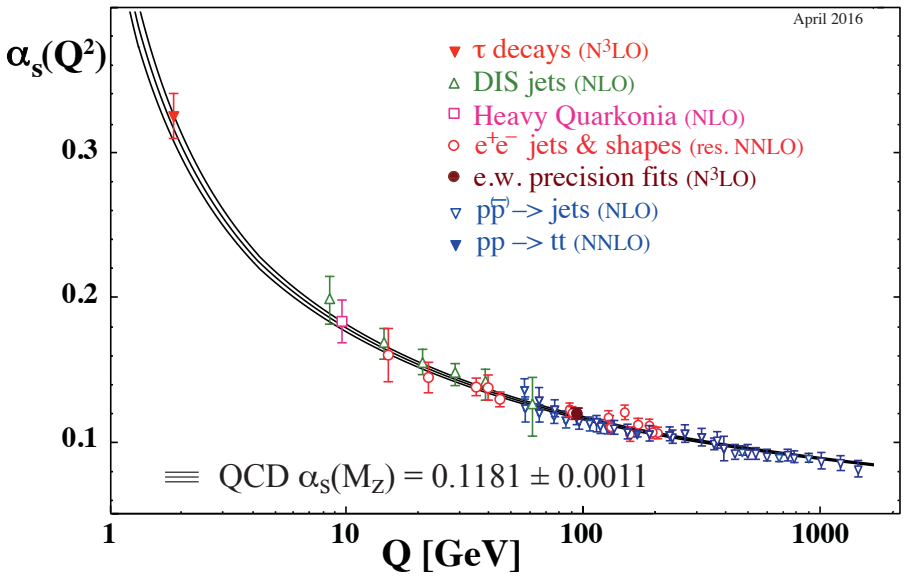

FIGURE 1.3: Running of the strong coupling constant. Figure taken from [4]

1.2.6 Factorization

As described in the previous section, in QCD two distinct regimes are present: the low-coupling regime where a perturbative theoretical treatment is possible and the low-scale regime of non-perturbative QCD where theoretical understanding is restricted to parametrization and phenomenological models. Detailed QCD predictions for hadron colliders are possible due to the factorization theorem [18], which separates perturbative and non-perturbative QCD. In particular, the cross-section for a process can be written as

$$\sigma(AB \to X) = \sum_{i,j} \int dx_i dx_j \, f_{i,A}(x_i, \mu_F^2) f_{j,B}(x_j, \mu_F^2) \, \hat{\sigma}_{i,j}^{(ij\to X)}(x_i, x_j, \alpha_s(\mu_R^2), \mu_F^2, \mu_R^2) \tag{1.41}$$

where $\hat{\sigma}_{ij}$ denotes the short-distance partonic cross-section, the function $f_{i,A}(x_i, \mu_F^2)$ is the probability to find a parton i with momentum fraction x_i inside a hadron A when probed at an energy scale μ_F. These probability densities, the so called Parton Distribution Functions (PDFs), are extremely non-perturbative and therefore uncalculable. Factorization allows to express a cross-section as a convolution between the PDFs and the hard sub-process. The success of factorization is due to the fact that PDFs are approximately universal and, once determined in a given process from data obtained in a particular experiment, they can be used to compute the cross-sections for other perturbative hadronic processes. The factorization scale μ_F is an arbitrary scale that originates from the same regularization and

renormalization techniques applied to the coupling costant. It allows to define the boundary between the kinematic region where infrared divergences, associated with soft and/or collinear emissions of one of the partons, are in the PDFs. The evolution of the PDFs at any scale μ^2 is theoretically predicted, similarly to the evolution of the strong coupling constant α_s, described in (1.39). The renormalization group equations governing the evolution of the PDFs are the Dokshitzer–Gribov–Lipatov–Altarelli–Parisi (DGLAP) [19–21],

$$\frac{d\, f_a(x,\mu^2)}{d\, \ln \mu^2} = \sum_b \int_0^1 \frac{dz}{z} P_{ab}(\alpha_s(\mu^2), z) f_a\left(\frac{x}{z}, \mu^2\right). \tag{1.42}$$

The kernels $P_{ab}(\alpha_s, z)$ are the Altarelli-Parisi splitting functions, that can be computed as an expantion series of α_s

$$P_{ab}(\alpha_s, z) = \alpha_s P_{ab}^{(\mathrm{LO})} + \alpha_s^2 P_{ab}^{(\mathrm{NLO})} + \alpha_s^3 P_{ab}^{(\mathrm{NNLO})} + O(\alpha_s^4). \tag{1.43}$$

There are no evolution equations as a function of x, so the PDFs cannot be calculated a priori and they are thus extracted from fits to cross-section measurements performed by various experiments. The fits these data are performed by collaborations, for example MMHT [22], CTEQ [23], NNPDF [24] and HERAPDF [25]. Examplary results of global fits by the NNPDF Collaboration for PDFs are shown in Figure 1.4. A more detailed description of factorization and DGLAP equations can be found in [26, 27].

1.3 The Top quark

The top quark is the u-type quark of the third generation and it is a special component of the SM. From a theoretical point of view, the existence of such a third generation quark doublet, in conjuction with the presence of three lepton generations, cancels chiral gauge anomalies [28] in the SM and it is therefore crucial for the renormalizability and self-consistency of the theory. In addition, the CKM mechanism needs mixing among three generations (and no fewer) to provide CP violation [15]. The first experimental evidence for the third-generation particles was the discovery of the τ lepton in 1975 [29] which opened the search for the third-generation quarks. Only few years later, in 1977, also the first third-generation quark, the b-quark, was discovered at Fermilab [30] and these results seemed to enforce the hints of a possible existence of an additional quark, the top quark. In 1995, the top quark has been finally discovered [31, 32] by the CDF [33] and D0 [34] Collaborations at the $p\bar{p}$ collider Tevatron. The most recent combination of the measurements of the top quark mass performed by ATLAS, CDF, CMS and D0 experiments [35] is

$$m_{\mathrm{top}} = 173.34 \pm 0.27(\mathrm{stat.}) \pm 0.71(\mathrm{syst.})\,\mathrm{GeV} \tag{1.44}$$

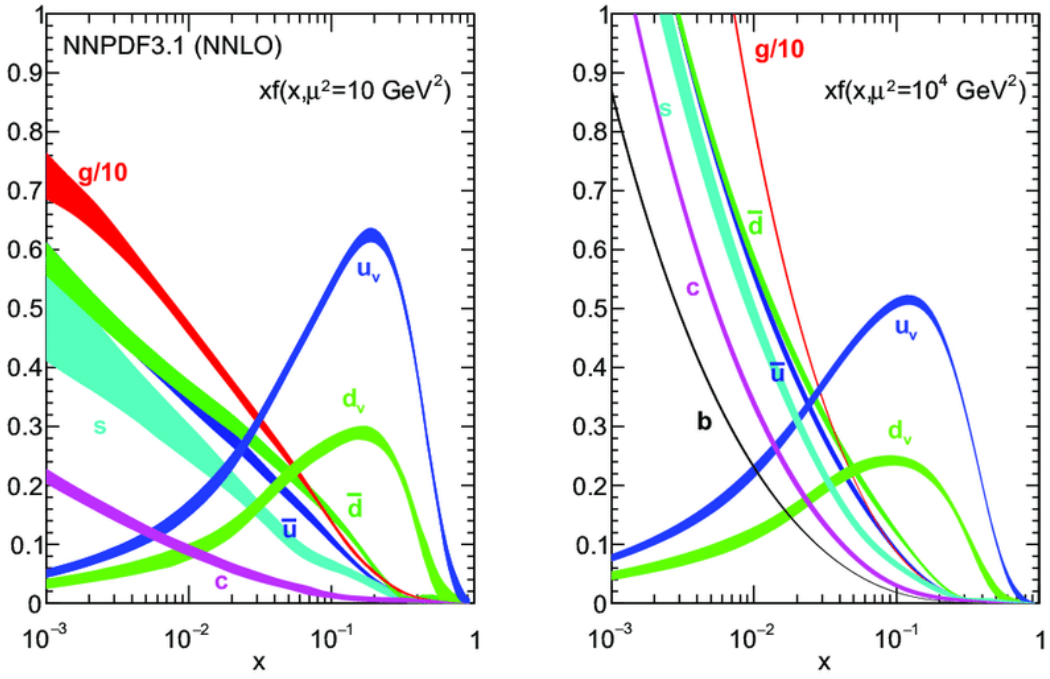

FIGURE 1.4: Results of the most recent global fits by the NNPDF Collaboration [24] for PDFs at factorization scales of 10 GeV^2 (on the left) and 10^4 GeV^2 (on the right).

and this value makes the top quark the heaviest known fundamental particle of the SM, 40 times heavier than the b-quark. A summary of the LHC and Tevatron+LHC combined measurements of the top quark mass is shown in Figure 1.5, while an overview of the SM particles and the orders of magnitude of their masses are shown in Figure 1.6.

The phenomenology of the top quark is driven by its relatively large mass. The lifetime of the top quark[2] is approximately 10^{-25} s, about one order of magnitude smaller than the characteristic time of the strong interaction ($\tau_s \approx 10^{-24}$ s), so the top quark decays before the hadronization process can occur. This offers an unique opportunity to study the properties of a bare quark and its decay products without perturbations due to hadronization and to test strong interactions, both in the perturbative and non-perturbative regimes. In addition, the top-quark large mass implies a Yukawa coupling $\lambda_{\text{top}} \approx 1$ to the Higgs boson, so top quark physics is fundamental in order to study Higgs boson related constraints.

[2]The lifetime of a particle is related to its width by the relation $\tau = \hbar/\Gamma$. For the top quark, the predicted width in SM at NLO is $\Gamma_t = 1.35$ GeV for a value of $m_t = 173.3$ GeV [4].

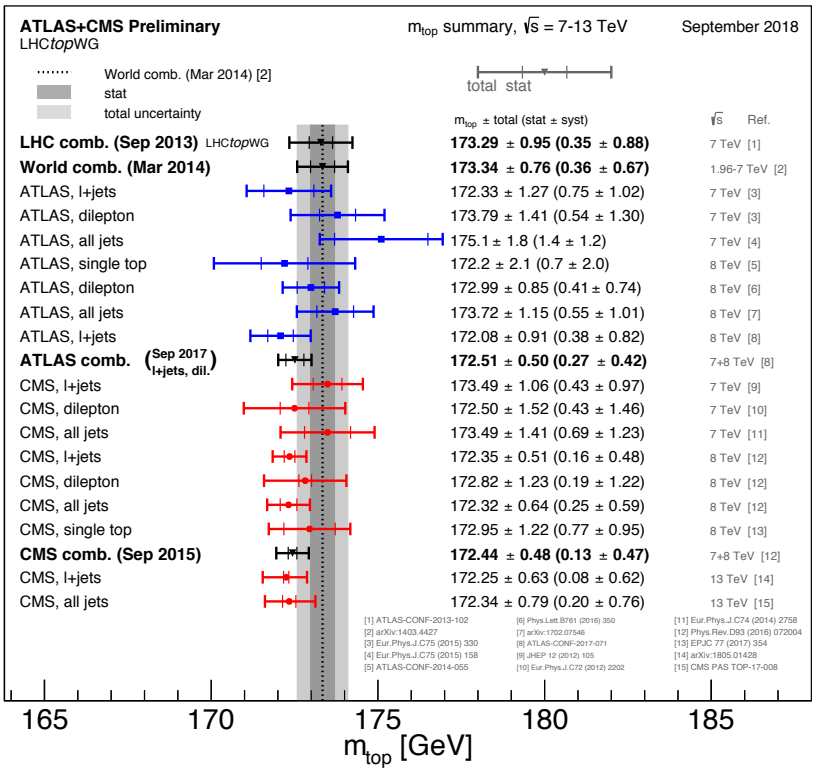

FIGURE 1.5: Summary of the ATLAS and CMS measurements of the top quark mass. The results are compared with the LHC and Tevatron+LHC m_t combinations.

1.3.1 Top quark production

Top quarks can be produced in hadron colliders, such as the Tevatron or the LHC, mostly in a top quark-antiquark pair via a strong interaction or on much rarer occasions singly via an electroweak interaction. The aim of the analysis described in this thesis is to measure $t\bar{t}$ production cross-section and therefore single top production will be considered as one of the background processes. In the following sections, the top-quark pair production will be presented and discussed in more details, together with a brief overiew on the status of both theoretical predictions and experimental results.

1.3.1.1 Top quark pair production

The $t\bar{t}$ pair production in hadron colliders occurs via strong interaction and the corresponding cross-section can be expressed as a convolution between the PDFs and the parton-parton hard scattering process by using the factorization theorem, described in Section 1.2.6. The LO diagrams for $t\bar{t}$ production come from gluon-gluon (gg) fusion and quark-antiquark ($q\bar{q}$) annihilation. The Feynman diagrams related to these processes are shown in Figure 1.7.

The relative contribution to the $t\bar{t}$ production cross-section of the two aforementioned mechanisms depends on the structure of the proton and, subsequently, on its PDFs. The proton is

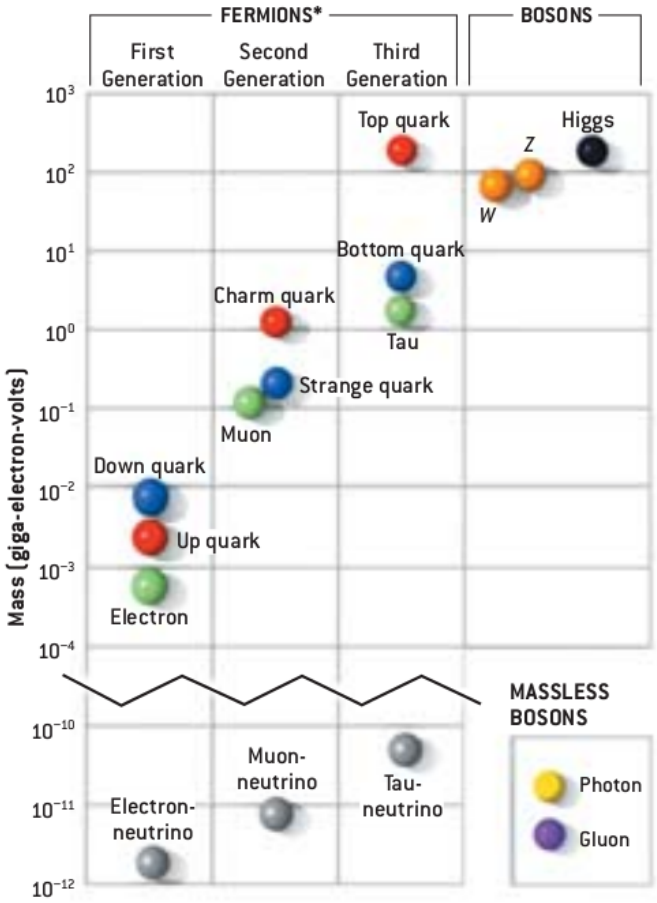

FIGURE 1.6: A graphical comparison of the masses of the SM particles.

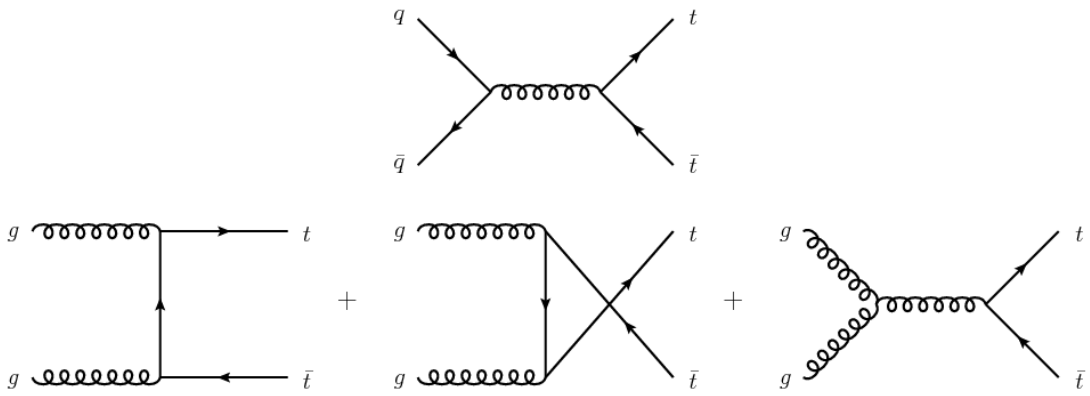

FIGURE 1.7: Feynman diagrams at leading order for $t\bar{t}$ pair production via quark/anti-quark annihilation (on top) and gluon-gluon fusion (on bottom).

a bound state of three valence quarks including sea partons. The probability to find a gluon with fraction x of the proton momentum rapidly increases as x decreases, as it is shown in Figure 1.4. At the Tevatron, x needs to be at least ~ 0.2 in order to reach the top-quark

$\sqrt{s}$	$\sigma_{t\bar{t}}^{\mathrm{NNLO}}$ [pb]	Scale + α_{S} uncertainty [pb]	PDF uncertainty [pb]
8 TeV	252.89	$^{+6.39}_{-8.64}$	$^{+11.67}_{-11.67}$
13 TeV	831.76	$^{+19.77}_{-29.20}$	$^{35.06}_{-35.06}$

TABLE 1.1: Predicted cross-sections for $t\bar{t}$ production at next-to-next-to leading order (NNLO) with next-to-next-to leading log (NNLL) soft gluon resummation [36] for the center-of-mass energies $\sqrt{s}$ of 8 TeV and 13 TeV. The values are obtained assuming a top quark mass of 172.5 GeV, using the TOP++2.0 [37] program. The first uncertainty comes from the independent variation of the factorisation and renormalisation scales, μ_{F} and μ_{R}, while the second one is associated to variations in the PDF and α_{S}, following the PDF4LHC prescription [38] with MSTW2008 68% CL NNLO , CT10 NNLO and NNPDF2.3 5f FFN PDF sets [39–41].

pair production[3] threshold of 350 GeV and therefore $t\bar{t}$ production is mostly ($\sim$ 85%) coming from annihilation between valence quarks ($q\bar{q}$). On the contrary, at the LHC x needs to be $\sim$ 0.02, due to higher centre-of-mass energy with respect to the Tevatron, so the gluon PDF is higher compared to valence quarks PDFs and gluon-gluon fusion process (gg) becomes dominant ($\sim$ 90%).

The total cross section of top quark pair production has a significant dependence on the top quark mass and on the center-of-mass energy of the colliding hadrons. The theoretical predictions for the production rates at the LHC are reported in Table 1.1.

1.3.2 Status of theoretical predictions for differential $t\bar{t}$ production

The inclusive cross-section $\sigma_{t\bar{t}}$ of top-quark pair production represents a theoretical result useful to test the pQCD, when compared with data. Nevertheless, an even more stringent test of the pQCD predictions is provided by the calculation of differential distributions of $\sigma_{t\bar{t}}$, where the cross-section value depends on the specific region of phase-space considered, and the comparison with precise measurements. Given the relatively large cross-section of top-quark pair production among the SM processes, as shown in Figure 1.8, $t\bar{t}$ production is suitable to perform differential measurements. In particular, the distribution of the differential $t\bar{t}$ cross-section as a function of the transverse momentum of the top quark has long shown tensions between NLO predictions and data. This discrepancy has long been a reason for concern and it could be due to higher-order SM corrections to $t\bar{t}$ production and mis-modeling of the NLO Monte Carlo generators used in the differential analyses. Nonetheless, any discrepancy in the SM description of this process could indicate the presence of new physics, given the fact that $t\bar{t}$ production represents one of the main source of background for new physics searches. That said, the improvements in the calculations of the differential $t\bar{t}$ cross-section has played a crucial role in top physics in the recent years.

[3] Considering $t\bar{t}$ production, x can be evaluated by the expression $x \sim \frac{2m_t}{\sqrt{s}}$.

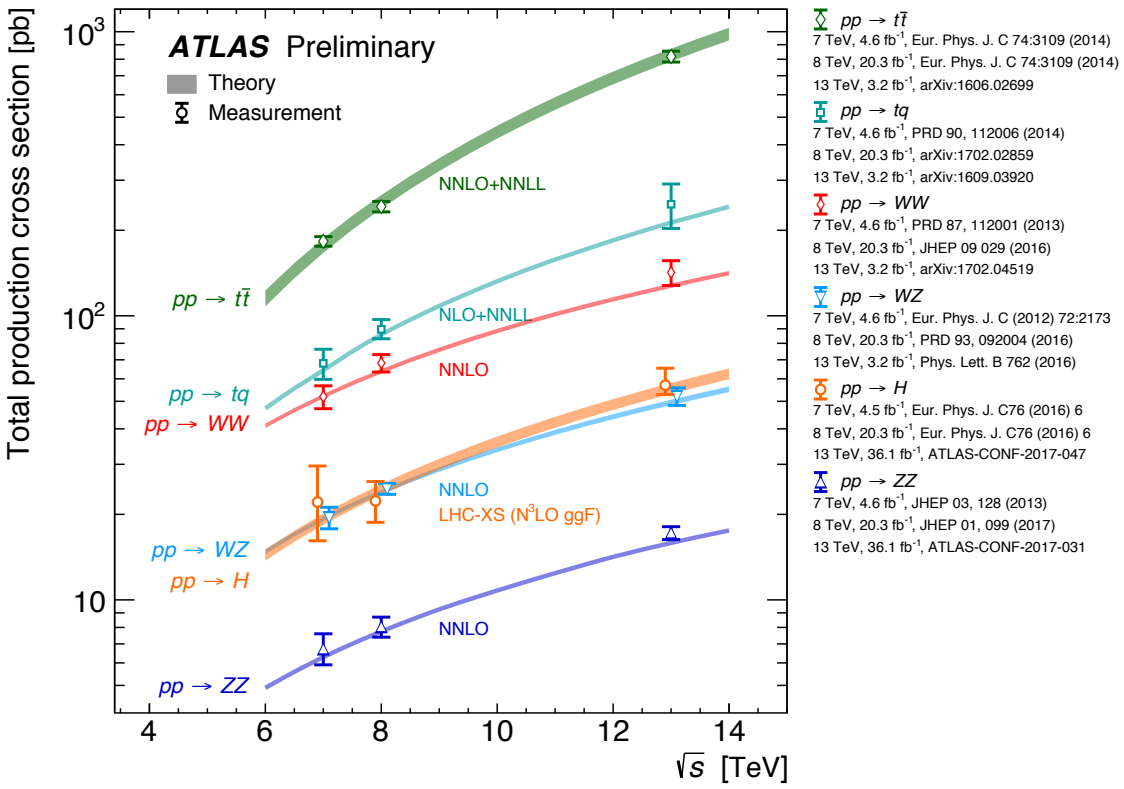

FIGURE 1.8: Summary of total production cross-section measurements by ATLAS presented as a function of centre-of-mass energy $\sqrt{s}$ from 7 to 13 TeV for a few selected processes. Some markers are displaced horizontally for better visibility

The inclusion of higher-order contributions to the differential $t\bar{t}$ cross-sections has been an area of theoretical activity in which the efforts have been mostly concentrated. The calculations of the differential cross-sections for $t\bar{t}$ production at NNLO accuracy [42] reduce the tensions with data. The NNLO predictions for the single differential cross-section as a function of the top quark pp_{T} are compared with LO and NLO predictions in Figure 1.9a and NNLO prediction tends to be lower at high-p_{T}. It is evident that for NNLO, the theoretical uncertainties are reduced, since the scale dependence decreases with the inclusion of higher-order terms. The NNLO predictions are in better agreement with data as shown in Figure 1.9b, where the predictions are compared with a CMS measurement at $\sqrt{s} = 8$ TeV [43].

A further improvement to the SM theoretical predictions for $t\bar{t}$ production is represented by the inclusion of the EW corrections on top of the NNLO QCD calculations, described before. Although the weak interactions are suppressed due to the fact that their coupling is relatively small compared to the strong coupling, the contribution of diagrams of the order $\alpha_{\mathrm{S}}^2\alpha_{\mathrm{EW}}$ can have a small impact at the level of the total cross-section, but sizable effect on differential distributions. The differential distributions of the $t\bar{t}$ production cross-section for NNLO QCD calculations that include NLO EW corrections at $\sqrt{s} = 13$ TeV [44] allow to evaluate the impact of such corrections in specific regions of phase-space. In Figure 1.10, a

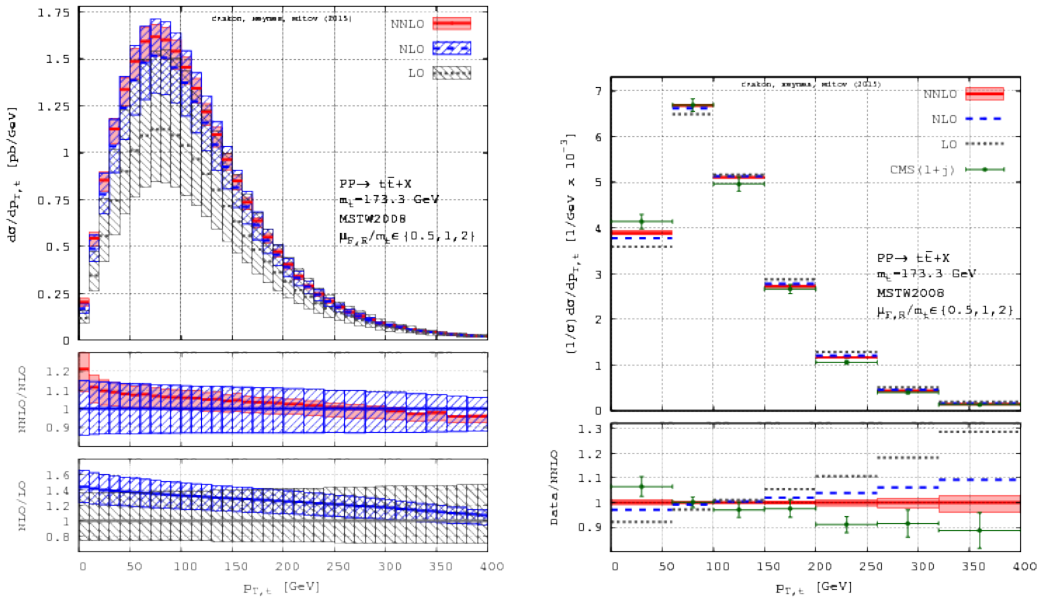

(A) (B)

FIGURE 1.9: Comparison between LO, NLO and NNLO QCD predictions for the the differential $t\bar{t}$ cross-section as a function of the transverse momentum of the top quark (a). The comparison is extended in (b) to the measurement performed by CMS at $\sqrt{s} = 8$ TeV [43]. The error bands represent the scale variation only. The vertical bars represent the uncertainty on the measurement. Figures are taken from [42].

comparison between the predictions obtained by pure QCD calculations at NNLO accuracy and the inclusion of EW contributions at NLO are shown for the top/antitop average and the invariant mass of the $t\bar{t}$ system.

Finally, the double differential NNLO QCD predictions have been calculated [42, 45], but are not yet publicly available. This major achievement in theoretical calculations of $t\bar{t}$ production cross-section can be used to further test the SM predictions in a more stringent way and in more specific regions of the phase-space.

1.3.2.1 Single quark top production

Top quarks can also be produced as single quarks via weak interactions. The cross-section of this process is lower by a factor ~ 3 with respect to $t\bar{t}$ production, even though single top production threshold is lower than $t\bar{t}$. This suppression is due to the fact that α_S is relatevely large compared to α_{EW}. Leading-order Feynman diagrams are the so called s-channel, t-channel and Wt-channel and they are shown in Fig 1.11.

These channels are proportional to the CKM matrix element $|V_{tb}|^2$ (1.35) and therefore the cross section measurement of any of these single top production mechanism is a direct extraction of this matrix element. The expected cross-sections for the different channels at $\sqrt{s} = 13$ TeV are listed in Table 1.2, where it is shown that the Wt-channel is the dominant

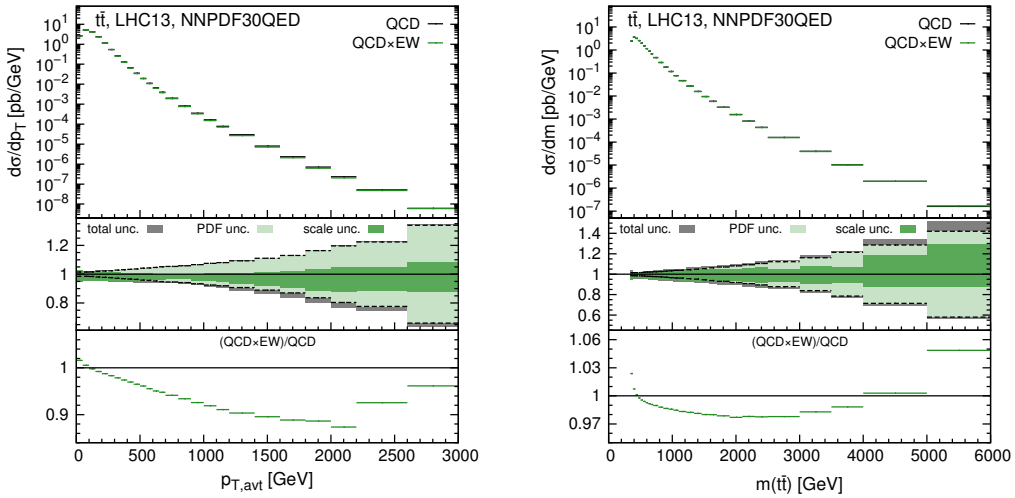

(A) (B)

FIGURE 1.10: Theoretical predictions of top-quark pair production in QCD at NNLO accuracy and the comparison with the inclusion of the NLO EW contributions for the top/antitop average p_T (a) and the invariant mass of the $t\bar{t}$ system (b) differential distributions. The uncertainty is shown for each QCD × EW distributions, including scale, PDF and total combined in quadrature uncertainties. The boundaries of the PDF variation band are marked with black dashed lines. Also shown is the ratio of central scales for the combined QCD and EW prediction with respect to the NNLO QCD one. Figures are taken from [44].

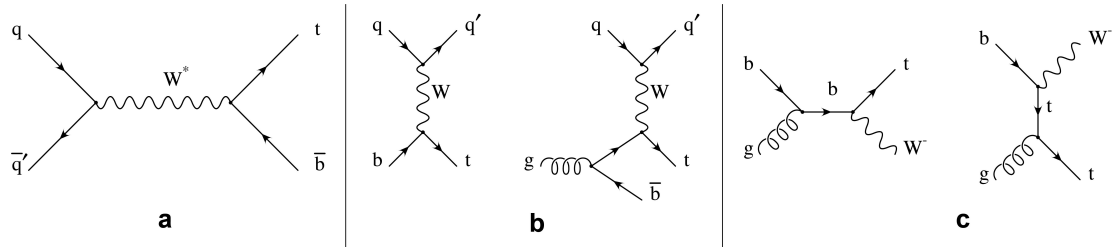

FIGURE 1.11: Single top production channels at leading order. From left to right s-channel (a), t-channel (b) and Wt-channel (c) are shown.

process at LHC. The single top production in the Wt-channel is one of the most important backgrounds present in the measurement of the $t\bar{t}$ cross-section. The reason for that is not only the similar final state, but also the overlap between diagrams between the two process. In fact, NLO diagrams of Wt-channel are the same of LO $t\bar{t}$ production. The contribution of these diagrams has a sizeble effect in the calculations of the single top cross-section in Wt-channel at NLO accuracy. So, two methods have been developed [50] to take into account this double-counting problem: the diagram removal procedure set to zero the amplitudes of doubly-resonant diagrams removing the interference term, while the diagram subtraction mantains the interference at the cost of an increase of the theoretical uncertainty.

Channel	Cross-section [pb]
t	$219.99^{+9.04}_{-7.71}$
Wt	71.7 ± 3.84
s	$10.32^{+0.40}_{-0.36}$

TABLE 1.2: Expected single top quark production cross sections in different channels at a center-of-mass energy of 13 TeV. The predicted single-top cross sections for pp collisions at a centre-of-mass energy of $\sqrt{s} = 13$ TeV is calculated for a top quark mass of 172.5 GeV at next-to-leading order (NLO) in QCD with Hathor v2.1 [46, 47]. PDF and α_S uncertainties are calculated using the PDF4LHC prescription [38] with the MSTW2008 68% CL NLO [48], CT10 NLO [49] and NNPDF2.3 [41] PDF sets, added in quadrature to the scale uncertainty.

Decay mode	Fraction
$e\nu_e$	$1/9$
$\mu\nu_\mu$	$1/9$
$\tau\nu_\tau$	$1/9$
$l\nu_l$	$3 \times 1/9 = 1/3$
$q\bar{q}$	$6 \times 1/9 = 2/3$

TABLE 1.3: W boson decay modes [4].

1.3.3 Top quark decay

The top quark decays via weak interaction into a W^+ (W^-) boson and a d-type quark (antiquark). Decay rates are proportional to the squares of the CKM matrix elements $|V_{tq}|^2$ where $q = b, s, d$. According to (1.35),

$$\mathrm{Br}(t \to Wb) = 0.998, \qquad \mathrm{Br}(t \to Ws) \approx 1.6 \times 10^3, \qquad \mathrm{Br}(t \to Wd) \approx 10^{-4}, \tag{1.45}$$

so the total decay rate is completely dominated by $t \to Wb$, while $t \to Ws$ and $t \to Wd$ are not considered in the following discussion.
Since the top quark decays into a W boson and a b-quark, $t\bar{t}$ event final state is determined exclusively by the decay of the two W bosons from t and $\bar{t}$, while b-quarks hadronise into b-flavoured hadrons. The W boson can hadronically decay into a quark-antiquark pair or leptonically into a lepton and a neutrino. Taking into account all the possible decay mode, there are nine possible W boson final states which are summarized in Table 1.3. So for $t\bar{t}$ events, the experimental final state can be classified into three different categories, which depend on the decay modes of the two W bosons:

- **All hadronic**: in this channel both W bosons hadronically decay ($W \to q\bar{q}$). In the final state there are two high-p_T b-quarks and four light quarks which hadronise into six jets. This is the only channel where all final state constituents are directly measured by the detector. Despite of a high branching ratio, this channel suffers from a large background, such as QCD multi-jet production which is not easy to deal with.

- **Dileptonic**: in this channel both W bosons decay into leptons ($W \to \ell\nu$) and thus events consist of two oppositely charged leptons, two b-quarks and large missing transverse energy due to the presence of two neutrinos. This is the cleanest channel in terms of background contamination, but its branching ratio is relatively small.
- **Semileptonic**: in this channel one W boson decays into leptons while the W boson into quark pair. The final state is characterized by one lepton, two b-quarks, two light quarks and relatively large missing transverse energy due to the neutrino presence. This channel is the best compromise between small background contamination and large branching ratio.

The branching ratios for the three different channels are show in Table 1.4 and graphically represented in Figure 1.12.

Decay modes	Process	Fraction
Dileptonic	$t\bar{t} \to W^+bW^-\bar{b} \to l^+\nu_l b l^-\bar{\nu}_l\bar{b}$	10.5%
Semileptonic	$t\bar{t} \to W^+bW^-\bar{b} \to q\bar{q}'bl^-\bar{\nu}_l\bar{b} + l^+\nu_l bq\bar{q}'\bar{b}$	43.8%
All hadronic	$t\bar{t} \to W^+bW^-\bar{b} \to q\bar{q}'bq''\bar{q}'''\bar{b}$	45.7%

TABLE 1.4: Top-quark pair decay modes and their branching ratios [4].

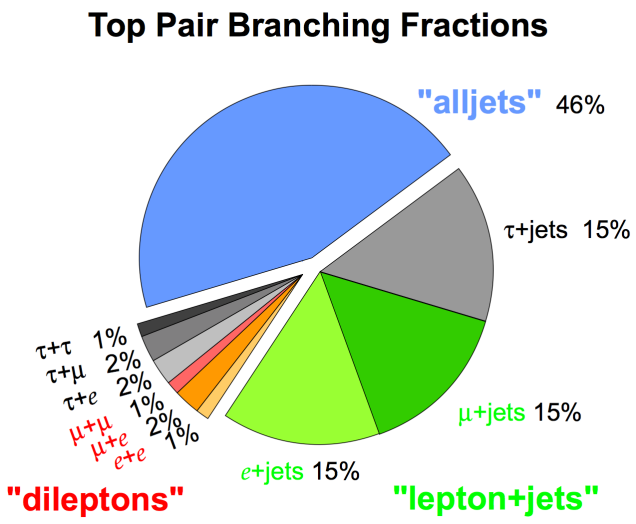

FIGURE 1.12: Pie diagram of top quark pair decay fractions.

The analysis presented in this thesis will focus on the semileptonic decay channel of the $t\bar{t}$ system, the so-called ℓ+jets channel. The process that will be the subject of study is

$$pp \to t\bar{t} \to W^+ b\, W^- \bar{b} \to \ell\nu_\ell\, b\, q\bar{q}\, \bar{b} \tag{1.46}$$

and one of the Feynman diagrams associated to ℓ+jets decay channel is shown in Fig. 1.13.

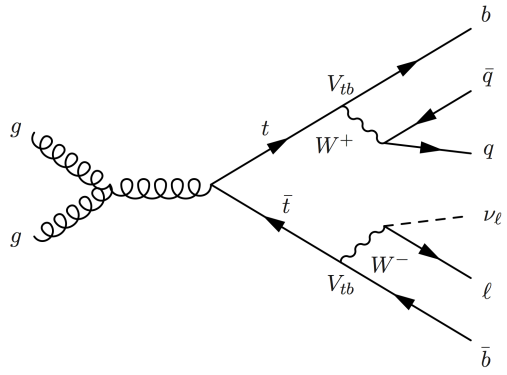

FIGURE 1.13: A Feynman diagram for the top quark pair decay into ℓ+jets channel.

Inclusive $t\bar{t}$ cross-section

In Fig. 1.14, a summary of the most precise measurements of $\sigma_{t\bar{t}}$ at $\sqrt{s}$ = 13 TeV are shown and compared with the latest theoretical prediction, previously presented in Table 1.1. These experimental results, obtained from the combination of measurements performed in different decay channels, are in good agreement with the predicted values. A comparison of the predicted inclusive $t\bar{t}$ cross-section as a function of the center-of-mass energy with the Tevatron and the LHC results is shown in Fig 1.15. The measurements are in good agreement with the SM predictions for all the range of energies covered by the hadron colliders.

1.3.4 Status of the differential cross-section measurements

Since the precision reached by the theoretical calculations has been increasing in recent years, the experimental differential results of $t\bar{t}$ production cross-section allow to more stringently test the predictions of pQCD. The differential cross-section measurements have been provided for all the decay channels and as a function of many kinematic variables and these results are compared with theoretical predictions to probe specific regions of the phase-space. The following discussion will be focused on the ℓ+jets channel since the analysis described in this thesis is performed in this channel. The differential cross-section measurements can be performed in the full phase-space, which are identified as *parton-level* measurements, or in a fiducial phase-space, denoted as *particle-level* analyses.

Particle-level measurements are based on selections that reproduce the acceptance of the detector and on objects similar to the reconstructed ones. This kind of measurements allows to reduce the uncertainties related to the extrapolation in regions of the phace-space not covered by the detector. On the contrary, particle-level analyses may not be suitable for combinations of measurements obtained by different experiments, since the fiducial cuts applied are detector-dependent. These measurements are particularly useful to discriminate between different predictions and to tune the parameters of the Monte Carlo generators.

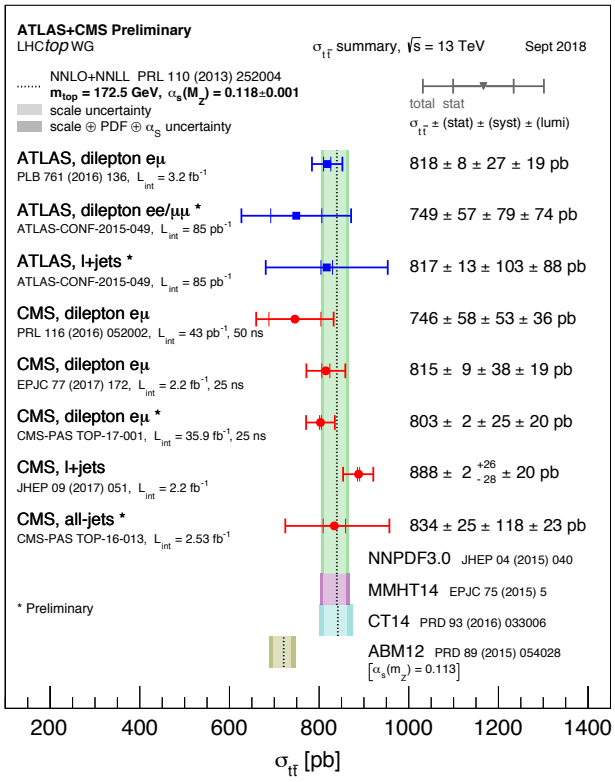

FIGURE 1.14: Top-pair prodcution cross-section measurements at 13 TeV by the ATLAS and CMS collaborations. The band shows the NNLO QCD calculation complemented with NNLL resummation (Top++2.0). The measurements and the theory calculation is quoted at $m_{\text{top}} = 172.5\,\text{GeV}$.

This aspect of the fiducial measurements will be discuss in more details in Section 3.10. In the $t\bar{t}$ cross-section analyses, it is often applied a further categorization based on the p_{T} of the top quark. For high-p_{T} top-quark events, the jets coming from the decay of the top are more collimated and could totally or partially overlap between each other. This leads to a different topology, called *boosted* topology, that requires dedicated reconstruction techniques. The low- and medium-p_{T} regions are denoted as *resolved* regime as the jets are more easily resolved in different objects.

The ATLAS Collaboration provided a particle-level measurement of the $t\bar{t}$ cross-section in the ℓ+jets channel at 13 TeV [51]. The differential distribution of the p_{T} of the hadronic top in the resolved regime is shown in Figure 1.16a, where it is evident that the slope between data and predictions is still present. The overlap between the two toplogies is shown in Figure 1.16b where it is possible to observe that the trend of the mis-modeling is similar between them.

Parton-level measurements are defined on the full phase-space and, subsequelty, are not experiment-dependent. For this reason, they are suitable for combinations and meaningful

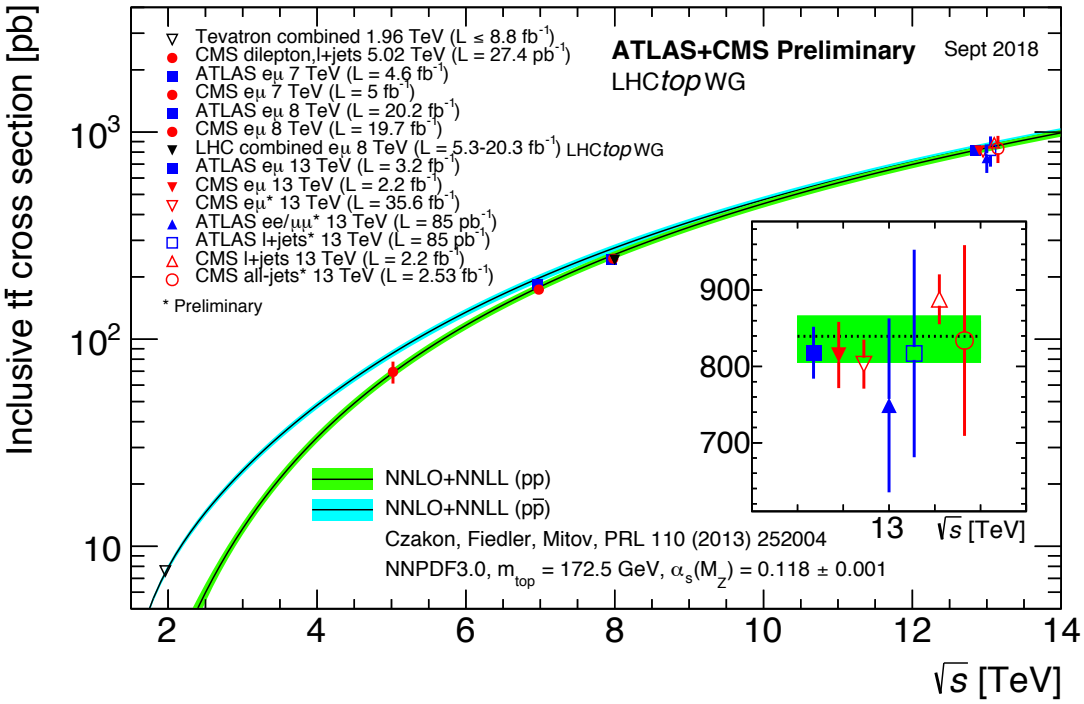

FIGURE 1.15: Summary of the LHC and the Tevatron measurements of the top-pair production cross-section as a function of the centre-of-mass energy compared to the NNLO QCD calculations complemented with NNLL resummation (Top++2.0). The theory calculation refer to $m_{\text{top}} = 172.5\,\text{GeV}$. Measurements made at the same centre-of-mass energy are slightly offset for clarity.

comparisons of measurements obtained with different experiments. In addition, parton-level distributions can be compared with the available theoretical predictions at a fixed-order accuracy and they represent powerful observables to test pQCD. In Figure 1.17, the comparison between the ATLAS and CMS parton-level results at 8 TeV for the invariant mass of the $t\bar{t}$ system is shown together with the NNLO and NLO theoretical predictions [45].

The most recent measurements provided by the ATLAS Collaboration in the ℓ+jets channel for parton level is performed at 8 TeV [52]. Currently, ATLAS has not published a parton-level result in ℓ+jets channel at 13 TeV. In addition to the aformentioned benefits of having parton-level measurements, these analyses are useful to derive PDFs, in particular the gluon PDF inside the proton, and to extract QCD parameters, such as α_S and m_t. A first result of PDF determination from ATLAS measurements, including $t\bar{t}$ cross-sections [52], was recently published [53].

The increasing statistics available from the LHC allows to further differentiate the cross-section distributions. A better understanding of the level of agreement between data and predictions can be reached by measuring double differential distributions. CMS presented double differential distributions at $\sqrt{s} = 13\,\text{TeV}$ [54]. A first attempt to measure double

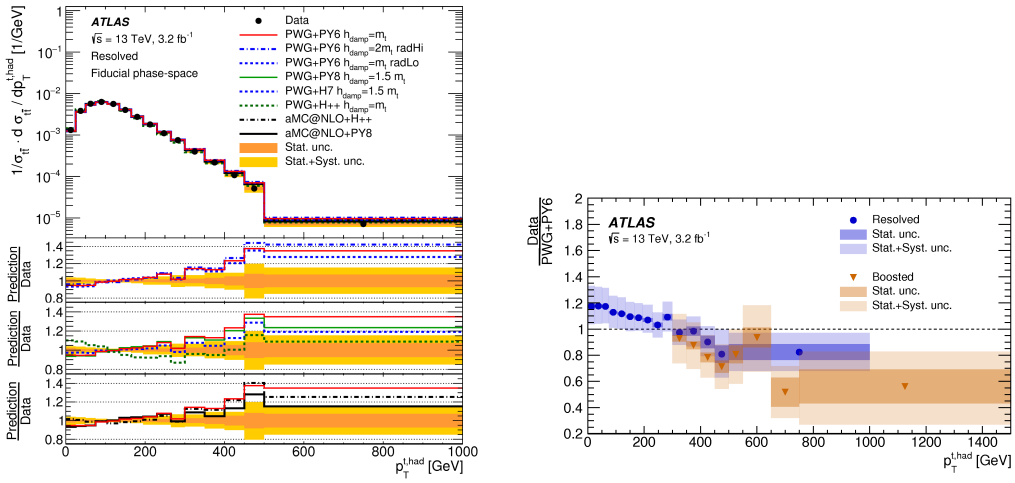

(A) (B)

FIGURE 1.16: Fiducial phase-space relative differential cross-sections as a function of the (a) transverse momentum of the hadronic top quark. The yellow band indicate the total uncertainty of the data in each bin. The lower panels show the ratio of different predictions to the data. In (b), it is shown the ratios of the measured fiducial phase-space differential cross-section to the prediction from POWHEG+PYTHIA 6 in the resolved and boosted topologies as a function of their respective transverse momentum of the hadronic top quark. The bands indicate the statistical and total uncertainties of the data in each bin. Figures are taken from [51].

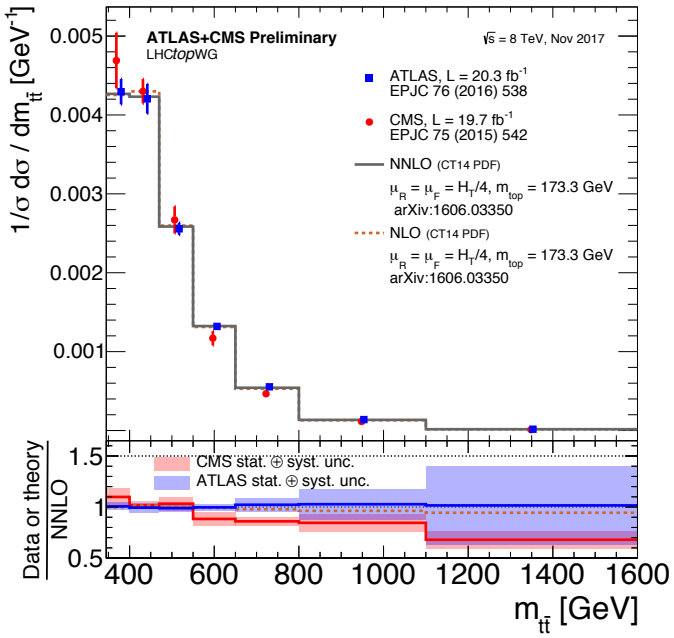

FIGURE 1.17: Full phase-space normalised differential ttbar cross-section as a function of the invariant mass of the top-quark pair. The CMS and ATLAS results are compared to the NLO and NNLO calculations from [45]. The shaded bands show the total uncertainty on the data measurements in each bin. The lower panel shows the ratio of the data measurements and NLO calculation to the NNLO calculation.

differential distributions in ℓ+jets channel for ATLAS was recently published [55] where an analysis strategy similar to the previously presented ℓ+jets analysis at 13 TeV [52] was used. The differential cross-sections are presented as a function of exclusive bins of jet multiplicity. From the distributions of p_{T} of the hadronic top in different bins of jet multiplicity, shown in Figure 1.19, it has been found that the dominant contribution to the tension between data and predictions is localized in the 4-jet exclusive region. It was not possible to find this result in the previous inclusive analysis. The discriminating power have the potential to futher constrain the MC models used to describe the top-quark pair production and provides hints of the benefits of having double differential cross-section results for a wider set of kinematic variables.

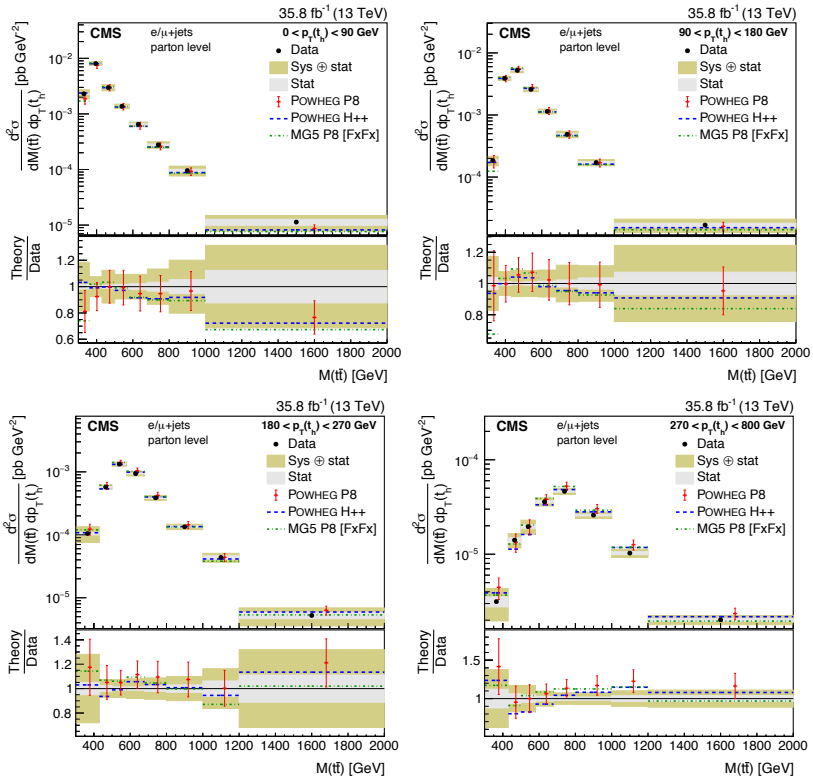

FIGURE 1.18: Double-differential cross section at the parton level as a function of p_{T} of the hadronic top vs invariant mass of the $t\bar{t}$ system. The data are shown as points with light (dark) bands indicating the statistical (statistical and systematic) uncertainties. The cross sections are compared to different predictions. The ratios of the various predictions to the measured cross sections are shown at the bottom of each panel [54].

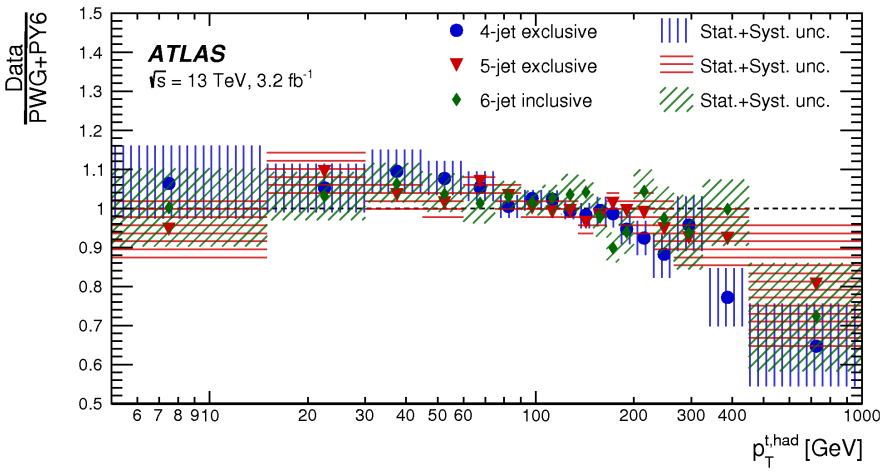

FIGURE 1.19: Normalised ratio of data to the nominal prediction as a function of p_{T} of the hadronic top in the 4-jet exclusive, 5-jet exclusive and 6-jet inclusive configurations [55].

Chapter 2

The LHC and the ATLAS experiment

2.1 The LHC

The Large Hadron Collider (LHC) [56] is a circular proton-proton collider situated astride the Franco-Swiss boarder in the Geneva area and it is currently the largest and most energetic particle accelerator in the world. It was built by the European Organization for Nuclear Research (CERN) and it is the most recent addition to the system of particle accelerators available at CERN. It is situated at a depth between 50 m and 175 m and consists of a 27 km ring of superconducting magnets in which protons circulate in two opposite beams. A scheme of the accelerator is shown in Figure 2.1. Before the injection in the LHC main ring, the protons are produced by ionization of hydrogen gas and then boosted by a system of accelerating structures. Each of the pre-accelerators work in sequence and bring protons to a larger energy compared to the previous step. The accelerating structures are:

- **LINAC2** that is responsible for accelerating the protons to 50 MeV. It is a linear accelerator that exploits radiofrequency cavities in order to charge cylindrical conductors, which are alternately positive or negative.
- **Proton Synchrotron Booster (PSB)** in which protons are accelerated to 1.4 GeV. It is made up of four superimposed synchrotron rings.
- **Proton Synchrotron (PS)** where protons reach 26 GeV. The PS was the first synchrotron at CERN and was for a brief period the world's highest energy particle accelerator. The weak neutral current, mediated by the Z boson, was discovered using this accelerator.
- **Super Proton Synchrotron (SPS)** accelerates protons to 450 GeV, that is the minimum energy at which the LHC can maintain a stable beam. The W and Z bosons were discovered in 1983 thanks to SPS, when this accelerator was running as proton-antiproton collider. It is the second largest machine available in the accelerator complex at CERN.

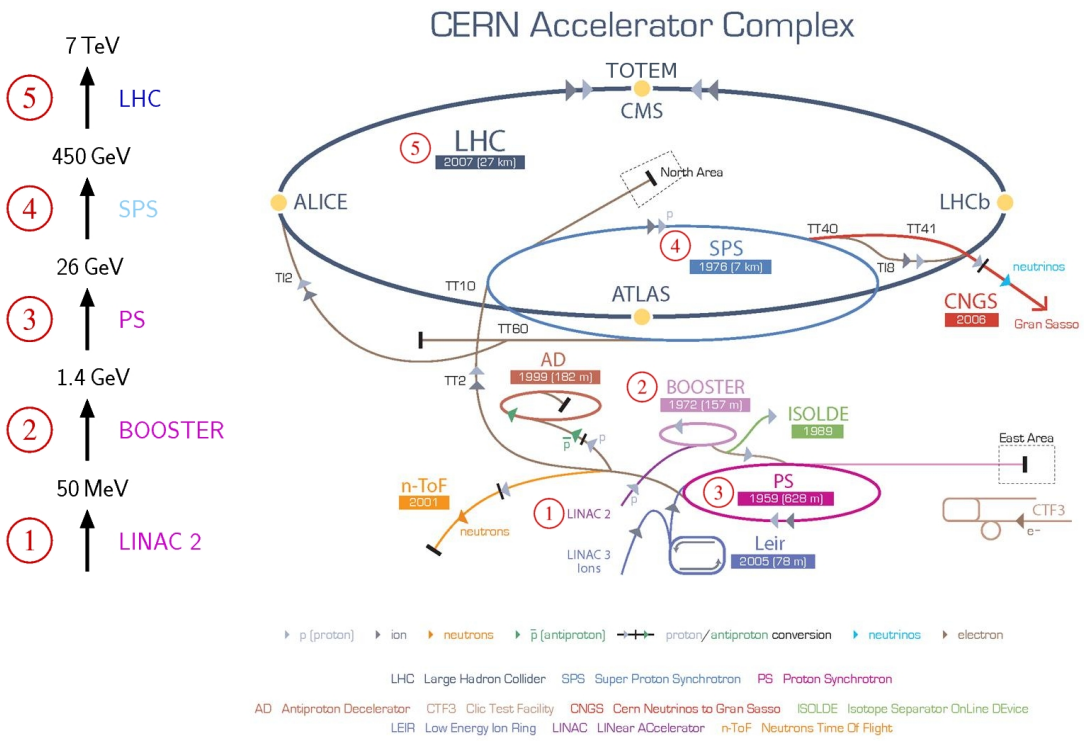

FIGURE 2.1: Overview of the accelerating steps and nominal energy reached (on the left) and schematic view of the LHC accelerator complex and particle detectors (on the right).

Protons circulating inside the LHC are distributed in bunches and each of these bunches contains about 10^{11} protons. The proton bunches are injected in the main ring and splitted into two opposite beams. The beams follow a circular trajectory due to the effect of a superconducting magnet system, which surrounds the main ring. It consists of coils of niobium-titanium (NbTi) wires which are cooled by a liquid-helium circuit. The magnetic field produced by the system reaches the value of 8.3 T in order to sufficiently bend and focus the beams and it operates at a temperature of 1.9 K to keep the coils in a superconducting status. A dipole system ensures that the proton beams are bended, while a multipole magnet system makes the proton beams squeezed and focused either vertically and horizontally. The two opposite beams of proton bunches collide in several interaction points, where detectors are installed in order to collect data from these collisions.

An important feature of a collider is the instantaneous luminosity, which is defined as

$$\mathcal{L}_{\text{ins}} = \frac{dN}{dt}\frac{1}{\sigma_{\text{event}}} \tag{2.1}$$

where dN/dt is the event rate and σ_{event} is the cross section of the particular event under study. The instataneous luminosity has the dimensions of number of events per unity of

Parameter	Design	2015	2016
Beam Energy [TeV]	7	6.5	6.5
Bunch Spacing [ns]	25	25	25
Number of bunches	2808	2232	2200
Number of particles per bunch	$1.15 \cdot 10^{11}$	$1.21 \cdot 10^{11}$	$1.15 \cdot 10^{11}$
β^* [m]	0.55	0.8	0.4
ε_n [μm rad]	3.75	3.3	2.1
Luminosity [$\text{cm}^{-2}\text{s}^{-1}$]	10^{34}	$5.02 \cdot 10^{33}$	$1.45 \cdot 10^{34}$
Total Luminosity delivered [fb^{-1}]	-	4.2	38.5

TABLE 2.1: An overview of the typical performance-related parameters of the LHC during operations in 2015-2016 years and their corresponding record values.

time and per area. It can be written, in general, as

$$\mathcal{L}_{\text{ins}} = \frac{N_b^2 n_b f}{4\pi\sigma_x^*\sigma_y^*} F, \tag{2.2}$$

Assuming round beams and equal values of the beta function for both beams, the instantaneous luminosity for the LHC may be expressed as

$$\mathcal{L}_{\text{ins}} = \frac{N_b^2 n_b f \gamma_r}{4\pi\varepsilon_n\beta^*} F, \tag{2.3}$$

where f is the frequency of bunch crossings, N_b the number of particles per bunch, n_b the number of bunches per beam, γ_r the relativistic gamma factor, ε_n the normalized transverse beam emittance, β^* the optical beta function, σ_x^* and σ_y^* are the horizontal and vertical beam sizes at the interaction point and F is the geometrical reduction factor, which is related to the effective area of the beams. Given the design parameters (see Table 2.1), the nominal luminosity of the LHC is of $10^{34}\,\text{cm}^{-2}\,\text{s}^{-1}$.

The quantity often used to measure the number of events delivered by a collider is the integrated luminosity

$$\mathcal{L} = \int \mathcal{L}_{\text{ins}}\, dt, \tag{2.4}$$

that measures the total numbers of collisions in a certain period of time.

2.1.1 The LHC Experiments

The experiments, situated along the main ring, use detectors in order to record and analyse the collisions delivered by the LHC. Currently, seven experiments are carried out at the LHC and each of them is carachterized by its detector. The main experiments, in terms of size and number of scientists involved, are four and they are situated in specific interaction points, which are shown in a schematic view in Figure 2.2. The four main experiments are:

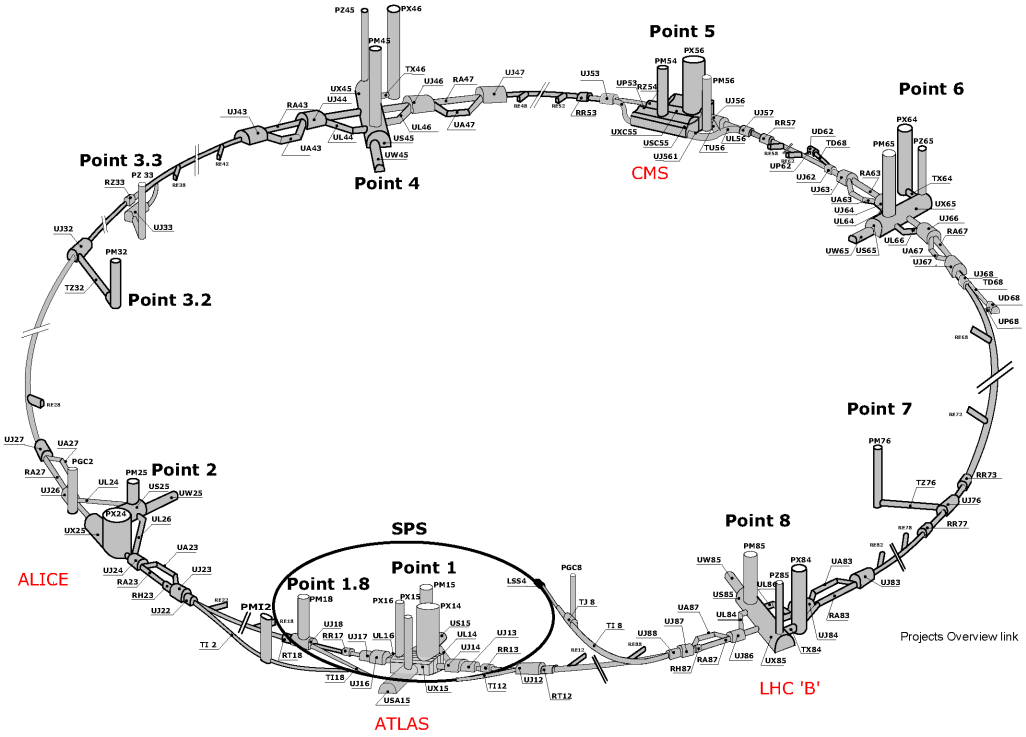

FIGURE 2.2: View of the LHC infrastructures and map of its experiments. Each of LHC experiments is indicated in red.

- **A Large Lhc Toroidal ApparatuS (ATLAS)** [57] is one of the two multipurpose experiments, which investigates a wide range of physics processes, from SM precise measurements to searches for signatures of new physics. The data analysed for this work have been collected with the ATLAS detector, so a more detailed description can be found in Section 2.2.

- **Compact Muon Solenoid (CMS)** [58] is also a multipurpose experiment and it has the same aim of ATLAS, but it uses different and complementary technologies, independent from ATLAS. Therefore, it is possible to cross-confirm a new discovery, e.g. the discovery of the Higgs boson, and perform a comparison or combination of the results obtained by two experiments.

- **Large Hadron Collider beauty (LHCb)** [59] is designed to focus on the study of flavour physics of the B mesons and possibly explain the CP-violation present in nature.

- **A Large Ion Collider Experiment (ALICE)** [60] is built to study quark-gluon plasma created in heavy-ion collisions. The LHC performs special runs in which heavy ions, e.g. lead, are used instead of the usual protons. The ion-ion and proton-ion collisions are the most relevant for this experiment.

There are also three smaller experiments along the LHC, which share the interaction points with the main detectors described above.

- **TOTal Elastic and diffractive cross section Measurement (TOTEM)** [61] is dedicated to measure the effective size of the proton and monitor the LHC luminosity. It is the longest experimental detector on the LHC and it is located around the CMS interaction point.
- **Large hadron Collider forward (LHCf)** [62] is designed to simulate and study cosmic rays, exploiting neutral particles emitted by LHC collisions in the forwar region, i.e. the directions at a small angle from the beamline. It is made up of two parts and they are situated at either side of the ATLAS interaction point.
- **Monopole and Exotics Detector at the LHC (MoEDAL)** [63] is intended for the direct search for the magnetic monopole, a hypothetical particle with a magnetic charge. It is deployed around the LHCb interaction point.

2.2 The ATLAS Detector

The ATLAS detector is a general purpose detector and its aim is to exploit the full discovery potential of the LHC and perform precise measurements of the SM physics processes. ATLAS is the largest detector currently present at the LHC as it is about 44 m long, 25 m high and it weighs 7000 tons. It is intended to be hermetic in order to detect all the identificable particles as precisely as possible and it is designed to handle the high-multiplicity and high-rate bunch crossing conditions of the LHC. The layout of the detector is based on the traditional onion-shell structure used in collider experiments and it has a cylindrical symmetry around the beam pipe. The ATLAS detector consists of a central part, *barrel*, and two side parts, *endcaps*.

Given the specific geometry of the ATLAS detector, it is convenient to define a standard spatial coordinate system taking the nominal interaction point as origin. The counterclockwise beam direction defines the z-axis and the x-y plane is transverse to the beam direction, with the x-axis pointing to the center of the LHC ring and the y-axis pointing upwards. The azimuthal angle ϕ is measured around the beam axis and the polar angle θ is measured from the z-axis. The side-A of the detector is defined as the side including positive values of z and side-C is the one with negative values of z. The transverse momentum p_{T}, the transverse energy E_{T} and the missing transverse energy $E_{\mathrm{T}}^{\mathrm{miss}}$ are defined in the $x-y$ plane unless stated otherwise.

In hadron-collider physics, the rapidity (y) is preferred over the polar angle because differences in rapidity are Lorentz invariant under boosts along the longitudinal axis and they

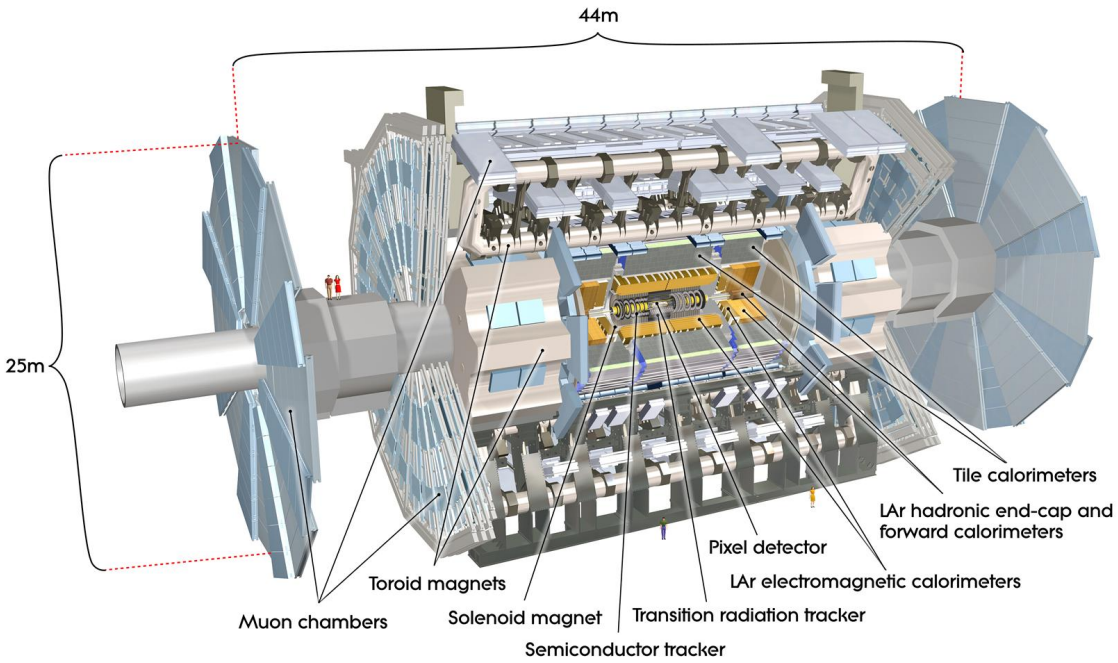

FIGURE 2.3: Schematic view of ATLAS detector.

transform additively. The expression of the rapidity is the following

$$y = \frac{1}{2} \ln \left(\frac{E + p_z}{E - p_z} \right), \tag{2.5}$$

where E is the energy and p_z is the longitudinal momentum (i.e. the component along the beam axis) of the particle. The polar angle θ is used to define an useful quantity, the pseudorapidity (η), describing the direction of a particle relative to the beam axis as

$$\eta = -\ln \left(\tan \frac{\theta}{2} \right). \tag{2.6}$$

In terms of the momentum, the pseudorapidity can be written as

$$\eta = \frac{1}{2} \ln \left(\frac{|\mathbf{p}| + p_z}{|\mathbf{p}| - p_z} \right) \tag{2.7}$$

where $\mathbf{p}$ is the three-momentum. In Figure 2.4 exemplary values of the polar angle θ are shown in association with their corresponding values of the pseudorapidity η. By comparing Equation 2.5 and Equation 2.7, it is evident that $\eta \simeq y$ in the ultra-relativistic limit $m \ll |\mathbf{p}| \rightarrow E \approx |\mathbf{p}|$.

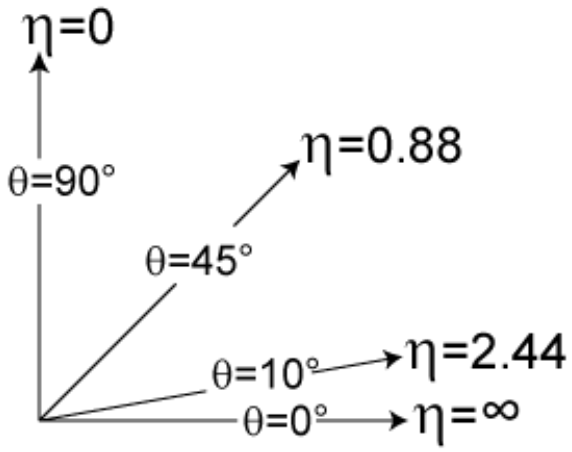

FIGURE 2.4: Example values of the polar angle and their corresponding values of the pseudorapidity.

The pseudorapidity is used to define a measure of the angular separation between particles in the $\eta - \phi$ space with angular-only quantities

$$\Delta R = \sqrt{(\Delta\eta)^2 + (\Delta\phi)^2} \tag{2.8}$$

which is Lorentz invariant if the involved particles are massless.

ATLAS is composed by different sub-components [64] and a schematic view of their names and collocation inside the detector is shown in Figure 2.3. In detail, it is composed by a magnetic system and five main sub-detectors (from the innermost to the outermost): the inner detector (ID), the electromagnetic liquid argon calorimeter (LAr), the hadronic calorimeter (Tile), the muon spectrometer (MS) and the forward detectors. The particular order and disposition of each of the sub-detectors is crucial in the reconstruction of the particles crossing the detector. The ID is a tracking system and it is immersed in a magnetic field. The presence of the magnetic field allows to bend the charged-particle trajectories and measure the momentum of the particles. The middle section of ATLAS is filled by the calorimetric system and it absorbes most of the particles and it measures their energy. Then, the MS is used for the identification and reconstruction of muons which reach the outermost part of the detector. The interaction of different type of particles with the sub-detectors is shown in Figure 2.5.

2.3 Magnet System

The magnet system of ATLAS is designed to provide magnetic field covering a volume of 12000 m^3 in order to bend the trajectories of charged particles. The deflection induced by the magnetic system is used to perform the measurement of the momenta of the charged particles. The magnetic field system of ATLAS is composed of:

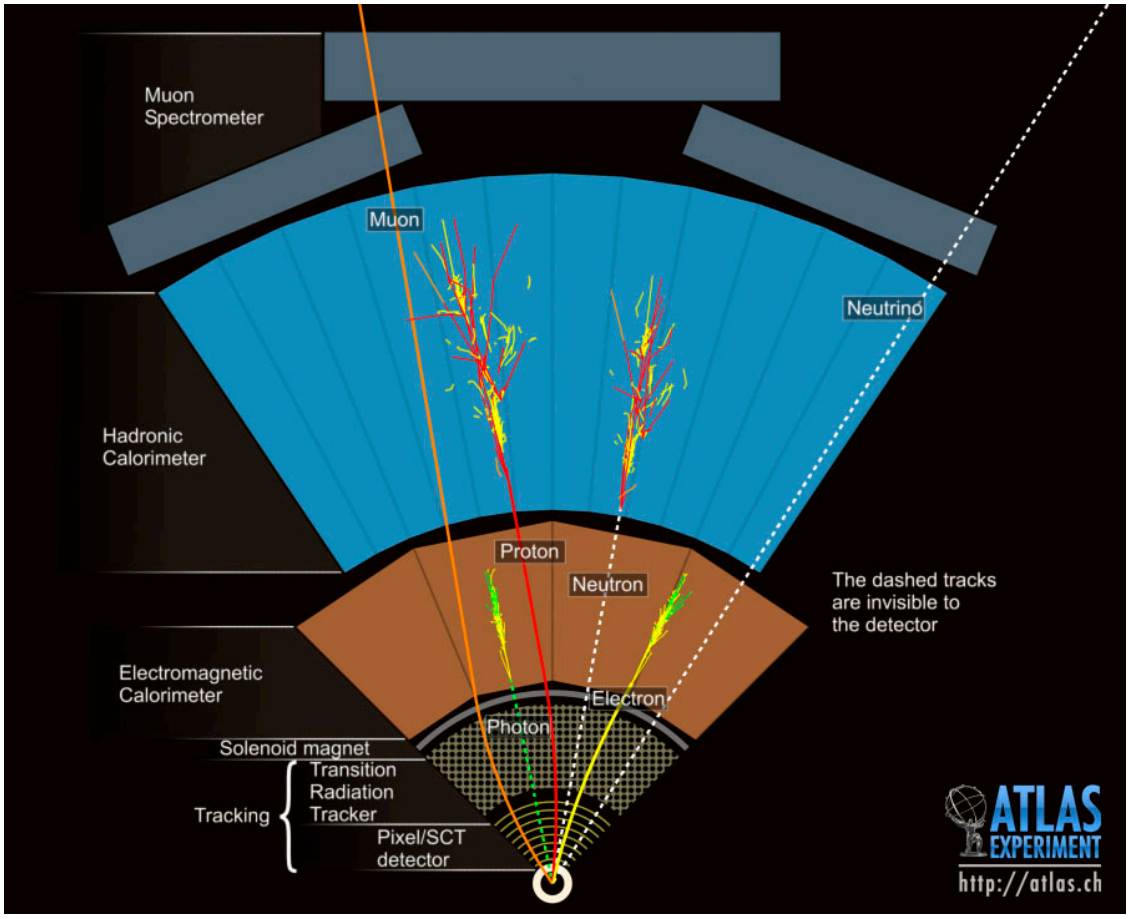

FIGURE 2.5: Section of the ATLAS detector and the interations that the particles undergo with each of the sub-detectors.

- a superconducting **central solenoid (CS)** which produces a magnetic field of 2 T directed along the beam line. It surrounds the ID and it is designed to be as thick as possible in order to minimize the impact on the energy measurement in calorimeters. It has a diameter of 2.4 m with a lenght of 5.3 m;
- a **toroid** system, which provides a $\simeq 4$ T field mostly orthogonal to the muon trajectories. It is constituted by a **barrel toroid (BT)** and two **end-cap toroids (ECT)**. The BT is composed by eight toroids 25 m long, with a inner core of 9.4 m and an outer diameter of 20.1 m. It provides the magnetic bending for particles in the region $|\eta| < 1$. The two ECTs are 5 m long with an inner core of 1.64 m and an outer diameter of 10.7 m. and they operate in region $1.4 \leq |\eta| < 2.7$. In the transition region, $1 \leq |\eta| < 1.4$, the magnetic deflection is provided by a combination of barrel and end-cap toroids.

An illustration of each component of the magnet system is shown in Figure 2.6.

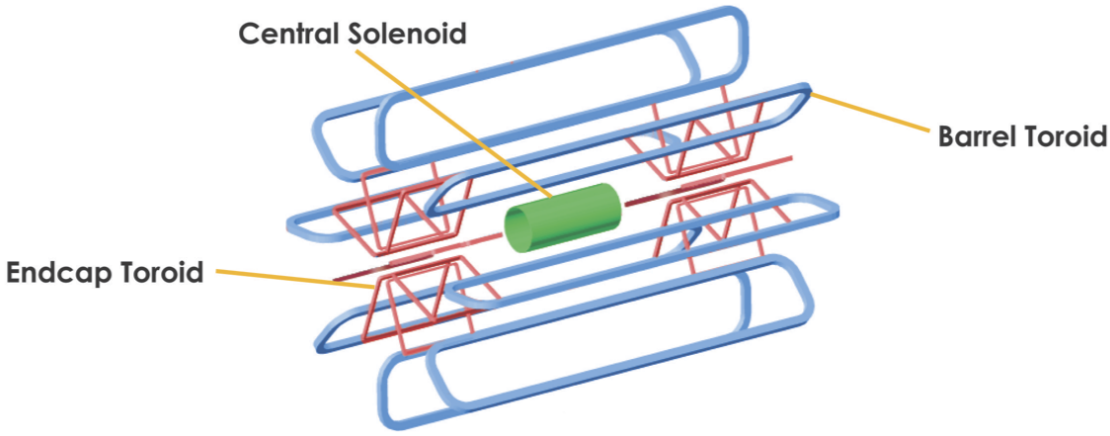

FIGURE 2.6: Overview of layout of the magnet system of ATLAS.

2.4 Inner Detector

The Inner Detector (ID) is the innermost part of the ATLAS detector and it surrounds the beam pipe and the nominal interaction point IP1. The ID is the ATLAS tracking system dedicated to identify and reconstruct tracks and vertices in the region $|\eta| < 2.5$. It is designed to handle the large density of particles coming from the pp collisions provided by the LHC. The average number of particle produced from the interaction point every 25 ns is of the order of the thousands. Given these challenging conditions, the ID needs to be sufficiently granular to discriminate the origin of tracks and measure the curvature of the charged particles due to the presence of the magnetic field. In particular, secondary vertex reconstruction is crucial for the identification of the jets containing B-hadrons, so called b-tagging. It is a 7 m long cylinder with a diameter of 2.5 m immersed in a 2 T magnetic field generated by the central solenoid. A schematic overall view of the ID with its general sizes is shown in Figure 2.7.

The ID consists of four independent but complementary sub-detectors: the Insertable B-Layer (IBL), the Pixel Detector, the Semi Conductor Tracker (SCT) and the Transition Radiation Tracker (TRT). The radial distance from the beam pipe of all the sub-components of the ID is shown in Figure 2.8. The highest granularity is achieved by the pixel and SCT, based on silicon technology and arranged on concentric cylinders around the beam pipe, while the performance of secondary vertex reconstruction is enhanced by the more recent IBL. The combination of silicon trackers in the innermost part with the TRT in the outermost part provides high-quality pattern recognition and transverse momentum resolution.

2.4.1 Insertable B-Layer

During the period of LHC shutdown in 2013, between Run 1 (2009-2012) and Run 2 (2015-2018), the Insertable B-Layer (IBL) and a new beam pipe were installed as the innermost

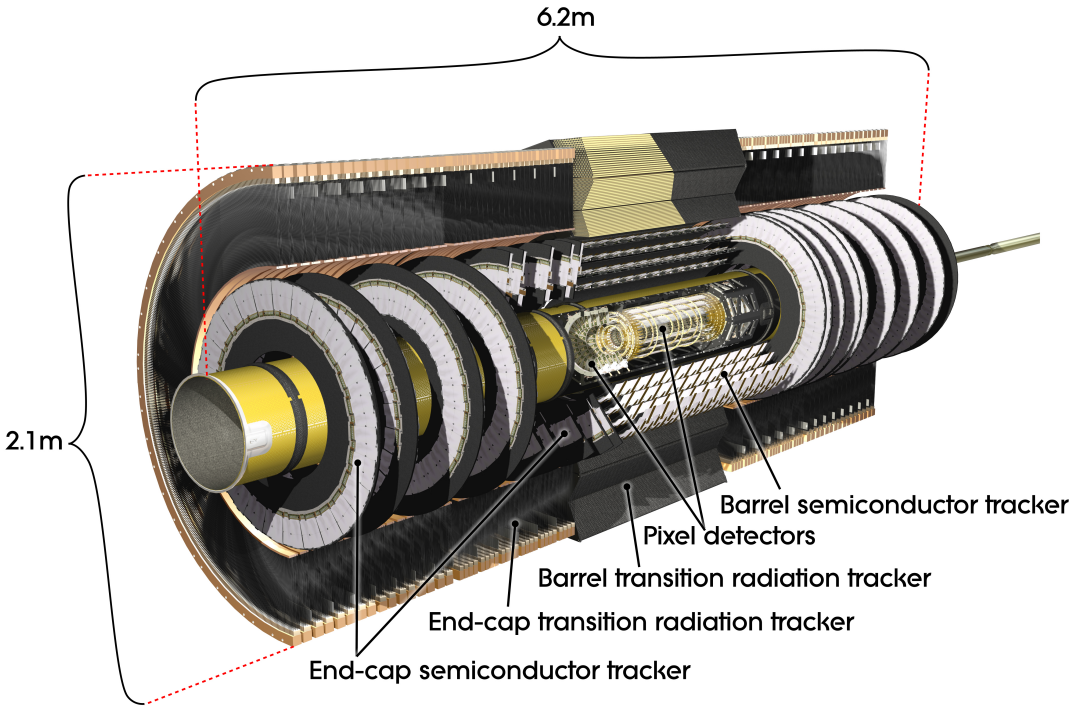

FIGURE 2.7: Overview of the Inner Detector layout [65].

layer of the ID instead of the original beam pipe. This additional layer is intended to handle the increase of the LHC luminosity between Run 1 and Run 2 and to mitigate the impact of radiation damage on the innermost part of the pixel detector. The IBL consists of a single cylindrical layer of silicon pixel and it contributes to measure the impact parameters and the decay vertices of short living particles, e.g. B-hadrons and τ leptons. The IBL is made up of 14 staves located at an average radial distance from the beam line of 35.7 mm. A schematic view of the IBL is shown in Figure 2.9. Its layout allows to fully cover the ϕ angle and to improves the resolution in x from 15 μm to 11 μm and in z from 34 μm to 24 μm [66, 67]. It is designed to increase the performances on the track and vertex reconstruction, providing an additional level of measurement closer to the interaction point. The impact of the IBL addition on the b-tagging performances will be further discussed in the dedicated Section 4.5.

2.4.2 Pixel Detector

The Pixel detector [68] is constitued by highly-granular silicon detectors and the system consists of three layers in the barrel, containing approximately 67 million of pixels, and three disks on each end-cap, containing 13 million of pixels. A scheme of the different layers of the Pixel detector is shown in Figure 2.10. The total readout channels of the Pixel detector are over 80 million distributed in 1744 modules. All the pixel sensors are identical and have a size in $R-\phi\times z$ of $50\times 400\,\mu\text{m}^2$ covering a total active area of about $1.7\,\text{m}^3$.

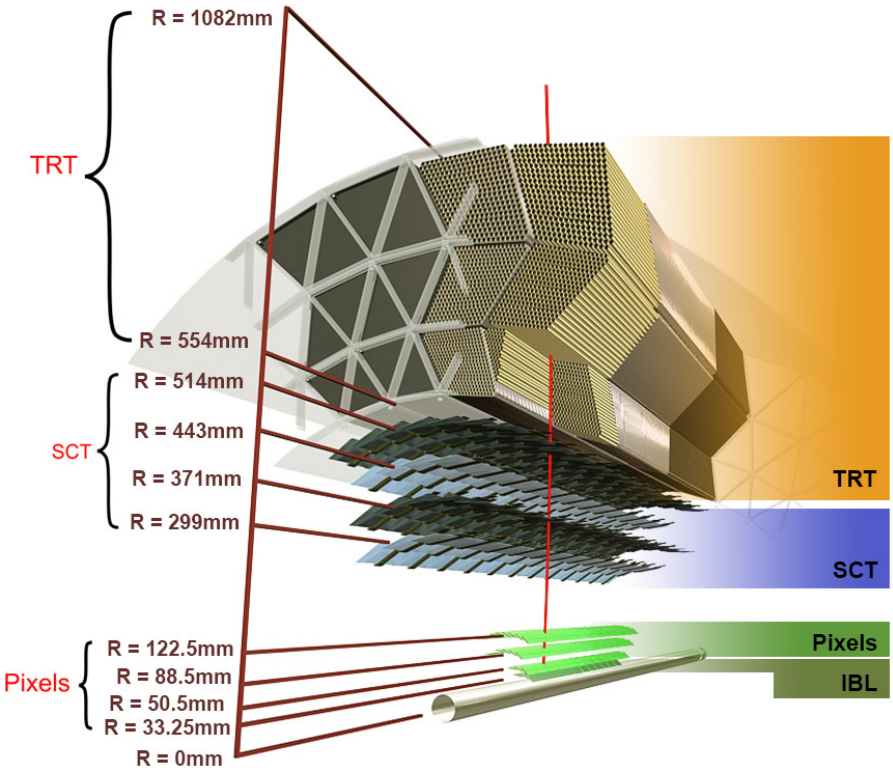

FIGURE 2.8: Scheme of the components of the Inner Detector showing distances from the interaction point.

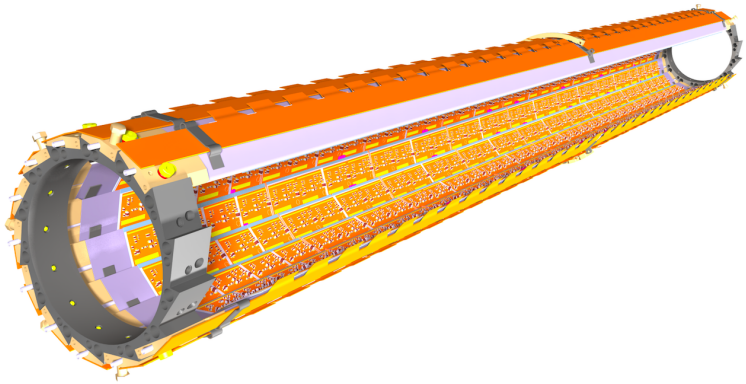

FIGURE 2.9: Schematic view of the IBL.

The system provides typically three precision points for tracks in the region $|\eta| < 2.5$ and it completely covers the ϕ angle. The resolution in R-ϕ direction is 10 μm and 115 μm in the z-axis direction.

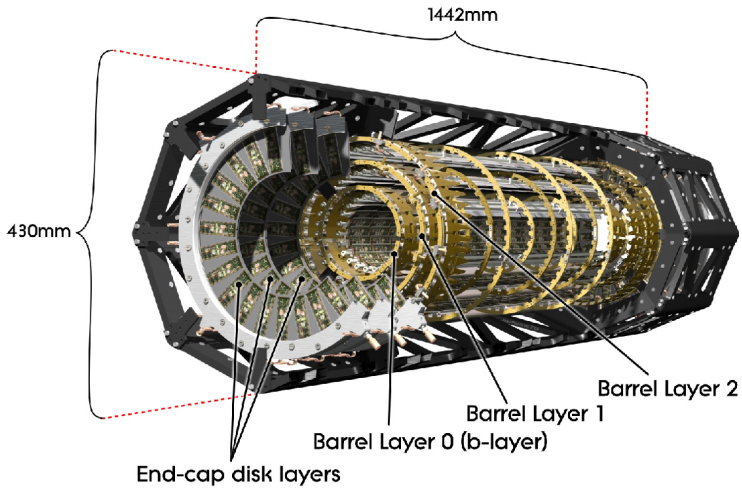

FIGURE 2.10: Schematic view of the Pixel detector showing the three concentric layers in the barrel and three disks on each of the two end-caps.

2.4.3 SemiConductor Tracker

The SemiConductor Tracker (SCT) [69] is a silicon strip detector built around the Pixel Detector and is designed to provide precise track measurements, contributing to improve identification of charged particles and momentum resolution of their tracks in the intermediate radial range. The SCT consists of four concentric layers around the pixel detector, placed at a radius in a range from 30 to 51 cm from the beam line and nine disk-shape layers in the endcap. It covers the region of $|\eta| < 2.5$ and the achieved resolution in R-ϕ direction is 17 μm and while in the z-axis direction is 580 μm.

2.4.4 Transition Radiation Tracker

The Transition Radiation Tracker (TRT) [70] is the outermost component of the Inner Detector and it is a combination of a drift tube tracker and a Transition Radiation detector useful for pattern recognition and particle discrimination, in fact the presence of several layers of material with different refration indices allows to produce transition radiation depending on the speed of the crossing particle. It consists of polymide drift (straw) tubes of 4 mm diameter that contain wires of tungsten plated in gold with a diameter of 31 μm. The gap between the straw and the wire is filled by a mixture of gases (70% Xe, 27% CO_2 and 3% O_2). The ionizing particles crossing TRT produce a low energy signal on the wires. In case of highly relativistic particles that pass from the gas to the polypropylene fibers, a transition radiation in the X-ray spectrum is emitted and absorbed by the Xe present in the gas mixture; the signal due to this kind of process is higher than the signal produced by ionisation. Therefore, this difference in amplitude gives the possibility to discriminate

between particles with high momentum (typically electrons) from other incident particles. TRT covers a region of $|\eta| < 2$ and measures $R - \phi$ coordinate of tracks with a resolution of 130 μm.

2.5 Calorimeters

The Calorimetric system of the ATLAS detector is designed to trigger and measure the energy of electrons, photons, jets, neutrons and $E_{\mathrm{T}}^{\mathrm{miss}}$. Particles typically interact with the materials of the calorimeter via a production of a cascade of secondary particles, called shower. ATLAS calorimeters are divided into two distinct sub-system, the electromagnetc calorimeter (EC) and the hadronic calorimeter (HC). A schematic view of the calorimetric system with all the sub-components is shown in Figure 2.11. The split of the calorimeters into two different categories is needed to discriminate between the electromagnetic shower and the hadronic one. An electromagnetic shower consists of electrons, positrons and photons and it is normally fully contained in the calorimeter; therefore, it can be fully absorbed. Hadronic showers involve different types of particles and they are characterized by a different longitudinal and transverse evolution. The typically involved particles are neutrons, muons and neutrinos, which tend to escape the detection. Containing of the electromagnetic and hadronic showers is crucial for energy measurement, but also for $E_{\mathrm{T}}^{\mathrm{miss}}$ measurement and to prevent to particles different to muons to arrive in the outermost component of the ATLAS detector, the Muon Spectrometer (MS). Both the EC and HC are composed by alternating layers of absorbing and active material. The absorbing material maximize the production of the showers, while the active material is used to measure the energy of the particles. This type of detectors are called sampling calorimeters.

The calorimeters are located outside the solenoid that surrounds the Inner Detector and cover the region of $|\eta| < 4.9$. Over the region matched to the Inner Detector, $|\eta| < 2.5$, the fine granularity of the electromagnetic calorimeter is designed to allow precision measurements of electrons and photons. The hadronic calorimeter has a coarser granularity that is sufficient to provide enough precision for jet recontruction and $E_{\mathrm{T}}^{\mathrm{miss}}$ measurement.

2.5.1 Electromagnetic Calorimeter

The Electromagnetic Calorimeter (EM, also referred to as LAr) [71] uses liquid argon as active material and lead as absorber detector material. The particles passing through the calorimeter ionize the LAr and the electrons drift towards the copper electrodes due to the presence of an electric field. The EM is divided into a barrel part ($|\eta| < 1.475$) and two end-cap components ($1.375 \leq |\eta| < 3.2$). The transition region between the barrel and the end-cap ($1.37 \leq |\eta| < 1.52$, called *crack* region, contains a large amount of additional material needed to instrument and cool the detector. In this transition region the energy resolution is significantly degraded and, in particular, the performance of electron reconstruction

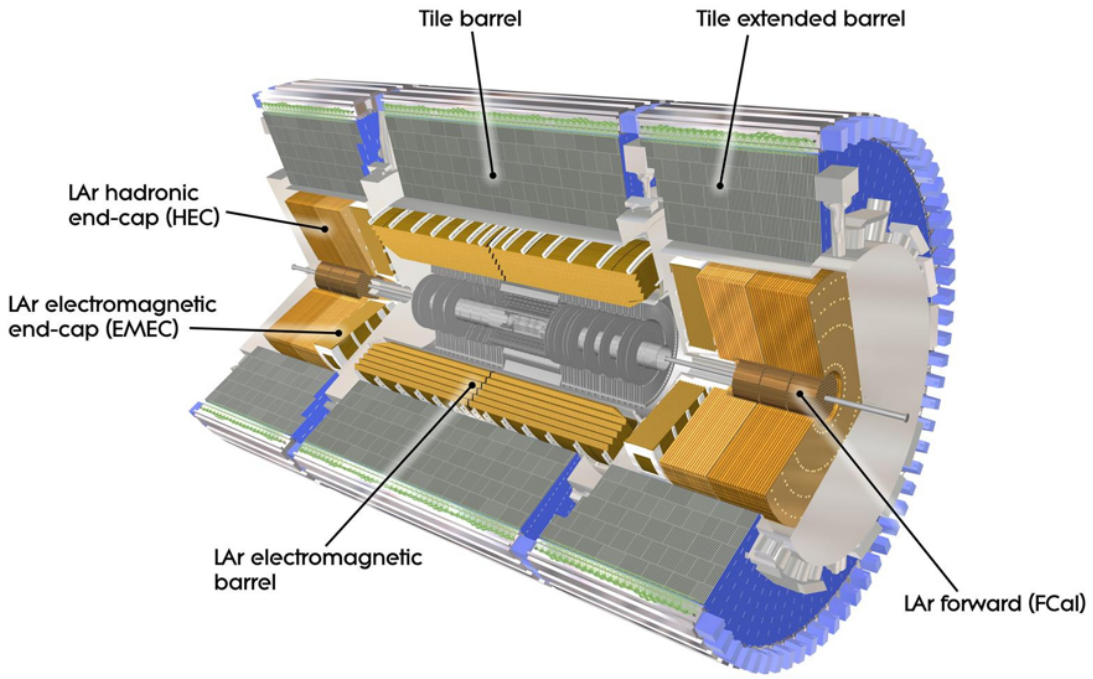

FIGURE 2.11: Section of the Calorimetric system of the ATLAS detector.

worsens. The peculiar accordion geometry of the EM, in which the lead is distributed in a series of plates and LAr fills the gaps between them, reduces the number of blind regions of the calorimeter and avoids azimuthal cracks, providing a full coverage in the ϕ angle.

2.5.2 Hadronic Calorimeter

The Hadronic Calorimeter (HCAL) is designed to absorb energy from hadronic showers produced by particles that pass through the EM. It is composed by two sub-detectors:

- **Tile Calorimeter** [72], placed directly outside the EM, it uses iron as absorber and plastic scintillating tiles as active component and covers a range of $|\eta| < 1.7$. It consists of a barrel covering the region $|\eta| < 0.8$ and two extended barrels, in the region between the barrel and the end-caps $0.8 \leq |\eta| < 1.7$.
- **Hadronic End-Cap Calorimeter** (HEC) is located just behind the end-cap eletromagnetic calorimeter. HEC uses liquid Argon as active medium and copper as absorber. It covers a region of $1.5 < |\eta| < 3.2$, overlapping with the Tile calorimeter on one side and the LAr Forward calorimeter on the other side, avoiding cracks in the transition regions.

2.5.3 Forward Calorimeter

The Forward Calorimeter (FCAL) [73] is an electromagnetic and hadronic calorimeter. The FCAL is composed by three sections in each end-cap: a copper section optimised for electromagnetic measurements and two sections with tungsten as passive material, useful for the measurement of the energy of hadronic showers. It covers the region near the beam pipe, $3.1 \leq |\eta| < 4.9$, to include even the most forward particles and it is located at a distance of 1.2 m from the EM front face in order to reduce the neutron flux. The FCAL must stand high radiation levels due to the high particle fluxes and energies in the forward region. The hermetic design ensures that the energy imbalance measurements can be done as precisely as possible.

2.6 Muon Spectrometer

The SM particles that can traverse the hadronic calorimeters are the muons and the neutrinos, a part from the particles produced by the showers not fully contained in the HC. In particular, muons are charged particles that in principle ionize the material of the calorimenters, but their energy loss is not enough to allow the full absorption of them. The Muon Spectrometer (MS) [74] is the outermost ATLAS detector and its main function is measuring the momentum of particles not fully absorbed in the calorimeters in the region of $|\eta| < 2.7$ and triggering on these particles in the region $|\eta| < 2.4$. The MS surrounds the calorimeters and uses magnetic deflection of tracks in order to precisely measure momentum and charge. In the region of $|\eta| < 1.4$, the bending is induced by the barrel solenoid magnet, while in the region $1.6 \leq |\eta| < 2.7$ the bending is due to the end-cap toroidal magnet. In the transition region, $1.4 \leq |\eta| < 1.6$, the two magnetic fields are overlapping. In general, the magnetic field is designed to be mostly orthogonal to the muon trajectories minimizing the degradation in resolution due to multiple scattering.

The reconstruction of muons employs a combination of trigger chambers, fast-response detectors with limited resolution for momentum measurements, and high-precision tracking chambers, with better resolution but slowly reacting. The trigger system consists of the Resistive Plate Chambers (RPC) and the Thin Gap Chambers (TGC), while the precise measurement of the track coordinates is performed by using the Monitor Drift Tubes (MDT) and he Cathode Strip Chambers (CSC). A schematic view of the MS with its sub-components is shown in Figure 2.12.

2.6.1 Monitored Drift Tubes

The Monitored Drift Tubes (MDT) chambers are designed for precision measurement of momentum and they cover the range $|\eta| < 2.7$. The MDT chambers consists of pressurised

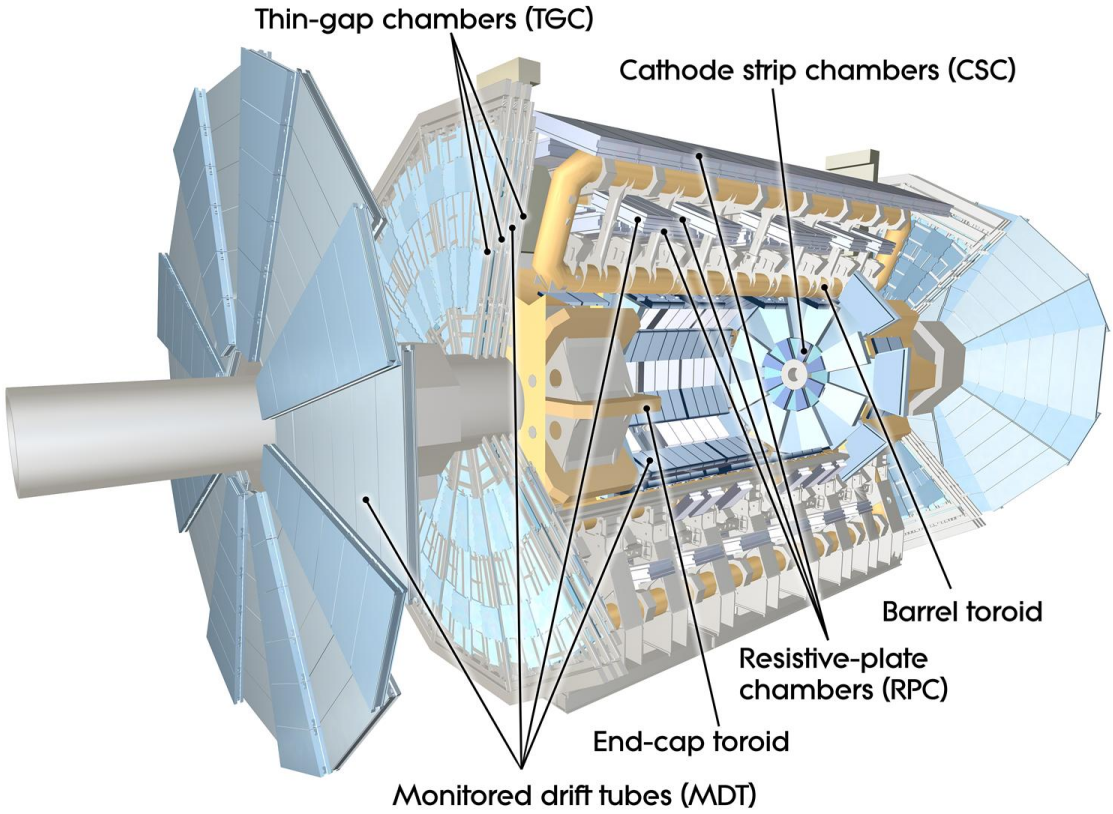

FIGURE 2.12: Schematic view of Muon Spectrometer and its sub-detectors.

tubes in aluminium with a diameter of 3 cm, operating with a mixture of Ar (93%) and CO_2 (7%) at 3 bar. At the center of the tube an anodic wire made of tungsten-rhenium with a diameter of 50 μm is located in order to collect the electrons resulting from ionisation in the gas induced by the crossing muons. By measuring the drift time, it is possible to have a precise measure of the drift distance. Each MDT chamber consists of two multilayers of tubes fixed at a supporting structure. The 1150 modules are organized into three layers in the barrel and four in the end-cap. The design of the MDT chambers allows to achieve a spatial resolution of 80 μm per tube layer, while the typical drift time is 700 ns. Given these performances, MDT chambers are suitable for precise measurements but too slow for triggering.

2.6.2 Catode Strip Chambers

The Catode Strip Chambers (CSC) are located in the innermost end-cap layer and they cover the region $2.0 \leq |\eta| < 2.7$. The CSCs are multiwire proportional chambers with the wires oriented in the radial direction with respct to the beam line. They consist of arrays of positevely-charged "anode" wires crossed with negatively-charged "cathode" strips within a gas volume (30% Ar, 50% CO_2 and 20% CF_4). The position of the track is obtained by interpolation between the charges induced on neighbouring cathode strips. The CSC system

consists of two disks with eight chambers each (eight small and eight large) and each chamber contains four CSC planes providing four different measurements in η and ϕ for each track. The achieved spatial resolution is of 60 μm.

2.6.3 Resistive Plate Chambers

The Resistive Plate Chambers (RPC) are fast gaseous detectors installed in the barrel region. The RPC consist of two parallel plates, a positively-charged anode and a negatively-charged cathode, made of resistive bakelite kept at a distance of 2 mm by polycarbonate spacers. The gap between the plates is filled by a gas mixture (94.7% $C_2H_2F_4$, 5% Iso-C_4H_{10} and 0.3% SF_6). After the passage of a particle inside the chamber, the primary ionization electrons are multiplied into avalanches by an high electric field of typically 4.9 kV/mm. The electrons are collected by external metallic strips after a precise time delay. A RPC trigger chamber consists of two independent detector layers, each one readout by two orthogonal series of strips. The strips parallel to the MDT wires provide the measurement for η and the ones orthogonal to the MDT wires the ϕ coordinate measurement. The spatial resolution of the RPCs is $\sim$ 1 cm, while the time resolution is 1 ns. Given these performances, RPCs play a crucial role in triggering muons and represent the only sub-detector in the MS to provide a ϕ measurement in the barrel region, $|\eta| < 1.05$.

2.6.4 Thin Gap Chambers

The Thin Gap Chambers (TGC) are multiwire proportional chambers installed in the endcap regions of the MS (referred as to *big wheels* in the ATLAS jargon). A TGC chamber consists of a plane of wires spaced by a distance of 1.8 mm and two cathode planes spaced by a distance of 1.4 mm, while the operational gas is a highly quenching mixture (55% CO_2 and 45% n-C_5H_{12}). The high electric field applied in the TGC in combination with the small distance between the wires leads to excellent time resolution (4 ns). The TGCs can provide spatial resolution of $\sim$ 5 mm. Given these preformances, the TGCs provide muon trigger capability and a measurement of the muon coordinate in the direction orthogonal to the one determined by using MDTs in the region $1.05 \leq |\eta| < 2.7$.

2.7 Forward Detectors

In addition to the main ATLAS detectors, special-purpose detectors are installed in the forward region:

- **LUminosity measurement using Cherenkov Integrating Detector (LUCID)** [75] is a Cherenkov detector located at a distance of $\pm$17 m from the interaction point, covering a region of $5.6 \leq |\eta| < 6$. It is used as the main relative luminosity monitor in

ATLAS. LUCID consists of aluminium tubes filled with gas (C_4F_{10}) that emits photons by Cherenkov effect when charged particles pass through it. The photons are then collected by photomultipliers (PMTs) situated at the end of each tube. From the number of tubes involved, it is possible to evaluate the average number of interactions per bunch crossing and extract the instantaneous luminosity.

- **Beam Conditions Monitor (BCM)** [76] consists of two stations located symmetrically around the interaction point ($z = \pm 184\,\text{cm}$ and $r = 55\,\text{mm}$ equivalent to a value of $\eta = 4.2$). BCM is dedicated to monitor the beam conditions and the potential detector damage resulting from their anomalies.

- **Zero Degree Calorimeter (ZDC)** is located at a distance of ±140 m from the interaction point and it is used for detecting forward neutrons ($|\eta| > 8.3$) in order to determine centrality of heavy-ion collisions.

- **Absolute Luminosity For ATLAS (ALFA)** is situated at a distance of ±240 m from the interaction point and its main function is measuring the absolute luminosity that is determined via elastic scattering at small angles.

2.8 ATLAS Performance during LHC Run 2 (2015 and 2016 only)

The LHC delivered 42.7 fb^{-1} of pp collision data at a center-of-mass energy of $\sqrt{s} = 13\,\text{TeV}$ in 2015 and 2016. The ATLAS detector recorded 39.5 fb^{-1} of pp collisions, corresponding to a data taking efficiency of ~ 92%.

The total integrated luminosity and data taking efficiency during stable beams and pp collisions at the LHC in 2015 and 2016 are shown in Figure 2.13. The cumulative luminosity versus time delivered to ATLAS is shown in green. It accounts for the luminosity delivered from the start of stable beams until the LHC requests ATLAS to put the detector in a safe standby mode to allow a beam dump or beam studies. The luminosity recorded by ATLAS is shown in yellow. The difference with the delivered luminosity reflects the inefficiency of the Data Acquisition System (DAQ, see Section 2.9.1), as well as the inefficiency of the so called *warm start*: when the stable beam flag is raised by the LHC, the ATLAS detectors undergo a ramp of the high-voltage before they start taking data.

2.8.1 Pileup effect on data

The pileup effect is reconstructing multiple pp interactions as part of the single event, intended as each time the proton bunches are made to collide. The main sources of pileup are:

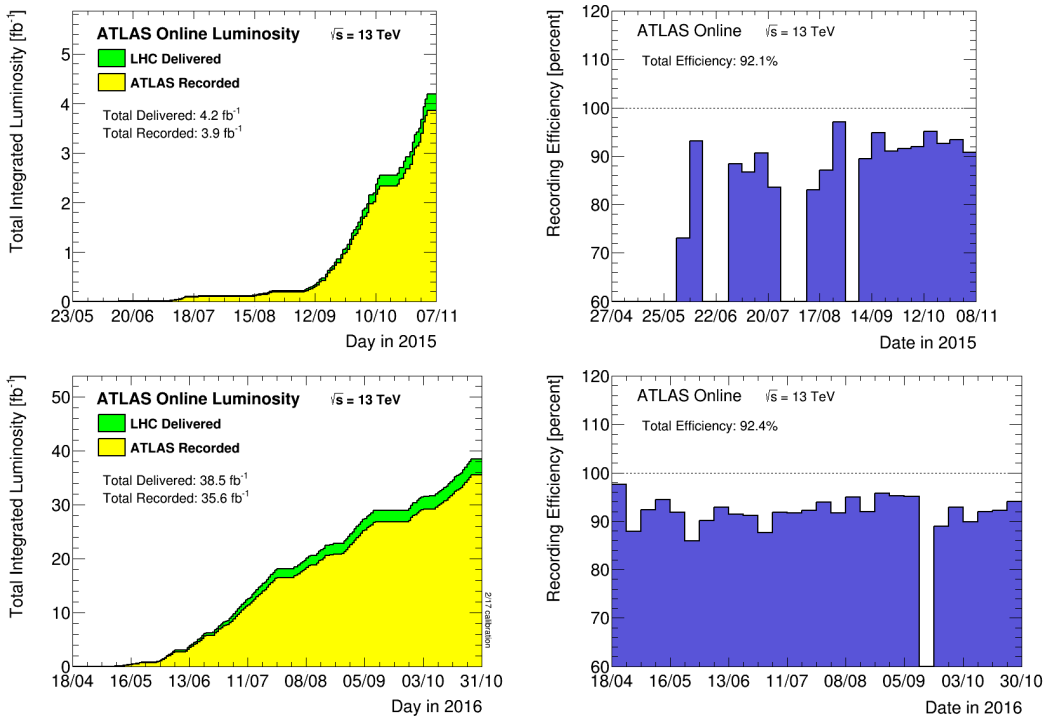

FIGURE 2.13: Total integrated luminosity of the ATLAS detector in 2015 (on top left) and 2016 (on bottom left). In addition, data taking efficiency per week is shown for 2015 (on top right) and 2016 (on bottom right) separately.O

- **In-time pileup**: the probability of multiple pp interactions increases with luminosity, so high luminosity implies an increase of pileup.
- **Out-of-time pileup**: the probability of multiple pp collisions depends also on spacing between the bunches. If the spacing is shorter than the response time of the detectors, the interactions in a specific bunch crossing can be misreconstructed as part of another bunch crossing, affecting the subsequent measurements.

The mean number of interactions per crossing is calculated from the instantaneous per bunch luminosity as

$$< \mu >= \frac{\mathcal{L}_{\text{ins}} \cdot \sigma_{\text{inel}}}{n_b \cdot f_r} \tag{2.9}$$

where $\mathcal{L}_{\text{ins}}$ is the average instantaneous luminosity over a large time period ($\Delta t \gg 600\,\text{ns}$), σ_{inel} is the total cross-section of the inelastic scattering (for 13 TeV collisions is 80 mb), n_b is the number of proton bunches and f_r is the LHC beam circulating frequency (11 KHz). The luminosity-weighted distribution of the mean number of interactions per crossing for 2015 and 2016 data in pp collisions at a centre-of-mass energy of 13 TeV is shown in Figure 2.14.

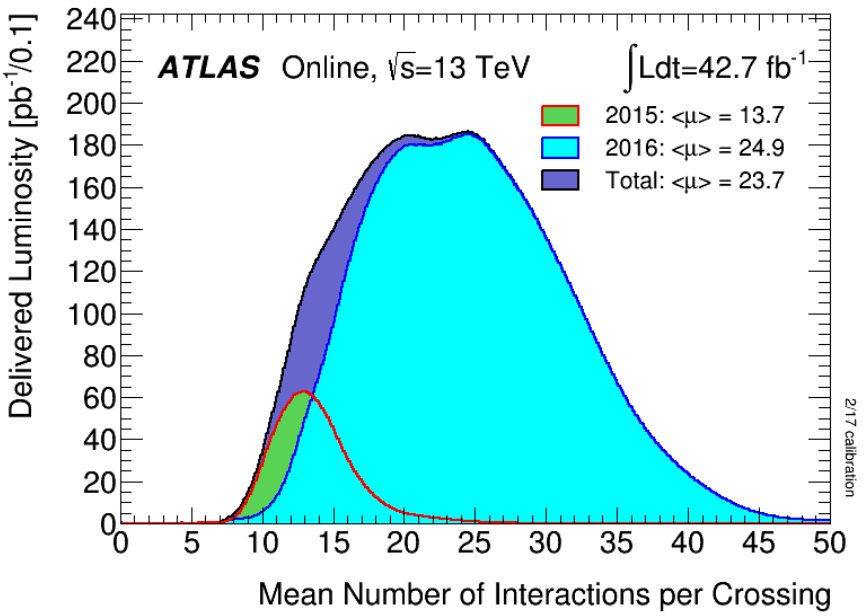

FIGURE 2.14: Luminosity-weighted distribution of the mean number of interactions per crossing for the combined 2015 and 2016 *pp* collision data at 13 TeV centre-of-mass energy. The mean number of interactions per crossing corresponds to the mean of the poisson distribution of the number of interactions per crossing calculated for each bunch.

2.9 Analysis of ATLAS data

The analysis of ATLAS data is a challenging task due to the high collision rate (40 MHz) provided by the LHC. The amount of data collected by the ATLAS detector per event makes the full recording impossible. Therefore, dedicated systems are needed in order to perform the selection and storage of the events of physics interest for the offline analysis.

2.9.1 TDAQ system

The Trigger and Data Acquisition (TDAQ) system is the ATLAS infrastructure dedicated to read, format and transfer the event data (DAQ) and to apply a selection in order to reduce the information rate (Trigger).

Trigger

The Trigger system is responsible for the selection of events particularly interesting for the ATLAS physics programme. The ATLAS trigger system is composed by two levels:

- **Level-1 (L1)** is a hardware-based trigger that, from detector information, searches for high transverse momentum objects in the events. The sub-detectors that provide inputs for L1 trigger are the Calorimeters and the MS trigger chambers, used to identify

the presence of a muon. L1 trigger, starting from the detector inputs, is able to quickly reconstruct electrons, photons, taus, jets, $E_{\mathrm{T}}^{\mathrm{miss}}$ and muons using simplified algorithms with respect to the full offline reconstruction. In addition to the reconstruction of the physics objects, L1 trigger defines one or more Region-of-Interest (RoI) in η and ϕ coordinates, where interesting features are identified. L1 trigger reduces the event rate from the initial value of 40 MHz to 100 kHz and it has a decision time of $\sim$ 2.5 μs. The events passing the L1-trigger selection are passed to the next level of the trigger system.

- **High Level Trigger (HLT)** is a software-based trigger that uses RoI information from L1 trigger and perform a reconstruction similar to the full offline one. HLT algorithms process the events in $\sim$ 200 ms and reduce the event rate to 1 kHz. The system unifies the Run 1 two stage system (L2 and Event Filter) to optmize the use of resources.

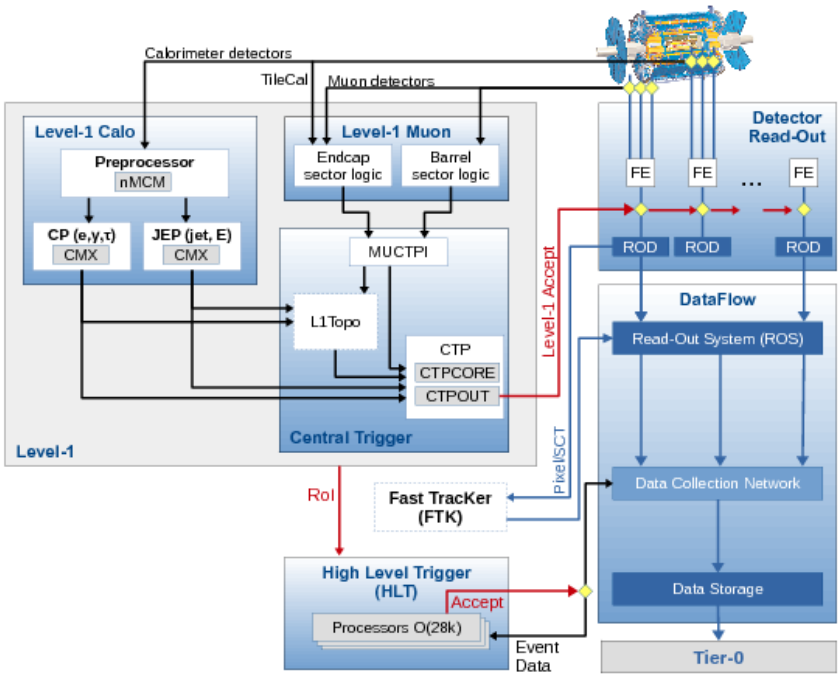

FIGURE 2.15: Schematic diagrams showing the triggering process.

Data Acquisition System

The ATLAS Data Acquisition system (DAQ) is responsible for reading, transferring and temporarily storing data from detectors. After an event is accepted by the L1 trigger, the data are transferred to the first step of the DAQ process, the Readout Drivers (ROD) system, which receives and temporarily stores the data. Event data associated with RoI from L1 trigger is sent to HLT for further selection. Events passing HLT are permanently stored at the CERN computer centre. A schematic view of DAQ process can be seen in Fig. 2.15.

2.9.2 Computing system

Storaging, transferring and processing of the recorded data is the main tasks of ATLAS offline computing system. The system also supports the production and the distribution of simulated data and detector modelling. It interconnects local computing centres by high-speed international networks and it is based on GRID technologies [77], making all computing and storage resources as a virtual single computer.

ATLAS computing model is based on a distributed tiered model [78], where CERN is the central production centre (Tier-0) that distributes in quasi-real time data to Tier-1 centres. At the moment, 13 Tier-1 centres work for the LHC, allowing to reprocess and analyze large amount of data also offline. Each Tier-1 centre provides services for a cloud of associated Tier-2 centres.

The processing and analysis of real and simulated data can be subdivided into four steps:

- **Raw Data Objects (RDO)** raw (unprocessed) data are transferred to Tier-0 centre for processing and archiving
- **ESD (Event Summary Data)** are generated by the application of algorithms in order to reconstruct particle information and are stored in Tier-1 centres.
- **Extended Analysis Object Data (xAOD)**, a compact format, designed to allow physics analysis, which further reduces the dimensions for storage and includes a summary of reconstruction. It is produced using the ATLAS software analysis release, `ATHENA` [79].
- **Derived Analysis Object Data (DxAOD)** is produced starting from the output of the general reconstruction framework in xAOD format and providing a similar output, but containing less information. Storage dimension becomes smaller than xAOD containers. The content of DxAOD is defined by the physics groups and has to be useful for subsequent analysis.

Chapter 3

Data sample and Monte Carlo simulation

3.1 Data sample

This analysis is based on data events collected with the ATLAS detector in pp collisions at the LHC in 2015 and 2016 at a center-of-mass energy of 13 TeV. The performances related to data-taking in the time period under study are presented in Section 2.8. The cumulative distributions of the total integrated luminosity delivered to and recorded by ATLAS are shown in Figure 2.13. Among all the recorded events, corresponding to an integrated luminosity of 39.5 fb^{-1}, only data taken in periods in which all the sub-detectors were fully functional are considered for this analysis. The data that satisfy this requirement corresponds to an integrated luminosity of 36.1 fb^{-1} and are included in the so-called Good Run List (GRL) and separated into periods according to the running conditions such as beam settings and trigger configurations.

3.2 Monte Carlo simulation

The Monte Carlo simulation is a crucial tool for the analyses in high-energy physics. It is used to estimate the acceptance and efficiency of the experimental apparatus, to model the physics processes that the analyses target as signal and to evaluate the impact of background processes which mimic the signal final state. The basic step to perform the MC simulation of one particular physics process is the calculation of the expected cross-section. Then, the MC simulation is performed in various steps: the hard scatter simulation, the showering, the hadronisation, the decay of the unstable particles and the evaluation of the underlying events. The MC samples need to take into account both theoretical predictions and phenomenological models as the physics processes involve interactions from

very short distance scales to the typical scale of hadron formation and decay. The QCD coupling costant is small at short distances (of the order of the femtometer) and that allows to deal with short-distance physics by using tools based on perturbation theory. Phenomena occurring at larger distances, like hadronisation and underlying events, cannot be described by first principles and they need phenomenological models for their simulation. The different steps of the MC simulation a pp collision are illustrated in Figure 3.1 and they will be described in more details in the following sections.

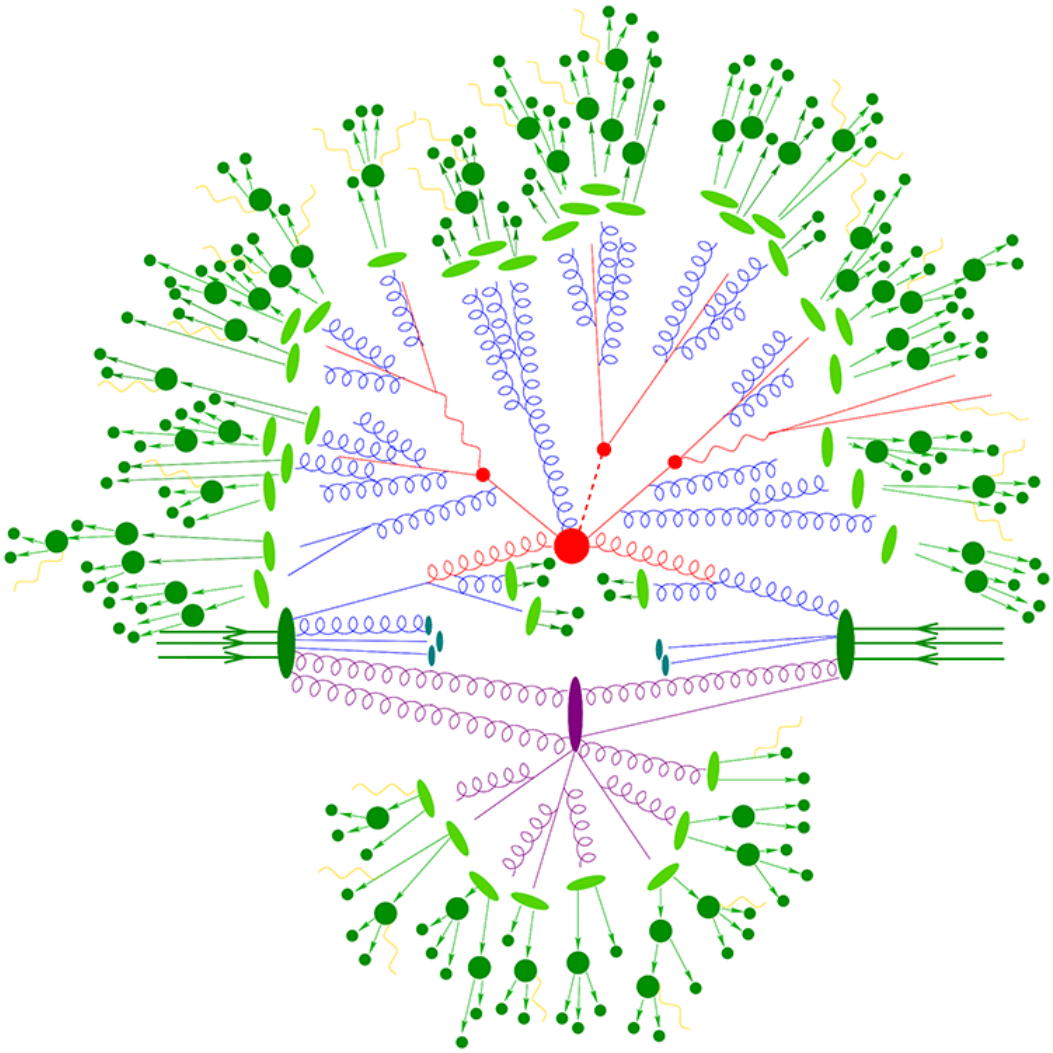

FIGURE 3.1: Sketch of a hadron-hadron collision as simulated by a Monte Carlo event generator. The red blob in the center represents the hard collision, surrounded by a tree like-like structure representing Bremsstrahlung as simulated by parton showers. The purple blob indicates a secondary interaction between other partons of the proton involving smaller momentum transfers. Light green blobs represent the parton-to-hadron transitions, the dark green blobs describe hadron decays, and the yellow lines indicate soft photon radiation. Figure is taken from [80].

3.3 Hard scattering process and Matrix Element generators

The evaluation of the scattering probability of the hard process is the first step of the event generation. It is performed by the calculation of the Matrix Elements (MEs) at a fixed perturbative order in the strong coupling costant α_s, evaluating the matrix element of a $2 \rightarrow n$ process. The cross-section for this type of process can be decomposed into three components at NLO order:

$$\sigma = \int_n \sigma^B + \int_n \sigma^V + \int_n \sigma^R, \tag{3.1}$$

where σ^B denotes the Born element which contains the diagrams with exactly n particles in the final state, σ^V indicates the virtual part (diagrams with n particles in the final state that include higher-order contributions) and σ^R is the component in which the real emission (diagrams with n+1 particles) is taken into account. An examplary set of Feynman diagrams for the $t\bar{t}$ production for the three components described above are shown in Figure 3.2. The matrix element generators can be divided according to which contributions in (3.1) are considered in the calculation:

- **Tree level:** it includes the diagrams with a fixed number of particles in the final state and the virtual contributions are not taken into account
- **NLO:** it considers all the diagrams that contribute to a physics process up to a fixed order in perturbation theory, including also the virtual contributions

The NLO generators ensure better accuracy in the description of the physics process compared to a LO description provided by Tree level generators. NNLO ME generators have increasingly been developed [81] but they are not currently available for $t\bar{t}$ production process.

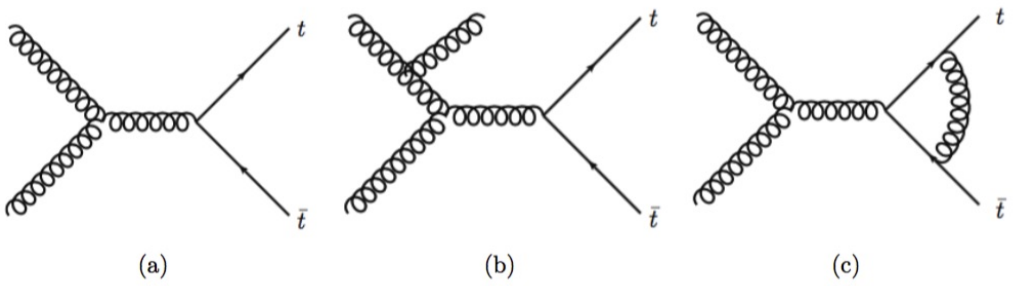

FIGURE 3.2: Example of Feynman diagrams for $t\bar{t}$ production at tree level (a), for a real emission (b) and a virtual contribution (c).

The momenta of partons in the initial state are distributed following the proton PDFs, while partons of the final state are spread in the avalable phase space. The calculation of the cross-section is then carried out by convoluting the PDFs with the hard-scatter cross-sections,

following the factorization theorem described in Section 1.2.6. When the partonic cross-sections are associated with soft interactions at long distance, collinear divergences could arise from the calculations. The introduction of a *factorization scale*, μ_F, allows to redefine the PDFs in order to absorbe the divergences. The factorization scale indicates at which energy the non perturbative part of the interaction, represented by the PDF, starts to dominate over the short-distance hard process. In general, the factorization scale is set to the same value of the *renormalization scale*, μ_R, and the choosen value is usually the characteristic momentum of the final state system.

3.4 Parton shower

The following step of the MC simulation is the Parton Shower (PS), which is responsible for providing a model for QCD radiation, indicated by the red lines in Figure 3.1. The QCD radiation is a cascade process, in which partons emit from the hard-scatter scale to the hadronization scale (~ 1GeV) due to higher order QCD effects which include the possibility for a parton to split into other partons. This process is called *splitting* and it is described by the Altarelli-Parisi splitting functions $P_{ab}(\alpha_s, z)$, described in Section 1.2.6. In QCD, the emission or splitting can occur via these processes: $q \rightarrow gq$, $g \rightarrow gg$ and $g \rightarrow q\bar{q}$. The typical phase-space in which the PS operates is characterized by soft emissions, in which the parton is emitted at low energy, and collinear emissions, in which two final state or a final state and an initial state particles are separated by a low angle. The use of ME generators in association with PS models can lead to a double counting of the considered diagrams in both steps. In order to avoid this possile double counting, a matching procedure is needed to separate the phase-spaces. This procedure is implemented by the introduction of a *matching scale* that separates the region where the full ME is exploited between the region in which the additional radiation is modeled by the PS. The PS is implemented in MC generators via the so-called Sudakov form factors:

$$\Delta_i(q_1^2, q_2^2) = \exp\left(-\sum_i \int_{q_2^2}^{q_1^2} \int_{z_{\min}}^{z_{\max}} dP_i(z, q^2)\right) \tag{3.2}$$

which represents the probability for a parton i to evolve from an initial scale q_1 to a lower scale q_2 without undergoing a splitting. The Sudakov form factor provides the scale q_2 at which the emission can occur and if the value is above the hadronization scale, the procedure is repeated using q_2 as initial scale. In case the evaluated value for q_2 is below the hadronization scale, the shower process is interrupted. The ordering used in the splitting characterizes the different PS models and it usually depends on angles or transverse momentum of the involved particles.

3.5 Underlying event

The Underlying event (UE), indicated in purple ovals in Figure 3.1, consists of the collection of soft processes, which are actually the dominant processes at the LHC, that accompany a hard-scattering interaction. The main contributions to the UE are coming from the interactions between the beam-beam remnants, i.e. the left-overs of the initial hadrons after the hard scattering, and the multiple parton interactions (MPI) that generate distinct scatters. The description of the UE cannot rely on perturbative QCD and therefore its description requires phenomenological models and a tuning of their parameters based on experimental data [82].

3.6 Hadronization

The following step of the MC simulation is the hadronization, in which the coloured partons generated by the PS and the UE are binded together into colorless baryons and mesons. This process starts at the scale of the PS cut-off and it is characterized by low energies and large distances, where perturbation theory is not valid anymore due to the increase of the strong coupling α_s. The dynamics of the hadronization requires non-perturbative models in order to be consistently described. The most common methods used to model the hadrization are the cluster fragmentation model [83, 84] and the Lund string model [85, 86].

- **Cluster fragmentation model** is based on the concept of the preconfinement [87] and it is an iterative process that starts with the non-perturbative splitting of the remaining gluons from the PS into color-singlet $q\bar{q}$ pairs. When the event consists of only color connected quarks and anti quarks, color-singlet combinations are grouped into clusters. The heaviest clusters are split into lower mass clusters and then are iteratively fragmented until stable hadrons are constituted. Clusters with a mass below $3-4\,\text{GeV}$ are replaced by a light hadron. A graphic scheme of the procedure used in the cluster model is shown in 3.3a

- **Lund string model** is based on linear confinement in which the potential among the partons linearly increases with their separation. In this model , the gluons between $q\bar{q}$ pairs are considered as color field lines that are attacted to each other as a consequence of the gluon self-interaction. As q and $\bar{q}$ move apart, the color strings are stretched until they break and form an additional $q\bar{q}$ pair, which is more energetically favorable. This process is iterated until the strings are too light to generate further fragmentation. A schematic overview of this technique is shown in 3.3b.

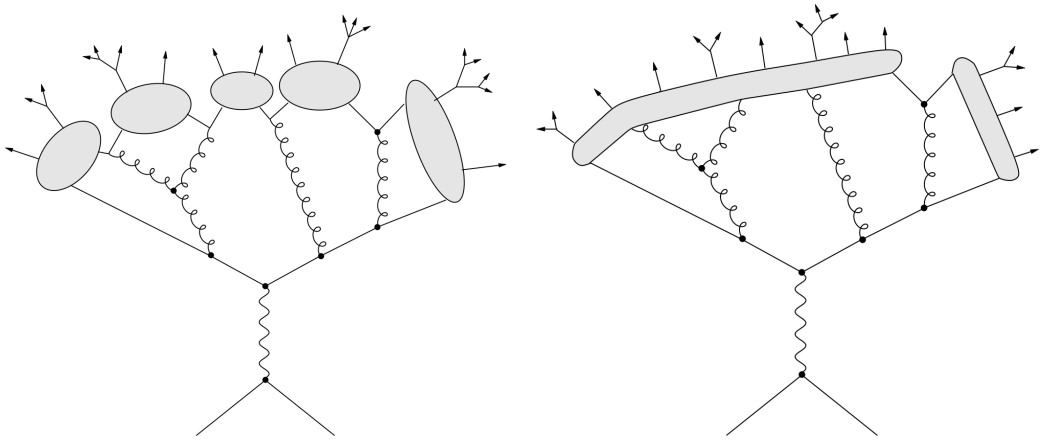

(A) (B)

FIGURE 3.3: Graphical scheme of the cluster model (a) and of the string model (b) used to describe the hadronization process.

3.7 Monte Carlo Generators

An overview of MC generators used in the analysis described in this thesis will be presented in the following sections. Each MC generator implements peculiar theoretical models and the choice among them has the aim to cover the theoretical uncertainty associated to a given MC generator prediction.

Matrix Element Generators

- POWHEG-BOX [88] is a matrix element generator which implements NLO calculations for a large number of physics processes using the POWHEG method (Positive Weight Hardest Emission Generator) [89, 90] with p_{T} ordered emissions. It needs to be matched with a parton shower generator in order to fully generate the event. The matching procedure has to be taken into account to avoid possible double counting between the ME generator and the PS. One of the main parameter used to separate the scales of the emissions is h_{damp} which determines the p_{T} of the first additional emission. It has been studied in the context of the ATLAS MC tuning.

- MADGRAPH5_aMC@NLO [91] is a MC generator suitable for automated computation of the ME at LO and NLO. The matching procedure to interface the ME generator with a PS follows the MC@NLO method [92], in which negative weights can be assigned to a small fraction of events.

Multi-purpose Generators

The Multi-purpose Generators are able to implement all the steps of the MC simulation described in the previous sections.

- PYTHIA [93] provides LO hard scattering simulations for several physics processes and can be interfaced with the aforementioned ME generators in order to simulate PS, hadronization and particle decay. The PS model used by PYTHIA is based on p_{T} ordering of the emissions and its model of the hadronization step is based on the Lund string model.
- HERWIG [94, 95] is a multi-purpose generator which can be interfaced with NLO ME generators to provide a PS and hadronization model. The PS follows an ordering of the emissions based on the opening angle and its hadronization model is based on the cluster model.

In the analysis presented in this thesis, the above generators are used to simulate the parton shower, hadronization and the underlying event.

Milti-purpose Generators including NLO Matrix Element

- SHERPA [96] (Simulation of High-Energy Reactions of PArticles) is a NLO/LO multi-purpose generator able to perform all the steps of MC simulation and it used to simulate several physics processes. The hadronization step is based on the cluster model.

3.8 MC samples used in the analysis

In this section, the MC samples used in the analysis described in this thesis will be presented. In particular, the MC samples used to simulate the signal process of $t\bar{t}$ production as well as MC samples used to simulate the background physics processes will be discussed.

As a common setting, all the MC samples are simulated taking into account the pileup conditions in 2015 and 2016, described in details in Section 2.8.1. In order to simulate the effects of pileup, the PYTHIA 8 (v8.186) [93] with the A14 [97] tune is used to generate additional soft QCD interactions to be overlaided to the event debribing the hard scatter. Therefore, simulated events are re-weighted so that the distribution of the average number of pp interactions per bunch crossing matches that observed in data. This procedure is called *pileup reweighting*.

3.8.1 Nominal $t\bar{t}$ signal sample

The generation of $t\bar{t}$ events is performed by using the POWHEG-BOX 2 [98] NLO generator with the NLO NNPDF3.0 [99] PDF set in the matrix element calculations. The h_{damp} parameter which regulates the p_{T} of the first additional emission is set to 1.5 times the top quark mass. This value has been thoroughly studied and this choice will be discuss in Section 3.10. The parton shower, hadronization and underlying event are simulated using PYTHIA 8 (v8.230) [93] with the LO NNPDF2.3 [41] PDF set and the appropriate A14 [97] set of tunable parameters. The normalization and factorization scales are set to the transverse mass of the top quark, defined as $m_{T,t} = \sqrt{m_t^2 + p_{T,t}^2}$, where $p_{T,t}$ is the transverse momentum of the top quark in the $t\bar{t}$ center-of-mass reference frame. The sample is normalized to the NNLO prediction of the inclusive cross-section $\sigma_{t\bar{t}} = 832^{+46}_{-51}$ pb, where the uncertainty includes PDF, μ_{R}, μ_{F} and α_{S} variations. The cross-section is calculated using the Top++2.0 [37] program and obtained from NNLO in QCD including resummation of NNLL soft gluon terms [36, 100–102] assuming a top quark mass $m_t = 172.5$ GeV. Events where both top quarks decay into hadronically-decaying W bosons are not included.

3.8.2 Alternative $t\bar{t}$ samples

A set of MC samples that simulate the $t\bar{t}$ production is used to asses the impact of the uncertainty due to the tune of the parameters and the choice of the models to describe parton shower, hadronization, PDF and underlying event.

Additional POWHEG+PYTHIA 8 samples are used to study the impact of the variations of the amount of additional radiation. The samples are generated by using different settings of POWHEG and tune parameters of PYTHIA 8:

- The sample with reduced QCD radiation is generated by multiplying μ_{R} and μ_{F} by a factor of 2.0, the h_{damp} remains at 1.5 times the top quark mass and the Var3c down [97] variation from A14 tune is used, which corresponds to a α_{S} variation
- The sample with increased QCD radiation is generated by multiplying μ_{R} and μ_{F} by a factor of 0.5, h_{damp} is increased up to 3.0 times the top quark mass and the Var3c up variation from A14 tune is used.

In order to evaluate the impact on the modeling of the parton shower, hadronization and underlying event, the previously described POWHEG generator is interfaced with HERWIG 7 (v7.0.1) [95] using the LO MMHT2014 PDF [22] set andthe H7-UE-MMHT tune [103].

The impact of the ME event generator choice is evaluated using events produced with SHERPA 2.2.1 [96] and the NNPDF3.0 PDF set at NNLO.

All the samples described in this section are normalized to the same value of the predicted inclusive cross-section used for the nominal $t\bar{t}$ sample.

3.8.3 MC samples for background processes

The selection of $t\bar{t}$ signal is affected by background contamination due to physics processes that mimic the same final state or misreconstruction of the objects entering the selection criteria. The processes considered as background that need to be simulated by MC samples are the single top quark production, V+jets production (W+ jets and Z + jets), diboson final states and $t\bar{t}$ production in association with an electroweak mediator.

Single top

The generator used to simulate the single top produced in $Wt-$ and $s-$ channel is POWHEG +PYTHIA 6 [104], where the CT10 [49] PDF set is used for the matrix calculation. The diagram removal scheme is used to remove the overlap between $t\bar{t}$ production and single top processes. The electroweak t-channel is simulated with POWHEG+PYTHIA 6 using the CTEQ6L1 [105] PDF set. All the single top samples are interfaced to PYTHIA 6 (v6.428) with Perugia 2012 [106] underlying-event tune. The $Wt-$, $t-$ and $s-$ channel samples are normalized to the approximate NNLO theoretical cross-sections [107–109].

V+jets

Events containing W or Z bosons with associated jets are simulated using the SHERPA 2.2.1 generator. The NNLO NNPDF3.0 PDF set is used with a dedicated parton shower tuning developed by the authors. The W+ jets and Z + jets samples are normalized to NNLO cross-sections. These samples are filtered according to the flavour of the additional jets to ensure enough statistics in all the regions of the phase-space.

Diboson

The electro-weak production of diboson (WW, WZ, ZZ) is simulated by the SHERPA 2.1.1 generator with the CT10 PDF set for the ME calculations. The CT10 PDF set is also used with a dedicated parton shower tuning developed by the authors. The generator cross-sections, already evaluated at NLO accuracy, are used in this case.

$t\bar{t}$ + V

Events with $t\bar{t}$ production in association with a vector boson are simulated using MADGRAPH5_aMC@NLO interfaced to PYTHIA 8 (v2.3.3 and v8.210 respectively). The $t\bar{t}$ + V samples use NLO NNPDF3.0 PDF set for the ME evaluation and the A14 tune with LO NNPDF2.3 PDF set for the parton shower.

3.9 ATLAS Simulation

The outcome of the MC generation of a physics event is the collection of the four-vectors of all the stable[1] particles after hadronization and decay of the intermediate unstable particles. This collection represents the so-called stable *particle level* and it is stored in EVNT format. After the physics processes generation, an accurate simulation of the interaction of the particles with the detector is needed in order to study its response and efficiencies in details. The ATLAS Collaboration developed a detector simulation that reproduces the output obtained by the ATLAS TDAQ system, described in Section 2.9.1. Therefore, the data acquisition process is performed also on the simulated samples using the same triggers and reconstruction algorithms as for real pp collisions. The ATLAS detector simulation is based on GEANT4 [110] framework. The simulation takes into account all the information regarding the real detector conditions, e.g. mis-alignments or subdetector issues. The interactions between particles and the detector generate energy deposits in the involved components and they are stored in HITS format. The simulation converts these energy deposits into simulated electronic signals in RDO format, described in Section 2.9.2, that can be processed by the reconstruction algorithms.

The most CPU intensive step of the detector simulation is the generation of the particle shower in the calorimeter system. Therefore, the full detector simulation, referred to as Fullsim, requires a significant amount of time. The Atlfast-II (AFII) simulation has been developed to provide a faster simulation by imposing a parametrized description of the particle showers in the calorimeters. Generally, the Fullsim simulation provides higher accuracy in the description of the response of the ATLAS compared to AFII. The samples used in the analysis described in this thesis are based on Fullsim simulation with the exception of the MC samples used to evaluate the uncertainties related to the $t\bar{t}$ modeling.

The MC events are corrected in order to improve the description of the detector effects on the reconstructed quantities. Comparisons between the reconstruction and identification efficiencies of the physics objects measured in data and evaluated in MC simulations allow to define multiplicative scale factors (SF) as

$$SF = \frac{\varepsilon_{\text{data}}}{\varepsilon_{\text{sim.}}} \tag{3.3}$$

applied to the simulated MC events in a per-event correction procedure referred to as calibration that will be futher discussed in the following chapter.

[1] A stable particle is defined as a final-state particle with mean lifetime $\tau > 3 \times 10^{-11}$ s.

3.10 Rivet framework and studies on $t\bar{t}$ modeling

The Rivet [111] toolkit (Robust Independent Validation of Experiment and Theory) is a system for validation, development and tuning of MC event generators. It is a framework based on C++ and it consists of a collection of routines which replicate the analysis chain using shared object definitions and reconstruction algorithms collected in the core libraries of the framework. Rivet allows to preserve analysis code from the LHC and other high-energy colliders for the comparison of the predictions with the published results. For this reason, it is highly recommended and requested that analyses performing a particle level measurement provide a Rivet routine to be included in the public database. Rivet is used by phenomenologists and MC generator developers to test theoretical models and to perform the parameter tuning. In particular, Rivet has been extensively used to perform studies on the $t\bar{t}$ modeling in recent years and it has been playing a crucial role in improving the understanding of $t\bar{t}$ production and, subsequently, reduce the related uncertainties.

During my PhD, I worked on the preparation and validation of several Rivet routines concerning ATLAS $t\bar{t}$ cross-section analyses, in particular, the differential measurement in the ℓ+jets channel at 8 TeV [52] and 13 TeV (2015 data) [51], already presented in Section 1.3.4. The aforementioned routines are published and available in the official release of Rivet [112, 113] and have been used to perform studies related to MC modeling of $t\bar{t}$ production. The optimisation of the h_{damp} parameter, as well as the scale variations for the nominal $t\bar{t}$ MC sample was performed by using these routines [114]. From the comparison between the MC samples generated with POWHEG+PYTHIA 8 using different values of $h_{\text{damp}}$and the measurements of the differential ℓ+jets cross-section analyses at 8 TeV and 13 TeV, it has been found that the best agreement between multiple centre-of-mass energies is obtained by using $h_{\text{damp}} = 1.5 \cdot m_t$ as the preferred value [114]. The comparisons between data and different configurations of POWHEG+PYTHIA 8 is shown in Figure 3.4. In addition, a first study on the sensitivity on the choice of the scale variations was performed [114] and it allows to set a configuration to estimate the uncertainties due to QCD radiation and scale dependance, as described in Section 3.8.2.

The continue effort to improve the $t\bar{t}$ modeling benefits from the availability of Rivet routines. The most recent NLO +PS MC generators used to model top-quark pair production have been optimized [115]. These studies are carried out using unfolded data of the previously cited ℓ+jets analysis at 13 TeV [51] and the related Rivet routine. A comparison between the settings used in early Run 2 analyses [115] and the updated configuration used in this analysis allows to asses the improvement in the modeling of $t\bar{t}$ production and the subsequently reduction of the uncertainties related to the choice of hard scatter generator, PS model and additional QCD radiation. A comparison between the setup for early Run 2 analyses and the current setup is shown in Figure 3.5. It is worth emphasizing that that the reduction of uncertainties is a crucial point for carrying out precision studies such as the measurement of $t\bar{t}$ production cross-section and the studies previously described were preparatory for the analysis setup.

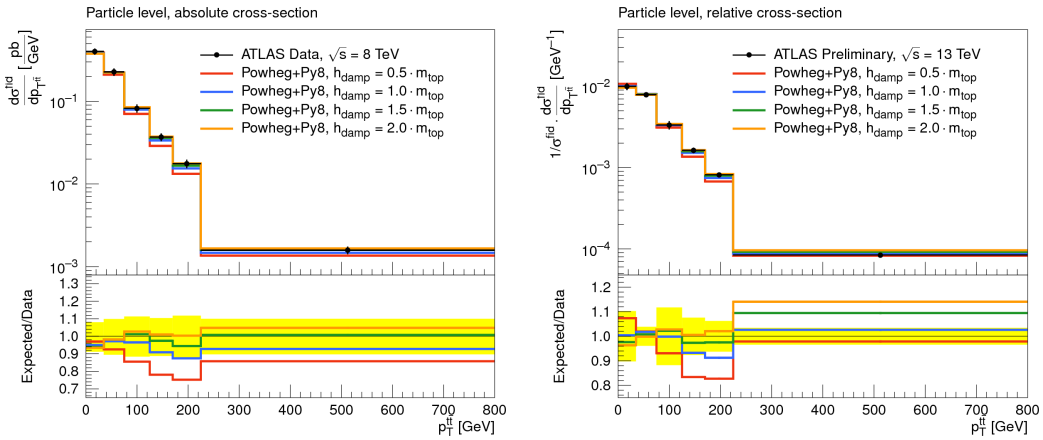

(A) (B)

FIGURE 3.4: The POWHEG+PYTHIA 8 samples with different h_{damp} variations are compared to ATLAS data unfolded to particle level as a function of the transverse momentum of the $t\bar{t}$ system at 8 TeV [52] (a) and 13 TeV [51] (b). The yellow band is the total experimental uncertainty on the data (statistical and systematic). The generator predictions are shown as solid colored lines. Figures are taken from [114].

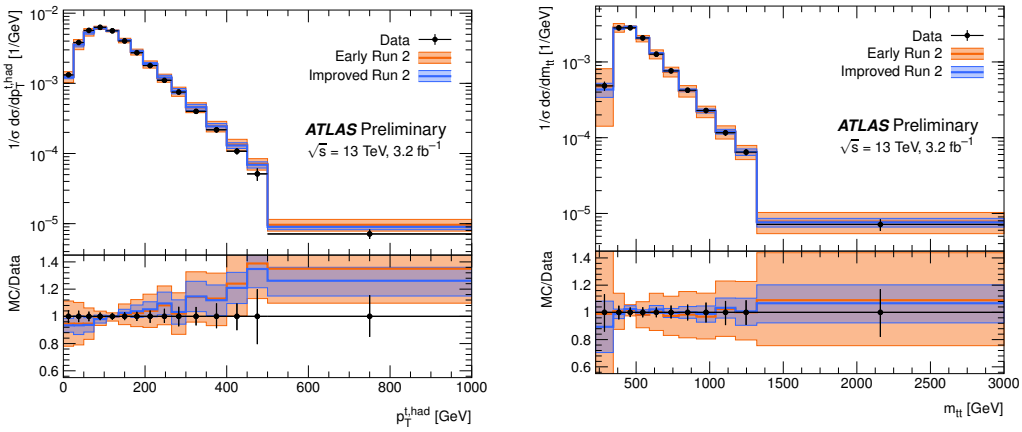

(A) (B)

FIGURE 3.5: Comparison of the generator setup defined for early Run 2 analyses (red) with the setup used in the analysis (blue), compared to ATLAS unfolded data to particle level as a function of the transverse momentum of the top quark (a) and of the invariant mass of the $t\bar{t}$ system (b) at 13 TeV [51]. The data are represented as closed (black) circles with the total experimental uncertainty on the data (statistical and systematic) indicated by the error bars. Figures are taken from [115].

Chapter 4

Object Definition

The final state that characterizes the ℓ+jets channel of the top-quark pair decay consists of charged leptons, neutrinos, light and heavy quarks. After the hadronization and the decay processes which these particles undergo, specific subdetectors of ATLAS are involved in the final state object reconstruction. Each object has a specific signature that depends on the particular response and interaction of the various subdetectors and the definition is strictly related to the characteristics of the ATLAS detector. The following sections will be dedicated to the overview of the reconstruction and definition of the objects used to select the $t\bar{t}$ signal of this analysis.

4.1 Tracks and Primary Vertices

The tracking reconstruction algorithm [116, 117] uses information collected by the inner detector. The track reconstruction is based on the combination of the hits in the different layers of the ID generated by charged particles. The trajectories of the incoming charged particles, curved by the effect of the magnetic field, are parametrized by a set of five quantities which exploit their geometry and kinematics:

$$(d_0, z_0, \phi, \theta, q/|\vec{p}|), \tag{4.1}$$

where d_0 and z_0 represent, respectively, the transverse and longitudinal impact parameters, ϕ and θ are the azimuthal and polar angle respectively while $q/|\vec{p}|$ expresses the ratio between the charge and the momentum. The impact parameters and the direction are usually calculated with respect to the primary vertex of the event.

The reconstruction proceeds through the application of a pattern recognition algorithm on the deposits present in the ID. From the deposits in the Pixel and the SCT, clusters are created and combined with the TRT raw timing information which are translated into calibrated drift circles. An *inside-out* algorithm [116] takes the Pixel and SCT space points as

seeds to perform track finding and then it extends the reconstruction outwards to the TRT. In addition, an *outside-in* procedure is applied to track reconstruction, known as back-tracking, in order to consider all the remaining hits. It esentially goes in the opposite direction of the previous algorithm, so it is seeded from TRT information and then it extrapolates the track to the silicon detectors.

Once the tracks have been reconstructed, a dedicated vertex finder [118, 119] is employed to find primary and secondary vertices. In order to enhance the resolution on the spatial position of the vertex, only vertices with at least two associated tracks with a $p_{\mathrm{T}} > 400\,\mathrm{MeV}$ are considered. The number of reconstructed vertices is proportional to pileup. The Primary Vertex (PV) of the event is the one with the highest sum of squared p_{T} of the associated tracks and it is considered the hardest pp interaction point in a bunch crossing. The remaining vertices are associated to the additional pileup interactions in the event. The reconstructed vertices which are not compatible with the estimated beam collision region are considered as secondary vertices. Secondary vertices are particularly important in b-tagging and they will be further discussed in Section 4.5.

4.2 Electrons

Electrons are reconstructed in the central region of the ATLAS detector within $|\eta| < 2.7$, but outside the transition region ($1.37 \leq |\eta| < 1.52$) between the barrel and the end-cap EM calorimeter. The reconstruction is based on the information collected by the electromagnetic calorimeter and the inner tracker. The information from the EM calorimeter defines the energy of the electron while the ID tracks give the angular direction at the production point.

The first step of the electron reconstruction is the creation of clusters in the calorimeter energy deposits. The electron candidate clusters are intially seeded from small groups of cells in the electromagnetic calorimeter with global $E_{\mathrm{T}} > 2.5\,\mathrm{GeV}$. This treshold is chosen in order to minimize the impact of electronic or pileup noise and maximize the reconstruction efficiency [120].

Once the seed clusters are created, an attempt to match them to the tracks reconstructed in the ID, according to the method described in Section 4.1, is made. Tracks are extrapolated from their last measured point in the ID to the EM calorimeter. Then, the extrapolated η and ϕ coordinates in the EM calorimeter are compared to the cluster coordinates. The matching is based on angular quantities: the track and the cluster are considered matched if the distance between the track impact point and the EM cluster barycentre is $|\Delta\eta| < 0.05$. In case there is no matching, the cluster is considered as an unconverted photon. In case of a matching but the track is not coming from a primary vertex, then the cluster is considered as a converted photon. The cluster is tagged as an electron if the matched track is originated from the primary vertex. Additional requirements are applied on track parameters,

$|d_0|/\sigma_{d_0} < 5$ and $|z_0 \sin\theta| < 0.5\,\text{mm}$ to improve the track association with the primary interaction vertex. The clusters are also extended in the ϕ direction in order to account for breamsstrahlung loss effects.

The reconstruction efficiency of electrons is defined as the ratio of the number of clusters matched to a track after passing the track quality criteria to the number of all clusters. This efficiency is measured using Z and J/ψ resonances with a tag-and-probe method. The efficiency of the electron reconstruction has a slight dependence on the transverse energy of the electron (E_T) and it varies between 97% for $E_\text{T} = 15\,\text{GeV}$ and 99% for $E_\text{T} > 50\,\text{GeV}$.

The identification of the electrons originating from the hard interaction, i.e. *prompt* electrons, has to be optimized in order to separate them from possible background sources, such as hadronic jets or converted photons. In order to reach a good separation between real and fake electrons, an identification algorithm (ID) [121] is applied to the electron candidates. The ID algorithm employs a likelihood-based method (LH) and it is based on a multivariate analysis technique which considers several properties of the candidate, including track quality, track-cluster matching and information from calorimeters and TRT, and combines them in a discriminant.

Three levels of identification working points are provided for electron ID, *loose*, *medium* and *tight* electrons, in order of increasing background rejection. They are defined in such a way that each operating point uses the same variables to define the LH discriminant but with a different cut value. The efficiencies for all the three working points are shown in Figure 4.1.

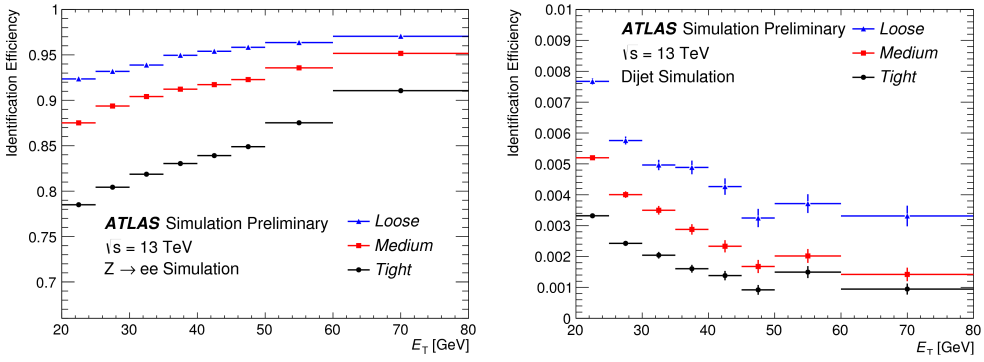

FIGURE 4.1: The efficiency to identify electrons (left) from $Z \to ee$ decays and the effiency to identify hadrons as electrons (background rejection, right) using simulated dijet samples for al. The efficiencies are shown as a function of the E_T of the candidate electron and for all the defined working points [121].

The working point used to identify electrons in this analysis is the *TightLH*. However, a looser identification operating point is used in the estimation of fake and non-prompt electrons as described in Section 5.4.2.

In addition to the identification criteria described above, isolation requirements are applied on the electron candidate in order to reduce the contamination from fake leptons. These requirements are based on two discrimating variables:.

- calorimetric isolation energy, $E_{\mathrm{T}}^{\mathrm{cone0.2}}$, defined as the sum of transverse energy of EM clusters within a cone of $\Delta R = 0.2$ around the electron candidate,
- a track isolation, $p_{\mathrm{T}}^{\mathrm{varcone0.2}}$, defined as the sum of transverse momenta of all the tracks within a cone of $\Delta R = \min(0.2, 10\,\mathrm{GeV}/E_{\mathrm{T}})$ around the track of the electron candidate originating from the primary vertex.

The isolation efficiency is defined as the ratio of the number of electrons that pass a certain criterion on the isolation variables to the total number of electron candidates passing the identification requirements. The electrons used in this analysis are selected by requiring a *Gradient* isolation working point, defined in such a way to provide isolation efficiency of at least 90% for electrons with $p_{\mathrm{T}} > 25\,\mathrm{GeV}$, increasing to 99% for electrons with $p_{\mathrm{T}} > 60\,\mathrm{GeV}$ [121]. In order to correct for the differences between the isolation efficiencies measured in data and estimated in MC, a per-event scale factor is applied in the analysis.

4.3 Muons

Muons are reconstructed in ATLAS combining information from the muon spectrometer and the inner detector. The first step of the reconstruction is performed independently in the two detectors. The track reconstruction in the inner detector is performed as already described in Section 4.1 for any charged particle. In the muon spectrometer, the first step of the reconstruction is the creation of segments in the MDT chambers. A Hough trasformation [122] is used to search for hits aligned on a trajectory in the bending plane of the detector. The RPC and TGC hits are used to measure the coordinate orthogonal to the bending plane. Segments in the CSC detector are built using a separate combinatorial search in the η and ϕ detector planes.

Muon track candidates are then built by fitting together hits from segments in different layers. At least two matching segments are required to build a track, except in the transition region between the barrel and the end-cap where a single high-quality segment with η and ϕ information can be used to build a track. In case of multiple tracks share the same segment, an overlap removal procedure is applied. In order to allow high efficiency for close-by muons, all the tracks with segments in three different layers of the spectrometer are not removed if they share segments in two of three layers, but not in the outermost one [123].

The combined reconstruction exploits the information coming from ID, MS and calorimeter and several algorithms are developed. Four different definitions of muon are defined based on the specific information used in the reconstruction:

- **Combined muon (CB)**: the track reconstruction is performed independently in the ID and MS, and a combined track is then build with a global refit that uses the hits from both the ID and MS subdetectors. Most part of the muons are reconstructed taking as

starting point the track in MS and then extrapolated inward and matched to the tracks in the inner detectors.

- **Segment-tagged (ST)**: a muon is reconstructed starting from a track in the ID which is extrapolated to the MS and associated with at least one segment in the MDT or CSC chambers.

- **Calorimeter tagged (CT)**: a track in the ID is identified as a muon if it can be matched to an energy deposit in calorimeters. This type of muon candidate has the lowest purity of all the muon types but it recovers acceptance in the regions of the MS that are only partially instrumented.

- **Extrapolated muons (ME)**: a muon is reconstructed using only the information from MS. ME muons are mainly used to extend the acceptance for muon reconstruction into the region $2.5 < |\eta| < 2.7$, which is not covered by the ID.

Similarly to the electrons, the reconstruction of muon candidates is followed by an identification procedure which is performed by applying quality requirements in order to improve the selection of prompt muons with high efficiency and measure the momentum with accuracy and, in parallel, to suppress the background due to fake muons. The muon identification is based on the following set of variables:

- $|q/p|$ significance, defined as the absolute value of the difference between the ratio of the charge q determined from the track curvature and the momentum p of the muons measured in the ID and MS divided by the sum in quadrature of the corresponding uncertainties,

- ρ', defined as the absolute value of the difference between the ratio of the transverse momentum measurements in the ID and MS divided by the p_{T} of the combined track,

- the normalized χ^2 of the combined track fit [123].

DIfferent working points are defined based on the requirements on the number of hits and on the aforementioned variables. Muons in this thesis are required to pass the *Medium* identification criteria. This identification selection minimizes systematic uncertainties associated with the calibration and reconstruction of muons. The requirements of this working point are:

- at least three hits in at least two MDT layers, with exception for the region $|\eta| < 0.1$ where one MDT layer and no hole[1] are sufficient,

- q/p significance less than 7,

[1] A hole is defined as an active sensor traversed by the track that does not contain any hits.

- at least 10% of the TRT hits assigned to the track are included in the fit within $0.1 \leq |\eta| < 1.9$,
- at least one Pixel hit, five SCT hits and less than three Pixel or SCT holes.

Also in the case of muons, additional requirements based on isolation allow to further discriminate between the prompt muons, considered as signal, and the non-prompt muons coming from the heavy-flavor hadron semi-leptonic decays. The track-based isolation variable, $p_{\mathrm{T}}^{\mathrm{varcone0.3}}$, is defined as the scalar sum of the transverse momenta of the tracks with $p_{\mathrm{T}} > 1\,\mathrm{GeV}$ in a cone size $\Delta R = \min(10\,\mathrm{GeV}/p_{\mathrm{T}}^{\mu}, 0.3)$, excluding the muon track itself. The calorimeter-based isolation variable, $E_{\mathrm{T}}^{\mathrm{topocone0.2}}$, is defined as the sum of the transverse energy of topological clusters in a cone of size $\Delta R = 0.2$ around the muon, after subtracting the contribution from the energy deposit of the muon itself and correcting for pile-up effects. Muons considered in this analysis are required to satisfy the *Gradient* isolation working point. The isolation efficiency is defined as the ratio of the number of muons passing a certain isolation selection to the total number of muons passing the *Medium* identification criteria. The Gradient working point is defined in such a way to provide an isolation that is at least of 90% at $p_{\mathrm{T}} = 25\,\mathrm{GeV}$ and 99% at $p_{\mathrm{T}} = 60\,\mathrm{GeV}$ [123]. The muon reconstruction and isolation efficiencies as a function of the p_{T} for the working point used in the analysis are show in Figure 4.2.

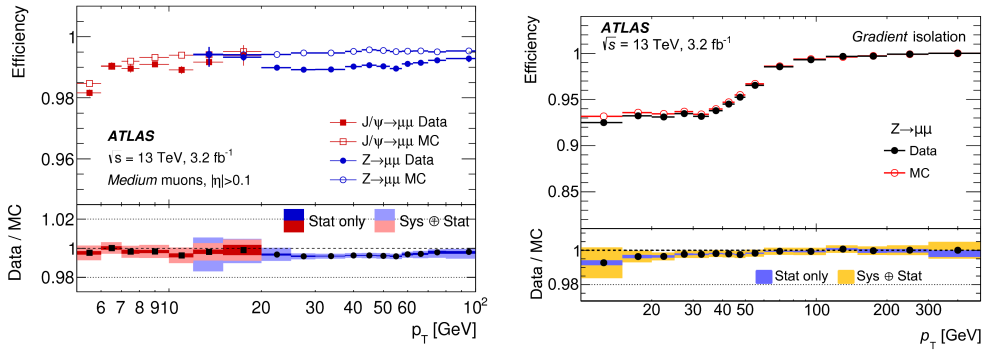

FIGURE 4.2: Reconstruction efficiency for the *Medium* muon selection (on the left) and isolation efficiency (on the right) for the *Gradient* working point as a function of the p_{T} of the muon [123].

4.4 Jets

The property of QCD known as confinement has already been discussed in Section 1.2.5. This property does not allow the gluons and quarks produced in the hadronic collisions to be observed as free states. They undergo the hadronization process in which color singlets are build from the additional gluons and quarks radiated due to the strong field between the partons. The jets are the collimated showers of hadrons as observed in the detector. The

aim of jet reconstruction is to identify physics objects with kinematics and properties related to the corresponding ones of the initial partons.

4.4.1 Jet reconstruction

The jet reconstruction is defined by the type of objects considered and the algorithms used to build them. A good jet definition can be applied to experimental measurements, to the output of parton-showering MC and to partonic calculations, and the resulting jets provide a common representation of all these different kinds of events. At the particle level, the jets are reconstructed from truth stable particles generated by the MC simulation. In ATLAS, the detector-level jets are initially reconstructed using the information collected by the cells in the calorimeters, but the association to the tracks present in the ID is crucial for their calibration and for the mitigation of pileup contributions. The starting point of the jet reconstruction is the creation of topologically adjacent clusters of calorimeter cells, referred as to topo-clusters. The topo-clusters are built up in an iterative process [124], starting from the most significant energy deposits. Then, the neighbouring cells are combined together into single topoclusters. The topo-clusters represent the first collection of proto-jets which serve as input for the particular jet algorithm in use.

Jet algorithms should follow general properties, known as *Snowmass accord* [125]:

1. Simple to implement in an experimental analysis;
2. Simple to implement in the theoretical calculation;
3. Defined at any order of perturbation theory;
4. Yields finite cross sections at any order of perturbation theory;
5. Yields a cross section that is relatively insensitive to hadronisation.

In particluar, the desirable property for a jet algorithm is the infrared and collinear safety:

- **Infrared safety**: If additional soft particles are present between two particles belonging to the same jet, this should not interfere with the recombination of these two particles into a jet and its reconstruction. So, if a soft particle is present, it should not affect the number of jets produced
- **Collinear safety** The jet should be reconstructed indipendently of the fact that an amount of transverse momentum is carried by only one particle or two splitted collinear particles.

The reasons for the requirement of the infrared and collinear safety could be summarized in few points [126]:

- Collinear splittings and soft emissions effectively occur through perturbative and non-perturbative effects. One of the reason to define jets is to establish a way of viewing events that is insensitive to all these effects, which is also connected with point 5 of the Snowmass accord.
- In fixed-order perturbative QCD calculations, soft emissions and collinear splittings are associated with divergent matrix elements. In addition, divergent loop matrix elements are present that enter in the calculations with the opposite sign. Generally, the two sources of divergence should cancel. For infrared and collinear unsafe jet algorithms the tree-level splittings may lead to one set of jets, while the loop diagrams may lead to another, breaking the cancellation and leading to infinite cross sections in perturbation theory (point 4 of the Snowmass conditions).
- The detector finite resolution and the non-zero momentum thresholds provide regularization of collinear and infrared unsafety, but it is specific of the apparatus. This does not allow to compare experimental results in case of unsafe algorithms to the predictions at the particle level.

The anti-k_t algorithm [127] successfully exhibits the aforementioned requirements and it combines the proto-jets as follows. Two distances in the $\eta - \phi$ plane are defined:

$$d_{ij} = \min(k_{Ti}^{2p}, k_{Tj}^{2p}) \frac{\Delta_{ij}^2}{R^2} \tag{4.2}$$

$$d_{iB} = k_{Ti}^{2p} \tag{4.3}$$

$$\Delta_{ij} = (\eta_i - \eta_j)^2 + (\phi_i - \phi_j)^2 \tag{4.4}$$

where d_{ij} represents the distance between two proto-jets (i and j), d_{iB} expresses the distance from the beam pipe of a proto-jet, k_{Ti} is the p_{T} of input i and R is the jet radius parameter used to define the final size of the jet. The algorithm follows an iterative procedure and compares the two distances d_{ij} and d_{iB}:

- if $d_{iB} < d_{ij}$, the proto-jet is considered a jet and removed from the proto-jet list
- if $d_{iB} > d_{ij}$, the proto-jets i and j are combined in a new proto-jet

The algorithm is defined by the R and p parameters. The anti-k_t algorithm has $p = -1$, the Cambridge–Aachen sets $p = 0$ and the k_t algorithm has $p = 1$. A comparison between the three algorithms for $R = 1.0$ is shown in Figure 4.3. The anti-k_t favours clustering that involves hard particles rather than clusterings that involve soft particles (k_T algorithm) or energy-independent clusterings (Cambridge–Aachen) and the jets tend to be more conical than the other two options. The disadvantage of the anti-k_t algorithm is that it does not allow to gather information about the substructure of the jets.

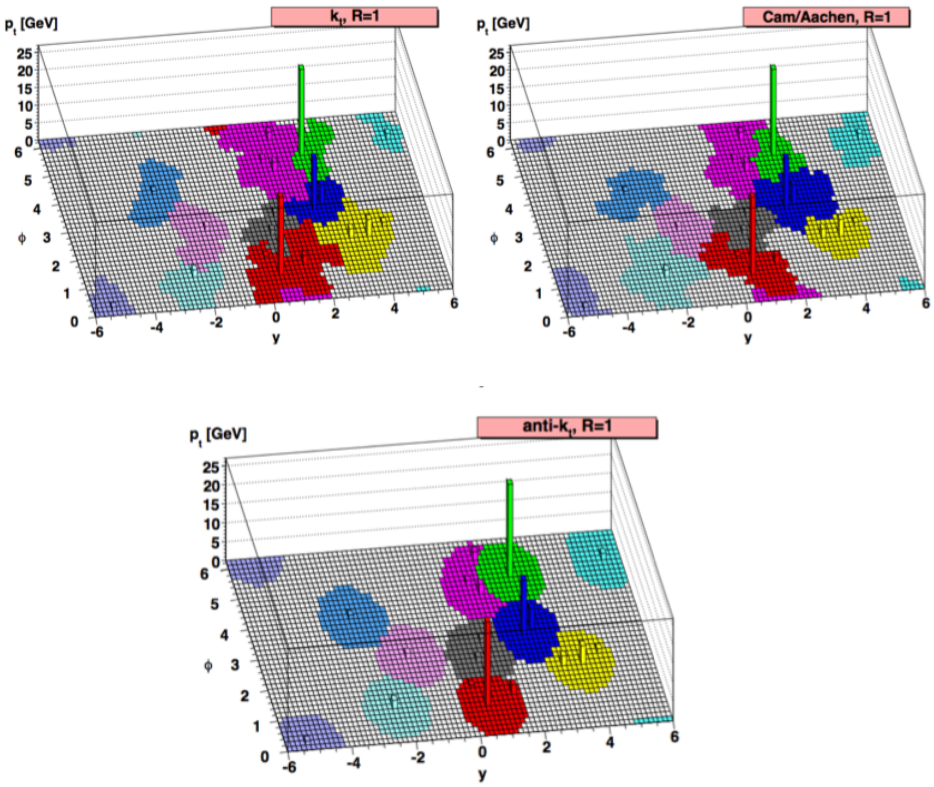

FIGURE 4.3: Comparison between the jets obtained by the k_t (top left), Cambridge–Aachen (top right) and anti-k_t (bottom) for a radius parameter $R = 1.0$ starting from the same inputs [126].

In the analysis described in this thesis, two sets of jets are used: the anti-k_t with a radius parameter $R = 0.4$ for the resolved topology while the $R = 1.0$ is choosen for the boosted topology.

4.4.2 Jet calibration

The jet calibration is the procedure used to correct the energy of the reconstructed jets in order to relate it to the energy of the initial parton. The corrections are derived from both MC simulation and data and the scheme used is the sequential calibration scheme [128], which will be described in the following. The first step consists in a correction on the jet direction to point toward the primary vertex. This improves the angular resolution of the jets. Then, the calibration corrects for the additional energy deposited within the jet radius due to in-time and out-of-time pileup. The additional energy due to pileup is subtracted from each jet according to its area A [129], defined using ghost association [130], where *ghost* particles of infinitesimal momentum are added uniformly to the event before jet reconstruction in order to test the jet area. The area is then defined as the fraction of momentum-less particles associated to each jet using ghost matching procedure. This procedure consists of a

re-clustering of the jets including infinitesimal momentum but specific direction, so this addition of particles does not affect the jet four momentum even if they are considered as jet constituents.

The following step of the calibration sequence is the jet energy scale and η correction obtained from MC simulation and it is used to correct the reconstructed jet energy at the electromagnetic scale to the energy scale of particle-level jets. The particle-level jets are matched to the reconstructed-level jets by applying an angular requirement $\Delta R(\text{truth}, \text{reco}) < 0.3$. The ratio between the energies of the reconstructed and the particle-level jets is parametrized as a function of the p_{T} and η of the reconstructed jet and its inverse is applied as a correction factor. Then, a Global Sequential Calibration (GSC) is performed to reduce the dependence of the jet energy on the different shower profiles between jets initiated by quarks and by gluons. In general, a quark-jet contains hadrons that carry large part of the jet p_{T}, while a gluon-initiated jet contains softer particles and produces a wider shower profile.

The last step of the jet calibration consists of a series of corrections derived from data, referred to as *in-situ* corrections. The aim of these corrections is to account for the differences in jets response between MC and data by balancing the jet p_{T} against well-measured physics objects (photons, Z bosons and calibrated jets).

4.4.3 Jet Vertex Tagger

Additional jets due to the pileup activity are often present and they are considered as background with respect to the jets coming from the hard-scatter interaction. The Jet Vertex Tagger (JVT) [131] has been developed in order to separate hard-scatter jets and pileup jets. This tagger is based on multivariate analysis and combines the information of two variables:

- corrJVF, which is the ratio of the sum of p_{T} of all the tracks coming from the hard-scatter primary vertex matched to the jet.
- $R_{p_{\text{T}}}$ is defined as the ratio of the scalar sum of p_{T} of the tracks associated with the jet and originate from the hard-scatter vertex to the calibrated jet p_{T} after pileup subtraction.

The distribution of the JVT disriminant output for pileup and hard-scatter jets is shown in Figure 4.4. In this analysis, a requirement on the JVT output, JVT > 0.59, is applied to jets with a p_{T} below 60 GeV and with $|\eta| < 2.4$ since the contribution of pileup jets at high p_{T} is negligible.

4.4.4 Jet reconstruction and calibration in boosted topology

During Run 2, the high energy and luminosity reached by the LHC allow to produce more often heavy particles such as W, Z, H and top quarks with large transverse momentum

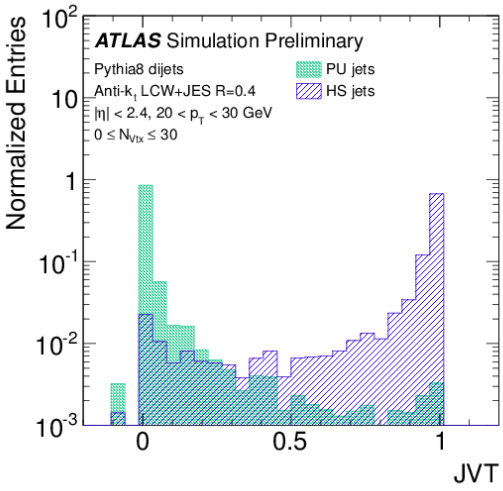

FIGURE 4.4: Distribution of JVT for pileup and hard-scatter jets with p_{T} between 20 and 30 GeV [131].

(*boosted particles*) that implies large Lorentz boost for their decay products. Therefore, boosted object decays are collimated along the momentum direction of the boosted mother particle in the detector rest frame. The angular separation between the W and b decay products of top quarks in simulated $Z' \to t\bar{t}$ events (Z' is an hypothetical massive gauge boson) as well as the separation between the light quarks of the hadronically-decaying W boson are shown in Figure 4.5. The angular separation of the decay products of an heavy particle is

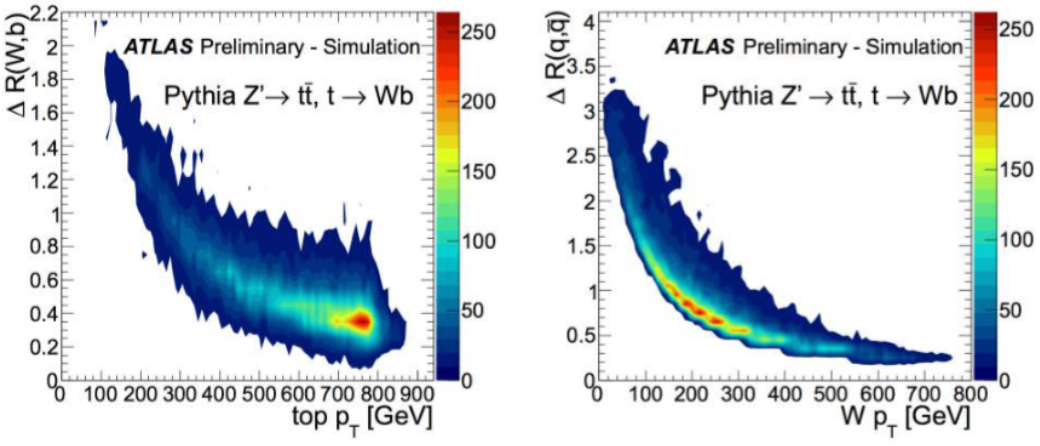

FIGURE 4.5: Opening angle between W and b in top decays $t \to Wb$ as a function of the top p_{T} (on the left) and opening angle of the $W \to q\bar{q}$ system from $t \to Wb$ decays as a function of the p_{T} of W boson.

approximately

$$\Delta R \approx \frac{2m}{p_{\mathrm{T}}} \tag{4.5}$$

where m and p_{T} refer to the decaying particle. So, for W boson with a p_{T} larger than 200 GeV the possibility to resolve each product of the hadronic decay using the small-R jets is reduced and for top quark with $p_{\mathrm{T}} > 350$ GeV the decay products tend to have a separation of $\Delta R < 1.0$. Subsequently, the decay products can be fully contained in a jet of radius $R = 1.0$.

The extensively method to reconstruct the decay products of boosted top quarks is to exploit large-R jets with radius $R = 1.0$. The inputs used are the calorimeter topological clusters similarly to the small-R jet case. The differences between the two sets of reconstructed jets is the energy corrections applied in the specific case (LCW clusters for boosted objects). A single large-R jet which contains the products of the decay of a top quark will have significantly different properties than a single large-R jet of the same p_{T} originating from a single light-quark or gluon. The characteristic three-body decay of a top quark results in a hard substructure (absent from the light-quark or gluon jets) that can be identified and exploited to discriminate signal from the multi-jet QCD background by removing soft radiation from jets. This procedure is generally referred to as jet *grooming*.

The standard grooming algorithm used in ATLAS is the trimming [132]. This procedure removes contamination from pile-up, initial- and final-state radiation and underlying events that are often much softer than hard-scattering parton products. The removal of these contributions is possible since their effect is usually the creation of new topological clusters in the calorimeter, instead of contributing to the clusters related the products of interest. The trimming procedure reconstructs the large-R jet with the k_t algorithm finding the pseudo-jets constituents with a smaller radius R_{sub}. Then, all the subjets i with $p_{\mathrm{T}}^{i}/p_{\mathrm{T}}^{\mathrm{jet}} < f_{\mathrm{cut}}$ are removed. Therefore, the parameters of the method are R_{sub} and f_{cut}. After this procedure, low-mass jets from a light quark or gluon usually loose 30-50% of their mass, while jets containing the decay products of a boosted top quark lose only a few percent of mass, mainly removing pile-up contribution; this is due to the large-R jet internal structure that is more uniform in the case of light quarks and gluons production. The effect of trimming increases the separation between signal and background distributions for substructure variables used in boosted top tagging [133]:

- m_{jet}: the jet mass is calculated from the energies and momenta of its constituents as

$$m_{\mathrm{jet}}^2 = \left(\sum_i E_i\right)^2 - \left(\sum_i p_i\right)^2 \tag{4.6}$$

  where E_i and p_i are the energy and momenta of the constituent i.

- N-subjettiness: the N-subjettiness variable [134, 135] is related to the pseudo-jet multiplicity. The τ_N variable is calculated by clustering with the k_t algorithm the constituents of the jet requiring exactly N pseudo-jets to be found. The clusterization process stops when exactly N pseduo-jets remain. The τ_N variables are defined as the

sum over all k constituents of the jet

$$\tau_N = \frac{1}{d_0} \sum_k p_{Tk} \times \min(\Delta R_{1k}, \Delta R_{2k}, \ldots, \Delta R_{Nk}), \quad \text{with} \quad d_0 = \sum_k p_{Tk} \times R \tag{4.7}$$

The quantity τ_N indicates how well the large-R jet can be described as containing N or fewer pseudo-jets, discriminating by how constituents are localized close to the pseudo-jet axes. In top tagging, the $\tau_{32} = \tau_3/\tau_2$ quantity is used which; its value is small if a three body hypothesis describes a large-R jet better than a two body one.

In the previous $t\bar{t}$ cross-section measurement in the ℓ+jets channel at 13 TeV with 2015 data [51], the boosted analysis was perfomed by using the large-R jets with $R_{\text{sub}} = 0.2$ and $f_{\text{cut}} = 0.05$ and by applying a combination of requirements on m_{jet} and τ_{32} to identify the hadronically decaying boosted top quark [133]. The dominant uncertainties are the systematic uncertainties, in particular the large-R jets JES.

In order to improve the reconstruction and calibrations of the large-R jets a new approach is use in the analysis described in this thesis. The jet reclustering [136] allows to apply the well known calibrations and uncertainties evaluated for the small-R jets to the large-R jets. In this approach, the calibrated small-R jets are considered as input for the anti-k_t algorithm with $R = 1.0$. The calibrations derived with reclustering have similar performances to the standard large-R jet calibrations, but the uncertainty related to JES is significantly smaller [137]. This technique has been tested to be un-biased and the small-R jet calibrations and uncertainties can be directly forwarded in the dense environment of the reclustered jet, without additional corrections or systematic [137]. The re-clustered jets rely mainly on the technique and cuts applied to remove the pile-up contribution in the calibration of the small-R jets. However, a trimming technique is applied also to the re-clustered jet after the formation, with the aim to remove soft small-R jets that could be originated entirely from pile-up. The trimming procedure removes all the small-R jets with fraction of p_T smaller than 0.05 of the re-clustered large-R jet p_T.

The interpretation of the sub-structure in the reclustered jets is complicated since these usually contains only 1 or 2 sub-jets, consequently the identification of the re-clustered jets originated from a top quark is done simply applying a mass window cut to the re-clustered jets around the nominal value of the top-quark mass, 120 GeV$< m_{\text{jet}} <$ 220 GeV.

A comparison between the mass responses and the JES uncertainty obtained with the reclustered and large-R jets are shown in Figure 4.6. Since the performances of the standard large-R jets and of the reclustered jets are at the same level, while the uncertainties due to jet energy scale are reduced by 50% using the re-clustering, the re-clustering approach is the method selected for this analysis. The reduction of the dominant uncertainty highly improves the sensitivity of the boosted analysis and allows to test top-quark pair production models in regions of the phase-space never investigated before, in particular in double differential cross-section measurements.

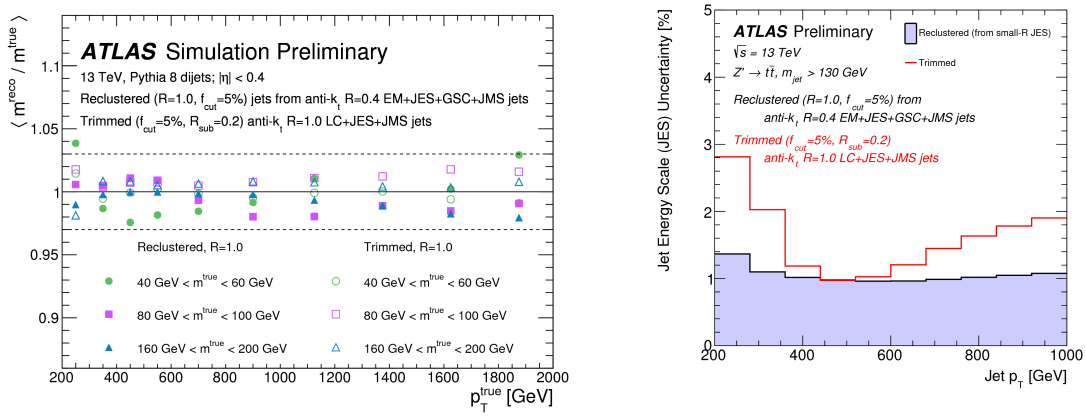

FIGURE 4.6: Reclustered and conventional trimmed large-R jet mass responses (on the left), shown as a function of the matched truth jet transverse momentum ($p_{\mathrm{T}}^{\mathrm{true}}$) in representative mass bins. The dashed lines indicate deviations from unity of 3%. The jet energy scale uncertainty as a function of p_{T} for reclustered jets and conventional large-R jets from $Z' \rightarrow t\bar{t}$ events. A requirement that the mass of the large-R jet be greater than 130 GeV is applied [137].

4.5 b-tagging

The identification of jets containing b-hadrons, referred to as b-tagging, plays a crucial role in the measurements of physics processes whose partonic final states have a b-quark. In particular, it is extremely relevant in $t\bar{t}$ cross-section measurements for discriminating top-quark pair events from the background.

The basis of b-tagging is the characteristic long lifetime ($\tau \approx 1.5\,\mathrm{ps}$, $c\tau \approx 450\,\mu\mathrm{m}$) and large mass of b-hadrons. A b-hadron in the energy range above 10 GeV has a significant mean flight path lenght $< l >= \beta\gamma c\tau$, thus it can travel on average about 3 mm in the transverse direction before its decay. Therefore, the topology of b-hadron decay is characterized by at least one vertex displaced from the interaction point of the hard-scatter collision. A graphical scheme of this topology is shown in Figure 4.7. The ability to find a secondary vertex of a jet, its distance to the primary vertex (decay lenght) and the mass of the associated particles to the reconstructed vertex help to identify this topology. In addition, the longitudinal and transverse impact parameters of the tracks in the analyzed jet play also an important role in b-tagging. The longitudinal and transverse impact parameters are defined as the minimum distance of the track to the primary vertex in the z direction and in the $x-y$ plane, respectively. The impact parameter is considered positive if the track extrapolation crosses the jet direction in front of the primary vertex, and negative otherwise. In general, the tracks from b-hadron decay products tend to have large and positive impact parameters which can be distinguished from tracks stemming from the primary vertex.

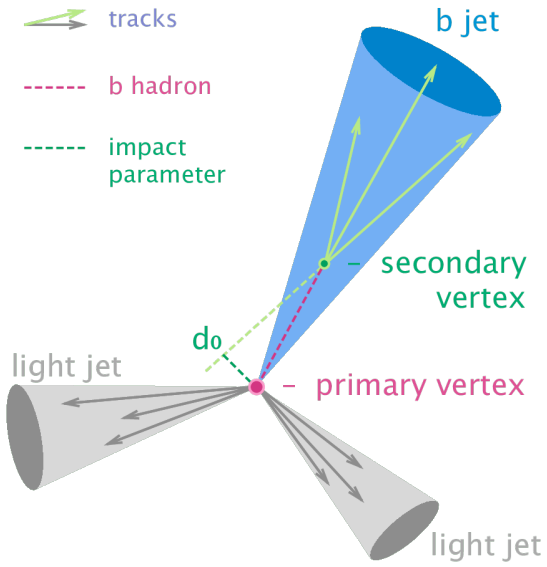

FIGURE 4.7: Characteristic topology of jets containing b-hadrons and graphical representation of the impact parameter.

4.5.1 b-tagging algorithms

In ATLAS b-tagging is based on different and complementary strategies that exploit the characteristic topology decribed above. Three basic algorithms have been developed to implement these strategies and they are described in the following.

IP2D and IP3D

The IP2D and IP3D [138] algorithms are based on the sign convention of the longitudinal and transverse impact parameters and the fact that secondary vertices originating from b-hadron decays are generally in front of the primary vertex. The IP2D tagger makes use of the transverse impact parameter significance, d_0/σ_{d_0}, as the discriminating variable while IP3D uses both the transverse and the longitudinal impact parameter significance, $z_0 \sin\theta/\sigma_{z_0 \sin\theta}$, in a two-dimensional template to account for their correlation. A loglikelihood ratio (LLR) discriminant is defined as

$$\sum_{i=1}^{N} \log\left(\frac{p_b}{p_u}\right), \tag{4.8}$$

where N is the number of tracks of the jet considered and p_b, p_u are the template probability density functions (PDF) for the b- and light-flavour jet hypothesis, respectively. In addition to the LLR separating b- and light-flavour jets, LLR functions are also computed to separate b- from c-jets, or c-jets from light-flavour jets. The information based on the knowledge of the detector geometry and inactive module maps whether a certain hit is expected or not in the innermost (IBL) and in the next-to-innermost (b-layer) layers of the ID is useful to assign a quality evaluation on the tracks and improve the discrimination. The log-lokelihood ratios

for IP2D and IP3D as ratio of the *b*- and light-flavour jet hypotheses are shown in Figure 4.8.

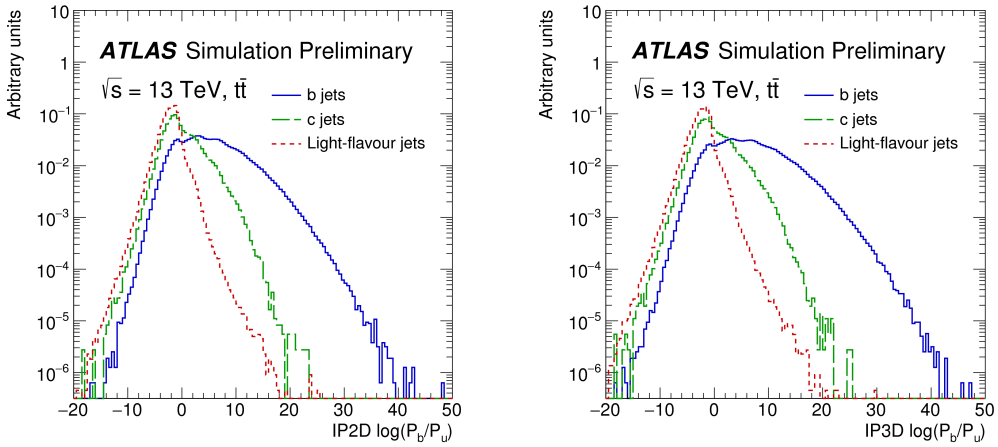

FIGURE 4.8: The log-likelihood ratios for the IP2D (on the left) and for the IP3D (on the right) b-tagging algorithms for *b*- (solid blue), *c*- (dashed green) and light-flavour (dotted red) jets in $t\bar{t}$ events. The log-likelihood ratios shown here are computed as ratio of the *b*- and light-flavour jet hypotheses. If no tracks are found in the jet, a large negative value that is not indicated in the plots is assigned as algorithm output [139].

Secondary Vertex Finding

The secondary vertex finding algorithm (SV) [140] explicitely reconstructs a displaced secondary vertex of the jet. All track pairs within a jet are tested for a two-track vertex hypothesis. A likelihood discriminant is constructed using several variables which characterize the secondary vertex and enhance the discriminating power, such as the invariant mass of all the associated tracks with the vertex, the number of two-track vertices (both shown in Figure 4.9), the decay length significance, and the fraction of the sum of the energies of the tracks in the vertex to the sum of the energies of all tracks in the jet.

JetFitter

The decay chain multi-vertex reconstruction algorithm, JetFitter [141], exploits the topological structure of weak *b*- and *c*-hadron decays inside the jet and tries to reconstruct the full *b*-hadron decay chain. A Kalman filter is used to find a common line on which the primary vertex and the *b*- and *c*-hadron vertices lie, approximating the *b*-hadron flight path, as well as their positions. JetFitter goes beyond the secondary vertex finding and it also searches for tertiary vertices.

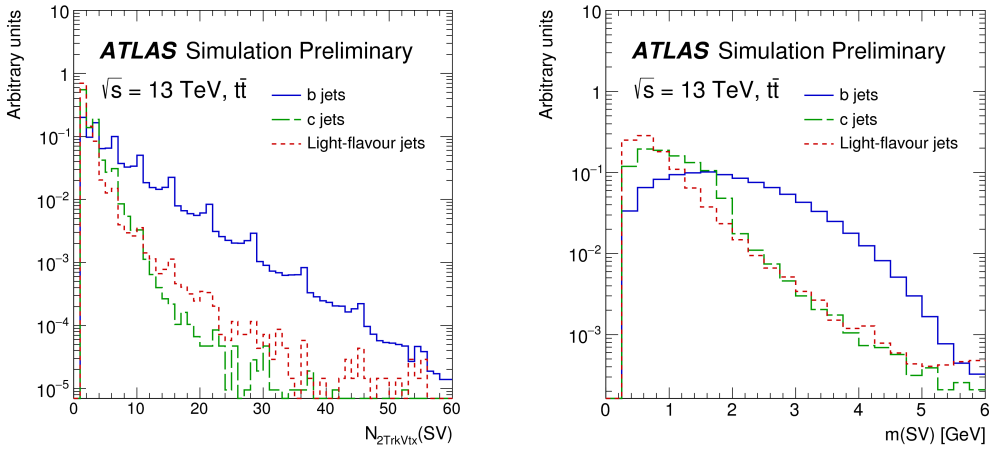

FIGURE 4.9: Properties of secondary vertices reconstructed by the SV algorithm for b- (solid blue), c- (dashed green) and light-flavour (dotted red) jets in $t\bar{t}$ events: the number of two-track vertices reconstructed within the jet (on the left) and the invariant mass (on the right) associated with the vertex [139].

MV2

A high-level tagger, MV2, which combines the output of the basic algorithms described above, has been developed in order to enhance the discrimination power between the different jet flavours. MV2 is a Boosted Decision Tree (BDT) algorithm, using the ROOT Toolkit for Mutivariate Data Analysis (TMVA). The list of the input variables is shown in Figure 4.10.

Input	Variable	Description
Kinematics	$p_T(jet)$	Jet transverse momentum
	$\eta(jet)$	Jet pseudo-rapidity
IP2D, IP3D	$\log(P_b/P_{\text{light}})$	Likelihood ratio between the b- and light jet hypotheses
	$\log(P_b/P_c)$	Likelihood ratio between the b- and c-jet hypotheses
	$\log(P_c/P_{\text{light}})$	Likelihood ratio between the c- and light jet hypotheses
SV	m(SV)	Invariant mass of tracks at the secondary vertex assuming pion masses
	f_E(SV)	Fraction of the charged jet energy in the secondary vertex
	N_{TrkAtVtx}(SV)	Number of tracks used in the secondary vertex
	N_{2TrkVtx}(SV)	Number of two track vertex candidates
	L_{xy}(SV)	Transverse distance between the primary and secondary vertices
	L_{xyz}(SV)	Distance between the primary and secondary vertices
	S_{xyz}(SV)	Distance between the primary and secondary vertices divided by its uncertainty
	ΔR(jet, SV)	ΔR between the jet axis and the direction of the secondary vertex relative to the primary vertex
Jet Fitter	N_{2TrkVtx}(JF)	Number of 2-track vertex candidates (prior to decay chain fit)
	m(JF)	Invariant mass of tracks from displaced vertices assuming pion masses
	S_{xyz}(JF)	Significance of the average distance between the primary and displaced vertices
	f_E(JF)	Fraction of the charged jet energy in the secondary vertices
	$N_{\text{1-trk vertices}}$(JF)	Number of displaced vertices with one track
	$N_{\geq\text{2-trk vertices}}$(JF)	Number of displaced vertices with more than one track
	N_{TrkAtVtx}(JF)	Number of tracks from displaced vertices with at least two tracks
	$\Delta R(\vec{p}_{\text{jet}}, \vec{p}_{\text{vtx}})$	ΔR between the jet axis and the vectorial sum of the momenta of all tracks attached to displaced vertices

FIGURE 4.10: The input variables of the MV2 b-tagging algorithm [142].

The training of the multivariate classifier is performed on jets from $t\bar{t}$ events with b-jets considered as signal and c- and light-flavour jets as background. Afterwards, the performances of the algorithm are checked on a statistically independent sample of $t\bar{t}$ events. The jet p_T

and $|\eta|$ are included in the training variables in order to exploit the correlations with other variables. However, the signal jets are reweighted in p_{T} and $|\eta|$ to match the spectrum of the light-flavour background jets, in order to avoid the possibility to use any discrepancy betweeen the kinematic spectra of b-jet and background jets as a discriminant variable.

Several versions of the algorithm have been developed and compared between each other with the purpose of finding the option that can provide the best performace in terms of c-jet and light-jet rejection. The variants are MV2c00, MV2c10 and MV2c20, where the names of the taggers indicate the c-jet fraction in the training. Therefore, the c-jet fraction of the training for MV2c20 is 15%, MV2c10 is trained on b-jets as signal and a mixture of 93% light-flavour jets and 7% c-jets as background, and for MV2c00 no c-jet contribution is present in the training.

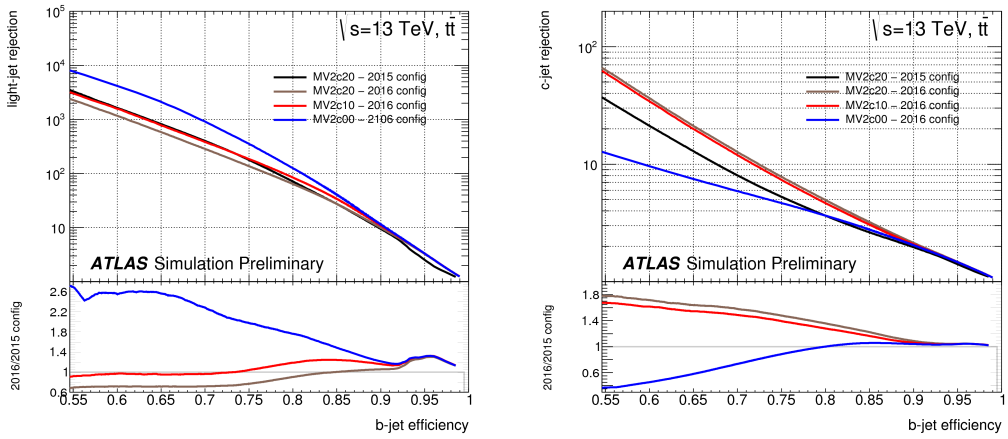

FIGURE 4.11: Light-flavour jet rejection (on the left) and c-jet rejection (on the right) versus b-jet efficiency for the previous (2015 config) and the current configuration (2016 config) of the MV2 b-tagging algorithm evaluated on $t\bar{t}$ events [139].

The performances of MV2c00, MV2c10 and MV2c20 b-tagging algorithms are compared in Figure 4.11 with MV2c20 which follows the previous configuration choosen for 2015 data. The main difference between the 2015 and 2016 configurations is the penalty factors applied in the training procedure. In the previous version of the algorithm, jets failing to produce results in any of the algorithms were given a penalty weight (10^{-6}) in the training procedure, while in the current procedure the penalty factor is applied if and only if all the three baseline algorithms are found to be invalid. The 2015 MV2c20 algorithm was used in previous $t\bar{t}$ cross-section analyses in the ℓ+jets channel at 13 TeV [51, 55]. It is clear that the current MV2c10 (2016 configuration) discriminant provides a similar light-flavour jet rejection to the 2015 MV2c20 configuration, but a significantly better c-jet rejection. The 2016 MV2c20 setup provides even better charm rejection, but at the expense of a reduced light-flavour jet rejection. The MV2c10 algorithm has therefore been chosen as the standard b-tagging discriminant for 2016 analyses.

The BDT score of the MV2c10 algorithm for signal and background components is shown in Figure 4.12. Four working points are defined by a cut value applied on the MV2c10 output

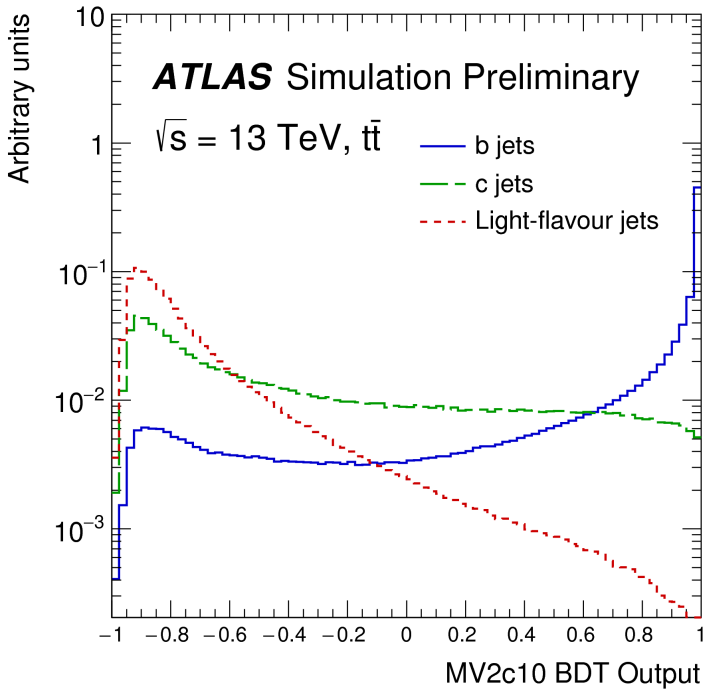

FIGURE 4.12: MV2c10 BDT output for b- (solid blue), c- (dashed green) and light-flavour (dotted red) jets evaluated with $t\bar{t}$ events [142].

BDT Cut Value	b-jet efficiency [%]	c-jet Rejection	Light-jet Rejection	τ-jet Rejection
0.9349	60	34	1538	184
0.8244	70	12	381	55
0.6459	77	6	134	22
0.1758	85	3.1	33	8.2

TABLE 4.1: Working points for the MV2c10 b-tagging algorithm, including benchmark numbers for the efficiency and rejections rates. These values have been extracted from $t\bar{t}$ events, the main requirement being jet p_{T} above 20 GeV [142].

in order to provide a specific b-tagging efficiency (85%, 77%, 70% and 60%), and they are listed in Table 4.1.

In the analysis described in this thesis, the MV2c10 algorithm at the 70% working point is used for b-tagging, instead of the 77% working point used in the previous analyses [51, 55]. The studies that have lead to this choice are presented in Appendix A.

4.5.2 b-tagging calibration

Since the efficiencies of the b-tagging algorithms for the working points listed in Table 4.1 are extracted from MC simulation, measurements of the b-tagging efficiency scale factors

are needed to correct for possibile differences between data and simulation. The scale factors are defined as $SF = \varepsilon_b^{\text{data}}/\varepsilon_b^{\text{sim.}}$, where $\varepsilon_b^{\text{data}}$ is the efficiency measured in data, while $\varepsilon_b^{\text{sim.}}$ represents the efficiency predicted by the simulation. The correction of the b-tagging efficiency in the simulation via a scale factor is referred to as a calibration of the b-tagging efficiency.

The b-tagging calibrations in ATLAS are performed using top-quark pair events as the decay of a $t\bar{t}$ pair provides a large sample of jets originating from the hadronisation of b-quarks. In particular, the standard b-tagging calibrations are based on dilepton $t\bar{t}$ events, since they provide a pure b-jet sample with low background contamination. The choice of dileptonic channel is due to the reduction of the systematic uncertainties related to the measurement. The methods used on dilepton $t\bar{t}$ events to calibrate the ATLAS b-tagging algorithms are the combinatorial likelihood method (dilepton $t\bar{t}$ PDF or LH method) and the tag-and-probe method (dilepton $t\bar{t}$ T&P) [143]. The two methods give compatible results, and achieve a similar level of precision, measuring data-to-simulation scale factors close to unity with uncertainties ranging from 2% to 12% depending on the jet transverse momentum. The scale factors are measured in a transverse momentum range from 20 to 300 GeV.

As the b-tagging algorithm can mistakenly tag a jet originating from a c-quark or a light-flavour parton (u-, d-, s-quark, or a gluon) as a b-jet, also the mistag efficiencies need a calibration to account for the differences in data and simulation. The measurement of b-tagging efficiency of c-jets is performed using single-lepton $t\bar{t}$ events, in which one of the W boson decays leptonically and the other decays hadronically in a c- and s-quark, or other quark pair combinations [144].

The evaluation of the misidentification rate of light-flavour jets for the b-tagging algorithm MV2c10 is performed using the negative tag method [145]. The negative-tag method relies to a large extent on the assumption that light-flavour jets are mistagged as b-jets mainly because of the finite resolution of the reconstructed inner detector track trajectories and impact parameters. It uses a flipped version of the algorithm in which the signs of impact parameter of the jet tracks and distributions related to secondary vertices are inverted. This implementation is expected to be a good approximation of the light-flavour jet mistag rate since the distributions of the impact parameters are symmetric around zero for light-flavour jets, while the b- and c-jets exhibit distributions with higher tails at large positive values.

4.5.3 Calibration of b-tagging algorithm using semileptonic $t\bar{t}$ events

During my qualification period, I performed a calibration of the b-tagging efficiencies of the MV2c10 algorithm using semileptonic $t\bar{t}$ events. The calibration is based on the tag-and-probe method already used during Run 1 [146]. The use of semileptonic $t\bar{t}$ decays gives a larger sample of jets than from the dilepton sample, allowing data-to-simulation scale factors to be measured with higher statistical precision and the measurement to be extended to higher jet p_{T}. The b-tagging efficiencies and the corresponding scale factors

for all the working points are presented as a function of the transverse momentum and the pseudorapidity of the jets. This calibration has been published by the ATLAS Collaboration in [147].

The results obtained by using the tag-and-probe method on selmiletptonic events, referred to as $t\bar{t}$ SL T&P method, are compared in Figures 4.13a-4.13c to the scale factors provided by the dilepton $t\bar{t}$ PDF and the dilepton $t\bar{t}$ T&P calibrations [143]. In general, all three methods are compatible within their combined statistical and systematic uncertainties. The comparison between the values obtained by the different methods is shown for the working points of 85%, 77% and 70%, respectively. The dominant uncertainty in the high-p_{T} region for the dilepton $t\bar{t}$ PDF and the dilepton $t\bar{t}$ T&P measurements is the statistical uncertainty. The tag-and-probe method on semileptonic $t\bar{t}$ events provides a scale factor for b-jets with a p_{T} between 300 GeV and 500 GeV. Thus the method described in [147] allows to extend the p_{T} region where data-to-simulation b-tagging scale factors can be derived compared to the measurements performed using dilepton $t\bar{t}$ events.

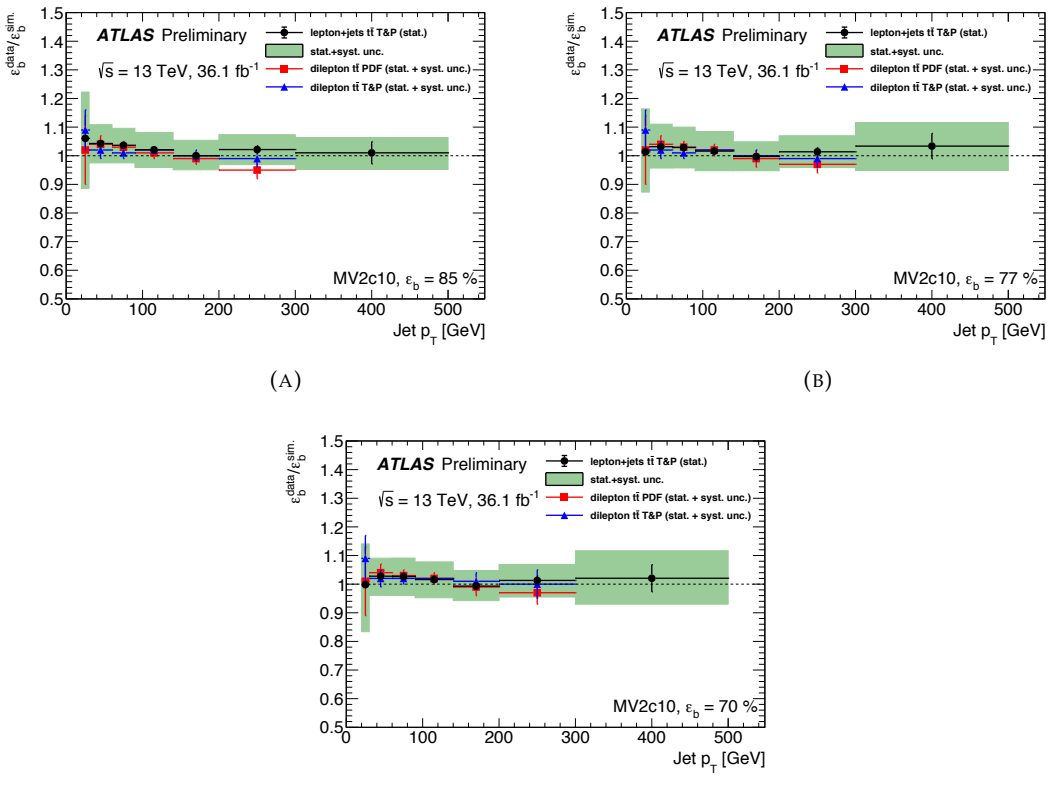

(A) (B)

(C)

FIGURE 4.13: Comparison between the data-to-simulation scale factors for the MV2c10 algorithm at the 85%(a), the 77%(b) and the 70%(c) working points obtained by using the tag-and-probe method (T&P) applied to $t\bar{t}$ single lepton (SL) candidate events and those obtained by using $t\bar{t}$ dilepton events. The results for the combinatorial likelihood (PDF) method using $t\bar{t}$ dilepton events [143] are presented as red squares and the scale factors measured with the tag-and-probe method (T&P) using $t\bar{t}$ dilepton events [143] are presented as blue triangles [147].

4.5.4 Performance enhancement due to the addition of the IBL

The addition of the IBL, presented in Section 2.4.1, has a significant impact on the performance of *b*-tagging during Run 2. Comparisons of the ligh-jet and *c*-jet rejection of the MV2c20 algorithm including or not the IBL in the simulated geometry of the detector are shown in Figure 4.14. The performance is evaulated at a fixed *b*-tagging efficiency of 70% and shown as a function of the jet p_{T}.

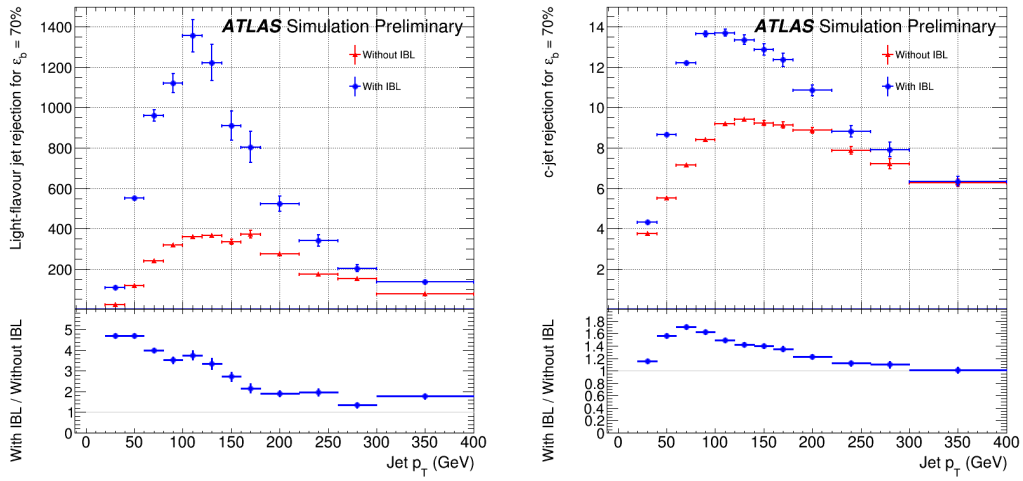

FIGURE 4.14: Performance of the *b*-tagging algorithm MV2c20 expressed in terms of light-jet (on the left) and *c* -jet (on the right) rejection as a function of jet transverse momentum (p_{T}), while keeping the *b*-tagging efficiency fixed at 70% in each p_{T} bin. The performance of the Run 1 ("Without IBL") and Run 2 ("With IBL") detector layouts are compared, where the latter includes IBL. The underlying algorithms are updated to the detector geometry in each case. Jets are required to be truth matched to a hard scatter jet. The rejection is defined as the inverse of the tagging efficiency.

The light-flavour jet rejection increases by a factor 4 in the p_{T} region of interest for the analysis described in this thesis, while the *c*-jet rejection is enhanced by a factor close to 2.

4.6 Missing Transverse Momentum

The transverse momenta sum of the collision products should be equal to zero given that the initial beam has zero transverse momentum because of the momentum conservation. Any imbalance in the sum of the visible transverse momenta is referred to as *missing transverse momentum*, or $E_{\mathrm{T}}^{\mathrm{miss}}$. It indicates the presence of undetectable particles that, in the case of the SM, are the neutrinos. The $E_{\mathrm{T}}^{\mathrm{miss}}$ is reconstructed as the magnitude of the negative vector sum of the momenta of all calibrated and reconstructed objects (hard term) and additional correction terms from tracking (soft term) [148]. The $\mathrm{E}_{\mathrm{T}}^{\mathrm{miss}}$ of an event is calculated as the

sum of a number of components:

$$E_{\mathrm{x(y)}}^{\mathrm{miss}} = E_{\mathrm{x(y)}}^{\mathrm{miss,e}} + E_{\mathrm{x(y)}}^{\mathrm{miss},\gamma} + E_{\mathrm{x(y)}}^{\mathrm{miss},\tau} + E_{\mathrm{x(y)}}^{\mathrm{miss,jets}} + E_{\mathrm{x(y)}}^{\mathrm{miss},\mu} + E_{\mathrm{x(y)}}^{\mathrm{miss,soft}}. \tag{4.9}$$

The terms for jets, charged leptons and photons are the negative sum of the energy projected in the $x-$ and $y-$ direction for the respective calibrated objects. From the components $\mathrm{E}_{\mathrm{x(y)}}^{\mathrm{miss}}$, the $\mathrm{E}_{\mathrm{T}}^{\mathrm{miss}}$ is calculated as:

$$E_{\mathrm{T}}^{\mathrm{miss}} = \sqrt{(E_{\mathrm{x}}^{\mathrm{miss}})^2 + (E_{\mathrm{y}}^{\mathrm{miss}})^2}. \tag{4.10}$$

In the above representation of $E_{\mathrm{T}}^{\mathrm{miss}}$, there is a need to consider effects due to energy deposits or track from pileup, detector miscalibration, limited coverage, finite resolution, dead material and electronic noise [148].

4.7 Overlap Removal

Detector reconstruction may produce objects that satisfy both the jet and lepton criteria. In order to match the detector information to a unique physics object, an overlap removal procedure is applied: double-counting of electron energy deposits as jets is prevented by discarding the closest jet lying a distance $\Delta R < 0.2$ from a reconstructed electron. Subsequently, if an electron lies $\Delta R < 0.4$ from a jet, the electron is discarded in order to reduce the impact of non-prompt leptons. In addition, if a jet has fewer than three associated tracks and lies $\Delta R < 0.4$ from a muon, the jet is discarded. Finally, any muon that lies $\Delta R < 0.4$ from a jet with at least three associated tracks is discarded.

Chapter 5

Event Selection and Reconstruction

5.1 Event Selection

The event selection consists a set of requirements applied on the reconstructed objects, defined in Chapter 4, that select out of an intial data sample of preselected-events those that better match the characteristics of the final state event topology. The events used in this analysis are selected using single-lepton triggers, where the detector read-out is triggered by the presence of an electron or muon at the level of HLT, described in Section 2.9.1. This specific sort of trigger is chosen since one electron or one muon are expected from semileptonic $t\bar{t}$ decay. Three different triggers are used in the e+jets channel and two triggers for the μ+jets channel. The available triggers differ for the 2015 and 2016 data taking periods and the list of triggers used in the analysis is presented in Table 5.1.

Object	2015	2016
electron	HLT_e24_lhmedium_L1EM20VH HLT_e60_lhmedium HLT_e120_lhloose	HLT_e26_lhtight_nod0_ivarloose HLT_e60_lhmedium_nod0 HLT_e140_lhloose_nod0
muon	HLT_mu20_iloose_L1MU15 HLT_mu50	HLT_mu26_ivarmedium HLT_mu50

TABLE 5.1: Single lepton triggers used in the analysis in 2015 and 2016 data taking. The identification operating points are represented by *lhtight*, *lhmedium*, *lhloose* and *loose*, while the isoltaion operating points are represented by *ivarloose* and *ivarmedium*.

Each event is required to pass the logical OR between the different triggers listed in Table 5.1 and to contain exactly one good electron or muon. For both channels the reconstructed lepton candidate must have a transverse momentum greater than 27 GeV and it has to be geometrically matched to the corresponding object at the trigger level.

Events are required to have one reconstructed primary vertex, defined in Section 4.1, in order to ensure originates from proton-proton collisions. After this first preselection, two different sets of cuts are applied for the resolved and boosted topologies.

Resolved selection At least four small-R jets (of which at least two b-tagged) are required. These criteria are sufficient to select a highly pure $t\bar{t}$ sample, as will be shown in Table 5.9. Two different approaches are studied to reconstruct the $t\bar{t}$ events: the pseudo-top and KLFitter algorithms. When KLFitter is used, an additional cut is applied on the likelihood value of the best permutation, that needs to be larger than -52. The validation of this cut is described in Appendix B. The details on the reconstruction of the $t\bar{t}$ system will be presented in the following sections.

Boosted selection It is required the presence of a re-clustered jet with $p_{\mathrm{T}} > 350\,\mathrm{GeV}$, called the *hadronic top candidate*. To reject fake lepton background, the missing transverse energy has to be larger than 20 GeV and the sum of $E_{\mathrm{T}}^{\mathrm{miss}}$and m_T^W (W transverse mass[1]) has to be larger than 60 GeV. Further selection is performed by requiring also the presence of at least one small-R jet close to the lepton (ΔR (lepton,small-R-jet) < 2.0). Additional requirements are applied to the hadronic top candidate: it has to be top-tagged, well angular-separated from the lepton ($\Delta\phi$(large-R jet, lepton) > 1.0) and from the small-R jet associated to the lepton (Δ R(large-R jet, small-R jet) > 1.5). In addition, it is required that at least one b-tagged small-R jet exists which must fulfill the following requirements: it is among the components of the reclustered jet or it is one of the small-R jet associated with the lepton. A detailed description of the boosted top reconstruction and tagging is presented in Section 5.9.

In order to make the samples selected in the boosted and resolved topology statistically independent, an additional cut is applied at reconstructed level: all the events that pass both resolved and boosted selection are removed from the resolved topology. Details on this cut, as well as its validation, are presented in Appendix C.

5.2 Particle-level objects reconstruction and fiducial phase-space definition

For the Monte Carlo signal samples, particle-level objects are also defined corresponding to reconstructed objects. Cuts applied to particle-level objects attempt to replicate the above fiducial selections for the reconstructed objects. The procedure explained in this section is applied to the $t\bar{t}$ signal only, since a background subtraction is performed before unfolding the real data.

[1] $m_T^W = \sqrt{2p_T^l E_T^{\mathrm{miss}}(1-\cos\Delta\phi(l, E_T^{\mathrm{miss}}))}$

Stable electrons and muons are required not to come from a hadron in the Monte Carlo truth record, either directly or through a decay of a τ lepton. This ensures that the lepton is from an electroweak decay without requiring a direct W-boson match. The four momenta of the bare leptons are then *dressed* by adding the four momenta of all stable photons within $\Delta R = 0.1$. The dressed leptons are required to have $p_{\mathrm{T}} > 27\,\mathrm{GeV}$ and $|\eta| < 2.5$.

Neutrinos from hadron decays either directly or via a decay of a τ-lepton are rejected. Particle-level missing transverse energy is calculated from the four-vector sum of the selected neutrinos.

Particle-level jets are clustered using the anti-k_t algorithm [127] with radius parameters $R = 0.4$ and $R = 1$, starting from all stable particles with $|\eta| < 5.0$, except for selected leptons (e, μ, ν) and the photons used to dress the leptons. Particle-level jets are required to have $p_{\mathrm{T}} > 25\,\mathrm{GeV}$ and $|\eta| < 2.5$. B-hadrons with $p_{\mathrm{T}} > 5\,\mathrm{GeV}$ are associated with jets through ghost matching [129]. Particle-level jets with at least one ghost-associated B-hadron are tagged as b-jets.

The re-clustered large-R jets are reconstructed at particle level starting from the particle-level jets with $R = 0.4$. The same trimming used at reconstructed level is applied also at particle: the sub-jets of the re-clustered jets with $p_T < 5\%$ of the jet p_T are removed from the jet. The trimmed re-clustered jets are considered b-tagged if at least one of the constituent small-R jets is b-tagged.

Particle-level objects are subject to different overlap removal criteria with respect to reconstructed objects, after dressing and jet reclustering. Muons and electrons with $\Delta R < 0.4$ of a jet are excluded. No electron-muon overlap removal is applied at the particle level.

Dilepton events with one lepton outside the acceptance of the particle level selection that pass all the selection requirements are considered signal.

In summary, events with an isolated electron or a muon in the final state are selected, meaning that leptonic decays of the τ are also considered. In more detail, at particle level, a direct lepton–W match (where direct match means the lepton must come directly from a W decay) is not required, but an indirect W match (a W must be one of the ancestors of the lepton) is required. With this requirement, the τ as a parent of the electron or a muon is accepetd only if the τ itself comes from a W. Leptons that come from a quark or a hadron are rejected. Therefore, the selected leptons come from a W without any hadron in between (i.e. $W \to \nu\tau(\to \text{hadron} \to \ell\nu)$ are not selected).

The event selection at both detector and particle levels is summarized in Tables 5.2 and 5.3[2]

[2]boosted needs corrections

Selection	Detector level		Particle level
	e + jets	μ + jets	
Leptons	One electron, no muons $\lvert d_0^{\mathrm{BL}}\text{sign.}\rvert < 5$ $\lvert \Delta z_0^{\mathrm{BL}} \sin\theta \rvert < 0.5\,\mathrm{mm}$ Track and calorimeter isolation $\lvert\eta\rvert$ <1.37 or 1.52 < $\lvert\eta\rvert$ < 2.47 $E_{\mathrm{T}} > 27\,\mathrm{GeV}$	One muon, no electrons $\lvert d_0^{\mathrm{BL}}\text{sign.}\rvert < 3$ $\lvert \Delta z_0^{\mathrm{BL}} \sin\theta \rvert < 0.5\,\mathrm{mm}$ Track and calorimeter isolation $\lvert\eta\rvert < 2.5$ $p_{\mathrm{T}} > 27\,\mathrm{GeV}$	One lepton (e/μ) $\lvert\eta\rvert < 2.5$ $p_{\mathrm{T}} > 27\,\mathrm{GeV}$
Anti-k_t $R = 0.4$ jets	$N^{\mathrm{jets}} \geq 4$ $\lvert\eta\rvert < 2.5$ $p_{\mathrm{T}} > 25\,\mathrm{GeV}$ JVT cut (if $p_{\mathrm{T}} < 60\,\mathrm{GeV}$ and $\lvert\eta\rvert < 2.4$) b-tagging: ≥ 2 jets with MV2c10 at 70%		$N^{\mathrm{jets}} \geq 4$ $\lvert\eta\rvert < 2.5$ $p_{\mathrm{T}} > 25\,\mathrm{GeV}$ b-tagging: Ghost-matched B-hadron
Overlap removal	If an electron shares a track with a muon: electron removed If $\Delta R(e, \mathrm{jet}_{R=0.4}) < 0.2$: jet removed then If $\Delta R(e, \mathrm{jet}_{R=0.4}) < 0.4$: e removed If $\Delta R(\mu, \mathrm{jet}_{R=0.4}) < 0.4$ and $n^{\mathrm{jet}}_{\mathrm{tracks}} \geq 3$: μ removed If $\Delta R(\mu, \mathrm{jet}_{R=0.4}) < 0.4$ and $n^{\mathrm{jet}}_{\mathrm{tracks}} < 3$: jet is removed		If $\Delta R(e, \mathrm{jet}_{R=0.4}) < 0.4$: e removed If $\Delta R(\mu, \mathrm{jet}_{R=0.4}) < 0.4$: μ removed
Top reconstruction quality	Remove events passing boosted selection. $\log L > -52$ for the best permutation from the kinematic fit		

TABLE 5.2: Summary of event selections for detector-level and MC-generated particle-level events in the resolved topology.

5.3 Parton-level objects and full phase-space definition

Parton-level objects are defined for simulated events. Only top quarks decaying directly to a W boson and a b-quark in the simulation are considered. The full phase space for the measurements presented in this thesis is defined by the set of $t\bar{t}$ pairs in which one top quark decays semileptonically (including τ leptons) and the other decays hadronically. In the boosted topology, the full phase space is limited to the region where the top quark is produced with a transverse momentum greater than 350 GeV. Events in which both top quarks decay leptonically are removed from the parton level signal simulation.

5.4 Background determination

The requirements on b-tagging and top-tagging allow to reduce the background contamination in the signal region. However, there are several processes that can pass the event selection and contribute to the background fraction. These background processes that can be reconstructed as a $t\bar{t}$ event are single top production, W+ jets, Z+jets, WW or WZ (diboson) and $t\bar{t}$ production in association with a vector boson.

Selection	Detector level		Particle level
	e + jets	μ + jets	
Leptons	One electron, no muons $\lvert d_0^{\mathrm{BL}}\text{sign.}\rvert < 5$ $\lvert\Delta z_0^{\mathrm{BL}}\sin\theta\rvert < 0.5$ mm Track and calorimeter isolation $\lvert\eta\rvert$ <1.37 or 1.52 < $\lvert\eta\rvert$ < 2.47 $E_{\mathrm{T}} > 27$ GeV	One muon, no electrons $\lvert d_0^{\mathrm{BL}}\text{sign.}\rvert < 3$ $\lvert\Delta z_0^{\mathrm{BL}}\sin\theta\rvert < 0.5$ mm Track and calorimeter isolation $\lvert\eta\rvert < 2.5$ $p_{\mathrm{T}} > 27$ GeV	One lepton (e/μ) $\lvert\eta\rvert < 2.5$ $p_{\mathrm{T}} > 27$ GeV
Reclustered $R=1.0$ jet	$p_{\mathrm{T}} > 350$ GeV, $\lvert\eta\rvert < 2.0$		
Anti-k_t $R = 0.4$ jets	≥ 1 jet $p_{\mathrm{T}} > 25$ GeV $\lvert\eta\rvert < 2.5$ JVT cut (if $p_{\mathrm{T}} < 60$ GeV and $\lvert\eta\rvert < 2.4$) b-tagging: ≥ 1 jets with MV2c10 at 70%		≥ 1 jet $\lvert\eta\rvert < 2.5$, $p_{\mathrm{T}} > 25$ GeV b-tagging: Ghost-matched B-hadron
Overlap removal	If an electron shares a track with a muon: electron removed If $\Delta R(e,\mathrm{jet}_{R=0.4}) < 0.2$: jet removed then If $\Delta R(e,\mathrm{jet}_{R=0.4}) < 0.4$: e removed If $\Delta R(\mu,\mathrm{jet}_{R=0.4}) < 0.4$ and $n_{\mathrm{tracks}}^{\mathrm{jet}} \geq 3$: μ removed If $\Delta R(\mu,\mathrm{jet}_{R=0.4}) < 0.4$ and $n_{\mathrm{tracks}}^{\mathrm{jet}} < 3$: jet is removed		If $\Delta R(e,\mathrm{jet}_{R=0.4})$ <0.4: e removed If $\Delta R(\mu,\mathrm{jet}_{R=0.4})$ <0.4: μ removed
$E_{\mathrm{T}}^{\mathrm{miss}}$, m_{T}^{W}	$E_{\mathrm{T}}^{\mathrm{miss}} > 20$ GeV, $E_{\mathrm{T}}^{\mathrm{miss}} + m_{\mathrm{T}}^{W} > 60$ GeV		
Leptonic top	At least one anti-k_t $R = 0.4$ jet with $\Delta R(\ell,\mathrm{jet}_{R=0.4}) < 2.0$		
Hadronic top	Top-tagging on the leading reclustered jet: 120 GeV < m_{jet} < 220 GeV, $\Delta R(\mathrm{jet}_{R=1.0},\mathrm{jet}_{R=0.4}) > 1.5$, $\lvert\Delta\phi(\ell,\mathrm{jet}_{R=1.0})\rvert > 1.0$		
b-jets	~~At least one of:~~ 1. one of the anti-k_t $R = 0.4$ jet with $\Delta R(\ell,\mathrm{jet}_{R=0.4}) < 2.0$ and $\Delta R(\mathrm{jet}_{R=1.0},\mathrm{jet}_{R=0.4}) > 1.5$ is b-tagged; 2. one of the anti-k_t $R = 0.4$ jet, component of the top-tagged reclustered jet, is b-tagged.		

TABLE 5.3: Summary of the requirements for detector-level and MC-generated particle-level events, for the boosted event selection. The description of the particle-level selection is in Section 5.2.

Single-top production background is one of the largest contribution in both resolved and boosted topologies as it is characterized by a similar final state to the $t\bar{t}$ production. The processes where W and Z bosons decay leptonically and are produced in association with jets share a similar final state with $t\bar{t}$ signal. In particular, if one or more of the additional jets are coming from heavy quark or are mis-tagged as b-jet, these processes can easily pass the event selection and be reconstructed as signal. The W+jets process contributes more to the background contamination with respect to Z+jets process. The diboson production where one boson decay leptonically while the other one hadronically can pass the selection cuts, but it gives a minor contribution. Finally, $t\bar{t}$ production in association with a vector boson has a final state close to the signal, but its cross-section is three order of magnitude lower than the $t\bar{t}$ production and, as a consequence, it represents a minor contribution.

An additional source of background is represented by multijet production processes, including all-hadronic $t\bar{t}$ production, which have a large cross-section and mimic the ℓ+jets final

state signature. The mis-reconstruction as $t\bar{t}$ signal is due to jets mis-identified as prompt leptons, referred as to fake leptons, or to semileptonic decays of heavy-flavour hadrons (non-prompt leptons). The multijet background is estimated directly from data and the technique used to estimate its contribution will be discussed in Section 5.4.2 in more details.

5.4.1 MC-based backgrounds

The single top quark, W+jets, Z+jets, diboson and $t\bar{t}$ +V background are estimated by using the MC samples, described in Section 3.8.3. For all the MC-based estimation, an overall uncertainty based on the calculation of the total cross-sections is applied to the MC samples, in order to take into account the theoretical uncertainties. For the dominating background components, additional systematic uncertainties that affect both normalization and shapes of the distributions are considered:

- For the W+jets background, additional uncertainties based on the variations of μ_{R} and μ_{F} scales, α_{S} and the heavy-flavor composition are applied, as described in Section 7.3.1;
- for the Z+jets background, additional uncertainties based on the jet multiplicity in each event are applied to take into account PDF, μ_{R}, μ_{F} and α_{S} variations. These uncertainties are documented in Reference [149] and are listed in Table 7.1;
- for the dominating components of the single top background, i.e. t- and Wt-channel, an uncertainty based on variations of the initial- and final-state radiation settings is applied and, for the Wt-channel only, also an uncertainty to consider the possible descriptions of the $Wt/t\bar{t}$ interference, described in Section 1.3.2.1.

5.4.2 Non-prompt and fake lepton background

Events with non-prompt leptons or jets identified as leptons may satisfy the selection criteria and contribute to one of the major background component, the so-called multijet/fakes background. The non-prompt and fake lepton background is estimated using a data-driven technique, the Matrix Method [150]. This method was originally developed in the D0 experiment [151] and it has been already extensively used in ATLAS analyses [51, 52, 55].

The first step of the method is to define two levels of lepton selection requirements, the *tight* selection, which is used in the nominal selection as described in Sections 4.2 and 4.3, and the *loose* selection, which applies less stringent identification and isolation requirements. The different requirements of the two lepton selections used in this analysis are summarized in Table 5.4.

The inclusive data sample S, selected by requiring exactly one loose lepton and at least one jet, can be divided into two disjoint sets of tight events T and exclusively loose events L

depending on whether the lepton passes the tight requirements or not. The subset of events can be divided also by looking for real leptons R and for fake/non-prompt leptons F, which are disjoint while $T + L = R + F = S$ holds. Background events that contribute to the analysis signal selection are defined by the intersection of T and F sets. The matrix method is based on the equation:

$$\begin{pmatrix} \langle n_T \rangle \\ \langle n_L \rangle \end{pmatrix} = \begin{pmatrix} \varepsilon_r & \varepsilon_f \\ \overline{\varepsilon_r} & \overline{\varepsilon_f} \end{pmatrix} \begin{pmatrix} n_R \\ n_F \end{pmatrix} \tag{5.1}$$

which relates the expected number of tight and loose events, $\langle n_T \rangle$ and $\langle n_L \rangle$, to the unknown true number of real and fake events, n_R and n_F. The coefficient ε_r (ε_f) represents the probability of a real (fake) lepton to fulfill the tight selection criteria and it is called the *real* (*fake*) *efficiency*. The coefficients $\overline{\varepsilon_i}$ are defined as $\overline{\varepsilon_i} = 1 - \varepsilon_i$. The ε_r and ε_f efficiencies are measured in dedicated control regions of data dominated by real and fake lepton events, respectively.

In order to estimate the number of fake leptons in the tight selection, which is $\varepsilon_f \langle n_T \rangle$, the Equation 5.1 can be inverted by assuming that $\varepsilon_r \neq \varepsilon_f$:

$$\begin{pmatrix} n_R \\ n_F \end{pmatrix} = \frac{1}{\varepsilon_r - \varepsilon_f} \begin{pmatrix} \overline{\varepsilon_f} & -\varepsilon_f \\ -\overline{\varepsilon_r} & \varepsilon_r \end{pmatrix} \begin{pmatrix} \langle n_T \rangle \\ \langle n_L \rangle \end{pmatrix} \tag{5.2}$$

and the estimator of n_{TF} can be constructed as:

$$\hat{n}_{TF} = \varepsilon_f \hat{n}_F = \frac{\varepsilon_f}{\varepsilon_r - \varepsilon_f} (\varepsilon_r (n_T + n_L) - n_T) \,. \tag{5.3}$$

by taking the observed number of tight and loose events.

The efficiencies ε_r and ε_f could depend on kinematic properties of an event, so they are parametrised in representative observables and calculated per-event accordingly. The practical estimate of the background in a given bin of a certain distribution is obtained by summing all loose and tight events i in that particular bin, weighted by:

$$w_i = \frac{\varepsilon_f}{\varepsilon_r - \varepsilon_f} (\varepsilon_r - \delta_{i \in T}) \tag{5.4}$$

where $\delta_{i \in T} = 1$ if the event passes the tight selection and 0 if this is not the case.

	Loose selection	**Tight selection**
Electron identification level	MediumLH	TightLH
Muon identification level	Medium	Medium
Lepton isolation requirement	None	Gradient

TABLE 5.4: Summary of differences between loose and tight lepton selection requirements.

Measurement and parametrisation of the fake efficiency

The fake efficiency is measured as the ratio between the number of tight lepton events and the number of all events in a control region enriched of non-prompt and fake-lepton events. The selection applied to define this control region is the following:

- exactly one loose or tight lepton
- at least one jet
- in the e+jets channel: $E_{\mathrm{T}}^{\mathrm{miss}} < 20$ GeV
- in the μ+jets channel: muon $|d_0^{\mathrm{sig}}| > 5$

The residual event yields from other processes ($t\bar{t}$, single top, W+jets, Z+jets) are estimated with MC simulation and subtracted separately in the numerator and denominator of the efficiency.

Measurement and parametrisation of the real efficiency

The real efficiency is measured by using the $Z \to \ell\ell$ tag-and-probe method, in which events with a pair of same-flavour opposite-sign loose or tight leptons are selected. In addition, at least one jet is required and the invariant mass of the dilepton system has to be between 60 and 120 GeV. If one of the two leptons passes the tight lepton requirements, it is considered a tag and the other lepton is considered a probe. The efficiency is measured by taking the ratio between the number of probes which pass the tight criteria and the number of all the probes. If both leptons pass the tight criteria, the procedure is performed twice by taking each lepton as probe one by one.

In order to correct the measurement for residual amount of fake leptons in the selection (originating mostly from $t\bar{t} \to \ell$+jets events with an additional fake lepton), a method based on $m_{\ell\ell}$ fit is employed. For each bin of an observable x in which the efficiency is measured, a fit of $m_{\ell\ell}$ is performed with a signal+background model including events only from this bin. The amount of signal (i.e. $Z \to \ell\ell$) is calculated as the number of events within the range 80 – 100 GeV minus the integral of the background function over this range. The same procedure is performed separately for the numerator and the denominator of the efficiency and the resulting numbers are divided to obtain the real efficiency in a given bin of x.

Trigger requirements

For the tight selection, the triggers already defined in Section 5.1 are used. For the 2015 data taking period, the lowest-p_{T} trigger for each channel is a non-isolated trigger with medium

or loose identification requirements. The leptons selected by this trigger are therefore not biased towards being tight. However, the lowest-p_{T} triggers used for 2016 data taking period apply isolation requirements and tightened ID requirements. So, the nominal triggers used on 2016 data are not suitable for the estimation of fakes background contribution as they are already selecting tight leptons. The triggers used for the 2016 data taking period for the resolved topology are summarized in Table 5.5.

Channel	Tight selection	Loose selection
e+jets	HLT_e26_lhtight_nod0_ivarloose HLT_e60_lhmedium_nod0 HLT_e140_lhloose_nod0	HLT_e26_lhvloose_nod0_L1EM20VH HLT_e60_lhmedium_nod0 HLT_e140_lhloose_nod0
μ+jets	HLT_mu26_ivarmedium HLT_mu50	HLT_mu24 HLT_mu50

TABLE 5.5: Different triggers used in the loose and tight lepton selection requirements for 2016 data taking period in the resolved topology.

As the two new low-p_{T} triggers are in fact prescaled triggers, the appropriate prescale must be applied on the fakes weight that is obtained for events in the low-p_{T} region. The prescale for the electron and muon triggers is 50. The boosted topology is less sensitive to the loose trigger used in the low-p_{T} region, thus the triggers employed in the fakes estimation are kept the same as the tight selection.

Efficiency parametrisations

The fake and real efficiencies are parametrised in terms of kinematic observables in order to better model the fake background contribution. The efficiencies are parametrized in the following observables:

- p_{T}^{ℓ}, the lepton transverse momentum,
- η^{ℓ}, the lepton pseudorapidity,
- $\Delta\phi$, the azimuthal angle difference between the lepton and the $E_{\mathrm{T}}^{\mathrm{miss}}$,
- $N_{b-\mathrm{jet}}$, the b-jet multiplicity,
- $p_{\mathrm{T}}^{\mathrm{jet1}}$, the leading jet transverse momentum,
- ΔR, the $\Delta R = \sqrt{(\Delta\phi)^2 + (\Delta\eta)^2}$ distance between the lepton and the closest jet,
- m_T^W, the transverse mass of the W boson.

These observables are further split in two groups, events with exactly one and events with two or more jets. When combining n different parametrisations, the individual efficiencies

resulting from the parametrisations $k \in \{0, 1, \ldots, n-1\}$ are multiplied according to

$$\varepsilon_{\text{combined}} = \varepsilon_{k=0} \cdot \prod_{k \in 1,\ldots,n-1} \frac{\varepsilon_k}{\bar{\varepsilon}}, \tag{5.5}$$

where $\bar{\varepsilon}$ is the average efficiency which is extracted by a linear fit to the parametrisation distribution.

A characteristic feature of the Matrix Method is the possibility that part of the weights in the fake-background estimation become negative. This leads to an unfortunate side-effect of the matrix method that it may provide a total negative fakes yield for particular bins of a distribution. This could be related to a too high granular binning, a targeted region with an expected low amount of fakes or a loose selection close to the tight one. This effect has been taken into account in the procedure of choosing the parametrization applied in this analysis, in combination with the agreeement between data observations and the combination of MC simulation and fakes estimate predictions. The set of parametrisations used in the analysis are shown in table 5.6.

Topology	Channel	Real efficiency parametrisation	Fake efficiency parametrisation
Resolved	e+jets	$\eta^{\ell} \oplus p_{\mathrm{T}}^{\mathrm{jet1}} \oplus \Delta R$	$\eta^{\ell} \oplus p_{\mathrm{T}}^{\mathrm{jet1}} \oplus \Delta R$
Resolved	μ+jets	$\eta^{\ell} \oplus p_{\mathrm{T}}^{\ell} \oplus \Delta R$	$\eta^{\ell} \oplus p_{\mathrm{T}}^{\ell} \oplus \Delta R$
Boosted	e+jets	$\eta^{\ell} \oplus p_{\mathrm{T}}^{\mathrm{jet1}} \oplus \Delta R$	$\eta^{\ell} \oplus p_{\mathrm{T}}^{\mathrm{jet1}} \oplus \Delta R$
Boosted	μ+jets	$\eta^{\ell} \oplus p_{\mathrm{T}}^{\ell} \oplus \Delta R$	$\eta^{\ell} \oplus p_{\mathrm{T}}^{\ell} \oplus \Delta R$

TABLE 5.6: Choosen fakes parametrisations for the different topologies and channels.

5.5 Combination ot the analysis channels

The event selection is performed on two independent samples defined by the flavour of the lepton that triggered the event. The yields of the two channels are shown in Table 5.7 and Table 5.8 for the resolved and boosted topologies, respectively.

The combination of the two channels is simply performed by adding together the events of the two channels after the selection cuts. This procedure can be done if the relative yield in data and predictions are consistent, which is the case, as it is previously shown. This approach allows to take into account properly the correlations among the uncertainties. The correlated uncertainties will be added linearly between the channels, while the uncorrelated uncertainties, which tipically affect only events in one particular channel, are added in quadrature to the other uncertainties. However, the dominant uncertainties are not channel-specific, so there is no gain from splitting the final result into different channels. The event yields are displayed in Table 5.9 for data, simulated signal and background sources in the combined ℓ+jets channel.

Sample	Yield resolved e+jets	Yield resolved μ+jets
$t\bar{t}$	593378 ± 46135	554618 ± 42210
W+jets	17747 ± 9712	17099 ± 9324
Z+jets	7532 ± 4210	4070 ± 2302
Single top	28145 ± 2689	26365 ± 2485
$t\bar{t}V$	2141 ± 131	1912 ± 116
Diboson	918 ± 100	805 ± 84
Fakes	30843 ± 17290	3030 ± 4578
Expected	680705 ± 55610	607897 ± 48441
Observed	657083	619957
Expected/Observed [%]	103 ± 8	98 ± 8

TABLE 5.7: Observed and expected number of events in the e+jets and in the μ+jets channels after the full event selection in the resolved analysis. The systematic uncertainties do not include the signal modelling ones. Symmetrised uncertainties are obtained by averaging the up- and down-uncertainty components.

Sample	Yield boosted e+jets	Yield boosted μ+jets
$t\bar{t}$	25064 ± 1098	19640 ± 805
W+jets	1707 ± 901	1120 ± 598
Z+jets	217 ± 121	167 ± 92
Single top	1139 ± 82	901 ± 62
$t\bar{t}V$	248 ± 11	191 ± 8
Diboson	105 ± 10	90 ± 8
Fakes	733 ± 368	279 ± 146
Expected	29211 ± 1654	22388 ± 1158
Observed	26528	21072
Expected/Observed [%]	101 ± 9	108 ± 6

TABLE 5.8: Observed and expected number of events in the e+jets and in the μ+jets channels after the full event selection in the boosted analysis. The systematic uncertainties do not include the signal modelling ones. Symmetrised uncertainties are obtained by averaging the up- and down-uncertainty components.

Sample	Yields resolved			Yields boosted		
$t\bar{t}$	1127390	±	93173	44703	±	1842
Single top	53649	±	5074	2040	±	139
Fakes	33946	±	16018	1012	±	396
W+jets	34386	±	18762	2827	±	1502
Z+jets	11515	±	6456	384	±	213
$t\bar{t}V$	3795	±	229	438	±	18
Diboson	1681	±	179	194	±	16
Expected	1266361	±	106689	51599	±	2740
Observed	1252692			47600		
Expected/Observed [%]	103	±	8	108	±	5

TABLE 5.9: Event yields after the resolved and boosted selections and the combination of the e+jets and μ+jets channels. Events that pass both resolved and boosted selections are removed from the resolved selection. The uncertainties include the combined statistical and systematic uncertainties, excluding the systematic uncertainties related to the modelling of the $t\bar{t}$ system, as described in Section 7.2. Symmetrised uncertainties are obtained by averaging the up- and down-uncertainty components.

5.6 Validation plots for kinematic variables

In this section, a comparison between data, signal MC model and the various backgound contributions (MC-based and data-driven contributions) will be shown for the ℓ+jets channel both in resolved and boosted topologies. In all the following plots, data distributions are compared to predictions that use the nominal sample as $t\bar{t}$ signal model. The predictions from the different signal and background processes are displayed in different colours and stacked together in order to allow a direct comparison with the data. The hashed area represents the combined statistical and systematic uncertainties on the total prediction, with the exception of the uncertainties related to the modeling of the $t\bar{t}$ system.

The comparison distributions between the data and the predictions of the kinematic variables for the resolved topology are shown in Figures 5.1 and 5.2, while for the boosted topology the distributions are shown in Figures 5.3-5.5. The comparisons show a good agreement between the data and the predictions within the uncertainties.

The kinematic variables shown in this set of validation plots enter as inputs in the algorithms used for the reconstruction of the $t\bar{t}$ system. A detailed description of such algorithms will be presented in the following sections.

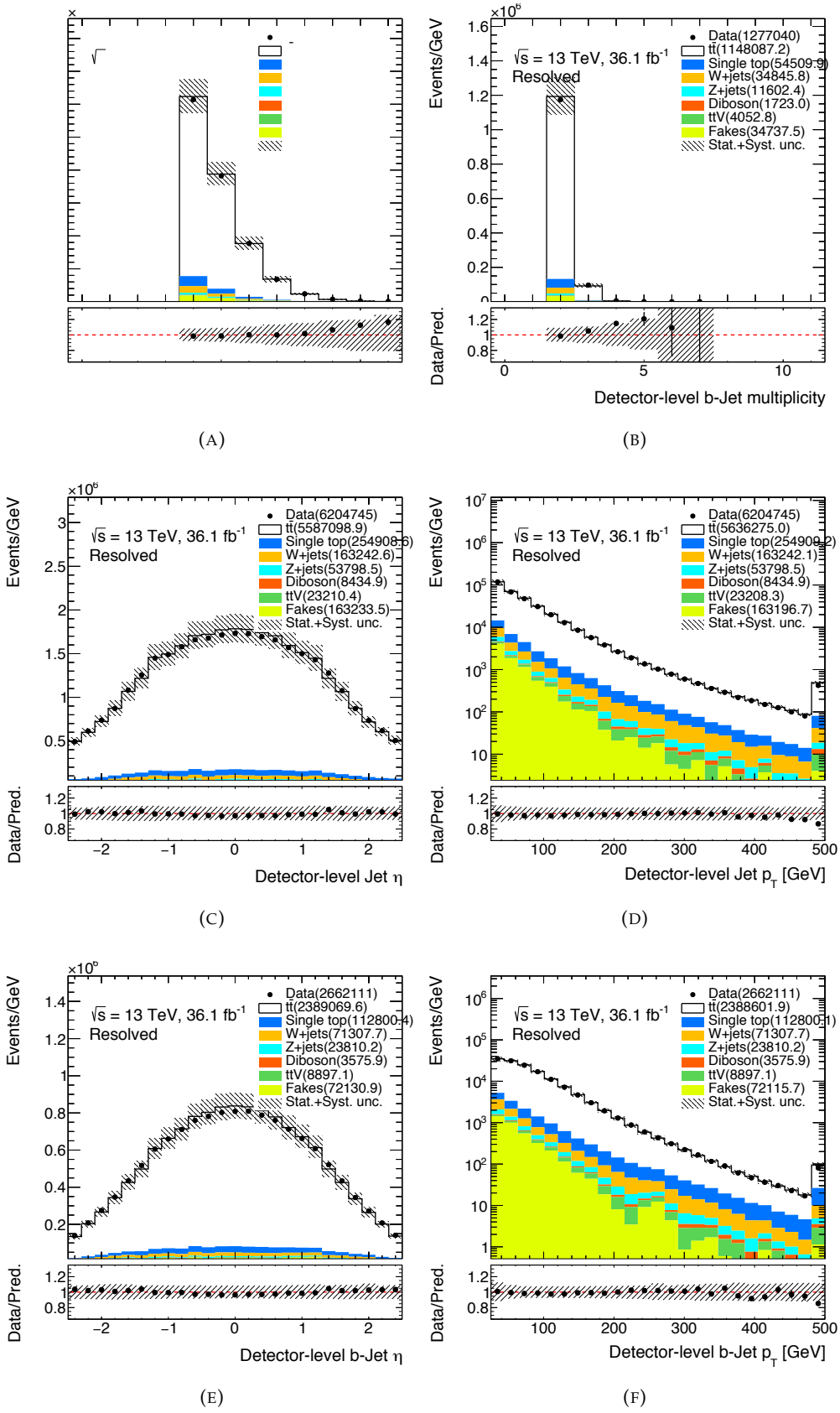

FIGURE 5.1: Comparison between data and predictions for basic jet kinematic distributions in the resolved topology for the combined ℓ+jets channel at the detector level: (a) jet multiplicity, (b) number of b-tagged jets, (c) pseudorapidity and (d) and transverse momentum of the jet, (e) pseudorapidity and (f) transverse momentum of the b-tagged jet. Events beyond the range of the horizontal axis are included in the last bin.

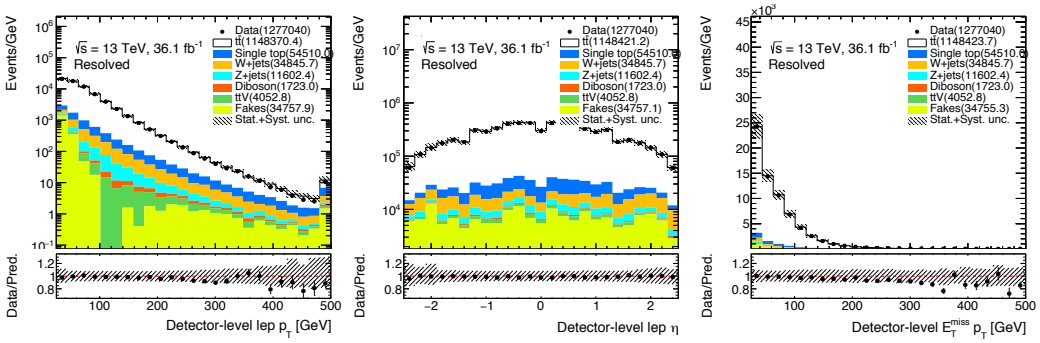

(A) (B) (C)

FIGURE 5.2: Comparison between data and predictions for basic kinematic distributions in the resolved topology for the combined ℓ+jets channel at the detector level: (a) transverse momentum and (b) pseudorapidity of the lepton and (c) missing transverse momentum. Events beyond the range of the horizontal axis are included in the last bin.

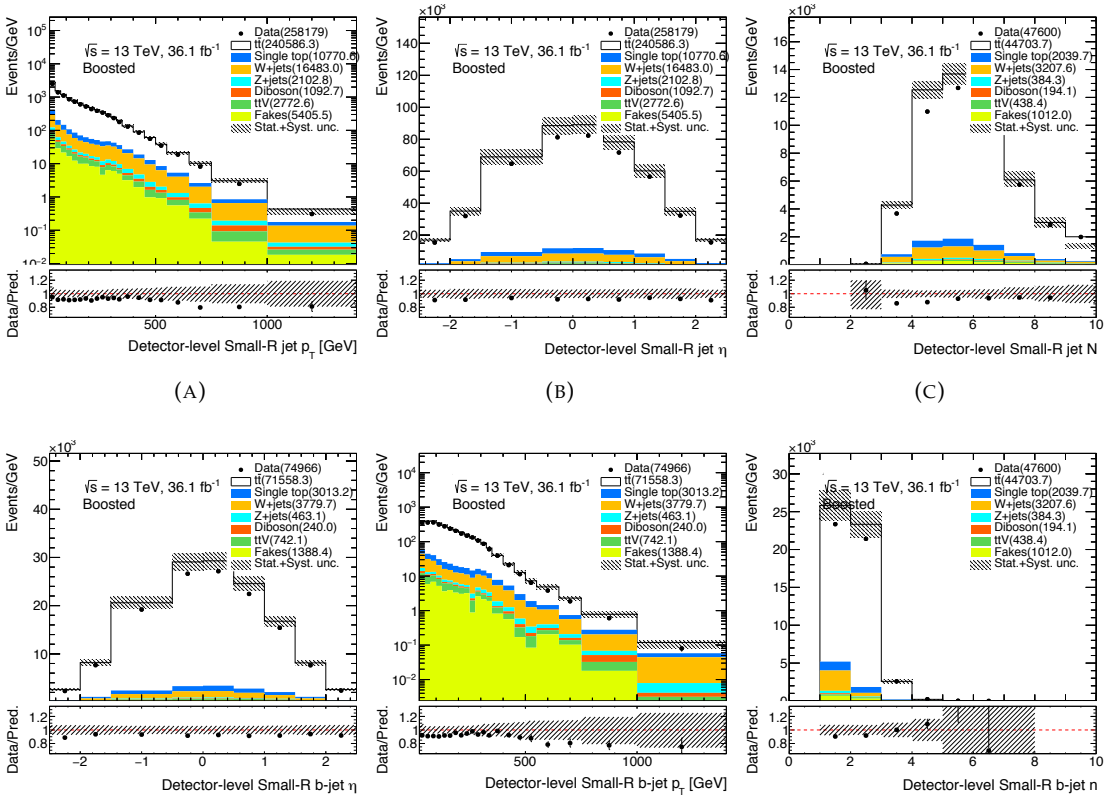

(A) (B) (C)

(D) (E) (F)

FIGURE 5.3: Comparison between data and predictions for basic kinematic distributions in the boosted topology for the combined ℓ+jets channel at the detector level: (a) transverse momentum and (b) pseudorapidity and (a) jet multiplicity of the small-R jet, (e) transverse momentum and (d) pseudorapidity and (f) jet multiplicity of the b-tagged small-R jet. Events beyond the range of the horizontal axis are included in the last bin.

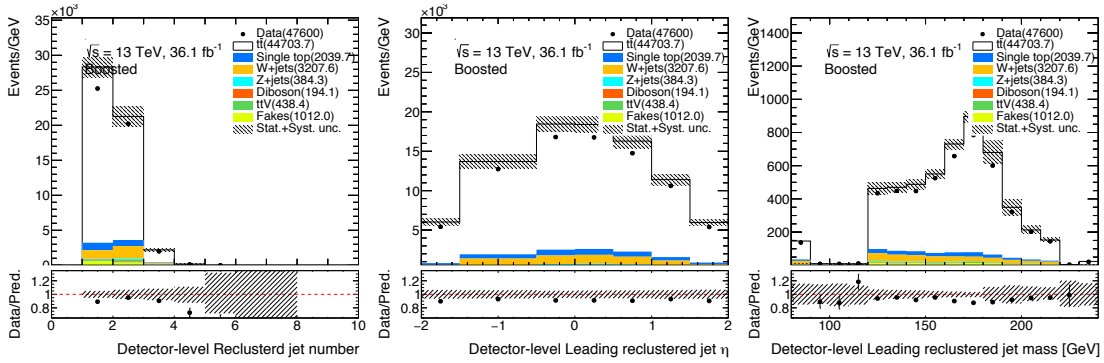

(A) (B) (C)

FIGURE 5.4: Comparison between data and predictions for basic kinematic distributions in the boosted topology for the combined ℓ+jets channel at the detector level: (a) multiplicity and (b) pseudorapidity and (c) mass of the re-clustered jet. Events beyond the range of the horizontal axis are included in the last bin.

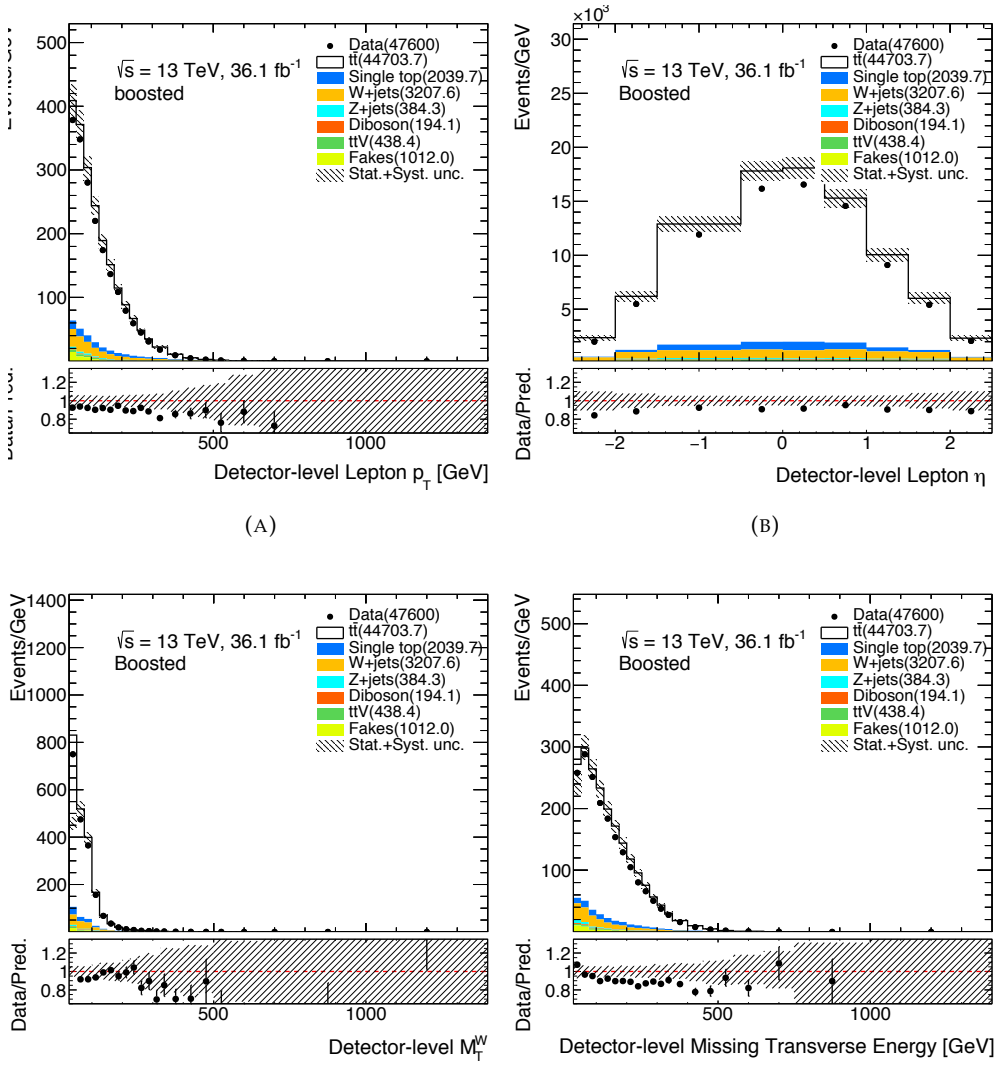

FIGURE 5.5: Comparison between data and predictions for basic kinematic distributions in the boosted topology for the combined ℓ+jets channel at the detector level: (a) transverse momentum and (b) pseudorapidity of the lepton, (c) W transverse mass and (d) missing transverse momentum. Events beyond the range of the horizontal axis are included in the last bin.

5.7 Pseudo-top reconstruction algorithm

The pseudo-top algorithm reconstructs the kinematics of the top quarks and their complete decay chain from final-state objects, namely the charged lepton (electron or muon), missing transverse momentum and four small-R jets, at least two of which identified as coming from the hadronization of a b-quark. In case more than two b-jets are present in an event, only the two hardest b-jet are considered as b-jets in the pseudo-top algorithm, the additional b-tagged jets are treated as light-jets.

The algorithm adopted in the analysis described in this thesis is exactly the same as the 8 TeV analysis [52] as well as 13 TeV pseudo-top analyses [51, 55]. The algorithm yields very good correlation between particle- and detector-level objects. The general idea is to keep the algorithm as simple as possible in order to facilitate the Rivet implementation and to reduce the dependence on the details of MC simulation. Moreover, no mass cuts on the hadronic W or on the reconstructed top-quark masses are applied in order to avoid differences on scales and resolutions between particle- and detector-levels. The same Pseudo-Top algorithm is applied on detector- and particle-level objects and it is used to perform the particle-level analysis in the resolved topology.

The algorithm is structured as follows:

1. Reconstruct the four-momentum of the neutrino which appears in the decay chain $t \to Wb \to \ell\nu b$:
   (a) Estimate the z-component of the neutrino momentum by applying the W boson mass constraint. If the resulting quadratic equation has two real solutions, take the one with smallest absolute value of $|p_z|$. If the determinant is negative, drop the imaginary part of the solution.
   (b) The components of the four-momentum of the neutrino in the (p_x, p_y, p_z, m) representation are given by:
   $$P^{\nu} = \left(E_x^{\text{miss}}, E_y^{\text{miss}}, p_z^{\nu}, 0\right), \tag{5.6}$$
   where the p_z^{ν} comes from the $m_{\ell\nu} = m_W$ constrain, applied at both detector and particle levels.
2. Reconstruct the leptonic W boson which underwent the leptonic decay $W \to \ell\nu$ from the system constituted by the charged lepton and the neutrino;
3. Reconstruct the leptonic top quark from the combination of the leptonic W and the b-tagged jet closest in ΔR to the charged lepton (among the two highest-p_T b-tagged jets);

4. Reconstruct the W boson which underwent the hadronic decay $W \rightarrow q\bar{q}'$ from the non-b-tagged jets pair whose invariant mass is the closest to the mass of the W boson, taken from the Particle Data Group [4].

5. Reconstruct the hadronic top quark from the sum of the hadronic W boson and the remaining b-jet.

The mass, transverse momentum and rapidity of the reconstructed leptonic and hadronic top quark by using the Pseudo-top algorithm are shown in Figure 5.6, while the mass, transverse momentum and rapidity of the reconstructed $t\bar{t}$ system are shown in Figure 5.7. The comparisons show a good level of agreement between data and predictions for the characteristic variables of the top quarks and the $t\bar{t}$ system at the detector-level.

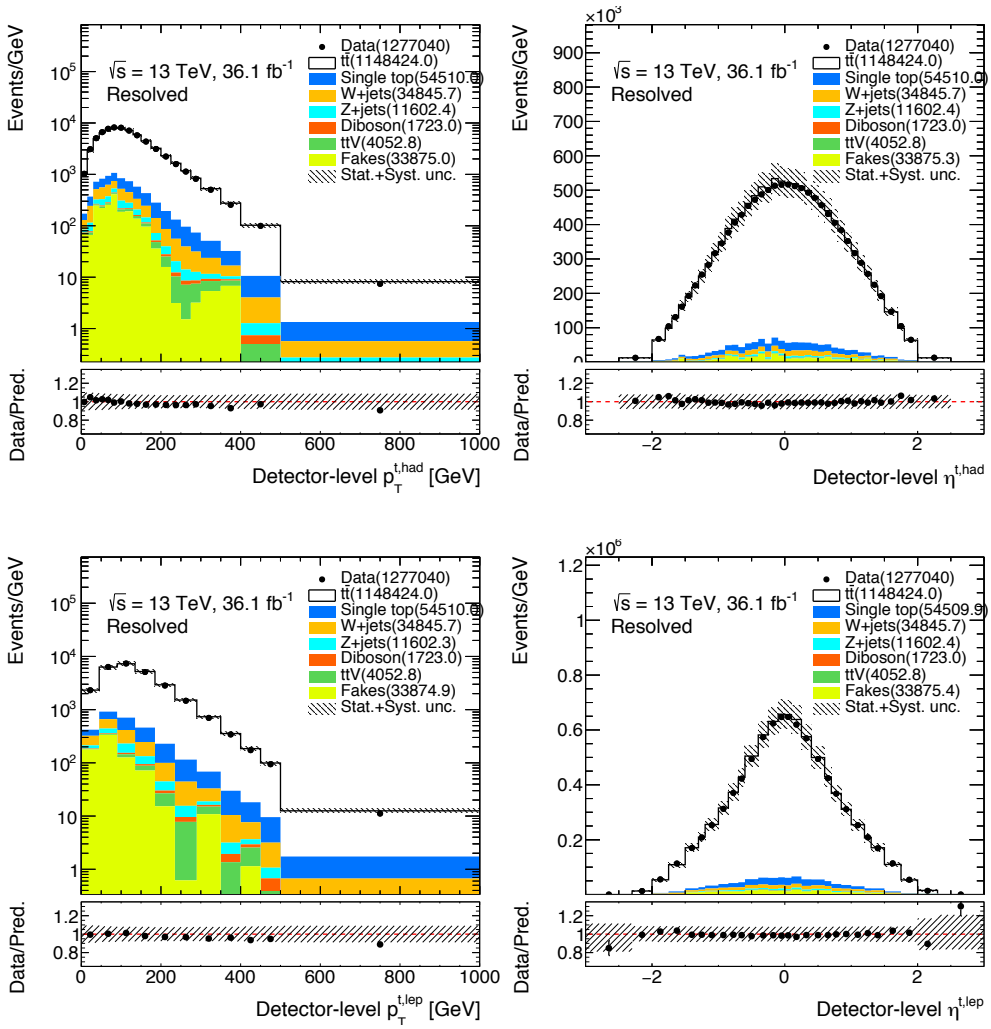

FIGURE 5.6: Transverse momentum (top left) and the rapidity (top right) of the hadronically decaying pseudo-top quark, and the transverse momentum (bottom left) and the rapidity (bottom right) of the leptonically decaying pseudo-top quark in the combined ℓ+jets channel. The shaded area represents the total statistical and systematic uncertainties on the expected number of events.

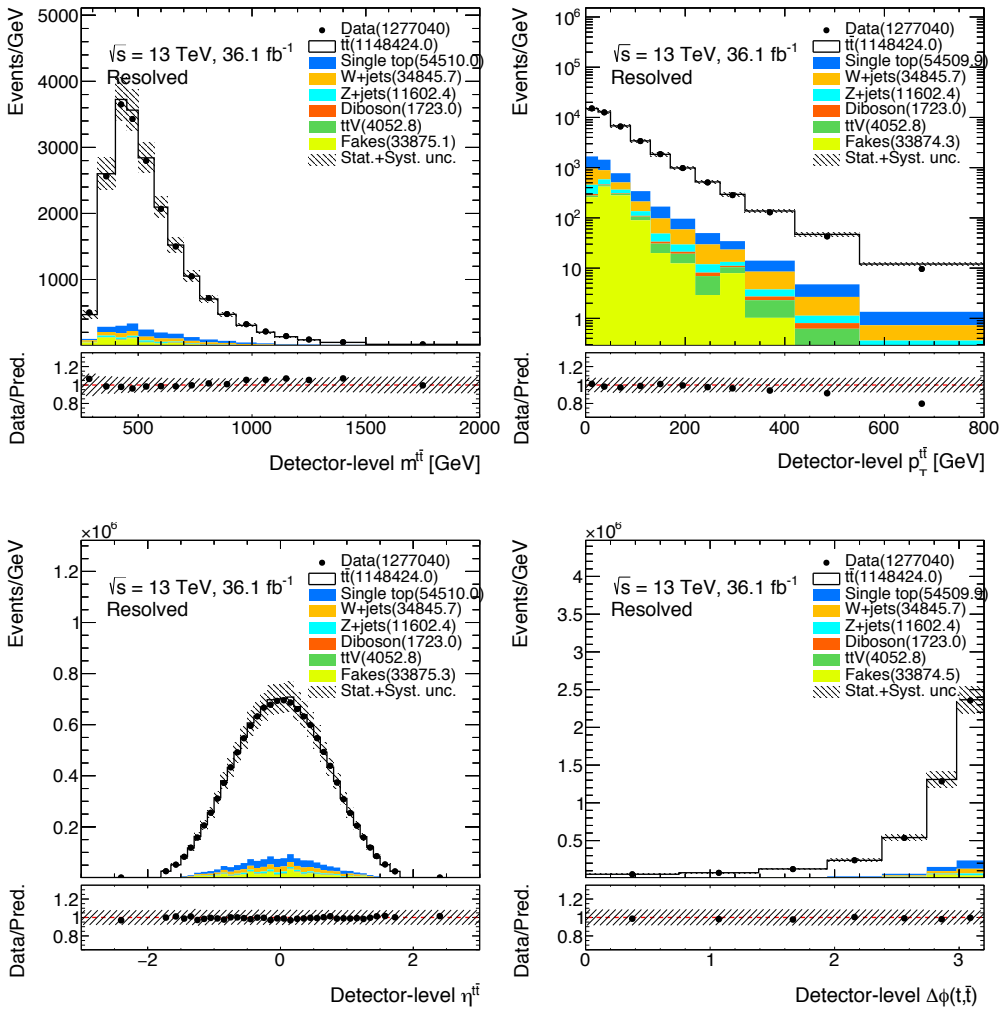

FIGURE 5.7: Invariant mass (top left), transverse momentum (top right) and the rapidity (bottom left) and the azimuthal angle difference (bottom right) of the reconstructed pseudo-$t\bar{t}$ pairs in the combined ℓ+jets channel. The shaded area represents the total statistical and systematic uncertainties on the expected number of events.

5.8 Reconstruction of the $t\bar{t}$ system via the kinematic likelihood fit

For the parton-level measurement, an alternative algorithm for the reconstruction of the $t\bar{t}$ system has been consider, in addition to the Pseudo-top algorithm described in the previous section. In order to evaluate the kinematic variables of the top quarks and of the $t\bar{t}$ system, the full $t\bar{t}$ system is reconstructed using a kinematic fit KLFitter [152] which assesses the compatibility of the observed event with the decays of a $t\bar{t}$ pair based on a likelihood approach. This approach was followed in the 7 TeV ℓ+jets analysis [153] and it is summarized in the following.

The likelihood takes as input the measured energies, pseudorapidities and azimuthal angles of four jets and the lepton, and the missing transverse momentum assumed to be related to a single neutrino. Such likelihood is a product of two terms. The first one is the product of Breit-Wigner distributions for the production of W bosons and top quarks, given the four momenta of the $t\bar{t}$ decay products. The second term is the probability to observe the energies of the $t\bar{t}$ products (lepton, jets, missing transverse momentum) times the probability to b-tag a certain jet given the parton it is supposed to derive from. The masses of both the W bosons and the top quarks are set to their respective measured (world-average) values [4]. A set of transfer functions (TFs) allows to map the reconstructed quantities to quarks and leptons produced in the hard scattering.

In the evaluation of the TFs, the following selection cuts were applied:

- at least one lepton with $p_{\mathrm{T}} \geq 20\,\mathrm{GeV}$;
- at least four jets with $p_{\mathrm{T}} \geq 20\,\mathrm{GeV}$;
- two b-tagged jets;
- $E_{\mathrm{T}}^{\mathrm{miss}} \geq 20\,\mathrm{GeV}$

After the selection, the reconstructed objects were matched to the truth level objects. Jets were matched to quarks by requiring $\Delta R\,(\mathrm{quark,jet}) \leq 0.3$, leptons were matched to the corresponding truth lepton if $\Delta R\,(\mathrm{reco,truth}) < 0.1$. No matching was required between the $E_{\mathrm{T}}^{\mathrm{miss}}$ and the neutrino. In the cases of not unique matching, the event was discarded.

A truth mapping was applied to separate b-jets from light-jets and each flavour of jets has a specific set of TF parameters. The TFs are thus derived using all the availaible truth information and are then applied to the particles of the corresponding assumed truth quality in the KLFitter, i.e. jets assumed to be mapped to a b-parton are fitted using b-jet TFs while the other jets using the light-jet TFs.

The likelihood is maximized with respect to the energies of the partons, the energy of the charged lepton and the components of the neutrino three-momentum. If there are more than four jets in the event satisfying $p_{\mathrm{T}} > 25\,\mathrm{GeV}$ and $|\eta| < 2.5$, all subsets of four jets from the

five jets collection are considered. The input jet collection is defined by taking the b-tagged jets with higher priority and then considering the hardest remaining light jets.

The assignment of jets to partons which gives the highest likelihood is selected. Figure 5.8 shows the log $\mathcal{L}$ distributions for the e+jets and μ+jets channels. Figures 5.9-5.10 show the reconstructed transverse momentum and rapidity of the hadronic and leptonic top and the reconstructed mass, transverse momentum and rapidity of the $t\bar{t}$ system.

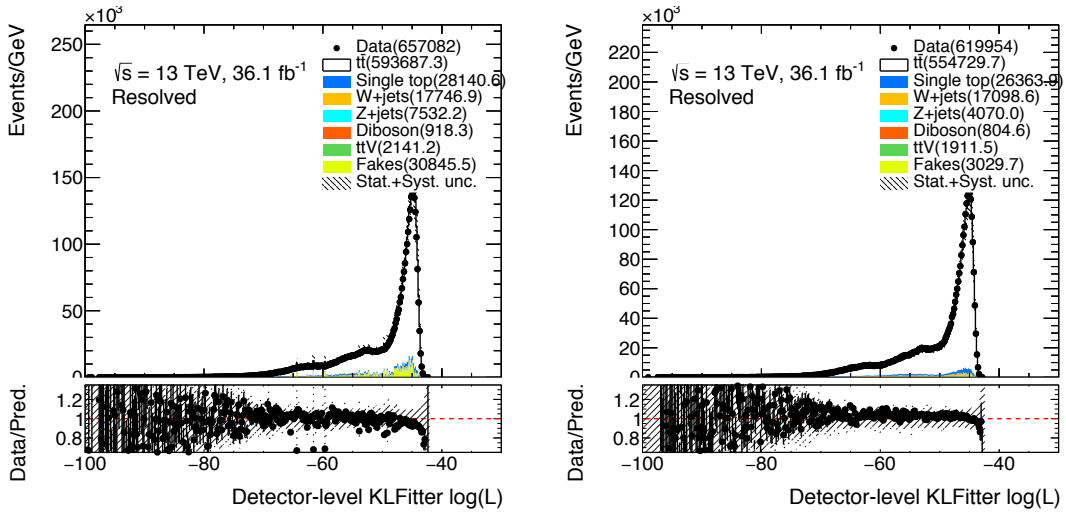

FIGURE 5.8: The kinematic likelihood fitter log $\mathcal{L}$ distributions for the e+jets channel (left) and μ+jets channel (right). All statistical and systematic uncertainties are taken into account in the error bands.

For the analysis of the $t\bar{t}$ system properties, in order to enhance the fraction of properly reconstructed $t\bar{t}$ events, a further selection cut on the likelihood value of the best permutation $\mathcal{L}$ is applied, $\mathcal{L} > -52$. The effect on the signal purity for the transverse momentum of the hadronic top and the mass of the $t\bar{t}$ system is shown in Figures 5.11 and 5.12. Further details on the KLFitter method are presented in Reference [154].

5.8.1 Comparison between 4- a 5-jet likelihood computation

The performances of the Pseudo-top and KLFitter (using 4 or 5 jets as input of the likelihood maximization, using both 8 TeV and 13 TeV TFs) methods have been compared in terms of *resolution* and *bias*, respectively defined as the RMS and Mean of the difference between the reconstructed and truth quantities. The results of this study are shown in Figs. 5.13 and 5.14. The RMS and Mean distributions in general show that the 4 jet configuration is not favored and that the differences between the PseudoTop and KLFitter with 5 jets are minimal (no difference is observed when using either the 8 TeV and 13 TeV transfer functions). In particular:

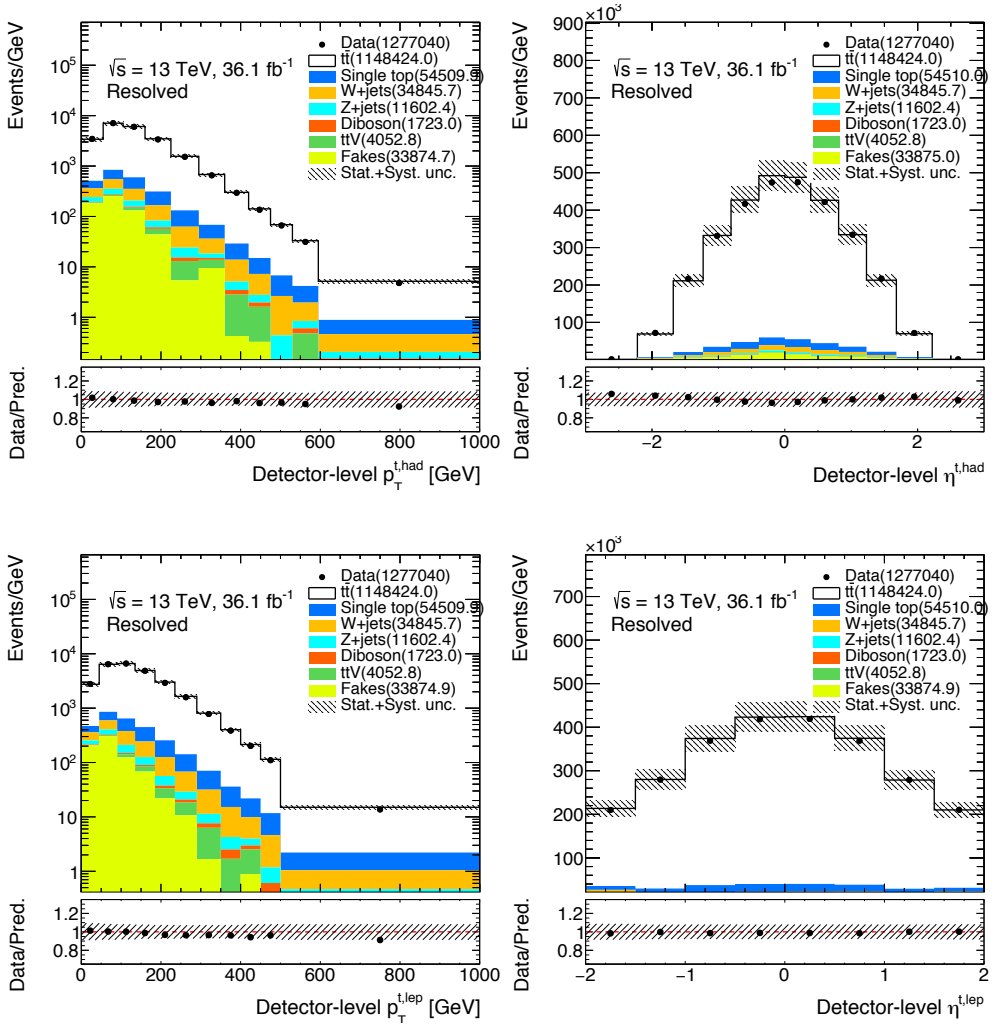

FIGURE 5.9: Transverse momentum (top left) and absolute value of the rapidity (top right) of the hadronically decaying top quark, and the transverse momentum (bottom left) and and absolute value of the rapidity (bottom right) of the leptonically decaying top quark in the combined ℓ+jets channel. The shaded area represents the total statistical and systematic uncertainties on the expected number of events.

- for the p_{T} and $|\eta|$ of the hadronically-decaying top the pseudotop method performs worse than the KLFitter in terms of bias;
- for the p_{T} of the leptonically-decaying top, the Pseudo-top method performs worse than the KLFitter in terms of bias but better in terms of RMS;
- for the η of leptonically-decaying top, the Pseudo-top method performs better with respect to the KLFitter in terms of RMS but much worse in terms of bias;
- for the p_{T} of the $t\bar{t}$ system, the Pseudo-top method performs slightly better with respect to the KLFitter in terms of RMS;

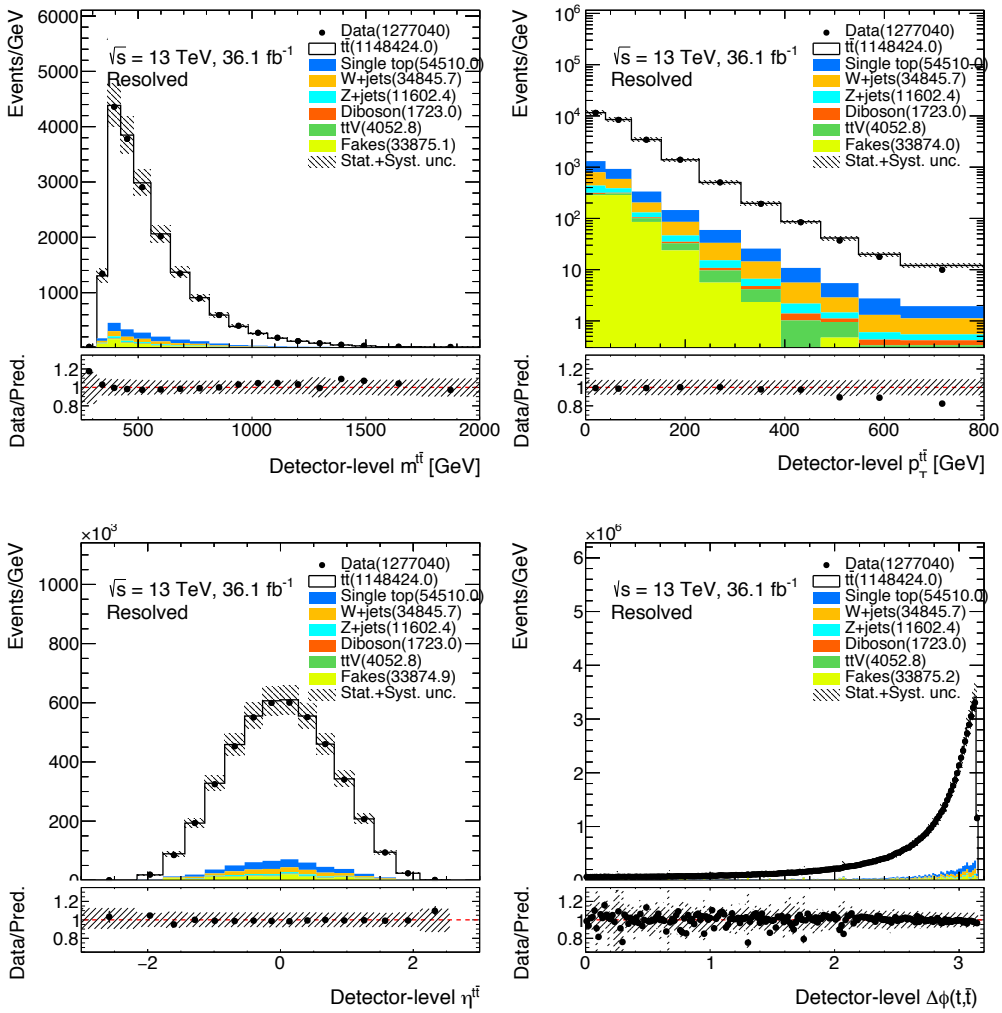

FIGURE 5.10: Invariant mass (top left), transverse momentum (top right) and the absolute value of the rapidity (bottom) and the azimuthal angle difference (bottom right) of the reconstructed $t\bar{t}$ pairs in the combined ℓ+jets channel. The shaded area represents the total statistical and systematic uncertainties on the expected number of events.

- for the $|\eta|$ of the $t\bar{t}$ system, no differences are observed among the three approaches;
- for the m of the $t\bar{t}$ system, the Pseudo-top method performs slightly worse with respect to the KLFitter in terms of RMS at low masses (also below the on-shell threshold) but performs better in terms of bias.

Despite the minimal differences in performances between the KLFitter and PseudoTop, since the KLFitter distributions shown in Figs. 5.13 and 5.14 were produced without applying the cut on the likelihood, it is important to compare the methods and test the impact on the performances of KLFitter with the inclusion of the additional likelihood cut. This comparison is shown in Figs. 5.15 and 5.16, where it is evident that KLFitter with the 5-jets

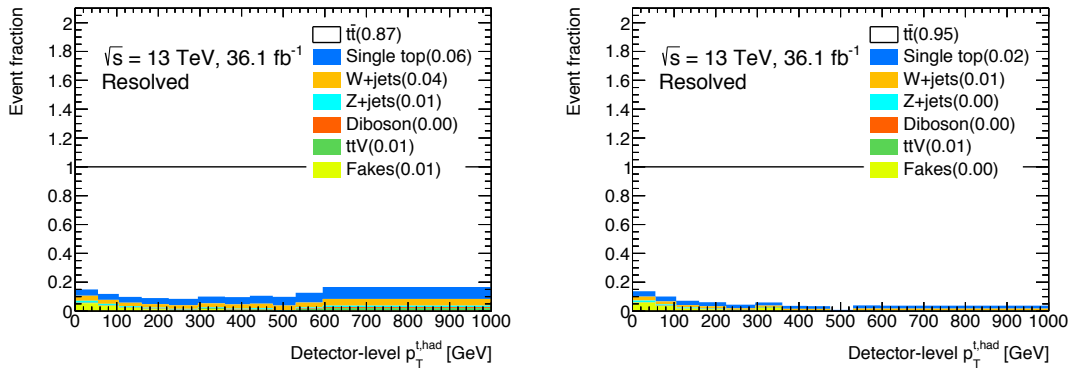

FIGURE 5.11: Sample compositions in the hadronic top p_T spectrum for a selection without (left) and with (right) likelihood cut in the ℓ+jets channel

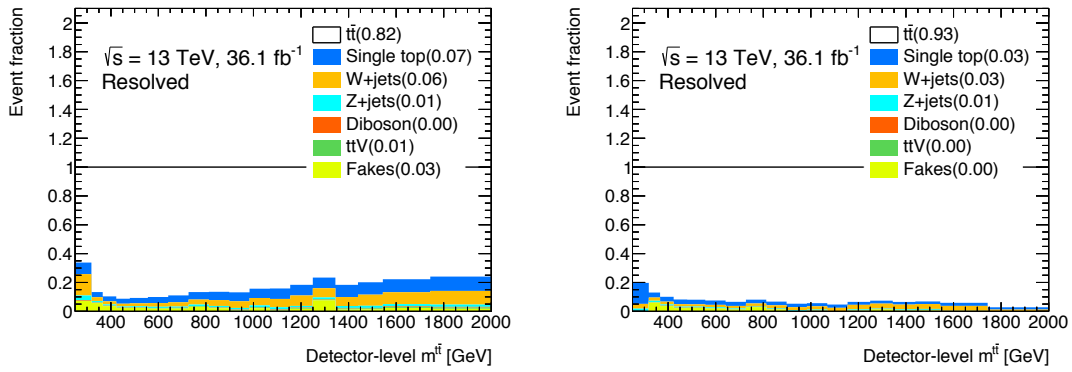

FIGURE 5.12: Sample compositions in $t\bar{t}$ mass spectrum for a selection without (left) and with (right) likelihood cut in the ℓ+jets channel

configuration becomes more performant than the PseudoTop method once the likelihood cut is applied. KLFitter with 5-jets configuration including the likelihood cut is the method used in the parton-level analysis described in this thesis.

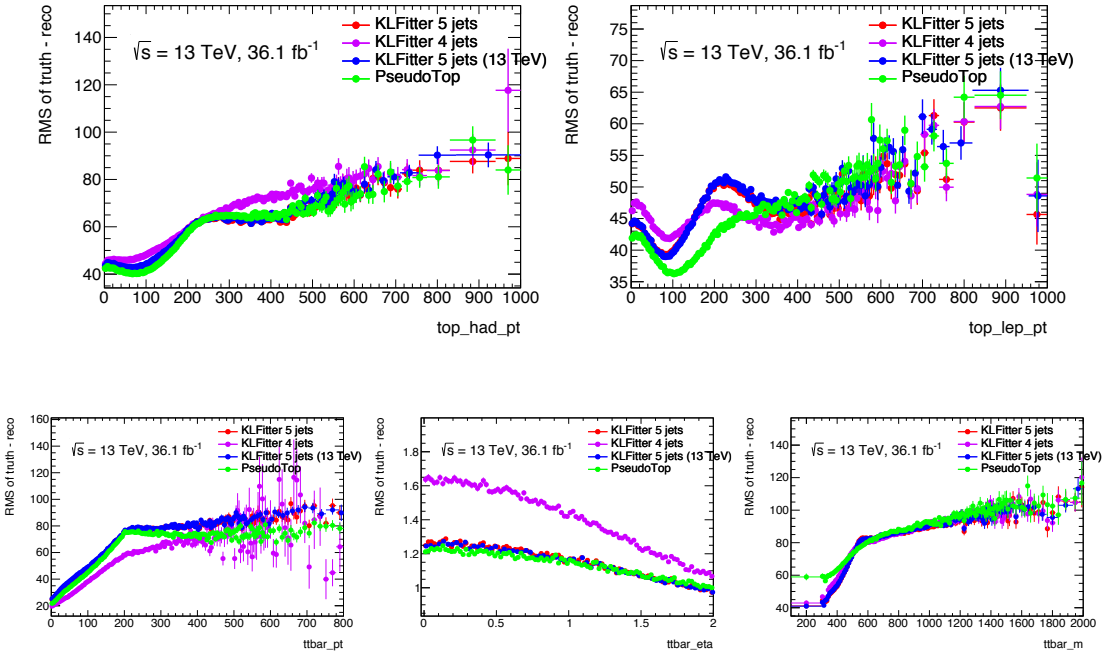

FIGURE 5.13: RMS of the reco/truth difference for basic $t\bar{t}$ observables, reconstructed using the PseudoTop, KLFitter fed with 4 jets (using 8 TeV TFs) and KLFitter fed with 5 jets (using both 8 TeV and 13 TeV TFs).

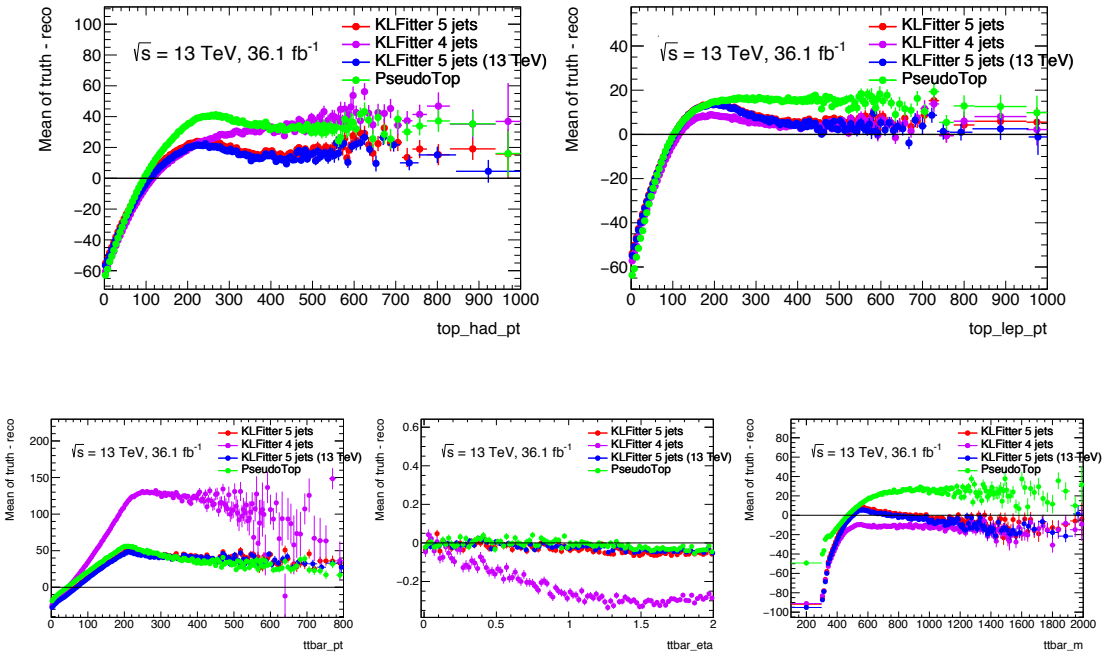

FIGURE 5.14: Mean of the reco/truth difference for basic $t\bar{t}$ observables, reconstructed using the PseudoTop, KLFitter fed with 4 jets (using 8 TeV TFs) and KLFitter fed with 5 jets (using both 8 TeV and 13 TeV TFs).

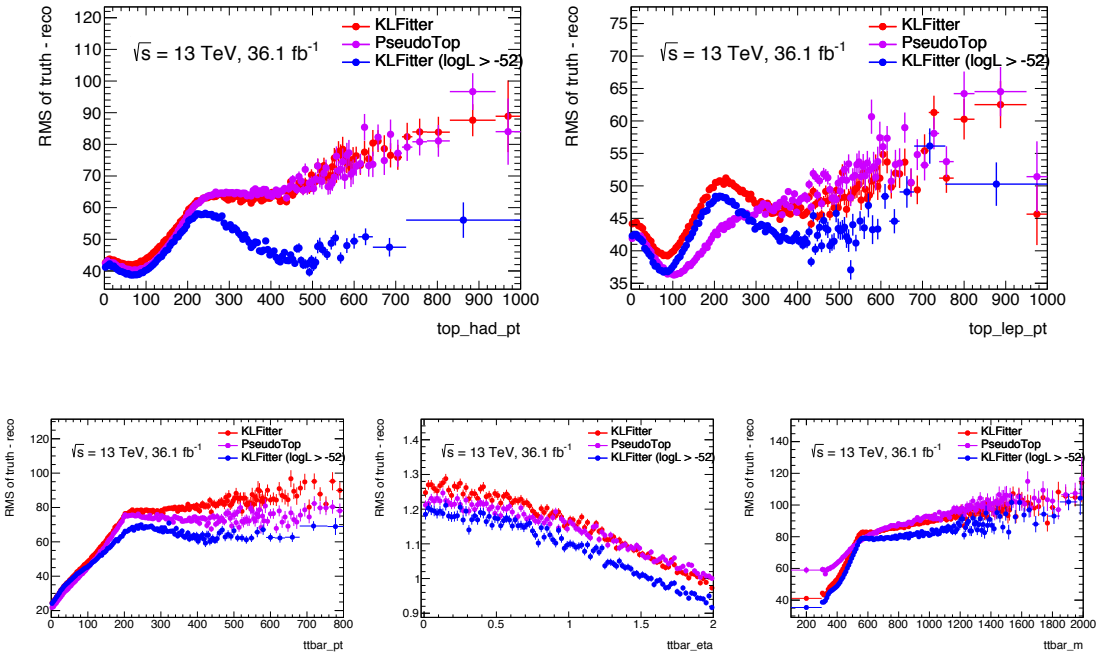

FIGURE 5.15: RMS of the reco/truth difference for basic $t\bar{t}$ observables, reconstructed using the PseudoTop, KLFitter fed with 5 jets with and without the likelihood cut.

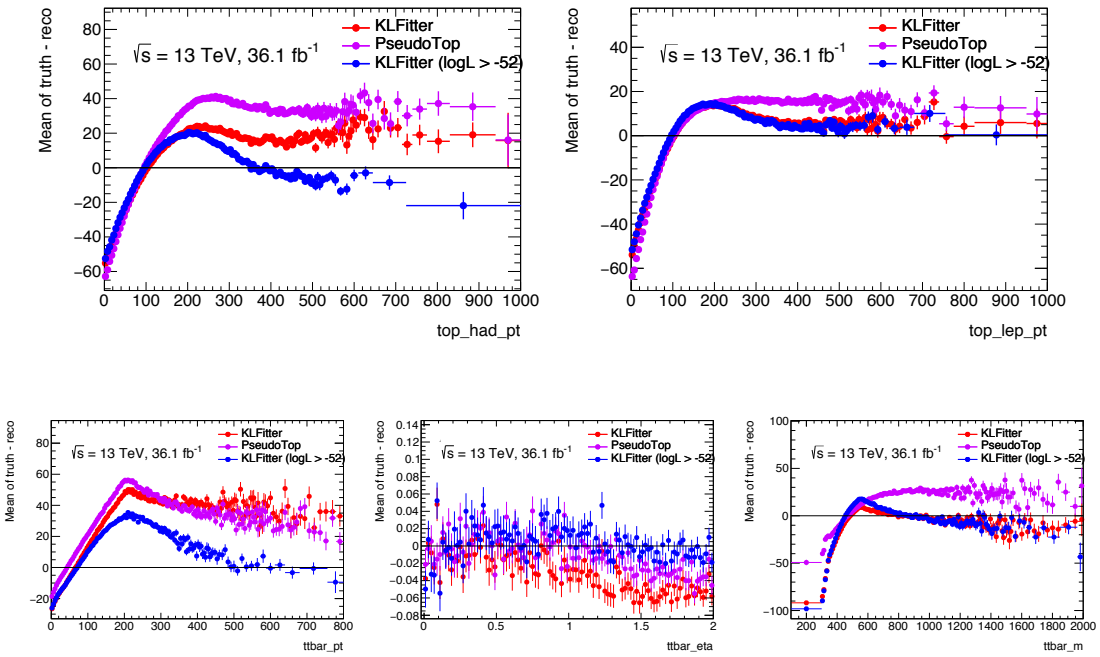

FIGURE 5.16: Mean of the reco/truth difference for basic $t\bar{t}$ observables, reconstructed using the PseudoTop, KLFitter fed with 5 jets with and without the likelihood cut.

5.9 Boosted top reconstruction and tagging

The reconstruction of the $t\bar{t}$ system in the boosted topology needs a specific procedure to take into account the different topology in the detector with respect to the resolved final state.

The leading re-clustered large-R jet that passes the selection described in Section 5.1 is directly considered the hadronic top. The top-tagging is performed by applying a mass window cut on the jet mass around the top-quark mass [120,220] GeV. This tagging differs from the method used to top-tag the large-R jet in the analysis on 2015 data [51], since only one sub-structure property is used and the cut is fixed on the entire jet p_{T} range. In the analysis on 2015 data, the top-tagging procedure employed p_T-dependent cuts using the m_{jet} and τ_{32} substructure variables [155].

The efficiency obtained using the mass window cut is shown in Figure 5.17, where the efficiency at detector-level and particle-level are shown as a function of the p_{T} of the leading jet and the top-matched jet . The relative background rejection is shown in Figure 5.17, where the only W+jets sample is used to estimate the background since this component represents the dominant one which does not contain top quarks. A positive consequence of having a simple mass window cut to identify the top candidate is the possibility to have complete compatibility between particle- and detector-level, that reflects in a flat acceptance correction in the unfolding procedure, discussed in the following section.

Once the candidate hadronic top is identified, the leptonic top is reconstructed using the leading b-tagged jet that fulfills the following requirements:

- ΔR((lepton, small-R jet) < 2.0
- ΔR(large-R jet,small-R jet) > 1.5

If there are no b-tagged jet that fulfill these requirements then the leading p_{T} jet is used. The procedure for the reconstruction of the leptonic top starting from the lepton, the missing transverse momentum and the selected jet is analogous to the pseudo-top reconstruction described in Section 5.7. The reconstructed mass, transverse momentum and rapidity of the hadronic and leptonic top quark, respectively are shown in Figures 5.18 and 5.19, while the reconstructed mass, transverse momentum and rapidity of the $t\bar{t}$ system are shown in Figure 5.20.

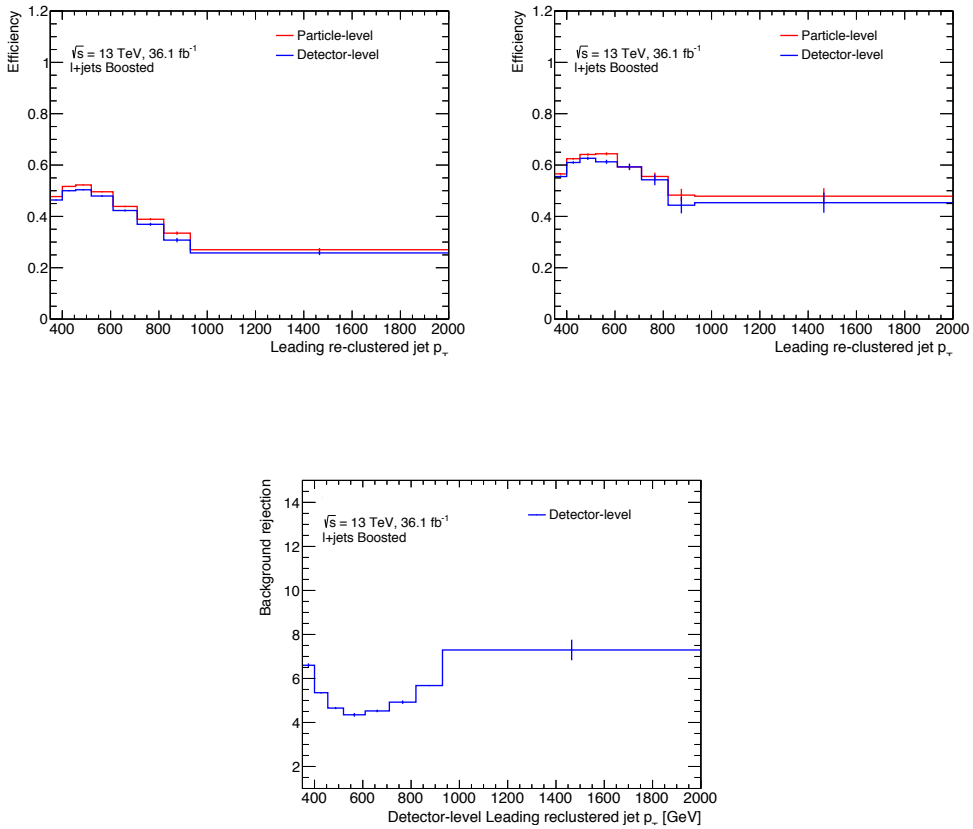

FIGURE 5.17: Efficiency and background rejection of the mass cut [120, 220] applied on the re-clustered jets to identify the top quarks as a function of the p_{T} of the leading re-clustered jet in the event. On the top-left the efficiency at detector level (blue) and particle level (red), evaluated as the ratio of the leading reclustered jet in the event that fulfills the mass window requirement and all the leading reclustered jets in the same p_{T} range is shown. In the top right only jets that matches $\Delta R(\text{RC jet, truth } t(\text{or } \bar{t})) < 0.75$ are considered. On the bottom the background rejection is defined as the opposite of the selection efficiency and it is derived using a W+jets sample. Only events containing a single lepton, with $E_{\mathrm{T}}^{\mathrm{miss}} > 20\,\mathrm{GeV}$, sum of $E_{\mathrm{T}}^{\mathrm{miss}}$and $m_{\mathrm{T}}^{W} > 60\,\mathrm{GeV}$ and containing at least a re-clustered jet with $p_{\mathrm{T}} > 200\,\mathrm{GeV}$ are used to obtain the efficiencies.

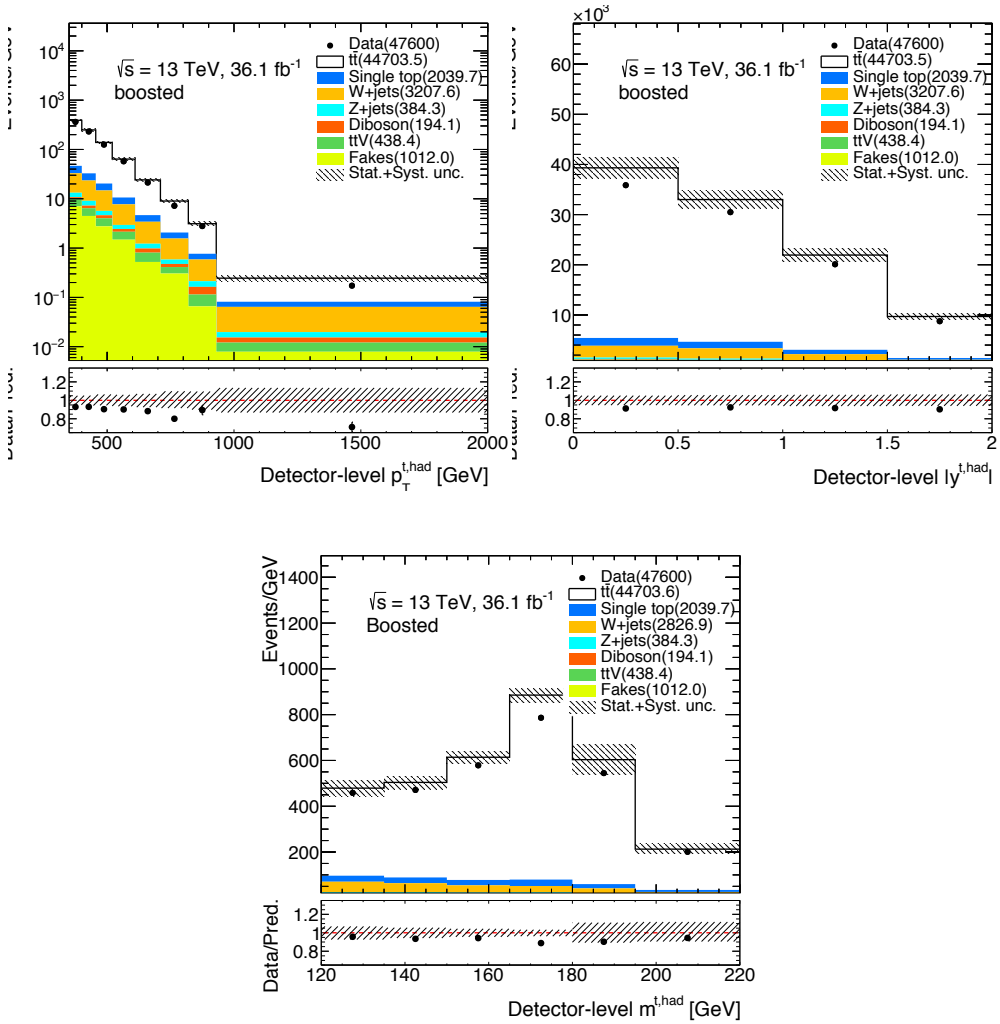

FIGURE 5.18: Transverse momentum (top left), absolute value of the rapidity (top right) and mass (bottom) of the hadronically decaying top quark in the combined ℓ+jets channel in the boosted topology. The shaded area represents the total statistical and systematic uncertainties on the expected number of events.

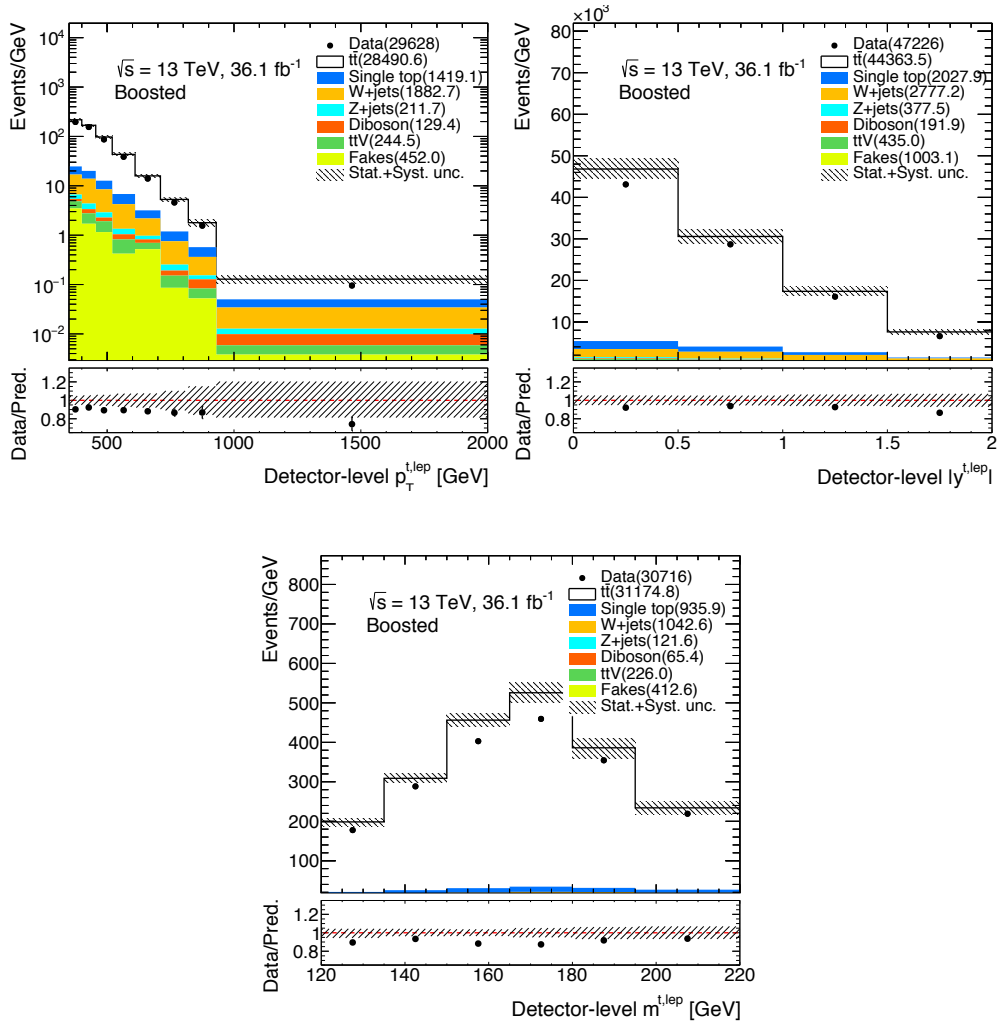

FIGURE 5.19: Transverse momentum (top left), absolute value of the rapidity (top right) and mass (bottom) of the leptonically decaying top quark in the combined ℓ+jets channel in the boosted topology. The shaded area represents the total statistical and systematic uncertainties on the expected number of events.

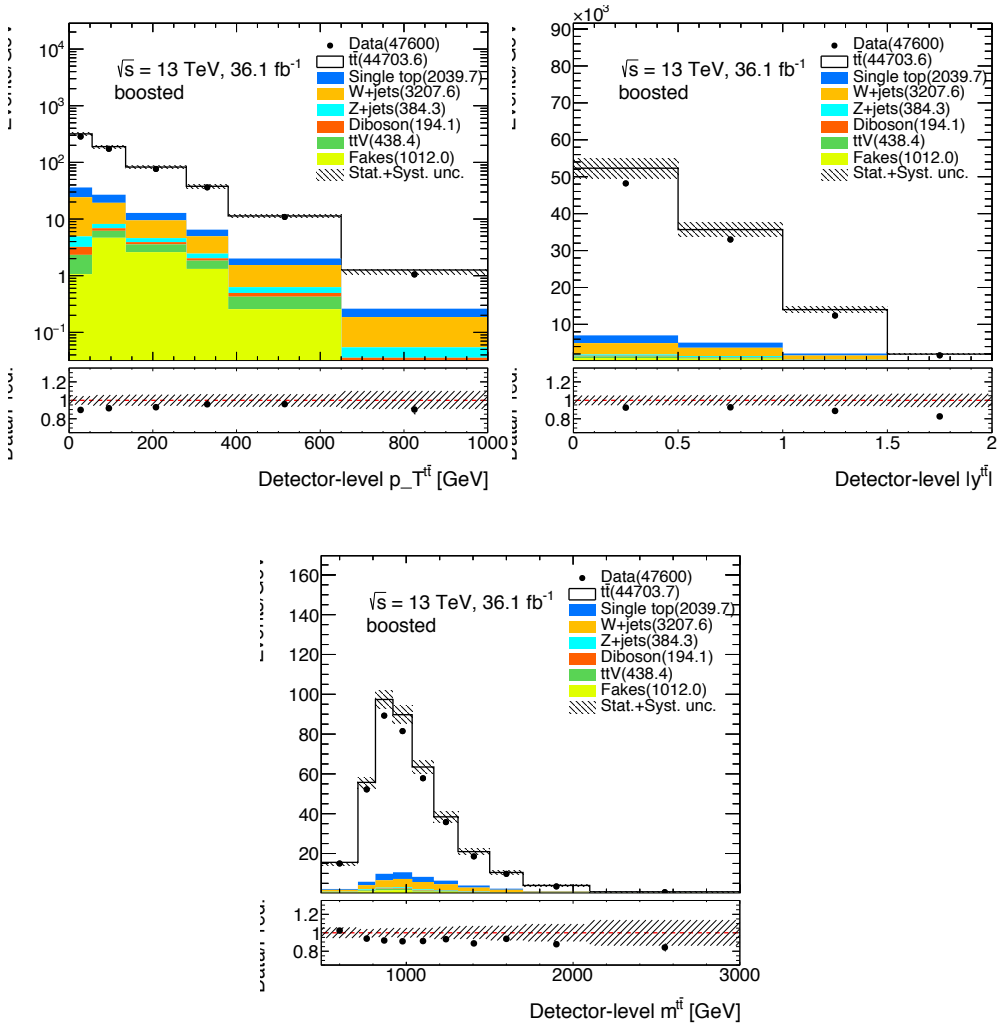

FIGURE 5.20: Invariant mass (top left), transverse momentum (top right) and the absolute value of the rapidity (bottom) of the reconstructed $t\bar{t}$ pairs in the combined ℓ+jets channel in the boosted topology. The shaded area represents the total statistical and systematic uncertainties on the expected number of events.

Chapter 6

Cross-Section Measurement

6.1 Unfolding

Measurements of physical observables are generally distorted or biased by the limited resolution and acceptance of the detector. So, a direct comparison of measured distributions with the theoretical predictions is not possible. Unfolding is the procedure that allows to correct for detector effects and makes possible such a comparison. The finite resolution effect is due to the limited accuracy of the detector and it causes a statistical smearing between the true variable x and the measured quantity y. From a mathematical point of view, this effect can be represented by the *Fredholm integral equation* [156]

$$g(y) = \int A(x,y) f(x)\, dx \tag{6.1}$$

where $g(y)$ is the measured distribution and the $f(x)$ is the true distribution. The resolution function $A(x,y)$ represents the distortion introduced by the detector. The unfolding consists in evaluating $f(x)$ from a given $g(y)$ and a $A(x,y)$. Therefore, the solution to this problem needs the calculation of the inverse of the resolution function $A^{-1}(x,y)$.
In case of differential cross-section measurements in high-energy physics, the considered distributions are discrete, so the resolution function becomes a discrete matrix, evaluated by Monte Carlo simulation, called Response Matrix (or Migration Matrix). In this case, a system of linear equations have to be solved. In addition, the response matrix itself can be affected by uncertainties. The inversion of a finite system of equations rarely admits an exact solution, so a series of different techniques have been developed. The four main unfolding methods used in high-energy physics analyses are:

- **Bin-by-bin** this technique extracts correction factors for each bin from the ratio of the reconstructed simulation over the theoretical prediction distribution. This is the simplest method and cannot be even stricly considered a proper unfolding technique since migration effects are not considered.

- **Simple matrix inversion** this technique numerically inverts the migration matrix to apply unfolding to the measured distribution.
- **Single Value Decomposition (SVD)** [157] is an extension of the simple inversion matrix. It is based on the decomposition of the A migration matrix into three matrices in order to make easier its inversion.
- **Iterative Bayesian** is a *cause-effect* procedure [158]. This is the technique employed in the analysis described in this thesis and will be described in the following.

6.1.1 Iterative Bayesian Unfolding Method

This procedure is based on the Bayes' theorem [159] and it leads to a cause-effect interpretation of the problem. Causes C_i correspond to the generated true value while effects E_j are the measured events. Each cause can produce different effects, but the exact corresponding cause for a given effect is unknown. From Monte Carlo simulation it is possible to evaluate the probability $P(E_j|C_i)$ for a cause to generate a specific effect. The Bayes theorem allows to estimate the probability $P(C_i|E_j)$ that cause C_i generates the effect E_j

$$P(C_i|E_j) = \frac{P(E_j|C_i) \cdot P_0(C_i)}{\sum_{k=1}^{n_C} P(E_j|C_k) \cdot P_0(C_k)} \tag{6.2}$$

where $P_0(C_i)$ is the prior probability for the cause C_i and n_C is the number of possible causes. The estimator for the number of causes in the $i-th$ bin can be expressed as

$$\hat{n}(C_i) = \frac{1}{\varepsilon_i} \sum_{j=1}^{n_E} n(E_j) \cdot P(C_i|E_j) \tag{6.3}$$

where $n(E_j)$ is the number of measured effects in the $j-th$ bin and ε_i is the efficiencies for each bin, evaluated from Monte Carlo. These efficiencies are defined as

$$\varepsilon_i = \sum_{j=1}^{n_E} \frac{n(E_j)^{MC}}{n(C_i)^{MC}} \tag{6.4}$$

The $P(C_i|E_j)$ can be considered equilavent to the elements of an inverted migration matrix

$$\mathcal{M}_{ij} = \frac{P(E_j|C_i) \cdot P_0(C_i)}{\sum_{h=1}^{n_E} P(C_i|E_h) \cdot \sum_{k=1}^{n_C} P(E_j|C_k) \cdot P_0(C_k)} \tag{6.5}$$

leading to the following unfolding equation

$$\hat{n}(C_i) = \sum_{j=1}^{n_E} \mathcal{M}_{ij} n(E_j) \tag{6.6}$$

The new causes probability

$$P_0'(C_i) = \frac{\hat{n}(C_i)}{\sum_{i=1}^{n_C} \hat{n}(C_i)} \tag{6.7}$$

replaces the initial prior $P_0(C_i)$ and the procedure is reiterated until $P_0(C_i)$ and $P_0'(C_i)$ converge. The stability of the method is reached when the result of the last iteration is similar to the one obtained from the previous iteration.

6.2 Binning choice and optimization

The optimization of the binning choice for the measured distributions of the differential cross-sections is based on the resolution of the ATLAS detector and of the reconstruction algorithms of the $t\bar{t}$ system. The optimization procedure used in this analysis will be described in this section and it is performed for each variable separately. The effect due to the detector resolution is described by the migration matrix which relates a given variable at truth and reconstructed level and the difference between the reconstructed level and truth level considered. Resolution matrices were evaluated on simulation using a fine binning as a starting point and the resolution is evaluated in each truth-level bin of the migration matrix by looking at the profile distribution.

This resolution-based binning has been derived by the following iterative formula from the profile distributions:

$$\delta \cdot \mathrm{Resol}(p_{\mathrm{N}-1}) \geq \frac{x_{\mathrm{N}} - x_{\mathrm{N}-1}}{2}, \tag{6.8}$$

where $\mathrm{Resol}(p_{N-1})$ is the resolution function for a given variable in the middle of the specified bin and x_N, x_{N-1} are bin edges. The parameter δ (usually greater than 1) is a conservative parameter to account for the non-gaussian shape of the resolution distributions. An additional requirement of an expected statistical error on the number of reconstructed events in the given bin lower than 5% is applied.

In general, good diagonality of the migration matrices is observed, with more than 50% of events staying on the diagonal. As this matrix represents a correction map of the bin-by-bin migrations between the truth-level and the detector-level distributions, the diagonal elements are related to the probability of a truth-level event to be reconstructed in the same bin of the detector-level. Bin edges were further rounded and the number of bins may be reduced when statistical fluctuations in MC closure tests occurred. Different binning is used for leptonic and hadronic top quarks, as the resolutions of their transverse momenta and rapidities are different.

6.2.1 Binning optimization for double differential distributions

For the double differential distributions, the complexity introduced by the additional dimension and the need to optimize two variables (X in bins of Y) at the same time, leads to

a slightly different binning optimization performed in the boosted and resolved topologies, driven also by the expected statistics in each topology.

Resolved For the measurement of a given spectrum X in bin of Y, a first optimization procedure is performed on the Y variable The procedure is similar to the one described above, with more stringent requirements, $\delta = 2$ and 0.5% as maximum statistical error, in order to guarantee enough granularity for the following step of the optimization. Then, the X variable is optimized in each bin of Y: in this case, the parameters have been relaxed by requiring $\delta = 2$ and 1% as maximum statistical error. Then, closure tests have been performed on the newly found binning and a by-hand rebinning is applied to cope for the eventual non-closure observed in the tests.

Boosted The statistics of the sample in the boosted topology does not allow to reach the same large number of bins as the resolved topology and subsequently the choice of the number of bins is highly dominated by the need to reduce statistical fluctuations in MC closure tests and not by the resolution. Consequently, the number of bins is fixed to 2, or 3 at maximum, of the *external* variable Y and the number of bins in the spectrum of the *internal* variable X is reduced with respect to the single differential case to guarantee a good closure and stress tests.

6.3 Correction evaluation

The use of the experimental apparatus to measure the original kinematic properties of the particles under study inevitably leads to differences between the observed and the *true* quantities. In particular, the differences between the reconstructed momentum, energy and position with respect to the corresponding *true* ones are due to the limited detector resolution. Moreover, a detector covers a specific region of the space, thus the limited acceptance may cause the loss of the particles produced outside the coverage region. In addition, the analysis strategy, aiming at separating the signal from the background, reduces the acceptance of the selection, i.e. reject events with all particle in the phase-space region covered by the detector. Therefore, the measured yields needs corrections to take into account all of these effects and the corrections factors are estimated by using MC distributions and detector simulation.

The definition of the *truth* level, where the particles have not interacted yet with the detector is crucial to define the corrections. This definition has to take into account the various processes (radiation, decay, hadronization) that top quarks and the other unstable particles undergo before the interaction with the detector. The truth level is defined by the stage at which the corrections are evaluated.

6.3.1 Fiducial phase-space (particle level)

The fiducial phase-space is defined by the selection criteria presented in Section 5.2, i.e. very close to the detector level.

The acceptance correction is obtained in simulation by taking the ratio between the number of events that pass both the reconstructed- and particle-level selections to the number of all events that pass reconstructed selection in the reconstructed bin j. The binning used for this correction is the same as for the reconstructed quantities:

$$f_{\text{acc}}^{j} \equiv \left(\frac{N_{\text{reco}\wedge\text{part}}}{N_{\text{reco}}} \right)^{j}.$$

The acceptance correction is a bin-by-bin factor which corrects for the selected reco-level events which were not selected at the particle level. These are considered as poorly reconstructed events as they do not belong to the fiducial volume of interest. In more detail, the values of $N^{j}_{\text{reco}\wedge\text{part}}$ (reco-level, entering the acceptance correction) and $N^{i}_{\text{reco}\wedge\text{part}}$ (particle-level, entering the efficiency correction described below) are obtained as the fully in-range projection of the response matrix onto the respective axes, in order to respect the restricted analysis bin range, thus excluding over- and under-flow bins.

In the resolved topology, in order to remove combinatorial migrations between the particle and detector levels, a matching correction is introduced which improves the diagonality of the migration matrix. A simple geometric ΔR algorithm matches reconstructed objects which constitute the pseudo-top quarks to particle-level objects that form the pseudo-top quarks at particle level and satisfy the fiducial requirements. Each particle-level lepton $e(\mu)$ is matched to the closest reconstructed lepton $e(\mu)$ within $\Delta R < 0.02$, respectively. Particle jets are geometrically matched to the closest reconstructed jet within $\Delta R_{\text{reco-jet,particle-jet}} < 0.35$. The matching correction can be expressed as

$$f_{\text{match}}^{j} \equiv \left(\frac{N_{\text{reco}\wedge\text{part}\wedge\text{matched}}}{N_{\text{reco}\wedge\text{part}}} \right)^{j}.$$

It is worth noting that in the boosted topology the matching between the detector-level objects and the particle-level objects is not required, in contrast to the resolved topology. This has a small effect and events that contain unmatched objects will tend to populate the off-diagonal regions of the response matrix. Since the response matrix is fairly diagonal, an extra matching correction is deemed unnecessary.

The resulting distribution is then unfolded to the particle using the unfolding procedure described in Section 6.4.

Finally, an efficiency correction is applied to the unfolded spectrum, in order to correct the result by a bin-by-bin factor to the fiducial phase-space. It corrects for events which pass the particle level selection but were not reconstructed at the detector (reco) level. It is defined

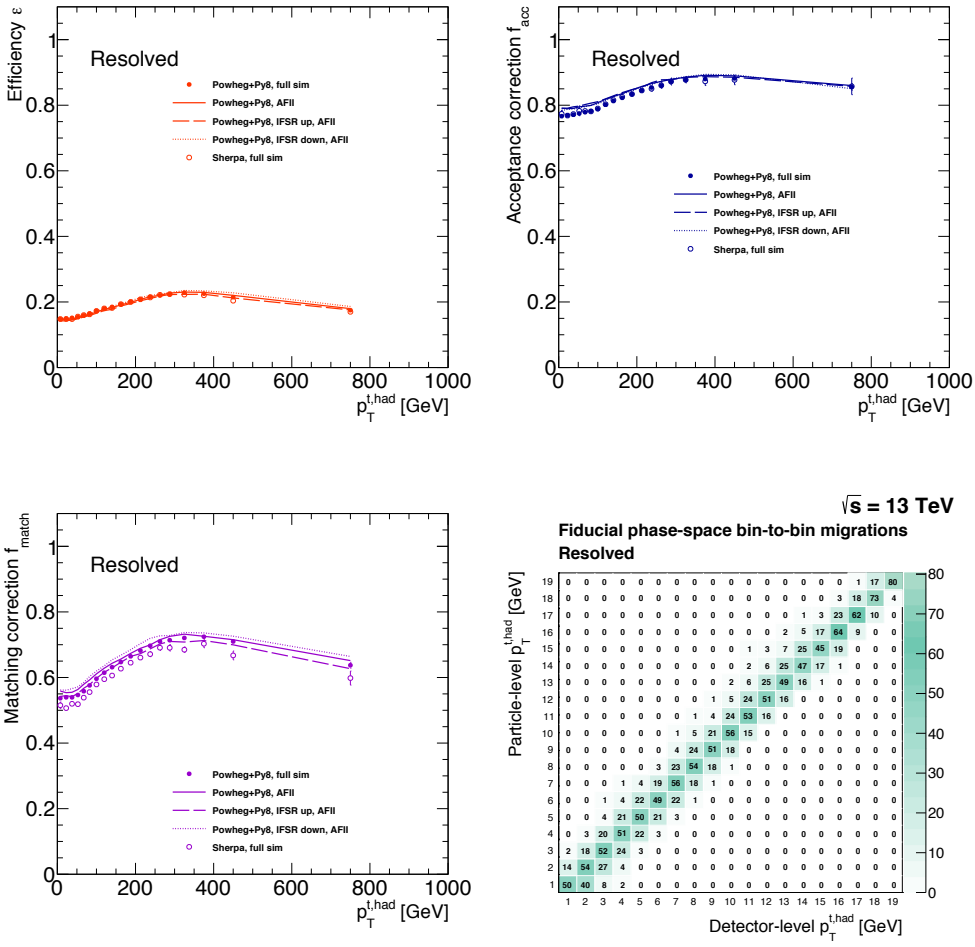

FIGURE 6.1: Efficiency f^j_{eff} and acceptance f^j_{acc} and matching f^j_{match} corrections and the migration matrix for the $p_{\text{T}}^{t,\text{had}}$ variable in the resolved topology at the particle level in the combined ℓ+jets channel.

as the number of events passing both the reconstructed and particle selection criteria, over the number of events passing the particle level selection, binned in the variable of interest:

$$\epsilon \equiv \left(\frac{N_{\text{reco}\wedge\text{part}}}{N_{\text{part}}} \right)^i .$$

A set of corrections for a selection of one-dimensional as well as two-dimensional spectra is shown in Figures 6.1–6.4.

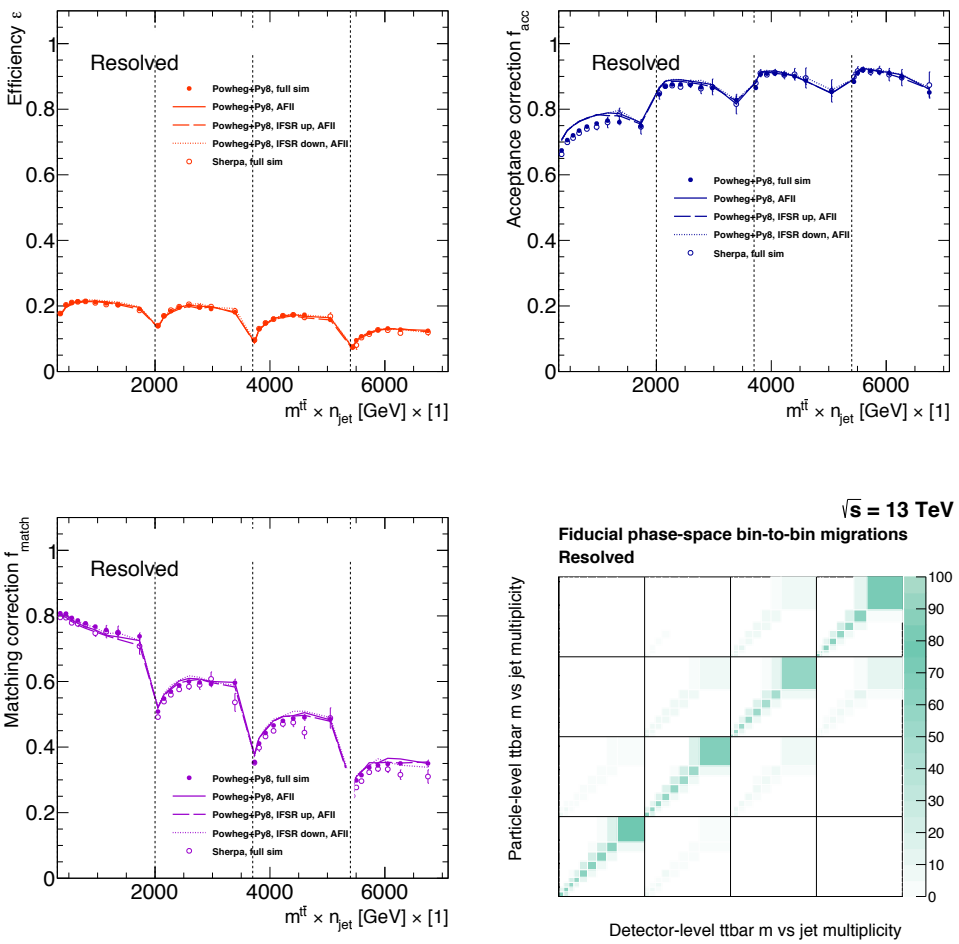

FIGURE 6.2: Efficiency f^j_{eff} and acceptance f^j_{acc} and matching f^j_{match} corrections and the migration matrix for the $m^{t\bar{t}} \times n_{\text{jet}}$ variable in the resolved topology at the particle level in the combined ℓ+jets channel.

6.3.2 Full phase space (parton level)

In order to unambiguously define leptonic and hadronic top quarks, the contribution of $t\bar{t}$ pairs decaying dileptonically is removed by applying a correction factor f_{ljets} (dilepton correction) which represents the fraction of $t\bar{t}$ single-lepton events in the nominal sample. The τ leptons from the leptonically decaying W bosons are considered as signal regardless of the τ decay mode. The cross-section measurements are defined with respect to the top quarks before the decay (parton level) and after QCD radiation. Observables related to top quarks are extrapolated to the full phase-space starting from top quarks decaying hadronically at the detector level.

The acceptance correction f_{acc} corrects for detector-level events which are reconstructed outside the parton-level bin range for a given variable. The migration matrix ($\mathcal{M}$) is derived

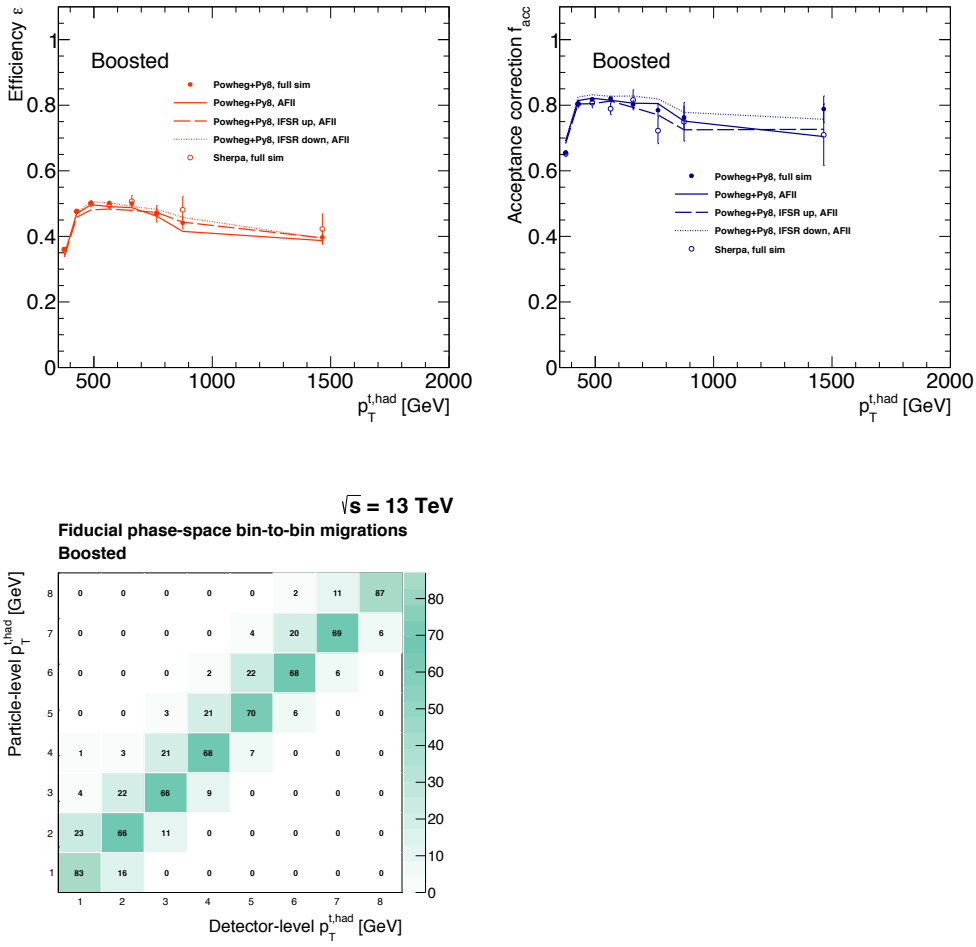

FIGURE 6.3: Efficiency f_{eff}^{j} and acceptance f_{acc}^{j} corrections and the migration matrix for the $p_{\text{T}}^{t,\text{had}}$ variable in the boosted topology at the particle level in the combined ℓ+jets channel.

from simulated $t\bar{t}$ events decaying in the single-lepton channel and the efficiency correction f_{eff} corrects for events which did not pass the detector-level selection.

All corrections are evaluated with simulation and are presented in Figures 6.5 and 6.6 for the case of the p_{T} of the top quark, in the resolved and boosted topology.

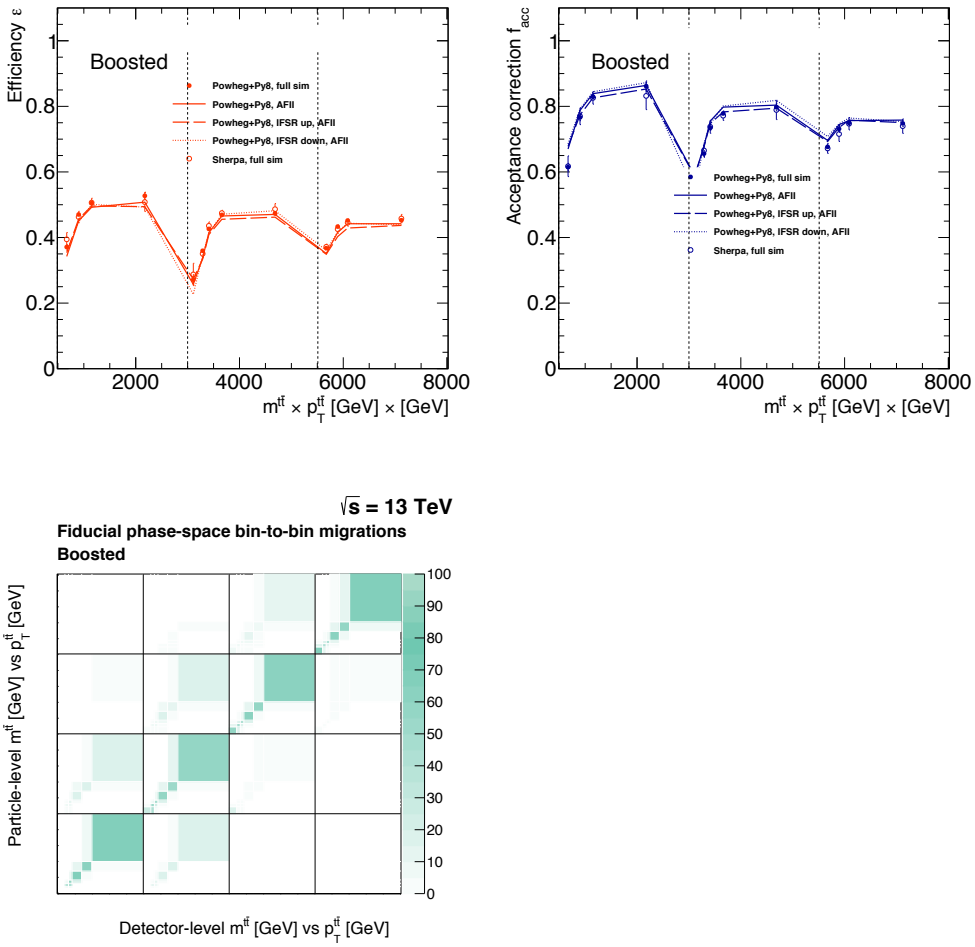

FIGURE 6.4: Efficiency f^j_{eff} and acceptance f^j_{acc} corrections and the migration matrix for the $m^{t\bar{t}} \times p^{t\bar{t}}_{\text{T}}$ variable in the boosted topology at the particle level in the combined ℓ+jets channel.

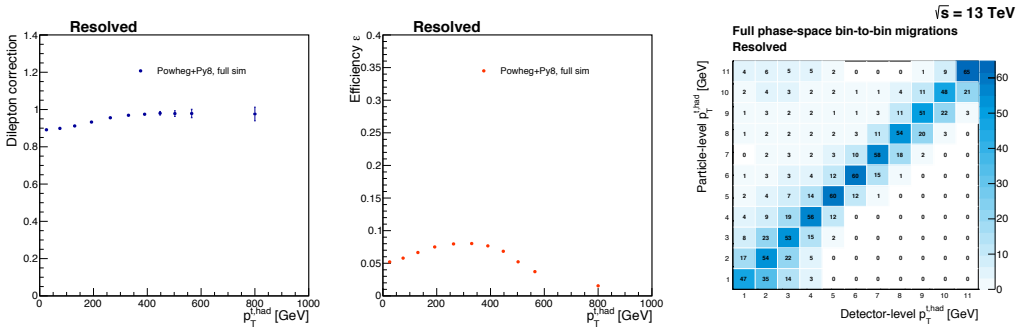

(A) (B) (C)

FIGURE 6.5: The (a) dilepton and (b) efficiency corrections (evaluated with several simulations samples), and the (c) detector-to-parton level migration matrix (evaluated with the nominal POWHEG+PYTHIA 8 simulation sample) for the hadronic top-quark transverse momentum in the resolved topology at parton level, for events selected with the kinematic likelihood cut.

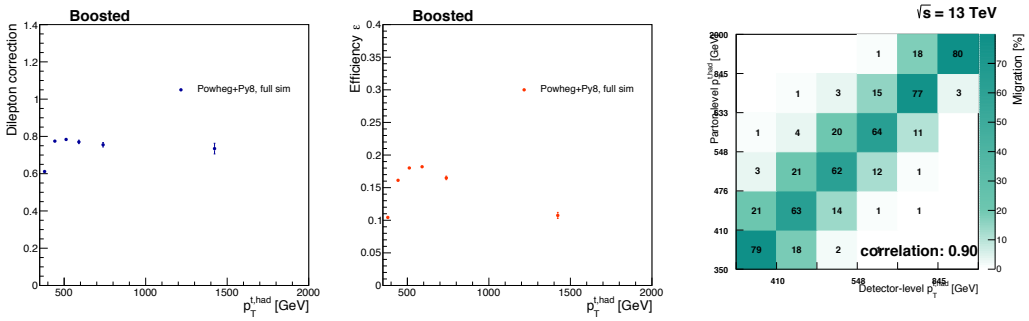

(A) (B) (C)

FIGURE 6.6: The (a) dilepton and (b) efficiency corrections (evaluated with several simulations samples), and the (c) detector-to-parton level migration matrix (evaluated with the nominal POWHEG+PYTHIA 8 simulation sample) for the hadronic top-quark transverse momentum in the boosted topology at parton level.

6.4 Unfolding procedure

The acceptance-corrected, background-subtracted distributions in data are unfolded to the particle or parton level (called truth level from now on) using the Iterative Bayesian method as implemented in RooUnfold [160]. Unfolding requires as input the response matrix between the truth-level and the measured distributions (corrected for acceptance and background as described above). For each spectrum, the response matrix is constructed from all events that pass both the truth and reconstructed level selection in the nominal $t\bar{t}$ MC sample. The migration matrix is then built from the response matrix by normalizing the reco bins in each truth-level bin to the sum of events in given truth-level bin. For all the variables, both at particle and parton level, the number of iterations has been set to 4. This value has not be optimized individually for each spectrum, but has been cross checked in terms of unfolding stability and bias.

6.5 Cross section extraction

The master formulas for the measurement of the differential cross-section in the fiducial phase-space in the resolved and boosted topologies then read

$$\frac{\mathrm{d}\sigma^{\mathrm{fid}}}{\mathrm{d}X^i} \equiv \frac{1}{\mathcal{L}\cdot\Delta X^i}\cdot\frac{1}{\epsilon^i}\cdot\sum_j \mathcal{M}_{ij}^{-1}\cdot f_{\mathrm{match}}^j\, f_{\mathrm{acc}}^j\cdot\left(N_{\mathrm{reco}}^j - N_{\mathrm{bkg}}^j\right)$$

and

$$\frac{\mathrm{d}\sigma^{\mathrm{fid}}}{\mathrm{d}X^i} \equiv \frac{1}{\mathcal{L}\cdot\Delta X^i}\cdot\frac{1}{\epsilon^i}\cdot\sum_j \mathcal{M}_{ij}^{-1}\cdot f_{\mathrm{acc}}^j\cdot\left(N_{\mathrm{reco}}^j - N_{\mathrm{bkg}}^j\right),$$

while the same formula for the full phase-space becomes

$$\frac{\mathrm{d}\sigma^{\text{full}}}{\mathrm{d}X^i} \equiv \frac{1}{\mathcal{L} \cdot \Delta X^i \cdot \text{BR}} \cdot \frac{1}{\epsilon^i} \cdot \sum_j \mathcal{M}_{ij}^{-1} \cdot f_{\text{dilep}}^j \cdot \left(N_{\text{reco}}^j - N_{\text{bkg}}^j \right),$$

where the inversion of the migration matrix symbolizes the regularized unfolding, index j stands for the reconstructed level while the i index labels bins at the particle level, ΔX^i is the bin width, $\mathcal{L}$ is the integrated luminosity and, for the full phase space unfolding only, BR is the branching fraction, which is needed to extrapolate the unfolded result in the ℓ+jets phase-space to the full phase-space. The unfolded differential cross-section is integrated to obtain the measured total cross-section, which is then used to define the normalized differential cross-section as

$$\frac{1}{\sigma} \frac{\mathrm{d}\sigma}{\mathrm{d}X^i}. \tag{6.9}$$

6.6 Unfolding validation

The unfolding procedure has been validated via closure and stress tests, described in the following sections.

6.6.1 Closure tests

Closure tests represent important checks of the consistency of the unfolding procedure. These tests allow to check that the unfolding procedure is able to correctly recover a statistically independent sample generated with the same modelling used in the production of the unfolding corrections.

The closure tests have been performed according to the following procedure:

1. the signal Monte Carlo sample is split in two, statistically-independent, halves. In these specific studies, the 'half-0' sample has been populated with events with even event number and the 'half-1' with events with odd event number;
2. one sample is taken as pseudo-data and the other one as signal Monte Carlo used in the evalution of the unfolding corrections. In these studies the half-0 sample has been used as pseudo-data and the half-1 as MC;
3. unfold the pseudo-data with the corrections obtained with the MC sample. In these tests the bayesian-inspired unfolding method, with a number of iterations set to 4, has been used;
4. check the compatibility of the unfolded pseudo-data and its corresponding true spectrum.

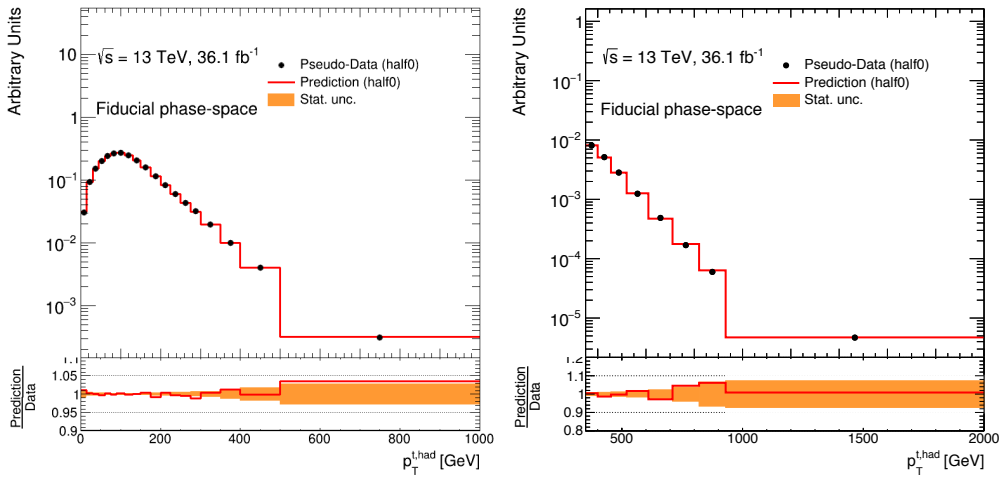

FIGURE 6.7: Closure tests for hadronic top p_{T} in the resolved and boosted topologies reconstructed using the pseudo top algorithm with matching selection

All the tests show that the unfolded results are in agreement with the pseudo-data within the only statistical uncertainties. An example of closure test for the p_{T} of the hadronically decaying top in the resolved and boosted topology is shown if Fig. 6.7.

6.6.2 Stress tests

Stress tests are additional checks performed by reweighting the MC in order to change the shapes of the distributions and then use this varied distribution as pseudo-data. Subsequently, the reweighted MC is unfolded with the nominal MC response and the unfolding result is compared to the reweighted MC particle-level distribution. Non-closure would indicate that the unfolding introduces a bias towards the training particle-level spectrum. Different reweight strategies have been used for the different spectra:

- linear reweighting as a function of the p_{T} of the hadronic top. The reweighting function for the resolved and boosted topologies has been defined as

$$f\left(p_{\mathrm{T}}^{t,\,\mathrm{had}}\right) = 1 + \frac{1}{800\mathrm{GeV}} \cdot p_{\mathrm{T}}^{t,\,\mathrm{had}}. \tag{6.10}$$

- reweighting based on the observed data/MC discrepancy:

$$f\left(X\right) = \frac{N_{\mathrm{Observed}}\left(X\right)}{N_{\mathrm{Expected}}\left(X\right)} \tag{6.11}$$

  where $X = p_{\mathrm{T}}^{t,\,\mathrm{had}}$, y^{had}, $m_{t\bar{t}}$, $p_{\mathrm{T}}^{t\bar{t}}$ in the resolved topology and $X = p_{\mathrm{T}}^{t\bar{t}}$, $m_{t\bar{t}}$ in the boosted topology.

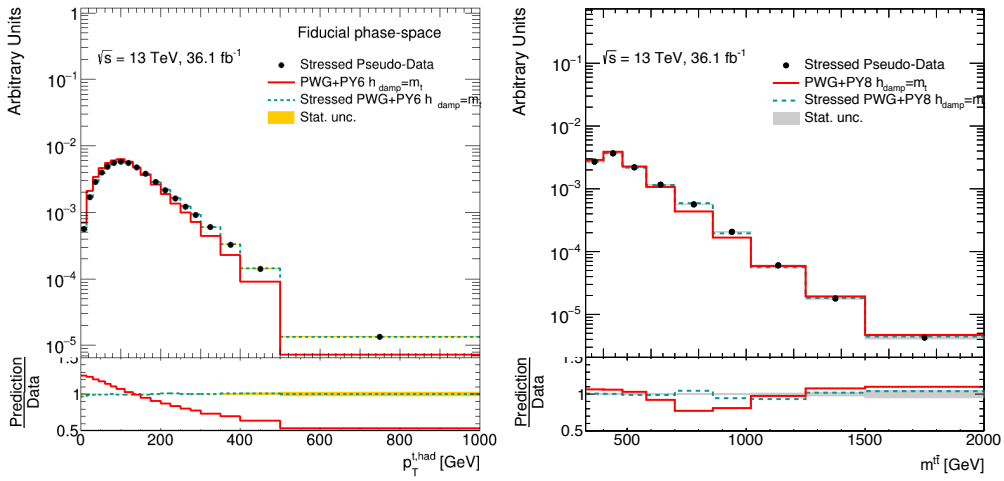

FIGURE 6.8: Stress test plots in the ℓ+jets channel performed by reweighting the p_{T} of the hadronic top (left) and the mass of the $t\bar{t}$ system (right) for the relative spectra.

- new physics stress test: a gaussian-shape bump has been introduced in the parton level $m_{t\bar{t}}$ spectrum:

$$f\left(m_{t\bar{t}}\right) = 1 + k \exp\left[-\left(\frac{m_{t\bar{t}} - m_0}{\sigma}\right)^2\right] \tag{6.12}$$

  where $m_0 = 800\,\mathrm{GeV}$, $\sigma = 100\,\mathrm{GeV}$ and $k = 0.5$.

Stress tests have been performed for each variable being unfolded using all the reweighting shapes. So, for example, the stress tests for the $m_{t\bar{t}}$ spectrum have been performed by reweighting the input spectrum using the input spectrum with all the shape functions described above: linear reweighting based on the p_{T} of the hadronic top and data/MC-based reweighting based on $m_{t\bar{t}}$, $p_{\mathrm{T}}^{t,\,\mathrm{had}}$, y^{had} and $p_{\mathrm{T}}^{t\bar{t}}$.

In general, the reweighting shapes based on the data/MC are not strong enough to put the unfolding procedure under a significant stress, while the linear reweighting based on the $p_{\mathrm{T}}^{t,\,\mathrm{had}}$ and gaussian reweightig based on $m_{t\bar{t}}$ are clearly unphysical but they are still recovered by the unfolding procedure, as shown in Figure 6.8.

All the stress tests show that the unfolding procedure correctly recovers the reweighted shape as indicated by the green line in plots which compares the stressed and unfolded distribution to the expected reweighted particle-level spectrum.

6.7 Rivet validation

The Rivet [111] toolkit (Robust Independent Validation of Experiment and Theory) has been already introduced and described in Section 3.10. Rivet is a system for the validation of Monte Carlo event generators, and it is used by phenomenologists, Monte Carlo generator

developers and experimentalists to compare the results of measurements in high energy physics with the theory predictions. Two routines are provided for the measurement described in this note, one routine that performs the same selection and reconstruction applied for the resolved topology and one for the boosted. The most important change in the implementation of the analysis workflow in the routines with respect to the previous $t\bar{t}\ell$+jets differential Rivet routines is the use of jet re-clustering in the boosted topology. The jet re-clustering has been implemented by exploiting the `FastJet` [161] classes and funcionalities in Rivet.

In order to validate the Rivet routines, a direct comparison is performed between the main objects and observables coming from the usual chain with the analysis framework and the ones that are the output of the Rivet routine. The closure tests have to be done running over the same Monte Carlo dataset. However, Rivet runs over EVNT files, not DxAOD such as the usual analyses. Therefore, it's necessary to use an EVNT file for Rivet and the exactly corresponding DxAOD for the analysis. The event and run numbers are not conserved between the EVNT file and the final DxAOD in the ATLAS production system, so an EVNT file and a DxAOD file have been provided with events in exactly the same order. Therefore, it was possible to do an event-by-event comparison.

Then, the particle-level prediction obtained by running the analysis framework on the whole nominal $t\bar{t}$ Monte Carlo sample (in DxAOD format), described in Sec. 3.8.1, is compared with the prediction coming from the Rivet routines running over the same $t\bar{t}$ sample (in EVNT format) for the full statistics available. There is a caveat for this comparison, indeed the EVNT file contains 60 millions of events while the DxAOD file consists of a subset of around 49 millions of those events. Therefore, the statistical unceratainty due to the number of generated events has to be taken into account to fairly compare the predictions. An example of this direct comparison is given in Figure 6.9 for the transverse momentum p_{T} of the hadronic pseudo-top quark.

Although Rivet is intended as a particle-level tool, it can access to the MC-truth record of the different Monte Carlo generators. So, it is possibile to get the informations of the simulated particles also at the parton level. This feature has been exploited to develop a partonic Rivet routine that faithfully reproduces the parton level results of the analysis. The partonic Rivet routine looses the generator-independency, but it gives robust results based on the *right definition* of the partonic top specific for each Monte Carlo generator. Once validated for a particular Monte Carlo generator, the Rivet routine at parton level could be used by all of the analyses that run over the same Monte Carlo generator. The phylosophy of the validation at particle level is the opposite: once validated for a Monte Carlo sample in an analysis, then all the simulated samples could be processed by the same Rivet routine at particle level.

The same procedure applied for the validation of the Rivet routine at particle level is used to validate the partonic Rivet routine. The parton-level prediction is obtained by runniing on the same DxAOD file as the particle level, while the partonic Rivet routine runs over the

same EVNT file as the particle level one. Then, the outputs are directly compared between each other and an example of this direct comparison is given in Figure 6.10 for the transverse momentum p_{T} of the top quark. The combination of both the particle- and parton-level Rivet routines provide a powerful tool to perform studies on the different Monte Carlo generators.

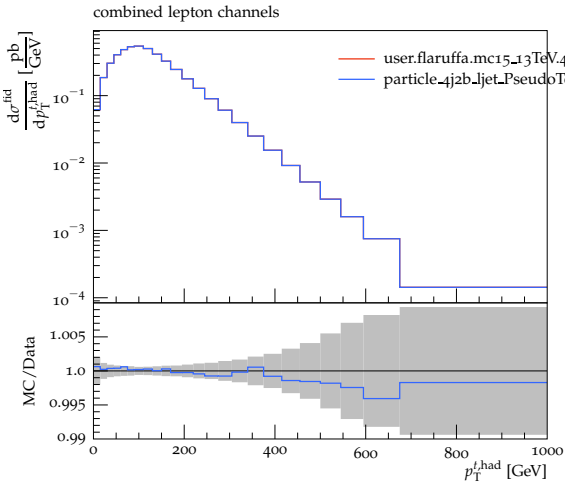

FIGURE 6.9: Particle level comparison between the nominal prediction obtained by running the analysis framework over the $t\bar{t}$ sample in DxAOD format (blue line) and the prediction coming from the resolved Rivet routine running over the same $t\bar{t}$ sample in EVNT format (red line) for the transverse momentum p_T of the hadronic pseudo-top quark in the ℓ+jets cahnnel. The grey band represents the statistical uncertainty.

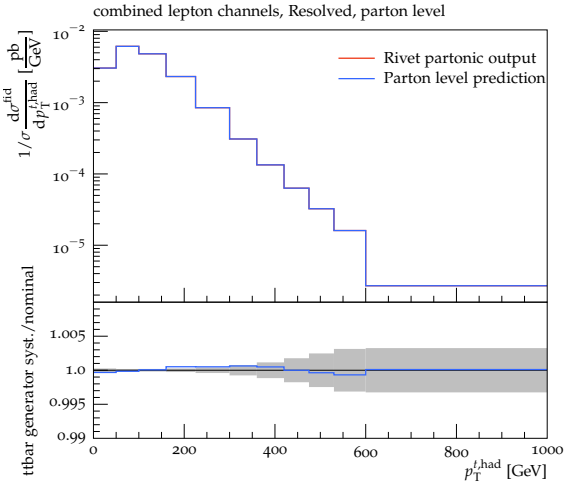

FIGURE 6.10: Parton level comparison between the nominal prediction obtained by running the analysis framework over the $t\bar{t}$ sample in DxAOD format (blue line) and the prediction coming from the resolved partonic Rivet routine running over the same $t\bar{t}$ sample in EVNT format (red line) for the transverse momentum p_T of the hadronic top quark in the ℓ+jets cahnnel. The grey band represents the statistical uncertainty.

Chapter 7

Systematic Uncertainties

Several sources of systematic uncertainty affect the measured differential cross-sections. The systematic uncertainties due to detector effects and the ones related to the modelling of the signal and background MC components, which are found to be the most relevant sources, are described in this Section.

To evaluate the impact of each uncertainty after the unfolding, the reconstructed distribution in simulation is varied, unfolded using corrections from the nominal POWHEG+PYTHIA8 signal sample, and the unfolded varied distribution is compared to the corresponding particle-level distribution. All detector- and background-related systematic uncertainties are evaluated using the same generator, while alternative generators and generator setups are employed to assess modelling systematic uncertainties. In these cases, the corrections, derived from one generator, are used to unfold the detector-level spectra of the alternative generator.

The detector-related uncertainties are described in Section 7.1 while the uncertainties on the $t\bar{t}$ signal and background modelling are discussed in Sections 7.2 and 7.3 respectively.

The complete breakdown of each source of systematic uncertainty on the final measurement is presented in Appendix F.

7.1 Detector systematics

The experimental uncertainties refer to the quality of the detector simulation to describe the detector response in data for each of the reconstructed objects. The systematics uncertainty is evaluated using the varied simulated signal to which a varied background is added and nominal background subtracted, followed by the unfolding procedure using the nominal correction factors.

7.1.1 Lepton reconstruction

The uncertainties related to the MC modeling of the lepton trigger, identification, energy or momentum resolution and reconstruction efficiencies are estimated from $Z \to ee/\mu\mu$, $J/\psi \to ee/\mu\mu$, and $W \to e\nu$ processes using techniques discussed in References [123, 162].

These uncertainties are relatively small, dominated by the lepton identification in the e+jets channel and the muon triggering efficiency in the μ+jets channel. They are specific to each lepton flavor and thus uncorrelated between the channels.

7.1.2 Jet reconstruction

The impact of the uncertainty on the Jet Energy Scale is estimated by varying the jet energies according to the uncertainties derived from simulation and in-situ calibration measurements using a model with a reduced set of 29 orthogonal components representing the steps of the calibration procedure [128].

The uncertainty due to the difference in Jet Energy Resolution between the data and MC events is evaluated by smearing the MC jet transverse momentum according to the jet resolution as a function of the jet p_{T} and η [128].

7.1.2.1 Jets from gluons and quarks response

The calorimeter response, defined as the ratio between the value of the p_{T} of the reconstructed jet and the p_{T} of the truth jet, depends on the flavor of the parton that initiates the jet and in particular whether this parton is a quark or gluon [**?**]. The flavor composition of each specific analysis could be different from the samples used for the calibration, so a systematic uncertainty is introduced to take into account this possible variation. This uncertainty is given by the following formula:

$$\Delta\mathcal{R}_S = \Delta f_g \times (\mathcal{R}_g - \mathcal{R}_q) \oplus f_g \times \Delta\mathcal{R}_g \tag{7.1}$$

where $\mathcal{R}_g$ and $\mathcal{R}_q$ represent the response of jets initiated by light quarks and gluons, respectively. $\Delta\mathcal{R}_g$ is the uncertainty associated to the response of the jets initiated by gluons while f_g and Δf_g are the fraction of the jets initiated by gluons and its corresponding uncertainty. The first term of the equation 7.1 is the uncertainty on the flavor composition while the second term is the uncertainty on the response of the jets initiated by gluons. In the previous analyses at 13 TeV in ℓ+jets channel [51, 55], the fraction of the jets initiated by gluons was set to a non-optimized value of 0.5 as well as the fraction of the jets initiated by light quarks with a 100% of uncertainty ($f_g = 0.5 \pm 0.5$). A specific study is performed to estimate a more realistic description of the fraction of the jets initiated by gluons for the selection applied in the analysis. The aim of this specific estimate is to reduce this uncertainty that is one of

the most significant component of the total JES uncertainty. The details of this study are presented in Appendix D.

The total jet reconstruction systematic uncertainties are for all the $t\bar{t}$ differential cross-sections in the resolved and boosted topologies at the level of 5–10%.

7.1.3 b-tagging

The systematic uncertainties associated with tagging jets originating from b-quarks are separated into three categories. These are the efficiency of the tagging algorithm (b-quark tagging efficiency), the mis-tag efficiency with which jets originating from c-quarks pass the b-tag requirement (c-quark misidentified tagging efficiency) and the rate at which light-flavour jets are tagged (light-quark misidentified tagging efficiency). The efficiencies are estimated from data and parameterised as a function of p_{T} and η. The systematic uncertainties arise from the scale factors used to correct the differences between the simulation and data in each of the categories, extensively described in Section 4.5. The uncertainties in the simulation modelling of the b-tagging performance are assessed by studying b-jets in dileptonic $t\bar{t}$ events [143]. The uncertainty associated to the b-tagging efficiency is a large contributor of about 10% to the overall systematic uncertainty and tends to slightly increase with p_{T}^{t}, but is much reduced for the relative cross-sections, though still dominant.

7.1.4 Missing transverse momentum

The systematic uncertainties associated with the momenta and energies of reconstructed objects (leptons and jets) are also propagated to the $E_{\mathrm{T}}^{\mathrm{miss}}$ calculation. The $E_{\mathrm{T}}^{\mathrm{miss}}$ reconstruction receives also contributions from the presence of low-p_{T} jets and calorimeter cells not included in reconstructed objects ("soft terms"). The systematic uncertainty on soft terms are evaluated using $Z \rightarrow \mu\mu$ events from the $E_{\mathrm{T}}^{\mathrm{miss}}$ data/MC ratio in events without jets and from the balance between soft terms and hard objects using methods similar to those used in [163]. The $E_{\mathrm{T}}^{\mathrm{miss}}$ measurement is affected by a small systematic uncertainty (below ±1%). In both topologies, the systematic uncertainty on this quantity affects in principle the reconstruction of the leptonic top and, as a consequence, of the $t\bar{t}$ system. Moreover, in the boosted topology it enters in the selection, where a requirement is applied on the $E_{\mathrm{T}}^{\mathrm{miss}}$ in the event. However, this uncertainty is sub-dominant for both boosted and resolved topologies.

7.1.5 Luminosity

The uncertainty on the combined 2015+2016 integrated luminosity is 2.1%. It is derived, following a methodology similar to that described in [164], from a calibration of the luminosity scale using $x - y$ beam-separation scans performed in August 2015 and May 2016.

7.2 Signal modelling systematics

The MC samples used as alternative $t\bar{t}$ samples to study the uncertainty related to the $t\bar{t}$ signal modeling have been already discussed in Section 3.8.2. In the following sections, the methodology followed in this analysis to evaluate these uncertainties is presented.

7.2.1 MC generator: matrix element and parton shower models

The choice of the MC generator used in the signal modelling affects the kinematic properties of simulated $t\bar{t}$ events and reconstruction efficiencies. For the purpose of addressing this effect, $t\bar{t}$ events simulated with different settings of POWHEG and aMC@NLO with various parton shower implementations and SHERPA have been used to assess the impact of different NLO matrix element calculations and parton shower models.

The uncertainty due to the choice of matrix element generator is determined by unfolding SHERPA sample using corrections and response matrices from the POWHEG+PYTHIA8 sample. The unfolded result is then compared to the particle level spectrum of the SHERPA sample and that relative uncertainty is used as the systematic uncertainty due to the choice of the ME generator. The resulting systematic uncertainty is found to be 5-10% and it strongly depends on the variable and bin under study, as the modelling is a dominant systematics for the normalized cross-sections. At the early stages of the analysis, the generator uncertainty was estimated using a $t\bar{t}$ sample generated with MADGRAPH5_aMC@NLO +PYTHIA8, still compared with the nominal $t\bar{t}$ sample produced using POWHEG+PYTHIA8. The large differences with the nominal generator for the particle-level distributions, shown in Appendix E, reflected in an unrealistic large uncertainty in various regions of the phase-space. These large differences are due to a non-optimal setting of the shower starting scale in the available MADGRAPH5_aMC@NLO +PYTHIA8 sample. In addtion, the large fraction of negative weights in MADGRAPH5_aMC@NLO, which reaches even the 40% of the total in the high $p_{\mathrm{T}}^{t}$and $p_{\mathrm{T}}^{t\bar{t}}$tails, caused an effective decrease in statistics and as a consequence an enhanced modeling uncertainty due to statistical fluctuations. This study are carried out by using the validated Rivet routines and performed at the particle and parton levels.

The uncertainty due to choice of parton shower/hadronization model is determined by unfolding a POWHEG +HERWIG7 AFII sample with respect to a POWHEG+PYTHIA8 AFII sample. The uncertainty is then projected onto the POWHEG+PYTHIA8 FullSim sample by taking the relative difference with respect to the POWHEG +HERWIG7 truth spectrum, and symmetrized.

7.2.2 Initial- and final-state QCD radiation for the signal sample

The amount of ISR/FSR changes in particular the number of jets in the event as well as the transverse momemtum of the $t\bar{t}$ system. In order to evaluate the uncertainty related to

the modelling of the ISR/FSR, $t\bar{t}$ MC samples with modified ISR/FSR modeling are used. In particular, the ufolding procedure is applied to a sample generated using POWHEG+PYTHIA8, where the factorization and renormalization scales, as well as the the h_{damp} parameter have been co-varied as follows [165]: one of the samples is defined as scaling μ_R and μ_F by 0.5 with respect to their nominal values, while simultaneously changing the h_{damp} to the value of $3m_t$, and using the Var3cUp eigentune from the A14 tune. The other variation, is defined by scaling μ_R and μ_F by 2, keeping $h_{\text{damp}} = 1.5m_t$ and using the Var3cDown eigentune from the A14. In each case, the spectrum unfolded using the nominal POWHEG+PYTHIA8 generator is compared to the truth-level spectrum of the corresponding generator.

7.2.3 Parton distribution functions

The impact of the choice of different PDF sets has been assessed by applying an event-by-event reweighting procedure to a $t\bar{t}$ sample generated with POWHEG+PYTHIA8 using the 30 PDF set of the PDF4LHC15 prescription [166] as well as using the central value of the NNPDF3.0 PDF set.

The effect of a different PDF choice modifies the efficiency, acceptance and potentially also the response matrix, i.e. the corrections used to correct the spectrum at the detector level to the particle and parton levels. The impact of the PDF choice has been evaluated by unfolding the nominal POWHEG+PYTHIA8 sample using differently PDF-reweighted corrections. The so-called "intra-PDF" variations using the PDF4LHC15 set are combined to define a relative uncertainty as

$$\delta_{\text{intra}} \equiv \frac{\sqrt{\sum_{i \in \text{sets}} (U_i \cdot R_0 - T_0)^2}}{T_0}$$

while the relative "inter-PDF" between the NNPDF3.0 and the PDF4LHC15 central is evaluated as

$$\delta_{\text{inter}} \equiv \frac{U_{\text{NNPDF3.0}} \cdot R_0 - T_0}{T_0}$$

where the 0 (i) subscripts denotes the PDF4LHC15 central (varied) PDF set, R represents the distribution at the detector level while T symbolizes the distribution at the truth level, and the unfolding procedure is shortened into the U factor, with subscript on each characterizing the PDF set used to evaluate the spectrum or the corrections. The resulting uncertainties are found to be at the sub-percent level, with few excesses to 1 or 2% in low-statistics bins.

7.2.4 MC generator: Finite sample statistics

To account for the limited statistics of the signal sample, pseudo-experiments are used to evaluate the impact of finite statistics. The number of events in each bin is smeared by a Gaussian shift with mean equal to the yield of the bin, and standard deviation equal to the uncertainty of the bin. Then, the smeared spectrum is unfolded and the procedure is

replicated ten thousand times. The final statistical uncertainty is evaluated from the average over the ten thousand toys. The resulting systematic uncertainty is found to be typically below 0.5%, increasing to 1 – 2% in the tails of particular distributions.

7.3 Background modelling systematics

The individual experimental and theoretical uncertainties are used to calculate the uncertainty of the background contributions determined by MC simulation. This translates into an uncertainty on the background subtraction used in the unfolding procedure. The systematic uncertainty is evaluated using the nominal simulated signal to which a varied background is added and nominal background subtracted, followed by the unfolding procedure using the nominal correction factors.

7.3.1 Systematics on W+jets

Two different uncertainty components, based on α_S and μ_R and μ_F scale variations and calculated following the prescriptions reported in Reference [149], are applied to the MC prediction of the W+jets samples. The scale uncertainty is calculated by evaluating the envelop of 6 variations, that differ for the values of the factorization and normalization scales:

- $\mu_r = 0.5 \cdot \mu_r^{\text{ref}}$ and $\mu_f = 0.5 \cdot \mu_f^{\text{ref}}$
- $\mu_r = 0.5 \cdot \mu_r^{\text{ref}}$ and $\mu_f = \mu_f^{\text{ref}}$
- $\mu_r = \mu_r^{\text{ref}}$ and $\mu_f = 0.5 \cdot \mu_f^{\text{ref}}$
- $\mu_r = 2 \cdot \mu_r^{\text{ref}}$ and $\mu_f = 2 \cdot \mu_f^{\text{ref}}$
- $\mu_r = 2 \cdot \mu_r^{\text{ref}}$ and $\mu_f = \mu_f^{\text{ref}}$
- $\mu_r = \mu_r^{\text{ref}}$ and $\mu_f = 2 \cdot \mu_f^{\text{ref}}$

and then considering the final scale uncertainty as symmetrized. The uncertainty due to the PDF variations is found to be sub-dominant and subsequently not included.

An additional uncertainty is considered on the fraction of the heavy-flavours components. This uncertainty is evaluated applying a 50% shift on the cross-section of the b-filtered sample and re-scaling also the other samples in order to keep constant the total W+jets cross section. This uncertainty is considered sufficient to cover a possible mis-modelling of the heavy-flavours composition since no disagreements among predictions and data has been observed.

7.3.2 Systematics on Z + jets

A global uncertainty, based on α_s, PDF and μ_F and μ_R scale variations and calculated in Reference [149], is applied to the MC prediction of the Z+jets background components. These uncertainties, evaluated in bins of jet multiplicity, are reported in Table 7.1.

N_{jet} bin	Uncertainty [%]
0	1.2
1	2.3
2	16.9
3	40.5
4	53.0
5	56.8
6	57.2
≥ 7	56.1

TABLE 7.1: Fractional uncertainty on the Z+jets prediction in exclusive bins of jet multiplicity.

7.3.3 Single top

For the single top background, three component of uncertainties are applied:

1. total normalization uncertainty: the cross-section of the single-top process has been varied within uncertainty for the t-channel [109], s-channel [108] and Wt associate production [107], shown in Table 1.2;
2. ISR/FSR uncertainty: single top (Wt- and t-channel) MC AFII samples with modified ISR/FSR modeling are used in a similar way of what has been done for the ISR/FSR systematics for the signal sample;
3. DR/DS uncertainty: the uncertainty due to the overlap of the Wt-channel of single top production and $t\bar{t}$ production has been evaluated by comparing the single top samples obtained using the diagram removal and diagram subtraction schemes [50].

7.3.4 Diboson and $t\bar{t}V$

A 40% uncertainty is applied to the diboson background, including the uncertainty on the cross-section and a contribution due to the presence of two additional jets.

For the $t\bar{t}V$ background, an overall uncertainty of 14% has been applied, covering the uncertainties related to the scale, α_S and PDF for the $t\bar{t}W^{\pm}$ and $t\bar{t}Z$ components.

7.3.5 Non-prompt and fake lepton background

The following components of systematic uncertainty of the non-prompt and fake lepton background estimates are evaluated:

Alternative parametrization An uncertainty due to the choice of the parametrization of the fake and real efficiencies has been assessed by using an alternative choice, based on the variables affected by the largest data/MC discrepancies. The alternative parametrisations used are shown in Table 7.2.

Overall normalization uncertainty Given the disagreements of the fake lepton background predictions with data for several variables in dedicated control regions, an additional overall 50% uncertainty on the fake lepton background yield has been assigned.

Topology	Channel	Alternative real efficiency parametrisation	Alternative fake efficiency parametrisation
Resolved	e+jets	$\eta^{\ell} \oplus p_{\mathrm{T}}^{\mathrm{jet1}} \oplus \Delta R$	$\eta^{\ell} \oplus p_{\mathrm{T}}^{\mathrm{jet1}} \oplus \Delta\phi$
Resolved	μ+jets	$\eta^{\ell} \oplus p_{\mathrm{T}}^{\ell} \oplus \Delta R$	$\eta^{\ell} \oplus p_{\mathrm{T}}^{\ell} \oplus \Delta\phi$
Boosted	e+jets	$\eta^{\ell} \oplus p_{\mathrm{T}}^{\mathrm{jet1}} \oplus \Delta R$	$\eta^{\ell} \oplus p_{\mathrm{T}}^{\mathrm{jet1}} \oplus \Delta\phi$
Boosted	μ+jets	$\eta^{\ell} \oplus p_{\mathrm{T}}^{\ell} \oplus \Delta R$	$\eta^{\ell} \oplus p_{\mathrm{T}}^{\mathrm{jet1}} \oplus \Delta\phi$

TABLE 7.2: Alternative fake parametrisation for the different topologies and channels used to evaluate a systematic uncertainty on the fake lepton background.

7.4 Unfolding systematics

The non-closure on MC, described in Section 6.6.1, is at a few per-cent level, but consistent with statistical fluctuations and MC statistical uncertainty. Therefore, non-closure is not assumed as a systematics, since the effect on simulation seems purely statistical.

Chapter 8

Results

In this Section, the measurements of the $t\bar{t}$ production cross-sections are presented as a function of kinematic observables. In the following, the indices *had* and *lep* refer to the hadronically and semileptonically decaying top quarks, respectively.

In general, a set of baseline observables is presented: transverse momentum ($p_{\mathrm{T}}^{t,\,\mathrm{had}}$) and absolute value of the rapidity (y^{had}) of the hadronic top quark, and the transverse momentum ($p_{\mathrm{T}}^{t\bar{t}}$)), rapidity ($y_{t\bar{t}}$) and invariant mass ($m_{t\bar{t}}$) of the $t\bar{t}$ system. These observables have been previously measured in the fiducial phase-space by the ATLAS experiment using the data collected in 2015 at 13 TeV [51], except for the $t\bar{t}$ system variables which have not been measured in the boosted topology. The level of agreement between data and predictions is within the quoted uncertainties. A trend is observed in the $p_{\mathrm{T}}^{t,\,\mathrm{had}}$ distribution, which is not well modelled by MC at high values.

The measurements of the differential $t\bar{t}$ cross-sections in the fiducial phase-space are presented in Section 8.1, for both the resolved and boosted topology. The absolute distributions are compared with several SM predictions obtained using different MC generators. The POWHEG-BOX generator, denoted "PWG" in the figures, is employed with two different parton-shower models, namely PYTHIA 8 and HERWIG 7, as well as two extra settings for radiation modeling. Finally, an additional NLO generator is compared to the data, namely SHERPA. All of these samples are described in detail in Section 3.8. The comparisons between data and predictions will be focused on the general agreement of the different MC models used to describe the $t\bar{t}$ production. For this reason, the differential cross-sections are also measured as a function of observables depending on the transverse momentum of the decay products of the top quark, since they have been found to be sensitive to higher-order corrections [167, 168]:

- the out-of-plane momentum ($p_{\mathrm{out}}^{t\bar{t}}$), i.e. the projection of top-quark three momentum onto the direction perpendicular to a plane defined by the other top quark and the

beam axis (z) in the laboratory frame [169]:

$$p_{\text{out}}^{t\bar{t}} = \vec{p}^{\,t,\text{had}} \cdot \frac{\vec{p}^{\,t,\text{lep}} \times \hat{z}}{\left|\vec{p}^{\,t,\text{lep}} \times \hat{z}\right|} \tag{8.1}$$

- the scalar sum of the transverse momenta of the two top quarks ($H_T^{t\bar{t}}$) [167, 168].

They have been previously measured in the resolved topology by the ATLAS experiment using the 8 TeV dataset [52] and the out-of-plane momentum also using the 13 TeV dataset, as a function of the jet multiplicity [170]. The level of agreement between data and prediction is within the quoted uncertainties. The inclusion of double differential measurements enhances the discriminating power between the different predictions and in this Section a set of the aforementioned observables is choosen to demonstrate sensitivity to the different aspects of the MC $t\bar{t}$ modelling.

The measurements of the differential $t\bar{t}$ cross-sections in the full phase-space are presented in Section 8.2, for both the resolved and boosted topology. A set of single and double differential NNLO QCD predictions have been provided by Czakon, Mitov and Papanastasiou following the procedure described in References [42, 45] with the optimised binning chosen for this analysis. Therefore, the parton-level distributions are compared with the NNLO QCD predictions in order to perform stringent tests of the pQCD. The availability of the theoretical distributions with the optimised binning ensures the best sensitivity for this study. The predictions have been provided for different sets of PDFs, in particular CT14, NNPDF31, MMHT2014, NNPDF31 and PDF4LHC15. Results are provided for 7 scale combinations: (μ_R, μ_F) = ((1,1), (2,1), (1,2), (0.5,1), (1,0.5), (0.5,0.5), (2,2)) $\times$ μ_0, where $\mu_0 = H_T/4$ for all the observables, apart from p_T of the top, for which is set to $M_t/2$. The uncertainty included in the following plots for the NNLO QCD predictions is evaluated by taking the envelope of all the μ_{R} and μ_{F} variations. NNPDF31 is taken as the reference PDF set. The results are not significantly affected by this arbitrariness as all the predictions with different PDFs are compatible within the scale uncertainty described below, even in the regions of the phase-space more sensitive to the PDF choice. In addition, SM predictions obtained using the nominal $t\bar{t}$ MC sample, namely POWHEG+PYTHIA8, are included in the comparisons. Also in the case of distributions in the full phase-space, the inclusion of double differential measurements enhances the discriminating power of the tests on the fixed-order calculations.

8.1 Results in the fiducial phase space

8.1.1 Resolved topology

In the resolved topology, single differential cross-sections have been measured in the fiducial phase-space as a function of the mass, transverse momentum and rapidity of the $t\bar{t}$

system, transverse momentum and rapidity of the top and as function of the additional variables $\left|p_{\text{out}}^{t\bar{t}}\right|$ and $H_T^{t\bar{t}}$.

Double differential cross-sections have been measured as a function of the p_{T} of the hadronically-decaying top in bins of the p_{T} of the $t\bar{t}$ system and the p_{T} of the $t\bar{t}$ system in bins of the mass of the $t\bar{t}$ system. Moreover, the distributions of the p_{T} and mass of the $t\bar{t}$ system have been measured as function of the jet multiplicity. All the measurements have been compared with the Monte Carlo predictions.

The Monte Carlo predictions show good agreement with the data in the single differential cross-section measurements, with the exception of the differential cross-section as a function of the p_{T} of the $t\bar{t}$ system shown in Figure 8.2b and the cross-section as a function of $H_T^{t\bar{t}}$ where all the MC predictions, except for the POWHEG+PYTHIA 8 prediction with the Var3cDown tuning, show a trend overestimating the data in the high-p_{T} regions. A similar trend is observed in the double-differential cross sections as a function of the p_{T} of the $t\bar{t}$ system in bins of jet multiplicity (Figures 8.6b and 8.7b).

The MC description of the p_{T} of the hadronic top is improved with respect to previous ATLAS analyses, even though a slight tension is still present in the high-p_{T} tail. The p_{T} of the $t\bar{t}$ system in bins of the mass of the $t\bar{t}$ system shows the discriminating power of a double differential cross-section at particle level, promising for future developments in MC tuning, similar to p_{T} of the $t\bar{t}$ system in bins of jet multiplicity already presented in Reference [55].

All the shown results for the absolute cross-section in the resolved topology at the particle level are tabulated and presented in Appendix F together with the complete breakdown of the systematic uncertainties and the corresponding relative cross-sections.

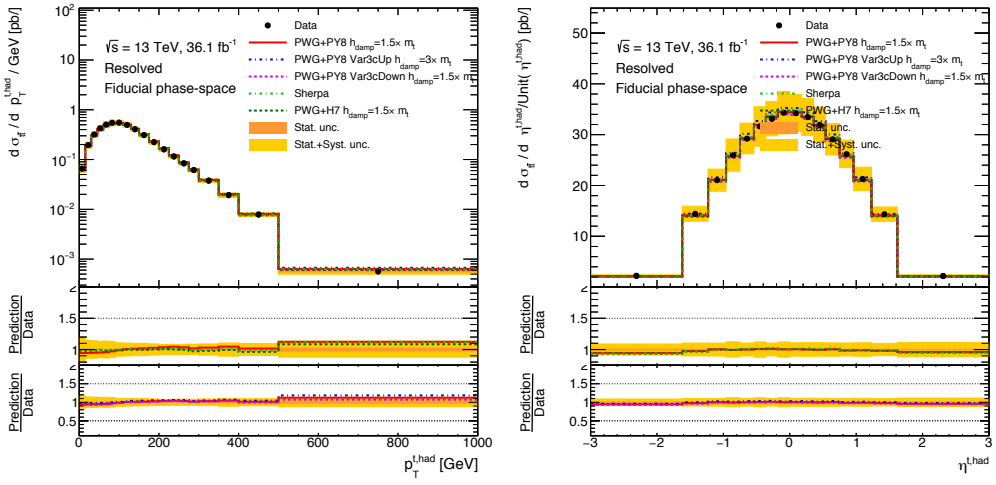

(A) (B)

FIGURE 8.1: Particle-level differential cross-sections as a function of p_{T} (a) and the rapidity (b) of the hadronically decaying top, compared with the nominal POWHEG+PYTHIA 8 prediction. The bands indicate the total uncertainty in the data in each bin. The POWHEG+PYTHIA 8 event generator is used as the nominal prediction to correct for detector effects, parton showering and hadronization.

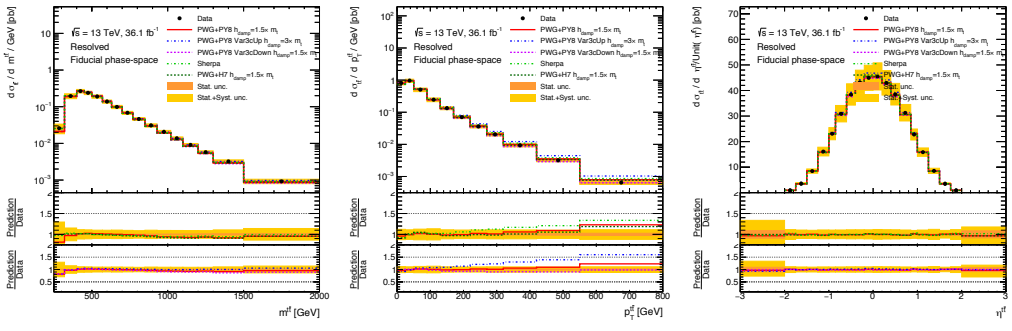

(A) (B) (C)

FIGURE 8.2: Particle-level differential cross-sections as a function of (a) the mass, (b) the transverse momentum and (c) the rapidity of the $t\bar{t}$ system in the resolved topology, compared with different Monte Carlo predictions. The bands indicate the total uncertainty in the data in each bin. The POWHEG+PYTHIA 8 event generator is used as the nominal prediction to correct for detector effects, parton showering and hadronization. Data points are placed at the center of each bin.

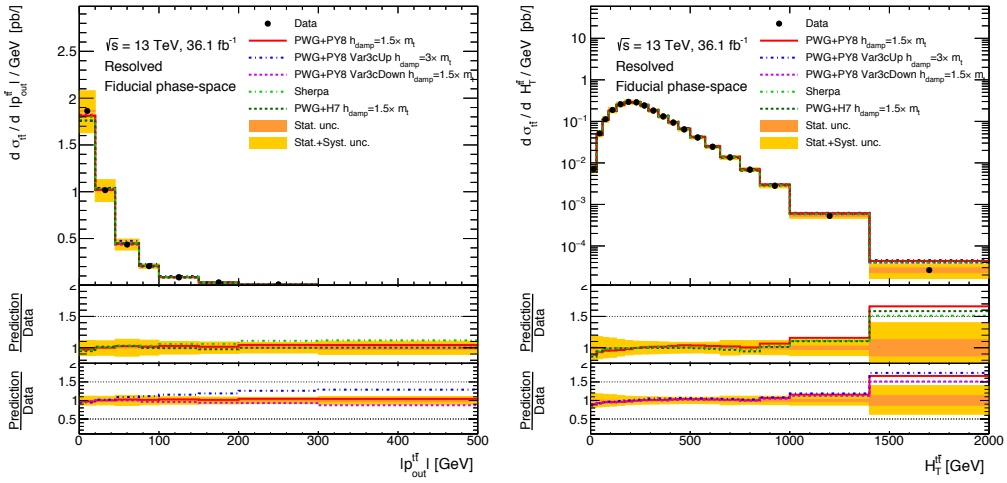

(A) (B)

FIGURE 8.3: Particle-level differential cross-sections as a function of (a) $|p_{\text{out}}^{t\bar{t}}|$ and (b) $H_T^{t\bar{t}}$ in the resolved topology, compared with different Monte Carlo predictions. The bands indicate the total uncertainty in the data in each bin. The POWHEG+PYTHIA 8 event generator is used as the nominal prediction to correct for detector effects, parton showering and hadronization. Data points are placed at the center of each bin.

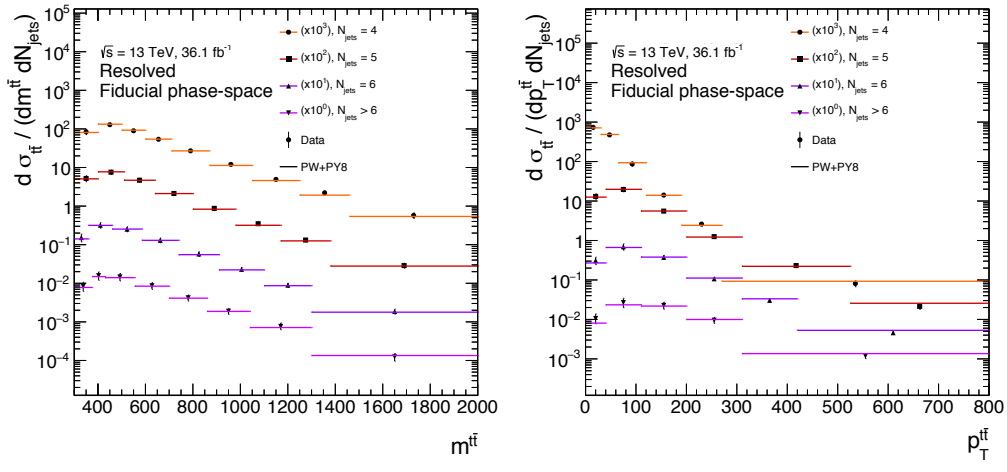

(A) (B)

FIGURE 8.4: Particle-level differential cross-sections as a function of (a) the mass of the $t\bar{t}$ system and (b) the p_{T} of the $t\bar{t}$ system in bins of jet multiplicity, compared with the nominal POWHEG+PYTHIA 8 prediction. The POWHEG+PYTHIA 8 event generator is used as the nominal prediction to correct for detector effects, parton showering and hadronization.

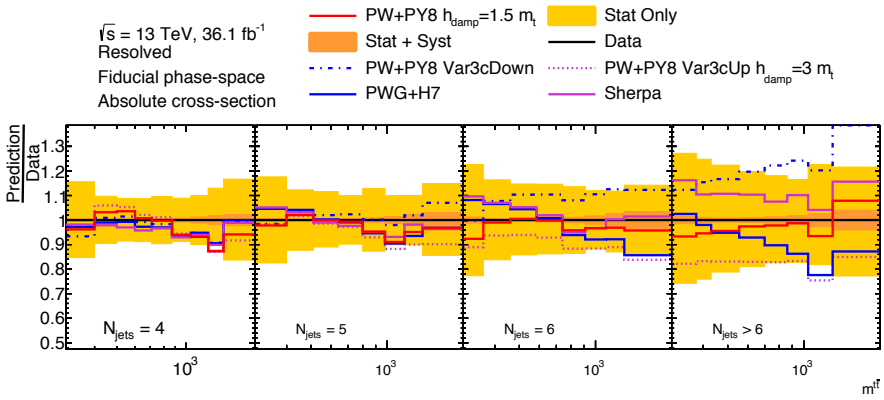

(A)

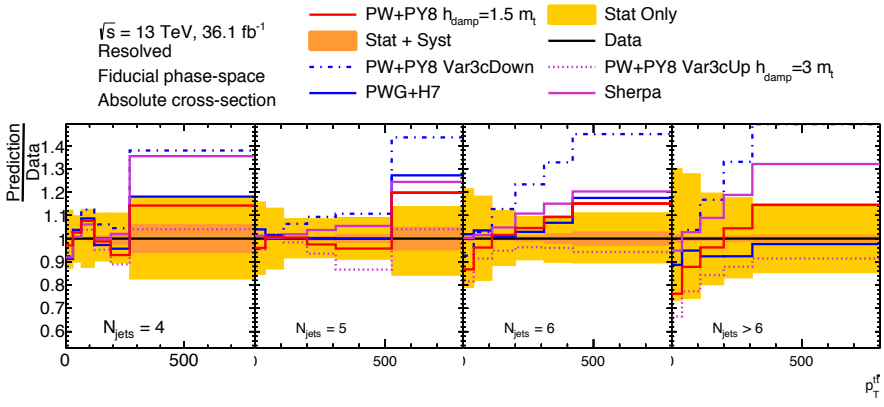

(B)

FIGURE 8.5: Ratios of the Monte Carlo predictions divided by the data for the particle-level differential cross-sections as a function of (a) the mass of the $t\bar{t}$ system and (b) the p_{T} of the $t\bar{t}$ system in bins of jet multiplicity. The bands indicate the total uncertainty in the data in each bin. The POWHEG+PYTHIA 8 event generator is used as the nominal prediction to correct for detector effects, parton showering and hadronization.

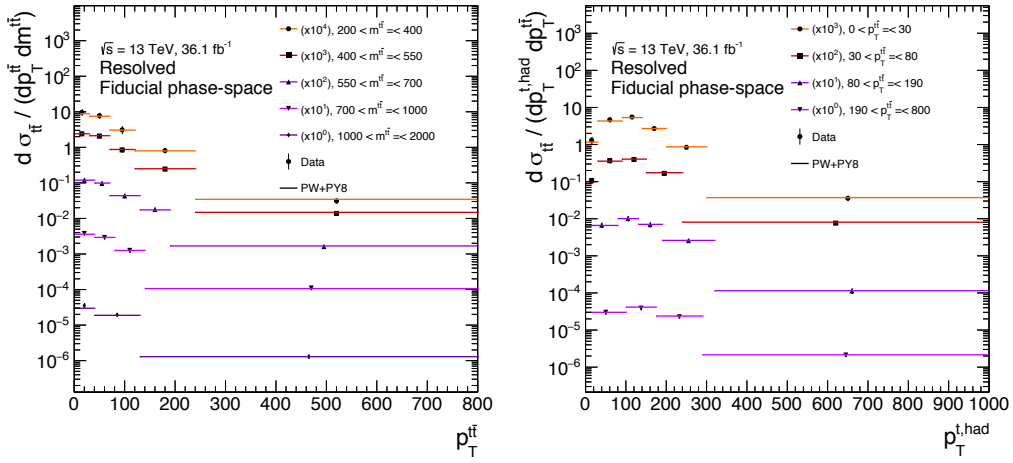

(A) (B)

FIGURE 8.6: Particle-level differential cross-sections as a function of the transverse momentum of the $t\bar{t}$ system in bins of the mass of the $t\bar{t}$ system (a) and (b) the transverse momenum of the hadronic top in bins of the p_{T} of the $t\bar{t}$ system, compared with the nominal POWHEG+PYTHIA 8 prediction. The POWHEG+PYTHIA 8 event generator is used as the nominal prediction to correct for detector effects, parton showering and hadronization.

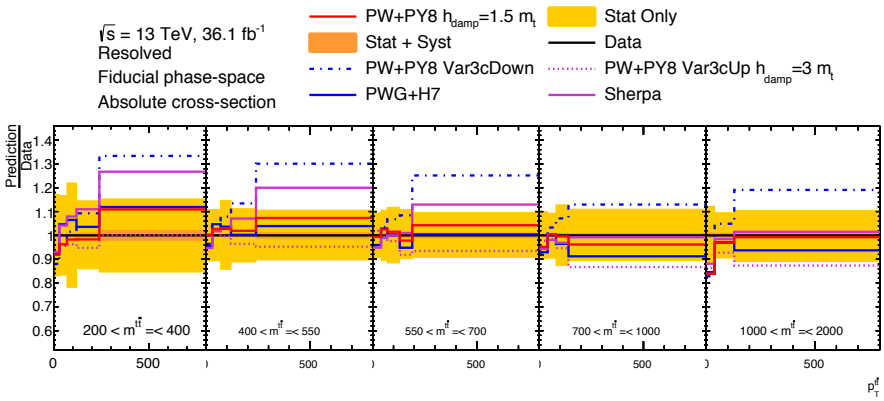

(A)

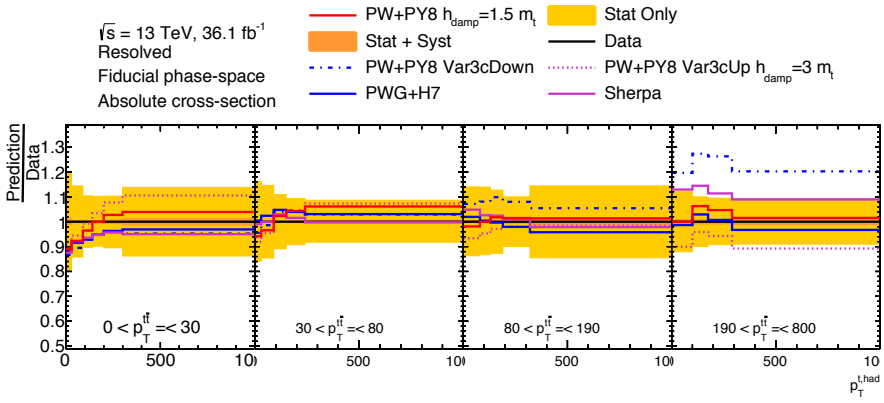

(B)

FIGURE 8.7: Ratios of the Monte Carlo predictions divided by the data for the particle-level differential cross-sections as a function of the $t\bar{t}$ system in bins of the mass of the $t\bar{t}$ system (a) and the transverse momenum of the hadronic top in bins of the p_{T} of the $t\bar{t}$ system (b). The bands indicate the total uncertainty in the data in each bin. The POWHEG+PYTHIA 8 event generator is used as the nominal prediction to correct for detector effects, parton showering and hadronization.

8.1.2 Boosted topology

In the boosted topology, single differential cross-sections have been measured in the fiducial phase-space as a function of the mass, transverse momentum and rapidity of the $t\bar{t}$ system, transverse momentum and rapidity of the top and as function of the additional variables $|p_{\text{out}}^{t\bar{t}}|$ and $H_T^{t\bar{t}}$.

Double differential cross-sections have been measured as a function of the p_{T} of the hadronically-decaying top and the mass and transverse momentum of the $t\bar{t}$ system in bins of the jet multiplicity, the p_{T} of the hadronic top in bins of the p_{T} of the $t\bar{t}$ system, the mass of the $t\bar{t}$ system in bins of the p_{T} of the $t\bar{t}$ system. All the measurements have been compared with the Monte Carlo samples.

The Monte Carlo predictions show tensions with the data in single differential cross-section measurements as a function of the p_{T} of the hadronic top, shown in Figure 8.8a, the mass of the $t\bar{t}$ system, shown in Figure 8.9a, and $H_T^{t\bar{t}}$, shown in Figure 8.10b, where all the MC predictions show a trend in overestimating the data in the tails of the distributions. To a smaller extent, tensions are observed in all predictions at high values in $y_{t\bar{t}}$ spectrum, shown in Figure 8.9c, and in the tails of the $|p_{\text{out}}^{t\bar{t}}|$ distribution, shown in 8.10a, where only the prediction by POWHEG+PYTHIA 8 Var3cDown and POWHEG +HERWIG 7 show good agreement with the data.

The mismodelling of the p_{T} of the hadronic top is observed in the double-differential cross section, in all the bins of $p_{\text{T}}^{t\bar{t}}$, shown in Figure 8.13b. Finally, Figure 8.11a shows that enhanced sensitivity can be gained by measuring double differential cross-section as a function of the p_{T} of hadronic top in bins of the additional jet multiplicity: in the low jet multiplicity region, the POWHEG+PYTHIA 8 predictions overshoot the data, while in the high jet multiplicity region the predictions from SHERPA and POWHEG+PYTHIA 8 show a significant disagreement with the data in the tails of the distributions.

In general, the double differential distributions show a high discriminating power that combined with the Rivet routine of this analysis can be exploited to further improve the MC modeling of the $t\bar{t}$ production in the specific phase-space of the boosted regime.

All the shown results for the absolute cross-section in the boosted topology at the particle level are tabulated and presented in Appendix F together with the complete breakdown of the systematic uncertainties and the corresponding relative cross-sections.

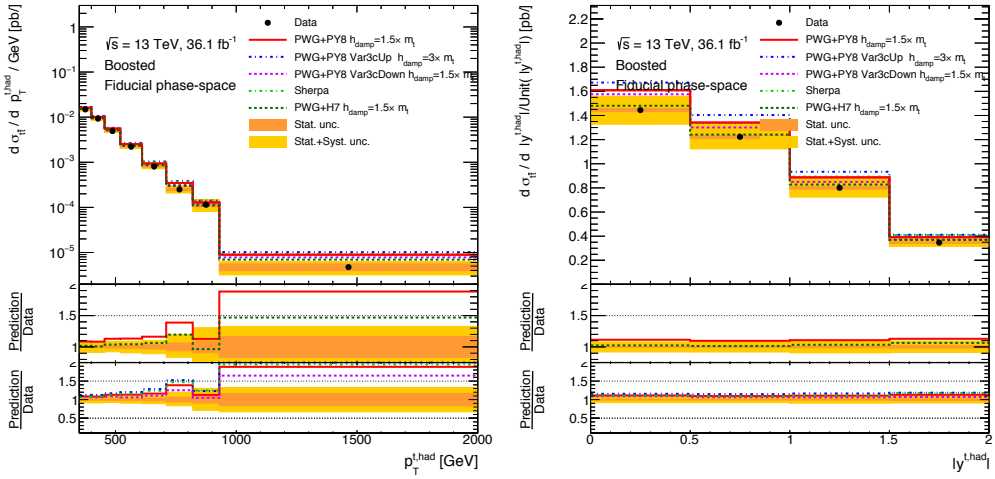

(A) (B)

FIGURE 8.8: Particle-level differential cross-sections as a function of (a) the p_{T} and (b) absolute value of the rapidity of the hadroncially-decaying top in the boosted topology, compared with different Monte Carlo predictions. The bands indicate the total uncertainty in the data in each bin. The POWHEG+PYTHIA 8 event generator is used as the nominal prediction to correct for detector effects, parton showering and hadronization. Data points are placed at the center of each bin.

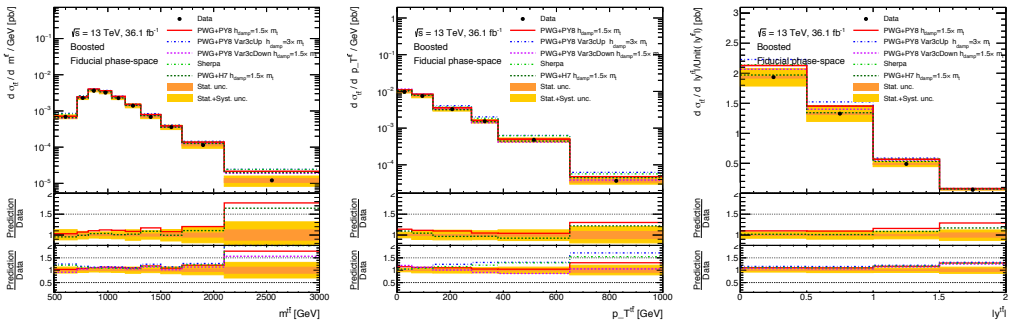

(A) (B) (C)

FIGURE 8.9: Particle-level differential cross-sections as a function of (a) the mass, (b) the transverse momentum and (c) the absolute value of the rapidity of the $t\bar{t}$ system in the boosted topology, compared with different Monte Carlo predictions. The bands indicate the total uncertainty in the data in each bin. The POWHEG+PYTHIA 8 event generator is used as the nominal prediction to correct for detector effects, parton showering and hadronization. Data points are placed at the center of each bin.

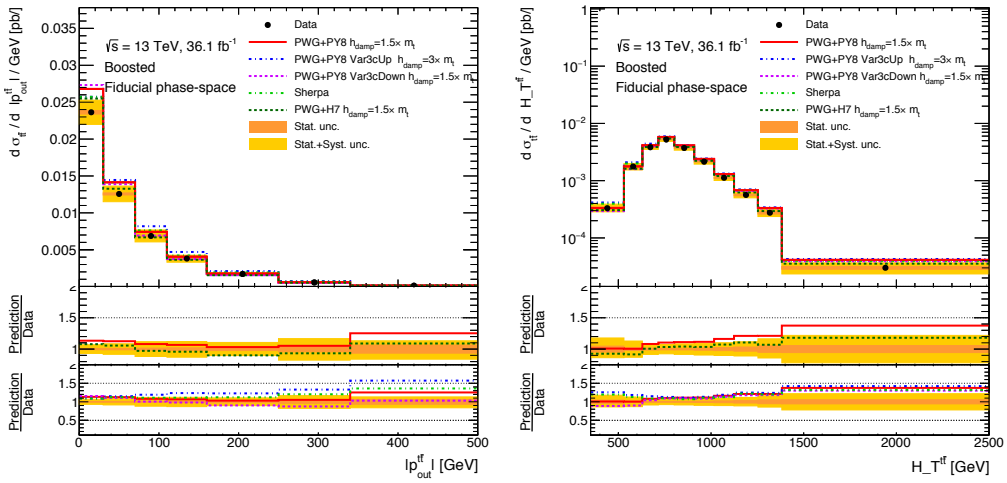

(A) (B)

FIGURE 8.10: Particle-level differential cross-sections as a function of $\left|p_{\text{out}}^{t\bar{t}}\right|$ (a) and $H_T^{t\bar{t}}$ (b), compared with different Monte Carlo predictions. The bands indicate the total uncertainty in the data in each bin. The POWHEG+PYTHIA 8 event generator is used as the nominal prediction to correct for detector effects, parton showering and hadronization. Data points are placed at the center of each bin.

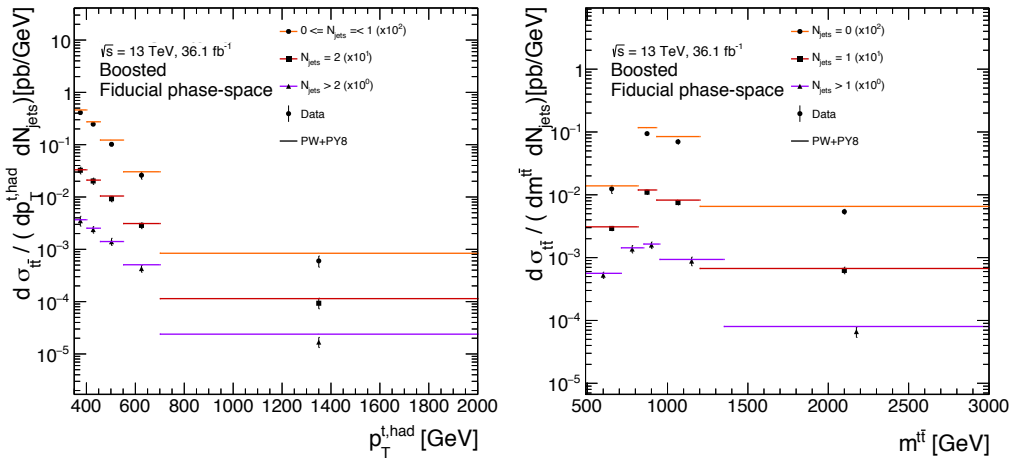

(A) (B)

FIGURE 8.11: Particle-level differential cross-sections as a function of the transverse momentum of the hadronically decaying top (a) and the mass of the $t\bar{t}$ system (b) in bins of jet multiplicity, compared with the nominal POWHEG+PYTHIA 8 prediction. The POWHEG+PYTHIA 8 event generator is used as the nominal prediction to correct for detector effects, parton showering and hadronization.

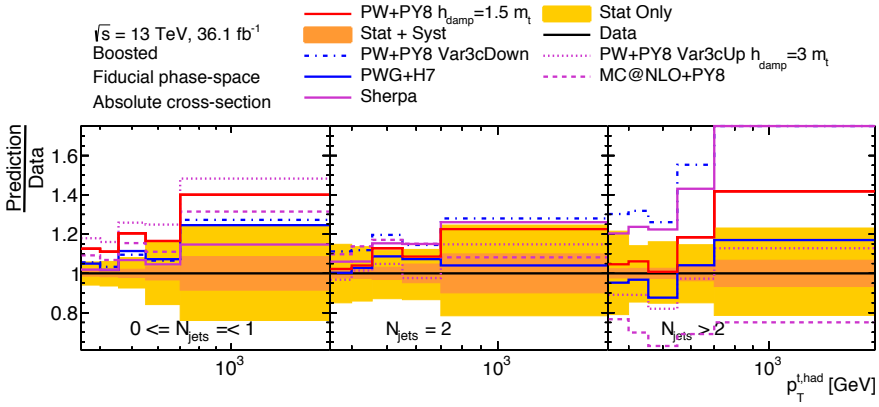

(A)

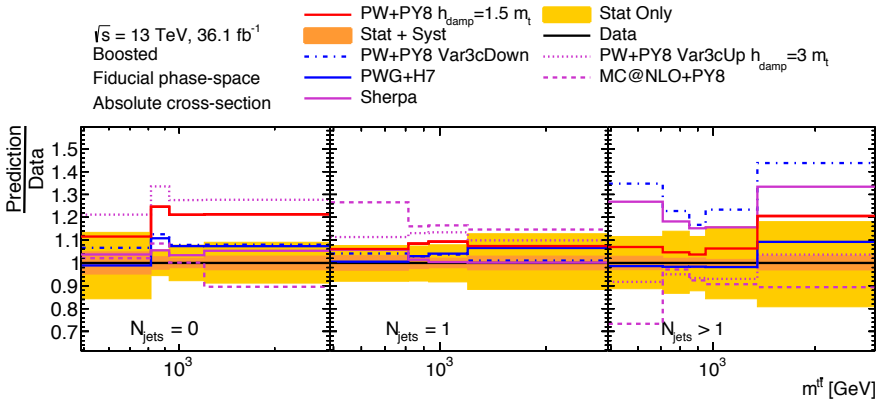

(B)

FIGURE 8.12: Ratios of the Monte Carlo predictions divided by the data for the particle-level differential cross-sections as a function of the transverse momentum of the hadronically decaying top (a) the mass of the $t\bar{t}$ system (b) in bins of jet multiplicity. The bands indicate the total uncertainty in the data in each bin. The event generator is used as POWHEG+PYTHIA 8 the nominal prediction to correct for detector effects, parton showering and hadronization.

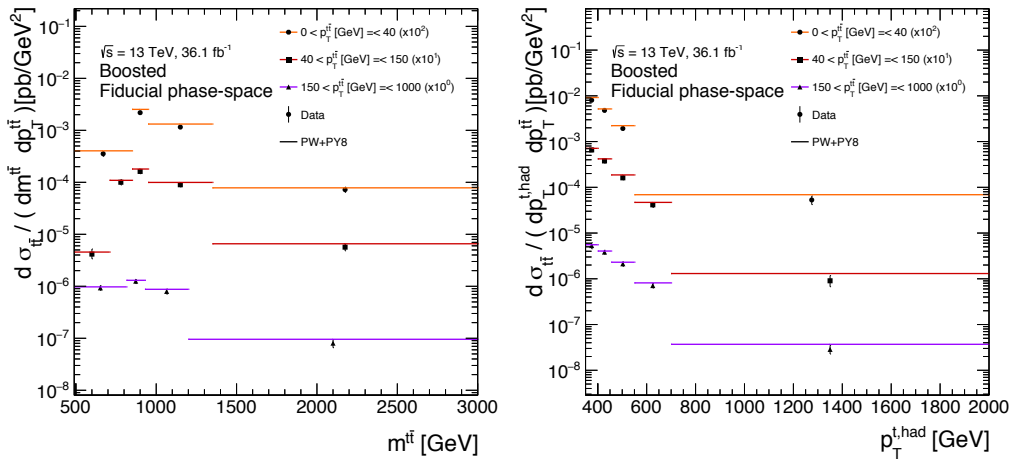

(A) (B)

FIGURE 8.13: Particle-level differential cross-sections as a function of the mass of the $t\bar{t}$ system (a) and the transverse momentum of the hadronically decaying top (b) in bins of the transverse momentum of the $t\bar{t}$ system, compared with the nominal POWHEG+PYTHIA 8 prediction. The POWHEG+PYTHIA 8 event generator is used as the nominal prediction to correct for detector effects, parton showering and hadronization.

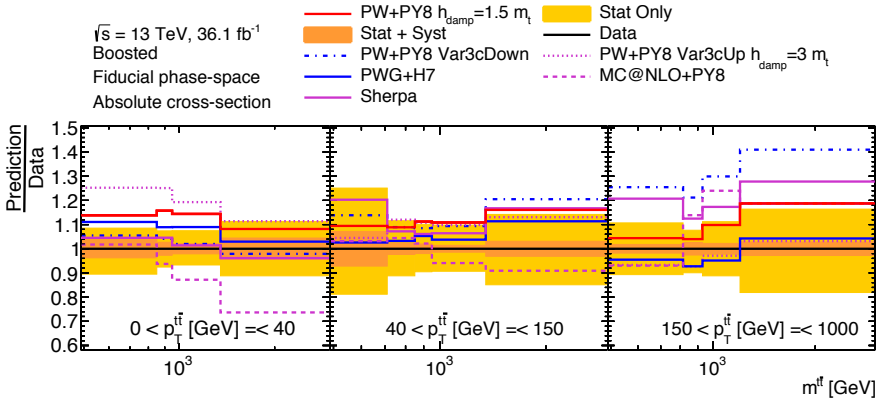

(A)

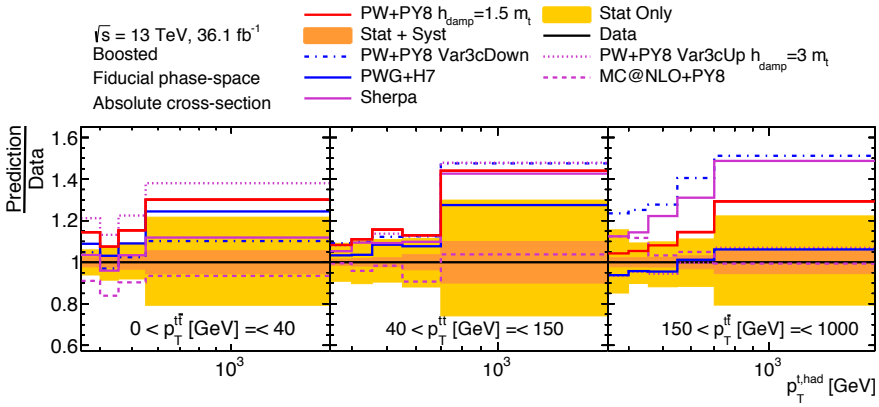

(B)

FIGURE 8.14: Ratios of the Monte Carlo predictions divided by the data for the particle-level differential cross-sections as a function of the mass of the $t\bar{t}$ system (a) and the transverse momentum of the hadronically decaying top (b) in bins of the transverse momentum of the $t\bar{t}$ system. The bands indicate the total uncertainty in the data in each bin. The event generator is used as POWHEG+PYTHIA 8 the nominal prediction to correct for detector effects, parton showering and hadronization.

8.2 Results in the full phase space

8.2.1 Resolved topology

In the resolved topology, single differential cross-sections have been measured in the full phase-space as a function of the mass, transverse momentum and rapidity of the $t\bar{t}$ system and transverse momentum and rapidity of the top quark.

Double differential cross-sections have been measured as a function of the p_{T} of the hadronic top in bins of the mass and p_{T} of the $t\bar{t}$ system and absolute value of the rapidity of the top, and the p_{T} of the $t\bar{t}$ system in bins of the mass of the $t\bar{t}$ system. All the measurements have been compared with the available NNLO predictions described before. In addition, the Monte Carlo POWHEG+PYTHIA 8 prediction is included in the comparisons.

Single differential cross section measurements are shown in Figures 8.15 and 8.16 for the basic kinematic variables of the top and $t\bar{t}$ system, respectively.

Double differential cross-section measurements are shown in Figures 8.17–8.20.

Figure 8.17 shows the comparison of the measured differential cross-section as a function of the p_{T} of the top and $t\bar{t}$ system in bins of the mass of the $t\bar{t}$ system, compared with the NNLO prediction, while Figure 8.18 shows the ratios of the POWHEG+PYTHIA 8 and NNLO predictions divided by the measured differential cross sections as a function of the same variables.

Finally, Figure 8.19 shows the comparison of the measured differential cross section as a function of the p_{T} of the top in bins of the p_{T} of the $t\bar{t}$ system and the absolute value of the rapidity of the top, compared with the NNLO prediction, while Figure 8.20 shows the ratios of the POWHEG+PYTHIA 8 and NNLO predictions divided by the measured differential cross sections as a function of the same variables.

The NNLO QCD predictions show a good agreement with the data in all the single differential cross-section measurements and all the double differential cross-section distributions within their uncertainties. In particular, exploting double differential cross-section measurements is possible to stringently test the pQCD predictions at NNLO in specific regions of the phase-space. The agreement with the data is better for NNLO fixed-order calculations than for the NLO+PS MC prediction. Therefore, higher-order calculations show an improved description of the $t\bar{t}$ production in the full-phase space. The reduction of both theoretical and experimental systematics could allow to further test the pQCD predictions.

All the shown results for the absolute cross-section in the resolved topology at the parton level are tabulated and presented in Appendix F together with the complete breakdown of the systematic uncertainties and the corresponding relative cross-sections.

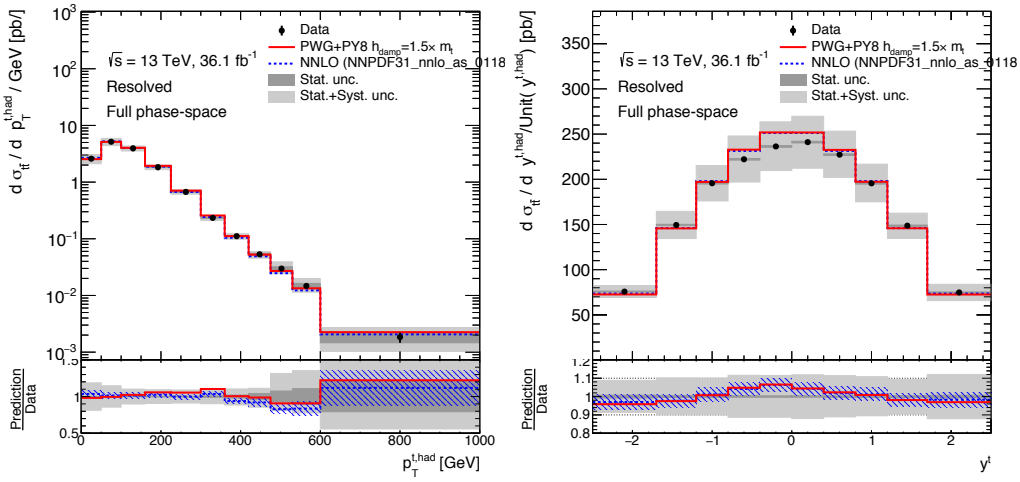

(A) (B)

FIGURE 8.15: Parton-level differential cross-sections as a function of (a) the transverse momentum and (b) the rapidity of the top quark in the resolved topology, compared with the NNLO prediction performed using the NNPDF31_nnlo_as_0118 PDF set and the POWHEG+PYTHIA 8 Monte Carlo generator. The grey and blue bands indicate the total uncertainty on the data and on the NNLO prediction in each bin, respectively. Data points are placed at the center of each bin.

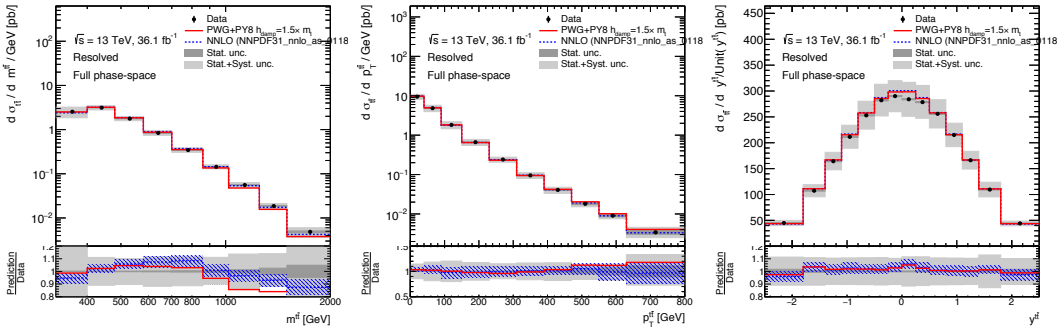

(A) (B) (C)

FIGURE 8.16: Parton-level differential cross-sections as a function of (a) the mass, (b) transverse momentum and (c) the rapidity of the $t\bar{t}$ system in the resolved topology, compared with the NNLO prediction performed using the NNPDF31_nnlo_as_0118 PDF set and the POWHEG+PYTHIA 8 Monte Carlo generator. The grey and blue bands indicate the total uncertainty on the data and on the NNLO prediction in each bin, respectively. Data points are placed at the center of each bin.

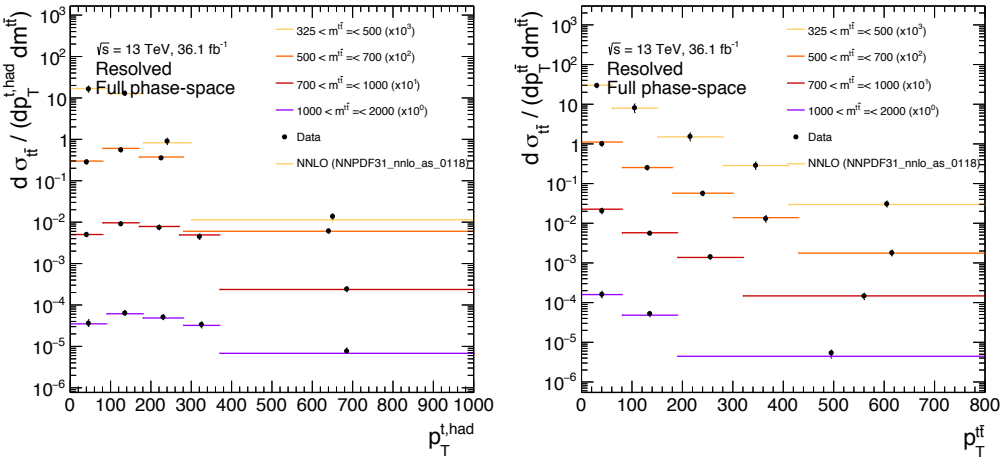

(A) (B)

FIGURE 8.17: Parton-level differential cross-sections as a function of the transverse momentum of (a) the top quark and (b) the $t\bar{t}$ system in bins of $m_{t\bar{t}}$, compared with the fixed order NNLO prediction performed using the NNPDF31_nnlo_as_0118 PDF set. Data points are placed at the center of each bin.

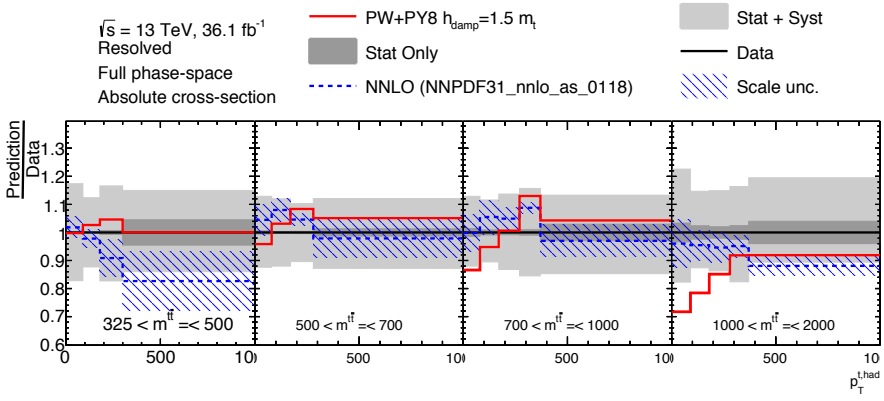

(A)

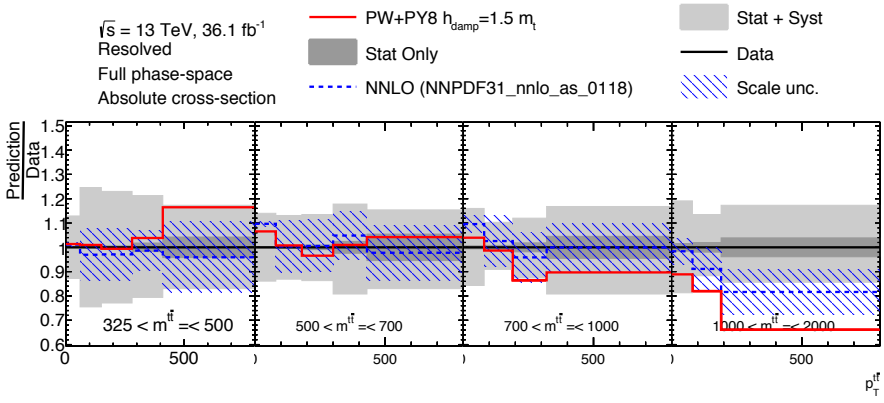

(B)

FIGURE 8.18: Ratios of the NNLO prediction and the POWHEG+PYTHIA 8 Monte Carlo prediction divided by the data for the parton-level differential cross-sections as a function of the transverse momentum of (a) the top quark and (b) the $t\bar{t}$ system in bins of the $m_{t\bar{t}}$ in the resolved topology. The grey and blue bands indicate the total uncertainty on the data and on the NNLO prediction in each bin, respectively.

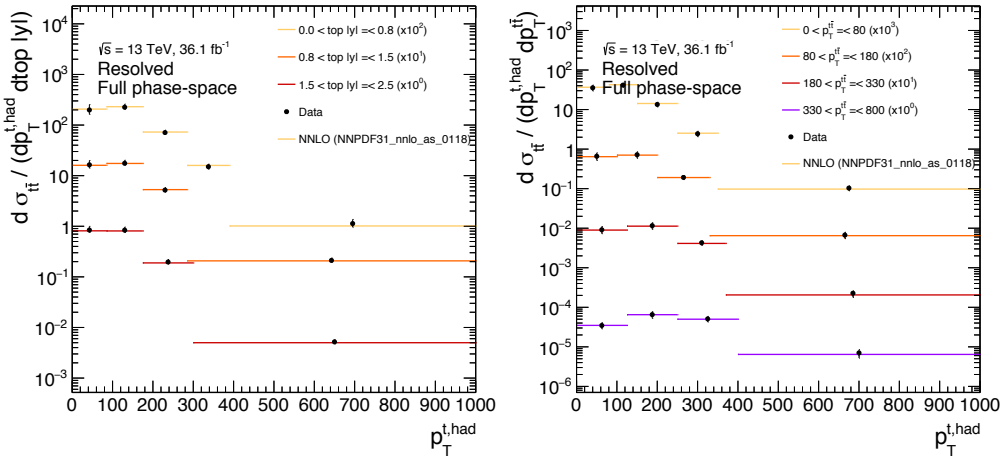

(A) (B)

FIGURE 8.19: Parton-level differential cross-sections as a function of the transverse momentum of the top in bins of (a) the absolute value of the rapidity of the top and (b) the p_{T} of the $t\bar{t}$ system, compared with the fixed order NNLO prediction performed using the NNPDF31_nnlo_as_0118 PDF set. Data points are placed at the center of each bin.

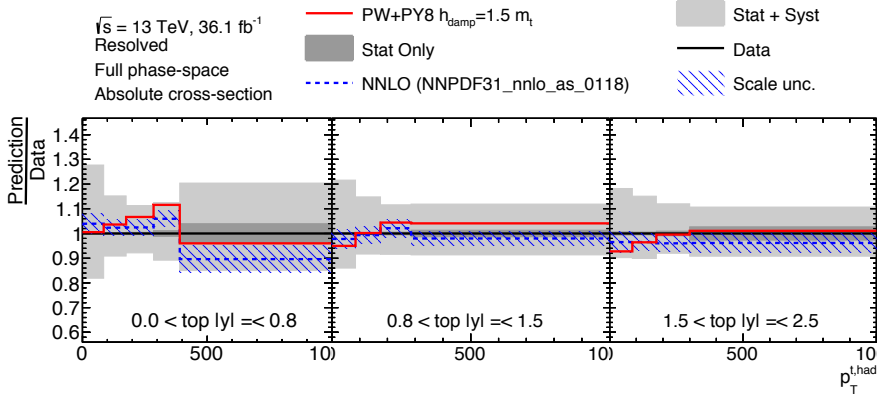

(A)

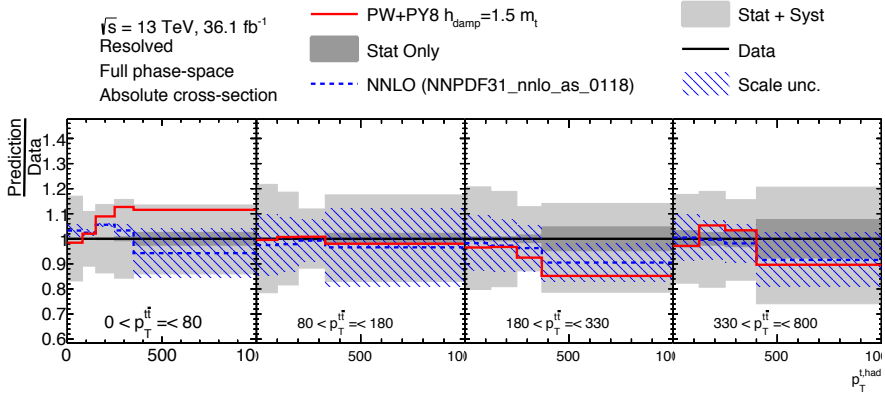

(B)

FIGURE 8.20: Ratios of the NNLO prediction and the POWHEG+PYTHIA 8 Monte Carlo prediction divided by the data for the parton-level differential cross-sections as a function of the p_{T} of the top in bins of (b) the transverse momentum of the $t\bar{t}$ system and (b) the absolute value of the rapidity of the top in the resolved topology. The grey and blue bands indicate the total uncertainty on the data and on the NNLO prediction in each bin, respectively.

8.2.2 Boosted topology

In the boosted topology, differential cross-sections have been measured at the parton level as a function of the mass of the $t\bar{t}$ system, the transverse momentum of the top and the mass of the $t\bar{t}$ system in bins of the p_{T} of the top. In this topology, the parton level phase space is defined as the region of the full phas- space where the top is produced with a p_{T} greater than 350 GeV.

Figure 8.21 shows the single differential cross sections as a function of the p_{T} of the top, compared to the fixed-order NNLO prediction, and as a function of the mass of the $t\bar{t}$ system, compared with different Monte Carlo generators, as the NNLO prediction is not available so far.

Figure 8.22 shows the comparison of the measured differential cross-section as a function of the mass of the $t\bar{t}$ system in bins of the p_{T} of the top, compared with the fixed order NNLO prediction, and the ratios of the POWHEG+PYTHIA 8 and NNLO predictions divided by the measured differential cross sections as a function of the same variables.

Tension between data and most MC predictions is observed in the case of the single differential cross-sections as a function of the mass of the $t\bar{t}$ system. In the case of the single differential cross-section as a funtion of the p_{T} of the hadronic top, the NNLO prediction decribes better the data compared to the MC prediction, even if a discrepancy is visible in the high-p_{T} region. The double differential cross-section as a function of $m_{t\bar{t}}$ in bins of the p_{T} of the top, shown in Figure 8.22, allows to further investigate this tension: the highest discrepancy is observed in the high-p_{T} region, while in the lower p_{T} region the mass spectrum predicted by the simulations shows better agreement with the data in full $m_{t\bar{t}}$ range.

All the shown results for the absolute cross-section in the boosted topology at the parton level are tabulated and presented in Appendix F together with the complete breakdown of the systematic uncertainties and the corresponding relative cross-sections.

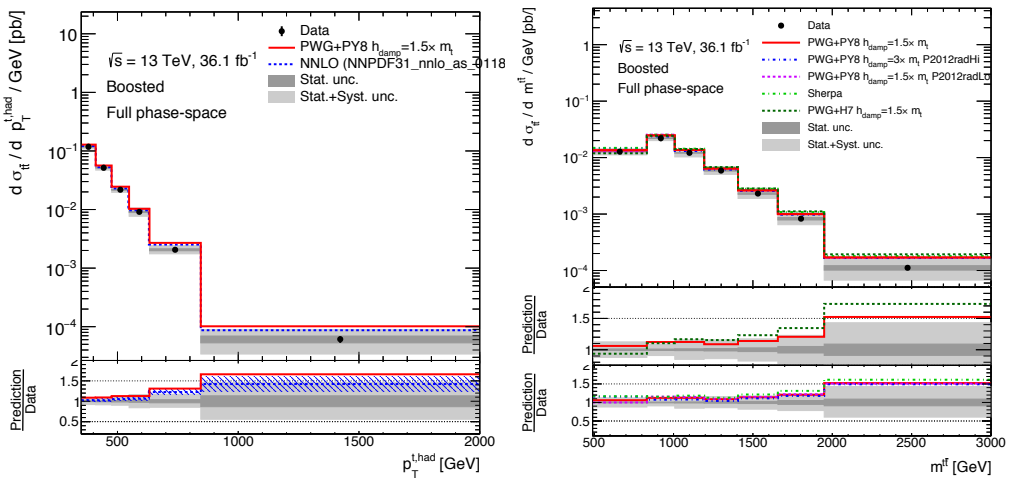

(A) (B)

FIGURE 8.21: (a): parton-level differential cross-sections as a function of the transverse momentum of the top in the boosted topology, compared with the NNLO prediction performed using the NNPDF31_nnlo_as_0118 PDF set and the POWHEG+PYTHIA 8 Monte Carlo generator. (b): parton-level differential cross-sections as a function of the mass of the $t\bar{t}$ system in the boosted topology, compared with different Monte Carlo predictions. The grey and blue bands indicate the total uncertainty on the data and on the NNLO prediction in each bin, respectively. Data points are placed at the center of each bin.

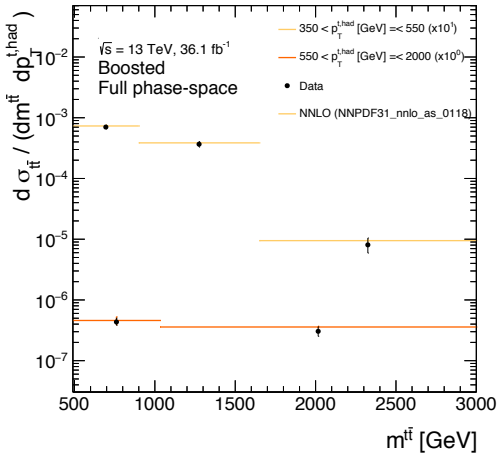

(A)

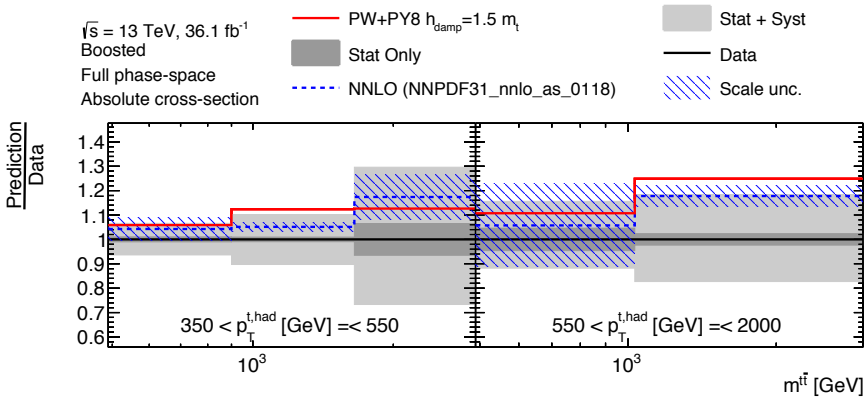

(B)

FIGURE 8.22: (a): parton-level differential cross-sections as a function of the mass of the $t\bar{t}$ system in bins of the transverse momentum of, compared with the nominal fixed order NNLO prediction performed using the NNPDF31_nnlo_as_0118 PDF set. (b): ratios of the NNLO prediction and the POWHEG+PYTHIA 8 Monte Carlo prediction divided by the data for the parton-level differential cross-sections as a function of the mass of the $t\bar{t}$ system in bins of the transverse momentum of the top quark in the boosted topology. The grey and blue bands indicate the total uncertainty on the data and on the NNLO prediction in each bin, respectively.

8.3 Comparisons with NNLO QCD+NLO EW theoretical predictions

In this section, a comparison between the measured differential cross-sections at parton level and the currently available theoretical predictions at NNLO QCD with the inclusion of NLO EW corrections [44] is carried out in order to make more stringent tests on perturbative QCD calculations. The NNLO QCD+NLO EW predictions presented in Reference [44], are available for different sets of PDF at NNLO QCD accuracy [99, 171, 172]. The predictions include the uncertainty relative to the choice of the renormalisation and factorisation scales and of the PDFs. The binning of the measured cross-sections at parton level is the same of the theoretical calculations and it is relative to an unpublished $t\bar{t}$ CMS analysis at 13 TeV. The binning used for this comparison is coarser than the optimised binning in the analysis described in this thesis and the common validation tests have been performed in order to check the stability of the unfolding procedure. The comparison has been carried out for the following distributions: the top-pair invariant mass $m^{t\bar{t}}$, the transverse momentum $p_T^{t\bar{t}}$ and the rapidity $y_{t\bar{t}}$ of the $t\bar{t}$ system. In addition, the comparison for the top/antitop average transverse momentum $p_T^{\mathrm{t,avg}}$ and rapidity $y^{\mathrm{t,avg}}$ are shown. The distributions of the top/antitop average are calculated not an event-by-event basis but by averaging the results of the histograms of the distributions of the top and antitop quark. In this case, the measured cross-sections at parton level used for the comparison shown in the following plots are taken as a function of the hadronic top quark. Further details on the theoretical predictions are documented in Reference [44].

The NNLO QCD and the NNLO QCD with the inclusion of NLO EW corrections show a good agreement for all the measured distributions. Moreover, no significant difference is found between the NNLO QCD predictions with or without the inclusion of the NLO EW corrections, since the largest effect are expected at very high values of the p_{T} of the quark top and in high mass regions of the $t\bar{t}$ system, as shown in Section 1.3.2. However, the possible inclusion of the NLO EW contributions for the already available NNLO QCD predictions could allow to test these effects more stringently, in particular exploiting the double differential cross-section measurements previously presented and the future full Run 2 analysis.

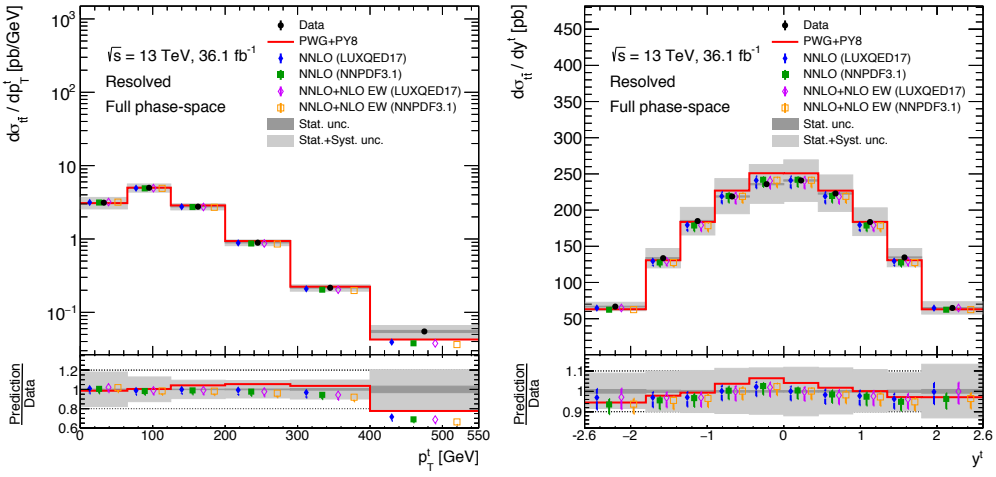

FIGURE 8.23: Absolute cross-section as a function of $p_T^{t,avg}$ (left) and $y^{t,avg}$ (right) parton level spectra in the resolved topology. The results are compared with NNLO QCD and NNLO QCD+NLO EW theoretical calculations in the ratio pads. The red solid line is the nominal NLO PowHeg showered with Pythia8 prediction, the black solid line represents data. The NNLO fixed-order calculations are represented using blue (LUXQED17 PDF set) and green (NNPDF3.1 PDF set) bullets. The NNLO fixed-order calculations including NLO ElectroWeak corrections are drawn as purple (LUXQED17 PDF set) and orange (NNPDF3.1 PDF set) bullets. The vertical bands on each marker represents the total uncertainty of the prediction. The lighter grey band represents the total uncertainty while the darker grey one the statistical uncertainty.

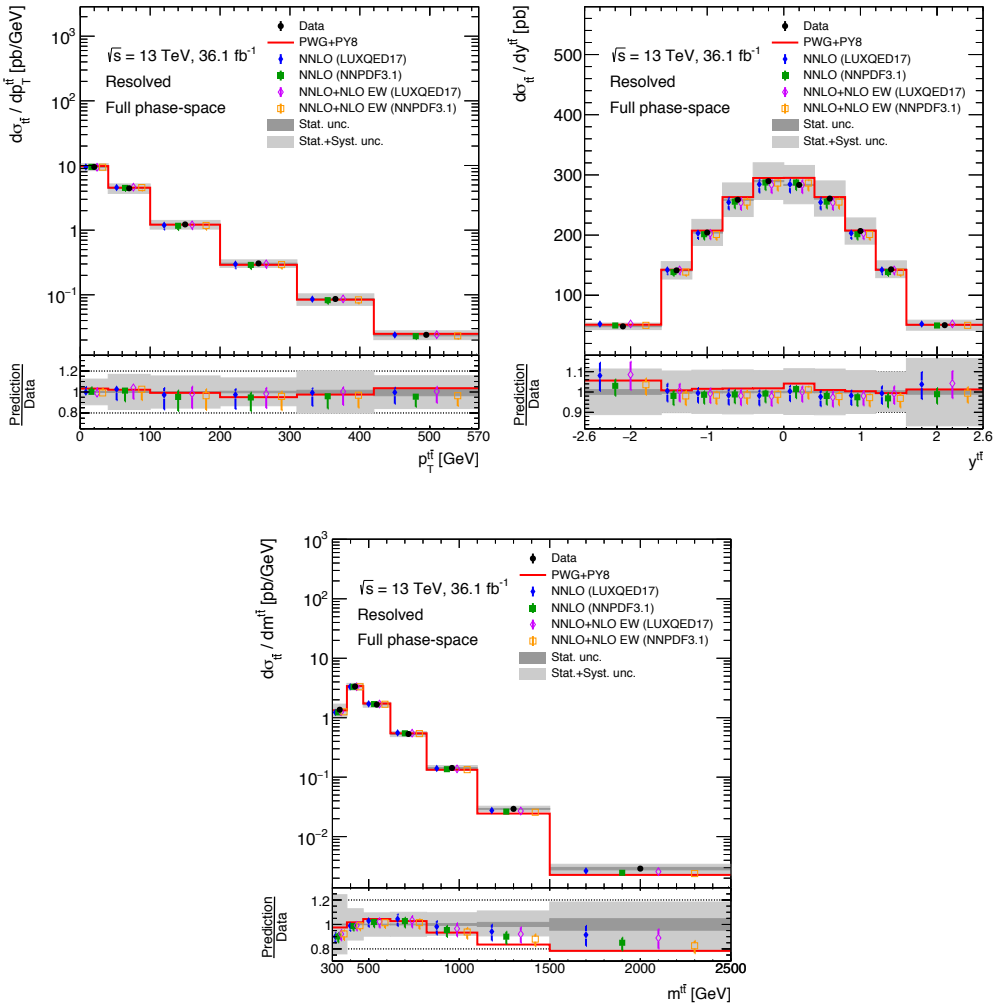

FIGURE 8.24: Absolute cross-section as a function of $p_T^{t\bar{t}}$ (top left) and $y_{t\bar{t}}$ (top right) and $m^{t\bar{t}}$ (bottom) parton level spectra in the resolved topology. The results are compared with NNLO QCD and NNLO QCD+NLO EW theoretical calculations in the ratio pads. The red solid line is the nominal NLO PowHeg showered with Pythia8 prediction, the black solid line represents data. The NNLO fixed-order calculations are represented using blue (LUXQED17 PDF set) and green (NNPDF3.1 PDF set) bullets. The NNLO fixed-order calculations including NLO ElectroWeak corrections are drawn as purple (LUXQED17 PDF set) and orange (NNPDF3.1 PDF set) bullets. The vertical bands on each marker represents the total uncertainty of the prediction. The lighter grey band represents the total uncertainty while the darker grey one the statistical uncertainty.

Conclusions

The measurement of the single and double differential cross-section for top-quark pair production using data collected by the ATLAS detector in 2015 and 2016 at $\sqrt{s} = 13\,\text{TeV}$ has been presented in this thesis. The selection and reconstruction of the $t\bar{t}$ events where one of the top decays hadronically while the othe decays leptonically are performed by using two different strategies according to the transverse momentum of the top quark. The resolved analysis selects events with at least four jets coming from the decay products of the top quarks and applies b-tagging requirements in order to improve the purity of the sample. The boosted analysis requires specific techniques to reconstruct the hadronic top when it is produced with high transverse momentum ($p_{\text{T}} > 350\,\text{GeV}$). The decay products of a boosted top quark tend to be more collimated and they may overlap due to the Lorentz boost. Therefore, they are less efficiently reconstructed as well-separated jets. Also the boosted analysis applies requirements based on b-tagging to ensure a sufficient signal purity and reconstruction efficiency. The application of the re-clustering technique allowed to reduce the dominant systematic uncertainty of the measurement with respect to previous analyses, and, as a consequence, to increase the discrimnating power of differential cross-sections in the boosted regime.

The single and double differential distributions are measured in a fiducial phase-space defined by the cuts introduced to take into acoount the limited coverage of the detector apparatus. The measurement is also extrapolated to the full phase-space. The differential cross-section results are presented as a function of the main kinematic variables of the hadronic top quark and of the $t\bar{t}$ system as well as observables sensitive to extra QCD radiation. Moreover, these observables are combined to define a set of double differential measurements particularly sensitive to specific aspects of the top-quark pair production. The study of the distributions in the fiducial phase-space is focused on the evaluation of the level of agreement of the MC description of the $t\bar{t}$ modeling. These distributions are relevant for the MC tuning and they can contribute to the improvement of the understanding of $t\bar{t}$ production. The aim is to reduce the systematic uncertainties related to top-quark modeling which are the dominant in the $t\bar{t}$ cross-section measurement. Therefore, a reduction of these systematic could lead to a more precise measurements in the top quark sector. On the other hand, the measured distributions in the full phase-space are particularly suited to perform stringent test of pQCD, thanks to the achievements in the theoretical calculations which provide precise predictions of $t\bar{t}$ production in both the resolved and boosted regime.

For these reasons, the measured spectra are compared with NLO+PS MC predictions and NNLO QCD calculations which represent the most advanced SM description of $t\bar{t}$ available so far.

In general, the predictions agree with the data over a wide kinematic region, but poor modeling of specific phase-spaces are found for NLO+PS MC predictions, in particular thanks to the double differential cross-sections. The inclusion of fixed-order calculations at NNLO accuracy in QCD enhanced the level of agreement between theoretical predictions and data, and the comparison of double differential distributions with NNLO predictions provide a stringent test of the SM description of $t\bar{t}$ production. The comparison with the currently available NNLO QCD predictions with the inclusion of NLO EW contributions shows that the tested region of the phase-space is not suitable to fully evaluate these effects, even though a further test on SM has been performed.

The measured distributions show high sensitivity to the different aspects of the MC generators. Therefore, the combination of these results with the provided Rivet routines could lead to a large discriminating power between different models of $t\bar{t}$ productions towards a full-Run 2 analysis of differential $t\bar{t}$ cross-sections. In addition, the measured spectra can be used to put stronger constraints on the gluon PDF inside the proton, extract the top quark mass, and, in general, perform detailed phenomenological studies.

Finally, the calibration of the b-tagging efficiencies using semileptonic $t\bar{t}$ events, recently published by the ATLAS Collaboration, extends the range of the jet p_{T} where the direct measurement of data-to-simulation scale factors is possible. This study is particularly interesting for the boosted topology towards the full-Run 2 analysis where the reconstruction strategy, which already exploits b-tagging calibration of the small-R jets, can benefit from a dedicated calibration in the high-p_{T} region in order to improve the efficiency and to reduce the uncertainties related to b-tagging.

Appendix A

Studies on the b-tagging working points

The final state of the $t\bar{t}$ decay contains two b-quark and consequently the choice of the b-tagging working point has an important role in the efficiency of the selection used to identify $t\bar{t}$ events, described in section 5.1, and on the capability to reject background events. The increase of a factor ten in statistics with respect to the analysis performed on 2015 data [51] allows to investigate the usage of a tighter working point than the one used before.

The advantage of a tighter b-tagging working point is a reduction of the amount of remaining background in the selected sample and the consequent reduction of the related uncertainty. The disadvantages of a tighter working point are the increase in the b-tagging uncertainty and the reduction of the statistics. The b-tagging efficiency has a shape in p_T, as shown in Figure A.1, where the efficiency of the b-tagging on small-R jets and reclustered jets is shown as a function of the jet p_T in a boosted region, where only events containing at least a reclustered jet with $p_T > 200\,\text{GeV}$ and high $E_{\text{T}}^{\text{miss}}$ ($E_{\text{T}}^{\text{miss}} > 20\,\text{GeV}$, $E_{\text{T}}^{\text{miss}} + m_{\text{T}}^{W} > 60\,\text{GeV}$) are included. Consequently the reduction in statistics could have a different impact in various regions of the phase-space. All these effects need to be considered in the choice of the b-tagging working point. In this appendix the change in statistics, the effect of the b-tagging systematics and the global effect on the measurement will be presented comparing two b-tagging working point: 77%, used in the analysis on 2015 data, and a tighter point at 70% of the efficiency.

A.1 Resolved topology

In Figure A.2 are presented the number of b-jets in the events selected in the resolved topology, as described in section 5.1, using a b-tagging working point of 77%, on the left and equal to 70% on the right. In Table A.1 is presented the fraction of all the different type of background that populate the selected sample using the two b-tagging working point.

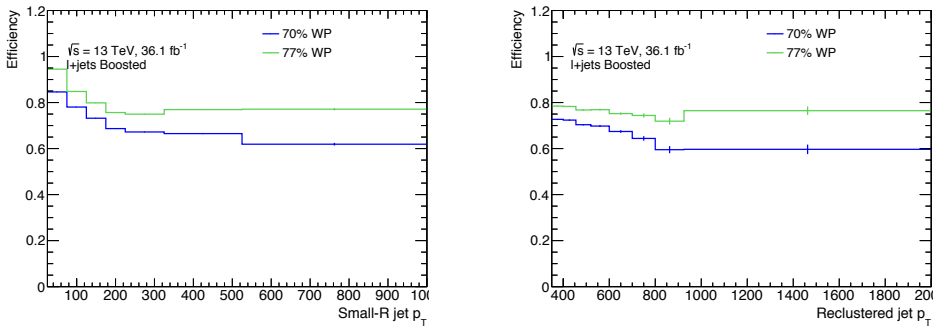

FIGURE A.1: *b*-tagging efficiency as a function of the p_T, for the small-R jets (left) and reclustered jets (right). The efficiency is calculated as the ratio between the number of *b*-tagged jets at detector level and the number of *b*-tagged jets in the same p_T bin at particle level, using a ghost B-hadron matching.

As expected, the tightest working point reduces the amount of background selected in the signal region, in particular the amount of Z+jets and W+jets events, where the presence of a real *b*-hadron is less expected, are highly reduced.

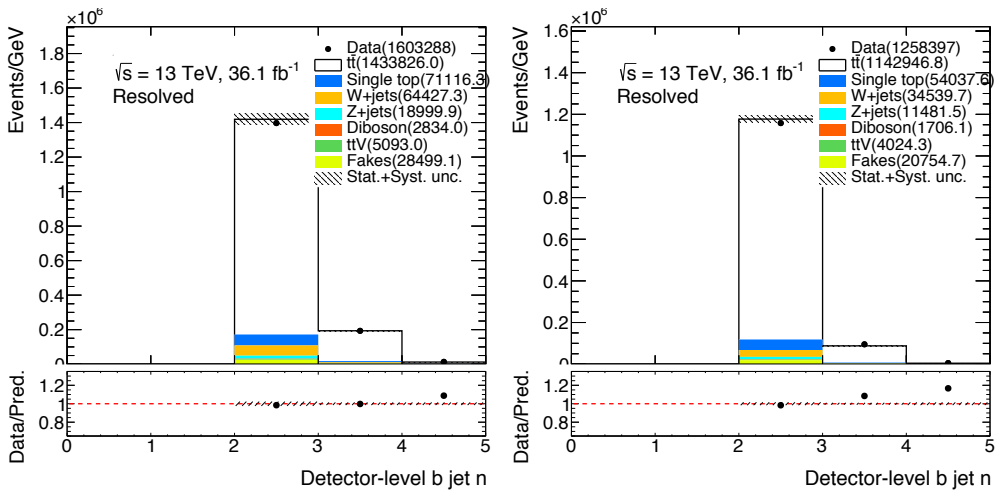

FIGURE A.2: Number of *b*-jets per event in the resolved topology, using a *b*-tagging working point of 77% on the left and 70% on the right.

In Figure A.3 is presented the systematic due to the *b*-tagging on the signal sample at detector level as a function of $p_T^{t,had}$, $\eta^{t,had}$, $|p_{out}^{t\bar{t}}|$, $m^{t\bar{t}}$, $\eta^{t\bar{t}}$ and $p_T^{t\bar{t}}$ in resolved topology, considering the two *b*-tagging working points. The overall increase of the systematic is of 10%.

A.2 Boosted topology

Figure A.4 shows the numer of *b*-jets in the events selected in the boosted topology, as described in section 5.1, using a *b*-tagging working point of 77%, on the left and equal to

Sample	Percentage of the total sample	
	77%	70%
Single Top	4.29	4.44
W+jets	4.02	2.74
Z+jets	1.19	0.91
Diboson	0.18	0.14
$t\bar{t}$V	0.32	0.32
Multijet	1.78	1.65
$t\bar{t}$	88.2 %	90 %

TABLE A.1: Percentage composition of the sample selected in the resolved signal region using the 77% *b*-tagging working point on the left and the 70% on the right.

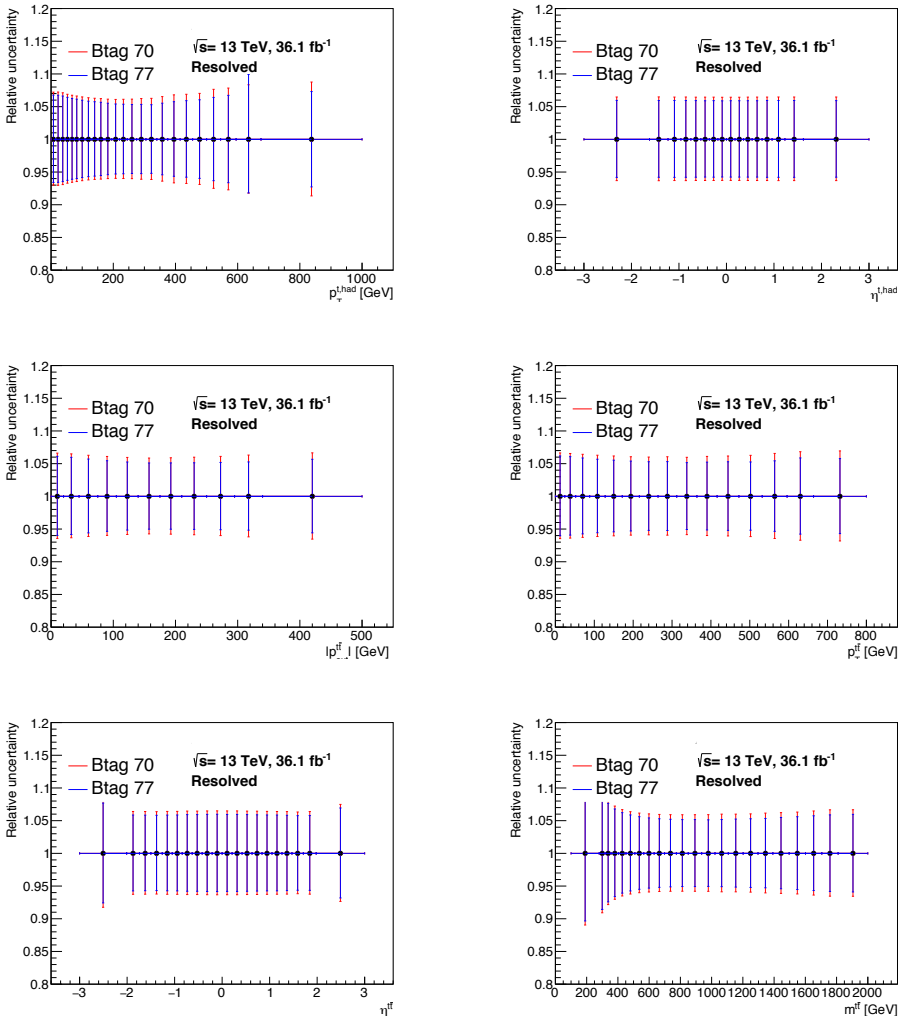

FIGURE A.3: Effect of the different *b*-tagging working points on the related uncertainty on the signal sample in the resolved topology.

70% on the right. In Table A.2 is presented the fraction of all the different type of background that populate the selected sample using the two *b*-tagging working points.

As expected, the tightest working point reduces the amount of background selected in the signal region, in particular the amount of *Z*+jets and *W*+jets events, where the presence of a real *b*-hadron is less expected, is reduced.

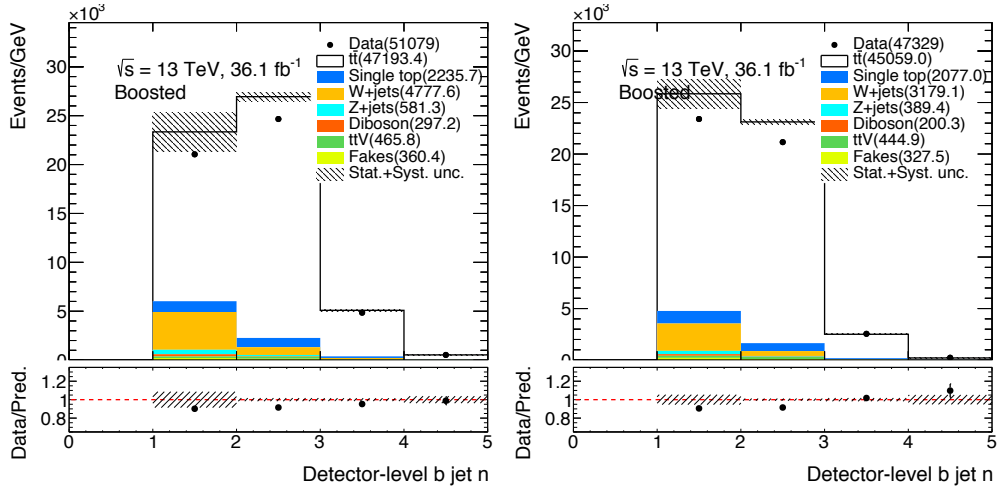

FIGURE A.4: Number of *b*-jets per event in the boosted topology, using a *b*-tagging working point of 77% on the left and 70% on the right.

Sample	Percentage of the total sample	
	77%	70%
Single Top	4.37	4.39
W+jets	9.34	6.71
Z+jets	1.14	0.82
Diboson	0.58	0.42
$t\bar{t}$V	0.92	0.94
Multijet	0.71	0.69
$t\bar{t}$	84.4 %	87.2% %

TABLE A.2: Percentage composition of the sample selected in the boosted signal region using the 77% *b*-tagging working point on the left and the 70% on the right.

Figure A.5 presents the systematic due to the *b*-tagging on the signal sample at detector level as a function of $p_T^{t,had}$, $\eta^{t,had}$, $m^{t\bar{t}}$ and $p_T^{t\bar{t}}$ in boosted topology, considering the two *b*-tagging working points. The overall increase of the systematics is of 15%, however this source of uncertainty is subdominant in boosted topology. As an example of the effect of a different working point, the total uncertainties affecting the measurement of the $d\sigma_{t\bar{t}}$ as a function of the $p_{\mathrm{T}}^{t,\mathrm{had}}$ and $m_{t\bar{t}}$ in boosted topology are presented in Figure A.6, considering the 77% WP on the left and the 70% WP on the right. The global effect of a different working point is a reduction of the total uncertainty. The uncertainties on fakes and single top background are not included in both plots.

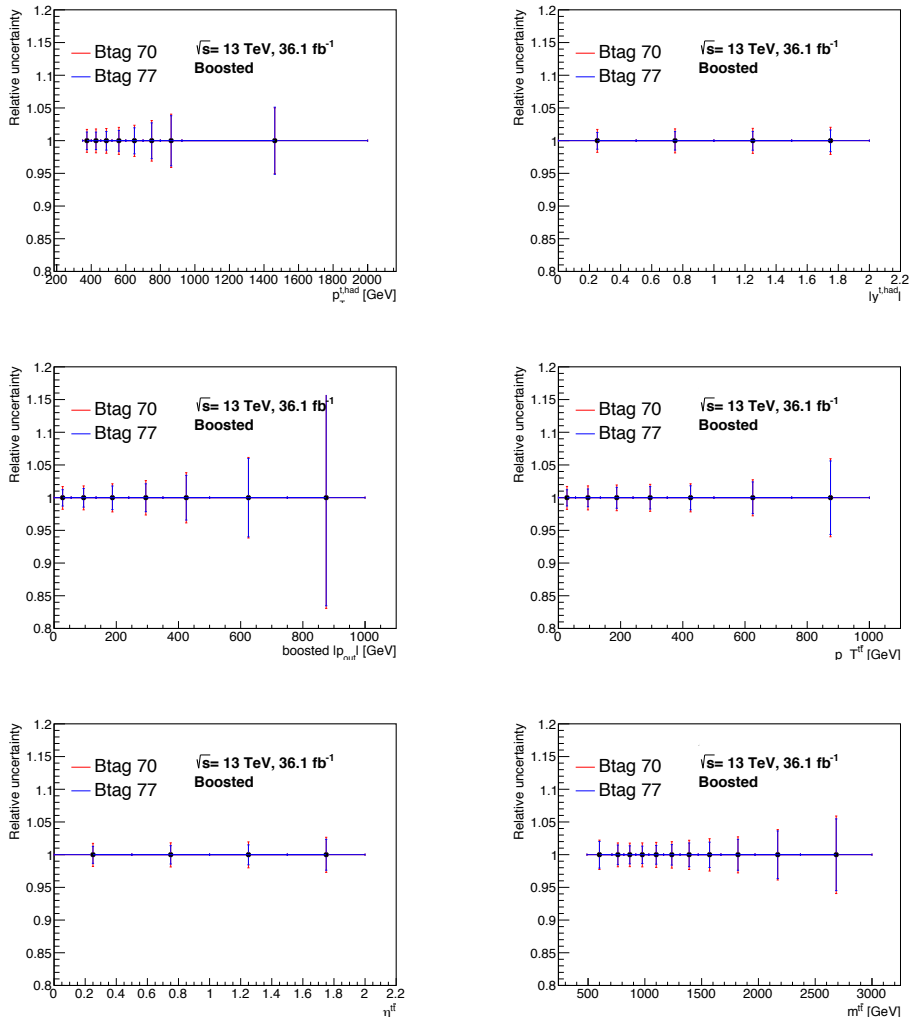

FIGURE A.5: Effect of the different *b*-tagging working point on the related uncertainty on the signal sample in the boosted topology.

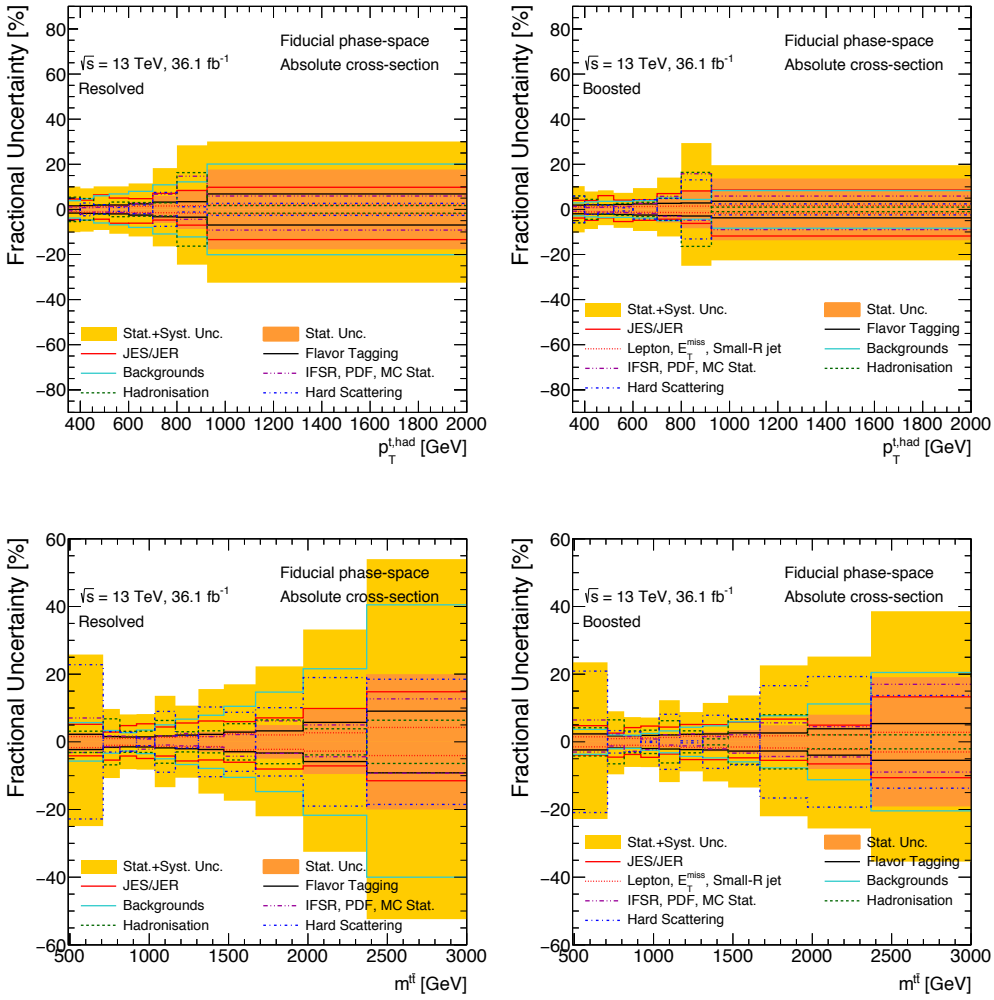

FIGURE A.6: Fractional uncertainty on the absolute particle level cross-section as a function of $p_{\mathrm{T}}^{t,\,\mathrm{had}}$ (top) and $m_{t\bar{t}}$ (bottom) using a 77% efficiency working point on the left and 70% on the right.

Appendix B

Validation of the KLFitter likelihood cut

The additional cut applied on the likelihood value of the KLFitter algorithm has been validated in data. In the validation process, the efficiency of the cut in data, defined as $N_{\text{goodlhood}}/N_{\text{Total}}$, has been compared with the same efficiency evaluated for the total signal+background prediction. The following plots show the agreement between the efficiencies in data and in the predictions.

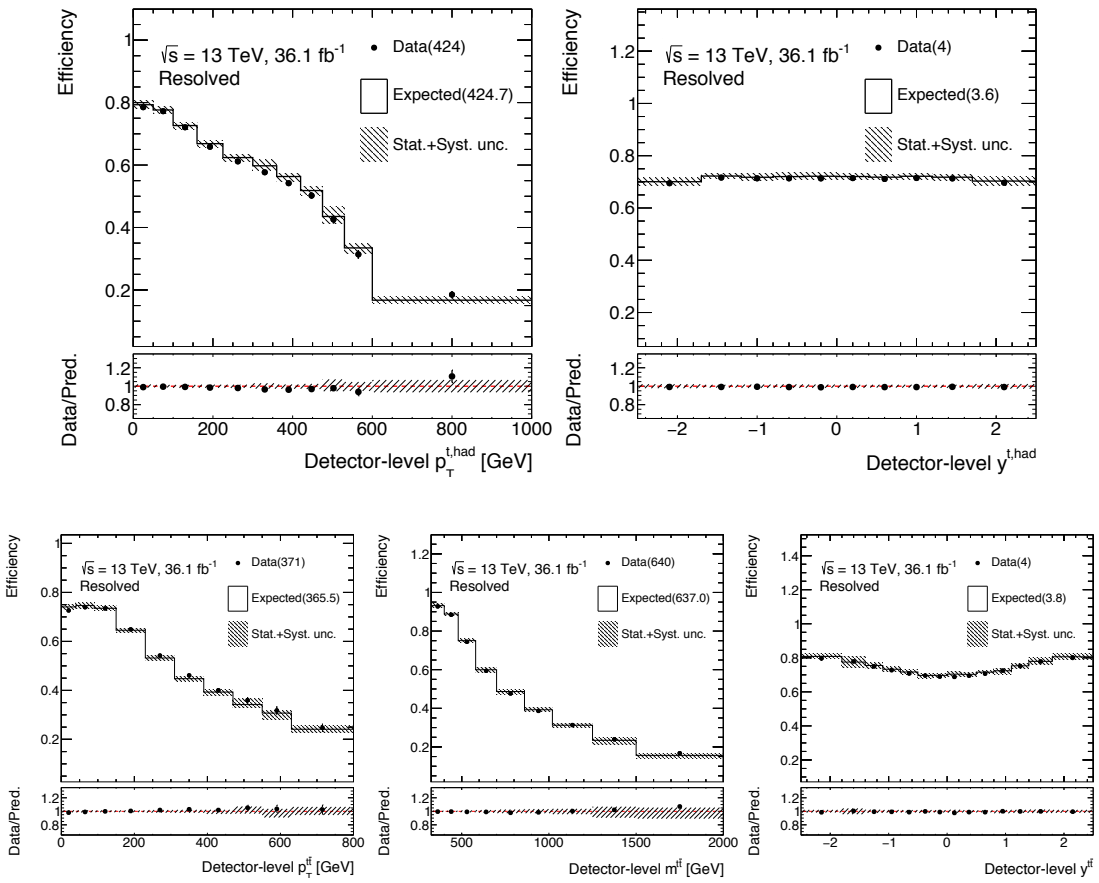

FIGURE B.1: Comparison between data and prediction efficiencies of the likelihood cut of basic top kinematic distributions.

Appendix C

Effects of the orthogonal selection

In order to provide statistically independent measurements in the resolved and boosted phase-spaces, events passing both the resolved and boosted selections are removed from the resolved samples (and kept in the boosted). This additional cut affects the final distributions in different ways:

- it can increase the overall systematic uncertainties, since the boosted selection contains cut on the p_T and mass of the reconstructed large-R jets.
- it will reduce the efficiency, and the overall available statistics in the high-p_T tails of the resolved distributions.

The event yields for all the sample after applying this additional cut (using RC-jets) is presented in Tables C.1-C.3.

Sample	Total resolved events without boost	Fraction wrt total
$t\bar{t}$	$1127389.50^{+92969.90}_{-93376.28}$	0.98
W+jets	$34386.04^{+18831.10}_{-18693.20}$	0.99
Z+jets	$11514.60^{+6463.07}_{-6448.50}$	0.99
Single top	$53648.77^{+5099.11}_{-5049.20}$	0.98
$t\bar{t}V$	$3795.38^{+229.42}_{-227.89}$	0.94
Diboson	$1680.80^{+191.89}_{-165.88}$	0.98
Fakes	$33945.99^{+16016.52}_{-16019.93}$	1.00
Expected	$1266361.00^{+106763.33}_{-106615.51}$	0.98
Observed	$1252692.00^{+1119.24}_{-1119.24}$	0.98

TABLE C.1: Observed and expected number of events in the ℓ+jets channel after the full event selection and the removal of the events passing the boosted selection in the resolved analysis. The systematic uncertainties do not include the signal modelling ones. The fraction with respect the total has been evaluated as $\frac{N_{noboost}}{N_{total}}$.

Sample	Total resolved events without boost	Fraction wrt total
$t\bar{t}$	$580125.81^{+45959.31}_{-44198.89}$	0.98
W+jets	$17466.97^{+9596.68}_{-9514.49}$	0.98
Z+jets	$7480.97^{+4182.72}_{-4179.11}$	0.99
Single top	$27669.57^{+2675.23}_{-2614.03}$	0.98
$t\bar{t}V$	$1997.32^{+122.64}_{-120.88}$	0.93
Diboson	$895.60^{+103.55}_{-92.77}$	0.98
Fakes	$30865.29^{+17302.69}_{-17302.69}$	1.00
Expected	$666501.56^{+55460.57}_{-53601.16}$	0.98
Observed	$643594.00^{+802.24}_{-802.24}$	0.98

TABLE C.2: Observed and expected number of events in the e+jets channel after the full event selection and the removal of the events passing the boosted selection in the resolved analysis. The systematic uncertainties do not include the signal modelling ones. The fraction with respect the total has been evaluated as $\frac{N_{noboost}}{N_{total}}$.

Sample	Total resolved events without boost	Fraction wrt total
$t\bar{t}$	$543977.94^{+42045.68}_{-40891.86}$	0.98
W+jets	$16919.07^{+9254.48}_{-9192.20}$	0.99
Z+jets	$4033.71^{+2288.62}_{-2274.31}$	0.99
Single top	$25978.96^{+2446.35}_{-2457.61}$	0.99
$t\bar{t}V$	$1798.13^{+109.12}_{-109.38}$	0.94
Diboson	$785.20^{+89.92}_{-75.37}$	0.98
Fakes	$3079.09^{+4588.37}_{-4588.37}$	1.02
Expected	$596572.12^{+48291.99}_{-46993.50}$	0.98
Observed	$609098.00^{+780.45}_{-780.45}$	0.98

TABLE C.3: Observed and expected number of events in the μ+jets channel after the full event selection and the removal of the events passing the boosted selection in the resolved analysis. The systematic uncertainties do not include the signal modelling ones. The fraction with respect the total has been evaluated as $\frac{N_{noboost}}{N_{total}}$. This ratio is greater than 1 in the Fakes sample because the "noboost" cut removes mostly negative-weighted events.

Both effects have been studied by comparing the reconstructed distributions obtained using the standard resolved selection (labelled 'Resolved' in the legend), the resolved selection removing the events passing the RC-jet based boosted selection (labelled 'Not boosted RC' in the legend) and removing the events passing the standard large-R jet based boosted selection (labelled 'Not boosted' in the legend). The standard control variables are shown in Fig. C.1, the reconstructed variables using the pseudo-top method in Fig. C.2 and the reconstructed variables using the KLFitter method in Fig. C.3. The uncertainty bands include the MC sample statistical uncertainty, small-R jet energy resolution and scale and, for the 'Not boosted' only distribution, large-R jet uncertainties.

From this set of plots, it is clear that the total loss of statistics is not significant (of the order of few percent) with a significant increase in the tails of the p_T distributions of jets and hadronic top. On the other hand, the distribution of the log $\mathcal{L}$ of the kinematic fit shows that the most important reduction of efficiency appears in the tail of the distribution. Therefore,

there is a hint that the discarded events would have been poorly reconstructed if they were included in the resolved selection. Finally, a small increase of the total uncertainty can be observed only in the 'Not boosted' distribution, that is caused by the addition of the large-R jet uncertainties.

The comparison of the efficiency and acceptance corrections between the 'resolved' and 'Not boosted' selections are shown in Figs. C.4–C.5. As expected, the efficiency correction shows a trend similar to the one observed in Fig. C.2, since the final particle level phas-space (denominator of the efficiency) is not affected by the removal of the reconstructed boosted events.

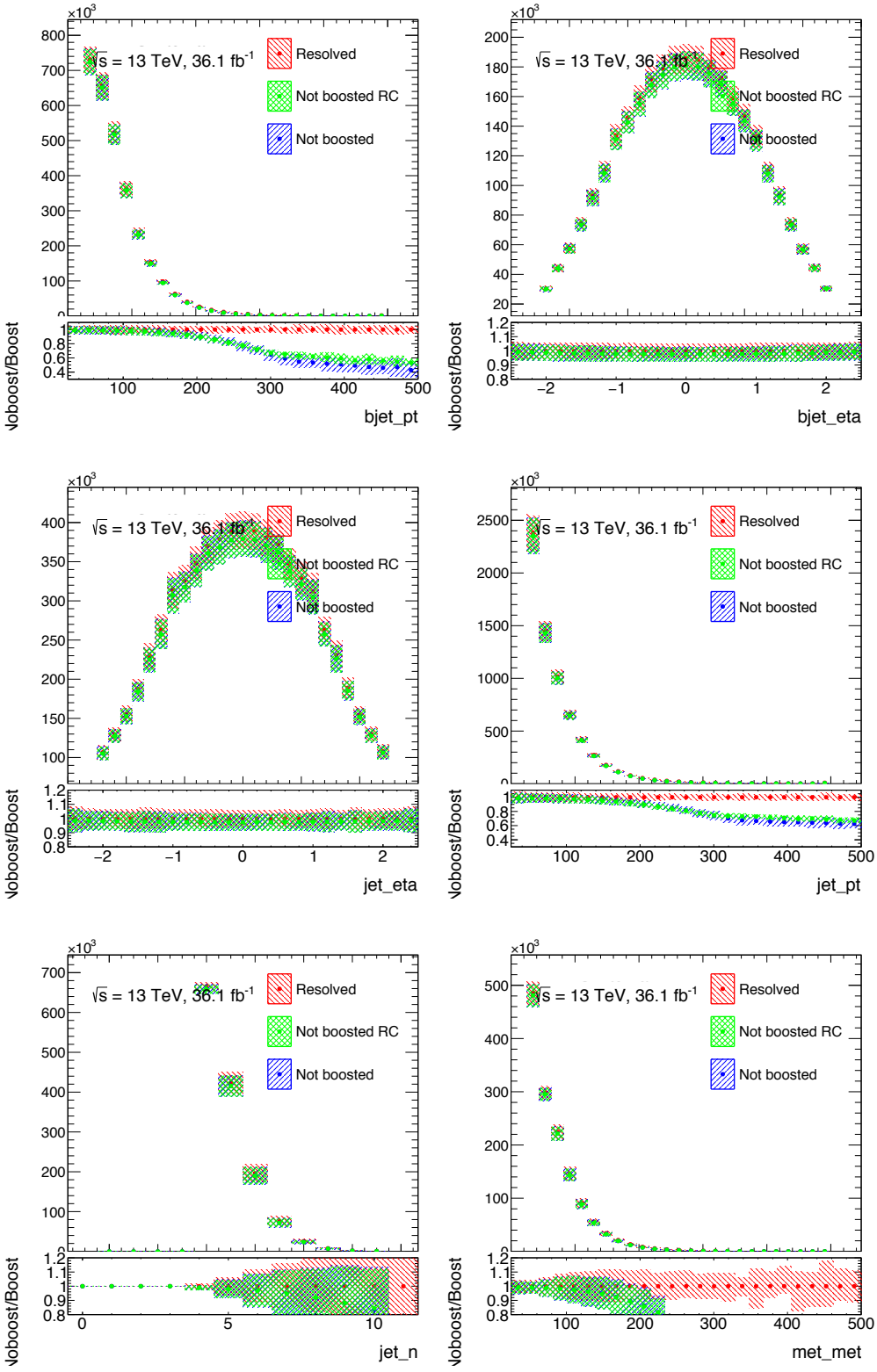

FIGURE C.1: Comparison between the resolved, resolved without RC boosted events and resolved without boosted events for basic kinematic distributions. The bottom pad shows the ratios of all the spectra divided by the spectrum obtained after the resolved selection.

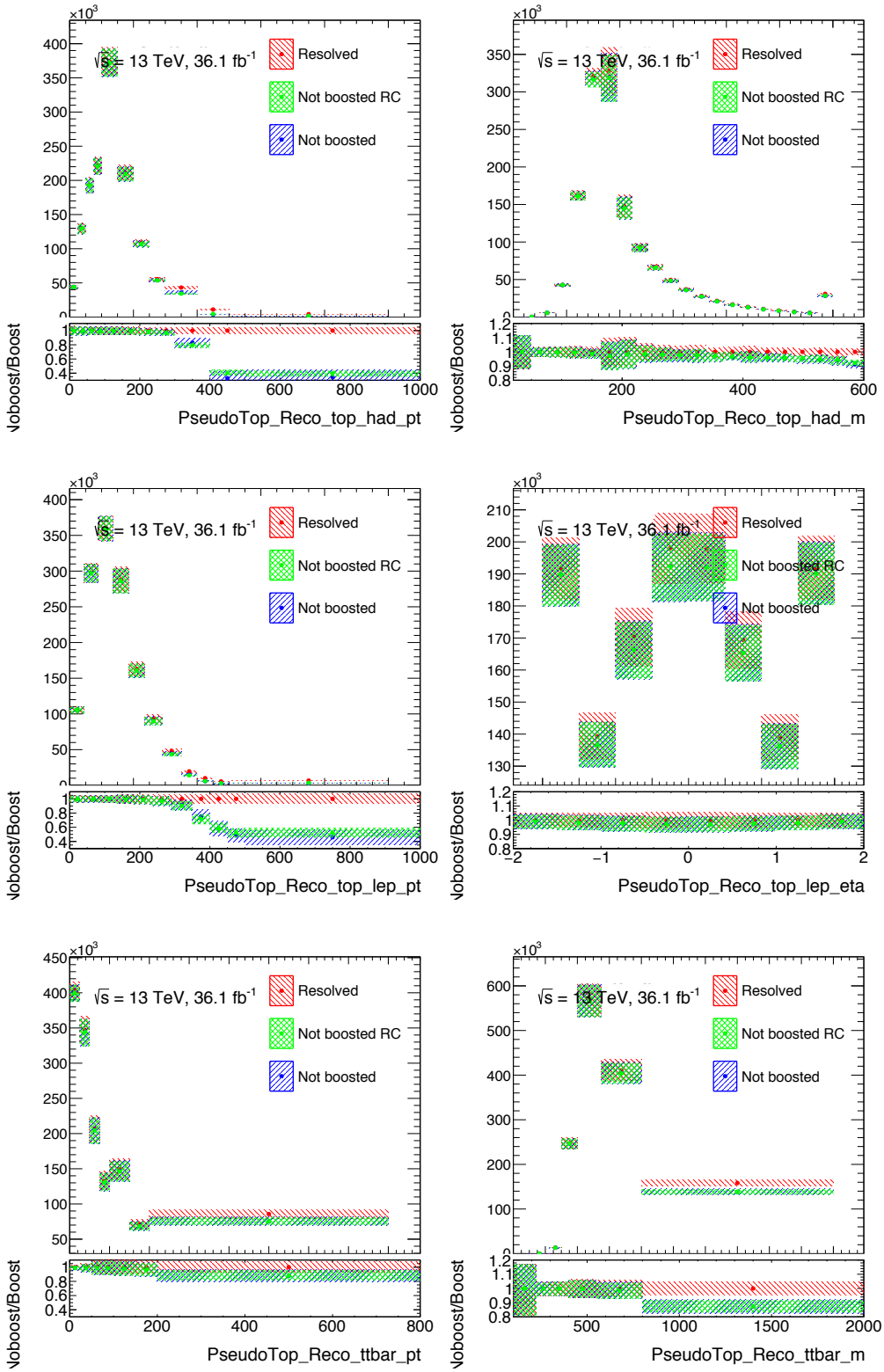

FIGURE C.2: Comparison between the resolved, resolved without RC boosted events and resolved without boosted events for basic pseudo-top kinematic distributions. The bottom pad shows the ratios of all the spectra divided by the spectrum obtained after the resolved selection.

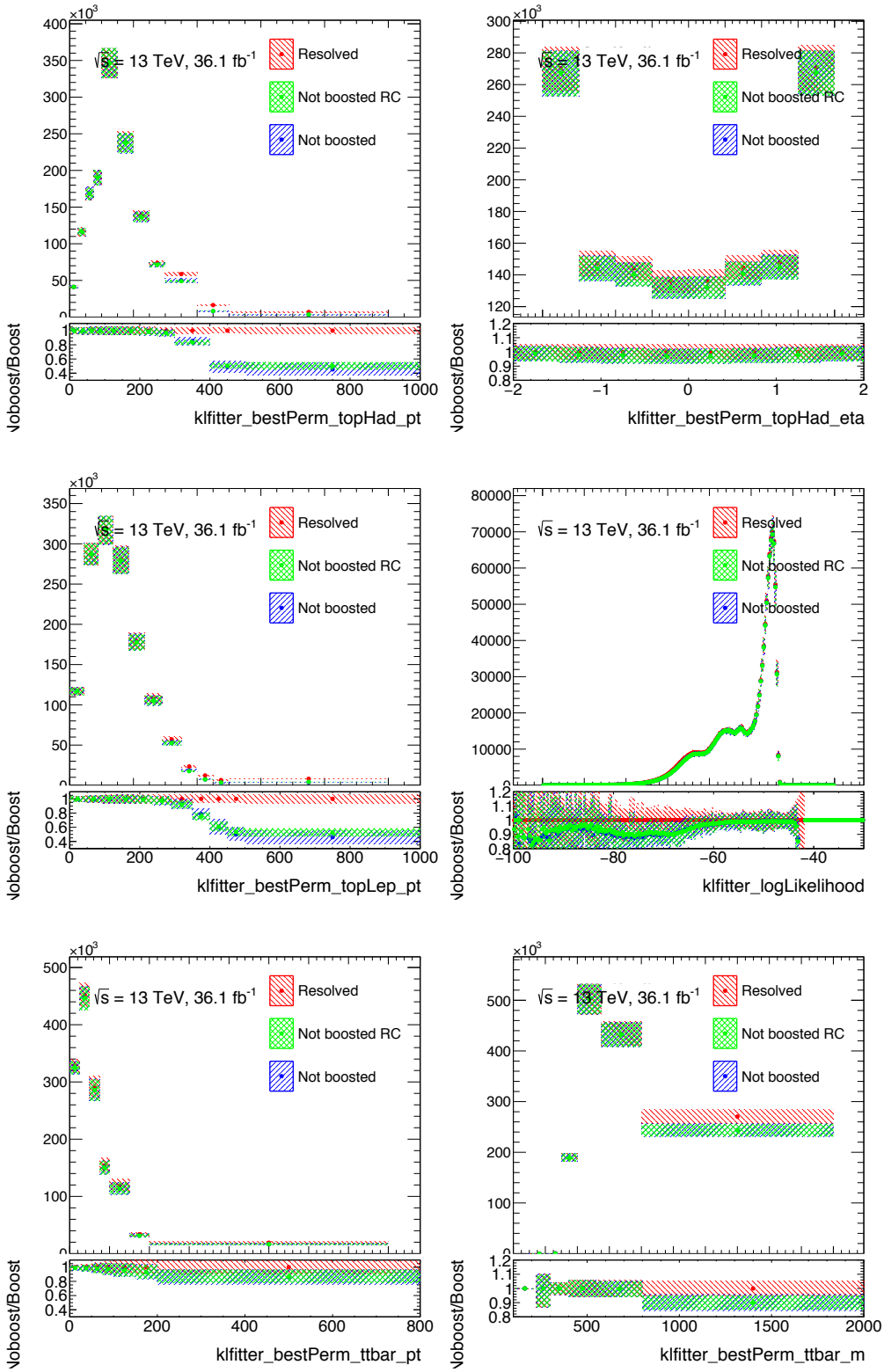

FIGURE C.3: Comparison between the resolved, resolved without RC boosted events and resolved without boosted events for basic KLFitter kinematic distributions. The bottom pad shows the ratios of all the spectra divided by the spectrum obtained after the resolved selection.

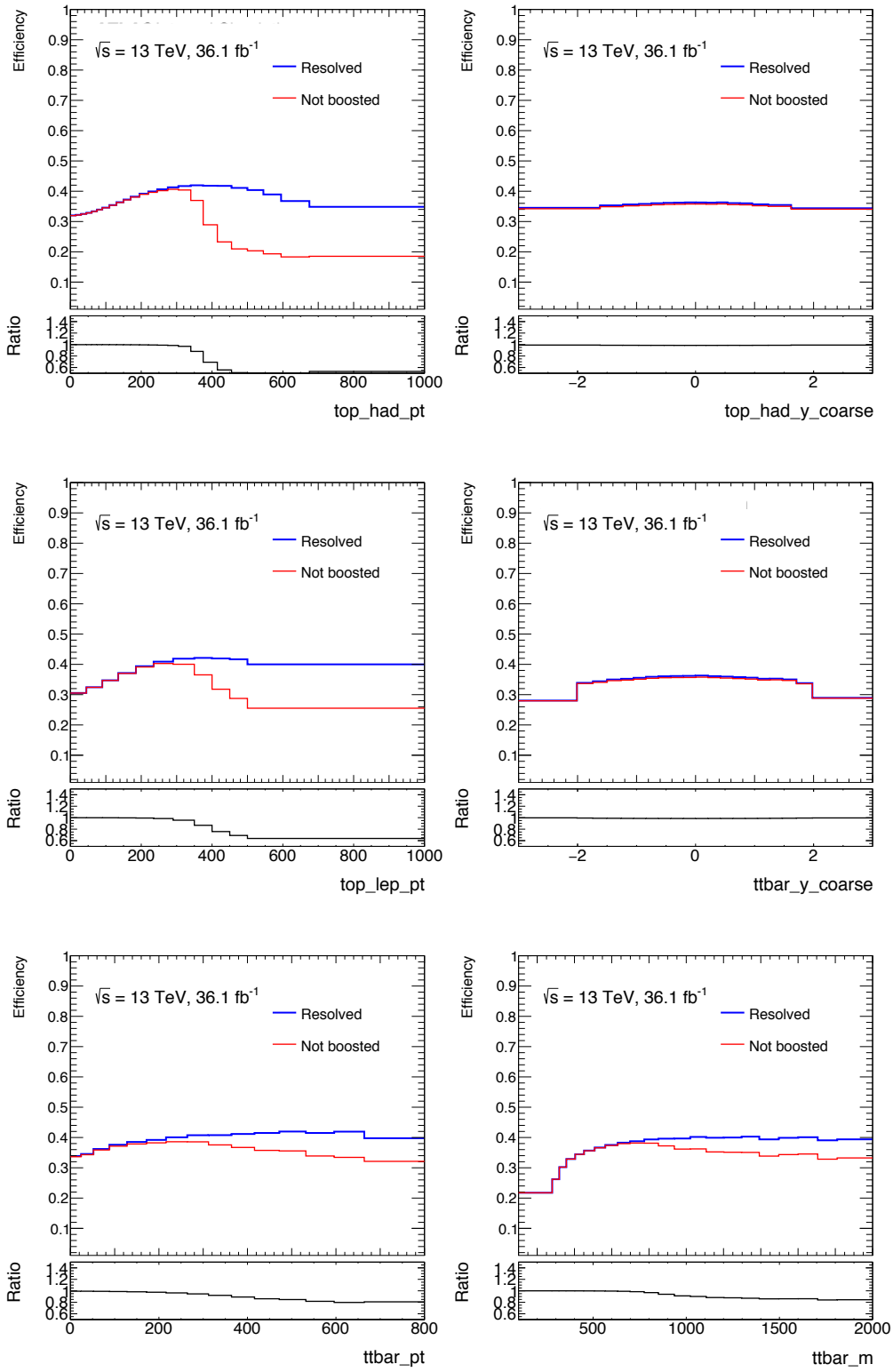

FIGURE C.4: Comparison between the resolved and resolved without boosted events for the efficiencies of basic pseudo-top kinematic distributions.

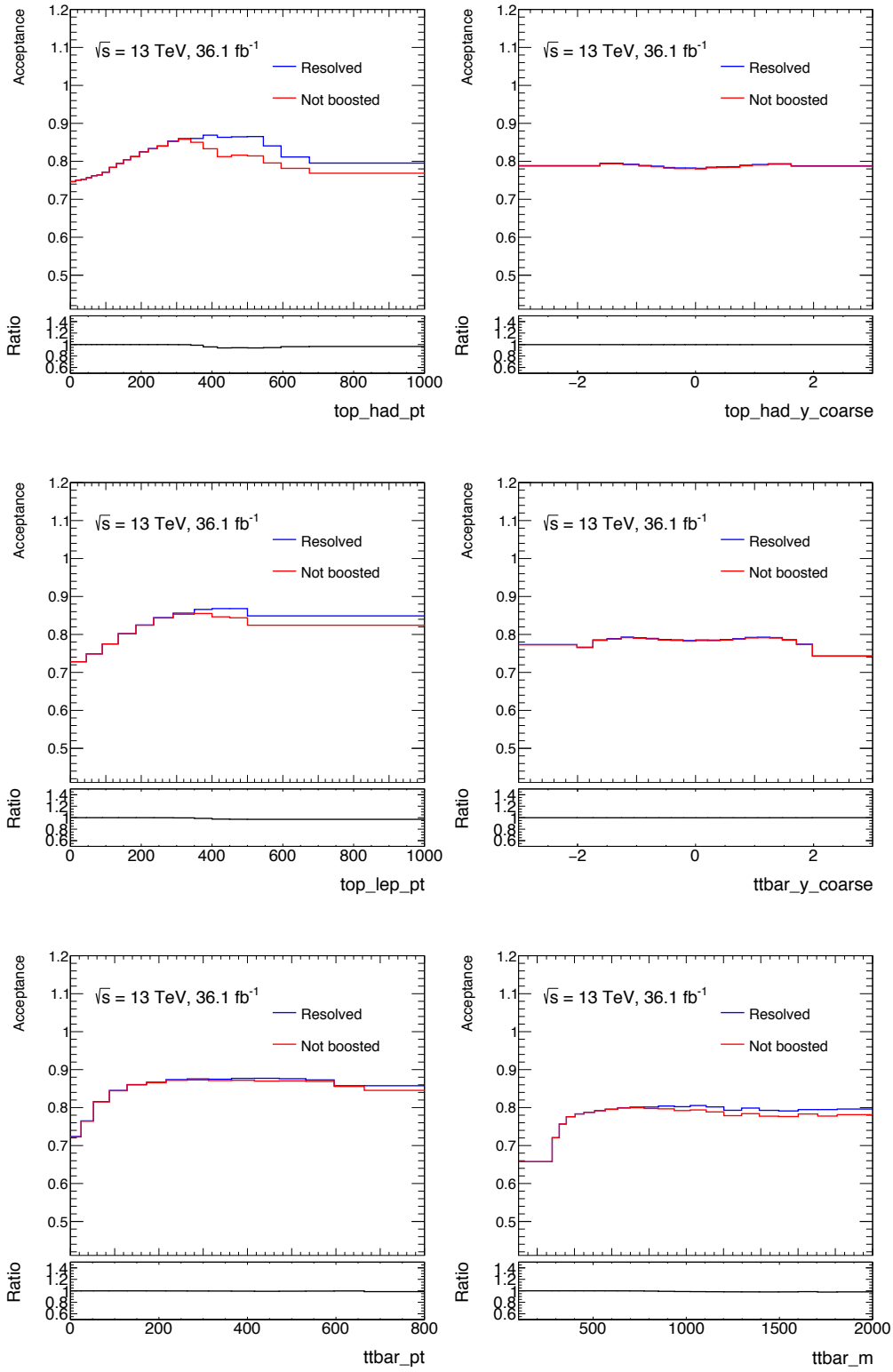

FIGURE C.5: Comparison between the resolved and resolved without boosted events for the efficiencies of basic pseudo-top kinematic distributions.

C.1 Validation of the orthogonal selection

The addition of the orthogonal selection has been validated in data. In the validation process, the efficiency of the 'Not boosted' cut in data, defined as $N_{\text{Noboost}}/N_{\text{Total}}$, has been compared with the same efficiency evaluated for the total signal+background prediction.

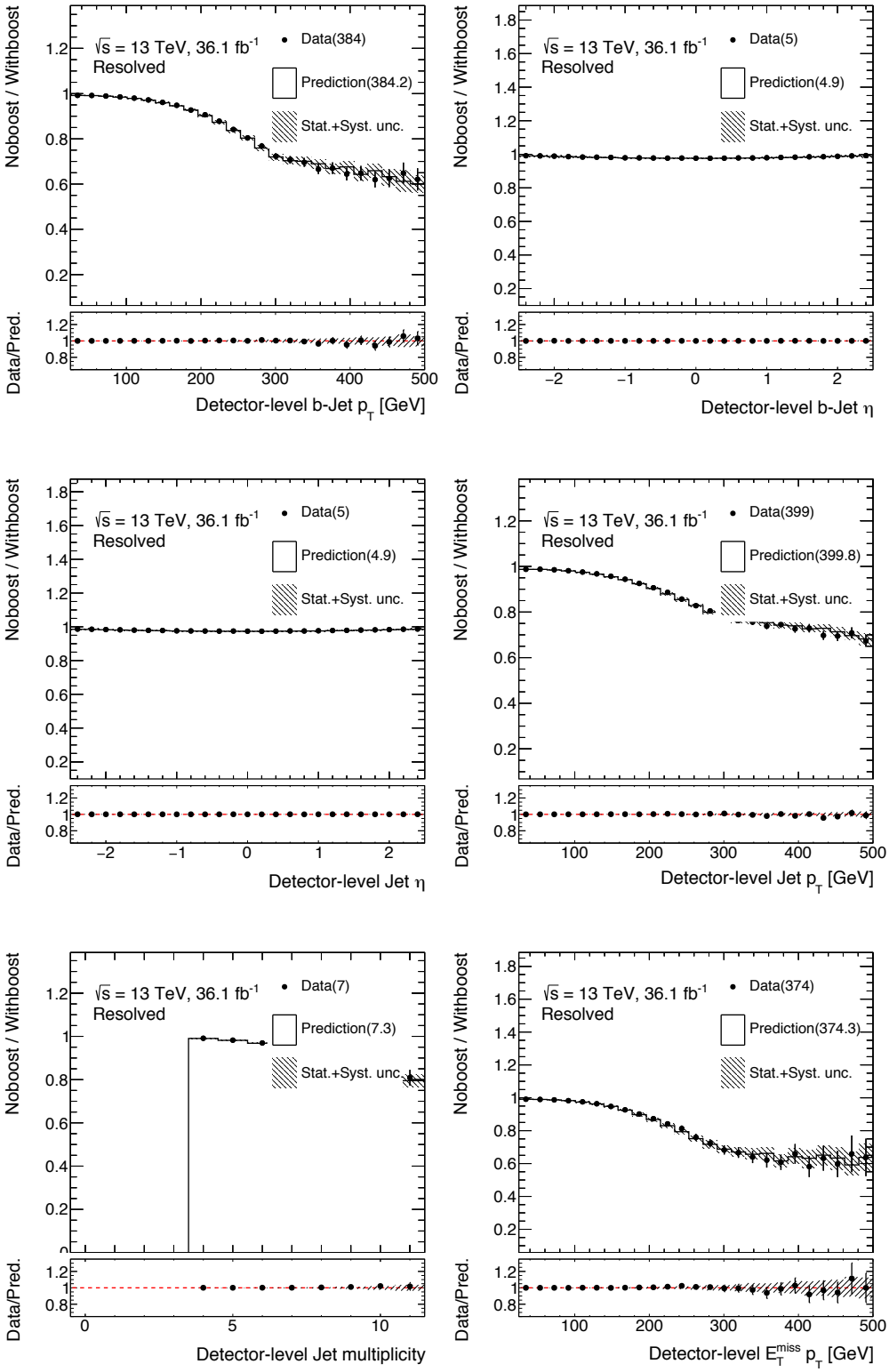

FIGURE C.6: Comparison between the ratio of the spectra after applying the resolved without boosted events selection and the spectra after applying the resolved selection obtained in data and prediction for basic kinematic variables.

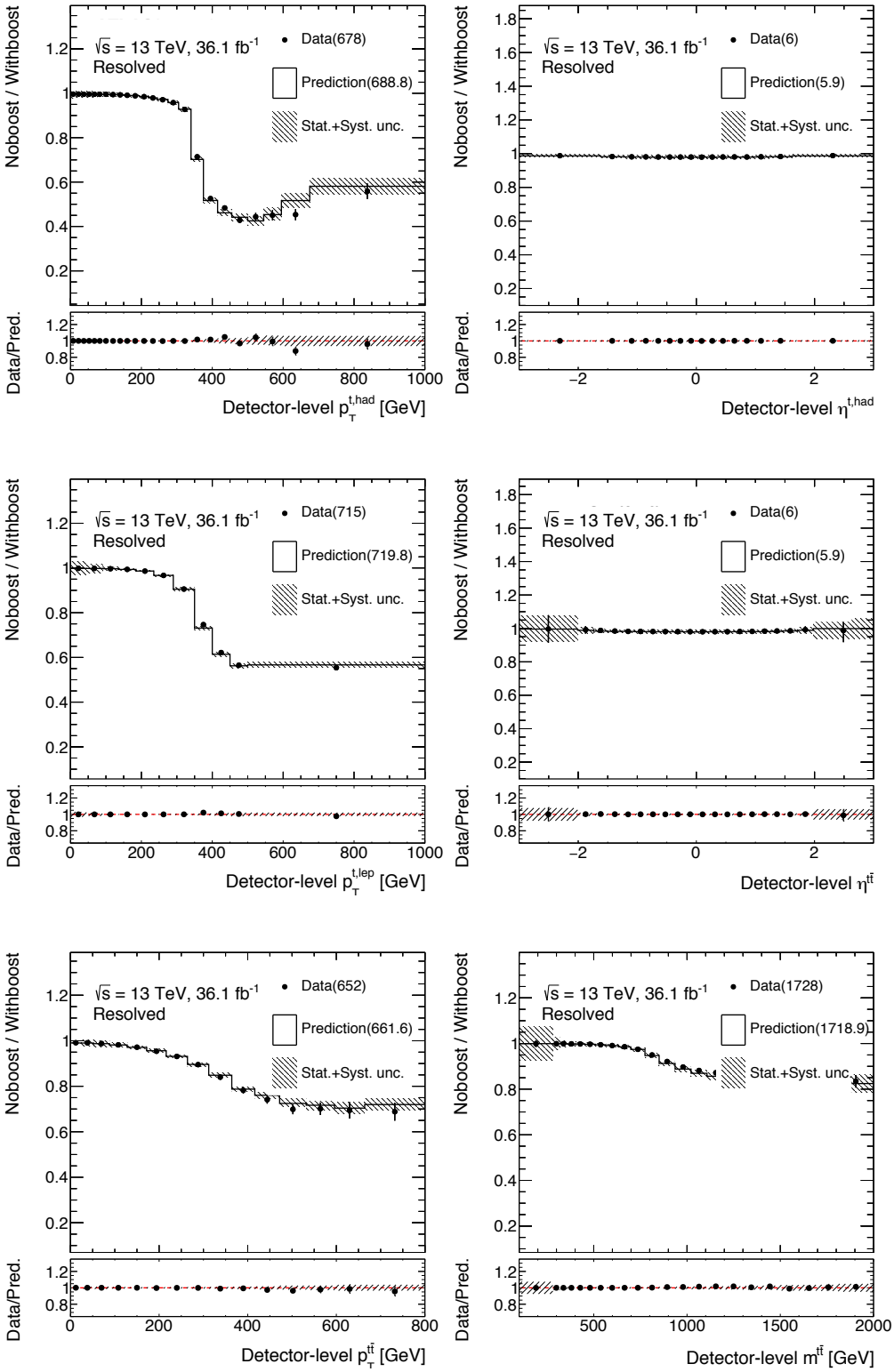

FIGURE C.7: Comparison between the ratio of the spectra after applying the resolved without boosted events selection and the spectra after applying the resolved selection obtained in data and prediction for basic pseudo top kinematic variables.

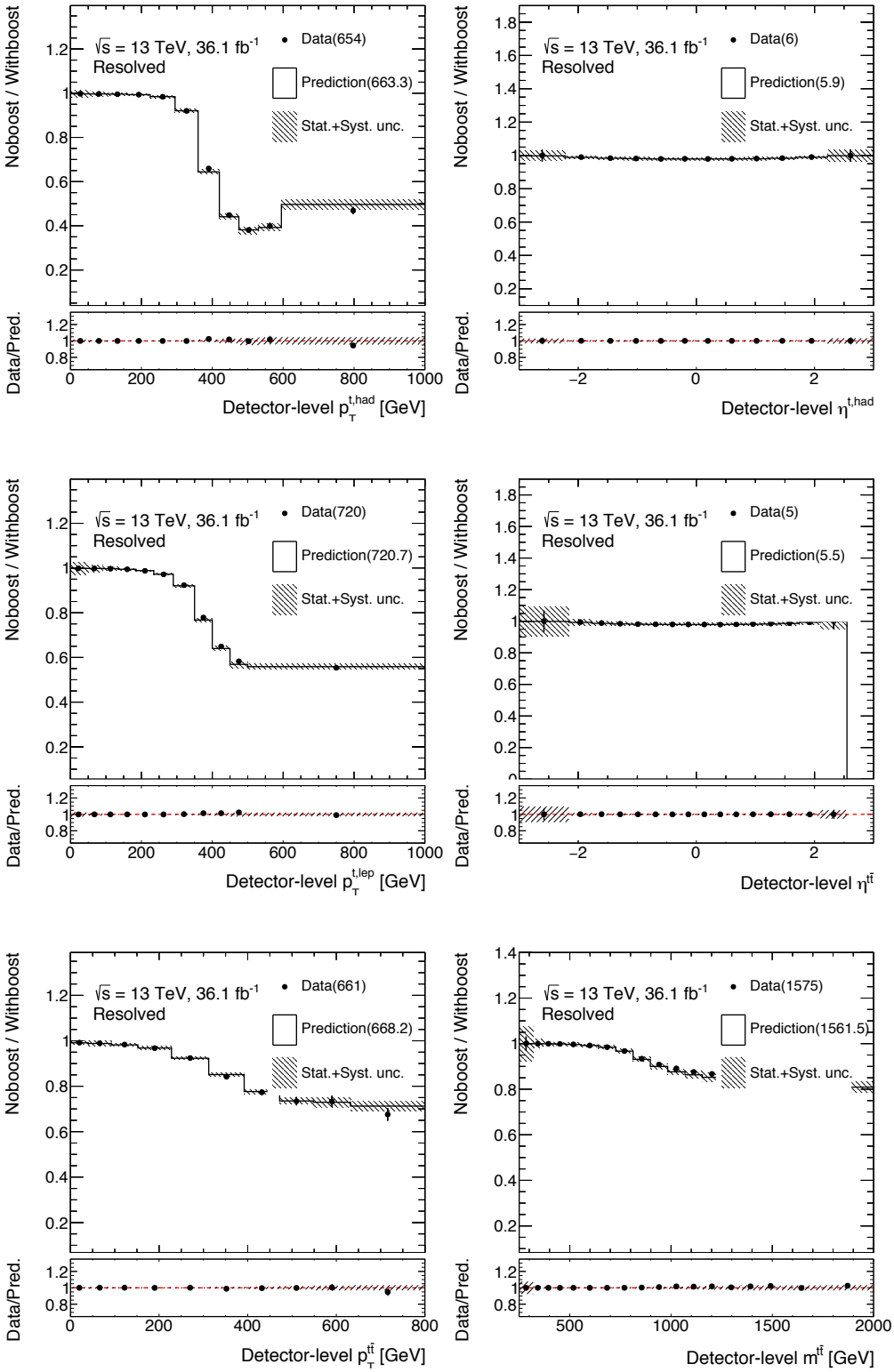

FIGURE C.8: Comparison between the ratio of the spectra after applying the resolved without boosted events selection and the spectra after applying the resolved selection obtained in data and prediction for basic klfitter kinematic variables.

C.2 Comparison of the two selection

In this appendix it has been shown that is possible to remove the events passing the boosted selection from the resolved without increasing the uncertainty in the resolved topology and maintainig a good compatibility among MC and data.

Figure C.3 shows that the larger part of the events passing both the boosted and the resolved selection is not well handled by the $t\bar{t}$ reconstruction at particle level in the resolved topology. An additional comparison of the reconstruction performace in the boosted and resolved topologies can be done on the events containing an high p_T top quark and with respect to the parton-level top. Figure C.9 shows the ΔR between the reconstructed and the parton-level top quark (left) and the relative difference between the reconstructed and the parton-level top quark p_{T} (right), for all the events passing the resolved or boosted selection containing a hadronic top with $p_{\mathrm{T}} > 350$ GeV.

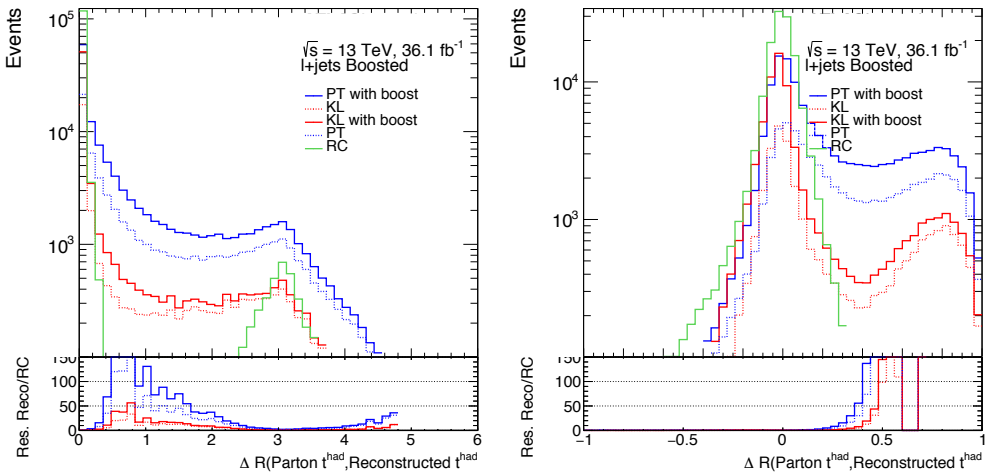

FIGURE C.9: Comparison between the reconstructed hadronic top and the parto- level top quark. Three different approaches are compared for the reconstruction of the hadronic top: the pseudo-top algorithm, klfitter and the boosted approach with reclustered jets. In case of klfitter and pseudo-top algorithm both the cases of retaining and removing the events passing the boosted selection are considered.

Appendix D

Estimation of the fraction of jets initiated by gluons

The flavour composition and flavour response uncertainties, which are two of the components of the Jet Energy Scale uncertainty, depend on the fraction of jets initiated by gluons. In the default configuration, the fraction of the jets initiated by gluons is set to 0.5 as well as the fraction of the jets initiated by light quarks with a 100% of uncertainty ($f_g = 0.5 \pm 0.5$). This setting is too conservative and it does not allow to have a proper evaluation of the uncertainties. So, the estimation of this fraction is studied for the specific topology of this analysis. The procedure to extract the quark-gluon fraction and its uncertainty is the following:

- **Truth jet matching** The jets at the detector level that pass all of the requirements are matched to jets at particle level ($\Delta R = 0.3$)
- **Particle matching** The partonic flavor of each jet is defined by the closest ($\Delta R < 0.4$) and more energetic parton based on MC truth information
- **Jet-flavour mapping** f_g depends on the p_{T} and the η of jets, so the jet flavour is evaluated in different regions of the phase-space.
- **Fraction** From the above mapping, the quark-gluon fraction is determined by taking the ratio:

$$f_{qg}(p_T, \eta) = \frac{N^{\text{jet}}_{\text{gluon}}}{N^{\text{jet}}_{\text{gluon}} + N^{\text{jet}}_{\text{non-gluon}}} \tag{D.1}$$

  where $N^{\text{jet}}_{\text{non-gluon}}$ is the number of jets assigned to light-flavour quarks (u, d and s quarks).
- **Uncertainty** The uncertainty $\sigma(f_{qg})$ is determined by comparing the f_{qg} coming from different MC samples, in particular:

- **MC generator** The absolute difference of f_{qg} between the nominal MC sample and the aMC@NLO +PYTHIA8 sample.
- **Hadronisation** The absolute difference of f_{qg} between the nominal MC sample and the POWHEG +HERWIG 7 sample.
- **ISR/FSR** The half of the absolute difference of f_{qg} between the nominal MC sample and the POWHEG+PYTHIA 8 samples used for the modeling of initial/final state radiation.

The final systematic uncertainty is defined as the quadratic sum of the different sources described above.

The events are selected by applying the same requirements applied of the nominal selection for both resolved and boosted topology, with the exception of the b-tagging selection to not create a possible bias in the estimation of the gluon fraction. In order to exploit the full MC statistics, the e+jets and μ+jets channel and the 2015 and 2016 data taking periods are combined together. It has been tested that there is no significant difference between the triggers used in the different channel and year configurations. The comparison between the results of the gluon fraction coming from the trigger requirements for each year and channel is shown in Figure D.1. The estimated gluon fraction used as input for the flavour composition and flavour response uncertainties is shown in Fig. D.2. Then, the expected reduction of the flavour composition and the flavour response uncertainties is evaluated by comparing the results using the gluon fraction estimation optimized for the topology of the analysis with the default one. In Figures D.3 and D.4 a comparison between the default and the more realistic flavour composition and the flavour response uncertainties are shown for the p_{T} and mass of the hadronic top and the $t\bar{t}$ system. The result is an overall reduction of these two uncertainty components of the JES uncertainty.

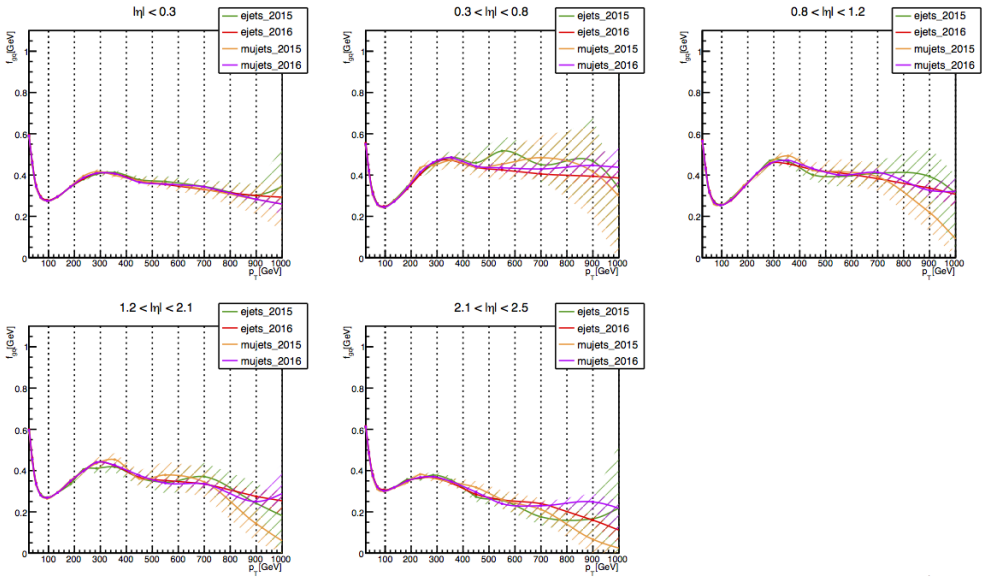

FIGURE D.1: Comparison between the gluon fractions estimated selecting a single lepton with the trigger requirements for e+jets and μ+jets channel and the 2015 and 2016 year. The shaded bands represent the uncertainty on the gluon fraction estimation.

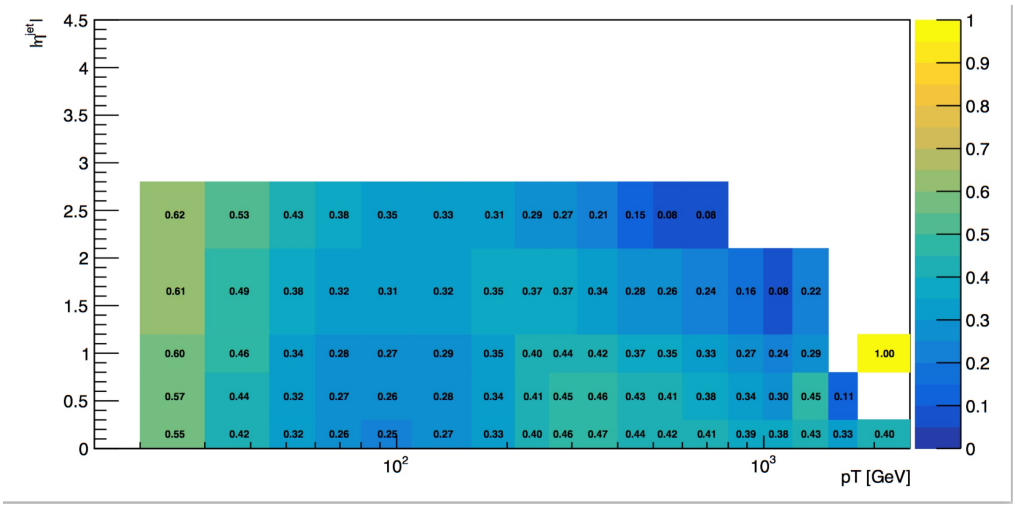

FIGURE D.2: Gluon fraction map in bins of the jet p_{T} and η estimated for the topology of the analysis.

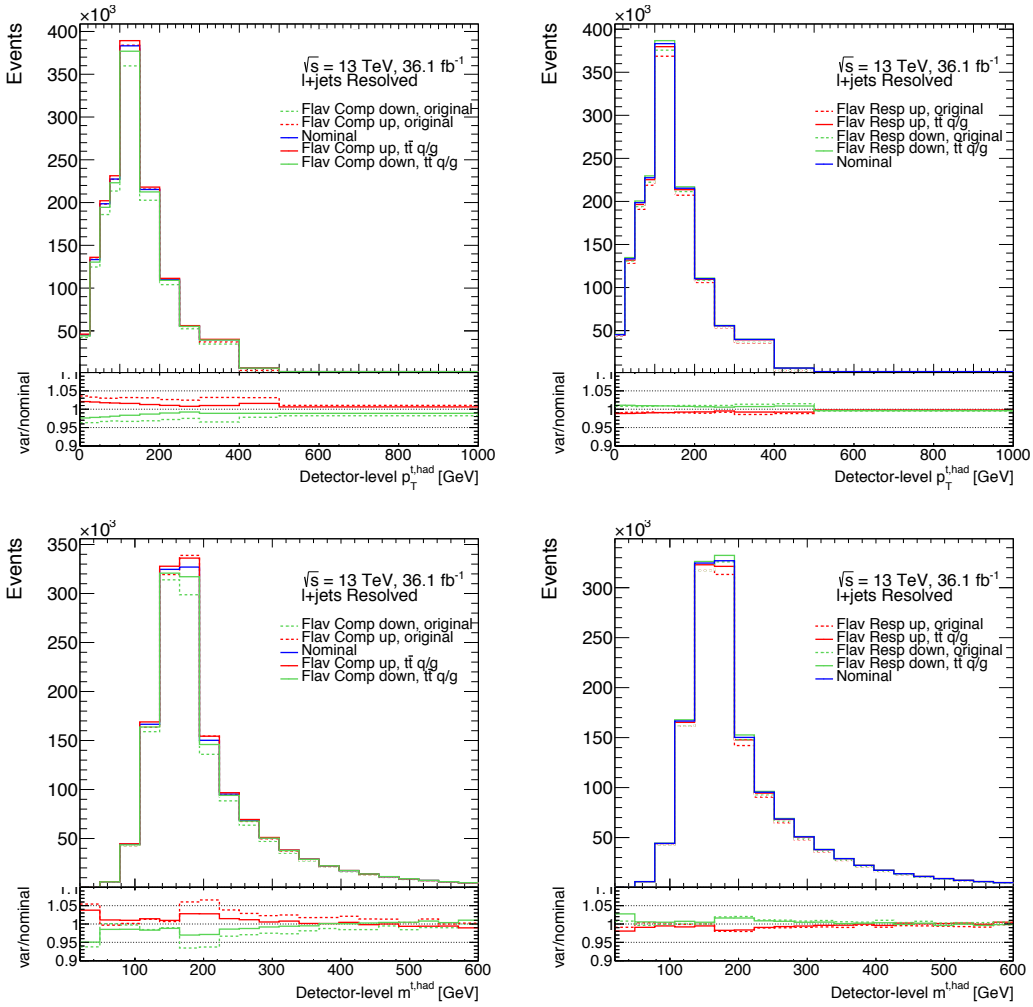

FIGURE D.3: Comparison between the default and the current flavour composition and (on the left) the flavour response uncertainties (on the right) for the p_{T} (on the top) and the mass (on bottom) of the hadronic top.

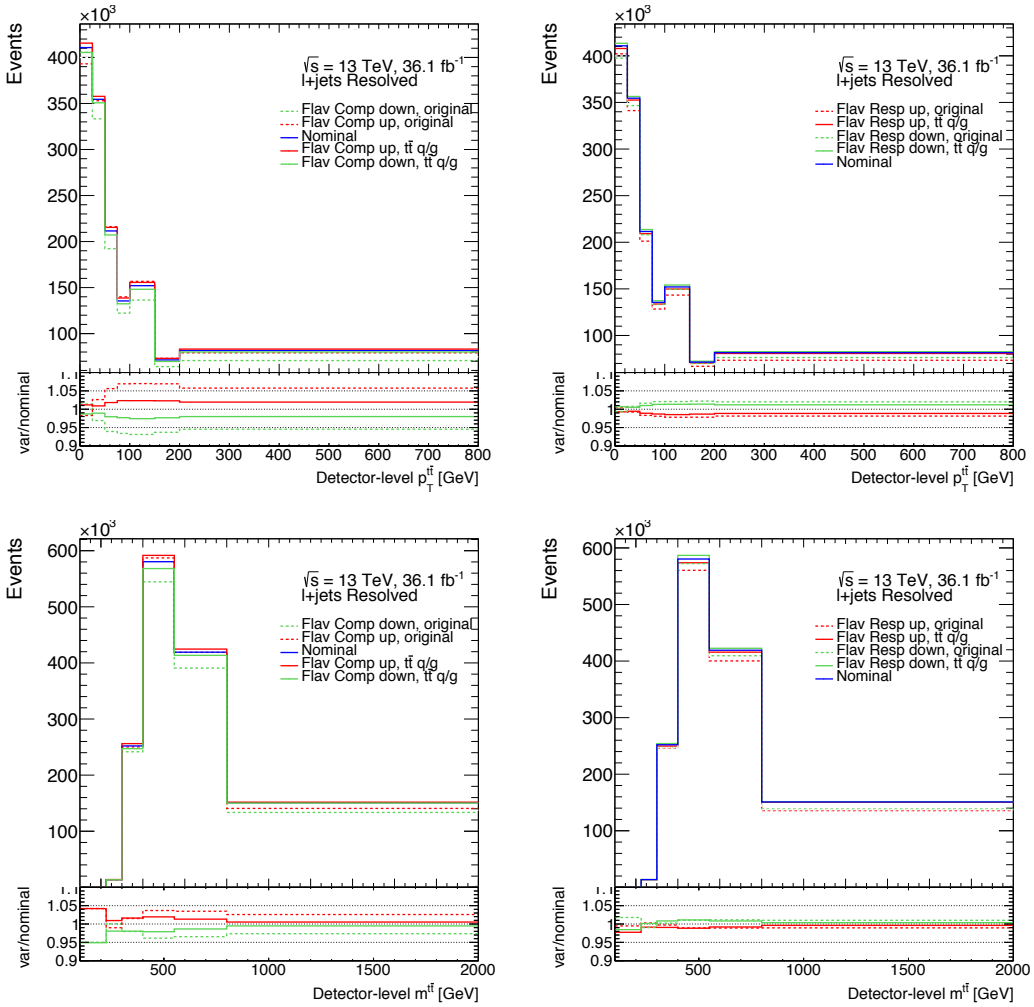

FIGURE D.4: Comparison between the default and the current flavour composition and (on the left) the flavour response uncertainties (on the right) for the p_{T} (on the top) and the mass (on bottom) of the $t\bar{t}$ system.

Appendix E

Comparison of different $t\bar{t}$ Monte Carlo Generators using Rivet

The systematic uncertainty related to the choice of the Monte Carlo generator used for the ME calculation is the most dominant among the uncertainties related to the $t\bar{t}$ modeling. A dedicated study on MC modeling has been carried out by using the Rivet routines validated for the analysis. The available version at the early stages of the analysis of MC@NLO interfaced with PYTHIA 8 for the parton shower used to estimate the hard scatter uncertainty , referred to as 'old' in the legend of the following plots, showed significant differences with respect to the nominal Monte Carlo sample generated with POWHEG interfaced with PYTHIA 8. The differences between these two predictions, together with the significant differences in the correction factors obtained from the two samples, led to a large uncertainty in the final unfolded measurement.

An updated version of MC@NLO +PYTHIA 8, labelled as 'new' in the legend of the plots showed in this Section, has been produced in which the scale choice is now dynamic and dependent on the value of H_T for each simulatated event, since this choice appears to be more suited to reproduce differential distributions [45]. A comparison of the normalised differential cross-section distributions as a function of several observables for the different Monte Carlo generators has been performed for both the resolved and boosted topology. In addition, a $t\bar{t}$ sample generated by using SHERPA is included in the study. The distributions are produced by running the Rivet routines on the EVNT files and so a comparison is possible for all the MC generators taken into account at both particle and parton level. The updated version of MC@NLO has been not available in xAOD format as the detector simulation was not performed for this particular sample. Therefore, a detector-level comparison was not possible among all the MC samples. The results are shown in Fig. E.1 for the resolved topology and in Fig. E.2 for the boosted one for the Rivet routine at particle level, while the partonic results are shown in Fig. E.3 and E.4 for the resolved and boosted topology, respectively.

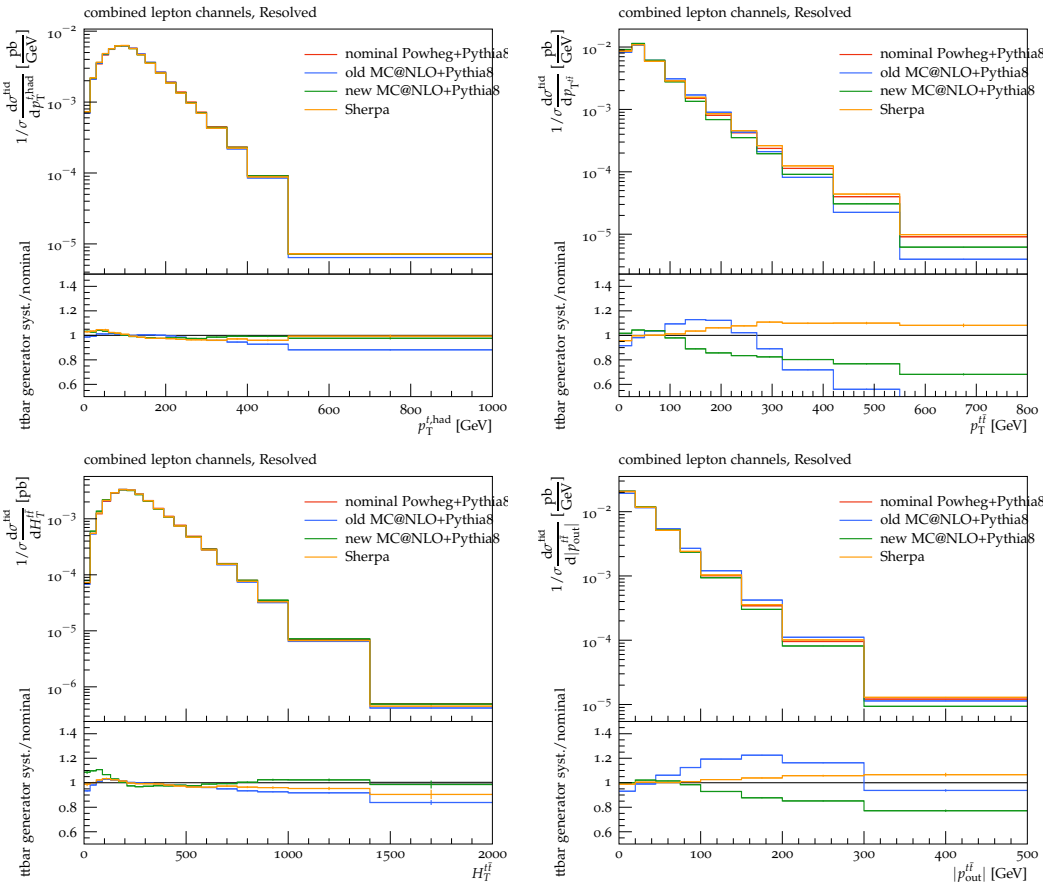

FIGURE E.1: Comparison of particle level predictions of different MC generators using the resolved Rivet routine. The normalized differential cross sections are shown as a function of p_T of hadronic pseudo-top (top left), the p_T of the $t\bar{t}$ system (top right), the scalar sum of the p_T of the top quarks H_T (bottom left) and the absolute value of $|p_{out}^{t\bar{t}}|$ (bottom right). The vertical bands on the distributions are the statistical uncertainties of MC samples.

The general comment on the results is that the prediction obtained by using SHERPA is closer to the POWHEG+PYTHIA 8 nominal prediction for all the observables taken into account for this study in the resolved topology. Indeed, for both the previous and the updated version of MC@NLO +PYTHIA 8 samples there are discrepancies with respect to the nominal prediction, in particular in the tails of the normalized differential cross-sections as a function of the p_T of the $t\bar{t}$ system. The predictions for the spcectrum of the p_T of the hadronic pseudo-top quark are much similar and the updated version of MC@NLO is closer to the nominal and the Sherpa sample. For the boosted topology, the general comment is still valid, but for the absolute value of the $|p_{out}^{t\bar{t}}|$ SHERPA shows very large discrepancies with respect to the nominal POWHEG+PYTHIA 8 prediction. Moreover, the differences between the MC predcitions of the generators are larger for observables more sensitive to extra radiation (e.g. p_T of the $t\bar{t}$ system).

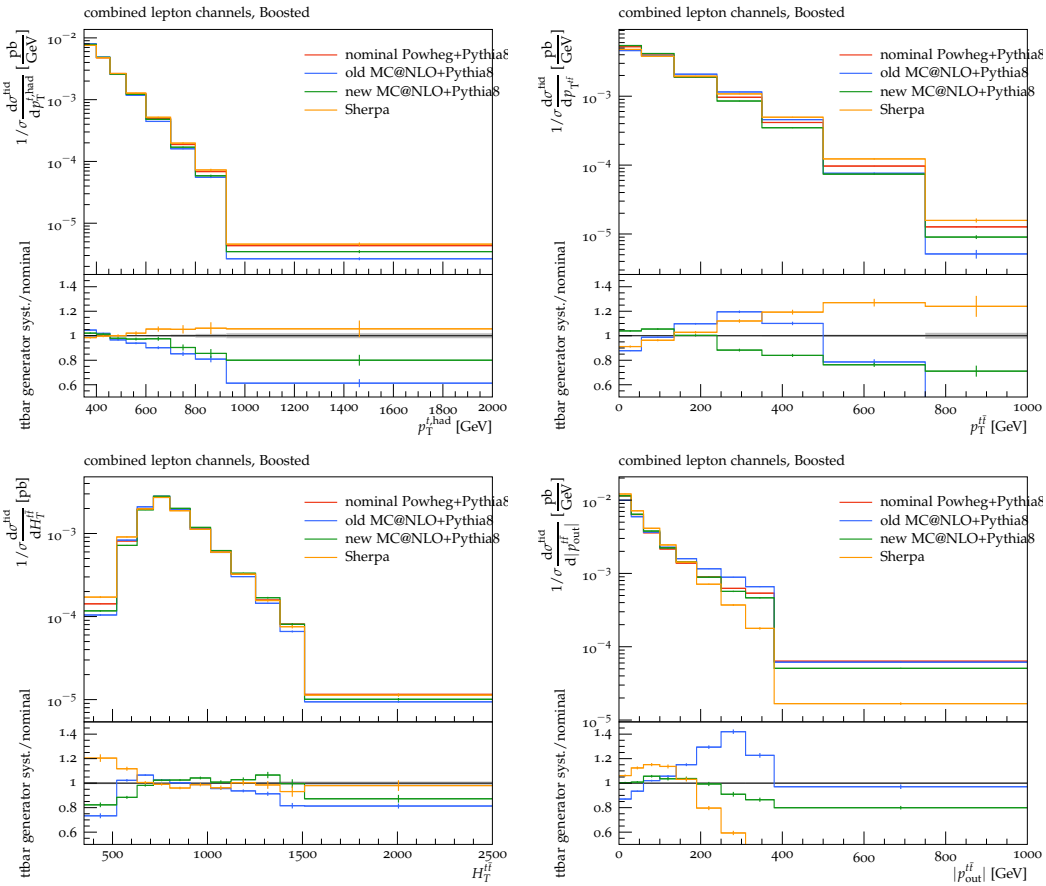

FIGURE E.2: Comparison of particle level predictions of different MC generators using the boosted Rivet routine. The normalized differential cross sections are shown as a function of p_T of hadronic pseudo-top (top left), the p_T of the $t\bar{t}$ system (top right), the scalar sum of the p_T of the top quarks H_T (bottom left) and the absolute value of $|p_{out}^{t\bar{t}}|$ (bottom right). The vertical bands on the distributions are the statistical uncertainties of MC samples.

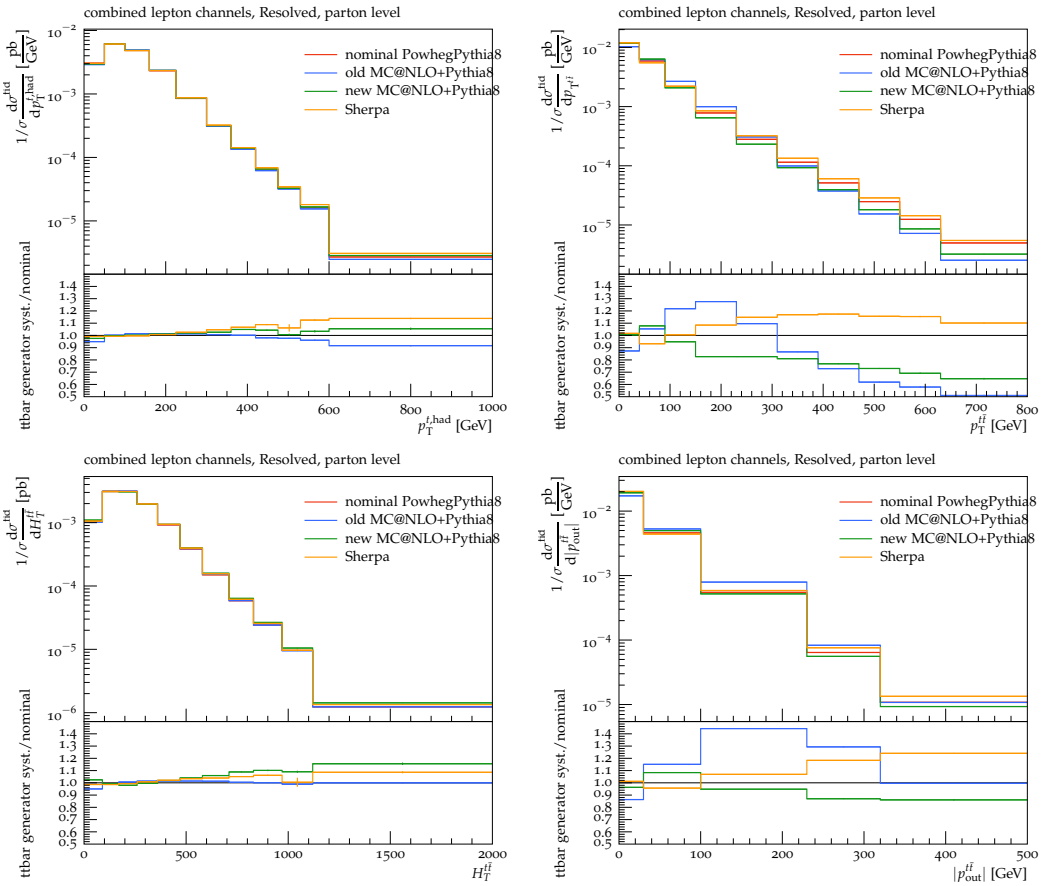

FIGURE E.3: Comparison of parton level predictions of different MC generators using the partonic resolved Rivet routine. The normalized differential cross sections are shown as a function of p_{T} of hadronic pseudo-top (top left), the p_{T} of the $t\bar{t}$ system (top right), the scalar sum of the p_{T} of the top quarks H_T (bottom left) and the absolute value of $|p_{\mathrm{out}}^{t\bar{t}}|$ (bottom right). The vertical bands on the distributions are the statistical uncertainties of MC samples.

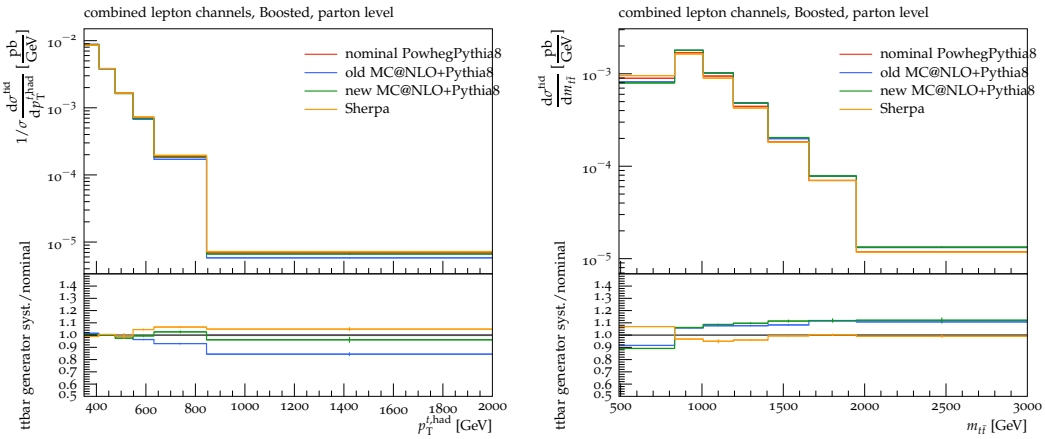

FIGURE E.4: Comparison of parton level predictions of different MC generators using the partonic boosted Rivet routine. The normalized differential cross sections are shown as a function of p_{T} of hadronic pseudo-top (left) and the m of the $t\bar{t}$ system (right). The vertical bands on the distributions are the statistical uncertainties of MC samples.

Appendix F

Systematic Tables

F.1 Particle level

F.1.1 Absolute differential cross section

F.1.1.1 Resolved topology

Bins [GeV]	0–20	20–45	45–75	75–100	100–150	150–200	200–300	300–500
$d\sigma$ / $d\lvert p_{out}^{t\bar{t}}\rvert$ [pb/GeV]	$1.86 \cdot 10^{0}$	$1.02 \cdot 10^{0}$	$4.35 \cdot 10^{-1}$	$2.05 \cdot 10^{-1}$	$8.57 \cdot 10^{-2}$	$2.95 \cdot 10^{-2}$	$7.98 \cdot 10^{-3}$	$1.01 \cdot 10^{-3}$
Total Uncertainty [%]	$^{+11.5}_{-12.5}$	$^{+11.0}_{-11.9}$	$^{+13.5}_{-13.3}$	$^{+12.1}_{-11.6}$	$^{+9.96}_{-10.0}$	$^{+9.21}_{-9.02}$	$^{+8.47}_{-8.29}$	$^{+10.4}_{-10.5}$
Statistics [%]	±0.1	±0.1	±0.2	±0.4	±0.5	±0.9	±1.3	±2.6
Systematics [%]	$^{+11.5}_{-12.5}$	$^{+11.0}_{-11.9}$	$^{+13.5}_{-13.3}$	$^{+12.0}_{-11.6}$	$^{+9.94}_{-9.99}$	$^{+9.13}_{-8.94}$	$^{+8.33}_{-8.14}$	$^{+10.0}_{-10.1}$
Jet energy resolution [%]	±0.28	±1.02	±1.60	±1.19	±1.08	∓1.06	∓1.33	∓0.80
b-Tagged jet energy scale (JES) [%]	±0.47	$^{+0.46}_{-0.49}$	$^{+0.54}_{-0.55}$	$^{+0.72}_{-0.59}$	$^{+0.60}_{-0.63}$	$^{+0.55}_{-0.61}$	$^{+0.62}_{-0.80}$	$^{+0.45}_{-0.36}$
Effective detector NP set 1 (JES) [%]	-	-	-	-	$^{+0.12}_{-0.10}$	-	$^{+0.22}_{-0.16}$	-
Effective detector NP set 2 (JES) [%]	-	-	-	-	-	-	$^{+0.15}_{-0.11}$	±0.13
Effective mixed NP set 1 (JES) [%]	-	-	$^{+0.20}_{-0.18}$	$^{+0.36}_{-0.24}$	$^{+0.34}_{-0.41}$	$^{+0.47}_{-0.44}$	$^{+0.68}_{-0.69}$	$^{+1.35}_{-1.22}$
Effective mixed NP set 2 (JES) [%]	-	-	-	-	-	-	$^{+0.10}_{-0.13}$	-
Effective modelling NP set 1 (JES) [%]	$^{+1.85}_{-1.74}$	$^{+2.36}_{-2.37}$	$^{+3.01}_{-2.94}$	$^{+2.84}_{-2.61}$	$^{+2.15}_{-2.22}$	$^{+1.55}_{-1.38}$	$^{+1.38}_{-1.18}$	$^{+0.87}_{-1.45}$
Effective modelling NP set 2 (JES) [%]	$^{+0.16}_{-0.16}$	$^{+0.22}_{-0.22}$	$^{+0.21}_{-0.21}$	-	-	$^{+0.11}_{-0.12}$	$^{+0.24}_{-0.17}$	$^{+0.57}_{-0.63}$
Effective modelling NP set 3 (JES) [%]	$^{+0.17}_{±0.12}$	$^{+0.21}_{-0.14}$	$^{+0.24}_{+0.12}$	$^{+0.19}_{-}$	$^{-0.17}_{+0.13}$	$^{+0.17}_{-0.15}$	$^{+0.43}_{-0.36}$	$^{+0.36}_{-0.58}$
Effective modelling NP set 4 (JES) [%]	-	$^{+0.10}_{-0.11}$	$^{+0.16}_{-0.15}$	$^{+0.17}_{-0.11}$	±0.14	-	$^{+0.24}_{-0.16}$	-
Effective statistical NP set 1 (JES) [%]	$^{+0.31}_{-0.30}$	$^{+0.43}_{-0.42}$	$^{+0.52}_{-0.49}$	$^{+0.45}_{-0.42}$	$^{+0.33}_{-0.35}$	$^{+0.16}_{-0.21}$	$^{+0.25}_{-0.20}$	-
Effective statistical NP set 2 (JES) [%]	$^{+0.26}_{+0.27}$	∓0.37	$^{+0.43}_{+0.45}$	$^{+0.35}_{+0.39}$	$^{+0.31}_{+0.29}$	$^{+0.16}_{+0.14}$	$^{+0.10}_{+0.12}$	-
Effective statistical NP set 3 (JES) [%]	-	-	-	-	-	-	-	$^{-0.69}_{+0.46}$
Effective statistical NP set 4 (JES) [%]	-	-	-	-	$^{+0.20}_{-0.23}$	$^{+0.20}_{-0.21}$	$^{+0.33}_{-0.35}$	$^{+0.21}_{-0.39}$
Effective statistical NP set 5 (JES) [%]	-	-	-	-	$^{-0.11}_{+0.10}$	-	$^{+0.19}_{-0.10}$	$^{+0.35}_{-0.38}$
Effective statistical NP set 6 (JES) [%]	-	-	-	-	-	$^{-0.15}_{-}$	-	$^{+0.12}_{-0.15}$
Effective statistical NP set 7 (JES) [%]	-	-	$^{+0.11}_{-}$	-	$^{+0.13}_{-0.12}$	$^{+0.10}_{-0.13}$	$^{+0.23}_{-0.19}$	±0.14
η intercalibration model (JES) [%]	$^{+0.52}_{-0.50}$	$^{+0.56}_{-0.61}$	$^{+0.83}_{-0.91}$	$^{+1.04}_{-0.84}$	$^{+0.79}_{-0.90}$	$^{+0.85}_{-0.83}$	$^{+0.74}_{-0.75}$	$^{+0.94}_{-0.63}$
η intercalibration non closure (JES) [%]	∓0.21	∓0.24	$^{-0.32}_{+0.35}$	$^{-0.34}_{+0.38}$	$^{-0.40}_{+0.33}$	∓0.27	$^{-0.34}_{+0.28}$	$^{-0.68}_{+0.73}$
η intercalibration total stat (JES) [%]	±0.32	±0.40	$^{+0.58}_{-0.54}$	$^{+0.63}_{-0.57}$	$^{+0.48}_{-0.52}$	$^{+0.32}_{-0.38}$	$^{+0.41}_{-0.39}$	$^{+0.15}_{-0.29}$
Flavour composition (JES) [%]	$^{+1.71}_{-1.79}$	$^{+1.81}_{-2.03}$	$^{+2.58}_{-2.63}$	$^{+2.75}_{-2.61}$	$^{+1.93}_{-2.25}$	$^{+1.48}_{-1.07}$	$^{+1.19}_{-1.09}$	$^{+0.84}_{-0.82}$
Flavour response (JES) [%]	∓0.85	$^{-0.93}_{+0.88}$	$^{-1.34}_{+1.29}$	$^{-1.37}_{+1.45}$	$^{-1.19}_{+1.01}$	$^{-0.79}_{+0.87}$	$^{-0.62}_{+0.63}$	$^{-0.78}_{+0.85}$
Pile-up offset μ (JES) [%]	∓0.11	$^{-0.12}_{+0.14}$	$^{-0.18}_{+0.21}$	$^{-0.25}_{+0.24}$	$^{-0.18}_{+0.16}$	-	$^{-0.13}_{+0.18}$	-
Pile-up offset N_{PV} (JES) [%]	$^{+0.36}_{-0.31}$	$^{+0.48}_{-0.51}$	$^{+0.65}_{-0.66}$	$^{+0.81}_{-0.53}$	$^{+0.48}_{-0.58}$	$^{+0.33}_{-0.37}$	$^{+0.40}_{-0.22}$	$^{+0.51}_{-0.36}$
Pile-up offset p_T (JES) [%]	-	$^{-0.11}_{+0.12}$	-	$^{+0.36}_{-0.25}$	$^{+0.40}_{-0.59}$	$^{+0.79}_{-0.71}$	$^{+0.65}_{-0.70}$	$^{+1.36}_{-1.22}$
Pile-up offset ρ topology (JES) [%]	$^{+2.60}_{-2.52}$	±3.48	$^{+4.69}_{-4.47}$	$^{+4.65}_{-4.15}$	$^{+3.52}_{-3.59}$	$^{+2.53}_{-2.35}$	$^{+2.21}_{-2.14}$	$^{+1.33}_{-1.35}$
Jet vertex fraction [%]	$^{+0.65}_{-0.68}$	$^{+0.73}_{-0.77}$	$^{+0.80}_{-0.83}$	$^{+0.72}_{-0.76}$	$^{+0.59}_{-0.62}$	$^{+0.44}_{-0.48}$	$^{+0.36}_{-0.40}$	$^{+0.24}_{-0.29}$
b-Quark tagging efficiency (eigenvector 0) [%]	$^{-6.70}_{+7.04}$	$^{-6.51}_{+6.74}$	$^{-6.15}_{+6.28}$	$^{-5.92}_{+6.04}$	$^{-5.77}_{+5.91}$	$^{-5.65}_{+5.79}$	$^{-5.74}_{+5.87}$	$^{-5.72}_{+5.85}$
b-Quark tagging efficiency (eigenvector 1) [%]	$^{-1.91}_{+1.86}$	$^{-1.92}_{+1.95}$	$^{-1.95}_{+1.97}$	$^{-2.02}_{+2.03}$	$^{-2.12}_{+2.14}$	$^{-2.37}_{+2.39}$	$^{-2.72}_{+2.75}$	$^{-3.35}_{+3.39}$
b-Quark tagging efficiency (eigenvector 2) [%]	$^{+1.32}_{-1.30}$	$^{+1.25}_{-1.24}$	±1.14	±1.05	$^{+0.97}_{-0.96}$	$^{+0.84}_{-0.83}$	±0.62	±0.22
b-Quark tagging efficiency (eigenvector 3) [%]	-	-	-	-	-	±0.12	-	-
c-Quark tagging efficiency (eigenvector 0) [%]	±0.26	±0.28	±0.29	±0.28	±0.25	±0.23	$^{+0.20}_{-0.19}$	±0.18
c-Quark tagging efficiency (eigenvector 1) [%]	∓0.21	∓0.23	∓0.26	$^{-0.27}_{+0.28}$	∓0.32	∓0.35	∓0.32	$^{-0.33}_{+0.34}$
Light-jet tagging efficiency (eigenvector 0) [%]	$^{-0.58}_{+0.59}$	$^{-0.70}_{+0.73}$	$^{-0.71}_{+0.73}$	$^{-0.74}_{+0.76}$	$^{-0.74}_{+0.75}$	$^{-0.85}_{+0.88}$	$^{-0.79}_{+0.82}$	$^{-0.80}_{+0.83}$
Light-jet tagging efficiency (eigenvector 1) [%]	$^{+0.21}_{-0.20}$	$^{+0.26}_{-0.25}$	$^{+0.25}_{-0.24}$	±0.20	±0.21	$^{+0.19}_{-0.18}$	±0.15	-
Light-jet tagging efficiency (eigenvector 3) [%]	-	-	-	-	-	∓0.10	-	-
Light-jet tagging efficiency (eigenvector 5) [%]	-	-	-	-	-	∓0.11	-	-
b-Quark tagging extrapolation [%]	-	-	-	-	±0.11	±0.17	±0.31	±0.94
Electron trigger efficiency [%]	±0.12	$^{+0.12}_{-0.11}$	±0.11	±0.11	±0.12	±0.11	±0.11	±0.12
Electron identification efficiency [%]	±0.41	±0.41	±0.41	±0.42	±0.44	±0.46	±0.48	±0.53
Electron isolation efficiency [%]	±0.10	±0.10	±0.11	±0.12	±0.14	±0.16	±0.19	±0.25
Muon trigger efficiency stat [%]	±0.30	±0.29	$^{+0.28}_{-0.29}$	$^{+0.28}_{-0.29}$	$^{+0.28}_{-0.29}$	±0.29	±0.28	$^{+0.28}_{-0.29}$
Muon trigger efficiency syst [%]	$^{+0.52}_{-0.51}$	$^{+0.51}_{-0.50}$	$^{+0.51}_{-0.50}$	±0.50	$^{+0.50}_{-0.49}$	$^{+0.51}_{-0.50}$	$^{+0.51}_{-0.50}$	$^{+0.50}_{-0.49}$
Muon identification stat [%]	-	-	-	-	-	-	-	-
Muon identification syst [%]	±0.38	±0.37	±0.37	±0.38	±0.38	$^{+0.40}_{-0.39}$	$^{+0.41}_{-0.40}$	±0.43
Muon isolation efficiency syst [%]	±0.11	±0.10	±0.10	±0.10	±0.10	±0.10	±0.10	±0.10
E_T^{miss} Soft jet resolution para [%]	-	-	±0.13	-	-	-	±0.39	∓0.10
E_T^{miss} Soft jet resolution perp [%]	-	-	-	±0.12	-	-	±0.16	±0.27
E_T^{miss} Soft jet scale [%]	-	-	$^{-0.10}_{+0.15}$	$^{-}_{+0.19}$	-	-	-	-
Luminosity [%]	∓2.02	∓2.04	∓2.06	∓2.06	∓2.05	∓2.05	∓2.05	∓2.05
Z+jets cross-section [%]	±0.60	±0.55	±0.45	±0.48	±0.46	±0.67	±0.53	±0.68
Monte Carlo sample statistics [%]	±0.11	±0.11	±0.23	±0.28	±0.32	±0.68	±0.78	±1.51
ISR/FSR + scale [%]	$^{-}_{-5.40}$	$^{-}_{-4.71}$	$^{+1.06}_{-0.76}$	$^{+0.92}_{-}$	$^{+0.99}_{-}$	$^{-}_{-0.95}$	$^{+0.77}_{-}$	$^{-1.04}_{+0.40}$
Alternate hard-scattering model [%]	±1.85	±3.68	±5.54	±3.86	±2.57	±3.70	±2.06	±1.65
Alternate parton-shower model [%]	∓5.06	∓1.71	±6.09	±5.27	±3.23	±2.23	±0.40	±4.31
Inter PDF [%]	-	-	-	-	-	-	∓0.12	±0.33
Intra PDF [%]	-	-	±0.10	±0.22	±0.31	±0.52	±0.61	±2.00
Fakes overall normalization, el [%]	±0.25	±0.89	$^{+1.36}_{-1.35}$	±1.05	±0.73	±0.50	±0.75	±0.66
Fakes overall normalization, mu [%]	-	-	-	-	-	∓0.13	∓0.22	∓0.51
Fakes alternative parametrization [%]	∓2.54	∓2.70	∓2.74	∓2.23	∓1.93	∓1.37	∓0.88	∓1.36
W+jets heavy flavour component [%]	±4.38	±3.95	±2.84	±1.90	±2.03	±0.11	∓0.18	±2.20

TABLE F.1: Table of systematics for the absolute differential cross-section at the particle level for the $\lvert P_{out}^{t\bar{t}} \rvert$ observable.

Bins [GeV]	0–30	30–60	60–90	90–130	130–170	170–210	210–250	250–290	290–340	340–390	390–440	440–500	500–575	575–650	650–750	750–850	850–1000	1000–1400	1400–2000.00
$d\sigma$ / $dH_T^{t\bar{t}}$ [pb/GeV]	$7.15 \cdot 10^{-3}$	$5.14 \cdot 10^{-2}$	$1.13 \cdot 10^{-1}$	$1.88 \cdot 10^{-1}$	$2.58 \cdot 10^{-1}$	$2.95 \cdot 10^{-1}$	$2.87 \cdot 10^{-1}$	$2.41 \cdot 10^{-1}$	$1.82 \cdot 10^{-1}$	$1.31 \cdot 10^{-1}$	$9.35 \cdot 10^{-2}$	$6.41 \cdot 10^{-2}$	$4.09 \cdot 10^{-2}$	$2.45 \cdot 10^{-2}$	$1.36 \cdot 10^{-2}$	$6.89 \cdot 10^{-3}$	$2.82 \cdot 10^{-3}$	$5.28 \cdot 10^{-4}$	$2.62 \cdot 10^{-5}$
Total Uncertainty [%]	$^{+19.0}_{-19.2}$	$^{+17.6}_{-17.5}$	$^{+16.4}_{-16.2}$	$^{+15.5}_{-15.2}$	$^{+13.2}_{-13.1}$	$^{+11.4}_{-11.3}$	$^{+10.5}_{-10.3}$	$^{+10.1}_{-9.95}$	$^{+9.83}_{-9.62}$	$^{+9.28}_{-8.99}$	$^{+8.62}_{-8.74}$	$^{+8.66}_{-8.44}$	$^{+8.54}_{-8.26}$	$^{+8.94}_{-8.78}$	±11.5	$^{+11.4}_{-10.2}$	$^{+11.4}_{-11.1}$	$^{+12.6}_{-12.5}$	$^{+39.9}_{-37.1}$
Statistics [%]	±1.8	±0.7	±0.4	±0.3	±0.2	±0.2	±0.2	±0.2	±0.3	±0.3	±0.4	±0.4	±0.5	±0.7	±0.9	±1.3	±1.8	±2.6	±12.
Systematics [%]	$^{+18.8}_{-19.1}$	$^{+17.6}_{-17.4}$	$^{+16.4}_{-16.2}$	$^{+15.5}_{-15.2}$	$^{+13.2}_{-13.1}$	$^{+11.4}_{-11.3}$	$^{+10.5}_{-10.3}$	$^{+10.1}_{-9.94}$	$^{+9.82}_{-9.61}$	$^{+9.27}_{-8.98}$	$^{+8.60}_{-8.72}$	$^{+8.64}_{-8.42}$	$^{+8.52}_{-8.24}$	$^{+8.90}_{-8.74}$	±11.5	$^{+11.3}_{-10.1}$	$^{+11.2}_{-10.9}$	$^{+12.3}_{-12.1}$	$^{+37.4}_{-34.3}$
Jet energy resolution [%]	±3.33	±1.83	±1.61	±2.05	±0.84	-	∓0.60	±0.23	±1.21	±0.58	±0.58	±0.71	±1.11	±2.07	±5.05	±2.77	±1.31	±2.23	±4.88
b-Tagged jet energy scale (JES) [%]	$^{-0.29}_{+0.28}$	-	-	-	$^{+0.24}_{-0.13}$	$^{+0.39}_{-0.37}$	$^{+0.57}_{-0.59}$	$^{+0.71}_{-0.78}$	$^{+0.75}_{-0.76}$	$^{+0.70}_{-0.64}$	$^{+0.66}_{-0.72}$	±0.68	$^{+0.58}_{-0.61}$	$^{+0.74}_{-0.67}$	$^{+0.69}_{-0.66}$	$^{+0.54}_{-0.57}$	±0.72	$^{+0.86}_{-0.70}$	$^{+0.56}_{-0.18}$
Effective detector NP set 1 (JES) [%]	-	-	-	-	-	-	-	-	-	$^{-}_{-0.11}$	±0.11	-	$^{+0.11}_{-}$	$^{+0.17}_{-0.12}$	$^{+0.16}_{-0.19}$	$^{+0.10}_{-0.15}$	$^{+0.27}_{-0.25}$	$^{+0.40}_{-0.17}$	$^{-}_{-1.19}$
Effective detector NP set 2 (JES) [%]	-	-	-	-	-	-	-	-	-	-	-	-	-	$^{+0.17}_{-0.12}$	$^{+0.10}_{-0.14}$	-	$^{+0.22}_{-0.18}$	$^{+0.25}_{-0.13}$	$^{-}_{-0.65}$
Effective mixed NP set 1 (JES) [%]	$^{-0.20}_{+0.33}$	$^{-0.19}_{+0.28}$	$^{-0.23}_{+0.21}$	$^{-0.19}_{+0.18}$	$^{-0.12}_{+0.17}$	-	-	±0.16	$^{+0.27}_{-0.23}$	$^{+0.30}_{-0.28}$	$^{+0.34}_{-0.44}$	$^{+0.49}_{-0.47}$	$^{+0.54}_{-0.53}$	$^{+0.91}_{-0.85}$	$^{+1.10}_{-1.31}$	$^{+1.24}_{-0.84}$	$^{+1.93}_{-1.79}$	$^{+2.84}_{-2.98}$	$^{+3.31}_{-4.96}$
Effective mixed NP set 2 (JES) [%]	-	-	-	-	-	-	-	-	-	-	-	-	-	$^{-0.11}_{+0.15}$	$^{-0.15}_{-}$	-	$^{-0.18}_{+0.23}$	$^{-0.14}_{+0.32}$	$^{-0.32}_{+0.28}$
Effective mixed NP set 3 (JES) [%]	-	-	-	-	-	-	-	-	-	-	-	-	-	-	-	-	-	-	$^{+0.15}_{-0.14}$
Effective modelling NP set 1 (JES) [%]	$^{+1.51}_{-1.19}$	$^{+2.48}_{-2.00}$	$^{+2.79}_{-2.60}$	$^{+2.61}_{-2.60}$	$^{+2.44}_{-2.42}$	$^{+2.35}_{-2.33}$	$^{+2.43}_{-2.31}$	$^{+2.45}_{-2.33}$	$^{+2.25}_{-2.18}$	$^{+1.98}_{-1.94}$	$^{+1.71}_{-1.93}$	$^{+1.67}_{-1.61}$	$^{+1.72}_{-1.37}$	$^{+1.47}_{-1.51}$	$^{+1.40}_{-1.56}$	$^{+1.47}_{-1.15}$	$^{+1.55}_{-0.84}$	$^{+1.46}_{-2.00}$	$^{+0.87}_{-1.13}$
Effective modelling NP set 2 (JES) [%]	$^{-0.19}_{+0.55}$	$^{-0.38}_{+0.49}$	$^{-0.48}_{+0.46}$	$^{-0.46}_{+0.42}$	$^{-0.41}_{+0.42}$	$^{-0.33}_{+0.34}$	$^{-0.24}_{+0.26}$	$^{-0.15}_{+0.19}$	-	-	-	$^{+0.10}_{-0.13}$	$^{+0.15}_{-0.20}$	$^{+0.42}_{-0.26}$	$^{+0.38}_{-0.49}$	$^{+0.44}_{-0.42}$	$^{+0.96}_{-0.86}$	$^{+1.44}_{-1.35}$	$^{+2.44}_{-4.45}$
Effective modelling NP set 3 (JES) [%]	$^{+0.41}_{-0.13}$	$^{+0.41}_{-0.33}$	$^{+0.40}_{-0.43}$	$^{+0.35}_{-0.39}$	$^{+0.35}_{-0.32}$	$^{+0.28}_{-0.27}$	±0.17	-	-	-	$^{-0.16}_{+0.17}$	$^{-0.23}_{+0.20}$	$^{-0.26}_{+0.21}$	$^{-0.34}_{+0.45}$	$^{-0.49}_{+0.41}$	$^{-0.31}_{+0.39}$	$^{-0.68}_{+0.53}$	$^{-0.53}_{+0.82}$	$^{-0.21}_{-}$
Effective modelling NP set 4 (JES) [%]	-	-	-	-	-	-	$^{+0.11}_{-0.10}$	$^{+0.16}_{-0.11}$	$^{+0.12}_{-0.13}$	$^{+0.13}_{-0.14}$	±0.14	$^{+0.12}_{-0.11}$	-	$^{+0.18}_{-0.14}$	$^{+0.16}_{-0.17}$	$^{-}_{-0.15}$	$^{+0.23}_{-0.13}$	$^{+0.45}_{-0.20}$	$^{-}_{-1.18}$
Effective statistical NP set 1 (JES) [%]	$^{+0.42}_{-}$	$^{+0.55}_{-0.32}$	$^{+0.52}_{-0.51}$	$^{+0.47}_{-0.49}$	$^{+0.46}_{-0.45}$	$^{+0.42}_{-0.45}$	$^{+0.42}_{-0.40}$	$^{+0.43}_{-0.36}$	±0.34	$^{+0.30}_{-0.31}$	$^{+0.26}_{-0.31}$	$^{+0.21}_{-0.22}$	$^{+0.19}_{-0.14}$	$^{+0.33}_{-0.17}$	$^{+0.22}_{-0.29}$	±0.15	$^{+0.23}_{-0.14}$	±0.62	$^{-}_{-0.84}$
Effective statistical NP set 2 (JES) [%]	$^{-0.13}_{+0.39}$	$^{-0.32}_{+0.54}$	$^{-0.44}_{+0.51}$	$^{-0.43}_{+0.42}$	$^{-0.41}_{+0.40}$	$^{-0.41}_{+0.37}$	$^{-0.36}_{+0.38}$	$^{-0.32}_{+0.40}$	∓0.32	$^{-0.29}_{+0.28}$	$^{-0.27}_{+0.21}$	∓0.18	$^{-}_{+0.14}$	-	$^{-0.14}_{-}$	-	$^{+0.27}_{-0.16}$	$^{+0.37}_{-0.28}$	$^{+1.05}_{-1.94}$
Effective statistical NP set 3 (JES) [%]	-	-	-	-	-	-	-	-	-	-	-	-	-	$^{-0.20}_{+0.28}$	$^{-0.37}_{+0.29}$	$^{-0.30}_{+0.33}$	$^{-0.89}_{+0.78}$	$^{-0.82}_{+1.19}$	$^{-0.84}_{+0.70}$
Effective statistical NP set 4 (JES) [%]	$^{-}_{+0.26}$	$^{-0.24}_{+0.27}$	$^{-0.27}_{+0.24}$	$^{-0.23}_{+0.20}$	$^{-0.16}_{+0.19}$	$^{-0.12}_{+0.11}$	-	-	$^{+0.11}_{-0.14}$	$^{+0.14}_{-0.15}$	$^{+0.25}_{-0.20}$	$^{+0.28}_{-0.24}$	$^{+0.19}_{-0.28}$	$^{+0.33}_{-0.24}$	$^{+0.34}_{-0.36}$	$^{+0.10}_{-0.18}$	$^{+0.19}_{-0.26}$	$^{+0.21}_{-}$	$^{-0.47}_{+0.25}$
Effective statistical NP set 5 (JES) [%]	-	-	-	-	-	-	-	-	-	-	-	-	-	$^{+0.16}_{-}$	$^{+0.17}_{-0.26}$	-	$^{+0.29}_{-0.32}$	-	$^{-0.99}_{-}$
Effective statistical NP set 6 (JES) [%]	-	-	±0.11	$^{-}_{-0.12}$	$^{+0.11}_{-0.10}$	-	-	-	-	-	-	-	-	-	-	-	$^{+0.12}_{-0.10}$	-	$^{-}_{-0.83}$
Effective statistical NP set 7 (JES) [%]	-	-	-	-	-	-	-	-	-	$^{+0.10}_{-0.12}$	$^{+0.13}_{-0.14}$	$^{+0.11}_{-0.13}$	±0.14	$^{+0.25}_{-0.14}$	$^{+0.21}_{-0.28}$	$^{+0.13}_{-0.14}$	$^{+0.37}_{-0.27}$	$^{+0.41}_{-0.33}$	$^{-}_{-0.72}$
η intercalibration model (JES) [%]	$^{+0.32}_{-0.30}$	$^{+0.38}_{-0.27}$	$^{+0.31}_{-0.40}$	$^{+0.37}_{-0.45}$	$^{+0.55}_{-0.45}$	$^{+0.46}_{-0.52}$	$^{+0.59}_{-0.63}$	$^{+0.76}_{-0.77}$	$^{+0.75}_{-0.73}$	$^{+0.71}_{-0.78}$	$^{+0.74}_{-0.88}$	$^{+0.84}_{-0.75}$	$^{+0.70}_{-0.71}$	$^{+0.84}_{-0.76}$	$^{+1.20}_{-1.02}$	$^{+0.96}_{-0.81}$	$^{+1.04}_{-1.03}$	$^{+1.72}_{-1.79}$	$^{+1.10}_{-1.89}$
η intercalibration non closure (JES) [%]	$^{-}_{-0.24}$	$^{-0.16}_{+0.11}$	$^{-0.19}_{+0.16}$	$^{-0.19}_{+0.26}$	$^{-0.15}_{+0.26}$	$^{-0.24}_{+0.16}$	$^{-0.25}_{+0.17}$	$^{-0.27}_{+0.29}$	$^{-0.26}_{+0.31}$	∓0.27	$^{-0.30}_{+0.23}$	$^{-0.34}_{+0.39}$	∓0.36	$^{-0.35}_{+0.39}$	$^{-0.49}_{+0.53}$	$^{-0.43}_{+0.59}$	$^{-0.55}_{+0.66}$	$^{-1.06}_{+0.66}$	$^{-0.42}_{+0.13}$
η intercalibration total stat (JES) [%]	-	$^{+0.37}_{-0.16}$	$^{+0.36}_{-0.30}$	±0.32	$^{+0.34}_{-0.32}$	$^{+0.33}_{-0.40}$	$^{+0.44}_{-0.42}$	$^{+0.53}_{-0.45}$	$^{+0.48}_{-0.49}$	$^{+0.45}_{-0.46}$	$^{+0.42}_{-0.50}$	±0.41	$^{+0.39}_{-0.35}$	$^{+0.49}_{-0.32}$	$^{+0.45}_{-0.46}$	$^{+0.20}_{-0.31}$	$^{+0.34}_{-0.35}$	$^{+0.59}_{-0.57}$	$^{-}_{-0.54}$
Flavour composition (JES) [%]	$^{+1.63}_{-2.05}$	$^{+1.85}_{-2.05}$	$^{+2.35}_{-2.19}$	$^{+2.51}_{-2.44}$	$^{+2.33}_{-2.45}$	$^{+1.94}_{-2.19}$	$^{+1.94}_{-2.20}$	$^{+2.12}_{-2.17}$	$^{+1.88}_{-1.94}$	$^{+1.66}_{-1.74}$	$^{+1.42}_{-1.85}$	$^{+1.50}_{-1.44}$	$^{+1.46}_{-1.21}$	$^{+1.33}_{-1.21}$	$^{+1.35}_{-1.60}$	$^{+1.22}_{-1.09}$	$^{+1.58}_{-0.93}$	$^{+1.99}_{-2.26}$	$^{+2.17}_{-4.30}$
Flavour response (JES) [%]	$^{-0.81}_{+0.77}$	$^{-0.85}_{+1.13}$	$^{-1.01}_{+1.25}$	$^{-1.09}_{+0.99}$	$^{-1.04}_{+0.95}$	$^{-1.02}_{+0.96}$	$^{-1.03}_{+0.99}$	$^{-1.03}_{+1.10}$	$^{-1.01}_{+1.02}$	$^{-1.00}_{+0.91}$	$^{-1.03}_{+0.79}$	$^{-0.87}_{+0.89}$	$^{-0.78}_{+0.90}$	$^{-0.61}_{+0.75}$	$^{-0.92}_{+0.78}$	$^{-0.57}_{+0.56}$	$^{-0.32}_{+0.67}$	$^{-0.89}_{+0.88}$	$^{-}_{-1.97}$
Pile-up offset μ (JES) [%]	-	-	$^{-}_{+0.17}$	$^{-0.14}_{+0.18}$	$^{-0.17}_{+0.16}$	$^{-0.15}_{+0.10}$	$^{-0.11}_{+0.14}$	$^{-0.13}_{+0.16}$	$^{-0.14}_{+0.12}$	∓0.18	$^{-0.16}_{+0.14}$	$^{-0.14}_{-}$	$^{-0.12}_{+0.11}$	$^{-0.11}_{+0.16}$	$^{-}_{+0.16}$	$^{-0.22}_{-}$	$^{-}_{+0.27}$	-	$^{-}_{-0.20}$
Pile-up offset N_{PV} (JES) [%]	$^{-}_{-0.23}$	$^{+0.50}_{-0.31}$	$^{+0.63}_{-0.54}$	$^{+0.48}_{-0.40}$	$^{+0.38}_{-0.32}$	$^{+0.40}_{-0.42}$	$^{+0.51}_{-0.56}$	$^{+0.64}_{-0.55}$	$^{+0.56}_{-0.47}$	$^{+0.37}_{-0.40}$	$^{+0.38}_{-0.55}$	$^{+0.47}_{-0.53}$	$^{+0.40}_{-0.23}$	$^{+0.45}_{-0.31}$	$^{+0.45}_{-0.49}$	±0.27	$^{+0.43}_{-}$	$^{+0.51}_{-0.49}$	$^{-}_{-0.41}$
Pile-up offset p_T (JES) [%]	$^{-0.63}_{+0.44}$	$^{-0.68}_{+0.67}$	∓0.68	$^{-0.59}_{+0.57}$	$^{-0.43}_{+0.52}$	$^{-0.39}_{+0.38}$	$^{-0.16}_{+0.11}$	$^{+0.13}_{-0.15}$	$^{+0.29}_{-0.25}$	$^{+0.33}_{-0.43}$	±0.56	$^{+0.62}_{-0.45}$	$^{+0.62}_{-0.76}$	$^{+0.94}_{-0.86}$	$^{+1.07}_{-1.08}$	$^{+1.00}_{-0.92}$	$^{+1.13}_{-1.41}$	$^{+1.87}_{-1.48}$	$^{+2.02}_{-1.98}$
Pile-up offset ρ topology (JES) [%]	$^{+1.12}_{-1.39}$	$^{+2.82}_{-2.62}$	$^{+3.53}_{-3.45}$	$^{+3.58}_{-3.49}$	$^{+3.39}_{-3.37}$	$^{+3.36}_{-3.31}$	$^{+3.60}_{-3.42}$	$^{+3.84}_{-3.65}$	$^{+3.61}_{-3.49}$	±3.20	$^{+2.93}_{-3.06}$	$^{+2.85}_{-2.65}$	$^{+2.59}_{-2.37}$	±2.35	$^{+2.24}_{-2.39}$	$^{+2.69}_{-1.62}$	$^{+2.01}_{-1.68}$	$^{+1.44}_{-2.12}$	$^{+0.94}_{-2.45}$
Punch-through (JES) [%]	-	-	-	-	-	-	-	-	-	-	-	-	-	-	-	-	-	-	$^{+0.35}_{-0.24}$
Jet vertex fraction [%]	$^{+0.88}_{-0.92}$	$^{+0.97}_{-1.00}$	$^{+1.00}_{-1.04}$	$^{+0.96}_{-1.00}$	$^{+0.90}_{-0.94}$	$^{+0.84}_{-0.87}$	$^{+0.76}_{-0.80}$	$^{+0.68}_{-0.71}$	$^{+0.59}_{-0.62}$	$^{+0.51}_{-0.55}$	$^{+0.45}_{-0.48}$	$^{+0.40}_{-0.43}$	$^{+0.35}_{-0.38}$	$^{+0.30}_{-0.34}$	$^{+0.26}_{-0.30}$	$^{+0.23}_{-0.27}$	$^{+0.18}_{-0.22}$	$^{+0.11}_{-0.15}$	$^{+0.16}_{-0.21}$
b-Quark tagging efficiency (eigenvector 0) [%]	$^{-8.11}_{+8.39}$	$^{-8.15}_{+8.43}$	$^{-7.95}_{+8.22}$	$^{-7.51}_{+7.75}$	$^{-7.07}_{+7.29}$	$^{-6.70}_{+6.90}$	$^{-6.41}_{+6.59}$	$^{-6.24}_{+6.41}$	$^{-6.08}_{+6.25}$	$^{-5.88}_{+6.04}$	$^{-5.72}_{+5.87}$	$^{-5.63}_{+5.77}$	$^{-5.60}_{+5.74}$	$^{-5.60}_{+5.74}$	$^{-5.70}_{+5.84}$	$^{-5.83}_{+5.98}$	$^{-5.99}_{+6.14}$	$^{-6.41}_{+6.58}$	$^{-5.75}_{+7.74}$
b-Quark tagging efficiency (eigenvector 1) [%]	$^{-1.19}_{+1.20}$	∓1.16	$^{-1.16}_{+1.17}$	∓1.24	$^{-1.36}_{+1.37}$	$^{-1.51}_{+1.52}$	$^{-1.67}_{+1.68}$	$^{-1.84}_{+1.85}$	$^{-2.08}_{+2.10}$	$^{-2.37}_{+2.40}$	$^{-2.65}_{+2.68}$	$^{-2.92}_{+2.96}$	$^{-3.21}_{+3.26}$	$^{-3.50}_{+3.55}$	$^{-3.85}_{+3.91}$	$^{-4.18}_{+4.25}$	$^{-4.48}_{+4.57}$	$^{-4.95}_{+5.05}$	$^{-5.62}_{+5.74}$
b-Quark tagging efficiency (eigenvector 2) [%]	$^{+1.72}_{-1.70}$	$^{+1.67}_{-1.66}$	$^{+1.62}_{-1.61}$	$^{+1.57}_{-1.56}$	$^{+1.51}_{-1.50}$	$^{+1.46}_{-1.45}$	±1.39	$^{+1.31}_{-1.30}$	$^{+1.19}_{-1.17}$	$^{+1.04}_{-1.03}$	±0.88	±0.72	±0.51	±0.29	-	∓0.18	∓0.42	$^{-0.77}_{+0.78}$	$^{-1.09}_{+1.10}$
b-Quark tagging efficiency (eigenvector 3) [%]	∓0.27	∓0.26	∓0.24	∓0.19	∓0.12	-	-	-	±0.17	±0.25	±0.28	±0.28	±0.23	±0.14	-	∓0.16	∓0.35	$^{-0.66}_{+0.67}$	∓1.04
b-Quark tagging efficiency (eigenvector 4) [%]	-	-	-	-	-	-	-	-	-	-	-	-	-	-	-	-	∓0.13	∓0.23	∓0.36
c-Quark tagging efficiency (eigenvector 0) [%]	±0.30	±0.38	±0.40	±0.41	±0.39	±0.34	±0.30	±0.26	±0.22	±0.18	±0.15	±0.13	±0.12	±0.10	-	-	-	-	±0.20
c-Quark tagging efficiency (eigenvector 1) [%]	∓0.14	$^{-0.12}_{+0.11}$	∓0.13	∓0.16	∓0.18	∓0.19	$^{-0.22}_{+0.23}$	∓0.25	$^{-0.26}_{+0.27}$	∓0.29	∓0.29	∓0.31	∓0.32	∓0.31	∓0.34	∓0.35	∓0.38	∓0.57	$^{-1.05}_{+1.06}$
c-Quark tagging efficiency (eigenvector 2) [%]	±0.11	±0.12	±0.14	±0.16	±0.16	±0.13	±0.11	-	-	-	-	-	-	-	∓0.11	∓0.11	∓0.15	∓0.23	∓0.45
Light-jet tagging efficiency (eigenvector 0) [%]	$^{-0.98}_{+1.13}$	$^{-1.02}_{+1.15}$	$^{-0.94}_{+1.00}$	$^{-0.81}_{+0.80}$	$^{-0.66}_{+0.65}$	∓0.62	$^{-0.68}_{+0.71}$	$^{-0.71}_{+0.75}$	$^{-0.61}_{+0.62}$	$^{-0.56}_{+0.57}$	$^{-0.53}_{+0.54}$	$^{-0.56}_{+0.57}$	$^{-0.57}_{+0.56}$	$^{-0.65}_{+0.67}$	$^{-0.67}_{+0.68}$	∓0.62	$^{-0.57}_{+0.58}$	$^{-1.05}_{+1.10}$	$^{-1.88}_{+2.04}$
Light-jet tagging efficiency (eigenvector 1) [%]	$^{+0.59}_{-0.52}$	$^{+0.70}_{-0.64}$	$^{+0.57}_{-0.55}$	±0.39	±0.32	$^{+0.27}_{-0.26}$	±0.24	$^{+0.22}_{-0.21}$	±0.17	±0.14	-	-	-	-	-	-	-	-	∓0.45
Light-jet tagging efficiency (eigenvector 2) [%]	-	-	-	-	-	-	-	-	-	-	-	-	-	-	-	-	-	-	∓0.28
Light-jet tagging efficiency (eigenvector 3) [%]	$^{+0.18}_{-0.17}$	$^{+0.20}_{-0.18}$	$^{+0.12}_{-0.11}$	-	-	-	-	-	-	-	-	∓0.11	∓0.12	∓0.13	∓0.11	∓0.11	∓0.14	∓0.23	$^{-0.13}_{+0.14}$
Light-jet tagging efficiency (eigenvector 4) [%]	-	-	-	-	-	-	-	-	-	-	-	-	-	-	-	-	-	-	±0.12
Light-jet tagging efficiency (eigenvector 5) [%]	-	-	-	-	-	-	-	-	-	-	-	-	-	-	-	-	-	-	±0.68
Light-jet tagging efficiency (eigenvector 6) [%]	-	-	-	-	-	-	-	-	-	-	-	-	-	-	-	-	-	-	∓0.19
Light-jet tagging efficiency (eigenvector 7) [%]	-	-	-	-	-	-	-	-	-	-	-	-	-	-	-	-	-	-	∓0.41
Light-jet tagging efficiency (eigenvector 8) [%]	-	-	-	-	-	-	-	-	-	-	-	-	-	-	-	-	-	-	±0.12
Light-jet tagging efficiency (eigenvector 9) [%]	-	-	-	-	-	-	-	-	-	-	-	-	-	-	-	-	-	-	∓0.10
b-Quark tagging extrapolation [%]	-	-	-	-	-	-	-	-	-	-	-	-	$^{+0.15}_{-0.14}$	±0.25	±0.51	±0.96	$^{+1.74}_{-1.73}$	$^{+3.29}_{-3.27}$	$^{+6.66}_{-6.55}$
Electron energy scale [%]	-	-	-	-	-	-	-	-	-	-	-	-	-	-	-	-	-	-	-
Electron trigger efficiency [%]	±0.14	±0.14	±0.14	±0.13	±0.12	±0.12	±0.11	±0.11	±0.11	±0.11	±0.11	±0.11	$^{+0.11}_{-0.10}$	$^{+0.11}_{-0.10}$	±0.11	±0.11	±0.11	±0.11	±0.12
Electron reconstruction efficiency [%]	-	-	-	-	-	-	-	-	-	-	-	-	-	±0.10	±0.10	±0.11	±0.11	±0.12	±0.14
Electron identification efficiency [%]	±0.36	±0.37	±0.36	±0.36	±0.36	±0.36	±0.37	±0.39	±0.42	±0.44	±0.47	±0.50	±0.53	±0.57	±0.61	±0.64	±0.68	±0.74	±0.89
Electron isolation efficiency [%]	-	-	-	-	-	-	-	-	-	$^{+0.11}_{-0.12}$	±0.15	±0.19	$^{+0.24}_{-0.25}$	±0.31	±0.40	±0.48	±0.57	±0.74	±1.29
Muon trigger efficiency stat [%]	$^{+0.33}_{-0.34}$	±0.32	$^{+0.31}_{-0.32}$	$^{+0.30}_{-0.31}$	±0.30	$^{+0.29}_{-0.30}$	±0.29	±0.29	$^{+0.28}_{-0.29}$	±0.28	±0.28	$^{+0.27}_{-0.28}$	$^{+0.27}_{-0.28}$	$^{+0.27}_{-0.28}$	$^{+0.27}_{-0.28}$	$^{+0.27}_{-0.28}$	±0.28	$^{+0.28}_{-0.29}$	±0.33
Muon trigger efficiency syst [%]	$^{+0.58}_{-0.56}$	$^{+0.57}_{-0.55}$	$^{+0.56}_{-0.54}$	$^{+0.54}_{-0.53}$	$^{+0.53}_{-0.52}$	$^{+0.52}_{-0.51}$	$^{+0.51}_{-0.50}$	$^{+0.51}_{-0.50}$	$^{+0.50}_{-0.49}$	$^{+0.50}_{-0.49}$	$^{+0.49}_{-0.48}$	$^{+0.49}_{-0.48}$	$^{+0.49}_{-0.47}$	$^{+0.48}_{-0.47}$	$^{+0.48}_{-0.47}$	$^{+0.48}_{-0.47}$	$^{+0.48}_{-0.47}$	$^{+0.50}_{-0.49}$	$^{+0.55}_{-0.54}$
Muon identification stat [%]	±0.11	±0.10	±0.10	±0.10	±0.10	-	-	-	-	-	-	-	-	-	-	-	-	-	±0.10
Muon identification syst [%]	±0.39	±0.38	±0.37	±0.36	±0.36	±0.36	±0.36	±0.36	±0.37	±0.38	±0.39	$^{+0.41}_{-0.40}$	±0.42	±0.45	$^{+0.48}_{-0.47}$	±0.50	±0.55	$^{+0.61}_{-0.60}$	$^{+0.72}_{-0.71}$
Muon isolation efficiency syst [%]	±0.12	±0.12	±0.11	±0.11	±0.11	±0.11	±0.10	±0.10	±0.10	±0.10	±0.10	±0.10	±0.10	±0.10	±0.10	±0.10	±0.10	±0.12	±0.20
E_T^{miss} Soft jet resolution para [%]	∓0.36	∓0.30	-	-	-	±0.14	-	-	-	∓0.10	∓0.11	-	-	-	∓0.31	∓0.20	-	∓0.40	∓0.26
E_T^{miss} Soft jet resolution perp [%]	∓1.36	∓0.35	∓0.24	-	±0.14	±0.19	-	-	-	-	∓0.12	-	-	∓0.28	∓0.19	-	∓0.37	∓0.48	∓0.46
E_T^{miss} Soft jet scale [%]	$^{-0.77}_{+0.17}$	-	-	-	$^{+0.11}_{-}$	$^{+0.12}_{-}$	$^{-}_{-0.12}$	-	-	$^{-0.12}_{+0.15}$	$^{-0.15}_{-}$	$^{-}_{+0.14}$	-	$^{-0.17}_{+0.22}$	$^{-0.34}_{+0.15}$	-	$^{-0.25}_{+0.26}$	$^{-0.43}_{+0.46}$	$^{-}_{-0.29}$
Luminosity [%]	∓2.05	∓2.05	∓2.05	∓2.05	∓2.05	∓2.05	∓2.05	∓2.05	∓2.05	∓2.05	∓2.05	∓2.05	∓2.05	∓2.05	∓2.05	∓2.05	∓2.05	∓2.05	∓2.05
Z+jets cross-section [%]	±0.58	±0.68	±0.77	±0.87	±0.83	±0.72	±0.60	±0.50	±0.39	±0.33	±0.29	±0.25	±0.24	±0.22	±0.21	±0.23	±0.26	±0.27	±0.54
Monte Carlo sample statistics [%]	±1.44	±0.64	±0.43	±0.32	±0.27	±0.20	±0.19	±0.19	±0.19	±0.22	±0.25	±0.29	±0.34	±0.45	±0.55	±0.82	±1.05	±1.51	±5.35
ISR/FSR + scale [%]	$^{-3.48}_{+1.23}$	$^{-}_{-1.39}$	$^{-}_{-0.51}$	$^{+1.89}_{-}$	$^{-0.37}_{+1.07}$	$^{+1.37}_{-}$	$^{+1.17}_{-}$	$^{-0.82}_{+0.35}$	$^{-0.42}_{+1.00}$	$^{-}_{+1.93}$	$^{+0.68}_{-}$	$^{-0.42}_{+0.59}$	$^{-0.43}_{+0.34}$	$^{+0.30}_{-0.77}$	$^{-}_{-0.24}$	$^{+3.97}_{-}$	$^{+1.03}_{-}$	$^{+2.14}_{-}$	$^{+16.4}_{-}$
Alternate hard-scattering model [%]	±5.34	±6.65	±5.62	±5.73	±4.74	±3.57	±3.63	±2.99	±1.84	±1.61	±1.48	±2.29	±1.22	∓0.54	±2.02	±1.48	∓4.80	±0.49	±27.8
Alternate parton-shower model [%]	∓3.59	∓0.69	-	±1.68	±2.30	±2.52	±2.01	±1.56	±2.18	±2.22	±1.33	±1.14	±1.14	∓0.53	±0.81	±3.53	±2.18	∓0.93	±10.9
Inter PDF [%]	±0.14	-	-	-	-	-	-	-	-	-	∓0.10	-	-	-	-	∓0.16	-	±0.16	-
Intra PDF [%]	±1.52	±0.47	±0.16	±0.27	-	-	±0.15	±0.11	±0.12	±0.13	±0.42	±0.30	±0.44	±0.20	±0.38	±1.17	±0.43	±1.20	±1.66
Fakes overall normalization, el [%]	$^{+0.96}_{-0.95}$	±1.89	$^{+2.29}_{-2.28}$	±2.14	$^{+1.48}_{-1.49}$	±0.90	±0.55	±0.36	±0.20	-	-	-	-	∓0.26	∓0.29	∓0.19	-	±0.34	±3.51
Fakes overall normalization, mu [%]	∓0.22	-	±0.16	±0.15	±0.14	$^{+0.18}_{-0.17}$	±0.19	±0.14	-	-	∓0.13	∓0.20	∓0.38	∓0.52	∓0.88	∓1.12	∓0.96	∓1.22	-
Fakes alternative parametrization [%]	∓5.93	∓6.75	∓7.31	∓6.71	∓4.95	∓3.55	∓2.35	∓1.72	∓1.32	∓0.79	∓0.34	±0.23	±0.72	±0.93	±1.67	±1.88	±1.58	±2.30	∓0.45
W+jets heavy flavour component [%]	±12.7	±10.3	±8.17	±6.81	±5.41	±3.90	±2.42	±2.53	±2.84	±2.10	±2.06	±1.36	±1.67	±2.48	±5.22	±2.46	±1.79	±3.48	±1.28

TABLE F.2: Table of systematics for the absolute differential cross-section at the particle level for the $H_T^{t\bar{t}}$ observable.

Bins [GeV]	0–15	15–30	30–45	45–60	60–75	75–90	90–110	110–130	130–150	150–175	175–200	200–225	225–250	250–275	275–300	300–350	350–400	400–500	500–1000.00
$d\sigma$ / dp^t_T [pb/GeV]	$6.56 \cdot 10^{-2}$	$1.96 \cdot 10^{-1}$	$3.18 \cdot 10^{-1}$	$4.25 \cdot 10^{-1}$	$5.03 \cdot 10^{-1}$	$5.47 \cdot 10^{-1}$	$5.50 \cdot 10^{-1}$	$4.96 \cdot 10^{-1}$	$4.07 \cdot 10^{-1}$	$3.10 \cdot 10^{-1}$	$2.23 \cdot 10^{-1}$	$1.60 \cdot 10^{-1}$	$1.15 \cdot 10^{-1}$	$8.38 \cdot 10^{-2}$	$6.15 \cdot 10^{-2}$	$3.77 \cdot 10^{-2}$	$1.93 \cdot 10^{-2}$	$7.86 \cdot 10^{-3}$	$5.64 \cdot 10^{-4}$
Total Uncertainty [%]	$^{+17.6}_{-17.3}$	$^{+14.4}_{-13.7}$	$^{+14.1}_{-13.8}$	$^{+12.9}_{-13.0}$	$^{+13.6}_{-13.4}$	$^{+13.1}_{-12.8}$	$^{+10.7}_{-10.5}$	$^{+10.4}_{-10.2}$	$^{+10.0}_{-9.77}$	$^{+9.88}_{-9.61}$	$^{+9.09}_{-8.74}$	$^{+8.08}_{-8.26}$	$^{+8.04}_{-8.11}$	$^{+8.52}_{-8.27}$	$^{+8.44}_{-8.11}$	$^{+9.03}_{-8.88}$	±10.5	$^{+9.76}_{-9.48}$	$^{+13.3}_{-12.1}$
Statistics [%]	±1.1	±0.5	±0.4	±0.3	±0.3	±0.3	±0.3	±0.3	±0.3	±0.3	±0.4	±0.5	±0.5	±0.6	±0.7	±0.7	±1.1	±1.3	±2.2
Systematics [%]	$^{+17.5}_{-17.3}$	$^{+14.3}_{-13.7}$	$^{+14.1}_{-13.8}$	$^{+12.9}_{-13.0}$	$^{+13.5}_{-13.4}$	$^{+13.1}_{-12.8}$	$^{+10.7}_{-10.5}$	$^{+10.4}_{-10.2}$	$^{+10.0}_{-9.76}$	$^{+9.87}_{-9.60}$	$^{+9.07}_{-8.73}$	$^{+8.06}_{-8.24}$	$^{+8.01}_{-8.08}$	$^{+8.48}_{-8.24}$	$^{+8.39}_{-8.05}$	$^{+8.98}_{-8.84}$	±10.4	$^{+9.64}_{-9.35}$	$^{+13.0}_{-11.8}$
Jet energy resolution [%]	±4.88	∓0.18	±1.64	∓0.25	±1.02	±2.78	∓0.63	±0.31	±1.19	±1.30	±0.41	∓0.39	∓0.44	∓0.39	±0.84	±2.54	±4.08	±0.67	±1.96
b-Tagged jet energy scale (JES) [%]	-	-	-	$^{+0.13}_{-0.15}$	$^{+0.25}_{-0.27}$	$^{+0.27}_{-0.22}$	$^{+0.47}_{-0.49}$	$^{+0.71}_{-0.67}$	$^{+0.73}_{-0.75}$	$^{+0.79}_{-0.77}$	$^{+0.74}_{-0.68}$	$^{+0.60}_{-0.75}$	$^{+0.64}_{-0.80}$	$^{+0.78}_{-0.62}$	$^{+0.60}_{-0.72}$	$^{+0.78}_{-0.67}$	$^{+0.58}_{-0.53}$	$^{+0.66}_{-0.79}$	$^{+0.88}_{-0.50}$
Effective detector NP set 1 (JES) [%]	-	-	-	-	-	-	-	-	-	-	$^{+0.11}_{-}$	-	-	-	-	$^{+0.20}_{-}$	-	$^{+0.20}_{-0.24}$	$^{+0.24}_{-0.32}$
Effective detector NP set 2 (JES) [%]	-	-	-	-	-	-	-	-	-	-	-	-	-	-	-	$^{+0.17}_{-}$	-	±0.19	$^{-}_{-0.23}$
Effective mixed NP set 1 (JES) [%]	$^{-0.13}_{+0.14}$	$^{-0.15}_{+0.19}$	$^{-}_{+0.16}$	-	-	$^{-}_{+0.12}$	-	$^{+0.13}_{-0.12}$	$^{+0.15}_{-0.18}$	$^{+0.28}_{-0.23}$	$^{+0.32}_{-0.23}$	$^{+0.31}_{-0.44}$	$^{+0.39}_{-0.54}$	$^{+0.64}_{-0.38}$	$^{+0.53}_{-0.57}$	$^{+0.82}_{-0.95}$	$^{+0.80}_{-0.73}$	$^{+1.59}_{-1.70}$	$^{+2.68}_{-2.34}$
Effective mixed NP set 2 (JES) [%]	-	-	-	-	-	-	-	-	-	-	-	-	-	-	-	$^{-}_{+0.16}$	-	$^{-0.16}_{+0.17}$	$^{-0.27}_{+0.17}$
Effective modelling NP set 1 (JES) [%]	$^{+2.75}_{-2.40}$	$^{+3.31}_{-2.73}$	$^{+3.07}_{-2.81}$	$^{+2.61}_{-2.86}$	$^{+2.60}_{-2.73}$	$^{+2.58}_{-2.36}$	$^{+2.40}_{-2.31}$	$^{+2.33}_{-2.28}$	$^{+2.23}_{-2.12}$	$^{+2.05}_{-1.94}$	$^{+1.71}_{-1.64}$	$^{+1.43}_{-1.69}$	$^{+1.46}_{-1.52}$	$^{+1.55}_{-1.20}$	$^{+1.32}_{-1.01}$	$^{+1.25}_{-1.34}$	$^{+0.73}_{-1.09}$	$^{+1.51}_{-1.10}$	$^{+1.14}_{-1.49}$
Effective modelling NP set 2 (JES) [%]	$^{-0.35}_{+0.29}$	$^{-0.43}_{+0.44}$	$^{-0.42}_{+0.45}$	$^{-0.42}_{+0.43}$	$^{-0.43}_{+0.40}$	$^{-0.33}_{+0.38}$	∓0.29	$^{-0.18}_{+0.20}$	$^{-}_{+0.11}$	-	-	-	$^{+0.11}_{-0.14}$	$^{+0.23}_{-0.15}$	$^{-}_{-0.24}$	$^{+0.36}_{-0.31}$	$^{+0.37}_{-0.29}$	±0.72	$^{+1.22}_{-1.23}$
Effective modelling NP set 3 (JES) [%]	$^{+0.32}_{-0.34}$	$^{+0.37}_{-0.36}$	$^{+0.36}_{-0.33}$	$^{+0.35}_{-0.34}$	$^{+0.33}_{-0.36}$	$^{+0.30}_{-0.26}$	$^{+0.21}_{-0.23}$	$^{+0.11}_{-0.10}$	-	-	-	$^{-0.20}_{+0.12}$	$^{-0.25}_{+0.22}$	$^{-0.22}_{+0.30}$	$^{-0.32}_{+0.15}$	$^{-0.34}_{+0.44}$	$^{-0.35}_{+0.38}$	$^{-0.63}_{+0.59}$	$^{-0.46}_{+0.49}$
Effective modelling NP set 4 (JES) [%]	-	-	-	-	$^{+0.12}_{-0.13}$	-	$^{-}_{-0.12}$	$^{+0.15}_{-0.13}$	-	$^{+0.14}_{-0.12}$	$^{+0.15}_{-0.11}$	$^{-}_{-0.14}$	$^{-}_{-0.13}$	-	-	$^{+0.19}_{-}$	-	$^{+0.16}_{-0.13}$	±0.34
Effective statistical NP set 1 (JES) [%]	$^{+0.39}_{-0.38}$	$^{+0.64}_{-0.49}$	$^{+0.54}_{-0.51}$	$^{+0.49}_{-0.54}$	$^{+0.54}_{-0.58}$	$^{+0.47}_{-0.41}$	$^{+0.38}_{-0.39}$	$^{+0.44}_{-0.41}$	$^{+0.36}_{-0.31}$	$^{+0.29}_{-0.31}$	±0.25	$^{+0.21}_{-0.29}$	$^{+0.21}_{-0.19}$	$^{+0.15}_{-0.10}$	$^{+0.11}_{-0.16}$	$^{+0.21}_{-}$	$^{-}_{-0.13}$	±0.24	$^{+0.35}_{-0.48}$
Effective statistical NP set 2 (JES) [%]	$^{-0.35}_{+0.34}$	$^{-0.43}_{+0.59}$	$^{-0.46}_{+0.50}$	$^{-0.47}_{+0.43}$	$^{-0.53}_{+0.46}$	$^{-0.37}_{+0.42}$	$^{-0.33}_{+0.35}$	$^{-0.37}_{+0.39}$	$^{-0.28}_{+0.32}$	∓0.26	$^{-0.22}_{+0.20}$	$^{-0.25}_{+0.20}$	$^{-0.17}_{+0.21}$	$^{-}_{+0.15}$	$^{-0.11}_{+0.14}$	-	-	-	$^{+0.29}_{-0.34}$
Effective statistical NP set 3 (JES) [%]	-	-	-	-	-	-	-	-	-	-	-	-	-	-	-	$^{-0.16}_{+0.26}$	$^{-0.24}_{+0.20}$	$^{-0.73}_{+0.60}$	$^{-0.85}_{+1.18}$
Effective statistical NP set 4 (JES) [%]	$^{-0.22}_{+0.23}$	$^{-0.22}_{+0.24}$	$^{-0.18}_{+0.20}$	∓0.18	∓0.15	$^{-0.14}_{+0.15}$	-	-	-	$^{+0.16}_{-0.14}$	$^{+0.17}_{-0.16}$	$^{+0.17}_{-0.26}$	$^{+0.26}_{-0.30}$	$^{+0.31}_{-0.21}$	$^{+0.21}_{-0.29}$	$^{+0.35}_{-0.29}$	$^{+0.28}_{-0.20}$	$^{+0.25}_{-0.31}$	-
Effective statistical NP set 5 (JES) [%]	-	-	-	-	-	-	-	-	-	-	-	-	-	-	-	$^{+0.20}_{-0.16}$	$^{+0.19}_{-0.21}$	±0.27	-
Effective statistical NP set 6 (JES) [%]	-	-	-	-	$^{+0.11}_{-0.13}$	$^{+0.12}_{-}$	±0.11	-	-	-	-	-	-	-	-	-	-	$^{+0.10}_{-0.13}$	-
Effective statistical NP set 7 (JES) [%]	-	-	-	-	-	-	-	-	-	-	$^{+0.12}_{-0.11}$	$^{-}_{-0.15}$	±0.13	$^{+0.13}_{-}$	$^{-}_{-0.16}$	$^{+0.23}_{-0.16}$	$^{+0.18}_{-0.13}$	$^{+0.25}_{-0.28}$	$^{+0.29}_{-0.35}$
η intercalibration model (JES) [%]	$^{+0.66}_{-0.77}$	$^{+0.47}_{-0.41}$	$^{+0.51}_{-0.49}$	$^{+0.54}_{-0.57}$	$^{+0.52}_{-0.66}$	$^{+0.50}_{-0.44}$	$^{+0.56}_{-0.54}$	$^{+0.68}_{-0.74}$	$^{+0.75}_{-0.77}$	$^{+0.73}_{-0.71}$	$^{+0.64}_{-0.59}$	$^{+0.74}_{-0.86}$	$^{+0.71}_{-0.77}$	$^{+0.83}_{-0.73}$	$^{+0.59}_{-0.63}$	$^{+0.72}_{-0.66}$	$^{+0.77}_{-0.67}$	$^{+1.34}_{-1.30}$	$^{+0.89}_{-0.96}$
η intercalibration non closure (JES) [%]	$^{-}_{+0.22}$	$^{-0.22}_{+0.24}$	$^{-0.25}_{+0.36}$	$^{-0.32}_{+0.22}$	$^{-0.31}_{+0.26}$	$^{-0.17}_{+0.26}$	∓0.22	$^{-0.25}_{+0.23}$	$^{-0.24}_{+0.23}$	$^{-0.21}_{+0.22}$	$^{-0.22}_{+0.24}$	$^{-0.35}_{+0.30}$	$^{-0.35}_{+0.27}$	$^{-0.26}_{+0.45}$	$^{-0.42}_{+0.24}$	$^{-0.35}_{+0.34}$	$^{-0.25}_{+0.50}$	$^{-0.66}_{+0.64}$	$^{-0.56}_{+0.31}$
η intercalibration total stat (JES) [%]	$^{+0.24}_{-0.23}$	$^{+0.52}_{-0.31}$	$^{+0.40}_{-0.30}$	$^{+0.34}_{-0.39}$	$^{+0.39}_{-0.49}$	$^{+0.35}_{-0.34}$	$^{+0.41}_{-0.36}$	$^{+0.51}_{-0.50}$	$^{+0.46}_{-0.42}$	$^{+0.47}_{-0.45}$	$^{+0.41}_{-0.39}$	$^{+0.34}_{-0.52}$	$^{+0.42}_{-0.43}$	$^{+0.38}_{-0.25}$	$^{+0.30}_{-0.27}$	$^{+0.41}_{-0.31}$	$^{+0.26}_{-0.33}$	$^{+0.40}_{-0.41}$	$^{+0.20}_{-0.50}$
Flavour composition (JES) [%]	$^{+2.78}_{-2.97}$	$^{+3.23}_{-2.77}$	$^{+2.64}_{-2.62}$	$^{+2.30}_{-2.88}$	$^{+2.56}_{-2.62}$	$^{+2.27}_{-2.31}$	$^{+1.99}_{-2.28}$	$^{+1.92}_{-2.09}$	$^{+1.95}_{-1.96}$	$^{+1.63}_{-1.64}$	$^{+1.32}_{-1.42}$	$^{+1.17}_{-1.47}$	$^{+1.22}_{-1.19}$	$^{+1.31}_{-0.98}$	$^{+1.07}_{-0.92}$	$^{+0.97}_{-1.03}$	$^{+0.42}_{-0.97}$	$^{+1.55}_{-1.00}$	$^{+1.51}_{-1.44}$
Flavour response (JES) [%]	$^{-1.07}_{+1.28}$	$^{-1.26}_{+1.60}$	$^{-1.32}_{+1.34}$	$^{-1.30}_{+1.00}$	$^{-1.22}_{+1.04}$	$^{-1.06}_{+1.12}$	$^{-1.00}_{+1.02}$	$^{-1.04}_{+0.97}$	∓0.99	$^{-0.81}_{+0.91}$	$^{-0.79}_{+0.75}$	$^{-0.92}_{+0.65}$	$^{-0.80}_{+0.68}$	$^{-0.56}_{+0.83}$	$^{-0.42}_{+0.56}$	$^{-0.59}_{+0.60}$	$^{-0.54}_{+0.25}$	$^{-0.74}_{+0.92}$	$^{-0.34}_{-}$
Pile-up offset μ (JES) [%]	$^{-0.12}_{-}$	$^{-}_{+0.21}$	$^{-0.12}_{+0.19}$	∓0.16	$^{-0.11}_{+0.12}$	∓0.11	$^{-0.17}_{+0.15}$	$^{-0.17}_{+0.16}$	$^{-0.18}_{+0.19}$	-	$^{-0.13}_{+0.16}$	$^{-0.17}_{-}$	$^{-0.13}_{-}$	$^{-0.12}_{+0.19}$	-	$^{-0.15}_{+0.21}$	$^{-0.13}_{+0.12}$	$^{-}_{+0.18}$	-
Pile-up offset N_{PV} (JES) [%]	$^{+0.44}_{-0.33}$	$^{+0.91}_{-0.38}$	$^{+0.71}_{-0.48}$	$^{+0.36}_{-0.58}$	$^{+0.36}_{-0.48}$	$^{+0.54}_{-0.39}$	±0.52	±0.48	$^{+0.48}_{-0.41}$	$^{+0.54}_{-0.49}$	$^{+0.43}_{-0.45}$	$^{+0.16}_{-0.46}$	$^{+0.37}_{-0.46}$	$^{+0.48}_{-0.27}$	$^{+0.40}_{-0.20}$	$^{+0.38}_{-0.18}$	$^{+0.30}_{-0.27}$	$^{+0.25}_{-0.23}$	$^{+0.28}_{-0.59}$
Pile-up offset p_T (JES) [%]	$^{-0.51}_{+0.56}$	$^{-0.59}_{+0.57}$	$^{-0.51}_{+0.66}$	$^{-0.57}_{+0.59}$	$^{-0.51}_{+0.33}$	$^{-0.34}_{+0.37}$	$^{-0.20}_{+0.26}$	-	$^{+0.21}_{-0.30}$	$^{+0.42}_{-0.31}$	$^{+0.37}_{-0.30}$	$^{+0.41}_{-0.61}$	$^{+0.66}_{-0.62}$	$^{+0.85}_{-0.76}$	$^{+0.52}_{-0.75}$	$^{+1.00}_{-0.85}$	$^{+0.80}_{-0.76}$	$^{+1.27}_{-1.40}$	$^{+1.42}_{-1.34}$
Pile-up offset ρ topology (JES) [%]	$^{+4.04}_{-3.47}$	$^{+4.48}_{-3.86}$	$^{+4.05}_{-3.81}$	$^{+3.59}_{-3.87}$	$^{+3.64}_{-3.69}$	$^{+3.66}_{-3.34}$	$^{+3.52}_{-3.41}$	$^{+3.48}_{-3.39}$	$^{+3.58}_{-3.45}$	$^{+3.30}_{-3.21}$	$^{+2.86}_{-2.75}$	$^{+2.41}_{-2.75}$	$^{+2.41}_{-2.49}$	$^{+2.66}_{-2.17}$	$^{+2.41}_{-1.93}$	$^{+2.02}_{-2.00}$	$^{+1.34}_{-1.80}$	$^{+2.17}_{-1.70}$	$^{+1.30}_{-1.46}$
Jet vertex fraction [%]	$^{+1.03}_{-1.07}$	$^{+1.04}_{-1.07}$	$^{+1.01}_{-1.05}$	$^{+0.96}_{-1.00}$	$^{+0.91}_{-0.94}$	$^{+0.85}_{-0.89}$	$^{+0.79}_{-0.82}$	$^{+0.70}_{-0.73}$	$^{+0.61}_{-0.65}$	$^{+0.53}_{-0.57}$	$^{+0.46}_{-0.50}$	$^{+0.41}_{-0.44}$	$^{+0.38}_{-0.41}$	$^{+0.33}_{-0.37}$	$^{+0.31}_{-0.34}$	$^{+0.27}_{-0.31}$	$^{+0.25}_{-0.28}$	$^{+0.19}_{-0.23}$	$^{+0.13}_{-0.18}$
b-Quark tagging efficiency (eigenvector 0) [%]	$^{-7.63}_{+7.87}$	$^{-7.74}_{+8.00}$	$^{-7.57}_{+7.81}$	$^{-7.22}_{+7.44}$	$^{-6.96}_{+7.17}$	$^{-6.77}_{+6.97}$	$^{-6.54}_{+6.72}$	$^{-6.30}_{+6.48}$	$^{-6.17}_{+6.34}$	$^{-6.04}_{+6.20}$	$^{-5.87}_{+6.03}$	$^{-5.77}_{+5.92}$	$^{-5.68}_{+5.82}$	$^{-5.67}_{+5.81}$	$^{-5.70}_{+5.84}$	$^{-5.68}_{+5.82}$	$^{-5.79}_{+5.93}$	$^{-5.84}_{+5.99}$	$^{-6.41}_{+6.57}$
b-Quark tagging efficiency (eigenvector 1) [%]	∓1.21	∓1.20	∓1.25	$^{-1.35}_{+1.36}$	$^{-1.45}_{+1.46}$	$^{-1.54}_{+1.55}$	$^{-1.66}_{+1.67}$	$^{-1.80}_{+1.82}$	$^{-1.97}_{+1.98}$	$^{-2.18}_{+2.20}$	$^{-2.43}_{+2.46}$	$^{-2.66}_{+2.70}$	$^{-2.89}_{+2.93}$	$^{-3.07}_{+3.12}$	$^{-3.23}_{+3.28}$	$^{-3.46}_{+3.52}$	$^{-3.78}_{+3.85}$	$^{-4.12}_{+4.20}$	$^{-4.65}_{+4.74}$
b-Quark tagging efficiency (eigenvector 2) [%]	$^{+1.52}_{-1.51}$	±1.51	$^{+1.51}_{-1.50}$	$^{+1.51}_{-1.50}$	$^{+1.49}_{-1.48}$	$^{+1.46}_{-1.45}$	$^{+1.41}_{-1.40}$	$^{+1.34}_{-1.33}$	±1.25	$^{+1.14}_{-1.13}$	$^{+1.00}_{-0.99}$	±0.86	$^{+0.72}_{-0.71}$	$^{+0.60}_{-0.59}$	±0.48	±0.31	-	∓0.19	$^{-0.61}_{+0.62}$
b-Quark tagging efficiency (eigenvector 3) [%]	∓0.19	∓0.19	∓0.18	∓0.14	∓0.10	-	-	-	±0.12	±0.19	$^{+0.25}_{-0.24}$	$^{+0.27}_{-0.26}$	±0.26	±0.23	±0.18	-	-	∓0.23	∓0.60
b-Quark tagging efficiency (eigenvector 4) [%]	-	-	-	-	-	-	-	-	-	-	-	-	-	-	-	-	-	∓0.10	∓0.21
c-Quark tagging efficiency (eigenvector 0) [%]	±0.42	±0.41	±0.38	±0.38	±0.39	±0.34	$^{+0.32}_{-0.31}$	$^{+0.27}_{-0.26}$	±0.23	±0.21	±0.18	±0.14	±0.13	±0.12	±0.11	±0.11	±0.12	-	±0.10
c-Quark tagging efficiency (eigenvector 1) [%]	∓0.14	∓0.12	∓0.13	∓0.16	∓0.17	∓0.19	∓0.22	∓0.24	∓0.26	∓0.28	∓0.30	∓0.31	∓0.31	∓0.30	∓0.31	∓0.31	∓0.36	$^{-0.33}_{+0.34}$	$^{-0.63}_{+0.64}$
c-Quark tagging efficiency (eigenvector 2) [%]	$^{+0.13}_{-0.14}$	±0.13	±0.15	±0.16	±0.15	±0.14	±0.12	-	-	-	-	-	-	-	-	-	∓0.10	∓0.10	∓0.25
Light-jet tagging efficiency (eigenvector 0) [%]	$^{-0.95}_{+0.99}$	$^{-0.72}_{+0.61}$	$^{-0.78}_{+0.80}$	$^{-0.87}_{+0.91}$	$^{-0.74}_{+0.76}$	∓0.59	$^{-0.69}_{+0.71}$	$^{-0.64}_{+0.66}$	$^{-0.59}_{+0.60}$	$^{-0.59}_{+0.61}$	$^{-0.63}_{+0.66}$	$^{-0.58}_{+0.60}$	∓0.58	$^{-0.54}_{+0.52}$	$^{-0.58}_{+0.59}$	$^{-0.67}_{+0.69}$	$^{-0.64}_{+0.65}$	$^{-0.72}_{+0.74}$	$^{-1.09}_{+1.14}$
Light-jet tagging efficiency (eigenvector 1) [%]	$^{+0.50}_{-0.46}$	$^{+0.48}_{-0.47}$	±0.47	$^{+0.42}_{-0.41}$	$^{+0.32}_{-0.31}$	±0.26	±0.24	$^{+0.22}_{-0.21}$	±0.16	$^{+0.17}_{-0.16}$	$^{+0.14}_{-0.13}$	±0.10	-	-	-	-	-	-	-
Light-jet tagging efficiency (eigenvector 2) [%]	-	$^{-0.28}_{+0.18}$	$^{-0.12}_{+0.10}$	-	-	-	-	-	-	-	-	-	-	-	-	-	-	-	-
Light-jet tagging efficiency (eigenvector 3) [%]	$^{+0.12}_{-0.13}$	-	-	-	-	-	-	-	-	-	-	-	-	∓0.11	∓0.11	$^{-0.11}_{+0.10}$	$^{-0.11}_{+0.10}$	∓0.15	∓0.20
Light-jet tagging efficiency (eigenvector 5) [%]	-	-	-	-	-	-	-	-	-	-	-	-	-	-	-	-	-	-	±0.15
b-Quark tagging extrapolation [%]	-	-	-	-	-	-	-	-	-	-	-	-	±0.10	±0.12	±0.18	±0.30	±0.63	±1.28	$^{+3.29}_{-3.26}$
Electron trigger efficiency [%]	±0.13	±0.13	±0.13	±0.13	±0.12	±0.12	±0.12	±0.11	±0.11	±0.11	±0.11	±0.11	±0.11	±0.11	±0.11	±0.11	±0.11	±0.11	±0.11
Electron reconstruction efficiency [%]	-	-	-	-	-	-	-	-	-	-	-	-	-	-	-	±0.10	±0.10	$^{+0.11}_{-0.10}$	±0.11
Electron identification efficiency [%]	±0.37	±0.38	±0.37	±0.37	±0.37	±0.37	±0.38	$^{+0.39}_{-0.38}$	±0.40	±0.42	±0.44	±0.47	±0.48	±0.50	±0.52	±0.55	±0.59	±0.63	±0.72
Electron isolation efficiency [%]	-	-	-	-	-	-	-	-	-	±0.10	±0.12	±0.15	$^{+0.17}_{-0.18}$	$^{+0.21}_{-0.20}$	±0.24	±0.29	±0.36	±0.45	±0.64
Muon trigger efficiency stat [%]	$^{+0.30}_{-0.31}$	$^{+0.30}_{-0.31}$	$^{+0.30}_{-0.31}$	±0.30	$^{+0.29}_{-0.30}$	$^{+0.29}_{-0.30}$	$^{+0.29}_{-0.30}$	±0.29	$^{+0.28}_{-0.29}$	$^{+0.28}_{-0.29}$	$^{+0.28}_{-0.29}$	±0.28	±0.28	±0.28	$^{+0.27}_{-0.28}$	$^{+0.27}_{-0.28}$	±0.28	±0.28	±0.29
Muon trigger efficiency syst [%]	$^{+0.55}_{-0.54}$	$^{+0.54}_{-0.53}$	$^{+0.54}_{-0.53}$	$^{+0.53}_{-0.52}$	$^{+0.52}_{-0.51}$	$^{+0.52}_{-0.51}$	$^{+0.52}_{-0.51}$	$^{+0.51}_{-0.50}$	$^{+0.50}_{-0.49}$	$^{+0.50}_{-0.49}$	$^{+0.50}_{-0.49}$	$^{+0.49}_{-0.48}$	$^{+0.49}_{-0.48}$	$^{+0.50}_{-0.48}$	$^{+0.49}_{-0.48}$	$^{+0.48}_{-0.47}$	$^{+0.49}_{-0.47}$	$^{+0.48}_{-0.47}$	$^{+0.50}_{-0.49}$
Muon identification stat [%]	±0.10	±0.10	±0.10	±0.10	-	-	-	-	-	-	-	-	-	-	-	-	-	-	-
Muon identification syst [%]	±0.37	±0.37	±0.37	±0.37	±0.36	±0.36	±0.36	±0.36	±0.37	±0.37	±0.38	±0.39	±0.40	±0.41	±0.42	±0.44	±0.46	±0.50	±0.57
Muon isolation efficiency syst [%]	±0.11	±0.11	±0.11	±0.11	±0.11	±0.10	$^{+0.10}_{-0.11}$	±0.10	±0.10	±0.10	±0.10	±0.10	±0.10	±0.10	±0.10	±0.10	±0.10	±0.10	±0.12
Luminosity [%]	∓2.05	∓2.05	∓2.05	∓2.05	∓2.05	∓2.05	∓2.05	∓2.05	∓2.05	∓2.05	∓2.05	∓2.05	∓2.05	∓2.05	∓2.05	∓2.05	∓2.05	∓2.05	∓2.05
Z+jets cross-section [%]	±0.56	±0.74	±0.74	±0.79	±0.74	±0.69	±0.69	±0.52	±0.44	±0.39	±0.38	±0.31	±0.28	±0.28	±0.28	±0.26	±0.29	±0.31	±0.45
Monte Carlo sample statistics [%]	±0.78	±0.54	±0.33	±0.29	±0.32	±0.32	±0.22	±0.20	±0.21	±0.23	±0.27	±0.30	±0.34	±0.39	±0.46	±0.48	±0.70	±0.78	±1.28
ISR/FSR + scale [%]	$^{-0.21}_{-}$	$^{-}_{-0.22}$	$^{-0.25}_{+0.53}$	$^{-0.14}_{+1.22}$	$^{+1.72}_{-}$	$^{+1.39}_{-}$	$^{-0.22}_{+0.73}$	$^{-0.43}_{+0.96}$	$^{-0.48}_{+1.38}$	$^{-0.59}_{+1.38}$	$^{+1.83}_{-}$	$^{+0.65}_{-}$	$^{-}_{-1.25}$	$^{-1.89}_{+0.54}$	$^{+1.26}_{-}$	$^{+0.35}_{-}$	$^{-0.22}_{+0.94}$	$^{-1.76}_{+1.72}$	$^{+5.33}_{-}$
Alternate hard-scattering model [%]	±6.43	±5.60	±4.46	±4.93	±6.36	±4.26	±2.75	±2.57	±1.99	±2.50	±1.83	±1.14	±1.35	±2.25	±0.65	±1.14	±0.52	∓1.58	±3.72
Alternate parton-shower model [%]	∓0.26	±0.48	±0.49	±1.43	±2.48	±2.20	±2.03	±2.62	±1.53	±1.70	±2.15	±0.52	∓0.20	∓0.13	±1.52	∓1.03	±1.63	±1.26	±2.43
Intra PDF [%]	±0.85	±0.21	-	±0.25	±0.18	±0.10	-	-	±0.23	-	±0.12	±0.21	±0.10	±0.33	±0.38	-	±0.36	±0.46	±0.41
Fakes overall normalization, el [%]	±0.84	±1.02	±1.15	±1.09	±0.99	±0.93	±0.75	±0.65	±0.61	±0.43	±0.36	±0.40	±0.39	±0.25	±0.11	±0.22	±0.31	±0.24	±1.37
Fakes overall normalization, mu [%]	±0.24	±0.32	±0.24	±0.16	±0.14	±0.20	±0.17	±0.13	-	-	-	∓0.16	∓0.27	∓0.34	∓0.43	∓0.67	∓0.87	∓0.82	∓1.15
Fakes alternative parametrization [%]	∓5.32	∓5.25	∓4.84	∓4.53	∓4.09	∓3.72	∓3.11	∓2.48	∓1.99	∓1.50	∓1.06	∓0.71	∓0.31	-	±0.62	±0.53	±0.90	±1.18	±1.54
W+jets heavy flavour component [%]	±10.2	±4.90	±6.40	±4.68	±4.85	±6.06	±3.14	±2.99	±3.11	±3.24	±2.13	±1.34	±0.83	±0.99	±1.59	±2.66	±4.93	±1.00	±2.57

TABLE F.3: Table of systematics for the absolute differential cross-section at the particle level for the $p_T^{t,had}$ observable.

Bins [Unit y^{t_h}]	-3—1.62	-1.62—1.23	-1.23—0.96	-0.96—0.75	-0.75—0.54	-0.54—0.36	-0.36—0.18	-0.18–0	0–0.18	0.18–0.36	0.36–0.54	0.54–0.75	0.75–0.96	0.96–1.23	1.23–1.62	1.62–3
$d\sigma$ / dy^{t_h} [pb/ Unit y^{t_h}]	$2.22 \cdot 10^{0}$	$1.44 \cdot 10^{1}$	$2.10 \cdot 10^{1}$	$2.59 \cdot 10^{1}$	$2.92 \cdot 10^{1}$	$3.16 \cdot 10^{1}$	$3.31 \cdot 10^{1}$	$3.43 \cdot 10^{1}$	$3.42 \cdot 10^{1}$	$3.35 \cdot 10^{1}$	$3.19 \cdot 10^{1}$	$2.91 \cdot 10^{1}$	$2.62 \cdot 10^{1}$	$2.13 \cdot 10^{1}$	$1.44 \cdot 10^{1}$	$2.19 \cdot 10^{0}$
Total Uncertainty [%]	$^{+8.89}_{-8.86}$	$^{+10.3}_{-10.1}$	±10.3	$^{+12.3}_{-12.0}$	$^{+10.4}_{-10.2}$	±12.2	$^{+10.4}_{-10.0}$	$^{+12.2}_{-12.1}$	$^{+10.7}_{-10.4}$	$^{+11.0}_{-10.7}$	$^{+10.9}_{-10.5}$	±10.6	$^{+10.5}_{-10.1}$	$^{+10.8}_{-10.6}$	$^{+9.91}_{-9.75}$	±11.4
Statistics [%]	±0.5	±0.4	±0.4	±0.4	±0.4	±0.4	±0.4	±0.4	±0.4	±0.4	±0.4	±0.4	±0.4	±0.4	±0.4	±0.5
Systematics [%]	$^{+8.86}_{-8.83}$	$^{+10.3}_{-10.0}$	$^{+10.3}_{-10.2}$	$^{+12.3}_{-12.0}$	$^{+10.4}_{-10.1}$	$^{+12.1}_{-12.2}$	$^{+10.3}_{-10.0}$	±12.1	$^{+10.7}_{-10.4}$	$^{+11.0}_{-10.7}$	$^{+10.9}_{-10.5}$	±10.6	$^{+10.4}_{-10.0}$	$^{+10.8}_{-10.6}$	$^{+9.90}_{-9.73}$	±11.4
Jet energy resolution [%]	∓0.16	±0.28	∓0.20	±3.64	∓1.25	±2.69	∓0.26	±3.02	∓0.53	-	±0.45	±1.09	∓0.44	±1.57	±1.45	±0.18
b-Tagged jet energy scale (JES) [%]	$^{+0.28}_{-0.29}$	$^{+0.43}_{-0.46}$	±0.49	$^{+0.47}_{-0.45}$	±0.57	$^{+0.55}_{-0.57}$	$^{+0.54}_{-0.57}$	$^{+0.58}_{-0.53}$	$^{+0.55}_{-0.59}$	±0.57	$^{+0.53}_{-0.47}$	$^{+0.51}_{-0.62}$	$^{+0.52}_{-0.42}$	±0.47	$^{+0.37}_{-0.44}$	±0.30
Effective mixed NP set 1 (JES) [%]	-	$^{+0.16}_{-0.12}$	$^{+0.14}_{-0.19}$	±0.13	±0.15	$^{+0.13}_{-0.17}$	$^{+0.19}_{-0.15}$	$^{+0.13}_{-0.15}$	$^{+0.17}_{-0.13}$	$^{+0.16}_{-0.17}$	$^{+0.18}_{-0.11}$	$^{+0.13}_{-0.15}$	$^{+0.17}_{-0.12}$	$^{+0.14}_{-0.18}$	$^{+0.11}_{-0.12}$	-
Effective modelling NP set 1 (JES) [%]	$^{+1.15}_{-1.17}$	$^{+2.05}_{-1.85}$	$^{+2.12}_{-2.16}$	$^{+2.30}_{-2.19}$	$^{+2.48}_{-2.40}$	$^{+2.40}_{-2.47}$	$^{+2.44}_{-2.30}$	$^{+2.34}_{-2.54}$	$^{+2.52}_{-2.34}$	$^{+2.29}_{-2.30}$	$^{+2.49}_{-2.27}$	$^{+2.37}_{-2.31}$	$^{+2.37}_{-2.17}$	$^{+2.15}_{-2.00}$	$^{+1.75}_{-1.84}$	$^{+1.43}_{-1.29}$
Effective modelling NP set 2 (JES) [%]	$^{-0.12}_{+0.15}$	$^{-0.12}_{+0.17}$	$^{-0.14}_{+0.12}$	$^{-0.22}_{+0.20}$	$^{-0.20}_{+0.15}$	$^{-0.18}_{+0.15}$	$^{-0.15}_{+0.22}$	∓0.16	$^{-0.19}_{+0.23}$	$^{-0.17}_{+0.19}$	∓0.17	∓0.18	$^{-0.15}_{+0.17}$	$^{-0.16}_{+0.14}$	$^{-0.12}_{+0.14}$	$^{-0.12}_{+0.11}$
Effective modelling NP set 3 (JES) [%]	-	-	-	$^{+0.13}_{-0.11}$	-	-	$^{+0.13}_{-}$	-	$^{+0.14}_{-0.11}$	$^{+0.11}_{-0.10}$	-	±0.10	$^{-}_{-0.11}$	-	-	-
Effective modelling NP set 4 (JES) [%]	-	-	±0.10	$^{+0.14}_{-0.12}$	$^{+0.11}_{-0.10}$	$^{-}_{-0.13}$	$^{+0.15}_{-0.12}$	$^{+0.10}_{-0.11}$	$^{+0.15}_{-0.13}$	$^{+0.13}_{-0.10}$	$^{+0.12}_{-0.13}$	$^{+0.11}_{-0.10}$	$^{+0.11}_{-0.10}$	$^{+0.11}_{-0.12}$	-	-
Effective statistical NP set 1 (JES) [%]	±0.22	$^{+0.36}_{-0.26}$	$^{+0.33}_{-0.40}$	$^{+0.47}_{-0.41}$	$^{+0.36}_{-0.42}$	$^{+0.38}_{-0.42}$	$^{+0.48}_{-0.37}$	$^{+0.31}_{-0.42}$	$^{+0.46}_{-0.41}$	±0.42	$^{+0.41}_{-0.34}$	$^{+0.40}_{-0.43}$	$^{+0.40}_{-0.35}$	$^{+0.35}_{-0.37}$	$^{+0.36}_{-0.31}$	$^{+0.19}_{-0.18}$
Effective statistical NP set 2 (JES) [%]	$^{-0.17}_{+0.21}$	$^{-0.22}_{+0.30}$	$^{-0.36}_{+0.28}$	$^{-0.35}_{+0.45}$	$^{-0.37}_{+0.30}$	$^{-0.37}_{+0.33}$	$^{-0.31}_{+0.42}$	$^{-0.35}_{+0.26}$	$^{-0.37}_{+0.41}$	$^{-0.34}_{+0.38}$	$^{-0.30}_{+0.34}$	$^{-0.39}_{+0.35}$	$^{-0.32}_{+0.35}$	$^{-0.33}_{+0.29}$	$^{-0.26}_{+0.32}$	$^{-0.16}_{+0.17}$
Effective statistical NP set 7 (JES) [%]	-	-	-	-	-	-	-	-	$^{+0.12}_{-0.11}$	-	-	-	-	-	-	-
η intercalibration model (JES) [%]	$^{+0.77}_{-0.75}$	$^{+1.05}_{-0.98}$	$^{+0.86}_{-1.00}$	$^{+0.64}_{-0.58}$	$^{+0.60}_{-0.56}$	$^{+0.44}_{-0.55}$	$^{+0.52}_{-0.41}$	$^{+0.34}_{-0.59}$	$^{+0.47}_{-0.45}$	$^{+0.40}_{-0.36}$	±0.49	$^{+0.59}_{-0.55}$	$^{+0.71}_{-0.62}$	$^{+0.82}_{-0.90}$	$^{+0.98}_{-1.00}$	$^{+0.76}_{-0.79}$
η intercalibration non closure (JES) [%]	$^{-0.10}_{+0.19}$	$^{-0.37}_{+0.43}$	$^{-0.54}_{+0.43}$	$^{-0.48}_{+0.52}$	$^{-0.44}_{+0.45}$	$^{-0.52}_{+0.37}$	$^{-0.27}_{+0.48}$	$^{-0.28}_{+0.22}$	$^{-0.28}_{+0.29}$	$^{-0.21}_{+0.26}$	$^{-0.20}_{+0.12}$	-	-	-	-	-
η intercalibration total stat (JES) [%]	±0.21	$^{+0.42}_{-0.34}$	$^{+0.38}_{-0.46}$	$^{+0.49}_{-0.42}$	$^{+0.41}_{-0.47}$	±0.43	$^{+0.52}_{-0.37}$	$^{+0.32}_{-0.43}$	$^{+0.49}_{-0.43}$	$^{+0.43}_{-0.46}$	$^{+0.46}_{-0.38}$	$^{+0.39}_{-0.46}$	$^{+0.45}_{-0.33}$	$^{+0.37}_{-0.44}$	$^{+0.39}_{-0.35}$	$^{+0.20}_{-0.21}$
Flavour composition (JES) [%]	$^{+0.81}_{-0.96}$	±1.73	$^{+1.82}_{-2.22}$	$^{+2.33}_{-2.06}$	$^{+2.33}_{-2.25}$	$^{+1.76}_{-2.34}$	$^{+2.14}_{-2.08}$	$^{+2.02}_{-2.36}$	$^{+2.20}_{-2.29}$	$^{+1.96}_{-2.13}$	$^{+2.23}_{-2.07}$	$^{+1.90}_{-2.21}$	$^{+2.06}_{-1.90}$	$^{+1.90}_{-1.95}$	$^{+1.58}_{-1.74}$	$^{+0.93}_{-1.01}$
Flavour response (JES) [%]	$^{-0.44}_{+0.46}$	$^{-0.89}_{+1.00}$	$^{-1.17}_{+0.97}$	∓0.99	$^{-1.08}_{+1.09}$	$^{-1.06}_{+0.93}$	$^{-1.04}_{+1.12}$	$^{-1.16}_{+0.96}$	$^{-1.07}_{+1.00}$	$^{-0.93}_{+0.91}$	$^{-1.05}_{+1.13}$	$^{-1.05}_{+1.04}$	$^{-1.04}_{+1.00}$	$^{-0.95}_{+0.92}$	$^{-0.83}_{+0.84}$	$^{-0.54}_{+0.59}$
Pile-up offset μ (JES) [%]	-	$^{-0.11}_{+0.18}$	$^{-0.15}_{-}$	$^{-0.13}_{+0.17}$	-	$^{-0.20}_{+0.18}$	$^{-0.13}_{+0.21}$	$^{-0.21}_{+0.16}$	$^{-0.10}_{+0.19}$	$^{-0.15}_{+0.14}$	$^{-}_{+0.17}$	$^{-0.18}_{+0.10}$	$^{-0.11}_{+0.19}$	$^{-0.17}_{-}$	$^{-0.11}_{+0.16}$	-
Pile-up offset N_{PV} (JES) [%]	$^{+0.18}_{-0.21}$	$^{+0.55}_{-0.26}$	$^{+0.45}_{-0.59}$	$^{+0.43}_{-0.40}$	$^{+0.56}_{-0.57}$	$^{+0.29}_{-0.46}$	$^{+0.56}_{-0.43}$	$^{+0.47}_{-0.63}$	$^{+0.61}_{-0.41}$	$^{+0.45}_{-0.64}$	$^{+0.54}_{-0.38}$	$^{+0.53}_{-0.62}$	$^{+0.60}_{-0.25}$	$^{+0.47}_{-0.48}$	$^{+0.33}_{-0.26}$	$^{+0.26}_{-0.27}$
Pile-up offset p_T (JES) [%]	-	-	-	-	-	-	-	-	-	-	-	-	-	-	-	-
Pile-up offset ρ topology (JES) [%]	$^{+1.58}_{-1.66}$	$^{+2.87}_{-2.75}$	$^{+3.18}_{-3.21}$	$^{+3.45}_{-3.35}$	$^{+3.72}_{-3.57}$	$^{+3.35}_{-3.64}$	$^{+3.75}_{-3.49}$	$^{+3.67}_{-3.72}$	$^{+3.79}_{-3.54}$	±3.53	$^{+3.70}_{-3.37}$	$^{+3.56}_{-3.57}$	$^{+3.54}_{-3.06}$	$^{+3.18}_{-3.09}$	$^{+2.71}_{-2.67}$	$^{+1.82}_{-1.78}$
Jet vertex fraction [%]	$^{+0.66}_{-0.69}$	$^{+0.70}_{-0.73}$	$^{+0.70}_{-0.74}$	$^{+0.69}_{-0.72}$	$^{+0.69}_{-0.72}$	$^{+0.69}_{-0.73}$	$^{+0.68}_{-0.72}$	$^{+0.69}_{-0.73}$	$^{+0.69}_{-0.73}$	$^{+0.69}_{-0.73}$	$^{+0.69}_{-0.73}$	$^{+0.68}_{-0.72}$	$^{+0.69}_{-0.72}$	$^{+0.70}_{-0.73}$	$^{+0.69}_{-0.72}$	$^{+0.66}_{-0.69}$
b-Quark tagging efficiency (eigenvector 0) [%]	$^{-6.31}_{+6.49}$	$^{-6.40}_{+6.58}$	$^{-6.40}_{+6.58}$	$^{-6.46}_{+6.65}$	$^{-6.48}_{+6.66}$	$^{-6.49}_{+6.68}$	$^{-6.50}_{+6.69}$	$^{-6.52}_{+6.70}$	$^{-6.50}_{+6.68}$	$^{-6.50}_{+6.68}$	$^{-6.51}_{+6.69}$	$^{-6.47}_{+6.66}$	$^{-6.45}_{+6.64}$	$^{-6.43}_{+6.62}$	$^{-6.36}_{+6.55}$	$^{-6.31}_{+6.49}$
b-Quark tagging efficiency (eigenvector 1) [%]	$^{-1.95}_{+1.97}$	$^{-1.94}_{+1.96}$	$^{-1.95}_{+1.97}$	$^{-1.96}_{+1.98}$	$^{-1.95}_{+1.97}$	$^{-1.97}_{+1.98}$	$^{-1.98}_{+1.99}$	$^{-1.96}_{+1.98}$	$^{-1.97}_{+1.99}$	$^{-1.97}_{+1.99}$	$^{-1.97}_{+1.99}$	$^{-1.97}_{+1.99}$	$^{-1.96}_{+1.99}$	$^{-1.95}_{+1.97}$	$^{-1.94}_{+1.96}$	$^{-1.96}_{+1.98}$
b-Quark tagging efficiency (eigenvector 2) [%]	$^{+1.22}_{-1.21}$	$^{+1.22}_{-1.21}$	$^{+1.22}_{-1.21}$	±1.21	$^{+1.21}_{-1.20}$	$^{+1.22}_{-1.21}$	±1.21	$^{+1.21}_{-1.20}$	±1.21	±1.21	±1.21	$^{+1.21}_{-1.20}$	$^{+1.22}_{-1.21}$	±1.22	±1.22	$^{+1.22}_{-1.21}$
c-Quark tagging efficiency (eigenvector 0) [%]	±0.26	±0.27	±0.27	±0.25	$^{+0.29}_{-0.28}$	±0.27	±0.28	±0.26	±0.28	±0.28	±0.28	±0.28	±0.26	±0.25	$^{+0.28}_{-0.27}$	±0.25
c-Quark tagging efficiency (eigenvector 1) [%]	∓0.20	∓0.20	∓0.23	∓0.22	∓0.25	∓0.24	∓0.25	∓0.25	∓0.25	∓0.26	∓0.25	∓0.24	∓0.23	∓0.22	∓0.21	∓0.20
Light-jet tagging efficiency (eigenvector 0) [%]	$^{-0.79}_{+0.82}$	∓0.58	$^{-0.69}_{+0.71}$	$^{-0.66}_{+0.69}$	$^{-0.54}_{+0.46}$	$^{-0.85}_{+0.94}$	$^{-0.55}_{+0.52}$	$^{-0.45}_{+0.43}$	$^{-0.70}_{+0.73}$	$^{-0.68}_{+0.70}$	∓0.63	$^{-0.68}_{+0.69}$	$^{-0.69}_{+0.73}$	$^{-0.76}_{+0.82}$	$^{-0.76}_{+0.80}$	$^{-0.70}_{+0.72}$
Light-jet tagging efficiency (eigenvector 1) [%]	±0.28	±0.19	$^{+0.25}_{-0.24}$	$^{+0.22}_{-0.21}$	$^{+0.17}_{-0.18}$	$^{+0.37}_{-0.34}$	±0.19	$^{+0.14}_{-0.15}$	$^{+0.24}_{-0.25}$	±0.26	$^{+0.18}_{-0.19}$	±0.24	$^{+0.22}_{-0.21}$	±0.24	$^{+0.24}_{-0.23}$	$^{+0.25}_{-0.24}$
Light-jet tagging efficiency (eigenvector 2) [%]	-	-	-	-	-	-	-	-	-	-	-	-	-	$^{+0.12}_{-0.11}$	-	-
Light-jet tagging efficiency (eigenvector 3) [%]	-	-	-	-	-	-	-	-	-	-	-	-	-	-	-	-
Electron trigger efficiency [%]	±0.12	±0.12	$^{+0.11}_{-0.12}$	$^{+0.12}_{-0.11}$	±0.12	±0.12	±0.12	$^{+0.11}_{-0.12}$	$^{+0.11}_{-0.12}$	$^{+0.11}_{-0.12}$	±0.12	$^{+0.11}_{-0.12}$	$^{+0.12}_{-0.11}$	$^{+0.11}_{-0.12}$	$^{+0.11}_{-0.12}$	±0.11
Electron identification efficiency [%]	±0.41	±0.41	±0.41	±0.41	±0.41	±0.42	±0.41	±0.41	±0.41	±0.41	±0.41	±0.41	±0.41	±0.41	±0.41	±0.41
Electron isolation efficiency [%]	±0.10	±0.10	±0.10	±0.10	±0.11	±0.11	±0.10	$^{+0.10}_{-0.11}$	±0.10	±0.11	±0.11	±0.11	±0.10	±0.10	±0.10	±0.10
Muon trigger efficiency stat [%]	$^{+0.28}_{-0.29}$	$^{+0.28}_{-0.29}$	±0.29	±0.29	±0.29	±0.29	±0.29	$^{+0.29}_{-0.30}$	$^{+0.29}_{-0.30}$	$^{+0.29}_{-0.30}$	±0.29	±0.29	±0.29	±0.29	±0.29	$^{+0.28}_{-0.29}$
Muon trigger efficiency syst [%]	$^{+0.51}_{-0.50}$	$^{+0.50}_{-0.49}$	$^{+0.51}_{-0.50}$	$^{+0.51}_{-0.50}$	$^{+0.51}_{-0.50}$	$^{+0.51}_{-0.50}$	±0.51	$^{+0.52}_{-0.51}$	$^{+0.52}_{-0.50}$	$^{+0.52}_{-0.51}$	$^{+0.51}_{-0.50}$	$^{+0.51}_{-0.50}$	$^{+0.51}_{-0.50}$	$^{+0.51}_{-0.50}$	$^{+0.51}_{-0.49}$	$^{+0.50}_{-0.49}$
Muon identification syst [%]	±0.37	±0.37	±0.37	±0.37	±0.37	$^{+0.37}_{-0.38}$	±0.37	±0.38	±0.38	±0.38	$^{+0.37}_{-0.38}$	±0.38	±0.38	±0.38	±0.38	±0.38
Muon isolation efficiency syst [%]	±0.10	±0.10	±0.10	±0.10	±0.10	$^{+0.10}_{-0.11}$	±0.10	±0.11	±0.10	$^{+0.11}_{-0.10}$	±0.10	±0.10	±0.10	±0.10	±0.10	±0.10
Luminosity [%]	∓2.05	∓2.05	∓2.05	∓2.05	∓2.05	∓2.05	∓2.05	∓2.05	∓2.05	∓2.05	∓2.05	∓2.05	∓2.05	∓2.05	∓2.05	∓2.05
Z+jets cross-section [%]	±0.40	±0.41	±0.49	±0.51	±0.61	±0.66	±0.53	±0.61	±0.63	±0.61	±0.59	±0.56	±0.54	±0.46	±0.51	±0.43
Monte Carlo sample statistics [%]	±0.37	±0.27	±0.28	±0.29	±0.34	±0.34	±0.37	±0.46	±0.31	±0.30	±0.30	±0.28	±0.30	±0.35	±0.31	±0.39
ISR/FSR + scale [%]	$^{-}_{-0.99}$	$^{-0.12}_{+0.90}$	$^{-0.14}_{+1.28}$	$^{+1.56}_{-}$	$^{-0.97}_{+1.42}$	$^{-0.22}_{+0.81}$	$^{-0.27}_{+1.08}$	$^{-0.14}_{+1.75}$	$^{+1.05}_{-}$	$^{-0.12}_{+1.82}$	$^{-0.15}_{+1.06}$	$^{-1.06}_{+0.86}$	$^{-0.33}_{+0.60}$	$^{-}_{+1.30}$	$^{-0.37}_{+1.27}$	$^{-}_{-1.62}$
Alternate hard-scattering model [%]	±1.94	±3.90	±3.63	±2.42	±2.64	±3.68	±1.82	±2.80	±3.39	±3.74	±3.37	±1.56	±3.68	±3.91	±2.15	±7.23
Alternate parton-shower model [%]	∓0.85	±1.37	±1.76	±0.88	±1.87	±1.51	±1.40	±1.88	±1.52	±1.84	±1.25	±2.32	±1.88	±0.64	±0.67	∓1.87
Intra PDF [%]	±0.25	±0.24	-	±0.12	±0.18	±0.16	±0.46	±0.40	±0.29	±0.17	±0.12	±0.17	±0.34	±0.20	±0.14	±0.18
Fakes overall normalization, el [%]	±0.37	±0.71	±0.64	±0.64	±0.71	±0.77	±0.85	±0.75	±0.72	±0.75	±0.72	±0.71	±0.67	±0.66	±0.56	±0.48
Fakes overall normalization, mu [%]	-	-	-	-	-	-	-	-	-	-	-	-	-	-	-	±0.10
Fakes alternative parametrization [%]	∓2.27	∓2.56	∓2.65	∓2.67	∓2.50	∓2.71	∓2.52	∓2.49	∓2.55	∓2.75	∓2.46	∓2.48	∓2.37	∓2.33	∓2.56	∓2.46
W+jets heavy flavour component [%]	±2.64	±2.82	±2.32	±6.42	±1.80	±6.07	±3.05	±5.99	±2.78	±3.35	±3.62	±3.95	±2.10	±3.91	±3.43	±2.42

TABLE F.4: Table of systematics for the absolute differential cross-section at the particle level for the $y^{t,had}$ observable.

Bins [GeV]	0–25	25–50	50–90	90–130	130–170	170–220	220–270	270–320	320–420	420–550	550–800.00
$d\sigma$ / $dp_T^{t\bar{t}}$ [pb/GeV]	$8.17 \cdot 10^{-1}$	$9.61 \cdot 10^{-1}$	$5.03 \cdot 10^{-1}$	$2.45 \cdot 10^{-1}$	$1.34 \cdot 10^{-1}$	$7.05 \cdot 10^{-2}$	$3.61 \cdot 10^{-2}$	$2.05 \cdot 10^{-2}$	$9.34 \cdot 10^{-3}$	$3.19 \cdot 10^{-3}$	$6.46 \cdot 10^{-4}$
Total Uncertainty [%]	+12.1 −12.6	+10.9 −11.9	+12.5 −12.9	+13.4 −13.2	+10.9 −10.7	+10.4 −10.1	+10.6 −10.1	+10.9 −10.7	±10.6	+10.0 −9.72	+11.2 −11.9
Statistics [%]	±0.2	±0.1	±0.2	±0.3	±0.4	±0.5	±0.7	±1.0	±1.1	±1.7	±2.7
Systematics [%]	+12.1 −12.6	+10.9 −11.9	+12.5 −12.9	+13.4 −13.2	+10.9 −10.7	+10.4 −10.1	+10.5 −10.1	+10.8 −10.7	±10.5	+9.85 −9.50	+10.7 −11.5
Jet energy resolution [%]	-	-	±1.66	±2.05	±0.46	±0.55	±0.31	±2.93	±1.13	±0.86	±0.96
b-Tagged jet energy scale (JES) [%]	+0.51 −0.50	+0.48 −0.50	+0.52 −0.51	±0.54	+0.52 −0.55	+0.49 −0.52	+0.51 −0.47	+0.37 −0.44	+0.33 −0.35	+0.48 −0.46	+0.22 −0.40
Effective detector NP set 1 (JES) [%]	-	-	-	-	-	-	-	-	-	+0.21 −0.13	+0.10 −0.18
Effective detector NP set 2 (JES) [%]	-	-	-	-	-	−0.13 -	-	-	-	-	-
Effective mixed NP set 1 (JES) [%]	-	-	-	+0.18 −0.21	±0.28	+0.35 −0.29	+0.45 −0.34	+0.61 −0.56	+0.63 −0.76	+1.43 −1.40	+2.17 −1.71
Effective mixed NP set 2 (JES) [%]	-	-	-	-	-	-	-	-	-	−0.13 +0.33	−0.15 -
Effective modelling NP set 1 (JES) [%]	+1.21 −1.10	±1.85	+2.91 −2.88	+3.23 −3.11	+3.01 −2.94	+2.64 −2.49	+2.59 −2.26	+2.31 −2.10	+1.92 −1.84	+1.53 −1.86	+1.71 −1.67
Effective modelling NP set 2 (JES) [%]	-	−0.19 +0.18	−0.28 +0.29	−0.21 +0.26	−0.17 -	-	-	-	-	+0.59 −0.51	+1.26 −1.08
Effective modelling NP set 3 (JES) [%]	-	±0.12	+0.19 −0.17	+0.13 −0.11	-	-	-	−0.15 +0.13	+0.14	−0.28 +0.20	∓0.26 +0.19
Effective modelling NP set 4 (JES) [%]	-	-	−0.13 +0.15	+0.16 −0.15	+0.17 −0.12	±0.15	+0.22 −0.14	+0.14 −0.19	-	+0.21 −0.15	−0.14 +0.14
Effective statistical NP set 1 (JES) [%]	+0.18 −0.15	+0.32 −0.33	±0.53	−0.56 −0.53	+0.47 −0.48	+0.37 −0.38	+0.43 −0.22	−0.42 −0.46	+0.30 −0.31	+0.52 −0.36	−0.39 −0.46
Effective statistical NP set 2 (JES) [%]	−0.14 +0.16	∓0.29	−0.46 +0.45	−0.46 +0.50	−0.41 +0.43	−0.37 +0.35	−0.23 +0.35	−0.36 +0.26	−0.19 +0.24	-	+0.29 −0.21
Effective statistical NP set 3 (JES) [%]	-	-	-	-	-	-	-	−0.20 +0.19	−0.28 +0.18	−0.70 +0.64	−0.52 +0.94
Effective statistical NP set 4 (JES) [%]	-	-	-	-	+0.14 −0.15	±0.19	+0.22 −0.10	+0.17 −0.26	-	-	-
Effective statistical NP set 5 (JES) [%]	-	-	-	-	−0.10 +0.13	-	+0.18 -	+0.23 −0.18	+0.20 −0.28	-	−0.25 +0.27
Effective statistical NP set 6 (JES) [%]	-	-	-	±0.10	-	-	-	+0.12 −0.10	+0.15 −0.17	-	-
Effective statistical NP set 7 (JES) [%]	-	-	-	+0.11 −0.10	+0.12 -	+0.16 −0.18	+0.20 −0.15	+0.13 −0.17	-	+0.22 −0.24	±0.12
η intercalibration model (JES) [%]	+0.42 −0.39	+0.43 −0.45	+0.71 −0.76	+0.95 −0.96	+0.89 −0.92	+0.95 −1.01	+0.91 −0.83	+0.87 −0.71	+0.91 −0.89	+1.20 −1.32	+1.50 −0.88
η intercalibration non closure (JES) [%]	−0.14 +0.18	−0.18 +0.19	−0.28 +0.26	−0.36 +0.34	−0.37 +0.40	−0.44 +0.40	−0.46 +0.53	−0.54 +0.53	−0.50 +0.41	−0.74 +0.66	−0.13 +0.55
η intercalibration total stat (JES) [%]	+0.25 −0.22	+0.30 −0.31	±0.50	+0.64 −0.62	+0.59 −0.63	+0.52 −0.48	+0.48 −0.28	+0.52 −0.59	+0.34 −0.44	+0.62 −0.32	+0.25 −0.27
Flavour composition (JES) [%]	+1.39 −1.43	+1.31 −1.42	+2.15 −2.33	+3.04 −3.22	+3.00 −3.13	+2.57 −2.46	+2.57 −2.49	+2.39 −2.24	+1.73 −1.96	+2.17 −2.26	+2.19 −2.09
Flavour response (JES) [%]	−0.65	−0.64	−1.12	−1.64	−1.67	−1.37	−1.18	−1.23	−1.26	−0.85	−0.65
Pile-up offset μ (JES) [%]	+0.67 -	+0.61 −0.10	+1.05 ∓0.19	+1.58 −0.20	+1.60 −0.22	+1.42 −0.14	+1.44 -	+1.31 −0.32	+1.09 -	+0.84 -	+0.75 -
Pile-up offset N_{PV} (JES) [%]	+0.26	+0.11 +0.36	+0.56	+0.23 +0.73	+0.19 +0.74	+0.17 +0.63	+0.17 +0.69	+0.28 +0.53	+0.47	+0.28 +0.42	+0.86
Pile-up offset p_T (JES) [%]	−0.16 -	−0.34 −0.13	−0.63 −0.18	−0.76 -	−0.73 +0.28	−0.47 +0.40	−0.47 −0.38	−0.34 +0.33	−0.51 +0.33	−0.25 ±0.63	−0.92 ±1.08
Pile-up offset ρ topology (JES) [%]	+1.68	+0.11 ±2.65	+0.14 +4.37	+5.01	−0.32 +4.26	−0.35 +4.23	−0.42 +3.96	−0.35 +3.46	−0.49 +2.72	+2.73	+2.21
Punch-through (JES) [%]	−1.58 -	-	−4.34 -	−4.88 -	−4.50 -	−3.76 -	−3.60 -	−3.16 -	−2.73 -	−2.55 -	−1.97 -
Jet vertex fraction [%]	+0.53 −0.57	+0.66 −0.69	+0.83 −0.86	+0.82 −0.85	+0.74 −0.77	+0.69 −0.72	+0.63 −0.67	+0.61 −0.65	+0.55 −0.59	+0.45 −0.49	+0.40 −0.44
b-Quark tagging efficiency (eigenvector 0) [%]	−6.81 +7.07	−6.64 +6.86	−6.35 +6.52	−6.16 +6.32	−6.10 +6.25	−6.00 +6.14	−5.88 +6.01	−5.86 +6.00	−5.72 +5.85	−5.73 +5.85	−5.64 +5.76
b-Quark tagging efficiency (eigenvector 1) [%]	−1.95 +1.98	−1.94 +1.97	−1.91 +1.93	−1.87 +1.89	−1.91 +1.93	−2.02 +2.04	−2.19 +2.20	−2.38 +2.40	−2.59 +2.62	−2.98 +3.01	−3.54 +3.59
b-Quark tagging efficiency (eigenvector 2) [%]	+1.36 −1.34	+1.31 −1.29	±1.20	+1.11 −1.10	+1.07 −1.06	+1.02 −1.01	+0.96 −0.95	+0.87 −0.86	±0.71	±0.43	-
b-Quark tagging efficiency (eigenvector 3) [%]	-	-	-	-	-	-	±0.10	±0.13	±0.11	-	∓0.13
c-Quark tagging efficiency (eigenvector 0) [%]	+0.26 −0.25	+0.27 −0.26	±0.28	±0.29	±0.30	±0.30	±0.26	±0.23	±0.24	±0.18	+0.16 −0.17
c-Quark tagging efficiency (eigenvector 1) [%]	∓0.20	∓0.22	∓0.26	∓0.26	∓0.24	−0.25 +0.24	∓0.24	∓0.25	∓0.30	∓0.31	−0.41 +0.42
Light-jet tagging efficiency (eigenvector 0) [%]	−0.59 +0.63	∓0.60	∓0.69	−0.75 +0.77	−0.76 +0.78	−0.79 +0.81	−0.79 +0.82	−0.67 +0.68	−0.77 +0.80	−0.56 +0.57	−0.84 +0.90
Light-jet tagging efficiency (eigenvector 1) [%]	+0.22 −0.21	+0.22 −0.21	±0.23	+0.27 −0.26	±0.26	+0.22 −0.21	±0.22	±0.23	±0.24	±0.18	+0.16 −0.17
Light-jet tagging efficiency (eigenvector 2) [%]	-	-	-	-	-	-	-	-	-	-	±0.10
Light-jet tagging efficiency (eigenvector 3) [%]	-	-	-	-	-	-	-	-	-	-	∓0.10
b-Quark tagging extrapolation [%]	-	-	-	-	-	-	+0.12 −0.11	±0.12	±0.13	±0.34	+0.97 −0.99
Electron trigger efficiency [%]	±0.12	±0.12	±0.11	±0.11	±0.11	+0.12 −0.11	±0.11	±0.11	±0.11	±0.11	±0.11
Electron reconstruction efficiency [%]	-	-	-	-	-	-	-	-	-	±0.10	±0.11
Electron identification efficiency [%]	+0.41 −0.40	±0.40	±0.40	±0.41	±0.43	±0.45	±0.47	±0.48	+0.52 −0.53	±0.57	±0.64
Electron isolation efficiency [%]	-	-	-	±0.10	±0.12	+0.15 −0.14	±0.17	±0.20	±0.26	±0.34	±0.50
Muon trigger efficiency stat [%]	±0.30	±0.29	+0.28 −0.29	±0.28	+0.28 −0.29	+0.28 −0.29	+0.28 −0.29	+0.28 −0.29	±0.28	+0.27 −0.28	±0.27
Muon trigger efficiency syst [%]	+0.52 −0.51	+0.52 −0.50	+0.51 −0.50	+0.51 −0.50	+0.50 −0.49	+0.51 −0.50	+0.50 −0.49	+0.51 −0.50	+0.49 −0.48	±0.48	+0.47 −0.46
Muon identification stat [%]	-	-	-	-	-	-	-	-	-	-	-
Muon identification syst [%]	±0.38	±0.37	±0.36	±0.37	±0.38	±0.39	±0.40	±0.42	±0.43	±0.45	±0.48
Muon isolation efficiency syst [%]	±0.11	±0.11	±0.10	±0.10	±0.10	±0.10	±0.10	±0.10	±0.10	±0.10	±0.10
E_T^{miss} Soft jet resolution para [%]	∓0.17	-	±0.17	-	∓0.11	±0.15	-	∓0.35	-	-	∓0.52
E_T^{miss} Soft jet resolution perp [%]	-	-	-	-	-	-	∓0.15	-	-	∓0.45	±0.10
E_T^{miss} Soft jet scale [%]	+0.27 −0.36	-	−0.19 +0.26	−0.17 +0.16	-	+0.22 -	−0.19 +0.11	-	-	−0.46 +0.29	−0.13 +0.48
Luminosity [%]	∓2.04	∓2.04	∓2.05	∓2.05	∓2.05	∓2.05	∓2.05	∓2.05	∓2.05	∓2.05	∓2.05
Z+jets cross-section [%]	±0.65	±0.60	±0.48	±0.43	±0.50	±0.54	±0.46	±0.46	±0.48	±0.42	±0.48
Monte Carlo sample statistics [%]	±0.15	±0.12	±0.16	±0.20	±0.27	±0.35	±0.46	±0.61	±0.66	±1.01	±1.43
ISR/FSR + scale [%]	- −3.92	- −4.98	- −3.55	+1.02 -	−0.90 +1.26	- −0.48	+0.48 -	- −1.60	+0.57 -	+2.03 -	- −5.15
Alternate hard-scattering model [%]	±1.45	±1.77	±5.28	±5.21	±2.78	±3.38	±4.12	±0.79	±4.12	∓1.61	±3.03
Alternate parton-shower model [%]	∓6.02	∓4.47	±3.67	±5.53	±2.73	±2.57	±2.95	±4.13	±4.89	±2.92	±2.17
Inter PDF [%]	-	-	-	-	-	-	-	-	-	±0.29	∓0.10
Intra PDF [%]	±0.13	-	-	-	±0.12	±0.21	±0.26	±0.20	±0.47	±1.45	±0.49
Fakes overall normalization, el [%]	∓0.13	+0.77 −0.78	±1.48	±0.92	±0.49	±0.39	±0.29	±0.31	±0.32	-	-
Fakes overall normalization, mu [%]	∓0.20	-	±0.27	±0.25	-	-	∓0.15	∓0.30	∓0.28	∓0.45	∓0.78
Fakes alternative parametrization [%]	∓2.51	∓2.88	∓3.09	∓2.51	∓1.97	∓1.13	∓0.74	∓0.87	±0.17	±1.23	±1.04
W+jets heavy flavour component [%]	±5.27	±3.96	±3.27	±2.80	±1.54	±1.83	±1.41	±3.69	±1.64	±1.84	±4.11

TABLE F.5: Table of systematics for the absolute differential cross-section at the particle level for the $p_T^{t\bar{t}}$ observable.

Bins [Unit $y^{t\bar{t}}$]	-3—2	-2—1.75	-1.75—1.50	-1.50—1.25	-1.25—1	-1—0.85	-0.85—0.60	-0.60—0.40	-0.40—0.20	-0.20—0	0–0.20	0.20–0.40	0.40–0.60	0.60–0.85	0.85–1	1–1.25	1.25–1.50	1.50–1.75	1.75–2	2–3
$d\sigma$ / $dy^{t\bar{t}}$ [pb/ Unit $y^{t\bar{t}}$]	$2.55 \cdot 10^{-2}$	$9.23 \cdot 10^{-1}$	$3.57 \cdot 10^{0}$	$8.48 \cdot 10^{0}$	$1.61 \cdot 10^{1}$	$2.31 \cdot 10^{1}$	$3.09 \cdot 10^{1}$	$3.84 \cdot 10^{1}$	$4.32 \cdot 10^{1}$	$4.49 \cdot 10^{1}$	$4.55 \cdot 10^{1}$	$4.30 \cdot 10^{1}$	$3.85 \cdot 10^{1}$	$3.12 \cdot 10^{1}$	$2.28 \cdot 10^{1}$	$1.59 \cdot 10^{1}$	$8.56 \cdot 10^{0}$	$3.52 \cdot 10^{0}$	$9.23 \cdot 10^{-1}$	$2.50 \cdot 10^{-2}$
Total Uncertainty [%]	$^{+33.6}_{-26.5}$	$^{+11.4}_{-12.1}$	$^{+10.3}_{-9.88}$	$^{+9.85}_{-9.93}$	$^{+10.6}_{-10.5}$	$^{+10.3}_{-10.2}$	$^{+10.5}_{-10.2}$	$^{+10.9}_{-10.7}$	$^{+11.0}_{-10.5}$	$^{+10.9}_{-10.8}$	$^{+11.7}_{-11.6}$	$^{+11.2}_{-11.0}$	$^{+11.0}_{-10.8}$	$^{+10.5}_{-10.1}$	$^{+9.44}_{-9.46}$	$^{+10.4}_{-10.2}$	±12.0	$^{+9.59}_{-8.83}$	$^{+11.4}_{-12.1}$	$^{+17.8}_{-30.0}$
Statistics [%]	±9.1	±2.5	±1.2	±0.7	±0.5	±0.6	±0.4	±0.4	±0.3	±0.3	±0.3	±0.3	±0.4	±0.3	±0.6	±0.5	±0.7	±1.2	±2.4	±8.4
Systematics [%]	$^{+31.7}_{-24.1}$	$^{+11.0}_{-11.7}$	$^{+10.2}_{-9.77}$	$^{+9.80}_{-9.88}$	±10.5	$^{+10.3}_{-10.1}$	$^{+10.5}_{-10.2}$	$^{+10.9}_{-10.7}$	$^{+11.0}_{-10.4}$	$^{+10.9}_{-10.8}$	$^{+11.7}_{-11.5}$	$^{+11.2}_{-11.0}$	$^{+11.0}_{-10.8}$	$^{+10.5}_{-10.1}$	$^{+9.41}_{-9.43}$	$^{+10.3}_{-10.2}$	$^{+11.9}_{-12.0}$	$^{+9.47}_{-8.70}$	$^{+11.0}_{-11.7}$	$^{+14.7}_{-28.3}$
Jet energy resolution [%]	∓1.85	∓1.91	∓1.68	±0.63	±1.05	±0.93	∓0.16	±1.54	±0.41	±0.61	±2.05	±1.24	±1.00	±0.47	∓0.91	±1.91	∓1.66	∓2.71	∓4.07	±3.09
b-Tagged jet energy scale (JES) [%]	$^{-}_{-1.14}$	$^{+0.35}_{-0.45}$	$^{+0.29}_{-0.25}$	$^{+0.39}_{-0.44}$	$^{+0.38}_{-0.44}$	$^{+0.58}_{-0.53}$	$^{+0.47}_{-0.46}$	$^{+0.53}_{-0.57}$	$^{+0.59}_{-0.51}$	$^{+0.54}_{-0.51}$	$^{+0.53}_{-0.60}$	±0.53	$^{+0.46}_{-0.51}$	$^{+0.53}_{-0.49}$	$^{+0.51}_{-0.54}$	$^{+0.35}_{-0.46}$	$^{+0.40}_{-0.41}$	$^{+0.39}_{-0.16}$	$^{-}_{-0.25}$	-
Effective detector NP set 1 (JES) [%]	$^{+0.29}_{-}$	-	-	-	-	-	-	-	-	-	-	-	-	-	-	-	-	-	-	-
Effective detector NP set 2 (JES) [%]	$^{+0.42}_{-}$	-	-	-	-	-	-	-	-	-	-	-	-	-	-	-	-	-	-	+0.24
Effective mixed NP set 1 (JES) [%]	$^{-0.19}_{+1.24}$	$^{-}_{-0.21}$	$^{+0.28}_{-0.14}$	-	±0.16	$^{+0.16}_{-0.12}$	$^{+0.13}_{-0.14}$	$^{+0.16}_{-0.12}$	$^{+0.14}_{-0.13}$	$^{+0.16}_{-0.17}$	$^{+0.16}_{-0.14}$	±0.14	$^{+0.15}_{-0.17}$	$^{+0.12}_{-0.11}$	$^{+0.10}_{-0.17}$	$^{+0.18}_{-}$	$^{-}_{-0.15}$	$^{+0.23}_{-}$	$^{-0.42}_{-}$	+0.33
Effective mixed NP set 2 (JES) [%]	$^{+0.42}_{-}$	-	-	-	-	-	-	-	-	-	-	-	-	-	-	-	-	-	-	+0.24
Effective mixed NP set 3 (JES) [%]	-	-	-	-	-	-	-	-	-	-	-	-	-	-	-	-	-	-	-	+0.24
Effective modelling NP set 1 (JES) [%]	$^{+1.88}_{-0.89}$	$^{+0.92}_{-1.60}$	$^{+1.73}_{-1.68}$	$^{+1.83}_{-1.89}$	$^{+1.97}_{-1.93}$	$^{+2.29}_{-2.11}$	$^{+2.06}_{-2.15}$	$^{+2.38}_{-2.19}$	$^{+2.58}_{-2.29}$	$^{+2.22}_{-2.34}$	$^{+2.50}_{-2.38}$	$^{+2.29}_{-2.36}$	$^{+2.20}_{-2.17}$	$^{+2.27}_{-2.03}$	$^{+2.10}_{-2.14}$	$^{+2.09}_{-1.93}$	$^{+1.56}_{-1.80}$	$^{+2.04}_{-1.18}$	$^{+0.47}_{-1.89}$	$^{+1.00}_{-1.31}$
Effective modelling NP set 2 (JES) [%]	$^{+0.98}_{-}$	$^{-0.51}_{+0.21}$	$^{-}_{+0.26}$	-	$^{-0.19}_{+0.20}$	-	∓0.18	∓0.17	$^{-0.15}_{+0.14}$	$^{-0.20}_{+0.19}$	$^{-0.20}_{+0.23}$	$^{-0.16}_{+0.15}$	$^{-0.20}_{+0.19}$	∓0.13	$^{-0.17}_{+0.13}$	$^{-0.11}_{+0.20}$	$^{-0.16}_{-}$	$^{+0.22}_{-}$	$^{-0.24}_{+0.14}$	$^{-0.51}_{+0.36}$
Effective modelling NP set 3 (JES) [%]	$^{+1.02}_{-0.33}$	$^{+0.20}_{-0.35}$	-	-	$^{+0.14}_{-}$	-	$^{+0.12}_{-0.11}$	$^{+0.11}_{-}$	-	$^{-}_{-0.11}$	$^{+0.13}_{-0.12}$	-	$^{-}_{-0.12}$	-	-	-	-	-	$^{+0.13}_{-0.23}$	$^{+0.11}_{-0.17}$
Effective modelling NP set 4 (JES) [%]	$^{-0.11}_{+0.30}$	$^{-}_{-0.20}$	$^{+0.15}_{-}$	-	±0.13	-	$^{+0.12}_{-0.11}$	-	±0.10	±0.12	$^{+0.14}_{-0.12}$	$^{+0.10}_{-0.11}$	$^{+0.14}_{-0.15}$	-	$^{-}_{-0.14}$	-	-	-	-	-
Effective statistical NP set 1 (JES) [%]	$^{+0.30}_{-}$	$^{-}_{-0.59}$	$^{+0.40}_{-0.29}$	$^{+0.30}_{-0.33}$	$^{+0.37}_{-0.39}$	$^{+0.27}_{-0.19}$	±0.39	$^{+0.39}_{-0.37}$	$^{+0.38}_{-0.40}$	$^{+0.44}_{-0.39}$	$^{+0.45}_{-0.42}$	$^{+0.34}_{-0.41}$	$^{+0.44}_{-0.38}$	$^{+0.36}_{-0.33}$	$^{+0.37}_{-0.47}$	$^{+0.40}_{-0.26}$	$^{+0.18}_{-0.25}$	$^{+0.49}_{-0.36}$	$^{-}_{-0.25}$	-
Effective statistical NP set 2 (JES) [%]	$^{+0.61}_{-}$	$^{-0.38}_{-}$	$^{-0.26}_{+0.37}$	$^{-0.28}_{+0.24}$	$^{-0.35}_{+0.33}$	$^{-0.15}_{+0.25}$	$^{-0.34}_{+0.32}$	$^{-0.32}_{+0.34}$	$^{-0.34}_{+0.31}$	$^{-0.34}_{+0.37}$	$^{-0.37}_{+0.43}$	$^{-0.36}_{+0.28}$	$^{-0.33}_{+0.39}$	$^{-0.29}_{+0.32}$	$^{-0.40}_{+0.31}$	$^{-0.22}_{+0.35}$	$^{-0.26}_{+0.14}$	$^{-0.22}_{+0.40}$	$^{-}_{-0.25}$	−0.28
Effective statistical NP set 3 (JES) [%]	$^{+0.60}_{-}$	-	-	-	-	-	-	-	-	-	-	-	-	-	-	-	-	-	-	-
Effective statistical NP set 4 (JES) [%]	$^{-}_{+0.85}$	$^{-0.21}_{+0.10}$	-	-	-	-	-	-	-	-	-	-	-	-	-	-	-	-	$^{-0.28}_{+0.12}$	$^{-0.15}_{+0.10}$
Effective statistical NP set 5 (JES) [%]	$^{+0.54}_{-}$	-	-	-	-	-	-	-	-	-	-	-	-	-	-	-	-	-	-	-
Effective statistical NP set 6 (JES) [%]	+0.41	-	-	-	-	-	-	-	-	-	-	-	-	-	-	-	-	-	-	$^{+0.10}_{-0.37}$
Effective statistical NP set 7 (JES) [%]	$^{+0.26}_{-}$	-	-	-	$^{+0.13}_{-}$	-	-	-	-	-	-	-	±0.10	-	-	-	-	-	-	-
η intercalibration model (JES) [%]	$^{+1.15}_{-0.70}$	$^{+0.77}_{-0.90}$	$^{+1.18}_{-0.71}$	$^{+0.77}_{-1.06}$	$^{+0.75}_{-0.77}$	$^{+0.97}_{-0.89}$	$^{+0.69}_{-0.66}$	$^{+0.52}_{-0.58}$	$^{+0.59}_{-0.55}$	$^{+0.50}_{-0.49}$	$^{+0.52}_{-0.56}$	$^{+0.49}_{-0.57}$	$^{+0.54}_{-0.53}$	$^{+0.74}_{-0.68}$	$^{+0.82}_{-1.01}$	$^{+0.84}_{-0.75}$	$^{+0.65}_{-0.88}$	$^{+1.25}_{-0.71}$	$^{-}_{-1.13}$	$^{+1.42}_{-0.14}$
η intercalibration non closure (JES) [%]	∓0.19	$^{-}_{-0.25}$	$^{-0.30}_{+0.48}$	$^{-0.45}_{+0.43}$	$^{-0.46}_{+0.41}$	$^{-0.32}_{+0.46}$	$^{-0.46}_{+0.42}$	$^{-0.32}_{+0.31}$	$^{-0.31}_{+0.41}$	$^{-0.32}_{+0.26}$	∓0.22	$^{-0.23}_{+0.20}$	$^{-0.14}_{-}$	$^{-}_{+0.17}$	-	$^{-}_{+0.16}$	$^{-0.16}_{-}$	$^{+0.20}_{-}$	-	$^{+0.17}_{-0.14}$
η intercalibration total stat (JES) [%]	+1.11	$^{-}_{-0.35}$	$^{+0.43}_{-0.38}$	$^{+0.35}_{-0.41}$	$^{+0.40}_{-0.42}$	$^{+0.36}_{-0.27}$	$^{+0.39}_{-0.43}$	$^{+0.43}_{-0.41}$	$^{+0.42}_{-0.38}$	$^{+0.47}_{-0.41}$	$^{+0.48}_{-0.43}$	$^{+0.36}_{-0.45}$	$^{+0.45}_{-0.41}$	$^{+0.40}_{-0.36}$	$^{+0.37}_{-0.51}$	$^{+0.48}_{-0.32}$	$^{+0.13}_{-0.28}$	$^{+0.54}_{-0.33}$	$^{-}_{-0.30}$	$^{+0.34}_{-0.24}$
Flavour composition (JES) [%]	+3.05	$^{+0.35}_{-1.12}$	$^{+1.62}_{-1.48}$	$^{+1.55}_{-1.80}$	$^{+1.73}_{-1.94}$	$^{+1.83}_{-2.12}$	$^{+1.94}_{-2.05}$	$^{+1.88}_{-2.02}$	$^{+2.34}_{-2.06}$	$^{+1.77}_{-2.14}$	$^{+2.06}_{-2.35}$	$^{+2.20}_{-2.16}$	$^{+1.89}_{-2.00}$	$^{+2.01}_{-1.88}$	$^{+1.74}_{-2.02}$	$^{+1.65}_{-1.81}$	$^{+1.57}_{-1.67}$	$^{+1.59}_{-1.41}$	$^{+0.96}_{-1.24}$	$^{-}_{-1.45}$
Flavour response (JES) [%]	+1.19	$^{-0.79}_{+0.12}$	$^{-0.73}_{+0.96}$	$^{-0.97}_{+0.82}$	$^{-0.93}_{+0.89}$	$^{-1.05}_{+0.90}$	$^{-0.94}_{+0.95}$	$^{-0.94}_{+0.95}$	$^{-1.03}_{+1.17}$	$^{-1.10}_{+0.91}$	$^{-1.06}_{+1.07}$	$^{-1.06}_{+0.98}$	$^{-1.01}_{+1.00}$	$^{-0.89}_{+0.92}$	$^{-1.09}_{+0.97}$	∓0.91	$^{-0.73}_{+0.60}$	$^{-0.69}_{+1.12}$	$^{-0.78}_{+0.11}$	$^{-0.66}_{+1.34}$
Pile-up offset μ (JES) [%]	+0.52	-	$^{-0.12}_{-}$	-	$^{-0.15}_{+0.18}$	$^{-}_{+0.11}$	$^{-0.14}_{+0.11}$	$^{-0.19}_{+0.17}$	$^{-0.13}_{+0.17}$	$^{-0.13}_{+0.15}$	$^{-0.10}_{+0.16}$	$^{-0.18}_{+0.13}$	$^{-0.14}_{+0.13}$	$^{-0.11}_{+0.17}$	$^{-0.21}_{+0.13}$	$^{-}_{+0.17}$	-	$^{-0.19}_{+0.31}$	$^{-}_{-0.46}$	$^{-0.17}_{+0.66}$
Pile-up offset N_{PV} (JES) [%]	$^{+0.32}_{-1.46}$	$^{-}_{-0.85}$	$^{+0.61}_{-0.24}$	$^{+0.33}_{-0.53}$	$^{+0.41}_{-0.33}$	$^{+0.50}_{-0.46}$	$^{+0.45}_{-0.46}$	$^{+0.43}_{-0.45}$	$^{+0.60}_{-0.45}$	$^{+0.45}_{-0.43}$	$^{+0.56}_{-0.49}$	$^{+0.44}_{-0.61}$	$^{+0.46}_{-0.44}$	$^{+0.58}_{-0.38}$	$^{+0.33}_{-0.45}$	$^{+0.42}_{-0.28}$	$^{+0.34}_{-0.52}$	$^{+0.58}_{-}$	$^{-}_{-0.65}$	$^{-}_{-0.50}$
Pile-up offset p_T (JES) [%]	$^{+1.14}_{-}$	$^{-0.57}_{+0.21}$	$^{+0.21}_{-}$	±0.10	-	$^{+0.13}_{-}$	-	-	-	-	-	-	-	-	$^{-}_{-0.14}$	-	-	-	$^{-0.67}_{+0.12}$	$^{-}_{-0.18}$
Pile-up offset ρ topology (JES) [%]	$^{+1.74}_{-1.59}$	$^{+1.21}_{-1.89}$	$^{+2.58}_{-2.22}$	$^{+2.55}_{-2.76}$	$^{+2.92}_{-2.99}$	$^{+3.22}_{-3.11}$	$^{+3.17}_{-3.24}$	$^{+3.43}_{-3.29}$	$^{+3.92}_{-3.45}$	$^{+3.33}_{-3.40}$	$^{+3.66}_{-3.63}$	$^{+3.55}_{-3.52}$	$^{+3.32}_{-3.22}$	$^{+3.34}_{-3.07}$	$^{+3.17}_{-3.21}$	$^{+3.04}_{-2.72}$	$^{+2.53}_{-2.69}$	$^{+2.85}_{-1.94}$	$^{+0.77}_{-2.22}$	$^{+0.32}_{-1.55}$
Jet vertex fraction [%]	$^{+0.53}_{-0.56}$	$^{+0.64}_{-0.66}$	$^{+0.70}_{-0.72}$	$^{+0.68}_{-0.71}$	$^{+0.69}_{-0.72}$	$^{+0.69}_{-0.72}$	$^{+0.69}_{-0.72}$	$^{+0.69}_{-0.73}$	$^{+0.68}_{-0.73}$	$^{+0.69}_{-0.73}$	$^{+0.69}_{-0.73}$	$^{+0.68}_{-0.72}$	$^{+0.70}_{-0.73}$	$^{+0.69}_{-0.73}$	$^{+0.68}_{-0.72}$	$^{+0.69}_{-0.72}$	$^{+0.68}_{-0.72}$	$^{+0.69}_{-0.71}$	$^{+0.63}_{-0.66}$	$^{+0.68}_{-0.69}$
b-Quark tagging efficiency (eigenvector 0) [%]	$^{-6.45}_{+6.64}$	$^{-6.12}_{+6.29}$	$^{-6.25}_{+6.43}$	$^{-6.29}_{+6.46}$	$^{-6.34}_{+6.52}$	$^{-6.39}_{+6.57}$	$^{-6.45}_{+6.64}$	$^{-6.46}_{+6.65}$	$^{-6.53}_{+6.71}$	$^{-6.54}_{+6.73}$	$^{-6.51}_{+6.70}$	$^{-6.52}_{+6.70}$	$^{-6.47}_{+6.66}$	$^{-6.45}_{+6.63}$	$^{-6.39}_{+6.58}$	$^{-6.33}_{+6.51}$	$^{-6.28}_{+6.46}$	$^{-6.20}_{+6.38}$	$^{-6.16}_{+6.34}$	$^{-6.16}_{+6.33}$
b-Quark tagging efficiency (eigenvector 1) [%]	$^{-2.15}_{+2.18}$	$^{-2.02}_{+2.04}$	$^{-1.97}_{+1.99}$	$^{-1.99}_{+2.01}$	$^{-1.98}_{+2.00}$	$^{-1.97}_{+1.99}$	$^{-1.96}_{+1.98}$	$^{-1.96}_{+1.98}$	$^{-1.95}_{+1.96}$	$^{-1.95}_{+1.97}$	$^{-1.95}_{+1.97}$	$^{-1.96}_{+1.98}$	$^{-1.95}_{+1.97}$	$^{-1.96}_{+1.98}$	$^{-1.98}_{+2.00}$	$^{-1.96}_{+1.98}$	$^{-1.99}_{+2.01}$	$^{-2.00}_{+2.02}$	$^{-2.09}_{+2.11}$	$^{-2.15}_{+2.17}$
b-Quark tagging efficiency (eigenvector 2) [%]	$^{+1.16}_{-1.15}$	±1.15	±1.20	$^{+1.21}_{-1.20}$	±1.21	±1.21	$^{+1.22}_{-1.21}$	$^{+1.22}_{-1.21}$	±1.21	$^{+1.22}_{-1.21}$	±1.21	$^{+1.21}_{-1.20}$	$^{+1.22}_{-1.21}$	$^{+1.22}_{-1.21}$	$^{+1.22}_{-1.21}$	$^{+1.22}_{-1.21}$	$^{+1.22}_{-1.21}$	±1.22	$^{+1.18}_{-1.17}$	$^{+1.14}_{-1.13}$
b-Quark tagging efficiency (eigenvector 3) [%]	±0.12	±0.11	-	-	-	-	-	-	-	-	-	-	-	-	-	-	-	-	±0.12	±0.11
c-Quark tagging efficiency (eigenvector 0) [%]	±0.14	±0.34	±0.31	±0.33	±0.28	±0.29	±0.27	±0.26	$^{+0.28}_{-0.27}$	±0.26	±0.27	±0.26	±0.26	±0.26	$^{+0.30}_{-0.29}$	±0.28	±0.29	±0.26	±0.31	±0.17
c-Quark tagging efficiency (eigenvector 1) [%]	$^{-0.29}_{+0.28}$	∓0.22	∓0.20	∓0.22	∓0.23	∓0.24	∓0.24	∓0.23	∓0.23	∓0.24	∓0.24	$^{-0.23}_{+0.24}$	$^{-0.24}_{+0.25}$	∓0.23	$^{-0.23}_{+0.22}$	∓0.23	∓0.25	∓0.23	∓0.25	∓0.20
Light-jet tagging efficiency (eigenvector 0) [%]	$^{-1.67}_{+1.65}$	$^{-0.84}_{+0.86}$	$^{-0.65}_{+0.62}$	$^{-0.80}_{+0.83}$	$^{-0.70}_{+0.73}$	$^{-0.70}_{+0.74}$	$^{-0.67}_{+0.71}$	∓0.61	$^{-0.48}_{+0.41}$	$^{-0.73}_{+0.78}$	$^{-0.70}_{+0.74}$	$^{-0.55}_{+0.54}$	$^{-0.72}_{+0.75}$	$^{-0.66}_{+0.67}$	$^{-0.73}_{+0.74}$	$^{-0.84}_{+0.90}$	∓0.63	$^{-0.67}_{+0.70}$	$^{-0.81}_{+0.86}$	$^{-1.28}_{+1.26}$
Light-jet tagging efficiency (eigenvector 1) [%]	±0.70	±0.40	±0.23	$^{+0.28}_{-0.27}$	$^{+0.26}_{-0.24}$	±0.25	$^{+0.25}_{-0.24}$	$^{+0.18}_{-0.19}$	±0.15	$^{+0.28}_{-0.27}$	±0.27	±0.22	$^{+0.24}_{-0.23}$	±0.19	±0.23	$^{+0.25}_{-0.24}$	±0.19	±0.26	±0.22	±0.49
Light-jet tagging efficiency (eigenvector 2) [%]	∓0.46	$^{-0.16}_{+0.15}$	∓0.14	-	-	-	-	-	-	-	-	-	$^{+0.11}_{-0.10}$	-	-	-	-	∓0.11	-	∓0.36
Light-jet tagging efficiency (eigenvector 3) [%]	∓0.49	∓0.11	$^{-0.18}_{+0.20}$	-	-	-	-	-	-	-	-	-	-	-	-	-	-	∓0.15	$^{-0.19}_{+0.20}$	∓0.39
Light-jet tagging efficiency (eigenvector 5) [%]	∓0.31	-	-	-	-	-	-	-	-	-	-	-	-	-	-	-	-	∓0.11	∓0.15	∓0.18
Light-jet tagging efficiency (eigenvector 6) [%]	±0.16	-	-	-	-	-	-	-	-	-	-	-	-	-	-	-	-	-	-	-
Light-jet tagging efficiency (eigenvector 7) [%]	∓0.19	-	-	-	-	-	-	-	-	-	-	-	-	-	-	-	-	-	-	-
Electron energy resolution [%]	$^{+0.57}_{-0.70}$	$^{-0.20}_{+0.25}$	-	-	-	-	-	-	-	-	-	-	-	-	-	-	-	-	-	$^{-}_{-0.56}$
Electron energy scale [%]	$^{+1.67}_{-}$	-	-	$^{-}_{-0.14}$	-	-	-	-	-	-	-	-	-	-	-	-	-	-	-	$^{-}_{-0.71}$
Electron trigger efficiency [%]	±0.23	±0.18	±0.15	±0.14	±0.13	±0.12	±0.12	±0.11	±0.11	±0.11	±0.11	±0.11	±0.11	±0.11	±0.12	±0.12	±0.13	±0.15	±0.18	±0.27
Electron reconstruction efficiency [%]	±0.10	-	-	-	-	-	-	-	-	-	-	-	-	-	-	-	-	-	-	±0.12
Electron identification efficiency [%]	±0.91	±0.70	±0.55	±0.47	±0.42	$^{+0.41}_{-0.40}$	±0.40	±0.40	±0.40	±0.40	±0.40	±0.40	±0.41	±0.41	±0.42	±0.42	±0.45	±0.52	±0.69	±0.96
Electron isolation efficiency [%]	±0.13	±0.13	±0.11	$^{+0.11}_{-0.10}$	±0.10	±0.10	±0.10	±0.10	±0.10	±0.10	±0.11	±0.10	±0.11	±0.10	±0.10	±0.10	±0.10	±0.11	±0.14	±0.18
Muon (ID) momentum resolution [%]	$^{-}_{+0.46}$	-	-	-	-	-	-	-	-	-	-	-	-	-	-	-	-	-	$^{-}_{-0.32}$	$^{+1.48}_{-}$
Muon (MS) momentum resolution [%]	$^{+0.28}_{-}$	-	-	-	-	-	-	-	-	-	-	-	-	-	-	-	$^{-}_{+0.20}$	-	$^{-}_{-0.22}$	$^{+0.53}_{-}$
Muon energy scale [%]	-	-	-	-	-	-	-	-	-	-	-	-	-	-	-	-	-	-	-	$^{+0.12}_{-0.35}$
Muon trigger efficiency stat [%]	±0.41	$^{+0.28}_{-0.29}$	±0.26	±0.27	±0.28	$^{+0.28}_{-0.29}$	±0.29	±0.29	$^{+0.29}_{-0.30}$	$^{+0.29}_{-0.30}$	$^{+0.29}_{-0.30}$	$^{+0.29}_{-0.30}$	$^{+0.29}_{-0.30}$	$^{+0.29}_{-0.30}$	±0.29	±0.29	$^{+0.27}_{-0.28}$	$^{+0.26}_{-0.27}$	$^{+0.28}_{-0.29}$	$^{+0.32}_{-0.33}$
Muon trigger efficiency syst [%]	$^{+0.57}_{-0.56}$	$^{+0.50}_{-0.49}$	$^{+0.50}_{-0.49}$	$^{+0.52}_{-0.51}$	$^{+0.52}_{-0.51}$	$^{+0.52}_{-0.51}$	$^{+0.52}_{-0.50}$	$^{+0.51}_{-0.50}$	$^{+0.51}_{-0.50}$	$^{+0.51}_{-0.50}$	$^{+0.51}_{-0.50}$	$^{+0.51}_{-0.50}$	$^{+0.51}_{-0.50}$	$^{+0.51}_{-0.50}$	$^{+0.51}_{-0.50}$	$^{+0.51}_{-0.50}$	±0.51	$^{+0.51}_{-0.50}$	±0.48	$^{+0.45}_{-0.44}$
Muon identification stat [%]	-	-	±0.10	±0.10	±0.10	-	-	-	-	-	-	-	-	-	-	±0.10	±0.10	±0.10	-	-
Muon identification syst [%]	±0.55	±0.49	±0.48	±0.46	±0.42	±0.39	±0.37	±0.35	±0.35	±0.34	$^{+0.35}_{-0.34}$	±0.35	±0.36	$^{+0.38}_{-0.39}$	±0.41	$^{+0.45}_{-0.44}$	±0.49	±0.52	±0.52	±0.49
Muon isolation efficiency syst [%]	±0.13	±0.11	±0.12	±0.12	±0.11	±0.11	$^{+0.11}_{-0.10}$	±0.10	±0.10	±0.10	±0.10	±0.10	±0.10	±0.10	±0.11	±0.11	±0.11	±0.12	±0.11	±0.10
E_T^{miss} Soft jet resolution para [%]	±2.28	∓0.30	±0.71	±0.12	±0.14	-	-	∓0.12	-	-	∓0.14	-	-	-	±0.13	-	±0.42	±0.28	±0.79	±0.98
E_T^{miss} Soft jet resolution perp [%]	∓2.34	±0.81	±0.32	±0.33	-	-	-	∓0.11	-	-	-	-	-	-	-	-	±0.54	±0.30	±0.33	∓0.74
E_T^{miss} Soft jet scale [%]	$^{+0.42}_{-}$	$^{+0.32}_{-0.50}$	$^{+0.43}_{-0.34}$	$^{+0.22}_{-0.31}$	$^{+0.19}_{-0.18}$	-	-	-	-	-	-	-	-	-	-	-	$^{+0.45}_{-0.22}$	$^{+0.51}_{-0.45}$	$^{+0.63}_{-0.64}$	$^{+0.62}_{-}$
Luminosity [%]	∓2.05	∓2.05	∓2.05	∓2.05	∓2.05	∓2.05	∓2.05	∓2.05	∓2.05	∓2.05	∓2.05	∓2.05	∓2.05	∓2.05	∓2.05	∓2.05	∓2.05	∓2.05	∓2.05	∓2.05
Z+jets cross-section [%]	±0.44	±0.42	±0.44	±0.49	±0.49	±0.56	∓0.51	±0.59	±0.55	±0.57	±0.58	±0.58	±0.55	±0.53	±0.50	±0.52	±0.47	±0.55	±0.43	±0.52
Monte Carlo sample statistics [%]	±6.42	±1.57	±0.86	±0.56	±0.36	±0.41	±0.26	±0.33	±0.30	±0.25	±0.25	±0.35	±0.31	±0.25	±0.46	±0.41	±0.49	±0.80	±1.57	±5.33
ISR/FSR + scale [%]	$^{+19.9}_{-}$	$^{-}_{-3.31}$	$^{-}_{+1.80}$	$^{-0.45}_{+0.30}$	$^{-0.65}_{+0.41}$	$^{-}_{-0.87}$	$^{-0.56}_{+2.21}$	$^{-0.30}_{+1.39}$	$^{-0.11}_{+1.33}$	$^{+1.21}_{-}$	$^{-0.41}_{+1.01}$	$^{-0.26}_{+1.38}$	$^{+1.40}_{-}$	$^{+1.27}_{-}$	$^{-0.48}_{+0.38}$	$^{-1.60}_{+0.49}$	$^{+0.43}_{-0.29}$	$^{-1.56}_{+1.86}$	$^{-}_{-2.47}$	$^{-}_{-23.9}$
Alternate hard-scattering model [%]	∓12.4	∓3.40	±4.57	±1.07	±3.84	±1.82	±2.73	±2.30	±3.49	±3.70	±3.84	±3.86	±3.79	±2.51	±0.75	±2.43	±7.94	∓0.17	∓4.03	∓0.60
Alternate parton-shower model [%]	±16.0	∓6.10	∓0.32	±1.00	±0.21	-	±2.32	±2.18	±1.83	±2.35	±1.51	±1.87	±2.21	±2.30	-	-	∓0.73	∓0.85	∓5.44	∓9.96
Inter PDF [%]	±1.11	∓0.34	-	-	-	-	-	-	-	-	-	-	-	-	-	-	-	-	-	∓0.13
Intra PDF [%]	±7.43	±0.79	±0.30	±0.24	±0.37	±0.32	±0.14	±0.18	±0.27	±0.30	±0.31	±0.10	±0.19	±0.24	±0.26	±0.25	±0.24	±0.46	±0.87	±1.85
Fakes overall normalization, el [%]	±1.62	±0.28	±0.21	±0.69	±0.57	±0.68	±0.74	±0.69	±0.75	±0.70	±0.66	±0.70	±0.77	±0.69	±0.66	±0.79	±0.45	±0.61	∓0.33	$^{-1.82}_{+1.83}$
Fakes overall normalization, mu [%]	-	-	-	-	-	±0.10	-	-	-	-	-	-	-	-	±0.10	-	-	-	±0.13	±0.21
Fakes alternative parametrization [%]	∓2.76	∓1.48	∓1.70	∓2.32	∓2.47	∓2.65	∓2.74	∓2.46	∓2.66	∓2.55	∓2.53	∓2.75	∓2.46	∓2.60	∓2.39	∓2.46	∓2.02	∓1.73	∓0.54	∓0.42
W+jets heavy flavour component [%]	±2.65	±2.65	±2.03	±4.31	±4.00	±4.07	±2.86	±4.43	±2.90	±3.51	±4.91	±3.79	±3.87	±3.25	±2.31	±4.18	±2.38	∓0.26	±0.58	±5.92

TABLE F.6: Table of systematics for the absolute differential cross-section at the particle level for the $y^{t\bar{t}}$ observable.

Bins [GeV]	250–320	320–400	400–450	450–500	500–570	570–630	630–700	700–770	770–850	850–930	930–1020	1020–1100	1100–1200	1200–1300	1300–1500	1500–2000
$\mathrm{d}\sigma$ / $\mathrm{d}m^{t\bar{t}}$ [pb/GeV]	$2.59 \cdot 10^{-2}$	$1.95 \cdot 10^{-1}$	$2.66 \cdot 10^{-1}$	$2.39 \cdot 10^{-1}$	$1.90 \cdot 10^{-1}$	$1.38 \cdot 10^{-1}$	$9.86 \cdot 10^{-2}$	$6.82 \cdot 10^{-2}$	$4.63 \cdot 10^{-2}$	$3.10 \cdot 10^{-2}$	$2.06 \cdot 10^{-2}$	$1.37 \cdot 10^{-2}$	$9.10 \cdot 10^{-3}$	$5.74 \cdot 10^{-3}$	$3.21 \cdot 10^{-3}$	$9.24 \cdot 10^{-4}$
Total Uncertainty [%]	$^{+29.6}_{-29.2}$	±15.2	$^{+11.2}_{-11.0}$	$^{+10.8}_{-10.6}$	$^{+10.1}_{-9.97}$	$^{+9.97}_{-9.65}$	$^{+10.3}_{-10.1}$	$^{+9.65}_{-9.57}$	$^{+8.95}_{-9.03}$	±10.0	$^{+9.44}_{-9.11}$	$^{+9.37}_{-9.00}$	$^{+9.18}_{-9.16}$	$^{+9.11}_{-9.35}$	$^{+10.7}_{-9.73}$	$^{+14.1}_{-13.7}$
Statistics [%]	±1.0	±0.2	±0.2	±0.2	±0.2	±0.3	±0.3	±0.4	±0.4	±0.5	±0.6	±0.8	±1.0	±1.2	±1.4	±1.7
Systematics [%]	$^{+29.5}_{-29.1}$	±15.2	$^{+11.2}_{-11.0}$	$^{+10.8}_{-10.6}$	$^{+10.1}_{-9.96}$	$^{+9.96}_{-9.64}$	$^{+10.2}_{-10.1}$	$^{+9.64}_{-9.56}$	$^{+8.93}_{-9.01}$	±10.0	$^{+9.40}_{-9.08}$	$^{+9.32}_{-8.94}$	$^{+9.08}_{-9.07}$	$^{+8.98}_{-9.22}$	$^{+10.5}_{-9.56}$	$^{+13.9}_{-13.5}$
Jet energy resolution [%]	±3.14	-	∓0.53	±0.93	±0.44	±0.80	±2.52	±2.07	±1.40	±2.66	±2.04	±0.29	∓0.11	-	±0.16	±5.43
b-Tagged jet energy scale (JES) [%]	$^{-3.49}_{+3.86}$	$^{-0.90}_{+0.87}$	$^{+0.43}_{-0.45}$	$^{+0.92}_{-0.90}$	$^{+0.93}_{-0.98}$	$^{+0.95}_{-0.96}$	$^{+0.94}_{-0.96}$	$^{+1.00}_{-0.95}$	$^{+0.94}_{-0.90}$	$^{+0.86}_{-0.96}$	$^{+1.14}_{-0.82}$	$^{+1.00}_{-0.81}$	$^{+0.57}_{-0.94}$	$^{+0.62}_{-0.95}$	$^{+0.69}_{-0.92}$	$^{+1.04}_{-0.65}$
Effective detector NP set 1 (JES) [%]	$^{-0.26}_{+0.31}$	-	-	-	-	$^{+0.10}_{-0.12}$	-	$^{+0.14}_{-0.11}$	$^{+0.12}_{-0.10}$	$^{-}_{-0.12}$	$^{+0.11}_{-0.12}$	$^{+0.14}_{-0.13}$	-	$^{-}_{-0.17}$	$^{-}_{-0.19}$	$^{+0.26}_{-}$
Effective detector NP set 2 (JES) [%]	$^{-0.19}_{+0.17}$	-	-	-	-	-	-	-	-	$^{-}_{-0.11}$	$^{-}_{-0.12}$	$^{+0.13}_{-0.14}$	-	-	$^{-}_{-0.14}$	$^{+0.15}_{-}$
Effective mixed NP set 1 (JES) [%]	$^{-1.09}_{+1.29}$	$^{-0.53}_{+0.55}$	-	$^{+0.12}_{-0.15}$	$^{+0.26}_{-0.31}$	$^{+0.38}_{-0.34}$	$^{+0.39}_{-0.37}$	$^{+0.55}_{-0.50}$	$^{+0.53}_{-0.57}$	$^{+0.53}_{-0.69}$	$^{+0.75}_{-0.68}$	$^{+0.88}_{-0.63}$	$^{+0.89}_{-0.84}$	$^{+0.80}_{-1.14}$	$^{+0.80}_{-1.22}$	$^{+1.58}_{-1.00}$
Effective mixed NP set 2 (JES) [%]	$^{+0.17}_{-0.16}$	-	-	-	-	-	-	-	-	-	-	∓0.13	-	-	$^{-0.17}_{-}$	$^{-}_{+0.21}$
Effective modelling NP set 1 (JES) [%]	$^{+2.04}_{-1.28}$	$^{+2.18}_{-2.13}$	$^{+2.73}_{-2.67}$	$^{+2.84}_{-2.75}$	$^{+2.54}_{-2.45}$	$^{+2.26}_{-2.20}$	$^{+1.98}_{-1.88}$	$^{+1.77}_{-1.65}$	$^{+1.37}_{-1.46}$	$^{+1.23}_{-1.34}$	$^{+1.30}_{-1.33}$	$^{+1.07}_{-0.97}$	$^{+0.62}_{-0.68}$	$^{+0.24}_{-0.71}$	$^{+0.24}_{-0.59}$	$^{+0.73}_{-0.20}$
Effective modelling NP set 2 (JES) [%]	$^{-1.06}_{+1.18}$	$^{-0.64}_{+0.70}$	$^{-0.36}_{+0.34}$	∓0.20	-	-	-	$^{+0.15}_{-}$	$^{+0.17}_{-0.14}$	$^{+0.11}_{-0.37}$	$^{+0.31}_{-0.25}$	$^{+0.55}_{-0.17}$	$^{+0.32}_{-0.37}$	$^{+0.37}_{-0.64}$	$^{+0.35}_{-0.59}$	$^{+0.94}_{-0.58}$
Effective modelling NP set 3 (JES) [%]	$^{+1.11}_{-1.06}$	$^{+0.66}_{-0.61}$	$^{+0.27}_{-0.29}$	$^{-}_{-0.12}$	-	$^{-0.10}_{+0.12}$	$^{-0.15}_{+0.11}$	$^{-0.18}_{+0.26}$	$^{-0.23}_{+0.25}$	$^{-0.36}_{+0.19}$	$^{-0.32}_{+0.36}$	$^{-0.34}_{+0.57}$	$^{-0.34}_{+0.47}$	$^{-0.64}_{+0.28}$	$^{-0.40}_{+0.23}$	$^{-0.43}_{+0.66}$
Effective modelling NP set 4 (JES) [%]	$^{-0.26}_{+0.34}$	-	$^{+0.11}_{-0.13}$	±0.15	$^{+0.16}_{-0.17}$	±0.17	$^{+0.11}_{-0.10}$	$^{+0.16}_{-0.12}$	$^{+0.13}_{-0.10}$	$^{-}_{-0.14}$	$^{-}_{-0.12}$	$^{+0.17}_{-0.10}$	$^{+0.11}_{-}$	-	-	$^{+0.29}_{-}$
Effective statistical NP set 1 (JES) [%]	$^{+0.67}_{-0.43}$	$^{+0.49}_{-0.45}$	$^{+0.47}_{-0.46}$	$^{+0.46}_{-0.47}$	$^{+0.42}_{-0.43}$	$^{+0.37}_{-0.33}$	$^{+0.24}_{-0.27}$	$^{+0.28}_{-0.25}$	$^{+0.21}_{-0.18}$	$^{-}_{-0.21}$	$^{+0.13}_{-0.12}$	$^{+0.17}_{-}$	-	$^{-}_{-0.21}$	-	$^{+0.36}_{-}$
Effective statistical NP set 2 (JES) [%]	$^{-0.33}_{+0.56}$	$^{-0.40}_{+0.44}$	$^{-0.43}_{+0.45}$	$^{-0.42}_{+0.41}$	$^{-0.37}_{+0.35}$	$^{-0.29}_{+0.32}$	$^{-0.24}_{+0.23}$	$^{-0.21}_{+0.25}$	$^{-0.15}_{+0.14}$	$^{-0.17}_{-}$	-	-	-	-	-	$^{+0.35}_{-0.10}$
Effective statistical NP set 3 (JES) [%]	$^{+0.12}_{-0.11}$	-	-	-	-	-	-	-	-	$^{-0.18}_{-}$	$^{-0.13}_{+0.19}$	$^{-}_{+0.32}$	$^{-0.23}_{+0.22}$	$^{-0.46}_{+0.23}$	$^{-0.41}_{+0.17}$	$^{-0.39}_{+0.69}$
Effective statistical NP set 4 (JES) [%]	$^{-1.02}_{+1.00}$	$^{-0.46}_{+0.48}$	∓0.11	-	$^{+0.13}_{-0.14}$	$^{+0.19}_{-0.20}$	$^{+0.18}_{-0.23}$	$^{+0.32}_{-0.25}$	$^{+0.31}_{-0.21}$	$^{+0.19}_{-0.34}$	$^{+0.29}_{-0.30}$	$^{+0.38}_{-0.25}$	$^{+0.27}_{-0.25}$	$^{+0.12}_{-0.33}$	$^{+0.11}_{-0.34}$	$^{+0.37}_{-}$
Effective statistical NP set 5 (JES) [%]	±0.56	$^{+0.15}_{-0.13}$	-	$^{-0.11}_{+0.12}$	∓0.12	-	-	-	-	-	$^{+0.12}_{-0.10}$	$^{+0.19}_{-}$	$^{+0.11}_{-0.14}$	$^{-}_{-0.29}$	-	$^{+0.26}_{-}$
Effective statistical NP set 6 (JES) [%]	$^{-}_{+0.24}$	$^{+0.13}_{-0.10}$	$^{+0.14}_{-0.15}$	$^{+0.11}_{-0.12}$	-	-	-	-	-	-	-	-	-	-	-	$^{+0.23}_{-}$
Effective statistical NP set 7 (JES) [%]	$^{-0.16}_{+0.17}$	-	-	-	$^{+0.11}_{-0.13}$	$^{+0.14}_{-0.15}$	$^{+0.11}_{-}$	$^{+0.16}_{-0.12}$	$^{+0.12}_{-0.13}$	$^{-}_{-0.19}$	$^{+0.18}_{-0.16}$	$^{+0.28}_{-0.11}$	$^{+0.15}_{-0.11}$	$^{-}_{-0.27}$	$^{-}_{-0.23}$	$^{+0.42}_{-}$
η intercalibration model (JES) [%]	$^{-1.29}_{+1.86}$	$^{-0.21}_{+0.15}$	$^{+0.50}_{-0.52}$	$^{+0.84}_{-0.79}$	$^{+0.87}_{-0.89}$	$^{+0.87}_{-0.91}$	±0.85	$^{+1.02}_{-0.99}$	$^{+0.91}_{-1.10}$	$^{+0.93}_{-1.05}$	$^{+1.15}_{-0.91}$	$^{+1.16}_{-1.02}$	$^{+1.04}_{-1.17}$	$^{+0.98}_{-1.24}$	$^{+0.99}_{-1.18}$	$^{+1.73}_{-1.22}$
η intercalibration non closure (JES) [%]	$^{+0.40}_{-}$	-	$^{-0.27}_{+0.25}$	$^{-0.29}_{+0.31}$	$^{-0.32}_{+0.28}$	∓0.23	$^{-0.22}_{+0.27}$	$^{-0.34}_{+0.42}$	$^{-0.38}_{+0.32}$	$^{-0.45}_{+0.29}$	$^{-0.26}_{+0.54}$	$^{-0.25}_{+0.32}$	$^{-0.55}_{+0.39}$	$^{-0.93}_{+0.25}$	$^{-0.49}_{+0.31}$	$^{-0.18}_{+0.79}$
η intercalibration total stat (JES) [%]	$^{-0.51}_{+0.86}$	-	$^{+0.44}_{-0.43}$	$^{+0.58}_{-0.57}$	$^{+0.57}_{-0.59}$	$^{+0.55}_{-0.49}$	$^{+0.42}_{-0.45}$	$^{+0.56}_{-0.48}$	$^{+0.41}_{-0.42}$	$^{+0.31}_{-0.52}$	$^{+0.42}_{-0.34}$	$^{+0.38}_{-0.23}$	$^{+0.22}_{-0.23}$	$^{+0.10}_{-0.44}$	$^{+0.13}_{-0.34}$	$^{+0.56}_{-0.12}$
Flavour composition (JES) [%]	$^{+2.91}_{-2.05}$	$^{+2.15}_{-2.36}$	$^{+2.39}_{-2.60}$	$^{+2.38}_{-2.63}$	$^{+2.15}_{-2.23}$	$^{+1.90}_{-1.81}$	$^{+1.53}_{-1.59}$	$^{+1.38}_{-1.44}$	$^{+1.04}_{-1.19}$	$^{+0.97}_{-1.00}$	$^{+0.92}_{-0.88}$	$^{+0.85}_{-0.66}$	$^{+0.66}_{-0.48}$	$^{+0.22}_{-0.40}$	-	$^{+0.45}_{-}$
Flavour response (JES) [%]	$^{+0.77}_{-}$	$^{-1.01}_{+0.89}$	$^{-1.28}_{+1.17}$	$^{-1.30}_{+1.32}$	$^{-1.12}_{+1.17}$	$^{-1.01}_{+0.98}$	$^{-0.83}_{+0.84}$	$^{-0.69}_{+0.83}$	$^{-0.65}_{+0.42}$	$^{-0.62}_{+0.40}$	$^{-0.49}_{+0.58}$	$^{-0.25}_{+0.46}$	$^{-0.23}_{+0.36}$	$^{-0.47}_{-}$	$^{-}_{-0.28}$	-
Pile-up offset μ (JES) [%]	$^{+0.20}_{-}$	-	$^{-0.15}_{+0.17}$	$^{-0.20}_{+0.17}$	$^{-0.20}_{+0.18}$	$^{-0.13}_{+0.18}$	$^{-0.13}_{-}$	$^{-0.11}_{+0.15}$	$^{-}_{+0.13}$	-	∓0.13	-	-	$^{-0.42}_{+0.20}$	-	-
Pile-up offset N_{PV} (JES) [%]	$^{+0.81}_{-}$	±0.26	$^{+0.50}_{-0.48}$	$^{+0.59}_{-0.56}$	$^{+0.60}_{-0.59}$	$^{+0.57}_{-0.60}$	$^{+0.55}_{-0.50}$	$^{+0.50}_{-0.38}$	$^{+0.34}_{-0.40}$	$^{+0.25}_{-0.54}$	$^{+0.40}_{-0.32}$	$^{+0.57}_{-0.30}$	$^{+0.15}_{-0.34}$	$^{-}_{-0.22}$	-	$^{+0.34}_{-0.30}$
Pile-up offset p_T (JES) [%]	$^{-2.83}_{+2.89}$	$^{-1.28}_{+1.29}$	$^{-0.29}_{+0.31}$	-	$^{+0.30}_{-0.31}$	$^{+0.47}_{-0.45}$	$^{+0.51}_{-0.52}$	$^{+0.66}_{-0.67}$	$^{+0.70}_{-0.82}$	$^{+0.82}_{-0.80}$	$^{+0.97}_{-0.68}$	$^{+1.03}_{-0.90}$	$^{+1.04}_{-1.13}$	$^{+0.73}_{-1.11}$	$^{+0.96}_{-1.20}$	$^{+1.41}_{-0.96}$
Pile-up offset ρ topology (JES) [%]	$^{+0.41}_{-}$	$^{+2.36}_{-2.47}$	$^{+4.07}_{-3.89}$	$^{+4.52}_{-4.26}$	$^{+4.02}_{-3.91}$	$^{+3.69}_{-3.52}$	$^{+3.21}_{-3.17}$	$^{+2.91}_{-2.83}$	$^{+2.39}_{-2.46}$	$^{+2.26}_{-2.37}$	$^{+2.11}_{-1.97}$	$^{+1.81}_{-1.43}$	$^{+1.10}_{-1.26}$	$^{+0.59}_{-1.15}$	$^{+0.69}_{-0.82}$	$^{+0.59}_{-0.33}$
Jet vertex fraction [%]	$^{+1.73}_{-1.75}$	$^{+1.13}_{-1.16}$	$^{+0.86}_{-0.89}$	$^{+0.72}_{-0.76}$	$^{+0.62}_{-0.65}$	$^{+0.53}_{-0.57}$	$^{+0.47}_{-0.51}$	$^{+0.41}_{-0.45}$	$^{+0.36}_{-0.41}$	$^{+0.32}_{-0.37}$	$^{+0.28}_{-0.33}$	$^{+0.25}_{-0.30}$	$^{+0.21}_{-0.27}$	$^{+0.18}_{-0.23}$	$^{+0.17}_{-0.22}$	-
b-Quark tagging efficiency (eigenvector 0) [%]	$^{-12.5}_{+13.2}$	$^{-7.97}_{+8.25}$	$^{-6.57}_{+6.77}$	$^{-6.16}_{+6.33}$	$^{-5.98}_{+6.14}$	$^{-5.85}_{+6.00}$	$^{-5.79}_{+5.93}$	$^{-5.76}_{+5.89}$	$^{-5.77}_{+5.91}$	$^{-5.81}_{+5.94}$	$^{-5.85}_{+5.99}$	$^{-5.95}_{+6.09}$	$^{-6.03}_{+6.17}$	$^{-6.09}_{+6.23}$	$^{-6.20}_{+6.34}$	$^{-6.45}_{+6.60}$
b-Quark tagging efficiency (eigenvector 1) [%]	±0.41	$^{-0.91}_{+0.92}$	$^{-1.49}_{+1.50}$	$^{-1.79}_{+1.80}$	$^{-2.02}_{+2.04}$	$^{-2.27}_{+2.29}$	$^{-2.50}_{+2.52}$	$^{-2.69}_{+2.72}$	$^{-2.87}_{+2.91}$	$^{-3.05}_{+3.09}$	$^{-3.24}_{+3.29}$	$^{-3.43}_{+3.48}$	$^{-3.61}_{+3.66}$	$^{-3.72}_{+3.78}$	$^{-3.88}_{+3.93}$	$^{-4.29}_{+4.35}$
b-Quark tagging efficiency (eigenvector 2) [%]	$^{+1.39}_{-1.38}$	$^{+1.56}_{-1.54}$	$^{+1.49}_{-1.48}$	$^{+1.38}_{-1.37}$	±1.25	$^{+1.13}_{-1.12}$	±1.01	±0.90	$^{+0.79}_{-0.78}$	±0.67	±0.56	$^{+0.47}_{-0.46}$	±0.39	±0.32	±0.20	-
b-Quark tagging efficiency (eigenvector 3) [%]	∓0.60	∓0.27	-	-	±0.15	±0.20	$^{+0.22}_{-0.23}$	±0.22	±0.19	±0.16	±0.12	-	-	-	-	∓0.16
b-Quark tagging efficiency (eigenvector 4) [%]	±0.14	-	-	-	-	-	-	-	-	-	-	-	-	-	-	∓0.10
c-Quark tagging efficiency (eigenvector 0) [%]	$^{+0.90}_{-0.89}$	±0.41	±0.29	±0.25	±0.24	±0.22	±0.21	$^{+0.21}_{-0.20}$	±0.20	$^{+0.17}_{-0.18}$	±0.18	±0.17	±0.13	±0.14	±0.13	±0.19
c-Quark tagging efficiency (eigenvector 1) [%]	±0.11	-	∓0.11	∓0.16	∓0.22	∓0.27	∓0.33	∓0.40	∓0.45	∓0.52	$^{-0.61}_{+0.62}$	∓0.67	∓0.65	∓0.74	∓0.85	$^{-1.04}_{+1.05}$
c-Quark tagging efficiency (eigenvector 2) [%]	±0.18	±0.17	$^{+0.14}_{-0.13}$	$^{+0.11}_{-0.10}$	-	-	-	-	-	-	$^{-0.14}_{+0.15}$	∓0.17	∓0.18	∓0.20	∓0.27	∓0.41
Light-jet tagging efficiency (eigenvector 0) [%]	$^{-1.05}_{+0.80}$	$^{-0.47}_{+0.46}$	$^{-0.45}_{+0.47}$	$^{-0.56}_{+0.60}$	$^{-0.52}_{+0.53}$	$^{-0.64}_{+0.65}$	$^{-0.73}_{+0.76}$	$^{-0.85}_{+0.88}$	$^{-1.07}_{+1.13}$	$^{-1.04}_{+1.05}$	$^{-1.17}_{+1.16}$	$^{-1.40}_{+1.46}$	$^{-1.25}_{+1.31}$	$^{-1.51}_{+1.56}$	$^{-2.19}_{+2.26}$	$^{-2.06}_{+2.10}$
Light-jet tagging efficiency (eigenvector 1) [%]	$^{+0.79}_{-0.77}$	±0.30	±0.22	$^{+0.23}_{-0.22}$	$^{+0.22}_{-0.21}$	±0.23	$^{+0.23}_{-0.22}$	±0.18	$^{+0.24}_{-0.22}$	±0.17	-	-	-	-	$^{+0.11}_{-0.12}$	∓0.21
Light-jet tagging efficiency (eigenvector 2) [%]	-	-	-	-	-	-	-	-	-	-	±0.10	$^{+0.13}_{-0.14}$	±0.12	±0.13	-	±0.19
Light-jet tagging efficiency (eigenvector 3) [%]	$^{+0.35}_{-0.43}$	$^{+0.10}_{-0.11}$	-	-	-	-	∓0.10	∓0.16	$^{-0.22}_{+0.21}$	∓0.23	∓0.30	∓0.36	∓0.30	∓0.39	∓0.65	$^{-0.67}_{+0.68}$
Light-jet tagging efficiency (eigenvector 5) [%]	-	-	-	-	-	-	-	-	∓0.10	∓0.11	∓0.13	∓0.12	-	-	$^{-0.13}_{+0.12}$	-
Light-jet tagging efficiency (eigenvector 8) [%]	-	-	-	-	-	-	-	-	-	-	-	-	-	∓0.11	∓0.19	∓0.22
b-Quark tagging extrapolation [%]	-	-	-	-	-	-	-	-	±0.11	±0.21	±0.36	±0.52	±0.65	±0.80	±1.07	$^{+1.67}_{-1.66}$
b-Quark tagging extrapolation from c-Quark [%]	-	-	-	-	-	-	-	-	-	-	-	-	-	-	±0.11	-
Electron energy resolution [%]	$^{-}_{-0.20}$	-	-	-	-	-	-	-	-	-	-	-	-	-	-	-
Electron energy scale [%]	$^{-0.12}_{-}$	-	-	-	-	-	-	-	$^{+0.11}_{-0.10}$	±0.11	$^{+0.17}_{-0.16}$	$^{+0.28}_{-0.17}$	$^{+0.24}_{-0.21}$	$^{-}_{-0.27}$	$^{+0.26}_{-0.16}$	$^{+0.37}_{-0.30}$
Electron trigger efficiency [%]	±0.15	±0.12	±0.11	±0.11	±0.11	±0.11	±0.11	±0.12	±0.12	±0.12	±0.12	±0.13	±0.13	±0.14	±0.15	±0.16
Electron reconstruction efficiency [%]	-	-	-	-	-	-	-	-	-	-	±0.10	±0.10	±0.11	±0.11	±0.12	±0.13
Electron identification efficiency [%]	±0.37	±0.34	±0.35	±0.37	±0.40	±0.42	±0.45	±0.48	±0.51	±0.53	±0.56	±0.60	$^{+0.62}_{-0.63}$	±0.65	±0.70	±0.80
Electron isolation efficiency [%]	-	-	-	-	-	±0.11	±0.13	±0.16	±0.19	±0.23	$^{+0.25}_{-0.26}$	±0.29	±0.31	±0.33	±0.37	±0.48
Muon (ID) momentum resolution [%]	-	-	-	-	-	-	-	-	-	-	-	-	-	-	-	-
Muon (MS) momentum resolution [%]	-	-	-	-	-	-	-	-	-	-	-	-	-	-	-	-
Muon energy scale [%]	-	-	-	-	-	-	-	-	-	-	-	-	-	-	-	-
Muon trigger efficiency stat [%]	$^{+0.32}_{-0.33}$	$^{+0.29}_{-0.30}$	±0.29	$^{+0.28}_{-0.29}$	$^{+0.28}_{-0.29}$	±0.29	±0.29	±0.29	$^{+0.29}_{-0.30}$	$^{+0.29}_{-0.30}$	±0.30	$^{+0.30}_{-0.31}$	$^{+0.30}_{-0.31}$	$^{+0.30}_{-0.31}$	$^{+0.31}_{-0.32}$	±0.32
Muon trigger efficiency syst [%]	$^{+0.57}_{-0.56}$	$^{+0.52}_{-0.50}$	$^{+0.51}_{-0.49}$	$^{+0.50}_{-0.49}$	$^{+0.50}_{-0.49}$	$^{+0.51}_{-0.49}$	$^{+0.51}_{-0.50}$	$^{+0.52}_{-0.51}$	$^{+0.52}_{-0.51}$	$^{+0.53}_{-0.52}$	$^{+0.54}_{-0.53}$	$^{+0.54}_{-0.53}$	$^{+0.55}_{-0.54}$	$^{+0.56}_{-0.54}$	$^{+0.57}_{-0.56}$	$^{+0.58}_{-0.56}$
Muon identification stat [%]	$^{+0.10}_{-0.11}$	-	-	-	-	-	-	-	±0.10	±0.10	±0.10	±0.10	±0.10	±0.10	±0.11	±0.11
Muon identification syst [%]	±0.38	±0.34	±0.34	±0.34	±0.36	$^{+0.38}_{-0.37}$	±0.39	±0.41	±0.44	±0.46	±0.48	$^{+0.51}_{-0.50}$	$^{+0.53}_{-0.52}$	±0.55	±0.59	±0.64
Muon isolation efficiency syst [%]	±0.12	±0.10	±0.10	±0.10	±0.10	±0.10	$^{+0.11}_{-0.10}$	$^{+0.11}_{-0.10}$	±0.11	±0.11	±0.11	±0.11	±0.12	±0.12	±0.12	±0.13
E_T^{miss} Soft jet resolution para [%]	±1.15	±0.67	±0.19	-	∓0.19	∓0.28	∓0.32	∓0.29	∓0.42	∓0.33	∓0.20	∓0.26	∓0.30	∓0.45	∓0.48	∓0.28
E_T^{miss} Soft jet resolution perp [%]	±1.07	±0.62	±0.19	-	∓0.18	∓0.25	∓0.25	∓0.34	∓0.33	∓0.19	∓0.37	∓0.62	∓0.44	∓0.21	∓0.49	∓0.44
E_T^{miss} Soft jet scale [%]	$^{+1.12}_{-0.97}$	$^{+0.72}_{-0.69}$	$^{+0.21}_{-0.24}$	-	$^{-0.19}_{+0.15}$	∓0.25	$^{-0.33}_{+0.32}$	$^{-0.29}_{+0.39}$	$^{-0.38}_{+0.36}$	$^{-0.38}_{+0.34}$	$^{-0.36}_{+0.44}$	$^{-0.37}_{+0.56}$	$^{-0.34}_{+0.39}$	$^{-0.45}_{+0.13}$	$^{-0.56}_{+0.59}$	$^{-0.35}_{+0.40}$
Luminosity [%]	∓2.05	∓2.05	∓2.05	∓2.05	∓2.05	∓2.05	∓2.05	∓2.05	∓2.05	∓2.05	∓2.05	∓2.05	∓2.05	∓2.05	∓2.05	∓2.05
Z+jets cross-section [%]	±1.83	$^{+0.60}_{-0.61}$	±0.40	±0.44	±0.47	±0.49	±0.53	±0.58	±0.68	±0.67	±0.72	±0.81	±0.87	±0.92	±0.97	±1.20
Monte Carlo sample statistics [%]	±1.22	±0.21	±0.17	±0.19	±0.21	±0.20	±0.22	±0.26	±0.35	±0.38	±0.45	±0.57	±0.84	±0.86	±1.04	±1.10
ISR/FSR + scale [%]	$^{-}_{-1.26}$	$^{-0.31}_{+0.30}$	$^{+1.38}_{-}$	$^{-0.89}_{+0.61}$	$^{-0.31}_{+0.81}$	$^{+1.60}_{-}$	$^{-0.84}_{+1.19}$	$^{-1.45}_{+0.42}$	$^{-}_{-1.30}$	$^{+1.02}_{-}$	$^{+1.10}_{-}$	$^{+0.41}_{-}$	$^{+0.62}_{-}$	$^{+0.44}_{-0.24}$	$^{-1.09}_{+1.19}$	$^{+0.55}_{-}$
Alternate hard-scattering model [%]	±16.7	±8.54	±3.09	±1.85	±1.77	±2.02	±2.60	±1.72	±1.04	±2.01	-	∓1.62	∓0.63	±0.53	±1.06	±3.56
Alternate parton-shower model [%]	∓1.40	±2.21	±2.64	±1.96	±2.61	±2.63	±1.58	±1.01	-	±1.09	±1.31	±2.53	±2.06	∓1.21	∓0.93	∓1.08
Inter PDF [%]	-	-	-	-	-	-	-	-	-	-	-	-	∓0.21	∓0.28	±0.12	±0.12
Intra PDF [%]	±0.42	-	±0.27	-	±0.10	±0.15	±0.19	±0.31	±0.42	±0.16	±0.17	±0.21	±1.21	±1.49	±0.92	±0.45
Fakes overall normalization, el [%]	$^{+3.96}_{-3.92}$	$^{+0.89}_{-0.90}$	±0.45	±0.46	±0.48	±0.55	±0.65	±0.66	±0.64	±0.69	±0.93	±1.19	±1.20	±1.19	±1.20	±3.17
Fakes overall normalization, mu [%]	±0.44	±0.15	-	-	-	-	-	-	∓0.16	∓0.30	∓0.30	∓0.35	∓0.44	∓0.32	∓0.46	∓0.71
Fakes alternative parametrization [%]	∓9.97	∓4.32	∓3.15	∓2.63	∓2.22	∓1.83	∓1.58	∓1.33	∓1.12	∓0.77	∓0.74	∓0.61	∓0.46	∓0.31	-	∓0.94
W+jets heavy flavour component [%]	±13.7	±5.77	±2.81	±3.24	±2.26	±2.38	±4.04	±3.69	±3.26	±4.66	±3.39	±2.11	±2.52	±2.72	±3.00	±6.77

TABLE F.7: Table of systematics for the absolute differential cross-section at the particle level for the $m^{t\bar{t}}$ observable.

Bins [Unit y^{t_h}]	-3—1.62	-1.62—1.23	-1.23—0.96	-0.96—0.75	-0.75—0.54	-0.54—0.36	-0.36—0.18	-0.18–0	0–0.18	0.18–0.36	0.36–0.54	0.54–0.75	0.75–0.96	0.96–1.23	1.23–1.62	1.62–3
dσ / dy^{t_h} [pb/ Unit y^{t_h}]	$2.22 \cdot 10^{0}$	$1.44 \cdot 10^{1}$	$2.10 \cdot 10^{1}$	$2.59 \cdot 10^{1}$	$2.92 \cdot 10^{1}$	$3.16 \cdot 10^{1}$	$3.31 \cdot 10^{1}$	$3.43 \cdot 10^{1}$	$3.42 \cdot 10^{1}$	$3.35 \cdot 10^{1}$	$3.19 \cdot 10^{1}$	$2.91 \cdot 10^{1}$	$2.62 \cdot 10^{1}$	$2.13 \cdot 10^{1}$	$1.44 \cdot 10^{1}$	$2.19 \cdot 10^{0}$
Total Uncertainty [%]	+8.89 −8.86	+10.3 −10.1	±10.3	+12.3 −12.0	+10.4 −10.2	±12.2	+10.4 −10.0	+12.2 −12.1	+10.7 −10.4	+11.0 −10.7	+10.9 −10.5	±10.6	+10.5 −10.1	+10.8 −10.6	+9.91 −9.75	±11.4
Statistics [%]	±0.5	±0.4	±0.4	±0.4	±0.4	±0.4	±0.4	±0.4	±0.4	±0.4	±0.4	±0.4	±0.4	±0.4	±0.4	±0.5
Systematics [%]	+8.86 −8.83	+10.3 −10.0	+10.3 −10.2	+12.3 −12.0	+10.4 −10.1	+12.1 −12.2	+10.3 −10.0	±12.1	+10.7 −10.4	+11.0 −10.7	+10.9 −10.5	±10.6	+10.4 −10.0	+10.8 −10.6	+9.90 −9.73	±11.4
Jet energy resolution [%]	∓0.16	±0.28	∓0.20	±3.64	∓1.25	±2.69	∓0.26	±3.02	∓0.53	-	±0.45	±1.09	∓0.44	±1.57	±1.45	±0.18
b-Tagged jet energy scale (JES) [%]	+0.28 −0.29	+0.43 −0.46	±0.49	+0.47 −0.45	±0.57	+0.55 −0.57	+0.54 −0.57	+0.58 −0.53	+0.55 −0.59	±0.57	+0.53 −0.47	+0.51 −0.62	+0.52 −0.42	±0.47	+0.37 −0.44	±0.30
Effective mixed NP set 1 (JES) [%]	-	+0.16 −0.12	+0.14 −0.19	±0.13	±0.15	+0.13 −0.17	+0.19 −0.15	+0.13 −0.15	+0.17 −0.13	+0.16 −0.17	+0.18 −0.11	+0.13 −0.15	+0.17 −0.12	+0.14 −0.18	+0.11 −0.12	-
Effective modelling NP set 1 (JES) [%]	+1.15 −1.17	+2.05 −1.85	+2.12 −2.16	+2.30 −2.19	+2.48 −2.40	+2.40 −2.47	+2.44 −2.30	+2.34 −2.54	+2.52 −2.34	+2.29 −2.30	+2.49 −2.27	+2.37 −2.31	+2.37 −2.17	+2.15 −2.00	+1.75 −1.84	+1.43 −1.29
Effective modelling NP set 2 (JES) [%]	−0.12 +0.15	−0.12 +0.17	−0.14 +0.12	−0.22 +0.20	−0.20 +0.15	−0.18 +0.15	−0.15 +0.22	∓0.16	−0.19 +0.23	−0.17 +0.19	∓0.17	∓0.18	−0.15 +0.17	−0.16 +0.14	−0.12 +0.14	−0.12 +0.11
Effective modelling NP set 3 (JES) [%]	-	-	-	+0.13 −0.11	-	-	+0.13 -	-	+0.14 −0.11	+0.11 −0.10	-	±0.10	- −0.11	-	-	-
Effective modelling NP set 4 (JES) [%]	-	-	±0.10	+0.14 −0.12	+0.11 −0.10	- −0.13	+0.15 −0.12	+0.10 −0.11	+0.15 −0.13	+0.13 −0.10	+0.12 −0.13	+0.11 −0.10	+0.11 −0.10	+0.11 −0.12	-	-
Effective statistical NP set 1 (JES) [%]	±0.22	+0.36 −0.26	+0.33 −0.40	+0.47 −0.41	+0.36 −0.42	+0.38 −0.42	+0.48 −0.37	+0.31 −0.42	+0.46 −0.41	±0.42	+0.41 −0.34	+0.40 −0.43	+0.40 −0.35	+0.35 −0.37	+0.36 −0.31	+0.19 −0.18
Effective statistical NP set 2 (JES) [%]	−0.17 +0.21	−0.22 +0.30	−0.36 +0.28	−0.35 +0.45	−0.37 +0.30	−0.37 +0.33	−0.31 +0.42	−0.35 +0.26	−0.37 +0.41	−0.34 +0.38	−0.30 +0.34	−0.39 +0.35	−0.32 +0.35	−0.33 +0.29	−0.26 +0.32	−0.16 +0.17
Effective statistical NP set 7 (JES) [%]	-	-	-	-	-	-	-	-	+0.12 −0.11	-	-	-	-	-	-	-
η intercalibration model (JES) [%]	+0.77 −0.75	+1.05 −0.98	+0.86 −1.00	+0.64 −0.58	+0.60 −0.56	+0.44 −0.55	+0.52 −0.41	+0.34 −0.59	+0.47 −0.45	+0.40 −0.36	±0.49	+0.59 −0.55	+0.71 −0.62	+0.82 −0.90	+0.98 −1.00	+0.76 −0.79
η intercalibration non closure (JES) [%]	−0.10 +0.19	−0.37 +0.43	−0.54 +0.43	−0.48 +0.52	−0.44 +0.45	−0.52 +0.37	−0.27 +0.48	−0.28 +0.22	−0.28 +0.29	−0.21 +0.26	−0.20 +0.12	-	-	-	-	-
η intercalibration total stat (JES) [%]	±0.21	+0.42 −0.34	+0.38 −0.46	+0.49 −0.42	+0.41 −0.47	±0.43	+0.52 −0.37	+0.32 −0.43	+0.49 −0.43	+0.43 −0.46	+0.46 −0.38	+0.39 −0.46	+0.45 −0.33	+0.37 −0.44	+0.39 −0.35	+0.20 −0.21
Flavour composition (JES) [%]	+0.81 −0.96	±1.73	+1.82 −2.22	+2.33 −2.06	+2.33 −2.25	+1.76 −2.34	+2.14 −2.08	+2.02 −2.36	+2.20 −2.29	+1.96 −2.13	+2.23 −2.07	+1.90 −2.21	+2.06 −1.90	+1.90 −1.95	+1.58 −1.74	+0.93 −1.01
Flavour response (JES) [%]	−0.44 +0.46	−0.89 +1.00	−1.17 +0.97	∓0.99	−1.08 +1.09	−1.06 +0.93	−1.04 +1.12	−1.16 +0.96	−1.07 +1.00	−0.93 +0.91	−1.05 +1.13	−1.05 +1.04	−1.04 +1.00	−0.95 +0.92	−0.83 +0.84	−0.54 +0.59
Pile-up offset μ (JES) [%]	-	−0.11 +0.18	−0.15 -	−0.13 +0.17	-	−0.20 +0.18	−0.13 +0.21	−0.21 +0.16	−0.10 +0.19	−0.15 +0.14	- +0.17	−0.18 +0.10	−0.11 +0.19	−0.17 -	−0.11 +0.16	-
Pile-up offset N_{PV} (JES) [%]	+0.18 −0.21	+0.55 −0.26	+0.45 −0.59	+0.43 −0.40	+0.56 −0.57	+0.29 −0.46	+0.56 −0.43	+0.47 −0.63	+0.61 −0.41	+0.45 −0.64	+0.54 −0.38	+0.53 −0.62	+0.60 −0.25	+0.47 −0.48	+0.33 −0.26	+0.26 −0.27
Pile-up offset p_T (JES) [%]	-	-	-	-	-	-	-	-	-	-	-	-	-	-	-	-
Pile-up offset ρ topology (JES) [%]	+1.58 −1.66	+2.87 −2.75	+3.18 −3.21	+3.45 −3.35	+3.72 −3.57	+3.35 −3.64	+3.75 −3.49	+3.67 −3.72	+3.79 −3.54	±3.53	+3.70 −3.37	+3.56 −3.57	+3.54 −3.06	+3.18 −3.09	+2.71 −2.67	+1.82 −1.78
Jet vertex fraction [%]	+0.66 −0.69	+0.70 −0.73	+0.70 −0.74	+0.69 −0.72	+0.69 −0.72	+0.69 −0.73	+0.68 −0.72	+0.69 −0.73	+0.69 −0.73	+0.69 −0.73	+0.69 −0.73	+0.68 −0.72	+0.69 −0.72	+0.70 −0.73	+0.69 −0.72	+0.66 −0.69
b-Quark tagging efficiency (eigenvector 0) [%]	−6.31 +6.49	−6.40 +6.58	−6.40 +6.58	−6.46 +6.65	−6.48 +6.66	−6.49 +6.68	−6.50 +6.69	−6.52 +6.70	−6.50 +6.68	−6.50 +6.68	−6.51 +6.69	−6.47 +6.66	−6.45 +6.64	−6.43 +6.62	−6.36 +6.55	−6.31 +6.49
b-Quark tagging efficiency (eigenvector 1) [%]	−1.95 +1.97	−1.94 +1.96	−1.95 +1.97	−1.96 +1.98	−1.95 +1.97	−1.97 +1.98	−1.98 +1.99	−1.96 +1.98	−1.97 +1.99	−1.97 +1.99	−1.97 +1.99	−1.97 +1.99	−1.96 +1.99	−1.95 +1.97	−1.94 +1.96	−1.96 +1.98
b-Quark tagging efficiency (eigenvector 2) [%]	+1.22 −1.21	+1.22 −1.21	+1.22 −1.21	±1.21	+1.21 −1.20	+1.22 −1.21	±1.21	+1.21 −1.20	±1.21	±1.21	±1.21	+1.21 −1.20	+1.22 −1.21	±1.22	±1.22	+1.22 −1.21
c-Quark tagging efficiency (eigenvector 0) [%]	±0.26	±0.27	±0.27	±0.25	+0.29 −0.28	±0.27	±0.28	±0.26	±0.28	±0.28	±0.28	±0.28	±0.26	±0.25	+0.28 −0.27	±0.25
c-Quark tagging efficiency (eigenvector 1) [%]	∓0.20	∓0.20	∓0.23	∓0.22	∓0.25	∓0.24	∓0.25	∓0.25	∓0.25	∓0.26	∓0.25	∓0.24	∓0.23	∓0.22	∓0.21	∓0.20
Light-jet tagging efficiency (eigenvector 0) [%]	−0.79 +0.82	∓0.58	−0.69 +0.71	−0.66 +0.69	−0.54 +0.46	−0.85 +0.94	−0.55 +0.52	−0.45 +0.43	−0.70 +0.73	−0.68 +0.70	∓0.63	−0.68 +0.69	−0.69 +0.73	−0.76 +0.82	−0.76 +0.80	−0.70 +0.72
Light-jet tagging efficiency (eigenvector 1) [%]	±0.28	±0.19	+0.25 −0.24	+0.22 −0.21	+0.17 −0.18	+0.37 −0.34	±0.19	+0.14 −0.15	+0.24 −0.25	±0.26	+0.18 −0.19	±0.24	+0.22 −0.21	±0.24	+0.24 −0.23	+0.25 −0.24
Light-jet tagging efficiency (eigenvector 2) [%]	-	-	-	-	-	-	-	-	-	-	-	-	-	+0.12 −0.11	-	-
Light-jet tagging efficiency (eigenvector 3) [%]	-	-	-	-	-	-	-	-	-	-	-	-	-	-	-	-
Electron trigger efficiency [%]	±0.12	±0.12	+0.11 −0.12	+0.12 −0.11	±0.12	±0.12	±0.12	+0.11 −0.12	+0.11 −0.12	+0.11 −0.12	±0.12	+0.11 −0.12	+0.12 −0.11	+0.11 −0.12	+0.11 −0.12	±0.11
Electron identification efficiency [%]	±0.41	±0.41	±0.41	±0.41	±0.41	±0.42	±0.41	±0.41	±0.41	±0.41	±0.41	±0.41	±0.41	±0.41	±0.41	±0.41
Electron isolation efficiency [%]	±0.10	±0.10	±0.10	±0.10	±0.11	±0.11	±0.10	+0.10 −0.11	±0.10	±0.11	±0.11	±0.11	±0.10	±0.10	±0.10	±0.10
Muon trigger efficiency stat [%]	+0.28 −0.29	+0.28 −0.29	±0.29	±0.29	±0.29	±0.29	±0.29	+0.29 −0.30	+0.29 −0.30	+0.29 −0.30	±0.29	±0.29	±0.29	±0.29	±0.29	+0.28 −0.29
Muon trigger efficiency syst [%]	+0.51 −0.50	+0.50 −0.49	+0.51 −0.50	+0.51 −0.50	+0.51 −0.50	+0.51 −0.50	±0.51	+0.52 −0.51	+0.52 −0.50	+0.52 −0.51	+0.51 −0.50	+0.51 −0.50	+0.51 −0.50	+0.51 −0.50	+0.51 −0.49	+0.50 −0.49
Muon identification syst [%]	±0.37	±0.37	±0.37	±0.37	±0.37	+0.37 −0.38	±0.37	±0.38	±0.38	±0.38	+0.37 −0.38	±0.38	±0.38	±0.38	±0.38	±0.38
Muon isolation efficiency syst [%]	±0.10	±0.10	±0.10	±0.10	±0.10	+0.10 −0.11	±0.10	±0.11	±0.10	+0.11 −0.10	±0.10	±0.10	±0.10	±0.10	±0.10	±0.10
Luminosity [%]	∓2.05	∓2.05	∓2.05	∓2.05	∓2.05	∓2.05	∓2.05	∓2.05	∓2.05	∓2.05	∓2.05	∓2.05	∓2.05	∓2.05	∓2.05	∓2.05
Z+jets cross-section [%]	±0.40	±0.41	±0.49	±0.51	±0.61	±0.66	±0.53	±0.61	±0.63	±0.61	±0.59	±0.56	±0.54	±0.46	±0.51	±0.43
Monte Carlo sample statistics [%]	±0.37	±0.27	±0.28	±0.29	±0.34	±0.34	±0.37	±0.46	±0.31	±0.30	±0.30	±0.28	±0.30	±0.35	±0.31	±0.39
ISR/FSR + scale [%]	- −0.99	−0.12 +0.90	−0.14 +1.28	+1.56 -	−0.97 +1.42	−0.22 +0.81	−0.27 +1.08	−0.14 +1.75	+1.05 -	−0.12 +1.82	−0.15 +1.06	−1.06 +0.86	−0.33 +0.60	- +1.30	−0.37 +1.27	- −1.62
Alternate hard-scattering model [%]	±1.94	±3.90	±3.63	±2.42	±2.64	±3.68	±1.82	±2.80	±3.39	±3.74	±3.37	±1.56	±3.68	±3.91	±2.15	±7.23
Alternate parton-shower model [%]	∓0.85	±1.37	±1.76	±0.88	±1.87	±1.51	±1.40	±1.88	±1.52	±1.84	±1.25	±2.32	±1.88	±0.64	±0.67	∓1.87
Intra PDF [%]	±0.25	±0.24	-	±0.12	±0.18	±0.16	±0.46	±0.40	±0.29	±0.17	±0.12	±0.17	±0.34	±0.20	±0.14	±0.18
Fakes overall normalization, el [%]	±0.37	±0.71	±0.64	±0.64	±0.71	±0.77	±0.85	±0.75	±0.72	±0.75	±0.72	±0.71	±0.67	±0.66	±0.56	±0.48
Fakes overall normalization, mu [%]	-	-	-	-	-	-	-	-	-	-	-	-	-	-	-	±0.10
Fakes alternative parametrization [%]	∓2.27	∓2.56	∓2.65	∓2.67	∓2.50	∓2.71	∓2.52	∓2.49	∓2.55	∓2.75	∓2.46	∓2.48	∓2.37	∓2.33	∓2.56	∓2.46
W+jets heavy flavour component [%]	±2.64	±2.82	±2.32	±6.42	±1.80	±6.07	±3.05	±5.99	±2.78	±3.35	±3.62	±3.95	±2.10	±3.91	±3.43	±2.42

TABLE F.8: Table of systematics for the absolute differential cross-section at the particle level for the $y^{t,had}$ observable.

Bins [GeV] x	300–400	400–500	500–600	600–710	710–870	870–1050	1050–1250	1250–1460	1460–2000	2000–2100	2100–2210	2210–2340	2340–2500	2500–2680	2680–2870	2870–3080	3080–3700	3700–3760	3760–3860	3860–3985	3985–4140	4140–4310	4310–4500	4500–4700	4700–5400	5400–5475.50	5475.50–5530	5530–5655	5655–5800	5800–5960	5960–6140	6140–6400	6400–7100
dσ / d$m^{t\bar{t}}$vs$y^{t,had}$ [pb/GeV x]	$8.41 \cdot 10^{-2}$	$1.28 \cdot 10^{-1}$	$8.94 \cdot 10^{-2}$	$5.40 \cdot 10^{-2}$	$2.70 \cdot 10^{-2}$	$1.20 \cdot 10^{-2}$	$4.93 \cdot 10^{-3}$	$2.20 \cdot 10^{-3}$	$5.73 \cdot 10^{-4}$	$5.20 \cdot 10^{-2}$	$7.57 \cdot 10^{-2}$	$4.68 \cdot 10^{-2}$	$2.13 \cdot 10^{-2}$	$8.72 \cdot 10^{-3}$	$3.50 \cdot 10^{-3}$	$1.32 \cdot 10^{-3}$	$2.88 \cdot 10^{-4}$	$1.53 \cdot 10^{-2}$	$3.20 \cdot 10^{-2}$	$2.53 \cdot 10^{-2}$	$1.30 \cdot 10^{-2}$	$5.75 \cdot 10^{-3}$	$2.30 \cdot 10^{-3}$	$8.94 \cdot 10^{-4}$	$1.86 \cdot 10^{-4}$	$8.36 \cdot 10^{-3}$	$1.58 \cdot 10^{-2}$	$1.46 \cdot 10^{-2}$	$8.64 \cdot 10^{-3}$	$4.21 \cdot 10^{-3}$	$1.89 \cdot 10^{-3}$	$7.64 \cdot 10^{-4}$	$1.25 \cdot 10^{-4}$
Total Uncertainty [%]	+15.6 −15.3	+9.69 −9.59	+8.82 −8.58	+8.75 −8.82	+9.62 −9.65	+8.89 −8.74	±10.0	+13.0 −10.4	+16.7 −16.3	+17.6 −17.5	±12.3	+11.6 −11.0	+10.0 −9.83	+12.8 −12.7	+9.98 −10.1	+10.0 −10.1	+14.9 −14.4	+22.6 −22.7	+16.4 −16.2	+14.7 −14.2	+14.6 −13.8	±13.6	+12.0 −11.8	+11.8 −13.0	+14.2 −14.3	+27.2 −25.8	+24.8 −24.1	+22.4 −21.2	+19.8 −19.0	+18.1 −17.4	+16.5 −17.3	+22.6 −18.2	+21.6 −22.8
Statistics [%]	±0.4	±0.3	±0.3	±0.4	±0.5	±0.8	±1.2	±1.8	±2.2	±0.5	±0.3	±0.4	±0.6	±0.9	±1.4	±2.2	±3.0	±1.1	±0.6	±0.6	±0.7	±1.1	±1.6	±2.6	±3.4	±1.4	±1.0	±0.8	±1.0	±1.3	±1.8	±2.6	±4.0
Systematics [%]	+15.6 −15.3	+9.68 −9.58	+8.80 −8.56	+8.73 −8.81	+9.60 −9.62	+8.83 −8.69	+9.96 −9.92	+12.8 −10.2	+16.5 −16.1	+17.6 −17.5	±12.3	+11.5 −11.0	+10.0 −9.80	+12.8 −12.6	+9.83 −9.96	+9.65 −9.81	+14.5 −13.9	+22.5 −22.6	+16.3 −16.2	+14.7 −14.1	+14.5 −13.8	±13.6	+11.8 −11.6	+11.4 −12.7	+13.6 −13.7	+27.1 −25.7	+24.7 −24.1	+22.3 −21.2	+19.8 −19.0	+18.1 −17.3	+16.4 −17.1	+22.4 −17.9	+21.1 −22.4
Jet energy resolution [%]	-	∓0.18	-	±0.41	±1.58	-	∓1.23	±2.25	±6.27	±0.31	±0.78	±2.20	±1.13	±6.40	±2.47	±2.12	±0.62	±6.08	∓1.16	∓0.19	±0.85	±4.00	±0.75	∓1.31	±1.09	±1.43	±1.00	±2.74	±6.27	±1.76	±1.67	∓9.11	±2.22
b-Tagged jet energy scale (JES) [%]	[illegible]	[illegible]	[illegible]	[illegible]	[illegible]	[illegible]	[illegible]	[illegible]	[illegible]	[illegible]	[illegible]	[illegible]	[illegible]	[illegible]	[illegible]	[illegible]	[illegible]	[illegible]	[illegible]	[illegible]	[illegible]	[illegible]	[illegible]	[illegible]	[illegible]	[illegible]	[illegible]	[illegible]	[illegible]	[illegible]	[illegible]	[illegible]	[illegible]
Effective detector NP set 1 (JES) [%]	[illegible]	[illegible]	[illegible]	[illegible]	[illegible]	[illegible]	[illegible]	[illegible]	[illegible]	[illegible]	[illegible]	[illegible]	[illegible]	[illegible]	[illegible]	[illegible]	[illegible]	[illegible]	[illegible]	[illegible]	[illegible]	[illegible]	[illegible]	[illegible]	[illegible]	[illegible]	[illegible]	[illegible]	[illegible]	[illegible]	[illegible]	[illegible]	[illegible]
Effective detector NP set 2 (JES) [%]	[illegible]	[illegible]	[illegible]	[illegible]	[illegible]	[illegible]	[illegible]	[illegible]	[illegible]	[illegible]	[illegible]	[illegible]	[illegible]	[illegible]	[illegible]	[illegible]	[illegible]	[illegible]	[illegible]	[illegible]	[illegible]	[illegible]	[illegible]	[illegible]	[illegible]	[illegible]	[illegible]	[illegible]	[illegible]	[illegible]	[illegible]	[illegible]	[illegible]
Effective mixed NP set 1 (JES) [%]	[illegible]	[illegible]	[illegible]	[illegible]	[illegible]	[illegible]	[illegible]	[illegible]	[illegible]	[illegible]	[illegible]	[illegible]	[illegible]	[illegible]	[illegible]	[illegible]	[illegible]	[illegible]	[illegible]	[illegible]	[illegible]	[illegible]	[illegible]	[illegible]	[illegible]	[illegible]	[illegible]	[illegible]	[illegible]	[illegible]	[illegible]	[illegible]	[illegible]
Effective mixed NP set 2 (JES) [%]	[illegible]	[illegible]	[illegible]	[illegible]	[illegible]	[illegible]	[illegible]	[illegible]	[illegible]	[illegible]	[illegible]	[illegible]	[illegible]	[illegible]	[illegible]	[illegible]	[illegible]	[illegible]	[illegible]	[illegible]	[illegible]	[illegible]	[illegible]	[illegible]	[illegible]	[illegible]	[illegible]	[illegible]	[illegible]	[illegible]	[illegible]	[illegible]	[illegible]
Effective mixed NP set 3 (JES) [%]	[illegible]	[illegible]	[illegible]	[illegible]	[illegible]	[illegible]	[illegible]	[illegible]	[illegible]	[illegible]	[illegible]	[illegible]	[illegible]	[illegible]	[illegible]	[illegible]	[illegible]	[illegible]	[illegible]	[illegible]	[illegible]	[illegible]	[illegible]	[illegible]	[illegible]	[illegible]	[illegible]	[illegible]	[illegible]	[illegible]	[illegible]	[illegible]	[illegible]
Effective modelling NP set 1 (JES) [%]	[illegible]	[illegible]	[illegible]	[illegible]	[illegible]	[illegible]	[illegible]	[illegible]	[illegible]	[illegible]	[illegible]	[illegible]	[illegible]	[illegible]	[illegible]	[illegible]	[illegible]	[illegible]	[illegible]	[illegible]	[illegible]	[illegible]	[illegible]	[illegible]	[illegible]	[illegible]	[illegible]	[illegible]	[illegible]	[illegible]	[illegible]	[illegible]	[illegible]
Effective modelling NP set 2 (JES) [%]	[illegible]	[illegible]	[illegible]	[illegible]	[illegible]	[illegible]	[illegible]	[illegible]	[illegible]	[illegible]	[illegible]	[illegible]	[illegible]	[illegible]	[illegible]	[illegible]	[illegible]	[illegible]	[illegible]	[illegible]	[illegible]	[illegible]	[illegible]	[illegible]	[illegible]	[illegible]	[illegible]	[illegible]	[illegible]	[illegible]	[illegible]	[illegible]	[illegible]
Effective modelling NP set 3 (JES) [%]	[illegible]	[illegible]	[illegible]	[illegible]	[illegible]	[illegible]	[illegible]	[illegible]	[illegible]	[illegible]	[illegible]	[illegible]	[illegible]	[illegible]	[illegible]	[illegible]	[illegible]	[illegible]	[illegible]	[illegible]	[illegible]	[illegible]	[illegible]	[illegible]	[illegible]	[illegible]	[illegible]	[illegible]	[illegible]	[illegible]	[illegible]	[illegible]	[illegible]
Effective modelling NP set 4 (JES) [%]	[illegible]	[illegible]	[illegible]	[illegible]	[illegible]	[illegible]	[illegible]	[illegible]	[illegible]	[illegible]	[illegible]	[illegible]	[illegible]	[illegible]	[illegible]	[illegible]	[illegible]	[illegible]	[illegible]	[illegible]	[illegible]	[illegible]	[illegible]	[illegible]	[illegible]	[illegible]	[illegible]	[illegible]	[illegible]	[illegible]	[illegible]	[illegible]	[illegible]
Effective statistical NP set 1 (JES) [%]	[illegible]	[illegible]	[illegible]	[illegible]	[illegible]	[illegible]	[illegible]	[illegible]	[illegible]	[illegible]	[illegible]	[illegible]	[illegible]	[illegible]	[illegible]	[illegible]	[illegible]	[illegible]	[illegible]	[illegible]	[illegible]	[illegible]	[illegible]	[illegible]	[illegible]	[illegible]	[illegible]	[illegible]	[illegible]	[illegible]	[illegible]	[illegible]	[illegible]
Effective statistical NP set 2 (JES) [%]	[illegible]	[illegible]	[illegible]	[illegible]	[illegible]	[illegible]	[illegible]	[illegible]	[illegible]	[illegible]	[illegible]	[illegible]	[illegible]	[illegible]	[illegible]	[illegible]	[illegible]	[illegible]	[illegible]	[illegible]	[illegible]	[illegible]	[illegible]	[illegible]	[illegible]	[illegible]	[illegible]	[illegible]	[illegible]	[illegible]	[illegible]	[illegible]	[illegible]
Effective statistical NP set 3 (JES) [%]	[illegible]	[illegible]	[illegible]	[illegible]	[illegible]	[illegible]	[illegible]	[illegible]	[illegible]	[illegible]	[illegible]	[illegible]	[illegible]	[illegible]	[illegible]	[illegible]	[illegible]	[illegible]	[illegible]	[illegible]	[illegible]	[illegible]	[illegible]	[illegible]	[illegible]	[illegible]	[illegible]	[illegible]	[illegible]	[illegible]	[illegible]	[illegible]	[illegible]
Effective statistical NP set 4 (JES) [%]	[illegible]	[illegible]	[illegible]	[illegible]	[illegible]	[illegible]	[illegible]	[illegible]	[illegible]	[illegible]	[illegible]	[illegible]	[illegible]	[illegible]	[illegible]	[illegible]	[illegible]	[illegible]	[illegible]	[illegible]	[illegible]	[illegible]	[illegible]	[illegible]	[illegible]	[illegible]	[illegible]	[illegible]	[illegible]	[illegible]	[illegible]	[illegible]	[illegible]
Effective statistical NP set 5 (JES) [%]	[illegible]	[illegible]	[illegible]	[illegible]	[illegible]	[illegible]	[illegible]	[illegible]	[illegible]	[illegible]	[illegible]	[illegible]	[illegible]	[illegible]	[illegible]	[illegible]	[illegible]	[illegible]	[illegible]	[illegible]	[illegible]	[illegible]	[illegible]	[illegible]	[illegible]	[illegible]	[illegible]	[illegible]	[illegible]	[illegible]	[illegible]	[illegible]	[illegible]
Effective statistical NP set 6 (JES) [%]	[illegible]	[illegible]	[illegible]	[illegible]	[illegible]	[illegible]	[illegible]	[illegible]	[illegible]	[illegible]	[illegible]	[illegible]	[illegible]	[illegible]	[illegible]	[illegible]	[illegible]	[illegible]	[illegible]	[illegible]	[illegible]	[illegible]	[illegible]	[illegible]	[illegible]	[illegible]	[illegible]	[illegible]	[illegible]	[illegible]	[illegible]	[illegible]	[illegible]
Effective statistical NP set 7 (JES) [%]	[illegible]	[illegible]	[illegible]	[illegible]	[illegible]	[illegible]	[illegible]	[illegible]	[illegible]	[illegible]	[illegible]	[illegible]	[illegible]	[illegible]	[illegible]	[illegible]	[illegible]	[illegible]	[illegible]	[illegible]	[illegible]	[illegible]	[illegible]	[illegible]	[illegible]	[illegible]	[illegible]	[illegible]	[illegible]	[illegible]	[illegible]	[illegible]	[illegible]
η intercalibration model (JES) [%]	[illegible]	[illegible]	[illegible]	[illegible]	[illegible]	[illegible]	[illegible]	[illegible]	[illegible]	[illegible]	[illegible]	[illegible]	[illegible]	[illegible]	[illegible]	[illegible]	[illegible]	[illegible]	[illegible]	[illegible]	[illegible]	[illegible]	[illegible]	[illegible]	[illegible]	[illegible]	[illegible]	[illegible]	[illegible]	[illegible]	[illegible]	[illegible]	[illegible]
η intercalibration non closure (JES) [%]	[illegible]	[illegible]	[illegible]	[illegible]	[illegible]	[illegible]	[illegible]	[illegible]	[illegible]	[illegible]	[illegible]	[illegible]	[illegible]	[illegible]	[illegible]	[illegible]	[illegible]	[illegible]	[illegible]	[illegible]	[illegible]	[illegible]	[illegible]	[illegible]	[illegible]	[illegible]	[illegible]	[illegible]	[illegible]	[illegible]	[illegible]	[illegible]	[illegible]
η intercalibration total stat (JES) [%]	[illegible]	[illegible]	[illegible]	[illegible]	[illegible]	[illegible]	[illegible]	[illegible]	[illegible]	[illegible]	[illegible]	[illegible]	[illegible]	[illegible]	[illegible]	[illegible]	[illegible]	[illegible]	[illegible]	[illegible]	[illegible]	[illegible]	[illegible]	[illegible]	[illegible]	[illegible]	[illegible]	[illegible]	[illegible]	[illegible]	[illegible]	[illegible]	[illegible]
Flavour composition (JES) [%]	[illegible]	[illegible]	[illegible]	[illegible]	[illegible]	[illegible]	[illegible]	[illegible]	[illegible]	[illegible]	[illegible]	[illegible]	[illegible]	[illegible]	[illegible]	[illegible]	[illegible]	[illegible]	[illegible]	[illegible]	[illegible]	[illegible]	[illegible]	[illegible]	[illegible]	[illegible]	[illegible]	[illegible]	[illegible]	[illegible]	[illegible]	[illegible]	[illegible]
Flavour response (JES) [%]	[illegible]	[illegible]	[illegible]	[illegible]	[illegible]	[illegible]	[illegible]	[illegible]	[illegible]	[illegible]	[illegible]	[illegible]	[illegible]	[illegible]	[illegible]	[illegible]	[illegible]	[illegible]	[illegible]	[illegible]	[illegible]	[illegible]	[illegible]	[illegible]	[illegible]	[illegible]	[illegible]	[illegible]	[illegible]	[illegible]	[illegible]	[illegible]	[illegible]
Pile-up offset μ (JES) [%]	[illegible]	[illegible]	[illegible]	[illegible]	[illegible]	[illegible]	[illegible]	[illegible]	[illegible]	[illegible]	[illegible]	[illegible]	[illegible]	[illegible]	[illegible]	[illegible]	[illegible]	[illegible]	[illegible]	[illegible]	[illegible]	[illegible]	[illegible]	[illegible]	[illegible]	[illegible]	[illegible]	[illegible]	[illegible]	[illegible]	[illegible]	[illegible]	[illegible]
Pile-up offset N_{PV} (JES) [%]	[illegible]	[illegible]	[illegible]	[illegible]	[illegible]	[illegible]	[illegible]	[illegible]	[illegible]	[illegible]	[illegible]	[illegible]	[illegible]	[illegible]	[illegible]	[illegible]	[illegible]	[illegible]	[illegible]	[illegible]	[illegible]	[illegible]	[illegible]	[illegible]	[illegible]	[illegible]	[illegible]	[illegible]	[illegible]	[illegible]	[illegible]	[illegible]	[illegible]
Pile-up offset p_T (JES) [%]	[illegible]	[illegible]	[illegible]	[illegible]	[illegible]	[illegible]	[illegible]	[illegible]	[illegible]	[illegible]	[illegible]	[illegible]	[illegible]	[illegible]	[illegible]	[illegible]	[illegible]	[illegible]	[illegible]	[illegible]	[illegible]	[illegible]	[illegible]	[illegible]	[illegible]	[illegible]	[illegible]	[illegible]	[illegible]	[illegible]	[illegible]	[illegible]	[illegible]
Pile-up offset ρ topology (JES) [%]	[illegible]	[illegible]	[illegible]	[illegible]	[illegible]	[illegible]	[illegible]	[illegible]	[illegible]	[illegible]	[illegible]	[illegible]	[illegible]	[illegible]	[illegible]	[illegible]	[illegible]	[illegible]	[illegible]	[illegible]	[illegible]	[illegible]	[illegible]	[illegible]	[illegible]	[illegible]	[illegible]	[illegible]	[illegible]	[illegible]	[illegible]	[illegible]	[illegible]
Jet vertex fraction [%]	[illegible]	[illegible]	[illegible]	[illegible]	[illegible]	[illegible]	[illegible]	[illegible]	[illegible]	[illegible]	[illegible]	[illegible]	[illegible]	[illegible]	[illegible]	[illegible]	[illegible]	[illegible]	[illegible]	[illegible]	[illegible]	[illegible]	[illegible]	[illegible]	[illegible]	[illegible]	[illegible]	[illegible]	[illegible]	[illegible]	[illegible]	[illegible]	[illegible]
b-Quark tagging efficiency (eigenvector 0) [%]	[illegible]	[illegible]	[illegible]	[illegible]	[illegible]	[illegible]	[illegible]	[illegible]	[illegible]	[illegible]	[illegible]	[illegible]	[illegible]	[illegible]	[illegible]	[illegible]	[illegible]	[illegible]	[illegible]	[illegible]	[illegible]	[illegible]	[illegible]	[illegible]	[illegible]	[illegible]	[illegible]	[illegible]	[illegible]	[illegible]	[illegible]	[illegible]	[illegible]
b-Quark tagging efficiency (eigenvector 1) [%]	[illegible]	[illegible]	[illegible]	[illegible]	[illegible]	[illegible]	[illegible]	[illegible]	[illegible]	[illegible]	[illegible]	[illegible]	[illegible]	[illegible]	[illegible]	[illegible]	[illegible]	[illegible]	[illegible]	[illegible]	[illegible]	[illegible]	[illegible]	[illegible]	[illegible]	[illegible]	[illegible]	[illegible]	[illegible]	[illegible]	[illegible]	[illegible]	[illegible]
b-Quark tagging efficiency (eigenvector 2) [%]	+1.67 −1.66	+1.52 −1.51	+1.33 −1.32	+1.16 −1.15	±0.97	+0.75 −0.74	±0.56	±0.40	±0.17	+1.52 −1.51	+1.39 −1.38	±1.12	±0.84	+0.57 −0.56	±0.33	±0.15	-	+1.39 −1.38	±1.37	+1.16 −1.15	+0.86 −0.85	+0.58 −0.57	±0.33	±0.16	-	+1.31 −1.30	±1.28	+1.10 −1.09	±0.81	±0.54	±0.31	-	∓0.20
b-Quark tagging efficiency (eigenvector 3) [%]	∓0.33	-	±0.15	±0.22	±0.22	±0.17	±0.10	-	∓0.10	∓0.29	-	±0.21	±0.24	±0.16	-	-	∓0.17	∓0.37	-	±0.15	±0.22	±0.16	-	-	∓0.18	∓0.29	-	+0.10 −0.11	±0.19	±0.14	-	-	∓0.19
b-Quark tagging efficiency (eigenvector 4) [%]	-	-	-	-	-	-	-	-	-	-	-	-	-	-	-	-	∓0.10	-	-	-	-	-	-	-	-	-	-	-	-	-	-	-	-
c-Quark tagging efficiency (eigenvector 0) [%]	±0.44	±0.27	±0.23	±0.20	±0.20	±0.19	±0.11	±0.13	±0.17	±0.41	±0.26	±0.22	±0.18	+0.17 −0.18	±0.16	±0.10	±0.19	±0.49	±0.33	±0.26	±0.21	±0.22	±0.18	+0.23 −0.22	±0.18	±0.47	±0.39	±0.32	±0.28	±0.24	±0.19	±0.17	±0.14
c-Quark tagging efficiency (eigenvector 1) [%]	-	∓0.13	∓0.21	∓0.27	−0.38 +0.39	∓0.50	∓0.52	−0.64 +0.65	−0.81 +0.82	-	∓0.14	∓0.26	∓0.39	∓0.52	∓0.71	∓0.87	−1.09 +1.10	±0.10	-	∓0.22	−0.37 +0.38	∓0.57	−0.77 +0.78	∓0.90	∓1.17	+0.10 −0.11	-	∓0.18	−0.41 +0.40	∓0.61	∓0.87	∓1.07	∓1.40
c-Quark tagging efficiency (eigenvector 2) [%]	±0.19	±0.12	-	-	-	-	∓0.11	−0.14 +0.15	∓0.28	±0.17	+0.11 −0.12	-	-	∓0.11	∓0.17	∓0.27	∓0.44	±0.13	±0.14	-	-	-	∓0.25	∓0.29	−0.48 +0.49	±0.17	±0.19	±0.10	-	∓0.10	∓0.27	−0.37 +0.36	∓0.61
Light-jet tagging efficiency (eigenvector 0) [%]	−0.46 +0.39	−0.49 +0.52	−0.42 +0.41	−0.65 +0.67	−0.92 +1.00	−0.90 +0.88	−0.96 +1.02	−1.70 +1.77	−1.88 +2.05	−0.47 +0.48	−0.58 +0.63	−0.59 +0.61	−0.82 +0.84	−1.04 +1.06	−1.37 +1.43	−1.88 +1.90	−2.17 +2.20	[illegible]	−0.41 +0.39	−0.64 +0.67	−0.96 +0.98	∓1.13	−1.79 +1.84	−1.91 +1.97	∓2.70	−0.58 +0.59	−0.55 +0.57	−0.61 +0.66	−0.81 +0.82	−1.20 +1.21	−1.81 +1.85	−2.19 +2.28	−2.88 +2.87
Light-jet tagging efficiency (eigenvector 1) [%]	±0.29	+0.21 −0.20	+0.18 −0.17	+0.21 −0.20	+0.26 −0.24	+0.11 −0.14	±0.11	±0.19	+0.20 −0.23	±0.26	±0.25	+0.23 −0.22	±0.18	±0.10	-	∓0.10	−0.24 +0.23	[illegible]	±0.27	±0.27	±0.27	+0.12 −0.11	+0.22 −0.21	-	−0.31 +0.30	±0.50	+0.41 −0.40	+0.29 −0.28	±0.28	±0.17	±0.13	-	∓0.34
Light-jet tagging efficiency (eigenvector 2) [%]	-	-	-	-	-	-	-	-	-	-	+0.12 −0.10	-	-	-	±0.17	±0.32	±0.18	[illegible]	-	-	-	-	-	±0.14	±0.23	-	-	-	-	-	±0.15	±0.13	±0.18
Light-jet tagging efficiency (eigenvector 3) [%]	-	-	-	-	∓0.15	∓0.18	∓0.17	∓0.44	−0.52 +0.53	±0.16	-	-	∓0.19	∓0.26	∓0.42	−0.50 +0.51	∓0.77	[illegible]	-	-	∓0.16	∓0.33	−0.47 +0.46	∓0.61	∓0.86	±0.31	±0.25	-	-	∓0.29	∓0.47	∓0.61	∓0.96
Light-jet tagging efficiency (eigenvector 5) [%]	-	-	-	-	-	-	-	−0.14 +0.15	-	-	-	-	∓0.10	∓0.11	∓0.12	∓0.13	-	-	-	-	−0.10 +0.11	∓0.15	∓0.21	∓0.11	-	-	-	-	-	∓0.13	∓0.19	-	-
Light-jet tagging efficiency (eigenvector 7) [%]	-	-	-	-	-	-	-	-	-	-	-	-	-	-	-	-	-	-	-	-	-	-	-	-	-	-	-	-	-	-	-	±0.12	-
Light-jet tagging efficiency (eigenvector 8) [%]	-	-	-	-	-	-	-	∓0.10	∓0.12	-	-	-	-	-	-	∓0.17	∓0.25	-	-	-	-	-	-	∓0.20	∓0.41	-	-	-	-	-	-	∓0.13	−0.40 +0.39
b-Quark tagging extrapolation [%]	-	-	-	-	-	±0.22	±0.47	±0.77	±1.28	-	-	-	-	±0.25	±0.59	±1.02	+1.80 −1.79	-	-	-	-	±0.20	±0.59	±0.97	+1.71 −1.70	-	-	-	-	±0.20	±0.53	+0.98 −0.99	+1.82 −1.81
b-Quark tagging extrapolation from c-Quark [%]	-	-	-	-	-	-	±0.10	±0.13	-	-	-	-	-	-	-	-	-	-	-	-	-	-	-	-	-	-	-	-	-	-	-	-	-
Electron energy resolution [%]	-	-	-	-	-	-	-	-	-	-	-	-	-	-	-	-	-	-	-	-	-	-	-	-	-	-	-	-	-	-	-	-	-
Electron energy scale [%]	-	-	-	-	+0.12 -	+0.18 -	+0.11 −0.26	+0.29 −0.18	+0.31 −0.38	-	-	-	- −0.12	+0.15 -	+0.14 −0.26	+0.34 −0.32	+0.43 −0.25	-	-	-	-	-	+0.21 −0.22	- −0.13	- −0.30	-	-	-	-	-	+0.11 -	+0.19 −0.12	+0.29 −0.26
Electron trigger efficiency [%]	±0.12	±0.12	±0.11	+0.11 −0.12	±0.12	±0.13	+0.14 −0.13	±0.15	±0.15	±0.12	±0.11	±0.11	±0.11	±0.12	±0.13	±0.14	±0.17	±0.12	±0.11	±0.11	±0.11	±0.11	±0.12	±0.13	±0.15	+0.11 −0.12	±0.11	±0.11	±0.11	±0.11	±0.12	±0.13	±0.15
Electron reconstruction efficiency [%]	-	-	-	-	-	±0.10	+0.11 −0.10	±0.11	±0.12	-	-	-	-	-	±0.11	±0.11	±0.13	-	-	-	-	-	±0.10	±0.11	±0.12	-	-	-	-	-	-	±0.10	±0.12
Electron identification efficiency [%]	±0.33	±0.36	±0.40	±0.44	±0.49	±0.55	+0.61 −0.62	±0.67	±0.77	±0.33	±0.36	+0.41 −0.42	±0.48	±0.54	±0.61	±0.68	±0.83	±0.33	±0.35	+0.40 −0.39	+0.46 −0.45	±0.51	+0.57 −0.58	±0.64	±0.75	±0.34	±0.36	±0.40	±0.45	±0.51	±0.55	±0.63	±0.75
Electron isolation efficiency [%]	-	-	-	±0.11	±0.16	±0.22	±0.28	±0.32	±0.46	-	-	±0.10	+0.17 −0.16	±0.24	±0.32	±0.37	±0.50	-	-	-	±0.15	+0.23 −0.22	±0.30	±0.36	±0.44	-	-	±0.10	±0.16	±0.23	±0.28	±0.34	±0.45
Muon (ID) momentum resolution [%]	-	-	-	-	-	-	-	−0.25	-	-	-	-	-	-	-	-	-	-	-	-	-	-	-	−0.27	+0.25	-	-	-	-	-	-	-	-
Muon (MS) momentum resolution [%]	-	-	-	-	-	-	-	-	-	-	-	-	-	-	-	−0.22	+0.21	-	-	-	-	-	-	-	-	-	-	-	-	-	−0.10 +0.11	-	-
Muon trigger efficiency stat [%]	±0.30	+0.29 −0.30	±0.29	+0.29 −0.30	±0.30	+0.30 −0.31	+0.31 −0.32	±0.33	+0.32 −0.33	±0.29	±0.28	±0.28	+0.28 −0.29	±0.29	±0.29	±0.30	±0.31	+0.28 −0.29	+0.28 −0.29	±0.28	±0.28	±0.28	±0.30	+0.30 −0.31	+0.31 −0.32	±0.28	±0.28	+0.27 −0.28	±0.28	+0.27 −0.28	±0.28	+0.28 −0.29	+0.29 −0.30
Muon trigger efficiency syst [%]	+0.52 −0.51	+0.51 −0.50	+0.51 −0.50	+0.52 −0.51	+0.53 −0.52	+0.55 −0.53	+0.56 −0.55	+0.58 −0.57	+0.60 −0.58	+0.51 −0.50	+0.50 −0.49	+0.50 −0.49	+0.51 −0.49	+0.52 −0.51	+0.53 −0.52	+0.56 −0.54	+0.56 −0.55	+0.49 −0.48	+0.50 −0.49	+0.49 −0.48	+0.50 −0.49	+0.51 −0.50	+0.54 −0.53	+0.54 −0.53	+0.55 −0.54	+0.51 −0.49	+0.50 −0.49	+0.49 −0.48	+0.49 −0.48	+0.50 −0.49	+0.51 −0.50	+0.51 −0.50	+0.54 −0.53
Muon identification stat [%]	-	-	-	-	±0.10	±0.10	±0.10	±0.11	±0.11	-	-	-	-	±0.10	±0.10	±0.10	±0.10	-	-	-	-	-	±0.10	±0.10	±0.11	-	-	-	-	-	-	-	±0.10
Muon identification syst [%]	±0.35	±0.34	±0.36	±0.39	±0.43	±0.47	±0.52	±0.57	+0.64 −0.63	±0.33	±0.34	+0.36 −0.37	±0.41	+0.47 −0.46	+0.52 −0.51	±0.57	±0.63	±0.32	±0.33	+0.36 −0.35	±0.39	±0.44	±0.50	±0.54	+0.64 −0.63	±0.33	±0.34	±0.35	±0.38	±0.42	±0.47	±0.51	±0.59
Muon isolation efficiency syst [%]	±0.11	±0.10	±0.10	±0.11	±0.11	±0.11	±0.12	±0.12	±0.13	±0.10	±0.10	±0.10	±0.10	±0.11	±0.11	±0.12	±0.13	±0.10	±0.10	±0.10	±0.10	+0.10 −0.11	±0.11	±0.11	±0.13	±0.10	±0.10	±0.10	±0.10	±0.10	±0.11	±0.11	±0.13
E_T^{miss} Soft jet resolution para [%]	±0.73	±0.10	∓0.24	∓0.32	∓0.29	∓0.32	∓0.13	∓0.92	∓0.15	±0.79	-	∓0.20	∓0.48	∓0.16	∓0.46	∓0.56	∓0.46	±1.15	±0.26	∓0.18	±0.26	∓0.31	∓0.54	±0.34	∓1.09	±0.86	±0.20	±0.15	∓0.26	∓0.43	∓0.54	±0.19	∓0.20
E_T^{miss} Soft jet resolution perp [%]	±0.70	-	∓0.17	∓0.19	∓0.35	∓0.38	∓0.43	∓0.24	∓0.32	±0.66	-	∓0.20	∓0.35	∓0.35	∓0.54	∓0.39	∓0.54	±0.84	±0.32	-	∓0.39	∓0.25	∓0.39	-	∓0.70	±0.98	±0.40	-	∓0.31	∓0.21	∓0.76	±0.41	∓0.47
E_T^{miss} Soft jet scale [%]	+0.76 −0.70	-	−0.20 +0.19	−0.27 +0.29	∓0.35	−0.30 +0.33	−0.47 +0.29	−0.55 +0.56	−0.25 +0.37	+0.80 −0.73	-	−0.26 +0.28	−0.42 +0.46	−0.32 +0.38	−0.46 +0.57	−0.55 +0.24	−0.42 +0.46	+1.13 −0.89	+0.31 −0.39	- +0.12	−0.40 +0.31	−0.39 +0.42	−0.47 +0.62	−0.20 +0.39	−0.52 +0.47	+0.97 −1.05	+0.36 −0.56	-	−0.35 +0.30	- +0.27	−0.68 +0.30	+0.74 -	−0.79 +0.55
Luminosity [%]	∓2.05	∓2.05	∓2.05	∓2.05	∓2.05	∓2.05	∓2.05	∓2.05	∓2.05	∓2.05	∓2.05	∓2.05	∓2.05	∓2.05	∓2.05	∓2.05	∓2.05	∓2.05	∓2.05	∓2.05	∓2.05	∓2.05	∓2.05	∓2.05	∓2.05	∓2.05	∓2.05	∓2.05	∓2.05	∓2.05	∓2.05	∓2.05	∓2.05
Z+jets cross-section [%]	±0.81	±0.55	±0.57	±0.64	±0.77	±0.76	±0.95	±1.00	±1.16	±0.46	±0.34	±0.38	±0.48	±0.60	±0.75	±0.93	±1.21	±0.52	±0.28	±0.27	±0.36	±0.50	±0.67	±0.82	±1.06	±0.36	±0.26	±0.25	±0.34	±0.42	±0.58	±0.70	±0.90
Monte Carlo sample statistics [%]	±0.38	±0.21	±0.34	±0.30	±0.41	±0.54	±1.03	±1.34	±1.63	±0.33	±0.30	±0.29	±0.38	±0.59	±0.95	±1.47	±1.86	±1.57	±0.38	±0.38	±0.49	±0.70	±1.09	±1.65	±2.16	±0.93	±0.66	±0.52	±0.60	±0.81	±1.16	±1.65	±2.33
ISR/FSR + scale [%]	- +2.04	−0.39 +0.71	−0.52 +1.26	−1.94 +1.07	−1.05 +0.66	+0.43 -	+2.03 -	−0.86 +0.68	−0.52 +0.11	+1.41 -	−0.28 +1.98	+1.57 -	−0.20 +0.67	−1.21 +0.79	- −1.47	+1.69 -	−0.13 +3.64	- −2.37	−0.16 +0.11	+0.20 −1.01	- −1.02	−0.66 +0.22	+1.34 −2.65	- −3.74	−2.75 +0.12	+2.90 -	+0.85 −0.74	+0.80 −0.83	+0.70 −0.57	+1.73 -	±4.94	+3.02 −0.90	+5.54 -
Alternate hard-scattering model [%]	±7.08	±1.22	∓0.16	±0.24	∓0.40	±0.50	∓2.52	∓1.23	∓2.32	±11.6	±3.12	±2.24	±2.38	±0.91	-	∓0.13	±9.06	±11.4	±5.36	±2.68	±5.55	±5.77	±1.43	-	±1.46	±13.7	±12.3	±8.30	±4.47	±6.88	±0.28	±2.25	±13.9
Alternate parton-shower model [%]	∓1.68	∓0.48	∓0.91	∓1.61	∓1.71	∓0.34	±1.10	∓2.05	∓5.06	±3.63	±4.26	±4.25	±2.45	±2.17	±1.60	∓0.21	±2.71	±2.69	±5.14	±4.63	±5.07	±2.54	±4.72	±4.62	±7.65	±10.8	±9.90	±8.88	±6.07	±4.82	±4.15	±8.60	±3.75
Inter PDF [%]	-	-	-	-	-	±0.11	-	-	-	-	-	-	-	-	∓0.42	±0.13	∓0.20	±0.11	∓0.14	-	-	-	-	∓0.24	-	±0.13	∓0.10	-	-	-	-	-	±0.51
Intra PDF [%]	-	-	±0.17	±0.32	±0.36	±0.56	±0.38	±0.44	±0.54	±0.11	±0.27	±0.15	±0.29	±0.16	±2.23	±1.09	±1.70	±0.63	±0.54	±0.14	±0.13	±0.23	±0.52	±1.62	±1.15	±1.09	±0.30	±0.75	±0.25	±0.56	±0.56	±0.65	±3.17
Fakes overall normalization, el [%]	±1.16	±0.65	±0.62	±0.84	±0.83	±1.10	+1.73 −1.72	±0.99	±2.79	±0.73	±0.34	±0.29	±0.55	±0.53	±0.56	±1.24	±2.68	±0.92	±0.34	±0.25	±0.45	±0.24	±0.75	±1.58	±2.86	±0.70	±0.40	±0.17	±0.57	±0.19	±0.32	±0.54	±1.38
Fakes overall normalization, mu [%]	±0.21	±0.14	±0.18	-	-	∓0.21	∓0.22	∓0.29	∓0.63	±0.11	-	-	∓0.11	∓0.32	∓0.52	∓0.52	∓0.52	-	-	-	∓0.10	∓0.48	∓0.45	∓0.45	∓0.85	∓0.17	-	∓0.18	∓0.25	∓0.34	∓0.46	∓0.76	∓0.67
Fakes alternative parametrization [%]	∓4.93	∓3.23	∓2.42	∓2.15	∓1.64	∓1.21	∓0.85	±0.40	∓1.11	∓4.06	∓2.70	∓1.51	∓0.97	∓0.82	∓0.22	±0.15	∓0.93	∓5.54	∓3.05	∓1.99	∓0.89	-	-	∓1.29	∓0.57	∓3.25	∓2.99	∓2.16	∓1.40	∓0.37	∓0.27	±0.74	∓0.27
W+jets heavy flavour component [%]	±7.68	±3.76	±2.78	±3.20	±4.92	±3.31	±3.15	±1.48	±9.57	±5.40	±2.93	±2.79	±2.29	±6.66	±3.29	±2.48	±1.72	±10.0	±1.30	-	±0.42	±3.04	±0.99	±1.51	±2.58	±5.11	±2.72	±1.85	±4.47	±1.54	±0.48	±4.78	±3.95

TABLE F.9: Table of systematics for the absolute differential cross-section at the particle level for the $m_{t\bar{t}}$ in bins of jet multiplicity observable.

Bins [GeV] x	0–30	30–65	65–120	120–190	190–270	270–800	800–840	840–910	910–1000	1000–1110	1110–1325	1325–1600	1600–1640	1640–1710	1710–1800	1800–1910	1910–2020	2020–2400	2400–2440	2440–2510	2510–2600	2600–2710	2710–3200
dσ / d$p_T^{tt} vsN.jets$ [pb/GeV x]	$7.36 \cdot 10^{-1}$	$4.74 \cdot 10^{-1}$	$8.66 \cdot 10^{-2}$	$1.41 \cdot 10^{-2}$	$2.60 \cdot 10^{-3}$	$8.12 \cdot 10^{-5}$	$1.31 \cdot 10^{-1}$	$1.96 \cdot 10^{-1}$	$5.56 \cdot 10^{-2}$	$1.25 \cdot 10^{-2}$	$2.32 \cdot 10^{-3}$	$2.14 \cdot 10^{-4}$	$3.11 \cdot 10^{-2}$	$6.93 \cdot 10^{-2}$	$3.73 \cdot 10^{-2}$	$1.07 \cdot 10^{-2}$	$3.05 \cdot 10^{-3}$	$4.60 \cdot 10^{-4}$	$1.06 \cdot 10^{-2}$	$2.67 \cdot 10^{-2}$	$2.27 \cdot 10^{-2}$	$9.55 \cdot 10^{-3}$	$1.19 \cdot 10^{-3}$
Total Uncertainty [%]	+12.2/−12.7	+9.82/−10.1	+12.6/−12.4	+11.0/−9.64	+11.0/−10.5	+17.3/−17.4	+15.8/−15.4	±13.1	+8.61/−8.32	+8.53/−8.25	+9.08/−8.92	+13.8/−15.8	+21.4/−21.1	+18.3/−18.0	+12.1/−11.6	+9.51/−9.14	+9.88/−10.2	+11.1/−10.5	+30.1/−26.5	+27.9/−25.7	+19.6/−19.9	+17.6/−16.9	+15.0/−14.7
Statistics [%]	±0.2	±0.1	±0.5	±1.2	±2.6	±6.0	±0.4	±0.2	±0.5	±1.0	±1.6	±4.8	±0.8	±0.4	±0.6	±1.0	±2.1	±2.8	±1.5	±0.7	±0.8	±1.1	±1.4
Systematics [%]	+12.2/−12.7	+9.82/−10.0	+12.6/−12.3	+10.9/−9.50	+10.5/−10.1	+15.9/−16.0	+15.7/−15.4	±13.1	+8.59/−8.30	+8.45/−8.16	+8.87/−8.70	+12.7/−14.9	+21.4/−21.0	+18.3/−18.0	+12.1/−11.5	+9.43/−9.06	+9.57/−9.99	+10.6/−10.0	+30.0/−26.5	+27.9/−25.6	+19.6/−19.8	+17.6/−16.8	+14.9/−14.6
Jet energy resolution [%]	∓0.35	-	±2.02	±1.43	±3.31	±0.52	±2.40	±1.48	±0.33	±0.84	±1.04	∓2.42	±2.03	±1.21	-	∓1.18	-	±3.38	±3.16	±5.59	±1.81	±1.86	±4.02
b-Tagged jet energy scale (JES) [%]	+0.52/−0.51	+0.47/−0.50	+0.47/−0.45	+0.44/−0.40	+0.31/−0.34	+0.20/−0.25	+0.42/−0.43	+0.51/−0.53	±0.52	+0.40/−0.46	+0.41/−0.33	+0.20/−0.32	+0.56/−0.43	+0.57/−0.60	±0.54	+0.48/−0.52	+0.21/−0.46	+0.38/−0.18	+0.57/−0.78	+0.73/−0.62	+0.47/−0.54	+0.63/−0.51	+0.42/−0.34
Effective detector NP set 1 (JES) [%]	-	-	-	-	-/+0.17	+0.24/-	-	-	-	-	±0.14	-	-	-	+0.12/−0.10	-	+0.15/-	+0.29/−0.23	+0.31/−0.13	+0.21/−0.16	-/−0.20	+0.13/-	-/−0.18
Effective detector NP set 2 (JES) [%]	-	-	-	-	-	-/+0.22	-	-	-	-	-/−0.16	−0.12/+0.35	-	-	-	-	+0.15/-	-	-	-	-	-	-
Effective mixed NP set 1 (JES) [%]	-	-	-	−0.14/-	−0.14/+0.17	-/+0.46	+0.11/-	+0.13/−0.10	+0.21/−0.28	+0.51/−0.46	+1.16/−0.96	+2.21/−2.43	+0.16/−0.20	+0.17/−0.18	+0.30/−0.31	+0.67/−0.36	+0.31/−0.77	+1.94/−1.50	+0.36/-	+0.30/−0.21	+0.26/−0.52	+0.54/−0.29	+0.96/−0.94
Effective mixed NP set 2 (JES) [%]	-	-	-	-	-	-	-	-	-	-	−0.13/-	−0.19/-	-	-	-	-	-	−0.19/+0.17	-	-	-	-	-
Effective mixed NP set 3 (JES) [%]	-	-	-	-	-	-	-	-	-	-	-	-	-	-	-	-	-	-	-	-	-	-	-
Effective modelling NP set 1 (JES) [%]	+0.93/−0.89	+0.59/−0.76	-/−0.31	-	−0.41/+0.33	−0.35/+2.69	+5.01/−4.57	+3.03/−2.95	+0.92/−1.20	+0.57/−0.48	+0.31/-	−1.36/+0.31	+7.74/−7.25	+6.12/−5.90	+4.02/−3.52	+2.45/−2.01	+1.12/−1.73	+0.86/−1.00	+11.2/−8.70	+9.47/−7.90	+6.66/−6.76	+5.39/−4.85	+4.16/−3.83
Effective modelling NP set 2 (JES) [%]	-	-	-	-	+0.16/−0.12	+0.59/-	−0.50/+0.52	−0.28/+0.30	-	+0.15/-	+0.30/−0.43	+1.34/−1.40	−0.85/+0.71	−0.61/+0.63	−0.15/+0.14	-	-/−0.18	+1.11/−0.91	−0.82/+0.72	−0.83/+0.96	−0.61/+0.51	−0.33/+0.35	+0.16/-
Effective modelling NP set 3 (JES) [%]	-	-	-	-	-/+0.17	+0.21/-	±0.37	+0.21/−0.18	−0.16/+0.13	−0.15/+0.21	−0.36/+0.30	−0.46/+0.18	+0.54/−0.65	+0.42/−0.41	-	−0.14/+0.27	−0.12/+0.23	−0.32/+0.40	+0.69/−0.37	+0.66/−0.55	+0.23/−0.36	-	−0.19/-
Effective modelling NP set 4 (JES) [%]	-	-	-	-	-/+0.16	+0.45/-	+0.19/−0.20	+0.17/−0.15	-	-	±0.10	-	+0.32/−0.34	±0.26	±0.20	+0.18/−0.12	+0.23/-	+0.17/−0.22	+0.43/−0.32	+0.44/−0.38	+0.33/−0.40	+0.29/−0.21	+0.17/−0.26
Effective statistical NP set 1 (JES) [%]	+0.15/−0.12	+0.13/−0.12	-	-	−0.22/+0.30	−0.11/+0.87	+0.83/−0.87	+0.54/−0.52	+0.14/−0.12	-	+0.22/−0.21	-	+1.32/−1.35	+1.06/−1.10	+0.67/−0.64	+0.28/-	+0.23/−0.20	+0.49/−0.43	+1.62/−1.29	+1.60/−1.43	+1.09/−1.25	+0.98/−0.80	+0.61/−0.75
Effective statistical NP set 2 (JES) [%]	−0.11/+0.13	−0.10/+0.12	-	-	+0.28/−0.14	+0.76/−0.10	−0.76/+0.74	−0.47/+0.48	−0.10/+0.13	−0.13/+0.10	+0.17/−0.25	+0.54/−0.28	−1.16/+1.18	−0.95/+0.94	−0.54/+0.57	−0.15/+0.23	−0.12/+0.22	+0.20/−0.21	−1.21/+1.44	−1.26/+1.36	−1.11/+0.99	−0.76/+0.87	−0.42/+0.33
Effective statistical NP set 3 (JES) [%]	-	-	-	-	-	-	-	-	-	-	−0.74/+0.67	−0.68/+0.53	-	-	-	-	−0.35/+0.28	−0.72/+0.76	-	+0.14/-	-	-	−0.33/+0.26
Effective statistical NP set 4 (JES) [%]	-	-	-	-	-	-	−0.10/+0.12	-	+0.20/−0.19	+0.21/−0.25	-	−0.45/+0.11	−0.18/+0.19	-	±0.14	+0.29/−0.20	-	-	+0.31/-	-	-	+0.11/−0.16	-
Effective statistical NP set 5 (JES) [%]	-	-	-	-	-	-	-	-	−0.12/+0.11	+0.25/−0.18	+0.25/−0.28	−0.31/+0.12	-	-	−0.14/-	+0.18/-	+0.28/−0.23	−0.14/+0.19	-/+0.21	−0.10/+0.11	−0.15/+0.13	-	-
Effective statistical NP set 6 (JES) [%]	-	-	-	-	-/+0.18	-/+0.24	+0.11/-	±0.14	-	-	+0.25/−0.29	−0.39/+0.31	+0.19/−0.23	+0.19/−0.18	-	-	+0.23/−0.16	-	+0.26/−0.22	+0.31/−0.29	+0.10/−0.16	-	-/−0.16
Effective statistical NP set 7 (JES) [%]	-	-	-	-	-/+0.17	-/+0.31	±0.17	+0.12/-	-	+0.11/−0.13	+0.17/−0.28	-/+0.18	+0.19/−0.23	+0.17/−0.18	+0.12/−0.15	+0.22/−0.11	+0.18/−0.14	+0.29/−0.23	+0.36/−0.21	+0.33/−0.25	+0.20/−0.29	+0.24/−0.19	+0.16/−0.23
η intercalibration model (JES) [%]	+0.35/−0.37	-	−0.23/+0.18	-	−0.70/+0.12	+1.08/-	+1.10/−1.05	+0.91/−0.92	+0.47/−0.44	+0.40/−0.28	+0.62/−0.32	-	+1.91/−2.12	+1.68/−1.77	+1.19/−1.15	+1.01/−0.88	+0.82/−1.10	+1.06/−1.26	+2.67/−2.35	+2.42/−2.26	+2.00/−2.32	+1.54/−1.47	+1.67/−1.59
η intercalibration non closure (JES) [%]	−0.14/+0.15	-	-	−0.19/-	-/−0.37	+0.53/-	−0.46/+0.45	−0.35/+0.32	−0.22/+0.16	−0.41/+0.40	−0.23/+0.45	−0.18/+0.42	−0.80/+0.60	−0.54/+0.65	−0.45/+0.39	−0.40/+0.59	−0.69/+0.65	−0.67/+0.57	−0.65/+0.94	−0.67/+1.07	−1.01/+0.66	−0.58/+0.78	−0.72/+0.58
η intercalibration total stat (JES) [%]	+0.22/−0.20	+0.11/-	-	-	−0.31/+0.30	+0.95/-	±0.73	+0.58/−0.59	+0.24/−0.21	+0.18/−0.12	+0.25/−0.20	-/−0.42	+1.18/−1.26	+1.10/−1.14	+0.81/−0.79	+0.40/−0.28	+0.35/−0.30	+0.43/−0.19	+1.56/−1.28	+1.68/−1.36	+1.19/−1.42	+0.97/−0.92	+0.73/−0.79
Flavour composition (JES) [%]	+0.99/−1.03	−0.42/+0.45	−1.93/+1.75	−0.93/+0.82	−1.12/+1.99	−0.22/+3.34	+4.72/−5.26	+2.92/−3.13	+0.51/−0.67	−0.30/+0.31	+0.35/-	-/−1.00	+8.08/−8.73	+6.64/−6.90	+4.00/−3.94	+2.29/−2.16	+0.73/−1.74	+1.00/−1.13	+11.8/−10.6	+10.1/−9.41	+7.57/−8.31	+6.30/−6.15	+4.65/−4.67
Flavour response (JES) [%]	∓0.45	+0.36/−0.35	+1.22/−1.20	+0.50/−0.75	+0.49/−1.02	+2.25/-	−2.63/+2.47	−1.58/+1.55	−0.38/+0.34	-	+0.14/−0.16	+0.42/−1.42	−4.70/+4.21	−3.62/+3.49	−2.05/+2.17	−0.99/+1.40	−1.13/+0.65	−0.28/+0.59	−5.21/+6.09	−5.06/+5.29	−4.52/+3.87	−3.24/+3.17	−2.45/+2.44
Pile-up offset μ (JES) [%]	-	-	-	-	−0.18/-	+0.38/-	−0.34/+0.28	−0.21/+0.22	-	-	-	-/−0.47	−0.31/+0.40	−0.37/+0.36	−0.20/+0.16	−0.19/+0.23	-	+0.25/-	−0.49/+0.63	−0.40/+0.62	−0.59/+0.37	−0.37/+0.47	−0.24/+0.16
Pile-up offset N_{PV} (JES) [%]	+0.22/−0.14	+0.10/−0.16	-	-/−0.30	−0.53/+1.03	+1.05/-	+0.76/−0.68	+0.60/−0.62	+0.32/−0.49	-	+0.10/−0.34	-/−0.17	+1.70/−1.60	+1.25/−1.31	+1.16/−0.79	+0.78/−0.31	+0.25/−0.21	+0.41/−0.11	+3.17/−2.32	+2.40/−1.42	+1.08/−1.54	+1.32/−0.96	+1.02/−0.99
Pile-up offset p_T (JES) [%]	-	-	−0.13/+0.14	-	-	-	−0.49/+0.48	-	+0.43/−0.48	+0.67/−0.48	+0.65/−0.49	+0.63/−1.08	−0.54/+0.59	−0.27/+0.29	+0.27/−0.32	+0.51/−0.36	+0.33/−0.62	+0.80/−0.86	−0.30/+0.81	−0.39/+0.58	-/−0.23	+0.28/−0.31	+0.54/−0.47
Pile-up offset ρ topology (JES) [%]	+1.32/−1.28	+0.92/−1.16	+0.17/−0.60	-/−0.24	-/+0.83	−0.51/+3.31	+6.97/−6.57	+4.50/−4.55	+1.66/−1.95	+0.45/−0.54	+0.41/-	−1.47/+0.18	+11.3/−10.3	+9.31/−8.55	+5.98/−5.30	+3.70/−3.37	+1.41/−2.28	+0.91/−0.79	+15.5/−12.8	+13.8/−11.3	+10.7/−10.0	+8.63/−7.83	+6.07/−5.52
Jet vertex fraction [%]	+0.49/−0.53	+0.46/−0.51	+0.38/−0.42	+0.33/−0.38	+0.27/−0.32	+0.23/−0.28	+1.16/−1.19	+0.85/−0.88	+0.42/−0.47	+0.26/−0.31	+0.18/−0.23	-	+1.56/−1.58	+1.28/−1.30	+0.87/−0.90	+0.59/−0.63	+0.43/−0.47	+0.28/−0.33	+1.86/−1.87	+1.73/−1.74	+1.41/−1.44	+1.14/−1.17	+0.88/−0.92
b-Quark tagging efficiency (eigenvector 0) [%]	−6.81/+7.07	−6.71/+6.93	−6.61/+6.79	−6.65/+6.83	−6.58/+6.76	−6.53/+6.72	−6.45/+6.63	−6.34/+6.51	−6.25/+6.41	−6.18/+6.34	−6.11/+6.26	−5.92/+6.06	−6.11/+6.26	−6.07/+6.22	−6.00/+6.15	−5.89/+6.03	−5.78/+5.91	−5.92/+6.07	−5.75/+5.86	−5.69/+5.80	−5.60/+5.70	−5.51/+5.62	−5.25/+5.35
b-Quark tagging efficiency (eigenvector 1) [%]	−1.95/+1.98	−1.97/+1.99	−2.05/+2.07	−2.29/+2.31	−2.54/+2.57	−2.97/+3.01	−1.91/+1.93	−1.89/+1.91	−1.90/+1.91	−2.29/+2.30	−2.90/+2.93	−3.70/+3.75	−1.82/+1.83	−1.81/+1.83	−1.89/+1.91	−2.16/+2.18	−2.54/+2.56	−3.28/+3.33	−1.63/+1.65	−1.68/+1.70	−1.83/+1.84	−2.09/+2.11	−2.66/+2.68
b-Quark tagging efficiency (eigenvector 2) [%]	+1.35/−1.34	+1.32/−1.31	+1.26/−1.25	±1.17	±1.04	±0.79	±1.28	+1.20/−1.19	+1.11/−1.10	±1.04	±0.71	-	+1.18/−1.17	+1.13/−1.12	+1.05/−1.04	±0.94	±0.75	±0.30	+1.04/−1.03	±1.02	±0.94	+0.85/−0.84	±0.47
b-Quark tagging efficiency (eigenvector 3) [%]	-	-	-	-	-	-	-	-	-	±0.12	±0.13	∓0.12	-	-	-	±0.10	±0.12	-	-	-	-	-	-
c-Quark tagging efficiency (eigenvector 0) [%]	+0.26/−0.25	±0.27	±0.29	±0.29	±0.26	+0.16/−0.15	±0.24	±0.26	±0.32	+0.27/−0.26	±0.22	-	±0.35	±0.28	±0.28	±0.24	±0.23	±0.17	±0.41	±0.36	±0.30	±0.28	±0.22
c-Quark tagging efficiency (eigenvector 1) [%]	−0.19/+0.20	∓0.23	−0.27/+0.28	∓0.32	∓0.34	∓0.35	−0.22/+0.21	∓0.23	−0.22/+0.21	∓0.25	∓0.28	∓0.45	∓0.31	∓0.29	∓0.22	∓0.21	∓0.27	∓0.32	∓0.41	∓0.40	∓0.33	∓0.26	∓0.34
c-Quark tagging efficiency (eigenvector 2) [%]	-	-	-	-	-	-	-	-	±0.10	-	-	-	-	-	-	-	-	-	-	-	-	-	-
Light-jet tagging efficiency (eigenvector 0) [%]	−0.55/+0.58	−0.58/+0.57	−0.78/+0.80	−1.12/+1.25	−0.71/+0.72	−0.94/+0.95	−0.80/+0.88	−0.63/+0.65	∓0.68	−0.69/+0.71	−0.75/+0.78	−0.75/+0.77	−0.95/+0.98	−0.69/+0.65	∓0.72	−0.75/+0.78	−0.93/+0.96	−0.47/+0.48	−1.14/+1.20	−1.09/+1.12	−0.95/+0.97	−0.69/+0.72	∓0.67
Light-jet tagging efficiency (eigenvector 1) [%]	±0.19	+0.24/−0.23	+0.32/−0.31	+0.17/−0.18	-	-	+0.30/−0.29	+0.20/−0.19	±0.25	±0.21	±0.28	+0.14/−0.13	±0.32	±0.21	±0.23	±0.25	+0.27/−0.26	±0.12	±0.31	±0.30	±0.30	+0.23/−0.22	+0.19/−0.20
Light-jet tagging efficiency (eigenvector 2) [%]	-	-	-	±0.17	-	±0.13	±0.11	-	-	-	-	±0.16	-	-	-	-	+0.16/−0.15	-	-	-	-	-	-
Light-jet tagging efficiency (eigenvector 3) [%]	-	-	-	−0.16/+0.18	∓0.13	∓0.20	-	-	-	-	-	-	∓0.10	−0.15/+0.14	-	-	-	-	−0.11/+0.12	-	-	-	-
Light-jet tagging efficiency (eigenvector 5) [%]	-	-	-	-	-	-	-	-	-	-	-	∓0.10	-	-	-	-	-	-	-	-	-	-	-
Light-jet tagging efficiency (eigenvector 7) [%]	-	-	-	+0.15/−0.14	-	-	-	-	-	-	-	-	-	-	-	-	-	-	-	-	-	-	-
Light-jet tagging efficiency (eigenvector 8) [%]	-	-	-	+0.14/−0.13	-	-	-	-	-	-	-	-	-	-	-	-	-	-	-	-	-	-	-
Light-jet tagging efficiency (eigenvector 9) [%]	-	-	-	−0.12/+0.13	-	-	-	-	-	-	-	-	-	-	-	-	-	-	-	-	-	-	-
b-Quark tagging extrapolation [%]	-	-	-	±0.10	±0.17	±0.34	-	-	-	±0.12	±0.12	+0.91/−0.93	-	-	-	-	±0.13	±0.59	-	-	±0.10	±0.10	±0.34
b-Quark tagging extrapolation from *c*-Quark [%]	-	-	-	-	-	-	-	-	-	-	-	±0.12	-	-	-	-	-	-	-	-	-	-	-
Electron energy scale [%]	-	-	-	-	-	-	-	-	-	-	-	-	-	-	-	-	-	-	-	-	-	-	-
Electron trigger efficiency [%]	±0.12	±0.12	±0.12	±0.12	±0.12	±0.12	+0.11/−0.12	±0.11	+0.11/−0.12	±0.12	±0.12	±0.12	±0.11	±0.11	±0.11	±0.11	±0.11	±0.11	±0.11	±0.11	±0.11	±0.11	±0.11
Electron reconstruction efficiency [%]	-	-	-	-	-	±0.10	-	-	-	-	±0.10	±0.11	-	-	-	-	-	±0.10	-	-	-	-	-
Electron identification efficiency [%]	+0.41/−0.40	±0.41	±0.42	±0.46	±0.48	±0.53	+0.38/−0.39	±0.39	±0.43	±0.48	+0.56/−0.55	±0.67	±0.38	±0.39	±0.42	±0.47	±0.51	±0.58	±0.38	±0.39	+0.43/−0.42	+0.47/−0.46	±0.55
Electron isolation efficiency [%]	-	-	±0.10	±0.13	±0.17	±0.26	-	-	±0.12	±0.17	±0.28	±0.45	-	-	±0.12	+0.18/−0.17	±0.24	±0.39	-	-	±0.12	±0.17	±0.33
Muon (ID) momentum resolution [%]	-	-	-	-	-	-	-	-	-	-	-	-	-	-	-	-	-	-	-	-	-	-	-
Muon (MS) momentum resolution [%]	-	-	-	-	-	-/+0.18	-	-	-	-	-	-	-	-	-	-	-	-	-	-	-	-	-
Muon trigger efficiency stat [%]	±0.30	+0.29/−0.30	+0.28/−0.29	±0.30	+0.30/−0.31	+0.29/−0.30	+0.28/−0.29	+0.28/−0.29	+0.28/−0.29	+0.29/−0.30	+0.28/−0.29	+0.27/−0.28	+0.28/−0.29	+0.28/−0.29	±0.28	+0.28/−0.29	±0.28	+0.28/−0.29	+0.28/−0.29	±0.28	±0.28	±0.28	±0.26
Muon trigger efficiency syst [%]	+0.52/−0.51	+0.52/−0.51	+0.52/−0.51	+0.53/−0.52	+0.53/−0.52	+0.53/−0.52	+0.50/−0.49	+0.51/−0.49	+0.51/−0.50	+0.52/−0.51	+0.51/−0.50	+0.46/−0.45	+0.51/−0.50	+0.50/−0.49	+0.50/−0.49	+0.50/−0.49	+0.49/−0.48	+0.50/−0.49	+0.51/−0.50	+0.51/−0.50	+0.50/−0.49	+0.49/−0.48	+0.47/−0.46
Muon identification stat [%]	±0.10	-	-	±0.10	-	-	-	-	-	-	-	-	-	-	-	-	-	-	±0.10	-	-	-	-
Muon identification syst [%]	±0.38	±0.37	±0.37	±0.40	±0.41	±0.44	±0.36	±0.36	±0.38	±0.41	±0.44	±0.48	±0.36	±0.36	+0.38/−0.37	±0.40	±0.43	±0.47	±0.37	±0.37	±0.37	+0.40/−0.39	±0.43
Muon isolation efficiency syst [%]	±0.11	+0.10/−0.11	±0.10	±0.11	±0.11	±0.11	±0.10	±0.10	±0.10	±0.10	±0.10	±0.10	±0.10	±0.10	±0.10	±0.10	±0.10	±0.10	±0.10	±0.10	±0.10	±0.10	±0.10
E_T^{miss} Soft jet resolution para [%]	∓0.47	±0.44	±0.64	∓0.54	∓0.43	∓1.18	-	-	-	∓0.10	-	∓0.46	±0.24	-	-	-	∓0.38	∓0.26	±0.20	-	-	-	-
E_T^{miss} Soft jet resolution perp [%]	∓0.45	±0.44	±0.49	∓0.47	∓0.45	∓0.62	-	-	∓0.11	-	±0.20	∓0.59	-	-	∓0.14	∓0.17	∓0.35	∓0.11	±0.36	-	∓0.12	-	-
E_T^{miss} Soft jet scale [%]	-	-	−0.28/+0.64	−0.70/+0.78	∓0.18	−0.27/+0.50	+0.12/−0.13	-	−0.11/+0.14	−0.13/+0.11	-/+0.17	−0.28/-	+0.23/−0.17	-	−0.12/+0.10	-	-/−0.22	−0.34/+0.48	-/−0.30	-	-	-	−0.17/+0.21
Luminosity [%]	∓2.03	∓2.05	∓2.06	∓2.05	∓2.05	∓2.05	∓2.06	∓2.05	∓2.05	∓2.05	∓2.05	∓2.05	∓2.05	∓2.05	∓2.05	∓2.05	∓2.05	∓2.05	∓2.05	∓2.05	∓2.05	∓2.05	∓2.05
Z+jets cross-section [%]	±0.65	±0.66	±0.70	±1.18	±0.76	±0.79	±0.40	±0.40	±0.52	±0.59	±0.65	±0.68	±0.38	±0.35	±0.36	±0.40	±0.45	±0.40	±0.37	±0.39	±0.36	±0.33	±0.32
Monte Carlo sample statistics [%]	±0.14	±0.18	±0.37	±1.12	±1.71	±3.35	±0.35	±0.19	±0.33	±0.63	±1.01	±2.58	±0.58	±0.38	±0.37	±0.64	±1.21	±1.57	±1.03	±0.52	±0.49	±0.67	±0.80
ISR/FSR + scale [%]	-/−3.89	-/−2.81	+0.92/−0.57	+5.20/-	+2.25/-	-/−6.81	−0.63/+2.32	+0.45/-	−0.93/+2.36	−0.62/+1.60	+0.88/-	-/−7.02	+0.95/-	+0.13/−0.42	-/−1.51	-/−1.67	-/−0.28	+2.93/−0.38	+4.41/−0.22	+1.87/−0.60	+0.86/−0.82	+1.26/-	+0.15/−1.38
Alternate hard-scattering model [%]	±1.81	±1.42	±2.05	±1.00	±4.73	∓4.50	±5.17	±5.16	±0.88	±1.32	∓0.47	∓8.34	±4.03	±7.20	±3.16	±1.48	±0.99	∓0.10	±7.89	±10.9	±6.21	±7.12	±6.06
Alternate parton-shower model [%]	∓6.38	∓2.19	±6.20	±3.12	±0.25	±10.8	±3.64	±5.36	±0.13	±0.72	±3.32	±0.93	±9.11	±5.53	±2.27	±2.18	±5.82	±3.78	±13.0	±10.2	±7.05	±6.63	±3.82
Inter PDF [%]	-	-	-	-	±0.23	-	∓0.10	-	-	∓0.12	-	-	∓0.19	∓0.12	-	-	∓0.18	±0.23	-	-	-	∓0.10	±0.17
Intra PDF [%]	±0.16	-	±0.27	±0.33	±0.83	±1.05	±0.31	±0.11	-	±0.70	±0.52	±0.75	±0.68	±0.34	-	±0.49	±0.71	±0.76	±0.50	±0.52	±0.26	±0.28	±1.37
Fakes overall normalization, el [%]	∓0.13	+1.43/−1.44	+3.38/−3.36	+1.97/−1.98	∓0.29	−0.11/+0.12	+0.39/−0.40	±0.46	±0.71	±0.50	±0.41	±0.57	±0.62	±0.56	±0.33	±0.26	±0.40	±0.15	±1.01	±0.89	±0.29	-	-
Fakes overall normalization, mu [%]	∓0.23	±0.23	±1.12	±0.88	-	-	∓0.12	-	±0.13	-	∓0.35	∓0.52	-	-	-	∓0.15	±0.21	±0.57	∓0.28	-	±0.16	±0.28	±0.57
Fakes alternative parametrization [%]	∓2.50	∓3.08	∓3.95	∓3.04	∓0.54	∓1.02	∓2.68	∓2.59	∓1.79	∓1.05	±0.69	±0.82	∓3.14	∓2.81	∓1.74	∓0.77	∓0.16	±0.56	∓3.37	∓3.57	∓1.62	∓0.60	±0.85
W+jets heavy flavour component [%]	±5.17	±3.97	±2.73	±1.00	±2.12	±2.96	±5.14	±3.36	±2.43	±2.96	±2.19	±3.71	±2.54	±2.00	±1.24	±0.24	±0.32	±3.03	±0.18	±4.90	±1.68	±1.74	±4.48

TABLE F.10: Table of systematics for the absolute differential cross-section at the particle level for the $p_T^{t\bar{t}}$ in bins of jet multiplicity observable.

Bins [GeV] x [GeV]	0–30	30–70	70–120	120–240	240–800	800–830	830–870	870–920	920–1040	1040–1600	1600–1640	1640–1670	1670–1730	1730–1790	1790–2400	2400–2440	2440–2480	2480–2540	2540–3200	3200–3240	3240–3330	3330–4000
dσ / d$m^{tt} vs p_T^{tt}$ [pb/GeV x GeV]	$1.93 \cdot 10^{-1}$	$1.56 \cdot 10^{-1}$	$6.22 \cdot 10^{-2}$	$1.62 \cdot 10^{-2}$	$6.23 \cdot 10^{-4}$	$3.60 \cdot 10^{-1}$	$3.11 \cdot 10^{-1}$	$1.27 \cdot 10^{-1}$	$3.67 \cdot 10^{-2}$	$2.07 \cdot 10^{-3}$	$1.80 \cdot 10^{-1}$	$1.45 \cdot 10^{-1}$	$6.47 \cdot 10^{-2}$	$2.67 \cdot 10^{-2}$	$2.42 \cdot 10^{-3}$	$1.13 \cdot 10^{-1}$	$8.73 \cdot 10^{-2}$	$3.79 \cdot 10^{-2}$	$3.31 \cdot 10^{-3}$	$3.55 \cdot 10^{-2}$	$1.94 \cdot 10^{-2}$	$1.30 \cdot 10^{-3}$
Total Uncertainty [%]	+17.2/−17.0	±16.7	+22.0/−21.8	+14.5/−14.1	+15.3/−15.4	+10.8/−10.7	+10.9/−10.7	+14.6/−14.3	±11.2	+10.6/−10.3	+9.43/−9.28	+10.6/−10.5	+11.8/−11.6	+10.8/−9.83	+9.54/−9.24	+9.98/−9.82	+9.35/−9.56	+12.8/−12.7	+11.0/−10.6	+12.2/−12.0	±9.50	+10.5/−11.0
Statistics [%]	±0.4	±0.3	±0.6	±0.8	±2.0	±0.3	±0.2	±0.4	±0.5	±1.0	±0.4	±0.3	±0.5	±0.8	±0.9	±0.5	±0.4	±0.7	±0.7	±0.9	±0.8	±1.2
Systematics [%]	+17.2/−17.0	+16.7/−16.6	+22.0/−21.8	+14.5/−14.0	±15.2	±10.7	+10.9/−10.7	+14.6/−14.3	±11.2	+10.5/−10.2	+9.41/−9.27	+10.6/−10.5	+11.7/−11.6	+10.8/−9.77	+9.47/−9.17	+9.96/−9.80	+9.33/−9.54	+12.8/−12.7	+10.9/−10.5	+12.2/−11.9	+9.44/−9.45	+10.4/−10.9
Jet energy resolution [%]	∓1.86	±0.10	±3.91	∓0.64	∓0.51	±0.11	±0.13	±0.60	-	±1.20	±0.50	±2.54	±2.14	±1.33	±0.64	±0.89	±1.85	±4.33	±1.95	±1.98	∓0.63	±2.17
b-Tagged jet energy scale (JES) [%]	−1.40/+1.41	−1.24/+1.17	−0.93/+1.02	−0.87/+0.97	−1.08/+0.98	+0.84/−0.86	+0.79/−0.77	+0.72/−0.73	+0.57/−0.67	+0.32/−0.31	+1.04/−1.07	+0.99/−1.08	+0.97/−1.05	+1.14/−0.97	+0.74/−0.71	+1.08/−0.93	+0.99/−0.94	+0.93/−0.90	+0.82/−0.76	+0.82/−0.92	+0.84/−0.90	+0.62/−0.90
Effective detector NP set 1 (JES) [%]	−0.14/+0.19	−0.13/+0.14	-	-	-	-	-	-/−0.11	-	-	-	-	+0.12/-	+0.10/−0.11	+0.20/−0.12	+0.14/-	-/−0.13	+0.12/−0.15	+0.17/−0.11	-	-	+0.15/−0.27
Effective detector NP set 2 (JES) [%]	−0.11/+0.16	−0.11/+0.13	-	-	-	-	-	-	-	-	-	-	-	-	+0.17/−0.12	-	-	-	+0.15/-	-	-	+0.15/−0.20
Effective mixed NP set 1 (JES) [%]	−0.79/+0.78	−0.71/+0.70	−0.47/+0.58	−0.29/+0.44	-	-	-	-/−0.14	+0.13/−0.18	+0.63/−0.50	+0.35/−0.37	+0.29/−0.27	+0.32/−0.36	+0.46/−0.36	+0.81/−0.68	+0.60/−0.53	+0.47/−0.54	+0.49/−0.55	+0.90/−0.72	+0.91/−0.75	+0.74/−0.91	+1.23/−1.41
Effective mixed NP set 2 (JES) [%]	+0.15/−0.10	+0.12/−0.11	-	-	-	-	-	-	-	-	-	-	-	-	−0.10/+0.13	-	-	-	-	-	-	−0.23/+0.15
Effective modelling NP set 1 (JES) [%]	+1.05/−0.78	+2.17/−2.35	+3.48/−3.33	+3.30/−2.83	+1.46/−1.52	+1.85/−1.83	+2.84/−2.76	+3.84/−3.61	+3.23/−3.24	+2.47/−2.22	+1.41/−1.37	+2.22/−2.27	+3.09/−3.00	+3.11/−2.83	+2.34/−1.97	+0.71/−0.56	+1.32/−1.59	+2.40/−2.51	+2.32/−2.13	−0.29/+0.73	+0.66/−1.03	+1.62/−1.66
Effective modelling NP set 2 (JES) [%]	−0.66/+0.73	−0.82/+0.83	−0.75/+0.90	−0.55/+0.64	-/+0.38	−0.15/+0.14	−0.28/+0.29	−0.34/+0.33	−0.20/+0.14	-	-	-	-	-	+0.14/−0.11	+0.29/−0.21	+0.10/−0.15	-	+0.30/−0.14	+0.45/−0.51	+0.33/−0.38	+0.62/−0.71
Effective modelling NP set 3 (JES) [%]	+0.74/−0.70	+0.81/−0.80	+0.78/−0.66	+0.53/−0.46	+0.45/-	-	+0.19/−0.18	+0.19/−0.21	-	-	−0.18/+0.12	-	-	−0.14/+0.24	−0.20/+0.18	−0.28/+0.34	∓0.22	−0.22/+0.20	−0.24/+0.41	−0.42/+0.43	−0.37/+0.31	−0.67/+0.55
Effective modelling NP set 4 (JES) [%]	-	-	-	-	-	-/−0.11	±0.13	+0.19/−0.22	+0.17/−0.21	+0.13/−0.16	+0.11/−0.13	+0.15/−0.14	+0.18/−0.16	+0.14/−0.15	+0.25/−0.19	+0.12/-	+0.12/−0.15	+0.14/−0.16	+0.18/−0.12	-	-	+0.14/−0.24
Effective statistical NP set 1 (JES) [%]	+0.30/−0.28	+0.54/−0.55	+0.76/−0.54	+0.60/−0.50	+0.54/−0.24	+0.32/−0.26	±0.50	+0.62/−0.68	+0.48/−0.53	+0.43/−0.45	+0.13/−0.19	+0.32/−0.35	+0.49/−0.44	+0.51/−0.41	+0.52/−0.35	-	+0.28/−0.27	+0.35/−0.44	+0.24/−0.18	−0.12/+0.17	-/−0.20	+0.28/−0.27
Effective statistical NP set 2 (JES) [%]	−0.23/+0.29	−0.49/+0.50	−0.52/+0.65	−0.44/+0.52	−0.12/+0.38	−0.24/+0.28	−0.45/+0.46	∓0.59	−0.50/+0.42	−0.32/+0.27	−0.16/+0.11	−0.32/+0.28	−0.42/+0.47	−0.39/+0.48	−0.27/+0.40	-	−0.20/+0.22	−0.39/+0.31	−0.12/+0.16	±0.20	-	-
Effective statistical NP set 3 (JES) [%]	-	+0.11/-	+0.12/−0.10	+0.12/−0.13	−0.19/+0.29	-	-	-	-	−0.19/+0.20	-	-	-	-	−0.20/+0.13	-	-	-	-/+0.15	−0.30/+0.27	−0.28/+0.25	−0.46/+0.40
Effective statistical NP set 4 (JES) [%]	−0.58/+0.60	−0.62/+0.61	−0.48/+0.53	−0.31/+0.34	−0.17/+0.47	-	-	-	+0.12/−0.13	-	+0.20/−0.25	+0.13/−0.14	+0.19/−0.20	+0.30/−0.28	+0.24/−0.26	+0.35/−0.26	+0.24/−0.28	±0.28	+0.36/−0.25	+0.26/−0.25	+0.15/−0.24	+0.38/−0.40
Effective statistical NP set 5 (JES) [%]	+0.25/−0.19	+0.21/−0.24	±0.13	-	+0.27/−0.13	−0.11/+0.10	-	−0.16/+0.15	−0.15/+0.11	+0.17/−0.16	−0.13/+0.10	−0.12/-	−0.13/+0.16	−0.15/+0.19	-	-	-	-	-	+0.16/−0.14	-	-
Effective statistical NP set 6 (JES) [%]	-	+0.12/−0.10	+0.16/-	-	+0.29/−0.15	+0.11/−0.12	+0.13/−0.12	+0.16/−0.18	-	-	-	-	-	-	-	-	-	-	-	-	-	-
Effective statistical NP set 7 (JES) [%]	-/+0.12	-	-	-	-	-	-	+0.12/−0.13	+0.10/−0.16	+0.12/−0.15	+0.11/−0.14	+0.11/-	+0.13/−0.10	+0.13/−0.11	+0.22/−0.19	+0.17/−0.12	+0.11/−0.15	+0.15/−0.14	+0.21/−0.15	+0.15/−0.11	-/−0.14	+0.23/−0.34
η intercalibration model (JES) [%]	−0.70/+0.74	−0.47/+0.31	-	+0.18/-	-	+0.55/−0.51	+0.64/−0.66	+0.97/−0.99	+0.92/−1.05	+0.89/−0.69	+0.73/−0.77	+0.83/−0.87	+1.10/−1.13	+1.25/−1.12	+1.03/−0.88	+0.80/−0.78	±1.03	+1.20/−1.21	+1.26/−1.21	+1.00/−0.96	+0.99/−1.22	+1.38/−1.53
η intercalibration non closure (JES) [%]	+0.14/-	-	−0.15/+0.31	−0.31/+0.27	−0.28/+0.14	−0.22/+0.23	−0.24/+0.25	−0.34/+0.31	−0.51/+0.40	−0.44/+0.47	−0.19/+0.13	−0.22/+0.24	−0.23/+0.30	−0.33/+0.40	−0.44/+0.56	−0.23/+0.34	−0.39/+0.33	−0.41/+0.42	−0.49/+0.54	−0.37/+0.44	−0.48/+0.31	−0.66/+0.55
η intercalibration total stat (JES) [%]	−0.22/+0.27	-	+0.33/−0.18	+0.29/−0.23	-	+0.41/−0.38	±0.51	+0.76/−0.73	+0.55/−0.65	+0.51/−0.56	+0.36/−0.39	+0.48/−0.47	+0.67/−0.71	+0.80/−0.64	+0.62/−0.39	+0.39/−0.28	+0.49/−0.46	+0.65/−0.71	+0.51/−0.43	-	+0.13/−0.32	+0.54/−0.56
Flavour composition (JES) [%]	+1.17/−1.26	+2.05/−2.31	+3.64/−3.67	+3.27/−3.46	+1.53/−2.38	+1.73/−1.92	+2.12/−2.38	+3.38/−3.35	+3.11/−3.33	+2.54/−2.41	±1.15	+1.42/−1.62	+2.52/−2.58	+2.99/−2.63	+2.20/−2.10	+0.36/−0.28	+0.85/−0.98	+2.02/−2.22	+2.38/−2.21	−0.54/+0.84	+0.18/−0.36	+1.93/−1.85
Flavour response (JES) [%]	−0.32/+0.35	−0.90/+0.63	−1.61/+1.68	−1.75/+1.71	−0.78/+1.04	−0.90/+0.91	−1.09/+1.11	−1.80/+1.76	−1.79/+1.69	−1.25/+1.39	−0.61/+0.51	−0.87/+0.75	−1.44/+1.41	−1.31/+1.63	−1.18/+1.21	−0.11/+0.23	−0.57/+0.46	−1.21/+1.05	−1.11/+1.29	+0.46/−0.22	-	−1.12/+0.96
Pile-up offset μ (JES) [%]	-	-	−0.19/+0.21	−0.19/+0.23	+0.27/-	-	∓0.21	−0.31/+0.26	−0.22/+0.18	-	-	−0.15/+0.13	−0.16/+0.21	−0.14/+0.20	−0.12/+0.17	-	−0.12/+0.16	−0.20/+0.11	−0.10/+0.20	-	−0.18/-	−0.16/+0.21
Pile-up offset N_{PV} (JES) [%]	-	+0.14/−0.27	+0.35/−0.51	+0.75/−0.23	+0.45/−0.44	+0.38/−0.37	+0.52/−0.47	+0.90/−0.81	+0.81/−0.93	+0.48/−0.27	+0.32/−0.35	+0.50/−0.59	+0.80/−0.83	+1.05/−0.65	+0.61/−0.56	+0.33/−0.21	+0.23/−0.46	+0.53/−0.62	+0.76/−0.47	-	+0.24/−0.40	+0.16/−0.34
Pile-up offset p_T (JES) [%]	−1.59/+1.60	−1.70/+1.71	−1.35/+1.41	−1.03/+0.86	−0.72/+1.03	-	∓0.13	-	+0.17/−0.18	±0.34	+0.54/−0.53	+0.34/−0.37	+0.41/−0.45	+0.74/−0.70	+0.54/−0.59	+0.76/−0.75	+0.63/−0.68	+0.76/−0.69	+1.05/−0.84	+1.06/−1.07	+0.86/−0.99	+1.21/−1.33
Pile-up offset ρ topology (JES) [%]	-	+2.07/−2.60	+4.61/−4.42	+4.36/−3.46	+1.11/−1.75	+2.89/−2.82	+4.38/−4.19	+6.01/−5.54	+5.21/−5.10	+3.50/−3.16	±2.37	+3.52/−3.62	+4.90/−4.81	+5.25/−4.49	+3.53/−3.33	+1.22/−1.09	+2.40/−2.65	+4.16/−4.00	+3.74/−3.42	−0.54/+0.73	+1.14/−1.54	+2.66/−2.59
Jet vertex fraction [%]	+1.08/−1.11	+1.28/−1.30	+1.35/−1.37	+1.18/−1.20	+0.85/−0.89	+0.60/−0.64	+0.79/−0.82	+0.90/−0.93	+0.80/−0.83	+0.66/−0.70	+0.36/−0.41	+0.54/−0.58	+0.65/−0.69	+0.60/−0.64	+0.53/−0.57	+0.20/−0.25	+0.39/−0.43	+0.52/−0.56	+0.44/−0.49	-	+0.26/−0.31	+0.32/−0.38
b-Quark tagging efficiency (eigenvector 0) [%]	−8.74/+9.09	−8.49/+8.81	−8.23/+8.52	−7.95/+8.22	−7.03/+7.23	−6.52/+6.72	−6.32/+6.50	−6.07/+6.22	−5.99/+6.14	−5.80/+5.94	−6.06/+6.23	−5.78/+5.92	−5.45/+5.57	−5.41/+5.53	−5.51/+5.62	−6.12/+6.27	−5.77/+5.91	−5.42/+5.53	−5.46/+5.57	−6.62/+6.79	−5.97/+6.11	−5.70/+5.81
b-Quark tagging efficiency (eigenvector 1) [%]	−0.80/+0.81	∓0.75	∓0.61	∓0.68	−1.42/+1.43	−1.75/+1.76	−1.72/+1.74	−1.65/+1.67	−1.64/+1.65	−2.19/+2.21	−2.38/+2.41	−2.36/+2.38	−2.30/+2.33	−2.23/+2.25	−2.51/+2.53	−2.94/+2.98	−2.89/+2.92	−2.83/+2.86	−2.91/+2.94	−3.89/+3.95	−3.69/+3.75	−3.65/+3.70
b-Quark tagging efficiency (eigenvector 2) [%]	+1.68/−1.67	+1.60/−1.58	+1.46/−1.45	±1.42	+1.19/−1.18	+1.49/−1.48	±1.43	+1.33/−1.32	+1.27/−1.26	±0.94	±1.19	±1.13	±1.02	+0.99/−0.98	+0.83/−0.82	+0.90/−0.89	±0.81	±0.68	±0.55	±0.43	+0.31/−0.30	±0.10
b-Quark tagging efficiency (eigenvector 3) [%]	∓0.36	∓0.34	−0.33/+0.32	∓0.24	-	-	-	-	-	±0.13	±0.23	±0.24	±0.23	±0.20	±0.17	±0.22	±0.22	±0.19	±0.11	-	-	∓0.10
c-Quark tagging efficiency (eigenvector 0) [%]	±0.45	±0.45	±0.48	±0.47	±0.34	±0.25	±0.26	±0.28	±0.31	±0.25	±0.19	±0.22	±0.23	+0.27/−0.26	±0.22	±0.17	±0.20	±0.21	±0.21	±0.10	±0.16	±0.21
c-Quark tagging efficiency (eigenvector 1) [%]	-	-	-	-	-	∓0.14	∓0.17	∓0.17	−0.11/+0.10	∓0.12	∓0.25	∓0.31	∓0.36	∓0.31	∓0.24	∓0.40	∓0.49	∓0.57	∓0.47	∓0.60	∓0.81	−0.93/+0.94
c-Quark tagging efficiency (eigenvector 2) [%]	±0.17	±0.18	±0.17	+0.20/−0.19	±0.12	±0.10	±0.11	±0.11	±0.15	±0.11	-	-	-	-	-	-	-	∓0.10	-	∓0.16	∓0.25	∓0.29
Light-jet tagging efficiency (eigenvector 0) [%]	−0.70/+0.75	−0.42/+0.32	−0.47/+0.42	−0.48/+0.50	−0.30/+0.32	−0.50/+0.55	−0.47/+0.48	∓0.52	−0.52/+0.53	−0.40/+0.41	−0.57/+0.60	−0.69/+0.72	−0.83/+0.86	−0.73/+0.74	−0.53/+0.54	−0.79/+0.81	−0.98/+1.01	−1.15/+1.16	−1.29/+1.37	−1.18/+1.19	−1.68/+1.74	−2.00/+2.06
Light-jet tagging efficiency (eigenvector 1) [%]	+0.42/−0.40	±0.29	±0.31	±0.37	±0.39	±0.20	+0.21/−0.20	±0.24	±0.27	+0.23/−0.22	+0.19/−0.18	±0.23	+0.30/−0.29	±0.27	±0.23	+0.16/−0.15	+0.23/−0.21	+0.20/−0.19	±0.18	-	-	-
Light-jet tagging efficiency (eigenvector 2) [%]	-	−0.13/-	-	-	-	-	-	-	-	-	-	-	-	-	-	-	-	-	±0.11	±0.16	-	±0.18
Light-jet tagging efficiency (eigenvector 3) [%]	+0.22/−0.21	-	+0.14/−0.15	+0.24/−0.23	±0.21	-	-	-	-	-	-	-	∓0.10	-	-	∓0.13	∓0.21	∓0.27	−0.28/+0.29	∓0.31	∓0.50	∓0.56
Light-jet tagging efficiency (eigenvector 5) [%]	-	-	-	-	-	-	-	-	-	-	-	-	-	-	-	-	∓0.10	∓0.13	∓0.13	-	∓0.11	-
Light-jet tagging efficiency (eigenvector 8) [%]	-	-	-	-	-	-	-	-	-	-	-	-	-	-	-	-	-	-	-	-	∓0.12	∓0.16
b-Quark tagging extrapolation [%]	-	-	-	-	-	-	-	-	-	-	-	-	-	-	-	-	±0.11	±0.15	+0.26/−0.27	+0.70/−0.69	±0.79	±1.20
b-Quark tagging extrapolation from *c*-Quark [%]	-	-	-	-	-	-	-	-	-	-	-	-	-	-	-	-	-	-	-	±0.10	-	-
Electron energy resolution [%]	-	-	-	-	-/+0.12	-	-	-	-	-	-	-	-	-	-	-	-	-	-	-	-	-
Electron energy scale [%]	-	-	-	-	∓0.10	-	-	-	-	-	-	-	-	-	-	+0.12/−0.13	+0.10/−0.11	+0.13/−0.10	-	+0.25/−0.20	±0.20	+0.13/−0.22
Electron trigger efficiency [%]	±0.13	±0.12	±0.12	±0.12	±0.11	+0.11/−0.12	±0.11	±0.11	±0.11	+0.11/−0.10	±0.11	±0.11	±0.11	±0.11	±0.11	±0.12	±0.12	±0.12	±0.12	±0.14	±0.14	±0.14
Electron reconstruction efficiency [%]	-	-	-	-	-	-	-	-	-	-	-	-	-	-	-	-	-	-	-	±0.11	±0.11	±0.12
Electron identification efficiency [%]	±0.33	±0.33	±0.33	±0.35	±0.43	+0.36/−0.37	±0.36	±0.36	±0.39	±0.45	±0.43	±0.42	±0.42	±0.44	±0.49	+0.51/−0.50	±0.50	±0.50	±0.55	±0.65	±0.65	±0.70
Electron isolation efficiency [%]	-	-	-	-	±0.10	-	-	-	-	±0.18	±0.10	±0.10	±0.10	±0.13	±0.22	±0.18	±0.18	±0.19	±0.27	±0.32	±0.32	±0.42
Muon (ID) momentum resolution [%]	-	-	-	-	-	-	-	-	-	-	-	-	-	-	-	-	-	-	-	-	-	-
Muon (MS) momentum resolution [%]	-	-	-	-	-	-	-	-	-	-	-	-	-	-	-	-	-	-	-	-	-	-
Muon trigger efficiency stat [%]	±0.31	+0.29/−0.30	±0.29	+0.29/−0.30	+0.27/−0.28	+0.29/−0.30	+0.28/−0.29	±0.28	±0.28	+0.27/−0.28	+0.29/−0.30	+0.28/−0.29	±0.28	±0.28	±0.28	+0.30/−0.31	±0.29	±0.28	+0.29/−0.30	±0.33	+0.30/−0.31	+0.29/−0.30
Muon trigger efficiency syst [%]	+0.53/−0.52	+0.52/−0.51	+0.51/−0.50	+0.51/−0.50	+0.47/−0.46	+0.51/−0.50	+0.51/−0.50	+0.50/−0.49	+0.50/−0.49	+0.48/−0.47	+0.51/−0.50	+0.51/−0.50	+0.50/−0.49	+0.50/−0.49	+0.49/−0.48	+0.53/−0.52	+0.52/−0.51	+0.52/−0.50	+0.52/−0.51	+0.59/−0.58	+0.55/−0.54	+0.53/−0.52
Muon identification stat [%]	±0.10	-	-	-	-	-	-	-	-	-	-	-	-	-	-	±0.10	-	-	-	±0.11	±0.10	±0.10
Muon identification syst [%]	±0.35	±0.34	+0.33/−0.34	±0.34	±0.35	±0.35	±0.34	±0.34	±0.35	+0.38/−0.37	±0.38	±0.37	±0.37	±0.38	±0.41	±0.44	±0.43	+0.43/−0.42	±0.46	+0.58/−0.57	±0.54	±0.55
Muon isolation efficiency syst [%]	±0.11	+0.11/−0.10	±0.10	±0.10	±0.10	±0.10	±0.10	±0.10	±0.10	±0.10	±0.10	±0.10	±0.10	±0.10	±0.10	±0.11	±0.11	±0.11	±0.11	±0.13	±0.12	±0.12
E_T^{miss} Soft jet resolution para [%]	±0.40	±1.02	±0.99	±0.62	±0.79	∓0.28	±0.19	±0.13	∓0.12	±0.18	∓0.35	∓0.14	∓0.50	-	∓0.31	∓0.44	∓0.13	∓0.32	∓0.27	∓0.93	-	∓0.26
E_T^{miss} Soft jet resolution perp [%]	±0.40	±0.90	±0.95	±0.57	±0.76	∓0.26	±0.19	-	-	±0.16	∓0.30	-	∓0.37	∓0.15	∓0.26	∓0.39	∓0.29	∓0.29	∓0.24	∓0.79	∓0.25	∓0.47
E_T^{miss} Soft jet scale [%]	+0.88/−0.91	+0.80/−0.79	+0.80/−0.65	+0.62/−0.55	+0.87/−0.39	+0.12/−0.25	-	−0.11/+0.26	-	-	-	−0.34/+0.29	−0.60/+0.59	−0.34/+0.52	−0.24/+0.19	−0.19/+0.17	−0.44/+0.50	−0.49/+0.86	−0.29/+0.22	−0.43/+0.44	−0.40/+0.36	−0.44/+0.49
Luminosity [%]	∓2.05	∓2.05	∓2.05	∓2.05	∓2.05	∓2.05	∓2.05	∓2.05	∓2.05	∓2.05	∓2.05	∓2.05	∓2.05	∓2.05	∓2.05	∓2.05	∓2.05	∓2.05	∓2.05	∓2.05	∓2.05	∓2.05
Z+jets cross-section [%]	±0.88	±0.72	±0.54	±0.49	±0.32	±0.52	±0.45	±0.32	±0.38	±0.26	±0.57	±0.51	±0.42	±0.39	±0.41	±0.69	±0.57	±0.55	±0.75	±0.99	±0.87	±0.98
Monte Carlo sample statistics [%]	±0.39	±0.39	±0.41	±0.52	±1.16	±0.23	±0.23	±0.26	±0.34	±0.62	±0.27	±0.24	±0.34	±0.53	±0.56	±0.33	±0.33	±0.46	±0.55	±0.82	±0.57	±0.77
ISR/FSR + scale [%]	−0.89/+1.76	+1.77/-	±0.17	-/−0.52	-/−0.69	−1.10/+1.24	−0.49/+1.10	-	−0.87/+1.38	+0.27/-	−1.01/+1.67	−0.82/+1.54	+0.84/−0.48	−0.66/+2.43	+0.94/−0.97	−0.78/+1.02	-/−1.89	+1.13/-	+0.77/−0.15	−1.13/+1.34	+1.09/-	+2.14/−3.86
Alternate hard-scattering model [%]	±8.97	±8.86	±14.2	±7.54	±10.4	-	±2.18	±5.45	±2.40	±4.15	±0.19	±2.54	±2.52	±2.10	±1.05	∓0.76	±0.75	±4.12	±3.54	∓0.13	±1.79	∓1.40
Alternate parton-shower model [%]	∓3.28	±2.38	±6.65	±1.62	±3.30	∓2.80	±2.72	±7.30	±3.35	±3.21	∓1.65	±2.35	±5.09	±2.02	±3.51	∓3.32	±1.32	±5.12	±4.13	∓3.14	±2.54	±2.18
Inter PDF [%]	-	-	-	-	±0.27	-	-	∓0.12	∓0.11	-	-	-	-	-	-	-	-	-	-	∓0.10	∓0.12	-
Intra PDF [%]	±0.19	±0.10	±0.17	±0.28	±1.54	-	-	±0.46	±0.37	±0.30	±0.24	±0.13	±0.28	±0.22	±0.40	±0.52	±0.11	±0.71	±0.18	±0.62	±0.78	±0.67
Fakes overall normalization, el [%]	+0.57/−0.58	+1.83/−1.82	±1.48	±0.44	±0.25	-	-	±0.89	±0.85	±0.18	-	∓0.14	±0.96	±1.11	±0.46	-	±0.15	±1.23	±1.24	±0.28	∓0.42	±2.59	±1.92
Fakes overall normalization, mu [%]	-	±0.26	±0.38	±0.28	-	∓0.11	±0.19	±0.38	-	∓0.24	∓0.13	±0.14	±0.30	-	∓0.30	∓0.35	-	±0.10	∓0.30	∓0.70	−0.23/+0.22	∓0.49
Fakes alternative parametrization [%]	∓5.07	∓5.53	∓4.92	∓2.92	∓0.97	∓2.76	∓3.13	∓2.95	∓2.02	∓0.22	∓1.71	∓2.16	∓2.18	∓1.18	∓0.11	∓1.14	∓1.50	∓1.06	∓0.20	±0.49	∓1.14	∓0.16
W+jets heavy flavour component [%]	±7.50	±6.68	±7.41	±3.77	±5.05	±4.63	±2.59	±1.27	±1.45	±2.37	±3.79	±3.80	±1.46	±0.10	±0.91	±4.56	±3.59	±3.92	±2.07	±7.13	±0.63	±2.31

TABLE F.11: Table of systematics for the absolute differential cross-section at the particle level for the $p_T^{t\bar{t}}$ vs $m^{t\bar{t}}$ observable.

Bins [GeV] x [GeV]	0–30	30–90	90–140	140–200	200–300	300–1000	1000–1030	1030–1090	1090–1150
$d\sigma$ / $dp_T^{t\bar{t}} vs p_T^{t,had}$ [pb/GeV x GeV]	$3.91 \cdot 10^{-2}$	$1.40 \cdot 10^{-1}$	$1.66 \cdot 10^{-1}$	$8.11 \cdot 10^{-2}$	$2.53 \cdot 10^{-2}$	$1.07 \cdot 10^{-3}$	$5.33 \cdot 10^{-2}$	$1.85 \cdot 10^{-1}$	$1.98 \cdot 10^{-1}$
Total Uncertainty [%]	$^{+19.4}_{-19.3}$	$^{+14.4}_{-14.2}$	$^{+10.4}_{-10.3}$	$^{+10.2}_{-9.85}$	$^{+10.3}_{-10.5}$	±13.8	$^{+16.2}_{-15.9}$	±14.6	±10.9
Statistics [%]	±1.0	±0.3	±0.3	±0.4	±0.7	±1.3	±0.8	±0.3	±0.2
Systematics [%]	±19.3	$^{+14.4}_{-14.2}$	$^{+10.4}_{-10.3}$	$^{+10.2}_{-9.84}$	$^{+10.3}_{-10.5}$	±13.7	$^{+16.1}_{-15.8}$	±14.6	±10.9
Jet energy resolution [%]	±0.44	±0.73	∓2.08	±0.76	∓0.31	±2.60	±0.32	±2.32	±0.26
b-Tagged jet energy scale (JES) [%]	$^{-}_{-0.32}$	$^{+0.13}_{-}$	$^{+0.63}_{-0.67}$	$^{+0.91}_{-0.79}$	$^{+0.65}_{-0.75}$	$^{+0.75}_{-0.66}$	-	$^{+0.17}_{-0.12}$	$^{+0.61}_{-0.66}$
Effective detector NP set 1 (JES) [%]	-	-	-	-	-	$^{+0.23}_{-0.17}$	-	-	-
Effective detector NP set 2 (JES) [%]	-	-	-	-	-	$^{+0.18}_{-0.15}$	-	-	-
Effective mixed NP set 1 (JES) [%]	$^{-0.29}_{+0.38}$	$^{-0.19}_{+0.22}$	-	$^{+0.33}_{-0.26}$	$^{+0.37}_{-0.44}$	±1.43	$^{-0.27}_{+0.23}$	$^{-0.22}_{+0.20}$	-
Effective mixed NP set 2 (JES) [%]	-	-	-	-	-	$^{-0.14}_{+0.18}$	-	-	-
Effective modelling NP set 1 (JES) [%]	$^{+1.86}_{-1.55}$	$^{+1.55}_{-1.46}$	$^{+1.42}_{-1.39}$	$^{+1.16}_{-0.91}$	$^{+0.48}_{-0.49}$	$^{+0.20}_{-0.25}$	$^{+3.02}_{-2.93}$	$^{+2.69}_{-2.80}$	$^{+2.47}_{-2.51}$
Effective modelling NP set 2 (JES) [%]	$^{-0.27}_{+0.40}$	$^{-0.35}_{+0.36}$	$^{-0.18}_{+0.15}$	-	$^{+0.18}_{-0.23}$	$^{+0.69}_{-0.68}$	$^{-0.60}_{+0.52}$	$^{-0.49}_{+0.48}$	$^{-0.28}_{+0.27}$
Effective modelling NP set 3 (JES) [%]	$^{+0.35}_{-0.25}$	±0.34	$^{+0.11}_{-0.17}$	$^{-0.12}_{+0.19}$	$^{-0.30}_{+0.19}$	$^{-0.55}_{+0.59}$	$^{+0.46}_{-0.54}$	$^{+0.41}_{-0.39}$	$^{+0.19}_{-0.21}$
Effective modelling NP set 4 (JES) [%]	-	-	-	$^{+0.13}_{-}$	-	$^{+0.17}_{-0.14}$	-	-	$^{+0.10}_{-0.11}$
Effective statistical NP set 1 (JES) [%]	$^{+0.63}_{-0.24}$	$^{+0.29}_{-0.31}$	$^{+0.21}_{-0.22}$	$^{+0.17}_{-}$	-	-	$^{+0.61}_{-0.56}$	$^{+0.54}_{-0.57}$	$^{+0.44}_{-0.43}$
Effective statistical NP set 2 (JES) [%]	$^{-0.21}_{+0.60}$	$^{-0.26}_{+0.27}$	∓0.19	$^{-}_{+0.13}$	-	$^{+0.19}_{-0.21}$	$^{-0.51}_{+0.56}$	$^{-0.52}_{+0.48}$	$^{-0.38}_{+0.40}$
Effective statistical NP set 3 (JES) [%]	-	-	-	-	-	$^{-0.46}_{+0.54}$	-	-	-
Effective statistical NP set 4 (JES) [%]	$^{-0.21}_{+0.27}$	$^{-0.19}_{+0.22}$	-	$^{+0.25}_{-0.17}$	$^{+0.25}_{-0.28}$	$^{+0.29}_{-0.30}$	$^{-0.35}_{+0.29}$	∓0.23	-
Effective statistical NP set 5 (JES) [%]	-	-	-	$^{-}_{+0.12}$	-	±0.29	-	-	-
Effective statistical NP set 6 (JES) [%]	-	±0.10	-	-	-	-	-	±0.12	±0.10
Effective statistical NP set 7 (JES) [%]	-	-	-	$^{+0.15}_{-}$	-	$^{+0.30}_{-0.26}$	-	-	-
η intercalibration model (JES) [%]	$^{+0.34}_{-0.14}$	$^{+0.22}_{-0.20}$	$^{+0.38}_{-0.45}$	$^{+0.62}_{-0.50}$	$^{+0.50}_{-0.53}$	$^{+0.81}_{-0.73}$	$^{+0.28}_{-0.45}$	$^{+0.41}_{-0.45}$	$^{+0.58}_{-0.68}$
η intercalibration non closure (JES) [%]	$^{-0.20}_{+0.11}$	$^{-}_{+0.14}$	$^{-0.12}_{+0.11}$	$^{-0.16}_{+0.26}$	$^{-0.25}_{+0.22}$	$^{-0.35}_{+0.54}$	-	∓0.23	$^{-0.21}_{+0.17}$
η intercalibration total stat (JES) [%]	$^{+0.42}_{-0.11}$	$^{+0.15}_{-0.19}$	$^{+0.28}_{-0.26}$	$^{+0.37}_{-0.29}$	$^{+0.17}_{-0.16}$	$^{+0.25}_{-0.30}$	$^{+0.39}_{-0.25}$	$^{+0.29}_{-0.38}$	$^{+0.44}_{-0.43}$
Flavour composition (JES) [%]	$^{+1.55}_{-1.86}$	$^{+1.70}_{-1.72}$	$^{+1.30}_{-1.45}$	$^{+1.12}_{-1.05}$	$^{+0.44}_{-0.50}$	$^{+0.43}_{-0.48}$	$^{+2.92}_{-2.80}$	$^{+2.08}_{-2.32}$	$^{+1.79}_{-2.09}$
Flavour response (JES) [%]	$^{-0.47}_{+1.09}$	$^{-0.69}_{+0.64}$	$^{-0.65}_{+0.64}$	$^{-0.54}_{+0.59}$	$^{-0.35}_{+0.29}$	$^{-0.26}_{+0.29}$	$^{-1.17}_{+1.05}$	$^{-1.08}_{+0.87}$	$^{-0.95}_{+0.87}$
Pile-up offset μ (JES) [%]	$^{+0.22}_{-}$	-	$^{-0.13}_{-}$	-	-	$^{-}_{+0.11}$	-	$^{-0.16}_{+0.13}$	∓0.17
Pile-up offset N_{PV} (JES) [%]	$^{+0.47}_{-}$	$^{+0.27}_{-0.12}$	$^{+0.32}_{-0.31}$	$^{+0.35}_{-0.18}$	-	$^{+0.21}_{-}$	$^{+0.43}_{-0.57}$	$^{+0.38}_{-0.50}$	$^{+0.50}_{-0.51}$
Pile-up offset p_T (JES) [%]	$^{-0.60}_{+0.59}$	$^{-0.50}_{+0.48}$	-	$^{+0.55}_{-0.44}$	$^{+0.64}_{-0.65}$	$^{+1.26}_{-1.20}$	$^{-0.88}_{+0.87}$	$^{-0.69}_{+0.70}$	$^{-0.20}_{+0.15}$
Pile-up offset ρ topology (JES) [%]	$^{+1.71}_{-2.03}$	$^{+1.85}_{-1.76}$	$^{+2.07}_{-2.00}$	$^{+1.97}_{-1.71}$	$^{+0.94}_{-0.95}$	$^{-}_{-0.28}$	$^{+4.57}_{-4.02}$	$^{+3.62}_{-3.77}$	$^{+3.72}_{-3.76}$
Jet vertex fraction [%]	$^{+0.92}_{-0.96}$	$^{+0.78}_{-0.82}$	$^{+0.58}_{-0.62}$	$^{+0.36}_{-0.40}$	$^{+0.17}_{-0.21}$	-	$^{+1.13}_{-1.16}$	$^{+0.99}_{-1.02}$	$^{+0.77}_{-0.80}$
b-Quark tagging efficiency (eigenvector 0) [%]	$^{-8.50}_{+8.81}$	$^{-7.60}_{+7.86}$	$^{-6.70}_{+6.91}$	$^{-6.26}_{+6.44}$	$^{-5.76}_{+5.91}$	$^{-5.94}_{+6.10}$	$^{-8.01}_{+8.27}$	$^{-7.17}_{+7.40}$	$^{-6.35}_{+6.54}$
b-Quark tagging efficiency (eigenvector 1) [%]	$^{-1.11}_{+1.12}$	∓1.37	$^{-1.72}_{+1.74}$	$^{-2.27}_{+2.29}$	$^{-3.14}_{+3.19}$	$^{-4.36}_{+4.45}$	∓1.08	∓1.35	$^{-1.75}_{+1.77}$
b-Quark tagging efficiency (eigenvector 2) [%]	$^{+1.73}_{-1.71}$	$^{+1.65}_{-1.64}$	$^{+1.49}_{-1.48}$	±1.21	$^{+0.73}_{-0.72}$	∓0.20	$^{+1.59}_{-1.58}$	$^{+1.54}_{-1.53}$	$^{+1.39}_{-1.38}$
b-Quark tagging efficiency (eigenvector 3) [%]	∓0.30	∓0.17	-	±0.24	±0.37	∓0.12	∓0.25	$^{-0.13}_{+0.14}$	-
c-Quark tagging efficiency (eigenvector 0) [%]	±0.44	$^{+0.38}_{-0.37}$	$^{+0.27}_{-0.26}$	±0.16	-	-	±0.42	±0.37	$^{+0.29}_{-0.28}$
c-Quark tagging efficiency (eigenvector 1) [%]	∓0.10	∓0.15	∓0.20	$^{-0.24}_{+0.23}$	∓0.25	∓0.26	∓0.13	∓0.18	∓0.26
c-Quark tagging efficiency (eigenvector 2) [%]	±0.11	$^{+0.16}_{-0.15}$	±0.10	-	-	-	±0.13	±0.15	-
Light-jet tagging efficiency (eigenvector 0) [%]	$^{-1.12}_{+1.25}$	$^{-0.78}_{+0.86}$	$^{-0.54}_{+0.56}$	$^{-0.47}_{+0.50}$	$^{-0.36}_{+0.35}$	$^{-0.62}_{+0.68}$	$^{-0.52}_{+0.16}$	∓0.69	$^{-0.67}_{+0.70}$
Light-jet tagging efficiency (eigenvector 1) [%]	$^{+0.77}_{-0.69}$	$^{+0.37}_{-0.36}$	$^{+0.18}_{-0.17}$	$^{+0.12}_{-0.11}$	-	-	$^{+0.33}_{-0.35}$	$^{+0.37}_{-0.36}$	$^{+0.22}_{-0.21}$
Light-jet tagging efficiency (eigenvector 2) [%]	-	-	-	-	-	$^{+0.14}_{-0.13}$	$^{-0.51}_{+0.34}$	-	-
Light-jet tagging efficiency (eigenvector 3) [%]	$^{+0.28}_{-0.27}$	$^{+0.12}_{-0.10}$	-	-	-	-	$^{-0.27}_{+0.17}$	-	-
b-Quark tagging extrapolation [%]	-	-	-	-	-	$^{+0.87}_{-0.86}$	-	-	-
Electron energy scale [%]	-	-	-	-	-	-	-	-	-
Electron trigger efficiency [%]	±0.15	±0.13	±0.12	±0.11	±0.11	±0.11	±0.14	$^{+0.12}_{-0.13}$	±0.11
Electron reconstruction efficiency [%]	-	-	-	-	-	±0.11	-	-	-
Electron identification efficiency [%]	±0.37	±0.36	±0.37	±0.42	±0.50	±0.64	±0.36	$^{+0.36}_{-0.35}$	±0.37
Electron isolation efficiency [%]	-	-	-	-	±0.18	±0.47	-	-	-
Muon trigger efficiency stat [%]	±0.33	$^{+0.31}_{-0.32}$	±0.30	±0.29	±0.28	±0.29	$^{+0.30}_{-0.31}$	$^{+0.29}_{-0.30}$	±0.29
Muon trigger efficiency syst [%]	$^{+0.58}_{-0.56}$	$^{+0.54}_{-0.53}$	$^{+0.52}_{-0.51}$	$^{+0.50}_{-0.49}$	$^{+0.49}_{-0.48}$	$^{+0.49}_{-0.48}$	$^{+0.55}_{-0.53}$	$^{+0.53}_{-0.52}$	$^{+0.51}_{-0.50}$
Muon identification stat [%]	±0.11	±0.10	-	-	-	-	±0.10	±0.10	-
Muon identification syst [%]	±0.39	±0.37	±0.36	$^{+0.38}_{-0.37}$	±0.41	±0.53	±0.36	±0.36	±0.36
Muon isolation efficiency syst [%]	±0.12	±0.11	$^{+0.11}_{-0.10}$	±0.10	±0.10	±0.10	±0.11	±0.11	±0.10
E_T^{miss} Soft jet resolution para [%]	∓0.45	∓0.35	∓0.29	∓0.36	∓0.38	∓0.53	±0.19	±0.29	±0.28
E_T^{miss} Soft jet resolution perp [%]	∓0.45	∓0.34	∓0.17	∓0.38	∓0.45	∓0.88	±0.18	±0.31	±0.20
E_T^{miss} Soft jet scale [%]	-	$^{+0.12}_{-0.28}$	$^{+0.20}_{-0.33}$	$^{-}_{-0.18}$	-	$^{-0.31}_{-}$	-	-	-
Luminosity [%]	∓2.05	∓2.05	∓2.05	∓2.05	∓2.05	∓2.05	∓2.05	∓2.05	∓2.05
Z+jets cross-section [%]	±0.73	±0.98	±0.69	±0.38	±0.20	±0.21	±0.71	±0.78	±0.55
Monte Carlo sample statistics [%]	±1.01	±0.33	±0.24	±0.31	±0.42	±0.82	±0.91	±0.31	±0.20
ISR/FSR + scale [%]	$^{-}_{-1.94}$	$^{-0.98}_{+2.16}$	$^{-1.78}_{+1.84}$	$^{-0.47}_{+2.21}$	$^{-2.08}_{+0.68}$	$^{-}_{-1.41}$	$^{+0.56}_{-}$	$^{+1.23}_{-}$	$^{-0.67}_{+0.88}$
Alternate hard-scattering model [%]	±7.86	±3.94	∓0.27	∓0.66	-	∓5.87	±6.68	±5.49	±3.07
Alternate parton-shower model [%]	∓4.34	∓2.38	∓3.40	∓4.10	∓6.36	∓7.08	±1.83	±3.89	±3.40
Intra PDF [%]	±0.59	±0.11	-	±0.16	±0.29	±0.40	±0.26	±0.11	±0.10
Fakes overall normalization, el [%]	±0.69	±0.66	∓0.11	$^{-0.50}_{+0.51}$	∓0.65	∓1.18	±1.89	±1.74	±1.25
Fakes overall normalization, mu [%]	∓0.13	-	-	∓0.22	∓0.54	∓1.36	±0.46	±0.32	±0.24
Fakes alternative parametrization [%]	∓6.44	∓5.24	∓2.34	∓0.85	±0.67	±1.98	∓7.53	∓5.19	∓2.88
W+jets heavy flavour component [%]	±11.9	±8.10	±3.25	±3.78	±2.78	±3.73	±5.52	±6.24	±2.89

Bins [GeV] x [GeV]	1150–1240	1240–2000	2000–2080	2080–2130	2130–2190	2190–2320	2320–3000	3000–3100	3100–3175	3175–3290	3290–4000
$d\sigma$ / $dp_T^{t\bar{t}} vs p_T^{t,had}$ [pb/GeV x GeV]	$8.35 \cdot 10^{-2}$	$3.81 \cdot 10^{-3}$	$7.40 \cdot 10^{-2}$	$1.11 \cdot 10^{-1}$	$7.62 \cdot 10^{-2}$	$2.82 \cdot 10^{-2}$	$1.25 \cdot 10^{-3}$	$1.83 \cdot 10^{-2}$	$2.38 \cdot 10^{-2}$	$1.39 \cdot 10^{-2}$	$1.29 \cdot 10^{-3}$
Total Uncertainty [%]	$^{+9.36}_{-9.25}$	$^{+8.62}_{-8.24}$	$^{+14.0}_{-13.7}$	$^{+13.9}_{-13.3}$	±12.7	$^{+10.0}_{-9.96}$	$^{+14.4}_{-14.5}$	$^{+12.3}_{-12.1}$	±10.0	$^{+9.45}_{-9.20}$	$^{+9.20}_{-9.03}$
Statistics [%]	±0.3	±0.5	±0.4	±0.5	±0.5	±0.6	±1.3	±0.7	±0.8	±0.9	±1.1
Systematics [%]	$^{+9.35}_{-9.24}$	$^{+8.59}_{-8.21}$	$^{+14.0}_{-13.7}$	$^{+13.9}_{-13.3}$	$^{+12.7}_{-12.6}$	$^{+9.98}_{-9.93}$	$^{+14.3}_{-14.4}$	$^{+12.3}_{-12.0}$	±10.0	$^{+9.39}_{-9.14}$	$^{+9.09}_{-8.93}$
Jet energy resolution [%]	±0.88	±1.19	±0.74	±1.53	±2.44	∓1.06	±5.88	±2.10	±1.59	∓0.70	±1.59
b-Tagged jet energy scale (JES) [%]	$^{+0.77}_{-0.78}$	$^{+0.73}_{-0.69}$	$^{+0.18}_{-0.28}$	$^{+0.63}_{-0.53}$	$^{+0.70}_{-0.74}$	$^{+0.65}_{-0.68}$	$^{+0.79}_{-0.75}$	$^{+0.29}_{-0.20}$	$^{+0.44}_{-0.46}$	$^{+0.49}_{-0.61}$	$^{+0.65}_{-0.62}$
Effective detector NP set 1 (JES) [%]	-	$^{+0.13}_{-0.10}$	-	-	$^{-}_{-0.12}$	$^{+0.11}_{-0.13}$	$^{+0.15}_{-0.18}$	-	$^{-}_{-0.12}$	$^{+0.17}_{-0.10}$	$^{+0.13}_{-0.14}$
Effective detector NP set 2 (JES) [%]	-	$^{+0.12}_{-0.10}$	-	-	-	-	$^{+0.11}_{-0.17}$	-	-	$^{+0.15}_{-}$	$^{+0.15}_{-0.10}$
Effective mixed NP set 1 (JES) [%]	$^{+0.27}_{-0.23}$	±0.81	-	$^{+0.21}_{-0.12}$	$^{+0.19}_{-0.27}$	$^{+0.39}_{-0.35}$	$^{+1.18}_{-1.42}$	$^{+0.51}_{-0.49}$	$^{+0.50}_{-0.53}$	$^{+0.69}_{-0.60}$	$^{+1.00}_{-0.99}$
Effective mixed NP set 2 (JES) [%]	-	$^{-}_{+0.11}$	-	-	-	-	$^{-0.15}_{+0.11}$	-	-	-	$^{-0.13}_{+0.12}$
Effective modelling NP set 1 (JES) [%]	$^{+1.91}_{-1.93}$	$^{+1.52}_{-1.27}$	$^{+4.04}_{-3.80}$	$^{+3.68}_{-3.21}$	$^{+2.81}_{-2.75}$	$^{+1.98}_{-2.12}$	$^{+1.27}_{-1.90}$	$^{+3.22}_{-3.00}$	$^{+2.16}_{-2.17}$	$^{+1.80}_{-1.63}$	$^{+1.34}_{-1.26}$
Effective modelling NP set 2 (JES) [%]	-	$^{+0.30}_{-0.28}$	$^{-0.40}_{+0.46}$	$^{-0.21}_{+0.36}$	-	-	$^{+0.58}_{-0.62}$	$^{-0.11}_{-}$	-	$^{+0.19}_{-0.17}$	$^{+0.43}_{-0.41}$
Effective modelling NP set 3 (JES) [%]	-	$^{-0.31}_{+0.36}$	±0.29	$^{+0.20}_{-}$	-	$^{-0.17}_{+0.16}$	∓0.50	-	-	$^{-0.27}_{+0.32}$	∓0.41
Effective modelling NP set 4 (JES) [%]	$^{+0.11}_{-0.10}$	$^{+0.14}_{-0.10}$	$^{+0.14}_{-0.13}$	$^{+0.20}_{-0.16}$	$^{+0.15}_{-0.14}$	$^{+0.17}_{-0.16}$	$^{+0.12}_{-0.13}$	±0.16	$^{+0.11}_{-0.18}$	$^{+0.17}_{-0.14}$	±0.11
Effective statistical NP set 1 (JES) [%]	$^{+0.30}_{-0.31}$	$^{+0.19}_{-0.18}$	$^{+0.67}_{-0.64}$	$^{+0.68}_{-0.53}$	$^{+0.40}_{-0.51}$	$^{+0.27}_{-0.35}$	$^{+0.28}_{-0.31}$	$^{+0.55}_{-0.50}$	$^{+0.33}_{-0.39}$	$^{+0.27}_{-0.20}$	$^{+0.18}_{-0.13}$
Effective statistical NP set 2 (JES) [%]	∓0.28	-	$^{-0.56}_{+0.61}$	$^{-0.49}_{+0.60}$	$^{-0.44}_{+0.38}$	$^{-0.34}_{+0.30}$	-	$^{-0.41}_{+0.38}$	$^{-0.28}_{+0.25}$	$^{-0.16}_{+0.22}$	-
Effective statistical NP set 3 (JES) [%]	-	$^{-0.20}_{+0.22}$	-	-	-	-	∓0.46	$^{-0.18}_{+0.16}$	$^{-0.17}_{+0.10}$	-	∓0.33
Effective statistical NP set 4 (JES) [%]	±0.14	$^{+0.27}_{-0.23}$	$^{-}_{+0.12}$	-	$^{+0.14}_{-0.20}$	±0.27	$^{+0.31}_{-0.25}$	-	$^{-}_{-0.16}$	$^{+0.30}_{-0.31}$	$^{+0.25}_{-0.26}$
Effective statistical NP set 5 (JES) [%]	-	$^{+0.12}_{-0.14}$	-	$^{-0.10}_{+0.14}$	$^{-0.18}_{+0.19}$	$^{-0.11}_{-}$	$^{+0.21}_{-0.18}$	$^{+0.21}_{-0.15}$	-	-	$^{+0.17}_{-0.15}$
Effective statistical NP set 6 (JES) [%]	-	-	-	-	-	-	-	-	-	-	-
Effective statistical NP set 7 (JES) [%]	-	$^{+0.18}_{-0.15}$	-	$^{+0.14}_{-}$	$^{-}_{-0.11}$	$^{+0.15}_{-0.13}$	±0.22	$^{+0.15}_{-0.18}$	$^{-}_{-0.21}$	$^{+0.22}_{-0.15}$	$^{+0.18}_{-0.14}$
η intercalibration model (JES) [%]	$^{+0.71}_{-0.70}$	$^{+0.77}_{-0.62}$	±0.91	$^{+1.07}_{-0.94}$	$^{+0.83}_{-0.98}$	$^{+0.90}_{-0.89}$	$^{+0.86}_{-1.20}$	$^{+0.95}_{-0.99}$	±0.93	$^{+0.86}_{-0.81}$	$^{+0.96}_{-0.81}$
η intercalibration non closure (JES) [%]	$^{-0.25}_{+0.26}$	∓0.36	$^{-0.35}_{+0.45}$	$^{-0.35}_{+0.44}$	$^{-0.35}_{+0.19}$	$^{-0.36}_{+0.37}$	$^{-0.45}_{+0.39}$	$^{-0.59}_{+0.63}$	$^{-0.53}_{+0.36}$	$^{-0.39}_{+0.34}$	$^{-0.39}_{+0.47}$
η intercalibration total stat (JES) [%]	$^{+0.45}_{-0.42}$	$^{+0.33}_{-0.31}$	$^{+0.65}_{-0.57}$	$^{+0.81}_{-0.65}$	$^{+0.54}_{-0.69}$	$^{+0.52}_{-0.57}$	$^{+0.37}_{-0.45}$	$^{+0.49}_{-0.42}$	$^{+0.46}_{-0.49}$	$^{+0.40}_{-0.45}$	$^{+0.36}_{-0.26}$
Flavour composition (JES) [%]	$^{+1.24}_{-1.40}$	$^{+1.01}_{-0.69}$	$^{+3.84}_{-3.99}$	$^{+3.43}_{-3.23}$	$^{+2.52}_{-2.64}$	$^{+1.76}_{-1.89}$	$^{+0.99}_{-1.80}$	$^{+3.35}_{-3.56}$	$^{+2.18}_{-2.30}$	$^{+1.76}_{-1.51}$	$^{+1.26}_{-1.03}$
Flavour response (JES) [%]	$^{-0.73}_{+0.70}$	$^{-0.42}_{+0.61}$	$^{-1.97}_{+2.06}$	$^{-1.62}_{+1.82}$	$^{-1.42}_{+1.33}$	$^{-1.10}_{+0.99}$	$^{-1.02}_{+0.58}$	$^{-1.69}_{+1.68}$	$^{-1.32}_{+1.26}$	$^{-0.95}_{+0.92}$	$^{-0.59}_{+0.69}$
Pile-up offset μ (JES) [%]	$^{-0.12}_{+0.15}$	$^{-}_{+0.12}$	$^{-0.20}_{+0.23}$	$^{-0.17}_{+0.26}$	$^{-0.29}_{+0.19}$	$^{-0.14}_{-}$	$^{-0.19}_{+0.27}$	$^{-0.11}_{+0.13}$	$^{-0.24}_{+0.14}$	$^{-0.10}_{+0.19}$	$^{-}_{+0.14}$
Pile-up offset N_{PV} (JES) [%]	$^{+0.40}_{-0.47}$	$^{+0.40}_{-0.31}$	$^{+0.83}_{-0.78}$	$^{+1.06}_{-0.70}$	$^{+0.69}_{-0.80}$	$^{+0.46}_{-0.65}$	$^{+0.17}_{-0.37}$	$^{+0.76}_{-0.62}$	$^{+0.42}_{-0.47}$	$^{+0.35}_{-0.40}$	$^{+0.44}_{-0.21}$
Pile-up offset p_T (JES) [%]	$^{+0.36}_{-0.30}$	$^{+0.73}_{-0.78}$	$^{-0.30}_{+0.34}$	-	$^{+0.32}_{-0.43}$	$^{+0.64}_{-0.55}$	$^{+1.11}_{-1.26}$	-	±0.44	$^{+0.66}_{-0.74}$	$^{+0.95}_{-1.04}$
Pile-up offset ρ topology (JES) [%]	$^{+3.13}_{-3.20}$	$^{+2.43}_{-1.98}$	$^{+5.84}_{-5.49}$	$^{+5.61}_{-4.96}$	$^{+4.75}_{-4.59}$	$^{+3.37}_{-3.48}$	$^{+2.11}_{-3.12}$	$^{+4.88}_{-4.51}$	$^{+3.18}_{-3.20}$	$^{+2.93}_{-2.53}$	$^{+2.11}_{-1.87}$
Jet vertex fraction [%]	$^{+0.49}_{-0.53}$	$^{+0.28}_{-0.31}$	$^{+1.06}_{-1.10}$	$^{+0.87}_{-0.91}$	$^{+0.67}_{-0.71}$	$^{+0.50}_{-0.53}$	$^{+0.31}_{-0.35}$	$^{+0.83}_{-0.87}$	$^{+0.61}_{-0.66}$	$^{+0.44}_{-0.48}$	$^{+0.32}_{-0.36}$
b-Quark tagging efficiency (eigenvector 0) [%]	$^{-5.89}_{+6.05}$	$^{-5.70}_{+5.85}$	$^{-6.73}_{+6.92}$	$^{-6.08}_{+6.24}$	$^{-5.78}_{+5.92}$	$^{-5.65}_{+5.78}$	$^{-5.74}_{+5.87}$	$^{-6.24}_{+6.39}$	$^{-5.61}_{+5.73}$	$^{-5.66}_{+5.79}$	$^{-5.76}_{+5.89}$
b-Quark tagging efficiency (eigenvector 1) [%]	$^{-2.45}_{+2.49}$	$^{-3.69}_{+3.76}$	$^{-1.32}_{+1.33}$	$^{-1.66}_{+1.68}$	$^{-1.98}_{+2.00}$	$^{-2.62}_{+2.65}$	$^{-3.94}_{+4.01}$	$^{-2.02}_{+2.03}$	$^{-2.33}_{+2.34}$	$^{-2.49}_{+2.51}$	$^{-3.09}_{+3.12}$
b-Quark tagging efficiency (eigenvector 2) [%]	$^{+1.04}_{-1.03}$	±0.25	$^{+1.35}_{-1.34}$	$^{+1.26}_{-1.25}$	±1.07	±0.70	∓0.12	$^{+1.01}_{-1.00}$	$^{+0.92}_{-0.91}$	±0.77	±0.34
b-Quark tagging efficiency (eigenvector 3) [%]	±0.28	±0.13	-	-	±0.14	±0.16	∓0.16	-	±0.17	±0.14	-
c-Quark tagging efficiency (eigenvector 0) [%]	±0.16	-	±0.40	±0.32	±0.26	±0.18	±0.11	±0.32	±0.22	±0.22	±0.21
c-Quark tagging efficiency (eigenvector 1) [%]	∓0.29	$^{-0.31}_{+0.32}$	∓0.14	$^{-0.24}_{+0.23}$	∓0.31	∓0.37	∓0.45	∓0.14	∓0.30	∓0.32	∓0.38
c-Quark tagging efficiency (eigenvector 2) [%]	-	∓0.10	±0.16	±0.12	-	-	∓0.17	±0.14	-	-	-
Light-jet tagging efficiency (eigenvector 0) [%]	$^{-0.56}_{+0.58}$	$^{-0.56}_{+0.57}$	$^{-0.74}_{+0.73}$	$^{-0.78}_{+0.81}$	$^{-0.75}_{+0.77}$	$^{-0.74}_{+0.75}$	∓0.78	$^{-0.74}_{+0.78}$	∓0.60	$^{-0.74}_{+0.76}$	$^{-0.88}_{+0.92}$
Light-jet tagging efficiency (eigenvector 1) [%]	±0.11	-	±0.39	$^{+0.27}_{-0.26}$	$^{+0.19}_{-0.18}$	±0.12	-	±0.32	$^{+0.20}_{-0.21}$	±0.21	±0.11
Light-jet tagging efficiency (eigenvector 2) [%]	-	-	-	-	-	-	-	-	-	-	-
Light-jet tagging efficiency (eigenvector 3) [%]	-	∓0.13	-	-	-	-	∓0.17	-	-	-	∓0.12
b-Quark tagging extrapolation [%]	-	±0.41	-	-	-	±0.12	$^{+1.13}_{-1.12}$	-	-	-	±0.87
Electron energy scale [%]	-	-	-	-	-	-	-	-	-	-	-
Electron trigger efficiency [%]	±0.11	±0.10	$^{+0.11}_{-0.12}$	±0.11	±0.11	±0.11	±0.11	±0.11	±0.11	±0.12	±0.12
Electron reconstruction efficiency [%]	-	±0.10	-	-	-	-	±0.11	-	-	-	-
Electron identification efficiency [%]	$^{+0.43}_{-0.44}$	±0.57	±0.38	±0.39	±0.41	±0.47	±0.63	±0.51	±0.49	±0.47	±0.52
Electron isolation efficiency [%]	±0.11	±0.32	-	-	±0.10	±0.17	±0.42	±0.22	±0.21	±0.19	±0.25
Muon trigger efficiency stat [%]	±0.28	$^{+0.27}_{-0.28}$	±0.29	$^{+0.28}_{-0.29}$	$^{+0.28}_{-0.29}$	±0.28	±0.27	±0.28	±0.28	$^{+0.28}_{-0.29}$	±0.29
Muon trigger efficiency syst [%]	$^{+0.50}_{-0.49}$	$^{+0.48}_{-0.47}$	$^{+0.51}_{-0.50}$	$^{+0.51}_{-0.50}$	$^{+0.50}_{-0.49}$	$^{+0.50}_{-0.48}$	$^{+0.47}_{-0.46}$	$^{+0.49}_{-0.48}$	$^{+0.49}_{-0.48}$	$^{+0.51}_{-0.50}$	$^{+0.50}_{-0.49}$
Muon identification stat [%]	-	-	-	-	-	-	-	-	-	-	-
Muon identification syst [%]	±0.37	±0.45	±0.36	±0.36	±0.37	±0.39	±0.47	±0.41	±0.41	$^{+0.41}_{-0.40}$	$^{+0.43}_{-0.42}$
Muon isolation efficiency syst [%]	±0.10	±0.10	±0.10	±0.10	±0.10	±0.10	±0.10	±0.10	±0.10	±0.10	±0.10
E_T^{miss} Soft jet resolution para [%]	±0.24	-	-	-	-	±0.13	±0.28	∓0.36	-	-	-
E_T^{miss} Soft jet resolution perp [%]	±0.28	±0.26	-	∓0.12	-	±0.14	-	∓0.39	-	-	-
E_T^{miss} Soft jet scale [%]	-	-	$^{-0.11}_{+0.17}$	$^{-0.20}_{+0.34}$	$^{-0.17}_{+0.16}$	-	-	$^{-0.31}_{+0.21}$	$^{-0.12}_{+0.13}$	-	$^{+0.11}_{-0.21}$
Luminosity [%]	∓2.05	∓2.05	∓2.05	∓2.05	∓2.05	∓2.05	∓2.05	∓2.05	∓2.05	∓2.05	∓2.05
Z+jets cross-section [%]	±0.30	±0.19	±0.56	±0.51	±0.45	±0.33	±0.22	±0.40	±0.41	±0.51	±0.63
Monte Carlo sample statistics [%]	±0.22	±0.35	±0.29	±0.32	±0.35	±0.37	±0.81	±0.49	±0.51	±0.54	±0.70
ISR/FSR + scale [%]	$^{-0.40}_{+0.84}$	$^{-0.64}_{+0.95}$	$^{-}_{+0.45}$	$^{+0.89}_{-0.12}$	$^{+0.61}_{-}$	$^{+1.21}_{-}$	$^{+2.66}_{-}$	$^{+0.61}_{-}$	$^{+1.10}_{-1.12}$	$^{+0.66}_{-0.74}$	$^{-}_{-1.03}$
Alternate hard-scattering model [%]	±2.03	±0.22	±6.10	±5.13	±4.06	±2.67	±7.40	±3.41	±3.26	±3.99	∓0.33
Alternate parton-shower model [%]	±2.53	±0.62	±3.60	±5.90	±6.03	±4.24	±3.10	±4.37	±2.60	±1.90	±1.74
Intra PDF [%]	±0.40	±0.30	±0.15	±0.11	±0.12	±0.47	±0.33	±0.37	±0.16	±0.20	±0.19
Fakes overall normalization, el [%]	±0.65	$^{+0.11}_{-0.12}$	±0.53	±0.86	±1.03	$^{+1.09}_{-1.08}$	±1.27	∓0.15	-	±0.53	±1.11
Fakes overall normalization, mu [%]	-	∓0.63	±0.42	±0.29	±0.22	-	∓0.87	∓0.25	∓0.17	∓0.28	∓0.36
Fakes alternative parametrization [%]	∓1.05	±0.94	∓2.77	∓3.07	∓2.73	∓0.86	±1.47	±0.58	∓0.17	∓1.20	∓0.97
W+jets heavy flavour component [%]	±2.40	±1.50	±2.18	±2.07	±2.59	∓0.13	±4.79	±3.27	±3.11	-	±2.91

TABLE F.12: Table of systematics for the absolute differential cross-section at the particle level for the $p_T^{t,had}$ vs $p_T^{t\bar{t}}$ observable.

F.1.1.2 Boosted topology

Bins [GeV]	350–400	400–455	455–520	520–610	610–710	710–820	820–930	930–2000
$d\sigma$ / $dp_T^{t,had}$ [pb/GeV]	$1.49 \cdot 10^{-2}$	$9.33 \cdot 10^{-3}$	$4.95 \cdot 10^{-3}$	$2.23 \cdot 10^{-3}$	$8.08 \cdot 10^{-4}$	$2.50 \cdot 10^{-4}$	$1.14 \cdot 10^{-4}$	$4.74 \cdot 10^{-6}$
Total Uncertainty [%]	+8.86 −8.74	+8.08 −8.85	+8.91 −7.74	+9.03 −9.52	+10.1 −10.8	+19.7 −16.5	+30.6 −29.0	+32.7 −32.8
Statistics [%]	±1.0	±1.2	±1.6	±2.0	±3.3	±6.2	±9.3	±16.
Systematics [%]	+8.77 −8.66	+7.94 −8.72	+8.72 −7.51	+8.70 −9.21	+9.43 −10.1	+18.5 −15.0	+28.6 −26.9	±27.5
b-Tagged jet energy scale (JES) [%]	+0.38 −0.39	+0.40 −0.64	+0.71 −0.38	+0.43 −0.59	+0.50 −0.63	+1.14 −0.39	- −0.97	+0.68 −0.78
Effective detector NP set 1 (JES) [%]	+0.12 −0.14	- −0.15	+0.33 -	- −0.16	- −0.31	+0.92 -	- −1.14	+1.15 −0.67
Effective detector NP set 2 (JES) [%]	+0.11 −0.13	- −0.14	+0.30 −0.10	- −0.14	-	+0.44 -	- −0.25	+0.26 −0.53
Effective mixed NP set 1 (JES) [%]	+0.66 −0.68	+0.91 −1.26	+1.80 −1.03	+1.54 −2.10	+2.19 −2.03	+4.38 −2.62	+0.26 −2.94	+6.12 −4.62
Effective mixed NP set 2 (JES) [%]	∓0.10	-	-	−0.20	-	+0.86 -	−0.25 -	−0.42
Effective mixed NP set 3 (JES) [%]	-	-	+0.29 -	+0.15 -	−0.29 -	- +0.39	- -	+0.10 -
Effective modelling NP set 1 (JES) [%]	+1.48 −1.34	+1.36 −1.63	+2.11 −1.55	+1.38 −1.67	+1.17 −1.65	- +3.10	−0.29 +0.77	- +2.31
Effective modelling NP set 2 (JES) [%]	+0.10 −0.16	+0.29 −0.44	+0.91 −0.47	+0.38 −0.88	±1.34	−2.09 +2.93	- +0.26	−1.87 +5.28
Effective modelling NP set 3 (JES) [%]	−0.30 +0.26	−0.58 +0.43	−0.42 +0.76	−0.58 +0.48	−0.66 +0.34	−1.02 +1.08	−1.91 -	−3.68 -
Effective modelling NP set 4 (JES) [%]	+0.13 −0.19	+0.13 −0.14	+0.28 −0.11	-	- −0.23	+1.17 −0.15	−0.65 - −1.42	−0.97 +0.95 −0.46
Effective statistical NP set 1 (JES) [%]	±0.11	+0.15 −0.20	+0.40 −0.21	+0.26 −0.34	+0.17 −0.51	+1.69 −0.75	−1.62 +1.56	+1.83 −2.06
Effective statistical NP set 2 (JES) [%]	−0.15	−0.25	+0.25	-	-	−1.56	∓1.53	+1.77
Effective statistical NP set 3 (JES) [%]	+0.16 -	+0.12 −0.45	−0.11 −0.64	−0.93	−0.49 −1.21	−0.68 −1.13	+0.79	−1.97 −0.62
Effective statistical NP set 4 (JES) [%]	+0.36	+0.17 +0.34	+1.02 +0.34	+0.73 -	+0.82 -	+1.97 -	−0.35 −0.37	+0.92 −0.12
Effective statistical NP set 5 (JES) [%]	−0.32 +0.11	−0.42 +0.30	−0.13 +0.46	+0.14	-	+0.43 −0.39	- -	+0.26 −0.50
Effective statistical NP set 6 (JES) [%]	−0.13 −0.13	−0.31 -	−0.26 +0.29	−0.21 -	−0.27 -	+1.10 -	−0.69 −0.52	+1.09 −0.51
Effective statistical NP set 7 (JES) [%]	+0.14 −0.18	+0.12 −0.23	−0.13 +0.47 −0.12	+0.18 −0.34	−0.30 - −0.28	+0.88 +0.86 -	- −0.79	+0.39 +1.10 −0.66
η intercalibration model (JES) [%]	+0.75 −0.62	+0.70 −1.12	+1.51 −0.72	+0.95 −1.17	+0.91 −1.58	+2.03 −1.30	+0.54 -	+2.23 −2.31
η intercalibration non closure (JES) [%]	−0.33 +0.44	−0.78 +0.47	−0.29 +0.87	−1.12 +0.44	−0.55 +0.11	−1.44 +1.58	−1.21 +1.32	−0.37 +0.54
η intercalibration total stat (JES) [%]	+0.31 −0.36	+0.40 −0.48	+0.49 −0.24	+0.24 −0.50	+0.23 −0.49	+1.05 -	−0.53	+1.18 −0.96
Flavour composition (JES) [%]	+1.71 −1.67	+1.72 −2.11	+2.50 −1.66	+2.00 −2.20	+2.12 −2.88	+3.75 −2.74	+3.06 −2.72	+4.14 −3.60
Flavour response (JES) [%]	−0.90 +0.89	−1.33 +1.07	−0.94 +1.41	−1.08 +0.81	−0.80 +0.43	−0.68 +1.43	+0.82 -	- −0.24
Pile-up offset μ (JES) [%]	−0.15 +0.16	−0.18 +0.10	-	-	-	- +0.38	−0.10 +0.44	−0.33
Pile-up offset N_{PV} (JES) [%]	+0.57 −0.39	+0.22 −0.46	+0.63 −0.33	+0.24 −0.49	+0.47 −0.48	+1.87 −0.39	- −0.94	+1.65 −0.32
Pile-up offset p_T (JES) [%]	+0.74 −0.86	+0.82 −1.13	+1.70 −0.79	+0.84 −1.33	±1.19	+2.35 −1.46	+0.83 −1.08	+1.29 −1.48
Pile-up offset ρ topology (JES) [%]	+2.49 −2.37	+2.23 −2.57	+2.82 −2.12	+1.97 −2.01	+1.47 −2.27	+3.24 −2.30	+1.86 −0.20	+1.88 −1.67
Punch-through (JES) [%]	-	-	-	-	-	-	- −0.62	+0.28 -
Single particle high-p_T (JES) [%]	-	-	-	-	-	-	-	−0.10 +0.11
Jet vertex fraction [%]	+0.27 −0.31	+0.29 −0.33	+0.25 −0.29	+0.23 −0.27	+0.22 −0.26	+0.25 −0.29	+0.13 −0.19	+0.37 −0.42
b-Quark tagging efficiency (eigenvector 0) [%]	−1.52	−1.39	−1.62	−1.74	−1.80	−1.99	−2.30	−2.54
b-Quark tagging efficiency (eigenvector 1) [%]	+1.46 −1.12	+1.52 −1.17	+1.55 −1.17	+1.66 −1.31	+1.73 −1.31	+1.91 −1.40	+2.23 −1.66	+2.45 −1.54
b-Quark tagging efficiency (eigenvector 2) [%]	+1.09 -	+1.13 -	+1.13 -	+1.27 ∓0.11	+1.26 -	+1.36 -	+1.63 ∓0.10	+1.48 ∓0.17
b-Quark tagging efficiency (eigenvector 3) [%]	-	-	-	∓0.10	−0.13 +0.12	∓0.13	∓0.15	−0.33 +0.32
b-Quark tagging efficiency (eigenvector 4) [%]	-	-	-	-	-	-	-	∓0.10
c-Quark tagging efficiency (eigenvector 0) [%]	-	-	-	-	-	±0.12	-	±0.15
c-Quark tagging efficiency (eigenvector 1) [%]	∓0.22	∓0.28	∓0.27	−0.28 +0.27	∓0.34	∓0.42	∓0.63	∓0.38
c-Quark tagging efficiency (eigenvector 2) [%]	-	∓0.10	-	-	∓0.13	∓0.14	−0.28 +0.27	-
Light-jet tagging efficiency (eigenvector 0) [%]	∓0.39	−0.47 +0.48	∓0.61	−0.58 +0.59	∓0.84	−1.15 +1.20	−1.08 +1.07	−2.42 +2.40
Light-jet tagging efficiency (eigenvector 1) [%]	-	-	-	-	-	−0.17 +0.19	-	∓0.90
Light-jet tagging efficiency (eigenvector 2) [%]	-	-	-	±0.10	-	-	∓0.16	∓0.12
Light-jet tagging efficiency (eigenvector 3) [%]	∓0.10	∓0.10	∓0.15	∓0.16	∓0.17	∓0.20	∓0.12	±0.28
Light-jet tagging efficiency (eigenvector 4) [%]	-	-	-	-	-	-	-	±0.36
Light-jet tagging efficiency (eigenvector 5) [%]	-	-	-	-	-	±0.24	±0.19	±0.58
Light-jet tagging efficiency (eigenvector 6) [%]	-	-	-	-	-	∓0.16	-	∓0.30
Light-jet tagging efficiency (eigenvector 7) [%]	-	-	-	-	-	∓0.21	∓0.13	∓0.50
Light-jet tagging efficiency (eigenvector 8) [%]	-	-	-	-	-	-	-	±0.16
Light-jet tagging efficiency (eigenvector 9) [%]	-	-	-	-	-	-	-	∓0.21
b-Quark tagging extrapolation [%]	-	±0.30	±0.39	±0.60	+0.85 −0.87	+1.06 −1.08	+1.70 −1.73	+1.94 −2.05
Electron energy scale [%]	-	-	-	-	-	-	- −0.25	-
Electron trigger efficiency [%]	±0.11	±0.11	±0.11	±0.12	±0.12	±0.12	±0.13	±0.14
Electron reconstruction efficiency [%]	±0.10	±0.10	±0.11	±0.11	±0.12	±0.12	±0.14	±0.15
Electron identification efficiency [%]	±0.57	±0.62	±0.65	±0.70	±0.73	±0.78	±0.81	±0.98
Electron isolation efficiency [%]	±0.33	±0.41	±0.48	±0.57	±0.62	±0.77	±0.85	±1.05
Muon trigger efficiency stat [%]	±0.28	+0.28 −0.29	±0.28	+0.27 −0.28	±0.29	±0.31	±0.30	±0.35
Muon trigger efficiency syst [%]	+0.49 −0.48	+0.49 −0.48	+0.49 −0.48	+0.49 −0.48	+0.52 −0.51	+0.50 −0.49	+0.52 −0.51	+0.57 −0.56
Muon identification stat [%]	-	-	-	-	-	-	±0.10	±0.10
Muon identification syst [%]	±0.46	±0.49	±0.51	±0.53	±0.58	±0.56	+0.61 −0.60	±0.65
Muon isolation efficiency syst [%]	±0.10	±0.10	±0.10	±0.11	±0.12	±0.12	±0.15	±0.18
E_T^{miss} Soft jet resolution para [%]	∓0.25	∓0.26	∓0.15	∓0.21	∓0.16	±0.21	∓0.11	∓0.25
E_T^{miss} Soft jet resolution perp [%]	∓0.21	∓0.17	-	∓0.16	∓0.19	±0.38	-	∓0.17
E_T^{miss} Soft jet scale [%]	−0.19 +0.15	−0.26 +0.14	- +0.13	−0.11 +0.13	-	- +0.27	- −0.34	-
Luminosity [%]	∓2.05	∓2.05	∓2.05	∓2.05	∓2.05	∓2.05	∓2.05	∓2.05
Z+jets cross-section [%]	±0.37	±0.46	±0.48	±0.51	±0.68	±0.84	±1.15	±1.46
Diboson cross-section [%]	-	-	-	-	-	-	±0.13	±0.11
$t\bar{t}V$ cross-section [%]	±0.10	±0.11	±0.13	±0.16	±0.19	±0.19	±0.27	±0.34
Monte Carlo sample statistics [%]	±0.62	±0.76	±0.93	±1.23	±1.89	±3.14	±5.38	±5.87
ISR/FSR + scale [%]	−0.47 +1.17	−2.02 +0.22	- −0.77	+0.41 -	+0.32 −0.56	+7.31 -	+10.7 -	- −5.17
Alternate hard-scattering model [%]	±1.26	±1.41	∓1.58	±0.84	∓2.68	±7.71	±13.8	±17.0
Alternate parton-shower model [%]	±6.00	±4.41	±2.03	±3.59	±0.93	±5.08	±18.8	±3.79
Fakes overall normalization, el [%]	±0.63	±0.68	±0.80	±1.14	±1.37	±2.34	±1.33	±3.06
Fakes overall normalization, mu [%]	±0.37	±0.33	±0.35	±0.27	-	-	-	∓0.70
Fakes alternative parametrization [%]	∓2.02	∓2.03	∓2.31	∓2.84	∓2.56	∓4.69	∓2.58	∓4.72
W+jets heavy flavour component [%]	±0.16	±0.10	-	-	-	-	±0.12	±0.35
W+jets Scales [%]	±2.46	±3.04	±3.50	±3.92	±5.00	±6.06	±6.73	±11.7
W+jets α_S [%]	−0.16 +0.18	−0.19 +0.22	−0.21 +0.24	−0.24 +0.29	−0.31 +0.37	−0.33 +0.47	−0.39 +0.53	−0.62 +1.07
Single Top DS/DR [%]	∓1.17	∓1.62	∓2.08	∓2.86	∓3.87	∓4.80	∓6.02	∓11.0
Single Top IFSR [%]	- −0.36	- −0.59	- −0.81	+0.18 −0.64	+0.63 −0.85	+0.57 −0.39	+3.35 −1.89	+2.63 −1.46

TABLE F.13: Table of systematics for the absolute differential cross-section at the particle level for the $p_{\mathrm{T}}^{t,\mathrm{had}}$ observable.

Bins [Unit $y^{t,had}$]	0–0.50	0.50–1	1–1.50	1.50–2
$d\sigma$ / $dy^{t,had}$ [pb/ Unit $y^{t,had}$]	$1.44 \cdot 10^{0}$	$1.22 \cdot 10^{0}$	$8.01 \cdot 10^{-1}$	$3.47 \cdot 10^{-1}$
Total Uncertainty [%]	$^{+7.93}_{-8.11}$	$^{+8.42}_{-8.15}$	$^{+9.37}_{-9.58}$	$^{+9.28}_{-9.02}$
Statistics [%]	±0.9	±0.9	±1.2	±1.8
Systematics [%]	$^{+7.86}_{-8.04}$	$^{+8.35}_{-8.07}$	$^{+9.26}_{-9.47}$	$^{+9.03}_{-8.75}$
b-Tagged jet energy scale (JES) [%]	$^{+0.47}_{-0.54}$	$^{+0.49}_{-0.41}$	$^{+0.46}_{-0.59}$	$^{+0.44}_{-0.41}$
Effective detector NP set 1 (JES) [%]	$^{+0.13}_{-0.17}$	$^{+0.18}_{-0.10}$	$^{+0.17}_{-0.16}$	±0.13
Effective detector NP set 2 (JES) [%]	$^{+0.12}_{-0.14}$	$^{+0.16}_{-0.10}$	$^{+0.15}_{-0.14}$	-
Effective mixed NP set 1 (JES) [%]	$^{+1.07}_{-1.17}$	$^{+1.22}_{-1.12}$	$^{+1.35}_{-1.34}$	$^{+1.31}_{-1.20}$
Effective mixed NP set 2 (JES) [%]	$^{-0.13}$	-	$^{-0.13}$	-
Effective modelling NP set 1 (JES) [%]	$^{+0.11}_{+1.44}$	$^{+0.16}_{+1.65}$	$^{+0.14}_{+1.67}$	$^{+1.51}$
Effective modelling NP set 2 (JES) [%]	$^{-1.48}_{+0.42}$	$^{-1.48}_{+0.50}$	$^{-1.75}_{+0.49}$	$^{-1.21}_{+0.50}$
Effective modelling NP set 3 (JES) [%]	$^{-0.49}_{-0.46}$	$^{-0.40}_{-0.38}$	$^{-0.58}_{-0.51}$	$^{-0.42}_{-0.40}$
Effective modelling NP set 4 (JES) [%]	$^{+0.41}_{+0.15}$	$^{+0.47}_{+0.17}$	$^{+0.48}_{+0.18}$	$^{+0.36}_{+0.11}$
Effective statistical NP set 1 (JES) [%]	$^{-0.18}$ ±0.19	$^{-0.11}_{-0.17}$	$^{-0.19}_{-0.30}$	$^{-0.16}_{-0.18}$
Effective statistical NP set 3 (JES) [%]	$^{-0.40}$	∓0.39	$^{-0.54}$	∓0.45
Effective statistical NP set 4 (JES) [%]	$^{+0.34}_{+0.24}$	$^{+0.29}$	$^{+0.43}$ ±0.31	$^{+0.26}$
Effective statistical NP set 5 (JES) [%]	$^{-0.27}_{+0.20}$	$^{-0.22}_{+0.22}$	$^{+0.18}$	$^{-0.20}_{+0.11}$
Effective statistical NP set 7 (JES) [%]	$^{-0.21}_{+0.20}$	$^{-0.15}_{+0.21}$	$^{-0.21}_{+0.23}$	$^{-0.18}_{+0.15}$
η intercalibration model (JES) [%]	$^{-0.23}$ ±0.11	$^{-0.15}_{+0.72}$	$^{-0.22}_{+2.02}$	$^{-0.19}_{+2.57}$
η intercalibration non closure (JES) [%]	-	$^{-0.55}_{-0.63}$	$^{-2.22}_{-1.11}$	$^{-2.28}_{-0.70}$
η intercalibration total stat (JES) [%]	$^{+0.32}$	$^{+0.70}_{+0.37}$	$^{+0.94}_{+0.48}$	$^{+1.01}_{+0.36}$
Flavour composition (JES) [%]	$^{-0.35}$	$^{-0.36}$	$^{-0.52}$	$^{-0.32}$
Flavour response (JES) [%]	$^{+1.71}_{-1.70}$	$^{+1.98}_{-2.04}$	$^{+2.26}_{-2.21}$	$^{+2.32}_{-1.95}$
Flavour response (JES) [%]	$^{-0.84}$	$^{-1.02}$	$^{-1.38}$	$^{-0.97}$
Pile-up offset μ (JES) [%]	$^{+0.80}_{-0.12}$	$^{+1.04}_{-}$	$^{+1.20}_{-0.16}$	$^{+1.34}_{-}$
Pile-up offset N_{PV} (JES) [%]	$^{+0.37}$	$^{+0.19}_{+0.55}$	$^{+0.47}$	$^{+0.50}$
Pile-up offset p_T (JES) [%]	$^{-0.44}_{+0.72}$	$^{-0.44}_{+1.09}$	$^{-0.37}_{+1.20}$	$^{-0.35}_{+1.45}$
Pile-up offset ρ topology (JES) [%]	$^{-0.87}_{+2.23}$	$^{-0.91}_{+2.56}$	$^{-1.22}_{+2.47}$	$^{-1.35}_{+2.19}$
Jet vertex fraction [%]	$^{-2.29}_{+0.25}$	$^{-2.33}_{+0.27}$	$^{-2.50}_{+0.28}$	$^{-1.98}_{+0.28}$
b-Quark tagging efficiency (eigenvector 0) [%]	$^{-0.29}_{-1.55}$	$^{-0.31}_{-1.63}$	$^{-0.32}_{-1.66}$	$^{-0.32}_{-1.72}$
b-Quark tagging efficiency (eigenvector 1) [%]	$^{+1.48}_{-1.17}$	$^{+1.56}_{-1.17}$	$^{+1.60}_{-1.22}$	$^{+1.65}_{-1.22}$
c-Quark tagging efficiency (eigenvector 1) [%]	$^{+1.13}$ ∓0.26	$^{+1.13}$ ∓0.27	$^{+1.18}$ ∓0.27	$^{+1.18}_{-0.27}$
Light-jet tagging efficiency (eigenvector 0) [%]	∓0.44	$^{-0.55}_{+0.56}$	∓0.54	$^{+0.26}_{-0.75}$
Light-jet tagging efficiency (eigenvector 2) [%]	-	-	-	$^{+0.76}$ ±0.11
Light-jet tagging efficiency (eigenvector 3) [%]	$^{-0.10}$	∓0.10	∓0.14	∓0.20
b-Quark tagging extrapolation [%]	$^{+0.11}_{+0.34}$	±0.33	±0.32	±0.25
Electron trigger efficiency [%]	$^{-0.35}$ ±0.11	±0.11	±0.11	±0.12
Electron reconstruction efficiency [%]	±0.11	±0.11	±0.11	±0.11
Electron identification efficiency [%]	±0.62	±0.63	±0.63	±0.64
Electron isolation efficiency [%]	±0.43	±0.44	±0.43	±0.43
Muon trigger efficiency stat [%]	±0.28	±0.28	±0.28	±0.28
Muon trigger efficiency syst [%]	$^{+0.50}_{-0.48}$	$^{+0.49}_{-0.48}$	$^{+0.50}_{-0.49}$	$^{+0.49}_{-0.48}$
Muon identification syst [%]	±0.49	$^{+0.50}_{-0.49}$	±0.49	±0.50
Muon isolation efficiency syst [%]	±0.10	±0.10	±0.10	±0.10
E_T^{miss} Soft jet resolution para [%]	∓0.20	∓0.23	∓0.22	∓0.23
E_T^{miss} Soft jet resolution perp [%]	∓0.14	∓0.15	∓0.18	∓0.18
E_T^{miss} Soft jet scale [%]	$^{-0.12}_{-}$	$^{-0.19}_{+0.17}$	$^{-0.22}_{+0.17}$	$^{-0.23}_{+0.11}$
Luminosity [%]	∓2.05	∓2.05	∓2.05	∓2.05
Z+jets cross-section [%]	±0.44	±0.46	±0.46	±0.58
$t\bar{t}V$ cross-section [%]	±0.12	±0.12	±0.12	±0.12
Monte Carlo sample statistics [%]	±0.53	±0.59	±0.71	±1.11
ISR/FSR + scale [%]	$^{-}_{-0.83}$	$^{-0.34}_{+1.41}$	$^{-}_{-0.32}$	$^{-}_{-1.16}$
Alternate hard-scattering model [%]	±0.88	±0.10	±2.12	±0.74
Alternate parton-shower model [%]	±4.20	±3.94	±4.95	±4.21
Fakes overall normalization, el [%]	±0.77	±0.84	±0.85	±0.84
Fakes overall normalization, mu [%]	±0.34	±0.33	±0.21	±0.30
Fakes alternative parametrization [%]	∓2.24	∓2.36	∓2.13	∓2.27
W+jets heavy flavour component [%]	±0.10	±0.11	±0.12	-
W+jets Scales [%]	±3.06	±3.23	±3.22	±3.92
W+jets α_S [%]	$^{-0.19}_{+0.22}$	$^{-0.20}_{+0.23}$	$^{-0.19}_{+0.23}$	$^{-0.22}_{+0.30}$
Single Top DS/DR [%]	∓1.96	∓2.01	∓1.89	∓1.48
Single Top IFSR [%]	$^{-}_{-0.59}$	$^{+0.12}_{-0.30}$	$^{-}_{-0.95}$	$^{+0.37}_{-0.63}$

TABLE F.14: Table of systematics for the absolute differential cross-section at the particle level for the y^{had}observable.

Bins [GeV]	0–55	55–135	135–280	280–380	380–650	650–1000
$d\sigma$ / $dp_T^{t\bar{t}}$ [pb/GeV]	$9.71 \cdot 10^{-3}$	$7.51 \cdot 10^{-3}$	$3.29 \cdot 10^{-3}$	$1.54 \cdot 10^{-3}$	$4.80 \cdot 10^{-4}$	$3.67 \cdot 10^{-5}$
Total Uncertainty [%]	$^{+6.66}_{-6.62}$	±10.6	$^{+11.6}_{-11.5}$	$^{+10.3}_{-11.0}$	$^{+12.4}_{-13.1}$	$^{+20.2}_{-18.8}$
Statistics [%]	±1.1	±1.2	±1.3	±2.5	±2.6	±8.5
Systematics [%]	$^{+6.52}_{-6.48}$	±10.5	$^{+11.5}_{-11.4}$	$^{+9.94}_{-10.6}$	$^{+12.0}_{-12.8}$	$^{+17.8}_{-16.2}$
b-Tagged jet energy scale (JES) [%]	$^{+0.46}_{-0.54}$	$^{+0.52}_{-0.49}$	$^{+0.43}_{-0.45}$	$^{+0.50}_{-0.52}$	$^{+0.43}_{-0.41}$	$^{+0.38}_{-0.79}$
Effective detector NP set 1 (JES) [%]	$^{+0.12}_{-0.18}$	$^{+0.16}_{-0.11}$	$^{+0.19}_{-0.12}$	$^{+0.19}_{-0.20}$	-	$^{+1.08}_{-0.26}$
Effective detector NP set 2 (JES) [%]	$^{+0.11}_{-0.16}$	$^{+0.14}_{-0.10}$	$^{+0.16}_{-}$	$^{+0.13}_{-0.12}$	-	$^{+0.63}_{-}$
Effective mixed NP set 1 (JES) [%]	$^{+1.17}_{-1.26}$	$^{+1.25}_{-1.29}$	$^{+1.06}_{-0.91}$	$^{+1.44}_{-1.39}$	$^{+0.90}_{-1.01}$	$^{+3.47}_{-2.83}$
Effective mixed NP set 2 (JES) [%]	$^{-0.15}_{+0.10}$	$^{-}_{+0.15}$	$^{-}_{+0.15}$	$^{-}_{+0.13}$	-	$^{+0.90}_{-}$
Effective mixed NP set 3 (JES) [%]	-	-	-	-	-	$^{+0.20}_{-}$
Effective modelling NP set 1 (JES) [%]	$^{+0.86}_{-0.92}$	$^{+1.79}_{-1.71}$	$^{+1.92}_{-1.74}$	$^{+1.90}_{-1.80}$	$^{+1.72}_{-1.97}$	$^{+3.11}_{-2.25}$
Effective modelling NP set 2 (JES) [%]	$^{+0.54}_{-0.56}$	$^{+0.45}_{-0.46}$	$^{+0.38}_{-0.39}$	$^{+0.45}_{-0.46}$	$^{+0.31}_{-0.32}$	$^{+2.19}_{-1.25}$
Effective modelling NP set 3 (JES) [%]	$^{-0.52}_{+0.50}$	$^{-0.41}_{+0.40}$	$^{-0.41}_{+0.35}$	$^{-0.39}_{+0.60}$	$^{-0.45}_{+0.39}$	$^{+1.08}_{-}$
Effective modelling NP set 4 (JES) [%]	$^{+0.14}_{-0.18}$	$^{+0.15}_{-0.15}$	$^{+0.21}_{-0.11}$	$^{+0.21}_{-0.24}$	-	$^{+1.08}_{-0.24}$
Effective statistical NP set 1 (JES) [%]	-	$^{+0.22}_{-0.26}$	$^{+0.30}_{-0.26}$	$^{+0.48}_{-0.15}$	$^{-0.21}_{-0.35}$	$^{+1.27}_{-0.78}$
Effective statistical NP set 2 (JES) [%]	-	-	-	-	-	$^{+0.46}_{-0.31}$
Effective statistical NP set 3 (JES) [%]	$^{-0.46}_{+0.40}$	$^{-0.42}_{+0.38}$	$^{+0.14}_{-0.33}$	$^{+0.23}_{-0.48}$	$^{-0.28}_{-0.61}$	$^{-0.86}_{-}$
Effective statistical NP set 4 (JES) [%]	$^{+0.30}_{-0.35}$	$^{+0.22}_{-0.19}$	$^{+0.24}_{-0.27}$	$^{+0.66}_{+0.26}$	$^{+0.47}_{-}$	$^{+1.23}_{+0.51}$
Effective statistical NP set 5 (JES) [%]	$^{+0.28}_{-0.30}$	$^{+0.20}_{-0.16}$	-	$^{-0.21}_{+0.10}$	$^{-0.26}_{+0.25}$	$^{-}_{-0.15}$
Effective statistical NP set 6 (JES) [%]	-	-	-	-	$^{-0.43}_{-}$	$^{+0.49}_{+0.44}$
Effective statistical NP set 7 (JES) [%]	$^{+0.20}_{-0.25}$	$^{+0.19}_{-0.15}$	$^{+0.21}_{-0.20}$	±0.26	$^{-0.22}_{-}$	$^{-}_{+1.10}$
η intercalibration model (JES) [%]	$^{+0.57}_{-0.79}$	$^{+0.96}_{-0.92}$	$^{+1.12}_{-0.71}$	$^{+1.37}_{-1.72}$	$^{-0.14}_{+1.05}$	$^{-0.12}_{+2.18}$
η intercalibration non closure (JES) [%]	$^{-0.55}_{+0.47}$	$^{-0.56}_{+0.50}$	$^{-0.33}_{+0.58}$	∓0.79	$^{-0.90}_{-0.46}$	$^{-1.41}_{-0.20}$
η intercalibration total stat (JES) [%]	±0.26	$^{+0.32}_{-0.44}$	$^{+0.38}_{-0.43}$	$^{+0.65}_{-0.51}$	$^{+0.52}_{-0.38}$	$^{+0.77}_{-0.46}$
Flavour composition (JES) [%]	$^{+0.97}_{-1.02}$	$^{+2.35}_{-2.27}$	$^{+2.38}_{-2.20}$	$^{+2.46}_{-2.73}$	$^{+2.26}_{-2.31}$	$^{+4.14}_{-4.73}$
Flavour response (JES) [%]	$^{+0.58}_{-0.63}$	$^{+1.07}_{-1.04}$	$^{+1.28}_{-1.27}$	$^{+1.46}_{-1.66}$	$^{+1.07}_{-0.96}$	$^{+1.92}_{-1.66}$
Pile-up offset μ (JES) [%]	-	-	$^{-0.14}_{+0.23}$	-	$^{-0.28}_{+0.10}$	$^{+0.64}_{-}$
Pile-up offset N_{PV} (JES) [%]	$^{+0.32}_{-0.26}$	$^{+0.53}_{-0.54}$	$^{+0.45}_{-0.36}$	$^{+0.69}_{-0.70}$	$^{+0.55}_{-0.52}$	$^{+0.49}_{-}$
Pile-up offset p_T (JES) [%]	$^{+1.00}_{-1.07}$	$^{+0.98}_{-1.11}$	$^{+1.06}_{-0.86}$	$^{+1.06}_{-0.86}$	$^{+0.66}_{-0.91}$	$^{+2.52}_{-0.97}$
Pile-up offset ρ topology (JES) [%]	$^{+1.25}_{-1.30}$	$^{+2.67}_{-2.81}$	$^{+3.07}_{-2.67}$	$^{+3.13}_{-2.86}$	$^{+2.56}_{-2.64}$	$^{+3.25}_{-2.30}$
Punch-through (JES) [%]	-	-	-	-	-	-
Jet vertex fraction [%]	$^{+0.11}_{-0.14}$	$^{+0.31}_{-0.35}$	$^{+0.35}_{-0.39}$	$^{+0.37}_{-0.41}$	$^{+0.34}_{-0.39}$	$^{+0.27}_{-0.32}$
b-Quark tagging efficiency (eigenvector 0) [%]	$^{-1.40}_{+1.33}$	$^{-1.55}_{+1.48}$	$^{-1.79}_{+1.73}$	$^{-1.84}_{+1.78}$	$^{-1.92}_{+1.84}$	$^{-2.32}_{+2.27}$
b-Quark tagging efficiency (eigenvector 1) [%]	$^{-1.33}_{+1.20}$	$^{-1.48}_{+1.24}$	$^{-1.72}_{+1.09}$	$^{-0.93}_{+0.90}$	$^{-0.96}_{+0.93}$	$^{-1.17}_{+1.14}$
b-Quark tagging efficiency (eigenvector 2) [%]	∓0.10	∓0.13	-	±0.25	±0.25	$^{+0.22}_{-0.21}$
c-Quark tagging efficiency (eigenvector 0) [%]	-	-	-	±0.13	±0.13	$^{+0.17}_{-0.18}$
c-Quark tagging efficiency (eigenvector 1) [%]	∓0.20	∓0.32	∓0.30	∓0.21	∓0.21	∓0.18
c-Quark tagging efficiency (eigenvector 2) [%]	-	∓0.11	∓0.10	-	-	-
Light-jet tagging efficiency (eigenvector 0) [%]	∓0.50	∓0.43	$^{-0.50}_{+0.51}$	$^{-0.72}_{+0.73}$	$^{-0.78}_{+0.80}$	$^{-1.64}_{+1.65}$
Light-jet tagging efficiency (eigenvector 1) [%]	-	-	-	-	-	$^{+0.20}_{-0.19}$
Light-jet tagging efficiency (eigenvector 2) [%]	-	-	-	±0.13	±0.11	-
Light-jet tagging efficiency (eigenvector 3) [%]	∓0.14	∓0.14	∓0.10	-	∓0.11	-
Light-jet tagging efficiency (eigenvector 5) [%]	-	-	-	-	-	±0.12
b-Quark tagging extrapolation [%]	±0.31	±0.41	±0.37	$^{+0.14}_{-0.15}$	-	-
Electron energy resolution [%]	-	-	-	-	-	-
Electron trigger efficiency [%]	±0.11	±0.11	±0.12	±0.12	±0.12	±0.12
Electron reconstruction efficiency [%]	±0.11	±0.11	±0.10	±0.10	±0.10	±0.11
Electron identification efficiency [%]	±0.66	±0.65	±0.60	±0.54	±0.55	±0.65
Electron isolation efficiency [%]	±0.52	±0.47	±0.36	±0.27	±0.27	±0.48
Muon trigger efficiency stat [%]	±0.28	$^{+0.27}_{-0.28}$	±0.28	$^{+0.29}_{-0.30}$	$^{+0.29}_{-0.30}$	$^{+0.33}_{-0.34}$
Muon trigger efficiency syst [%]	$^{+0.49}_{-0.48}$	$^{+0.49}_{-0.48}$	$^{+0.49}_{-0.48}$	$^{+0.53}_{-0.51}$	$^{+0.52}_{-0.51}$	$^{+0.56}_{-0.55}$
Muon identification stat [%]	-	-	-	-	-	±0.11
Muon identification syst [%]	±0.54	±0.50	±0.46	±0.43	±0.45	±0.55
Muon isolation efficiency syst [%]	±0.10	±0.10	±0.10	±0.11	±0.11	±0.12
E_T^{miss} Soft jet resolution para [%]	∓0.36	∓0.40	-	±0.47	∓0.52	∓0.74
E_T^{miss} Soft jet resolution perp [%]	∓0.59	-	±0.16	±0.29	∓0.46	±0.30
E_T^{miss} Soft jet scale [%]	$^{-0.45}_{+0.19}$	$^{-}_{+0.30}$	-	$^{+0.38}_{-}$	-	$^{-}_{+0.26}$
Luminosity [%]	∓2.05	∓2.05	∓2.05	∓2.05	∓2.05	∓2.05
Z+jets cross-section [%]	±0.27	±0.42	±0.55	±0.79	±0.81	±1.05
$t\bar{t}V$ cross-section [%]	-	±0.11	±0.18	±0.22	±0.24	±0.25
Monte Carlo sample statistics [%]	±0.69	±0.72	±0.80	±1.59	±1.55	±4.37
ISR/FSR + scale [%]	$^{-1.26}_{+2.17}$	$^{-0.40}_{+1.30}$	$^{+0.78}_{-2.04}$	$^{-}_{-3.26}$	$^{+0.51}_{-3.24}$	$^{+4.97}_{-}$
Alternate hard-scattering model [%]	∓3.21	±2.22	±5.20	±2.88	∓4.84	±3.47
Alternate parton-shower model [%]	±0.30	±6.94	±5.52	±1.45	±6.90	±10.8
Fakes overall normalization, el [%]	∓0.14	±0.91	±1.61	±1.67	±0.95	-
Fakes overall normalization, mu [%]	-	±0.49	±0.36	±0.58	±0.39	±0.12
Fakes alternative parametrization [%]	±0.30	∓2.82	∓3.96	∓4.51	∓2.69	∓0.12
W+jets heavy flavour component [%]	±0.18	-	-	-	-	-
W+jets Scales [%]	±2.52	±3.13	±3.45	±3.92	±4.98	±6.07
W+jets α_S [%]	$^{-0.18}_{+0.20}$	$^{-0.20}_{+0.22}$	$^{-0.19}_{+0.25}$	$^{-0.22}_{+0.27}$	$^{-0.27}_{+0.35}$	$^{-0.32}_{+0.47}$
Single Top DS/DR [%]	∓1.33	∓1.92	∓2.13	∓2.37	∓2.89	∓4.36
Single Top IFSR [%]	-	$^{-}_{-0.81}$	$^{+0.21}_{-0.58}$	$^{-}_{-1.94}$	$^{+0.78}_{-0.32}$	$^{+1.31}_{-1.87}$

TABLE F.15: Table of systematics for the absolute differential cross-section at the particle level for the $p_{\mathrm{T}}^{t\bar{t}}$ observable.

Bins [GeV]	490–710	710–815	815–920	920–1035	1035–1165	1165–1310	1310–1500	1500–1700	1700–2100	2100–3000
$d\sigma$ / $dm^{t\bar{t}}$ [pb/GeV]	$6.88 \cdot 10^{-4}$	$2.28 \cdot 10^{-3}$	$3.63 \cdot 10^{-3}$	$3.24 \cdot 10^{-3}$	$2.27 \cdot 10^{-3}$	$1.39 \cdot 10^{-3}$	$6.80 \cdot 10^{-4}$	$3.57 \cdot 10^{-4}$	$1.14 \cdot 10^{-4}$	$1.21 \cdot 10^{-5}$
Total Uncertainty [%]	$^{+12.8}_{-11.4}$	$^{+8.82}_{-9.40}$	$^{+7.01}_{-7.21}$	$^{+7.58}_{-7.79}$	$^{+9.37}_{-9.03}$	$^{+12.6}_{-12.5}$	$^{+10.4}_{-9.83}$	$^{+13.2}_{-14.2}$	$^{+19.5}_{-18.5}$	$^{+31.6}_{-31.5}$
Statistics [%]	±2.5	±1.8	±1.3	±1.3	±1.5	±1.9	±2.5	±3.6	±4.8	±12.
Systematics [%]	$^{+12.5}_{-11.0}$	$^{+8.55}_{-9.16}$	$^{+6.83}_{-7.04}$	$^{+7.41}_{-7.63}$	$^{+9.18}_{-8.84}$	±12.3	$^{+10.0}_{-9.37}$	$^{+12.5}_{-13.5}$	$^{+18.7}_{-17.6}$	$^{+28.7}_{-28.6}$
b-Tagged jet energy scale (JES) [%]	$^{+0.32}_{-0.25}$	$^{-}_{-0.48}$	±0.41	$^{+0.62}_{-0.59}$	$^{+0.53}_{-0.38}$	$^{+0.57}_{-0.78}$	$^{+0.87}_{-0.44}$	$^{+0.46}_{-0.49}$	$^{+0.45}_{-0.81}$	$^{+0.42}_{-0.45}$
Effective detector NP set 1 (JES) [%]	-	$^{-}_{-0.30}$	$^{+0.24}_{-0.10}$	$^{+0.15}_{-0.11}$	$^{-}_{-0.17}$	$^{+0.13}_{-0.25}$	$^{+0.46}_{-}$	$^{-}_{-0.29}$	$^{+0.18}_{-0.33}$	$^{+0.72}_{-}$
Effective detector NP set 2 (JES) [%]	-	$^{-}_{-0.27}$	$^{+0.25}_{-0.10}$	$^{+0.13}_{-0.10}$	-	$^{+0.18}_{-0.16}$	$^{+0.29}_{-}$	$^{-}_{-0.26}$	$^{-}_{-0.20}$	$^{+0.38}_{-}$
Effective mixed NP set 1 (JES) [%]	$^{+0.50}_{-}$	$^{+0.27}_{-0.93}$	$^{+0.60}_{-0.86}$	$^{+1.37}_{-1.38}$	$^{+1.11}_{-0.93}$	$^{+1.85}_{-1.63}$	$^{+2.39}_{-1.66}$	$^{+1.84}_{-2.45}$	$^{+2.87}_{-2.60}$	$^{+2.64}_{-3.61}$
Effective mixed NP set 2 (JES) [%]	-	$^{-}_{-0.21}$	$^{-}_{+0.23}$	$^{-}_{-}$	$^{-0.13}_{-}$	$^{-0.18}_{+0.14}$	$^{-}_{+0.37}$	$^{-0.37}_{+0.11}$	$^{-0.24}_{+0.21}$	$^{+0.43}_{-}$
Effective mixed NP set 3 (JES) [%]	-	-	-	-	-	-	-	-	±0.12	-
Effective modelling NP set 1 (JES) [%]	$^{+1.91}_{-1.47}$	$^{+0.92}_{-1.64}$	$^{+1.56}_{-1.41}$	$^{+1.72}_{-1.53}$	$^{+1.33}_{-1.16}$	$^{+1.82}_{-1.93}$	$^{+1.86}_{-1.63}$	$^{+1.28}_{-1.84}$	$^{+1.53}_{-1.27}$	$^{+2.19}_{-1.79}$
Effective modelling NP set 2 (JES) [%]	-	$^{-}_{-0.35}$	$^{+0.24}_{-0.28}$	$^{+0.35}_{-0.50}$	$^{+0.51}_{-0.28}$	$^{+0.67}_{-0.74}$	$^{+1.22}_{-0.66}$	$^{+0.72}_{-1.24}$	$^{+1.77}_{-1.59}$	$^{+1.85}_{-1.61}$
Effective modelling NP set 3 (JES) [%]	$^{-}_{+0.18}$	$^{-}_{-0.55}$	$^{-}_{+0.39}$	$^{-0.34}_{+0.57}$	$^{-0.53}_{+0.56}$	$^{-0.36}_{+0.53}$	$^{-0.75}_{-0.33}$	$^{-0.53}_{+0.40}$	$^{-0.51}_{+0.52}$	$^{-0.14}_{+0.50}$
Effective modelling NP set 4 (JES) [%]	-	$^{-}_{-0.36}$	$^{-}_{-0.10}$	$^{+0.16}_{-0.13}$	$^{-}_{-0.17}$	$^{+0.10}_{-0.15}$	$^{+0.52}_{-}$	$^{+0.12}_{-0.59}$	$^{-}_{\pm 0.21}$	$^{+0.72}_{-}$
Effective statistical NP set 1 (JES) [%]	$^{+0.20}_{-}$	$^{-}_{-0.36}$	$^{+0.34}_{-0.15}$	$^{-}_{-}$	$^{+0.13}_{-0.22}$	±0.34	$^{+0.44}_{-0.15}$	$^{+0.35}_{-0.38}$	$^{+0.41}_{-0.47}$	$^{+0.72}_{-0.57}$
Effective statistical NP set 2 (JES) [%]	$^{-0.23}_{+0.20}$	$^{-0.33}_{-}$	$^{-}_{+0.18}$	$^{-}_{-}$	$^{-}_{-}$	$^{-}_{-}$	$^{+0.43}_{-}$	$^{-}_{-0.47}$	$^{+0.35}_{-0.28}$	$^{+0.60}_{-0.53}$
Effective statistical NP set 3 (JES) [%]	-	$^{-}_{-0.56}$	$^{-0.19}_{+0.16}$	$^{-0.45}_{+0.44}$	$^{-0.28}_{+0.64}$	$^{-0.76}_{+0.59}$	$^{-0.74}_{+0.96}$	$^{-0.41}_{+0.64}$	$^{-1.10}_{+0.59}$	$^{-0.33}_{+0.83}$
Effective statistical NP set 4 (JES) [%]	$^{+0.12}_{-0.17}$	$^{-}_{-0.44}$	$^{+0.46}_{-0.29}$	$^{+0.42}_{-0.31}$	$^{+0.23}_{-0.18}$	$^{+0.22}_{-0.39}$	$^{+0.24}_{-}$	$^{-}_{-}$	$^{-}_{-}$	$^{-}_{-}$
Effective statistical NP set 5 (JES) [%]	$^{-}_{-0.21}$	$^{-}_{-0.34}$	$^{+0.24}_{-0.15}$	$^{+0.34}_{-0.22}$	$^{+0.17}_{-0.23}$	$^{+0.29}_{-0.40}$	$^{+0.36}_{+0.28}$	$^{-}_{-0.31}$	$^{-}_{-}$	$^{+0.24}_{-}$
Effective statistical NP set 6 (JES) [%]	-	$^{-}_{-0.20}$	$^{-}_{-}$	$^{-}_{-}$	$^{-}_{-}$	±0.10	$^{-}_{-}$	$^{-}_{-0.24}$	$^{+0.15}_{+0.21}$	$^{+0.39}_{-}$
Effective statistical NP set 7 (JES) [%]	-	$^{-}_{-0.49}$	$^{+0.22}_{-0.15}$	$^{+0.21}_{-0.14}$	$^{+0.19}_{-0.18}$	$^{+0.30}_{-0.37}$	$^{+0.36}_{-}$	$^{+0.25}_{-0.39}$	$^{+0.21}_{-0.34}$	$^{+0.59}_{-}$
η intercalibration model (JES) [%]	$^{+0.95}_{-0.20}$	$^{+0.61}_{-0.63}$	$^{+0.64}_{-0.63}$	±0.84	$^{+0.73}_{-0.97}$	$^{+1.34}_{-1.19}$	$^{+1.45}_{-1.16}$	$^{+1.00}_{-1.84}$	$^{+2.34}_{-1.57}$	$^{+2.98}_{-2.71}$
η intercalibration non closure (JES) [%]	$^{+0.26}_{-}$	$^{-}_{-0.46}$	$^{-0.49}_{+0.58}$	$^{-0.54}_{+0.58}$	$^{-0.48}_{+0.42}$	$^{-0.56}_{+0.91}$	$^{-0.90}_{+0.75}$	$^{-1.45}_{+0.67}$	$^{-0.17}_{+0.92}$	$^{-0.54}_{+1.09}$
η intercalibration total stat (JES) [%]	$^{+0.29}_{-0.25}$	$^{+0.17}_{-0.67}$	$^{+0.45}_{-0.32}$	$^{+0.35}_{-0.36}$	$^{+0.51}_{-0.29}$	$^{+0.46}_{-0.48}$	$^{+0.55}_{-0.31}$	$^{+0.27}_{-0.65}$	$^{+0.41}_{-0.23}$	$^{+0.78}_{-0.55}$
Flavour composition (JES) [%]	$^{+2.05}_{-1.70}$	$^{+1.37}_{-1.98}$	$^{+1.22}_{-1.69}$	$^{+1.96}_{-1.91}$	$^{+1.88}_{-1.56}$	$^{+2.17}_{-2.39}$	$^{+2.59}_{-1.89}$	$^{+2.55}_{-2.90}$	$^{+2.74}_{-2.86}$	$^{+4.72}_{-4.42}$
Flavour response (JES) [%]	$^{-1.12}_{+0.99}$	$^{-1.25}_{+0.62}$	$^{-0.95}_{+1.03}$	$^{-1.00}_{+1.08}$	$^{-0.92}_{+1.04}$	$^{-1.26}_{+1.18}$	$^{-0.91}_{+1.03}$	$^{-1.14}_{+1.05}$	$^{-0.60}_{+0.86}$	$^{-0.68}_{+0.41}$
Pile-up offset μ (JES) [%]	$^{-0.20}_{+0.22}$	$^{-}_{-0.26}$	$^{-}_{+0.21}$	$^{-}_{+0.20}$	$^{-0.18}_{+0.10}$	$^{-}_{-}$	$^{-0.10}_{+0.39}$	$^{-0.58}_{-}$	$^{-}_{-}$	$^{-}_{+0.16}$
Pile-up offset N_{PV} (JES) [%]	$^{+0.50}_{-0.28}$	$^{-}_{-0.72}$	$^{+0.73}_{-0.46}$	$^{+0.51}_{-0.39}$	$^{+0.30}_{-0.21}$	$^{+0.52}_{-0.74}$	$^{+0.75}_{-0.23}$	$^{+0.41}_{-0.46}$	$^{+0.42}_{-}$	$^{+0.31}_{-0.57}$
Pile-up offset p_T (JES) [%]	$^{+0.38}_{-0.51}$	$^{+0.41}_{-0.63}$	$^{+0.83}_{-0.97}$	$^{+1.02}_{-1.13}$	$^{+1.29}_{-0.98}$	$^{+1.25}_{-1.30}$	$^{+1.52}_{-0.84}$	$^{+1.46}_{-1.80}$	$^{+1.19}_{-1.89}$	$^{+2.28}_{-1.93}$
Pile-up offset ρ topology (JES) [%]	$^{+0.59}_{-2.24}$	$^{+0.83}_{-2.51}$	$^{+1.07}_{-2.20}$	$^{+1.18}_{-2.52}$	$^{+1.21}_{-2.05}$	$^{+1.33}_{-2.62}$	$^{+1.40}_{-2.03}$	$^{+1.50}_{-2.47}$	$^{+1.60}_{-1.67}$	$^{+2.01}_{-3.43}$
Punch-through (JES) [%]	-	-	-	-	-	-	-	-	$^{-}_{-0.16}$	-
Jet vertex fraction [%]	$^{+0.45}_{-0.49}$	$^{+0.31}_{-0.35}$	$^{+0.25}_{-0.29}$	$^{+0.24}_{-0.28}$	$^{+0.25}_{-0.29}$	$^{+0.22}_{-0.27}$	$^{+0.21}_{-0.26}$	$^{+0.26}_{-0.30}$	$^{+0.31}_{-0.35}$	$^{+0.34}_{-0.41}$
b-Quark tagging efficiency (eigenvector 0) [%]	$^{-2.16}_{+2.10}$	$^{-1.54}_{+1.48}$	$^{-1.47}_{+1.40}$	$^{-1.32}_{+1.45}$	$^{-1.56}_{+1.49}$	$^{-1.59}_{+1.51}$	$^{-1.68}_{+1.61}$	$^{-1.86}_{+1.78}$	$^{-1.86}_{+1.77}$	$^{-2.55}_{+2.47}$
b-Quark tagging efficiency (eigenvector 1) [%]	$^{-0.60}_{+0.59}$	$^{-0.83}_{+0.83}$	$^{-1.11}_{+1.07}$	$^{-1.22}_{+1.18}$	$^{-1.26}_{+1.21}$	$^{-1.37}_{+1.33}$	$^{-1.35}_{+1.40}$	$^{-1.55}_{+1.50}$	$^{-1.64}_{+1.60}$	$^{-2.06}_{+2.01}$
b-Quark tagging efficiency (eigenvector 2) [%]	±0.46	±0.18	-	-	-	∓0.19	∓0.20	∓0.18	$^{-0.25}_{+0.24}$	∓0.38
b-Quark tagging efficiency (eigenvector 3) [%]	-	-	-	-	-	-	∓0.13	∓0.14	∓0.19	∓0.31
b-Quark tagging efficiency (eigenvector 4) [%]	-	-	-	-	-	-	-	-	-	∓0.11
c-Quark tagging efficiency (eigenvector 0) [%]	±0.17	-	-	-	-	-	-	-	-	±0.17
c-Quark tagging efficiency (eigenvector 1) [%]	∓0.11	∓0.16	$^{-0.20}_{+0.19}$	∓0.19	∓0.28	∓0.36	∓0.36	∓0.57	∓0.66	$^{-1.20}_{+1.21}$
c-Quark tagging efficiency (eigenvector 2) [%]	-	-	-	-	∓0.11	∓0.12	∓0.10	∓0.24	∓0.30	∓0.51
Light-jet tagging efficiency (eigenvector 0) [%]	$^{-0.73}_{+0.75}$	$^{-0.28}_{+0.27}$	∓0.39	$^{-0.29}_{+0.31}$	∓0.53	∓0.65	$^{-0.71}_{+0.72}$	$^{-0.88}_{+0.87}$	$^{-1.25}_{+1.23}$	∓2.80
Light-jet tagging efficiency (eigenvector 1) [%]	±0.15	-	-	-	-	-	∓0.11	-	∓0.28	$^{-0.96}_{+0.95}$
Light-jet tagging efficiency (eigenvector 2) [%]	$^{+0.19}_{-0.18}$	-	-	-	-	±0.10	±0.10	-	-	-
Light-jet tagging efficiency (eigenvector 3) [%]	-	-	-	-	∓0.15	∓0.16	∓0.20	∓0.28	∓0.34	∓0.61
Light-jet tagging efficiency (eigenvector 4) [%]	-	-	-	-	-	-	-	-	-	±0.14
Light-jet tagging efficiency (eigenvector 5) [%]	-	-	-	-	-	-	-	-	±0.21	$^{+0.59}_{-0.60}$
Light-jet tagging efficiency (eigenvector 6) [%]	-	-	-	-	-	-	-	-	∓0.17	$^{-0.16}_{+0.17}$
Light-jet tagging efficiency (eigenvector 7) [%]	-	-	-	-	-	-	-	-	∓0.11	∓0.33
Light-jet tagging efficiency (eigenvector 8) [%]	-	-	-	-	-	-	-	-	-	∓0.10
Light-jet tagging efficiency (eigenvector 9) [%]	-	-	-	-	-	-	-	-	-	∓0.17
b-Quark tagging extrapolation [%]	-	-	±0.11	±0.20	±0.39	$^{+0.52}_{-0.53}$	$^{+0.69}_{-0.70}$	$^{+0.91}_{-0.93}$	$^{+1.20}_{-1.22}$	$^{+2.43}_{-2.47}$
Electron energy resolution [%]	-	$^{-0.18}_{-}$	-	-	-	-	-	$^{+0.20}_{-}$	-	$^{+0.24}_{-}$
Electron energy scale [%]	-	$^{-}_{-0.22}$	-	-	-	-	-	$^{+0.36}_{-}$	$^{-0.27}_{+0.14}$	$^{-0.12}_{+0.37}$
Electron trigger efficiency [%]	±0.12	±0.11	±0.10	±0.11	±0.11	±0.11	±0.12	±0.13	±0.16	±0.20
Electron reconstruction efficiency [%]	-	-	±0.10	±0.11	±0.11	±0.11	±0.12	±0.12	±0.15	±0.18
Electron identification efficiency [%]	±0.40	±0.53	±0.58	±0.63	±0.65	±0.69	±0.73	±0.77	±0.92	±1.18
Electron isolation efficiency [%]	-	±0.23	±0.36	±0.45	±0.50	±0.55	±0.61	±0.68	±0.75	±0.98
Muon (ID) momentum resolution [%]	-	-	-	-	-	-	$^{+0.28}_{-}$	-	$^{+0.29}_{-0.29}$	$^{-1.08}_{+1.04}$
Muon (MS) momentum resolution [%]	-	-	-	-	-	-	-	$^{+0.22}_{-0.19}$	$^{-0.19}_{+0.20}$	$^{+0.24}_{-0.38}$
Muon energy scale [%]	-	-	-	-	-	-	-	$^{-0.19}_{-0.20}$	$^{-}_{-}$	$^{-}_{-}$
Muon trigger efficiency stat [%]	±0.31	$^{+0.27}_{-0.28}$	±0.27	±0.27	±0.28	±0.29	$^{+0.29}_{-0.30}$	$^{+0.30}_{-0.31}$	±0.31	$^{+0.37}_{-0.38}$
Muon trigger efficiency syst [%]	$^{+0.53}_{-0.52}$	$^{+0.47}_{-0.46}$	$^{+0.47}_{-0.46}$	$^{+0.48}_{-0.47}$	$^{+0.49}_{-0.48}$	$^{+0.51}_{-0.50}$	$^{+0.52}_{-0.51}$	$^{+0.54}_{-0.53}$	$^{+0.55}_{-0.54}$	$^{+0.68}_{-0.67}$
Muon identification stat [%]	±0.10	-	-	-	-	-	-	±0.10	±0.11	±0.13
Muon identification syst [%]	±0.37	±0.40	±0.44	±0.48	±0.52	±0.56	±0.60	±0.66	±0.68	$^{+0.96}_{-0.95}$
Muon isolation efficiency syst [%]	±0.11	±0.10	-	±0.10	±0.10	±0.11	±0.12	±0.14	±0.14	±0.20
E_T^{miss} Soft jet resolution para [%]	±0.31	±0.20	-	∓0.32	∓0.36	∓0.70	∓0.50	∓0.51	∓0.54	∓0.46
E_T^{miss} Soft jet resolution perp [%]	±0.79	-	-	∓0.13	∓0.44	∓0.73	∓0.13	∓0.58	∓0.58	∓0.44
E_T^{miss} Soft jet scale [%]	$^{+0.88}_{-0.91}$	-	-	$^{-0.18}_{+0.24}$	$^{-0.33}_{+0.22}$	$^{-0.53}_{+0.59}$	$^{-0.33}_{+0.41}$	$^{-0.95}_{+0.63}$	$^{-0.61}_{+0.43}$	$^{-0.59}_{+0.84}$
Luminosity [%]	∓2.05	∓2.05	∓2.05	∓2.05	∓2.05	∓2.05	∓2.05	∓2.05	∓2.05	∓2.05
Z+jets cross-section [%]	±0.74	±0.35	±0.24	±0.31	±0.39	±0.52	±0.68	±0.90	±1.29	±2.52
Diboson cross-section [%]	-	-	-	-	-	-	-	-	-	±0.13
$t\bar{t}V$ cross-section [%]	±0.17	±0.13	±0.10	±0.10	±0.12	±0.13	±0.15	±0.15	±0.18	±0.25
Monte Carlo sample statistics [%]	±1.51	±1.08	±0.80	±0.82	±0.94	±1.19	±1.47	±2.24	±2.71	±4.83
ISR/FSR + scale [%]	$^{+6.27}_{-2.59}$	$^{-0.52}_{+2.09}$	$^{-2.65}_{+1.34}$	$^{-}_{-2.15}$	$^{+1.91}_{-}$	$^{+2.07}_{-}$	$^{-}_{-1.92}$	$^{-}_{-2.68}$	$^{+6.70}_{-2.84}$	$^{+5.57}_{-1.91}$
Alternate hard-scattering model [%]	±5.90	±1.29	∓0.59	∓0.95	∓0.57	±8.01	∓1.65	-	±3.53	±7.56
Alternate parton-shower model [%]	±4.18	±6.50	±3.22	±3.45	±6.23	±3.28	±1.26	±7.03	±8.46	±2.88
Fakes overall normalization, el [%]	$^{+1.12}_{-1.11}$	±0.72	±0.54	±0.62	±0.59	±0.70	±0.96	±1.43	±2.60	±5.98
Fakes overall normalization, mu [%]	±0.52	±0.26	±0.27	±0.35	±0.10	±0.50	±0.35	±0.24	±0.69	±0.71
Fakes alternative parametrization [%]	∓3.29	∓1.97	∓1.63	∓1.95	∓1.40	∓2.42	∓2.62	∓3.35	∓6.59	∓10.5
W+jets heavy flavour component [%]	-	±0.13	±0.14	±0.11	-	-	-	±0.10	±0.15	±0.24
W+jets Scales [%]	±3.83	±1.92	±1.74	±2.14	±2.90	±4.16	±5.11	±6.06	±9.34	±19.5
W+jets α_S [%]	$^{-0.21}_{+0.25}$	$^{-0.11}_{+0.13}$	$^{-0.11}_{+0.12}$	∓0.15	$^{-0.19}_{+0.21}$	$^{-0.25}_{+0.31}$	$^{-0.30}_{+0.37}$	$^{-0.42}_{+0.46}$	$^{-0.51}_{+0.69}$	$^{-1.16}_{+1.49}$
Single Top DS/DR [%]	∓1.02	∓0.90	∓1.09	∓1.31	∓1.86	∓2.97	∓3.50	∓4.35	∓5.01	∓9.07
Single Top IFSR [%]	$^{+0.43}_{-0.40}$	$^{-}_{-0.36}$	$^{-}_{-0.46}$	$^{-}_{-0.54}$	$^{-}_{-0.47}$	$^{+0.46}_{-0.89}$	$^{+0.57}_{-0.78}$	$^{-}_{-0.57}$	$^{+0.84}_{-0.65}$	$^{+1.12}_{-4.53}$

TABLE F.16: Table of systematics for the absolute differential cross-section at the particle level for the $m_{t\bar{t}}$observable.

Bins [Unit $y^{t\bar{t}}$]	0–0.50	0.50–1	1–1.50	1.50–2
$d\sigma$ / $dy^{t\bar{t}}$ [pb/ Unit $y^{t\bar{t}}$]	$1.93 \cdot 10^{0}$	$1.33 \cdot 10^{0}$	$4.90 \cdot 10^{-1}$	$6.28 \cdot 10^{-2}$
Total Uncertainty [%]	$^{+7.50}_{-7.63}$	$^{+9.85}_{-9.74}$	$^{+9.20}_{-9.11}$	$^{+12.2}_{-12.8}$
Statistics [%]	±0.7	±0.9	±1.6	±4.9
Systematics [%]	$^{+7.44}_{-7.58}$	$^{+9.78}_{-9.67}$	$^{+8.99}_{-8.90}$	$^{+10.8}_{-11.5}$
b-Tagged jet energy scale (JES) [%]	$^{+0.43}_{-0.49}$	$^{+0.49}_{-0.48}$	$^{+0.57}_{-0.58}$	$^{+0.59}_{-0.54}$
Effective detector NP set 1 (JES) [%]	$^{+0.15}_{-0.13}$	$^{+0.16}_{-0.15}$	$^{+0.12}_{-0.14}$	$^{+0.39}_{-0.33}$
Effective detector NP set 2 (JES) [%]	$^{+0.14}_{-0.11}$	$^{+0.12}_{-0.14}$	$^{+0.16}_{-0.14}$	- $^{-}_{-0.20}$
Effective mixed NP set 1 (JES) [%]	$^{+1.03}_{-1.10}$	$^{+1.34}_{-1.24}$	$^{+1.41}_{-1.40}$	$^{+1.43}_{-1.30}$
Effective mixed NP set 2 (JES) [%]	$^{-0.10}_{+0.13}$	∓0.13	$^{-0.12}_{+0.15}$	-
Effective modelling NP set 1 (JES) [%]	$^{+1.48}_{-1.51}$	$^{+1.62}_{-1.49}$	$^{+1.74}_{-1.53}$	$^{+1.38}_{-1.57}$
Effective modelling NP set 2 (JES) [%]	±0.42	$^{+0.51}_{-0.52}$	$^{+0.55}_{-0.54}$	$^{+0.44}_{-0.47}$
Effective modelling NP set 3 (JES) [%]	$^{-0.43}_{+0.40}$	$^{-0.42}_{+0.47}$	$^{-0.53}_{+0.51}$	$^{-0.34}_{+0.53}$
Effective modelling NP set 4 (JES) [%]	$^{+0.16}_{-0.15}$	$^{+0.16}_{-0.17}$	±0.16	$^{+0.15}_{-0.33}$
Effective statistical NP set 1 (JES) [%]	$^{+0.22}_{-0.17}$	$^{+0.19}_{-0.23}$	$^{+0.22}_{-0.24}$	$^{+0.57}_{-0.31}$
Effective statistical NP set 2 (JES) [%]	-	-	-	$^{-0.13}_{+0.24}$
Effective statistical NP set 3 (JES) [%]	$^{-0.38}_{+0.36}$	$^{-0.44}_{+0.41}$	$^{-0.61}_{+0.39}$	$^{-0.38}_{+0.62}$
Effective statistical NP set 4 (JES) [%]	$^{+0.25}_{-0.23}$	$^{+0.30}_{-0.27}$	$^{+0.28}_{-0.30}$	$^{+0.19}_{-0.27}$
Effective statistical NP set 5 (JES) [%]	$^{+0.20}_{-0.18}$	$^{+0.19}_{-0.17}$	$^{+0.16}_{-0.25}$	$^{+0.54}_{-0.13}$
Effective statistical NP set 6 (JES) [%]	-	-	-	$^{-}_{+0.36}$
Effective statistical NP set 7 (JES) [%]	$^{+0.21}_{-0.18}$	$^{+0.19}_{-0.21}$	$^{+0.21}_{-0.24}$	$^{+0.41}_{-0.29}$
η intercalibration model (JES) [%]	$^{+0.38}_{-0.42}$	$^{+1.25}_{-1.10}$	$^{+1.95}_{-1.82}$	$^{+2.66}_{-3.12}$
η intercalibration non closure (JES) [%]	∓0.29	$^{-0.66}_{+0.69}$	$^{-0.92}_{+1.04}$	$^{-0.54}_{+0.79}$
η intercalibration total stat (JES) [%]	±0.34	$^{+0.39}_{-0.42}$	$^{+0.40}_{-0.44}$	$^{+0.69}_{-0.59}$
Flavour composition (JES) [%]	$^{+1.80}_{-1.90}$	$^{+2.09}_{-1.93}$	$^{+2.23}_{-2.04}$	$^{+2.33}_{-2.47}$
Flavour response (JES) [%]	$^{-0.96}_{+0.91}$	$^{-1.05}_{+1.10}$	$^{-1.14}_{+1.10}$	$^{-1.31}_{+1.40}$
Pile-up offset μ (JES) [%]	$^{-0.11}_{+0.13}$	$^{-0.12}_{+0.11}$	$^{-0.14}_{+0.12}$	-
Pile-up offset N_{PV} (JES) [%]	±0.40	$^{+0.54}_{-0.41}$	$^{+0.48}_{-0.47}$	$^{+0.45}_{-0.59}$
Pile-up offset p_T (JES) [%]	$^{+0.81}_{-0.87}$	$^{+1.12}_{-1.01}$	$^{+1.36}_{-1.48}$	$^{+1.54}_{-1.14}$
Pile-up offset ρ topology (JES) [%]	$^{+2.31}_{-2.35}$	$^{+2.41}_{-2.35}$	$^{+2.57}_{-2.11}$	$^{+2.17}_{-2.30}$
Jet vertex fraction [%]	$^{+0.26}_{-0.30}$	$^{+0.27}_{-0.31}$	$^{+0.27}_{-0.30}$	$^{+0.28}_{-0.32}$
b-Quark tagging efficiency (eigenvector 0) [%]	$^{-1.57}_{+1.50}$	$^{-1.64}_{+1.57}$	$^{-1.71}_{+1.65}$	$^{-1.54}_{+1.47}$
b-Quark tagging efficiency (eigenvector 1) [%]	$^{-1.16}_{+1.12}$	$^{-1.21}_{+1.17}$	$^{-1.21}_{+1.18}$	$^{-1.22}_{+1.19}$
c-Quark tagging efficiency (eigenvector 1) [%]	∓0.26	∓0.26	$^{-0.27}_{+0.26}$	∓0.25
Light-jet tagging efficiency (eigenvector 0) [%]	∓0.46	$^{-0.52}_{+0.51}$	∓0.75	$^{-0.80}_{+0.82}$
Light-jet tagging efficiency (eigenvector 1) [%]	-	-	-	∓0.11
Light-jet tagging efficiency (eigenvector 2) [%]	-	-	±0.11	-
Light-jet tagging efficiency (eigenvector 3) [%]	-	∓0.14	∓0.17	∓0.33
Light-jet tagging efficiency (eigenvector 8) [%]	-	-	-	∓0.10
b-Quark tagging extrapolation [%]	$^{+0.33}_{-0.34}$	±0.32	$^{+0.30}_{-0.31}$	±0.24
Electron energy resolution [%]	-	-	-	- $^{+0.34}$
Electron energy scale [%]	-	-	-	$^{+0.20}_{-}$
Electron trigger efficiency [%]	±0.10	±0.11	±0.14	±0.20
Electron reconstruction efficiency [%]	±0.10	±0.10	±0.12	±0.13
Electron identification efficiency [%]	±0.61	±0.61	±0.68	±1.00
Electron isolation efficiency [%]	±0.44	±0.43	±0.40	±0.44
Muon (ID) momentum resolution [%]	-	-	-	-
Muon (MS) momentum resolution [%]	-	-	-	- $^{-0.33}$
Muon energy scale [%]	-	-	-	- $^{+0.19}$
Muon trigger efficiency stat [%]	$^{+0.28}_{-0.29}$	±0.28	$^{+0.27}_{-0.28}$	±0.25
Muon trigger efficiency syst [%]	$^{+0.49}_{-0.48}$	$^{+0.50}_{-0.49}$	$^{+0.51}_{-0.50}$	$^{+0.51}_{-0.50}$
Muon identification stat [%]	-	-	±0.10	±0.10
Muon identification syst [%]	±0.46	$^{+0.50}_{-0.49}$	±0.59	$^{+0.72}_{-0.71}$
Muon isolation efficiency syst [%]	±0.10	±0.11	±0.11	±0.12
E_T^{miss} Soft jet resolution para [%]	∓0.25	∓0.18	∓0.31	±0.69
E_T^{miss} Soft jet resolution perp [%]	∓0.25	-	∓0.17	∓0.25
E_T^{miss} Soft jet scale [%]	$^{-0.24}_{+0.13}$	$^{-0.11}_{+0.20}$	-	$^{+0.61}_{-}$
Luminosity [%]	∓2.05	∓2.05	∓2.05	∓2.05
Z+jets cross-section [%]	±0.43	±0.46	±0.56	±0.70
$t\bar{t}V$ cross-section [%]	±0.12	±0.12	±0.12	±0.14
Monte Carlo sample statistics [%]	±0.46	±0.60	±0.97	±2.73
ISR/FSR + scale [%]	$^{-}_{-0.29}$	$^{-1.29}_{+1.30}$	$^{+0.62}_{-}$	$^{-}_{-3.80}$
Alternate hard-scattering model [%]	±0.36	±2.56	∓0.41	∓5.59
Alternate parton-shower model [%]	±3.37	±5.88	±3.93	±1.12
Fakes overall normalization, el [%]	±0.72	±0.90	±0.89	±1.35
Fakes overall normalization, mu [%]	±0.26	±0.30	±0.47	±0.66
Fakes alternative parametrization [%]	∓1.96	∓2.42	∓2.72	∓4.04
W+jets heavy flavour component [%]	-	±0.11	±0.14	±0.15
W+jets Scales [%]	±3.00	±3.30	±3.70	±4.46
W+jets α_S [%]	$^{-0.19}_{+0.21}$	$^{-0.20}_{+0.24}$	$^{-0.19}_{+0.27}$	∓0.29
Single Top DS/DR [%]	∓2.09	∓1.71	∓1.87	∓1.39
Single Top IFSR [%]	$^{-}_{-0.61}$	$^{-}_{-0.46}$	$^{-}_{-0.74}$	$^{-}_{-0.73}$

TABLE F.17: Table of systematics for the absolute differential cross-section at the particle level for the $y_{t\bar{t}}$observable.

Bins [GeV]	350–530	530–629.50	629.50–715.50	715.50–801.50	801.50–909	909–1016.50	1016.50–1124	1124–1253	1253–1382	1382–2500
$d\sigma$ / $dH_T^{t\bar{t}}$ [pb/GeV]	$3.31 \cdot 10^{-4}$	$1.77 \cdot 10^{-3}$	$3.85 \cdot 10^{-3}$	$5.25 \cdot 10^{-3}$	$3.73 \cdot 10^{-3}$	$2.15 \cdot 10^{-3}$	$1.12 \cdot 10^{-3}$	$5.63 \cdot 10^{-4}$	$2.75 \cdot 10^{-4}$	$3.01 \cdot 10^{-5}$
Total Uncertainty [%]	+17.7 −13.7	+12.8 −13.0	+8.16 −8.52	+7.33 −7.57	+8.36 −8.48	+9.18 −9.51	+10.2 −10.1	+11.6 −11.0	+16.4 −14.2	+21.8 −21.9
Statistics [%]	±4.7	±2.2	±1.4	±1.2	±1.3	±1.7	±2.4	±3.3	±5.1	±5.6
Systematics [%]	+16.8 −12.6	+12.6 −12.8	+7.97 −8.34	+7.19 −7.43	+8.22 −8.34	+8.94 −9.28	+9.80 −9.78	+11.0 −10.3	+15.3 −12.9	+20.9 −21.0
b-Tagged jet energy scale (JES) [%]	+1.23 -	- −0.74	+0.24 −0.51	+0.52 −0.38	+0.56 −0.55	+0.51 −0.52	+0.39 −0.45	+0.85 −0.53	+0.71 −0.58	+0.61 −0.93
Effective detector NP set 1 (JES) [%]	+0.35 -	- -	- -	+0.23 −0.20	+0.19 −0.22	- -	+0.31 -	+0.28 −0.36	- -	+0.41 −0.55
Effective detector NP set 2 (JES) [%]	+0.35 -	- -	- -	+0.20 −0.18	+0.20 −0.15	+0.13 -	+0.15 −0.11	+0.12 −0.10	- -	+0.14 −0.32
Effective mixed NP set 1 (JES) [%]	+1.13 -	+0.26 −0.20	+0.39 -	+1.03 −0.83	+1.22 −1.20	+1.49 −1.50	+1.36 −2.01	+3.23 −1.94	+2.43 −2.32	+4.31 −4.33
Effective mixed NP set 2 (JES) [%]	+0.37 -	−0.67 -	−0.78 -	−0.14 +0.19	−0.16 +0.19	- -	−0.12 +0.19	−0.25 +0.28	+0.30 -	−0.39 +0.18
Effective mixed NP set 3 (JES) [%]	-	-	-	-	-	-	-	-	-	+0.10 −0.18
Effective modelling NP set 1 (JES) [%]	+3.00 −0.83	+1.53 −2.24	+1.57 −1.60	+1.50 −1.03	+1.48 −1.60	+1.61 −1.94	+1.25 −1.42	+1.79 −1.36	+2.10 −1.41	+1.45 −1.50
Effective modelling NP set 2 (JES) [%]	+0.90 -	- −0.36	- −0.36	+0.32 -	+0.48 −0.24	+0.72 −0.23	+0.56 −0.39	+1.35 −0.37	+1.23 −0.94	+3.14 −2.68
Effective modelling NP set 3 (JES) [%]	+0.49 -	−0.42 -	−0.39 +0.20	−0.28 +0.55	−0.24 +0.45	−0.23 +0.59	−0.39 +0.54	−0.42 +0.80	−0.10 +0.40	−0.67 +0.37
Effective modelling NP set 4 (JES) [%]	+0.43 -	- -	- -	+0.29 −0.21	+0.21 −0.16	- -	+0.21 −0.14	+0.22 −0.25	- -	+0.55 −0.63
Effective statistical NP set 1 (JES) [%]	+0.54 -	+0.21 −0.10	- -	+0.31 −0.15	+0.34 −0.27	+0.18 −0.21	+0.34 −0.76	+0.57 −0.58	+0.36 -	+0.67 −0.63
Effective statistical NP set 2 (JES) [%]	−0.24 +0.37	−0.20 +0.35	−0.25 -	- -	- -	- -	+0.13 −0.15	+0.42 −0.21	+0.30 -	+0.57 −0.86
Effective statistical NP set 3 (JES) [%]	+0.78 -	- −0.24	- −0.38	- +0.31	−0.48 +0.46	−0.82 +0.60	−0.90 +0.65	−1.02 +1.25	−0.76 +1.26	−3.05 +3.80
Effective statistical NP set 4 (JES) [%]	+0.79 -	+0.10 −0.50	+0.16 −0.35	+0.48 −0.33	+0.32 −0.35	+0.33 −0.17	- -	+0.14 -	+0.24 -	−0.24 -
Effective statistical NP set 5 (JES) [%]	+0.25 -	- −0.21	+0.15 −0.16	+0.19 −0.18	+0.32 −0.43	+0.37 −0.21	+0.20 -	- -	+0.39 -	−0.63 +0.49
Effective statistical NP set 6 (JES) [%]	-	−0.20 -	-	-	-	+0.13 −0.15	+0.23 -	-	+0.24 -	−0.37 +0.25
Effective statistical NP set 7 (JES) [%]	+0.38	-	-	+0.28 −0.22	+0.29 −0.21	+0.24 −0.17	+0.31 −0.14	+0.32 −0.21	- -	+0.37 −0.48
η intercalibration model (JES) [%]	+2.58 −0.58	+1.13 −0.75	+0.44 −0.62	+0.90 −0.80	+0.91 −0.77	+0.70 −1.22	+1.04 −1.39	+1.34 −1.37	+1.32 −0.41	+1.62 −1.78
η intercalibration non closure (JES) [%]	+1.57 -	−0.53 +0.38	−0.62 +0.39	−0.38 +0.57	−0.46 +0.49	−0.72 +0.50	−0.87 +0.47	−0.57 +0.71	+0.83 -	−1.15 +1.16
η intercalibration total stat (JES) [%]	+0.92 −0.13	+0.29 −0.54	+0.11 −0.36	+0.52 −0.34	+0.40 −0.49	+0.26 −0.27	+0.35 −0.34	+0.55 −0.52	+0.26 -	+0.46 −0.64
Flavour composition (JES) [%]	+3.31 −0.84	+1.70 −2.58	+1.88 −1.74	+1.78 −1.50	+1.86 −2.12	+2.02 −2.07	+1.77 −2.19	+2.47 −1.88	+2.90 −1.66	+3.88 −3.78
Flavour response (JES) [%]	−1.08 +2.06	−1.30 +1.04	−0.96 +0.85	−0.85 +1.11	−1.26 +1.11	−1.28 +0.94	−0.95 +0.87	−0.62 +0.67	+0.94 -	−0.73 +0.47
Pile-up offset μ (JES) [%]	−0.37 +0.95	- −0.23	- -	−0.13 +0.26	−0.14 +0.16	- -	- -	- -	+0.29 -	−0.31 +0.16
Pile-up offset N_{PV} (JES) [%]	- +1.09	−1.14 −0.58	+0.54 -	+0.57 -	+0.39 −0.72	+0.25 −0.36	+0.57 −0.47	+0.60 -	+0.84 -	+0.43 −0.70
Pile-up offset p_T (JES) [%]	+0.75 -	+0.50 −0.93	+0.50 −0.81	+0.97 −0.72	+1.26 −1.32	+1.25 −1.15	+0.73 −1.19	+1.47 −0.92	+2.60 −0.94	+1.42 −2.10
Pile-up offset ρ topology (JES) [%]	+4.78 −1.31	+2.59 −3.47	+2.52 −2.86	+2.52 −1.82	+2.40 −2.41	+2.31 −2.49	+1.89 −2.13	+1.91 −1.21	+1.92 −1.57	+2.28 −2.49
Punch-through (JES) [%]	+0.21 -	-	-	-	-	-	-	-	−0.25 -	-
Jet vertex fraction [%]	+0.48 −0.53	+0.42 −0.47	+0.32 −0.36	+0.23 −0.26	+0.26 −0.29	+0.26 −0.30	+0.19 −0.23	+0.18 −0.22	−0.73 +0.18 −0.24	+0.23 −0.28
b-Quark tagging efficiency (eigenvector 0) [%]	−2.44 +2.36	−1.88 +1.83	−1.49 +1.43	−1.44 +1.37	−1.58 +1.50	−1.64 +1.57	−1.68 +1.61	−1.76 +1.68	−1.93 +1.85	−2.23 +2.17
b-Quark tagging efficiency (eigenvector 1) [%]	−0.36 +0.55	−0.71 +0.69	−1.00 +0.97	−1.15 +1.11	−1.27 +1.22	−1.32 +1.28	−1.45 +1.41	−1.42 +1.37	−1.52 +1.47	−1.83 +1.77
b-Quark tagging efficiency (eigenvector 2) [%]	±0.59	±0.36	±0.10	-	-	∓0.14	∓0.19	∓0.21	∓0.20	∓0.32
b-Quark tagging efficiency (eigenvector 3) [%]	-	-	-	-	-	-	∓0.14	∓0.16	∓0.17	∓0.30
b-Quark tagging efficiency (eigenvector 4) [%]	-	-	-	-	-	-	-	-	-	∓0.10
c-Quark tagging efficiency (eigenvector 0) [%]	±0.21	±0.16	-	-	-	-	-	-	±0.11	-
c-Quark tagging efficiency (eigenvector 1) [%]	∓0.14	∓0.18	∓0.22	∓0.24	∓0.25	∓0.31	∓0.37	∓0.28	∓0.33	∓0.68
c-Quark tagging efficiency (eigenvector 2) [%]	-	-	-	-	-	∓0.10	∓0.14	-	-	∓0.33
Light-jet tagging efficiency (eigenvector 0) [%]	−0.85 +0.91	−0.57 +0.59	−0.43 +0.42	−0.38 +0.39	∓0.49	−0.53 +0.54	∓0.61	∓0.74	−0.88 +0.92	−1.39 +1.38
Light-jet tagging efficiency (eigenvector 1) [%]	±0.14	±0.18	-	-	-	-	-	∓0.12	-	∓0.46
Light-jet tagging efficiency (eigenvector 2) [%]	+0.16 −0.15	-	±0.10	-	-	-	-	-	+0.11 −0.13	∓0.11
Light-jet tagging efficiency (eigenvector 3) [%]	-	-	∓0.10	∓0.12	∓0.13	∓0.15	∓0.18	∓0.23	∓0.11	∓0.22
Light-jet tagging efficiency (eigenvector 5) [%]	-	-	-	-	-	-	-	-	±0.13	±0.42
Light-jet tagging efficiency (eigenvector 6) [%]	-	-	-	-	-	-	-	-	∓0.12	∓0.17
Light-jet tagging efficiency (eigenvector 7) [%]	-	-	-	-	-	-	-	-	-	∓0.32
b-Quark tagging extrapolation [%]	-	-	-	±0.13	±0.28	±0.52	+0.73 −0.74	+0.78 −0.80	+1.05 −1.08	+2.14 −2.20
Electron energy resolution [%]	-	-	-	-	-	-	-	-	-	-
Electron energy scale [%]	±0.13	-	-	-	-	-	-	-	-	-
Electron trigger efficiency [%]	±0.14	±0.11	±0.11	±0.11	±0.11	±0.11	±0.12	±0.11	±0.12	±0.13
Electron reconstruction efficiency [%]	-	-	±0.10	±0.10	±0.11	±0.11	±0.12	±0.12	±0.13	±0.14
Electron identification efficiency [%]	±0.37	±0.44	±0.54	±0.61	±0.65	±0.70	±0.73	±0.75	±0.80	±0.92
Electron isolation efficiency [%]	-	-	±0.24	±0.38	±0.48	±0.57	±0.64	±0.71	±0.78	±1.05
Muon (ID) momentum resolution [%]	- −0.26	-	-	-	-	-	-	-	-	-
Muon (MS) momentum resolution [%]	+0.11 −0.37	-	-	-	-	-	-	-	-	-
Muon trigger efficiency stat [%]	+0.31 −0.32	+0.30 −0.31	+0.27 −0.28	±0.27	±0.28	+0.27 −0.28	±0.28	±0.29	±0.29	+0.32 −0.33
Muon trigger efficiency syst [%]	+0.58 −0.57	+0.53 −0.52	+0.49 −0.48	+0.49 −0.48	+0.49 −0.48	+0.48 −0.47	+0.50 −0.49	+0.51 −0.50	+0.51 −0.50	+0.53 −0.52
Muon identification stat [%]	±0.11	-	-	-	-	-	-	-	-	±0.10
Muon identification syst [%]	±0.37	±0.38	±0.42	±0.47	±0.52	±0.54	±0.57	+0.62 −0.61	±0.62	+0.67 −0.66
Muon isolation efficiency syst [%]	±0.12	±0.11	±0.10	±0.10	±0.10	±0.10	±0.11	±0.12	±0.13	±0.17
E_T^{miss} Soft jet resolution para [%]	∓0.49	±0.19	±0.25	∓0.38	∓0.36	∓0.35	-	∓0.38	∓0.80	∓0.23
E_T^{miss} Soft jet resolution perp [%]	±0.28	-	±0.26	-	∓0.46	∓0.18	∓0.51	∓0.27	∓0.57	-
E_T^{miss} Soft jet scale [%]	−0.27 +0.40	-	+0.27 −0.43	∓0.16	−0.33 +0.31	−0.46 +0.30	−0.36 +0.16	−0.22 +0.52	+0.69 -	- −0.59
Luminosity [%]	∓2.05	∓2.05	∓2.05	∓2.05	∓2.05	∓2.05	∓2.05	∓2.05	∓2.05	∓2.05
Z+jets cross-section [%]	±1.25	±0.76	±0.43	±0.34	±0.40	±0.42	±0.47	±0.56	±0.60	±0.95
Diboson cross-section [%]	-	-	-	-	-	-	-	-	-	±0.10
$t\bar{t}V$ cross-section [%]	±0.19	±0.19	±0.12	-	±0.10	±0.13	±0.14	±0.16	±0.19	±0.24
Monte Carlo sample statistics [%]	±2.91	±1.38	±0.91	±0.72	±0.78	±1.05	±1.42	±1.87	±2.78	±2.87
ISR/FSR + scale [%]	+8.02 -	+4.03 −2.22	- −0.89	−3.51 +1.49	+0.72 −0.54	- −0.98	+3.33 -	+1.55 −0.50	+9.10 −6.56	+4.18 -
Alternate hard-scattering model [%]	±7.53	±5.16	±2.76	∓0.25	±0.17	∓2.21	±4.58	∓2.13	±4.61	±10.2
Alternate parton-shower model [%]	±3.60	±6.79	±3.88	±3.24	±4.62	±4.79	±2.20	±4.55	±4.35	±8.12
Fakes overall normalization, el [%]	±2.15	±1.92	±1.16	±0.54	±0.47	±0.57	±0.72	±0.66	+1.07 −1.08	±1.72
Fakes overall normalization, mu [%]	±0.45	±0.51	±0.15	±0.33	±0.40	±0.45	-	±0.29	±0.13	±0.17
Fakes alternative parametrization [%]	∓5.20	∓4.87	∓2.65	∓1.76	∓1.74	∓2.03	∓1.26	∓1.91	∓2.42	∓3.81
W+jets heavy flavour component [%]	±0.10	-	±0.13	±0.19	-	-	-	-	-	-
W+jets Scales [%]	±5.61	±3.59	±2.53	±2.43	±2.98	±3.38	±3.93	±4.61	±5.52	±7.96
W+jets α_S [%]	−0.33 +0.37	−0.19 +0.25	−0.15 +0.17	−0.16 +0.18	−0.19 +0.22	−0.22 +0.24	−0.24 +0.28	−0.28 +0.34	−0.33 +0.42	−0.47 +0.68
Single Top DS/DR [%]	∓0.69	∓1.23	∓0.98	∓1.26	∓1.63	∓2.11	∓3.67	∓4.17	∓3.87	∓9.10
Single Top IFSR [%]	+0.52 −0.73	- −0.53	- −0.76	-	- −0.50	+0.34 −0.70	- −1.39	+0.80 −1.56	+2.20 -	+1.29 −2.31

TABLE F.18: Table of systematics for the absolute differential cross-section at the particle level for the $H_T^{t\bar{t}}$ observable.

Bins [GeV]	0–30	30–70	70–110	110–160	160–250	250–340	340–500
$d\sigma$ / dp_{out}^{tt} [pb/GeV]	$2.36 \cdot 10^{-2}$	$1.26 \cdot 10^{-2}$	$6.87 \cdot 10^{-3}$	$3.81 \cdot 10^{-3}$	$1.72 \cdot 10^{-3}$	$5.69 \cdot 10^{-4}$	$1.28 \cdot 10^{-4}$
Total Uncertainty [%]	$^{+6.95}_{-6.96}$	$^{+8.52}_{-8.38}$	±11.8	$^{+12.0}_{-12.9}$	$^{+10.6}_{-10.3}$	$^{+16.7}_{-17.6}$	$^{+13.2}_{-16.1}$
Statistics [%]	±1.0	±1.1	±1.5	±2.0	±2.3	±4.3	±6.4
Systematics [%]	±6.85	$^{+8.42}_{-8.28}$	±11.6	$^{+11.8}_{-12.7}$	$^{+10.2}_{-10.0}$	$^{+15.9}_{-16.9}$	$^{+11.0}_{-14.3}$
b-Tagged jet energy scale (JES) [%]	$^{+0.40}_{-0.49}$	$^{+0.52}_{-0.42}$	$^{+0.49}_{-0.65}$	$^{+0.48}_{-0.70}$	$^{+0.66}_{-0.30}$	$^{+0.35}_{-0.44}$	$^{+0.20}_{-0.53}$
Effective detector NP set 1 (JES) [%]	$^{+0.12}_{-0.16}$	$^{+0.18}_{-0.11}$	$^{+0.20}_{-0.16}$	$^{+0.15}_{-0.14}$	-	$^{+0.47}_{-}$	-
Effective detector NP set 2 (JES) [%]	$^{+0.12}_{-0.13}$	$^{+0.15}_{-0.11}$	$^{+0.18}_{-0.14}$	-	$^{-0.17}_{-}$	$^{-}_{+0.25}$	$^{-0.38}_{-}$
Effective mixed NP set 1 (JES) [%]	$^{+1.10}_{-1.17}$	$^{+1.22}_{-1.16}$	±1.23	$^{+1.03}_{-0.95}$	$^{+1.42}_{-1.20}$	$^{+1.69}_{-2.06}$	$^{+1.37}_{-2.11}$
Effective mixed NP set 2 (JES) [%]	∓0.11	$^{-0.11}_{+0.16}$	$^{-0.13}_{+0.17}$	-	-	$^{+0.36}_{-}$	$^{-0.33}_{-}$
Effective modelling NP set 1 (JES) [%]	$^{+0.94}_{-0.91}$	$^{+1.75}_{-1.79}$	$^{+2.25}_{-2.17}$	$^{+2.06}_{-1.63}$	$^{+2.01}_{-1.79}$	$^{+1.68}_{-1.88}$	$^{+1.79}_{-2.97}$
Effective modelling NP set 2 (JES) [%]	$^{+0.42}_{-0.53}$	$^{+0.51}_{-0.46}$	$^{+0.33}_{-0.43}$	$^{+0.46}_{-0.12}$	$^{+0.55}_{-0.39}$	$^{+0.59}_{-1.26}$	$^{+1.15}_{-1.00}$
Effective modelling NP set 3 (JES) [%]	$^{-0.50}_{+0.42}$	$^{-0.40}_{+0.44}$	$^{-0.34}_{+0.38}$	$^{-0.28}_{+0.41}$	$^{-0.56}_{+0.50}$	$^{-0.64}_{+0.76}$	$^{-0.34}_{+0.67}$
Effective modelling NP set 4 (JES) [%]	$^{+0.10}_{-0.19}$	$^{+0.19}_{-0.12}$	$^{+0.23}_{-0.13}$	$^{+0.15}_{-0.21}$	$^{-}_{-0.16}$	$^{+0.43}_{-}$	$^{+0.13}_{-0.41}$
Effective statistical NP set 1 (JES) [%]	$^{+0.10}_{-0.13}$	$^{+0.29}_{-0.18}$	$^{+0.34}_{-0.32}$	$^{+0.28}_{-0.33}$	$^{-}_{-0.27}$	$^{+0.69}_{-}$	$^{+0.23}_{-1.01}$
Effective statistical NP set 2 (JES) [%]	-	-	-	-	$^{-0.24}_{+0.16}$	$^{+0.54}_{-}$	$^{-}_{-0.52}$
Effective statistical NP set 3 (JES) [%]	−0.45	−0.40	−0.42	−0.29	−0.45	−0.75	−0.78
Effective statistical NP set 4 (JES) [%]	$^{+0.32}_{+0.24}$	$^{+0.45}_{+0.51}$	$^{+0.37}_{+0.26}$	$^{+0.31}_{+0.33}$	$^{+0.41}_{+0.27}$	$^{+0.78}_{+0.23}$	$^{+0.69}_{+0.17}$
Effective statistical NP set 5 (JES) [%]	$^{-0.30}_{+0.20}$	$^{-0.24}_{+0.24}$	$^{-0.19}_{+0.11}$	$^{-0.23}_{+0.17}$	$^{-0.30}_{+0.19}$	$^{-0.10}_{+0.39}$	$^{-0.26}_{-}$
Effective statistical NP set 6 (JES) [%]	$^{-0.21}_{-}$	$^{-0.22}_{-}$	$^{-}_{-}$	$^{-}_{-}$	$^{-0.33}_{-}$	$^{-}_{+0.27}$	$^{-0.37}_{-}$
Effective statistical NP set 7 (JES) [%]	$^{+0.16}_{-0.21}$	$^{+0.23}_{-0.17}$	$^{+0.24}_{-0.19}$	$^{+0.19}_{-0.25}$	$^{+0.12}_{-0.25}$	$^{+0.59}_{-}$	$^{-0.22}_{+0.21}$
η intercalibration model (JES) [%]	$^{+0.64}_{-0.77}$	$^{+1.08}_{-0.82}$	$^{+1.13}_{-0.98}$	$^{+0.92}_{-1.02}$	$^{+1.30}_{-1.04}$	$^{+1.09}_{-1.75}$	$^{-0.40}_{+1.65}$
η intercalibration non closure (JES) [%]	−0.57	−0.35	−0.49	−0.71	−0.34	−0.72	−1.41
η intercalibration total stat (JES) [%]	$^{+0.43}_{+0.22}$	$^{+0.58}_{+0.43}$	$^{+0.60}_{+0.54}$	$^{+0.70}_{+0.42}$	$^{+0.57}_{+0.42}$	$^{+0.76}_{+0.69}$	$^{-1.26}_{+0.52}$
Flavour composition (JES) [%]	$^{-0.36}_{+1.26}$	$^{-0.33}_{+2.08}$	$^{-0.49}_{+2.59}$	$^{-0.44}_{+2.86}$	$^{-0.44}_{+2.69}$	$^{-}_{+2.05}$	$^{+0.38}_{-0.94}$
Flavour response (JES) [%]	$^{-1.25}_{-0.77}$	$^{-2.14}_{-1.02}$	$^{-2.55}_{-1.29}$	$^{-2.35}_{-1.14}$	$^{-2.26}_{-1.37}$	$^{-2.51}_{-1.30}$	$^{+2.49}_{-5.08}$
Pile-up offset μ (JES) [%]	+0.59	+1.15	+1.37	+1.40	+1.42	+0.95	−2.15
Pile-up offset N_{PV} (JES) [%]	-	$^{-}_{+0.22}$	$^{-0.17}_{+0.31}$	$^{-0.22}_{+0.21}$	-	$^{+0.35}_{-}$	+1.15
Pile-up offset p_T (JES) [%]	$^{+0.22}_{-0.40}$	$^{+0.60}_{-0.43}$	$^{+0.46}_{-0.37}$	$^{+0.63}_{-0.25}$	+0.83	+0.92	$^{-0.40}_{+0.30}$
Pile-up offset ρ topology (JES) [%]	$^{+0.91}_{-1.04}$	$^{+0.98}_{-0.88}$	$^{+0.98}_{-1.02}$	$^{+1.14}_{-1.19}$	$^{+1.42}_{-0.79}$	$^{+0.93}_{-1.20}$	$^{-0.70}_{+1.14}$
Punch-through (JES) [%]	$^{+1.39}_{-1.41}$	$^{+2.55}_{-2.71}$	$^{+3.60}_{-3.30}$	$^{+3.46}_{-2.71}$	$^{+3.32}_{-2.78}$	$^{+1.90}_{-2.41}$	$^{-1.42}_{+2.34}$
Jet vertex fraction [%]	-	-	-	-	-	$^{-}_{-0.24}$	$^{-4.43}_{-}$
b-Quark tagging efficiency (eigenvector 0) [%]	$^{+0.18}_{-0.21}$	$^{+0.30}_{-0.34}$	$^{+0.36}_{-0.40}$	$^{+0.33}_{-0.38}$	$^{+0.33}_{-0.37}$	$^{+0.34}_{-0.38}$	$^{+0.25}_{-0.30}$
b-Quark tagging efficiency (eigenvector 1) [%]	$^{-1.48}_{+1.41}$	$^{-1.63}_{+1.55}$	$^{-1.66}_{+1.59}$	$^{-1.75}_{+1.69}$	$^{-1.81}_{+1.75}$	$^{-2.06}_{+2.01}$	$^{-1.92}_{+1.87}$
b-Quark tagging efficiency (eigenvector 2) [%]	$^{-1.17}_{+1.13}$	$^{-1.16}_{+1.12}$	$^{-1.11}_{+1.07}$	$^{-1.16}_{+1.12}$	$^{-1.36}_{+1.33}$	$^{-1.46}_{+1.43}$	$^{-1.72}_{+1.68}$
c-Quark tagging efficiency (eigenvector 0) [%]	-	-	-	-	±0.10	-	∓0.18
c-Quark tagging efficiency (eigenvector 1) [%]	∓0.24	∓0.26	∓0.28	∓0.30	∓0.30	∓0.31	$^{-0.28}_{+0.29}$
c-Quark tagging efficiency (eigenvector 2) [%]	-	-	-	∓0.10	-	∓0.14	-
Light-jet tagging efficiency (eigenvector 0) [%]	∓0.53	$^{-0.48}_{+0.49}$	∓0.56	$^{-0.51}_{+0.50}$	∓0.53	∓0.61	$^{-0.67}_{+0.65}$
Light-jet tagging efficiency (eigenvector 1) [%]	-	-	-	-	-	∓0.15	-
Light-jet tagging efficiency (eigenvector 2) [%]	-	-	-	-	-	-	±0.13
Light-jet tagging efficiency (eigenvector 3) [%]	∓0.13	∓0.10	∓0.13	$^{-0.12}_{+0.13}$	∓0.13	∓0.24	-
Light-jet tagging efficiency (eigenvector 5) [%]	-	-	-	-	-	-	±0.12
Light-jet tagging efficiency (eigenvector 6) [%]	-	-	-	-	-	-	∓0.14
b-Quark tagging extrapolation [%]	±0.33	±0.33	$^{+0.26}_{-0.27}$	$^{+0.29}_{-0.30}$	±0.34	±0.46	±0.60
Electron energy resolution [%]	-	-	-	-	-	-	-
Electron trigger efficiency [%]	±0.11	±0.11	±0.11	±0.12	±0.11	±0.11	±0.12
Electron reconstruction efficiency [%]	±0.11	±0.10	±0.10	±0.10	±0.10	±0.11	±0.12
Electron identification efficiency [%]	±0.65	±0.62	±0.59	±0.60	±0.61	±0.66	±0.79
Electron isolation efficiency [%]	±0.47	±0.42	±0.36	±0.36	±0.39	±0.48	±0.74
Muon (ID) momentum resolution [%]	-	-	-	-	-	-	-
Muon (MS) momentum resolution [%]	-	-	-	-	-	-	-
Muon trigger efficiency stat [%]	±0.28	±0.28	$^{+0.28}_{-0.29}$	$^{+0.28}_{-0.29}$	±0.29	$^{+0.28}_{-0.29}$	±0.29
Muon trigger efficiency syst [%]	$^{+0.48}_{-0.47}$	$^{+0.50}_{-0.49}$	$^{+0.50}_{-0.49}$	$^{+0.50}_{-0.49}$	$^{+0.51}_{-0.50}$	$^{+0.51}_{-0.49}$	$^{+0.47}_{-0.46}$
Muon identification syst [%]	$^{+0.51}_{-0.50}$	±0.49	±0.48	±0.47	±0.49	±0.52	±0.56
Muon isolation efficiency syst [%]	±0.10	±0.10	±0.11	±0.10	±0.11	±0.11	±0.11
E_T^{miss} Soft jet resolution para [%]	∓0.22	∓0.18	∓0.33	-	∓0.23	∓0.43	∓0.35
E_T^{miss} Soft jet resolution perp [%]	-	∓0.31	∓0.36	±0.24	-	-	∓0.82
E_T^{miss} Soft jet scale [%]	-	$^{-0.19}_{+0.28}$	$^{-0.43}_{+0.17}$	$^{-0.17}_{+0.36}$	-	-	$^{-0.59}_{+0.46}$
Luminosity [%]	∓2.05	∓2.05	∓2.05	∓2.05	∓2.05	∓2.05	∓2.05
Z+jets cross-section [%]	±0.36	±0.48	±0.59	±0.58	±0.52	±0.54	±0.45
$t\bar{t}V$ cross-section [%]	-	±0.12	±0.16	±0.18	±0.21	±0.24	±0.28
Monte Carlo sample statistics [%]	±0.60	±0.67	±0.95	±1.20	±1.44	±2.52	±3.56
ISR/FSR + scale [%]	$^{+1.41}_{-}$	$^{-0.32}_{+1.46}$	$^{-1.22}_{-}$	$^{+0.34}_{-5.44}$	$^{-}_{-2.22}$	$^{-4.39}_{+2.37}$	$^{-}_{-5.39}$
Alternate hard-scattering model [%]	∓1.47	±0.53	±3.18	±7.93	±1.72	∓1.45	∓3.75
Alternate parton-shower model [%]	±2.79	±3.93	±7.63	±2.96	±5.35	±13.2	±3.24
Fakes overall normalization, el [%]	±0.86	±0.86	±0.92	±0.72	±0.60	±0.37	±0.32
Fakes overall normalization, mu [%]	±0.28	±0.28	±0.31	±0.49	±0.32	±0.23	±0.51
Fakes alternative parametrization [%]	∓2.29	∓2.29	∓2.47	∓2.45	∓1.85	∓1.22	∓1.67
W+jets heavy flavour component [%]	±0.16	±0.10	-	-	-	-	-
W+jets Scales [%]	±2.85	±3.32	±3.52	±3.57	±3.53	±3.60	±3.84
W+jets α_S [%]	$^{-0.20}_{+0.21}$	$^{-0.20}_{+0.23}$	$^{-0.21}_{+0.24}$	$^{-0.20}_{+0.27}$	$^{-0.18}_{+0.26}$	$^{-0.20}_{+0.28}$	$^{-0.23}_{+0.28}$
Single Top DS/DR [%]	∓1.33	∓1.75	∓2.00	∓2.05	∓3.22	∓4.44	∓6.14
Single Top IFSR [%]	$^{-}_{-0.15}$	$^{-}_{-0.75}$	$^{-}_{-1.04}$	$^{+0.35}_{-0.69}$	$^{-}_{-0.33}$	$^{+0.19}_{-1.90}$	$^{+0.41}_{-1.57}$

TABLE F.19: Table of systematics for the absolute differential cross-section at the particle level for the $p_{\mathrm{out}}^{t\bar{t}}$observable.

Bins [GeV] x	490–815	815–930	930–1200	1200–3000	3000–3325	3325–3440	3440–3710	3710–5510	5510–5730	5730–5870	5870–5970	5970–6370	6370–8020.00
$d\sigma$ / $dm^{t\bar{t}}[GeV]vsextrajetN$ [pb/GeV x]	$1.24 \cdot 10^{-4}$	$9.41 \cdot 10^{-4}$	$6.98 \cdot 10^{-4}$	$5.39 \cdot 10^{-5}$	$2.91 \cdot 10^{-4}$	$1.10 \cdot 10^{-3}$	$7.53 \cdot 10^{-4}$	$6.25 \cdot 10^{-5}$	$5.26 \cdot 10^{-4}$	$1.37 \cdot 10^{-3}$	$1.59 \cdot 10^{-3}$	$8.80 \cdot 10^{-4}$	$6.65 \cdot 10^{-5}$
Total Uncertainty [%]	+13.4 −15.7	+5.77 −5.55	+7.79 −7.77	+9.07 −8.82	+7.64 −8.01	+7.42 −7.92	+7.96 −8.30	+12.8 −11.6	+11.6 −11.3	+13.9 −13.3	+11.6 −12.2	+15.8 −15.7	+18.1 −19.2
Statistics [%]	±4.8	±2.7	±2.0	±3.0	±3.1	±2.4	±2.1	±3.0	±2.9	±2.0	±2.1	±1.5	±3.0
Systematics [%]	+12.2 −14.6	+4.85 −4.59	+7.41 −7.39	+8.36 −8.09	+6.69 −7.11	+6.83 −7.38	+7.57 −7.93	+12.3 −11.1	+11.0 −10.8	+13.7 −13.1	+11.4 −11.9	+15.7 −15.6	+17.7 −18.9
b-Tagged jet energy scale (JES) [%]	-	+0.60	+0.44	+0.59	-	+0.22	+0.74	+0.66	+0.45	+0.32	+0.52	+0.64	+0.43
Effective detector NP set 1 (JES) [%]	−1.69	−0.56 +0.33	−0.60	−0.45 +0.17	−0.32	−0.11	−0.72	−0.42 +0.10	−0.42	−0.40	−0.11 +0.24	−0.65 +0.20	−0.80 +0.35
Effective detector NP set 2 (JES) [%]	−0.88	+0.40	+0.16	−0.21	-	-	±0.13	−0.14 +0.16	-	±0.19	−0.18 +0.20	−0.16 +0.16	−0.44
Effective mixed NP set 1 (JES) [%]	−0.93 −1.51	+0.44	−0.12 +1.13	−0.15 +2.09	−0.20 +0.51	-	−0.18 +1.22	+2.04	+0.66	−0.17 +0.82	−0.15 +0.76	−0.13 +1.60	−0.16 +2.48
Effective mixed NP set 2 (JES) [%]	+0.64	−0.92	−1.75 −0.17	−1.48 −0.18	−1.10	−0.65	−1.56 −0.10	−1.61 −1.61	-	−0.82 −0.14	−0.72	−1.77 −1.77	−2.58 −0.58
Effective mixed NP set 3 (JES) [%]	−0.86 −0.39	+0.39	+0.12	+0.14	-	-	+0.17	+0.20	-	+0.13	+0.15	+0.14	+0.16
Effective modelling NP set 1 (JES) [%]	- −3.96	- −0.56	- -	- −0.49	- -	- +1.02	- +1.32	- +0.74	- +2.38	- +2.90	- +3.32	- +3.72	- +3.14
Effective modelling NP set 2 (JES) [%]	+2.71 -	+0.65 +0.70	−0.80 +0.50	+1.31 +1.15	−0.63	−1.05	−0.28 +0.75	−0.66 +1.09	−1.84	−2.74 +0.20	−3.40	−3.40 +0.37	−3.53 +1.25
Effective modelling NP set 3 (JES) [%]	−1.04	−0.48 −0.56	+0.63 −0.68	−0.84 −0.59	−0.31	-	−0.83 ∓0.76	−0.88 −0.52	-	−0.21 −0.39	+0.21	−0.31 −0.41	−1.43 −0.60
Effective modelling NP set 4 (JES) [%]	−0.74 -	+0.85 +0.24	+0.59 -	+0.63 +0.17	−0.46	+0.22	+0.16	+0.44	+0.34	+0.50 +0.22	+0.27	+0.42 +0.20	+0.52 +0.47
Effective statistical NP set 1 (JES) [%]	−0.88 −1.51	-	−0.19	−0.11	−0.31	-	-	−0.21 +0.10	+0.28	−0.20 +0.43	−0.23 +0.63	−0.22 +0.55	−0.37 +0.70
Effective statistical NP set 2 (JES) [%]	+0.42 +0.44	-	+0.12	+0.47	-	+0.29	+0.26	+0.13 +0.13	−0.33 −0.33	−0.46 −0.34	−0.64 −0.58	−0.48 −0.28	+0.96 +0.10
Effective statistical NP set 3 (JES) [%]	−0.49 -	−0.15 -	−0.43 −0.76	−0.39 -	-	-	−0.22 -	−0.26 −0.61	+0.21 -	+0.45 +0.38	+0.50 +0.30	+0.37 +0.61	−0.22 −1.07
Effective statistical NP set 4 (JES) [%]	−1.85 -	+0.41 +0.55	+0.50 +0.45	+0.62 +0.15	−0.40 -	+0.43	+0.50 +0.40	+0.69 -	+0.22	+0.28 +0.28	+0.29	+0.48 +0.28	+0.80 -
Effective statistical NP set 5 (JES) [%]	−0.99 -	−0.30 +0.44	−0.43 +0.45	+0.73 +0.10	−0.36 -	−0.12 +0.19	−0.32 +0.36	+0.20	−0.17 +0.13	−0.21 +0.13	−0.31 +0.24	−0.25 +0.20	−0.25
Effective statistical NP set 6 (JES) [%]	−0.77 -	- -	−0.36 -	−0.19 -	−0.30 -	−0.10 -	−0.25 -	- -	−0.17 -	−0.22 -	−0.12 -	−0.22 -	+0.11 -
Effective statistical NP set 7 (JES) [%]	−0.78 -	+0.23 +0.32	+0.18	+0.21	-	-	+0.23	-	−0.15	-	±0.22	−0.17 +0.33	+0.42
η intercalibration model (JES) [%]	−0.90 −1.74	-	−0.14 −0.22	−0.25 −0.76	−0.35 +0.20	+0.59	−0.19 +0.56	−0.20 +1.00	+1.20	−0.26 +1.64	+1.19	−0.29 +1.37	−0.41 +2.73
η intercalibration non closure (JES) [%]	+0.59 +0.21	−0.25	−0.42 −0.58	−0.32 −0.44	−0.14	−0.17	−1.06 −0.75	−1.16 −0.38	−0.47 +0.34	−0.84 −0.57	−1.47 −0.86	−1.36 −0.55	−2.59 −1.46
η intercalibration total stat (JES) [%]	- −1.27	+0.57 +0.25 −0.16	+0.32	+0.58	-	+0.65 +0.32	+0.47 +0.26 −0.12	+0.73 +0.31 −0.18	+0.48 −0.40	+0.88 +0.58 −0.75	+0.65 +0.82 −0.81	+0.65 +0.72 −0.61	+0.95 +0.60 −1.09
Flavour composition (JES) [%]	−4.84 +2.77	−0.65 +0.90	−1.00 +0.54	−0.33 +1.30	+0.30 -	+1.11 −1.14	+1.33 −0.88	+1.74 −1.19	+2.46 −2.31	+3.43 −3.30	+4.24 −4.47	+4.40 −4.62	+4.89 −5.25
Flavour response (JES) [%]	+2.06 −2.39	+0.87 −0.24	-	+0.92 −0.30	−0.60	−0.72 +0.91	−0.52 +0.52	−0.45 +0.34	−1.33 +1.40	−2.11 +2.13	−2.50 +2.19	−2.17 +2.38	−2.59 +1.81
Pile-up offset μ (JES) [%]	- −0.99	+0.40 -	-	−0.18 +0.22	-	-	−0.15 +0.17	+0.13 +0.33	−0.92 -	-	−0.31 +0.37	-	−0.26 +0.13
Pile-up offset N_{PV} (JES) [%]	-	+0.75	-	−0.19 +0.47	-	+0.41 +0.74 -	+0.40 -	+0.79 −0.16	+0.49 −0.11	+0.83 −0.77	+0.35 −0.73	+1.00 −1.02	+0.76 −0.81
Pile-up offset p_T (JES) [%]	−2.33 -	+0.64	−0.42 +1.27	+1.52	−0.35 +0.33	±0.80	+1.11	+1.66	±0.52	+0.96	+0.71	+1.17	+1.29
Pile-up offset ρ topology (JES) [%]	−1.12 −1.71	−1.28 −0.72	−1.25 −1.26	−1.07 −0.95	−0.93	+1.84	−1.57 +2.25	−1.18 +1.21	+4.03	−0.34 +4.65	−0.57 +4.87	−0.94 +5.29	−1.56 +4.40
Punch-through (JES) [%]	+2.84 -	+0.37 -	- -	+1.32 -	−0.75 -	−1.55 -	−1.47 -	−0.39 -	−2.98 -	−4.00 -	−5.06 -	−5.17 -	−4.79 -
Jet vertex fraction [%]	−0.12	-	-	−0.18	-	+0.17	+0.12	-	+0.52	+0.56	+0.60	+0.57	+0.58
b-Quark tagging efficiency (eigenvector 0) [%]	−1.19 +1.12	−1.24 +1.17	−1.45 +1.38	+0.15 −1.64 +1.56	−1.63 +1.56	−0.20 −1.55 +1.49	−0.16 −1.59 +1.52	−1.62 +1.52	−2.21 +2.15	−1.59 +1.53	−1.62 +1.54	−1.60 +1.54	−1.98 +1.91
b-Quark tagging efficiency (eigenvector 1) [%]	−0.82 +0.78	−1.04 +1.00	−1.18 +1.13	−1.30 +1.24	−0.73 ∓0.70	+1.18	−1.31 +1.27	−1.46 +1.41	−0.59 +0.58	−0.88 +0.86	−1.19 +1.15	−1.30 +1.26	−1.76 +1.72
b-Quark tagging efficiency (eigenvector 2) [%]	-	-	-	∓0.11	∓0.26 −0.25	-	∓0.14	∓0.21	±0.46	±0.19	-	∓0.10	∓0.29
b-Quark tagging efficiency (eigenvector 3) [%]	-	-	-	-	-	-	-	∓0.12	-	-	-	-	∓0.21
c-Quark tagging efficiency (eigenvector 0) [%]	-	-	-	-	-	-	-	-	±0.18	-	-	-	-
c-Quark tagging efficiency (eigenvector 1) [%]	∓0.27	∓0.18	∓0.14	∓0.34	−0.18 +0.17	∓0.21	∓0.18	−0.47 +0.46	-	∓0.15	∓0.19	∓0.36	∓0.71
c-Quark tagging efficiency (eigenvector 2) [%]	∓0.11	-	-	∓0.13	-	-	-	∓0.14	-	-	-	∓0.14	∓0.29
Light-jet tagging efficiency (eigenvector 0) [%]	∓0.20	−0.33 +0.34	∓0.34	∓0.68	∓0.34	∓0.26	∓0.39	∓1.05	−0.71 +0.72	∓0.40	−0.48 +0.50	−0.53 +0.54	−1.09 +1.08
Light-jet tagging efficiency (eigenvector 1) [%]	-	-	-	∓0.13	-	-	-	∓0.19	∓0.13 −0.12	-	-	-	∓0.28 +0.22
Light-jet tagging efficiency (eigenvector 2) [%]	-	-	-	-	-	±0.10	-	∓0.12	−0.32 −0.21	-	-	-	-
Light-jet tagging efficiency (eigenvector 3) [%]	∓0.11	-	∓0.12	∓0.19	-	-	∓0.14	∓0.31	-	∓0.10	-	∓0.13	∓0.30
Light-jet tagging efficiency (eigenvector 5) [%]	-	-	-	-	-	-	-	-	-	-	-	-	±0.15
Light-jet tagging efficiency (eigenvector 6) [%]	-	-	-	-	-	-	-	-	-	-	-	-	±0.10
b-Quark tagging extrapolation [%]	-	±0.12	+0.25 −0.26	+0.60 −0.61	-	±0.11	+0.35 −0.36	+0.77 −0.79	-	-	-	±0.38	+1.27 −1.29
Electron energy resolution [%]	-	-	-	-	-	-	-	-	-	-	-	-	-
Electron energy scale [%]	- −0.61	-	∓0.11	+0.12 −0.16	−0.29	−0.13	-	-	-	-	+0.26 -	+0.15	+0.23 −0.16
Electron trigger efficiency [%]	±0.11	±0.10	±0.10	±0.12	±0.11	±0.10	±0.10	±0.13	±0.12	±0.11	±0.11	±0.11	±0.14
Electron reconstruction efficiency [%]	±0.11	±0.10	±0.11	±0.12	-	±0.10	±0.11	±0.13	-	-	±0.10	±0.11	±0.13
Electron identification efficiency [%]	±0.59	±0.60	±0.66	±0.77	±0.51	±0.58	±0.64	±0.80	±0.40	±0.51	±0.58	±0.64	±0.83
Electron isolation efficiency [%]	±0.33	±0.44	±0.52	±0.68	±0.21	±0.36	±0.49	±0.68	-	±0.20	±0.34	±0.45	±0.68
Muon (ID) momentum resolution [%]	-	-	-	-	-	-	-	-	-	-	-	-	-
Muon (MS) momentum resolution [%]	-	-	-	-	-	-	-	-	-	-	-	-	-
Muon trigger efficiency stat [%]	+0.25 −0.26	±0.26	±0.27	±0.28	±0.28	+0.27 −0.28	+0.27 −0.28	+0.30 −0.31	+0.30 −0.31	±0.28	+0.26 −0.27	±0.29	+0.31 −0.32
Muon trigger efficiency syst [%]	+0.44 −0.43	+0.46 −0.45	+0.46 −0.45	+0.51 −0.50	+0.48 −0.47	+0.48 −0.47	+0.48 −0.47	+0.54 −0.53	+0.53 −0.52	+0.48 −0.47	+0.47 −0.46	+0.51 −0.50	+0.56 −0.55
Muon identification stat [%]	-	-	-	-	-	-	-	±0.10	±0.10	-	-	-	±0.10
Muon identification syst [%]	±0.41	±0.47	±0.50	±0.63	±0.39	±0.45	±0.50	±0.66	±0.37	±0.39	±0.41	±0.51	±0.66
Muon isolation efficiency syst [%]	-	-	-	±0.11	±0.10	±0.10	±0.10	±0.13	±0.11	±0.10	-	±0.10	±0.14
E_T^{miss} Soft jet resolution para [%]	±1.13	-	∓0.27	∓0.59	±0.32	±0.11	∓0.73	∓0.33	±0.11	±0.31	-	∓0.40	∓0.85
E_T^{miss} Soft jet resolution perp [%]	±0.60	±0.49	∓0.44	∓0.42	±0.60	±0.14	∓0.73	∓0.40	±0.56	±0.15	∓0.23	∓0.29	∓0.60
E_T^{miss} Soft jet scale [%]	+0.79 −1.55	-	−0.33 +0.22	−0.54 +0.43	+0.41 −0.72	+0.29	−0.56 +0.18	−0.35 +0.54	+0.87 −0.97	-	−0.20 +0.48	−0.40 +0.35	−0.68 +0.31
Luminosity [%]	∓2.05	∓2.05	∓2.05	∓2.05	∓2.05	∓2.05	∓2.05	∓2.05	∓2.05	∓2.05	∓2.05	∓2.05	∓2.05
Z+jets cross-section [%]	±0.17	±0.13	±0.16	±0.32	±0.42	±0.17	±0.32	±0.89	±0.72	±0.40	±0.37	±0.58	±1.34
$t\bar{t}V$ cross-section [%]	-	-	-	-	-	-	-	±0.10	±0.19	±0.18	±0.20	±0.21	±0.26
Monte Carlo sample statistics [%]	±2.95	±1.52	±1.18	±1.82	±1.86	±1.49	±1.27	±1.87	±1.72	±1.24	±1.32	±0.95	±1.65
ISR/FSR + scale [%]	+3.55	+0.73	+2.32	-	+2.36	−3.78	-	+4.65	+2.35	−2.70	-	+0.89	-
Alternate hard-scattering model [%]	∓7.73	∓1.71	∓4.40	∓1.71	∓3.69	−0.37 ∓0.50	+1.96 ∓3.64	−2.75 ∓1.40	−2.08 ∓4.96	+3.20 ∓6.46	−2.16 ∓0.65	−0.76 ∓5.68	−4.15 ∓6.61
Alternate parton-shower model [%]	±0.42	±0.74	±3.17	±1.34	±0.91	±3.80	∓2.05	±0.32	±4.79	±7.83	±6.40	±9.87	±7.12
Fakes overall normalization, el [%]	±1.42	±0.45	±0.48	±1.40	±1.09	±0.41	±0.53	±1.38	±0.92	±0.56	±0.59	±0.82	±1.70
Fakes overall normalization, mu [%]	±1.13	±0.13	-	±0.30	-	±0.31	±0.39	±0.66	±0.38	±0.27	±0.50	±0.29	±0.19
Fakes alternative parametrization [%]	±5.10	±1.17	±1.08	±3.42	±2.28	±1.46	±1.85	±4.08	±2.62	±1.68	±2.19	±2.24	±3.79
W+jets heavy flavour component [%]	±0.13	±0.26	±0.12	±0.10	±0.11	±0.14	-	-	-	±0.11	-	-	-
W+jets Scales [%]	±1.20	±1.03	±1.74	±3.87	±2.54	±2.04	±2.53	±7.62	±3.58	±2.08	±2.09	±3.43	±8.69
W+jets α_S [%]	-	-	−0.14 +0.15	−0.29 +0.35	−0.16 +0.17	−0.13 +0.14	−0.17 +0.19	−0.45 +0.54	−0.20 +0.24	−0.11 +0.14	−0.12 +0.13	−0.21 +0.22	−0.49 +0.63
Single Top DS/DR [%]	±0.28	∓0.83	∓0.77	∓2.65	±1.19	∓0.77	∓1.38	∓4.08	±0.90	∓1.00	∓1.61	∓2.87	∓5.35
Single Top IFSR [%]	+0.10 −0.27	-	−0.22 +0.12	−0.61	−0.48	−0.59	+0.58	+0.74	+0.83 -	−0.49	−1.26	−1.57	+1.09 −2.16

TABLE F.20: Table of systematics for the absolute differential cross-section at the particle level for the $m^{t\bar{t}}$ vs extra jet N observable.

Bins [GeV] x [GeV]	350–400	400–455	455–550	550–2000	2000–2050	2050–2105	2105–2200	2200–2350	2350–3650	3650–3700	3700–3755	3755–3850	3850–4000	4000–5300
$d\sigma$ / $dp_T^{had}[GeV]vsp_T^{t\bar{t}}$ [pb/GeV x GeV]	$3.21 \cdot 10^{-3}$	$1.93 \cdot 10^{-3}$	$7.73 \cdot 10^{-4}$	$2.12 \cdot 10^{-5}$	$7.22 \cdot 10^{-3}$	$4.15 \cdot 10^{-3}$	$1.77 \cdot 10^{-3}$	$4.56 \cdot 10^{-4}$	$9.95 \cdot 10^{-6}$	$4.53 \cdot 10^{-3}$	$3.26 \cdot 10^{-3}$	$1.81 \cdot 10^{-3}$	$6.04 \cdot 10^{-4}$	$2.43 \cdot 10^{-5}$
Total Uncertainty [%]	+5.97 −6.13	+6.93 −8.61	+9.19 −8.03	+21.7 −20.7	+9.12 −9.15	±10.3	+10.9 −9.54	+11.5 −11.9	+29.9 −25.8	+15.6 −14.8	+9.29 −10.2	+9.79 −11.8	+11.2 −11.6	+22.3 −20.6
Statistics [%]	±2.2	±2.5	±3.3	±5.5	±1.5	±1.8	±2.2	±3.6	±10.	±2.1	±2.2	±2.2	±3.1	±5.4
Systematics [%]	+5.39 −5.56	+6.23 −8.06	+8.35 −7.05	+20.7 −19.8	+8.94 −8.97	±10.1	+10.6 −9.19	+10.8 −11.7	+27.7 −23.2	+15.4 −14.6	+8.93 −9.91	+9.43 −11.5	+10.7 −11.0	+21.5 −19.6
b-Tagged jet energy scale (JES) [%]	±0.21	±0.33	±0.96	±0.57	±0.43	±0.43	±0.67	±0.95	±0.44	±0.49	±0.43	±0.22	±0.51	±0.76
Effective detector NP set 1 (JES) [%]	−0.41 -	−1.09 -	−0.66 -	+0.25	−0.50 +0.10	−0.41 +0.15	−0.54 +0.31	−0.50 +0.33	−0.73 +0.25	−0.16 +0.23	−0.63 -	−0.56 +0.20	−0.34 -	−0.56 +0.52
Effective detector NP set 2 (JES) [%]	−0.13 -	−0.23 -	- -	+0.24	−0.16 +0.18	−0.12 -	+0.22 +0.24	−0.18 +0.15	−0.53 +0.21	−0.10 -	- -	- +0.22	−0.17 -	−0.19 +0.18
Effective mixed NP set 1 (JES) [%]	- +0.66	−0.24 +0.53	- +2.51	- +2.67	−0.17 +0.74	−0.10 +1.03	−0.18 +1.77	−0.11 +2.92	−0.18 +3.61	- +0.57	- +1.00	−0.13 +0.85	- +1.52	−0.11 +3.63
Effective mixed NP set 2 (JES) [%]	−0.41 -	−2.16 −0.20	−1.61 -	−1.72 -	−0.82 −0.15	−1.24 -	−1.77 −0.19	−2.04 −0.21	−4.54 −0.40	−0.60 -	−0.66 -	−1.67 -	−1.34 −0.15	−2.43 −0.11
Effective mixed NP set 3 (JES) [%]	-	-	-	+0.15	+0.26	+0.10	-	+0.27	+0.33	-	-	-	+0.18	+0.11	+0.35
Effective modelling NP set 1 (JES) [%]	+0.36	+0.34	+1.15	+0.68	+1.78	+1.88	+2.02	+2.15	+1.63	+1.99	+1.34	+1.89	+1.50	+2.52
Effective modelling NP set 2 (JES) [%]	−0.22 -	−1.46 -	−0.91 +1.22	+1.77	−1.76 +0.17	−1.68 +0.33	−1.87 +0.76	−1.20 +1.55	−1.96 +2.70	−1.55 -	−1.62 +0.37	−2.64 +0.26	−1.47 +0.58	−1.30 +2.37
Effective modelling NP set 3 (JES) [%]	- −0.29	−1.17 −1.00	−0.79 −0.78	−0.46 +0.56	−0.29 −0.42	−0.36 −0.35	−0.72 −0.50	−0.70 −0.38	−3.07 -	- -	−0.14 −0.57	−0.88 −0.68	−0.60 −0.37	−1.17 −0.17
Effective modelling NP set 4 (JES) [%]	+0.28 -	+0.52 -	+0.88 -	+0.40	+0.30 +0.12	+0.39 +0.21	+0.65 +0.22	+0.78 ±0.11	−0.25 +0.69	+0.19 +0.20	+0.43 -	+0.50 +0.18	+0.60 -	+0.45 +0.87
Effective statistical NP set 1 (JES) [%]	−0.26 -	−0.17 -	- -	+0.29	−0.19 +0.20	+0.30	−0.23 +0.31	+0.49 -	−0.67 +0.77	−0.11 +0.23	−0.17 -	−0.11 +0.39	+0.16	−0.55 +0.86
Effective statistical NP set 2 (JES) [%]	- -	−0.35 -	- +0.49	+0.70	−0.15 −0.12	−0.20	−0.38 +0.28	−0.30 +0.28	−1.67 -	−0.10 −0.16	−0.25 −0.36	−0.40 -	−0.34 -	−0.22 +0.22
Effective statistical NP set 3 (JES) [%]	- -	−0.21 -	−0.17 −0.90	−0.14 −0.28	+0.22 -	+0.16 −0.34	−0.24 −0.40	−0.26 −0.23	−0.65 −0.78	+0.20 -	+0.25 −0.17	- −0.90	−0.80	−0.11 −0.39
Effective statistical NP set 4 (JES) [%]	+0.31	−1.04 +0.35	+1.31 +0.24	+1.30 -	+0.33 +0.32	+0.33 +0.23	+0.89 +0.23	+1.34 +0.27	+0.92 −0.31	- +0.47	+0.23 +0.31	+0.65 +0.50	+0.69 -	+1.05 -
Effective statistical NP set 5 (JES) [%]	−0.80 −0.13	−0.67 +0.51	+0.59 -	- -	−0.32 -	−0.29 +0.23	−0.22 +0.22	- -	- −0.69	−0.24 -	−0.43 +0.18	−0.24 -	- -	+0.22 −0.17
Effective statistical NP set 6 (JES) [%]	−0.14 −0.48	−0.56 -	−0.33 -	−0.23 -	−0.19 -	−0.27 +0.27	−0.37 -	- -	+0.52 −0.78	- -	−0.31 -	−0.41 +0.30	- -	+0.56 −0.14
Effective statistical NP set 7 (JES) [%]	+0.18 -	−0.25 +0.12	- +0.26	- +0.40	- +0.12	- +0.21	−0.19 +0.19	- +0.44	+0.11 -	- +0.23	- -	−0.19 +0.12	- +0.11	+0.29 +0.57
η intercalibration model (JES) [%]	−0.19 -	−0.33 +0.63	−0.12 +1.16	- +0.82	−0.24 +0.95	−0.18 +0.81	−0.29 +1.21	−0.17 +1.38	−0.51 +1.38	- +1.40	−0.23 +0.59	−0.18 +1.18	−0.27 +1.25	- +1.84
η intercalibration non closure (JES) [%]	−0.36 -	−1.67 −1.08	−0.92 −0.46	−0.17 −0.33	−0.85 −0.49	−0.85 −0.62	−0.94 −0.50	−0.54 −0.61	−1.72 −0.35	−0.37 -	−1.08 −0.78	−1.32 −0.43	−1.05 −0.59	−1.37 −0.48
η intercalibration total stat (JES) [%]	−0.25 -	+0.36 +0.24	+1.02 +0.46	+0.98 +0.41	+0.67 +0.56	+0.52 +0.49	+0.46 +0.31	+0.29 +0.52	+0.99 -	+0.63 +0.50	+0.52 +0.38	+0.32 +0.49	+0.57 +0.15	+1.03 +0.90
Flavour composition (JES) [%]	−0.33 +0.35	−0.63 +0.21	- +1.76	+1.42	−0.29 +2.04	−0.27 +2.51	−0.45 +2.36	−0.48 +2.91	−1.14 +4.18	−0.29 +2.20	−0.66 +1.92	−0.44 +2.16	−0.41 +2.27	−0.18 +4.09
Flavour response (JES) [%]	−0.28 −0.38	−2.22 −1.36	−0.68 −0.50	−0.83 +0.49	−2.03 −0.88	−2.06 −1.38	−1.91 −0.80	−1.66 −0.15	−4.20 −1.14	−1.35 -	−2.05 −1.25	−2.98 −1.90	−2.28 −1.05	−2.57 −0.29
Pile-up offset μ (JES) [%]	+0.12 -	+0.38 −0.28	+0.92 +0.50	+0.33	+1.10 -	+1.06 −0.12	+1.09 −0.21	+0.75 −0.16	+0.81 -	+1.25 −0.19	+1.16 -	+1.47 −0.16	+0.90 -	+1.10 -
Pile-up offset N_{PV} (JES) [%]	−0.20 -	+0.11 -	−0.10 +0.37	+0.98	+0.84	+0.22 +0.56	+0.11 +0.62	+0.20 -	−0.31 -	+0.47 +0.61	+0.22	+0.20 +0.34	+0.63	+1.35
Pile-up offset p_T (JES) [%]	- +0.75	−1.07 +0.80	−0.35 +1.49	+1.59	−0.52 +0.86	−0.21 +0.84	−0.32 +1.38	+1.84	−0.64 +0.96	−0.41 +0.59	−0.39 +0.77	−0.80 +1.37	−0.60 +0.64	−0.16 +2.17
Pile-up offset ρ topology (JES) [%]	−0.89 +0.39	−1.90 +0.49	−1.29 +1.66	−0.44 −0.50	−0.93 +2.93	−0.96 +2.97	−0.95 +2.71	−1.05 +2.48	−1.25 +2.34	−0.63 +3.66	−0.81 +2.30	−1.26 +2.76	−0.92 +2.30	−0.92 +2.91
Punch-through (JES) [%]	−0.71 -	−2.38 -	−0.58 -	- -	−2.94 -	−2.53 -	−2.04 -	−1.77 -	−2.65 -	−2.84 -	−2.72 -	−3.46 -	−2.17 -	−1.59 +0.29
Jet vertex fraction [%]	-	−0.11	-	-	+0.32	+0.33	+0.27	+0.24	−0.37 +0.18	-	+0.38	+0.31	+0.31	+0.29
b-Quark tagging efficiency (eigenvector 0) [%]	-1.31	−1.43	−1.44	−1.67	−0.36 −1.44	−0.37 −1.47	−0.28 −1.35	−0.28 −1.81	−0.24 −2.12	−0.43 −1.87	−0.42 −1.85	−0.36 −1.81	−0.36 −1.84	−0.34 −2.16
b-Quark tagging efficiency (eigenvector 1) [%]	+1.24 −1.12	+1.36 −1.33	+1.26 −1.28	+1.57 −1.59	+1.38 −1.16	+1.40 −1.40	+1.46 −1.42	+1.58 −1.58	+2.07 −1.86	+1.82 −1.84	+1.29 −1.69	+1.74 −1.61	+1.77 −1.13	+2.08 −2.04
b-Quark tagging efficiency (eigenvector 2) [%]	+1.08 -	+1.29 ∓0.11	+1.19 ∓0.17	+1.32 ∓0.15	+1.12 -	+1.19 ∓0.13	+1.29 -	+1.53 ∓0.31	+1.80 ∓0.43	+1.02 ±0.22	+0.96 ±0.18	+0.98 +0.15	+1.10 -	+1.31 -
b-Quark tagging efficiency (eigenvector 3) [%]	-	-	∓0.11	±0.13	-	-	∓0.12	±0.20	−0.37 +0.36	-	-	−0.14 -	-	±0.10
b-Quark tagging efficiency (eigenvector 4) [%]	-	-	-	-	-	-	-	-	∓0.14	-	-	-	-	-
c-Quark tagging efficiency (eigenvector 0) [%]	-	-	-	-	-	-	-	-	-	-	±0.11	-	±0.12	±0.16
c-Quark tagging efficiency (eigenvector 1) [%]	∓0.18	∓0.19	∓0.16	∓0.16	±0.25	±0.31	−0.36 +0.35	±0.43 +0.57	−0.58 +0.52	±0.20	±0.29	±0.28	±0.22	±0.36
c-Quark tagging efficiency (eigenvector 2) [%]	-	-	-	-	-	±0.11	∓0.13	±0.15	±0.30	-	-	-	-	-
Light-jet tagging efficiency (eigenvector 0) [%]	−0.32 +0.31	−0.46 +0.45	∓0.65	±1.06 −0.15	±0.35	−0.47 +0.48	∓0.48	−0.63 +0.62	−1.26 +1.25	−0.54 +0.55	∓0.47	±0.69	−0.75 +0.78	−1.00 +1.05
Light-jet tagging efficiency (eigenvector 1) [%]	-	-	∓0.12	±0.14	-	-	-	±0.10	±0.80	-	-	-	-	-
Light-jet tagging efficiency (eigenvector 2) [%]	±0.10	-	-	-	-	-	-	-	∓0.23 +0.24	-	-	-	±0.15	±0.12 −0.14
Light-jet tagging efficiency (eigenvector 3) [%]	∓0.10	∓0.11	±0.21	±0.24	−0.13 +0.12	±0.10	∓0.17	±0.21	±0.21	-	±0.10	±0.12	±0.12	-
Light-jet tagging efficiency (eigenvector 4) [%]	-	-	-	-	-	-	-	-	±0.13	-	-	-	-	-
Light-jet tagging efficiency (eigenvector 5) [%]	-	-	-	±0.18	-	-	-	-	±0.61	-	-	-	-	-
Light-jet tagging efficiency (eigenvector 6) [%]	-	-	-	-	-	-	-	-	∓0.36	-	-	-	-	-
Light-jet tagging efficiency (eigenvector 7) [%]	-	-	-	-	-	-	-	-	∓0.55	-	-	-	-	-
Light-jet tagging efficiency (eigenvector 9) [%]	-	-	±0.11	-	-	-	-	-	∓0.12	-	-	-	-	-
b-Quark tagging extrapolation [%]	-	±0.30	+0.51 −0.52	+0.87 −0.89	-	±0.34	±0.61	+1.00 −1.03	+2.88 −2.92	-	±0.22	±0.23	±0.43	+0.75 −0.77
Electron energy resolution [%]	-	-	-	-	-	-	-	-	−0.18 +0.11	-	-	-	-	-
Electron energy scale [%]	-	-	-	-	-	-	-	-	-	-	-	-	-	-
Electron trigger efficiency [%]	±0.11	±0.11	±0.11	±0.11	±0.11	±0.11	±0.11	±0.11	±0.13	±0.11	±0.12	±0.12	±0.12	±0.13
Electron reconstruction efficiency [%]	±0.11	±0.11	±0.11	±0.12	±0.10	±0.10	±0.11	±0.12	±0.14	-	±0.10	±0.10	±0.11	±0.13
Electron identification efficiency [%]	±0.61	±0.67	±0.70	±0.76	±0.59	±0.65	±0.71	±0.79	±0.91	±0.52	±0.54	±0.59	±0.65	±0.78
Electron isolation efficiency [%]	±0.42	±0.53	±0.62	±0.79	±0.34	±0.46	±0.59	±0.76	±1.08	±0.22	±0.24	±0.33	±0.44	±0.69
Muon (MS) momentum resolution [%]	-	-	-	-	-	-	-	-	-	-	-	-	-	-
Muon energy scale [%]	-	-	-	-	-	-	-	-	-	-	-	-	-	-
Muon trigger efficiency stat [%]	±0.27	±0.29	+0.27 −0.28	±0.31	+0.27 −0.28	±0.28	±0.27	+0.28 −0.30	±0.32	±0.29	+0.29 −0.30	±0.28	±0.28	+0.29 −0.30
Muon trigger efficiency syst [%]	±0.48 −0.47	±0.48 −0.47	+0.48 −0.47	±0.54 −0.53	+0.49 −0.48	±0.49 −0.48	±0.48 −0.47	+0.50 −0.49	±0.54 −0.53	±0.51 −0.50	+0.50 −0.49	±0.51 −0.50	±0.50 −0.49	+0.49 −0.48
Muon identification stat [%]	-	-	-	-	-	-	-	-	±0.10	-	-	-	-	-
Muon identification syst [%]	±0.49	+0.55 −0.54	±0.59	+0.70 −0.69	±0.46	±0.50	±0.54	±0.60	+0.68 −0.67	±0.42	±0.44	±0.44	+0.49 −0.48	+0.51 −0.50
Muon isolation efficiency syst [%]	±0.10	±0.10	±0.10	±0.15	±0.10	±0.10	±0.10	±0.11	±0.16	±0.11	±0.11	±0.10	±0.11	±0.11
E_T^{miss} Soft jet resolution para [%]	±0.86	∓0.22	∓1.16	∓1.66	-	±0.29	-	±0.41	∓1.72	-	∓0.28	-	±0.10	±0.78
E_T^{miss} Soft jet resolution perp [%]	±1.19	∓0.46	∓0.45	∓0.91	±0.21	±0.16	-	±0.46	±1.39	±0.10	-	±0.11	-	±0.29
E_T^{miss} Soft jet scale [%]	−0.50 +0.13	−0.22 +0.41	−0.53 +0.21	- −0.75	- +0.22	−0.37 -	- +0.32	−0.19 +0.67	+0.31 -	-	−0.13 +0.10	- -	- −0.34	+0.14 -
Luminosity [%]	±2.05	∓2.05	∓2.05	∓2.05	∓2.05	±2.05	±2.05	±2.05	±2.05	±2.05	±2.05	±2.05	±2.05	±2.05
Z+jets cross-section [%]	±0.20	±0.25	±0.16	±0.36	±0.33	±0.41	±0.46	±0.58	±1.02	±0.61	±0.67	±0.68	±0.64	±1.03
Diboson cross-section [%]	-	-	-	-	-	-	-	-	±0.12	-	-	-	-	-
$t\bar{t}V$ cross-section [%]	-	-	-	-	±0.10	±0.11	±0.14	±0.20	±0.20	±0.18	±0.19	±0.23	±0.23	±0.27
Monte Carlo sample statistics [%]	±1.31	±1.60	±1.93	±2.93	±0.93	±1.08	±1.27	±2.07	±5.21	±1.32	±1.34	±1.35	±1.78	±2.79
ISR/FSR + scale [%]	−1.13 +1.38	+2.40	−2.57 +3.27	−2.32 −5.62	−1.88 +1.44	−2.21 +1.05	+4.37	+0.49 −5.33	+15.3	+4.05 −1.25	- −3.44	+0.14 −5.11	- −2.96	+6.81 −1.44
Alternate hard-scattering model [%]	∓2.81	∓2.79	±0.99	∓16.8	±0.99	±2.46	±2.27	±0.31	±3.26	±5.39	±2.90	±0.10	±4.91	±14.8
Alternate parton-shower model [%]	±0.90	±1.44	∓2.44	∓6.08	±5.64	±6.60	±4.58	±3.51	±15.2	±10.9	±3.00	±3.79	±2.80	±4.90
Fakes overall normalization, el [%]	∓0.27	∓0.37	∓0.50	∓0.40	±0.75	±0.75	±1.03	+1.12 −1.13	±2.40	±1.23	±1.27	±1.39	±1.81	±2.57
Fakes overall normalization, mu [%]	±0.24	∓0.34	±0.13	∓0.47	±0.32	±0.40	±0.58	-	±0.40	±0.55	±0.68	±0.33	±0.18	±0.25
Fakes alternative parametrization [%]	-	±1.45	±0.74	±1.77	∓2.15	∓2.33	∓3.24	∓2.10	∓5.62	∓3.57	∓3.91	∓3.45	∓4.00	∓4.63
W+jets heavy flavour component [%]	±0.33	±0.21	-	±0.10	±0.12	-	-	-	-	-	-	-	-	-
W+jets Scales [%]	±1.62	±2.49	±2.50	±4.83	±2.46	±2.89	±3.46	±4.56	±9.44	±3.24	±3.58	±4.11	±4.49	±5.78
W+jets α_S [%]	−0.14 +0.15	∓0.20	−0.17 +0.20	−0.32 +0.37	−0.15 +0.16	−0.18 +0.20	−0.23 +0.24	−0.28 +0.33	−0.55 +0.75	−0.19 +0.24	−0.20 +0.25	−0.22 +0.28	−0.24 +0.32	−0.32 +0.45
Single Top DS/DR [%]	∓0.69 −0.35	∓1.04 -	∓2.01 -	±3.22 −1.16	±0.97 -	±1.55 -	±2.05 -	±4.44 +0.22	∓7.58 +4.00	±1.96 -	±2.06 -	±2.37 +0.32	±3.06 +0.69	±4.78 +0.98
Single Top IFSR [%]	+0.31	−0.56	-	+0.85	−0.25	−0.50	−1.00	−1.61	−1.31	−1.19	−0.76	−0.76	−0.59	−1.51

TABLE F.21: Table of systematics for the absolute differential cross-section at the particle level for the $p_T^{had}vsp_T^{t\bar{t}}$ observable.

Bins [GeV] x	350–400	400–455	455–550	550–700	700–2000	2000–2050	2050–2105	2105–2200	2200–2350	2350–3650	3650–3700	3700–3755	3755–3850	3850–4000	4000–5300
$d\sigma$ / $dp_T^{t,had}[GeV]vsextrajetN$ [pb/GeV x]	$8.20 \cdot 10^{-3}$	$4.93 \cdot 10^{-3}$	$2.03 \cdot 10^{-3}$	$5.21 \cdot 10^{-4}$	$1.20 \cdot 10^{-5}$	$3.24 \cdot 10^{-3}$	$2.02 \cdot 10^{-3}$	$9.25 \cdot 10^{-4}$	$2.86 \cdot 10^{-4}$	$9.32 \cdot 10^{-6}$	$3.52 \cdot 10^{-3}$	$2.39 \cdot 10^{-3}$	$1.40 \cdot 10^{-3}$	$4.28 \cdot 10^{-4}$	$1.69 \cdot 10^{-5}$
Total Uncertainty [%]	+5.84 −5.96	+6.09 −6.43	+8.03 −7.45	+16.3 −15.9	+23.8 −24.0	+14.8 −15.0	+13.6 −14.1	+11.8 −12.9	+12.2 −13.4	+24.6 −21.6	+21.5 −21.0	+14.1 −14.6	+16.1 −15.2	+14.6 −15.0	+23.1 −21.4
Statistics [%]	±1.4	±1.7	±2.0	±3.3	±8.5	±2.3	±2.6	±3.1	±4.7	±9.9	±2.3	±2.5	±2.6	±3.7	±6.7
Systematics [%]	+5.60 −5.73	+5.74 −6.11	+7.65 −7.05	+15.9 −15.4	+21.8 −22.0	+14.5 −14.8	+13.2 −13.7	+11.3 −12.4	+10.9 −12.2	+21.9 −18.5	+21.3 −20.9	+13.8 −14.3	+15.8 −14.8	+13.9 −14.4	+21.8 −20.0
b-Tagged jet energy scale (JES) [%]	+0.34 −0.44	+0.33 −0.56	+0.64 −0.62	+0.69 −0.20	+0.53 −0.45	+0.23 −0.43	+0.36 −0.61	+0.65 −0.67	+0.99 −0.43	+0.58 −1.20	+0.70 −0.19	+0.61 −0.81	+0.30 −0.44	+0.53 −0.36	+0.62 −0.46
Effective detector NP set 1 (JES) [%]	-	-	+0.23 -	+0.21 −0.15	- −0.20	- −0.34	+0.20 −0.17	+0.20 −0.23	+0.63 -	+0.10 −0.36	+0.37 -	±0.15	+0.28 -	- −0.23	+0.79 −0.26
Effective detector NP set 2 (JES) [%]	-	- −0.17	+0.17 −0.12	+0.18 −0.11	-	- −0.26	+0.17 -	+0.29 −0.16	-	±0.20	+0.33 −0.12	-	+0.29 -	-	+0.24 -
Effective mixed NP set 1 (JES) [%]	+0.75 −0.65	+0.62 −1.35	+1.49 −1.53	+2.45 −1.45	+3.60 −4.58	+0.26 −0.67	+0.76 −1.20	+2.08 −1.40	+1.74 −1.84	+3.36 −3.08	+0.87 −0.64	+1.67 −1.08	+1.21 −1.56	+2.05 −1.28	+3.97 −2.65
Effective mixed NP set 2 (JES) [%]	-	-	−0.12 +0.22	−0.15 +0.27	- −0.25	- −0.23	-	−0.23 +0.14	−0.16 +0.44	−0.26 +0.11	- +0.30	-	- +0.23	−0.15 +0.10	- +0.38
Effective mixed NP set 3 (JES) [%]	-	-	-	-	-	-	-	-	-	- −0.24	+0.14 −0.10	-	-	-	+0.20 -
Effective modelling NP set 1 (JES) [%]	+0.32 -	- −0.42	+0.14 −0.44	+0.75 -	−0.60 +0.95	+2.21 −2.53	+2.81 −2.31	+2.54 −2.75	+2.23 −2.11	- −0.50	+4.13 −3.90	+4.18 −4.15	+4.23 −3.81	+3.36 −2.72	+4.41 −3.12
Effective modelling NP set 2 (JES) [%]	+0.31 −0.20	+0.23 −0.69	+0.88 −1.03	+1.50 −0.29	+2.82 −2.95	- −0.45	- −0.36	+0.71 −0.47	+1.06 −0.73	+3.00 −2.46	+0.31 -	+0.58 -	+0.17 −0.71	+0.54 −0.45	+2.25 −1.24
Effective modelling NP set 3 (JES) [%]	−0.38 +0.35	−0.70 +0.41	−0.75 +0.80	−0.31 +0.73	- −0.51	- −0.54	−0.51 +0.40	−0.46 +0.67	+1.10 -	−0.32 +0.12	+0.39	−0.34 +0.51	−0.52 +0.29	−0.33 +0.40	- +0.47
Effective modelling NP set 4 (JES) [%]	+0.12 −0.11	-	+0.12 -	-	+0.51 −0.56	- −0.42	+0.20 −0.11	+0.25 −0.18	+0.55	+0.11 −0.36	+0.49 −0.18	+0.31 −0.20	+0.29 −0.19	-	+1.13 −0.63
Effective statistical NP set 1 (JES) [%]	- +0.20	−0.19 -	-	+0.23 -	-	- −0.47	+0.40 −0.43	+0.50 −0.59	+0.52	+0.27 −0.74	+0.78 −0.61	+0.71 −0.50	+0.81 −0.56	+0.41 −0.84	+1.25 −0.57
Effective statistical NP set 2 (JES) [%]	-	-	±0.47	+0.47 −0.18	+0.69 −0.95	- −0.52	−0.43 +0.36	- +0.21	+0.43 −0.26	+0.21 −0.54	−0.62 +0.71	−0.44 +0.67	−0.11 +0.17	- −0.36	+0.60 -
Effective statistical NP set 3 (JES) [%]	-	−0.57 -	−0.98 +0.91	−0.40 +1.30	−0.64 +0.83	- −0.24	−0.47 -	−0.69 +1.00	−0.83 +0.96	−0.61 +0.80	-	−0.12 +0.49	−1.01 +0.68	−0.94 +0.81	−0.47 +1.08
Effective statistical NP set 4 (JES) [%]	+0.41 −0.33	+0.32 −0.48	+0.23 −0.20	-	- −0.21	- −0.43	+0.54 −0.44	+0.31 −0.26	−0.10 +0.16	−0.28 +0.22	+0.50 −0.18	+0.21 −0.26	+0.25 −0.14	−0.15	+0.20 -
Effective statistical NP set 5 (JES) [%]	+0.16 −0.14	+0.35 −0.36	+0.37 −0.32	+0.21	−0.35 +0.50	- −0.36	+0.42 −0.43	+0.28 −0.41	- +0.32	−0.47 +0.12	+0.22 -	+0.11 −0.10	+0.35 −0.32	-	−0.45 +0.70
Effective statistical NP set 6 (JES) [%]	−0.13 +0.14	-	+0.21 −0.11	-	−0.34 -	- −0.29	+0.24 −0.17	+0.29 −0.15	+0.26 -	−0.38 +0.27	-	+0.24 −0.13	+0.34 −0.21	-	+0.42 -
Effective statistical NP set 7 (JES) [%]	+0.10 −0.13	- −0.21	+0.28 −0.15	+0.35 −0.24	- −0.21	- −0.36	+0.27 −0.20	+0.39 −0.34	+0.59	- −0.22	+0.47 −0.10	+0.17 −0.28	+0.37 −0.25	+0.10 −0.33	+0.77 −0.12
η intercalibration model (JES) [%]	+0.27 −0.30	- −0.62	+0.64 −0.81	+0.97 −0.17	+0.74 −0.30	±0.96	+1.01 −1.40	+1.55 −0.88	+1.61 −1.22	+2.26 −1.34	+2.00 −1.09	+1.79 −1.97	+1.91 −1.59	+1.51 −1.44	+1.85 −2.10
η intercalibration non closure (JES) [%]	−0.26 +0.25	−0.50 +0.31	−0.59 +0.64	−0.20 +0.48	+0.80 -	−0.20	−0.86 +0.51	−0.22 +0.55	−0.60 +1.28	−0.16 +1.01	−0.60 +1.43	−1.32 +0.83	−0.43 +0.52	−0.92 +0.75	−0.88 +0.98
η intercalibration total stat (JES) [%]	+0.16 -	- −0.21	-	+0.37 -	−0.39 +0.29	- −0.72	+0.59 −0.69	+0.58 −0.66	+0.55 −0.25	- −0.75	+1.05 −0.81	+1.13 −0.91	+0.85 −0.58	+0.25 −0.73	+1.45 −0.55
Flavour composition (JES) [%]	+0.25	- −0.32	+0.12	+0.79	+1.06 −0.53	+2.43 −2.63	+3.21 −3.24	+3.01 −4.00	+1.67 −2.84	+0.86 −1.15	+5.24 −5.76	+5.10 −5.39	+5.20 −4.37	+5.08 −4.12	+6.55 −5.60
Flavour response (JES) [%]	-	- −0.34	-	+0.79	+0.98 −1.53	−1.88 +1.17	−2.00 +2.14	−1.98 +1.65	−1.10 +0.84	+1.13 -	−2.51 +2.83	−3.00 +2.76	−2.52 +2.87	−1.76 +1.89	−1.90 +2.44
Pile-up offset μ (JES) [%]	-	−0.23 -	-	-	+0.34 −0.35	- −0.38	-	- +0.19	+0.26 -	−0.20 -	−0.38 +0.69	−0.18 -	+0.23 -	−0.39 +0.16	- +0.21
Pile-up offset N_{PV} (JES) [%]	+0.45 -	- −0.23	+0.15 −0.23	+0.20	+0.75 −0.13	+0.60 −1.04	+0.80 −0.98	- −1.09	+0.37 −0.15	−1.04	+0.93 −0.69	+0.76 −0.82	+1.52 −0.63	+1.01 −0.45	+2.08 −0.85
Pile-up offset p_T (JES) [%]	+0.82 −1.16	+0.80 −1.30	+1.33 −1.21	+1.82 −0.89	+1.17 −1.41	+0.90 −0.48	+0.42 −0.98	+1.62 −1.17	+1.13 −0.93	+2.10 −0.77	+0.48 −0.28	+1.14 −0.83	+1.30 −1.16	+0.64 −0.70	+1.89 −1.05
Pile-up offset ρ topology (JES) [%]	+0.55 −0.49	- −0.53	+0.18 -	−0.49 +0.80	−1.24 +1.29	+4.01 −3.74	+3.47 −3.86	+3.23 −4.03	+2.28 −2.51	−0.46 +0.25	+6.62 −6.34	+6.46 −6.08	+6.29 −5.13	+4.74 −4.06	+5.93 −4.48
Punch-through (JES) [%]	-	-	-	-	-	-	-	-	-	- −0.22	-	-	-	-	+0.41 −0.10
Jet vertex fraction [%]	-	-	-	−0.14 +0.10	−0.19 +0.14	+0.44 −0.48	+0.42 −0.46	+0.30 −0.35	+0.17 −0.22	+0.10 −0.15	+0.82 −0.86	+0.77 −0.81	+0.71 −0.75	+0.69 −0.74	+0.59 −0.64
b-Quark tagging efficiency (eigenvector 0) [%]	−1.41 +1.35	−1.52 +1.45	−1.56 +1.47	−1.74 +1.66	−1.81 +1.72	−1.63 +1.56	−1.62 +1.54	−1.65 +1.57	−2.00 +1.92	−2.53 +2.45	−1.75 +1.69	−1.72 +1.66	−1.74 +1.69	−1.74 +1.68	−2.16 +2.09
b-Quark tagging efficiency (eigenvector 1) [%]	−1.10 +1.06	−1.22 +1.17	−1.21 +1.16	−1.44 +1.39	−1.27 +1.20	−1.08 +1.05	−1.18 +1.14	−1.25 +1.20	−1.39 +1.34	−1.82 +1.78	−1.20 +1.18	−1.07 +1.04	−1.13 +1.10	−1.17 +1.13	−1.45 +1.42
b-Quark tagging efficiency (eigenvector 2) [%]	-	-	∓0.12	∓0.18	∓0.15	-	-	-	-	∓0.23	±0.12	±0.10	-	-	-
b-Quark tagging efficiency (eigenvector 3) [%]	-	-	-	∓0.12	∓0.16	-	-	-	∓0.14	∓0.21	-	-	-	-	∓0.16
c-Quark tagging efficiency (eigenvector 0) [%]	-	-	-	-	-	-	-	-	±0.10	-	-	±0.11	-	±0.13	±0.16
c-Quark tagging efficiency (eigenvector 1) [%]	∓0.21	∓0.22	∓0.24	∓0.22	−0.55 +0.56	∓0.22	∓0.43	∓0.38	−0.28 +0.27	∓0.68	∓0.24	∓0.28	∓0.32	∓0.29	∓0.29
c-Quark tagging efficiency (eigenvector 2) [%]	-	-	-	-	∓0.23	-	∓0.17	∓0.14	-	∓0.29	-	-	-	-	-
Light-jet tagging efficiency (eigenvector 0) [%]	−0.31 +0.32	−0.47 +0.48	∓0.53	−0.63 +0.62	∓1.26	−0.53 +0.52	∓0.50	∓0.58	−0.84 +0.88	−0.99 +1.01	−0.47 +0.49	∓0.45	−0.75 +0.74	−0.67 +0.69	−1.43 +1.47
Light-jet tagging efficiency (eigenvector 1) [%]	-	-	-	-	∓0.34	-	-	-	-	−0.43 +0.42	-	-	-	-	−0.10 +0.12
Light-jet tagging efficiency (eigenvector 2) [%]	-	-	-	-	-	-	-	-	-	-	-	±0.13	-	±0.10	-
Light-jet tagging efficiency (eigenvector 3) [%]	∓0.11	∓0.11	∓0.17	∓0.16	∓0.13	-	∓0.11	∓0.20	−0.16 +0.17	-	−0.10 +0.11	-	∓0.11	∓0.15	∓0.11
Light-jet tagging efficiency (eigenvector 5) [%]	-	-	-	-	±0.35	-	-	-	-	±0.31	-	-	-	-	±0.24
Light-jet tagging efficiency (eigenvector 6) [%]	-	-	-	-	∓0.11	-	-	-	-	∓0.24	-	-	-	-	-
Light-jet tagging efficiency (eigenvector 7) [%]	-	-	-	-	∓0.22	-	-	-	-	∓0.31	-	-	-	-	−0.18 +0.19
Light-jet tagging efficiency (eigenvector 8) [%]	-	-	-	-	-	-	-	-	-	-	-	-	-	-	±0.10
b-Quark tagging extrapolation [%]	-	±0.31	+0.48 −0.49	+0.77 −0.79	+1.48 −1.55	-	±0.30	±0.45	+0.78 −0.80	+1.87 −1.88	-	±0.24	±0.37	±0.50	+1.00 −1.03
Electron energy resolution [%]	-	-	-	-	+0.13 −0.11	-	-	-	-	-	-	-	-	-	-
Electron energy scale [%]	-	−0.18 -	-	-	-	-	- −0.26	-	-	+0.39 -	+0.37 -	+0.51 -	+0.25 -	-	-
Electron trigger efficiency [%]	±0.11	±0.11	±0.11	±0.11	±0.13	±0.11	±0.11	±0.12	±0.12	±0.13	±0.11	±0.11	±0.12	±0.12	±0.12
Electron reconstruction efficiency [%]	±0.10	±0.11	±0.11	±0.12	±0.14	±0.10	±0.10	±0.11	±0.11	±0.13	-	±0.10	±0.10	±0.11	±0.12
Electron identification efficiency [%]	±0.59	±0.65	±0.70	±0.77	±0.90	±0.56	±0.61	±0.65	±0.72	±0.86	±0.53	±0.56	±0.60	±0.65	±0.73
Electron isolation efficiency [%]	±0.37	±0.47	±0.59	±0.73	±1.05	±0.28	±0.36	±0.45	±0.59	±0.87	±0.24	±0.29	±0.35	±0.45	±0.66
Muon (MS) momentum resolution [%]	-	-	-	-	-	-	-	-	-	-	-	-	-	-	-
Muon energy scale [%]	-	-	-	-	-	-	-	-	-	-	-	-	-	-	-
Muon trigger efficiency stat [%]	±0.27	±0.28	±0.27	+0.27 −0.28	+0.32 −0.33	±0.28	±0.30	+0.28 −0.29	±0.29	+0.31 −0.32	+0.28 −0.29	±0.29	±0.28	+0.28 −0.29	+0.30 −0.31
Muon trigger efficiency syst [%]	+0.48 −0.47	+0.48 −0.47	+0.48 −0.47	+0.49 −0.48	+0.51 −0.50	+0.50 −0.49	+0.51 −0.50	+0.51 −0.50	+0.51 −0.50	+0.52 −0.51	+0.51 −0.50	+0.50 −0.49	+0.51 −0.50	+0.51 −0.50	+0.53 −0.52
Muon identification syst [%]	±0.47	±0.51	±0.54	+0.60 −0.59	±0.64	±0.45	±0.49	±0.51	±0.55	+0.62 −0.61	±0.43	±0.44	±0.46	±0.51	±0.54
Muon isolation efficiency syst [%]	±0.10	±0.10	±0.10	±0.12	±0.15	±0.10	±0.11	±0.11	±0.11	±0.15	±0.11	±0.10	±0.10	±0.11	±0.12
E_T^{miss} Soft jet resolution para [%]	∓0.29	∓0.20	∓0.27	-	-	∓0.28	∓0.39	∓0.10	∓0.41	±0.11	-	∓0.30	-	∓0.40	-
E_T^{miss} Soft jet resolution perp [%]	∓0.26	∓0.17	∓0.14	∓0.11	±0.30	∓0.13	∓0.31	∓0.18	∓0.24	∓0.25	∓0.17	-	±0.14	∓0.39	±0.28
E_T^{miss} Soft jet scale [%]	−0.19 +0.14	−0.24 +0.10	-	-	-	−0.24 +0.22	−0.34 +0.23	−0.10 +0.20	- −0.26	-	−0.15 +0.12	−0.23 +0.16	- +0.25	−0.28 -	-
Luminosity [%]	∓2.05	∓2.05	∓2.05	∓2.05	∓2.05	∓2.05	∓2.05	∓2.05	∓2.05	∓2.05	∓2.05	∓2.05	∓2.05	∓2.05	∓2.05
Z+jets cross-section [%]	±0.27	±0.32	±0.31	±0.32	±0.74	±0.49	±0.58	±0.67	±0.76	±1.23	±0.54	±0.67	±0.69	±0.71	±1.08
$t\bar{t}V$ cross-section [%]	-	-	-	-	±0.13	±0.14	±0.16	±0.17	±0.20	±0.21	±0.22	±0.22	±0.26	±0.26	±0.31
Monte Carlo sample statistics [%]	±0.84	±1.03	±1.22	±1.98	±4.52	±1.50	±1.58	±1.84	±2.78	±5.33	±1.43	±1.54	±1.57	±2.02	±3.14
ISR/FSR + scale [%]	+0.48 −0.96	−0.33 +1.36	+3.10 -	+1.67 −1.72	+2.89 -	−4.09 +4.04	- −2.19	- −3.03	−5.57 +1.91	+12.0 -	+3.26 -	- −3.94	+2.84 −2.82	- −5.74	+5.11 −2.11
Alternate hard-scattering model [%]	∓2.78	∓1.28	∓2.72	∓12.5	±11.2	±2.37	±7.48	±2.07	∓0.94	±3.29	±10.6	±2.40	±5.88	∓1.28	±14.5
Alternate parton-shower model [%]	±1.22	±2.48	∓0.71	∓5.29	±11.2	±11.5	±6.51	±5.56	±1.97	±11.2	±13.6	±6.72	±7.91	±8.60	±2.47
Fakes overall normalization, el [%]	±0.59	±0.63	±0.80	±1.41	±3.14	±0.72	±0.83	±1.05	±1.79	±2.41	±0.65	±0.64	±0.90	±0.72	±1.23
Fakes overall normalization, mu [%]	±0.35	±0.10	±0.61	∓0.11	∓0.19	±0.15	±0.47	±0.29	±0.11	∓0.60	±0.61	±0.72	±0.10	-	-
Fakes alternative parametrization [%]	∓1.90	∓1.47	∓2.83	∓2.61	∓5.89	∓1.75	∓2.60	∓2.69	∓3.81	∓3.61	∓2.55	∓2.73	∓2.01	∓1.61	∓2.67
W+jets heavy flavour component [%]	±0.21	±0.11	-	-	-	-	±0.10	-	-	±0.13	-	-	-	-	-
W+jets Scales [%]	±2.10	±2.67	±3.07	±4.18	±7.23	±3.02	±3.85	±4.33	±5.31	±9.32	±2.95	±3.15	±3.85	±4.07	±6.00
W+jets α_S [%]	−0.15 +0.16	−0.18 +0.20	−0.19 +0.24	−0.25 +0.32	−0.45 +0.59	−0.18 +0.21	−0.23 +0.26	−0.27 +0.28	−0.30 +0.37	−0.55 +0.77	−0.16 +0.20	−0.18 +0.20	−0.22 +0.25	−0.23 +0.27	−0.28 +0.47
Single Top DS/DR [%]	∓0.82	∓1.34	∓1.75	∓2.73	∓7.95	∓1.17	∓1.86	∓3.35	∓4.54	∓5.78	∓2.15	∓1.99	∓2.09	∓3.41	∓4.62
Single Top IFSR [%]	-	- −0.57	- +0.25	−0.15 -	+1.55 -	- −0.56	-	- −2.02	- −1.63	+0.22 −1.73	- −1.51	+0.11 −1.06	+1.24 −1.54	+1.45 −1.25	+1.91 −1.81

TABLE F.22: Table of systematics for the absolute differential cross-section at the particle level for the $p_T^{t,had}vsextrajetN$ observable.

Bins [GeV] x [GeV]	490–850	850–950	950–1350	1350–3000	3000–3220	3220–3360	3360–3460	3460–3860	3860–5510	5510–5835	5835–5950	5950–6220	6220–8020.00
$d\sigma$ / $dm^{t\bar{t}}[GeV]vsp_T^{t\bar{t}}$ [pb/GeV x GeV]	$1.42 \cdot 10^{-4}$	$8.74 \cdot 10^{-4}$	$4.62 \cdot 10^{-4}$	$2.90 \cdot 10^{-5}$	$4.58 \cdot 10^{-5}$	$1.10 \cdot 10^{-3}$	$1.78 \cdot 10^{-3}$	$9.88 \cdot 10^{-4}$	$6.23 \cdot 10^{-5}$	$7.93 \cdot 10^{-4}$	$1.07 \cdot 10^{-3}$	$6.77 \cdot 10^{-4}$	$6.85 \cdot 10^{-5}$
Total Uncertainty [%]	$^{+8.54}_{-10.5}$	$^{+7.41}_{-7.57}$	$^{+7.47}_{-6.71}$	$^{+11.3}_{-11.2}$	$^{+25.1}_{-18.8}$	$^{+11.6}_{-11.2}$	$^{+10.1}_{-9.52}$	$^{+9.79}_{-9.31}$	$^{+14.2}_{-14.9}$	±10.7	$^{+7.66}_{-9.93}$	±11.2	$^{+16.4}_{-18.1}$
Statistics [%]	±3.7	±2.6	±2.1	±4.4	±7.1	±2.3	±2.0	±1.4	±3.1	±1.8	±2.5	±2.2	±2.7
Systematics [%]	$^{+7.36}_{-9.64}$	$^{+6.73}_{-6.89}$	$^{+7.06}_{-6.24}$	$^{+10.0}_{-9.97}$	$^{+23.7}_{-16.9}$	$^{+11.2}_{-10.9}$	$^{+9.93}_{-9.24}$	$^{+9.64}_{-9.16}$	$^{+13.8}_{-14.5}$	±10.5	$^{+7.02}_{-9.45}$	±10.9	$^{+16.1}_{-17.8}$
b-Tagged jet energy scale (JES) [%]	$^{-0.79}_{+0.10}$	$^{+0.23}_{-0.59}$	$^{+0.78}_{-0.86}$	$^{+0.65}_{-0.37}$	$^{+0.18}_{-1.42}$	$^{+0.62}_{-0.24}$	$^{+0.62}_{-0.30}$	$^{+0.63}_{-0.64}$	$^{+0.60}_{-0.47}$	$^{+0.30}_{-0.36}$	$^{+0.39}_{-0.30}$	$^{+0.57}_{-0.48}$	$^{+0.42}_{-0.66}$
Effective detector NP set 1 (JES) [%]	-	-	$^{+0.21}_{+0.16}$	-	-	-	-	$^{+0.17}_{-0.16}$	$^{+0.16}_{-0.46}$	-	$^{+0.13}_{-0.11}$	$^{+0.19}_{-0.18}$	$^{+0.19}_{-0.25}$
Effective detector NP set 2 (JES) [%]	$^{-0.31}_{-}$	$^{+0.20}_{-}$	$^{+0.19}_{+0.20}$	-	$^{-0.50}_{+0.15}$	$^{-0.17}_{+0.31}$	$^{+0.31}_{-}$	$^{+0.15}_{+0.16}$	$^{-0.24}_{+2.24}$	$^{+0.15}_{+0.46}$	$^{-}_{+0.16}$	$^{\pm0.19}_{+1.70}$	$^{-}_{+2.08}$
Effective mixed NP set 1 (JES) [%]	$^{-0.49}_{-}$	$^{+0.31}_{-1.16}$	$^{+1.74}_{-1.40}$	$^{+2.40}_{-2.07}$	$^{-1.08}_{+1.47}$	$^{+0.76}_{-0.34}$	$^{+0.76}_{-1.27}$	$^{+1.44}_{-1.18}$	$^{+2.24}_{-2.49}$	$^{+0.46}_{-0.61}$	$^{+0.16}_{-1.12}$	$^{-1.06}_{+1.11}$	$^{-2.20}_{+0.19}$
Effective mixed NP set 2 (JES) [%]	$^{-0.24}_{-}$	$^{-}_{+0.21}$	$^{-0.16}_{+0.21}$	$^{-}_{-}$	$^{-0.80}_{+0.40}$	$^{-0.13}_{-}$	$^{+0.26}_{-}$	±0.14	$^{-0.37}_{+0.14}$	$^{-}_{-}$	$^{-}_{-}$	$^{+0.20}_{-}$	$^{+0.16}_{-}$
Effective mixed NP set 3 (JES) [%]	-	-	-	-	$^{+0.14}_{-}$	-	-	-	-	-	-	-	-
Effective modelling NP set 1 (JES) [%]	$^{-0.55}_{-}$	$^{+0.25}_{-0.96}$	$^{+0.93}_{-0.83}$	$^{+0.68}_{+0.24}$	$^{-1.82}_{-}$	$^{+1.59}_{-1.12}$	$^{+2.00}_{-1.92}$	$^{+2.11}_{-1.58}$	$^{+1.40}_{-2.00}$	$^{+1.68}_{-1.70}$	$^{+1.20}_{-2.07}$	$^{+1.94}_{-1.58}$	$^{+1.97}_{-2.24}$
Effective modelling NP set 2 (JES) [%]	$^{-0.42}_{+0.23}$	-	$^{+0.83}_{-0.65}$	$^{+0.92}_{-0.97}$	$^{-}_{-1.56}$	$^{+0.39}_{-0.35}$	$^{+0.34}_{-0.13}$	$^{+0.48}_{-0.41}$	$^{+1.04}_{-1.29}$	$^{-}_{-}$	$^{+0.28}_{-0.17}$	$^{+0.52}_{-0.41}$	$^{+1.18}_{-1.37}$
Effective modelling NP set 3 (JES) [%]	-	$^{-0.46}_{+0.39}$	$^{-0.77}_{+0.76}$	$^{+0.23}_{+0.49}$	$^{-}_{-0.77}$	$^{-}_{+0.45}$	$^{-}_{+0.45}$	$^{-0.51}_{+0.47}$	$^{-0.59}_{+0.39}$	$^{-0.27}_{+0.21}$	$^{-0.28}_{+0.57}$	$^{-0.44}_{+0.47}$	$^{-0.73}_{+0.60}$
Effective modelling NP set 4 (JES) [%]	$^{-}_{-0.43}$	$^{+0.33}_{+0.19}$	$^{+0.17}_{-0.14}$	$^{+0.23}_{-}$	$^{-}_{-0.29}$	$^{+0.42}_{-0.20}$	$^{+0.32}_{-}$	±0.16	$^{+0.13}_{-0.38}$	$^{-}_{-}$	$^{-}_{-}$	$^{+0.20}_{-0.14}$	$^{+0.24}_{-0.29}$
Effective statistical NP set 1 (JES) [%]	$^{-0.61}_{-}$	$^{+0.18}_{-0.16}$	$^{-}_{-0.16}$	$^{+0.30}_{-}$	$^{-}_{-0.57}$	$^{+0.20}_{-0.10}$	$^{+0.38}_{-}$	$^{+0.26}_{-0.19}$	$^{+0.33}_{-0.79}$	$^{+0.23}_{-0.21}$	$^{+0.10}_{-0.20}$	$^{+0.34}_{-0.23}$	$^{+0.32}_{-0.44}$
Effective statistical NP set 2 (JES) [%]	$^{-0.45}_{+0.21}$	$^{+0.23}_{+0.32}$	$^{+0.23}_{-0.24}$	$^{+0.30}_{-}$	$^{-0.57}_{+0.42}$	$^{+0.15}_{-0.24}$	$^{+0.33}_{-}$	$^{-}_{-0.58}$	$^{-0.18}_{-0.54}$	$^{-0.23}_{+0.22}$	$^{-}_{-0.26}$	$^{-}_{-0.39}$	$^{-}_{-0.90}$
Effective statistical NP set 3 (JES) [%]	$^{-0.41}_{-}$	$^{+0.50}_{-0.33}$	$^{+0.20}_{+0.25}$	$^{+0.51}_{+0.28}$	$^{-1.38}_{-}$	$^{-}_{+0.19}$	$^{+0.31}_{+0.51}$	$^{+0.51}_{+0.30}$	$^{+0.66}_{-}$	$^{-}_{+0.20}$	$^{+0.27}_{+0.33}$	$^{+0.61}_{+0.42}$	$^{+0.68}_{-}$
Effective statistical NP set 4 (JES) [%]	$^{-0.25}_{-}$	$^{+0.26}_{+0.47}$	$^{-0.49}_{+0.47}$	$^{-}_{-}$	$^{-0.81}_{-}$	$^{-0.37}_{-}$	$^{-0.25}_{+0.38}$	$^{-0.24}_{+0.29}$	$^{-}_{-}$	$^{-0.22}_{+0.17}$	$^{-}_{+0.17}$	$^{-0.36}_{+0.23}$	$^{-0.15}_{-}$
Effective statistical NP set 5 (JES) [%]	$^{-0.21}_{-}$	$^{-}_{-}$	$^{-0.56}_{-}$	$^{-}_{-}$	$^{-0.85}_{-0.25}$	$^{-0.27}_{-}$	$^{-}_{-}$	$^{-0.25}_{+0.14}$	$^{-0.20}_{-}$	$^{-0.21}_{-}$	$^{-}_{-}$	$^{-0.26}_{-}$	$^{+0.16}_{-}$
Effective statistical NP set 6 (JES) [%]	$^{-0.59}_{-}$	$^{+0.27}_{+0.21}$	$^{-}_{-}$	$^{-}_{-}$	$^{-}_{-}$	$^{-}_{+0.12}$	$^{-}_{+0.33}$	$^{-0.12}_{+0.24}$	$^{-}_{+0.17}$	$^{-}_{-}$	$^{-}_{+0.14}$	$^{-}_{+0.28}$	$^{-}_{+0.29}$
Effective statistical NP set 7 (JES) [%]	$^{-}_{-0.32}$	$^{-}_{-}$	$^{+0.25}_{-0.29}$	$^{-}_{-}$	$^{-}_{-}$	$^{+0.12}_{-0.30}$	$^{-}_{-}$	$^{-0.21}_{+0.97}$	$^{-0.41}_{+1.35}$	$^{-}_{+0.97}$	$^{-0.13}_{+0.63}$	$^{-0.21}_{+1.02}$	$^{-0.34}_{+1.97}$
η intercalibration model (JES) [%]	$^{+0.10}_{+0.35}$	$^{-0.69}_{-}$	$^{+0.97}_{-0.71}$	$^{+0.72}_{-0.84}$	$^{-1.70}_{-}$	$^{-0.12}_{-0.13}$	$^{+1.00}_{-0.88}$	$^{-0.90}_{-0.44}$	$^{-1.79}_{-1.19}$	$^{-0.60}_{-0.86}$	$^{-0.65}_{-0.48}$	$^{-1.12}_{-0.55}$	$^{-1.74}_{-0.58}$
η intercalibration non closure (JES) [%]	$^{-0.68}_{-}$	$^{+0.28}_{+0.58}$	$^{+0.84}_{+0.84}$	$^{+0.32}_{+0.32}$	$^{-1.24}_{-}$	$^{+0.93}_{+0.93}$	$^{+0.61}_{+0.61}$	$^{+0.41}_{+0.41}$	$^{+0.84}_{+0.84}$	$^{+0.37}_{+0.37}$	$^{+0.24}_{+0.24}$	$^{+0.46}_{+0.46}$	$^{+0.97}_{+0.97}$
η intercalibration total stat (JES) [%]	$^{-0.44}_{-}$	$^{+0.39}_{+0.39}$	$^{+0.80}_{+0.80}$	$^{+1.44}_{+1.44}$	$^{-0.88}_{-}$	$^{+0.34}_{+0.34}$	$^{+0.22}_{+0.22}$	$^{+0.40}_{+0.40}$	$^{+0.66}_{+0.66}$	$^{+0.44}_{+0.44}$	$^{+0.32}_{+0.32}$	$^{+0.37}_{+0.37}$	$^{+0.62}_{+0.62}$
Flavour composition (JES) [%]	$^{-0.70}_{-}$	$^{-0.95}_{-0.77}$	$^{-1.10}_{-0.83}$	$^{-0.84}_{+0.49}$	$^{-2.48}_{-}$	$^{-1.31}_{-0.71}$	$^{-1.90}_{-0.91}$	$^{-1.94}_{-0.95}$	$^{-3.25}_{-1.25}$	$^{-1.98}_{-1.33}$	$^{-2.58}_{-1.53}$	$^{-2.31}_{-1.19}$	$^{-2.72}_{-1.58}$
Flavour response (JES) [%]	$^{-0.33}_{-}$	$^{+0.35}_{-}$	$^{+0.57}_{-}$	$^{+0.22}_{-}$	$^{-1.76}_{-}$	$^{+1.22}_{-}$	$^{+1.30}_{+0.31}$	$^{+1.25}_{\pm0.15}$	$^{+0.52}_{-0.28}$	$^{+1.05}_{-}$	$^{+1.12}_{-0.22}$	$^{+1.37}_{-}$	$^{+1.30}_{-}$
Pile-up offset μ (JES) [%]	$^{-0.74}_{-}$	$^{+0.31}_{-0.32}$	$^{+0.27}_{-0.44}$	$^{+0.49}_{-}$	$^{-0.82}_{-1.30}$	$^{+0.67}_{-0.35}$	$^{+0.78}_{-0.17}$	$^{+0.63}_{-0.34}$	$^{+0.11}_{-0.52}$	$^{+0.21}_{+0.42}$	$^{+0.10}_{+0.10}$	$^{+0.25}_{\pm0.66}$	$^{-0.29}_{+0.71}$
Pile-up offset N_{PV} (JES) [%]	$^{-0.98}_{-}$	$^{+0.54}_{-1.14}$	$^{+1.53}_{-1.35}$	$^{+1.39}_{-0.84}$	$^{-}_{-1.13}$	$^{+0.61}_{-0.18}$	$^{+1.09}_{-0.92}$	$^{+1.18}_{-1.04}$	$^{+1.15}_{-1.68}$	$^{+0.44}_{-0.65}$	$^{+0.70}_{-1.03}$	$^{+1.34}_{-1.04}$	$^{+1.60}_{-1.33}$
Pile-up offset p_T (JES) [%]	$^{-1.02}_{-1.13}$	$^{+0.41}_{-1.91}$	$^{+1.16}_{-1.06}$	$^{+0.60}_{-0.64}$	$^{+1.53}_{-2.71}$	$^{+2.65}_{-1.82}$	$^{+3.12}_{-3.13}$	$^{+3.02}_{-2.46}$	$^{+2.12}_{-2.72}$	$^{+2.82}_{-2.52}$	$^{+2.17}_{-3.25}$	$^{+3.12}_{-2.73}$	$^{+2.87}_{-2.99}$
Pile-up offset ρ topology (JES) [%]	-	-	-	-	-	-	-	-	-	-	-	-	-
Punch-through (JES) [%]	-	-	-	-	-	-	-	-	-	-	-	-	-
Jet vertex fraction [%]	-	-	-	-	$^{+0.46}_{-0.42}$	$^{+0.34}_{-0.37}$	$^{+0.31}_{-0.35}$	$^{+0.28}_{-0.32}$	$^{+0.31}_{-0.36}$	$^{+0.40}_{-0.44}$	$^{+0.32}_{-0.37}$	$^{+0.30}_{-0.35}$	$^{+0.33}_{-0.38}$
b-Quark tagging efficiency (eigenvector 0) [%]	$^{-1.14}_{+1.07}$	$^{-1.19}_{+1.11}$	$^{-1.50}_{+1.43}$	$^{-1.70}_{+1.61}$	$^{-1.95}_{+1.88}$	$^{-1.15}_{+1.36}$	$^{-1.40}_{+1.45}$	$^{-1.48}_{+1.41}$	$^{-2.77}_{+1.70}$	$^{-1.49}_{+1.91}$	$^{-1.74}_{+1.67}$	$^{-1.41}_{+1.68}$	$^{-1.80}_{+1.83}$
b-Quark tagging efficiency (eigenvector 1) [%]	$^{-0.95}_{+0.92}$	$^{-1.12}_{+1.08}$	$^{-1.31}_{+1.26}$	$^{-1.36}_{+1.31}$	$^{-0.78}_{+0.76}$	$^{-0.95}_{+0.91}$	$^{-1.20}_{+1.16}$	$^{-1.30}_{+1.25}$	$^{-1.67}_{+1.62}$	$^{-0.70}_{+0.68}$	$^{-1.05}_{+1.03}$	$^{-1.21}_{+1.17}$	$^{-1.48}_{+1.44}$
b-Quark tagging efficiency (eigenvector 2) [%]	-	-	∓0.11	∓0.10	±0.19	-	-	∓0.18	∓0.32	±0.39	±0.19	-	∓0.16
b-Quark tagging efficiency (eigenvector 3) [%]	-	-	-	∓0.12	-	-	-	-	±0.19	-	-	-	∓0.15
c-Quark tagging efficiency (eigenvector 0) [%]	-	-	-	-	-	-	-	-	-	±0.15	-	-	±0.10
c-Quark tagging efficiency (eigenvector 1) [%]	∓0.21	∓0.11	∓0.14	∓0.38	-	∓0.18	∓0.25	∓0.30	∓0.60	∓0.14	∓0.13	∓0.28	∓0.56
c-Quark tagging efficiency (eigenvector 2) [%]	-	-	-	∓0.16	±0.12	-	-	∓0.10	∓0.24	-	-	∓0.11	±0.19
Light-jet tagging efficiency (eigenvector 0) [%]	±0.19	$^{-0.36}_{+0.35}$	∓0.39	$^{-1.46}_{+1.47}$	∓0.20	∓0.23	∓0.28	$^{-0.46}_{+0.47}$	$^{-0.99}_{+0.97}$	∓0.58	$^{-0.58}_{+0.62}$	$^{-0.48}_{+0.49}$	∓0.88
Light-jet tagging efficiency (eigenvector 1) [%]	-	-	-	∓0.24	-	-	-	-	$^{-0.25}_{+0.24}$	±0.11	-	-	∓0.11
Light-jet tagging efficiency (eigenvector 2) [%]	±0.10	±0.13	-	-	-	-	-	-	-	-	-	-	$^{+0.11}_{-0.12}$
Light-jet tagging efficiency (eigenvector 3) [%]	-	-	∓0.13	∓0.42	-	-	-	∓0.14	∓0.32	-	∓0.10	∓0.11	∓0.20
Light-jet tagging efficiency (eigenvector 5) [%]	-	-	-	±0.17	-	-	-	-	$^{+0.13}_{-0.12}$	-	-	-	-
Light-jet tagging efficiency (eigenvector 6) [%]	-	-	-	∓0.12	-	-	-	-	±0.11	-	-	-	-
b-Quark tagging extrapolation [%]	-	±0.11	±0.32	$^{+0.74}_{-0.76}$	-	-	±0.16	$^{+0.41}_{-0.42}$	$^{+1.19}_{-1.20}$	-	-	±0.25	$^{+0.88}_{-0.89}$
Electron energy resolution [%]	$^{-}_{-0.16}$	-	$^{-0.12}_{-}$	-	-	-	-	-	-	-	-	-	-
Electron energy scale [%]	$^{-0.15}_{+0.17}$	-	-	$^{+0.48}_{-}$	-	$^{-0.24}_{-}$	-	-	-	-	-	-	$^{+0.13}_{-0.16}$
Electron trigger efficiency [%]	±0.10	±0.10	±0.11	±0.13	±0.10	±0.10	±0.10	±0.11	±0.14	±0.11	±0.11	±0.11	±0.14
Electron reconstruction efficiency [%]	±0.10	±0.11	±0.11	±0.13	-	±0.10	±0.10	±0.11	±0.13	-	±0.10	±0.11	±0.13
Electron identification efficiency [%]	±0.59	±0.60	±0.66	±0.83	±0.47	±0.56	±0.60	±0.66	±0.84	±0.45	±0.55	±0.62	±0.78
Electron isolation efficiency [%]	±0.41	±0.45	±0.53	±0.73	±0.14	±0.29	±0.40	±0.51	±0.71	±0.10	±0.26	±0.41	±0.63
Muon (ID) momentum resolution [%]	-	$^{-0.22}_{-}$	-	-	$^{+0.23}_{-0.48}$	-	-	-	-	-	-	-	-
Muon (MS) momentum resolution [%]	-	-	-	-	-	-	-	-	-	-	-	-	-
Muon energy scale [%]	-	-	-	-	-	-	-	-	-	-	-	-	-
Muon trigger efficiency stat [%]	$^{+0.26}_{-0.27}$	±0.27	$^{+0.28}_{-0.29}$	±0.31	±0.26	$^{+0.26}_{-0.27}$	±0.27	$^{+0.27}_{-0.28}$	$^{+0.31}_{-0.32}$	±0.30	±0.26	±0.28	$^{+0.29}_{-0.30}$
Muon trigger efficiency syst [%]	$^{+0.45}_{-0.44}$	$^{+0.46}_{-0.45}$	$^{+0.49}_{-0.47}$	$^{+0.57}_{-0.55}$	$^{+0.47}_{-0.46}$	$^{+0.47}_{-0.46}$	$^{+0.47}_{-0.46}$	$^{+0.39}_{-0.48}$	$^{+0.55}_{-0.54}$	$^{+0.51}_{-0.50}$	$^{+0.47}_{-0.46}$	$^{+0.50}_{-0.49}$	$^{+0.53}_{-0.51}$
Muon identification stat [%]	-	-	-	±0.10	-	-	-	-	±0.10	-	-	-	±0.10
Muon identification syst [%]	±0.45	$^{+0.49}_{-0.48}$	±0.55	$^{+0.75}_{-0.74}$	±0.37	±0.41	±0.46	±0.52	±0.68	±0.37	±0.39	±0.48	±0.59
Muon isolation efficiency syst [%]	-	±0.10	±0.15	±0.10	-	-	±0.10	±0.13	±0.10	-	±0.10	±0.12	
E_T^{miss} Soft jet resolution para [%]	∓0.37	∓0.65	∓1.00	∓0.79	±2.94	±0.53	±0.44	∓0.33	∓0.91	-	∓0.57	-	-
E_T^{miss} Soft jet resolution perp [%]	∓0.62	∓0.68	∓0.95	∓0.59	±3.07	±0.73	±0.55	∓0.30	∓0.83	±0.19	±0.11	∓0.24	±0.19
E_T^{miss} Soft jet scale [%]	$^{+0.30}_{-0.89}$	$^{-0.18}_{+0.20}$	$^{-0.78}_{+0.45}$	$^{-0.36}_{+0.24}$	$^{+1.99}_{-2.24}$	±0.42	$^{+0.34}_{-}$	$^{-0.32}_{+0.34}$	$^{-0.82}_{+0.70}$	±0.24	$^{-}_{-0.48}$	$^{-0.12}_{+0.18}$	$^{-0.48}_{+0.40}$
Luminosity [%]	∓2.05	∓2.05	∓2.05	∓2.05	∓2.05	∓2.05	∓2.05	∓2.05	∓2.05	∓2.05	∓2.05	∓2.05	∓2.05
Z+jets cross-section [%]	-	±0.13	±0.18	±0.67	±0.29	±0.20	±0.21	±0.40	±1.07	±0.65	±0.41	±0.53	±1.09
tWV cross-section [%]	-	-	-	-	±0.11	-	-	±0.11	±0.14	±0.17	±0.19	±0.22	±0.26
Monte Carlo sample statistics [%]	±2.16	±1.56	±1.23	±2.70	±4.05	±1.42	±1.17	±0.85	±1.79	±1.09	±1.60	±1.35	±1.59
ISR/FSR + scale [%]	$^{-}_{-5.26}$	$^{+2.46}_{-}$	$^{-0.93}_{+3.48}$	$^{+0.26}_{-}$	$^{+17.8}_{-}$	$^{-2.14}_{+1.96}$	$^{-3.02}_{+4.13}$	$^{-0.40}_{+0.70}$	$^{-0.18}_{+0.79}$	$^{+2.00}_{-}$	$^{-}_{-4.80}$	$^{+1.38}_{-3.43}$	$^{+0.13}_{-7.04}$
Alternate hard-scattering model [%]	∓6.41	∓4.84	∓1.65	∓1.50	±11.7	±6.74	±3.33	∓0.47	±0.19	±2.02	∓1.59	±1.03	±8.44
Alternate parton-shower model [%]	±0.20	∓0.18	-	∓2.02	±6.13	±6.68	±4.87	±6.01	±4.81	±7.06	±0.77	±6.14	±4.79
Fakes overall normalization, el [%]	∓0.12	∓0.29	$^{-0.37}_{+0.38}$	$^{-0.62}_{+0.63}$	$^{+2.14}_{-2.13}$	±0.68	±0.40	$^{+0.75}_{-0.76}$	±2.06	±1.04	±1.15	±1.30	$^{+2.60}_{-2.59}$
Fakes overall normalization, mu [%]	±0.26	∓0.29	∓0.15	∓0.38	±0.29	±0.11	±0.55	±0.31	±0.60	±0.49	±0.22	±0.61	±0.23
Fakes alternative parametrization [%]	∓0.27	±1.19	±0.44	±2.05	∓4.84	±1.60	∓1.91	∓2.14	∓5.34	∓3.08	∓2.76	∓3.84	∓5.67
W+jets heavy flavour component [%]	±0.29	±0.27	±0.18	±0.23	±0.16	±0.13	±0.10	-	-	-	-	-	-
W+jets Scales [%]	±0.60	±0.93	±2.29	±6.81	±1.91	±1.39	±1.68	±2.89	±8.35	±3.31	±2.61	±3.29	±6.73
W+jets α_S [%]	-	-	$^{-0.17}_{+0.18}$	$^{-0.50}_{+0.58}$	$^{-0.10}_{+0.12}$	-	$^{-0.11}_{+0.12}$	±0.20	$^{-0.48}_{+0.59}$	$^{-0.19}_{+0.23}$	$^{-0.15}_{+0.17}$	$^{-0.17}_{+0.23}$	$^{-0.37}_{+0.51}$
Single Top DS/DR [%]	-	∓0.58	∓1.35	∓3.62	∓1.28	∓0.72	∓0.85	∓1.81	∓4.30	∓1.01	∓2.06	∓2.62	∓5.11
Single Top IFSR [%]	$^{+0.13}_{-0.77}$	$^{-}_{-0.36}$	$^{-0.24}_{+0.69}$	$^{-}_{-1.24}$	$^{-0.36}_{-}$	$^{-}_{-0.32}$	$^{-}_{-0.51}$	$^{+0.11}_{-0.70}$	$^{+0.57}_{-1.10}$	$^{+0.26}_{-0.33}$	$^{-}_{-1.10}$	$^{-}_{-0.90}$	$^{+1.13}_{-1.75}$

TABLE F.23: Table of systematics for the absolute differential cross-section at the particle level for the $m^{t\bar{t}}[GeV]vsp_T^{t\bar{t}}$.

F.1.2 Relative differential cross section

F.1.2.1 Resolved topology

Bins [GeV]	0–20	20–45	45–75	75–100	100–150	150–200	200–300	300–500
$1/\sigma \cdot \mathrm{d}\sigma$ / $\mathrm{d}\lvert p_{out}^{t\bar{t}}\rvert$	$2.13 \cdot 10^{-2}$	$1.16 \cdot 10^{-2}$	$4.97 \cdot 10^{-3}$	$2.34 \cdot 10^{-3}$	$9.78 \cdot 10^{-4}$	$3.37 \cdot 10^{-4}$	$9.10 \cdot 10^{-5}$	$1.16 \cdot 10^{-5}$
Total Uncertainty [%]	+4.48 −4.95	+1.08 −2.11	+9.33 −8.10	+8.37 −6.98	+6.67 −4.99	+6.42 −5.76	+7.22 −5.75	+8.93 −8.47
Statistics [%]	±0.1	±0.1	±0.2	±0.4	±0.5	±0.9	±1.3	±2.6
Systematics [%]	+4.48 −4.95	+1.07 −2.10	+9.32 −8.09	+8.35 −6.96	+6.65 −4.95	+6.31 −5.64	+7.05 −5.54	+8.38 −7.89
Jet energy resolution [%]	∓0.46	±0.26	±0.84	±0.43	±0.32	∓1.80	∓2.07	∓1.54
b-Tagged jet energy scale (JES) [%]	-	-	-	+0.22 -	+0.10 −0.12	-	+0.12 −0.29	-
Effective detector NP set 1 (JES) [%]	-	-	-	-	-	-	+0.17 −0.11	-
Effective detector NP set 2 (JES) [%]	-	-	-	-	-	-	+0.12 -	±0.10
Effective mixed NP set 1 (JES) [%]	-	-	-	+0.22 -	+0.19 −0.27	+0.33 −0.30	+0.53 −0.55	+1.20 −1.08
Effective mixed NP set 2 (JES) [%]	-	-	-	-	-	-	- +0.11	-
Effective modelling NP set 1 (JES) [%]	−0.38 +0.44	+0.11 −0.20	+0.75 −0.78	+0.58 −0.45	-	−0.67 +0.80	−0.84 +1.01	−1.34 +0.73
Effective modelling NP set 2 (JES) [%]	-	-	-	-	+0.20 −0.25	+0.27 −0.29	+0.41 −0.34	+0.73 −0.80
Effective modelling NP set 3 (JES) [%]	-	-	-	-	−0.27 +0.22	−0.25 +0.26	−0.46 +0.52	−0.68 +0.46
Effective modelling NP set 4 (JES) [%]	-	-	-	-	-	-	-	−0.11 +0.13
Effective statistical NP set 1 (JES) [%]	-	-	+0.13 −0.12	-	-	−0.22 +0.16	−0.13 +0.17	−0.37 +0.29
Effective statistical NP set 2 (JES) [%]	-	-	∓0.11	-	-	+0.15 −0.18	+0.22 −0.20	±0.32
Effective statistical NP set 3 (JES) [%]	-	-	-	-	-	-	-	−0.70
Effective statistical NP set 4 (JES) [%]	-	-	-	-	+0.19 −0.22	+0.19 −0.20	+0.13 +0.32 −0.34	+0.47 +0.20 −0.38
Effective statistical NP set 5 (JES) [%]	-	-	-	-	-	-	+0.22 −0.12	+0.38 −0.41
Effective statistical NP set 6 (JES) [%]	-	-	-	-	-	−0.21 +0.12	-	-
Effective statistical NP set 7 (JES) [%]	-	-	-	-	-	-	+0.15 −0.10	-
η intercalibration model (JES) [%]	−0.11 +0.14	-	+0.19 −0.26	+0.40 −0.20	+0.15 −0.26	+0.21 −0.19	+0.10 −0.11	+0.30
η intercalibration non closure (JES) [%]	-	-	-	-	−0.14	-	-	−0.42 +0.46
η intercalibration total stat (JES) [%]	-	-	+0.16 −0.13	+0.12 +0.21 −0.17	-	-	-	−0.26 +0.11
Flavour composition (JES) [%]	−0.22 +0.25	-	+0.63 −0.60	+0.79 −0.58	- −0.21	−0.44 +0.99	−0.72 +0.96	−1.07 +1.24
Flavour response (JES) [%]	+0.14 −0.11	-	−0.34 +0.32	−0.37 +0.48	−0.20 -	+0.20 -	+0.37 −0.33	+0.21 −0.11
Pile-up offset μ (JES) [%]	-	-	-	−0.11 -	-	-	-	- −0.22
Pile-up offset N_{PV} (JES) [%]	−0.11 +0.14	-	+0.17 −0.21	+0.33 -	-	−0.14 -	-	-
Pile-up offset p_T (JES) [%]	-	−0.12 +0.13	-	+0.35 −0.23	+0.39 −0.57	+0.78 −0.70	+0.64 −0.69	+1.35 −1.21
Pile-up offset ρ topology (JES) [%]	−0.71 +0.74	+0.13 −0.24	+1.30 −1.27	+1.26 −0.93	+0.17 −0.35	−0.78 +0.92	−1.08 +1.13	−1.94 +1.95
Jet vertex fraction [%]	-	-	+0.10 −0.11	-	∓0.10	∓0.24	∓0.32	−0.44 +0.43
b-Quark tagging efficiency (eigenvector 0) [%]	−0.28 +0.33	-	+0.30 −0.38	+0.55 −0.60	+0.71 −0.72	±0.84	+0.74 −0.76	+0.76 −0.78
b-Quark tagging efficiency (eigenvector 1) [%]	-	-	-	-	−0.17 +0.14	−0.41 +0.39	−0.77 +0.74	−1.42 +1.37
b-Quark tagging efficiency (eigenvector 2) [%]	-	-	-	−0.17 +0.15	−0.25 +0.24	∓0.38	∓0.59	−0.98 +0.99
b-Quark tagging efficiency (eigenvector 3) [%]	-	-	-	-	-	-	-	∓0.12
c-Quark tagging efficiency (eigenvector 1) [%]	-	-	-	-	-	∓0.11	-	-
c-Quark tagging efficiency (eigenvector 2) [%]	-	-	-	-	-	-	∓0.11	∓0.15
Light-jet tagging efficiency (eigenvector 0) [%]	-	-	-	-	-	−0.18 +0.20	−0.13 +0.14	−0.14 +0.15
Light-jet tagging efficiency (eigenvector 1) [%]	-	-	-	-	-	-	-	−0.13 +0.12
b-Quark tagging extrapolation [%]	-	-	-	-	-	±0.10	±0.24	±0.87 −0.88
Electron identification efficiency [%]	-	-	-	-	-	-	-	±0.11
Electron isolation efficiency [%]	-	-	-	-	-	-	-	±0.14
E_T^{miss} Soft jet resolution para [%]	-	-	±0.13	-	-	-	±0.39	∓0.10
E_T^{miss} Soft jet resolution perp [%]	-	-	-	±0.12	-	-	±0.16	±0.27
E_T^{miss} Soft jet scale [%]	-	-	−0.10 +0.15	- +0.19	-	-	-	-
Z+jets cross-section [%]	-	-	-	-	-	±0.12	-	±0.13
Monte Carlo sample statistics [%]	-	-	±0.21	±0.28	±0.32	±0.68	±0.77	±1.51
ISR/FSR + scale [%]	- −2.11	- −1.79	+4.57 -	+4.43 -	+4.50 -	+2.60 -	+4.27 -	+3.28 -
Alternate hard-scattering model [%]	∓1.25	±0.52	±2.33	±0.69	∓0.55	±0.54	∓1.04	∓1.44
Alternate parton-shower model [%]	∓3.97	∓0.58	±7.31	±6.48	±4.42	±3.40	±1.56	±5.51
Inter PDF [%]	-	-	-	-	-	±0.10	-	±0.36
Intra PDF [%]	-	-	-	±0.12	±0.20	±0.41	±0.50	±1.89
Fakes overall normalization, el [%]	−0.43 +0.44	±0.20	+0.66 −0.67	±0.36	-	∓0.18	-	-
Fakes overall normalization, mu [%]	-	-	-	∓0.10	∓0.10	∓0.16	∓0.25	∓0.54
Fakes alternative parametrization [%]	-	∓0.17	∓0.21	±0.31	±0.61	±1.19	±1.69	±1.20
W+jets heavy flavour component [%]	±0.72	±0.31	∓0.76	∓1.67	∓1.53	∓3.39	∓3.68	∓1.37

TABLE F.24: Table of systematics for the relative differential cross-section at the particle level for the $\lvert P_{out}^{t\bar{t}} \rvert$ observable.

Bins [GeV]	0–30	30–60	60–90	90–130	130–170	170–210	210–250	250–290	290–340	340–390	390–440	440–500	500–575	575–650	650–750	750–850	850–1000	1000–1400	1400–2000.00
$1/\sigma \cdot \mathrm{d}\sigma / \mathrm{d}H_T^{t\bar{t}}$	$8.16 \cdot 10^{-5}$	$5.86 \cdot 10^{-4}$	$1.29 \cdot 10^{-3}$	$2.14 \cdot 10^{-3}$	$2.94 \cdot 10^{-3}$	$3.36 \cdot 10^{-3}$	$3.27 \cdot 10^{-3}$	$2.75 \cdot 10^{-3}$	$2.07 \cdot 10^{-3}$	$1.50 \cdot 10^{-3}$	$1.07 \cdot 10^{-3}$	$7.31 \cdot 10^{-4}$	$4.66 \cdot 10^{-4}$	$2.79 \cdot 10^{-4}$	$1.55 \cdot 10^{-4}$	$7.85 \cdot 10^{-5}$	$3.21 \cdot 10^{-5}$	$6.02 \cdot 10^{-6}$	$2.99 \cdot 10^{-7}$
Total Uncertainty [%]	$^{+12.3}_{-12.9}$	$^{+9.39}_{-9.46}$	$^{+7.71}_{-7.87}$	$^{+6.42}_{-6.39}$	$^{+3.75}_{-3.74}$	$^{+1.82}_{-1.80}$	$^{+2.04}_{-2.02}$	$^{+1.80}_{-1.85}$	±2.32	$^{+3.32}_{-3.19}$	$^{+3.71}_{-3.82}$	$^{+4.44}_{-4.38}$	$^{+5.23}_{-5.16}$	$^{+6.80}_{-6.92}$	$^{+7.49}_{-7.65}$	$^{+8.01}_{-7.13}$	$^{+10.8}_{-10.7}$	$^{+10.2}_{-10.0}$	$^{+35.6}_{-32.2}$
Statistics [%]	±1.8	±0.7	±0.4	±0.3	±0.2	±0.2	±0.2	±0.2	±0.2	±0.3	±0.4	±0.4	±0.5	±0.7	±0.9	±1.3	±1.7	±2.6	±12.
Systematics [%]	$^{+12.1}_{-12.7}$	$^{+9.34}_{-9.40}$	$^{+7.68}_{-7.84}$	$^{+6.40}_{-6.37}$	$^{+3.73}_{-3.72}$	$^{+1.79}_{-1.77}$	$^{+2.01}_{-1.99}$	$^{+1.77}_{-1.82}$	$^{+2.30}_{-2.29}$	$^{+3.29}_{-3.16}$	$^{+3.68}_{-3.79}$	$^{+4.40}_{-4.34}$	$^{+5.19}_{-5.12}$	$^{+6.74}_{-6.86}$	$^{+7.41}_{-7.58}$	$^{+7.86}_{-6.95}$	$^{+10.6}_{-10.5}$	$^{+9.79}_{-9.61}$	$^{+32.7}_{-29.0}$
Jet energy resolution [%]	±2.54	±1.06	±0.84	±1.28	-	∓0.67	∓1.35	∓0.52	±0.44	∓0.17	∓0.17	-	±0.34	±1.30	±4.26	±1.99	±0.55	±1.45	±4.09
b-Tagged jet energy scale (JES) [%]	∓0.79	$^{-0.50}_{+0.51}$	$^{-0.51}_{+0.38}$	$^{-0.44}_{+0.36}$	$^{-0.25}_{+0.37}$	$^{-0.10}_{+0.13}$	-	$^{+0.21}_{-0.27}$	$^{+0.25}_{-0.26}$	$^{+0.20}_{-0.14}$	$^{+0.16}_{-0.22}$	±0.18	-	$^{+0.24}_{-0.17}$	$^{+0.20}_{-0.15}$	-	±0.22	$^{+0.36}_{-0.19}$	$^{+0.32}_{-}$
Effective detector NP set 1 (JES) [%]	-	-	-	-	-	-	-	-	-	-	-	-	-	-	$^{+0.10}_{-0.14}$	-	$^{+0.21}_{-0.20}$	$^{+0.34}_{-0.12}$	$^{-}_{-1.14}$
Effective detector NP set 2 (JES) [%]	-	-	-	-	-	-	-	-	-	-	-	-	-	$^{+0.14}_{-}$	$^{-}_{-0.12}$	-	$^{+0.19}_{-0.15}$	$^{+0.23}_{-0.10}$	$^{-}_{-0.62}$
Effective mixed NP set 1 (JES) [%]	$^{-0.34}_{+0.47}$	$^{-0.33}_{+0.42}$	$^{-0.37}_{+0.35}$	$^{-0.33}_{+0.32}$	$^{-0.27}_{+0.31}$	$^{-0.24}_{+0.22}$	$^{-0.13}_{+0.10}$	-	$^{+0.13}_{-}$	$^{+0.16}_{-0.14}$	$^{+0.20}_{-0.30}$	$^{+0.35}_{-0.33}$	$^{+0.40}_{-0.39}$	$^{+0.76}_{-0.71}$	$^{+0.95}_{-1.17}$	$^{+1.10}_{-0.70}$	$^{+1.78}_{-1.65}$	$^{+2.69}_{-2.84}$	$^{+3.16}_{-4.83}$
Effective mixed NP set 2 (JES) [%]	-	-	-	-	-	-	-	-	-	-	-	-	-	$^{-}_{+0.13}$	$^{-0.13}_{-}$	-	$^{-0.17}_{+0.21}$	$^{-0.12}_{+0.30}$	$^{-0.31}_{+0.26}$
Effective mixed NP set 3 (JES) [%]	-	-	-	-	-	-	-	-	-	-	-	-	-	-	-	-	-	-	$^{+0.15}_{-0.14}$
Effective modelling NP set 1 (JES) [%]	$^{-0.71}_{+1.00}$	$^{+0.22}_{-}$	$^{+0.53}_{-0.42}$	$^{+0.36}_{-0.43}$	$^{+0.19}_{-0.24}$	$^{+0.10}_{-0.15}$	$^{+0.17}_{-0.13}$	$^{+0.20}_{-0.15}$	-	$^{-0.25}_{+0.23}$	$^{-0.52}_{+0.24}$	$^{-0.56}_{+0.58}$	$^{-0.51}_{+0.82}$	$^{-0.75}_{+0.67}$	$^{-0.82}_{+0.62}$	$^{-0.75}_{+1.04}$	$^{-0.68}_{+1.36}$	$^{-0.76}_{+0.18}$	$^{-1.34}_{+1.07}$
Effective modelling NP set 2 (JES) [%]	$^{-}_{+0.38}$	$^{-0.21}_{+0.31}$	$^{-0.31}_{+0.28}$	$^{-0.29}_{+0.25}$	∓0.24	∓0.16	-	-	-	$^{+0.15}_{-0.14}$	±0.23	$^{+0.27}_{-0.30}$	$^{+0.32}_{-0.37}$	$^{+0.59}_{-0.44}$	$^{+0.55}_{-0.67}$	$^{+0.61}_{-0.59}$	$^{+1.13}_{-1.03}$	$^{+1.62}_{-1.53}$	$^{+2.62}_{-4.62}$
Effective modelling NP set 3 (JES) [%]	$^{+0.31}_{-}$	$^{+0.31}_{-0.24}$	$^{+0.29}_{-0.34}$	$^{+0.25}_{-0.30}$	$^{+0.25}_{-0.22}$	±0.17	-	-	$^{-0.13}_{+0.12}$	$^{-0.16}_{+0.18}$	∓0.26	$^{-0.33}_{+0.30}$	$^{-0.36}_{+0.31}$	$^{-0.44}_{+0.55}$	$^{-0.59}_{+0.51}$	$^{-0.41}_{+0.48}$	$^{-0.78}_{+0.63}$	$^{-0.63}_{+0.92}$	$^{-0.32}_{+0.10}$
Effective modelling NP set 4 (JES) [%]	$^{-}_{+0.17}$	-	-	-	-	-	-	-	-	-	-	-	-	-	-	-	-	$^{+0.34}_{-}$	$^{-}_{-1.07}$
Effective statistical NP set 1 (JES) [%]	$^{+0.36}_{-}$	-	±0.13	$^{-}_{-0.12}$	-	-	-	-	-	-	-	$^{-0.16}_{+0.15}$	$^{-0.19}_{+0.23}$	$^{-}_{+0.20}$	$^{-0.16}_{-}$	$^{-0.23}_{+0.22}$	$^{-0.15}_{+0.23}$	$^{+0.23}_{-0.24}$	$^{-}_{-0.57}$
Effective statistical NP set 2 (JES) [%]	-	$^{+0.20}_{-}$	$^{-0.11}_{+0.17}$	-	-	-	-	-	-	-	-	$^{+0.14}_{-0.15}$	$^{+0.23}_{-0.18}$	$^{+0.29}_{-0.18}$	$^{+0.18}_{-0.24}$	$^{+0.27}_{-0.37}$	$^{+0.60}_{-0.49}$	$^{+0.70}_{-0.62}$	$^{+1.39}_{-2.27}$
Effective statistical NP set 3 (JES) [%]	-	-	-	-	-	-	-	-	-	-	-	-	-	$^{-0.21}_{+0.29}$	$^{-0.38}_{+0.30}$	$^{-0.31}_{+0.33}$	$^{-0.89}_{+0.78}$	$^{-0.83}_{+1.19}$	$^{-0.85}_{+0.71}$
Effective statistical NP set 4 (JES) [%]	$^{-}_{+0.26}$	$^{-0.24}_{+0.28}$	$^{-0.28}_{+0.25}$	$^{-0.24}_{+0.20}$	$^{-0.16}_{+0.20}$	$^{-0.13}_{+0.12}$	-	-	$^{+0.11}_{-0.13}$	$^{+0.13}_{-0.15}$	$^{+0.24}_{-0.19}$	$^{+0.28}_{-0.24}$	$^{+0.19}_{-0.27}$	$^{+0.33}_{-0.24}$	$^{+0.33}_{-0.36}$	$^{+0.10}_{-0.17}$	$^{+0.18}_{-0.26}$	$^{+0.20}_{-}$	$^{-0.48}_{+0.26}$
Effective statistical NP set 5 (JES) [%]	-	-	-	-	-	-	-	-	-	-	-	-	-	$^{+0.19}_{-0.11}$	$^{+0.20}_{-0.29}$	-	$^{+0.32}_{-0.35}$	-	$^{-0.97}_{-}$
Effective statistical NP set 6 (JES) [%]	-	-	-	-	-	-	-	-	-	-	-	$^{-0.13}_{+0.10}$	$^{-0.11}_{+0.14}$	-	-	-	-	-	$^{-}_{-0.89}$
Effective statistical NP set 7 (JES) [%]	-	-	-	-	-	-	-	-	-	-	-	-	-	$^{+0.17}_{-}$	$^{+0.12}_{-0.19}$	-	$^{+0.28}_{-0.19}$	$^{+0.32}_{-0.25}$	$^{-}_{-0.64}$
η intercalibration model (JES) [%]	$^{-0.30}_{+0.34}$	$^{-0.24}_{+0.37}$	$^{-0.32}_{+0.24}$	$^{-0.26}_{+0.19}$	$^{-}_{+0.19}$	$^{-0.16}_{+0.12}$	-	$^{+0.13}_{-0.12}$	$^{+0.12}_{-}$	$^{-}_{-0.14}$	$^{+0.10}_{-0.24}$	$^{+0.21}_{-0.10}$	-	$^{+0.20}_{-0.11}$	$^{+0.56}_{-0.37}$	$^{+0.32}_{-0.17}$	$^{+0.41}_{-0.39}$	$^{+1.08}_{-1.15}$	$^{+0.47}_{-1.26}$
η intercalibration non closure (JES) [%]	$^{-}_{-0.41}$	$^{-}_{-0.15}$	-	-	-	-	-	-	-	-	-	$^{-}_{+0.13}$	-	$^{-}_{+0.13}$	$^{-0.23}_{+0.26}$	$^{+0.32}_{-0.20}$	$^{-0.29}_{+0.40}$	$^{-0.80}_{+0.40}$	-
η intercalibration total stat (JES) [%]	$^{-0.35}_{+0.38}$	$^{-}_{+0.23}$	-	-	-	-	-	-	-	-	-	-	-	-	-	-	-	$^{+0.18}_{-0.17}$	$^{-}_{-0.95}$
Flavour composition (JES) [%]	$^{-}_{-0.30}$	-	$^{+0.40}_{-0.15}$	$^{+0.55}_{-0.40}$	$^{+0.37}_{-0.41}$	-	-	$^{+0.17}_{-0.13}$	-	$^{-0.27}_{+0.30}$	$^{-0.51}_{+0.19}$	$^{-0.42}_{+0.61}$	$^{-0.47}_{+0.84}$	$^{-0.59}_{+0.84}$	$^{-0.57}_{+0.44}$	$^{-0.70}_{+0.97}$	$^{-0.35}_{+1.13}$	$^{-}_{-0.22}$	$^{+0.23}_{-2.29}$
Flavour response (JES) [%]	$^{+0.18}_{-0.20}$	-	$^{-}_{+0.28}$	-	-	-	-	-	-	-	-	-	$^{+0.21}_{-}$	$^{+0.38}_{-0.21}$	$^{-}_{-0.18}$	$^{+0.42}_{-0.40}$	$^{+0.67}_{-0.29}$	-	$^{+1.07}_{-2.91}$
Pile-up offset μ (JES) [%]	$^{+0.14}_{-}$	-	-	-	-	-	-	-	-	-	-	-	-	-	-	-	-	-	$^{-}_{-0.30}$
Pile-up offset N_{PV} (JES) [%]	$^{-0.46}_{+0.21}$	-	$^{+0.15}_{-}$	-	$^{-}_{+0.12}$	-	-	$^{+0.16}_{-0.10}$	-	-	-	-	$^{-}_{+0.22}$	-	-	$^{-0.19}_{+0.18}$	$^{-}_{+0.39}$	-	$^{-0.88}_{+0.35}$
Pile-up offset p_T (JES) [%]	$^{-0.63}_{+0.44}$	∓0.68	∓0.68	$^{-0.59}_{+0.57}$	$^{-0.43}_{+0.52}$	∓0.39	$^{-0.17}_{+0.11}$	$^{+0.13}_{-0.15}$	$^{+0.29}_{-0.25}$	$^{+0.33}_{-0.43}$	$^{+0.55}_{-0.56}$	$^{+0.61}_{-0.44}$	$^{+0.62}_{-0.75}$	$^{+0.94}_{-0.86}$	±1.07	$^{+1.00}_{-0.92}$	$^{+1.13}_{-1.40}$	$^{+1.86}_{-1.48}$	$^{+2.02}_{-1.97}$
Pile-up offset ρ topology (JES) [%]	$^{-2.14}_{+1.91}$	$^{-0.50}_{+0.64}$	$^{+0.18}_{-0.21}$	$^{+0.23}_{-0.25}$	-	-	$^{+0.25}_{-0.17}$	$^{+0.47}_{-0.41}$	$^{+0.26}_{-0.25}$	-	$^{-0.39}_{+0.18}$	$^{-0.47}_{+0.61}$	$^{-0.72}_{+0.90}$	$^{-0.96}_{+0.92}$	$^{-1.06}_{+0.88}$	$^{-0.63}_{+1.68}$	$^{-1.28}_{+1.61}$	$^{-1.83}_{+1.15}$	$^{-2.31}_{+0.82}$
Punch-through (JES) [%]	-	-	-	-	-	-	-	-	-	-	-	-	-	-	-	-	-	-	$^{+0.35}_{-0.24}$
Jet vertex fraction [%]	±0.18	±0.27	$^{+0.30}_{-0.31}$	$^{+0.26}_{-0.27}$	$^{+0.20}_{-0.21}$	±0.14	-	-	∓0.10	∓0.18	∓0.24	∓0.29	∓0.34	$^{-0.38}_{+0.39}$	∓0.43	$^{-0.45}_{+0.46}$	$^{-0.50}_{+0.51}$	$^{-0.58}_{+0.57}$	$^{-0.52}_{+0.51}$
b-Quark tagging efficiency (eigenvector 0) [%]	$^{-1.75}_{+1.63}$	$^{-1.79}_{+1.66}$	$^{-1.58}_{+1.46}$	$^{-1.11}_{+1.02}$	$^{-0.64}_{+0.59}$	$^{-0.24}_{+0.22}$	-	$^{+0.25}_{-0.22}$	$^{+0.42}_{-0.38}$	$^{+0.63}_{-0.58}$	$^{+0.80}_{-0.74}$	$^{+0.90}_{-0.83}$	$^{+0.92}_{-0.85}$	$^{+0.93}_{-0.86}$	$^{+0.82}_{-0.76}$	$^{+0.68}_{-0.63}$	$^{+0.51}_{-0.48}$	-	$^{-1.15}_{+1.01}$
b-Quark tagging efficiency (eigenvector 1) [%]	$^{+0.77}_{-0.76}$	$^{+0.80}_{-0.79}$	$^{+0.80}_{-0.78}$	$^{+0.72}_{-0.71}$	$^{+0.60}_{-0.59}$	$^{+0.45}_{-0.44}$	±0.28	±0.11	∓0.12	$^{-0.42}_{+0.41}$	$^{-0.71}_{+0.70}$	$^{-0.98}_{+0.96}$	$^{-1.28}_{+1.26}$	$^{-1.57}_{+1.55}$	$^{-1.93}_{+1.90}$	$^{-2.26}_{+2.23}$	$^{-2.57}_{+2.54}$	$^{-3.06}_{+3.02}$	$^{-3.74}_{+3.69}$
b-Quark tagging efficiency (eigenvector 2) [%]	±0.49	$^{+0.44}_{-0.45}$	$^{+0.39}_{-0.40}$	±0.34	$^{+0.28}_{-0.29}$	±0.23	±0.17	-	-	∓0.18	∓0.33	$^{-0.49}_{+0.50}$	$^{-0.69}_{+0.71}$	$^{-0.91}_{+0.93}$	$^{-1.15}_{+1.17}$	$^{-1.39}_{+1.41}$	$^{-1.62}_{+1.65}$	$^{-1.97}_{+2.02}$	$^{-2.29}_{+2.34}$
b-Quark tagging efficiency (eigenvector 3) [%]	∓0.31	∓0.30	∓0.27	∓0.22	∓0.16	-	-	-	±0.13	±0.21	±0.25	±0.24	±0.20	±0.10	-	∓0.20	∓0.38	∓0.70	∓1.08
b-Quark tagging efficiency (eigenvector 4) [%]	-	-	-	-	-	-	-	-	-	-	-	-	-	-	-	-	-	∓0.19	∓0.32
c-Quark tagging efficiency (eigenvector 0) [%]	-	±0.10	±0.12	±0.13	±0.11	-	-	-	-	-	∓0.12	∓0.14	∓0.15	∓0.17	$^{-0.18}_{+0.17}$	∓0.17	∓0.23	∓0.20	-
c-Quark tagging efficiency (eigenvector 1) [%]	-	±0.11	±0.10	-	-	-	-	-	-	-	-	-	-	-	∓0.10	∓0.11	∓0.14	∓0.33	∓0.82
c-Quark tagging efficiency (eigenvector 2) [%]	-	-	-	-	-	-	-	-	-	-	∓0.10	∓0.13	∓0.15	∓0.16	∓0.18	∓0.18	∓0.21	∓0.29	∓0.52
Light-jet tagging efficiency (eigenvector 0) [%]	$^{-0.32}_{+0.44}$	$^{-0.35}_{+0.46}$	$^{-0.28}_{+0.32}$	$^{-0.14}_{+0.11}$	-	-	-	-	-	±0.10	$^{+0.13}_{-0.14}$	$^{+0.10}_{-0.11}$	$^{-}_{-0.11}$	-	-	-	-	$^{-0.38}_{+0.41}$	$^{-1.22}_{+1.34}$
Light-jet tagging efficiency (eigenvector 1) [%]	$^{+0.35}_{-0.29}$	$^{+0.46}_{-0.40}$	$^{+0.33}_{-0.32}$	$^{+0.15}_{-0.16}$	-	-	-	-	-	-	∓0.14	$^{-0.16}_{+0.15}$	$^{-0.20}_{+0.19}$	$^{-0.21}_{+0.20}$	$^{-0.18}_{+0.17}$	∓0.24	∓0.28	∓0.27	∓0.68
Light-jet tagging efficiency (eigenvector 2) [%]	-	-	-	-	-	-	-	-	-	-	-	-	-	-	-	-	-	-	∓0.31
Light-jet tagging efficiency (eigenvector 3) [%]	$^{+0.20}_{-0.19}$	$^{+0.22}_{-0.20}$	$^{+0.13}_{-0.12}$	-	-	-	-	-	-	-	-	-	∓0.10	∓0.11	-	-	∓0.12	$^{-0.21}_{+0.22}$	$^{-0.11}_{+0.12}$
Light-jet tagging efficiency (eigenvector 4) [%]	-	-	-	-	-	-	-	-	-	-	-	-	-	-	-	-	-	-	±0.12
Light-jet tagging efficiency (eigenvector 5) [%]	-	-	-	-	-	-	-	-	-	-	-	-	-	-	-	-	-	±0.13	±0.72
Light-jet tagging efficiency (eigenvector 6) [%]	-	-	-	-	-	-	-	-	-	-	-	-	-	-	-	-	-	-	∓0.20
Light-jet tagging efficiency (eigenvector 7) [%]	-	-	-	-	-	-	-	-	-	-	-	-	-	-	-	-	-	-	∓0.42
Light-jet tagging efficiency (eigenvector 8) [%]	-	-	-	-	-	-	-	-	-	-	-	-	-	-	-	-	-	-	±0.10
b-Quark tagging extrapolation [%]	-	-	-	-	-	-	-	-	-	-	-	-	-	±0.18	±0.44	±0.90	±1.67	$^{+3.22}_{-3.20}$	$^{+6.59}_{-6.49}$
Electron identification efficiency [%]	-	-	-	-	-	-	-	-	-	-	-	-	±0.12	±0.15	±0.19	$^{+0.22}_{-0.23}$	±0.26	±0.33	±0.48
Electron isolation efficiency [%]	-	-	-	-	-	-	-	-	-	-	-	-	±0.14	±0.20	±0.29	±0.37	±0.47	±0.63	±1.18
Muon (MS) momentum resolution [%]	-	-	-	-	-	-	-	-	-	-	-	-	-	-	-	-	-	-	-
Muon identification syst [%]	-	-	-	-	-	-	-	-	-	-	-	-	-	-	±0.10	±0.12	±0.17	$^{+0.23}_{-0.22}$	±0.34
E_T^{miss} Soft jet resolution para [%]	∓0.36	∓0.30	-	-	-	±0.14	-	-	-	∓0.10	∓0.11	-	-	-	∓0.31	∓0.20	-	∓0.40	∓0.26
E_T^{miss} Soft jet resolution perp [%]	∓1.36	∓0.35	∓0.24	-	±0.14	±0.19	-	-	-	-	∓0.12	-	-	∓0.28	∓0.19	-	∓0.38	∓0.48	∓0.46
E_T^{miss} Soft jet scale [%]	$^{-0.77}_{+0.17}$	-	-	-	$^{+0.11}_{-}$	$^{+0.12}_{-}$	$^{-}_{-0.12}$	-	-	$^{-0.12}_{+0.15}$	$^{-0.15}_{-}$	$^{-}_{+0.14}$	-	$^{-0.17}_{+0.22}$	$^{-0.34}_{+0.15}$	-	$^{-0.25}_{+0.26}$	$^{-0.43}_{+0.46}$	$^{-}_{-0.29}$
Z+jets cross-section [%]	-	∓0.12	∓0.22	$^{+0.31}_{-0.32}$	$^{+0.27}_{-0.28}$	∓0.16	-	-	∓0.16	$^{-0.21}_{+0.22}$	∓0.26	$^{-0.29}_{+0.30}$	∓0.31	$^{-0.32}_{+0.33}$	∓0.33	$^{-0.31}_{+0.32}$	∓0.28	∓0.28	-
Monte Carlo sample statistics [%]	±1.43	±0.63	±0.42	±0.30	±0.25	±0.19	±0.18	±0.18	±0.18	±0.21	±0.25	±0.29	±0.34	±0.45	±0.55	±0.81	±1.04	±1.51	±5.35
ISR/FSR + scale [%]	$^{-3.29}_{+0.24}$	$^{-}_{-1.19}$	$^{-}_{-1.48}$	$^{+0.89}_{-}$	$^{-0.17}_{-}$	$^{+0.38}_{-}$	$^{+0.34}_{-}$	$^{-}_{-0.62}$	$^{-0.22}_{-}$	$^{+0.93}_{-}$	$^{+0.24}_{-0.30}$	$^{-}_{-0.39}$	$^{-}_{-0.64}$	$^{+0.50}_{-1.74}$	$^{-}_{-0.99}$	$^{+2.95}_{-}$	$^{+1.24}_{-0.66}$	$^{+2.35}_{-0.48}$	$^{+16.6}_{-}$
Alternate hard-scattering model [%]	±2.08	±3.35	±2.35	±2.46	±1.50	±0.36	±0.43	∓0.19	∓1.30	∓1.53	∓1.65	∓0.87	∓1.90	∓3.61	∓1.13	∓1.65	∓7.75	∓2.61	±23.8
Alternate parton-shower model [%]	∓5.27	∓2.41	∓1.64	-	±0.52	±0.74	±0.24	∓0.19	±0.40	±0.44	∓0.42	∓0.61	∓0.61	∓2.26	∓0.93	±1.73	±0.40	∓2.65	±9.00
Inter PDF [%]	±0.17	-	-	-	-	-	-	-	-	-	-	-	-	-	-	∓0.13	-	±0.19	-
Intra PDF [%]	±1.33	±0.28	-	-	∓0.11	∓0.11	-	-	-	-	∓0.22	±0.11	±0.24	-	±0.19	±0.97	±0.23	±1.00	±1.47
Fakes overall normalization, el [%]	$^{+0.25}_{-0.24}$	$^{+1.17}_{-1.19}$	$^{+1.56}_{-1.59}$	$^{+1.42}_{-1.44}$	$^{+0.77}_{-0.78}$	±0.19	$^{-0.15}_{+0.16}$	∓0.34	∓0.50	$^{-0.68}_{+0.69}$	$^{-0.68}_{+0.69}$	$^{-0.67}_{+0.68}$	$^{-0.75}_{+0.76}$	$^{-0.96}_{+0.97}$	$^{-0.99}_{+1.00}$	$^{-0.89}_{+0.90}$	$^{-0.62}_{+0.63}$	$^{-0.36}_{+0.37}$	$^{+2.78}_{-2.82}$
Fakes overall normalization, mu [%]	∓0.25	-	±0.12	±0.12	±0.10	±0.14	±0.16	±0.10	-	-	∓0.16	∓0.23	∓0.41	∓0.56	∓0.91	∓1.15	∓1.00	∓1.26	-
Fakes alternative parametrization [%]	∓3.43	∓4.28	∓4.84	∓4.23	∓2.43	∓0.98	±0.24	±0.88	±1.29	±1.84	±2.30	±2.89	±3.40	±3.61	±4.37	±4.59	±4.28	±5.01	±2.18
W+jets heavy flavour component [%]	±8.71	±6.43	±4.34	±3.03	±1.68	±0.22	∓1.20	∓1.09	∓0.79	∓1.51	∓1.55	∓2.21	∓1.92	∓1.14	±1.49	∓1.16	∓1.81	∓0.18	∓2.29

TABLE F.25: Table of systematics for the relative differential cross-section at the particle level for the $H_T^{t\bar{t}}$ observable.

Bins [GeV]	0–15	15–30	30–45	45–60	60–75	75–90	90–110	110–130	130–150	150–175	175–200	200–225	225–250	250–275	275–300	300–350	350–400	400–500	500–1000.00
$1/\sigma \cdot \mathrm{d}\sigma / \mathrm{d}p_T^{t}$	$7.49 \cdot 10^{-4}$	$2.23 \cdot 10^{-3}$	$3.63 \cdot 10^{-3}$	$4.84 \cdot 10^{-3}$	$5.74 \cdot 10^{-3}$	$6.24 \cdot 10^{-3}$	$6.28 \cdot 10^{-3}$	$5.66 \cdot 10^{-3}$	$4.64 \cdot 10^{-3}$	$3.53 \cdot 10^{-3}$	$2.55 \cdot 10^{-3}$	$1.83 \cdot 10^{-3}$	$1.32 \cdot 10^{-3}$	$9.57 \cdot 10^{-4}$	$7.02 \cdot 10^{-4}$	$4.30 \cdot 10^{-4}$	$2.20 \cdot 10^{-4}$	$8.97 \cdot 10^{-5}$	$6.44 \cdot 10^{-6}$
Total Uncertainty [%]	$^{+9.31}_{-9.35}$	$^{+5.13}_{-4.99}$	$^{+4.69}_{-4.64}$	$^{+3.50}_{-3.72}$	$^{+4.15}_{-4.18}$	$^{+3.79}_{-3.72}$	$^{+1.83}_{-1.86}$	$^{+1.48}_{-1.49}$	±1.59	$^{+1.84}_{-1.74}$	$^{+3.07}_{-2.92}$	$^{+4.24}_{-4.41}$	$^{+5.03}_{-5.33}$	$^{+5.22}_{-5.20}$	$^{+5.70}_{-5.38}$	$^{+6.05}_{-6.02}$	$^{+6.88}_{-7.12}$	$^{+8.19}_{-8.20}$	$^{+10.1}_{-8.39}$
Statistics [%]	±1.1	±0.5	±0.4	±0.3	±0.3	±0.3	±0.2	±0.3	±0.3	±0.3	±0.4	±0.4	±0.5	±0.6	±0.7	±0.7	±1.1	±1.3	±2.2
Systematics [%]	$^{+9.21}_{-9.25}$	$^{+5.07}_{-4.93}$	$^{+4.66}_{-4.61}$	$^{+3.47}_{-3.69}$	$^{+4.12}_{-4.15}$	$^{+3.76}_{-3.70}$	$^{+1.79}_{-1.83}$	$^{+1.43}_{-1.45}$	$^{+1.55}_{-1.54}$	$^{+1.79}_{-1.68}$	$^{+3.03}_{-2.88}$	$^{+4.20}_{-4.38}$	$^{+4.98}_{-5.29}$	$^{+5.17}_{-5.15}$	$^{+5.63}_{-5.30}$	$^{+5.98}_{-5.95}$	$^{+6.74}_{-6.99}$	±8.05	$^{+9.76}_{-7.98}$
Jet energy resolution [%]	±4.09	∓0.93	±0.88	∓1.00	±0.26	±2.01	∓1.37	∓0.44	±0.43	±0.53	∓0.33	∓1.14	∓1.19	∓1.14	-	±1.77	±3.30	-	±1.20
b-Tagged jet energy scale (JES) [%]	$^{-0.54}_{+0.43}$	$^{-0.56}_{+0.44}$	$^{-0.40}_{+0.43}$	$^{-0.36}_{+0.35}$	$^{-0.24}_{+0.23}$	$^{-0.22}_{+0.29}$	-	$^{+0.20}_{-0.16}$	$^{+0.22}_{-0.25}$	$^{+0.28}_{-0.26}$	$^{+0.24}_{-0.17}$	$^{+0.10}_{-0.24}$	$^{+0.14}_{-0.29}$	$^{+0.28}_{-0.11}$	$^{-}_{-0.21}$	$^{+0.27}_{-0.16}$	-	$^{+0.15}_{-0.28}$	$^{+0.38}_{-}$
Effective detector NP set 1 (JES) [%]	-	-	-	-	-	-	-	-	-	-	-	-	-	-	-	-	-	$^{+0.15}_{-0.19}$	$^{+0.18}_{-0.27}$
Effective detector NP set 2 (JES) [%]	-	-	-	-	-	-	-	-	-	-	-	-	-	-	-	$^{+0.14}_{-}$	-	±0.16	$^{-0.20}_{-}$
Effective mixed NP set 1 (JES) [%]	∓0.28	$^{-0.30}_{+0.33}$	$^{-0.23}_{+0.30}$	$^{-0.24}_{+0.21}$	$^{-0.24}_{+0.19}$	$^{-0.23}_{+0.26}$	$^{-0.14}_{+0.15}$	-	-	$^{+0.13}_{-}$	$^{+0.17}_{-}$	$^{+0.16}_{-0.30}$	$^{+0.24}_{-0.40}$	$^{+0.49}_{-0.23}$	$^{+0.38}_{-0.43}$	$^{+0.67}_{-0.80}$	$^{+0.65}_{-0.59}$	$^{+1.44}_{-1.56}$	$^{+2.53}_{-2.20}$
Effective mixed NP set 2 (JES) [%]	-	-	-	-	-	-	-	-	-	-	-	-	-	-	-	-	-	$^{-0.14}_{+0.16}$	$^{-0.25}_{+0.15}$
Effective modelling NP set 1 (JES) [%]	$^{+0.50}_{-0.23}$	$^{+1.05}_{-0.57}$	$^{+0.81}_{-0.65}$	$^{+0.36}_{-0.70}$	$^{+0.35}_{-0.57}$	$^{+0.33}_{-0.19}$	$^{+0.15}_{-0.13}$	-	-	$^{-0.18}_{+0.23}$	$^{-0.51}_{+0.54}$	$^{-0.78}_{+0.48}$	$^{-0.75}_{+0.66}$	$^{-0.66}_{+0.99}$	$^{-0.89}_{+1.19}$	$^{-0.96}_{+0.85}$	$^{-1.47}_{+1.10}$	$^{-0.71}_{+1.09}$	$^{-1.07}_{+0.70}$
Effective modelling NP set 2 (JES) [%]	$^{-0.18}_{+0.11}$	$^{-0.26}_{+0.27}$	$^{-0.25}_{+0.28}$	$^{-0.25}_{+0.26}$	$^{-0.26}_{+0.23}$	$^{-0.17}_{+0.20}$	$^{-0.12}_{+0.11}$	-	-	$^{+0.16}_{-0.15}$	±0.17	$^{+0.21}_{-0.27}$	$^{+0.27}_{-0.31}$	$^{+0.39}_{-0.32}$	$^{+0.20}_{-0.41}$	$^{+0.53}_{-0.48}$	$^{+0.54}_{-0.46}$	±0.89	$^{+1.38}_{-1.41}$
Effective modelling NP set 3 (JES) [%]	$^{+0.22}_{-0.24}$	±0.27	$^{+0.26}_{-0.24}$	$^{+0.25}_{-0.24}$	$^{+0.23}_{-0.26}$	$^{+0.21}_{-0.17}$	$^{+0.11}_{-0.14}$	-	-	$^{-0.14}_{+0.18}$	$^{-0.19}_{+0.18}$	$^{-0.30}_{+0.21}$	$^{-0.35}_{+0.32}$	$^{-0.32}_{+0.39}$	$^{-0.42}_{+0.24}$	$^{-0.44}_{+0.54}$	$^{-0.44}_{+0.48}$	$^{-0.73}_{+0.68}$	$^{-0.55}_{+0.59}$
Effective modelling NP set 4 (JES) [%]	-	-	-	-	-	-	-	-	-	-	-	-	-	-	-	-	-	-	$^{+0.23}_{-0.22}$
Effective statistical NP set 1 (JES) [%]	-	$^{+0.25}_{-0.12}$	$^{+0.15}_{-0.14}$	$^{+0.10}_{-0.17}$	$^{+0.15}_{-0.20}$	-	-	-	-	-	$^{-0.13}_{+0.12}$	$^{-0.17}_{-}$	$^{-0.16}_{+0.18}$	$^{-0.22}_{+0.27}$	$^{-0.27}_{+0.21}$	$^{-0.16}_{+0.27}$	$^{-0.31}_{+0.24}$	∓0.13	-
Effective statistical NP set 2 (JES) [%]	-	$^{-0.11}_{+0.25}$	$^{-0.14}_{+0.16}$	$^{-0.14}_{-}$	$^{-0.21}_{+0.13}$	-	-	-	-	-	$^{+0.10}_{-0.13}$	-	$^{+0.15}_{-0.12}$	$^{+0.23}_{-0.18}$	$^{+0.21}_{-0.19}$	$^{+0.28}_{-0.29}$	$^{+0.25}_{-0.36}$	$^{+0.42}_{-0.36}$	$^{+0.62}_{-0.68}$
Effective statistical NP set 3 (JES) [%]	-	-	-	-	-	-	-	-	-	-	-	-	-	-	-	$^{-0.17}_{+0.26}$	$^{-0.24}_{+0.20}$	$^{-0.73}_{+0.60}$	$^{-0.86}_{+1.18}$
Effective statistical NP set 4 (JES) [%]	∓0.23	$^{-0.23}_{+0.25}$	$^{-0.19}_{+0.21}$	∓0.19	∓0.16	$^{-0.15}_{+0.16}$	$^{-0.12}_{-}$	-	-	$^{+0.15}_{-0.13}$	$^{+0.16}_{-0.15}$	$^{+0.16}_{-0.25}$	$^{+0.25}_{-0.29}$	$^{+0.30}_{-0.20}$	$^{+0.20}_{-0.28}$	$^{+0.34}_{-0.28}$	$^{+0.27}_{-0.19}$	$^{+0.24}_{-0.30}$	-
Effective statistical NP set 5 (JES) [%]	-	-	-	-	-	-	-	-	-	-	-	-	-	-	-	$^{+0.22}_{-0.19}$	$^{+0.22}_{-0.24}$	±0.30	-
Effective statistical NP set 6 (JES) [%]	-	-	-	-	-	-	-	-	-	-	-	$^{-0.14}_{+0.11}$	$^{-0.14}_{+0.11}$	$^{-0.14}_{+0.13}$	-	$^{-}_{+0.15}$	-	-	-
Effective statistical NP set 7 (JES) [%]	-	-	-	-	-	-	-	-	-	-	-	-	-	-	-	$^{+0.15}_{-}$	-	$^{+0.16}_{-0.19}$	$^{+0.21}_{-0.27}$
η intercalibration model (JES) [%]	-	$^{-0.15}_{+0.23}$	$^{-0.12}_{+0.15}$	-	-	$^{-0.13}_{+0.20}$	-	-	$^{+0.11}_{-0.12}$	-	-	$^{+0.10}_{-0.22}$	$^{-}_{-0.12}$	$^{+0.19}_{-}$	-	-	-	$^{+0.70}_{-0.65}$	$^{+0.25}_{-0.31}$
η intercalibration non closure (JES) [%]	$^{+0.21}_{-}$	-	-	-	-	-	-	-	-	-	-	-	-	-	-	-	$^{+0.24}_{-}$	$^{-0.40}_{+0.38}$	$^{-0.30}_{-}$
η intercalibration total stat (JES) [%]	$^{-0.17}_{+0.16}$	-	-	-	-	-	-	-	-	-	-	-	-	-	$^{-0.11}_{+0.13}$	-	$^{-0.15}_{-}$	-	$^{-}_{-0.20}$
Flavour composition (JES) [%]	$^{+0.82}_{-0.95}$	$^{+1.26}_{-0.75}$	$^{+0.69}_{-0.59}$	$^{+0.36}_{-0.86}$	$^{+0.61}_{-0.59}$	$^{+0.33}_{-0.28}$	$^{-}_{-0.25}$	-	-	$^{-0.29}_{+0.40}$	$^{-0.60}_{+0.63}$	$^{-0.74}_{+0.58}$	$^{-0.69}_{+0.86}$	$^{-0.61}_{+1.07}$	$^{-0.85}_{+1.14}$	$^{-0.94}_{+1.02}$	$^{-1.48}_{+1.08}$	$^{-0.38}_{+1.05}$	$^{-0.41}_{+0.61}$
Flavour response (JES) [%]	$^{-}_{+0.30}$	$^{-0.27}_{+0.62}$	$^{-0.32}_{+0.37}$	$^{-0.30}_{-}$	$^{-0.23}_{-}$	$^{-}_{+0.15}$	-	-	-	$^{+0.18}_{-}$	$^{+0.20}_{-0.21}$	$^{-}_{-0.31}$	$^{+0.19}_{-0.28}$	$^{+0.43}_{-0.13}$	$^{+0.57}_{-0.40}$	$^{+0.40}_{-0.36}$	$^{+0.45}_{-0.70}$	$^{+0.25}_{-}$	$^{+0.65}_{-0.87}$
Pile-up offset μ (JES) [%]	-	-	-	-	-	-	-	-	-	-	-	-	-	-	-	-	-	-	-
Pile-up offset N_{PV} (JES) [%]	-	$^{+0.43}_{-}$	$^{+0.24}_{-}$	-	-	-	-	-	-	-	-	$^{-}_{-0.30}$	-	-	$^{-}_{+0.24}$	$^{-}_{+0.27}$	$^{-0.16}_{+0.18}$	∓0.22	-
Pile-up offset p_T (JES) [%]	$^{-0.52}_{+0.58}$	$^{-0.60}_{+0.58}$	$^{-0.52}_{+0.68}$	$^{-0.58}_{+0.60}$	$^{-0.52}_{+0.34}$	$^{-0.36}_{+0.38}$	$^{-0.22}_{+0.27}$	-	$^{+0.20}_{-0.29}$	$^{+0.40}_{-0.30}$	$^{+0.35}_{-0.29}$	$^{+0.40}_{-0.60}$	$^{+0.64}_{-0.61}$	$^{+0.84}_{-0.74}$	$^{+0.51}_{-0.74}$	$^{+0.99}_{-0.83}$	$^{+0.79}_{-0.74}$	$^{+1.26}_{-1.39}$	$^{+1.41}_{-1.33}$
Pile-up offset ρ topology (JES) [%]	$^{+0.68}_{-0.23}$	$^{+1.10}_{-0.64}$	$^{+0.69}_{-0.58}$	$^{+0.24}_{-0.65}$	$^{+0.29}_{-0.46}$	$^{+0.31}_{-}$	±0.17	$^{+0.13}_{-0.15}$	$^{+0.23}_{-0.21}$	-	$^{-0.46}_{+0.50}$	$^{-0.90}_{+0.51}$	$^{-0.89}_{+0.77}$	$^{-0.65}_{+1.11}$	$^{-0.89}_{+1.35}$	$^{-1.27}_{+1.28}$	$^{-1.93}_{+1.48}$	$^{-1.13}_{+1.58}$	$^{-1.96}_{+1.84}$
Jet vertex fraction [%]	±0.34	±0.34	±0.32	±0.27	±0.21	±0.16	-	-	-	∓0.15	∓0.23	∓0.28	$^{-0.30}_{+0.31}$	∓0.35	∓0.38	∓0.41	∓0.44	∓0.49	∓0.55
b-Quark tagging efficiency (eigenvector 0) [%]	$^{-1.25}_{+1.15}$	$^{-1.37}_{+1.27}$	$^{-1.18}_{+1.09}$	$^{-0.81}_{+0.74}$	$^{-0.54}_{+0.50}$	$^{-0.33}_{+0.30}$	-	$^{+0.16}_{-0.14}$	$^{+0.31}_{-0.28}$	$^{+0.44}_{-0.40}$	$^{+0.62}_{-0.57}$	$^{+0.73}_{-0.67}$	$^{+0.82}_{-0.76}$	$^{+0.84}_{-0.77}$	$^{+0.80}_{-0.74}$	$^{+0.83}_{-0.77}$	$^{+0.71}_{-0.66}$	$^{+0.65}_{-0.61}$	-
b-Quark tagging efficiency (eigenvector 1) [%]	$^{+0.77}_{-0.75}$	$^{+0.78}_{-0.76}$	$^{+0.73}_{-0.71}$	$^{+0.62}_{-0.61}$	$^{+0.52}_{-0.51}$	±0.42	±0.31	$^{+0.16}_{-0.15}$	-	∓0.21	$^{-0.47}_{+0.46}$	$^{-0.71}_{+0.69}$	$^{-0.94}_{+0.92}$	$^{-1.13}_{+1.11}$	$^{-1.29}_{+1.27}$	$^{-1.53}_{+1.50}$	$^{-1.85}_{+1.82}$	$^{-2.20}_{+2.17}$	$^{-2.74}_{+2.70}$
b-Quark tagging efficiency (eigenvector 2) [%]	±0.30	$^{+0.29}_{-0.30}$	±0.29	±0.29	±0.27	$^{+0.23}_{-0.24}$	±0.19	$^{+0.13}_{-0.12}$	-	-	∓0.21	$^{-0.34}_{+0.35}$	∓0.49	$^{-0.60}_{+0.62}$	$^{-0.72}_{+0.73}$	$^{-0.89}_{+0.91}$	$^{-1.14}_{+1.16}$	$^{-1.39}_{+1.42}$	$^{-1.81}_{+1.85}$
b-Quark tagging efficiency (eigenvector 3) [%]	∓0.23	∓0.23	∓0.22	∓0.18	∓0.14	-	-	-	-	±0.15	±0.20	$^{+0.23}_{-0.22}$	±0.22	±0.19	±0.14	-	-	∓0.27	∓0.64
b-Quark tagging efficiency (eigenvector 4) [%]	-	-	-	-	-	-	-	-	-	-	-	-	-	-	-	-	-	-	∓0.17
c-Quark tagging efficiency (eigenvector 0) [%]	±0.14	±0.13	±0.11	±0.11	±0.11	-	-	-	-	-	-	∓0.13	$^{-0.14}_{+0.13}$	∓0.15	∓0.16	∓0.16	∓0.15	∓0.18	$^{-0.17}_{+0.16}$
c-Quark tagging efficiency (eigenvector 1) [%]	-	±0.11	±0.10	-	-	-	-	-	-	-	-	-	-	-	-	-	∓0.12	∓0.10	∓0.39
c-Quark tagging efficiency (eigenvector 2) [%]	-	-	-	-	-	-	-	-	-	-	-	∓0.12	∓0.14	$^{-0.13}_{+0.14}$	∓0.15	∓0.16	∓0.17	∓0.17	∓0.32
Light-jet tagging efficiency (eigenvector 0) [%]	$^{-0.29}_{+0.30}$	-	∓0.12	$^{-0.20}_{+0.23}$	-	-	-	-	-	-	-	-	-	$^{+0.12}_{-0.15}$	-	-	-	-	$^{-0.42}_{+0.45}$
Light-jet tagging efficiency (eigenvector 1) [%]	$^{+0.27}_{-0.23}$	$^{+0.25}_{-0.24}$	$^{+0.23}_{-0.24}$	$^{+0.19}_{-0.18}$	-	-	-	-	-	-	-	∓0.12	∓0.16	$^{-0.21}_{+0.19}$	$^{-0.18}_{+0.17}$	∓0.18	∓0.21	∓0.21	∓0.30
Light-jet tagging efficiency (eigenvector 2) [%]	-	$^{-0.32}_{+0.22}$	$^{-0.15}_{+0.14}$	-	-	-	-	-	-	-	-	-	-	-	-	-	-	-	-
Light-jet tagging efficiency (eigenvector 3) [%]	$^{+0.14}_{-0.15}$	-	-	±0.10	-	-	-	-	-	-	-	-	-	-	-	-	-	$^{-0.13}_{+0.14}$	∓0.18
Light-jet tagging efficiency (eigenvector 5) [%]	-	-	-	-	-	-	-	-	-	-	-	-	-	-	-	-	-	-	±0.19
b-Quark tagging extrapolation [%]	-	-	-	-	-	-	-	-	-	-	-	-	-	-	±0.11	±0.23	±0.56	±1.21	$^{+3.22}_{-3.19}$
Electron identification efficiency [%]	-	-	-	-	-	-	-	-	-	-	-	-	-	-	±0.11	±0.14	±0.17	$^{+0.21}_{-0.22}$	±0.30
Electron isolation efficiency [%]	-	-	-	-	-	-	-	-	-	-	-	-	-	±0.10	±0.13	±0.18	±0.25	$^{+0.34}_{-0.35}$	±0.53
Muon identification syst [%]	-	-	-	-	-	-	-	-	-	-	-	-	-	-	-	-	-	±0.12	±0.19
Z+jets cross-section [%]	-	±0.19	±0.19	±0.24	±0.19	±0.14	±0.14	-	∓0.10	∓0.15	$^{-0.16}_{+0.17}$	$^{-0.23}_{+0.24}$	∓0.26	∓0.26	∓0.26	∓0.28	∓0.25	∓0.23	-
Monte Carlo sample statistics [%]	±0.77	±0.53	±0.33	±0.29	±0.30	±0.30	±0.21	±0.20	±0.21	±0.22	±0.26	±0.29	±0.34	±0.39	±0.46	±0.48	±0.70	±0.78	±1.28
ISR/FSR + scale [%]	$^{-}_{-0.96}$	$^{-}_{-1.19}$	$^{-}_{-0.49}$	-	$^{+0.68}_{-}$	$^{+0.35}_{-}$	$^{-}_{-0.29}$	$^{-}_{-0.22}$	$^{-0.27}_{+0.34}$	$^{-0.38}_{+0.34}$	$^{+0.79}_{-}$	$^{+0.69}_{-0.37}$	$^{-}_{-1.67}$	$^{-}_{-1.68}$	$^{+1.48}_{-0.39}$	$^{+0.50}_{-0.66}$	-	$^{-1.55}_{+0.68}$	$^{+5.56}_{-}$
Alternate hard-scattering model [%]	±3.22	±2.41	±1.30	±1.76	±3.15	±1.11	∓0.34	∓0.51	∓1.08	∓0.59	∓1.24	∓1.91	∓1.71	∓0.83	∓2.38	∓1.91	∓2.51	∓4.55	±0.58
Alternate parton-shower model [%]	∓1.83	∓1.09	∓1.09	∓0.16	±0.86	±0.59	∓0.42	±1.00	-	±0.10	±0.54	∓1.05	∓1.77	∓1.71	-	∓2.58	-	∓0.33	±0.82
Inter PDF [%]	±0.11	-	-	-	-	-	-	-	-	-	-	-	-	-	-	-	-	-	-
Intra PDF [%]	±0.69	-	-	-	-	-	-	-	-	-	-	-	-	±0.17	±0.22	-	±0.19	±0.30	±0.25
Fakes overall normalization, el [%]	±0.15	$^{+0.32}_{-0.33}$	±0.46	$^{+0.39}_{-0.40}$	±0.30	$^{+0.23}_{-0.24}$	-	-	-	$^{-0.25}_{+0.26}$	$^{-0.32}_{+0.33}$	∓0.29	∓0.29	$^{-0.43}_{+0.44}$	$^{-0.57}_{+0.58}$	$^{-0.46}_{+0.47}$	$^{-0.37}_{+0.38}$	∓0.45	$^{+0.67}_{-0.68}$
Fakes overall normalization, mu [%]	±0.21	±0.29	±0.21	±0.13	±0.11	±0.16	±0.14	-	-	-	∓0.12	∓0.20	∓0.30	∓0.38	∓0.47	∓0.70	∓0.90	∓0.85	∓1.18
Fakes alternative parametrization [%]	∓2.86	∓2.79	∓2.36	∓2.05	∓1.59	∓1.22	∓0.59	-	±0.54	±1.05	±1.50	±1.86	±2.27	±2.63	±3.24	±3.14	±3.52	±3.81	±4.18
W+jets heavy flavour component [%]	±6.37	±1.23	±2.68	±1.02	±1.18	±2.35	∓0.46	∓0.61	∓0.49	∓0.36	∓1.44	∓2.20	∓2.69	∓2.54	∓1.96	∓0.92	±1.25	∓2.53	∓1.01

TABLE F.26: Table of systematics for the relative differential cross-section at the particle level for the $p_T^{t,had}$ observable.

Bins [Unit y^{t_h}]	-3—1.62	-1.62—1.23	-1.23—0.96	-0.96—0.75	-0.75—0.54	-0.54—0.36	-0.36—0.18	-0.18–0	0–0.18	0.18–0.36	0.36–0.54	0.54–0.75	0.75–0.96	0.96–1.23	1.23–1.62	1.62–3
$1/\sigma \cdot d\sigma$ / dy^{t_h}	$2.54 \cdot 10^{-2}$	$1.65 \cdot 10^{-1}$	$2.40 \cdot 10^{-1}$	$2.96 \cdot 10^{-1}$	$3.33 \cdot 10^{-1}$	$3.61 \cdot 10^{-1}$	$3.78 \cdot 10^{-1}$	$3.91 \cdot 10^{-1}$	$3.90 \cdot 10^{-1}$	$3.82 \cdot 10^{-1}$	$3.64 \cdot 10^{-1}$	$3.32 \cdot 10^{-1}$	$2.98 \cdot 10^{-1}$	$2.43 \cdot 10^{-1}$	$1.64 \cdot 10^{-1}$	$2.49 \cdot 10^{-2}$
Total Uncertainty [%]	+4.09 -4.22	+1.57 -1.48	+1.82 -1.89	+4.16 -4.09	+2.91 -2.96	+3.21 -3.29	+1.98 -1.88	+3.45 -3.49	+1.90 -1.74	+1.53 -1.38	+0.98 -0.79	+2.00 -2.19	+2.16 -2.18	+1.54 -1.51	+1.76 -1.80	+5.80 -5.99
Statistics [%]	±0.5	±0.4	±0.4	±0.4	±0.4	±0.4	±0.4	±0.4	±0.4	±0.4	±0.4	±0.4	±0.4	±0.4	±0.4	±0.5
Systematics [%]	+4.01 -4.17	+1.49 -1.39	+1.75 -1.82	+4.12 -4.05	+2.85 -2.91	+3.15 -3.24	+1.90 -1.79	+3.39 -3.44	+1.82 -1.65	+1.44 -1.27	+0.82 -0.58	+1.94 -2.12	+2.09 -2.11	+1.43 -1.40	+1.68 -1.72	+5.76 -5.95
Jet energy resolution [%]	∓0.90	∓0.46	∓0.94	±2.87	∓1.99	±1.93	∓1.00	±2.26	∓1.27	∓0.79	∓0.29	±0.34	∓1.18	±0.81	±0.70	∓0.56
b-Tagged jet energy scale (JES) [%]	∓0.21	-	-	-	-	-	-	-	-	-	-	-	-	-	-	-0.19 +0.20
Effective mixed NP set 1 (JES) [%]	-	-	-	-	-	-	-	-	-	-	-	-	-	-	-	+0.12
Effective modelling NP set 1 (JES) [%]	-1.08 +1.01	-0.17 +0.32	-	-	±0.24	+0.17 -0.31	+0.20 -0.13	+0.10 -0.38	+0.28 -0.17	-	+0.25 -0.11	+0.13 -0.14	-	- +0.17	-0.46 +0.33	-0.78 +0.89
Effective statistical NP set 1 (JES) [%]	+0.15	-	-	-	-	-	-	-	-	-	-	-	-	-	-	∓0.18
Effective statistical NP set 2 (JES) [%]	+0.15 -0.15	-	-	-	-	-	-	-	-	-	-	-	-	-	-	±0.16
η intercalibration model (JES) [%]	-0.15 -0.10	+0.41 -0.33	+0.21 -0.35	-	-	-0.19 +0.10	-0.12 +0.24	-0.29	-0.16 +0.19	-0.23 +0.28	-0.14 +0.15	-	-	+0.18 -0.25	+0.33 +0.35	+0.12 -0.14
η intercalibration non closure (JES) [%]	-0.15	-0.17	-0.28	-0.22	∓0.18	+0.20	-	-	-	-	-	±0.24	+0.27	+0.18	+0.16	-0.16
η intercalibration total stat (JES) [%]	-0.20	+0.16	+0.16	+0.25	-	+0.11	+0.21	-	-	-	-	-	-0.19	-0.20	-0.21	-0.15 -0.28
Flavour composition (JES) [%]	+0.39 -1.09	-	-	-	-	-	-	-	-	-	-	-	-	-	-	+0.19 -0.17
Flavour response (JES) [%]	-1.08 +1.08	-0.19 +0.30	-	+0.39 -	+0.39 -0.23	- -0.32	+0.20 -	- -0.33	+0.27 -0.26	-	+0.29 -	-	-	-	-0.33 +0.75	+1.04
Pile-up offset N_{PV} (JES) [%]	-0.50 -0.28	-	-	-	+0.12 -	-	-	-	-	-	+0.16 -	-	-	-	-0.12 -0.14	-0.36 -0.20
Pile-up offset p_T (JES) [%]	+0.23	-	-	-	-0.12	-	-	-	-	-	-	-0.17	-	-	+0.18	+0.17
Pile-up offset ρ topology (JES) [%]	-1.69 +1.62	-0.44 +0.50	-	±0.12	+0.38 -0.35	- -0.42	+0.41 -0.27	+0.33 -0.50	+0.45 -0.31	+0.19 -0.30	+0.36 -0.14	+0.22 -0.35	+0.21 -	-0.13 +0.14	-0.59 +0.57	-1.45 +1.50
b-Quark tagging efficiency (eigenvector 0) [%]	-0.13	-	-	-	-	-	-	-	-	-	-	-	-	-	-	+0.15 -0.13
Light-jet tagging efficiency (eigenvector 0) [%]	+0.14	-	-	-	+0.12 -0.21	-0.18 +0.26	+0.10 -0.15	+0.21 -0.24	-	-	-	-	-	-0.10 +0.14	+0.12	-
Light-jet tagging efficiency (eigenvector 1) [%]	-	-	-	-	-	+0.14 -0.11	-	-	-	-	-	-	-	-	-	-
Z+jets cross-section [%]	∓0.14	∓0.13	-	-	-	±0.11	-	-	-	-	-	-	-	-	-	∓0.11
Monte Carlo sample statistics [%]	±0.37	±0.27	±0.28	±0.29	±0.33	±0.34	±0.36	±0.44	±0.31	±0.29	±0.29	±0.28	±0.30	±0.34	±0.30	±0.38
ISR/FSR + scale [%]	-	+0.19 -0.20	- -	+0.50 -	-0.65 +0.30	- -0.29	-	+0.63 -	+0.63 -	+0.70 -	+0.16 -	-	-0.50	+0.31 -	+0.16	-1.47
Alternate hard-scattering model [%]	∓1.16	±0.73	±0.47	∓0.70	∓0.48	±0.52	∓1.28	∓0.33	±0.24	±0.58	±0.22	∓1.53	±0.51	±0.74	∓0.95	±3.96
Alternate parton-shower model [%]	∓2.14	-	±0.44	∓0.42	±0.55	±0.20	-	±0.56	±0.21	±0.52	-	±0.99	±0.56	∓0.65	∓0.62	∓3.14
Intra PDF [%]	-	-	∓0.14	-	-	-	±0.23	±0.18	-	-	∓0.10	-	±0.11	-	-	-
Fakes overall normalization, el [%]	-0.31 +0.32	-	-	-	-	-	+0.15 -0.16	-	-	-	-	-	-	-	∓0.12	±0.20
Fakes alternative parametrization [%]	±0.27	-	∓0.11	∓0.13	-	∓0.18	-	-	-	∓0.22	-	-	±0.16	±0.20	-	-
W+jets heavy flavour component [%]	∓0.93	∓0.75	∓1.24	±2.71	∓1.74	±2.37	∓0.53	±2.30	∓0.79	∓0.24	-	±0.33	∓1.45	±0.28	∓0.17	∓1.14

TABLE F.27: Table of systematics for the relative differential cross-section at the particle level for the $y^{t,had}$ observable.

Bins [GeV]	0–25	25–50	50–90	90–130	130–170	170–220	220–270	270–320	320–420	420–550	550–800.00
$1/\sigma \cdot d\sigma$ / $dp_T^{t\bar{t}}$	$9.32 \cdot 10^{-3}$	$1.10 \cdot 10^{-2}$	$5.75 \cdot 10^{-3}$	$2.80 \cdot 10^{-3}$	$1.53 \cdot 10^{-3}$	$8.05 \cdot 10^{-4}$	$4.12 \cdot 10^{-4}$	$2.33 \cdot 10^{-4}$	$1.07 \cdot 10^{-4}$	$3.64 \cdot 10^{-5}$	$7.37 \cdot 10^{-6}$
Total Uncertainty [%]	+6.64 -6.78	+4.31 -4.86	+5.46 -5.62	+8.21 -7.23	+5.72 -4.58	+4.92 -4.20	+5.96 -4.95	+6.55 -6.26	+7.75 -6.99	+9.48 -8.13	+7.20 -7.59
Statistics [%]	±0.1	±0.1	±0.2	±0.3	±0.4	±0.5	±0.7	±1.0	±1.1	±1.7	±2.7
Systematics [%]	+6.64 -6.78	+4.30 -4.86	+5.45 -5.61	+8.20 -7.22	+5.70 -4.56	+4.88 -4.15	+5.89 -4.88	+6.45 -6.14	+7.64 -6.87	+9.26 -7.86	+6.51 -6.94
Jet energy resolution [%]	∓0.74	∓0.68	±0.89	±1.28	∓0.29	∓0.20	∓0.43	±2.16	±0.37	±0.10	±0.20
b-Tagged jet energy scale (JES) [%]	-	-	-	-	-	-	-	-	-0.16 +0.15	- +0.23	-0.28 +0.10
Effective detector NP set 1 (JES) [%]	-	-	-	-	-	-	-	-	-	+0.15 -	-
Effective detector NP set 2 (JES) [%]	-	-	-	-	-	-	-	-	-	-	-
Effective mixed NP set 1 (JES) [%]	-	-	-	-	+0.13 -0.14	+0.21 -0.15	+0.31 -0.20	+0.47 -0.42	+0.49 -0.62	+1.29 -1.26	+2.03 -1.57
Effective mixed NP set 2 (JES) [%]	-	-	-	-	-	-	-	-	-	-0.11 +0.17	-
Effective modelling NP set 1 (JES) [%]	-1.00 +1.09	-0.37 +0.33	+0.65 -0.72	+0.97 -0.96	+0.75 -0.78	+0.39 -0.32	+0.34 -	-	-0.30 +0.33	-0.30 +0.31	-0.51 +0.50
Effective modelling NP set 2 (JES) [%]	-	-	∓0.11	-	-	+0.11 -0.10	+0.21 -	+0.22 -0.19	-	+0.76 -0.69	+1.43 -1.25
Effective modelling NP set 3 (JES) [%]	-	-	-	-	-0.12 +0.10	-0.18 +0.18	-0.15 +0.23	-0.25 +0.22	-0.19 +0.24	-0.38 +0.29	-0.36 +0.35
Effective modelling NP set 4 (JES) [%]	-	-	-	-	-	-	-	-	-	-	-
Effective statistical NP set 1 (JES) [%]	-0.19 +0.21	-	+0.14 -0.15	+0.18 -0.15	-	-	-	-	-	-	-
Effective statistical NP set 2 (JES) [%]	+0.18 -0.16	-	-0.13 +0.12	-0.13 +0.16	-	-	-	-	+0.13 -	+0.26 -0.30	+0.62 -0.55
Effective statistical NP set 3 (JES) [%]	-	-	-	-	-	-	-	∓0.20	-0.28 +0.18	-0.71 +0.64	-0.53 +0.94
Effective statistical NP set 4 (JES) [%]	-	-	-	-	+0.13 -0.14	±0.18	+0.21 -	+0.16 -0.25	-	-	-
Effective statistical NP set 5 (JES) [%]	-	-	-	-	-	-	+0.21 -0.10	+0.26 -0.21	+0.23 -0.30	-	-0.23 +0.24
Effective statistical NP set 6 (JES) [%]	-	-	-	-	-	∓0.12	-	-	-	-	-0.26
Effective statistical NP set 7 (JES) [%]	-	-	-	-	-	-	-	-	-0.11 -	+0.13 -0.15	-
η intercalibration model (JES) [%]	-0.20 +0.25	∓0.19	- -0.12	+0.31 -0.32	+0.25 -0.28	+0.32 -0.37	+0.27 -0.19	+0.23 -	+0.28 -0.25	+0.56 -0.68	+0.86 -0.23
η intercalibration non closure (JES) [%]	-	-	-	-	-0.11 +0.14	-0.18 +0.14	-0.20 +0.27	-0.28 +0.26	-0.24 +0.15	-0.48 +0.40	+0.29 -
η intercalibration total stat (JES) [%]	-0.16 +0.18	-	-	+0.23 -0.22	+0.18 -0.22	-	-	+0.10 -0.19	-	+0.21 -	-0.15 +0.12
Flavour composition (JES) [%]	+0.52 +0.61	-0.60 +0.62	+0.22 -0.30	+1.08 -1.21	+1.05 -1.11	+0.63 -0.44	+0.62 -0.47	+0.45 -0.20	-0.19 -	±0.23 -	+0.26 -
Flavour response (JES) [%]	+0.34 -0.29	±0.34 -	-0.13 -	-0.65 +0.60	-0.68 +0.63	-0.38 +0.45	-0.19 +0.46	-0.24 +0.34	-0.27 +0.13	+0.14 -0.11	+0.34 -0.20
Pile-up offset μ (JES) [%]	-	-	-	-	-	-	-	-0.18 +0.13	+0.10 -0.15	-	-
Pile-up offset N_{PV} (JES) [%]	-0.20 +0.29	∓0.11	-	+0.25 -0.31	+0.26 -0.28	-	+0.21 -	-	-	-	-0.28 +0.38
Pile-up offset p_T (JES) [%]	-	-0.13 +0.12	-0.18 -0.19	-	+0.27 -0.31	+0.39 -0.34	+0.38 -0.41	+0.52 -0.35	+0.32 -0.48	+0.20 ±0.62	-0.47 +1.08
Pile-up offset ρ topology (JES) [%]	-1.60 +1.71	-0.66 +0.61	+0.15 +1.00 -1.13	+1.61 -1.69	+1.37 -1.30	+0.86 -0.53	+0.60 -0.36	-	-0.59 +0.53	-0.59 +0.71	-1.07 -1.08 +1.31
Punch-through (JES) [%]	-	-	-	-	-	-	-	-	-	-	-
Jet vertex fraction [%]	∓0.15	-	±0.13	±0.13	-	-	-	-	-0.14 +0.13	∓0.23	∓0.29
b-Quark tagging efficiency (eigenvector 0) [%]	∓0.38	∓0.19	+0.11 -0.12	±0.31	+0.38 -0.37	+0.48 -0.47	+0.61 -0.59	+0.63 -0.61	+0.78 -0.75	+0.77 -0.74	+0.87 -0.83
b-Quark tagging efficiency (eigenvector 1) [%]	-	-	-	-	-	-	-0.23 +0.22	-0.43 +0.41	-0.64 +0.62	-1.04 +1.01	-1.61 +1.57
b-Quark tagging efficiency (eigenvector 2) [%]	±0.13	-	-	-0.11 +0.10	-0.15 +0.14	∓0.19	∓0.26	∓0.34	∓0.50	-0.77 +0.78	-1.14 +1.15
b-Quark tagging efficiency (eigenvector 3) [%]	-	-	-	-	-	-	-	-	-	-	∓0.17
c-Quark tagging efficiency (eigenvector 0) [%]	-	-	-	-	-	-	-	-	-	-	∓0.10
c-Quark tagging efficiency (eigenvector 1) [%]	-	-	-	-	-	-	-	-	-	-	∓0.18
c-Quark tagging efficiency (eigenvector 2) [%]	-	-	-	-	-	-	-	-	-	-	∓0.14
Light-jet tagging efficiency (eigenvector 0) [%]	-	-	-	-	-	-0.12 +0.13	-0.13 +0.14	-	∓0.11	-	-0.18 +0.22
b-Quark tagging extrapolation [%]	-	-	-	-	-	-	-	-	-	-0.11 ±0.28	+0.91 -
Electron identification efficiency [%]	-	-	-	-	-	-	-	-	±0.11	±0.16	-0.92 +0.22
Electron isolation efficiency [%]	-	-	-	-	-	-	-	-	±0.15	±0.24	-0.23 ±0.39
Muon identification syst [%]	-	-	-	-	-	-	-	-	-	-	±0.10
E_T^{miss} Soft jet resolution para [%]	∓0.17	-	±0.17	-	∓0.11	±0.15	-	∓0.35	-	-	∓0.52
E_T^{miss} Soft jet resolution perp [%]	-	-	-	-	-	-	∓0.15	-	-	∓0.45	±0.10
E_T^{miss} Soft jet scale [%]	+0.27 -0.36	-	-0.19 +0.26	-0.17 +0.16	-	+0.22 -	-0.19 +0.11	-	-	-0.46 +0.29	-0.13 +0.48
Z+jets cross-section [%]	±0.10	-	-	∓0.11	-	-	-	-	-	∓0.12	-
Monte Carlo sample statistics [%]	±0.13	-	±0.14	±0.19	±0.27	±0.34	±0.45	±0.61	±0.66	±1.01	±1.43
ISR/FSR + scale [%]	-1.15	-	+0.28 -1.50	+3.93	+3.42	+2.38	+3.12	+1.86	+3.47	+4.87 -	- -3.13
Alternate hard-scattering model [%]	∓1.59	∓1.28	±2.12	±2.05	∓0.30	±0.27	±0.99	∓2.23	±0.99	∓4.57	-
Alternate parton-shower model [%]	∓5.43	∓3.87	±4.32	±6.19	±3.38	±3.22	±3.60	±4.79	±5.55	±3.57	±2.81
Inter PDF [%]	-	-	-	-	-	-	-	-	-	±0.32	-
Intra PDF [%]	-	-	-	-	-	-	±0.13	-	±0.34	±1.32	±0.36
Fakes overall normalization, el [%]	-0.82 +0.83	-	+0.78 -0.79	±0.22	-0.20 +0.21	∓0.30	-0.40 +0.41	-0.38 +0.39	∓0.37	-0.65 +0.66	-0.65 +0.66
Fakes overall normalization, mu [%]	∓0.23	-	±0.23	±0.22	-	∓0.11	∓0.18	∓0.33	∓0.32	∓0.48	∓0.82
Fakes alternative parametrization [%]	-	∓0.34	∓0.56	-	±0.59	±1.44	±1.85	±1.72	±2.79	±3.88	±3.68
W+jets heavy flavour component [%]	±1.58	±0.31	∓0.35	∓0.80	∓2.01	∓1.73	∓2.14	-	∓1.92	∓1.73	±0.46

TABLE F.28: Table of systematics for the relative differential cross-section at the particle level for the $p_T^{t\bar{t}}$ observable.

Bins [Unit $y^{t\bar{t}}$]	-3—2	-2—1.75	-1.75—1.50	-1.50—1.25	-1.25—1	-1—0.85	-0.85—0.60	-0.60—0.40	-0.40—0.20	-0.20–0
$1/\sigma \cdot \mathrm{d}\sigma$ / $\mathrm{d}y^{t\bar{t}}$	$2.91 \cdot 10^{-4}$	$1.05 \cdot 10^{-2}$	$4.07 \cdot 10^{-2}$	$9.67 \cdot 10^{-2}$	$1.84 \cdot 10^{-1}$	$2.63 \cdot 10^{-1}$	$3.52 \cdot 10^{-1}$	$4.38 \cdot 10^{-1}$	$4.93 \cdot 10^{-1}$	$5.13 \cdot 10^{-1}$
Total Uncertainty [%]	$^{+32.9}_{-25.6}$	$^{+11.0}_{-12.2}$	$^{+4.58}_{-4.34}$	$^{+2.53}_{-2.90}$	$^{+1.81}_{-1.99}$	$^{+2.29}_{-2.54}$	$^{+1.89}_{-1.61}$	$^{+1.66}_{-1.64}$	$^{+1.43}_{-1.10}$	$^{+1.47}_{-1.18}$
Statistics [%]	±9.1	±2.5	±1.2	±0.7	±0.5	±0.6	±0.3	±0.4	±0.3	±0.3
Systematics [%]	$^{+30.9}_{-23.0}$	$^{+10.6}_{-11.8}$	$^{+4.32}_{-4.07}$	$^{+2.34}_{-2.73}$	$^{+1.68}_{-1.88}$	$^{+2.16}_{-2.42}$	$^{+1.83}_{-1.54}$	$^{+1.58}_{-1.56}$	$^{+1.35}_{-1.00}$	$^{+1.40}_{-1.09}$
Jet energy resolution [%]	∓2.57	∓2.63	∓2.40	∓0.10	±0.31	±0.19	∓0.89	±0.79	∓0.32	∓0.12
b-Tagged jet energy scale (JES) [%]	$^{-}_{-1.29}$	-	$^{-0.20}_{+0.25}$	-	-	-	-	-	-	-
Effective detector NP set 1 (JES) [%]	$^{+0.35}_{-}$	-	-	-	-	-	-	-	-	-
Effective detector NP set 2 (JES) [%]	$^{+0.45}_{-}$	-	-	-	-	-	-	-	-	-
Effective mixed NP set 1 (JES) [%]	$^{-0.34}_{+1.38}$	$^{-}_{-0.35}$	-	-	-	-	-	-	-	-
Effective mixed NP set 2 (JES) [%]	$^{+0.44}_{-}$	-	-	-	-	-	-	-	-	-
Effective mixed NP set 3 (JES) [%]	-	-	-	-	-	-	-	-	-	-
Effective modelling NP set 1 (JES) [%]	$^{-0.34}_{+1.30}$	$^{-1.28}_{+0.57}$	$^{-0.48}_{+0.50}$	$^{-0.39}_{+0.28}$	$^{-0.25}_{+0.24}$	-	-	-	$^{+0.33}_{-0.12}$	-
Effective modelling NP set 2 (JES) [%]	$^{+0.81}_{-}$	$^{-0.35}_{-}$	-	-	-	-	-	-	-	-
Effective modelling NP set 3 (JES) [%]	$^{+0.92}_{-0.24}$	$^{+0.10}_{-0.26}$	-	-	-	-	-	-	-	-
Effective modelling NP set 4 (JES) [%]	$^{-0.22}_{+0.41}$	-	-	-	-	-	-	-	-	-
Effective statistical NP set 1 (JES) [%]	$^{-}_{+0.39}$	$^{-}_{-0.31}$	-	-	-	$^{-0.11}_{+0.18}$	-	-	-	-
Effective statistical NP set 2 (JES) [%]	$^{+0.40}_{-}$	$^{-}_{-0.30}$	-	-	-	$^{+0.17}_{-}$	-	-	-	-
Effective statistical NP set 3 (JES) [%]	$^{+0.60}_{-}$	-	-	-	-	-	-	-	-	-
Effective statistical NP set 4 (JES) [%]	$^{-}_{+0.86}$	$^{-0.22}_{+0.11}$	-	-	-	-	-	-	-	-
Effective statistical NP set 5 (JES) [%]	$^{+0.57}_{-}$	-	-	-	-	-	-	-	-	-
Effective statistical NP set 6 (JES) [%]	$^{+0.46}_{-}$	-	-	-	-	-	-	-	-	-
Effective statistical NP set 7 (JES) [%]	$^{+0.34}_{-}$	-	-	-	-	-	-	-	-	-
η intercalibration model (JES) [%]	$^{+0.51}_{-}$	$^{+0.13}_{-0.25}$	$^{+0.54}_{-}$	$^{+0.12}_{-0.42}$	$^{+0.11}_{-0.12}$	$^{+0.32}_{-0.24}$	-	-	-	$^{-0.14}_{+0.16}$
η intercalibration non closure (JES) [%]	-	$^{-}_{-0.44}$	$^{-}_{+0.21}$	$^{-0.18}_{+0.17}$	$^{-0.20}_{+0.15}$	$^{-}_{+0.19}$	$^{-0.20}_{+0.15}$	-	$^{-}_{+0.15}$	-
η intercalibration total stat (JES) [%]	$^{+0.69}_{-}$	$^{-0.47}_{-}$	-	-	-	-	-	-	-	-
Flavour composition (JES) [%]	$^{+2.21}_{-}$	$^{-1.54}_{+0.93}$	$^{-0.30}_{+0.56}$	$^{-0.37}_{+0.24}$	$^{-0.19}_{-}$	-	-	-	$^{+0.40}_{-}$	-
Flavour response (JES) [%]	$^{+1.39}_{-}$	$^{+0.19}_{-0.83}$	$^{+0.25}_{-}$	-	-	-	-	-	$^{-}_{+0.20}$	-
Pile-up offset μ (JES) [%]	$^{+0.67}_{-}$	$^{+0.13}_{-0.33}$	-	-	-	-	-	-	-	-
Pile-up offset N_{PV} (JES) [%]	$^{-}_{-1.02}$	$^{-}_{-0.53}$	$^{+0.20}_{-}$	-	-	-	-	-	-	-
Pile-up offset p_T (JES) [%]	$^{+1.15}_{-}$	$^{-0.58}_{+0.22}$	$^{+0.20}_{-}$	-	-	+0.12	-	-	-	-
Pile-up offset ρ topology (JES) [%]	$^{-1.53}_{+1.69}$	$^{-2.05}_{+1.38}$	$^{-0.72}_{+1.04}$	$^{-0.75}_{+0.49}$	$^{-0.40}_{+0.25}$	$^{-0.10}_{+0.13}$	-	-	$^{+0.56}_{-0.22}$	-
Jet vertex fraction [%]	$^{-0.15}_{+0.16}$	-	-	-	-	-	-	-	-	-
b-Quark tagging efficiency (eigenvector 0) [%]	-	$^{+0.35}_{-0.32}$	$^{+0.21}_{-0.19}$	$^{+0.18}_{-0.16}$	$^{+0.12}_{-0.10}$	-	-	-	-	-
b-Quark tagging efficiency (eigenvector 1) [%]	∓0.19	-	-	-	-	-	-	-	-	-
c-Quark tagging efficiency (eigenvector 0) [%]	$^{-0.13}_{+0.12}$	-	-	-	-	-	-	-	-	-
Light-jet tagging efficiency (eigenvector 0) [%]	$^{-1.01}_{+0.96}$	$^{-0.17}_{+0.18}$	-	$^{-0.13}_{+0.15}$	-	-	-	-	$^{+0.18}_{-0.26}$	-
Light-jet tagging efficiency (eigenvector 1) [%]	±0.47	±0.17	-	-	-	-	-	-	-	-
Light-jet tagging efficiency (eigenvector 2) [%]	$^{-0.49}_{+0.50}$	∓0.19	$^{-0.17}_{+0.18}$	-	-	-	-	-	-	-
Light-jet tagging efficiency (eigenvector 3) [%]	∓0.47	-	$^{-0.16}_{+0.18}$	-	-	-	-	-	-	-
Light-jet tagging efficiency (eigenvector 5) [%]	$^{-0.27}_{+0.26}$	-	-	-	-	-	-	-	-	-
Light-jet tagging efficiency (eigenvector 6) [%]	±0.16	-	-	-	-	-	-	-	-	-
Light-jet tagging efficiency (eigenvector 7) [%]	∓0.20	-	-	-	-	-	-	-	-	-
Light-jet tagging efficiency (eigenvector 8) [%]	-	-	-	-	-	-	-	-	-	-
Electron energy resolution [%]	$^{+0.57}_{-0.70}$	$^{-0.19}_{+0.25}$	-	-	-	-	-	-	-	-
Electron energy scale [%]	$^{+1.63}_{-}$	-	$^{-0.11}_{+0.12}$	-	-	-	-	-	-	-
Electron trigger efficiency [%]	±0.11	-	-	-	-	-	-	-	-	-
Electron identification efficiency [%]	$^{+0.49}_{-0.50}$	±0.28	±0.13	-	-	-	-	-	-	-
Muon (ID) momentum resolution [%]	$^{-}_{+0.45}$	-	-	-	-	-	-	-	-	-
Muon (MS) momentum resolution [%]	$^{+0.28}_{-}$	-	-	-	-	-	-	-	-	-
Muon energy scale [%]	-	-	-	-	-	-	-	-	-	-
Muon trigger efficiency stat [%]	$^{+0.12}_{-0.11}$	-	-	-	-	-	-	-	-	-
Muon identification syst [%]	±0.17	±0.11	±0.10	-	-	-	-	-	-	-
E_T^{miss} Soft jet resolution para [%]	±2.27	∓0.30	±0.70	±0.12	±0.14	-	-	∓0.12	-	-
E_T^{miss} Soft jet resolution perp [%]	∓2.34	±0.81	±0.32	±0.33	-	-	-	∓0.11	-	-
E_T^{miss} Soft jet scale [%]	$^{+0.43}_{-}$	$^{+0.32}_{-0.49}$	$^{+0.42}_{-0.33}$	$^{+0.21}_{-0.31}$	$^{+0.19}_{-0.18}$	-	-	-	-	-
Z+jets cross-section [%]	∓0.10	∓0.12	∓0.10	-	-	-	-	-	-	-
Monte Carlo sample statistics [%]	±6.42	±1.57	±0.85	±0.55	±0.35	±0.41	±0.25	±0.31	±0.29	±0.25
ISR/FSR + scale [%]	$^{+20.1}_{-}$	$^{-}_{-4.38}$	$^{+0.67}_{-}$	$^{-}_{-0.80}$	$^{-}_{-0.70}$	$^{-}_{-1.16}$	$^{-0.31}_{+1.07}$	$^{-}_{+0.27}$	$^{+0.20}_{-}$	$^{+0.90}_{-}$
Alternate hard-scattering model [%]	∓15.0	∓6.33	±1.39	∓1.99	±0.69	∓1.26	∓0.38	∓0.79	±0.35	±0.55
Alternate parton-shower model [%]	±14.3	∓7.52	∓1.81	∓0.51	∓1.28	∓1.54	±0.78	±0.65	±0.30	±0.81
Inter PDF [%]	±1.13	∓0.33	-	-	-	-	-	-	-	-
Intra PDF [%]	±7.17	±0.54	-	-	±0.12	-	∓0.10	-	-	-
Fakes overall normalization, el [%]	$^{+0.92}_{-0.93}$	∓0.41	$^{-0.47}_{+0.48}$	-	∓0.11	-	-	-	-	-
Fakes overall normalization, mu [%]	-	-	-	-	-	-	-	-	-	-
Fakes alternative parametrization [%]	∓0.23	±1.07	±0.85	±0.21	-	∓0.12	∓0.22	-	∓0.13	-
W+jets heavy flavour component [%]	∓0.93	∓0.93	∓1.53	±0.67	±0.37	±0.44	∓0.72	±0.79	∓0.68	-

Bins [Unit $y^{t\bar{t}}$]	0–0.20	0.20–0.40	0.40–0.60	0.60–0.85	0.85–1	1–1.25	1.25–1.50	1.50–1.75	1.75–2	2–3
$1/\sigma \cdot \mathrm{d}\sigma$ / $\mathrm{d}y^{t\bar{t}}$	$5.19 \cdot 10^{-1}$	$4.90 \cdot 10^{-1}$	$4.39 \cdot 10^{-1}$	$3.56 \cdot 10^{-1}$	$2.60 \cdot 10^{-1}$	$1.81 \cdot 10^{-1}$	$9.76 \cdot 10^{-2}$	$4.02 \cdot 10^{-2}$	$1.05 \cdot 10^{-2}$	$2.85 \cdot 10^{-4}$
Total Uncertainty [%]	$^{+2.06}_{-2.10}$	$^{+1.21}_{-1.24}$	$^{+1.23}_{-1.17}$	$^{+1.28}_{-1.17}$	$^{+3.58}_{-3.71}$	$^{+2.39}_{-2.68}$	$^{+6.10}_{-6.27}$	$^{+7.14}_{-6.94}$	$^{+12.1}_{-13.1}$	$^{+16.6}_{-30.2}$
Statistics [%]	±0.3	±0.3	±0.4	±0.3	±0.6	±0.5	±0.7	±1.2	±2.4	±8.4
Systematics [%]	$^{+2.01}_{-2.05}$	$^{+1.10}_{-1.13}$	$^{+1.12}_{-1.05}$	$^{+1.19}_{-1.08}$	$^{+3.50}_{-3.63}$	$^{+2.28}_{-2.59}$	$^{+6.03}_{-6.20}$	$^{+6.98}_{-6.78}$	$^{+11.7}_{-12.8}$	$^{+13.3}_{-28.5}$
Jet energy resolution [%]	±1.30	±0.50	±0.26	∓0.26	∓1.64	±1.16	∓2.39	∓3.43	∓4.78	±2.33
b-Tagged jet energy scale (JES) [%]	-	-	-	-	-	-	-	$^{-0.10}_{+0.34}$	$^{-0.49}_{+0.26}$	$^{-0.51}_{+0.46}$
Effective detector NP set 1 (JES) [%]	-	-	-	-	-	-	-	-	$^{-0.16}_{+0.11}$	-
Effective detector NP set 2 (JES) [%]	-	-	-	-	-	-	-	-	∓0.10	$^{+0.21}_{-}$
Effective mixed NP set 1 (JES) [%]	-	-	-	-	-	-	-	-	$^{-0.56}_{+0.16}$	-
Effective mixed NP set 2 (JES) [%]	-	-	-	-	-	-	-	-	-	$^{+0.22}_{-}$
Effective mixed NP set 3 (JES) [%]	-	-	-	-	-	-	-	-	-	$^{+0.23}_{-}$
Effective modelling NP set 1 (JES) [%]	$^{+0.26}_{-0.22}$	$^{-}_{-0.19}$	-	-	-	$^{-0.14}_{+0.24}$	$^{-0.65}_{+0.37}$	$^{-0.18}_{+1.00}$	$^{-1.72}_{+0.28}$	$^{-1.20}_{+0.87}$
Effective modelling NP set 2 (JES) [%]	-	-	-	-	-	-	-	-	-	$^{-0.35}_{+0.18}$
Effective modelling NP set 3 (JES) [%]	-	-	-	-	-	-	-	-	-	-
Effective modelling NP set 4 (JES) [%]	-	-	-	-	-	-	-	-	$^{-0.18}_{+0.11}$	$^{-0.12}_{+0.13}$
Effective statistical NP set 1 (JES) [%]	-	-	-	-	-	-	$^{-0.19}_{+0.12}$	-	$^{-0.56}_{+0.11}$	$^{-0.52}_{+0.43}$
Effective statistical NP set 2 (JES) [%]	-	-	-	-	-	-	$^{-}_{-0.18}$	-	$^{-}_{-0.40}$	$^{-}_{-0.46}$
Effective statistical NP set 3 (JES) [%]	-	-	-	-	-	-	-	-	-	-
Effective statistical NP set 4 (JES) [%]	-	-	-	-	-	-	-	-	$^{-0.29}_{+0.13}$	$^{-0.16}_{+0.11}$
Effective statistical NP set 5 (JES) [%]	-	-	-	-	-	-	-	-	-	-
Effective statistical NP set 6 (JES) [%]	-	-	-	-	-	-	-	-	-	$^{-}_{-0.32}$
Effective statistical NP set 7 (JES) [%]	-	-	-	-	-	-	-	-	$^{-0.16}_{+0.13}$	-
η intercalibration model (JES) [%]	-	$^{-0.14}_{-}$	$^{-}_{+0.11}$	-	$^{+0.18}_{-0.37}$	$^{+0.20}_{-0.10}$	$^{-}_{-0.23}$	$^{+0.60}_{-}$	$^{-}_{-0.70}$	$^{+0.77}_{-}$
η intercalibration non closure (JES) [%]	-	-	$^{+0.11}_{-0.16}$	$^{+0.19}_{-}$	$^{-}_{-0.23}$	$^{+0.18}_{-}$	$^{+0.10}_{-0.21}$	$^{+0.28}_{-}$	$^{+0.27}_{-0.36}$	$^{+0.43}_{-0.40}$
η intercalibration total stat (JES) [%]	-	-	-	-	-	-	$^{-0.27}_{+0.12}$	-	$^{-0.72}_{+0.20}$	$^{-}_{+0.16}$
Flavour composition (JES) [%]	$^{+0.13}_{-0.31}$	$^{+0.26}_{-0.12}$	-	-	-	$^{-0.27}_{+0.22}$	$^{-0.35}_{+0.37}$	$^{-0.32}_{+0.63}$	$^{-0.95}_{+0.81}$	$^{-2.47}_{+0.59}$
Flavour response (JES) [%]	-	-	-	-	-	-	$^{+0.25}_{-0.36}$	$^{+0.30}_{-}$	$^{+0.21}_{-0.84}$	$^{+0.37}_{-}$
Pile-up offset μ (JES) [%]	-	-	-	-	-	-	-	$^{-}_{+0.16}$	$^{-}_{-0.32}$	$^{-}_{+0.51}$
Pile-up offset N_{PV} (JES) [%]	-	-	-	-	-	$^{-}_{+0.16}$	-	$^{+0.41}_{-}$	$^{-1.12}_{+0.30}$	$^{-0.97}_{-}$
Pile-up offset p_T (JES) [%]	-	-	-	-	-	-	-	-	$^{-0.68}_{+0.13}$	$^{-}_{-0.17}$
Pile-up offset ρ topology (JES) [%]	$^{+0.32}_{-0.40}$	$^{+0.20}_{-0.29}$	-	-	-	$^{-0.27}_{+0.53}$	$^{-0.77}_{+0.56}$	$^{-0.46}_{+1.34}$	$^{-2.47}_{+1.04}$	$^{-2.91}_{+1.74}$
Jet vertex fraction [%]	-	-	-	-	-	-	-	-	-	-
b-Quark tagging efficiency (eigenvector 0) [%]	-	-	-	-	-	$^{+0.12}_{-0.11}$	$^{+0.18}_{-0.16}$	$^{+0.27}_{-0.24}$	$^{+0.31}_{-0.27}$	$^{+0.31}_{-0.29}$
b-Quark tagging efficiency (eigenvector 1) [%]	-	-	-	-	-	-	-	-	∓0.12	$^{-0.19}_{+0.18}$
c-Quark tagging efficiency (eigenvector 0) [%]	-	-	-	-	-	-	-	-	-	∓0.10
Light-jet tagging efficiency (eigenvector 0) [%]	-	$^{+0.11}_{-0.14}$	-	-	-	$^{-0.17}_{+0.21}$	-	-	$^{-0.15}_{+0.17}$	$^{-0.61}_{+0.57}$
Light-jet tagging efficiency (eigenvector 1) [%]	-	-	-	-	-	-	-	-	-	$^{+0.26}_{-0.27}$
Light-jet tagging efficiency (eigenvector 2) [%]	-	-	-	-	-	-	-	∓0.14	-	∓0.39
Light-jet tagging efficiency (eigenvector 3) [%]	-	-	-	-	-	-	-	∓0.13	$^{-0.17}_{+0.18}$	∓0.37
Light-jet tagging efficiency (eigenvector 5) [%]	-	-	-	-	-	-	-	-	∓0.10	∓0.13
Light-jet tagging efficiency (eigenvector 6) [%]	-	-	-	-	-	-	-	-	-	-
Light-jet tagging efficiency (eigenvector 7) [%]	-	-	-	-	-	-	-	-	-	-
Light-jet tagging efficiency (eigenvector 8) [%]	-	-	-	-	-	-	-	-	-	∓0.11
Electron energy resolution [%]	-	-	-	-	-	-	-	-	-	$^{-}_{-0.57}$
Electron energy scale [%]	-	-	-	-	-	-	-	-	-	$^{-}_{-0.75}$
Electron trigger efficiency [%]	-	-	-	-	-	-	-	-	-	±0.15
Electron identification efficiency [%]	-	-	-	-	-	-	-	±0.10	±0.27	$^{+0.54}_{-0.55}$
Muon (ID) momentum resolution [%]	-	-	-	-	-	-	-	-	$^{-}_{-0.32}$	$^{+1.48}_{-}$
Muon (MS) momentum resolution [%]	-	-	-	-	-	-	$^{-}_{+0.20}$	-	$^{-}_{-0.22}$	$^{+0.53}_{-}$
Muon energy scale [%]	-	-	-	-	-	-	-	-	-	$^{+0.15}_{-0.37}$
Muon trigger efficiency stat [%]	-	-	-	-	-	-	-	-	-	-
Muon identification syst [%]	-	-	-	-	-	-	±0.11	±0.14	±0.14	±0.11
E_T^{miss} Soft jet resolution para [%]	∓0.15	-	-	-	±0.13	-	±0.42	±0.27	±0.79	±0.97
E_T^{miss} Soft jet resolution perp [%]	-	-	-	-	-	-	±0.53	±0.30	±0.32	∓0.75
E_T^{miss} Soft jet scale [%]	-	-	-	-	-	-	$^{+0.44}_{-0.21}$	$^{+0.51}_{-0.45}$	$^{+0.63}_{-0.64}$	$^{+0.61}_{-}$
Z+jets cross-section [%]	-	-	-	-	-	-	-	-	∓0.11	-
Monte Carlo sample statistics [%]	±0.25	±0.33	±0.30	±0.24	±0.45	±0.40	±0.49	±0.80	±1.57	±5.33
ISR/FSR + scale [%]	-	$^{-}_{+0.25}$	$^{+0.37}_{-}$	$^{+0.36}_{-}$	$^{-}_{-0.72}$	$^{-}_{-1.36}$	$^{+0.67}_{-1.39}$	$^{-1.32}_{+0.73}$	$^{-}_{-3.56}$	$^{-}_{-24.7}$
Alternate hard-scattering model [%]	±0.69	±0.71	±0.64	∓0.59	∓2.29	∓0.67	±4.67	∓3.20	∓6.94	∓3.62
Alternate parton-shower model [%]	-	±0.34	±0.67	±0.77	∓1.59	∓1.54	∓2.22	∓2.34	∓6.86	∓11.3
Inter PDF [%]	-	-	-	-	-	-	-	-	-	∓0.12
Intra PDF [%]	-	∓0.13	-	-	-	-	-	±0.21	±0.62	±1.60
Fakes overall normalization, el [%]	-	-	-	-	-	-	∓0.23	-	$^{-1.02}_{+1.03}$	$^{-2.50}_{+2.54}$
Fakes overall normalization, mu [%]	-	-	-	-	-	-	-	-	-	±0.17
Fakes alternative parametrization [%]	-	∓0.23	-	-	±0.14	-	±0.52	±0.81	±2.03	±2.16
W+jets heavy flavour component [%]	±1.24	±0.16	±0.25	∓0.34	∓1.26	±0.54	∓1.19	∓3.74	∓2.93	±2.22

TABLE F.29: Table of systematics for the relative differential cross-section at the particle level for the $y^{t\bar{t}}$ observable.

Bins [GeV]	250–320	320–400	400–450	450–500	500–570	570–630	630–700	700–770	770–850	850–930	930–1020	1020–1100	1100–1200	1200–1300	1300–1500	1500–2000
$1/\sigma \cdot d\sigma$ / $dm^{t\bar{t}}$	$2.95 \cdot 10^{-4}$	$2.23 \cdot 10^{-3}$	$3.04 \cdot 10^{-3}$	$2.72 \cdot 10^{-3}$	$2.16 \cdot 10^{-3}$	$1.58 \cdot 10^{-3}$	$1.13 \cdot 10^{-3}$	$7.78 \cdot 10^{-4}$	$5.28 \cdot 10^{-4}$	$3.53 \cdot 10^{-4}$	$2.36 \cdot 10^{-4}$	$1.57 \cdot 10^{-4}$	$1.04 \cdot 10^{-4}$	$6.55 \cdot 10^{-5}$	$3.67 \cdot 10^{-5}$	$1.05 \cdot 10^{-5}$
Total Uncertainty [%]	+22.2 −22.1	+6.78 −6.88	+2.37 −2.32	+2.35 −2.38	±2.66	+2.73 −2.56	+2.84 −2.87	+3.47 −3.56	+4.31 −4.52	±4.53	+5.61 −5.26	+7.05 −6.66	+6.67 −6.66	+6.97 −7.63	+8.96 −7.73	+9.93 −9.19
Statistics [%]	±1.0	±0.2	±0.2	±0.2	±0.2	±0.3	±0.3	±0.4	±0.4	±0.5	±0.6	±0.8	±1.0	±1.2	±1.4	±1.7
Systematics [%]	+22.1 −22.0	+6.77 −6.87	+2.35 −2.30	+2.33 −2.36	±2.64	+2.70 −2.53	+2.82 −2.84	+3.43 −3.52	+4.27 −4.48	+4.48 −4.47	+5.55 −5.19	+6.97 −6.59	+6.54 −6.53	+6.79 −7.48	+8.78 −7.52	+9.71 −8.96
Jet energy resolution [%]	±2.37	∓0.83	∓1.27	±0.18	∓0.30	-	±1.76	±1.32	±0.65	±1.90	±1.28	∓0.45	∓0.85	∓0.83	∓0.57	±4.65
b-Tagged jet energy scale (JES) [%]	−3.94 +4.35	−1.35 +1.34	-	+0.45 −0.43	+0.46 −0.52	+0.48 −0.49	+0.48 −0.49	+0.53 −0.48	+0.48 −0.44	+0.40 −0.49	+0.67 −0.36	+0.53 −0.35	+0.10 −0.47	+0.16 −0.48	+0.23 −0.45	+0.57 −0.18
Effective detector NP set 1 (JES) [%]	−0.31 +0.36	−0.13 +0.16	-	-	-	-	-	-	-	-	-	-	-	-	- −0.15	+0.21 -
Effective detector NP set 2 (JES) [%]	−0.22 +0.19	−0.10 +0.13	-	-	-	-	-	-	-	-	-	±0.11	-	-	-	-
Effective mixed NP set 1 (JES) [%]	−1.21 +1.41	−0.65 +0.67	−0.19 +0.21	-	+0.13 −0.19	+0.25 −0.22	+0.27 −0.25	+0.43 −0.38	+0.40 −0.45	+0.41 −0.57	+0.63 −0.57	+0.75 −0.51	+0.76 −0.72	+0.67 −1.02	+0.67 −1.10	+1.46 −0.88
Effective mixed NP set 2 (JES) [%]	+0.18 −0.17	+0.11 -	-	-	-	-	-	-	-	-	-	−0.12 +0.11	-	-	-	- +0.20
Effective modelling NP set 1 (JES) [%]	−0.20 +0.91	-	+0.47 −0.50	+0.58 −0.59	±0.28	-	−0.25 +0.30	−0.46 +0.53	−0.85 +0.72	−0.98 +0.85	−0.92 +0.86	−1.14 +1.22	−1.59 +1.52	−1.95 +1.49	−1.96 +1.62	−1.48 +2.02
Effective modelling NP set 2 (JES) [%]	−0.88 +0.99	−0.46 +0.51	−0.18 +0.14	-	-	±0.18	+0.20 −0.25	+0.34 −0.27	+0.36 −0.34	+0.29 −0.56	+0.49 −0.44	+0.73 −0.36	+0.50 −0.57	+0.56 −0.83	+0.53 −0.78	+1.12 −0.77
Effective modelling NP set 3 (JES) [%]	+1.00 −0.95	+0.55 −0.50	+0.15 −0.18	-	−0.12 +0.11	−0.21 +0.23	−0.26 +0.22	−0.29 +0.37	−0.34 +0.36	−0.48 +0.30	−0.43 +0.47	−0.46 +0.68	−0.45 +0.58	−0.75 +0.39	−0.51 +0.34	−0.54 +0.77
Effective modelling NP set 4 (JES) [%]	−0.37 +0.45	- +0.13	-	-	-	-	-	-	-	-	-	-	-	-	-	-
Effective statistical NP set 1 (JES) [%]	+0.28 -	-	-	-	-	-	−0.14 +0.10	−0.11 +0.12	−0.18 +0.19	−0.29 +0.16	−0.25 +0.26	−0.21 +0.29	−0.33 +0.25	−0.43 +0.16	−0.43 +0.34	- +0.31
Effective statistical NP set 2 (JES) [%]	- +0.21	-	−0.10 +0.11	-	-	-	-	-	+0.17 −0.19	+0.15 −0.28	+0.33 −0.27	+0.35 −0.29	+0.27 −0.44	+0.31 −0.44	+0.40 −0.37	+0.69 −0.44
Effective statistical NP set 3 (JES) [%]	+0.11 −0.10	-	-	-	-	-	-	-	-	−0.18 -	−0.14 +0.20	- +0.33	−0.24 +0.23	−0.46 +0.24	−0.41 +0.18	−0.40 +0.70
Effective statistical NP set 4 (JES) [%]	−1.01 +0.99	−0.45 +0.47	∓0.11	-	+0.13 −0.14	±0.20	+0.19 −0.23	+0.32 −0.26	+0.31 −0.22	+0.20 −0.34	+0.29 −0.30	+0.39 −0.26	+0.27 −0.26	+0.13 −0.34	+0.12 −0.34	+0.37 -
Effective statistical NP set 5 (JES) [%]	+0.59 −0.58	+0.17 −0.16	-	-	-	-	-	-	-	-	+0.15 −0.12	+0.22 -	+0.13 −0.16	- −0.31	-	+0.28 -
Effective statistical NP set 6 (JES) [%]	−0.15 +0.30	-	-	-	-	-	-	-	-	−0.18 +0.10	−0.14 -	-	-	−0.21 -	−0.19 -	-
Effective statistical NP set 7 (JES) [%]	∓0.24	−0.11 +0.14	-	-	-	-	-	-	-	-	-	+0.20 -	-	-	-	+0.34 -
η intercalibration model (JES) [%]	−1.89 +2.50	−0.82 +0.78	-	+0.23 −0.17	+0.25 −0.27	+0.26 −0.30	+0.23 −0.24	+0.40 −0.37	+0.30 −0.48	+0.32 −0.43	+0.53 −0.29	+0.54 −0.40	+0.42 −0.56	+0.36 −0.62	+0.38 −0.57	+1.11 −0.61
η intercalibration non closure (JES) [%]	+0.65 −0.21	+0.16 −0.17	-	-	-	-	-	- +0.16	-	−0.19 -	- +0.28	-	−0.30 +0.13	- −0.68	−0.24 -	+0.53 -
η intercalibration total stat (JES) [%]	−0.91 +1.26	∓0.33	-	±0.18	+0.17 −0.19	+0.14 -	-	+0.15 -	-	-	-	-	−0.18 +0.16	- −0.30	−0.27 -	+0.27 -
Flavour composition (JES) [%]	+0.94 -	+0.19 −0.31	+0.43 −0.55	+0.42 −0.59	+0.20 −0.18	- +0.24	−0.41 +0.47	−0.55 +0.62	−0.89 +0.87	−0.96 +1.07	−1.01 +1.20	−1.07 +1.42	−1.26 +1.60	−1.69 +1.68	−2.01 +1.95	−1.46 +2.28
Flavour response (JES) [%]	+1.08 −0.19	-	−0.28 +0.19	−0.31 +0.34	−0.12 +0.19	-	+0.15 −0.12	+0.30 −0.13	+0.34 −0.54	+0.37 −0.56	+0.50 −0.38	+0.74 −0.49	+0.76 −0.60	+0.52 −0.89	+1.04 −1.24	+1.10 −0.76
Pile-up offset μ (JES) [%]	+0.34 -	-	-	-	-	-	-	-	-	-	-	+0.16 -	-	−0.29 -	-	+0.22 -
Pile-up offset N_{PV} (JES) [%]	- +1.26	−0.20 +0.18	-	+0.12 −0.11	+0.13 −0.15	- −0.16	-	-	-	- −0.22	-	-	−0.32 +0.10	−0.69 +0.36	−0.37 +0.38	∓0.13
Pile-up offset p_T (JES) [%]	−2.80 +2.86	−1.25 +1.26	−0.26 +0.29	- −0.12	+0.33 −0.34	+0.50 −0.48	±0.54	+0.69 −0.70	+0.73 −0.85	+0.85 −0.83	+0.99 −0.71	+1.06 −0.93	+1.07 −1.16	+0.76 −1.13	+0.99 −1.23	+1.44 −0.99
Pile-up offset ρ topology (JES) [%]	−2.89 +3.76	−0.92 +0.78	+0.72 −0.68	+1.16 −1.07	+0.68 −0.70	+0.35 −0.30	-	−0.39 +0.41	−0.89 +0.78	−1.02 +0.88	−1.16 +1.29	−1.46 +1.85	−2.14 +2.02	−2.64 +2.14	−2.54 +2.48	−2.64 +2.98
Jet vertex fraction [%]	±1.02	±0.42	±0.15	-	-	∓0.17	∓0.23	−0.29 +0.28	−0.34 +0.33	−0.38 +0.37	∓0.41	−0.44 +0.43	−0.48 +0.47	−0.52 +0.51	−0.53 +0.52	−0.64 +0.62
b-Quark tagging efficiency (eigenvector 0) [%]	−6.43 +6.13	−1.57 +1.45	-	+0.36 −0.34	+0.55 −0.51	+0.69 −0.65	+0.76 −0.71	+0.80 −0.75	+0.78 −0.73	+0.74 −0.70	+0.69 −0.66	+0.59 −0.56	+0.50 −0.49	+0.44 −0.43	±0.33	-
b-Quark tagging efficiency (eigenvector 1) [%]	+2.38 −2.31	+1.03 −1.00	+0.44 −0.43	+0.14 −0.13	-	−0.35 +0.34	−0.58 +0.56	−0.78 +0.76	−0.96 +0.94	−1.15 +1.12	−1.34 +1.31	−1.53 +1.51	−1.71 +1.68	−1.83 +1.80	−1.99 +1.95	−2.40 +2.36
b-Quark tagging efficiency (eigenvector 2) [%]	+0.15 −0.16	+0.32 −0.33	±0.26	±0.15	-	∓0.10	∓0.21	∓0.32	−0.43 +0.44	∓0.55	−0.65 +0.66	−0.75 +0.76	−0.82 +0.84	−0.89 +0.91	−1.01 +1.02	−1.21 +1.23
b-Quark tagging efficiency (eigenvector 3) [%]	∓0.63	∓0.31	-	-	±0.12	±0.17	±0.19	±0.19	±0.16	+0.12 −0.13	-	-	-	-	-	−0.20 +0.19
b-Quark tagging efficiency (eigenvector 4) [%]	±0.18	-	-	-	-	-	-	-	-	-	-	-	-	-	-	-
c-Quark tagging efficiency (eigenvector 0) [%]	±0.61	±0.13	-	-	-	-	-	-	-	∓0.10	-	∓0.10	∓0.14	∓0.14	∓0.14	-
c-Quark tagging efficiency (eigenvector 1) [%]	±0.34	±0.18	±0.11	-	-	-	-	−0.17 +0.16	∓0.22	∓0.29	∓0.38	∓0.44	∓0.42	∓0.51	∓0.62	∓0.81
c-Quark tagging efficiency (eigenvector 2) [%]	+0.10 −0.11	±0.10	-	-	-	-	-	-	∓0.12	∓0.16	∓0.22	∓0.24	∓0.25	∓0.27	∓0.34	∓0.48
Light-jet tagging efficiency (eigenvector 0) [%]	−0.40 +0.13	+0.18 −0.20	+0.20 −0.19	-	+0.13 −0.14	-	-	−0.19 +0.20	−0.41 +0.46	−0.38 +0.37	−0.51 +0.49	−0.75 +0.78	−0.60 +0.63	−0.85 +0.88	−1.54 +1.58	−1.41 +1.42
Light-jet tagging efficiency (eigenvector 1) [%]	+0.55 −0.54	-	-	-	-	-	-	-	-	-	−0.16 +0.14	−0.16 +0.15	∓0.18	−0.17 +0.18	−0.12 +0.10	−0.45 +0.44
Light-jet tagging efficiency (eigenvector 2) [%]	-	-	-	-	-	-	-	-	-	-	-	±0.10	-	-	-	±0.16
Light-jet tagging efficiency (eigenvector 3) [%]	+0.36 −0.44	±0.12	-	-	-	-	-	−0.14 +0.15	∓0.20	∓0.21	∓0.29	−0.34 +0.35	∓0.29	∓0.37	−0.63 +0.64	−0.66 +0.67
Light-jet tagging efficiency (eigenvector 8) [%]	-	-	-	-	-	-	-	-	-	-	-	-	∓0.11	∓0.13	∓0.21	∓0.24
b-Quark tagging extrapolation [%]	-	-	-	-	-	-	-	-	-	±0.15	±0.30	±0.46	±0.59	±0.74	±1.01	±1.60
Electron energy resolution [%]	- −0.20	-	-	-	-	-	-	-	-	-	-	-	-	-	-	-
Electron energy scale [%]	−0.15 +0.13	-	-	-	-	-	-	-	-	-	±0.13	+0.24 −0.13	+0.21 −0.17	- −0.23	+0.23 −0.12	+0.34 −0.26
Electron identification efficiency [%]	-	-	-	-	-	-	-	-	-	±0.12	±0.15	±0.18	±0.21	±0.24	±0.29	+0.38 −0.39
Electron isolation efficiency [%]	-	-	-	-	-	-	-	-	-	±0.12	±0.15	±0.18	±0.21	±0.23	±0.26	±0.38
Muon (ID) momentum resolution [%]	-	-	-	-	-	-	-	-	-	-	-	-	-	-	-	-
Muon (MS) momentum resolution [%]	-	-	-	-	-	-	-	-	-	-	-	-	-	-	-	-
Muon identification syst [%]	-	-	-	-	-	-	-	-	-	-	±0.10	±0.13	±0.15	±0.17	±0.21	±0.26
E_T^{miss} Soft jet resolution para [%]	±1.13	±0.65	±0.17	-	∓0.21	∓0.29	∓0.34	∓0.31	∓0.44	∓0.35	∓0.21	∓0.28	∓0.32	∓0.47	∓0.50	∓0.30
E_T^{miss} Soft jet resolution perp [%]	±1.05	±0.60	±0.17	-	∓0.20	∓0.26	∓0.27	∓0.36	∓0.35	∓0.20	∓0.39	∓0.63	∓0.46	∓0.23	∓0.51	∓0.46
E_T^{miss} Soft jet scale [%]	+1.10 −0.95	+0.70 −0.68	+0.19 −0.22	-	−0.21 +0.17	−0.27 +0.26	−0.35 +0.34	−0.31 +0.41	−0.40 +0.38	−0.40 +0.36	−0.38 +0.46	−0.39 +0.58	−0.36 +0.41	−0.47 +0.15	−0.57 +0.61	−0.37 +0.42
Z+jets cross-section [%]	+1.27 −1.28	-	∓0.14	∓0.11	-	-	-	-	±0.12	±0.11	±0.17	±0.25	+0.31 −0.32	+0.36 −0.37	+0.41 −0.42	+0.64 −0.65
Monte Carlo sample statistics [%]	±1.20	±0.19	±0.16	±0.18	±0.19	±0.19	±0.22	±0.25	±0.34	±0.37	±0.44	±0.57	±0.83	±0.86	±1.04	±1.09
ISR/FSR + scale [%]	- −2.01	- −0.45	+0.61 -	- −0.61	-	+0.83 -	−0.56 +0.42	- −1.18	- −1.03	+1.30 -	+1.38 −0.70	+0.66 −0.34	+0.90 −0.28	+0.72 −1.00	−0.82 +0.42	+0.73 −0.21
Alternate hard-scattering model [%]	±12.9	±4.99	∓0.28	∓1.48	∓1.55	∓1.31	∓0.75	∓1.60	∓2.26	∓1.33	∓3.30	∓4.84	∓3.89	∓2.75	∓2.24	±0.17
Alternate parton-shower model [%]	∓3.31	±0.23	±0.65	-	±0.62	±0.64	∓0.38	∓0.93	∓1.89	∓0.86	∓0.64	±0.55	-	∓3.12	∓2.85	∓3.00
Inter PDF [%]	-	-	-	-	-	-	-	-	-	-	-	-	∓0.19	∓0.26	±0.14	±0.14
Intra PDF [%]	±0.23	∓0.10	-	∓0.14	-	-	-	±0.12	±0.23	-	-	-	±1.01	±1.29	±0.73	±0.26
Fakes overall normalization, el [%]	+3.24 −3.25	±0.20	∓0.24	−0.22 +0.23	∓0.21	−0.13 +0.14	-	-	-	-	±0.23	+0.49 −0.50	±0.50	±0.49	±0.50	+2.45 −2.49
Fakes overall normalization, mu [%]	±0.41	±0.11	-	-	-	-	-	-	∓0.20	∓0.33	∓0.34	∓0.39	∓0.48	∓0.36	∓0.50	∓0.74
Fakes alternative parametrization [%]	∓7.56	∓1.77	∓0.56	-	±0.39	±0.78	±1.04	±1.30	±1.51	±1.87	±1.90	±2.04	±2.19	±2.35	±2.69	±1.70
W+jets heavy flavour component [%]	±9.68	±2.01	∓0.84	∓0.42	∓1.36	∓1.25	±0.34	-	∓0.40	±0.94	∓0.27	∓1.51	∓1.11	∓0.93	∓0.66	±2.98

TABLE F.30: Table of systematics for the relative differential cross-section at the particle level for the $m^{t\bar{t}}$ observable.

Bins [GeV] x	300–400	400–500	500–600	600–710	710–870	870–1050	1050–1250	1250–1460	1460–2000	2000–2100	2100–2210
$1/\sigma \cdot d\sigma$ / $dm^{t\bar{t}}vsy^{t,had}$	$9.67 \cdot 10^{-4}$	$1.48 \cdot 10^{-3}$	$1.03 \cdot 10^{-3}$	$6.21 \cdot 10^{-4}$	$3.11 \cdot 10^{-4}$	$1.38 \cdot 10^{-4}$	$5.66 \cdot 10^{-5}$	$2.53 \cdot 10^{-5}$	$6.59 \cdot 10^{-6}$	$5.98 \cdot 10^{-4}$	$8.71 \cdot 10^{-4}$
Total Uncertainty [%]	+9.77 −9.57	+3.90 −4.02	+5.04 −4.92	+6.04 −6.25	+7.15 −7.68	±7.10	+9.63 −10.0	+14.4 −11.7	+15.4 −14.4	+9.57 −9.60	+3.83 −4.10
Statistics [%]	±0.4	±0.3	±0.3	±0.4	±0.5	±0.8	±1.2	±1.8	±2.2	±0.5	±0.3
Systematics [%]	+9.76 −9.55	+3.88 −4.00	+5.02 −4.90	+6.01 −6.23	+7.12 −7.65	±7.03	+9.50 −9.88	+14.3 −11.4	+15.1 −14.1	+9.55 −9.58	+3.80 −4.07
Jet energy resolution [%]	∓0.71	∓0.96	∓0.85	∓0.37	±0.79	∓0.76	∓2.00	∓3.01	±5.45	∓0.46	-
b-Tagged jet energy scale (JES) [%]	−1.69 +1.77	+0.14 −0.15	+0.58 −0.56	+0.47 −0.51	+0.40 −0.45	+0.47 −0.40	+0.23 −0.42	+0.52 −0.24	+0.28 −0.40	−1.45 +1.50	+0.10 −0.20
Effective detector NP set 1 (JES) [%]	−0.21 +0.22	-	-	-	-	-	-	-	-	−0.10 +0.16	-
Effective detector NP set 2 (JES) [%]	−0.16 +0.17	-	-	-	-	-	-	-	-	- +0.11	-
Effective mixed NP set 1 (JES) [%]	−0.90 +0.91	−0.20 +0.18	+0.14 −0.12	+0.16 −0.14	+0.18 −0.30	+0.46 −0.50	+0.50 −0.52	+0.96 −0.67	+1.02 −1.12	−0.63 +0.70	-
Effective mixed NP set 2 (JES) [%]	+0.15 −0.14	-	-	-	-	-	-	- +0.12	-	-	-
Effective mixed NP set 3 (JES) [%]	-	-	-	-	-	-	-	-	-	-	-
Effective modelling NP set 1 (JES) [%]	−1.83 +1.93	−1.00 +0.81	−1.07 +1.16	−1.79 +1.63	−2.44 +2.07	−2.61 +2.38	−3.21 +2.75	−3.47 +3.87	−2.65 +3.49	+0.47 −0.44	+1.09 −1.26
Effective modelling NP set 2 (JES) [%]	−0.43 +0.46	-	+0.23 −0.29	+0.36 −0.32	+0.41 −0.52	+0.56 −0.48	+0.61 −0.78	+0.91 −0.64	+1.03 −0.99	−0.52 +0.57	−0.18 +0.11
Effective modelling NP set 3 (JES) [%]	+0.57 −0.54	-	−0.26 +0.21	−0.27 +0.35	−0.46 +0.38	−0.46 +0.54	−0.59 +0.55	−0.65 +0.75	−0.64 +0.50	+0.60 −0.54	- −0.15
Effective modelling NP set 4 (JES) [%]	−0.20 +0.23	-	-	-	-	-	-	-	−0.27 +0.13	- +0.15	-
Effective statistical NP set 1 (JES) [%]	−0.19 +0.18	−0.13 +0.18	−0.25 +0.21	−0.34 +0.35	−0.43 +0.42	−0.58 +0.54	−0.52 +0.43	−0.46 +0.70	−0.62 +0.54	+0.19 −0.10	+0.15 −0.26
Effective statistical NP set 2 (JES) [%]	±0.14	+0.14 −0.10	+0.19 −0.23	±0.29	+0.35 −0.40	+0.51 −0.48	+0.47 −0.62	+0.83 −0.55	+0.58 −0.61	−0.12 +0.17	−0.24 +0.15
Effective statistical NP set 3 (JES) [%]	-	-	-	-	-	- +0.15	−0.31 +0.16	−0.43 +0.52	∓0.46	-	-
Effective statistical NP set 4 (JES) [%]	∓0.57	-	+0.16 −0.20	+0.22 −0.18	+0.24 −0.30	+0.30 −0.21	+0.18 −0.37	+0.30 −0.24	+0.16 −0.12	−0.45 +0.50	-
Effective statistical NP set 5 (JES) [%]	+0.24 −0.23	-	-	-	-	±0.15	-	+0.46 −0.21	- −0.22	+0.19 −0.16	-
Effective statistical NP set 6 (JES) [%]	-	-	-	−0.11 +0.14	−0.15 +0.11	∓0.15	−0.16 +0.13	-	-	-	-
Effective statistical NP set 7 (JES) [%]	−0.21 +0.22	-	-	-	-	-	-	-	-	- +0.15	-
η intercalibration model (JES) [%]	−1.47 +1.56	−0.44 +0.47	−0.12 +0.13	−0.23 +0.12	−0.25 -	-	- −0.21	-	+0.44 -	−0.69 +0.76	+0.23 −0.35
η intercalibration non closure (JES) [%]	+0.45 −0.39	+0.20 −0.15	+0.14 −0.13	+0.12 −0.16	-	-	-	-	+0.21 -	- −0.12	−0.22 -
η intercalibration total stat (JES) [%]	−0.73 +0.74	−0.14 +0.20	-	−0.13 +0.20	−0.30 +0.18	−0.39 +0.32	−0.45 +0.34	−0.18 +0.50	−0.37 +0.39	−0.25 +0.33	+0.13 −0.32
Flavour composition (JES) [%]	−1.65 +2.17	−1.34 +1.24	−1.54 +1.74	−2.15 +2.48	−2.89 +2.66	−2.99 +3.18	−3.55 +3.60	−4.43 +4.95	−3.14 +4.63	+0.80 −1.16	+1.06 −1.45
Flavour response (JES) [%]	+1.34 −1.27	+0.76 −0.73	+0.91 −0.74	+1.18 −1.15	+1.44 −1.62	+1.49 −1.57	+1.68 −1.79	+2.22 −2.01	+2.15 −1.59	−0.45 +0.41	−0.86 +0.60
Pile-up offset μ (JES) [%]	+0.18 −0.15	-	-	+0.10 −0.11	+0.12 −0.19	-	+0.13 −0.22	+0.25 -	+0.22 −0.11	-	−0.20 -
Pile-up offset N_{PV} (JES) [%]	−0.44 +0.58	−0.30 +0.27	-	−0.41 +0.32	−0.63 +0.23	−0.59 +0.41	−0.54 +0.52	−0.28 +0.69	−0.67 +0.89	−0.32 +0.15	- −0.31
Pile-up offset p_T (JES) [%]	−1.52 +1.50	∓0.15	+0.47 −0.40	+0.51 −0.57	+0.72 −0.81	+0.97 −0.92	+0.85 −0.83	+1.12 −1.19	+1.21 −1.27	−1.24 +1.34	-
Pile-up offset ρ topology (JES) [%]	−3.71 +3.85	−1.32 +1.22	∓1.34	−2.37 +2.16	−3.21 +2.75	−3.37 +3.39	−4.69 +4.22	−5.27 +5.28	−4.41 +5.51	-	+1.59 −1.89
Jet vertex fraction [%]	±0.26	∓0.11	∓0.33	−0.45 +0.44	∓0.55	−0.65 +0.64	−0.73 +0.72	−0.77 +0.76	−0.86 +0.85	±0.53	+0.18 −0.17
b-Quark tagging efficiency (eigenvector 0) [%]	−2.10 +1.97	−0.26 +0.25	+0.26 −0.23	+0.34 −0.32	+0.35 −0.33	+0.29 −0.28	-	−0.20 +0.16	−0.33 +0.27	−1.61 +1.50	+0.23 −0.21
b-Quark tagging efficiency (eigenvector 1) [%]	+1.05 −1.03	±0.32	−0.14 +0.13	−0.50 +0.49	−0.86 +0.84	−1.26 +1.24	−1.70 +1.67	−1.97 +1.94	−2.33 +2.29	+1.14 −1.12	±0.29
b-Quark tagging efficiency (eigenvector 2) [%]	+0.43 −0.44	±0.29	-	-	∓0.25	−0.47 +0.48	−0.65 +0.66	−0.81 +0.82	−1.04 +1.06	±0.29	+0.15 −0.16
b-Quark tagging efficiency (eigenvector 3) [%]	∓0.36	-	±0.12	±0.19	±0.18	±0.13	-	-	∓0.14	∓0.32	-
c-Quark tagging efficiency (eigenvector 0) [%]	±0.16	-	-	-	-	-	∓0.16	∓0.14	∓0.10	±0.14	-
c-Quark tagging efficiency (eigenvector 1) [%]	±0.16	-	-	-	∓0.15	∓0.27	∓0.28	−0.41 +0.42	∓0.58	±0.21	-
c-Quark tagging efficiency (eigenvector 2) [%]	±0.12	-	-	-	-	∓0.15	∓0.18	∓0.22	∓0.35	-	-
Light-jet tagging efficiency (eigenvector 0) [%]	+0.17 −0.26	+0.15 −0.13	+0.22 −0.24	-	−0.28 +0.34	−0.26 +0.22	−0.32 +0.36	−1.06 +1.05	−1.24 +1.39	+0.16 −0.17	-
Light-jet tagging efficiency (eigenvector 1) [%]	-	-	-	-	-	-	∓0.10	-	-	-	-
Light-jet tagging efficiency (eigenvector 2) [%]	−0.13 +0.10	-	-	-	-	-	-	-	-	-	-
Light-jet tagging efficiency (eigenvector 3) [%]	-	-	-	-	∓0.12	∓0.16	∓0.15	∓0.41	−0.50 +0.51	±0.18	+0.13 −0.11
Light-jet tagging efficiency (eigenvector 5) [%]	-	-	-	-	-	-	-	∓0.10	-	-	-
Light-jet tagging efficiency (eigenvector 7) [%]	-	-	-	-	-	-	-	-	-	-	-
Light-jet tagging efficiency (eigenvector 8) [%]	-	-	-	-	-	-	-	∓0.12	∓0.14	-	-
b-Quark tagging extrapolation [%]	-	-	-	-	-	±0.16	±0.41	±0.71	±1.22	-	-
Electron energy resolution [%]	-	-	-	-	-	-	-	-	-	-	-
Electron energy scale [%]	-	-	-	-	-	-	- −0.23	+0.25 −0.14	+0.28 −0.34	-	-
Electron identification efficiency [%]	-	-	-	-	-	±0.14	±0.20	±0.26	±0.36	-	-
Electron isolation efficiency [%]	-	-	-	-	-	±0.12	±0.18	±0.22	±0.35	-	-
Muon (ID) momentum resolution [%]	-	-	-	-	-	-	-	- −0.26	-	-	-
Muon (MS) momentum resolution [%]	-	-	-	-	-	-	-	-	-	-	-
Muon identification syst [%]	-	-	-	-	-	-	±0.14	±0.19	±0.26	-	-
E_T^{miss} Soft jet resolution para [%]	±0.72	-	∓0.25	∓0.33	∓0.31	∓0.34	∓0.15	∓0.94	∓0.16	±0.78	-
E_T^{miss} Soft jet resolution perp [%]	±0.68	-	∓0.18	∓0.20	∓0.36	∓0.40	∓0.45	∓0.25	∓0.33	±0.64	-
E_T^{miss} Soft jet scale [%]	+0.75 −0.69	-	−0.22 +0.20	−0.29 +0.30	∓0.36	−0.32 +0.35	−0.49 +0.31	−0.57 +0.58	−0.27 +0.39	+0.78 −0.72	-
Z+jets cross-section [%]	±0.27	-	-	±0.10	±0.23	±0.22	+0.41 −0.42	+0.45 −0.46	±0.62	-	∓0.19
Monte Carlo sample statistics [%]	±0.36	±0.20	±0.32	±0.29	±0.40	±0.54	±1.02	±1.34	±1.63	±0.33	±0.29
ISR/FSR + scale [%]	+1.14 -	-	−0.22 +0.36	−1.64 +0.18	- −0.75	+0.36 −0.45	+1.31 -	- −0.56	- −0.76	+0.52 -	+1.08 -
Alternate hard-scattering model [%]	±3.73	∓1.94	∓2.96	∓2.89	∓3.51	∓2.64	∓5.57	∓4.32	∓5.37	±8.16	-
Alternate parton-shower model [%]	∓3.24	∓2.06	∓2.48	∓3.17	∓3.27	∓1.92	∓0.49	∓3.61	∓6.56	±1.98	±2.61
Inter PDF [%]	-	-	-	-	-	±0.13	-	-	±0.10	-	-
Intra PDF [%]	∓0.18	∓0.18	-	-	-	±0.29	±0.11	±0.17	±0.28	∓0.15	-
Fakes overall normalization, el [%]	+0.50 −0.51	-	-	±0.18	±0.17	±0.44	+1.06 −1.08	+0.33 −0.34	+2.12 −2.15	-	∓0.31
Fakes overall normalization, mu [%]	±0.18	±0.11	±0.15	-	-	∓0.24	∓0.25	∓0.33	∓0.67	-	-
Fakes alternative parametrization [%]	∓2.46	∓0.72	±0.10	±0.38	±0.91	±1.34	±1.72	±3.00	±1.44	∓1.57	∓0.17
W+jets heavy flavour component [%]	±3.90	±0.11	∓0.82	∓0.42	±1.24	∓0.31	∓0.47	∓2.08	±5.72	±1.70	∓0.67

Bins [GeV] x	2210–2340	2340–2500	2500–2680	2680–2870	2870–3080	3080–3700	3700–3760	3760–3860	3860–3985	3985–4140	4140–4310
$1/\sigma \cdot d\sigma$ / $dm^{t\bar{t}}vsy^{t,had}$	$5.39 \cdot 10^{-4}$	$2.45 \cdot 10^{-4}$	$1.00 \cdot 10^{-4}$	$4.02 \cdot 10^{-5}$	$1.52 \cdot 10^{-5}$	$3.31 \cdot 10^{-6}$	$1.76 \cdot 10^{-4}$	$3.68 \cdot 10^{-4}$	$2.91 \cdot 10^{-4}$	$1.49 \cdot 10^{-4}$	$6.62 \cdot 10^{-5}$
Total Uncertainty [%]	+4.33 −4.04	+3.38 −3.35	+7.59 −7.54	+6.09 −6.31	+7.10 −7.36	+9.87 −9.45	+13.9 −14.4	+8.90 −9.18	+8.56 −8.49	+8.11 −7.82	+6.72 −6.89
Statistics [%]	±0.4	±0.6	±0.9	±1.4	±2.2	±3.0	±1.1	±0.6	±0.6	±0.7	±1.1
Systematics [%]	+4.29 −4.00	+3.30 −3.27	+7.51 −7.46	+5.85 −6.07	+6.57 −6.85	+9.20 −8.75	+13.8 −14.2	+8.87 −9.15	+8.53 −8.46	+8.05 −7.76	+6.59 −6.77
Jet energy resolution [%]	±1.40	±0.34	±5.57	±1.67	±1.32	∓0.16	±5.25	∓1.93	∓0.97	-	±3.19
b-Tagged jet energy scale (JES) [%]	+0.59 −0.55	+0.49 −0.47	+0.47 −0.46	+0.40 −0.39	-	+0.35 −0.25	−2.03 +2.07	−0.31 +0.21	+0.45 −0.47	+0.42 −0.39	+0.36 −0.33
Effective detector NP set 1 (JES) [%]	-	-	+0.14 -	-	+0.12 −0.19	-	−0.17 +0.20	-	-	-	- −0.18
Effective detector NP set 2 (JES) [%]	-	-	+0.14 -	- −0.13	+0.21 −0.19	-	- +0.17	-	-	-	-
Effective mixed NP set 1 (JES) [%]	+0.35 −0.21	+0.35 −0.44	+0.78 −0.53	+0.60 −0.84	+0.44 −1.29	+1.36 −0.90	−0.73 +0.74	∓0.12	+0.27 −0.25	+0.42 −0.40	+0.45 −0.56
Effective mixed NP set 2 (JES) [%]	-	-	- +0.13	-	−0.14 +0.19	-	+0.10 −0.11	-	-	-	-
Effective mixed NP set 3 (JES) [%]	-	-	-	-	+0.14 −0.10	-	-	-	-	-	-
Effective modelling NP set 1 (JES) [%]	+0.79 −0.63	-	−0.48 +0.58	−0.84 +0.80	−1.26 +0.62	−1.47 +1.35	+2.31 −2.35	±3.26	+2.87 −2.75	+2.43 −1.92	+1.37 −1.52
Effective modelling NP set 2 (JES) [%]	-	+0.35 −0.33	+0.42 −0.34	+0.46 −0.52	+0.52 −0.73	+0.80 −0.63	−0.74 +0.75	−0.42 +0.43	−0.15 +0.20	-	- −0.23
Effective modelling NP set 3 (JES) [%]	−0.10 +0.16	−0.36 +0.35	−0.35 +0.43	−0.52 +0.45	−0.46 +0.50	−0.55 +0.48	+0.68 −0.78	+0.34 −0.35	-	−0.17 +0.16	−0.18 +0.10
Effective modelling NP set 4 (JES) [%]	-	-	-	-	±0.10	-	-	+0.12 −0.16	+0.19 −0.11	+0.15 −0.13	-
Effective statistical NP set 1 (JES) [%]	+0.16 -	-	−0.21 -	−0.13 +0.23	- −0.29	−0.24 +0.32	+0.59 −0.76	+0.56 −0.57	+0.54 −0.47	+0.33 −0.24	- −0.38
Effective statistical NP set 2 (JES) [%]	- +0.14	-	- −0.19	+0.33 −0.32	+0.20 −0.27	+0.44 −0.39	−0.56 +0.45	−0.52 +0.53	−0.43 +0.49	−0.17 +0.27	- −0.31
Effective statistical NP set 3 (JES) [%]	-	-	-	−0.26 +0.27	−0.21 +0.28	−0.44 +0.31	+0.10 −0.11	-	-	-	-
Effective statistical NP set 4 (JES) [%]	+0.20 −0.13	+0.33 −0.31	+0.32 −0.27	+0.26 −0.31	+0.33 −0.25	+0.26 −0.31	−0.67 +0.62	−0.17 +0.13	-	+0.21 −0.24	±0.20
Effective statistical NP set 5 (JES) [%]	- +0.12	-	-	+0.14 −0.11	+0.15 −0.13	-	+0.29 −0.23	-	-	-	-
Effective statistical NP set 6 (JES) [%]	-	-	- +0.14	-	-	-	-	+0.11 −0.14	-	-	-
Effective statistical NP set 7 (JES) [%]	-	-	-	+0.14 −0.17	+0.17 −0.15	-	−0.11 -	-	+0.13 -	+0.10 −0.11	- −0.20
η intercalibration model (JES) [%]	+0.56 −0.37	+0.57 −0.59	+0.61 −0.30	+0.42 −0.69	+0.57 −0.80	+0.69 −0.45	- −0.48	+0.61 −0.67	+0.97 −1.05	±0.97	+0.93 −0.87
η intercalibration non closure (JES) [%]	- +0.16	-	- +0.14	−0.30 +0.17	−0.62 -	−0.19 +0.51	-	−0.30 +0.24	−0.30 +0.39	−0.38 +0.28	−0.18 +0.30
η intercalibration total stat (JES) [%]	+0.34 −0.17	+0.15 −0.12	-	-	- −0.24	-	- −0.18	+0.44 −0.54	+0.73 −0.61	+0.44 −0.46	+0.32 −0.54
Flavour composition (JES) [%]	+0.78 −0.60	+0.21 −0.19	−0.40 +0.74	−0.56 +0.47	−0.42 +0.86	−1.24 +0.70	+3.35 −4.23	+3.62 −4.22	+3.30 −3.42	+2.78 −2.53	+2.09 −2.23
Flavour response (JES) [%]	−0.33 +0.56	−0.21 +0.27	+0.23 -	+0.45 −0.46	+0.17 −0.32	+0.97 −0.82	−2.15 +1.66	−2.20 +2.00	−1.99 +1.96	−1.39 +1.68	−1.12 +1.02
Pile-up offset μ (JES) [%]	-	-	-	-	−0.43 -	+0.12 -	- −0.35	−0.19 +0.17	- +0.20	-	- −0.27
Pile-up offset N_{PV} (JES) [%]	+0.26 −0.11	+0.21 -	+0.28 −0.18	-	−1.02 +0.47	+0.52 −0.36	+0.12 −0.32	+0.58 −0.63	+0.97 −0.69	+0.83 −0.55	+0.36 −0.43
Pile-up offset p_T (JES) [%]	+0.54 −0.41	+0.66 −0.65	+0.85 −0.81	+0.77 −1.14	+1.29 −0.97	+1.39 −1.14	−1.47 +1.66	−0.51 +0.45	+0.15 −0.14	+0.55 −0.61	±0.71
Pile-up offset ρ topology (JES) [%]	+1.36 −1.23	+0.56 −0.60	−0.55 +0.50	−1.00 +1.02	−1.36 +0.73	−1.96 +1.97	+2.80 −2.59	+4.61 −4.48	+4.64 −4.25	+3.54 −3.15	+2.32 −2.39
Jet vertex fraction [%]	-	∓0.19	−0.30 +0.29	∓0.41	−0.49 +0.47	−0.55 +0.54	+0.91 −0.90	±0.58	+0.32 −0.31	±0.12	-
b-Quark tagging efficiency (eigenvector 0) [%]	+0.84 −0.78	+0.93 −0.87	+0.86 −0.81	+0.76 −0.72	+0.62 −0.59	+0.10 −0.13	−2.27 +2.12	-	+0.92 −0.86	+1.23 −1.15	+1.20 −1.12
b-Quark tagging efficiency (eigenvector 1) [%]	−0.29 +0.28	−0.79 +0.77	−1.26 +1.24	−1.64 +1.60	−1.94 +1.91	−2.52 +2.47	+1.62 −1.57	+0.68 −0.66	-	−0.52 +0.50	−0.96 +0.94
b-Quark tagging efficiency (eigenvector 2) [%]	∓0.10	∓0.38	−0.65 +0.66	−0.88 +0.90	−1.06 +1.08	−1.30 +1.32	+0.15 −0.16	±0.14	-	−0.36 +0.37	−0.64 +0.65
b-Quark tagging efficiency (eigenvector 3) [%]	+0.17 −0.18	±0.20	±0.12	-	-	∓0.21	∓0.41	∓0.11	±0.11	±0.18	±0.12
c-Quark tagging efficiency (eigenvector 0) [%]	-	-	-	∓0.10	∓0.17	-	+0.21 −0.22	-	-	-	-
c-Quark tagging efficiency (eigenvector 1) [%]	-	∓0.16	∓0.28	∓0.48	−0.63 +0.64	∓0.86	±0.34	±0.17	-	∓0.14	∓0.34
c-Quark tagging efficiency (eigenvector 2) [%]	-	∓0.10	∓0.18	∓0.24	∓0.34	∓0.52	-	-	-	-	∓0.16
Light-jet tagging efficiency (eigenvector 0) [%]	-	∓0.18	∓0.40	−0.73 +0.76	∓1.24	∓1.53	+0.72 −0.96	+0.23 −0.26	-	−0.32 +0.33	−0.49 +0.47
Light-jet tagging efficiency (eigenvector 1) [%]	-	-	∓0.12	∓0.25	∓0.33	−0.46 +0.45	-	-	-	-	∓0.10
Light-jet tagging efficiency (eigenvector 2) [%]	-	-	-	±0.14	±0.29	±0.15	−0.47 +0.38	-	-	-	-
Light-jet tagging efficiency (eigenvector 3) [%]	-	−0.16 +0.17	∓0.24	−0.39 +0.40	−0.48 +0.49	∓0.75	−0.17 +0.10	±0.11	-	−0.13 +0.14	−0.30 +0.31
Light-jet tagging efficiency (eigenvector 5) [%]	-	-	-	-	-	-	-	-	-	-	∓0.11
Light-jet tagging efficiency (eigenvector 7) [%]	-	-	-	-	-	-	-	-	-	-	-
Light-jet tagging efficiency (eigenvector 8) [%]	-	-	-	-	∓0.19	∓0.27	-	-	-	-	-
b-Quark tagging extrapolation [%]	-	-	±0.19	±0.53	±0.96	±1.73	-	-	-	-	±0.14
Electron energy resolution [%]	-	-	-	-	-	-	-	-	-	-	-
Electron energy scale [%]	-	-	-	+0.11 −0.22	+0.31 −0.28	+0.40 −0.21	-	-	-	-	-
Electron identification efficiency [%]	-	-	±0.13	±0.20	±0.27	±0.42	-	-	-	-	±0.10
Electron isolation efficiency [%]	-	-	±0.14	±0.21	±0.27	±0.39	-	-	-	-	±0.12
Muon (ID) momentum resolution [%]	-	-	-	-	-	-	-	-	-	-	-
Muon (MS) momentum resolution [%]	-	-	-	-	- −0.21	+0.22 -	-	-	-	-	-
Muon identification syst [%]	-	-	-	±0.14	±0.19	±0.25	-	-	-	-	-
E_T^{miss} Soft jet resolution para [%]	∓0.22	∓0.50	∓0.17	∓0.47	∓0.58	∓0.48	±1.14	±0.25	∓0.20	∓0.27	∓0.32
E_T^{miss} Soft jet resolution perp [%]	∓0.22	∓0.36	∓0.36	∓0.56	∓0.40	∓0.55	±0.83	±0.30	∓0.11	∓0.41	∓0.27
E_T^{miss} Soft jet scale [%]	−0.28 +0.29	−0.43 +0.47	−0.34 +0.39	−0.47 +0.58	−0.57 +0.25	−0.43 +0.47	+1.11 −0.88	+0.29 −0.38	−0.10 +0.13	−0.41 +0.33	−0.40 +0.44
Z+jets cross-section [%]	∓0.15	-	-	±0.21	±0.39	+0.67 −0.68	-	−0.25 +0.26	∓0.26	∓0.17	-
Monte Carlo sample statistics [%]	±0.28	±0.38	±0.58	±0.95	±1.47	±1.86	±1.55	±0.38	±0.38	±0.49	±0.69
ISR/FSR + scale [%]	+0.67 -	- −0.21	- −0.91	- −1.18	+1.47 -	+2.73 -	- −2.11	+0.13 −0.76	+0.50 −1.88	- −1.90	- −0.65
Alternate hard-scattering model [%]	∓0.95	∓0.82	∓2.24	∓3.13	∓3.26	±5.65	∓7.98	±2.06	∓0.52	±2.25	±2.46
Alternate parton-shower model [%]	±2.60	±0.83	±0.55	-	∓1.79	±1.08	±1.06	±3.47	∓2.97	±3.40	±0.92
Inter PDF [%]	-	-	-	∓0.40	±0.14	∓0.18	±0.13	∓0.12	-	-	-
Intra PDF [%]	∓0.10	-	∓0.10	±1.96	±0.82	±1.43	±0.37	±0.27	∓0.12	∓0.13	-
Fakes overall normalization, el [%]	∓0.36	∓0.10	∓0.12	-	+0.58 −0.59	+2.01 −2.04	±0.27	−0.30 +0.31	−0.39 +0.40	∓0.19	∓0.40
Fakes overall normalization, mu [%]	-	∓0.14	∓0.35	∓0.56	∓0.55	∓0.55	∓0.12	-	-	∓0.13	−0.51 +0.52
Fakes alternative parametrization [%]	±1.04	±1.59	±1.75	±2.36	±2.75	±1.63	∓3.09	∓0.53	±0.54	±1.67	±2.51
W+jets heavy flavour component [%]	∓0.81	∓1.30	±2.91	∓0.33	∓1.11	∓1.84	±6.13	∓2.25	∓3.42	∓3.09	∓0.57

Bins [GeV] x	4310–4500	4500–4700	4700–5400	5400–5475.50	5475.50–5530	5530–5655	5655–5800	5800–5960	5960–6140	6140–6400	6400–7100
$1/\sigma \cdot d\sigma$ / $dm^{t\bar{t}}vsy^{t,had}$	$2.65 \cdot 10^{-5}$	$1.03 \cdot 10^{-5}$	$2.14 \cdot 10^{-6}$	$9.61 \cdot 10^{-5}$	$1.81 \cdot 10^{-4}$	$1.68 \cdot 10^{-4}$	$9.94 \cdot 10^{-5}$	$4.84 \cdot 10^{-5}$	$2.18 \cdot 10^{-5}$	$8.78 \cdot 10^{-6}$	$1.43 \cdot 10^{-6}$
Total Uncertainty [%]	+6.98 −7.60	+7.83 −9.08	+9.70 −9.93	+19.2 −18.2	+17.2 −17.1	+15.3 −14.7	+12.8 −12.5	+11.6 −11.1	+11.9 −13.2	+17.0 −13.2	+15.6 −16.5
Statistics [%]	±1.6	±2.6	±3.4	±1.4	±1.0	±0.8	±0.9	±1.3	±1.8	±2.6	±4.0
Systematics [%]	+6.69 −7.33	+7.19 −8.53	+8.79 −9.05	+19.1 −18.1	+17.2 −17.0	+15.3 −14.7	+12.8 −12.4	+11.5 −11.0	+11.7 −13.0	+16.7 −12.8	+14.8 −15.8
Jet energy resolution [%]	-	∓2.08	±0.30	±0.64	±0.21	±1.94	±5.44	±0.97	±0.87	±8.26	±1.42
b-Tagged jet energy scale (JES) [%]	+0.37 −0.38	+0.57 −0.41	+0.17 −0.33	−1.47 +1.41	−0.47 +0.48	+0.41 −0.34	+0.40 −0.32	+0.18 −0.14	+0.21 −0.55	+0.74 −0.11	- −0.32
Effective detector NP set 1 (JES) [%]	-	+0.21 -	+0.36 −0.14	-	-	-	+0.19 −0.15	+0.20 −0.22	-	+0.18 −0.13	-
Effective detector NP set 2 (JES) [%]	-	+0.21 -	+0.21 -	-	-	-	+0.11 −0.10	+0.14 −0.15	-	+0.17 −0.12	-
Effective mixed NP set 1 (JES) [%]	+0.49 −0.68	+1.51 −0.71	+1.51 −1.26	−0.32 +0.39	−0.22 +0.10	+0.23 −0.19	+0.44 −0.45	+0.73 −0.49	+0.38 −1.18	+2.00 −0.37	- −1.74
Effective mixed NP set 2 (JES) [%]	-	-	-	-	-	-	-	∓0.11	-	−0.19 +0.14	-
Effective mixed NP set 3 (JES) [%]	-	-	-	-	-	-	-	-	-	-	-
Effective modelling NP set 1 (JES) [%]	+0.87 −0.83	- −0.79	−0.36 +0.49	+5.38 −4.42	+5.45 −4.93	+5.21 −4.60	+4.23 −4.07	+3.88 −3.76	+3.59 −3.87	+4.42 −1.46	+1.93 −3.85
Effective modelling NP set 2 (JES) [%]	+0.28 −0.52	+0.58 -	+0.40 −0.63	−0.95 +0.94	−0.58 +0.60	−0.45 +0.37	−0.22 +0.27	- +0.22	- −0.28	+1.19 -	- −1.07
Effective modelling NP set 3 (JES) [%]	−0.79 +0.29	- +0.57	−0.29 +0.27	+0.88 −0.87	±0.49	+0.19 −0.25	-	-	-	−0.34 +1.25	- −0.39
Effective modelling NP set 4 (JES) [%]	-	+0.23 -	+0.26 -	- −0.20	+0.13 −0.24	+0.28 −0.20	+0.29 −0.31	+0.26 −0.18	+0.15 −0.20	+0.22 −0.20	-
Effective statistical NP set 1 (JES) [%]	-	+0.49 -	−0.20 -	+1.16 −0.98	±0.78	+0.76 −0.75	+0.77 −0.91	+0.75 −0.59	+0.55 −0.60	+0.61 −0.18	+0.41 −0.23
Effective statistical NP set 2 (JES) [%]	-	+0.20 -	+0.33 −0.37	−0.85 +0.97	−0.67 +0.65	−0.69 +0.66	−0.75 +0.66	−0.54 +0.68	−0.45 +0.47	−0.10 +0.28	- +0.22
Effective statistical NP set 3 (JES) [%]	−0.25 -	−0.32 +0.34	−0.45 +0.32	- −0.13	-	-	-	-	-	−0.11 +0.58	−0.44 +0.19
Effective statistical NP set 4 (JES) [%]	+0.23 −0.43	+0.25 −0.13	+0.16 −0.26	−0.54 +0.56	−0.29 +0.20	-	+0.26 −0.13	+0.23 −0.12	- −0.25	+0.80 −0.43	-
Effective statistical NP set 5 (JES) [%]	+0.12 −0.31	-	-	±0.18	-	−0.10 +0.13	−0.11 +0.14	-	- −0.25	+0.20 -	-
Effective statistical NP set 6 (JES) [%]	-	-	+0.26 −0.11	-	+0.16 −0.20	+0.16 −0.14	-	-	-	- +0.20	-
Effective statistical NP set 7 (JES) [%]	- −0.22	+0.31 −0.14	+0.27 −0.10	-	- −0.18	±0.11	+0.32 −0.21	+0.19 −0.25	+0.12 −0.13	+0.55 −0.22	-
η intercalibration model (JES) [%]	+1.19 −0.86	+1.71 −1.28	+1.38 −1.27	+0.73 −0.51	+0.94 −1.06	+1.46 −1.32	+1.49 −1.48	+1.46 −1.82	+1.34 −1.90	+2.60 −1.18	+1.38 −2.67
η intercalibration non closure (JES) [%]	−0.18 +0.17	- +0.34	−0.16 -	−0.43 +0.72	−0.43 +0.38	∓0.52	−0.49 +0.60	−0.22 +0.36	−1.01 +0.54	−0.56 +1.23	−0.74 +0.16
η intercalibration total stat (JES) [%]	+0.17 −0.21	+0.67 -	+0.44 -	+0.78 −0.46	+0.53 −0.68	+0.93 −0.88	+0.86 −0.98	+0.98 −0.69	+0.67 −0.89	+1.02 −0.32	+0.27 −0.62
Flavour composition (JES) [%]	+1.44 −1.37	+0.68 −1.94	+0.66 −0.30	+6.88 −6.44	+6.20 −6.81	+6.17 −6.23	+5.27 −5.37	+4.91 −4.99	+4.28 −5.20	+5.88 −2.77	+3.87 −5.48
Flavour response (JES) [%]	−0.76 +0.73	−0.80 +0.62	-	−3.03 +3.67	−3.60 +3.37	−3.34 +3.16	−3.00 +2.81	−2.87 +2.61	−3.20 +2.24	−1.67 +3.28	−2.25 +1.61
Pile-up offset μ (JES) [%]	-	+0.37 -	- −0.32	−0.17 +0.37	−0.41 +0.31	−0.29 +0.36	−0.40 +0.25	−0.30 +0.28	-	−0.11 +0.91	-
Pile-up offset N_{PV} (JES) [%]	+0.50 −0.41	−0.26 +0.13	−0.44 -	+1.71 −0.49	+0.83 −0.49	+1.03 −1.05	+1.28 −1.04	+1.23 −0.93	+0.79 −1.34	+1.71 -	+0.11 −0.84
Pile-up offset p_T (JES) [%]	+0.59 −0.64	+1.34 −0.82	+1.54 −1.10	∓1.59	−0.71 +0.58	-	+0.23 −0.26	+0.87 −0.53	+0.13 −0.66	+1.74 −0.74	+0.31 −2.07
Pile-up offset ρ topology (JES) [%]	+1.55 −1.06	- −1.55	−0.30 +0.47	+7.24 −6.82	+7.86 −7.15	+8.06 −7.12	+6.84 −6.03	+5.98 −5.55	+5.43 −5.84	+5.88 −2.51	+3.28 −4.91
Jet vertex fraction [%]	-	∓0.13	−0.28 +0.26	+1.21 −1.20	+0.97 −0.96	+0.74 −0.73	±0.53	+0.43 −0.44	+0.33 −0.34	±0.32	+0.23 −0.25
b-Quark tagging efficiency (eigenvector 0) [%]	+1.01 −0.96	+0.92 −0.87	+0.61 −0.60	−1.57 +1.43	-	+1.17 −1.11	+1.52 −1.43	+1.62 −1.53	+1.39 −1.50	+1.53 −1.44	+1.48 −1.39
b-Quark tagging efficiency (eigenvector 1) [%]	−1.39 +1.36	−1.77 +1.74	−2.05 +2.00	+1.54 −1.50	+0.85 −0.83	±0.19	−0.33 +0.32	−0.66 +0.64	−1.00 +0.97	−1.34 +1.30	−1.83 +1.79
b-Quark tagging efficiency (eigenvector 2) [%]	−0.88 +0.89	−1.05 +1.07	−1.29 +1.32	-	-	−0.13 +0.12	∓0.41	−0.68 +0.69	−0.90 +0.91	−1.13 +1.14	−1.41 +1.44
b-Quark tagging efficiency (eigenvector 3) [%]	-	-	∓0.22	∓0.33	∓0.13	-	+0.15 −0.16	±0.10	-	∓0.10	−0.22 +0.23
c-Quark tagging efficiency (eigenvector 0) [%]	-	-	-	+0.19 −0.20	±0.12	-	-	-	-	-	∓0.12
c-Quark tagging efficiency (eigenvector 1) [%]	∓0.54	∓0.66	−0.94 +0.93	±0.34	±0.21	-	∓0.17	∓0.38	∓0.64	−0.84 +0.83	∓1.17
c-Quark tagging efficiency (eigenvector 2) [%]	∓0.32	∓0.36	∓0.56	±0.10	±0.11	-	-	∓0.17	∓0.34	∓0.44	∓0.68
Light-jet tagging efficiency (eigenvector 0) [%]	−1.15 +1.17	−1.27 +1.31	−2.06 +2.03	-	-	-	−0.17 +0.16	−0.56 +0.55	−1.17 +1.18	−1.55 +1.61	−2.24 +2.20
Light-jet tagging efficiency (eigenvector 1) [%]	-	∓0.25	∓0.53	+0.28 −0.27	±0.18	-	-	-	-	−0.13 +0.16	−0.57 +0.56
Light-jet tagging efficiency (eigenvector 2) [%]	-	±0.11	±0.20	-	-	-	-	-	±0.12	±0.10	+0.16 −0.15
Light-jet tagging efficiency (eigenvector 3) [%]	∓0.44	∓0.59	∓0.84	+0.34 −0.33	+0.28 −0.27	-	-	−0.26 +0.27	−0.44 +0.45	−0.58 +0.59	∓0.94
Light-jet tagging efficiency (eigenvector 5) [%]	∓0.17	-	-	-	-	-	-	-	∓0.14	-	-
Light-jet tagging efficiency (eigenvector 7) [%]	-	-	-	-	-	-	-	-	-	±0.11	-
Light-jet tagging efficiency (eigenvector 8) [%]	-	∓0.22	∓0.44	-	-	-	-	-	-	∓0.15	∓0.42
b-Quark tagging extrapolation [%]	±0.53	±0.91	+1.65 −1.64	-	∓0.10	-	-	±0.14	±0.47	+0.92 −0.93	±1.76
Electron energy resolution [%]	-	-	-	-	-	-	-	-	-	-	-
Electron energy scale [%]	+0.17 −0.18	-	- −0.26	−0.12 +0.11	-	-	-	-	-	+0.16 -	+0.26 −0.22
Electron identification efficiency [%]	±0.16	±0.23	±0.34	-	-	-	-	-	±0.14	+0.21 −0.22	±0.34
Electron isolation efficiency [%]	±0.19	±0.25	+0.33 −0.34	-	-	-	-	±0.12	+0.17 −0.18	±0.24	±0.34
Muon (ID) momentum resolution [%]	-	- −0.27	- +0.24	-	-	-	-	-	-	-	-
Muon (MS) momentum resolution [%]	-	-	-	-	-	-	-	-	−0.10 +0.11	-	-
Muon identification syst [%]	±0.12	±0.16	±0.26	-	-	-	-	-	-	±0.13	±0.22
E_T^{miss} Soft jet resolution para [%]	∓0.56	±0.33	∓1.10	±0.85	±0.18	±0.14	∓0.28	∓0.45	∓0.55	±0.17	∓0.21
E_T^{miss} Soft jet resolution perp [%]	∓0.40	-	∓0.72	±0.96	±0.39	-	∓0.32	∓0.23	∓0.77	±0.40	∓0.48
E_T^{miss} Soft jet scale [%]	−0.48 +0.63	−0.21 +0.40	−0.53 +0.48	+0.95 −1.03	+0.34 −0.55	-	−0.37 +0.32	−0.10 +0.28	−0.69 +0.31	+0.75 -	−0.81 +0.56
Z+jets cross-section [%]	+0.13 −0.14	±0.28	±0.52	∓0.17	∓0.27	−0.27 +0.28	∓0.19	∓0.11	-	±0.16	+0.36 −0.37
Monte Carlo sample statistics [%]	±1.09	±1.65	±2.15	±0.93	±0.66	±0.52	±0.60	±0.81	±1.16	±1.65	±2.33
ISR/FSR + scale [%]	+1.65 −3.51	- −4.59	- −2.46	+3.21 −0.78	+1.15 −1.62	+1.10 −1.70	+1.00 −1.45	+2.04 -	+5.26 −5.78	+3.33 −1.77	+5.86 -
Alternate hard-scattering model [%]	±1.73	∓3.07	∓1.71	±10.2	±8.81	±4.91	±1.20	±3.53	∓2.85	∓0.94	±10.3
Alternate parton-shower model [%]	∓3.06	±2.96	±5.95	±9.10	±8.16	±7.15	±4.38	±3.15	±2.50	±6.88	±2.11
Inter PDF [%]	-	∓0.22	-	±0.15	-	-	-	-	-	-	±0.52
Intra PDF [%]	±0.25	±1.35	±0.88	±0.82	-	±0.48	-	±0.29	±0.30	±0.39	±2.90
Fakes overall normalization, el [%]	±0.10	+0.92 −0.93	+2.19 −2.22	-	−0.24 +0.25	∓0.47	-	∓0.46	∓0.33	−0.10 +0.11	+0.72 −0.73
Fakes overall normalization, mu [%]	∓0.48	∓0.49	∓0.88	±0.14	-	∓0.21	∓0.28	∓0.37	∓0.50	∓0.79	∓0.71
Fakes alternative parametrization [%]	±2.59	±1.26	±2.00	∓0.74	∓0.48	±0.37	±1.15	±2.20	±2.31	±3.36	±2.87
W+jets heavy flavour component [%]	∓2.54	∓2.05	∓1.02	±1.42	∓0.88	∓1.72	±0.80	∓2.02	∓3.04	±1.10	±0.30

TABLE F.31: Table of systematics for the relative differential cross-section at the particle level for the $m_{t\bar{t}}$ in bins of jet multiplicity observable.

Bins [GeV] x	0–30	30–65	65–120	120–190	190–270	270–800	800–840	840–910	910–1000	1000–1110	1110–1325	1325–1600	1600–1640	1640–1710	1710–1800	1800–1910	1910–2020	2020–2400	2400–2440	2440–2510	2510–2600	2600–2710	2710–3200
$1/\sigma \cdot d\sigma$ / $dp_T^{t\bar{t}} vs N.jets$	$8.39 \cdot 10^{-3}$	$5.41 \cdot 10^{-3}$	$9.88 \cdot 10^{-4}$	$1.61 \cdot 10^{-4}$	$2.97 \cdot 10^{-5}$	$9.26 \cdot 10^{-7}$	$1.49 \cdot 10^{-3}$	$2.24 \cdot 10^{-3}$	$6.34 \cdot 10^{-4}$	$1.43 \cdot 10^{-4}$	$2.64 \cdot 10^{-5}$	$2.45 \cdot 10^{-6}$	$3.55 \cdot 10^{-4}$	$7.90 \cdot 10^{-4}$	$4.26 \cdot 10^{-4}$	$1.22 \cdot 10^{-4}$	$3.47 \cdot 10^{-5}$	$5.25 \cdot 10^{-6}$	$1.20 \cdot 10^{-4}$	$3.04 \cdot 10^{-4}$	$2.59 \cdot 10^{-4}$	$1.09 \cdot 10^{-4}$	$1.36 \cdot 10^{-5}$
Total Uncertainty [%]	+8.10/−8.56	+5.39/−5.57	+10.0/−9.59	+9.88/−7.40	+9.55/−8.01	+18.4/−16.8	+7.60/−7.15	+5.78/−5.60	+4.81/−3.93	+5.78/−5.07	+8.34/−7.66	+14.8/−17.1	±15.0	±11.1	+5.17/−4.76	+5.23/−5.08	+7.75/−8.06	+9.49/−8.27	+24.3/−21.1	+20.9/−19.0	+13.3/−13.8	+11.4/−10.8	+8.62/−8.41
Statistics [%]	±0.1	±0.1	±0.5	±1.2	±2.6	±6.0	±0.4	±0.2	±0.5	±1.0	±1.6	±4.8	±0.8	±0.4	±0.6	±1.0	±2.1	±2.8	±1.5	±0.7	±0.7	±1.1	±1.4
Systematics [%]	+8.10/−8.55	+5.39/−5.57	+10.0/−9.57	+9.74/−7.21	+9.02/−7.36	+17.1/−15.3	+7.58/−7.13	+5.77/−5.59	+4.77/−3.88	+5.65/−4.93	+8.11/−7.42	+13.8/−16.1	+14.9/−15.0	+11.1/−11.0	+5.12/−4.71	+5.08/−4.93	+7.36/−7.68	+8.90/−7.59	+24.2/−21.0	+20.9/−19.0	+13.2/−13.8	+11.4/−10.7	+8.46/−8.24
Jet energy resolution [%]	∓1.11	∓0.68	±1.24	±0.65	±2.51	∓0.24	±1.62	±0.70	∓0.43	-	±0.26	∓3.17	±1.25	±0.43	∓0.83	∓1.94	∓0.80	±2.59	±2.36	±4.78	±1.03	±1.08	±3.22
b-Tagged jet energy scale (JES) [%]	-	-	-	-	−0.18/+0.17	−0.30/+0.26	-	-	-	-	-/+0.18	−0.30/+0.18	-	-	-	-	−0.28/-	−0.12/+0.32	-/−0.27	+0.22/−0.11	-	-	-/+0.16
Effective detector NP set 1 (JES) [%]	-	-	-	-	-/+0.22	-/+0.29	-	-	-	-	-	−0.17/-	-	-	-	-	-	+0.24/−0.18	+0.26/-	+0.15/−0.10	-	-	-
Effective detector NP set 2 (JES) [%]	-	-	-	-	-	-/+0.25	-	-	-	-	-	−0.15/+0.38	-	-	-	-	-	-	-	-	-	-	-
Effective mixed NP set 1 (JES) [%]	-	−0.11/+0.10	−0.17/+0.15	−0.28/+0.20	−0.28/+0.31	−0.21/+0.60	-	-	-/−0.14	+0.37/−0.32	+1.02/−0.82	+2.07/−2.29	-	-	+0.16/−0.17	+0.52/−0.22	+0.17/−0.63	+1.79/−1.36	+0.22/-	+0.16/-	+0.12/−0.38	+0.40/−0.15	+0.82/−0.80
Effective mixed NP set 2 (JES) [%]	-	-	-	-	-	-	-	-	-	-	-	−0.18/-	-	-	-	-	-	−0.17/+0.16	-	-	-	-	-
Effective mixed NP set 3 (JES) [%]	-	-	-	-	-	-	-	-	-	-	-	-	-	-	-	-	-	-	-	-	-	-	-
Effective modelling NP set 1 (JES) [%]	−1.30/+1.33	−1.64/+1.46	−2.17/+1.93	−2.30/+2.11	−2.62/+2.59	−2.56/+5.00	+2.67/−2.42	+0.75/−0.77	−1.31/+1.01	−1.65/+1.75	−1.91/+2.36	−3.55/+2.56	+5.35/−5.16	+3.77/−3.78	+1.71/−1.35	-	−1.11/+0.47	−1.37/+1.22	+8.80/−6.65	+7.04/−5.82	+4.29/−4.66	+3.05/−2.71	+1.84/−1.66
Effective modelling NP set 2 (JES) [%]	+0.11/−0.10	+0.11/−0.12	+0.13/−0.18	+0.20/−0.31	+0.34/−0.29	+0.76/−0.25	−0.33/+0.34	−0.11/+0.12	+0.24/−0.25	+0.33/−0.25	+0.48/−0.61	+1.52/−1.58	−0.68/+0.53	−0.44/+0.45	-	+0.28/−0.15	+0.23/−0.36	+1.29/−1.09	−0.65/+0.54	−0.66/+0.78	−0.44/+0.33	−0.16/+0.17	+0.33/−0.27
Effective modelling NP set 3 (JES) [%]	-	-	∓0.13	−0.20/+0.12	−0.16/+0.27	-/+0.31	±0.27	-	−0.26/+0.23	−0.25/+0.30	−0.46/+0.40	−0.56/+0.28	+0.44/−0.56	+0.32/−0.31	-	−0.24/+0.37	−0.22/+0.33	−0.42/+0.50	+0.58/−0.27	+0.56/−0.45	+0.13/−0.27	-	−0.29/+0.17
Effective modelling NP set 4 (JES) [%]	-	-	−0.14/+0.13	−0.21/+0.14	−0.20/+0.27	-/+0.56	-	-	-	-	-	-	+0.21/−0.23	+0.14/−0.15	-	-	-	-	+0.32/−0.21	+0.33/−0.27	+0.21/−0.29	+0.17/−0.10	-/−0.15
Effective statistical NP set 1 (JES) [%]	−0.23/+0.25	∓0.25	−0.35/+0.32	−0.53/+0.30	−0.61/+0.69	−0.50/+1.26	+0.44/−0.49	+0.15/−0.14	−0.24/+0.25	−0.37/+0.33	−0.16/+0.17	−0.32/+0.33	+0.93/−0.97	+0.66/−0.72	+0.27/−0.25	−0.10/+0.30	−0.16/+0.17	-	+1.23/−0.91	+1.21/−1.05	+0.69/−0.87	+0.59/−0.42	+0.22/−0.37
Effective statistical NP set 2 (JES) [%]	+0.21/−0.20	±0.22	+0.28/−0.31	+0.30/−0.47	+0.62/−0.48	+1.09/−0.44	−0.43/+0.40	∓0.14	+0.22/−0.20	+0.19/−0.24	+0.50/−0.59	+0.88/−0.62	−0.83/+0.84	−0.62/+0.59	−0.21/+0.23	+0.17/−0.10	+0.20/−0.11	+0.54/−0.55	−0.88/+1.10	−0.93/+1.02	−0.78/+0.64	−0.43/+0.53	-
Effective statistical NP set 3 (JES) [%]	-	-	-	-	-	-	-	-	-	-	−0.74/+0.67	−0.69/+0.53	-	-	-	-	−0.36/+0.28	−0.73/+0.76	-	-	-	-	−0.34/+0.27
Effective statistical NP set 4 (JES) [%]	-	-	-	-	-	-	−0.11/+0.13	-	+0.19/−0.18	+0.20/−0.24	-	−0.46/+0.12	−0.19/+0.20	−0.12/-	±0.13	+0.28/−0.20	-	-	+0.32/-	-/+0.11	-	+0.10/−0.15	-
Effective statistical NP set 5 (JES) [%]	-	-	-	-	-	+0.22	-	-	-	+0.28/−0.21	+0.28/−0.31	−0.28/-	-	-	-	+0.21/-	+0.31/−0.26	−0.12/+0.16	-	-	−0.12/+0.10	-	-/−0.15
Effective statistical NP set 6 (JES) [%]	-	-	−0.12/+0.10	-	−0.11/+0.24	−0.10/+0.29	-	-	−0.14/+0.13	-	+0.19/−0.24	−0.45/+0.37	+0.13/−0.17	±0.13	-	-	+0.17/−0.10	-	+0.20/−0.16	+0.25/−0.23	-	-	-
Effective statistical NP set 7 (JES) [%]	-	-	−0.14/+0.13	−0.12/+0.11	−0.14/+0.25	−0.10/+0.39	-	-	-	-	-/−0.20	−0.17/+0.26	+0.11/−0.15	-	-	-	-	+0.21/−0.15	+0.28/−0.13	+0.24/−0.17	+0.12/−0.21	+0.15/−0.11	-/−0.14
η intercalibration model (JES) [%]	∓0.28	−0.57/+0.58	−0.87/+0.84	−0.75/+0.71	−1.33/+0.78	−0.58/+1.74	+0.45/−0.40	±0.27	−0.16/+0.20	−0.23/+0.37	-/+0.32	−0.44/+0.63	+1.26/−1.48	+1.04/−1.12	+0.55/−0.50	+0.36/−0.23	+0.18/−0.45	+0.41/−0.61	+2.02/−1.71	+1.77/−1.62	+1.35/−1.68	+0.89/−0.82	+1.02/−0.94
η intercalibration non closure (JES) [%]	+0.12/−0.11	+0.22/−0.21	±0.32	-/−0.19	+0.34/−0.63	+0.79/−0.14	−0.19/+0.18	-	-	−0.14/+0.13	-	-	−0.54/+0.34	−0.28/+0.39	−0.19/+0.12	−0.14/+0.32	−0.43/+0.38	−0.40/+0.31	−0.39/+0.67	−0.41/+0.80	−0.75/+0.39	−0.32/+0.52	−0.46/+0.31
η intercalibration total stat (JES) [%]	−0.19/+0.20	−0.30/+0.32	∓0.46	−0.55/+0.35	−0.72/+0.71	−0.37/+1.37	+0.31/−0.32	+0.16/−0.18	−0.17/+0.19	−0.23/+0.29	−0.15/+0.20	−0.84/+0.32	+0.76/−0.86	+0.68/−0.74	+0.39/−0.38	-	-	+0.21/-	+1.14/−0.87	+1.26/−0.96	+0.77/−1.01	+0.55/−0.52	+0.31/−0.38
Flavour composition (JES) [%]	−0.95/+1.05	−2.34/+2.57	−3.82/+3.90	−2.84/+2.96	−3.02/+4.15	−2.15/+5.52	+2.70/−3.26	+0.93/−1.09	∓1.42	−2.22/+2.43	−1.79/+2.47	−2.91/+1.85	+6.00/−6.80	+4.58/−4.94	+1.99/−1.91	+0.32/−0.10	−1.21/+0.32	−0.94/+0.95	+9.66/−8.74	+8.01/−7.49	+5.50/−6.38	+4.25/−4.17	+2.63/−2.66
Flavour response (JES) [%]	+0.55/−0.52	+1.39/−1.32	+2.26/−2.17	+1.53/−1.72	+1.52/−1.98	+3.29/−0.83	−1.64/+1.47	−0.58/+0.56	+0.63/−0.62	+1.20/−0.84	+1.16/−1.14	+1.45/−2.38	−3.73/+3.19	−2.64/+2.48	−1.05/+1.18	+0.41/-	-/−0.32	+0.73/−0.38	−4.24/+5.06	−4.09/+4.26	−3.55/+2.86	−2.25/+2.16	−1.46/+1.44
Pile-up offset μ (JES) [%]	-	-	+0.12/−0.16	-/−0.32	-	+0.53/-	−0.20/+0.13	-	-	+0.22/−0.13	-/−0.16	-/−0.53	−0.17/+0.26	−0.23/+0.21	-	-	+0.20/-	+0.40/-	−0.35/+0.48	−0.26/+0.47	−0.45/+0.22	−0.23/+0.32	-
Pile-up offset N_{PV} (JES) [%]	−0.25/+0.31	−0.37/+0.29	−0.56/+0.39	−0.61/+0.15	−1.01/+1.50	−0.39/+1.51	+0.27/−0.22	+0.12/−0.16	-	−0.39/+0.43	−0.37/+0.10	−0.43/+0.28	+1.21/−1.15	+0.77/−0.86	+0.67/−0.33	+0.29	−0.23/+0.24	-/+0.33	+2.67/−1.88	+1.91/−0.97	+0.59/−1.09	+0.83/−0.50	±0.53
Pile-up offset p_T (JES) [%]	-	-	−0.13/+0.14	-	-	-	∓0.49	-	+0.42/−0.48	+0.67/−0.48	+0.65/−0.48	+0.63/−1.07	−0.54/+0.59	−0.27/+0.30	+0.27/−0.31	-/+0.51	+0.33/−0.62	+0.80/−0.86	−0.30/+0.82	−0.40/+0.59	-/−0.22	+0.28/−0.30	+0.54/−0.46
Pile-up offset ρ topology (JES) [%]	−1.98/+2.06	−2.37/+2.18	−3.10/+2.76	−3.21/+3.13	−3.34/+4.25	−3.76/+6.81	+3.47/−3.40	+1.08/−1.31	−1.66/+1.37	∓2.83	−2.87/+3.41	−4.69/+3.57	+7.65/−7.31	+5.73/−5.45	+2.51/−2.09	−0.36/+0.30	−1.90/+1.02	−2.38/+2.57	+11.7/−9.87	+10.0/−8.29	+7.13/−7.04	+5.07/−4.70	+2.60/−2.31
Jet vertex fraction [%]	∓0.20	∓0.22	−0.31/+0.30	∓0.35	∓0.41	−0.46/+0.45	+0.46/−0.45	±0.15	−0.27/+0.26	−0.43/+0.42	∓0.50	∓0.61	+0.86/−0.85	+0.58/−0.57	±0.17	-	−0.26/+0.25	∓0.40	+1.15/−1.14	+1.02/−1.01	±0.71	±0.44	±0.18
b-Quark tagging efficiency (eigenvector 0) [%]	−0.38/+0.39	−0.27/+0.26	−0.16/+0.13	−0.20/+0.17	−0.13/+0.10	-	-	±0.12	±0.22	±0.29	±0.36	+0.56/−0.55	±0.36	+0.40/−0.39	+0.48/−0.47	+0.60/−0.58	+0.72/−0.69	+0.57/−0.54	+0.75/−0.74	+0.81/−0.79	+0.91/−0.88	+1.00/−0.96	+1.28/−1.21
b-Quark tagging efficiency (eigenvector 1) [%]	-	-	-	−0.33/+0.32	−0.59/+0.57	−1.03/+1.00	-	-	-	−0.33/+0.31	−0.96/+0.93	−1.77/+1.73	±0.14	±0.14	-	−0.20/+0.19	−0.59/+0.57	−1.35/+1.32	+0.33/−0.32	±0.27	+0.13/−0.14	−0.13/+0.12	−0.71/+0.68
b-Quark tagging efficiency (eigenvector 2) [%]	+0.13/−0.12	-	-	-	∓0.17	∓0.42	-	-	∓0.10	∓0.17	∓0.50	−1.11/+1.12	-	-	∓0.16	∓0.27	−0.45/+0.46	−0.90/+0.92	∓0.17	∓0.19	∓0.27	−0.36/+0.37	−0.74/+0.75
b-Quark tagging efficiency (eigenvector 3) [%]	-	-	-	-	-	-	-	-	-	-	-	∓0.16	-	-	-	-	-	-	-	-	-	-	-
c-Quark tagging efficiency (eigenvector 0) [%]	-	-	-	-	-	∓0.11	-	-	-	-	-	∓0.18	-	-	-	-	-	-	±0.13	-	-	-	-
c-Quark tagging efficiency (eigenvector 1) [%]	-	-	-	-	∓0.10	∓0.11	-	-	-	-	-	∓0.21	-	-	-	-	-	-	−0.18/+0.17	∓0.16	-	-	∓0.10
c-Quark tagging efficiency (eigenvector 2) [%]	-	-	-	-	-	∓0.11	-	-	-	-	-	∓0.11	-	-	-	-	-	-	-	-	-	-	∓0.10
Light-jet tagging efficiency (eigenvector 0) [%]	+0.11/-	-	−0.12/+0.11	−0.46/+0.57	-	−0.28/+0.27	−0.13/+0.19	-	-	-	-	-	−0.29/+0.30	-	-	-	−0.26/+0.28	+0.18/−0.20	−0.47/+0.51	−0.43/+0.44	∓0.29	-	-
Light-jet tagging efficiency (eigenvector 1) [%]	-	-	-	-	−0.12/+0.13	∓0.21	-	-	-	-	-	-	-	-	-	-	-	−0.11/+0.10	-	-	-	-	-
Light-jet tagging efficiency (eigenvector 2) [%]	-	-	-	+0.14/−0.13	-	-	-	-	-	-	-	+0.13/−0.12	-	−0.11/+0.10	-	-	±0.12	-	-	-	-	-	-
Light-jet tagging efficiency (eigenvector 3) [%]	-	-	-	−0.14/+0.16	−0.11/+0.12	∓0.18	-	-	-	-	-	-	-	−0.13/+0.12	-	-	-	-	-	-	-	-	-
Light-jet tagging efficiency (eigenvector 7) [%]	-	-	-	+0.14/−0.13	-	-	-	-	-	-	-	-	-	-	-	-	-	-	-	-	-	-	-
Light-jet tagging efficiency (eigenvector 8) [%]	-	-	-	±0.11	-	-	-	-	-	-	-	-	-	-	-	-	-	-	-	-	-	-	-
Light-jet tagging efficiency (eigenvector 9) [%]	-	-	-	−0.11/+0.12	-	-	-	-	-	-	-	-	-	-	-	-	-	-	-	-	-	-	-
b-Quark tagging extrapolation [%]	-	-	-	-	±0.11	±0.28	-	-	-	-	-	+0.85/−0.86	-	-	-	-	-	+0.52/−0.53	-	-	-	-	±0.28
Electron identification efficiency [%]	-	-	-	-	-	±0.12	-	-	-	-	±0.14	+0.25/−0.26	-	-	-	-	±0.10	±0.17	-	-	-	-	±0.14
Electron isolation efficiency [%]	-	-	-	-	-	±0.15	-	-	-	-	±0.17	±0.35	-	-	-	-	±0.13	±0.28	-	-	-	-	±0.22
Muon (ID) momentum resolution [%]	-	-	-	-	-	-	-	-	-	-	-	-	-	-	-	-	-	-	-	-	-	-	-
Muon (MS) momentum resolution [%]	-	-	-	-	-	-/+0.19	-	-	-	-	-	-	-	-	-	-	-	-	-	-	-	-	-
Muon identification syst [%]	-	-	-	-	-	-	-	-	-	-	-	±0.10	-	-	-	-	-	-	-	-	-	-	-
E_T^{miss} Soft jet resolution para [%]	∓0.47	±0.44	±0.64	∓0.54	∓0.43	∓1.18	-	-	-	∓0.10	-	∓0.47	±0.24	-	-	-	∓0.38	∓0.27	±0.20	-	-	-	-
E_T^{miss} Soft jet resolution perp [%]	∓0.45	±0.44	±0.48	∓0.47	∓0.46	∓0.62	-	-	∓0.11	-	±0.20	∓0.60	-	-	∓0.14	±0.17	∓0.35	∓0.11	±0.36	-	∓0.12	-	-
E_T^{miss} Soft jet scale [%]	-	-	−0.28/+0.64	−0.70/+0.78	−0.18/+0.19	−0.27/+0.50	+0.12/−0.13	-	−0.12/+0.14	−0.13/+0.11	-/+0.17	−0.28/-	+0.23/−0.17	-	−0.12/+0.10	-	-/−0.23	−0.34/+0.48	-/−0.30	-	-	-	−0.17/+0.21
Z+jets cross-section [%]	±0.10	±0.11	±0.15	+0.63/−0.64	±0.21	+0.23/−0.24	−0.14/+0.15	∓0.14	-	-	±0.10	±0.13	∓0.16	∓0.19	−0.18/+0.19	∓0.14	-	∓0.14	∓0.17	∓0.15	∓0.18	∓0.21	∓0.22
Monte Carlo sample statistics [%]	±0.13	±0.14	±0.36	±1.11	±1.71	±3.35	±0.34	±0.18	±0.33	±0.63	±1.01	±2.58	±0.58	±0.37	±0.37	±0.64	±1.21	±1.57	±1.03	±0.51	±0.49	±0.67	±0.80
ISR/FSR + scale [%]	-/−2.56	−1.41/-	+2.37/-	+6.71/-	+3.71/-	-/−6.19	+2.99/-	+1.72/-	+3.03/-	+2.26/-	+1.69/-	+0.16/−6.41	+2.40/-	+1.56/-	-	-/−0.26	+1.14/-	+4.41/-	+5.91/-	+3.34/-	+2.31/−0.17	+2.71/-	+1.59/−0.73
Alternate hard-scattering model [%]	∓1.28	∓1.66	∓1.05	∓2.06	±1.54	∓7.41	±1.97	±1.96	∓2.18	±1.76	±3.50	∓11.1	±0.86	±3.94	-	∓1.60	∓2.07	∓3.14	±4.61	±7.56	∓2.98	±3.86	±2.83
Alternate parton-shower model [%]	∓6.92	∓2.76	±5.58	±2.53	∓0.32	±10.2	±3.04	±4.75	∓0.44	±0.13	±2.72	∓1.50	±8.48	±4.92	±1.68	±1.58	±5.20	±3.18	±12.3	±9.56	±6.43	±6.02	±3.22
Inter PDF [%]	-	-	-	-	±0.26	-	-	-	-	-	-	-	∓0.16	-	-	-	∓0.14	±0.26	-	-	-	-	±0.21
Intra PDF [%]	-	∓0.11	-	±0.12	±0.61	±0.83	±0.10	-	∓0.11	±0.49	±0.31	±0.54	±0.47	±0.13	∓0.12	±0.28	±0.50	±0.55	±0.29	±0.31	-	-	±1.15
Fakes overall normalization, el [%]	−0.83/+0.84	+0.73/−0.74	+2.66/−2.67	+1.26/−1.28	−0.98/+1.00	−0.81/+0.82	−0.29/+0.30	∓0.23	-	∓0.19	±0.28	∓0.12	-	∓0.13	∓0.36	−0.42/+0.43	∓0.29	−0.54/+0.55	±0.31	±0.19	∓0.40	−0.66/+0.67	−0.74/+0.75
Fakes overall normalization, mu [%]	∓0.26	±0.19	+1.09/−1.08	±0.84	∓0.10	∓0.13	∓0.16	-	-	-	∓0.39	∓0.56	∓0.13	∓0.13	-	∓0.19	∓0.24	∓0.61	∓0.32	∓0.10	∓0.19	∓0.32	∓0.61
Fakes alternative parametrization [%]	-	∓0.55	∓1.44	∓0.50	±2.05	±1.56	∓0.13	-	±0.77	±1.53	±3.33	±3.46	∓0.60	∓0.26	±0.83	±1.82	±2.45	±3.19	∓0.84	∓1.04	±0.95	±1.99	±3.49
W+jets heavy flavour component [%]	±1.47	±0.31	∓0.87	∓2.54	∓1.46	∓0.65	±1.45	∓0.26	∓1.16	∓0.65	∓1.40	-	∓1.05	∓1.57	∓2.31	∓3.27	∓3.19	∓0.58	∓3.33	±1.21	∓1.88	∓1.82	±0.81

TABLE F.32: Table of systematics for the relative differential cross-section at the particle level for the $p_T^{t\bar{t}}$ in bins of jet multiplicity observable.

Bins [GeV] x [GeV]	0–30	30–70	70–120	120–240	240–800	800–830	830–870	870–920	920–1040	1040–1600	1600–1640	1640–1670	1670–1730	1730–1790	1790–2400	2400–2440	2440–2480	2480–2540	2540–3200	3200–3240	3240–3330	3330–4000
$1/\sigma \cdot d\sigma$ / $dm^{t\bar{t}} vs p_T^{t\bar{t}}$	$2.20 \cdot 10^{-3}$	$1.78 \cdot 10^{-3}$	$7.10 \cdot 10^{-4}$	$1.85 \cdot 10^{-4}$	$7.11 \cdot 10^{-6}$	$4.11 \cdot 10^{-3}$	$3.55 \cdot 10^{-3}$	$1.45 \cdot 10^{-3}$	$4.20 \cdot 10^{-4}$	$2.36 \cdot 10^{-5}$	$2.06 \cdot 10^{-3}$	$1.65 \cdot 10^{-3}$	$7.39 \cdot 10^{-4}$	$3.05 \cdot 10^{-4}$	$2.77 \cdot 10^{-5}$	$1.29 \cdot 10^{-3}$	$9.97 \cdot 10^{-4}$	$4.33 \cdot 10^{-4}$	$3.78 \cdot 10^{-5}$	$4.05 \cdot 10^{-4}$	$2.22 \cdot 10^{-4}$	$1.48 \cdot 10^{-5}$
Total Uncertainty [%]	±11.0	+8.37/−8.54	±13.7	+5.94/−5.88	+8.98/−9.21	+5.79/−5.90	+2.65/−2.60	+7.65/−7.52	+4.21/−4.38	+4.06/−4.02	+5.10/−5.13	+2.99/−2.94	+5.68/−5.64	+5.47/−4.79	+5.47/−5.56	+7.67/−7.52	+4.19/−4.50	+6.56/−6.24	+5.24/−4.97	+10.4/−9.95	+6.40/−6.65	+7.64/−8.72
Statistics [%]	±0.4	±0.3	±0.6	±0.8	±2.0	±0.3	±0.2	±0.4	±0.5	±1.0	±0.3	±0.3	±0.5	±0.8	±0.9	±0.5	±0.4	±0.7	±0.7	±0.9	±0.8	±1.2
Systematics [%]	±11.0	+8.35/−8.52	±13.7	+5.85/−5.80	+8.66/−8.90	+5.78/−5.89	+2.63/−2.58	+7.64/−7.51	+4.16/−4.33	+3.87/−3.83	+5.07/−5.11	+2.96/−2.90	+5.65/−5.61	+5.37/−4.68	+5.36/−5.45	+7.65/−7.50	+4.15/−4.46	+6.50/−6.18	+5.15/−4.89	+10.3/−9.87	+6.32/−6.57	+7.50/−8.59
Jet energy resolution [%]	∓2.57	∓0.62	±3.16	∓1.36	∓1.23	∓0.61	∓0.59	∓0.13	∓0.67	±0.47	∓0.22	±1.79	±1.40	±0.59	-	±0.16	±1.11	±3.57	±1.21	±1.23	∓1.35	±1.43
b-Tagged jet energy scale (JES) [%]	−1.86/+1.90	−1.70/+1.66	−1.39/+1.50	−1.33/+1.45	−1.54/+1.46	+0.37/−0.39	+0.32/−0.30	±0.25	+0.10/−0.20	−0.14/+0.16	+0.56/−0.60	+0.52/−0.61	+0.50/−0.58	+0.67/−0.50	+0.27/−0.23	+0.61/−0.46	+0.52/−0.47	+0.46/−0.42	+0.35/−0.29	+0.35/−0.45	+0.37/−0.43	+0.16/−0.43
Effective detector NP set 1 (JES) [%]	−0.19/+0.23	∓0.18	−0.10/+0.17	-/+0.15	-	-	-	-	-	-	-	-	-	-	+0.15/-	-	-	-	-	-	-	+0.10/−0.23
Effective detector NP set 2 (JES) [%]	−0.13/+0.18	−0.14/+0.15	-/+0.13	-	-	-	-	-	-	-	-	-	-	-	+0.15/-	-	-	-	-	-	-	+0.12/−0.18
Effective mixed NP set 1 (JES) [%]	−0.91/+0.89	−0.83/+0.82	−0.59/+0.70	−0.41/+0.56	-/+0.24	-	-	-	-	+0.51/−0.38	+0.23/−0.25	+0.17/−0.15	+0.20/−0.24	+0.33/−0.25	+0.68/−0.56	+0.48/−0.41	+0.35/−0.42	+0.36/−0.43	+0.78/−0.60	+0.78/−0.63	+0.62/−0.79	+1.10/−1.29
Effective mixed NP set 2 (JES) [%]	+0.16/−0.11	±0.13	+0.11/-	-	-	-	-	-	-	-	-	-	-	-	-/+0.12	-	-	-	-	-	-	−0.21/+0.14
Effective modelling NP set 1 (JES) [%]	−1.17/+1.43	-	+1.20/−1.17	+1.02/−0.66	−0.77/+0.67	−0.39/+0.35	+0.57/−0.59	+1.55/−1.45	+0.95/−1.08	+0.21/-	−0.81/+0.82	-	+0.82/−0.83	+0.84/−0.66	+0.21/-	−1.50/+1.66	−0.90/+0.60	+0.14/−0.33	-	−2.49/+2.98	−1.55/+1.17	−0.61/+0.53
Effective modelling NP set 2 (JES) [%]	−0.48/+0.53	−0.63/+0.64	−0.56/+0.71	−0.37/+0.44	-	-	∓0.10	−0.15/+0.14	-	+0.14/−0.20	+0.25/−0.32	+0.13/−0.17	±0.10	+0.23/−0.10	+0.33/−0.30	+0.47/−0.40	+0.29/−0.34	+0.23/−0.26	+0.49/−0.33	+0.64/−0.71	+0.51/−0.57	+0.80/−0.90
Effective modelling NP set 3 (JES) [%]	+0.62/−0.59	±0.69	+0.67/−0.55	+0.42/−0.35	+0.33/-	-	-	-	-	−0.17/-	−0.30/+0.23	−0.16/+0.17	−0.18/+0.17	−0.26/+0.35	−0.31/+0.29	−0.39/+0.45	∓0.33	−0.33/+0.31	−0.36/+0.52	∓0.54	−0.49/+0.42	−0.79/+0.66
Effective modelling NP set 4 (JES) [%]	−0.18/+0.22	∓0.13	-	-	-/+0.15	-	-	-/−0.12	-	-	-	-	-	-	+0.14/-	-	-	-	-	-	-	-
Effective statistical NP set 1 (JES) [%]	-	+0.14/−0.17	+0.37/−0.16	+0.21/−0.12	-	-	+0.11/−0.12	+0.22/−0.30	-/−0.15	-	−0.25/+0.18	-	-	-	-	−0.30/+0.34	−0.11/+0.10	-	−0.14/+0.19	−0.51/+0.55	−0.33/+0.17	−0.10/+0.11
Effective statistical NP set 2 (JES) [%]	-	−0.16/+0.15	−0.19/+0.30	−0.11/+0.17	+0.20	-	−0.12/+0.11	−0.26/+0.25	−0.17/-	-	+0.16/−0.23	-	-/+0.12	-	-	+0.30/−0.27	+0.12/−0.11	-	+0.20/−0.17	+0.53/−0.54	+0.31/−0.40	+0.34/−0.30
Effective statistical NP set 3 (JES) [%]	-	-	+0.11/-	+0.11/−0.12	−0.20/+0.29	-	-	-	-	−0.19/+0.21	-	-	-	-	−0.21/+0.13	-	-	-	-/+0.16	−0.31/+0.27	−0.29/+0.26	−0.47/+0.41
Effective statistical NP set 4 (JES) [%]	−0.57/+0.59	∓0.61	−0.48/+0.53	−0.30/+0.34	−0.16/+0.46	-	-	-	+0.12/−0.14	-	+0.21/−0.25	+0.13/−0.15	+0.20/−0.21	+0.30/−0.28	+0.24/−0.26	+0.36/−0.27	+0.25/−0.28	+0.29/−0.28	+0.36/−0.25	+0.27/−0.25	+0.15/−0.25	+0.38/−0.40
Effective statistical NP set 5 (JES) [%]	+0.28/−0.22	+0.24/−0.26	+0.15/−0.16	-	+0.29/−0.15	-	-	∓0.13	−0.12/-	+0.20/−0.19	-	-	−0.11/+0.13	−0.13/+0.17	-	-	-	-	+0.15/-	+0.18/−0.17	-/−0.11	-/−0.16
Effective statistical NP set 6 (JES) [%]	-	-	-	-	+0.23/-	-	-	-/−0.13	-	-	-	-	-	-/+0.11	-	−0.10/+0.12	-	-	-/+0.14	-	-	−0.20/+0.10
Effective statistical NP set 7 (JES) [%]	−0.18/+0.19	∓0.15	-/+0.18	-	-	-	-	-	-	-	-	-	-	-	+0.14/−0.11	-	-	-	+0.13/-	-	-	+0.15/−0.26
η intercalibration model (JES) [%]	−1.31/+1.37	−1.07/+0.93	−0.51/+0.61	−0.42/+0.54	−0.47/+0.59	-	-	+0.36/−0.37	+0.31/−0.43	+0.27/-	+0.12/−0.15	+0.21/−0.25	+0.49/−0.51	+0.64/−0.50	+0.41/−0.25	+0.19/−0.15	±0.41	+0.58/−0.59	+0.65/−0.59	+0.38/−0.34	+0.38/−0.60	+0.77/−0.91
η intercalibration non closure (JES) [%]	+0.39/−0.32	+0.21/−0.24	-	-	-	-	-	-	−0.26/+0.14	−0.19/+0.21	-	-	-	-/+0.14	−0.19/+0.30	-	−0.14/-	−0.15/+0.16	−0.23/+0.28	−0.12/+0.18	−0.23/-	−0.40/+0.29
η intercalibration total stat (JES) [%]	−0.63/+0.67	−0.47/+0.42	-/+0.20	−0.11/+0.16	−0.31/+0.51	-	+0.10/−0.11	+0.35/−0.34	+0.14/−0.25	+0.11/−0.16	-	-	+0.26/−0.32	+0.39/−0.24	+0.21/-	-	-	+0.24/−0.32	-	−0.38/+0.27	−0.26/-	+0.13/−0.16
Flavour composition (JES) [%]	−0.75/+0.80	+0.10/−0.26	+1.66/−1.64	+1.30/−1.43	-/−0.40	−0.21/+0.13	+0.17/−0.33	+1.40/−1.32	+1.13/−1.30	+0.57/−0.36	−0.77/+0.92	−0.52/+0.44	+0.56/−0.53	+1.02/−0.59	+0.24/-	−1.55/+1.81	−1.07/+1.09	-/−0.17	+0.42/−0.16	−2.44/+2.96	−1.73/+1.72	-/+0.20
Flavour response (JES) [%]	+0.68/−0.61	-/−0.33	−0.61/+0.70	−0.76/+0.73	+0.21/-	-	−0.10/+0.14	−0.81/+0.78	−0.79/+0.71	−0.25/+0.41	+0.39/−0.45	+0.12/−0.21	−0.45/+0.43	−0.31/+0.65	−0.18/+0.23	+0.89/−0.73	+0.43/−0.50	−0.21/-	−0.11/+0.31	+1.47/−1.19	+0.83/−1.06	-
Pile-up offset μ (JES) [%]	+0.17/-	-	-	-	+0.27/-	-	-	−0.18/+0.11	-	-	-	-	-	-	-	-	-	-	-	+0.11/−0.12	-	-
Pile-up offset N_{PV} (JES) [%]	−0.33/+0.64	−0.33/+0.17	-	+0.28/-	-	-	-	+0.42/−0.36	+0.33/−0.49	-	−0.14/-	-	+0.32/−0.38	+0.57/−0.20	+0.13/−0.11	−0.13/+0.23	-/−0.24	-/−0.18	+0.28/-	−0.43/+0.46	−0.22/-	−0.30/+0.10
Pile-up offset p_T (JES) [%]	−1.56/+1.58	−1.67/+1.68	−1.33/+1.39	−1.00/+0.83	−0.69/+1.01	-/−0.11	∓0.10	-	+0.20/−0.21	±0.37	+0.57/−0.56	+0.37/−0.40	+0.44/−0.48	+0.77/−0.72	+0.57/−0.62	+0.79/−0.78	+0.66/−0.71	+0.79/−0.72	+1.08/−0.87	+1.09/−1.10	+0.89/−1.02	+1.24/−1.36
Pile-up offset ρ topology (JES) [%]	−3.15/+3.35	−1.22/+0.65	+1.24/−1.22	+1.00/−0.23	−2.15/+1.53	∓0.42	+1.01/−0.98	+2.59/−2.38	+1.82/−1.92	-	−0.92/+0.89	+0.18/−0.39	+1.52/−1.62	+1.86/−1.30	+0.19/−0.10	−2.04/+2.21	−0.89/+0.60	+0.80/−0.79	+0.40/−0.18	−3.75/+4.10	−2.12/+1.75	−0.65/+0.66
Jet vertex fraction [%]	±0.37	+0.57/−0.56	+0.64/−0.63	+0.47/−0.46	+0.15/−0.14	∓0.10	-	±0.19	-	-	−0.34/+0.33	∓0.16	-	∓0.10	∓0.17	−0.50/+0.49	−0.31/+0.30	∓0.18	−0.26/+0.25	−0.73/+0.72	∓0.43	−0.37/+0.36
b-Quark tagging efficiency (eigenvector 0) [%]	−2.39/+2.25	−2.12/+1.98	−1.85/+1.71	−1.55/+1.43	−0.56/+0.51	-	+0.19/−0.17	+0.46/−0.43	+0.54/−0.51	+0.74/−0.70	+0.46/−0.43	+0.77/−0.71	+1.12/−1.04	+1.16/−1.08	+1.06/−0.99	+0.41/−0.38	+0.78/−0.72	+1.16/−1.08	+1.11/−1.04	−0.12/-	+0.56/−0.54	+0.85/−0.82
b-Quark tagging efficiency (eigenvector 1) [%]	+1.14/−1.11	+1.20/−1.17	+1.34/−1.30	+1.27/−1.24	+0.51/−0.50	±0.17	±0.20	±0.27	±0.28	−0.27/+0.26	−0.46/+0.45	−0.44/+0.43	∓0.38	−0.30/+0.29	−0.59/+0.57	−1.03/+1.01	−0.98/+0.96	−0.91/+0.90	−1.00/+0.97	−2.00/+1.97	−1.80/+1.77	−1.76/+1.72
b-Quark tagging efficiency (eigenvector 2) [%]	+0.44/−0.45	±0.36	+0.22/−0.23	±0.19	-	+0.25/−0.26	±0.20	-	-	∓0.28	-	-	∓0.20	−0.23/+0.24	−0.39/+0.40	−0.32/+0.33	∓0.41	−0.54/+0.55	−0.66/+0.67	−0.78/+0.80	−0.91/+0.92	−1.12/+1.14
b-Quark tagging efficiency (eigenvector 3) [%]	∓0.39	−0.37/+0.38	∓0.36	∓0.27	-	-	-	-	-	±0.10	±0.20	±0.20	±0.20	±0.17	±0.13	±0.19	±0.18	±0.15	-	-	-	∓0.13
c-Quark tagging efficiency (eigenvector 0) [%]	±0.17	±0.17	±0.20	±0.19	-	-	-	-	-	-	-	-	-	-	-	∓0.10	-	-	-	∓0.17	∓0.11	-
c-Quark tagging efficiency (eigenvector 1) [%]	±0.18	±0.18	±0.24	±0.30	±0.25	-	-	-	±0.12	+0.11/−0.10	-	-	−0.12/+0.13	-	-	∓0.17	−0.26/+0.25	∓0.34	∓0.24	∓0.37	∓0.58	−0.71/+0.70
c-Quark tagging efficiency (eigenvector 2) [%]	±0.10	±0.11	±0.10	±0.12	-	-	-	-	-	-	-	-	-	-	-	∓0.10	∓0.13	−0.17/+0.18	∓0.13	∓0.23	∓0.32	∓0.37
Light-jet tagging efficiency (eigenvector 0) [%]	-	+0.23/−0.34	+0.18/−0.24	±0.17	+0.35/−0.34	+0.15/−0.11	+0.18/−0.19	+0.13/−0.14	±0.13	±0.25	-	-	−0.18/+0.19	-	±0.12	∓0.14	−0.32/+0.33	−0.49/+0.48	−0.63/+0.69	−0.53/+0.51	−1.03/+1.06	−1.36/+1.38
Light-jet tagging efficiency (eigenvector 1) [%]	+0.18/−0.17	-	-	+0.13/−0.14	±0.16	-	-	-	-	-	-	-	-	-	-	-	-	-	-	−0.28/+0.24	−0.19/+0.18	∓0.25
Light-jet tagging efficiency (eigenvector 2) [%]	-	−0.17/+0.12	-	-	-	-	-	-	-	-	-	-	-	-	-	-	-	-	-	+0.13/−0.12	-	+0.15/−0.14
Light-jet tagging efficiency (eigenvector 3) [%]	+0.24/−0.22	-	+0.15/−0.17	±0.25	±0.22	-	-	-	-	-	-	-	-	-	-	∓0.12	∓0.20	∓0.26	∓0.27	∓0.30	∓0.49	−0.54/+0.55
Light-jet tagging efficiency (eigenvector 8) [%]	-	-	-	-	-	-	-	-	-	-	-	-	-	-	-	-	-	-	-	∓0.10	∓0.15	∓0.18
b-Quark tagging extrapolation [%]	-	-	-	-	∓0.15	-	-	-	-	∓0.10	-	-	-	-	-	-	-	-	+0.20/−0.21	+0.64/−0.63	±0.73	±1.14
Electron energy resolution [%]	-	-	-	-	-	-	-	-	-	-	-	-	-	-	-	-	-	-	-	-	-	-
Electron energy scale [%]	-	-	-	−0.10/+0.12	∓0.14	-	-	-	-	-	-	-	-	-	-	-	-	-	-	+0.21/−0.17	±0.16	+0.10/−0.19
Electron identification efficiency [%]	-	-	-	-	-	-	-	-	-	-	-	-	-	-	-	-	-	-	±0.13	±0.24	±0.24	±0.29
Electron isolation efficiency [%]	-	-	-	-	-	-	-	-	-	-	-	-	-	-	+0.11/−0.12	-	-	-	±0.16	±0.21	±0.22	+0.31/−0.32
Muon (ID) momentum resolution [%]	-	-	-	-	-	-	-	-	-	-	-	-	-	-	-	-	-	-	-	-	-	-
Muon (MS) momentum resolution [%]	-	-	-	-	-	-	-	-	-	-	-	-	-	-	-	-	-	-	-	-	-	-
Muon identification syst [%]	-	-	-	-	-	-	-	-	-	-	-	-	-	-	-	-	-	-	-	±0.20	±0.16	±0.18
E_T^{miss} Soft jet resolution para [%]	±0.38	±1.00	±0.97	±0.60	±0.77	∓0.30	±0.17	±0.11	∓0.14	±0.15	∓0.37	∓0.16	∓0.52	-	∓0.33	∓0.46	∓0.15	∓0.34	∓0.29	∓0.95	∓0.11	∓0.28
E_T^{miss} Soft jet resolution perp [%]	±0.38	±0.88	±0.93	±0.55	±0.75	∓0.28	±0.17	-	-	±0.14	∓0.32	∓0.10	∓0.39	∓0.17	∓0.28	∓0.41	∓0.31	∓0.31	∓0.26	∓0.81	∓0.27	∓0.49
E_T^{miss} Soft jet scale [%]	+0.86/−0.89	+0.78/−0.77	+0.78/−0.63	+0.60/−0.54	+0.85/−0.37	+0.10/−0.23	-	−0.13/+0.28	-	-	−0.16/-	−0.36/+0.31	−0.62/+0.61	−0.36/+0.54	−0.26/+0.20	−0.21/+0.19	−0.46/+0.52	−0.51/+0.88	−0.31/+0.24	−0.45/+0.46	−0.42/+0.38	−0.46/+0.50
Z+jets cross-section [%]	+0.32/−0.33	±0.17	-	-	−0.22/+0.23	-	∓0.10	∓0.23	∓0.16	∓0.28	-	-	∓0.12	−0.15/+0.16	∓0.13	∓0.14	-	-	∓0.20	+0.43/−0.44	+0.31/−0.32	+0.42/−0.43
Monte Carlo sample statistics [%]	±0.38	±0.37	±0.40	±0.52	±1.15	±0.22	±0.20	±0.26	±0.34	±0.62	±0.26	±0.24	±0.34	±0.53	±0.56	±0.33	±0.32	±0.46	±0.55	±0.81	±0.57	±0.77
ISR/FSR + scale [%]	−0.47/+0.87	+0.88/-	+0.59/−1.04	-/−1.02	+0.46/−1.56	−0.68/+0.36	-/+0.22	+0.36/−0.88	−0.46/+0.50	+0.70/−0.83	−0.59/+0.78	−0.40/+0.66	+1.26/−1.34	−0.24/+1.54	+1.37/−1.83	−0.36/+0.14	-/−1.48	+1.56/−0.43	+1.19/−1.02	−0.71/+0.46	+0.95/-	+2.57/−4.70
Alternate hard-scattering model [%]	±5.48	±5.37	±10.5	±4.09	±6.94	∓3.14	∓1.09	±2.07	∓0.87	±0.81	∓3.01	∓0.74	∓0.75	∓1.17	∓2.18	∓3.94	∓2.47	±0.78	±0.23	∓3.32	∓1.46	∓4.56
Alternate parton-shower model [%]	∓4.74	±0.84	±5.05	-	±1.75	∓4.27	±1.18	±5.69	±1.80	±1.66	∓3.13	±0.81	±3.51	±0.49	±1.95	∓4.78	∓0.20	±3.54	±2.57	∓4.60	±1.00	±0.64
Inter PDF [%]	-	-	-	-	±0.29	-	-	∓0.10	-	-	-	-	-	-	-	±0.10	-	±0.10	-	-	∓0.10	-
Intra PDF [%]	-	∓0.15	-	-	±1.29	∓0.15	∓0.19	±0.21	±0.12	-	-	∓0.11	-	-	±0.15	±0.27	∓0.13	±0.46	-	±0.37	±0.53	±0.42
Fakes overall normalization, el [%]	∓0.12	+1.12/−1.13	+0.77/−0.78	∓0.25	−0.44/+0.45	−0.77/+0.78	±0.19	+0.14/−0.15	−0.51/+0.52	−0.63/+0.64	−0.55/+0.56	±0.26	±0.41	∓0.23	−0.64/+0.65	−0.54/+0.55	+0.52/−0.53	±0.54	−0.40/+0.41	−1.11/+1.13	+1.88/−1.91	+1.21/−1.23
Fakes overall normalization, mu [%]	-	±0.22	±0.34	±0.24	-	∓0.15	±0.14	±0.34	-	∓0.28	∓0.17	±0.10	±0.26	-	∓0.34	∓0.40	-	-	∓0.34	∓0.74	∓0.27	∓0.53
Fakes alternative parametrization [%]	∓2.53	∓3.01	∓2.38	∓0.32	±1.66	±0.16	∓0.54	∓0.36	±0.59	±2.44	±0.91	±0.45	±0.43	±1.46	±2.55	±1.49	±1.13	±1.57	±2.46	±3.18	±1.49	±2.50
W+jets heavy flavour component [%]	±3.67	±2.88	±3.59	-	±1.31	±0.91	∓1.05	∓2.33	∓2.15	∓1.26	-	±0.10	∓2.14	∓3.45	∓2.67	±0.84	-	±0.22	∓1.55	±3.31	∓2.94	∓1.32

TABLE F.33: Table of systematics for the relative differential cross-section at the particle level for the $p_T^{t\bar{t}}$ vs $m^{t\bar{t}}$ observable.

Bins [GeV] x [GeV]	0–30	30–90	90–140	140–200	200–300	300–1000	1000–1030	1030–1090	1090–1150	1150–1240	1240–2000	2000–2080	2080–2130	2130–2190	2190–2320	2320–3000	3000–3100	3100–3175	3175–3290	3290–4000
$1/\sigma \cdot d\sigma \ / \ dp_T^{t\bar{t}} vs p_T^{t,had}$	$4.46 \cdot 10^{-4}$	$1.60 \cdot 10^{-3}$	$1.89 \cdot 10^{-3}$	$9.25 \cdot 10^{-4}$	$2.89 \cdot 10^{-4}$	$1.22 \cdot 10^{-5}$	$6.08 \cdot 10^{-4}$	$2.11 \cdot 10^{-3}$	$2.26 \cdot 10^{-3}$	$9.52 \cdot 10^{-4}$	$4.35 \cdot 10^{-5}$	$8.44 \cdot 10^{-4}$	$1.27 \cdot 10^{-3}$	$8.70 \cdot 10^{-4}$	$3.22 \cdot 10^{-4}$	$1.42 \cdot 10^{-5}$	$2.09 \cdot 10^{-4}$	$2.71 \cdot 10^{-4}$	$1.59 \cdot 10^{-4}$	$1.47 \cdot 10^{-5}$
Total Uncertainty [%]	$^{+12.3}_{-12.4}$	$^{+7.24}_{-7.28}$	$^{+7.09}_{-7.28}$	$^{+7.73}_{-7.55}$	$^{+10.1}_{-10.3}$	$^{+14.6}_{-14.7}$	$^{+7.41}_{-7.37}$	$^{+5.64}_{-5.65}$	$^{+2.47}_{-2.50}$	$^{+3.04}_{-2.93}$	$^{+6.28}_{-6.07}$	$^{+5.63}_{-5.53}$	$^{+6.32}_{-5.88}$	$^{+5.47}_{-5.49}$	$^{+5.78}_{-5.60}$	$^{+9.16}_{-9.28}$	$^{+5.47}_{-5.41}$	$^{+3.72}_{-4.04}$	$^{+4.79}_{-4.89}$	$^{+5.33}_{-5.52}$
Statistics [%]	±1.0	±0.3	±0.3	±0.4	±0.7	±1.3	±0.8	±0.2	±0.2	±0.3	±0.5	±0.4	±0.4	±0.5	±0.6	±1.3	±0.7	±0.8	±0.9	±1.1
Systematics [%]	$^{+12.2}_{-12.3}$	$^{+7.23}_{-7.26}$	$^{+7.08}_{-7.27}$	$^{+7.71}_{-7.53}$	$^{+10.0}_{-10.3}$	±14.6	$^{+7.31}_{-7.26}$	$^{+5.62}_{-5.63}$	$^{+2.45}_{-2.48}$	$^{+3.01}_{-2.90}$	$^{+6.24}_{-6.03}$	$^{+5.60}_{-5.51}$	$^{+6.29}_{-5.85}$	$^{+5.43}_{-5.45}$	$^{+5.73}_{-5.56}$	$^{+9.02}_{-9.15}$	$^{+5.39}_{-5.33}$	$^{+3.59}_{-3.91}$	$^{+4.67}_{-4.77}$	$^{+5.14}_{-5.35}$
Jet energy resolution [%]	∓0.30	-	∓2.82	-	∓1.06	±1.83	∓0.43	±1.55	∓0.48	±0.12	±0.43	-	±0.77	±1.67	∓1.81	±5.08	±1.33	±0.83	∓1.45	±0.83
b-Tagged jet energy scale (JES) [%]	$^{-0.82}_{+0.41}$	$^{-0.36}_{+0.42}$	$^{+0.13}_{-0.16}$	$^{+0.40}_{-0.28}$	$^{+0.14}_{-0.24}$	$^{+0.24}_{-0.15}$	$^{-0.64}_{+0.46}$	$^{-0.33}_{+0.38}$	$^{+0.11}_{-0.15}$	$^{+0.26}_{-0.27}$	$^{+0.22}_{-0.18}$	$^{-0.31}_{+0.22}$	-	$^{+0.20}_{-0.23}$	$^{+0.15}_{-0.17}$	$^{+0.29}_{-0.25}$	$^{-0.20}_{+0.30}$	-	-	$^{+0.15}_{-0.11}$
Effective detector NP set 1 (JES) [%]	$^{-}_{+0.17}$	-	-	-	-	$^{+0.18}_{-0.12}$	-	-	-	-	-	-	-	-	-	$^{+0.10}_{-0.13}$	-	-	-	-
Effective detector NP set 2 (JES) [%]	$^{-}_{+0.16}$	-	-	-	-	$^{+0.15}_{-0.12}$	-	-	-	-	-	-	-	-	-	$^{-}_{-0.14}$	-	-	-	-
Effective mixed NP set 1 (JES) [%]	$^{-0.43}_{+0.52}$	$^{-0.34}_{+0.36}$	$^{-0.15}_{+0.10}$	$^{+0.18}_{-0.12}$	$^{+0.23}_{-0.30}$	±1.29	$^{-0.41}_{+0.37}$	$^{-0.36}_{+0.34}$	$^{-0.14}_{+0.11}$	$^{+0.13}_{-}$	±0.67	$^{-}_{+0.14}$	-	-	$^{+0.25}_{-0.21}$	$^{+1.04}_{-1.28}$	$^{+0.37}_{-0.35}$	$^{+0.35}_{-0.39}$	$^{+0.55}_{-0.46}$	±0.85
Effective mixed NP set 2 (JES) [%]	$^{+0.15}_{-}$	-	-	-	-	$^{-0.13}_{+0.16}$	-	-	-	-	-	-	-	-	-	$^{-0.13}_{-}$	-	-	-	$^{-0.11}_{+0.10}$
Effective mixed NP set 3 (JES) [%]	-	-	-	-	-	-	-	-	-	-	-	-	-	-	-	-	-	-	-	-
Effective modelling NP set 1 (JES) [%]	$^{-0.37}_{+0.63}$	$^{-0.67}_{+0.72}$	$^{-0.79}_{+0.80}$	$^{-1.05}_{+1.29}$	∓1.72	$^{-1.99}_{+1.96}$	±0.77	$^{+0.44}_{-0.64}$	$^{+0.23}_{-0.34}$	$^{-0.31}_{+0.25}$	$^{-0.70}_{+0.92}$	$^{+1.76}_{-1.66}$	$^{+1.41}_{-1.06}$	$^{+0.55}_{-0.59}$	$^{-0.24}_{-}$	$^{-0.94}_{+0.27}$	$^{+0.95}_{-0.84}$	-	$^{-0.43}_{+0.55}$	$^{-0.87}_{+0.93}$
Effective modelling NP set 2 (JES) [%]	$^{-0.10}_{+0.22}$	$^{-0.18}_{+0.19}$	-	$^{+0.30}_{-0.24}$	$^{+0.35}_{-0.41}$	±0.86	$^{-0.43}_{+0.34}$	$^{-0.32}_{+0.30}$	$^{-0.11}_{-}$	$^{+0.13}_{-0.14}$	$^{+0.47}_{-0.46}$	$^{-0.23}_{+0.28}$	$^{-}_{+0.18}$	-	$^{+0.20}_{-0.19}$	$^{+0.75}_{-0.79}$	-	$^{+0.16}_{-0.26}$	$^{+0.36}_{-0.35}$	$^{+0.61}_{-0.59}$
Effective modelling NP set 3 (JES) [%]	$^{+0.25}_{-0.16}$	$^{+0.24}_{-0.25}$	-	$^{-0.22}_{+0.28}$	$^{-0.40}_{+0.29}$	$^{-0.65}_{+0.69}$	$^{+0.36}_{-0.45}$	$^{+0.31}_{-0.30}$	$^{-}_{-0.11}$	$^{-0.16}_{+0.18}$	$^{-0.41}_{+0.46}$	±0.19	-	$^{-0.15}_{+0.10}$	$^{-0.27}_{+0.26}$	$^{-0.60}_{+0.59}$	-	$^{-0.26}_{+0.11}$	$^{-0.37}_{+0.42}$	$^{-0.51}_{+0.50}$
Effective modelling NP set 4 (JES) [%]	$^{-}_{+0.14}$	-	-	-	-	-	-	-	-	-	-	-	-	-	-	-	-	-	-	-
Effective statistical NP set 1 (JES) [%]	$^{+0.24}_{-}$	-	$^{-0.17}_{+0.15}$	$^{-0.21}_{+0.28}$	$^{-0.39}_{+0.42}$	$^{-0.31}_{+0.41}$	$^{+0.22}_{-0.19}$	$^{+0.15}_{-0.19}$	-	-	$^{-0.19}_{+0.18}$	$^{+0.28}_{-0.27}$	$^{+0.29}_{-0.15}$	-	-	-	$^{+0.17}_{-0.12}$	-	$^{-0.11}_{+0.17}$	$^{-0.20}_{+0.24}$
Effective statistical NP set 2 (JES) [%]	$^{+0.26}_{-}$	-	$^{+0.13}_{-0.14}$	$^{+0.23}_{-0.20}$	$^{+0.35}_{-0.32}$	$^{+0.52}_{-0.55}$	$^{-0.18}_{+0.22}$	$^{-0.20}_{+0.14}$	-	-	$^{+0.24}_{-0.26}$	$^{-0.24}_{+0.27}$	$^{-0.17}_{+0.26}$	-	-	$^{+0.35}_{-0.34}$	-	-	$^{+0.16}_{-0.11}$	$^{+0.32}_{-0.31}$
Effective statistical NP set 3 (JES) [%]	-	-	-	-	-	$^{-0.46}_{+0.54}$	-	-	-	-	$^{-0.21}_{+0.22}$	-	-	-	-	$^{-0.47}_{+0.46}$	$^{-0.18}_{+0.16}$	$^{-0.18}_{+0.10}$	-	∓0.33
Effective statistical NP set 4 (JES) [%]	$^{-0.21}_{+0.28}$	$^{-0.20}_{+0.23}$	-	$^{+0.24}_{-0.16}$	$^{+0.24}_{-0.27}$	$^{+0.28}_{-0.29}$	$^{-0.36}_{+0.30}$	$^{-0.24}_{+0.23}$	-	$^{+0.13}_{-0.14}$	$^{+0.26}_{-0.22}$	$^{-}_{+0.13}$	-	$^{+0.13}_{-0.19}$	±0.26	$^{+0.30}_{-0.24}$	-	$^{-}_{-0.15}$	$^{+0.29}_{-0.30}$	$^{+0.24}_{-0.25}$
Effective statistical NP set 5 (JES) [%]	-	-	-	-	-	±0.32	$^{-}_{-0.13}$	-	-	-	$^{+0.15}_{-0.17}$	-	-	∓0.16	-	$^{+0.24}_{-0.20}$	$^{+0.24}_{-0.18}$	-	-	$^{+0.20}_{-0.18}$
Effective statistical NP set 6 (JES) [%]	-	-	-	-	$^{-0.18}_{+0.11}$	-	-	-	-	-	$^{-0.11}_{+0.13}$	-	-	-	∓0.11	-	-	-	$^{-}_{+0.12}$	-
Effective statistical NP set 7 (JES) [%]	$^{-}_{+0.16}$	-	-	-	-	$^{+0.22}_{-0.18}$	-	-	-	-	-	-	-	-	-	$^{+0.13}_{-0.14}$	-	-	$^{+0.14}_{-}$	-
η intercalibration model (JES) [%]	$^{-0.28}_{+0.50}$	$^{-0.40}_{+0.44}$	$^{-0.24}_{+0.19}$	-	$^{-0.12}_{+0.11}$	$^{+0.18}_{-}$	$^{-0.34}_{+0.18}$	$^{-0.21}_{+0.19}$	-	-	-	$^{+0.28}_{-0.27}$	$^{+0.44}_{-0.29}$	$^{+0.20}_{-0.34}$	$^{+0.26}_{-0.25}$	$^{+0.23}_{-0.56}$	$^{+0.32}_{-0.35}$	$^{+0.30}_{-0.28}$	$^{+0.23}_{-0.16}$	$^{+0.32}_{-0.17}$
η intercalibration non closure (JES) [%]	$^{-}_{-0.14}$	$^{+0.16}_{-0.12}$	$^{+0.13}_{-0.14}$	-	-	$^{-}_{+0.28}$	$^{+0.14}_{-0.22}$	-	-	-	∓0.10	$^{-}_{+0.18}$	$^{-0.10}_{+0.17}$	-	∓0.10	$^{-0.19}_{+0.13}$	$^{-0.33}_{+0.36}$	$^{-0.27}_{-}$	$^{-0.13}_{-}$	$^{-0.13}_{+0.21}$
η intercalibration total stat (JES) [%]	$^{+0.29}_{-}$	$^{-0.25}_{+0.21}$	∓0.13	-	$^{-0.23}_{+0.24}$	$^{-0.15}_{+0.10}$	-	-	-	-	-	$^{+0.23}_{-0.17}$	$^{+0.39}_{-0.24}$	$^{+0.12}_{-0.28}$	$^{+0.11}_{-0.16}$	-	-	-	-	-
Flavour composition (JES) [%]	$^{-0.37}_{+0.17}$	$^{-0.22}_{+0.32}$	$^{-0.61}_{+0.59}$	$^{-0.79}_{+1.00}$	$^{-1.46}_{+1.57}$	$^{-1.47}_{+1.58}$	$^{+0.97}_{-0.78}$	$^{+0.15}_{-0.28}$	-	$^{-0.67}_{+0.64}$	$^{-0.90}_{+1.36}$	$^{+1.87}_{-1.99}$	$^{+1.47}_{-1.21}$	$^{+0.58}_{-0.62}$	$^{-0.16}_{+0.14}$	$^{-0.92}_{+0.24}$	$^{+1.39}_{-1.55}$	$^{+0.24}_{-0.27}$	$^{-0.16}_{+0.53}$	$^{-0.65}_{+1.02}$
Flavour response (JES) [%]	$^{+0.52}_{-}$	$^{+0.30}_{-0.32}$	$^{+0.34}_{-0.32}$	$^{+0.45}_{-0.36}$	$^{+0.64}_{-0.66}$	$^{+0.73}_{-0.66}$	$^{-0.17}_{-}$	-	-	±0.26	$^{+0.57}_{-0.35}$	$^{-0.98}_{+1.09}$	$^{-0.63}_{+0.84}$	$^{-0.43}_{+0.36}$	-	$^{-}_{-0.37}$	$^{-0.70}_{+0.71}$	$^{-0.33}_{+0.29}$	-	$^{+0.40}_{-0.27}$
Pile-up offset μ (JES) [%]	$^{+0.31}_{-}$	-	-	-	-	-	-	-	-	-	-	-	-	-	-	-	-	-	-	-
Pile-up offset N_{PV} (JES) [%]	$^{+0.49}_{-}$	$^{-0.20}_{+0.33}$	∓0.14	$^{-0.12}_{+0.26}$	$^{-0.42}_{+0.36}$	$^{-0.26}_{+0.61}$	-	-	-	-	$^{-}_{+0.14}$	$^{+0.35}_{-0.33}$	$^{+0.58}_{-0.25}$	$^{+0.22}_{-0.35}$	$^{-}_{-0.20}$	$^{-0.30}_{-}$	$^{+0.28}_{-0.17}$	-	-	$^{-}_{+0.23}$
Pile-up offset p_T (JES) [%]	$^{-0.61}_{+0.59}$	$^{-0.51}_{+0.49}$	-	$^{+0.54}_{-0.43}$	±0.64	$^{+1.25}_{-1.19}$	$^{-0.89}_{+0.88}$	$^{-0.69}_{+0.70}$	$^{-0.20}_{+0.15}$	$^{+0.35}_{-0.29}$	$^{+0.72}_{-0.77}$	$^{-0.31}_{+0.35}$	-	$^{+0.31}_{-0.43}$	$^{+0.63}_{-0.54}$	$^{+1.11}_{-1.25}$	-	$^{+0.44}_{-0.43}$	$^{+0.66}_{-0.73}$	$^{+0.94}_{-1.03}$
Pile-up offset ρ topology (JES) [%]	$^{-1.57}_{+1.24}$	$^{-1.44}_{+1.52}$	$^{-1.22}_{+1.28}$	$^{-1.31}_{+1.58}$	$^{-2.32}_{+2.37}$	$^{-3.14}_{+3.05}$	$^{+1.19}_{-0.80}$	$^{+0.27}_{-0.54}$	$^{+0.37}_{-0.53}$	$^{-0.19}_{-}$	$^{-0.87}_{+1.30}$	$^{+2.42}_{-2.32}$	$^{+2.20}_{-1.77}$	$^{+1.37}_{-1.39}$	$^{-}_{-0.24}$	$^{-1.18}_{+0.12}$	$^{+1.49}_{-1.30}$	-	$^{-0.39}_{+0.73}$	$^{-1.18}_{+1.41}$
Jet vertex fraction [%]	$^{+0.22}_{-0.23}$	-	∓0.10	∓0.32	$^{-0.51}_{+0.52}$	$^{-0.68}_{+0.69}$	±0.43	$^{+0.29}_{-0.30}$	-	∓0.19	∓0.41	±0.37	±0.18	-	∓0.19	$^{-0.37}_{+0.38}$	±0.14	-	∓0.25	∓0.36
b-Quark tagging efficiency (eigenvector 0) [%]	$^{-2.18}_{+2.02}$	$^{-1.21}_{+1.13}$	$^{-0.25}_{+0.24}$	$^{+0.22}_{-0.19}$	$^{+0.75}_{-0.69}$	$^{+0.56}_{-0.51}$	$^{-1.64}_{+1.52}$	$^{-0.75}_{+0.70}$	$^{+0.11}_{-0.10}$	$^{+0.61}_{-0.56}$	$^{+0.81}_{-0.75}$	$^{-0.28}_{+0.25}$	$^{+0.40}_{-0.38}$	$^{+0.72}_{-0.68}$	$^{+0.86}_{-0.81}$	$^{+0.77}_{-0.72}$	±0.23	$^{+0.91}_{-0.86}$	$^{+0.85}_{-0.80}$	$^{+0.74}_{-0.70}$
b-Quark tagging efficiency (eigenvector 1) [%]	$^{+0.85}_{-0.84}$	$^{+0.59}_{-0.58}$	±0.23	∓0.31	$^{-1.21}_{+1.19}$	$^{-2.45}_{+2.43}$	$^{+0.89}_{-0.87}$	$^{+0.61}_{-0.60}$	±0.20	$^{-0.51}_{+0.50}$	$^{-1.77}_{+1.74}$	$^{+0.64}_{-0.63}$	±0.29	-	$^{-0.67}_{+0.66}$	$^{-2.03}_{+2.00}$	-	$^{-0.38}_{+0.36}$	$^{-0.54}_{+0.52}$	$^{-1.15}_{+1.12}$
b-Quark tagging efficiency (eigenvector 2) [%]	±0.50	$^{+0.42}_{-0.43}$	$^{+0.26}_{-0.27}$	-	$^{-0.48}_{+0.49}$	$^{-1.40}_{+1.43}$	$^{+0.36}_{-0.37}$	$^{+0.31}_{-0.32}$	±0.16	$^{-0.17}_{+0.18}$	$^{-0.95}_{+0.97}$	±0.13	-	∓0.14	∓0.51	$^{-1.33}_{+1.35}$	∓0.21	$^{-0.29}_{+0.30}$	$^{-0.44}_{+0.45}$	$^{-0.86}_{+0.88}$
b-Quark tagging efficiency (eigenvector 3) [%]	∓0.34	∓0.21	-	±0.20	±0.33	∓0.16	∓0.29	∓0.17	-	±0.24	-	$^{-0.11}_{+0.12}$	-	±0.10	±0.12	∓0.20	-	±0.13	±0.10	∓0.12
c-Quark tagging efficiency (eigenvector 0) [%]	±0.16	±0.10	-	∓0.11	∓0.19	∓0.22	±0.14	±0.10	-	∓0.10	∓0.20	±0.12	-	-	-	∓0.15	-	-	-	-
c-Quark tagging efficiency (eigenvector 1) [%]	±0.13	-	-	-	-	-	±0.10	-	-	-	-	-	-	-	∓0.13	∓0.21	-	-	-	∓0.14
c-Quark tagging efficiency (eigenvector 2) [%]	-	-	-	-	∓0.13	∓0.15	-	-	-	∓0.10	∓0.17	-	-	-	∓0.15	∓0.23	-	-	-	∓0.15
Light-jet tagging efficiency (eigenvector 0) [%]	$^{-0.45}_{+0.56}$	$^{-0.12}_{+0.17}$	$^{+0.12}_{-0.11}$	$^{+0.19}_{-0.17}$	$^{+0.30}_{-0.32}$	-	$^{+0.14}_{-0.51}$	-	-	±0.10	±0.10	-	$^{-0.11}_{+0.13}$	-	-	$^{-0.11}_{-}$	-	-	-	$^{-0.21}_{+0.23}$
Light-jet tagging efficiency (eigenvector 1) [%]	$^{+0.53}_{-0.46}$	±0.13	-	$^{-0.10}_{+0.11}$	$^{-0.21}_{+0.19}$	∓0.22	$^{+0.10}_{-0.12}$	±0.13	-	∓0.11	$^{-0.24}_{+0.23}$	$^{+0.15}_{-0.16}$	-	-	∓0.10	∓0.26	-	-	-	∓0.12
Light-jet tagging efficiency (eigenvector 2) [%]	-	-	-	-	-	$^{+0.11}_{-0.10}$	$^{-0.54}_{+0.37}$	-	-	-	-	-	-	-	-	-	-	-	-	-
Light-jet tagging efficiency (eigenvector 3) [%]	$^{+0.30}_{-0.29}$	$^{+0.14}_{-0.12}$	-	-	-	-	$^{-0.26}_{+0.15}$	-	-	-	∓0.11	-	-	-	-	∓0.15	-	-	-	$^{-0.10}_{+0.11}$
Light-jet tagging efficiency (eigenvector 5) [%]	-	-	-	-	-	-	-	-	-	-	-	-	-	-	-	±0.11	-	-	-	-
b-Quark tagging extrapolation [%]	-	-	-	-	-	±0.80	-	-	-	-	±0.35	-	-	-	-	$^{+1.07}_{-1.06}$	-	-	-	$^{+0.80}_{-0.81}$
Electron identification efficiency [%]	-	-	-	-	-	±0.22	-	-	-	-	±0.15	-	-	-	-	±0.21	±0.10	-	-	±0.11
Electron isolation efficiency [%]	-	-	-	-	-	±0.37	-	-	-	-	±0.21	-	-	-	-	±0.31	$^{+0.12}_{-0.11}$	±0.10	-	±0.14
Muon identification syst [%]	-	-	-	-	-	±0.15	-	-	-	-	-	-	-	-	-	-	-	-	-	-
E_T^{miss} Soft jet resolution para [%]	∓0.45	∓0.35	∓0.29	∓0.37	∓0.38	∓0.53	±0.19	±0.29	±0.28	±0.24	-	-	-	-	±0.13	±0.28	∓0.37	-	-	-
E_T^{miss} Soft jet resolution perp [%]	∓0.45	∓0.34	∓0.17	∓0.39	∓0.46	∓0.88	±0.18	±0.31	±0.19	±0.28	±0.25	-	∓0.12	-	±0.14	-	∓0.39	-	-	-
E_T^{miss} Soft jet scale [%]	-	$^{+0.12}_{-0.28}$	$^{+0.19}_{-0.33}$	$^{-}_{-0.18}$	-	$^{-0.31}_{-}$	-	-	-	-	-	$^{-0.11}_{+0.17}$	$^{-0.20}_{+0.34}$	$^{-0.17}_{+0.16}$	-	-	$^{-0.31}_{+0.21}$	$^{-0.12}_{+0.13}$	-	$^{+0.10}_{-0.21}$
Z+jets cross-section [%]	±0.18	$^{+0.42}_{-0.43}$	±0.13	∓0.17	∓0.35	$^{-0.33}_{+0.34}$	±0.15	$^{+0.22}_{-0.23}$	-	$^{-0.24}_{+0.25}$	$^{-0.35}_{+0.36}$	-	-	-	∓0.21	∓0.32	∓0.15	∓0.13	-	-
Monte Carlo sample statistics [%]	±1.00	±0.31	±0.23	±0.31	±0.42	±0.82	±0.90	±0.28	±0.19	±0.22	±0.35	±0.29	±0.32	±0.35	±0.37	±0.81	±0.49	±0.51	±0.53	±0.70
ISR/FSR + scale [%]	$^{-}_{-1.63}$	$^{-0.67}_{+1.22}$	$^{-1.48}_{+0.90}$	$^{-0.16}_{+1.27}$	$^{-}_{-1.77}$	$^{-}_{-1.10}$	$^{+0.88}_{-0.40}$	$^{+0.52}_{-}$	$^{-}_{-0.36}$	-	$^{-0.33}_{-}$	$^{+0.30}_{-0.47}$	$^{+1.20}_{-1.04}$	$^{+0.50}_{-0.31}$	$^{+1.53}_{-0.80}$	$^{+1.78}_{-}$	$^{+0.92}_{-0.73}$	$^{+1.42}_{-2.04}$	$^{+0.98}_{-1.66}$	$^{+0.22}_{-1.94}$
Alternate hard-scattering model [%]	±4.62	±0.82	∓3.26	∓3.65	∓2.93	∓8.69	±3.48	±2.33	-	∓1.03	∓2.78	±2.92	±1.97	±0.94	∓0.40	±4.18	±0.31	±0.16	±0.87	∓3.32
Alternate parton-shower model [%]	∓5.78	∓3.85	∓4.85	∓5.54	∓7.77	∓8.47	±0.30	±2.33	±1.85	±0.99	∓0.89	±2.04	±4.31	±4.43	±2.67	±1.54	±2.80	±1.06	±0.37	±0.20
Intra PDF [%]	±0.39	-	∓0.10	-	±0.10	±0.20	-	-	-	±0.21	±0.10	-	-	-	±0.28	±0.14	±0.17	-	-	-
Fakes overall normalization, el [%]	-	-	$^{-0.81}_{+0.82}$	$^{-1.20}_{+1.22}$	$^{-1.35}_{+1.37}$	$^{-1.87}_{+1.90}$	$^{+1.17}_{-1.19}$	$^{+1.03}_{-1.04}$	$^{+0.54}_{-0.55}$	-	∓0.58	∓0.17	$^{+0.15}_{-0.16}$	$^{+0.32}_{-0.33}$	±0.38	$^{+0.56}_{-0.57}$	$^{-0.85}_{+0.86}$	$^{-0.75}_{+0.77}$	∓0.16	$^{+0.40}_{-0.41}$
Fakes overall normalization, mu [%]	∓0.16	-	-	∓0.26	∓0.58	$^{-1.39}_{+1.40}$	±0.42	±0.29	±0.21	-	∓0.67	±0.39	±0.25	±0.19	∓0.13	∓0.90	∓0.29	∓0.20	∓0.32	∓0.40
Fakes alternative parametrization [%]	∓3.97	∓2.74	±0.23	±1.76	±3.32	±4.67	∓5.09	∓2.68	∓0.31	±1.55	±3.60	∓0.20	∓0.52	∓0.16	±1.75	±4.15	±3.24	±2.46	±1.40	±1.63
W+jets heavy flavour component [%]	±8.00	±4.29	∓0.38	±0.13	∓0.83	-	±1.80	±2.50	∓0.72	∓1.19	∓2.07	∓1.41	∓1.52	∓1.02	∓3.65	±1.10	∓0.36	∓0.51	∓3.43	∓0.70

TABLE F.34: Table of systematics for the relative differential cross-section at the particle level for the $p_T^{t,had}$ vs $p_T^{t\bar{t}}$ observable.

F.1.2.2 Boosted topology

Bins [GeV]	350–400	400–455	455–520	520–610	610–710	710–820	820–930	930–2000
$1/\sigma \cdot \mathrm{d}\sigma \,/\, \mathrm{d}p_T^{t,had}$	$7.83 \cdot 10^{-3}$	$4.89 \cdot 10^{-3}$	$2.60 \cdot 10^{-3}$	$1.17 \cdot 10^{-3}$	$4.23 \cdot 10^{-4}$	$1.31 \cdot 10^{-4}$	$5.99 \cdot 10^{-5}$	$2.48 \cdot 10^{-6}$
Total Uncertainty [%]	$^{+2.44}_{-2.34}$	$^{+1.57}_{-2.30}$	$^{+4.30}_{-3.92}$	$^{+3.14}_{-3.27}$	$^{+7.04}_{-7.37}$	$^{+15.1}_{-11.3}$	$^{+26.1}_{-23.5}$	$^{+28.8}_{-29.0}$
Statistics [%]	±0.8	±1.1	±1.5	±2.0	±3.2	±6.2	±9.2	±16.
Systematics [%]	$^{+2.21}_{-2.11}$	$^{+0.78}_{-1.85}$	$^{+3.91}_{-3.49}$	$^{+2.10}_{-2.29}$	$^{+5.96}_{-6.34}$	$^{+13.4}_{-9.03}$	$^{+23.8}_{-20.9}$	$^{+22.7}_{-23.0}$
b-Tagged jet energy scale (JES) [%]	-	-	$^{+0.23}_{-}$	-	-	$^{+0.67}_{-}$	-	$^{+0.21}_{-0.29}$
Effective detector NP set 1 (JES) [%]	-	-	-	-	-	$^{-}_{+0.76}$	$^{-0.70}_{-}$	$^{+0.99}_{-0.52}$
Effective detector NP set 2 (JES) [%]	-	-	-	-	$^{-}_{-0.20}$	$^{-}_{+0.30}$	$^{-0.99}_{-}$	$^{+0.12}_{-0.40}$
Effective mixed NP set 1 (JES) [%]	∓0.50	$^{-}_{-0.25}$	$^{+0.61}_{-}$	$^{+0.35}_{-0.94}$	$^{+1.00}_{-0.86}$	$^{+3.17}_{-1.45}$	$^{-0.21}_{-1.78}$	$^{-}_{+4.89}$
Effective mixed NP set 2 (JES) [%]	-	-	-	-	$^{-}_{-0.21}$	$^{+0.73}_{-}$	-	$^{-}_{-3.48}$
Effective mixed NP set 3 (JES) [%]	-	-	-	-	-	$^{-}_{+0.35}$	$^{-}_{-0.26}$	$^{-0.30}_{-}$
Effective modelling NP set 1 (JES) [%]	-	-	$^{+0.54}_{-}$	-	-	$^{-}_{+1.51}$	$^{-1.50}_{-1.84}$	$^{+0.74}_{+1.61}$
Effective modelling NP set 2 (JES) [%]	$^{+0.16}_{-0.34}$	-	$^{-}_{+0.45}$	-	$^{-0.38}_{\pm 0.88}$	$^{-0.60}_{+2.46}$	$^{+2.31}_{-}$	$^{-0.37}_{+4.80}$
Effective modelling NP set 3 (JES) [%]	$^{+0.29}_{+0.13}$	-	$^{-}_{+0.33}$	$^{-0.41}_{-}$	$^{-}_{-0.23}$	$^{-0.56}_{+0.65}$	$^{-1.45}_{-}$	$^{-3.23}_{+0.16}$
Effective modelling NP set 4 (JES) [%]	$^{-0.16}_{-}$	-	$^{-}_{-}$	$^{-}_{-0.13}$	$^{-}_{-0.20}$	$^{+1.01}_{-}$	$^{-0.52}_{-1.26}$	$^{-0.48}_{+0.79}$
Effective statistical NP set 1 (JES) [%]	-	-	-	-	-	$^{-}_{+1.47}$	$^{-}_{-1.84}$	$^{-0.29}_{+1.61}$
Effective statistical NP set 2 (JES) [%]	$^{-0.10}_{+0.12}$	$^{-0.20}_{-}$	$^{+0.30}_{-0.15}$	$^{+0.12}_{-}$	$^{-0.31}_{-}$	$^{-0.55}_{+1.60}$	$^{+1.77}_{-1.48}$	$^{-1.86}_{+1.52}$
Effective statistical NP set 3 (JES) [%]	±0.38	-	$^{-0.23}_{+0.65}$	$^{-0.51}_{+0.36}$	$^{-0.53}_{-0.80}$	$^{-0.71}_{-0.72}$	$^{+1.49}_{+1.21}$	$^{-2.01}_{-0.20}$
Effective statistical NP set 4 (JES) [%]	-	$^{-}_{-0.16}$	$^{-}_{-}$	$^{+0.27}_{+0.20}$	$^{+0.45}_{-0.38}$	$^{+1.59}_{-0.32}$	$^{-0.72}_{-0.64}$	$^{+0.55}_{-0.40}$
Effective statistical NP set 5 (JES) [%]	-	$^{+0.11}_{-0.13}$	$^{+0.27}_{-}$	$^{-}_{-}$	$^{+0.12}_{-0.47}$	$^{+0.70}_{-0.58}$	$^{+0.34}_{-}$	$^{+0.52}_{-0.69}$
Effective statistical NP set 6 (JES) [%]	$^{-0.14}_{+0.11}$	-	$^{+0.28}_{-0.10}$	-	$^{-}_{-0.27}$	$^{+1.29}_{+0.91}$	$^{-0.88}_{-0.54}$	$^{+1.28}_{-0.52}$
Effective statistical NP set 7 (JES) [%]	-	-	$^{+0.26}_{-}$	-	$^{-}_{-0.25}$	$^{+0.65}_{-}$	$^{-}_{-0.58}$	$^{+0.42}_{+0.90}$
η intercalibration model (JES) [%]	$^{-0.17}_{+0.27}$	$^{-}_{-0.23}$	$^{+0.58}_{-}$	$^{-}_{-0.28}$	$^{-}_{-0.70}$	$^{+1.09}_{-0.42}$	$^{-0.37}_{+1.01}$	$^{-0.45}_{+1.29}$
η intercalibration non closure (JES) [%]	$^{+0.17}_{-}$	$^{-}_{-0.27}$	$^{+0.33}_{-}$	$^{-}_{-0.22}$	$^{-}_{-0.42}$	$^{+1.03}_{-}$	$^{-0.71}_{+0.77}$	$^{-1.43}_{-}$
η intercalibration total stat (JES) [%]	-	-	-	-	-	$^{-}_{+0.67}$	$^{-}_{-0.53}$	$^{+0.80}_{-0.57}$
Flavour composition (JES) [%]	$^{-0.24}_{+0.26}$	$^{-}_{-0.22}$	$^{+0.53}_{-}$	$^{-}_{-0.27}$	$^{+0.16}_{-0.96}$	$^{+1.76}_{-0.82}$	$^{+1.08}_{-0.80}$	$^{+2.14}_{-1.71}$
Flavour response (JES) [%]	±0.11	$^{-0.31}_{-}$	$^{-}_{+0.40}$	-	$^{+0.21}_{-0.56}$	$^{+0.42}_{-}$	$^{+1.75}_{-0.17}$	$^{+1.04}_{-1.24}$
Pile-up offset μ (JES) [%]	-	-	-	-	$^{-}_{-0.19}$	$^{+0.25}_{-}$	$^{+0.31}_{-}$	$^{+0.20}_{-0.46}$
Pile-up offset N_{PV} (JES) [%]	-	$^{-}_{-0.24}$	-	$^{-}_{-0.22}$	-	$^{-}_{+1.39}$	-	$^{+1.17}_{-}$
Pile-up offset p_T (JES) [%]	$^{-0.24}_{+0.14}$	-	$^{+0.70}_{-}$	$^{-}_{-0.34}$	$^{-}_{\pm 0.19}$	$^{+1.35}_{-0.46}$	$^{-1.40}_{-}$	$^{+0.29}_{-0.48}$
Pile-up offset ρ topology (JES) [%]	-	$^{-}_{-0.26}$	$^{+0.42}_{-}$	$^{-0.40}_{+0.32}$	$^{-0.88}_{-}$	$^{+0.84}_{-}$	$^{-0.51}_{+2.17}$	$^{-0.78}_{+0.66}$
Punch-through (JES) [%]	-	-	-	-	-	-	-	$^{+0.26}_{-}$
Single particle high-p_T (JES) [%]	-	-	-	-	-	-	$^{-0.62}_{-}$	$^{-0.10}_{+0.11}$
Jet vertex fraction [%]	-	-	-	-	-	-	$^{-0.13}_{+0.11}$	$^{+0.10}_{-0.11}$
b-Quark tagging efficiency (eigenvector 0) [%]	-	-	-	$^{-0.12}_{+0.11}$	$^{-0.19}_{+0.18}$	$^{-0.38}_{+0.36}$	$^{-0.70}_{+0.67}$	$^{-0.94}_{+0.89}$
b-Quark tagging efficiency (eigenvector 1) [%]	-	-	-	$^{-0.13}_{+0.12}$	$^{-0.12}_{+0.11}$	$^{-0.22}_{+0.21}$	$^{+0.48}_{+0.47}$	$^{+0.36}_{+0.33}$
b-Quark tagging efficiency (eigenvector 2) [%]	-	-	-	-	-	-	-	∓0.15
b-Quark tagging efficiency (eigenvector 3) [%]	-	-	-	-	∓0.10	∓0.11	∓0.13	$^{-0.31}_{+0.30}$
c-Quark tagging efficiency (eigenvector 1) [%]	-	-	-	-	-	∓0.15	∓0.37	∓0.11
c-Quark tagging efficiency (eigenvector 2) [%]	-	-	-	-	-	-	∓0.19	-
Light-jet tagging efficiency (eigenvector 0) [%]	±0.12	-	-	-	$^{-0.32}_{+0.31}$	$^{-0.63}_{+0.67}$	$^{-0.56}_{+0.54}$	$^{-1.90}_{+1.87}$
Light-jet tagging efficiency (eigenvector 1) [%]	-	-	-	-	-	$^{-0.14}_{+0.16}$	±0.11	∓0.87
Light-jet tagging efficiency (eigenvector 2) [%]	-	-	-	-	-	-	∓0.23	∓0.19
Light-jet tagging efficiency (eigenvector 3) [%]	-	-	-	-	-	-	-	±0.40
Light-jet tagging efficiency (eigenvector 4) [%]	-	-	-	-	-	-	-	±0.36
Light-jet tagging efficiency (eigenvector 5) [%]	-	-	-	-	-	±0.22	±0.17	±0.56
Light-jet tagging efficiency (eigenvector 6) [%]	-	-	-	-	-	∓0.12	-	∓0.26
Light-jet tagging efficiency (eigenvector 7) [%]	-	-	-	-	-	∓0.24	∓0.16	∓0.53
Light-jet tagging efficiency (eigenvector 8) [%]	-	-	-	-	-	-	±0.10	±0.16
Light-jet tagging efficiency (eigenvector 9) [%]	-	-	-	-	-	-	-	∓0.23
Light-jet tagging efficiency (eigenvector 11) [%]	-	-	-	-	-	-	-	∓0.10
b-Quark tagging extrapolation [%]	∓0.24	-	-	±0.28	$^{+0.53}_{-0.55}$	$^{+0.74}_{-0.76}$	$^{+1.38}_{-1.41}$	$^{+1.62}_{-1.73}$
Electron energy scale [%]	-	-	-	-	-	-	$^{-}_{-0.25}$	-
Electron identification efficiency [%]	-	-	-	-	±0.10	±0.15	±0.18	$^{+0.34}_{-0.35}$
Electron isolation efficiency [%]	∓0.10	-	-	±0.14	$^{+0.18}_{-0.19}$	±0.34	±0.42	$^{+0.61}_{-0.62}$
Muon identification syst [%]	-	-	-	-	-	-	±0.11	±0.15
E_T^{miss} Soft jet resolution para [%]	-	-	-	-	-	±0.43	±0.10	-
E_T^{miss} Soft jet resolution perp [%]	-	-	-	-	-	±0.55	-	-
E_T^{miss} Soft jet scale [%]	-	-	-	-	$^{-}_{-0.18}$	-	$^{+0.18}_{-0.47}$	$^{+0.27}_{-}$
Z+jets cross-section [%]	-	-	-	-	±0.21	±0.38	$^{+0.68}_{-0.69}$	$^{+0.99}_{-1.00}$
Diboson cross-section [%]	-	-	-	-	-	-	±0.11	-
$t\bar{t}V$ cross-section [%]	-	-	-	-	-	-	±0.14	±0.22
Monte Carlo sample statistics [%]	±0.51	±0.70	±0.89	±1.19	±1.86	±3.13	±5.36	±5.86
ISR/FSR + scale [%]	$^{+0.64}_{-}$	$^{-}_{-1.44}$	$^{-}_{-0.70}$	$^{+1.02}_{-0.36}$	$^{+0.92}_{-1.08}$	$^{+7.95}_{-}$	$^{+11.4}_{-}$	$^{-}_{-5.67}$
Alternate hard-scattering model [%]	±0.39	±0.54	∓2.42	-	∓3.51	±6.79	±12.9	±16.0
Alternate parton-shower model [%]	±1.46	-	∓2.33	∓0.83	∓3.39	±0.58	±13.7	∓0.65
Fakes overall normalization, el [%]	∓0.17	$^{-0.12}_{+0.13}$	-	±0.33	$^{+0.55}_{-0.56}$	$^{+1.52}_{-1.54}$	$^{+0.51}_{-0.52}$	$^{+2.23}_{-2.27}$
Fakes overall normalization, mu [%]	-	-	-	-	$^{-0.40}_{+0.41}$	∓0.31	∓0.35	∓1.01
Fakes alternative parametrization [%]	±0.23	±0.22	-	∓0.60	∓0.31	∓2.50	∓0.34	∓2.53
W+jets heavy flavour component [%]	-	-	-	-	-	-	-	±0.24
W+jets Scales [%]	∓0.71	∓0.15	±0.29	±0.69	±1.74	±2.77	±3.42	±8.29
W+jets α_S [%]	-	-	-	-	$^{-0.11}_{+0.13}$	$^{-0.12}_{+0.23}$	$^{-0.19}_{+0.29}$	$^{-0.42}_{+0.83}$
Single Top DS/DR [%]	±0.73	±0.27	∓0.19	∓0.98	∓2.01	∓2.96	∓4.21	∓9.31
Single Top IFSR [%]	$^{-0.16}_{+0.20}$	-	$^{-}_{-0.24}$	$^{+0.14}_{-}$	$^{+0.59}_{-0.29}$	$^{+0.53}_{-}$	$^{+3.32}_{-1.33}$	$^{+2.59}_{-0.89}$

TABLE F.35: Table of systematics for the relative differential cross-section at the particle level for the $p_{\mathrm{T}}^{t,\,\mathrm{had}}$ observable.

Bins [Unit $y^{t,had}$]	0–0.50	0.50–1	1–1.50	1.50–2
$1/\sigma \cdot \mathrm{d}\sigma \,/\, \mathrm{d}y^{t,had}$	$7.57 \cdot 10^{-1}$	$6.41 \cdot 10^{-1}$	$4.20 \cdot 10^{-1}$	$1.82 \cdot 10^{-1}$
Total Uncertainty [%]	$^{+1.31}_{-1.45}$	$^{+1.77}_{-1.31}$	$^{+2.35}_{-2.63}$	$^{+2.95}_{-2.76}$
Statistics [%]	±0.7	±0.8	±1.0	±1.7
Systematics [%]	$^{+1.02}_{-1.19}$	$^{+1.48}_{-0.89}$	$^{+1.99}_{-2.31}$	$^{+2.11}_{-1.84}$
Effective mixed NP set 1 (JES) [%]	-	-	$^{+0.15}_{-0.14}$	-
Effective modelling NP set 1 (JES) [%]	-	-	$^{+0.10}_{-0.24}$	$^{-}_{+0.30}$
Effective modelling NP set 2 (JES) [%]	-	-	-	-
Effective statistical NP set 3 (JES) [%]	-	-	-	-
η intercalibration model (JES) [%]	$^{-0.81}_{+0.78}$	$^{-0.20}_{+0.34}$	$^{+1.08}_{-1.33}$	$^{+1.62}_{-1.39}$
η intercalibration non closure (JES) [%]	$^{+0.48}_{-0.47}$	$^{-0.12}_{+0.16}$	$^{-0.60}_{+0.39}$	$^{-0.19}_{+0.47}$
η intercalibration total stat (JES) [%]	-	-	$^{+0.11}_{-0.13}$	-
Flavour composition (JES) [%]	$^{-0.25}_{+0.24}$	-	$^{+0.28}_{-0.27}$	$^{-}_{+0.34}$
Flavour response (JES) [%]	$^{+0.18}_{-0.20}$	-	$^{-0.35}_{+0.18}$	$^{-}_{+0.32}$
Pile-up offset p_T (JES) [%]	$^{-0.28}_{+0.13}$	-	$^{+0.19}_{-0.22}$	$^{-}_{+0.44}$
Pile-up offset ρ topology (JES) [%]	-	-	$^{-}_{-0.19}$	$^{-0.35}_{-0.18}$
b-Quark tagging efficiency (eigenvector 0) [%]	-	-	-	$^{-}_{+0.34}$
Light-jet tagging efficiency (eigenvector 0) [%]	-	-	-	∓0.10
Z+jets cross-section [%]	-	-	-	∓0.22
Monte Carlo sample statistics [%]	±0.42	±0.49	±0.64	±1.06
ISR/FSR + scale [%]	$^{-}_{-0.39}$	$^{+1.06}_{-}$	$^{+0.50}_{-0.67}$	$^{-}_{-0.61}$
Alternate hard-scattering model [%]	-	∓0.77	±1.23	∓0.13
Alternate parton-shower model [%]	-	∓0.31	±0.64	-
Fakes alternative parametrization [%]	-	-	±0.12	-
W+jets Scales [%]	∓0.15	-	-	±0.67
Single Top DS/DR [%]	-	-	-	±0.44
Single Top IFSR [%]	-	$^{+0.27}_{-}$	$^{-}_{-0.37}$	$^{+0.33}_{-}$

TABLE F.36: Table of systematics for the relative differential cross-section at the particle level for the y^{had}observable.

Bins [GeV]	0–55	55–135	135–280	280–380	380–650	650–1000
$1/\sigma \cdot \mathrm{d}\sigma \,/\, \mathrm{d}p_T^{t\bar{t}}$	$5.09 \cdot 10^{-3}$	$3.93 \cdot 10^{-3}$	$1.72 \cdot 10^{-3}$	$8.09 \cdot 10^{-4}$	$2.52 \cdot 10^{-4}$	$1.92 \cdot 10^{-5}$
Total Uncertainty [%]	$^{+7.13}_{-6.89}$	$^{+3.56}_{-3.31}$	$^{+5.22}_{-5.45}$	$^{+5.42}_{-6.60}$	$^{+7.43}_{-8.31}$	$^{+15.0}_{-13.4}$
Statistics [%]	±1.0	±1.0	±1.2	±2.5	±2.5	±8.4
Systematics [%]	$^{+7.02}_{-6.78}$	$^{+3.34}_{-3.06}$	$^{+5.03}_{-5.26}$	$^{+4.54}_{-5.90}$	$^{+6.81}_{-7.76}$	$^{+11.6}_{-9.53}$
b-Tagged jet energy scale (JES) [%]	-	-	-	-	-	-
Effective detector NP set 1 (JES) [%]	-	-	-	-	-	$^{-0.29}_{+0.92}$
Effective detector NP set 2 (JES) [%]	-	-	-	-	-	$^{-0.12}_{+0.49}$
Effective mixed NP set 1 (JES) [%]	-	-	$^{-0.12}_{+0.28}$	$^{+0.24}_{-0.20}$	$^{-0.28}_{+0.18}$	$^{-}_{+2.25}$
Effective mixed NP set 2 (JES) [%]	-	-	-	-	-	$^{-1.66}_{+0.77}$
Effective mixed NP set 3 (JES) [%]	-	-	-	-	-	-
Effective modelling NP set 1 (JES) [%]	$^{-0.70}_{+0.60}$	$^{+0.21}_{-0.19}$	$^{+0.34}_{-0.22}$	$^{+0.33}_{-0.28}$	$^{+0.14}_{-0.45}$	$^{+1.51}_{-0.74}$
Effective modelling NP set 2 (JES) [%]	-	-	-	-	∓0.14	$^{+1.71}_{-0.78}$
Effective modelling NP set 3 (JES) [%]	-	-	-	-	-	$^{+0.63}_{-}$
Effective modelling NP set 4 (JES) [%]	-	-	-	-	-	$^{+0.92}_{-}$
Effective statistical NP set 1 (JES) [%]	$^{-0.12}_{+0.14}$	-	-	$^{+0.25}_{-}$	-	$^{+1.05}_{-0.57}$
Effective statistical NP set 2 (JES) [%]	-	-	-	-	-	$^{+0.51}_{-0.34}$
Effective statistical NP set 3 (JES) [%]	-	-	$^{-}_{-0.14}$	$^{-}_{+0.27}$	$^{-0.24}_{-0.18}$	$^{-0.43}_{+0.84}$
Effective statistical NP set 4 (JES) [%]	-	-	-	-	-	$^{+0.77}_{-}$
Effective statistical NP set 5 (JES) [%]	-	-	$^{-}_{+0.12}$	-	$^{-0.26}_{-0.23}$	$^{-0.34}_{+0.68}$
Effective statistical NP set 6 (JES) [%]	-	-	-	-	-	$^{+0.42}_{-}$
Effective statistical NP set 7 (JES) [%]	-	-	-	-	-	$^{+0.89}_{-}$
η intercalibration model (JES) [%]	$^{-0.36}_{+0.10}$	-	-	$^{+0.43}_{-0.83}$	-	$^{+1.23}_{-0.51}$
η intercalibration non closure (JES) [%]	-	-	-	$^{-0.28}_{+0.24}$	-	$^{+0.31}_{-}$
η intercalibration total stat (JES) [%]	$^{-0.11}_{+0.13}$	-	-	$^{+0.27}_{-0.12}$	-	$^{+0.89}_{-}$
Flavour composition (JES) [%]	$^{-0.98}_{+0.94}$	$^{+0.36}_{-0.32}$	$^{+0.39}_{-0.25}$	$^{+0.47}_{-0.79}$	$^{+0.27}_{-0.37}$	$^{+2.12}_{-2.83}$
Flavour response (JES) [%]	$^{+0.40}_{-0.43}$	-	$^{-0.24}_{+0.26}$	$^{-0.63}_{+0.43}$	-	$^{-0.64}_{+0.89}$
Pile-up offset μ (JES) [%]	-	-	-	-	-	$^{+0.52}_{-}$
Pile-up offset N_{PV} (JES) [%]	$^{-0.14}_{+0.16}$	-	-	$^{+0.23}_{-0.27}$	-	$^{+0.40}_{-}$
Pile-up offset p_T (JES) [%]	-	-	-	-	$^{-}_{-0.33}$	$^{-}_{+1.50}$
Pile-up offset ρ topology (JES) [%]	$^{-1.11}_{+1.05}$	$^{+0.27}_{-0.49}$	$^{+0.66}_{-0.34}$	$^{+0.71}_{-0.53}$	$^{-}_{+0.16}$ $^{-0.31}$	$^{-}_{+0.83}$ $^{-}$
Punch-through (JES) [%]	-	-	-	-	-	-
Jet vertex fraction [%]	$^{-0.15}_{+0.16}$	-	-	-	-	-
b-Quark tagging efficiency (eigenvector 0) [%]	±0.22	-	∓0.17	$^{-0.22}_{+0.23}$	$^{-0.30}_{+0.28}$	∓0.71
b-Quark tagging efficiency (eigenvector 1) [%]	-	-	-	$^{+0.26}_{-0.24}$	$^{+0.22}_{-0.21}$	-
b-Quark tagging efficiency (eigenvector 2) [%]	-	∓0.11	-	±0.28	±0.27	±0.24
c-Quark tagging efficiency (eigenvector 0) [%]	-	-	-	-	-	$^{+0.11}_{-0.12}$
Light-jet tagging efficiency (eigenvector 0) [%]	-	-	-	∓0.20	$^{-0.26}_{+0.27}$	$^{-1.12}_{+1.11}$
Light-jet tagging efficiency (eigenvector 1) [%]	-	-	-	$^{+0.12}_{-0.11}$	-	±0.23
Light-jet tagging efficiency (eigenvector 5) [%]	-	-	-	-	-	±0.10
Light-jet tagging efficiency (eigenvector 7) [%]	-	-	-	-	-	∓0.11
b-Quark tagging extrapolation [%]	-	-	-	$^{-0.17}_{+0.18}$	∓0.25	∓0.28
Electron energy resolution [%]	-	-	-	-	-	-
Electron isolation efficiency [%]	-	-	-	$^{-0.15}_{+0.16}$	∓0.16	-
E_T^{miss} Soft jet resolution para [%]	∓0.14	∓0.18	±0.29	±0.69	∓0.30	∓0.53
E_T^{miss} Soft jet resolution perp [%]	∓0.44	-	±0.31	±0.44	∓0.30	±0.46
E_T^{miss} Soft jet scale [%]	$^{-0.27}_{-}$	-	$^{+0.14}_{-0.31}$	$^{+0.26}_{-}$	$^{-}_{-0.20}$	-
Z+jets cross-section [%]	$^{-0.19}_{+0.20}$	-	-	$^{+0.31}_{-0.32}$	±0.34	±0.58
$t\bar{t}V$ cross-section [%]	-	-	-	-	±0.11	±0.12
Monte Carlo sample statistics [%]	±0.62	±0.63	±0.72	±1.55	±1.51	±4.37
ISR/FSR + scale [%]	$^{-0.89}_{+2.07}$	$^{-}_{+1.20}$	$^{+1.16}_{-2.14}$	$^{-}_{-3.35}$	$^{+0.89}_{-3.33}$	$^{+5.37}_{-}$
Alternate hard-scattering model [%]	∓4.17	±1.20	±4.15	±1.86	∓5.79	±2.45
Alternate parton-shower model [%]	∓3.82	±2.55	±1.18	∓2.71	±2.50	±6.32
Fakes overall normalization, el [%]	$^{-0.97}_{+0.99}$	-	$^{+0.77}_{-0.78}$	$^{+0.83}_{-0.84}$	$^{+0.11}_{-0.12}$	$^{-0.89}_{+0.90}$
Fakes overall normalization, mu [%]	∓0.32	±0.17	-	±0.26	-	∓0.19
Fakes alternative parametrization [%]	±2.67	∓0.52	∓1.70	∓2.26	∓0.40	±2.23
W+jets Scales [%]	∓0.69	∓0.10	±0.21	±0.66	±1.68	±2.74
W+jets α_S [%]	-	-	-	-	-	$^{-0.12}_{+0.24}$
Single Top DS/DR [%]	±0.59	-	∓0.21	∓0.46	∓0.98	∓2.48
Single Top IFSR [%]	$^{-0.17}_{+0.57}$	$^{-}_{-0.22}$	-	$^{-}_{-1.35}$	$^{+0.73}_{-}$	$^{+1.26}_{-1.29}$

TABLE F.37: Table of systematics for the relative differential cross-section at the particle level for the $p_{\mathrm{T}}^{t\bar{t}}$ observable.

Bins [GeV]	490–710	710–815	815–920	920–1035	1035–1165	1165–1310	1310–1500	1500–1700	1700–2100	2100–3000
$1/\sigma \cdot \mathrm{d}\sigma$ / $\mathrm{d}m^{t\bar{t}}$	$3.63 \cdot 10^{-4}$	$1.20 \cdot 10^{-3}$	$1.91 \cdot 10^{-3}$	$1.70 \cdot 10^{-3}$	$1.19 \cdot 10^{-3}$	$7.35 \cdot 10^{-4}$	$3.58 \cdot 10^{-4}$	$1.88 \cdot 10^{-4}$	$6.01 \cdot 10^{-5}$	$6.37 \cdot 10^{-6}$
Total Uncertainty [%]	+9.26 −7.20	+3.97 −4.17	+3.37 −3.96	+3.02 −3.53	+3.76 −3.30	+7.96 −7.64	+6.04 −5.87	+6.85 −7.67	+13.5 −11.9	+27.3 −27.0
Statistics [%]	±2.4	±1.7	±1.2	±1.2	±1.4	±1.9	±2.5	±3.6	±4.8	±12.
Systematics [%]	+8.80 −6.61	+3.40 −3.64	+3.04 −3.69	+2.62 −3.20	+3.34 −2.80	+7.64 −7.31	+5.30 −5.10	+5.38 −6.40	+12.3 −10.5	+23.9 −23.7
b-Tagged jet energy scale (JES) [%]	−0.13 +0.24	−0.50 -	-	+0.16 -	-	+0.11 −0.29	+0.40 -	-	- −0.31	-
Effective detector NP set 1 (JES) [%]	−0.11 +0.27	-	-	-	-	-	+0.30 -	-	- −0.19	+0.56
Effective detector NP set 2 (JES) [%]	-	-	-	-	-	-	-	-	-	+0.25
Effective mixed NP set 1 (JES) [%]	−0.65 +1.27	−0.89 +0.25	−0.56 +0.32	+0.20 −0.19	- +0.25	+0.67 −0.45	+1.21 −0.49	+0.66 −1.28	+1.68 −1.43	+1.45 −2.45
Effective mixed NP set 2 (JES) [%]	+0.17 −0.10	-	-	-	-	-	+0.23 -	- −0.25	−0.13 -	+0.30 -
Effective mixed NP set 3 (JES) [%]	-	-	-	-	-	-	-	-	-	-
Effective modelling NP set 1 (JES) [%]	+0.35 -	- −0.62	-	- -	−0.21 +0.35	+0.26 −0.42	+0.30 −0.11	- −0.33	- +0.24	+0.63 −0.28
Effective modelling NP set 2 (JES) [%]	−0.62 +0.38	−0.61 +0.11	−0.20 +0.18	-	-	+0.22 −0.27	+0.76 −0.19	+0.27 −0.77	+1.31 −1.13	+1.39 −1.14
Effective modelling NP set 3 (JES) [%]	+0.40 -	-	-	-	-	−0.31 -	+0.27 -	-	-	+0.29 -
Effective modelling NP set 4 (JES) [%]	−0.25 −0.12	−0.41 -	-	+0.13 -	-	-	+0.36 -	-	-	+0.56 -
Effective statistical NP set 1 (JES) [%]	+0.16 -	−0.20 -	-	- −0.13	-	+0.12	+0.22	−0.43 +0.13	+0.19	+0.50
Effective statistical NP set 2 (JES) [%]	+0.20 −0.18	−0.22 −0.29	-	+0.11 -	-	−0.13 +0.12	+0.47	−0.18 -	−0.26 +0.39	−0.37 +0.65
Effective statistical NP set 3 (JES) [%]	+0.17 +0.54	- -	+0.23	-	+0.26	−0.10 −0.33	−0.31	−0.50 −0.38	−0.32 −0.68	−0.57 +0.45
Effective statistical NP set 4 (JES) [%]	−0.31 −0.15	−0.61 -	−0.20 +0.18	- +0.15	-	+0.22 -	+0.58 -	+0.27 −0.13	+0.22 −0.25	−0.35 -
Effective statistical NP set 5 (JES) [%]	-	−0.23 -	-	-	-	+0.10	+0.23 +0.41	+0.28 −0.50	+0.28 −0.33	+0.34 −0.15
Effective statistical NP set 6 (JES) [%]	-	-	-	-	-	−0.20 -	+0.26	+0.16 -	+0.74 −0.10	+0.43 +0.43
Effective statistical NP set 7 (JES) [%]	−0.17 +0.39	−0.21 -	-	-	-	-	-	−0.26 -	+0.19 -	+0.39
η intercalibration model (JES) [%]	+0.58 +0.72	−0.31 +0.25	−0.27 +0.25	-	-	+0.41 −0.30	+0.52 −0.27	- −0.96	+1.40 −0.69	+2.04 −1.84
η intercalibration non closure (JES) [%]	−0.26	−0.53	-	-	-	+0.38	+0.22	−0.94 +0.14	+0.39 -	-
η intercalibration total stat (JES) [%]	+0.13	−0.27	-	-	-	-	-	-	-	+0.56 +0.41
Flavour composition (JES) [%]	+0.24 -	- −0.57	−0.32 +0.25	-	- +0.38	+0.21 −0.45	+0.62 -	−0.26 +0.59 −0.98	+0.77 −0.93	−0.16 +2.71 −2.53
Flavour response (JES) [%]	-	- −0.37	-	-	-	−0.22 +0.18	-	-	+0.43 −0.13	+0.35 −0.57
Pile-up offset μ (JES) [%]	-	- −0.26	-	-	-	+0.11 −0.27	+0.27 -	- −0.26	-	-
Pile-up offset N_{PV} (JES) [%]	-	- −0.55	+0.26 -	-	−0.15 +0.22	- −0.31	+0.29 -	-	- +0.41	-
Pile-up offset p_T (JES) [%]	−0.61 +0.49	−0.58 +0.37	-	- -	+0.29 -	+0.25 −0.29	+0.51 -	+0.46 −0.80	+0.10 −0.60	+1.27 -
Pile-up offset ρ topology (JES) [%]	+0.91 -	- −0.76	-	+0.23 −0.20	−0.37 +0.27	+0.23 −0.31	+0.29 -	- −0.47	−0.47 +0.66	+0.15 −1.14
Punch-through (JES) [%]	-	-	-	-	-	-	-	-	- −0.16	-
Jet vertex fraction [%]	+0.17 −0.18	-	-	-	-	-	-	-	-	-
b-Quark tagging efficiency (eigenvector 0) [%]	∓0.54	-	±0.14	-	-	-	-	−0.24 +0.22	−0.24 +0.21	−0.94 +0.91
b-Quark tagging efficiency (eigenvector 1) [%]	+0.57 −0.53	+0.32 −0.30	-	-	-	−0.19 +0.18	−0.27 +0.26	−0.38 +0.35	−0.47 +0.45	−0.89 +0.86
b-Quark tagging efficiency (eigenvector 2) [%]	±0.48	±0.19	-	-	-	∓0.17	∓0.18	−0.17 +0.16	∓0.23	∓0.36
b-Quark tagging efficiency (eigenvector 3) [%]	-	-	-	-	-	-	∓0.11	∓0.12	∓0.16	∓0.29
c-Quark tagging efficiency (eigenvector 0) [%]	±0.11	-	-	-	-	-	-	-	-	±0.11
c-Quark tagging efficiency (eigenvector 1) [%]	±0.15	-	-	-	-	-	-	−0.31 +0.30	∓0.39	∓0.94
c-Quark tagging efficiency (eigenvector 2) [%]	+0.15 −0.14	-	-	-	-	-	-	∓0.15	∓0.21	∓0.42
Light-jet tagging efficiency (eigenvector 0) [%]	−0.21 +0.22	+0.23 −0.24	±0.12	+0.22 −0.21	-	∓0.13	∓0.19	−0.36 +0.34	−0.73 +0.70	−2.29 +2.27
Light-jet tagging efficiency (eigenvector 1) [%]	±0.18	-	-	-	-	-	-	-	∓0.25	−0.93 +0.92
Light-jet tagging efficiency (eigenvector 2) [%]	+0.12 −0.11	-	-	-	-	-	-	-	-	-
Light-jet tagging efficiency (eigenvector 3) [%]	+0.17 −0.16	-	-	-	-	-	-	−0.16 +0.15	∓0.22	−0.49 +0.48
Light-jet tagging efficiency (eigenvector 4) [%]	-	-	-	-	-	-	-	-	-	±0.14
Light-jet tagging efficiency (eigenvector 5) [%]	-	-	-	-	-	-	-	-	±0.19	+0.57 −0.58
Light-jet tagging efficiency (eigenvector 6) [%]	-	-	-	-	-	-	-	-	∓0.13	−0.12 +0.13
Light-jet tagging efficiency (eigenvector 7) [%]	-	-	-	-	-	-	-	-	∓0.14	∓0.36
Light-jet tagging efficiency (eigenvector 9) [%]	-	-	-	-	-	-	-	-	-	∓0.19
b-Quark tagging extrapolation [%]	−0.31 +0.32	∓0.29	−0.20 +0.21	∓0.11	-	±0.20	+0.37 −0.38	+0.59 −0.61	+0.88 −0.90	+2.11 −2.16
Electron energy resolution [%]	-	−0.17 -	-	-	-	-	-	+0.20 -	- −0.27	+0.25 −0.12
Electron energy scale [%]	-	−0.22 -	-	-	-	-	-	+0.36 -	+0.14 −0.17	+0.37 −0.42
Electron identification efficiency [%]	−0.21 +0.22	-	-	-	-	-	+0.10 −0.11	±0.14	∓0.28 −0.29	±0.55
Electron isolation efficiency [%]	∓0.37	∓0.19	-	-	-	±0.12	+0.17 −0.18	±0.25	±0.32	±0.55
Muon (ID) momentum resolution [%]	-	-	-	-	-	-	+0.29 -	- −0.29	+0.29 -	- −1.08
Muon (MS) momentum resolution [%]	-	-	-	-	-	-	-	+0.21 −0.17	−0.20 -	+0.23 −0.36
Muon energy scale [%]	-	-	-	-	-	-	-	-	-	-
Muon trigger efficiency syst [%]	-	-	-	-	-	-	-	-	-	±0.18
Muon identification syst [%]	∓0.12	-	-	-	-	-	±0.10	±0.16	±0.18	±0.46
E_T^{miss} Soft jet resolution para [%]	±0.53	±0.42	±0.23	∓0.11	∓0.14	∓0.48	∓0.29	∓0.30	∓0.32	∓0.25
E_T^{miss} Soft jet resolution perp [%]	±0.95	±0.11	±0.22	-	∓0.29	∓0.58	-	∓0.43	∓0.42	∓0.29
E_T^{miss} Soft jet scale [%]	+1.06 −1.03	+0.13 −0.30	+0.13 −0.16	-	−0.16 +0.10	−0.36 +0.47	−0.16 +0.79	−0.78 +0.51	−0.44 +0.31	−0.42 +0.72
Z+jets cross-section [%]	±0.28	∓0.11	∓0.22	∓0.15	-	-	±0.21	±0.43	∓0.32	+2.05 −2.07
Diboson cross-section [%]	-	-	-	-	-	-	-	-	-	±0.10
$t\bar{t}V$ cross-section [%]	-	-	-	-	-	-	-	-	-	±0.12
Monte Carlo sample statistics [%]	±1.47	±1.03	±0.74	±0.76	±0.89	±1.14	±1.43	±2.21	±2.68	±4.81
ISR/FSR + scale [%]	+6.55 −2.84	−0.25 +1.84	−2.39 +1.08	- −1.88	+1.65 -	+2.34 -	- −1.66	- −2.42	+6.98 −3.08	+5.85 −2.15
Alternate hard-scattering model [%]	±4.77	±0.22	∓1.65	∓2.01	∓1.63	±6.87	∓2.70	∓1.15	±2.43	±6.42
Alternate parton-shower model [%]	∓0.11	±2.11	∓1.02	∓0.80	±1.85	∓0.96	∓2.90	±2.62	±3.99	∓6.88
Fakes overall normalization, el [%]	±0.30	-	−0.26 +0.27	∓0.19	−0.21 +0.22	∓0.11	±0.14	+0.61 −0.62	+1.77 −1.80	+5.12 −5.20
Fakes overall normalization, mu [%]	±0.21	-	-	-	∓0.20	±0.19	-	-	±0.38	∓1.02
Fakes alternative parametrization [%]	∓1.06	±0.28	±0.63	±0.30	±0.87	∓0.17	∓0.37	∓1.12	∓4.44	∓8.47
W+jets heavy flavour component [%]	-	-	-	-	-	-	-	-	-	±0.14
W+jets Scales [%]	±0.61	∓1.23	∓1.40	∓1.02	∓0.28	±0.93	±1.85	±2.77	±5.95	±15.8
W+jets α_S [%]	-	-	-	-	-	-	−0.10 +0.13	−0.22 +0.23	−0.31 +0.46	−0.96 +1.26
Single Top DS/DR [%]	±0.88	±1.00	±0.81	±0.59	-	∓1.09	∓1.64	∓2.51	∓3.17	∓7.31
Single Top IFSR [%]	+0.38 -	−0.11 +0.21	−0.10 +0.11	−0.38 -	−0.17 +0.10	+0.41 −0.31	+0.52 −0.20	-	+0.79 -	+1.07 −3.97

TABLE F.38: Table of systematics for the relative differential cross-section at the particle level for the $m_{t\bar{t}}$observable.

Bins [Unit $y^{t\bar{t}}$]	0–0.50	0.50–1	1–1.50	1.50–2
$1/\sigma \cdot \mathrm{d}\sigma \ / \ \mathrm{d}y^{t\bar{t}}$	$1.01 \cdot 10^{0}$	$6.96 \cdot 10^{-1}$	$2.57 \cdot 10^{-1}$	$3.29 \cdot 10^{-2}$
Total Uncertainty [%]	$^{+1.44}_{-1.57}$	$^{+2.72}_{-2.62}$	$^{+2.99}_{-2.78}$	$^{+9.79}_{-10.6}$
Statistics [%]	±0.5	±0.8	±1.5	±4.9
Systematics [%]	$^{+1.27}_{-1.41}$	$^{+2.54}_{-2.44}$	$^{+2.36}_{-2.09}$	$^{+8.00}_{-9.02}$
b-Tagged jet energy scale (JES) [%]	-	-	-	-
Effective detector NP set 1 (JES) [%]	-	-	-	$^{+0.23}_{-0.18}$
Effective mixed NP set 1 (JES) [%]	−0.16	-	+0.20	+0.23
Effective modelling NP set 1 (JES) [%]	-	-	−0.21	−0.10
Effective modelling NP set 4 (JES) [%]	-	-	-	-
Effective statistical NP set 1 (JES) [%]	-	-	-	$^{+0.35}_{-0.10}$
Effective statistical NP set 2 (JES) [%]	-	-	-	-
Effective statistical NP set 3 (JES) [%]	-	-	-	$^{+0.21}_{+0.23}$
Effective statistical NP set 5 (JES) [%]	-	-	-	-
Effective statistical NP set 6 (JES) [%]	-	-	-	$^{+0.34}_{-}$
Effective statistical NP set 7 (JES) [%]	-	-	-	$^{+0.20}_{-}$
η intercalibration model (JES) [%]	$^{-0.54}_{+0.47}$	$^{+0.31}_{-0.20}$	$^{+1.00}_{-0.93}$	$^{+1.70}_{-2.24}$
η intercalibration non closure (JES) [%]	$^{+0.21}_{-0.24}$	∓0.15	$^{-0.41}_{+0.49}$	$^{-}_{+0.24}$
η intercalibration total stat (JES) [%]	-	-	-	$^{+0.31}_{-0.20}$
Flavour composition (JES) [%]	−0.16	-	+0.26	$^{+0.35}_{-0.54}$
Flavour response (JES) [%]	-	-	−0.10	$^{-}_{-0.29}$
Pile-up offset N_{PV} (JES) [%]	-	-	-	+0.38
Pile-up offset p_T (JES) [%]	−0.19	-	+0.35	+0.53
Pile-up offset ρ topology (JES) [%]	+0.13	-	−0.47	−0.13
b-Quark tagging efficiency (eigenvector 0) [%]	-	-	∓0.10	-
Light-jet tagging efficiency (eigenvector 0) [%]	-	-	$^{-0.23}_{+0.22}$	∓0.28
Light-jet tagging efficiency (eigenvector 3) [%]	-	-	-	∓0.20
Light-jet tagging efficiency (eigenvector 8) [%]	-	-	-	∓0.10
Electron energy resolution [%]	-	-	-	-
Electron energy scale [%]	-	-	-	$^{+0.34}_{+0.21}$
Electron identification efficiency [%]	-	-	-	-
Muon (ID) momentum resolution [%]	-	-	-	$^{+0.36}_{-0.37}$
Muon (MS) momentum resolution [%]	-	-	-	-
Muon energy scale [%]	-	-	-	-
Muon identification syst [%]	-	-	-	$^{-0.35}_{+0.17}$
E_T^{miss} Soft jet resolution para [%]	-	-	-	±0.22
E_T^{miss} Soft jet resolution perp [%]	-	±0.14	-	±0.91
E_T^{miss} Soft jet scale [%]	-	-	-	-
Z+jets cross-section [%]	-	-	-	$^{+0.79}_{-0.14}$
Monte Carlo sample statistics [%]	±0.34	±0.50	±0.91	±0.23
ISR/FSR + scale [%]	$^{+0.26}_{-0.53}$	$^{-0.73}_{+0.92}$	$^{+1.19}_{-}$	±2.71
Alternate hard-scattering model [%]	∓0.53	±1.64	∓1.30	$^{-}_{-4.16}$
Alternate parton-shower model [%]	∓0.86	±1.55	∓0.32	∓6.43
Fakes overall normalization, el [%]	-	-	-	∓3.01
Fakes overall normalization, mu [%]	-	-	±0.15	$^{+0.53}_{-0.54}$
Fakes alternative parametrization [%]	±0.30	∓0.16	∓0.47	$^{+0.34}_{-0.35}$
W+jets Scales [%]	∓0.21	-	±0.46	∓1.81
Single Top DS/DR [%]	∓0.17	±0.20	-	±1.19
Single Top IFSR [%]	-	-	-	±0.53
				$^{-}_{-0.43}$

TABLE F.39: Table of systematics for the relative differential cross-section at the particle level for the $y_{t\bar{t}}$observable.

Bins [GeV]	350–530	530–629.50	629.50–715.50	715.50–801.50	801.50–909	909–1016.50	1016.50–1124	1124–1253	1253–1382	1382–2500
$1/\sigma \cdot \mathrm{d}\sigma \,/\, \mathrm{d}H_T^{t\bar{t}}$	$1.73 \cdot 10^{-4}$	$9.25 \cdot 10^{-4}$	$2.01 \cdot 10^{-3}$	$2.75 \cdot 10^{-3}$	$1.95 \cdot 10^{-3}$	$1.12 \cdot 10^{-3}$	$5.87 \cdot 10^{-4}$	$2.95 \cdot 10^{-4}$	$1.44 \cdot 10^{-4}$	$1.57 \cdot 10^{-5}$
Total Uncertainty [%]	+13.5 −9.54	+7.28 −6.89	+2.72 −3.25	+3.25 −4.39	+2.30 −2.28	+4.20 −4.39	+6.25 −5.52	+6.90 −6.32	+12.5 −10.0	+16.0 −15.8
Statistics [%]	±4.6	±2.1	±1.3	±1.1	±1.2	±1.7	±2.4	±3.2	±5.1	±5.5
Systematics [%]	+12.3 −7.82	+6.83 −6.41	+2.18 −2.82	+2.98 −4.19	+1.81 −1.78	+3.70 −3.91	+5.60 −4.77	+5.78 −5.08	+11.1 −8.23	+14.7 −14.5
b-Tagged jet energy scale (JES) [%]	+0.78 -	-	-	-	-	-	-	+0.37 -	+0.23 -	+0.14 −0.44
Effective detector NP set 1 (JES) [%]	- +0.45	−0.47 -	−0.22 −0.23	-	-	-	-	- +0.12	-	+0.25 −0.41
Effective detector NP set 2 (JES) [%]	+0.38 -	-	-	-	-	-	-	−0.22 -	+0.25 −0.11	-
Effective mixed NP set 1 (JES) [%]	- +1.64	−0.89 +0.49	−0.77 +0.39	−0.14 +0.33	-	+0.31 −0.34	+0.18 −0.86	+2.03 −0.78	+0.32 +1.24 −1.17	−0.19 ±3.10
Effective mixed NP set 2 (JES) [%]	+0.48 -	-	−0.22	-	-	-	-	−0.14 +0.15	+0.29 -	−0.28 -
Effective mixed NP set 3 (JES) [%]	-	-	-	-	-	-	-	-	-	−0.15
Effective modelling NP set 1 (JES) [%]	+1.40 -	- −0.73	-	+0.48	-	−0.43	−0.32 -	+0.21 -	+0.52 -	-
Effective modelling NP set 2 (JES) [%]	- +1.36	−0.76 -	−0.37 -	−0.13 +0.39	-	+0.27 −0.28	+0.10 −0.32	+0.89 -	+0.77 −0.48	+2.67 −2.23
Effective modelling NP set 3 (JES) [%]	+0.92 -	-	-	-	−0.23	−0.22	-	−0.52 +0.36	+0.32	-
Effective modelling NP set 4 (JES) [%]	- +0.38	−0.37 -	−0.23 -	-	-	+0.15 -	-	-	+0.27	+0.39
Effective statistical NP set 1 (JES) [%]	- +0.32	-	−0.26 −0.32	-	-	+0.12 -	-	-	-	−0.46 +0.41
Effective statistical NP set 2 (JES) [%]	- −0.19	−0.15	−0.21	-	-	+0.10	+0.18	+0.34 +0.46	+0.35	−0.43 +0.62
Effective statistical NP set 3 (JES) [%]	+0.33 +1.20	+0.31 +0.17	-	+0.36	-	−0.14 −0.41	−0.19 −0.48	−0.38 −0.25 −0.60	- −0.35	−0.90 −0.54
Effective statistical NP set 4 (JES) [%]	−0.16 +0.51	−0.56 -	−0.38 -	+0.20	-	+0.22 -	+0.28 −0.27	+0.88 −0.34	+0.88 -	+0.48 −0.51
Effective statistical NP set 5 (JES) [%]	- +0.39	−0.24 -	-	-	-	-	+0.25 -	+0.40 −0.24	+0.43 -	+0.27 −0.82
Effective statistical NP set 6 (JES) [%]	- -	−0.20 −0.21	-	-	+0.13 −0.24	- ±0.12	- +0.22	+0.15 -	+0.58 +0.27	+0.68 −0.38
Effective statistical NP set 7 (JES) [%]	+0.58	−0.13	−0.30	-	-	-	-	±0.12	-	+0.28 +0.17
η intercalibration model (JES) [%]	+1.62	+0.12 -	−0.49	-	-	-	+0.12	+0.59	+0.23 +0.47	+0.28 +0.67
η intercalibration non closure (JES) [%]	- +1.57	-	+0.25 -	-	-	−0.34 -	−0.51 -	−0.49 -	+0.84	−0.90 −0.65
η intercalibration total stat (JES) [%]	- +0.54	-	−0.26 -	-	-	- ∓0.11	−0.38 -	+0.16 +0.17	−0.11	+0.61
Flavour composition (JES) [%]	+1.30 -	-	-	−0.19	-	-	-	−0.13 +0.48	+0.44 +0.90	−0.25 +1.86
Flavour response (JES) [%]	- +1.03	−0.66 −0.28 -	+0.19 -	+0.43 -	−0.24	-	−0.26 -	- +0.40	- +1.50	−1.88 +0.29
Pile-up offset μ (JES) [%]	−0.24 -	-	−0.16 -	-	-	−0.26 -	−0.14 -	−0.33 -	+0.41	−0.54 −0.18
Pile-up offset N_{PV} (JES) [%]	+0.82 −0.54	-	−0.20 -	+0.37	-	−0.21	-	+0.35	−0.10 +0.63	-
Pile-up offset p_T (JES) [%]	+1.51 −0.23	−0.73 −0.48	−0.16 −0.47	-	−0.31 +0.27	+0.24	-	+0.47	+1.59	−0.29 +0.43
Pile-up offset ρ topology (JES) [%]	+0.93 +2.32	+0.18	+0.17 +0.10	+0.27 -	−0.33 -	−0.16 -	−0.25 −0.50	−0.48	−0.47	−1.12 -
Punch-through (JES) [%]	+0.21 -	−1.16 -	−0.54 -	+0.52 -	-	-	+0.20 -	+1.14 -	+0.28 -	-
Jet vertex fraction [%]	±0.21	±0.15	-	-	-	-	-	-	−0.22 -	-
b-Quark tagging efficiency (eigenvector 0) [%]	−0.82	∓0.26	+0.14	+0.18	-	-	-	−0.13	−0.31	−0.63
b-Quark tagging efficiency (eigenvector 1) [%]	+0.79 +0.61	+0.46	−0.12 +0.17	−0.17 -	-	−0.15	−0.28	+0.12 −0.25	+0.29 −0.35	+0.60 −0.66
b-Quark tagging efficiency (eigenvector 2) [%]	−0.57 ±0.60	−0.43 ±0.37	−0.16 ±0.11	-	-	+0.14 ∓0.13	+0.27 ∓0.18	+0.23 ∓0.20	+0.33 ∓0.19	+0.63 ∓0.31
b-Quark tagging efficiency (eigenvector 3) [%]	-	±0.10	-	-	-	-	∓0.12	∓0.14	∓0.15	∓0.28
c-Quark tagging efficiency (eigenvector 0) [%]	±0.15	±0.10	-	-	-	-	-	-	-	-
c-Quark tagging efficiency (eigenvector 1) [%]	±0.11	-	-	-	-	-	∓0.10	-	-	∓0.42
c-Quark tagging efficiency (eigenvector 2) [%]	±0.14	-	-	-	-	-	-	-	-	∓0.24
Light-jet tagging efficiency (eigenvector 0) [%]	−0.32 +0.37	-	-	±0.14	-	-	-	∓0.21	−0.35 +0.39	−0.87 +0.84
Light-jet tagging efficiency (eigenvector 1) [%]	±0.17	±0.21	-	-	-	-	-	-	-	∓0.43
Light-jet tagging efficiency (eigenvector 2) [%]	-	-	-	-	-	-	-	-	-	∓0.18
Light-jet tagging efficiency (eigenvector 3) [%]	-	±0.15	-	-	-	-	-	∓0.10	-	∓0.10
Light-jet tagging efficiency (eigenvector 5) [%]	-	-	-	-	-	-	-	-	±0.11	±0.41
Light-jet tagging efficiency (eigenvector 6) [%]	-	-	-	-	-	-	-	-	-	∓0.13
Light-jet tagging efficiency (eigenvector 7) [%]	-	-	-	-	-	-	-	-	-	∓0.35
b-Quark tagging extrapolation [%]	∓0.30	∓0.29	∓0.27	∓0.18	-	+0.20 −0.21	±0.42	+0.47 −0.48	+0.73 −0.77	+1.82 −1.88
Electron energy resolution [%]	-	-	-	-	-	-	-	-	-	-
Electron energy scale [%]	+0.12 −0.13	-	-	-	-	-	-	-	-	-
Electron identification efficiency [%]	∓0.25	−0.17 +0.18	-	-	-	-	±0.11	±0.13	±0.17	±0.29
Electron isolation efficiency [%]	−0.40 +0.41	−0.33 +0.34	∓0.17	-	-	±0.15	±0.22	±0.29	±0.35	±0.63
Muon (ID) momentum resolution [%]	- −0.26	-	-	-	-	-	-	-	-	-
Muon (MS) momentum resolution [%]	+0.10 −0.35	-	-	-	-	-	-	-	-	-
Muon identification syst [%]	∓0.11	∓0.10	-	-	-	-	-	±0.12	±0.13	±0.17
E_T^{miss} Soft jet resolution para [%]	∓0.28	±0.39	±0.46	∓0.17	∓0.15	∓0.14	±0.12	∓0.18	∓0.59	-
E_T^{miss} Soft jet resolution perp [%]	±0.42	±0.14	±0.40	-	∓0.31	-	∓0.37	∓0.13	∓0.43	±0.22
E_T^{miss} Soft jet scale [%]	−0.11 +0.28	+0.25 −0.20	+0.44 −0.55	-	−0.16 +0.19	−0.29 +0.18	−0.19 -	- +0.40	+0.57 -	- −0.42
Z+jets cross-section [%]	+0.76 −0.77	±0.28	-	∓0.13	-	-	-	-	±0.12	±0.47
$t\bar{t}V$ cross-section [%]	-	-	-	-	-	-	-	-	-	±0.11
Monte Carlo sample statistics [%]	±2.88	±1.33	±0.84	±0.66	±0.73	±1.01	±1.38	±1.84	±2.76	±2.84
ISR/FSR + scale [%]	+8.02 -	+4.03 −2.27	- −0.95	−3.51 +1.44	+0.72 −0.59	- −0.98	+3.27 -	+1.55 −0.56	+9.10 −6.61	+4.12 -
Alternate hard-scattering model [%]	±6.09	±3.76	±1.38	∓1.58	∓1.16	∓3.51	±3.18	∓3.44	±3.21	±8.76
Alternate parton-shower model [%]	∓0.62	±2.43	∓0.35	∓0.96	±0.35	±0.51	∓1.96	±0.28	-	±3.71
Fakes overall normalization, el [%]	+1.29 −1.31	+1.05 −1.07	+0.30 −0.31	∓0.30	−0.37 +0.38	∓0.28	±0.12	∓0.18	±0.22	+0.86 −0.88
Fakes overall normalization, mu [%]	±0.13	±0.20	∓0.15	-	-	±0.13	−0.40 +0.41	-	−0.17 +0.18	∓0.13
Fakes alternative parametrization [%]	∓2.94	∓2.60	∓0.32	±0.58	±0.60	±0.30	±1.09	±0.42	-	∓1.51
W+jets Scales [%]	±2.29	±0.34	∓0.69	∓0.78	∓0.25	±0.13	±0.67	±1.32	±2.20	±4.57
W+jets α_S [%]	∓0.13	-	-	-	-	-	-	-	−0.13	−0.26
Single Top DS/DR [%]	±1.22	±0.66	±0.92	±0.63	±0.25	∓0.22	∓1.81	∓2.32	+0.18 ∓2.03	+0.44 ∓7.35
Single Top IFSR [%]	+0.48 −0.15	−0.50 -	-	−0.21 +0.48	-	+0.31 −0.12	- −0.81	+0.76 −0.98	+2.42 -	+1.25 −1.74

TABLE F.40: Table of systematics for the relative differential cross-section at the particle level for the $H_T^{t\bar{t}}$ observable.

Bins [GeV]	0–30	30–70	70–110	110–160	160–250	250–340	340–500
$1/\sigma \cdot d\sigma$ / $dp_{out}^{t\bar{t}}$	$1.24 \cdot 10^{-2}$	$6.60 \cdot 10^{-3}$	$3.61 \cdot 10^{-3}$	$2.00 \cdot 10^{-3}$	$9.03 \cdot 10^{-4}$	$2.99 \cdot 10^{-4}$	$6.72 \cdot 10^{-5}$
Total Uncertainty [%]	$^{+3.45}_{-3.32}$	$^{+1.82}_{-1.38}$	$^{+4.66}_{-4.69}$	$^{+7.78}_{-9.56}$	$^{+3.75}_{-3.89}$	$^{+10.9}_{-11.8}$	$^{+10.0}_{-12.4}$
Statistics [%]	±0.8	±0.9	±1.4	±1.9	±2.2	±4.2	±6.4
Systematics [%]	$^{+3.31}_{-3.17}$	$^{+1.42}_{-0.78}$	$^{+4.32}_{-4.36}$	$^{+7.43}_{-9.28}$	$^{+2.61}_{-2.81}$	$^{+9.79}_{-10.7}$	$^{+6.84}_{-10.0}$
b-Tagged jet energy scale (JES) [%]	-	-	-	$^{-}_{-0.20}$	$^{+0.20}_{-}$	-	$^{-}_{-0.26}$
Effective detector NP set 1 (JES) [%]	-	-	-	-	-	$^{+0.31}_{-}$	-
Effective detector NP set 2 (JES) [%]	-	-	-	-	-	-	$^{-}_{-0.24}$
Effective mixed NP set 1 (JES) [%]	-	-	-	$^{-}_{-0.15}$	$^{+0.23}_{-}$	$^{-}_{+0.50}$	$^{-}_{+0.17}$
Effective mixed NP set 2 (JES) [%]	-	-	-	$^{+0.23}_{-}$	-	$^{-0.88}_{+0.23}$	$^{-0.20}_{-0.92}$
Effective modelling NP set 1 (JES) [%]	$^{-0.61}_{+0.60}$	$^{+0.18}_{-0.28}$	$^{+0.68}_{-0.67}$	$^{+0.48}_{-0.12}$	$^{+0.44}_{-0.28}$	$^{+0.11}_{-0.36}$	$^{-0.21}_{+0.22}$
Effective modelling NP set 2 (JES) [%]	-	-	-	$^{+0.35}_{-}$	-	$^{+0.12}_{-0.79}$	$^{-1.48}_{+0.68}$
Effective modelling NP set 3 (JES) [%]	-	-	-	-	-	$^{-0.20}_{+0.32}$	$^{-0.52}_{+0.23}$
Effective modelling NP set 4 (JES) [%]	-	-	-	-	-	$^{+0.27}_{-}$	-
Effective statistical NP set 1 (JES) [%]	-	-	±0.12	-	-	$^{-}_{+0.47}$	$^{-0.25}_{-}$
Effective statistical NP set 2 (JES) [%]	-	-	-	-	$^{-0.20}_{+0.13}$	$^{-}_{+0.58}$	$^{-0.80}_{-}$
Effective statistical NP set 3 (JES) [%]	-	-	-	$^{+0.13}_{-}$	-	$^{-}_{-0.32}$	$^{-0.48}_{-0.35}$
Effective statistical NP set 4 (JES) [%]	-	-	-	-	-	$^{+0.39}_{-}$	$^{+0.30}_{-}$
Effective statistical NP set 5 (JES) [%]	-	-	-	-	-	-	-
Effective statistical NP set 6 (JES) [%]	-	-	-	-	-	$^{-}_{+0.25}$	$^{-0.23}_{-}$
Effective statistical NP set 7 (JES) [%]	-	-	-	-	-	$^{-}_{+0.38}$	-
η intercalibration model (JES) [%]	$^{-0.28}_{+0.12}$	-	$^{+0.19}_{-}$	-	$^{+0.36}_{-0.15}$	$^{+0.15}_{-0.87}$	$^{+0.71}_{-0.52}$
η intercalibration non closure (JES) [%]	-	-	-	$^{-0.20}_{+0.15}$	-	$^{-0.21}_{+0.22}$	$^{-}_{-0.75}$
η intercalibration total stat (JES) [%]	-	-	$^{+0.17}_{-0.10}$	-	-	$^{+0.33}_{-}$	$^{-}_{-0.56}$
Flavour composition (JES) [%]	$^{-0.68}_{+0.69}$	$^{+0.10}_{-0.20}$	$^{+0.61}_{-0.62}$	$^{+0.87}_{-0.42}$	$^{+0.71}_{-0.33}$	$^{-}_{-0.58}$	$^{+0.51}_{-3.20}$
Flavour response (JES) [%]	$^{+0.25}_{-0.41}$	-	$^{-0.27}_{+0.36}$	$^{-0.12}_{+0.38}$	$^{-0.35}_{+0.41}$	$^{-}_{-0.27}$	$^{-1.13}_{+0.14}$
Pile-up offset μ (JES) [%]	-	-	-	-	-	$^{+0.23}_{-}$	-
Pile-up offset N_{PV} (JES) [%]	$^{-0.23}_{-}$	-	$^{+0.19}_{-}$	-	$^{+0.36}_{-0.19}$	$^{+0.46}_{-0.33}$	$^{-0.28}_{-0.28}$
Pile-up offset p_T (JES) [%]	-	-	-	$^{+0.14}_{-0.19}$	$^{+0.41}_{-}$	$^{-}_{-0.20}$	$^{+0.13}_{-0.42}$
Pile-up offset ρ topology (JES) [%]	$^{-0.97}_{+0.92}$	$^{+0.16}_{-0.40}$	$^{+1.18}_{-1.00}$	$^{+1.05}_{-0.40}$	$^{+0.91}_{-0.47}$	$^{-}_{-0.46}$	$^{-}_{-2.16}$
Punch-through (JES) [%]	-	-	-	-	-	$^{-}_{-0.25}$	-
b-Quark tagging efficiency (eigenvector 0) [%]	±0.13	-	-	$^{-0.13}_{+0.14}$	$^{-0.19}_{+0.20}$	∓0.45	$^{-0.30}_{+0.32}$
b-Quark tagging efficiency (eigenvector 1) [%]	-	-	-	-	$^{-0.17}_{+0.18}$	∓0.27	$^{-0.53}_{+0.52}$
b-Quark tagging efficiency (eigenvector 2) [%]	-	-	-	-	-	-	∓0.15
Light-jet tagging efficiency (eigenvector 0) [%]	-	-	-	-	-	-	$^{-0.14}_{+0.12}$
Light-jet tagging efficiency (eigenvector 1) [%]	-	-	-	-	-	∓0.12	-
Light-jet tagging efficiency (eigenvector 3) [%]	-	-	-	-	-	∓0.12	±0.17
Light-jet tagging efficiency (eigenvector 5) [%]	-	-	-	-	-	-	±0.10
Light-jet tagging efficiency (eigenvector 6) [%]	-	-	-	-	-	-	∓0.10
b-Quark tagging extrapolation [%]	-	-	-	-	-	±0.13	±0.27
Electron energy resolution [%]	-	-	-	-	-	-	-
Electron identification efficiency [%]	-	-	-	-	-	-	$^{+0.15}_{-0.16}$
Electron isolation efficiency [%]	-	-	-	-	-	-	±0.31
Muon (ID) momentum resolution [%]	-	-	-	-	-	-	-
Muon (MS) momentum resolution [%]	-	-	-	-	-	-	-
E_T^{miss} Soft jet resolution para [%]	-	-	∓0.11	±0.18	-	∓0.21	∓0.14
E_T^{miss} Soft jet resolution perp [%]	-	∓0.15	∓0.20	±0.40	-	±0.24	∓0.66
E_T^{miss} Soft jet scale [%]	$^{-}_{-0.14}$	-	$^{-0.26}_{-}$	$^{+0.22}_{-}$	$^{+0.16}_{-0.20}$	$^{+0.36}_{-}$	$^{-0.42}_{+0.32}$
Z+jets cross-section [%]	∓0.10	-	±0.12	±0.11	-	-	-
$t\bar{t}V$ cross-section [%]	-	-	-	-	-	±0.11	±0.15
Monte Carlo sample statistics [%]	±0.50	±0.58	±0.89	±1.16	±1.40	±2.50	±3.54
ISR/FSR + scale [%]	$^{+1.08}_{-}$	$^{+1.13}_{-}$	$^{-}_{-0.71}$	$^{+0.86}_{-5.74}$	$^{-}_{-1.72}$	$^{-3.90}_{+2.04}$	$^{-}_{-5.70}$
Alternate hard-scattering model [%]	∓2.29	∓0.30	±2.32	±7.03	±0.87	∓2.27	∓4.55
Alternate parton-shower model [%]	∓1.40	∓0.31	±3.23	∓1.24	±1.04	±8.59	∓0.98
Fakes overall normalization, el [%]	-	-	±0.10	-	∓0.21	$^{-0.43}_{+0.44}$	$^{-0.49}_{+0.50}$
Fakes overall normalization, mu [%]	-	-	-	±0.18	-	-	±0.20
Fakes alternative parametrization [%]	-	-	∓0.21	∓0.18	±0.42	±1.06	±0.61
W+jets heavy flavour component [%]	-	-	-	-	-	∓0.10	∓0.11
W+jets Scales [%]	∓0.35	-	±0.28	±0.33	±0.29	±0.36	±0.59
Single Top DS/DR [%]	±0.56	±0.14	∓0.11	∓0.16	∓1.35	∓2.60	∓4.33
Single Top IFSR [%]	$^{+0.41}_{-}$	-	$^{-}_{-0.48}$	$^{+0.31}_{-0.13}$	$^{-}_{+0.23}$	$^{+0.15}_{-1.34}$	$^{+0.37}_{-1.01}$

TABLE F.41: Table of systematics for the relative differential cross-section at the particle level for the $p_{\mathrm{out}}^{t\bar{t}}$observable.

Bins [GeV] x	490–815	815–930	930–1200	1200–3000	3000–3325	3325–3440	3440–3710	3710–5510	5510–5730	5730–5870	5870–5970	5970–6370	6370–8020.00
$1/\sigma \cdot d\sigma$ / $d m^{t\bar{t}}[GeV] vs extra jet N$	$6.55 \cdot 10^{-5}$	$4.96 \cdot 10^{-4}$	$3.68 \cdot 10^{-4}$	$2.84 \cdot 10^{-5}$	$1.53 \cdot 10^{-4}$	$5.79 \cdot 10^{-4}$	$3.97 \cdot 10^{-4}$	$3.29 \cdot 10^{-5}$	$2.77 \cdot 10^{-4}$	$7.21 \cdot 10^{-4}$	$8.35 \cdot 10^{-4}$	$4.63 \cdot 10^{-4}$	$3.50 \cdot 10^{-5}$
Total Uncertainty [%]	+15.6 −18.5	+7.92 −7.61	+7.83 −8.24	+8.44 −7.44	+7.82 −8.31	+4.69 −5.41	+8.33 −8.49	+9.70 −8.31	+6.91 −6.66	+8.58 −8.18	+5.76 −6.42	+8.95 −9.00	+11.1 −12.5
Statistics [%]	±4.8	±2.6	±2.0	±2.9	±3.1	±2.4	±2.0	±2.9	±2.8	±1.9	±2.1	±1.4	±3.0
Systematics [%]	+14.6 −17.7	+7.31 −6.96	+7.47 −7.91	+7.69 −6.59	+6.93 −7.47	+3.74 −4.61	+7.98 −8.15	+9.05 −7.54	+6.05 −5.77	+8.26 −7.85	+5.20 −5.91	+8.78 −8.83	+10.6 −12.0
b-Tagged jet energy scale (JES) [%]	−2.14	+0.14	-	-	−0.39	−0.23	+0.22	+0.20	-	−0.13	+0.39	+0.18	-
Effective detector NP set 1 (JES) [%]	+0.17 −1.03	- -	-	-	+0.17 -	+0.38 -	−0.22 -	- -	- -	- -	- -	−0.15 -	+0.31 +0.30
Effective detector NP set 2 (JES) [%]	- -	+0.27 -	-	-	-	+0.17 -	-	-	+0.23 -	-	-	-	−0.30 -
Effective mixed NP set 1 (JES) [%]	−1.06 2.65	−0.51 +0.25	-	+0.92 −0.31	−0.64 -	−0.76 +0.53	- −0.39	+0.86 −0.47	−0.49 +1.15	−0.34 +0.24	−0.37 +0.46	+0.43 −0.21	+1.29 −1.40
Effective mixed NP set 2 (JES) [%]	- −0.99	+0.26 -	-	-	-	-	-	-	+0.15 -	-	-	-	−0.22 -
Effective mixed NP set 3 (JES) [%]	−0.43 -	- -	-	-	−0.18 −0.15	-	-	-	-	-	-	-	-
Effective modelling NP set 1 (JES) [%]	−5.42	−2.08	−2.31	−2.01	−1.56	−0.51	−0.22	−0.79	+0.82	+1.33	+1.75	+2.13	+1.56
Effective modelling NP set 2 (JES) [%]	+4.30 -	+2.20 +0.24	+1.48 -	+2.87 +0.69	+0.90 −0.65	+0.47 −0.50	+0.74 +0.30	+0.86 +0.61	−0.32 −0.58	−1.24 −0.24	−1.95 −0.29	−1.91 -	−2.94 +0.83
Effective modelling NP set 3 (JES) [%]	−1.48 -	−0.12 -	−0.16 −0.15	−0.37 −0.34	+0.16 -	+0.54 +0.33	−0.36 −0.30	−0.41 -	+0.46 +0.34	+0.25 -	+0.53 +0.50	+0.15 -	−0.96 −0.16
Effective modelling NP set 4 (JES) [%]	−1.17 −1.03	+0.41 -	+0.15 -	+0.19 -	−0.77 -	−0.20 +0.20	+0.32 -	- -	- -	- -	−0.22 -	- -	+0.31 −0.21
Effective statistical NP set 1 (JES) [%]	−1.92	-0.40	−0.31	−0.32	+0.50	−0.25	-	-	+0.11 -	+0.21	+0.41	+0.33	+0.48
Effective statistical NP set 2 (JES) [%]	+0.63 +0.48	+0.29 +0.10	+0.30 +0.17	+0.26 +0.52	+0.24 -	- +0.25	+0.26 +0.31	+0.17	-0.28	−0.25 −0.30	−0.43 −0.53	−0.27 −0.25	−0.73 +0.14
Effective statistical NP set 3 (JES) [%]	−0.52 -	−0.19 -	−0.26 -	−0.42 −0.33	- -	- +0.48	−0.25 −0.24	−0.39 −0.18	+0.18 +0.55	+0.24 -	+0.48 +0.46	+0.34 −0.18	−0.29 −0.64
Effective statistical NP set 4 (JES) [%]	−2.21 -	+0.28	+0.19	+0.30 -	−0.56 -	−0.34 -	+0.22 +0.13	+0.32 −0.12	−0.24 -	- -	- -	+0.11 -	+0.43 ±0.25
Effective statistical NP set 5 (JES) [%]	−1.26 -	- +0.26	−0.17 +0.26	-	−0.22 -	-	−0.11 +0.19	+0.24 -	-	-	-	-	−0.43
Effective statistical NP set 6 (JES) [%]	−0.96 -	−0.11 -	−0.16 -	-	−0.30 -	-	-	-	-	-	-	-	+0.30 -
Effective statistical NP set 7 (JES) [%]	−0.76 -	+0.27 -	-	-	-	−0.11 +0.33	-	-	-0.37	-	-	+0.17 −0.13	+0.22
η intercalibration model (JES) [%]	−1.10 2.64	−1.05	−0.69	−0.15	−0.71	−0.53	-	-	+0.42	+0.71	+0.27	+0.44	+0.24 +1.76
η intercalibration non closure (JES) [%]	+1.49 +1.12	+0.72 +0.25	+0.47 -	+0.57 -	+0.75 +0.31	+0.72 +0.47	−0.35 -	+0.71 -	+0.65 -	- -	−0.58 −0.36	−0.47 -	−1.72 −0.62
η intercalibration total stat (JES) [%]	−2.43 1.63	−0.10	−0.35	−0.40	−0.68 −0.53	- -	−0.23 -	- -	−0.17 -	+0.37 +0.21	+0.12 +0.46	+0.36	+0.42 +0.23
Flavour composition (JES) [%]	+0.26 −6.66	+0.23 −2.55	+0.21 −2.90	+0.38 −2.23	+0.17 −1.61	+0.54 −0.82	+0.26 −0.60	+0.20 −0.20	+0.50	−0.36 +1.45	−0.41 +2.25	−0.21 +2.40	+0.70 +2.88
Flavour response (JES) [%]	+4.81 +3.12	+2.90 +1.92	+2.53 +0.86	+3.31 +1.95	+1.97 +0.56	+0.81 +0.31	+1.08 +0.51	+0.76 +0.58	−0.37 −0.30	−1.39 −1.09	−2.58 −1.40	−2.73 −1.15	−3.37 −1.38
Pile-up offset μ (JES) [%]	−3.35 -	−1.23 +0.52	−1.16 -	−1.28 -	−1.59 -	+0.29 -	−0.46 -	−0.65 +0.25	+0.39 −0.20	+1.12 -	+1.18 −0.19	+1.37 -	+0.80 -
Pile-up offset N_{PV} (JES) [%]	−1.10 −2.27	+0.50	−0.26 −0.75	-	−0.43	+0.45	-	−0.21 +0.33	+0.21 +0.31	-	+0.25 +0.37	-	+0.30
Pile-up offset p_T (JES) [%]	+0.14 −2.89	- -	+0.28	−0.64 +0.90 +0.52	−0.65	−0.18	+0.32 +0.17	+0.66	−0.46	−0.30 −0.27	−0.30 +0.42	+0.54 −0.59 -	−0.38 +0.30
Pile-up offset ρ topology (JES) [%]	+0.74 −5.21	−0.34 −3.25	−0.35 −3.42	−3.04	−2.62	+0.20 −0.80	−0.58 −3.38	−0.18 −1.88	+0.48 +1.31	+0.66 +2.23	+0.42 +2.61	+2.84	+0.56 +1.59
Punch-through (JES) [%]	+5.29 -	+2.76 -	+2.46 -	+3.73 -	+1.61 -	+0.79 -	+0.86 -	+1.97 -	−0.67 -	−1.71 -	−2.80 -	−2.92 -	−2.52 -
Jet vertex fraction [%]	∓0.40	−0.36	−0.35	−0.45	−0.25	∓0.10	∓0.14	−0.20	±0.25	±0.28	±0.32	+0.30	+0.31
b-Quark tagging efficiency (eigenvector 0) [%]	+0.42	+0.37 +0.37	+0.36 ±0.16	+0.46 -	+0.24 -	-	-	+0.19 -	−0.60	-	-	−0.31 -	−0.32 −0.36
b-Quark tagging efficiency (eigenvector 1) [%]	−0.41 +0.36	−0.36 ±0.13	-	−0.12	+0.45	-	−0.13	−0.28	+0.59 +0.59	+0.29	-	∓0.12	+0.35 −0.58
b-Quark tagging efficiency (eigenvector 2) [%]	−0.35 -	-	-	+0.10 -	−0.42 ±0.27	-	+0.12 −0.12	+0.26 ∓0.19	−0.55 ±0.48	−0.27 ±0.21	-	-	+0.57 ∓0.27
b-Quark tagging efficiency (eigenvector 3) [%]	±0.10	-	-	-	-	-	+0.13 -	∓0.10	-	±0.10	-	-	∓0.19
c-Quark tagging efficiency (eigenvector 0) [%]	-	-	-	-	-	-	-	-	±0.12	-	-	-	-
c-Quark tagging efficiency (eigenvector 1) [%]	-	-	±0.11	-	-	-	-	∓0.20	±0.19	±0.11	-	-	∓0.44
c-Quark tagging efficiency (eigenvector 2) [%]	-	-	-	-	-	-	-	-	±0.17	-	-	-	∓0.20
Light-jet tagging efficiency (eigenvector 0) [%]	±0.31	±0.18	±0.17	−0.16 +0.15	±0.17	±0.25	±0.12	−0.54 +0.52	∓0.19	+0.11 −0.12	-	-	−0.57 +0.55
Light-jet tagging efficiency (eigenvector 1) [%]	-	-	-	-	-	-	-	∓0.16	+0.16 −0.15	-	±0.13	-	∓0.19
Light-jet tagging efficiency (eigenvector 2) [%]	-	-	-	-	-	-	-	-	∓0.15	-	-	-	-
Light-jet tagging efficiency (eigenvector 3) [%]	-	-	-	-	±0.10	-	-	∓0.19	−0.14 +0.19 −0.18	-	-	-	∓0.18
Light-jet tagging efficiency (eigenvector 5) [%]	-	-	-	-	-	-	-	-	-	-	-	-	±0.13
b-Quark tagging extrapolation [%]	−0.24 +0.25	∓0.19	-	+0.28 −0.29	∓0.28	∓0.20	-	+0.45 −0.47	−0.31 +0.32	−0.29 +0.30	∓0.24	-	+0.95 −0.97
Electron energy resolution [%]	-	-	-	-	-	-	-	-	-	-	-	-	-
Electron energy scale [%]	−0.60	-	∓0.11	+0.12 −0.15	−0.28 -	−0.13 -	-	-	+0.14 -	-	+0.26 -	+0.15 -	+0.23 −0.16
Electron identification efficiency [%]	-	-	-	±0.14	∓0.11	-	-	±0.17	∓0.22	∓0.11	-	-	±0.20
Electron isolation efficiency [%]	-	-	-	±0.25	∓0.21	-	-	±0.25	∓0.37	∓0.22	-	-	+0.24 −0.25
Muon (MS) momentum resolution [%]	-	-	-	-	-	-	-	-	-	-	-	-	-
Muon identification syst [%]	-	-	-	±0.14	-	-	-	±0.16	∓0.12	∓0.10	-	-	±0.16
E_T^{miss} Soft jet resolution para [%]	±1.34	±0.17	-	∓0.38	±0.53	±0.32	∓0.51	∓0.12	±0.33	±0.52	±0.11	∓0.19	∓0.64
E_T^{miss} Soft jet resolution perp [%]	±0.75	±0.64	∓0.29	∓0.27	±0.75	±0.29	∓0.58	∓0.25	±0.71	±0.30	-	∓0.14	∓0.45
E_T^{miss} Soft jet scale [%]	+0.96 −1.66	+0.32 -	−0.16 ±0.11	−0.37 +0.32	∓0.58 −0.83	+0.45 -	−0.40 -	−0.19 +0.43	+1.04 −1.08	- -	- +0.37	−0.23 +0.24	−0.52 +0.20
Z+jets cross-section [%]	∓0.29	−0.32	∓0.30	∓0.14	-	∓0.28	∓0.14	±0.43	±0.26	-	-	±0.11	±0.87 −0.88
$t\bar{t}V$ cross-section [%]	±0.10	+0.33 ±0.11	±0.10	-	-	-	-	-	-	-	-	-	±0.13
Monte Carlo sample statistics [%]	±2.92	±1.49	±1.15	±1.79	±1.83	±1.46	±1.23	±1.83	±1.67	±1.19	±1.29	±0.89	±1.62
ISR/FSR + scale [%]	+3.75 ∓8.42	+0.53 ±2.45	+2.52 ±5.12	- ±2.45	+2.55 −0.57 ∓4.41	−3.60 +1.76 ±1.25	- −2.56 ∓4.37	+4.44 ±2.14	+2.54 −2.28 ±4.17	−2.52 +2.99 ±5.66	- −1.98 ±1.40	+1.08 −0.96 ±4.88	- −4.34 ±5.81
Alternate hard-scattering model [%]	∓3.68	±3.38	∓1.04	∓2.80	∓3.22	∓0.44	∓6.06	∓4.40	±0.50	±3.41	±2.04	±5.37	±2.73
Alternate parton-shower model [%]	+0.60 −0.61	−0.35 +0.36	−0.32 +0.33	+0.58 −0.59	+0.27 −0.28	−0.39 +0.40	∓0.28	+0.56 −0.57	+0.10 −0.11	−0.24 +0.25	−0.21 +0.22	-	+0.87 −0.89
Fakes overall normalization, el [%]	±0.82	+0.17 +0.18	−0.25 +0.26	-	∓0.26	-	-	+0.34 −0.35	-	-	±0.18	-	∓0.11
Fakes overall normalization, mu [%]	∓2.91	±1.10	±1.20	∓1.19	-	±0.81	±0.40	∓1.87	±0.37	±0.58	-	-	∓1.57
Fakes alternative parametrization [%]	-	±0.15	-	-	-	-	-	-	-	-	-	-	-
W+jets heavy flavour component [%]	∓1.92	±2.09	∓1.40	±0.65	∓0.62	∓1.10	∓0.63	±4.29	±0.37	∓1.07	∓1.06	±0.23	±5.33
W+jets Scales [%]	+0.13 −0.14	+0.12 −0.14	-	-	-	-	-	−0.25 +0.31	-	-	-	-	−0.29 +0.40
W+jets α_S [%]	±2.22	±1.07	±1.14	+0.12 ∓0.77	±0.71	±1.13	±0.52	∓2.22	±1.00	±0.90	±0.28	∓1.00	∓3.53
Single Top DS/DR [%]	+0.31 -	−0.18 +0.58	−0.27 +0.71	−0.41	−0.53 +0.13	−0.34	+1.17	+0.73 -	+0.78 -	-	−0.68	−0.99	+1.04 −1.58
Single Top IFSR [%]													

TABLE F.42: Table of systematics for the relative differential cross-section at the particle level for the $m^{t\bar{t}}$ vs extra jet N observable.

Bins [GeV] x [GeV]	350–400	400–455	455–550	550–2000	2000–2050	2050–2105	2105–2200	2200–2350	2350–3650	3650–3700	3700–3755	3755–3850	3850–4000	4000–5300
$1/\sigma \cdot d\sigma$ / $dp_T^{had}[GeV]vsp_T^{t\bar{t}}$	$1.68 \cdot 10^{-3}$	$1.01 \cdot 10^{-3}$	$4.05 \cdot 10^{-4}$	$1.11 \cdot 10^{-5}$	$3.78 \cdot 10^{-3}$	$2.17 \cdot 10^{-3}$	$9.29 \cdot 10^{-4}$	$2.39 \cdot 10^{-4}$	$5.21 \cdot 10^{-6}$	$2.37 \cdot 10^{-3}$	$1.71 \cdot 10^{-3}$	$9.48 \cdot 10^{-4}$	$3.16 \cdot 10^{-4}$	$1.27 \cdot 10^{-5}$
Total Uncertainty [%]	+7.63 −7.69	+7.58 −7.98	+9.80 −9.00	+23.1 −22.3	+3.16 −3.15	+3.55 −3.90	+5.40 −3.21	+6.31 −8.00	+24.5 −19.2	+9.37 −8.37	+4.01 −5.19	+3.53 −6.71	+7.67 −8.24	+18.0 −16.4
Statistics [%]	±2.1	±2.5	±3.3	±5.5	±1.4	±1.7	±2.1	±3.5	±9.9	±2.0	±2.1	±2.2	±3.0	±5.4
Systematics [%]	+7.20 −7.27	+6.96 −7.40	+9.03 −8.15	+22.2 −21.5	±2.68	+2.91 −3.33	+4.80 −2.03	+4.77 −6.85	+21.8 −15.6	+9.06 −8.02	+3.13 −4.54	+2.42 −6.19	+6.80 −7.44	+17.0 −15.2
b-Tagged jet energy scale (JES) [%]	−0.23	-	+0.49	+0.51	-	-	+0.20	+0.47	-	+0.32	-	-	-	+0.28
Effective detector NP set 1 (JES) [%]	-	−0.60	−0.17	-	-	-	+0.15	+0.17	−0.23	-	-	−0.24	-	+0.36
Effective detector NP set 2 (JES) [%]	-	-	-	-	-	-	-	-	−0.39	-	-	-	-	-
Effective mixed NP set 1 (JES) [%]	-	-	-	-	-	-	-	-	-	-	-	-	-	-
Effective mixed NP set 2 (JES) [%]	−0.50	-	+1.32	+1.48	−0.42	-	+0.58	+1.72	+2.41	−0.59	−0.17	-	+0.34	+2.43
Effective mixed NP set 3 (JES) [%]	+0.77	−1.00	−0.45	−0.56	+0.34	-	−0.10	−0.88	−3.41	+0.57	+0.51	−0.51	−0.17	−1.27
Effective modelling NP set 1 (JES) [%]	-	-	-	-	-	-	-	-	-	-	-	-	-	+0.22
Effective modelling NP set 2 (JES) [%]	-	-	-	-	-	-	+0.14	+0.20	−0.29	-	-	-	-	-
Effective modelling NP set 3 (JES) [%]	-	-	-	-	-	-	-	-	-	-	-	-	-	-
Effective modelling NP set 4 (JES) [%]	−1.19	−1.21	−0.42	−0.87	+0.20	+0.29	+0.44	+0.56	-	+0.40	-	+0.31	-	+0.92
Effective statistical NP set 1 (JES) [%]	+1.31	-	+0.61	+1.60	−0.25	−0.16	-	-	−0.45	-	−0.23	−1.14	-	-
Effective statistical NP set 2 (JES) [%]	−0.32	-	+0.75	+1.31	−0.28	−0.11	+0.31	+1.09	+2.24	−0.42	-	-	+0.12	+1.91
Effective statistical NP set 3 (JES) [%]	+0.45	−0.71	−0.34	-	+0.16	+0.19	−0.27	−0.24	−2.63	+0.41	+0.31	−0.42	−0.14	−0.72
Effective statistical NP set 4 (JES) [%]	+0.13	−0.57	−0.35	+0.60	-	-	-	+0.34	+0.17	+0.32	-	−0.25	-	+0.25
Effective statistical NP set 5 (JES) [%]	−0.14	-	+0.45	-	-	-	+0.21	-	−0.62	−0.23	-	-	-	-
Effective statistical NP set 6 (JES) [%]	-	-	-	+0.24	-	-	-	-	+0.33	-	-	-	−0.28	+0.71
Effective statistical NP set 7 (JES) [%]	-	-	-	-	-	-	-	-	−0.50	-	-	-	-	−0.29
Effective statistical model (JES) [%]	−0.38	-	+0.28	+0.49	-	-	-	+0.27	+0.55	-	-	+0.16	-	+0.53
Effective statistical NP set 1 (JES) [%]	+0.18	−0.24	-	-	-	-	−0.18	−0.10	−1.47	-	-	−0.20	-	-
Effective statistical NP set 2 (JES) [%]	-	-	+0.54	+0.75	-	−0.15	+0.30	+0.33	+0.10	−0.11	−0.31	-	-	+0.67
Effective statistical NP set 3 (JES) [%]	+0.57	-	−0.21	−0.18	+0.18	+0.12	−0.28	−0.39	−0.69	+0.16	+0.21	-	−0.22	−0.15
Effective statistical NP set 4 (JES) [%]	−0.35	−0.63	+0.93	−0.52	−0.35	-	+0.52	+0.96	+0.55	−0.46	+0.34	−0.49	−0.39	+0.68
Effective statistical NP set 5 (JES) [%]	-	-	-	−0.21	-	-	-	−0.26	−0.59	−0.43	−0.13	+0.28	+0.32	-
Effective statistical NP set 6 (JES) [%]	-	−0.41	+0.20	+0.39	-	-	-	+0.53	+0.31	-	−0.17	-	+0.23	−0.30
Effective statistical NP set 7 (JES) [%]	-	+0.24	+0.20	−0.23	-	-	-	−0.33	−0.84	-	-	+0.10	−0.13	+0.48
Flavour composition (JES) [%]	-	−0.37	−0.15	+0.18	-	-	-	+0.21	+0.94	+0.22	-	−0.22	+0.25	−0.57
Flavour response (JES) [%]	+0.29	-	-	-	-	-	+0.36	-	−0.41	−0.14	-	+0.19	-	+0.75
Pile-up offset μ (JES) [%]	+0.21	−0.22	-	-	-	-	−0.16	+0.23	+0.14	-	-	−0.16	-	−0.51
Pile-up offset N_{PV} (JES) [%]	-	-	-	-	-	-	+0.17	-	-	-	-	-	-	+0.42
η intercalibration model (JES) [%]	−1.20	-	+0.25	−0.11	-	-	+0.27	+0.63	−0.31	+0.51	-	+0.23	+0.31	+0.89
η intercalibration non closure (JES) [%]	+0.52	−0.79	-	+0.71	-	-	-	-	+0.89	-	−0.34	−0.44	−0.20	−0.39
η intercalibration total stat (JES) [%]	+0.24	-	+0.47	+0.44	-	-	-	−0.11	+0.45	+0.42	-	-	-	+0.48
Flavour composition (JES) [%]	−0.70	−0.58	-	-	-	-	-	+0.24	-	-	−0.28	−0.22	-	-
Flavour response (JES) [%]	−0.34	-	+0.43	+0.70	-	-	-	+0.14	-	-	-	-	-	+0.52
Pile-up offset μ (JES) [%]	-	−0.24	-	-	-	-	-	-	−0.76	-	−0.27	-	−0.22	-
Pile-up offset N_{PV} (JES) [%]	−1.59	-	−0.21	−0.54	-	+0.32	+0.37	+0.91	+2.15	+0.41	-	+0.18	+0.29	+2.06
Flavour response (JES) [%]	+1.69	−1.70	+1.28	+1.13	-	−0.12	-	-	−2.30	−0.26	-	−1.06	−0.34	−1.84
Pile-up offset μ (JES) [%]	+0.64	-	+0.53	+1.41	-	−0.35	+0.22	+0.88	-	−0.33	−0.22	−0.88	-	+0.74
Pile-up offset N_{PV} (JES) [%]	−0.89	−0.62	-	−0.52	-	+0.33	-	−0.26	−0.20	+0.23	+0.13	+0.45	-	-
Pile-up offset p_T (JES) [%]	-	-	+0.62	+0.45	-	-	-	-	-	-	-	-	-	+0.27
Pile-up offset ρ topology (JES) [%]	-	-	−0.23	-	-	-	-	-	−0.43	+0.34	-	-	-	-
Punch-through (JES) [%]	−0.43	-	-	+0.50	+0.37	−0.11	-	−0.29	-	-	−0.25	-	+0.16	+0.87
Jet vertex fraction [%]	+0.32	−0.66	-	-	−0.10	+0.20	-	+0.60	−0.40	-	-	−0.38	−0.18	-
b-Quark tagging efficiency (eigenvector 0) [%]	−0.23	-	+0.49	+0.59	-	-	+0.38	+0.84	-	−0.39	−0.21	±0.37	−0.34	+1.16
b-Quark tagging efficiency (eigenvector 1) [%]	-	−0.92	−0.30	-	-	-	-	-	−0.26	+0.36	+0.17	-	-	-
b-Quark tagging efficiency (eigenvector 2) [%]	−1.97	-	−0.74	−2.66	+0.50	+0.53	+0.30	+0.58	-	+1.21	-	+0.36	−0.11	+0.77
b-Quark tagging efficiency (eigenvector 3) [%]	+1.66	−1.88	+1.79	+2.47	−0.61	−0.20	-	-	−0.31	−0.51	−0.39	−1.14	+0.17	-
b-Quark tagging efficiency (eigenvector 4) [%]	-	-	-	-	-	-	-	-	−0.37	-	-	-	-	+0.28
c-Quark tagging efficiency (eigenvector 0) [%]	−0.22	−0.17	−0.21	−0.31	-	-	-	-	-	+0.11	+0.10	-	-	-
c-Quark tagging efficiency (eigenvector 1) [%]	+0.23	+0.19	+0.22	+0.32	-	-	-	-	−0.55	−0.12	−0.11	-	-	-
c-Quark tagging efficiency (eigenvector 2) [%]	+0.31	+0.18	±0.18	-	+0.17	±0.14	-	∓0.19	±0.51	±0.26	−0.24	∓0.19	∓0.22	−0.54
b-Quark tagging efficiency (eigenvector 1) [%]	−0.30	−0.19	-	−0.20	−0.16	-	−0.15	−0.40	−0.68	+0.14	+0.23	-	-	+0.52
b-Quark tagging efficiency (eigenvector 2) [%]	-	−0.15	-	-	-	-	+0.14	+0.38	+0.65	−0.12	+0.19	±0.16	-	∓0.16
b-Quark tagging efficiency (eigenvector 3) [%]	-	+0.14	-	+0.17	-	-	-	-	-	-	−0.18	-	-	-
b-Quark tagging efficiency (eigenvector 4) [%]	-	-	∓0.15	∓0.13	-	∓0.11	∓0.21	∓0.29	∓0.41	±0.24	+0.18	±0.16	-	-
c-Quark tagging efficiency (eigenvector 0) [%]	-	-	-	∓0.11	-	-	∓0.10	∓0.18	∓0.34	-	−0.19	-	-	-
c-Quark tagging efficiency (eigenvector 1) [%]	-	-	-	-	-	-	-	-	∓0.12	-	-	-	-	-
c-Quark tagging efficiency (eigenvector 2) [%]	-	-	±0.10	±0.10	-	-	-	∓0.16	∓0.31	-	-	-	-	±0.10
Light-jet tagging efficiency (eigenvector 0) [%]	±0.20	-	∓0.13	∓0.54	±0.17	-	-	-	∓0.21	-	-	-	-	-
Light-jet tagging efficiency (eigenvector 1) [%]	-	-	-	∓0.11	-	-	-	-	∓0.76	+0.12	-	−0.17	−0.23	−0.48
Light-jet tagging efficiency (eigenvector 2) [%]	-	-	-	-	-	-	-	-	-	−0.11	-	+0.16	+0.25	+0.52
Light-jet tagging efficiency (eigenvector 3) [%]	-	-	-	-	-	-	-	-	−0.30	-	-	-	-	-
Light-jet tagging efficiency (eigenvector 4) [%]	-	-	-	∓0.12	-	-	-	-	+0.31	-	-	-	-	±0.13
Light-jet tagging efficiency (eigenvector 5) [%]	-	-	-	±0.16	-	-	-	-	±0.59	-	-	-	-	-
Light-jet tagging efficiency (eigenvector 6) [%]	-	-	-	-	-	-	-	-	∓0.32	-	-	-	-	-
Light-jet tagging efficiency (eigenvector 7) [%]	-	-	-	∓0.12	-	-	-	-	∓0.58	-	-	-	-	-
Light-jet tagging efficiency (eigenvector 9) [%]	-	-	-	-	-	-	-	-	∓0.14	-	-	-	-	-
b-Quark tagging extrapolation [%]	−0.25	-	+0.19	+0.55	−0.23	-	±0.29	+0.68	+2.55	−0.24	-	-	±0.11	+0.43
Electron energy resolution [%]	+0.26	-	−0.20	−0.57	+0.24	-	-	−0.71	−2.64	+0.25	-	-	-	−0.45
Electron energy scale [%]	-	-	-	-	-	-	-	-	±0.19	-	-	-	-	-
Electron identification efficiency [%]	-	-	-	+0.13	-	-	-	±0.16	+0.11	±0.10	-	-	-	±0.15
Electron isolation efficiency [%]	-	±0.10	+0.19	−0.14	-	-	±0.16	±0.33	±0.28	∓0.10	-	-	-	+0.26
Muon identification syst [%]	-	-	±0.10	−0.20	-	-	-	±0.10	±0.65	∓0.20	∓0.18	-	-	−0.27
Muon identification stat [%]	∓0.65	-	∓0.94	±0.20	±0.19	-	±0.30	±0.63	±0.18	±0.18	-	-	-	-
E_T^{miss} Soft jet resolution para [%]	∓1.04	∓0.30	∓0.29	±1.45	±0.19	-	±0.30	±0.63	∓1.51	±0.11	-	±0.28	±0.10	±1.00
E_T^{miss} Soft jet resolution perp [%]	−0.33	-	−0.35	∓0.76	±0.37	-	-	±0.31	±1.55	-	±0.13	±0.27	-	±0.45
E_T^{miss} Soft jet scale [%]	-	+0.27	-	-0.57	-	-	-	+0.54	+0.49	-	-	+0.29	+0.10	+0.32
Z+jets cross-section [%]	−0.26	∓0.21	−0.29	∓0.10	∓0.13	-	-	±0.11	±0.55	±0.14	±0.20	−0.19	−0.47	−0.22
$t\bar{t}V$ cross-section [%]	±0.27	∓0.10	+0.30	-	-	-	-	-	-	-	-	±0.10	±0.11	±0.56
Monte Carlo sample statistics [%]	±1.28	±1.58	±1.91	±2.91	±0.86	±1.03	±1.23	±2.04	±5.18	±1.25	±1.30	±1.32	±1.76	±0.14
ISR/FSR + scale [%]	−0.87	+2.67	−2.31	−2.06	−1.63	−1.95	+4.19	+0.76	+15.1	+4.32	-	+0.41	-	±2.77
Alternate hard-scattering model [%]	+1.21	-	+3.10	+5.43	+1.27	+0.88	-	−5.49	-	−1.42	−3.18	−5.27	−3.12	+7.09
Alternate parton-shower model [%]	∓3.75	∓3.72	-	∓17.6	-	±1.47	±1.29	±0.65	±2.27	±4.37	±1.91	±0.85	∓5.83	−2.10
Fakes overall normalization, el [%]	∓3.46	∓2.94	∓6.66	∓10.1	±1.07	±1.98	-	±0.96	±10.2	±6.14	∓1.45	±0.69	∓1.64	±13.7
Fakes overall normalization, mu [%]	−1.09	−1.19	−1.31	−1.22	-	-	+0.20	+0.29	+1.56	±0.40	±0.44	+0.55	+0.97	±0.36
Fakes alternative parametrization [%]	+1.11	+1.21	+1.34	+1.24	-	-	−0.21	−0.30	−1.58	-	-	−0.56	−0.99	+1.73
Fakes overall normalization, mu [%]	-	∓0.66	∓0.18	∓0.79	-	-	±0.26	±0.40	-	±0.23	±0.36	-	∓0.13	−1.76
Fakes alternative parametrization [%]	±2.41	±3.83	±3.11	±4.16	±0.14	-	∓0.97	±0.19	∓3.40	±1.30	∓1.65	±1.18	±1.74	∓0.57
W+jets heavy flavour component [%]	±0.23	±0.10	-	-	-	-	-	-	-	-	-	-	-	∓2.39
W+jets Scales [%]	∓1.54	∓0.69	∓0.68	±1.56	∓0.72	∓0.31	±0.24	±1.30	±6.03	-	±0.35	±0.86	±1.23	±2.49
W+jets α_S [%]	-	-	-	−0.12	-	-	-	-	−0.35	-	-	-	-	−0.12
Single Top DS/DR [%]	±1.22	±0.87	∓0.11	+0.14 ∓1.34	±0.94	±0.35	∓0.16	∓2.59	+0.51 ±5.79	-	∓0.16	∓0.48	±1.18	+0.22 ∓2.94
Single Top IFSR [%]	−0.39	−0.25	+0.57	−1.19	+0.33	−0.17	-	+0.18	+3.96	-	-	+0.28	+0.65	+0.94
	+0.90	-	-	+1.45	-	-	−0.42	−1.03	−0.73	−0.60	-	−0.18	-	−0.93

TABLE F.43: Table of systematics for the relative differential cross-section at the particle level for the $p_T^{had}vsp_T^{t\bar{t}}$ observable.

Bins [GeV] x	350–400	400–455	455–550	550–700	700–2000	2000–2050	2050–2105	2105–2200	2200–2350	2350–3650	3650–3700	3700–3755	3755–3850	3850–4000	4000–5300
$1/\sigma \cdot d\sigma$ / $d p_T^{t,had}[GeV]vsextrajetN$	$4.29 \cdot 10^{-3}$	$2.58 \cdot 10^{-3}$	$1.07 \cdot 10^{-3}$	$2.73 \cdot 10^{-4}$	$6.28 \cdot 10^{-6}$	$1.70 \cdot 10^{-3}$	$1.06 \cdot 10^{-3}$	$4.84 \cdot 10^{-4}$	$1.50 \cdot 10^{-4}$	$4.88 \cdot 10^{-6}$	$1.84 \cdot 10^{-3}$	$1.25 \cdot 10^{-3}$	$7.31 \cdot 10^{-4}$	$2.24 \cdot 10^{-4}$	$8.82 \cdot 10^{-6}$
Total Uncertainty [%]	+6.51 −6.24	+5.00 −5.73	+8.16 −7.55	+17.8 −17.3	+19.3 −19.4	+8.62 −8.92	+7.93 −8.39	+4.97 −6.40	+7.96 −9.39	+20.3 −16.4	+15.3 −14.8	+7.34 −8.42	+9.73 −8.86	+7.95 −9.42	+18.8 −17.3
Statistics [%]	±1.2	±1.6	±2.0	±3.3	±8.5	±2.2	±2.5	±3.1	±4.7	±9.9	±2.2	±2.4	±2.5	±3.7	±6.6
Systematics [%]	+6.33 −6.06	+4.61 −5.40	+7.81 −7.18	+17.4 −16.8	+16.7 −16.8	+8.18 −8.50	+7.34 −7.83	+3.43 −5.30	+5.77 −7.63	+16.9 −12.0	+15.0 −14.6	+6.74 −7.90	+9.27 −8.34	+6.72 −8.41	+17.3 −15.7
b-Tagged jet energy scale (JES) [%]	-	-	+0.17 −0.13	+0.29 -	-	−0.24 -	-	+0.18 −0.17	+0.52 -	+0.11 −0.71	+0.29 -	+0.13 −0.32	−0.16 -	-	-
Effective detector NP set 1 (JES) [%]	-	-	-	-	−0.36	-	-	-	+0.47	-	+0.21	-	-	-	+0.63
Effective detector NP set 2 (JES) [%]	-	-	-	-	-	−0.20	-	-	-	−0.22	-	-	-	−0.21	−0.11
Effective mixed NP set 1 (JES) [%]	−0.41	-	+0.31	+1.26	+0.25 +2.39	−0.22 −0.90	-	+0.89	+0.56	+2.15	−0.30	+0.48	-	+0.86	+2.76
Effective mixed NP set 2 (JES) [%]	+0.52	−0.55	−0.36	−0.28	−3.45	+0.50	−0.41	−0.23	−0.68	−1.93	+0.53	-	−0.39	−0.10	−1.50
Effective mixed NP set 3 (JES) [%]	-	-	-	-	−0.24	−0.28	-	-	+0.30	-	-	−0.12	-	-	+0.24
Effective modelling NP set 1 (JES) [%]	−1.25	−1.99	−1.43	−1.57	−2.17	+0.60	+1.19	+0.93	+0.62	−0.91 −2.06	+2.49	+0.10 +2.53	+2.58	+1.73	+2.76
Effective modelling NP set 2 (JES) [%]	+1.56 −0.14	+1.32	+1.11 +0.43	+2.32 +1.04	+2.54 +2.36	−1.90 −0.75	−0.78 −0.57	−1.23 +0.25	−0.57 +0.60	+1.13 +2.52	−2.39 −0.43	−2.64 +0.7	−2.30	−1.20	−1.60 +1.79
Effective modelling NP set 3 (JES) [%]	+0.25	−0.24	−0.38 −0.32	+0.29	−2.51	-	-	-	+0.27 +0.66	−2.91 +0.17	+0.75 +0.45	-	−0.28	-	−0.79 −0.57
Effective modelling NP set 4 (JES) [%]	-	−0.27	+0.37	−0.15 +0.38	−0.56	−0.52	-	+0.24	-	−0.31	-	-	-	-	-
Effective statistical NP set 1 (JES) [%]	−0.26	−0.42	−0.22	+0.12 −0.12	−0.80 −0.80	−0.34	+0.17	+0.27	+0.38 +0.29	−0.20	+0.33 +0.56	+0.48	+0.58	+0.18	+0.82 +1.06
Effective statistical NP set 2 (JES) [%]	+0.41 +0.21	+0.23	+0.14 ±0.52	-	−0.20 +0.75	−0.31	−0.22 −0.38	−0.38	-	−0.53	−0.40 −0.57	−0.29 −0.38	−0.35	−0.63	−0.76 +0.28
Effective statistical NP set 3 (JES) [%]	+0.40	−0.23	−0.57	+0.52 +0.92	−0.99 −0.23	−0.47 +0.26	+0.31	−0.28	+0.49 −0.32	−0.32 −0.20	−0.58 +0.52	−0.67 +0.52	-	−0.30 −0.33	-
Effective statistical NP set 4 (JES) [%]	−0.31 +0.13	−0.32	+0.54	-	−0.46 −0.49	−0.61	−0.29 +0.26	+0.63	+0.59 −0.38	+0.43 −0.56	−0.30 +0.22	+0.52	−0.60 +0.31	+0.44 +0.43	+0.71 −0.25
Effective statistical NP set 5 (JES) [%]	-	−0.22 ±0.15	+0.18	−0.17 +0.42	+0.11 −0.34	-	−0.18 +0.23	-	+0.47 −0.27	+0.49 −0.66	+0.31	-	+0.15	+0.34 −0.32	+0.46 −0.68
Effective statistical NP set 6 (JES) [%]	−0.15	−0.18	−0.13 +0.20	-	+0.69 −0.55	−0.32	−0.25 +0.23	−0.23 +0.28	+0.50 +0.29	+0.31 −0.39	-	+0.23	−0.13 +0.33	+0.17	+0.89
Effective statistical NP set 7 (JES) [%]	±0.17	-	-	-	-	−0.30	−0.14	−0.12 +0.18	+0.38	+0.30	-	−0.10	−0.18 +0.16	-	+0.45 +0.56
η intercalibration model (JES) [%]	-	-	-	-	−0.42	−0.28	-	−0.14	-	-	+0.26	-	-	-	-
η intercalibration non closure (JES) [%]	−0.66 +0.59	−0.84 +0.27	−0.29	+0.72	−0.19 +0.59	-	−0.51	+0.60	+0.66 −0.33	+1.30 −0.45	+1.04 −0.20	+0.84 −1.08	+0.96 −0.70	+0.56 −0.55	+0.90 −1.22
η intercalibration total stat (JES) [%]	+0.24 −0.29	−0.23	-	+0.30	+0.55	+0.30 −0.50	−0.36	+0.28	−0.10 +0.73	+0.46 -	+0.88	−0.82 +0.28	-	−0.42 +0.20	−0.38 +0.43
Flavour composition (JES) [%]	+0.21 +0.33	−0.37 +0.18	−0.29 +0.28	-	−0.77 +0.69	−0.50 −0.34	+0.21 −0.30	+0.20 −0.27	-	−0.63	+0.66 −0.41	+0.78 −0.51	+0.47 −0.18	−0.34	+1.06 −0.15
Flavour response (JES) [%]	+1.72 +2.18	−2.28 +1.81	−1.84 +1.92	−1.40 +2.82	−0.93 +3.47	+0.41 −0.82	+1.17 −1.99	+0.98 −2.02	−0.88	−1.12 +0.85	+3.16 −3.06	+3.03 −3.47	+3.13 −3.48	+3.01 −2.98	+4.45 −3.60
Flavour response (JES) [%]	−0.89	+0.31 −1.08	±0.93	+1.84 −0.99	+3.44 −2.74	−0.82 +0.13	−1.99 +1.10	−2.02 +0.61	-	+1.25 −1.06	−3.06 +1.78	−3.47 +1.70	−3.48 +1.82	−2.98 +0.85	−3.60 +1.39
Pile-up offset μ (JES) [%]	+0.14	-	-	+0.29 −0.14	+0.46 −0.48	-	-	-	+0.29	-	−0.18 +0.26	-	-	−0.27 -	-
Pile-up offset N_{PV} (JES) [%]	-	−0.70	−0.32	−0.45	−0.73	−0.26	+0.32	-	−0.10	−1.52	+0.47	+0.28	+1.04	+0.53	+1.60
Pile-up offset p_T (JES) [%]	+0.37	+0.31	+0.19 +0.34	+0.45 +0.82	−0.62	−0.62	−0.55 −0.56	−0.67 +0.62	+0.27	+0.45 +1.10	−0.37 −0.50	−0.39	−0.31 +0.31	−0.34	−0.42 +0.39
Pile-up offset ρ topology (JES) [%]	-	−0.31 −2.49	−0.22 −2.21	−2.88	+0.17 −0.45 −3.60	+0.31 +1.23	+0.99	−0.18 +0.78	-	−2.85	+0.71 +4.07	+3.91	−0.17 +3.74	+0.29 +2.23	+3.40
Punch-through (JES) [%]	+1.93 -	+1.89 -	+2.35 -	+3.26 -	+3.76 -	−1.39 -	−1.51 -	−1.69 -	-	+2.70 -	−4.06 -	−3.79 -	−2.82 -	−1.72 -	−2.15 +0.40
Jet vertex fraction [%]	−0.25 +0.26	−0.23 +0.24	∓0.30	∓0.42 −0.12	∓0.46 −0.19	±0.16	±0.14	-	-	−0.77 +0.16	+0.54 −0.55	±0.49	+0.43 −0.44	+0.41 −0.42	−0.10 +0.31 −0.32
b-Quark tagging efficiency (eigenvector 0) [%]	−0.20 −0.19	-	-	+0.11 −0.26	+0.16	-	-	-	−0.39 +0.36	−0.92 +0.89	−0.13 +0.14	−0.10 +0.11	−0.13 +0.14	∓0.13	−0.55 +0.53
b-Quark tagging efficiency (eigenvector 1) [%]	-	-	-	+0.24	-	-	-	-	+0.20 +0.19	−0.82 +0.63	-	−0.11 −0.10	-	-	∓0.27
b-Quark tagging efficiency (eigenvector 2) [%]	-	-	∓0.10	∓0.16	∓0.13	-	-	-	-	∓0.21	±0.14	±0.11	-	-	
b-Quark tagging efficiency (eigenvector 3) [%]	-	-	-	∓0.10	∓0.14	-	-	-	∓0.12	∓0.19	±0.10	-	-	-	∓0.14
c-Quark tagging efficiency (eigenvector 0) [%]	-	-	-	-	-	-	-	-	-	-	-	-	-	-	±0.10
c-Quark tagging efficiency (eigenvector 1) [%]	-	-	-	-	∓0.29	-	∓0.16	∓0.11	-	∓0.42	-	-	-	-	-
c-Quark tagging efficiency (eigenvector 2) [%]	-	-	-	-	∓0.14	-	-	-	-	∓0.20	-	-	-	-	-
Light-jet tagging efficiency (eigenvector 0) [%]	±0.20	-	-	-	−0.75 +0.73	-	-	-	−0.32 +0.35	−0.47 +0.48	-	-	−0.23 +0.21	−0.15 +0.16	−0.91 +0.94
Light-jet tagging efficiency (eigenvector 1) [%]	-	-	-	-	∓0.30	+0.13	-	-	-	∓0.39	-	-	-	-	-
Light-jet tagging efficiency (eigenvector 2) [%]	-	-	-	-	−0.12 +0.13	−0.12	-	-	-	-	-	-	-	-	-
Light-jet tagging efficiency (eigenvector 5) [%]	-	-	-	-	±0.33	-	-	-	-	±0.29	-	-	-	-	±0.23
Light-jet tagging efficiency (eigenvector 6) [%]	-	-	-	-	-	-	-	-	-	∓0.20	-	-	-	-	-
Light-jet tagging efficiency (eigenvector 7) [%]	-	-	-	-	∓0.25	-	-	-	-	∓0.34	-	-	-	-	∓0.21
Light-jet tagging efficiency (eigenvector 8) [%]	-	-	-	-	-	-	-	-	-	-	-	-	-	-	±0.10
b-Quark tagging extrapolation [%]	−0.24 ±0.25	-	+0.16 −0.17	+0.45 −0.47	+1.16 −1.24	∓0.23	-	±0.13	+0.46 −0.48	+1.55 −1.57	∓0.24	-	-	±0.18	+0.68 −0.71
Electron energy resolution [%]	-	-	-	-	+0.14 −0.11	-	-	-	-	-	-	-	-	-	-
Electron energy scale [%]	-	−0.19	-	-	-	-	-	-	-	+0.39	+0.36	+0.50	+0.24	-	-
Electron identification efficiency [%]	-	-	-	±0.14	+0.27 −0.28	-	−0.26	-	-	±0.23	-	-	-	-	±0.10
Electron isolation efficiency [%]	-	-	±0.16	±0.30	+0.61 −0.62	∓0.14	-	-	±0.16	+0.43 −0.44	∓0.18	∓0.13	-	-	±0.23
Muon (MS) momentum resolution [%]	-	-	-	-	-	-	-	-	-	-	-	-	-	-	-
Muon energy scale [%]	-	-	-	-	-	-	-	-	-	-	-	-	-	-	-
Muon identification syst [%]	-	-	-	±0.10	±0.14	-	-	-	-	±0.12	-	-	-	-	-
E_T^{miss} Soft jet resolution para [%]	-	-	-	±0.21	±0.31	-	∓0.17	±0.11	∓0.19	±0.33	±0.12	-	±0.26	∓0.18	±0.26
E_T^{miss} Soft jet resolution perp [%]	-	-	-	-	±0.47	-	∓0.15	-	-	-	-	-	±0.31	∓0.23	±0.45
E_T^{miss} Soft jet scale [%]	-	-	-	-	-	-	−0.16	-	-	-	-	-	-	-	+0.22
Z+jets cross-section [%]	−0.18	∓0.14	∓0.15	∓0.14	±0.27	-	+0.11	±0.20	−0.27 ±0.29	−0.16 +0.75	+0.20	-	±0.22	±0.25	+0.61
$t\bar{t}V$ cross-section [%]	+0.19	-	-	-	-	-	−0.12	-	-	−0.76	−0.21 ±0.10	-	±0.13	±0.13	−0.62 ±0.18
Monte Carlo sample statistics [%]	±0.77	±0.99	±1.18	±1.96	±4.50	±1.46	±1.55	±1.82	±2.77	±5.32	±1.38	±1.51	±1.54	±2.00	±3.12
ISR/FSR + scale [%]	+0.67 −1.12	−0.15 +1.19	+2.93	+1.86 −1.86	+2.72	−3.91 +3.87	-	-	−5.40 +1.74	+12.2	+3.45	-	+3.03 −3.76	+0.23 −5.89	+5.31 −2.27
Alternate hard-scattering model [%]	∓3.55	∓2.07	∓3.49	∓13.2	±10.4	±1.55	±6.62	±1.26	∓1.73	±2.46	±9.72	±1.59	±5.04	∓2.06	±13.6
Alternate parton-shower model [%]	∓3.18	∓1.98	∓5.03	∓9.42	±6.37	±6.67	±1.87	±0.96	∓2.47	±6.40	±8.73	±2.07	±3.21	±3.87	∓1.99
Fakes overall normalization, el [%]	∓0.21	∓0.17	-	+0.60 −0.61	+2.31 −2.35	-	-	+0.23 −0.24	+0.97 −0.99	+1.59 −1.61	∓0.15	−0.16 +0.17	-	-	+0.42 −0.43
Fakes overall normalization, mu [%]	-	∓0.21	±0.29	∓0.42	−2.50 +0.51	∓0.16	±0.15	-	∓0.20	∓0.92	±0.30	+0.40 −0.41	∓0.21	∓0.23	∓0.21
Fakes alternative parametrization [%]	±0.35	±0.79	∓0.59	∓0.36	∓3.72	±0.51	∓0.36	∓0.44	∓1.59	∓1.38	±0.30	∓0.49	±0.24	±0.65	∓0.42
W+jets heavy flavour component [%]	±0.10	-	-	-	-	-	-	-	-	-	-	-	-	-	-
W+jets Scales [%]	∓1.07	∓0.52	∓0.13	±0.94	±3.89	∓0.17	±0.62	±1.08	±2.04	±5.92	∓0.25	-	±0.62	±0.84	±2.70
W+jets α_S [%]	-	-	-	-	−0.25 +0.35	-	-	-	-	−0.35 +0.53	-	-	-	-	+0.74
Single Top DS/DR [%]	±1.09	±0.56	±0.14	∓0.85	∓6.17	±0.73	-	∓1.48	∓2.70	∓3.96	±0.25	-	∓0.20	∓1.54	∓2.78
Single Top IFSR [%]	−0.12 +0.69	−0.26 -	−0.10 ±0.84	−0.18 ±0.65	+1.51 -	−0.21 -	-	−1.44	−1.05	+0.18 −1.15	−0.93	−0.48	+1.20 −0.96	+1.41 −0.67	+1.87 −1.23

TABLE F.44: Table of systematics for the relative differential cross-section at the particle level for the $p_T^{t,had}vsextrajetN$ observable.

Bins [GeV] x [GeV]	490–850	850–950	950–1350	1350–3000	3000–3220	3220–3360	3360–3460	3460–3860	3860–5510	5510–5835	5835–5950	5950–6220	6220–8020.00
$1/\sigma \cdot d\sigma$ / $dm^{t\bar{t}}[GeV]vsp_T^{t\bar{t}}$	$7.47 \cdot 10^{-5}$	$4.61 \cdot 10^{-4}$	$2.43 \cdot 10^{-4}$	$1.53 \cdot 10^{-5}$	$2.41 \cdot 10^{-5}$	$5.81 \cdot 10^{-4}$	$9.39 \cdot 10^{-4}$	$5.20 \cdot 10^{-4}$	$3.28 \cdot 10^{-5}$	$4.18 \cdot 10^{-4}$	$5.62 \cdot 10^{-4}$	$3.57 \cdot 10^{-4}$	$3.61 \cdot 10^{-5}$
Total Uncertainty [%]	+11.1 −13.2	+9.75 −9.76	+7.74 −6.91	+11.0 −10.8	+23.6 −16.4	+7.67 −7.46	+5.72 −4.84	+3.00 −2.78	+8.03 −8.36	+4.67 −4.31	+5.50 −7.68	+4.27 −5.20	+10.4 −12.8
Statistics [%]	±3.7	±2.6	±2.0	±4.4	±7.1	±2.2	±1.9	±1.3	±3.0	±1.7	±2.5	±2.1	±2.7
Systematics [%]	+10.3 −12.4	+9.25 −9.26	+7.36 −6.48	+9.77 −9.57	+22.2 −14.2	+7.19 −6.97	+5.27 −4.30	+2.57 −2.31	+7.22 −7.58	+4.23 −3.82	+4.62 −7.07	+3.44 −4.54	+9.98 −12.4
b-Tagged jet energy scale (JES) [%]	−1.25	-	+0.31	-	-	−0.28	-	+0.16	-	−0.15	-	-	-
Effective detector NP set 1 (JES) [%]	+0.60 -	−0.23 -	−0.36 -	−0.16 +0.18	−1.73 −0.34	+0.25 -	-	−0.14 -	- −0.31	+0.13 -	+0.19 -	-	-
Effective detector NP set 2 (JES) [%]	−0.46 -	-	-	−0.10 -	-	-	-	-	-	-	-	-	-
Effective mixed NP set 1 (JES) [%]	−0.42 +1.64	−0.84	+0.57	+0.16 +1.21	−0.41 −2.23	−0.40	-	+0.27	+1.07	−0.69	−0.99	+0.52	+0.90
Effective mixed NP set 2 (JES) [%]	+1.18 -	-	−0.22	−0.90	+2.68 -	+0.84	−0.40	-	−1.33 −0.24	+0.57	-	-	−1.03
Effective mixed NP set 3 (JES) [%]	−0.37 -	-	-	-	−0.47 −0.32	-	-	-	- -	-	-	-	-
Effective modelling NP set 1 (JES) [%]	−0.20 −2.08	-	-	-	+0.17 -	-	-	-	-	-	-	-	-
Effective modelling NP set 2 (JES) [%]	+1.62 −0.87	+0.56 −0.42	+0.69 +0.37	+1.29 +0.46	−1.46 -	-	−0.45 −0.10	-	−0.58 +0.58	−0.18 −0.51	−0.56 −0.17	-	+0.40 −0.73 +0.72
Effective modelling NP set 3 (JES) [%]	+0.74 +0.23	-	−0.18 −0.33	−0.50 +0.20	−2.00 -	-	+0.33 +0.36	-	−0.82 -	+0.35 +0.17	+0.29 -	-	−0.90 −0.29
Effective modelling NP set 4 (JES) [%]	−0.63 -	-	+0.32 -	-	−1.21 -	-	-	-	-	−0.23 -	-	-	+0.15 -
Effective statistical NP set 1 (JES) [%]	−0.48 −0.83	-	−0.14	-	−0.39 −0.31	-	-	-	−0.22 +0.10	-	-	-	−0.13 +0.10
Effective statistical NP set 2 (JES) [%]	+0.10 -	−0.20	+0.11 +0.28	+0.51 +0.35	+0.19 −0.52	-	-	-	−0.59 +0.23	−0.20	-	-	−0.24 -
Effective statistical NP set 3 (JES) [%]	−0.41 +0.64	+0.29 +0.21	−0.27 −0.17	−0.52	+0.45 +0.71	+0.18	+0.29 +0.39	−0.15	−0.58 −0.47	+0.18 +0.19	+0.16	+0.24	−0.15 −0.47
Effective statistical NP set 4 (JES) [%]	−0.79 −0.26	−0.36 +0.22	+0.32 -	+0.13 +0.29	−1.75 -	−0.34	+0.24	+0.13	+0.29 −0.26	−0.29 -	−0.10 -	-	+0.30 −0.19
Effective statistical NP set 5 (JES) [%]	- −0.41	+0.26	−0.23 +0.28	- +0.20	−0.55 -	-	-	-	+0.25 −0.40	-	-	+0.14 −0.10	+0.10 −0.23
Effective statistical NP set 6 (JES) [%]	- −0.61	- -	−0.37 -	-	−1.04 −0.27	-	-	+0.12	- −0.13	-	-	-	+0.35 -
Effective statistical NP set 7 (JES) [%]	- -	+0.30 -	-	−0.14	+0.12 0.00	-	-	-	- -	-	-	-	-
η intercalibration model (JES) [%]	−0.41 +1.00	−0.97	-	+0.13 +1.20	+0.20 −2.00	-	-	-	−0.21 −0.41	+0.15 +0.28	−0.28	-	+0.14 +1.05
η intercalibration non closure (JES) [%]	+0.86 -	+0.19 -	−0.25 −0.22	-	+0.75 -	+0.57 +0.58	−0.14	-	−1.06 −0.68	+0.24 -	+0.23 -	−0.24 -	−0.86 −0.28
η intercalibration total stat (JES) [%]	−1.20 −0.81	−0.76 -	+0.28 -	+0.53	−0.73 -	-	+0.23	-	+0.11 -	−0.26 -	−0.14	-	+0.43 +0.12
Flavour composition (JES) [%]	- −2.61	−1.53	−0.90	−0.50	−0.96 -	−0.16	+0.47	+0.36	−0.27 +0.74	-	- +0.44	+0.44	−0.23 +1.07
Flavour response (JES) [%]	+1.58 +0.76	+1.00 +0.26	+0.85 +0.20	+1.12 +1.30	−1.99 -	+0.64 +0.52	+0.28	+0.24	−1.34 -	−0.29	−0.65 −0.50	−0.38 −0.16	−1.35 −0.55
Pile-up offset μ (JES) [%]	−1.32 -	−0.64 -	−0.43 +0.16	−0.51 -	−2.35 -	-	-	-	−0.47 -	-	+0.11 -	+0.36 -	+0.28 -
Pile-up offset N_{PV} (JES) [%]	−0.62 −1.31	- +0.10	−0.15 -	-	−0.70 −1.76	-	-	-	- −0.35	-	- −0.36	- −0.24	+0.24 -
Pile-up offset p_T (JES) [%]	- −0.93	−0.47	+0.33 −0.35	+0.39 -	−1.79	−0.38 +0.82	-	+0.18	+0.15 −0.68	−0.54 +0.24	−0.28	+0.54 -	+0.60 −0.33
Pile-up offset ρ topology (JES) [%]	−3.43 +2.44	−1.91 +0.42	−0.78 +1.29	−1.73 +1.72	- −0.82	+0.51 -	+0.72 −0.83	+0.62 −0.13	- −0.41	+0.23 −0.19	- −0.94	+0.73 −0.41	+0.48 −0.68
Punch-through (JES) [%]	-	-	-	-	-	-	-	-	-	-	-	-	-
Jet vertex fraction [%]	−0.23 +0.24	−0.19 +0.21	−0.21 +0.22	−0.22 +0.23	±0.18 -	-	-	-	-	+0.12 −0.13	-	-	-
b-Quark tagging efficiency (eigenvector 0) [%]	+0.47 −0.46	+0.43 −0.42	±0.11	-	−0.34 +0.32	+0.19 −0.17	±0.12	±0.13	−0.16 +0.14	∓0.36	∓0.12	∓0.13	−0.29 +0.28
b-Quark tagging efficiency (eigenvector 1) [%]	+0.22 −0.21	-	−0.13 +0.11	−0.18 +0.16	+0.39 −0.37	+0.23 −0.22	-	−0.12 +0.11	−0.49 +0.47	+0.48 −0.44	+0.12 −0.11	-	−0.30 +0.29
b-Quark tagging efficiency (eigenvector 2) [%]	-	-	-	-	±0.21	-	-	∓0.16	±0.30	±0.41	±0.21	-	∓0.15
b-Quark tagging efficiency (eigenvector 3) [%]	-	-	-	∓0.10	-	-	-	-	∓0.17	-	±0.10	-	∓0.13
c-Quark tagging efficiency (eigenvector 1) [%]	-	±0.14	+0.11 −0.12	∓0.12	+0.34 −0.33	-	-	-	∓0.33	±0.12	±0.12	-	∓0.29
c-Quark tagging efficiency (eigenvector 2) [%]	-	-	-	-	±0.20	-	-	-	∓0.15	+0.11 −0.10	-	-	∓0.10
Light-jet tagging efficiency (eigenvector 0) [%]	±0.32	+0.15 −0.16	±0.12	−0.95 +0.94	±0.31	±0.28	±0.23	-	−0.47 +0.45	-	-	-	∓0.36
Light-jet tagging efficiency (eigenvector 1) [%]	-	-	-	∓0.21	-	-	-	-	∓0.21	±0.14	±0.12	-	-
Light-jet tagging efficiency (eigenvector 3) [%]	-	-	-	∓0.29	±0.14	-	-	-	∓0.20	±0.10	-	-	-
Light-jet tagging efficiency (eigenvector 5) [%]	-	-	-	±0.15	-	-	-	-	±0.11	-	-	-	-
b-Quark tagging extrapolation [%]	−0.26 +0.27	∓0.20	-	+0.42 −0.44	−0.37 +0.38	−0.27 +0.28	∓0.15	-	+0.86 −0.88	∓0.31	∓0.27	-	+0.56 −0.57
Electron energy resolution [%]	−0.16 −0.19	-	−0.11 +0.10	-	-	-	-	-	-	-	-	-	-
Electron energy scale [%]	+0.17 -	-	-	+0.48 -	-	−0.24 -	-	-	-	-	-	-	+0.13 −0.16
Electron identification efficiency [%]	-	-	-	±0.20	∓0.15	-	-	-	±0.21	−0.17 +0.18	-	-	±0.15
Electron isolation efficiency [%]	-	-	±0.10	+0.30 −0.31	∓0.28 +0.22	∓0.13	-	-	+0.28 −0.29	∓0.32	∓0.16	-	±0.20
Muon (ID) momentum resolution [%]	-	−0.23 -	-	-	−0.48 -	-	-	-	-	-	-	-	-
Muon (MS) momentum resolution [%]	-	-	-	-	-	-	-	-	-	-	-	-	-
Muon energy scale [%]	-	-	-	-	-	-	-	-	-	-	-	-	-
Muon identification syst [%]	-	-	-	±0.25	∓0.12	-	-	-	±0.18	∓0.12	∓0.10	-	-
E_T^{miss} Soft jet resolution para [%]	∓0.16	∓0.44	∓0.79	∓0.58	±3.15	±0.74	±0.65	∓0.12	±0.70	±0.30	∓0.36	±0.22	±0.14
E_T^{miss} Soft jet resolution perp [%]	∓0.47	∓0.53	∓0.80	∓0.44	±3.23	±0.88	±0.70	∓0.15	±0.68	±0.34	±0.26	-	-
E_T^{miss} Soft jet scale [%]	+0.47 −1.01	-	−0.62 +0.33	−0.19 +0.12	+2.16 −2.35	+0.59 −0.54	+0.26	−0.15 +0.22	−0.66 +0.57	+0.41 −0.37	- −0.60	-	−0.31 +0.28
Z+jets cross-section [%]	−0.36 +0.37	−0.32 +0.33	−0.27 +0.28	±0.21	±0.16	−0.25 +0.26	−0.24 +0.25	-	±0.61	±0.19	-	-	±0.62 −0.63
$t\bar{t}V$ cross-section [%]	∓0.11	±0.11	-	-	-	-	-	-	-	-	-	-	±0.14
Monte Carlo sample statistics [%]	±2.14	±1.54	±1.20	±2.68	±4.03	±1.37	±1.12	±0.79	±1.75	±1.03	±1.57	±1.31	±1.55
ISR/FSR + scale [%]	- −4.92	+2.83	−0.58 +3.24	+0.61 −0.17	+18.2	−1.79 +1.73	−2.68 +3.90	+0.47	+0.56	+2.36	- −5.02	+1.74 −3.65	+0.49 −7.26
Alternate hard-scattering model [%]	∓7.37	∓5.82	±2.67	±2.52	±10.6	±5.64	±2.26	∓1.50	±1.22	±0.96	±2.61	-	±7.32
Alternate parton-shower model [%]	∓3.99	∓4.36	∓4.19	∓6.13	±1.68	±2.21	±0.47	±1.57	±0.42	±2.57	∓3.44	±1.69	±0.40
Fakes overall normalization, el [%]	−0.93 +0.95	−1.10 +1.12	−1.18 +1.20	−1.43 +1.46	+1.31 −1.33	∓0.13	−0.40 +0.41	-	+1.23 −1.25	±0.22	+0.33 −0.34	±0.48	+1.76 −1.79
Fakes overall normalization, mu [%]	-	∓0.61	∓0.15	−0.69 +0.70	-	∓0.19	±0.23	-	+0.28 −0.29	±0.18	-	±0.30	-
Fakes alternative parametrization [%]	±2.04	±3.53	±2.77	±4.41	±2.64	±0.67	±0.35	±0.12	∓3.14	±0.84	±0.50	±1.61	∓3.48
W+jets heavy flavour component [%]	±0.18	±0.17	-	±0.12	-	-	-	-	-	-	-	-	-
W+jets Scales [%]	∓2.49	∓2.17	∓0.86	±3.52	∓1.23	∓1.73	∓1.45	±0.28	±5.00	±0.12	∓0.54	±0.10	±3.43
W+jets α_S [%]	+0.14 −0.17	+0.10 −0.14	-	−0.30 +0.34	±0.10	+0.11 −0.14	-	-	−0.28 +0.36	-	-	-	−0.17 +0.27
Single Top DS/DR [%]	±1.86	±1.32	±0.54	∓1.77	±0.61	±1.18	±1.05	-	∓2.46	±0.89	±0.18	∓0.75	∓3.28
Single Top IFSR [%]	- −0.19	−0.30 +0.21	−0.29 +1.27	−1.28	−0.41 +0.61	−0.37 +0.40	-	-	+0.52 −0.53	+0.24 -	- −0.52	−0.32	+1.08 −1.17

TABLE F.45: Table of systematics for the relative differential cross-section at the particle level for the $m^{t\bar{t}}[GeV]vsp_T^{t\bar{t}}$.

F.2 Parton level

F.2.1 Absolute differential cross section

F.2.1.1 Resolved topology

Bins [GeV]	0–50	50–100	100–160	160–225	225–300	300–360	360–420	420–475	475–530	530–600	600–1000
$d\sigma$ / dp_T^t [pb/GeV]	$2.59 \cdot 10^{0}$	$5.15 \cdot 10^{0}$	$3.94 \cdot 10^{0}$	$1.83 \cdot 10^{0}$	$6.71 \cdot 10^{-1}$	$2.33 \cdot 10^{-1}$	$1.11 \cdot 10^{-1}$	$5.33 \cdot 10^{-2}$	$2.98 \cdot 10^{-2}$	$1.47 \cdot 10^{-2}$	$1.84 \cdot 10^{-3}$
Total Uncertainty [%]	±18.6	+14.6 −14.4	±10.1	+9.35 −9.38	+8.99 −8.82	+9.90 −9.75	+10.3 −11.5	+11.2 −14.5	+31.4 −18.9	+35.3 −22.4	+47.6 −44.1
Statistics [%]	±0.3	±0.2	±0.2	±0.3	±0.5	±1.0	±2.0	±4.2	±7.5	±10.	±20.
Systematics [%]	±18.6	+14.6 −14.4	±10.1	+9.34 −9.37	+8.97 −8.80	+9.83 −9.67	+10.0 −11.3	+10.1 −13.6	+30.2 −16.8	+33.0 −18.5	+41.1 −37.0
Jet energy resolution [%]	∓2.10	∓1.78	∓1.61	∓1.65	∓1.26	∓1.18	∓0.70	-	±0.97	∓4.03	∓12.7
b-Tagged jet energy scale (JES) [%]	−0.47 +0.34	-	+0.70 −0.74	+0.82 −1.03	+0.82 −0.66	+0.35 -	- −0.95	−0.10 +2.27	+5.82 -	+4.19 −1.74	- −3.92
Effective detector NP set 1 (JES) [%]	-	-	-	−0.15	-	-	−0.91	−0.73	+3.20	+1.76	−6.72
Effective detector NP set 2 (JES) [%]	-	-	-	-	-	-	−0.75	−0.74	+3.09	−1.17	-
Effective mixed NP set 1 (JES) [%]	−0.42	-	+0.17	+0.27	+0.14	+0.33	-	+0.36	+6.50	+3.30 +10.5	−6.13 +3.50
Effective mixed NP set 2 (JES) [%]	+0.27 -	+0.24 -	−0.14 -	−0.31 -	−0.27 -	−0.24 -	−1.24 -	−2.67 +0.68	+3.50	+1.08	−2.68 +0.66
Effective mixed NP set 3 (JES) [%]	-	-	-	-	-	-	−1.12 +1.44	- +3.10	- +2.45	-	−5.92 -
Effective modelling NP set 1 (JES) [%]	+2.76	+2.90	+2.79	+2.21	+1.60	+1.04	−1.17	+0.23	+4.66	+9.55	−2.88
Effective modelling NP set 2 (JES) [%]	−2.59 −0.69	−2.72 −0.56	−2.77 −0.23	−2.31 -	−1.48 -	−0.97 -	−1.01 -	−2.82 +0.87	−0.51 +3.83	−0.59 +4.24	−6.96 +0.76
Effective modelling NP set 3 (JES) [%]	+0.44 +0.48	+0.57 +0.45	+0.20 +0.11	- -	- -	- -	−0.68 -	−0.93 −1.56	- +3.48	- +4.09	−3.37 −2.94
Effective modelling NP set 4 (JES) [%]	−0.73 -	−0.27 +0.20	−0.10 +0.12	+0.12	+0.18 +0.12	-	−1.01 -	- -	- +3.23	- +2.36	+2.88 -
Effective statistical NP set 1 (JES) [%]	−0.25 +0.50	+0.57	−0.15 +0.45	−0.14 +0.33	−0.42 +0.24	-	−1.25 -	−2.00 -	- +1.40	- +4.15	−2.42 +2.23
Effective statistical NP set 2 (JES) [%]	−0.67 −0.56	−0.46 −0.37	−0.41 −0.43	−0.39 −0.34	−0.30 −0.20	∓0.11	−0.91 -	−1.09 -	- +2.19	- +2.56	−5.39 +0.50
Effective statistical NP set 3 (JES) [%]	+0.46 -	+0.55 -	+0.36 -	+0.33 -	+0.29 -	-	−0.80 -	−1.59 -	+5.62 -	+6.45 -	−4.44 -
Effective statistical NP set 4 (JES) [%]	−0.49	−0.16	-	±0.21	-	-	−0.78	−2.25 +0.50	- +1.50	- +1.87	−4.74 +1.79
Effective statistical NP set 5 (JES) [%]	+0.40 -	+0.33 -	-	−0.18 +0.10	∓0.10	-	−0.78 -	−1.74 -	−0.82 +3.89	+3.12	−1.63 +1.93
Effective statistical NP set 6 (JES) [%]	−0.14 -	- +0.18	-	-	-	+0.40	−1.30 -	−1.13 +1.77	- +3.03	- +1.84	- -
Effective statistical NP set 7 (JES) [%]	-	-	−0.15 +0.11	-	-	+0.40	−1.48 -	−0.80 -	- +3.74	- +5.31	−8.34 +2.57
η intercalibration model (JES) [%]	+0.14	+0.61	+0.67	+0.75	+0.53	−0.43 +0.37	−1.41 -	−1.31 +0.15	- +2.36	−2.06 +4.90	−1.98 −0.50
η intercalibration non closure (JES) [%]	−0.33 −0.34	−0.44 −0.17	−0.73 −0.33	−0.83 −0.25	−0.55 −0.25	−0.11 -	−0.80 -	−1.48 -	+0.44	+2.44	+4.28 -
η intercalibration total stat (JES) [%]	+0.12 +0.19	+0.33 +0.32	+0.28 +0.35	+0.32 +0.37	+0.17 +0.29	−0.31 -	−0.77 -	−0.85 -	+2.60	−1.28 +1.00	−3.31 +2.73
Flavour composition (JES) [%]	−0.30 +2.70	−0.30 +2.70	−0.55 +2.39	−0.52 +1.70	−0.40 +1.30	+0.50	−0.71 +0.14	−0.81 +1.06	−1.27 +2.41	−1.93 +6.60	−3.19 +1.67
Flavour response (JES) [%]	−2.83 −1.31	−2.79 −1.26	−2.60 −1.31	−1.90 −1.08	−1.19 −0.83	−0.79 −0.30	−1.34 -	−3.13 −2.37	−0.55 +2.75	- +3.86	- +2.81
Pile-up offset μ (JES) [%]	+1.92 −0.25	+1.34 -	+1.26 −0.23	+0.90 −0.10	+0.82 -	+0.21 -	−0.63 -	- -	+3.52	+2.07	- -
Pile-up offset N_{PV} (JES) [%]	+0.10 +0.21	+0.22 +0.21	+0.15 +0.25	+0.20 +0.22	−0.25 +0.47	-	−0.67 -	−1.10 +0.39	+3.06	+6.07	−2.94 +6.06
Pile-up offset p_T (JES) [%]	−0.25 −0.96	−0.40 −0.56	−0.58 -	−0.66 +0.43	−0.34 +0.31	+0.18	−0.60 −0.56	−1.25 -	+1.50	+2.79	+3.65 -
Pile-up offset ρ topology (JES) [%]	+0.92 +3.45	+0.61 +3.90	+4.27	−0.45 +3.40	−0.30 +2.39	−0.39 +1.13	+0.52	−1.36 -	+1.34	+5.39	−0.57 +6.35
Punch-through (JES) [%]	−3.33 -	−3.76 -	−4.17 -	−3.68 -	−2.52 -	−1.27 +0.16	−1.12 −0.37	−1.79 -	−0.11 +1.40	- -	−3.70 −3.01
Single particle high-p_T (JES) [%]	-	-	-	-	-	-	-	−0.29 -	- +1.75	+1.26 +1.61	+2.53 +2.08
Jet vertex fraction [%]	+1.17	+1.00	+0.77	+0.54	+0.40	+0.35	+0.41	−1.11 +0.48	+0.49	+0.60	+0.43
b-Quark tagging efficiency (eigenvector 0) [%]	−1.20 −7.90	−1.04 −7.24	−0.80 −6.37	−0.57 −5.58	−0.42 −5.15	−0.38 −5.15	−0.43 −5.73	−0.51 −6.29	−0.53 −6.77	−0.62 −6.58	−0.47 −5.88
b-Quark tagging efficiency (eigenvector 1) [%]	+8.18 −0.99	+7.48 −1.26	+6.55 −1.72	+5.22 −2.29	+5.27 −2.82	+5.27 −3.22	+5.88 −3.27	+6.47 −3.35	+6.96 −3.73	+6.77 −3.76	+6.03 −3.85
b-Quark tagging efficiency (eigenvector 2) [%]	+1.90 +1.27	+1.27 +1.32	+1.73 +1.39	+2.31 +0.99	+2.86 ±0.63	+3.27 ±0.31	+3.32 ±0.11	+3.40 ∓0.11	+3.79 ∓0.40	+3.81 ∓0.47	+3.92 ∓0.32
b-Quark tagging efficiency (eigenvector 3) [%]	−1.69 ∓0.33	−1.56 ∓0.17	−1.31 -	−0.98 +0.28 −0.27	±0.31	±0.16	∓0.12	∓0.35	±0.47	∓0.54	∓0.37
b-Quark tagging efficiency (eigenvector 4) [%]	-	-	-	-	-	-	-	-	∓0.11	∓0.16	∓0.18
c-Quark tagging efficiency (eigenvector 0) [%]	±0.44	+0.36 −0.35	±0.26	±0.21	±0.15	±0.14	±0.15	±0.17	-	±0.20	±0.13
c-Quark tagging efficiency (eigenvector 1) [%]	-	-	∓0.17	∓0.27	∓0.34	±0.41	∓0.48	∓0.51	∓0.48	±0.25	∓0.35
c-Quark tagging efficiency (eigenvector 2) [%]	±0.19	±0.15	-	-	-	∓0.10	∓0.17	∓0.17	∓0.18	-	-
Light-jet tagging efficiency (eigenvector 0) [%]	−0.56 +0.52	∓0.58	−0.51 +0.52	−0.49 +0.50	−0.48 +0.49	∓0.47	−0.64 +0.66	−1.01 +1.00	−1.28 +1.31	−1.28 +1.38	−0.76 +0.74
Light-jet tagging efficiency (eigenvector 1) [%]	+0.35 −0.34	±0.29	+0.20 −0.19	±0.12	-	-	-	±0.31	+0.12 −0.13	-	∓0.13
Light-jet tagging efficiency (eigenvector 2) [%]	-	-	-	-	-	-	-	∓0.12	+0.12 −0.13	+0.19 −0.21	±0.49
Light-jet tagging efficiency (eigenvector 3) [%]	+0.11 −0.12	-	-	-	-	∓0.11	∓0.12	∓0.20	∓0.29	∓0.26	±0.16
Light-jet tagging efficiency (eigenvector 5) [%]	-	-	-	-	-	-	-	-	∓0.14	-	±0.13
Light-jet tagging efficiency (eigenvector 6) [%]	-	-	-	-	-	-	-	-	-	−0.10 +0.11	∓0.15
Light-jet tagging efficiency (eigenvector 7) [%]	-	-	-	-	-	-	-	-	-	±0.13	-
Light-jet tagging efficiency (eigenvector 11) [%]	-	-	-	-	-	-	-	-	-	-	±0.19
b-Quark tagging extrapolation [%]	-	-	-	-	-	±0.14	±0.49	+1.11 −1.10	+1.72 −1.71	+2.27 −2.26	+3.13 −3.09
Electron energy resolution [%]	-	-	-	-	-	-	-	-	+2.09	−1.25	−0.84
Electron energy scale [%]	-	-	-	-	-	-	−0.71 −0.65	−0.56 -	- +2.09	−0.40 -	+0.18 +0.13
Electron trigger efficiency [%]	±0.12	±0.12	±0.11	±0.11	±0.10	±0.10	±0.10	−0.83 ±0.11	±0.12	±0.11	−2.17 ±0.11
Electron reconstruction efficiency [%]	-	-	-	-	-	-	±0.10	±0.10	±0.11	±0.10	±0.10
Electron identification efficiency [%]	±0.34	±0.35	±0.38	±0.43	±0.48	±0.54	±0.57	±0.59	±0.64	±0.58	±0.60
Electron isolation efficiency [%]	-	-	-	±0.11	±0.18	±0.28	±0.36	±0.41	±0.52	±0.50	±0.51
Muon (ID) momentum resolution [%]	-	-	-	-	-	-	-	-	+3.01	+1.31	-
Muon (MS) momentum resolution [%]	−0.21 -	-	-	-	-	-	−0.62 -	−0.33 −0.79	+4.37	+4.63	−3.89 +0.85
Muon (ID) sagitta ρ [%]	-	-	-	-	-	-	-	+0.35 -	+1.24	+1.38	−1.43 +2.41
Muon (ID) sagitta o [%]	−0.14	-	-	-	-	-	−0.33	−0.78	+3.39	+2.25	-
Muon energy scale [%]	-	-	-	-	-	+0.20 -	−0.43	−0.97	-	-	−2.29
Muon trigger efficiency stat [%]	±0.30	+0.29 −0.30	±0.28	±0.27	±0.26	±0.26	±0.26	±0.27	±0.27	±0.28	+0.26 −0.27
Muon trigger efficiency syst [%]	+0.53 −0.52	+0.51 −0.50	+0.49 −0.48	+0.48 −0.47	+0.46 −0.45	+0.45 −0.44	+0.45 −0.44	+0.44 −0.43	+0.43 −0.42	+0.46 −0.45	+0.50 −0.49
Muon identification stat [%]	±0.10	-	-	-	-	-	-	-	-	-	±0.11
Muon identification syst [%]	±0.35	±0.35	±0.34	±0.35	±0.38	±0.41	±0.44	±0.45	±0.45	±0.49	+0.53 −0.52
Muon isolation efficiency syst [%]	±0.11	±0.10	±0.10	±0.10	-	-	-	-	±0.10	±0.11	±0.10
E_T^{miss} Soft jet resolution para [%]	-	±0.22	±0.14	±0.13	±0.14	±0.36	∓0.36	±0.42	±1.44	±3.45	±1.81
E_T^{miss} Soft jet resolution perp [%]	-	±0.16	±0.19	-	±0.24	±0.20	∓0.82	∓0.87	±2.14	±0.51	∓2.59
E_T^{miss} Soft jet scale [%]	- −0.32	+0.19 −0.11	+0.21 −0.15	+0.15 −0.26	+0.20 −0.16	+0.18 -	- −0.96	- −1.21	+2.98 -	+3.44 -	−1.67 +0.80
Luminosity [%]	∓2.05	∓2.05	∓2.05	∓2.05	∓2.05	∓2.05	∓2.05	∓2.05	∓2.05	∓2.05	∓2.05
Z+jets cross-section [%]	±0.85	±0.61	±0.33	±0.15	±0.13	-	±0.14	±0.22	±0.32	±0.39	±0.43
Monte Carlo sample statistics [%]	±0.39	±0.15	±0.14	±0.20	±0.31	±0.58	±1.22	±2.58	±4.56	±6.43	±12.3
ISR/FSR + scale [%]	+0.54 -	+0.56 −0.15	±0.21	- +0.59	−0.46 +0.84	−3.11 +3.46	+2.14 -	- −4.92	+14.7 −4.20	+8.69 -	−8.82 +22.1
Alternate hard-scattering model [%]	±13.5	±9.58	±2.91	∓1.97	∓2.68	∓4.62	±1.19	±2.38	±0.22	∓9.68	∓21.9
Alternate parton-shower model [%]	±5.55	±2.83	∓0.70	∓2.97	∓3.75	∓3.02	±6.20	∓3.58	±11.9	±8.95	∓4.47
Inter PDF [%]	∓0.27	∓0.24	∓0.19	∓0.13	-	-	-	∓0.10	∓0.39	∓0.61	∓0.25
Intra PDF [%]	±0.76	±0.78	±0.77	±0.69	±0.57	±0.41	±0.22	±0.21	±0.87	±1.14	±0.67
Fakes overall normalization, el [%]	+3.84 −3.82	+2.12 −2.13	+0.62 −0.63	±0.24	±0.19	±1.65	∓0.50	∓0.30	±0.42	±0.47	-
Fakes overall normalization, mu [%]	±0.26	±0.17	±0.11	-	-	-	-	∓0.15	∓0.12	∓0.29	-
Fakes alternative parametrization [%]	∓0.80	∓0.60	-	∓0.29	±0.22	∓0.69	±0.95	∓0.23	∓0.26	±0.76	±4.02
W+jets heavy flavour component [%]	±1.45	±1.05	±0.67	±0.41	±0.19	±0.10	-	-	-	-	±0.18
W+jets Scales [%]	±1.32	±1.09	±0.76	±0.56	±0.45	±0.44	±0.69	±0.89	±1.62	±2.10	±1.27
Single Top DS/DR [%]	∓0.19	∓0.23	∓0.30	∓0.52	∓0.61	∓0.52	∓0.76	∓2.33	∓2.67	∓1.22	∓1.53
Single Top IFSR [%]	- −0.57	- −0.41	- −0.36	- −0.31	- −0.33	- −0.39	+0.20 −0.44	+0.41 -	+0.39 −2.43	- −3.00	+0.26 −2.11

TABLE F.46: Table of systematics for the absolute differential cross-section at the parton level for the $p_T^{t,had}$ observable.

Bins [Unit y^{th}]	-2.50—1.70	-1.70—1.20	-1.20—0.80	-0.80—0.40	-0.40–0	0–0.40	0.40–0.80	0.80–1.20	1.20–1.70	1.70–2.50
$d\sigma$ / dy^{th} [pb/ Unit y^{th}]	$7.58 \cdot 10^1$	$1.49 \cdot 10^2$	$1.96 \cdot 10^2$	$2.22 \cdot 10^2$	$2.36 \cdot 10^2$	$2.41 \cdot 10^2$	$2.27 \cdot 10^2$	$1.96 \cdot 10^2$	$1.49 \cdot 10^2$	$7.48 \cdot 10^1$
Total Uncertainty [%]	$^{+8.84}_{-8.64}$	$^{+10.1}_{-10.0}$	±10.0	$^{+11.6}_{-11.3}$	$^{+11.5}_{-11.2}$	$^{+11.8}_{-11.9}$	$^{+11.4}_{-11.0}$	$^{+10.8}_{-10.4}$	$^{+9.35}_{-9.50}$	±12.0
Statistics [%]	±0.7	±0.4	±0.4	±0.4	±0.3	±0.3	±0.4	±0.4	±0.4	±0.7
Systematics [%]	$^{+8.79}_{-8.59}$	$^{+10.1}_{-9.98}$	±10.0	$^{+11.5}_{-11.3}$	$^{+11.5}_{-11.2}$	$^{+11.8}_{-11.9}$	$^{+11.4}_{-11.0}$	$^{+10.8}_{-10.4}$	$^{+9.33}_{-9.48}$	±12.0
Jet energy resolution [%]	∓2.11	∓2.02	∓1.28	∓1.65	∓2.44	∓1.74	∓1.39	∓1.24	∓1.25	∓1.91
b-Tagged jet energy scale (JES) [%]	$^{+0.35}_{-0.53}$	$^{+0.51}_{-0.43}$	$^{+0.49}_{-0.50}$	$^{+0.35}_{-0.42}$	$^{+0.42}_{-0.27}$	$^{+0.23}_{-0.38}$	$^{+0.42}_{-0.40}$	$^{+0.57}_{-0.34}$	$^{+0.36}_{-0.52}$	$^{+0.33}_{-0.45}$
Effective detector NP set 1 (JES) [%]	-	-	-	-	-	-	-	-	-	-
Effective detector NP set 2 (JES) [%]	-	-	$^{+0.22}_{-}$	-	-	-	-	-	-	-
Effective mixed NP set 1 (JES) [%]	-	-	$^{-}_{-0.20}$	$^{+0.24}_{-}$	-	-	-	-	$^{-}_{-0.20}$	-
Effective mixed NP set 2 (JES) [%]	-	-	-	-	-	-	-	-	-	-
Effective mixed NP set 3 (JES) [%]	-	-	-	-	-	-	-	-	-	-
Effective modelling NP set 1 (JES) [%]	$^{+1.51}_{-1.37}$	$^{+2.06}_{-2.08}$	$^{+2.58}_{-2.63}$	$^{+3.01}_{-2.72}$	$^{+2.89}_{-2.83}$	$^{+2.76}_{-2.88}$	$^{+2.84}_{-2.59}$	$^{+2.69}_{-2.32}$	$^{+1.88}_{-2.24}$	$^{+1.34}_{-1.41}$
Effective modelling NP set 2 (JES) [%]	$^{-0.22}_{+0.39}$	$^{-0.31}_{+0.18}$	$^{-0.34}_{+0.33}$	$^{-0.15}_{+0.22}$	$^{-0.24}_{+0.43}$	$^{-0.44}_{+0.30}$	$^{-0.24}_{+0.32}$	$^{-0.22}_{+0.35}$	$^{-0.34}_{+0.11}$	$^{-}_{-0.23}$
Effective modelling NP set 3 (JES) [%]	$^{+0.17}_{-}$	$^{+0.18}_{-}$	$^{-}_{-}$	$^{+0.42}_{-0.31}$	$^{+0.18}_{-0.20}$	$^{-}_{-0.24}$	$^{+0.33}_{-0.26}$	$^{+0.19}_{-}$	$^{-}_{-}$	$^{-}_{-}$
Effective modelling NP set 4 (JES) [%]	$^{+0.16}_{-0.23}$	$^{-}_{-}$	$^{-}_{-0.15}$	$^{+0.36}_{-0.18}$	$^{-}_{-}$	$^{-}_{-}$	$^{+0.17}_{-}$	$^{+0.12}_{-0.11}$	$^{-}_{-}$	±0.13
Effective statistical NP set 1 (JES) [%]	$^{+0.28}_{-0.21}$	$^{+0.40}_{-0.35}$	$^{+0.38}_{-0.42}$	$^{+0.56}_{-0.42}$	$^{+0.58}_{-0.55}$	$^{+0.45}_{-0.60}$	$^{+0.49}_{-0.41}$	$^{+0.45}_{-0.29}$	$^{+0.19}_{-0.44}$	$^{+0.25}_{-0.49}$
Effective statistical NP set 2 (JES) [%]	$^{-0.27}_{+0.25}$	$^{-0.36}_{+0.35}$	$^{-0.43}_{+0.27}$	$^{-0.33}_{+0.58}$	$^{-0.41}_{+0.48}$	$^{-0.60}_{+0.37}$	$^{-0.37}_{+0.47}$	$^{-0.25}_{+0.52}$	$^{-0.34}_{+0.20}$	$^{-0.35}_{+0.17}$
Effective statistical NP set 3 (JES) [%]	-	-	-	-	-	-	-	-	$^{-}_{-0.20}$	$^{-0.17}_{-}$
Effective statistical NP set 4 (JES) [%]	$^{+0.18}_{-}$	-	-	-	-	-	-	-	-	-
Effective statistical NP set 5 (JES) [%]	-	$^{-}_{+0.18}$	-	-	-	-	-	-	-	-
Effective statistical NP set 6 (JES) [%]	-	-	$^{+0.20}_{-}$	$^{+0.16}_{-}$	-	-	-	-	-	$^{-}_{-0.16}$
Effective statistical NP set 7 (JES) [%]	$^{+0.13}_{-}$	-	-	-	$^{+0.19}_{-0.11}$	-	-	-	-	$^{-}_{-0.31}$
η intercalibration model (JES) [%]	$^{+0.91}_{-0.77}$	$^{+1.12}_{-1.14}$	$^{+0.84}_{-0.94}$	$^{+0.48}_{-0.42}$	$^{+0.30}_{-}$	$^{+0.10}_{-0.32}$	$^{+0.31}_{-0.38}$	$^{+0.92}_{-0.70}$	$^{+1.02}_{-1.16}$	$^{+0.54}_{-0.83}$
η intercalibration non closure (JES) [%]	$^{-}_{+0.25}$	$^{-0.31}_{+0.29}$	$^{-0.50}_{+0.36}$	$^{-0.62}_{+0.69}$	$^{-0.38}_{+0.57}$	$^{-0.43}_{-}$	$^{-}_{-}$	$^{-}_{-}$	$^{-}_{-}$	$^{-0.23}_{+0.17}$
η intercalibration total stat (JES) [%]	$^{+0.28}_{-0.31}$	$^{+0.43}_{-0.38}$	$^{+0.40}_{-0.50}$	$^{+0.47}_{-0.44}$	$^{+0.47}_{-0.39}$	$^{+0.39}_{-0.48}$	$^{+0.37}_{-0.36}$	$^{+0.55}_{-0.38}$	$^{+0.38}_{-0.53}$	$^{+0.20}_{-0.34}$
Flavour composition (JES) [%]	$^{+1.11}_{-1.18}$	$^{+1.94}_{-2.20}$	$^{+2.33}_{-2.46}$	$^{+2.67}_{-2.62}$	$^{+2.42}_{-2.76}$	$^{+2.43}_{-2.81}$	$^{+2.49}_{-2.42}$	±2.42	$^{+1.76}_{-1.98}$	±0.96
Flavour response [%]	$^{-0.58}_{+0.55}$	$^{-1.00}_{+1.19}$	$^{-1.44}_{+1.17}$	$^{-1.29}_{+1.20}$	$^{-1.17}_{+1.30}$	$^{-1.41}_{+1.15}$	$^{-1.20}_{+1.22}$	$^{-1.15}_{+1.23}$	$^{-1.07}_{+0.78}$	$^{-0.82}_{+0.51}$
Pile-up offset μ [%]	-	$^{-}_{+0.27}$	$^{-0.16}_{-}$	$^{+0.33}_{-}$	$^{-0.14}_{+0.12}$	$^{-0.30}_{-}$	$^{-0.12}_{+0.15}$	$^{-}_{+0.39}$	$^{-0.20}_{+0.18}$	$^{-}_{-0.33}$
Pile-up offset N_{PV} (JES) [%]	$^{+0.56}_{-0.43}$	$^{+0.41}_{-0.37}$	$^{+0.67}_{-0.62}$	$^{+0.35}_{-0.40}$	$^{+0.74}_{-0.46}$	$^{+0.35}_{-0.52}$	$^{+0.74}_{-0.50}$	$^{+0.67}_{-0.40}$	$^{+0.11}_{-0.48}$	$^{-}_{-0.38}$
Pile-up offset p_T (JES) [%]	-	-	-	$^{-0.17}_{+0.27}$	$^{-0.26}_{+0.33}$	$^{-0.35}_{+0.17}$	$^{-0.18}_{+0.21}$	$^{-}_{+0.15}$	$^{-0.13}_{+0.18}$	$^{-0.43}_{+0.12}$
Pile-up offset ρ topology (JES) [%]	$^{+2.19}_{-2.11}$	±3.08	$^{+3.77}_{-3.84}$	$^{+4.24}_{-4.16}$	$^{+4.31}_{-3.95}$	$^{+4.18}_{-4.19}$	$^{+4.07}_{-3.73}$	$^{+3.79}_{-3.53}$	$^{+3.01}_{-3.06}$	$^{+1.90}_{-2.21}$
Punch-through (JES) [%]	-	-	-	-	-	-	-	-	-	-
Single particle high-p_T (JES) [%]	-	-	-	-	-	-	-	-	-	-
Jet vertex fraction [%]	$^{+0.71}_{-0.74}$	$^{+0.79}_{-0.82}$	$^{+0.82}_{-0.85}$	$^{+0.82}_{-0.85}$	$^{+0.82}_{-0.85}$	$^{+0.83}_{-0.86}$	$^{+0.82}_{-0.85}$	$^{+0.81}_{-0.85}$	$^{+0.78}_{-0.81}$	$^{+0.70}_{-0.73}$
b-Quark tagging efficiency (eigenvector 0) [%]	$^{-6.09}_{+6.26}$	$^{-6.41}_{+6.59}$	$^{-6.57}_{+6.77}$	$^{-6.64}_{+6.84}$	$^{-6.64}_{+6.84}$	$^{-6.68}_{+6.88}$	$^{-6.64}_{+6.84}$	$^{-6.55}_{+6.75}$	$^{-6.36}_{+6.55}$	$^{-6.13}_{+6.30}$
b-Quark tagging efficiency (eigenvector 1) [%]	$^{-1.82}_{+1.84}$	$^{-1.75}_{+1.77}$	$^{-1.72}_{+1.74}$	$^{-1.71}_{+1.72}$	$^{-1.70}_{+1.72}$	$^{-1.70}_{+1.71}$	$^{-1.71}_{+1.73}$	$^{-1.72}_{+1.74}$	$^{-1.76}_{+1.77}$	$^{-1.83}_{+1.85}$
b-Quark tagging efficiency (eigenvector 2) [%]	$^{+1.24}_{-1.25}$	±1.30	$^{+1.31}_{-1.30}$	$^{+1.30}_{-1.29}$	±1.29	±1.29	$^{+1.29}_{-1.28}$	±1.30	$^{+1.51}_{-1.30}$	$^{+1.27}_{-1.26}$
c-Quark tagging efficiency (eigenvector 0) [%]	±0.31	±0.30	±0.28	±0.28	±0.29	$^{+0.31}_{-0.30}$	$^{+0.29}_{-0.28}$	±0.29	±0.30	±0.29
c-Quark tagging efficiency (eigenvector 1) [%]	∓0.22	∓0.17	∓0.17	∓0.17	∓0.17	∓0.17	∓0.16	∓0.16	∓0.18	$^{-0.23}_{+0.24}$
c-Quark tagging efficiency (eigenvector 2) [%]	-	±0.10	-	-	-	-	-	-	±0.11	-
Light-jet tagging efficiency (eigenvector 0) [%]	$^{-0.76}_{+0.79}$	∓0.58	$^{-0.54}_{+0.58}$	$^{-0.33}_{+0.24}$	$^{-0.62}_{+0.66}$	$^{-0.50}_{+0.53}$	$^{-0.48}_{+0.49}$	$^{-0.43}_{+0.40}$	$^{-0.64}_{+0.66}$	$^{-0.82}_{+0.87}$
Light-jet tagging efficiency (eigenvector 1) [%]	$^{+0.33}_{-0.32}$	±0.24	$^{+0.27}_{-0.25}$	$^{+0.11}_{-0.12}$	$^{+0.23}_{-0.22}$	±0.18	$^{+0.15}_{-0.18}$	$^{+0.23}_{-0.23}$	±0.26	±0.28
Light-jet tagging efficiency (eigenvector 2) [%]	$^{-0.11}_{+0.12}$	-	-	-	$^{+0.18}_{-0.16}$	±0.11	-	-	-	-
Light-jet tagging efficiency (eigenvector 3) [%]	∓0.14	-	-	-	$^{+0.13}_{-0.12}$	-	-	-	-	$^{-0.20}_{+0.21}$
Light-jet tagging efficiency (eigenvector 5) [%]	∓0.13	-	-	-	-	-	-	-	-	$^{-0.17}_{+0.18}$
Light-jet tagging efficiency (eigenvector 7) [%]	-	-	-	-	-	-	-	-	-	∓0.10
Electron energy resolution [%]	-	-	-	-	-	-	-	-	-	$^{-}_{-0.20}$
Electron energy scale [%]	-	-	-	-	-	-	-	-	$^{-}_{-0.19}$	-
Electron trigger efficiency [%]	±0.12	±0.12	±0.12	±0.11	±0.11	±0.11	±0.11	±0.11	±0.12	±0.12
Electron identification efficiency [%]	±0.40	±0.39	±0.39	±0.39	±0.38	±0.38	±0.39	±0.39	±0.39	±0.40
Muon (ID) momentum resolution [%]	-	-	-	-	-	-	-	-	-	-
Muon (MS) momentum resolution [%]	-	-	-	-	-	-	-	-	-	-
Muon (ID) sagitta ρ [%]	-	-	-	-	-	-	-	-	-	-
Muon energy scale [%]	-	-	-	-	-	-	-	-	$^{-}_{-0.26}$	-
Muon trigger efficiency stat [%]	$^{+0.27}_{-0.28}$	±0.28	±0.28	±0.28	$^{+0.28}_{-0.29}$	$^{+0.28}_{-0.29}$	$^{+0.28}_{-0.29}$	$^{+0.28}_{-0.29}$	±0.28	±0.28
Muon trigger efficiency syst [%]	$^{+0.50}_{-0.49}$	$^{+0.50}_{-0.49}$	$^{+0.50}_{-0.49}$	$^{+0.50}_{-0.49}$	$^{+0.50}_{-0.49}$	$^{+0.50}_{-0.49}$	$^{+0.50}_{-0.49}$	$^{+0.50}_{-0.49}$	$^{+0.49}_{-0.48}$	$^{+0.50}_{-0.49}$
Muon identification syst [%]	±0.36	±0.35	±0.35	±0.35	±0.35	±0.35	±0.35	±0.35	±0.36	±0.37
Muon isolation efficiency syst [%]	±0.10	±0.10	±0.10	±0.10	±0.10	±0.10	±0.10	±0.10	±0.10	±0.10
E_T^{miss} Soft jet resolution para [%]	±0.10	±0.11	±0.16	±0.17	±0.22	-	±0.26	±0.12	-	±0.13
E_T^{miss} Soft jet resolution perp [%]	±0.31	±0.10	-	±0.16	±0.20	-	±0.24	±0.23	-	±0.26
E_T^{miss} Soft jet scale [%]	$^{+0.27}_{-0.22}$	$^{+0.24}_{-0.20}$	$^{+0.20}_{-0.14}$	$^{+0.31}_{-0.19}$	-	$^{-}_{-0.31}$	$^{+0.34}_{-0.18}$	$^{+0.27}_{-0.13}$	$^{-}_{-0.32}$	$^{+0.12}_{-0.19}$
Luminosity [%]	∓2.05	∓2.05	∓2.05	∓2.05	∓2.05	∓2.05	∓2.05	∓2.05	∓2.05	∓2.05
Z+jets cross-section [%]	±0.35	±0.39	±0.41	±0.43	±0.44	±0.43	±0.42	±0.44	±0.39	±0.47
Monte Carlo sample statistics [%]	±0.48	±0.31	±0.31	±0.33	±0.27	±0.23	±0.25	±0.45	±0.34	±0.54
ISR/FSR + scale [%]	$^{+0.32}_{-}$	$^{+0.73}_{-}$	$^{+0.70}_{-}$	$^{+0.52}_{-0.27}$	$^{-0.16}_{+0.17}$	$^{+0.29}_{-}$	$^{+0.41}_{-}$	$^{-0.24}_{-}$	$^{-}_{-0.27}$	$^{+0.91}_{-0.20}$
Alternate hard-scattering model [%]	±1.46	±4.11	±2.85	±5.22	±4.59	±6.20	±5.57	±4.81	±2.86	±7.82
Alternate parton-shower model [%]	∓2.54	∓1.01	±0.30	±1.54	±1.57	±1.70	±1.18	±0.76	∓1.80	∓4.12
Inter PDF [%]	-	-	∓0.11	∓0.16	∓0.15	∓0.16	∓0.15	∓0.11	-	-
Intra PDF [%]	±0.59	±0.29	±0.31	±0.30	±0.29	±0.30	±0.30	±0.31	±0.28	±0.60
Fakes overall normalization, el [%]	±0.84	±0.95	±0.83	±1.89	±2.32	±1.43	±1.05	±1.18	±0.71	±1.03
Fakes overall normalization, mu [%]	±0.22	±0.13	-	±0.15	-	±0.14	±0.11	-	±0.11	±0.30
Fakes alternative parametrization [%]	±0.20	∓0.45	∓0.64	∓0.38	∓0.50	∓0.28	-	∓0.41	±0.17	∓0.14
W+jets heavy flavour component [%]	±0.60	±0.73	±0.74	±0.79	±0.80	±0.86	±0.82	±0.79	±0.70	±0.65
W+jets Scales [%]	±0.82	±0.87	±0.85	±0.84	±0.92	±0.93	±0.93	±0.78	±0.72	±0.82
Single Top DS/DR [%]	±0.21	∓0.32	∓0.32	∓0.45	∓0.33	∓0.36	∓0.34	∓0.29	∓0.31	∓0.32
Single Top IFSR [%]	$^{-}_{-0.34}$	$^{-}_{-0.55}$	$^{-}_{-0.33}$	$^{-}_{-0.43}$	$^{-}_{-0.20}$	$^{-}_{-0.29}$	$^{-}_{-0.34}$	$^{-}_{-0.52}$	$^{-}_{-0.48}$	$^{-}_{-0.28}$

TABLE F.47: Table of systematics for the absolute differential cross-section at the parton level for the $y^{t,had}$ observable.

Bins [GeV]	0–40	40–90	90–150	150–230	230–310	310–390	390–470	470–550	550–630	630–800
$d\sigma$ / $dp_T^{t\bar{t}}$ [pb/GeV]	$9.46 \cdot 10^{0}$	$4.84 \cdot 10^{0}$	$1.82 \cdot 10^{0}$	$6.63 \cdot 10^{-1}$	$2.41 \cdot 10^{-1}$	$9.53 \cdot 10^{-2}$	$4.07 \cdot 10^{-2}$	$1.81 \cdot 10^{-2}$	$9.08 \cdot 10^{-3}$	$3.44 \cdot 10^{-3}$
Total Uncertainty [%]	$^{+14.6}_{-14.5}$	±18.4	$^{+20.4}_{-20.2}$	$^{+17.4}_{-17.3}$	$^{+15.1}_{-14.5}$	$^{+16.6}_{-16.5}$	$^{+17.0}_{-18.1}$	$^{+12.7}_{-15.9}$	$^{+13.5}_{-17.1}$	$^{+33.4}_{-27.1}$
Statistics [%]	±0.2	±0.1	±0.2	±0.4	±0.9	±1.6	±2.8	±4.6	±6.8	±11.
Systematics [%]	$^{+14.6}_{-14.5}$	±18.4	$^{+20.4}_{-20.2}$	$^{+17.4}_{-17.3}$	$^{+15.1}_{-14.5}$	$^{+16.5}_{-16.4}$	$^{+16.7}_{-17.8}$	$^{+11.5}_{-15.0}$	$^{+11.0}_{-15.2}$	$^{+30.8}_{-23.9}$
Jet energy resolution [%]	∓3.79	∓0.96	±0.87	±1.03	∓0.20	∓1.26	∓1.93	∓3.69	±0.98	∓0.28
b-Tagged jet energy scale (JES) [%]	$^{+0.23}_{-0.35}$	$^{+0.41}_{-0.39}$	$^{+0.74}_{-0.58}$	$^{+0.79}_{-0.44}$	$^{+0.35}_{-0.40}$	$^{-0.27}_{-}$	$^{-}_{-0.47}$	$^{+0.67}_{-0.36}$	$^{+0.46}_{-1.83}$	$^{+0.98}_{+1.46}$
Effective detector NP set 1 (JES) [%]	-	-	-	-	$^{+0.44}_{-0.29}$	$^{-}_{-0.38}$	$^{+0.42}_{-}$	-	$^{-}_{-0.83}$	$^{-}_{+3.42}$
Effective detector NP set 2 (JES) [%]	-	-	-	-	$^{+0.34}_{-0.27}$	$^{-}_{-0.27}$	$^{-}_{-0.13}$	$^{+0.42}_{-}$	$^{-}_{-0.95}$	$^{-}_{+4.02}$
Effective mixed NP set 1 (JES) [%]	-	-	$^{+0.18}_{-}$	$^{+0.31}_{-0.26}$	$^{+0.83}_{-0.12}$	$^{+0.60}_{-0.54}$	$^{+0.20}_{-1.64}$	$^{+0.16}_{-0.82}$	$^{-}_{-1.42}$	$^{-}_{-1.79}$
Effective mixed NP set 2 (JES) [%]	-	-	-	-	$^{+0.39}_{+0.25}$	$^{-}_{-}$	$^{+0.19}_{+0.36}$	$^{-}_{+1.19}$	$^{-}_{-0.82}$	$^{+0.24}_{-0.20}$
Effective mixed NP set 3 (JES) [%]	-	-	-	-	$^{-}_{+2.81}$	$^{-}_{+1.23}$	$^{-}_{+0.64}$	$^{+0.26}_{+2.18}$	$^{-}_{+1.52}$	$^{+3.77}_{+6.11}$
Effective modelling NP set 1 (JES) [%]	±1.88	$^{+2.79}_{-2.76}$	$^{+3.60}_{-3.32}$	±3.26	$^{-2.29}_{-2.20}$	$^{-1.59}_{-0.20}$	$^{-1.43}_{-}$	$^{-1.74}_{+0.74}$	$^{-1.62}_{+1.17}$	$^{-2.24}_{+2.49}$
Effective modelling NP set 2 (JES) [%]	$^{-0.24}_{+0.23}$	∓0.35	$^{-0.22}_{+0.34}$	$^{-0.20}_{+0.12}$	$^{-}_{-0.26}$	$^{-}_{-}$	$^{-0.23}_{-}$	$^{-}_{+0.56}$	$^{-0.73}_{-2.12}$	$^{-0.78}_{+1.74}$
Effective modelling NP set 3 (JES) [%]	$^{+0.22}_{-0.21}$	$^{+0.20}_{-0.23}$	$^{+0.21}_{-}$	$^{-}_{-}$	$^{-}_{-0.23}$	$^{-}_{-0.23}$	$^{-}_{-0.26}$	$^{-}_{-0.57}$	$^{-}_{+0.71}$	$^{-}_{+2.84}$
Effective modelling NP set 4 (JES) [%]	-	$^{+0.12}_{-0.15}$	$^{+0.33}_{-0.16}$	$^{+0.20}_{-0.24}$	$^{+0.45}_{-0.26}$	$^{-}_{-0.25}$	$^{-}_{-0.32}$	$^{-}_{-0.96}$	$^{-0.86}_{+0.28}$	$^{-}_{+3.81}$
Effective statistical NP set 1 (JES) [%]	$^{+0.36}_{-0.35}$	$^{+0.45}_{-0.50}$	$^{+0.58}_{-0.50}$	$^{+0.51}_{-0.52}$	$^{+0.79}_{-0.52}$	$^{-}_{-0.47}$	$^{-}_{-0.53}$	$^{-}_{-0.32}$	$^{-}_{-1.81}$	$^{-}_{+3.74}$
Effective statistical NP set 2 (JES) [%]	$^{-0.31}_{+0.33}$	$^{-0.45}_{+0.40}$	$^{-0.46}_{+0.56}$	$^{-0.53}_{+0.48}$	$^{-}_{+0.68}$	$^{-0.31}_{+0.28}$	$^{-}_{-}$	$^{-}_{-0.91}$	$^{-2.36}_{-}$	$^{-}_{-0.90}$
Effective statistical NP set 3 (JES) [%]	-	-	-	-	-	$^{-0.71}_{+0.31}$	$^{-0.72}_{+1.29}$	$^{+0.60}_{+0.38}$	$^{-}_{-2.07}$	$^{+2.49}_{-0.63}$
Effective statistical NP set 4 (JES) [%]	-	$^{-0.16}_{-}$	$^{-}_{-}$	$^{-}_{-0.16}$	$^{+0.41}_{-}$	$^{-}_{-}$	$^{+0.51}_{-}$	$^{-}_{-}$	$^{-}_{-1.12}$	$^{+2.35}_{-}$
Effective statistical NP set 5 (JES) [%]	-	-	$^{-}_{+0.17}$	$^{-}_{-}$	$^{+0.27}_{+0.39}$	$^{+0.35}_{-0.21}$	$^{+0.33}_{-}$	$^{+0.62}_{-0.40}$	$^{+0.35}_{-2.36}$	$^{-1.18}_{+3.84}$
Effective statistical NP set 6 (JES) [%]	-	-	$^{-}_{-}$	$^{-}_{-}$	$^{-}_{+0.30}$	$^{-0.25}_{-}$	$^{+0.87}_{+0.48}$	$^{-}_{+0.41}$	$^{-}_{-1.87}$	$^{+0.42}_{+1.29}$
Effective statistical NP set 7 (JES) [%]	-	-	-	$^{+0.10}_{-0.15}$	$^{-}_{-0.31}$	$^{-}_{-0.43}$	$^{-0.32}_{-}$	$^{-}_{+0.38}$	$^{-1.61}_{+0.50}$	$^{-}_{+2.42}$
η intercalibration model (JES) [%]	$^{+0.32}_{-0.35}$	$^{+0.59}_{-0.68}$	$^{+0.99}_{-0.85}$	$^{+0.98}_{-0.96}$	$^{+0.94}_{-0.50}$	$^{+0.79}_{-0.50}$	$^{-}_{-1.35}$	$^{-}_{-1.11}$	$^{+0.80}_{-0.48}$	$^{-}_{-1.14}$
η intercalibration non closure (JES) [%]	$^{-0.18}_{+0.12}$	$^{-0.28}_{+0.24}$	$^{-0.39}_{+0.54}$	$^{-0.47}_{+0.45}$	$^{-0.13}_{+0.47}$	$^{-0.34}_{+0.45}$	$^{-}_{-1.18}$	$^{+0.91}_{+0.48}$	$^{+1.21}_{+0.50}$	$^{-1.56}_{+0.45}$
η intercalibration total stat (JES) [%]	$^{+0.30}_{-0.25}$	$^{+0.36}_{-0.51}$	$^{+0.70}_{-0.60}$	$^{+0.68}_{-0.65}$	$^{+1.03}_{-0.32}$	$^{-}_{-0.56}$	$^{-0.48}_{+0.32}$	$^{-}_{-0.87}$	$^{-}_{-1.20}$	$^{+1.45}_{-}$
Flavour composition (JES) [%]	$^{+1.56}_{-1.70}$	$^{+2.41}_{-2.60}$	$^{+3.36}_{-3.43}$	$^{+3.25}_{-3.37}$	$^{+2.32}_{-2.27}$	$^{+0.91}_{-1.72}$	$^{+0.80}_{-2.43}$	$^{+2.74}_{-1.56}$	$^{+3.47}_{-0.74}$	$^{+2.73}_{-2.35}$
Flavour response (JES) [%]	$^{-0.78}_{+0.77}$	$^{-1.32}_{+1.19}$	$^{-1.80}_{+1.70}$	$^{-1.78}_{+1.50}$	$^{-1.02}_{+1.43}$	$^{-1.05}_{+1.20}$	$^{-1.41}_{+0.51}$	$^{-}_{-}$	$^{+1.26}_{-}$	$^{+4.01}_{+2.70}$
Pile-up offset μ (JES) [%]	$^{-0.15}_{+0.17}$	$^{-0.19}_{+0.10}$	$^{-0.16}_{+0.24}$	$^{-0.16}_{+0.28}$	$^{+0.22}_{-0.16}$	$^{-}_{-0.24}$	$^{-0.45}_{+0.14}$	$^{-0.38}_{+0.71}$	$^{+0.16}_{-0.22}$	$^{-}_{+1.14}$
Pile-up offset N_{PV} (JES) [%]	$^{+0.26}_{-0.28}$	$^{+0.53}_{-0.54}$	$^{+0.91}_{-0.73}$	$^{+0.98}_{-0.77}$	$^{+0.59}_{-}$	$^{-}_{-0.20}$	$^{-}_{-0.64}$	$^{-}_{-0.36}$	$^{+0.34}_{-0.42}$	$^{-}_{+3.01}$
Pile-up offset p_T (JES) [%]	$^{-0.35}_{+0.21}$	$^{-0.25}_{+0.26}$	$^{+0.13}_{-}$	$^{+0.27}_{-0.19}$	$^{-}_{-}$	$^{-}_{-0.54}$	$^{-}_{-1.09}$	$^{-}_{+0.27}$	$^{-}_{-0.78}$	$^{-}_{+3.15}$
Pile-up offset ρ topology (JES) [%]	$^{+2.66}_{-2.65}$	$^{+4.09}_{-4.00}$	$^{+5.43}_{-5.09}$	$^{+5.23}_{-4.97}$	$^{+3.52}_{-3.11}$	$^{+1.95}_{-2.30}$	$^{+1.52}_{-2.08}$	$^{+1.44}_{-2.00}$	$^{+2.43}_{-0.79}$	$^{-}_{+1.57}$
Punch-through (JES) [%]	-	-	-	-	$^{-}_{+0.13}$	$^{-}_{+0.30}$	$^{-}_{-}$	$^{+0.37}_{-0.83}$	$^{-}_{-1.22}$	$^{-}_{+1.06}$
Single particle high-p_T (JES) [%]	-	-	-	-	$^{-}_{+0.69}$	$^{-}_{+0.63}$	$^{-}_{+0.57}$	$^{-0.21}_{+0.49}$	$^{-0.65}_{+0.39}$	$^{-}_{+0.48}$
Jet vertex fraction [%]	$^{+0.77}_{-0.80}$	$^{+0.85}_{-0.88}$	$^{+0.85}_{-0.88}$	$^{+0.77}_{-0.81}$	$^{-0.73}$	$^{-0.67}$	$^{-0.60}$	$^{-0.53}$	$^{-0.52}$	$^{-0.51}$
b-Quark tagging efficiency (eigenvector 0) [%]	$^{-6.93}_{+7.16}$	$^{-6.54}_{+6.74}$	$^{-5.96}_{+6.11}$	$^{-5.78}_{+5.91}$	$^{-6.03}_{+6.17}$	$^{-6.22}_{+6.37}$	$^{-6.10}_{+6.24}$	$^{-5.91}_{+6.07}$	$^{-5.65}_{+5.79}$	$^{-5.33}_{+5.45}$
b-Quark tagging efficiency (eigenvector 1) [%]	$^{-2.19}_{+1.58}$	$^{-2.63}_{+1.91}$	$^{-2.91}_{+2.27}$	$^{-2.77}_{+2.22}$	$^{-2.52}_{+2.55}$	$^{-2.53}_{+2.56}$	$^{-2.67}_{+2.69}$	$^{-2.93}_{+2.96}$	$^{-3.21}_{+3.26}$	$^{-3.42}_{+3.59}$
b-Quark tagging efficiency (eigenvector 2) [%]	$^{+1.38}_{-1.42}$	$^{+1.67}_{-1.34}$	±1.17	$^{+2.29}_{+0.90}$	±0.67	±0.59	±0.53	±0.44	±0.26	-
b-Quark tagging efficiency (eigenvector 3) [%]	-	-	±0.11	±0.17	-	-	-	-	-	-
c-Quark tagging efficiency (eigenvector 0) [%]	±0.30	$^{+0.30}_{-0.29}$	±0.27	±0.27	±0.30	±0.32	±0.20	±0.18	±0.16	±0.26
c-Quark tagging efficiency (eigenvector 1) [%]	∓0.12	∓0.16	∓0.22	∓0.32	∓0.39	∓0.42	∓0.39	∓0.31	$^{-0.31}_{+0.30}$	∓0.51
c-Quark tagging efficiency (eigenvector 2) [%]	±0.11	±0.10	-	-	-	-	-	-	-	-
Light-jet tagging efficiency (eigenvector 0) [%]	$^{-0.45}_{+0.47}$	$^{-0.52}_{+0.51}$	$^{-0.58}_{+0.57}$	$^{-0.77}_{+0.79}$	$^{-0.94}_{+0.97}$	$^{-0.96}_{+0.98}$	$^{-0.63}_{+0.64}$	∓0.26	$^{-0.59}_{+0.62}$	$^{-1.28}_{+1.30}$
Light-jet tagging efficiency (eigenvector 1) [%]	$^{+0.22}_{-0.21}$	±0.23	±0.19	±0.17	±0.17	$^{+0.20}_{-0.19}$	-	-	$^{+0.11}_{-0.12}$	±0.44
Light-jet tagging efficiency (eigenvector 2) [%]	-	-	-	-	$^{+0.13}_{-0.12}$	$^{+0.12}_{-0.11}$	$^{+0.20}_{-0.19}$	-	-	-
Light-jet tagging efficiency (eigenvector 5) [%]	-	-	-	-	-	-	-	-	$^{+0.12}_{-0.11}$	±0.10
Light-jet tagging efficiency (eigenvector 6) [%]	-	-	-	-	-	-	-	-	-	∓0.10
Light-jet tagging efficiency (eigenvector 7) [%]	-	-	-	-	-	-	-	-	-	±0.10
b-Quark tagging extrapolation [%]	-	-	-	-	±0.15	±0.40	±0.54	$^{+0.60}_{-0.59}$	±0.70	±0.83
b-Quark tagging extrapolation from c-Quark [%]	-	-	-	-	-	-	±0.10	-	-	-
Electron energy resolution [%]	-	-	-	-	-	$^{-}_{-0.36}$	-	-	$^{-}_{-0.90}$	$^{+1.20}_{+0.30}$
Electron energy scale [%]	-	-	-	-	-	$^{-}_{-0.35}$	$^{-}_{-0.24}$	$^{-}_{-0.52}$	-	-
Electron trigger efficiency [%]	±0.12	±0.11	±0.11	±0.11	±0.11	±0.11	±0.10	±0.10	±0.11	±0.11
Electron reconstruction efficiency [%]	-	-	-	-	-	-	±0.10	±0.10	±0.10	±0.11
Electron identification efficiency [%]	±0.37	±0.38	±0.40	±0.43	±0.48	±0.53	±0.55	±0.58	±0.61	±0.61
Electron isolation efficiency [%]	-	-	-	±0.12	±0.18	±0.24	±0.32	±0.38	±0.42	±0.49
Muon (ID) momentum resolution [%]	-	-	-	-	$^{+0.26}_{-}$	$^{-}_{-0.29}$	$^{-}_{-0.39}$	$^{-0.34}_{+0.10}$	$^{+0.43}_{-1.51}$	$^{+2.33}_{+1.07}$
Muon (MS) momentum resolution [%]	-	-	-	-	$^{+0.45}_{-}$	$^{+0.23}_{-0.10}$	$^{-}_{-0.21}$	$^{-0.51}_{+1.00}$	$^{+0.47}_{-}$	$^{-}_{+0.59}$
Muon (ID) sagitta ρ [%]	-	-	-	-	$^{+0.26}_{-}$	$^{-}_{-}$	$^{-0.40}_{+0.14}$	$^{-}_{-0.39}$	$^{-}_{+0.33}$	$^{-}_{+1.28}$
Muon energy scale [%]	-	-	-	-	$^{+0.32}_{-}$	$^{-}_{-}$	$^{-}_{-}$	$^{-}_{-0.54}$	$^{-}_{-0.72}$	$^{-}_{-}$
Muon trigger efficiency stat [%]	$^{+0.28}_{-0.29}$	±0.28	±0.28	±0.28	±0.28	$^{+0.27}_{-0.28}$	±0.28	$^{+0.26}_{-0.27}$	±0.27	±0.26
Muon trigger efficiency syst [%]	$^{+0.50}_{-0.49}$	$^{+0.50}_{-0.49}$	$^{+0.49}_{-0.48}$	$^{+0.49}_{-0.48}$	$^{+0.49}_{-0.48}$	$^{+0.49}_{-0.48}$	$^{+0.48}_{-0.47}$	$^{+0.45}_{-0.44}$	$^{+0.44}_{-0.43}$	$^{+0.47}_{-0.46}$
Muon identification syst [%]	±0.35	±0.35	±0.35	±0.36	±0.38	±0.40	±0.43	±0.44	±0.41	±0.50
Muon isolation efficiency syst [%]	±0.10	±0.10	±0.10	±0.10	±0.10	±0.10	±0.10	-	-	±0.10
E_T^{miss} Soft jet resolution para [%]	-	±0.28	±0.25	-	±0.45	±0.48	∓1.07	∓0.52	±2.08	∓0.58
E_T^{miss} Soft jet resolution perp [%]	-	±0.31	±0.30	±0.21	±0.27	±0.17	∓0.91	±0.50	∓0.21	±0.82
E_T^{miss} Soft jet scale [%]	$^{-}_{-0.26}$	$^{+0.26}_{-0.23}$	$^{+0.29}_{-}$	$^{-}_{-}$	$^{+0.25}_{-}$	$^{-}_{-0.45}$	$^{-}_{-0.31}$	$^{+1.16}_{-}$	$^{-}_{-1.27}$	$^{-1.30}_{+2.21}$
Luminosity [%]	∓2.05	∓2.05	∓2.05	∓2.05	∓2.05	∓2.05	∓2.05	∓2.05	∓2.05	∓2.05
Z+jets cross-section [%]	±0.48	±0.39	±0.33	±0.40	±0.43	±0.41	±0.33	±0.19	±0.15	±0.22
Monte Carlo sample statistics [%]	±0.13	±0.14	±0.19	±0.30	±0.55	±1.00	±1.66	±2.65	±3.65	±6.03
ISR/FSR + scale [%]	$^{-0.78}_{+1.01}$	±0.38	$^{+0.62}_{-0.80}$	$^{-}_{-0.89}$	$^{+1.70}_{-}$	$^{-1.11}_{+3.35}$	$^{-4.44}_{+1.44}$	$^{-}_{-9.82}$	$^{-}_{-8.90}$	$^{-3.69}_{+12.3}$
Alternate hard-scattering model [%]	∓2.88	±14.2	±8.94	±4.60	±5.35	±9.34	±2.92	∓1.42	±3.36	±21.8
Alternate parton-shower model [%]	∓10.3	±6.53	±14.8	±13.2	±10.1	±9.97	±13.9	±5.73	±3.48	±0.32
Inter PDF [%]	∓0.23	∓0.14	∓0.22	∓0.24	∓0.15	-	-	-	-	±0.19
Intra PDF [%]	±0.82	±0.72	±0.57	±0.41	±0.27	±0.29	±0.40	±0.49	±0.56	±0.58
Fakes overall normalization, el [%]	±1.33	±1.67	±1.23	±0.56	±0.13	±0.51	$^{-0.13}_{+0.14}$	±0.15	±0.45	∓0.11
Fakes overall normalization, mu [%]	-	±0.16	±0.22	±0.17	±0.21	±0.22	±0.24	∓0.19	±0.13	-
Fakes alternative parametrization [%]	∓0.27	∓0.37	∓0.34	-	±0.34	∓0.97	∓0.34	±0.60	∓0.12	±0.12
W+jets heavy flavour component [%]	±0.89	±0.77	±0.65	±0.65	±0.38	-	-	-	±0.11	-
W+jets Scales [%]	±0.78	±0.75	±0.98	±1.26	±1.59	±1.69	±1.49	±0.94	±1.02	±0.94
Single Top DS/DR [%]	∓0.14	∓0.31	∓0.49	∓0.79	∓1.38	∓1.99	∓1.59	∓1.68	∓2.51	∓1.28
Single Top IFSR [%]	$^{-0.43}_{-}$	$^{-}_{-0.37}$	$^{-}_{-0.41}$	$^{-}_{-0.47}$	$^{-}_{-0.92}$	$^{-}_{-1.08}$	$^{+0.27}_{-1.50}$	$^{+0.58}_{-}$	$^{+1.42}_{-}$	$^{+1.51}_{-1.08}$

TABLE F.48: Table of systematics for the absolute differential cross-section at the parton level for the $p_T^{t\bar{t}}$ observable.

Bins [GeV]	325–400	400–480	480–580	580–700	700–860	860–1020	1020–1250	1250–1500	1500–2000
$d\sigma$ / $dm^{t\bar{t}}$ [pb/GeV]	$2.54 \cdot 10^{0}$	$3.13 \cdot 10^{0}$	$1.77 \cdot 10^{0}$	$8.40 \cdot 10^{-1}$	$3.44 \cdot 10^{-1}$	$1.43 \cdot 10^{-1}$	$5.56 \cdot 10^{-2}$	$1.86 \cdot 10^{-2}$	$4.84 \cdot 10^{-3}$
Total Uncertainty [%]	+27.2 −27.0	+11.0 −10.9	+10.1 −10.2	+11.7 −11.8	+11.7 −11.3	+11.1 −9.94	+13.7 −13.4	+14.0 −11.9	+24.0 −24.9
Statistics [%]	±0.2	±0.2	±0.2	±0.3	±0.5	±0.8	±1.3	±2.5	±4.9
Systematics [%]	+27.2 −27.0	+11.0 −10.9	+10.1 −10.2	+11.7 −11.8	+11.7 −11.3	+11.0 −9.88	+13.6 −13.3	+13.7 −11.4	+23.2 −24.1
Jet energy resolution [%]	∓2.09	∓1.71	∓1.60	∓1.47	∓1.48	∓0.62	∓0.38	∓2.74	∓2.09
b-Tagged jet energy scale (JES) [%]	−0.42 +0.46	+0.48 −0.51	+0.79 −0.80	+0.71 −0.77	+0.51 −0.52	+0.73 -	+0.42 −0.22	+1.42 −0.18	- −2.92
Effective detector NP set 1 (JES) [%]	+0.20 -	-	-	+0.13 −0.19	-	+0.28 -	-	+0.92 -	- −1.66
Effective detector NP set 2 (JES) [%]	-	-	-	-	+0.18 −0.10	+0.49 -	−0.25	+0.47 -	- −2.89
Effective mixed NP set 1 (JES) [%]	−0.21 +0.49	-	+0.10 −0.26	+0.18 −0.26	+0.27 −0.26	+0.70 -	+0.42 −0.32	+1.45 -	- −2.91
Effective mixed NP set 2 (JES) [%]	-	-	-	-	-	+0.56 -	+0.22 -	-	- −1.63
Effective mixed NP set 3 (JES) [%]	-	-	-	-	-	-	-	+0.42 −0.14	- −1.46
Effective modelling NP set 1 (JES) [%]	+2.66 −2.43	+2.84 −2.77	+2.49 −2.62	+2.28 −2.25	+2.01 −1.74	+2.28 −1.25	+1.40 −1.97	+2.39 −1.91	+1.19 −1.80
Effective modelling NP set 2 (JES) [%]	−0.46 +0.68	−0.32 +0.28	−0.25 -	−0.12 -	-	+0.45 -	-	−0.14 +0.40	- −0.91
Effective modelling NP set 3 (JES) [%]	+0.71 −0.47	+0.16 −0.25	-	-	−0.10 +0.12	+0.28 -	-	+1.33 -	- −1.84
Effective modelling NP set 4 (JES) [%]	+0.22 -	-	−0.24	+0.14 −0.19	+0.20 -	+0.52 -	-	+0.45 -	- −1.45
Effective statistical NP set 1 (JES) [%]	+0.56 −0.47	±0.48	+0.36 −0.49	+0.33 −0.41	+0.28 −0.30	+0.57 -	−0.24 +0.81 −0.37	+1.08 -	- −1.92
Effective statistical NP set 2 (JES) [%]	−0.41 +0.57	−0.43 +0.40	−0.43 +0.27	−0.41 +0.40	−0.31 +0.43	+0.44 -	−0.26 +0.28	+0.82 -	- −2.18
Effective statistical NP set 3 (JES) [%]	-	-	-	-	-	-	+0.48 -	+0.33 -	- −1.77
Effective statistical NP set 4 (JES) [%]	−0.25 +0.51	-	−0.23	-	-	-	-	+1.57 -	- −1.73
Effective statistical NP set 5 (JES) [%]	-	-	-	-	-	+0.30 -	−0.45 -	+1.35 -	- −2.22
Effective statistical NP set 6 (JES) [%]	+0.26 -	-	-	-	-	+0.35 -	-	-	- −2.09
Effective statistical NP set 7 (JES) [%]	-	−0.15 -	-	-	+0.28 -	+0.27 -	−0.12 +0.25	+1.41 +1.26	- −1.48
η intercalibration model (JES) [%]	+0.28	+0.51 −0.54	+0.63 −0.85	+0.82 −0.85	+0.90 −0.71	+1.12 −0.74	+0.80 −1.02	+2.06 −0.93	+2.37 −3.09
η intercalibration non closure (JES) [%]	−0.12 +0.32	−0.34 +0.26	−0.34 +0.18	−0.25 +0.20	−0.17 +0.32	- +0.79	−0.32 -	+0.23 -	- −1.68
η intercalibration total stat (JES) [%]	+0.31 −0.15	+0.46 −0.50	+0.49 −0.55	+0.34 −0.54	+0.37 −0.27	+0.57 −0.12	+0.66 −0.65	+0.87 -	- −2.22
Flavour composition (JES) [%]	+2.64 −2.71	+2.48 −2.70	+2.06 −2.24	+1.72 −2.09	+1.85 −1.61	+2.07 −1.44	+2.35 −1.90	+2.14 −0.66	+0.57 −2.44
Flavour response (JES) [%]	−1.15 +1.73	−1.33 +1.19	−1.26 +1.06	−1.08 +0.99	−0.74 +0.96	−0.72 +1.17	−1.38 +0.93	−0.78 +1.21	- −2.21
Pile-up offset μ (JES) [%]	+0.24 -	−0.25 +0.19	−0.24 -	−0.16 +0.10	−0.14 +0.10	+0.59 -	+0.42 -	−0.19 +1.71	- −1.53
Pile-up offset N_{PV} (JES) [%]	+0.44 −0.24	+0.53 −0.54	+0.55 −0.58	+0.53 −0.48	+0.39 −0.43	+0.59 -	+0.48 −0.75	+1.09 −0.23	- −1.50
Pile-up offset p_T (JES) [%]	−0.83 +1.00	−0.28 +0.27	- −0.22	+0.11 −0.33	+0.36 −0.10	+0.50 -	- −0.72	+0.93 -	- −1.25
Pile-up offset ρ topology (JES) [%]	+3.38 −2.94	+4.20 −4.15	+3.94 −4.09	+3.43 −3.52	+2.95 −2.63	+3.45 −2.23	+3.60 −2.89	+3.85 −1.73	+1.12 −3.05
Punch-through (JES) [%]	-	-	-	-	-	-	-	+0.29 −0.10	- −1.91
Single particle high-p_T (JES) [%]	-	-	-	-	-	-	-	-	- −1.67
Jet vertex fraction [%]	+1.08 −1.11	+0.88 −0.91	+0.70 −0.73	+0.60 −0.63	+0.55 −0.58	+0.57 −0.60	+0.57 −0.60	+0.57 −0.60	+0.61 −0.63
b-Quark tagging efficiency (eigenvector 0) [%]	−7.53	−6.76	−6.15	−5.83	−5.72	−5.85	−5.99	−5.89	−5.89
b-Quark tagging efficiency (eigenvector 1) [%]	+7.79 ∓1.11	+6.96 −1.50	+6.32 −1.92	+5.98 −2.28	+5.87 −2.51	+6.00 −2.55	+6.14 −2.55	+6.04 −2.60	+6.03 −2.81
b-Quark tagging efficiency (eigenvector 2) [%]	+1.60 −1.59	+1.51 +1.44 −1.43	+1.94 ±1.21	+2.30 +1.00 −0.99	+2.54 ±0.82	+2.58 +0.77 −0.76	+2.58 ±0.74	+2.63 ±0.69	+2.86 ±0.58
b-Quark tagging efficiency (eigenvector 3) [%]	∓0.23	-	±0.12	±0.19	±0.17	±0.12	+0.11 −0.10	±0.11	±0.11
c-Quark tagging efficiency (eigenvector 0) [%]	±0.38	±0.31	±0.26	±0.23	±0.21	±0.22	±0.24	±0.30	±0.28
c-Quark tagging efficiency (eigenvector 1) [%]	-	∓0.14	∓0.20	∓0.25	∓0.28	∓0.30	∓0.34	∓0.33	−0.46 +0.47
c-Quark tagging efficiency (eigenvector 2) [%]	±0.16	±0.11	-	-	-	-	-	-	-
Light-jet tagging efficiency (eigenvector 0) [%]	−0.56 +0.55	−0.53 +0.54	−0.49 +0.48	−0.49 +0.50	∓0.54	−0.70 +0.73	−0.89 +0.95	∓1.22	−0.73 +0.71
Light-jet tagging efficiency (eigenvector 1) [%]	+0.31 −0.30	±0.23	±0.16	±0.14	±0.15	±0.22	+0.33 −0.31	+0.33 −0.34	-
Light-jet tagging efficiency (eigenvector 3) [%]	-	-	-	-	-	∓0.11	∓0.14	∓0.25	∓0.30
Light-jet tagging efficiency (eigenvector 5) [%]	-	-	-	-	-	-	∓0.10	∓0.15	∓0.17
b-Quark tagging extrapolation [%]	-	-	-	-	-	±0.12	±0.17	+0.21 −0.20	±0.27
Electron energy resolution [%]	-	-	-	-	-	-	-	+0.19 −0.48	- −1.09
Electron energy scale [%]	-	-	-	-	-	-	+0.16 −0.15	-	- −1.92
Electron trigger efficiency [%]	±0.12	±0.11	±0.11	±0.11	±0.11	±0.12	±0.14	±0.15	±0.16
Electron reconstruction efficiency [%]	-	-	-	-	-	-	±0.10	±0.10	±0.11
Electron identification efficiency [%]	±0.32	±0.36	±0.40	±0.45	±0.49	±0.52	±0.55	±0.61	±0.68
Electron isolation efficiency [%]	-	-	-	±0.13	±0.19	±0.22	±0.22	±0.23	±0.25
Muon (ID) momentum resolution [%]	-	-	-	-	-	-	+0.29 -	+0.87 -	- −2.30
Muon (MS) momentum resolution [%]	-	-	-	-	-	-	-	+1.17 -	−0.69 -
Muon (ID) sagitta ρ [%]	-	-	-	-	-	-	−0.21 -	-	- −0.65
Muon energy scale [%]	-	-	-	-	-	-	-	+0.57 -	- −2.18
Muon trigger efficiency stat [%]	±0.30	+0.28 −0.29	+0.27 −0.28	±0.27	+0.26 −0.27	+0.26 −0.27	−0.31 ±0.26	+0.25 −0.26	±0.25
Muon trigger efficiency syst [%]	+0.52 −0.51	+0.50 −0.49	+0.49 −0.48	+0.48 −0.47	+0.48 −0.47	+0.48 −0.47	+0.49 −0.48	+0.49 −0.48	+0.48 −0.47
Muon identification syst [%]	±0.33	±0.33	±0.35	±0.37	±0.41	±0.45	±0.48	+0.52 −0.51	±0.53
Muon isolation efficiency syst [%]	±0.10	±0.10	±0.10	±0.10	±0.10	±0.10	±0.11	±0.11	±0.11
E_T^{miss} Soft jet resolution para [%]	±0.28	±0.14	-	±0.12	-	±0.39	±0.29	±0.61	∓1.83
E_T^{miss} Soft jet resolution perp [%]	±0.21	±0.10	±0.14	±0.16	-	±0.41	±0.46	±0.32	∓3.48
E_T^{miss} Soft jet scale [%]	+0.30 −0.21	+0.13 −0.25	+0.14 −0.21	+0.19 -	-	+0.22 -	±0.19	+0.45 -	- −2.03
Luminosity [%]	∓2.05	∓2.05	∓2.05	∓2.05	∓2.05	∓2.05	∓2.05	∓2.05	∓2.05
Z+jets cross-section [%]	±0.65	±0.46	±0.33	±0.25	±0.25	±0.36	±0.45	±0.34	±0.47
Monte Carlo sample statistics [%]	±0.24	±0.12	±0.21	±0.21	±0.31	±0.56	±0.94	±1.80	±3.52
ISR/FSR + scale [%]	−0.42 +0.21	+0.65 −0.34	+0.50 -	−0.53 +0.82	−0.47 +1.79	+1.60 -	+1.35 -	+2.93 -	−1.28 +9.96
Alternate hard-scattering model [%]	±21.8	±4.21	∓1.09	∓4.03	∓4.84	∓1.83	∓6.26	±1.40	±12.8
Alternate parton-shower model [%]	±12.2	±1.43	∓3.87	∓6.79	∓6.08	∓5.56	∓7.63	∓6.65	∓13.0
Inter PDF [%]	∓0.28	∓0.19	∓0.18	∓0.20	∓0.23	∓0.27	∓0.24	-	±0.41
Intra PDF [%]	±0.59	±0.65	±0.71	±0.75	±0.83	±1.03	±1.24	±1.37	±1.75
Fakes overall normalization, el [%]	+2.57 −2.56	±1.42	+0.94 −0.95	±0.33	±1.43	-	∓0.40	-	−1.95 +1.96
Fakes overall normalization, mu [%]	±0.14	±0.12	±0.11	±0.11	-	-	-	±0.48	+0.58 −0.57
Fakes alternative parametrization [%]	∓0.28	∓0.37	∓0.32	-	∓0.38	∓0.39	∓0.34	±1.46	∓0.55
W+jets heavy flavour component [%]	±0.97	±0.75	±0.65	±0.68	±0.74	±1.00	±1.50	±1.85	±1.57
W+jets Scales [%]	±1.05	±0.78	±0.64	±0.82	±1.01	±1.57	±2.27	±2.98	±3.58
Single Top DS/DR [%]	∓0.19	∓0.29	∓0.42	∓0.53	∓0.44	∓0.21	∓0.17	±0.21	∓0.12
Single Top IFSR [%]	- −0.44	- −0.35	- −0.30	- −0.38	- −0.37	- −0.43	+0.13 −0.33	+0.19 −0.74	- −0.67

TABLE F.49: Table of systematics for the absolute differential cross-section at the parton level for the $m^{t\bar{t}}$ observable.

Bins [Unit $y^{t\bar{t}}$]	-2.50—1.80	-1.80—1.40	-1.40—1.10	-1.10—0.80	-0.80—0.50	-0.50—0.25	-0.25–0	0–0.25	0.25–0.50	0.50–0.80	0.80–1.10	1.10–1.40	1.40–1.80	1.80–2.50
$d\sigma$ / $dy^{t\bar{t}}$ [pb/ Unit $y^{t\bar{t}}$]	$4.49 \cdot 10^1$	$1.07 \cdot 10^2$	$1.64 \cdot 10^2$	$2.11 \cdot 10^2$	$2.53 \cdot 10^2$	$2.82 \cdot 10^2$	$2.90 \cdot 10^2$	$2.84 \cdot 10^2$	$2.79 \cdot 10^2$	$2.56 \cdot 10^2$	$2.15 \cdot 10^2$	$1.66 \cdot 10^2$	$1.10 \cdot 10^2$	$4.42 \cdot 10^1$
Total Uncertainty [%]	+11.3 −10.9	+10.8 −10.9	+10.5 −10.1	+10.6 −10.3	+10.8 −10.5	+10.9 −10.7	±10.3	±11.5	+11.5 −11.2	±10.6	±10.5	+10.4 −10.2	+13.0 −12.9	+10.1 −10.3
Statistics [%]	±1.6	±0.7	±0.5	±0.4	±0.3	±0.3	±0.3	±0.3	±0.3	±0.3	±0.4	±0.5	±0.7	±1.6
Systematics [%]	+11.1 −10.7	±10.8	+10.4 −10.0	+10.6 −10.3	+10.7 −10.5	+10.9 −10.7	±10.3	±11.5	+11.5 −11.2	±10.6	±10.5	+10.3 −10.1	+13.0 −12.8	+9.93 −10.1
Jet energy resolution [%]	∓1.97	∓2.18	∓1.59	∓1.20	∓2.04	∓1.98	∓1.79	∓1.47	∓1.71	∓1.69	∓1.84	∓1.41	±0.84	±1.44
b-Tagged jet energy scale (JES) [%]	-	+0.33 −0.20	+0.32 −0.40	+0.38 −0.58	+0.49 −0.42	+0.48 −0.28	+0.39 −0.48	+0.42 −0.45	+0.46 −0.27	+0.43 −0.40	+0.40 −0.58	+0.33 −0.46	+0.22 −0.16	-
Effective detector NP set 1 (JES) [%]	+0.55	-	-	-	-	-	-	-	-	-	-	-	+0.28 -	−0.28
Effective detector NP set 2 (JES) [%]	-	-	+0.25 -	-	+0.11 −0.12	-	-	-	-	-	−0.24	-	+0.16 -	+0.39 -
Effective mixed NP set 1 (JES) [%]	+0.30	−0.18 -	-	+0.25 ±0.27	-	-	-	-	-	-	-	-	−0.19 -	−0.40 -
Effective mixed NP set 2 (JES) [%]	+0.27	−0.31 -	-	-	-	-	-	-	-	−0.14 -	-	-	-	-
Effective mixed NP set 3 (JES) [%]	+0.27	-	-	-	-	-	-	-	-	-	-	-	−0.25 +0.22	-
Effective modelling NP set 1 (JES) [%]	+2.07 −1.79	+2.02 −2.06	+2.33 −2.17	+2.73 −2.27	+2.72 −2.51	+2.61 −2.70	+2.70 −2.83	+2.72 −2.69	+2.71 −2.60	+2.56 −2.62	+2.54 −2.47	−0.20 +2.33 −2.19	+1.79 −1.55	+1.19 −1.45
Effective modelling NP set 2 (JES) [%]	+0.79	−0.21 +0.38	−0.11 +0.37	−0.33 +0.19	∓0.35	−0.23 +0.31	−0.29 +0.23	−0.29 +0.35	−0.22 +0.40	−0.38 +0.29	−0.50 -	- -	−0.22 +0.18	−0.12 +0.42
Effective modelling NP set 3 (JES) [%]	+0.39	−0.38 −0.10	+0.27 -	+0.28 −0.16	+0.16 −0.18	+0.22 −0.16	+0.12 −0.24	+0.15 −0.19	+0.30 −0.13	+0.19 −0.23	+0.11 −0.22	+0.13 −0.20	-	+0.34 −0.16
Effective modelling NP set 4 (JES) [%]	+0.51	+0.32 -	+0.10 −0.11	+0.17 -	-	+0.18 −0.17	-	−0.13 −0.10	+0.22 -	-	-	+0.13 −0.16	-	-
Effective statistical NP set 1 (JES) [%]	+0.47	+0.49	−0.15 +0.36	+0.36	+0.54	+0.47	+0.36	−0.18 +0.48	+0.58	−0.24 +0.36	+0.34	−0.16 +0.34	+0.28	+0.36
Effective statistical NP set 2 (JES) [%]	−0.19	−0.48 +0.11	−0.28 −0.19	−0.37 −0.18	−0.50 −0.30	−0.46 −0.48	−0.56 −0.48	−0.43 −0.48	−0.45 −0.45	−0.44 −0.44	−0.53 −0.32	−0.53 −0.36	−0.75 −0.13	−0.30 −0.49
Effective statistical NP set 3 (JES) [%]	+0.59	+0.11 -	+0.65 -	+0.35 -	+0.36 -	+0.50 -	+0.36 -	+0.51 -	+0.48 -	+0.29 -	+0.40 -	+0.41 -	+0.22 -	- −0.30
Effective statistical NP set 4 (JES) [%]	−0.22 +0.38	−0.23	-	−0.17 -	−0.10	-	-	-	-	-	-	-	-	+0.13 −0.11
Effective statistical NP set 5 (JES) [%]	+0.52	+0.19 -	-	+0.20 -	+0.12 -	-	-	-	-	-	-	-	-	+0.21 +0.19
Effective statistical NP set 6 (JES) [%]	+0.24	-	+0.32	-	-	-	-	-	+0.18	-	-	-	-	−0.47 -
Effective statistical NP set 7 (JES) [%]	+0.40	-	+0.19	-	-	-	-	-	-	-	-	−0.32 -	-	−0.12 -
η intercalibration model (JES) [%]	+0.95	+0.75	−0.10 +0.90	+0.72	+0.71	+0.54	+0.37	+0.34	+0.49	+0.53	−0.22 +0.61	−0.19 +0.70	+0.85	−0.33 +0.51
η intercalibration non closure (JES) [%]	−0.55 −0.12	−0.74 −0.16	−0.60 −0.37	−0.70 −0.47	−0.57 −0.34	−0.59 −0.32	−0.50 −0.35	−0.38 −0.31	−0.29 −0.10	−0.56 −0.34	−0.79 -	−0.79 -	−0.99 −0.16	−1.02 -
η intercalibration total stat (JES) [%]	+0.37	+0.38	+0.28 +0.50	+0.69 +0.40	+0.51 ±0.38	+0.41 +0.51	+0.16 +0.41	+0.24 +0.48	+0.30 +0.39	+0.14 +0.31	+0.42	+0.48	+0.30 ±0.34	+0.15 -
Flavour composition (JES) [%]	+1.70	−0.13 +1.67	+0.31 +2.31	+0.53 +2.39	+2.14	−0.37 +2.39	−0.51 +2.34	−0.41 +2.48	−0.44 +2.46	−0.44 +2.44	−0.55 +2.17	−0.42 +2.30	+1.82	+0.78
Flavour response (JES) [%]	−1.79 −0.71	−2.11 −1.22	−2.14 −1.05	−2.43 −1.14	−2.63 −1.15	−2.65 −1.23	−2.60 −1.09	−2.58 −1.22	−2.50 −1.08	−2.49 −1.19	−2.31 −1.25	−2.23 −1.01	−1.63 −0.89	−2.04 −1.04
Pile-up offset μ (JES) [%]	+1.14	+0.89	+1.08 −0.14	+1.08 +0.46	+1.19 -	+1.14 −0.14	+1.19 -	+1.11 −0.19	+1.21 −0.21	+1.04 −0.14	+1.18 -	+1.07 -	+0.66 −0.11	+0.63 -
Pile-up offset N_{PV} (JES) [%]	+0.60	+0.15	+0.61	+0.53	±0.43 -	+0.52	+0.53	±0.32 -	±0.24 -	±0.19 -	+0.42	+0.53	±0.36 -	−0.35 -
Pile-up offset p_T (JES) [%]	−0.89	−0.42 −0.48	−0.21 -	−0.47 −0.16	−0.47 -	−0.50 −0.41	−0.50 −0.41	−0.44 −0.38	−0.47 -	−0.52 −0.26	−0.58 −0.27	−0.71 −0.31	−0.45 −0.27	−0.79 −0.71
Pile-up offset ρ topology (JES) [%]	+0.69 +2.11	+0.18 +2.55	+3.54	+0.15 +3.66	+0.19 +4.03	+0.32 +4.03	+0.19 +3.91	+0.11 +3.90	+4.22	+0.19 +3.84	+0.17 +3.64	+0.29 +3.58	+0.22 +2.69	+0.13 +1.50
Punch-through (JES) [%]	−1.29	−2.95	−3.30	−3.59	−3.67	−3.83	−4.00	−4.16	−3.81	−3.72	−3.56	−3.04	−2.53	−2.35
Single particle high-p_T (JES) [%]	- −0.72	-	-	-	-	-	-	-	-	-	-	-	-	+0.38 -
Jet vertex fraction [%]	+0.74	+0.77	+0.79	+0.81	+0.82	+0.82	+0.82	+0.82	+0.81	+0.81	+0.81	+0.79	+0.77	+0.78
b-Quark tagging efficiency (eigenvector 0) [%]	−0.76 −6.42	−0.80 −6.31	−0.82 −6.39	−0.84 −6.52	−0.85 −6.59	−0.85 −6.61	−0.85 −6.63	−0.85 −6.63	−0.84 −6.60	−0.84 −6.57	−0.84 −6.53	−0.81 −6.43	−0.79 −6.26	−0.80 −6.30
b-Quark tagging efficiency (eigenvector 1) [%]	+6.60 −1.75	+6.49 −1.77	+6.58 −1.76	+6.72 −1.73	+6.78 −1.71	+6.80 −1.71	+6.84 −1.72	+6.83 −1.71	+6.80 −1.72	+6.76 −1.73	+6.73 −1.73	+6.62 −1.75	+6.44 −1.78	+6.48 −1.74
b-Quark tagging efficiency (eigenvector 2) [%]	+1.77 +1.31	+1.76 +1.30	+1.77 +1.30	+1.75 +1.30	+1.72 ±1.29	+1.74 +1.29	+1.73 +1.30	+1.73 +1.29	+1.73 +1.29	+1.74 +1.30	+1.75 +1.30	+1.77 +1.31	+1.80 +1.31	+1.76 +1.31
c-Quark tagging efficiency (eigenvector 0) [%]	±0.36	−1.30 +0.36 −0.35	−1.32 +0.32 −0.31	−1.29 ±0.29	−1.28 ±0.28	−1.28 +0.29 −0.28	−1.29 ±0.29	−1.28 ±0.29	−1.28 ±0.29	−1.29 ±0.28	−1.29 ±0.30	−1.30 ±0.30	−1.30 ±0.29	−1.30 ±0.37
c-Quark tagging efficiency (eigenvector 1) [%]	∓0.19	∓0.18	∓0.18	∓0.17	∓0.18	−0.17 +0.18	∓0.16	∓0.16	∓0.16	∓0.17	∓0.17	∓0.18	∓0.20	∓0.24
c-Quark tagging efficiency (eigenvector 2) [%]	±0.10	-	±0.10	-	-	±0.10	-	-	-	-	±0.10	±0.10	±0.10	±0.12
Light-jet tagging efficiency (eigenvector 0) [%]	−0.84 +0.88	−0.76 +0.81	−0.57 +0.58	−0.29 +0.15	−0.58 +0.61	−0.58 +0.63	∓0.48	−0.40 +0.38	−0.54 +0.56	−0.54 +0.56	−0.60 +0.61	−0.64 +0.66	−0.60 +0.61	±0.80 -
Light-jet tagging efficiency (eigenvector 1) [%]	±0.40	+0.33 −0.32	+0.23 −0.22	+0.10 −0.11	±0.21	+0.22 −0.26	±0.19	±0.19	±0.23	±0.20	±0.21	±0.20	±0.23	±0.46
Light-jet tagging efficiency (eigenvector 2) [%]	−0.15 +0.14	-	-	−0.13 +0.13	-	-	-	-	-	-	-	-	-	±0.25
Light-jet tagging efficiency (eigenvector 3) [%]	+0.12	-	-	+0.13	-	-	-	-	-	-	-	-	-	∓0.14
Light-jet tagging efficiency (eigenvector 5) [%]	∓0.12	-	-	-	-	-	-	-	-	-	-	-	-	∓0.12
Electron energy resolution [%]	+0.22	−0.37	+0.26	-	-	-	-	-	-	-	-	-	-	+0.11 −0.13
Electron energy scale [%]	-	-	-	-	-	-	-	-	-	-	-	-	-	+0.20 -
Electron trigger efficiency [%]	±0.17	±0.15	±0.13	±0.12	±0.11	±0.11	±0.11	±0.11	±0.11	±0.11	±0.11	±0.12	±0.14	±0.17
Electron identification efficiency [%]	±0.59	±0.47	±0.39	±0.37	±0.36	±0.37	±0.38	±0.38	±0.38	±0.38	±0.39	±0.40	±0.46	±0.59
Electron isolation efficiency [%]	±0.10	-	-	-	-	-	-	-	-	-	-	-	-	±0.10
Muon (ID) momentum resolution [%]	−0.21	-	-	-	-	-	-	-	-	-	-	-	-	−0.11 +0.24
Muon (MS) momentum resolution [%]	-	-	-	+0.20	-	-	-	-	-	-	-	-	-	+0.13 -
Muon (ID) sagitta ρ [%]	-	-	-	-	-	-	-	-	-	-	-	-	-	+0.11 -
Muon energy scale [%]	−0.51 +0.30	-	-	-	-	-	-	-	-	-	-	-	−0.23	+0.29 -
Muon trigger efficiency stat [%]	±0.27	+0.26	+0.27	+0.27	+0.28	+0.28	+0.28	±0.29	±0.29	+0.28	+0.28	±0.28	+0.26	±0.26
Muon trigger efficiency syst [%]	+0.50 −0.49	+0.51 −0.50	+0.51 −0.50	+0.48 −0.49	+0.50 −0.49	+0.50 −0.48	+0.49 −0.48	+0.49 −0.48	+0.49 −0.48	+0.49 −0.48	+0.50 −0.49	+0.50 −0.49	+0.51 −0.50	+0.49 −0.48
Muon identification stat [%]	-	±0.10	±0.10	-	-	-	-	-	-	-	-	±0.10	±0.10	-
Muon identification syst [%]	±0.47	±0.44	±0.41	±0.36	±0.33	±0.32	±0.31	±0.31	±0.32	+0.35 −0.34	±0.38	±0.43	+0.48 −0.47	±0.49
Muon isolation efficiency syst [%]	±0.12	±0.11	±0.11	±0.10	±0.10	±0.10	-	-	±0.10	±0.10	±0.10	±0.11	±0.11	±0.11
E_T^{miss} Soft jet resolution para [%]	±0.27	±0.17	±0.20	-	±0.27	±0.18	±0.14	±0.11	±0.31	±0.12	-	±0.11	-	-
E_T^{miss} Soft jet resolution perp [%]	±0.73	±0.27	±0.23	±0.29	-	±0.29	±0.18	±0.11	±0.14	±0.18	-	±0.14	±0.18	-
E_T^{miss} Soft jet scale [%]	+0.67	-	+0.20	+0.35	-	+0.25	+0.22	+0.20	+0.23	-	-	+0.15	+0.10	+0.33
Luminosity [%]	∓2.05	−0.32 ∓2.05	−0.21 ∓2.05	−0.24 ∓2.05	∓2.05	∓2.05	−0.28 ∓2.05	−0.18 ∓2.05	−0.10 ∓2.05	−0.18 ∓2.05	−0.21 ∓2.05	−0.26 ∓2.05	−0.24 ∓2.05	−0.16 ∓2.05
Z+jets cross-section [%]	+0.59	±0.43	±0.40	±0.42	±0.39	±0.41	±0.43	±0.43	±0.44	±0.43	±0.40	±0.48	±0.43	±0.49
Monte Carlo sample statistics [%]	−0.58 ±1.07	±0.53	±0.34	±0.40	±0.30	±0.28	±0.23	±0.35	±0.26	±0.24	±0.29	±0.36	±0.45	±1.09
ISR/FSR + scale [%]	−1.67 +1.17	+1.44	−0.41 +1.38	−0.16 +0.33	+0.43	+0.53	+0.49 −0.52	−0.71	+0.25	+0.79	−0.15 +0.32	−0.99 +0.77	−0.80	−1.40 +2.97
Alternate hard-scattering model [%]	±3.82	±4.33	±4.19	±4.12	±4.33	±4.75	±3.23	±5.85	±5.76	±4.74	±4.63	±4.41	±8.75	±3.29
Alternate parton-shower model [%]	∓4.57	∓0.46	±0.23	±0.84	±0.90	±0.78	±0.72	±0.37	±0.82	±0.87	±0.76	±0.55	∓3.73	∓2.67
Inter PDF [%]	±0.93	-	-	-	-	-	-	-	-	-	-	-	-	±0.94
Intra PDF [%]	±2.25	±0.38	±0.17	±0.11	-	-	-	-	-	-	±0.12	±0.18	±0.38	±2.22
Fakes overall normalization, el [%]	±0.43	±3.41	±1.73	±1.99	±1.22	±0.68	±1.06	±2.29	+1.21 −1.22	±0.58	±0.85	±1.52	±1.88	±0.14
Fakes overall normalization, mu [%]	±0.48	±0.17	±0.12	-	±0.10	±0.13	±0.18	±0.11	-	-	±0.13	±0.13	±0.14	±0.27
Fakes alternative parametrization [%]	±0.62	±2.71	±0.95	±1.20	-	±0.46	±0.26	±0.39	±0.21	-	±0.19	±1.11	±1.60	±0.98
W+jets heavy flavour component [%]	±0.83	±0.78	±0.75	±0.79	±0.75	±0.75	±0.75	±0.78	±0.76	±0.78	±0.85	±0.83	±0.80	±1.01
W+jets Scales [%]	±1.05	±1.05	±0.94	±0.78	±0.84	±0.86	±0.78	±0.78	±0.99	±0.89	±0.74	±0.97	±0.97	±0.73
Single Top DS/DR [%]	∓0.23	∓0.23	∓0.41	∓0.30	∓0.30	∓0.35	∓0.44	∓0.37	∓0.31	∓0.26	∓0.45	∓0.33	±0.19	∓0.12
Single Top IFSR [%]	−0.37 -	−0.43	−0.57	−0.33	−0.36	−0.23	−0.35	−0.40	−0.40	−0.33	−0.40	−0.36	-	- −1.35

TABLE F.50: Table of systematics for the absolute differential cross-section at the parton level for the $y^{t\bar{t}}$ observable.

Bins [GeV] x [GeV]	0–90	90–180	180–300	300–1000	1000–1080	1080–1170	1170–1280	1280–2000	2000–2080	2080–2170	2170–2270	2270–2370	2370–3000	3000–3090	3090–3180	3180–3280	3280–3370	3370–4000
$d\sigma$ / $dm^{t\bar{t}}vsp_{T}^{t,had}$ [pb/GeV x GeV]	$2.90 \cdot 10^{0}$	$2.27 \cdot 10^{0}$	$1.59 \cdot 10^{-1}$	$2.42 \cdot 10^{-3}$	$5.72 \cdot 10^{-1}$	$1.12 \cdot 10^{0}$	$7.16 \cdot 10^{-1}$	$1.23 \cdot 10^{-2}$	$1.51 \cdot 10^{-1}$	$2.74 \cdot 10^{-1}$	$2.25 \cdot 10^{-1}$	$1.35 \cdot 10^{-1}$	$7.32 \cdot 10^{-3}$	$3.65 \cdot 10^{-2}$	$6.43 \cdot 10^{-2}$	$5.12 \cdot 10^{-2}$	$3.38 \cdot 10^{-2}$	$7.72 \cdot 10^{-3}$
Total Uncertainty [%]	$^{+17.4}_{-17.2}$	$^{+12.4}_{-12.3}$	$^{+16.6}_{-17.3}$	$^{+15.0}_{-14.0}$	$^{+12.9}_{-12.4}$	±12.0	$^{+10.3}_{-10.4}$	$^{+12.1}_{-12.8}$	$^{+12.9}_{-12.0}$	$^{+11.6}_{-10.5}$	$^{+13.7}_{-13.2}$	$^{+15.7}_{-15.5}$	$^{+13.3}_{-14.7}$	$^{+22.6}_{-17.7}$	$^{+14.7}_{-12.6}$	$^{+14.9}_{-13.7}$	$^{+16.4}_{-17.6}$	$^{+19.5}_{-10.6}$
Statistics [%]	±0.2	±0.2	±0.6	±4.5	±0.5	±0.3	±0.4	±1.3	±1.3	±0.9	±0.8	±0.9	±2.9	±3.3	±2.3	±2.0	±2.4	±3.9
Systematics [%]	$^{+17.4}_{-17.2}$	$^{+12.4}_{-12.3}$	$^{+16.6}_{-17.3}$	$^{+14.1}_{-13.0}$	$^{+12.9}_{-12.4}$	±12.0	$^{+10.3}_{-10.4}$	$^{+12.0}_{-12.7}$	$^{+12.8}_{-11.9}$	$^{+11.5}_{-10.4}$	$^{+13.7}_{-13.1}$	$^{+15.7}_{-15.5}$	$^{+12.8}_{-14.3}$	$^{+22.2}_{-17.1}$	$^{+14.4}_{-12.2}$	$^{+14.7}_{-13.5}$	$^{+16.1}_{-17.4}$	$^{+18.9}_{-9.50}$
Jet energy resolution [%]	∓2.35	∓1.37	∓0.93	∓1.57	∓0.65	∓1.61	∓1.89	∓0.21	±0.43	∓1.57	∓1.65	∓1.40	±0.39	∓1.14	±1.14	∓0.39	∓2.39	∓0.52
b-Tagged jet energy scale (JES) [%]	$^{-0.19}_{+0.27}$	$^{+0.61}_{-0.65}$	$^{+0.71}_{-1.11}$	$^{+1.24}_{-}$	$^{+0.35}_{-0.12}$	$^{+0.69}_{-0.82}$	$^{+0.88}_{-0.97}$	$^{+0.39}_{-0.54}$	$^{-}_{-0.23}$	$^{+0.69}_{-0.71}$	$^{+0.72}_{-0.59}$	$^{+0.58}_{-0.14}$	∓0.13	$^{+1.37}_{-}$	$^{+1.29}_{-}$	$^{+1.08}_{-}$	$^{-}_{-1.06}$	$^{-1.07}_{+1.29}$
Effective detector NP set 1 (JES) [%]	-	-	$^{-}_{-0.32}$	$^{+1.24}_{-}$	-	-	$^{-}_{-0.17}$	$^{-}_{-0.45}$	-	-	-	$^{+0.25}_{-}$	$^{-}_{-0.89}$	$^{+1.74}_{-}$	$^{+0.52}_{-}$	$^{+0.46}_{-}$	$^{-}_{-1.03}$	$^{-0.61}_{+0.60}$
Effective detector NP set 2 (JES) [%]	-	-	$^{-}_{-0.26}$	$^{+1.21}_{-}$	-	-	-	$^{-}_{-0.25}$	-	$^{+0.23}_{-0.24}$	$^{+0.30}_{-}$	$^{+0.20}_{-}$	$^{-}_{-0.86}$	$^{+0.85}_{-}$	-	$^{+0.51}_{-}$	$^{-}_{-0.62}$	$^{-}_{-0.65}$
Effective mixed NP set 1 (JES) [%]	$^{-0.28}_{+0.32}$	$^{+0.14}_{-}$	$^{+0.12}_{-0.26}$	$^{+1.39}_{-0.45}$	-	$^{-}_{-0.28}$	$^{+0.29}_{-0.28}$	$^{-}_{-0.60}$	$^{+0.32}_{-}$	$^{+0.47}_{-0.20}$	$^{+0.28}_{-0.42}$	$^{+0.35}_{-0.24}$	$^{-}_{-1.14}$	$^{+1.09}_{-}$	$^{+0.93}_{-}$	$^{+1.09}_{-}$	$^{-}_{-0.61}$	$^{+1.16}_{-0.35}$
Effective mixed NP set 2 (JES) [%]	-	-	$^{-0.38}_{+0.11}$	$^{+0.82}_{-}$	-	-	-	-	-	-	-	-	$^{-}_{-1.13}$	$^{+0.93}_{-}$	$^{+0.27}_{-}$	$^{+0.83}_{-}$	$^{-}_{-0.52}$	$^{-}_{-0.76}$
Effective mixed NP set 3 (JES) [%]	-	-	$^{-}_{-0.23}$	$^{+0.34}_{-}$	$^{+0.23}_{-}$	-	-	$^{-}_{-0.37}$	$^{+0.33}_{-0.13}$	$^{-}_{-0.26}$	$^{+0.36}_{-}$	$^{+0.15}_{-0.17}$	$^{-}_{-1.05}$	$^{+0.67}_{-}$	$^{-}_{+0.37}$	-	$^{-}_{-0.46}$	$^{-}_{-0.39}$
Effective modelling NP set 1 (JES) [%]	$^{+2.81}_{-2.64}$	$^{+2.80}_{-2.75}$	$^{+1.89}_{-2.39}$	$^{+1.98}_{-1.48}$	$^{+3.26}_{-3.01}$	$^{+2.75}_{-2.77}$	$^{+1.84}_{-1.99}$	$^{+0.35}_{-1.12}$	$^{+2.46}_{-2.66}$	$^{+2.90}_{-2.34}$	$^{+2.26}_{-1.77}$	$^{+1.23}_{-0.84}$	$^{-}_{-0.32}$	$^{+2.93}_{-0.28}$	$^{+3.08}_{-2.12}$	$^{+2.33}_{-1.58}$	$^{+0.40}_{-2.58}$	$^{+1.45}_{-0.55}$
Effective modelling NP set 2 (JES) [%]	$^{-0.50}_{+0.58}$	$^{-0.26}_{+0.23}$	$^{-0.14}_{-}$	$^{+0.40}_{-0.60}$	$^{-0.40}_{+0.58}$	$^{-0.28}_{+0.12}$	-	-	$^{-0.15}_{+0.18}$	$^{-0.19}_{+0.24}$	$^{+0.25}_{-}$	-	$^{-}_{-1.17}$	$^{+0.44}_{-}$	$^{+0.43}_{-}$	$^{+1.26}_{-}$	$^{-}_{-0.95}$	$^{+1.82}_{-}$
Effective modelling NP set 3 (JES) [%]	$^{+0.54}_{-0.53}$	$^{+0.12}_{-0.11}$	-	$^{-}_{-0.44}$	$^{+0.46}_{-0.36}$	-	$^{-0.10}_{+0.18}$	$^{-}_{-0.34}$	$^{+0.53}_{-}$	-	$^{-}_{+0.18}$	$^{-}_{+0.26}$	$^{-}_{-1.11}$	$^{+2.12}_{-}$	$^{+0.81}_{-}$	$^{+0.68}_{-}$	$^{-}_{-0.71}$	$^{-}_{+0.45}$
Effective modelling NP set 4 (JES) [%]	$^{+0.15}_{-}$	-	$^{+0.12}_{-0.49}$	$^{+1.90}_{-0.90}$	$^{+0.19}_{-0.17}$	$^{-}_{-0.23}$	$^{-}_{-0.11}$	$^{-}_{-0.58}$	$^{+0.25}_{-}$	$^{+0.54}_{-0.16}$	$^{+0.22}_{-}$	$^{+0.20}_{-}$	$^{-}_{-2.15}$	$^{+1.10}_{-}$	$^{+0.77}_{-}$	$^{+0.34}_{-}$	$^{-}_{-0.90}$	$^{-0.20}_{+0.12}$
Effective statistical NP set 1 (JES) [%]	$^{+0.57}_{-0.52}$	$^{+0.47}_{-0.44}$	$^{+0.16}_{-0.48}$	$^{+0.39}_{-1.28}$	$^{+0.66}_{-0.58}$	$^{+0.34}_{-0.55}$	$^{+0.26}_{-0.31}$	$^{-}_{-0.42}$	$^{+0.48}_{-0.17}$	$^{+0.43}_{-0.46}$	$^{+0.48}_{-}$	-	$^{-}_{-0.94}$	$^{+2.60}_{-}$	$^{+2.43}_{-0.46}$	$^{+1.08}_{-}$	$^{-}_{-0.94}$	$^{+0.59}_{-0.70}$
Effective statistical NP set 2 (JES) [%]	$^{-0.42}_{+0.50}$	∓0.42	$^{-0.45}_{+0.31}$	$^{+0.59}_{-}$	$^{-0.31}_{+0.74}$	$^{-0.55}_{+0.33}$	$^{-0.24}_{+0.21}$	$^{-}_{-0.56}$	$^{-0.12}_{+0.50}$	$^{-0.45}_{+0.48}$	$^{-0.20}_{+0.56}$	$^{-0.13}_{+0.35}$	$^{-0.60}_{-}$	$^{+0.73}_{-}$	$^{-0.54}_{+1.48}$	$^{+0.37}_{-}$	$^{-}_{-0.82}$	$^{+0.81}_{-}$
Effective statistical NP set 3 (JES) [%]	-	-	$^{-}_{-0.25}$	$^{-}_{-0.83}$	-	-	-	$^{-}_{-0.61}$	$^{+0.28}_{-}$	-	-	-	$^{-0.80}_{+0.30}$	$^{+1.49}_{-}$	$^{+0.63}_{-}$	$^{+0.62}_{-}$	-	$^{-}_{-1.64}$
Effective statistical NP set 4 (JES) [%]	$^{-0.31}_{+0.43}$	-	$^{+0.14}_{-0.22}$	$^{-}_{-0.35}$	$^{-0.12}_{+0.14}$	$^{-}_{-0.22}$	$^{+0.18}_{-0.23}$	$^{-}_{-0.59}$	$^{-0.33}_{+0.44}$	-	$^{+0.26}_{-0.19}$	$^{+0.23}_{-}$	$^{-}_{-0.99}$	$^{-0.56}_{+1.15}$	$^{+0.11}_{-0.22}$	$^{+0.65}_{-}$	$^{-}_{-1.63}$	$^{+0.55}_{+0.80}$
Effective statistical NP set 5 (JES) [%]	-	-	$^{-}_{-0.34}$	$^{+1.03}_{-}$	$^{+0.24}_{-}$	-	$^{-0.14}_{+0.13}$	$^{-}_{-0.27}$	-	$^{-0.11}_{+0.42}$	-	-	$^{-}_{-1.17}$	$^{-0.27}_{+1.12}$	$^{+0.97}_{-}$	$^{+0.46}_{-}$	$^{-}_{-0.68}$	$^{-}_{+0.69}$
Effective statistical NP set 6 (JES) [%]	$^{+0.16}_{-}$	$^{-}_{-0.16}$	-	$^{+1.51}_{-}$	-	-	-	$^{-}_{-0.26}$	-	-	-	$^{+0.27}_{-}$	$^{+0.46}_{-0.92}$	$^{+0.37}_{-}$	$^{+0.79}_{-0.15}$	$^{-0.10}_{+0.47}$	$^{-}_{-0.90}$	-
Effective statistical NP set 7 (JES) [%]	-	±0.11	$^{-}_{-0.21}$	$^{+0.76}_{-0.33}$	-	-	-	$^{-}_{-0.60}$	$^{+0.31}_{-}$	$^{+0.37}_{-0.10}$	$^{+0.32}_{-}$	$^{+0.31}_{-}$	$^{-}_{-1.63}$	$^{+3.30}_{-}$	$^{+0.37}_{-}$	$^{+0.57}_{-0.20}$	$^{-}_{-0.35}$	$^{+0.43}_{-}$
η intercalibration model (JES) [%]	$^{+0.32}_{-0.27}$	$^{+0.59}_{-0.55}$	$^{+0.52}_{-0.56}$	$^{-}_{-0.29}$	$^{+1.25}_{-1.03}$	$^{+0.75}_{-1.00}$	$^{+0.52}_{-0.73}$	$^{-0.24}_{-}$	±1.44	$^{+1.15}_{-1.16}$	$^{+1.25}_{-0.71}$	$^{+0.35}_{-0.28}$	$^{+0.17}_{-0.16}$	$^{+2.39}_{-0.81}$	$^{+1.84}_{-1.21}$	$^{+1.90}_{-0.86}$	$^{+0.69}_{-2.06}$	$^{+0.59}_{-}$
η intercalibration non closure (JES) [%]	$^{-0.27}_{+0.26}$	$^{-0.27}_{+0.31}$	$^{-0.58}_{+0.35}$	$^{-}_{-0.58}$	$^{-}_{+0.37}$	$^{-0.35}_{+0.19}$	$^{-0.21}_{+0.15}$	$^{-}_{-0.46}$	$^{-0.12}_{+0.30}$	$^{-0.19}_{+0.45}$	$^{-}_{+0.48}$	$^{-0.12}_{+0.44}$	$^{-}_{-0.99}$	$^{+0.65}_{-}$	$^{-0.28}_{+0.31}$	$^{-0.30}_{+0.24}$	$^{-}_{-0.94}$	$^{-}_{-0.31}$
η intercalibration total stat (JES) [%]	$^{+0.37}_{-0.26}$	$^{+0.48}_{-0.52}$	$^{+0.39}_{-0.62}$	$^{+0.51}_{-1.55}$	$^{+0.66}_{-0.41}$	$^{+0.39}_{-0.58}$	$^{+0.37}_{-0.48}$	$^{-}_{-0.40}$	$^{+0.43}_{-0.27}$	$^{+0.50}_{-0.49}$	$^{+0.54}_{-0.39}$	$^{+0.43}_{-}$	$^{-}_{-1.33}$	$^{+0.87}_{-}$	$^{+1.40}_{-0.43}$	$^{+0.92}_{-0.31}$	$^{-}_{-1.01}$	$^{+0.68}_{-0.11}$
Flavour composition (JES) [%]	$^{+2.73}_{-2.81}$	$^{+2.37}_{-2.63}$	$^{+1.63}_{-2.22}$	$^{-}_{-0.44}$	$^{+2.78}_{-2.87}$	$^{+2.31}_{-2.47}$	$^{+1.28}_{-1.59}$	$^{+0.15}_{-0.91}$	$^{+3.19}_{-2.76}$	$^{+2.46}_{-2.24}$	$^{+2.22}_{-1.70}$	$^{+1.08}_{-0.49}$	$^{+0.13}_{-0.82}$	$^{+7.78}_{-1.50}$	$^{+3.20}_{-1.30}$	$^{+2.21}_{-1.23}$	$^{-}_{-3.33}$	$^{+3.42}_{-0.84}$
Flavour response (JES) [%]	$^{-1.28}_{+1.19}$	$^{-1.31}_{+1.22}$	$^{-1.16}_{+0.64}$	$^{+2.72}_{-}$	$^{-1.31}_{+1.51}$	$^{-1.33}_{+1.23}$	$^{-0.93}_{+0.80}$	$^{-}_{-0.74}$	$^{-1.26}_{+1.35}$	$^{-1.14}_{+1.23}$	$^{-0.78}_{+1.25}$	$^{-0.27}_{+0.69}$	$^{+0.44}_{-0.71}$	$^{-0.76}_{+1.89}$	$^{-1.08}_{+0.74}$	$^{-1.05}_{+1.58}$	$^{-}_{-2.14}$	$^{-0.97}_{+1.19}$
Pile-up offset μ (JES) [%]	$^{-}_{+0.17}$	$^{-0.28}_{+0.17}$	$^{-}_{-0.27}$	-	$^{-0.21}_{+0.40}$	$^{-0.18}_{+0.14}$	-	$^{-}_{-0.50}$	-	-	$^{-0.33}_{+0.30}$	$^{+0.30}_{-}$	$^{-}_{-1.09}$	$^{+1.09}_{-0.58}$	$^{+0.79}_{-}$	$^{+1.22}_{-}$	$^{-}_{-0.65}$	$^{+0.57}_{-}$
Pile-up offset N_{PV} (JES) [%]	$^{+0.43}_{-0.34}$	$^{+0.54}_{-0.56}$	$^{+0.40}_{-0.87}$	$^{-}_{-0.51}$	$^{+0.73}_{-0.38}$	$^{+0.65}_{-0.51}$	$^{+0.48}_{-0.51}$	$^{+0.18}_{-0.34}$	$^{+0.41}_{-0.74}$	$^{+0.49}_{-0.56}$	$^{+0.50}_{-0.34}$	$^{+0.26}_{-0.11}$	$^{+0.49}_{-}$	$^{+2.18}_{-0.94}$	$^{+0.70}_{-0.52}$	$^{+0.83}_{-0.20}$	$^{+0.39}_{-1.75}$	$^{+0.22}_{-}$
Pile-up offset p_T (JES) [%]	$^{-0.80}_{+0.83}$	$^{-0.13}_{+0.17}$	$^{+0.19}_{-0.30}$	$^{+0.48}_{-}$	$^{-0.38}_{+0.39}$	-	$^{+0.42}_{-0.51}$	$^{-}_{-0.65}$	$^{+0.59}_{-}$	$^{+0.13}_{-0.18}$	$^{+0.45}_{-}$	$^{+0.65}_{-0.16}$	$^{+0.74}_{-}$	$^{+1.08}_{-}$	$^{-}_{-0.21}$	$^{+0.99}_{-0.20}$	$^{-}_{-2.27}$	$^{+0.47}_{-}$
Pile-up offset ρ topology (JES) [%]	$^{+3.64}_{-3.49}$	$^{+4.25}_{-4.06}$	$^{+3.70}_{-4.02}$	$^{-}_{-2.40}$	$^{+4.30}_{-4.22}$	$^{+4.31}_{-4.21}$	$^{+3.03}_{-3.29}$	$^{+0.96}_{-1.69}$	$^{+3.90}_{-3.31}$	$^{+4.24}_{-3.69}$	$^{+3.57}_{-2.92}$	$^{+1.63}_{-1.13}$	$^{-}_{-0.82}$	$^{+8.31}_{-0.23}$	$^{+4.29}_{-3.40}$	$^{+4.30}_{-3.23}$	$^{+1.43}_{-2.92}$	$^{+2.57}_{-0.56}$
Punch-through (JES) [%]	-	-	$^{-}_{-0.25}$	$^{+0.49}_{-0.19}$	-	-	-	$^{-}_{-0.48}$	$^{-}_{-0.19}$	-	$^{+0.19}_{-}$	-	$^{-0.38}_{+0.18}$	$^{-}_{-0.19}$	$^{+0.30}_{-}$	-	-	$^{-0.43}_{+0.13}$
Single particle high-p_T (JES) [%]	-	-	-	$^{+0.88}_{-}$	-	-	-	-	$^{-}_{-0.24}$	-	$^{+0.26}_{-}$	-	$^{-}_{-0.33}$	$^{+0.54}_{-}$	$^{-}_{-0.42}$	$^{-}_{-0.48}$	$^{-}_{-0.32}$	$^{+0.35}_{-0.74}$
Jet vertex fraction [%]	$^{+1.08}_{-1.11}$	$^{+0.81}_{-0.84}$	$^{+0.58}_{-0.61}$	$^{+0.43}_{-0.46}$	$^{+1.05}_{-1.09}$	$^{+0.74}_{-0.77}$	$^{+0.46}_{-0.49}$	$^{+0.37}_{-0.40}$	$^{+1.12}_{-1.15}$	$^{+0.79}_{-0.82}$	$^{+0.47}_{-0.50}$	$^{+0.33}_{-0.36}$	$^{+0.42}_{-0.45}$	$^{+1.18}_{-1.21}$	$^{+0.84}_{-0.87}$	$^{+0.47}_{-0.50}$	$^{+0.31}_{-0.34}$	$^{+0.39}_{-0.42}$
b-Quark tagging efficiency (eigenvector 0) [%]	$^{-7.55}_{+7.81}$	$^{-6.49}_{+6.68}$	$^{-5.47}_{+5.60}$	$^{-5.22}_{+5.34}$	$^{-7.42}_{+7.66}$	$^{-6.28}_{+6.46}$	$^{-5.36}_{+5.49}$	$^{-5.02}_{+5.13}$	$^{-7.54}_{+7.78}$	$^{-6.50}_{+6.68}$	$^{-5.33}_{+5.46}$	$^{-5.13}_{+5.24}$	$^{-5.95}_{+6.11}$	$^{-7.74}_{+7.97}$	$^{-6.75}_{+6.94}$	$^{-5.53}_{+5.67}$	$^{-5.17}_{+5.29}$	$^{-6.17}_{+6.35}$
b-Quark tagging efficiency (eigenvector 1) [%]	∓1.11	$^{-1.62}_{+1.64}$	$^{-2.31}_{+2.33}$	$^{-3.22}_{+3.26}$	$^{-1.27}_{+1.28}$	$^{-1.84}_{+1.85}$	$^{-2.50}_{+2.53}$	$^{-3.01}_{+3.05}$	$^{-1.31}_{+1.32}$	$^{-1.81}_{+1.82}$	$^{-2.63}_{+2.66}$	$^{-3.25}_{+3.30}$	$^{-3.30}_{+3.35}$	$^{-1.36}_{+1.37}$	$^{-1.82}_{+1.83}$	$^{-2.61}_{+2.64}$	$^{-3.25}_{+3.30}$	$^{-3.57}_{+3.63}$
b-Quark tagging efficiency (eigenvector 2) [%]	$^{+1.63}_{-1.62}$	$^{+1.37}_{-1.36}$	±0.96	±0.29	$^{+1.65}_{-1.64}$	$^{+1.26}_{-1.25}$	$^{+0.86}_{-0.85}$	±0.47	$^{+1.70}_{-1.68}$	$^{+1.28}_{-1.27}$	±0.75	±0.31	-	$^{+1.65}_{-1.64}$	$^{+1.27}_{-1.26}$	±0.76	±0.23	∓0.15
b-Quark tagging efficiency (eigenvector 3) [%]	∓0.24	-	±0.24	-	∓0.23	±0.11	±0.32	±0.25	∓0.24	-	±0.30	±0.20	∓0.19	∓0.19	-	±0.29	±0.14	∓0.34
c-Quark tagging efficiency (eigenvector 0) [%]	±0.39	±0.27	±0.22	±0.16	±0.41	±0.27	±0.18	±0.15	±0.43	±0.31	$^{+0.19}_{-0.18}$	±0.11	±0.15	±0.49	$^{+0.35}_{-0.34}$	±0.26	±0.16	±0.11
c-Quark tagging efficiency (eigenvector 1) [%]	-	∓0.15	∓0.31	∓0.61	-	∓0.18	∓0.29	∓0.41	∓0.11	∓0.20	∓0.31	∓0.36	∓0.51	∓0.15	∓0.32	∓0.36	∓0.37	∓0.46
c-Quark tagging efficiency (eigenvector 2) [%]	±0.16	±0.10	-	∓0.14	±0.17	-	-	-	±0.19	±0.12	-	∓0.10	∓0.19	±0.19	-	-	-	∓0.17
Light-jet tagging efficiency (eigenvector 0) [%]	$^{-0.59}_{+0.58}$	∓0.49	$^{-0.57}_{+0.59}$	$^{-0.57}_{+0.60}$	$^{-0.38}_{+0.31}$	$^{-0.53}_{+0.55}$	$^{-0.46}_{+0.47}$	∓0.58	∓0.93	$^{-0.75}_{+0.79}$	$^{-0.49}_{+0.48}$	∓0.40	$^{-0.61}_{+0.65}$	$^{-1.93}_{+2.09}$	$^{-1.70}_{+1.93}$	$^{-0.73}_{+0.74}$	$^{-0.50}_{+0.51}$	∓0.55
Light-jet tagging efficiency (eigenvector 1) [%]	±0.32	±0.19	$^{+0.10}_{-0.11}$	-	$^{+0.27}_{-0.26}$	$^{+0.20}_{-0.19}$	-	-	±0.51	$^{+0.34}_{-0.33}$	±0.10	-	-	$^{+0.75}_{-0.74}$	$^{+0.77}_{-0.74}$	±0.27	-	-
Light-jet tagging efficiency (eigenvector 2) [%]	-	-	±0.10	$^{+0.22}_{-0.21}$	-	-	-	-	-	-	-	-	-	-	$^{-0.12}_{+0.14}$	∓0.11	-	±0.16
Light-jet tagging efficiency (eigenvector 3) [%]	-	-	-	-	$^{+0.15}_{-0.16}$	-	-	∓0.10	-	-	-	-	∓0.18	$^{-0.26}_{+0.27}$	∓0.18	∓0.15	$^{-0.24}_{+0.25}$	-
Light-jet tagging efficiency (eigenvector 5) [%]	-	-	-	-	-	-	-	-	-	-	-	-	-	$^{-0.33}_{+0.34}$	$^{-0.24}_{+0.25}$	-	-	-
Light-jet tagging efficiency (eigenvector 6) [%]	-	-	-	-	-	-	-	-	-	-	-	-	-	±0.15	±0.11	-	-	-
Light-jet tagging efficiency (eigenvector 7) [%]	-	-	-	-	-	-	-	-	-	-	-	-	-	∓0.16	∓0.12	-	-	-
b-Quark tagging extrapolation [%]	-	-	-	±0.39	-	-	-	±0.12	-	-	-	±0.12	±0.59	-	-	-	±0.21	$^{+1.15}_{-1.14}$
b-Quark tagging extrapolation from c-Quark [%]	-	-	-	-	-	-	-	-	-	-	-	-	-	±0.10	-	-	-	-
Electron energy resolution [%]	-	-	-	$^{-0.13}_{+0.45}$	-	-	-	$^{-}_{-0.37}$	$^{-}_{-0.46}$	-	$^{+0.25}_{-}$	$^{+0.27}_{-}$	$^{-}_{-0.41}$	$^{-}_{-0.35}$	-	$^{-}_{-0.21}$	-	$^{-}_{-0.81}$
Electron energy scale [%]	-	-	-	-	-	-	-	$^{-}_{-0.62}$	-	-	-	-	$^{-0.50}_{-}$	$^{+0.73}_{-0.42}$	-	$^{-0.15}_{+0.18}$	$^{-}_{-0.80}$	$^{-}_{-0.33}$
Electron trigger efficiency [%]	±0.12	±0.11	±0.11	±0.12	±0.13	±0.11	±0.10	±0.10	±0.15	±0.13	±0.11	±0.10	±0.10	±0.19	±0.17	±0.14	±0.11	±0.11
Electron reconstruction efficiency [%]	-	-	-	-	-	-	-	-	-	-	-	±0.10	±0.10	-	-	±0.10	±0.10	±0.11
Electron identification efficiency [%]	±0.34	±0.36	±0.37	±0.38	±0.38	±0.41	±0.45	±0.46	±0.44	±0.44	±0.50	±0.56	±0.58	±0.57	±0.55	±0.56	±0.58	±0.67
Electron isolation efficiency [%]	-	-	-	-	-	-	±0.13	±0.16	-	-	±0.19	±0.32	±0.40	-	±0.10	±0.18	±0.32	±0.54
Muon (ID) momentum resolution [%]	-	-	$^{-}_{-0.20}$	$^{-0.44}_{-}$	$^{+0.24}_{-}$	-	-	$^{-}_{-0.43}$	$^{-0.42}_{-}$	$^{-0.37}_{+0.12}$	$^{+0.24}_{-}$	-	$^{-}_{-0.96}$	$^{+0.83}_{-}$	$^{-0.57}_{+0.62}$	$^{+0.84}_{-}$	$^{-0.32}_{+0.27}$	$^{-}_{-0.75}$
Muon (MS) momentum resolution [%]	-	-	$^{-}_{-0.29}$	$^{-0.94}_{+0.97}$	$^{+0.25}_{-}$	-	-	$^{-0.13}_{+0.17}$	-	-	-	-	$^{-}_{-0.62}$	$^{+0.73}_{-}$	$^{-}_{-0.16}$	$^{+0.84}_{-}$	$^{-}_{-0.68}$	$^{+1.05}_{-}$
Muon (ID) sagitta o [%]	-	-	-	-	$^{+0.15}_{-}$	-	-	-	$^{-}_{-0.14}$	-	-	-	$^{+0.48}_{-0.26}$	$^{-}_{-0.52}$	$^{-}_{-0.21}$	-	$^{-}_{-0.18}$	$^{-}_{-0.44}$
Muon energy scale [%]	-	-	-	$^{+1.09}_{-}$	-	-	-	-	-	-	-	-	$^{-}_{-0.45}$	$^{+1.25}_{-}$	$^{+0.38}_{-0.25}$	$^{-}_{-0.66}$	$^{-0.55}_{+0.31}$	±0.49
Muon trigger efficiency stat [%]	$^{+0.29}_{-0.30}$	$^{+0.28}_{-0.29}$	±0.28	$^{+0.27}_{-0.28}$	$^{+0.29}_{-0.30}$	$^{+0.27}_{-0.28}$	$^{+0.26}_{-0.27}$	$^{+0.26}_{-0.27}$	$^{+0.29}_{-0.30}$	±0.28	±0.26	$^{+0.25}_{-0.26}$	±0.27	$^{+0.29}_{-0.30}$	$^{+0.27}_{-0.28}$	±0.25	$^{+0.25}_{-0.26}$	±0.24
Muon trigger efficiency syst [%]	$^{+0.52}_{-0.51}$	$^{+0.50}_{-0.48}$	$^{+0.49}_{-0.48}$	$^{+0.48}_{-0.47}$	$^{+0.53}_{-0.52}$	$^{+0.49}_{-0.48}$	$^{+0.47}_{-0.46}$	$^{+0.46}_{-0.45}$	$^{+0.55}_{-0.54}$	$^{+0.51}_{-0.50}$	$^{+0.47}_{-0.46}$	$^{+0.44}_{-0.43}$	$^{+0.45}_{-0.44}$	$^{+0.55}_{-0.54}$	$^{+0.55}_{-0.54}$	$^{+0.48}_{-0.47}$	$^{+0.45}_{-0.44}$	$^{+0.43}_{-0.42}$
Muon identification stat [%]	-	-	-	-	±0.10	-	-	-	±0.10	±0.10	-	-	-	±0.10	±0.10	-	-	-
Muon identification syst [%]	±0.34	±0.33	±0.33	±0.33	±0.39	±0.36	±0.35	±0.35	±0.46	±0.43	±0.40	±0.42	±0.44	±0.52	±0.51	±0.48	±0.48	±0.50
Muon isolation efficiency syst [%]	±0.10	±0.10	±0.10	-	±0.11	±0.10	-	-	±0.12	±0.11	±0.10	-	-	±0.13	±0.13	±0.11	±0.10	-
E_T^{miss} Soft jet resolution para [%]	±0.18	±0.23	-	±1.10	±0.19	-	±0.15	±0.29	±0.30	∓0.11	±0.31	±0.16	∓0.36	±1.22	∓0.70	±0.17	±0.15	±0.62
E_T^{miss} Soft jet resolution perp [%]	-	±0.22	±0.14	±0.26	±0.38	±0.16	±0.10	-	±0.39	-	±0.27	-	∓0.34	±0.89	-	±0.63	∓0.28	∓0.25
E_T^{miss} Soft jet scale [%]	$^{+0.21}_{-0.17}$	$^{+0.18}_{-0.24}$	$^{+0.35}_{-0.41}$	$^{+1.52}_{-}$	$^{+0.38}_{-0.21}$	$^{-}_{-0.16}$	$^{+0.14}_{-0.15}$	$^{-}_{-0.54}$	$^{+0.18}_{-0.19}$	-	-	-	$^{-}_{-1.25}$	$^{+0.35}_{-0.36}$	$^{-}_{-0.24}$	$^{+0.47}_{-}$	$^{+0.13}_{-0.67}$	$^{-0.13}_{+0.16}$
Luminosity [%]	∓2.05	∓2.05	∓2.05	∓2.05	∓2.05	∓2.05	∓2.05	∓2.05	∓2.05	∓2.05	∓2.05	∓2.05	∓2.05	∓2.05	∓2.05	∓2.05	∓2.05	∓2.05
Z+jets cross-section [%]	±0.68	±0.35	±0.24	±0.44	±0.87	±0.33	±0.11	±0.11	±1.22	±0.53	±0.10	-	±0.13	±1.42	±0.95	±0.21	-	±0.18
Monte Carlo sample statistics [%]	±0.20	±0.15	±0.40	±2.72	±0.81	±0.23	±0.24	±0.75	±0.98	±0.56	±0.49	±0.55	±1.73	±2.66	±1.72	±1.38	±1.59	±2.52
ISR/FSR + scale [%]	$^{+0.24}_{-}$	$^{+0.54}_{-0.46}$	$^{-3.96}_{+1.78}$	$^{-4.32}_{+4.94}$	$^{+2.20}_{-0.54}$	$^{+0.23}_{-0.35}$	$^{+0.80}_{-}$	$^{-4.31}_{+3.33}$	$^{+3.42}_{-}$	$^{+3.57}_{-}$	$^{+0.80}_{-}$	$^{-1.79}_{+1.64}$	$^{-1.84}_{+0.84}$	$^{+0.24}_{-2.04}$	$^{+3.72}_{-}$	$^{+0.81}_{-}$	$^{-2.13}_{+4.72}$	$^{+15.4}_{-}$
Alternate hard-scattering model [%]	±12.3	±6.87	±8.32	±8.99	±5.43	∓2.21	∓3.96	±0.70	±2.08	±0.12	∓5.79	∓10.1	∓2.52	∓11.0	∓4.01	∓2.11	∓2.00	±3.70
Alternate parton-shower model [%]	±5.35	±3.57	±11.6	±1.14	∓0.99	∓6.72	∓5.12	±9.36	∓1.42	∓2.98	∓8.74	∓9.13	±9.90	∓0.59	∓2.85	∓10.3	∓13.3	∓1.44
Inter PDF [%]	∓0.27	∓0.18	-	-	∓0.37	∓0.27	-	-	∓0.59	∓0.53	∓0.27	-	-	∓0.49	∓0.38	∓0.14	-	∓0.32
Intra PDF [%]	±0.64	±0.60	±0.43	±0.55	±1.17	±0.93	±0.58	±0.46	±1.41	±1.26	±0.92	±0.44	±0.17	±2.25	±1.91	±1.61	±1.03	±0.41
Fakes overall normalization, el [%]	±2.85	$^{+0.67}_{-0.68}$	-	$^{-0.45}_{+0.46}$	±2.63	$^{+1.20}_{-1.21}$	∓0.19	-	±2.91	±2.07	±0.12	±1.43	$^{-0.42}_{+0.43}$	±0.52	$^{-0.48}_{+0.49}$	$^{-0.70}_{+0.71}$	∓0.44	∓0.37
Fakes overall normalization, mu [%]	±0.18	-	-	∓0.24	±0.35	±0.13	-	±0.11	±0.52	±0.15	-	-	-	∓0.17	±0.23	±0.42	∓0.20	-
Fakes alternative parametrization [%]	∓0.72	±0.21	±0.28	±0.56	∓1.28	∓0.59	-	±0.58	∓0.24	±0.45	∓0.35	∓0.67	∓0.27	∓0.87	∓0.11	±0.44	∓0.79	-
W+jets heavy flavour component [%]	±1.07	±0.58	±0.32	∓0.11	±1.80	±0.80	±0.24	-	±3.11	±1.70	±0.41	-	±0.14	±5.37	±2.98	±1.18	±0.21	-
W+jets Scales [%]	±1.06	±0.61	±0.69	±1.81	±1.57	±0.92	±0.33	±0.53	±3.39	±2.33	±0.59	±0.26	±0.64	±6.35	±5.22	±1.81	±0.70	±0.69
Single Top DS/DR [%]	∓0.20	∓0.28	∓0.55	∓0.52	∓0.34	∓0.34	∓0.65	∓0.93	∓0.38	∓0.33	∓0.35	∓0.38	∓1.09	±0.27	-	-	-	∓0.69
Single Top IFSR [%]	$^{-}_{-0.45}$	$^{-}_{-0.30}$	$^{-}_{-0.37}$	-	$^{-}_{-0.80}$	$^{-}_{-0.44}$	$^{-}_{-0.22}$	$^{-}_{-0.74}$	$^{-}_{-1.31}$	$^{-}_{-0.67}$	$^{-0.40}_{-}$	-	$^{+0.11}_{-0.74}$	$^{-}_{-2.05}$	$^{-}_{+0.37}$	$^{-}_{-0.83}$	$^{+0.32}_{-}$	$^{+1.25}_{-0.33}$

TABLE F.51: Table of systematics for the absolute differential cross-section at the parton level for the $p_T^{t,had}$ vs $m^{t\bar{t}}$ observable.

Bins [GeV] x [GeV]	0–60	60–150	150–280	280–410	410–800	800–880	880–980	980–1100	1100–1230	1230–1600	1600–1680	1680–1790	1790–1920	1920–2400	2400–2480	2480–2590	2590–3200
$d\sigma$ / $dm^{t\bar{t}}vsp_{T}^{t\bar{t}}$ [pb/GeV x GeV]	$5.23 \cdot 10^{0}$	$1.43 \cdot 10^{0}$	$2.71 \cdot 10^{-1}$	$5.04 \cdot 10^{-2}$	$5.42 \cdot 10^{-3}$	$2.03 \cdot 10^{0}$	$5.05 \cdot 10^{-1}$	$1.14 \cdot 10^{-1}$	$2.64 \cdot 10^{-2}$	$3.62 \cdot 10^{-3}$	$6.20 \cdot 10^{-1}$	$1.68 \cdot 10^{-1}$	$4.30 \cdot 10^{-2}$	$4.43 \cdot 10^{-3}$	$1.62 \cdot 10^{-1}$	$5.29 \cdot 10^{-2}$	$5.44 \cdot 10^{-3}$
Total Uncertainty [%]	$^{+12.9}_{-12.8}$	$^{+24.6}_{-24.5}$	$^{+23.0}_{-22.9}$	$^{+21.3}_{-20.6}$	$^{+17.3}_{-17.0}$	$^{+14.0}_{-13.9}$	±13.1	$^{+13.5}_{-13.7}$	$^{+17.8}_{-19.2}$	$^{+15.4}_{-17.0}$	$^{+16.0}_{-15.7}$	$^{+10.3}_{-9.07}$	$^{+12.0}_{-12.6}$	$^{+16.8}_{-19.2}$	$^{+19.1}_{-18.7}$	$^{+13.5}_{-11.7}$	$^{+17.3}_{-14.4}$
Statistics [%]	±0.2	±0.2	±0.6	±1.7	±4.2	±0.3	±0.4	±0.9	±2.4	±5.4	±0.6	±0.8	±1.8	±4.5	±1.5	±1.9	±3.8
Systematics [%]	$^{+12.9}_{-12.8}$	$^{+24.6}_{-24.5}$	$^{+23.0}_{-22.8}$	$^{+21.2}_{-20.5}$	$^{+16.6}_{-16.3}$	±13.9	$^{+13.1}_{-13.0}$	$^{+13.5}_{-13.6}$	$^{+17.5}_{-19.0}$	$^{+14.0}_{-15.8}$	$^{+16.0}_{-15.7}$	$^{+10.2}_{-9.02}$	$^{+11.8}_{-12.4}$	$^{+15.9}_{-18.5}$	$^{+19.0}_{-18.6}$	$^{+13.2}_{-11.4}$	$^{+16.6}_{-13.6}$
Jet energy resolution [%]	∓3.17	∓0.12	±1.08	∓1.54	∓3.36	∓2.44	±0.71	±0.79	∓2.34	∓1.75	∓2.11	-	∓0.72	±2.10	∓2.17	±0.88	±3.23
b-Tagged jet energy scale (JES) [%]	-	$^{+0.37}_{-0.48}$	$^{+0.61}_{-0.40}$	$^{+0.37}_{-}$	$^{-}_{-0.65}$	$^{+0.69}_{-0.76}$	$^{+0.93}_{-0.87}$	$^{+0.55}_{-0.46}$	$^{-}_{-0.85}$	$^{-}_{-0.61}$	$^{+0.45}_{-0.55}$	$^{+0.88}_{-0.33}$	$^{+0.30}_{-0.71}$	$^{+1.02}_{-0.35}$	$^{+0.33}_{-}$	$^{+0.40}_{-0.35}$	$^{+2.11}_{-0.52}$
Effective detector NP set 1 (JES) [%]	-	-	-	$^{+0.34}_{-}$	$^{+1.24}_{-}$	-	$^{+0.10}_{-0.16}$	$^{-}_{-0.29}$	$^{-}_{-1.17}$	$^{-}_{-1.29}$	-	$^{+0.33}_{-}$	$^{-0.56}_{-}$	$^{-0.12}_{+0.19}$	-	$^{+0.36}_{-}$	-
Effective detector NP set 2 (JES) [%]	-	-	-	$^{+0.35}_{-0.24}$	$^{+0.47}_{-}$	-	-	-	$^{-}_{-0.57}$	$^{-0.52}_{-}$	$^{+0.15}_{-}$	$^{+0.49}_{-}$	$^{-}_{-0.61}$	$^{-0.88}_{+0.48}$	$^{+0.36}_{-}$	$^{-}_{-0.23}$	$^{+0.50}_{-}$
Effective mixed NP set 1 (JES) [%]	$^{-0.25}_{+0.15}$	-	$^{+0.41}_{-0.21}$	$^{+0.30}_{-}$	$^{-}_{-1.20}$	$^{+0.12}_{-0.18}$	$^{+0.18}_{-0.32}$	$^{+0.15}_{-0.27}$	$^{+0.33}_{-0.93}$	$^{+1.22}_{-2.45}$	$^{+0.25}_{-0.23}$	$^{+0.43}_{-0.30}$	$^{-}_{-0.39}$	$^{+1.24}_{-1.66}$	$^{+0.51}_{-0.21}$	$^{+0.49}_{-}$	$^{-0.52}_{+2.64}$
Effective mixed NP set 2 (JES) [%]	-	-	$^{-}_{+0.20}$	$^{-0.12}_{+0.63}$	$^{-0.11}_{+1.03}$	-	-	$^{-0.28}_{+0.15}$	$^{-}_{-0.56}$	$^{-}_{-0.52}$	-	-	$^{-}_{-0.75}$	$^{+0.82}_{-0.32}$	$^{+0.51}_{-}$	-	$^{-}_{-0.53}$
Effective mixed NP set 3 (JES) [%]	-	-	-	-	-	-	-	-	$^{-}_{-0.60}$	$^{+0.85}_{-}$	-	-	$^{-}_{-0.96}$	$^{+0.21}_{-0.48}$	-	$^{-}_{+0.39}$	$^{+0.19}_{+0.51}$
Effective modelling NP set 1 (JES) [%]	$^{+2.22}_{-2.27}$	$^{+3.61}_{-3.33}$	$^{+3.48}_{-3.30}$	$^{+2.10}_{-1.49}$	$^{+1.40}_{-2.19}$	$^{+2.07}_{-2.13}$	$^{+3.27}_{-3.23}$	$^{+2.81}_{-2.76}$	$^{+0.71}_{-1.79}$	$^{+1.86}_{-2.93}$	$^{+1.66}_{-1.47}$	$^{+2.76}_{-1.96}$	$^{+1.70}_{-2.30}$	$^{+1.35}_{-2.21}$	$^{+1.28}_{-1.44}$	$^{+2.61}_{-1.93}$	$^{+4.48}_{-1.96}$
Effective modelling NP set 2 (JES) [%]	$^{-0.38}_{+0.37}$	$^{-0.42}_{+0.45}$	$^{-0.24}_{+0.28}$	$^{+0.34}_{-}$	$^{-0.40}_{+0.21}$	∓0.15	$^{-0.22}_{-}$	$^{-}_{-0.45}$	$^{-}_{-0.79}$	$^{+0.13}_{-0.49}$	-	-	$^{-}_{-0.45}$	-	$^{+0.20}_{-}$	$^{+0.92}_{-}$	$^{+1.66}_{-}$
Effective modelling NP set 3 (JES) [%]	$^{+0.29}_{-0.36}$	$^{+0.38}_{-0.32}$	$^{+0.23}_{-}$	$^{+0.21}_{-0.27}$	$^{+0.17}_{-0.87}$	-	-	$^{-}_{-0.36}$	$^{-}_{-0.51}$	$^{-0.20}_{+1.02}$	-	$^{-0.21}_{+0.32}$	$^{-}_{-0.76}$	$^{+1.01}_{-}$	$^{+0.41}_{-}$	$^{+0.35}_{-}$	$^{+0.56}_{-}$
Effective modelling NP set 4 (JES) [%]	-	$^{+0.26}_{-0.15}$	$^{+0.28}_{-}$	$^{+0.40}_{-}$	$^{+0.32}_{-}$	$^{-}_{-0.14}$	$^{+0.21}_{-0.22}$	$^{+0.12}_{-0.39}$	$^{-}_{-0.52}$	$^{-}_{-0.93}$	$^{+0.21}_{-}$	$^{+0.28}_{-}$	$^{-}_{-1.10}$	$^{-0.16}_{+0.38}$	$^{+0.49}_{-}$	$^{+0.12}_{-0.72}$	$^{-}_{-0.51}$
Effective statistical NP set 1 (JES) [%]	$^{+0.39}_{-0.43}$	$^{+0.68}_{-0.59}$	$^{+0.55}_{-0.47}$	$^{+0.51}_{-0.26}$	$^{+1.11}_{-}$	$^{+0.31}_{-0.35}$	$^{+0.45}_{-0.57}$	$^{+0.55}_{-0.83}$	$^{-}_{-1.10}$	$^{+0.38}_{-2.06}$	$^{+0.18}_{-0.24}$	$^{+0.57}_{-}$	$^{-}_{-0.60}$	$^{-0.59}_{+0.68}$	$^{+1.08}_{-0.22}$	$^{+0.95}_{-0.57}$	$^{+2.24}_{-}$
Effective statistical NP set 2 (JES) [%]	$^{-0.42}_{+0.38}$	$^{-0.43}_{+0.52}$	$^{-0.45}_{+0.61}$	$^{-0.51}_{+0.68}$	$^{-}_{+0.83}$	$^{-0.29}_{+0.31}$	$^{-0.54}_{+0.44}$	$^{-0.64}_{+0.16}$	$^{-}_{-0.94}$	$^{-}_{-1.01}$	$^{-0.18}_{+0.40}$	$^{-}_{-0.32}$	$^{-}_{-0.89}$	$^{+0.81}_{-}$	$^{-0.26}_{-}$	$^{-}_{+0.42}$	$^{-}_{+2.27}$
Effective statistical NP set 3 (JES) [%]	-	-	$^{+0.27}_{-}$	$^{+0.54}_{-}$	$^{-0.89}_{+1.31}$	-	-	$^{-}_{-0.34}$	$^{-}_{-0.57}$	$^{-}_{-0.62}$	-	$^{+0.51}_{+0.17}$	$^{-}_{-0.79}$	$^{-}_{-0.30}$	$^{+0.40}_{-}$	$^{-}_{+0.45}$	$^{+2.07}_{-}$
Effective statistical NP set 4 (JES) [%]	$^{-0.21}_{+0.17}$	$^{-0.12}_{+0.26}$	-	$^{-}_{+0.29}$	$^{-0.64}_{+0.96}$	-	$^{+0.20}_{-0.17}$	$^{+0.19}_{-0.62}$	$^{-}_{-0.99}$	$^{-}_{-0.59}$	-	$^{+0.33}_{-}$	$^{-}_{-0.70}$	$^{+0.32}_{+0.31}$	-	-	$^{+0.48}_{-}$
Effective statistical NP set 5 (JES) [%]	-	-	-	$^{+0.70}_{-0.13}$	$^{+0.59}_{-}$	-	$^{-}_{+0.18}$	-	$^{-}_{-0.33}$	-	-	$^{-}_{+0.28}$	$^{-}_{-1.21}$	$^{+1.51}_{-}$	-	$^{-0.45}_{+0.32}$	$^{+0.87}_{-}$
Effective statistical NP set 6 (JES) [%]	$^{+0.10}_{-0.13}$	$^{+0.10}_{-0.15}$	-	$^{+0.26}_{-}$	$^{+0.75}_{-}$	-	-	$^{-0.18}_{-}$	$^{-}_{-0.71}$	$^{+0.31}_{-1.89}$	-	$^{+0.32}_{-}$	$^{-}_{-0.50}$	$^{+0.92}_{-}$	-	$^{-0.30}_{+0.17}$	$^{-0.53}_{+0.48}$
Effective statistical NP set 7 (JES) [%]	-	-	-	$^{+0.25}_{-}$	$^{-0.49}_{+0.41}$	-	±0.19	$^{-}_{-0.69}$	$^{-}_{-0.77}$	$^{+0.59}_{-1.31}$	$^{+0.25}_{-}$	$^{+0.55}_{-}$	$^{-}_{-1.04}$	$^{+1.05}_{-0.17}$	$^{+0.53}_{-}$	$^{+0.20}_{-}$	$^{+0.91}_{-}$
η intercalibration model (JES) [%]	$^{+0.22}_{-0.23}$	$^{+0.70}_{-0.69}$	$^{+1.02}_{-0.78}$	$^{+1.09}_{-}$	$^{+0.23}_{-}$	$^{+0.62}_{-0.74}$	$^{+1.00}_{-1.09}$	$^{+0.54}_{-1.07}$	$^{+0.10}_{-2.47}$	$^{+0.77}_{-0.17}$	$^{+0.93}_{-0.71}$	$^{+1.04}_{-0.70}$	$^{-}_{-1.33}$	$^{+0.10}_{-0.94}$	$^{+1.10}_{-1.07}$	$^{+1.78}_{-1.17}$	$^{+3.13}_{-0.46}$
η intercalibration non closure (JES) [%]	$^{-0.17}_{+0.14}$	$^{-0.41}_{+0.48}$	$^{-0.63}_{+0.46}$	$^{-0.27}_{+0.56}$	$^{+0.76}_{-}$	$^{-0.20}_{+0.14}$	$^{-0.42}_{+0.29}$	$^{-0.29}_{+0.34}$	$^{-}_{-1.02}$	$^{-0.23}_{+0.67}$	$^{-}_{+0.33}$	$^{-0.23}_{+0.58}$	$^{-0.40}_{-}$	$^{-}_{+0.29}$	$^{-0.34}_{+0.11}$	$^{-0.69}_{+0.45}$	$^{+0.36}_{-1.23}$
η intercalibration total stat (JES) [%]	±0.26	$^{+0.63}_{-0.58}$	$^{+0.76}_{-0.72}$	$^{+0.48}_{-0.23}$	$^{-0.40}_{-}$	$^{+0.31}_{-0.44}$	$^{+0.67}_{-0.66}$	$^{+0.65}_{-0.70}$	$^{-}_{-0.83}$	$^{+1.01}_{-0.88}$	$^{+0.35}_{-0.15}$	$^{+0.65}_{-0.44}$	$^{-}_{-0.79}$	$^{-}_{-0.33}$	$^{+0.53}_{-0.32}$	$^{+0.46}_{-0.62}$	$^{+2.03}_{-}$
Flavour composition (JES) [%]	$^{+2.00}_{-2.15}$	$^{+3.21}_{-3.52}$	$^{+3.56}_{-3.63}$	$^{+1.85}_{-1.69}$	$^{+2.28}_{-1.57}$	$^{+1.48}_{-1.72}$	$^{+2.98}_{-3.00}$	$^{+2.67}_{-3.15}$	$^{-}_{-2.25}$	$^{+1.08}_{-1.39}$	$^{+1.54}_{-1.30}$	$^{+2.68}_{-1.91}$	$^{+1.27}_{-2.35}$	$^{+1.24}_{-2.51}$	$^{+2.23}_{-0.92}$	$^{+2.41}_{-2.85}$	$^{+2.70}_{-2.78}$
Flavour response (JES) [%]	$^{-0.98}_{+0.89}$	$^{-1.75}_{+1.64}$	$^{-1.81}_{+1.45}$	$^{-0.77}_{+1.20}$	$^{-0.95}_{+1.34}$	$^{-0.87}_{+0.89}$	$^{-1.69}_{+1.49}$	$^{-2.00}_{+1.46}$	$^{-2.01}_{+0.34}$	$^{+1.03}_{-}$	$^{-0.68}_{+0.81}$	$^{-0.84}_{+1.34}$	$^{-1.16}_{+1.31}$	$^{-0.44}_{+1.34}$	$^{-0.78}_{+0.63}$	$^{-1.87}_{+0.92}$	$^{-2.31}_{+1.94}$
Pile-up offset μ (JES) [%]	-	$^{-0.23}_{+0.32}$	$^{-0.11}_{+0.36}$	-	$^{-0.42}_{-}$	$^{-0.16}_{+0.15}$	$^{-0.24}_{+0.26}$	$^{-}_{-0.38}$	$^{-}_{-0.60}$	$^{+0.15}_{-0.29}$	$^{-0.10}_{+0.16}$	$^{-}_{+0.30}$	$^{-0.95}_{+0.27}$	$^{-1.69}_{+0.84}$	$^{+0.41}_{-}$	$^{+0.58}_{-0.25}$	$^{+2.73}_{-}$
Pile-up offset N_{PV} (JES) [%]	$^{+0.30}_{-0.34}$	$^{+0.70}_{-0.68}$	$^{+0.91}_{-0.71}$	$^{+0.53}_{-}$	$^{+0.73}_{-}$	$^{+0.44}_{-0.31}$	$^{+0.96}_{-0.84}$	$^{+1.09}_{-0.80}$	$^{-}_{-0.89}$	$^{+0.35}_{-1.05}$	$^{+0.19}_{-0.40}$	$^{+0.88}_{-0.25}$	$^{-0.97}_{-}$	$^{-}_{-0.77}$	$^{+0.51}_{-0.38}$	$^{+1.03}_{-1.21}$	$^{+2.18}_{-0.42}$
Pile-up offset p_T (JES) [%]	$^{-0.63}_{+0.62}$	$^{-0.27}_{+0.30}$	-	$^{-}_{+0.54}$	$^{+0.14}_{-0.47}$	$^{-}_{-0.18}$	$^{+0.21}_{-0.36}$	$^{+0.23}_{-0.52}$	$^{-}_{-1.51}$	$^{+0.17}_{-2.05}$	$^{+0.37}_{-}$	$^{+0.57}_{-}$	$^{-}_{-0.35}$	$^{+1.09}_{-1.06}$	$^{+0.16}_{-0.64}$	$^{+0.32}_{-0.28}$	$^{+0.26}_{-0.48}$
Pile-up offset ρ topology (JES) [%]	$^{+3.02}_{-3.05}$	$^{+5.22}_{-4.89}$	$^{+5.48}_{-4.92}$	$^{+2.58}_{-2.69}$	$^{+2.94}_{-2.10}$	$^{+3.17}_{-3.25}$	$^{+5.16}_{-5.14}$	$^{+4.52}_{-4.17}$	$^{+1.03}_{-3.24}$	$^{+1.49}_{-1.19}$	$^{+2.54}_{-2.24}$	$^{+4.03}_{-3.12}$	$^{+2.80}_{-3.51}$	$^{+2.51}_{-2.06}$	$^{+3.05}_{-2.29}$	$^{+4.83}_{-3.03}$	$^{+4.68}_{-2.68}$
Punch-through (JES) [%]	-	-	-	$^{+0.18}_{-}$	$^{-}_{-0.26}$	-	-	$^{-}_{-0.23}$	$^{-}_{-0.33}$	$^{-}_{-0.47}$	-	$^{+0.24}_{-}$	-	$^{-}_{-0.73}$	-	$^{-}_{-0.27}$	$^{+0.99}_{-}$
Single particle high-p_T (JES) [%]	-	-	-	$^{+0.26}_{-}$	$^{-}_{-0.32}$	-	-	-	$^{+0.10}_{-0.16}$	$^{+0.52}_{-}$	-	$^{+0.34}_{-}$	$^{+0.41}_{-}$	$^{-}_{-0.78}$	$^{+0.11}_{-0.10}$	$^{-}_{-0.64}$	$^{-}_{-0.51}$
Jet vertex fraction [%]	$^{+0.92}_{-0.95}$	$^{+0.98}_{-1.01}$	$^{+0.88}_{-0.92}$	$^{+0.70}_{-0.75}$	$^{+0.58}_{-0.60}$	$^{+0.63}_{-0.66}$	$^{+0.71}_{-0.75}$	$^{+0.66}_{-0.70}$	$^{+0.62}_{-0.66}$	$^{+0.45}_{-0.49}$	$^{+0.51}_{-0.54}$	$^{+0.60}_{-0.63}$	$^{+0.61}_{-0.64}$	$^{+0.53}_{-0.56}$	$^{+0.55}_{-0.57}$	$^{+0.60}_{-0.64}$	$^{+0.51}_{-0.55}$
b-Quark tagging efficiency (eigenvector 0) [%]	$^{-7.34}_{+7.59}$	$^{-6.56}_{+6.75}$	$^{-6.09}_{+6.23}$	$^{-6.26}_{+6.41}$	$^{-5.90}_{+6.05}$	$^{-6.14}_{+6.32}$	$^{-5.61}_{+5.75}$	$^{-5.75}_{+5.88}$	$^{-6.16}_{+6.31}$	$^{-5.92}_{+6.06}$	$^{-5.80}_{+5.96}$	$^{-5.44}_{+5.56}$	$^{-5.82}_{+5.95}$	$^{-6.40}_{+6.56}$	$^{-6.13}_{+6.31}$	$^{-5.62}_{+5.75}$	$^{-6.04}_{+6.16}$
b-Quark tagging efficiency (eigenvector 1) [%]	$^{-1.24}_{+1.25}$	$^{-1.49}_{+1.50}$	$^{-2.03}_{+2.04}$	$^{-2.29}_{+2.30}$	$^{-2.69}_{+2.72}$	$^{-2.01}_{+2.03}$	$^{-2.17}_{+2.19}$	$^{-2.56}_{+2.58}$	$^{-2.67}_{+2.70}$	$^{-3.04}_{+3.08}$	$^{-2.50}_{+2.54}$	$^{-2.56}_{+2.59}$	$^{-2.86}_{+2.89}$	$^{-3.09}_{+3.13}$	$^{-2.50}_{+2.53}$	$^{-2.64}_{+2.67}$	$^{-3.08}_{+3.12}$
b-Quark tagging efficiency (eigenvector 2) [%]	$^{+1.59}_{-1.58}$	±1.42	$^{+1.03}_{-1.02}$	±0.75	±0.57	$^{+1.18}_{-1.17}$	$^{+1.04}_{-1.03}$	±0.70	±0.50	$^{+0.29}_{-0.30}$	$^{+0.85}_{-0.84}$	±0.76	±0.47	±0.28	±0.78	±0.70	±0.34
b-Quark tagging efficiency (eigenvector 3) [%]	∓0.16	-	±0.10	-	-	±0.14	±0.20	±0.15	-	-	±0.17	±0.21	-	∓0.17	±0.10	±0.14	-
c-Quark tagging efficiency (eigenvector 0) [%]	±0.35	±0.30	$^{+0.30}_{-0.29}$	±0.33	±0.22	±0.24	±0.25	±0.28	±0.32	±0.16	±0.19	±0.24	±0.28	±0.15	±0.27	±0.22	$^{+0.32}_{-0.31}$
c-Quark tagging efficiency (eigenvector 1) [%]	-	∓0.14	∓0.29	∓0.40	∓0.38	∓0.19	∓0.27	∓0.38	∓0.43	$^{-0.31}_{+0.30}$	∓0.26	∓0.33	∓0.42	$^{-0.52}_{+0.53}$	$^{-0.32}_{+0.33}$	∓0.37	∓0.40
c-Quark tagging efficiency (eigenvector 2) [%]	±0.15	±0.11	-	-	-	-	-	-	-	-	-	-	-	∓0.13	-	-	-
Light-jet tagging efficiency (eigenvector 0) [%]	$^{-0.51}_{+0.52}$	$^{-0.55}_{+0.53}$	$^{-0.76}_{+0.77}$	$^{-1.02}_{+1.06}$	$^{-0.44}_{+0.45}$	$^{-0.39}_{+0.37}$	$^{-0.59}_{+0.60}$	$^{-0.91}_{+0.97}$	$^{-1.02}_{+1.04}$	$^{-0.49}_{+0.50}$	∓0.49	$^{-0.68}_{+0.71}$	$^{-0.86}_{+0.88}$	$^{-1.06}_{+1.08}$	$^{-0.86}_{+0.92}$	$^{-1.21}_{+1.32}$	∓0.99
Light-jet tagging efficiency (eigenvector 1) [%]	$^{+0.28}_{-0.27}$	±0.23	±0.19	±0.18	-	±0.15	±0.14	$^{+0.14}_{-0.13}$	$^{+0.19}_{-0.18}$	$^{+0.10}_{-0.11}$	$^{+0.16}_{-0.15}$	±0.18	±0.17	$^{+0.14}_{-0.15}$	$^{+0.24}_{-0.23}$	±0.45	$^{+0.23}_{-0.24}$
Light-jet tagging efficiency (eigenvector 2) [%]	-	-	±0.10	$^{+0.17}_{-0.16}$	-	-	-	$^{+0.11}_{-}$	$^{+0.14}_{-0.13}$	-	-	-	-	±0.19	-	$^{-0.10}_{+0.11}$	-
Light-jet tagging efficiency (eigenvector 3) [%]	-	-	-	-	-	-	-	$^{-0.15}_{+0.16}$	-	-	-	-	∓0.11	-	$^{-0.16}_{+0.15}$	$^{-0.19}_{+0.20}$	∓0.23
Light-jet tagging efficiency (eigenvector 5) [%]	-	-	-	-	-	-	-	-	-	-	-	-	-	-	∓0.12	∓0.15	-
b-Quark tagging extrapolation [%]	-	-	-	±0.26	±0.39	-	-	-	±0.43	±0.79	-	-	±0.22	±0.87	±0.14	±0.19	±0.51
b-Quark tagging extrapolation from c-Quark [%]	-	-	-	-	-	-	-	-	-	±0.11	-	-	-	-	-	-	-
Electron energy resolution [%]	-	-	-	-	$^{+0.62}_{-}$	-	-	$^{-}_{-0.28}$	$^{-}_{-0.47}$	$^{+0.45}_{-0.49}$	-	-	-	$^{-}_{-0.78}$	$^{-}_{-0.40}$	$^{-}_{+0.45}$	$^{-}_{-0.59}$
Electron energy scale [%]	-	-	-	-	$^{+0.23}_{-0.27}$	-	-	$^{-}_{-0.21}$	$^{-}_{-0.35}$	$^{+0.99}_{-}$	-	$^{+0.36}_{-}$	$^{-}_{-0.42}$	$^{-}_{-1.26}$	$^{-}_{-0.53}$	$^{+0.41}_{-}$	$^{+0.41}_{-}$
Electron trigger efficiency [%]	±0.12	±0.11	±0.11	±0.11	±0.10	±0.11	±0.11	±0.11	±0.11	±0.10	±0.11	±0.12	±0.12	±0.12	±0.14	±0.14	±0.14
Electron reconstruction efficiency [%]	-	-	-	-	-	-	-	-	±0.10	±0.11	-	-	±0.10	±0.11	±0.10	±0.10	±0.11
Electron identification efficiency [%]	±0.34	±0.35	±0.39	±0.46	±0.52	±0.41	±0.43	±0.49	±0.56	±0.60	±0.49	±0.51	±0.57	±0.63	±0.57	±0.57	±0.65
Electron isolation efficiency [%]	-	-	-	±0.16	±0.28	-	±0.11	±0.17	±0.29	±0.43	±0.18	±0.20	±0.28	±0.47	±0.21	±0.23	±0.36
Muon (ID) momentum resolution [%]	-	-	-	$^{+0.37}_{-}$	$^{+0.26}_{-0.62}$	-	-	$^{+0.17}_{-0.15}$	$^{-}_{-0.61}$	$^{-}_{+0.77}$	-	-	$^{-0.39}_{-}$	$^{-0.72}_{+0.37}$	$^{+0.83}_{-}$	$^{-0.42}_{-}$	$^{-}_{-0.48}$
Muon (MS) momentum resolution [%]	-	-	-	$^{+0.27}_{-}$	$^{-0.35}_{+0.16}$	-	-	-	∓0.16	$^{+0.95}_{-}$	-	-	$^{+0.15}_{-0.58}$	$^{-}_{-0.57}$	$^{+0.37}_{-}$	$^{+0.11}_{-0.29}$	$^{+0.64}_{-}$
Muon (ID) sagitta ρ [%]	-	-	-	-	$^{+0.52}_{-}$	-	-	-	$^{-}_{-0.25}$	$^{+0.62}_{-}$	-	-	-	$^{-}_{-1.03}$	$^{-}_{-0.31}$	$^{-}_{-0.20}$	$^{+0.74}_{-}$
Muon energy scale [%]	-	-	$^{+0.12}_{-}$	$^{+0.37}_{-}$	$^{-}_{-0.50}$	-	-	-	$^{+0.52}_{-0.29}$	$^{-0.23}_{-}$	-	$^{+0.42}_{-}$	$^{-}_{-0.39}$	$^{-}_{-0.43}$	-	$^{+0.20}_{-0.34}$	$^{-0.21}_{+0.41}$
Muon trigger efficiency stat [%]	$^{+0.29}_{-0.30}$	$^{+0.28}_{-0.29}$	±0.29	±0.28	$^{+0.27}_{-0.28}$	$^{+0.27}_{-0.28}$	$^{+0.27}_{-0.28}$	$^{+0.27}_{-0.28}$	±0.27	±0.27	$^{+0.26}_{-0.27}$	±0.27	$^{+0.27}_{-0.28}$	$^{+0.27}_{-0.28}$	$^{+0.25}_{-0.26}$	$^{+0.26}_{-0.27}$	$^{+0.26}_{-0.27}$
Muon trigger efficiency syst [%]	$^{+0.51}_{-0.50}$	$^{+0.50}_{-0.49}$	$^{+0.50}_{-0.49}$	$^{+0.49}_{-0.48}$	$^{+0.45}_{-0.44}$	$^{+0.48}_{-0.47}$	$^{+0.49}_{-0.48}$	$^{+0.49}_{-0.48}$	$^{+0.48}_{-0.47}$	$^{+0.47}_{-0.46}$	$^{+0.47}_{-0.46}$	$^{+0.48}_{-0.47}$	$^{+0.49}_{-0.48}$	$^{+0.50}_{-0.49}$	$^{+0.48}_{-0.47}$	$^{+0.50}_{-0.49}$	±0.48
Muon identification syst [%]	±0.33	±0.33	±0.34	±0.36	$^{+0.40}_{-0.39}$	±0.36	±0.36	±0.38	±0.41	±0.45	±0.41	±0.42	±0.44	±0.50	±0.48	±0.50	$^{+0.53}_{-0.52}$
Muon isolation efficiency syst [%]	±0.10	±0.10	±0.10	±0.10	-	±0.10	±0.10	±0.10	±0.10	-	±0.10	±0.10	±0.10	±0.11	±0.11	±0.11	±0.11
E_{T}^{miss} Soft jet resolution para [%]	±0.14	±0.29	±0.21	±0.50	∓0.16	-	±0.11	-	∓0.10	∓0.12	-	±0.27	±0.27	±1.03	∓0.17	±0.30	±2.05
E_{T}^{miss} Soft jet resolution perp [%]	-	±0.24	±0.16	±0.24	∓0.61	±0.15	±0.23	±0.12	∓0.21	∓1.01	±0.13	-	±0.38	±1.07	±0.41	∓0.27	±0.70
E_{T}^{miss} Soft jet scale [%]	$^{+0.12}_{-0.27}$	$^{+0.34}_{-0.18}$	$^{+0.21}_{-}$	$^{+0.34}_{-0.31}$	$^{+0.89}_{-}$	$^{+0.20}_{-0.25}$	-	$^{-0.24}_{+0.12}$	$^{-}_{-0.68}$	$^{-0.20}_{+1.12}$	-	-	-	$^{-}_{-1.98}$	$^{+0.18}_{-}$	$^{-}_{-0.57}$	$^{+1.06}_{-}$
Luminosity [%]	∓2.05	∓2.05	∓2.05	∓2.05	∓2.05	∓2.05	∓2.05	∓2.05	∓2.05	∓2.05	∓2.05	∓2.05	∓2.05	∓2.05	∓2.05	∓2.05	∓2.05
Z+jets cross-section [%]	±0.58	±0.41	±0.41	±0.47	±0.27	±0.29	±0.27	±0.52	±0.40	±0.20	±0.24	±0.30	±0.45	±0.30	±0.34	±0.57	±0.76
Monte Carlo sample statistics [%]	±0.16	±0.22	±0.36	±1.02	±2.34	±0.25	±0.25	±0.66	±1.47	±3.22	±0.37	±0.50	±1.19	±2.93	±1.09	±1.37	±2.75
ISR/FSR + scale [%]	$^{-0.18}_{+0.54}$	$^{+0.32}_{-0.85}$	$^{-}_{-1.45}$	$^{-1.68}_{+4.53}$	$^{-3.57}_{+2.98}$	$^{-0.11}_{+0.79}$	$^{+0.64}_{-1.01}$	$^{+0.24}_{-}$	$^{-}_{-0.89}$	$^{-6.77}_{+3.73}$	$^{-0.78}_{+1.78}$	$^{+1.49}_{-}$	$^{+3.36}_{-}$	$^{+0.50}_{-8.90}$	$^{+0.80}_{-}$	$^{+5.29}_{-}$	$^{-1.93}_{+1.79}$
Alternate hard-scattering model [%]	∓7.52	±14.0	∓8.52	±13.6	±11.3	∓4.20	±3.22	±1.96	∓7.45	∓0.87	∓7.23	±0.36	∓0.22	±6.04	∓9.06	±5.57	∓7.16
Alternate parton-shower model [%]	∓2.24	±17.1	±18.4	±12.6	±5.82	∓9.90	∓7.69	∓9.11	±13.3	∓9.76	∓11.3	±3.54	∓7.22	±10.2	∓13.6	±2.36	±3.93
Inter PDF [%]	∓0.21	∓0.22	∓0.28	-	-	∓0.21	∓0.15	∓0.10	-	±0.14	∓0.29	∓0.16	∓0.11	∓0.22	∓0.27	-	∓0.20
Intra PDF [%]	±0.71	±0.51	±0.31	±0.18	±0.44	±0.87	±0.65	±0.42	±0.36	±0.45	±0.93	±0.73	±0.47	±0.44	±1.46	±1.27	±0.95
Fakes overall normalization, el [%]	±1.76	±1.84	$^{+0.99}_{-1.00}$	±0.59	±0.14	±0.93	±0.74	$^{-0.40}_{+0.41}$	$^{-0.31}_{+0.32}$	∓0.26	±1.14	±1.47	$^{-0.66}_{+0.67}$	∓0.22	∓0.46	∓0.63	∓0.29
Fakes overall normalization, mu [%]	±0.10	±0.19	±0.14	±0.10	-	-	±0.14	±0.25	±0.66	±0.19	-	±0.11	±0.17	-	-	±0.41	-
Fakes alternative parametrization [%]	∓0.13	∓0.38	∓0.36	∓0.62	±0.25	∓0.34	∓0.73	±0.40	∓0.95	±0.71	∓0.13	∓0.87	-	-	∓0.10	∓0.75	±0.73
W+jets heavy flavour component [%]	±0.94	±0.68	±0.59	-	-	±0.72	±0.58	±0.51	-	∓0.10	±0.84	±0.76	±0.66	-	±1.65	±1.58	±1.01
W+jets Scales [%]	±0.85	±0.80	±1.13	±1.44	±0.86	±0.59	±0.88	±1.44	±1.51	±1.14	±0.90	±1.36	±2.28	±2.23	±2.21	±3.08	±3.19
Single Top DS/DR [%]	∓0.17	∓0.31	∓0.60	∓1.12	∓1.25	∓0.28	∓0.66	∓1.71	∓2.91	∓1.03	∓0.15	∓0.64	∓1.90	∓3.10	±0.37	∓0.49	∓1.38
Single Top IFSR [%]	$^{-0.44}_{-}$	$^{-}_{-0.37}$	$^{-}_{-0.48}$	$^{+0.40}_{-0.18}$	$^{-}_{-0.75}$	$^{-}_{-0.39}$	$^{-}_{-0.57}$	$^{-}_{-0.60}$	$^{-}_{-1.86}$	$^{+2.10}_{-}$	$^{-}_{-0.42}$	$^{-0.25}_{+0.13}$	$^{-}_{-0.64}$	$^{-}_{-1.95}$	$^{-}_{-0.26}$	$^{-}_{-0.36}$	$^{+2.20}_{-0.99}$

TABLE F.52: Table of systematics for the absolute differential cross-section at the parton level for the $p_{T}^{t\bar{t}}$ vs $m^{t\bar{t}}$ observable.

Bins [GeV]x[GeV]	0–85	85–175	175–285	285–390	390–1000	1000–1085	1085–1175	1175–1285	1285–2000	2000–2085	2085–2175	2175–2300	2300–3000
$d\sigma$ / $d\|y^{t,had}\|vsp_T^{t,had}$ [pb/GeVxGeV]	$1.49 \cdot 10^{0}$	$1.69 \cdot 10^{0}$	$5.33 \cdot 10^{-1}$	$1.13 \cdot 10^{-1}$	$8.49 \cdot 10^{-3}$	$1.23 \cdot 10^{0}$	$1.32 \cdot 10^{0}$	$3.89 \cdot 10^{-1}$	$1.59 \cdot 10^{-2}$	$8.42 \cdot 10^{-1}$	$8.37 \cdot 10^{-1}$	$1.96 \cdot 10^{-1}$	$5.20 \cdot 10^{-3}$
Total Uncertainty [%]	+27.7 −18.1	+15.2 −9.14	+11.3 −7.85	+12.5 −10.8	+20.4 −15.0	+21.6 −14.0	+14.8 −8.32	+11.6 −8.43	+11.9 −8.67	+18.2 −9.79	+15.1 −10.1	+12.0 −8.01	+10.7 −9.19
Statistics [%]	±0.3	±0.2	±0.4	±1.1	±3.9	±0.3	±0.3	±0.5	±1.3	±0.6	±0.5	±0.9	±2.6
Systematics [%]	+27.7 −18.1	+15.2 −9.14	+11.3 −7.83	+12.4 −10.7	+19.9 −14.2	+21.6 −14.0	+14.8 −8.31	+11.5 −8.40	+11.8 −8.53	+18.2 −9.76	+15.1 −10.1	+12.0 −7.93	+10.2 −8.61
Jet energy resolution [%]	∓0.61	∓0.91	∓0.89	∓0.83	±1.91	∓0.13	∓0.31	∓0.97	∓0.85	∓1.48	±1.23	∓0.98	∓0.63
b-Tagged jet energy scale (JES) [%]	+2.05 -	+1.38 -	+1.46 −0.42	+0.85 -	+1.80 -	+1.46 -	+1.59 -	+1.29 −0.43	+0.70 -	+1.19 -	+1.51 -	+0.98 -	+0.64 -
Effective detector NP set 1 (JES) [%]	+2.04 -	+1.01 -	+0.62 -	+0.42 -	−0.22 -	+1.28 -	+0.95 -	−0.61 -	+0.31 -	+1.05 -	+0.88 -	+0.61 -	−0.65 -
Effective detector NP set 2 (JES) [%]	+1.87 -	+0.83 -	+0.55 -	+0.51 -	+1.63 +0.99	+1.41 -	+0.97 -	+0.54 -	+0.58 -	+1.18 -	+0.92 -	+0.53 -	+0.21 −0.21
Effective mixed NP set 1 (JES) [%]	+2.17 -	+0.97 -	+0.81 -	+0.41 -	+1.35 -	+1.46 -	+1.01 -	+0.69 -	+0.64 -	+1.25 -	+0.95 -	+0.89 -	−0.58 +0.31
Effective mixed NP set 2 (JES) [%]	+1.81 -	+0.83 -	+0.51 -	+0.53 -	−0.43 +1.03	+1.30 -	+0.91 -	+0.48 -	+0.48 -	+1.22 -	+0.90 -	+0.65 -	+0.68 -
Effective mixed NP set 3 (JES) [%]	+1.78 -	+0.79 -	+0.53 -	+0.39 -	+0.98 -	+1.34 -	+0.96 -	+0.58 -	+0.37 -	+1.07 -	+0.85 -	+0.66 -	+0.30 -
Effective modelling NP set 1 (JES) [%]	+4.94 −1.32	+3.96 −2.26	+2.56 −1.54	+0.93 −0.55	+4.43 -	+4.00 −1.24	+3.58 −1.77	+2.33 −1.37	+1.04 −0.98	+2.84 −0.37	+2.62 −1.00	+2.05 −0.81	+0.66 −0.33
Effective modelling NP set 2 (JES) [%]	+2.32 -	+1.07 -	+0.59 -	+0.47 -	+0.96 -	+1.93 -	+1.04 -	+0.52 -	+0.71 -	+1.46 -	+1.01 -	+0.62 -	−0.25 -
Effective modelling NP set 3 (JES) [%]	+2.37 -	+0.90 -	+0.68 -	+0.45 -	+0.66 -	+1.72 -	+0.99 -	+0.63 -	+0.39 -	+1.58 -	+0.97 -	+0.56 -	+0.31 -
Effective modelling NP set 4 (JES) [%]	+1.95 -	+0.90 -	+0.63 -	+0.40 -	+0.52 -	+1.34 -	+0.99 -	+0.56 -	+0.35 -	+1.18 -	+1.08 -	+0.72 -	+0.74 -
Effective statistical NP set 1 (JES) [%]	+2.32 -	+1.37 -	+0.84 -	+0.37 -	+1.01 -	+1.85 -	+1.30 -	+0.66 -	+0.58 -	+1.59 -	+0.99 -	+0.85 -	+0.47 -
Effective statistical NP set 2 (JES) [%]	+2.32 -	+1.25 -	+0.84 -	+0.31 -	- -	+1.77 -	+1.29 -	+0.72 -	+0.33 -	+1.54 -	+1.07 -	+0.94 -	−0.29 -
Effective statistical NP set 3 (JES) [%]	+1.79 -	+0.84 -	+0.54 -	+0.35 -	+1.90 +1.24	+1.37 -	+0.92 -	+0.61 -	+0.30 -	+1.17 -	+0.82 -	+0.58 -	+0.44 -
Effective statistical NP set 4 (JES) [%]	+2.23 -	+0.80 -	+0.78 -	+0.48 -	+1.86 -	+1.51 -	+0.87 -	+0.63 -	+0.27 -	+1.32 -	+0.97 -	+0.47 -	- -
Effective statistical NP set 5 (JES) [%]	+1.86 -	+0.85 -	+0.61 -	+0.39 -	−0.13 +1.64	+1.35 -	+1.01 -	+0.54 -	+0.24 -	+1.27 -	+0.86 -	+0.83 -	−0.12 +0.97
Effective statistical NP set 6 (JES) [%]	+1.86 -	+0.88 -	+0.55 -	+0.70 -	+2.45 -	+1.43 -	+1.00 -	+0.45 -	+0.60 -	+1.24 -	+0.91 -	+0.60 -	−0.14 +0.56
Effective statistical NP set 7 (JES) [%]	+1.76 -	+0.98 -	+0.54 -	+0.39 -	+1.31 -	+1.31 -	+0.93 -	+0.60 -	+0.41 -	+1.11 -	+0.92 -	+0.71 -	+0.51 -
η intercalibration model (JES) [%]	+1.96 -	+1.13 -	+0.78 -	+0.56 -	+1.55 -	+1.99 -	+1.95 −0.14	+1.61 −0.57	+1.32 −0.50	+1.64 −0.21	+1.72 −0.64	+1.89 −0.64	−0.52 −0.42
η intercalibration non closure (JES) [%]	+2.30 -	+1.18 -	+0.69 -	+0.27 -	+0.84 -	+1.21 -	+1.05 -	+0.82 -	+0.30 -	+1.23 -	+1.12 -	+1.17 -	−0.56 +0.38
η intercalibration total stat (JES) [%]	+2.05 -	+1.26 -	+0.99 -	+0.47 -	+1.91 -	+1.70 -	+1.43 -	+0.90 -	+0.56 -	+1.62 -	+1.20 -	+0.89 -	+0.24 -
Flavour composition (JES) [%]	+4.85 −1.53	+3.41 −2.06	+2.11 −1.13	+0.83 −0.26	+3.05 −0.75	+4.14 −1.54	+3.25 −1.63	+1.96 −1.18	+1.10 −0.71	+2.46 -	+2.10 −0.73	+1.77 −0.59	+0.26 -
Flavour response (JES) [%]	+3.08 -	−0.60 -	−0.33 -	+0.84 -	−0.44 -	−1.54 -	−0.47 -	−0.42 -	−0.19 -	−1.85 -	+1.78 -	−0.41 -	−0.90 -
Pile-up offset μ (JES) [%]	+1.85 -	+2.11 +0.98	+1.36 +0.66	+0.35 -	+1.84 +0.61	+2.57 +1.49	+2.12 +1.09	+1.32 +0.69	+0.68 +0.63	+1.29 -	+1.01 -	+1.17 +0.47	+0.15 +0.79
Pile-up offset N_{PV} (JES) [%]	+2.13 -	+1.47 -	+1.04 -	+0.54 -	+2.39 -	+1.78 -	+1.47 -	+1.01 −0.35	+0.61 -	+1.53 -	+1.19 -	+0.85 −0.28	+0.43 +0.71
Pile-up offset p_T (JES) [%]	+2.58 -	+0.94 -	+0.96 -	- -	+2.17 -	+1.97 -	+0.91 -	+0.95 -	+0.74 -	+1.84 -	+0.91 -	+0.93 -	+0.38 −1.29
Pile-up offset ρ topology (JES) [%]	+5.95 −2.39	+5.59 −3.23	+3.97 −2.97	+1.54 −0.82	+2.53 -	+4.90 −1.24	+4.97 −1.07	+3.69 −0.75	+1.51 −1.42	+3.26 −0.78	+3.19 −1.86	+3.17 −1.60	+0.28 +0.44
Punch-through (JES) [%]	+1.72 -	+0.85 -	+0.53 -	+0.52 -	+0.72 -	+1.33 -	+0.88 -	+0.52 -	+0.51 -	+1.15 -	+0.88 -	+0.57 -	+0.60 -
Single particle high-p_T (JES) [%]	+1.72 -	+0.85 -	+0.55 -	+0.52 -	+1.40 -	+1.35 -	+0.88 -	+0.52 -	+0.51 -	+1.00 -	+0.85 -	+0.57 -	+0.34 -
Jet vertex fraction [%]	+2.82 -	+1.65 -	+0.93 -	+0.82 -	+1.45 -	+2.35 -	+1.63 -	+0.96 -	+0.95 -	+2.31 -	+1.55 -	+0.99 -	+0.73 -
b-Quark tagging efficiency (eigenvector 0) [%]	−6.12 +9.78	−5.66 −7.55	−4.87 +5.97	−4.63 +5.73	−5.18 +7.31	−6.27 +9.04	−5.58 +7.44	−4.85 −5.96	−4.57 +5.89	−5.50 +8.38	−5.44 +7.71	−4.79 +6.04	−4.59 +5.53
b-Quark tagging efficiency (eigenvector 1) [%]	+2.76 -	−0.83 -	−2.07 +3.93	−2.76 +3.79	−2.45 +4.48	+2.39 -	−0.85 +2.54	−2.06 +3.97	−2.64 +3.80	+2.62 -	−0.91 +2.54	−1.97 +3.12	−2.89 +3.78
b-Quark tagging efficiency (eigenvector 2) [%]	+3.33 -	+2.54 −2.18	+1.98 -	+0.79 -	+1.73 -	+2.92 -	−2.18 -	−1.32 -	+0.87 -	+3.00 -	+2.13 -	+1.37 -	+0.60 -
b-Quark tagging efficiency (eigenvector 3) [%]	+1.96 -	−0.48 −0.90	−0.36 −0.78	- +0.67	- +1.34	−0.38 +1.52	−0.50 +0.89	−0.34 +0.40	- +0.75	−0.31 +1.35	−0.50 +0.87	−0.25 +0.87	- +0.56
b-Quark tagging efficiency (eigenvector 4) [%]	+1.72 -	+0.91 -	+0.47 -	+0.52 -	+1.04 -	+1.29 -	+0.90 -	+0.49 -	+0.62 -	+1.40 -	+0.87 -	+0.56 -	+0.45 -
b-Quark tagging efficiency (eigenvector 5) [%]	+1.70 -	+0.85 -	+0.47 -	+0.49 -	+1.00 -	+1.27 -	+0.84 -	+0.49 -	+0.60 -	+1.35 -	+0.81 -	+0.56 -	+0.42 -
c-Quark tagging efficiency (eigenvector 0) [%]	+2.10 -	+1.12 -	+0.65 -	+0.63 -	+1.14 -	+1.65 -	+1.11 -	+0.68 -	+0.71 -	+1.73 -	+1.11 -	+0.74 -	+0.52 -
c-Quark tagging efficiency (eigenvector 1) [%]	+1.76 -	+1.00 -	+0.77 -	+0.90 -	+1.71 -	+1.34 -	+1.00 -	+0.78 -	+0.96 -	+1.46 -	+1.00 -	+0.89 -	−0.10 +0.93
c-Quark tagging efficiency (eigenvector 2) [%]	+1.86 -	+0.94 -	+0.47 -	+0.60 -	+1.26 -	+1.43 -	+0.93 -	+0.50 -	+0.68 -	+1.53 -	+0.92 -	+0.56 -	+0.61 -
Light-jet tagging efficiency (eigenvector 0) [%]	+2.21 -	+1.32 -	+0.89 -	+0.88 -	+1.63 -	+1.81 -	+1.37 -	+0.97 -	- -	+2.12 -	+1.53 -	−0.22 -	- -
Light-jet tagging efficiency (eigenvector 1) [%]	+1.95 -	+1.02 -	+0.53 -	+0.50 -	+1.03 -	+1.63 -	+1.06 -	+0.59 -	+1.23 +0.66	+1.75 -	+1.12 -	+1.67 -	+0.89 +0.50
Light-jet tagging efficiency (eigenvector 2) [%]	+1.74 -	+0.93 -	+0.59 -	+0.58 -	+1.10 -	+1.27 -	+0.85 -	+0.51 -	+0.63 -	+1.45 -	+0.93 -	+0.57 -	+0.43 -
Light-jet tagging efficiency (eigenvector 3) [%]	+1.79 -	+0.90 -	+0.47 -	+0.57 -	+1.06 -	+1.39 -	+0.84 -	+0.57 -	+0.75 -	+1.37 -	+0.93 -	+0.80 -	+0.54 -
Light-jet tagging efficiency (eigenvector 4) [%]	+1.70 -	+0.85 -	+0.46 -	+0.49 -	+0.98 -	+1.27 -	+0.84 -	+0.49 -	+0.60 -	+1.35 -	+0.81 -	+0.56 -	+0.41 -
Light-jet tagging efficiency (eigenvector 5) [%]	+1.70 -	+0.85 -	+0.47 -	+0.49 -	+1.00 -	+1.28 -	+0.88 -	+0.53 -	+0.63 -	+1.43 -	+0.92 -	+0.74 -	+0.45 -
Light-jet tagging efficiency (eigenvector 6) [%]	+1.70 -	+0.85 -	+0.48 -	+0.52 -	+1.03 -	+1.27 -	+0.85 -	+0.49 -	+0.62 -	+1.38 -	+0.86 -	+0.64 -	+0.43 -
Light-jet tagging efficiency (eigenvector 7) [%]	+1.71 -	+0.87 -	+0.50 -	+0.54 -	+1.05 -	+1.28 -	+0.84 -	+0.50 -	+0.64 -	+1.40 -	+0.87 -	+0.64 -	+0.42 -
Light-jet tagging efficiency (eigenvector 8) [%]	+1.71 -	+0.87 -	+0.50 -	+0.52 -	+0.99 -	+1.27 -	+0.86 -	+0.51 -	+0.60 -	+1.37 -	+0.82 -	+0.58 -	+0.49 -
Light-jet tagging efficiency (eigenvector 9) [%]	+1.71 -	+0.87 -	+0.48 -	+0.49 -	+1.02 -	+1.27 -	+0.85 -	+0.50 -	+0.60 -	+1.34 -	+0.81 -	+0.56 -	+0.44 -
Light-jet tagging efficiency (eigenvector 10) [%]	+1.69 -	+0.84 -	+0.46 -	+0.49 -	+0.98 -	+1.26 -	+0.84 -	+0.49 -	+0.61 -	+1.35 -	+0.81 -	+0.58 -	+0.43 -
Light-jet tagging efficiency (eigenvector 11) [%]	+1.70 -	+0.85 -	+0.46 -	+0.50 -	+0.99 -	+1.26 -	+0.84 -	+0.49 -	+0.61 -	+1.34 -	+0.81 -	+0.56 -	+0.42 -
Light-jet tagging efficiency (eigenvector 12) [%]	+1.69 -	+0.84 -	+0.46 -	+0.49 -	+0.98 -	+1.25 -	+0.84 -	+0.49 -	+0.60 -	+1.34 -	+0.81 -	+0.57 -	+0.42 -
Light-jet tagging efficiency (eigenvector 13) [%]	+1.69 -	+0.85 -	+0.46 -	+0.49 -	+1.00 -	+1.26 -	+0.83 -	+0.49 -	+0.60 -	+1.34 -	+0.81 -	+0.56 -	+0.41 -
Light-jet tagging efficiency (eigenvector 14) [%]	+1.69 -	+0.84 -	+0.46 -	+0.49 -	+0.99 -	+1.26 -	+0.83 -	+0.49 -	+0.60 -	+1.34 -	+0.80 -	+0.56 -	+0.41 -
Light-jet tagging efficiency (eigenvector 15) [%]	+1.69 -	+0.84 -	+0.46 -	+0.49 -	+0.98 -	+1.25 -	+0.83 -	+0.48 -	+0.60 -	+1.34 -	+0.80 -	+0.56 -	+0.42 -
b-Quark tagging extrapolation [%]	+1.69 -	+0.85 -	+0.50 -	+0.66 -	+2.13 −0.35	+1.26 -	+0.84 -	+0.52 -	+0.78 -	+1.34 -	+0.81 -	+0.59 -	+0.65 -
b-Quark tagging extrapolation from c-Quark [%]	+1.73 -	+0.87 -	+0.47 -	+0.49 -	+0.99 -	+1.30 -	+0.87 -	+0.49 -	+0.61 -	+1.37 -	+0.83 -	+0.57 -	+0.42 -
Electron energy resolution [%]	+1.73 -	+0.83 -	+0.46 -	+0.49 -	+0.99 -	+1.28 -	+0.88 -	+0.49 -	+0.60 -	+1.31 -	+0.90 -	+0.57 -	- -
Electron energy scale [%]	+1.77 -	+0.89 -	+0.48 -	+0.36 -	- +0.76	+1.33 -	+0.85 -	+0.45 -	+0.51 -	+1.37 -	+0.89 -	+0.67 -	+0.26 -
Electron trigger efficiency [%]	+1.82 -	+0.96 -	+0.57 -	+0.59 -	+1.10 -	+1.38 -	+0.95 -	+0.59 -	+0.70 -	+1.46 -	+0.92 -	+0.67 -	+0.52 -
Electron reconstruction efficiency [%]	+1.76 -	+0.92 -	+0.55 -	+0.58 -	+1.09 -	+1.32 -	+0.91 -	+0.57 -	+0.70 -	+1.40 -	+0.88 -	+0.65 -	+0.52 -
Electron identification efficiency [%]	+2.04 -	+1.22 -	+0.91 -	+1.02 -	+1.60 -	+1.61 -	+1.22 -	+0.94 -	+1.15 -	+1.69 -	+1.19 -	+1.03 -	+0.99 −0.45
Electron isolation efficiency [%]	+1.74 -	+0.91 -	+0.60 -	+0.77 -	+1.42 -	+1.31 -	+0.90 -	+0.63 -	+0.89 -	+1.39 -	+0.88 -	+0.70 -	+0.74 -
Muon (ID) momentum resolution [%]	+1.76 -	+0.83 -	+0.54 -	+0.45 -	+1.12 -	+1.35 -	+0.94 -	+0.47 -	+0.58 -	+1.18 -	+0.77 -	+0.50 -	+0.74 -
Muon (MS) momentum resolution [%]	+1.78 -	+0.78 -	+0.59 -	+0.63 -	+0.56 -	+1.29 -	+0.86 -	+0.51 -	+0.40 -	+1.28 -	+0.80 -	+0.56 -	+0.71 -
Muon (ID) sagitta ρ [%]	+1.76 -	+0.84 -	+0.51 -	+0.60 -	+0.63 -	+1.36 -	+0.85 -	+0.52 -	+0.64 -	+1.04 -	+0.84 -	+0.62 -	- +0.18
Muon energy scale [%]	+1.75 -	+0.88 -	+0.58 -	+0.50 -	+1.01 -	+1.24 -	+0.87 -	+0.47 -	+0.62 -	+1.52 -	+0.86 -	+0.53 -	- +0.26
Muon trigger efficiency stat [%]	+1.99 -	+1.13 -	+0.73 -	+0.75 -	+1.25 -	+1.55 -	+1.12 -	+0.75 -	+0.86 -	+1.63 -	+1.09 -	+0.82 -	+0.67 -
Muon trigger efficiency syst [%]	+2.22 -	+1.34 -	+0.93 -	+0.94 -	+1.43 -	+1.78 -	+1.33 -	+0.96 -	+1.05 -	+1.85 -	+1.30 -	+1.03 -	+0.85 -
Muon identification stat [%]	+1.79 -	+0.94 -	+0.55 -	+0.57 -	+1.07 -	+1.35 -	+0.93 -	+0.57 -	+0.68 -	+1.43 -	+0.90 -	+0.65 -	+0.50 -
Muon identification syst [%]	+2.04 -	+1.19 -	+0.83 -	+0.90 -	+1.42 -	+1.61 -	+1.18 -	+0.85 -	+1.01 -	+1.69 -	+1.16 -	+0.93 -	+0.85 -
Muon isolation efficiency stat [%]	+1.70 -	+0.85 -	+0.47 -	+0.50 -	+1.00 -	+1.26 -	+0.84 -	+0.50 -	+0.61 -	+1.34 -	+0.81 -	+0.57 -	+0.43 -
Muon isolation efficiency syst [%]	+1.80 -	+0.95 -	+0.56 -	+0.58 -	+1.08 -	+1.37 -	+0.94 -	+0.58 -	+0.69 -	+1.44 -	+0.91 -	+0.65 -	+0.51 -
Muon TTVA efficiency stat [%]	+1.73 -	+0.88 -	+0.50 -	+0.52 -	+1.02 -	+1.30 -	+0.87 -	+0.52 -	+0.63 -	+1.38 -	+0.84 -	+0.59 -	+0.45 -
Muon TTVA efficiency syst [%]	+1.73 -	+0.88 -	+0.50 -	+0.52 -	+1.01 -	+1.29 -	+0.87 -	+0.52 -	+0.63 -	+1.37 -	+0.84 -	+0.59 -	+0.44 -
E_T^{miss} Soft jet resolution para [%]	±1.80	±1.04	±0.73	±0.64	±1.47	±1.42	±0.97	±0.56	±0.68	±1.41	±0.91	±0.84	±0.31
E_T^{miss} Soft jet resolution perp [%]	±1.83	±1.04	±0.57	±0.34	±1.50	±1.36	±1.06	±0.72	±0.32	±1.10	±1.08	±0.73	±0.54
E_T^{miss} Soft jet scale [%]	+1.99 -	+0.88 -	+0.61 -	+0.57 -	+0.40 -	+1.45 -	+1.08 -	+0.84 -	+0.57 -	+1.38 -	+1.02 -	+0.62 -	+0.75 -
Luminosity [%]	±2.05	±2.05	±2.05	±2.05	±2.05	±2.05	±2.05	±2.05	±2.05	±2.05	±2.05	±2.05	±2.05
Z+jets cross-section [%]	±0.77	±0.37	±0.10	-	±0.26	±0.75	±0.34	±0.12	-	±0.58	±0.34	±0.27	-
Monte Carlo sample statistics [%]	±0.26	±0.17	±0.27	±0.65	±2.35	±0.26	±0.21	±0.34	±0.79	±0.40	±0.36	±0.67	±1.71
ISR/FSR + scale [%]	-	+0.26 −0.31	+0.76 -	−3.94 +2.67	- −2.95	+0.76 -	+0.45 -	- −1.41	−2.15 +3.66	+1.73 −0.23	+1.36 −0.37	+1.97 -	−1.16 -
Alternate hard-scattering model [%]	±14.1	±3.42	±1.95	∓6.46	±8.65	±10.4	±2.72	∓2.34	∓4.80	±6.25	±6.51	±3.57	±5.46
Alternate parton-shower model [%]	±5.85	±0.99	∓2.91	∓3.95	±7.60	±3.72	∓1.00	∓4.01	∓2.32	∓0.80	∓2.99	∓2.97	∓1.06
Inter PDF [%]	±0.22	∓0.12	∓0.11	-	-	-	-	-	-	∓0.21	-	±0.23	±0.24
Intra PDF [%]	±0.33	±0.32	±0.22	±0.19	±0.30	±0.28	±0.32	±0.30	±0.47	±0.68	±0.79	±0.89	±0.78
Fakes overall normalization, el [%]	+3.72 −3.71	+0.95 −0.96	∓0.31	±2.11	∓0.53	+2.10 −2.11	+0.82 −0.83	∓0.17	∓0.23	±1.83	±1.21	±0.14	∓0.24
Fakes overall normalization, mu [%]	±0.20	±0.12	-	-	-	±0.18	-	-	∓0.10	±0.27	±0.22	-	±0.33
Fakes alternative parametrization [%]	∓0.91	±0.15	±0.21	∓0.96	±0.36	∓0.93	∓0.45	-	±0.28	∓0.44	-	±0.19	∓0.10
W+jets heavy flavour component [%]	±3.07	±1.57	±0.75	±0.55	±1.02	±2.45	±1.53	±0.80	±0.69	±2.26	±1.49	±0.88	±0.47
W+jets Scales [%]	±3.07	±1.64	±0.89	±0.93	±2.06	±2.39	±1.66	±0.98	±1.01	±2.15	±1.55	±1.19	±0.94
Single Top DS/DR [%]	∓0.24	±0.35	∓0.56	±0.66	∓2.23	∓0.19	∓0.26	±0.65	∓0.48	∓0.22	∓0.14	∓0.57	-
Single Top IFSR [%]	- −0.51	−0.29 -	- -	- −0.56	- −1.32	- −0.48	- −0.46	- −0.45	- −0.37	- −0.55	- −0.26	- −0.36	+1.02 -

TABLE F.53: Table of systematics for the absolute differential cross-section at the parton level for the $p_T^{t,had}$ vs $|y|_T^{t,had}$ observable.

Bins [GeV] x [GeV]	0–80	80–150	150–250	250–350	350–1000	1000–1100	1100–1200	1200–1330	1330–2000	2000–2125	2125–2250	2250–2370	2370–3000	3000–3125	3125–3250	3250–3400	3400–4000
$d\sigma$ / $dp_{T}^{t\bar{t}} vs p_{T}^{t,had}$ [pb/GeV x GeV]	$2.84 \cdot 10^{0}$	$3.32 \cdot 10^{0}$	$1.08 \cdot 10^{0}$	$1.96 \cdot 10^{-1}$	$8.28 \cdot 10^{-3}$	$6.60 \cdot 10^{-1}$	$7.20 \cdot 10^{-1}$	$1.92 \cdot 10^{-1}$	$6.71 \cdot 10^{-3}$	$1.37 \cdot 10^{-1}$	$1.74 \cdot 10^{-1}$	$6.42 \cdot 10^{-2}$	$3.41 \cdot 10^{-3}$	$1.63 \cdot 10^{-2}$	$3.07 \cdot 10^{-2}$	$2.39 \cdot 10^{-2}$	$3.30 \cdot 10^{-3}$
Total Uncertainty [%]	$^{+17.0}_{-16.8}$	±10.9	$^{+13.7}_{-13.6}$	±15.7	$^{+13.5}_{-14.0}$	$^{+21.7}_{-21.5}$	$^{+18.6}_{-18.4}$	$^{+11.9}_{-11.7}$	$^{+17.5}_{-17.0}$	$^{+20.7}_{-20.2}$	$^{+18.9}_{-19.1}$	±12.8	$^{+14.1}_{-21.3}$	±17.7	$^{+18.9}_{-19.3}$	$^{+15.6}_{-16.5}$	$^{+20.6}_{-25.9}$
Statistics [%]	±0.3	±0.2	±0.3	±0.7	±2.5	±0.3	±0.3	±0.6	±2.1	±0.8	±0.8	±1.5	±4.7	±3.2	±2.5	±3.1	±7.6
Systematics [%]	$^{+17.0}_{-16.8}$	±10.9	$^{+13.7}_{-13.6}$	±15.7	$^{+13.2}_{-13.7}$	$^{+21.7}_{-21.5}$	$^{+18.6}_{-18.4}$	$^{+11.8}_{-11.6}$	$^{+17.3}_{-16.8}$	$^{+20.7}_{-20.2}$	$^{+18.9}_{-19.0}$	±12.7	$^{+12.9}_{-20.6}$	$^{+17.2}_{-17.3}$	$^{+18.6}_{-19.1}$	$^{+15.1}_{-16.1}$	$^{+18.5}_{-24.2}$
Jet energy resolution [%]	∓3.05	∓2.39	∓2.22	∓1.77	∓2.79	±0.46	±0.36	∓0.11	∓0.47	±0.76	∓0.32	±1.24	±1.84	∓1.32	∓2.27	∓2.09	∓2.43
b-Tagged jet energy scale (JES) [%]	∓0.42	$^{+0.50}_{-0.49}$	$^{+0.90}_{-0.99}$	$^{+0.56}_{-0.33}$	$^{-}_{-0.70}$	$^{+0.46}_{-0.42}$	$^{+0.91}_{-0.93}$	$^{+0.76}_{-0.68}$	$^{+0.59}_{-}$	$^{+0.42}_{-}$	$^{+0.47}_{-0.77}$	$^{+0.72}_{-}$	$^{-}_{-2.85}$	$^{-0.37}_{+0.49}$	$^{-}_{-0.73}$	$^{+0.77}_{-0.65}$	$^{-2.53}_{+2.35}$
Effective detector NP set 1 (JES) [%]	-	-	-	-	$^{-}_{-1.25}$	-	-	$^{-}_{-0.20}$	-	$^{+0.30}_{-}$	$^{+0.16}_{-0.22}$	-	$^{-}_{-2.02}$	$^{+0.64}_{-}$	$^{-}_{-0.37}$	$^{-}_{-0.32}$	$^{+0.15}_{-1.64}$
Effective detector NP set 2 (JES) [%]	-	-	-	-	$^{-}_{-1.04}$	-	$^{+0.11}_{-0.17}$	-	$^{+0.29}_{-0.13}$	-	-	-	$^{-}_{-1.90}$	$^{+0.48}_{-}$	-	$^{-0.38}_{+0.22}$	$^{-0.78}_{-}$
Effective mixed NP set 1 (JES) [%]	$^{-0.39}_{+0.40}$	-	$^{+0.22}_{-0.27}$	$^{+0.28}_{-0.19}$	$^{-}_{-1.12}$	-	$^{+0.25}_{-0.13}$	$^{+0.32}_{-0.43}$	$^{+0.37}_{-0.47}$	$^{+0.35}_{-0.17}$	$^{+0.36}_{-0.40}$	$^{-}_{+0.31}$	$^{-}_{-2.79}$	$^{+0.74}_{-1.43}$	$^{-}_{-1.13}$	$^{+0.46}_{-0.16}$	$^{+1.01}_{-2.06}$
Effective mixed NP set 2 (JES) [%]	$^{+0.11}_{-}$	-	-	-	$^{-}_{-1.12}$	-	-	-	$^{-}_{-0.40}$	$^{-}_{+0.29}$	$^{-0.19}_{+0.20}$	-	$^{-}_{-3.40}$	$^{-0.26}_{-}$	-	$^{-0.23}_{+0.71}$	$^{+0.19}_{-0.48}$
Effective mixed NP set 3 (JES) [%]	-	-	-	-	$^{-}_{-1.21}$	-	-	$^{+0.17}_{-0.12}$	-	-	-	$^{+0.23}_{-}$	$^{-}_{-2.34}$	$^{+0.42}_{-0.21}$	$^{-}_{-0.40}$	$^{-}_{-0.21}$	$^{+0.92}_{-}$
Effective modelling NP set 1 (JES) [%]	$^{+2.39}_{-2.29}$	$^{+2.51}_{-2.55}$	$^{+1.91}_{-1.93}$	$^{+1.06}_{-0.70}$	$^{-}_{-1.25}$	$^{+3.84}_{-3.55}$	$^{+3.65}_{-3.47}$	$^{+2.43}_{-2.32}$	$^{+0.70}_{-0.63}$	$^{+3.86}_{-3.38}$	$^{+2.91}_{-2.84}$	$^{+1.26}_{-1.55}$	$^{-}_{-2.24}$	$^{+2.62}_{-2.38}$	$^{+1.16}_{-2.19}$	$^{+0.45}_{-1.63}$	$^{-}_{-1.50}$
Effective modelling NP set 2 (JES) [%]	$^{-0.51}_{+0.61}$	$^{-0.32}_{+0.25}$	-	-	$^{-}_{-0.83}$	$^{-0.40}_{+0.46}$	$^{-0.24}_{+0.22}$	-	$^{-}_{-0.14}$	$^{-0.20}_{+0.42}$	-	$^{-}_{-0.62}$	$^{-}_{-2.02}$	$^{-0.86}_{+0.36}$	$^{-}_{-0.24}$	$^{-0.66}_{-}$	$^{+3.13}_{-1.64}$
Effective modelling NP set 3 (JES) [%]	±0.57	±0.15	-	$^{+0.20}_{-}$	$^{-}_{-0.95}$	$^{+0.40}_{-0.30}$	-	$^{-}_{+0.30}$	$^{-}_{-0.37}$	-	-	$^{-}_{-0.42}$	$^{-}_{-4.27}$	$^{+0.68}_{-0.18}$	$^{-0.48}_{+0.17}$	$^{-0.34}_{-}$	$^{+1.47}_{-}$
Effective modelling NP set 4 (JES) [%]	$^{+0.11}_{-0.10}$	-	-	-	$^{-}_{-1.00}$	$^{+0.30}_{-}$	$^{+0.25}_{-0.16}$	$^{+0.17}_{-0.25}$	$^{+0.18}_{-0.99}$	$^{+0.40}_{-}$	$^{+0.38}_{-0.46}$	±0.50	$^{-}_{-2.36}$	$^{-}_{-0.33}$	$^{-}_{-0.33}$	$^{-}_{-0.95}$	$^{+0.45}_{-}$
Effective statistical NP set 1 (JES) [%]	$^{+0.52}_{-0.44}$	$^{+0.41}_{-0.43}$	$^{+0.27}_{-0.35}$	$^{+0.25}_{-0.19}$	$^{-}_{-1.57}$	$^{+0.65}_{-0.66}$	$^{+0.62}_{-0.52}$	$^{+0.14}_{-0.15}$	$^{+1.06}_{-}$	$^{+0.70}_{-0.63}$	$^{+0.57}_{-0.69}$	$^{+0.48}_{-0.23}$	$^{-}_{-2.37}$	$^{+0.86}_{-0.45}$	$^{-}_{-0.90}$	$^{-}_{-0.55}$	$^{+1.56}_{-}$
Effective statistical NP set 2 (JES) [%]	$^{-0.44}_{+0.51}$	$^{-0.41}_{+0.33}$	$^{-0.26}_{+0.27}$	$^{+0.27}_{-}$	$^{-}_{-0.52}$	$^{-0.46}_{+0.62}$	$^{-0.46}_{+0.49}$	$^{-0.45}_{+0.29}$	$^{-}_{-0.32}$	$^{-0.53}_{+0.67}$	$^{-0.56}_{+0.69}$	$^{-0.33}_{+0.11}$	$^{-}_{-2.93}$	-	$^{-}_{-0.61}$	$^{-0.61}_{+0.39}$	$^{+2.93}_{-1.01}$
Effective statistical NP set 3 (JES) [%]	-	-	-	-	$^{-}_{-0.35}$	-	-	-	∓0.35	$^{+0.57}_{-}$	-	$^{-}_{-0.82}$	$^{-}_{-1.52}$	$^{-0.41}_{+1.45}$	$^{-0.83}_{+0.69}$	$^{-}_{-0.79}$	$^{-}_{-0.46}$
Effective statistical NP set 4 (JES) [%]	$^{-0.37}_{+0.36}$	-	$^{+0.11}_{-0.20}$	-	$^{-}_{-0.90}$	$^{-0.10}_{+0.24}$	$^{+0.21}_{-}$	$^{+0.25}_{-0.14}$	$^{-}_{-0.36}$	-	$^{-}_{-0.24}$	$^{+0.19}_{-0.25}$	$^{-}_{-3.47}$	$^{-0.34}_{+1.46}$	$^{-}_{-0.52}$	$^{-}_{-0.98}$	$^{-}_{-1.97}$
Effective statistical NP set 5 (JES) [%]	-	-	$^{-0.19}_{-}$	-	$^{-}_{-1.02}$	-	$^{-0.17}_{+0.23}$	$^{-}_{+0.23}$	$^{+0.48}_{-0.32}$	$^{+0.42}_{-}$	-	$^{+0.34}_{-0.18}$	$^{-}_{-2.18}$	$^{+0.33}_{-}$	$^{-}_{-0.88}$	$^{-}_{+0.28}$	$^{+1.49}_{-}$
Effective statistical NP set 6 (JES) [%]	$^{+0.16}_{-}$	$^{-}_{-0.16}$	-	-	$^{-}_{-1.10}$	-	$^{+0.13}_{-0.14}$	-	$^{+0.66}_{-}$	-	-	$^{+0.10}_{-0.31}$	$^{-}_{-1.66}$	$^{+0.63}_{-0.60}$	$^{-}_{-0.37}$	$^{-}_{+0.24}$	$^{+2.30}_{-3.89}$
Effective statistical NP set 7 (JES) [%]	-	-	$^{-}_{-0.17}$	-	$^{-}_{-0.63}$	-	$^{+0.18}_{-}$	$^{+0.22}_{-0.19}$	$^{-}_{-0.29}$	$^{+0.30}_{-}$	$^{-}_{-0.33}$	$^{-}_{-0.90}$	$^{-}_{-2.65}$	$^{-0.23}_{+0.17}$	$^{+0.36}_{-0.31}$	$^{-}_{-0.51}$	$^{+2.13}_{-3.14}$
η intercalibration model (JES) [%]	$^{+0.21}_{-0.22}$	$^{+0.49}_{-0.53}$	$^{+0.62}_{-0.68}$	$^{+0.47}_{-0.25}$	$^{-}_{-1.60}$	$^{+0.94}_{-0.86}$	$^{+1.01}_{-0.98}$	$^{+0.80}_{-0.92}$	$^{+0.77}_{-}$	$^{+1.23}_{-0.94}$	$^{+0.96}_{-1.10}$	$^{+0.44}_{-}$	$^{-}_{-0.32}$	$^{+1.06}_{-0.55}$	$^{+0.14}_{-0.64}$	$^{+0.13}_{-0.81}$	$^{-}_{-2.54}$
η intercalibration non closure (JES) [%]	$^{-0.19}_{+0.14}$	$^{-0.17}_{+0.15}$	$^{-0.24}_{+0.23}$	$^{-}_{+0.31}$	$^{-}_{-1.39}$	$^{-0.46}_{+0.68}$	$^{-0.48}_{+0.53}$	$^{-0.32}_{+0.10}$	$^{+0.14}_{-0.35}$	$^{-0.59}_{+0.51}$	$^{-0.47}_{+0.28}$	∓0.38	$^{-}_{-2.05}$	$^{-0.49}_{+0.76}$	$^{-0.58}_{-}$	$^{-}_{-0.92}$	$^{+2.43}_{-2.38}$
η intercalibration total stat (JES) [%]	$^{+0.26}_{-0.17}$	$^{+0.37}_{-0.41}$	$^{+0.37}_{-0.48}$	-	$^{-}_{-0.99}$	$^{+0.70}_{-0.55}$	$^{+0.74}_{-0.65}$	$^{+0.44}_{-0.73}$	$^{+0.68}_{-}$	$^{+0.81}_{-0.84}$	$^{+0.64}_{-0.77}$	$^{+0.56}_{-}$	$^{-}_{-3.08}$	$^{+0.21}_{-0.50}$	$^{-}_{-0.19}$	$^{-}_{-1.16}$	$^{+1.03}_{-}$
Flavour composition (JES) [%]	$^{+2.41}_{-2.40}$	$^{+1.97}_{-2.35}$	$^{+1.38}_{-1.35}$	$^{+0.40}_{-0.55}$	$^{-}_{-1.22}$	$^{+3.73}_{-3.79}$	$^{+3.33}_{-3.45}$	$^{+2.28}_{-2.18}$	$^{+1.15}_{-0.41}$	$^{+3.91}_{-3.74}$	$^{+2.77}_{-3.35}$	$^{+1.61}_{-1.62}$	$^{-}_{-3.26}$	$^{+2.92}_{-4.03}$	$^{+0.41}_{-1.84}$	$^{-}_{-1.19}$	$^{-}_{-1.62}$
Flavour response (JES) [%]	∓1.01	$^{-1.20}_{+1.02}$	$^{-0.76}_{+0.80}$	$^{-0.15}_{+0.40}$	$^{-}_{-1.41}$	$^{-1.90}_{+1.75}$	∓1.79	$^{-1.21}_{+0.98}$	$^{-}_{-0.25}$	$^{-1.74}_{+1.93}$	$^{-1.85}_{+1.55}$	$^{-1.57}_{+0.95}$	$^{-1.27}_{+0.83}$	$^{-1.58}_{+0.94}$	$^{-0.92}_{+0.62}$	$^{-0.90}_{+0.35}$	$^{-1.04}_{+1.57}$
Pile-up offset μ (JES) [%]	$^{-}_{+0.19}$	$^{-0.26}_{+0.13}$	$^{-0.14}_{-}$	$^{-}_{+0.33}$	$^{-}_{-1.41}$	$^{-}_{+0.23}$	$^{-0.16}_{+0.28}$	$^{-0.36}_{+0.13}$	$^{-}_{-0.81}$	-	$^{-0.20}_{-}$	$^{-}_{-0.28}$	$^{-}_{-1.85}$	$^{+0.67}_{-}$	$^{+0.21}_{-}$	$^{-1.00}_{+0.31}$	$^{+2.13}_{-}$
Pile-up offset N_{PV} (JES) [%]	$^{+0.29}_{-0.19}$	$^{+0.43}_{-0.53}$	$^{+0.41}_{-0.31}$	$^{+0.24}_{-0.21}$	$^{-}_{-0.67}$	$^{+0.84}_{-0.69}$	$^{+0.83}_{-0.77}$	$^{+0.88}_{-0.86}$	$^{+0.59}_{-}$	$^{+1.32}_{-0.80}$	$^{+0.86}_{-0.87}$	$^{+0.82}_{-0.12}$	$^{+0.34}_{-1.47}$	$^{-0.61}_{-}$	$^{-}_{-0.84}$	$^{-1.20}_{+0.26}$	$^{-0.73}_{+1.93}$
Pile-up offset p_T (JES) [%]	$^{-0.96}_{+0.94}$	$^{-0.30}_{+0.26}$	$^{+0.39}_{-0.41}$	$^{+0.51}_{-0.24}$	$^{-}_{-1.15}$	$^{-0.25}_{+0.31}$	$^{+0.19}_{-0.13}$	$^{+0.40}_{-0.28}$	-	$^{+0.21}_{-0.22}$	$^{+0.14}_{-0.21}$	-	$^{-}_{-1.53}$	$^{-0.88}_{+0.26}$	$^{-}_{-0.74}$	$^{-}_{-0.61}$	$^{+0.76}_{-3.81}$
Pile-up offset ρ topology (JES) [%]	$^{+3.02}_{-2.90}$	$^{+3.66}_{-3.74}$	$^{+3.23}_{-3.08}$	$^{+1.38}_{-1.29}$	$^{-1.46}_{+0.13}$	$^{+5.54}_{-5.11}$	$^{+5.63}_{-5.33}$	$^{+3.88}_{-3.87}$	$^{+1.97}_{-0.37}$	$^{+5.54}_{-4.82}$	$^{+4.38}_{-4.52}$	$^{+2.86}_{-2.28}$	$^{+2.09}_{-3.06}$	$^{+2.85}_{-3.75}$	$^{+2.27}_{-2.77}$	$^{-}_{-1.46}$	$^{-1.99}_{+1.15}$
Punch-through (JES) [%]	-	-	-	-	$^{-}_{-0.58}$	-	-	-	$^{-0.52}_{+0.43}$	-	-	-	$^{-}_{-0.46}$	$^{+0.71}_{-}$	$^{+0.20}_{-0.19}$	$^{-}_{-0.64}$	$^{-}_{-1.08}$
Single particle high-p_T (JES) [%]	-	-	-	-	$^{-}_{-0.74}$	-	-	-	$^{+0.44}_{-}$	-	-	$^{+0.33}_{-}$	$^{-}_{-0.46}$	$^{+0.72}_{-}$	$^{+0.40}_{-}$	$^{-}_{-0.45}$	$^{+0.95}_{-1.25}$
Jet vertex fraction [%]	$^{+1.10}_{-1.13}$	$^{+0.82}_{-0.85}$	$^{+0.50}_{-0.53}$	$^{+0.30}_{-0.32}$	$^{+0.34}_{-0.37}$	$^{+1.04}_{-1.07}$	$^{+0.82}_{-0.85}$	$^{+0.51}_{-0.55}$	$^{+0.42}_{-0.45}$	$^{+0.97}_{-1.01}$	$^{+0.72}_{-0.76}$	$^{+0.44}_{-0.48}$	$^{+0.48}_{-0.52}$	$^{+0.92}_{-0.96}$	$^{+0.61}_{-0.65}$	$^{+0.40}_{-0.44}$	$^{+0.52}_{-0.54}$
b-Quark tagging efficiency (eigenvector 0) [%]	$^{-7.90}_{+8.18}$	$^{-6.78}_{+6.99}$	$^{-5.68}_{+5.83}$	$^{-5.14}_{+5.27}$	$^{-5.81}_{+5.97}$	$^{-6.67}_{+6.86}$	$^{-5.83}_{+5.97}$	$^{-5.06}_{+5.17}$	$^{-5.43}_{+5.55}$	$^{-6.58}_{+6.75}$	$^{-5.88}_{+6.01}$	$^{-5.21}_{+5.32}$	$^{-6.08}_{+6.25}$	$^{-7.22}_{+7.41}$	$^{-6.27}_{+6.42}$	$^{-5.43}_{+5.56}$	$^{-5.96}_{+6.09}$
b-Quark tagging efficiency (eigenvector 1) [%]	∓0.98	$^{-1.49}_{+1.50}$	$^{-2.28}_{+2.30}$	$^{-3.14}_{+3.19}$	$^{-3.56}_{+3.62}$	$^{-1.48}_{+1.49}$	$^{-1.93}_{+1.94}$	$^{-2.61}_{+2.64}$	$^{-3.15}_{+3.20}$	$^{-1.99}_{+2.01}$	$^{-2.31}_{+2.34}$	$^{-2.92}_{+2.95}$	$^{-3.15}_{+3.19}$	$^{-2.34}_{+2.36}$	$^{-2.49}_{+2.51}$	$^{-2.83}_{+2.86}$	$^{-3.06}_{+3.09}$
b-Quark tagging efficiency (eigenvector 2) [%]	$^{+1.74}_{-1.73}$	$^{+1.46}_{-1.45}$	$^{+1.01}_{-1.00}$	±0.42	∓0.10	$^{+1.42}_{-1.41}$	±1.19	±0.76	±0.25	±0.99	±0.85	±0.48	±0.15	±0.61	$^{+0.67}_{-0.66}$	±0.51	$^{+0.10}_{-0.11}$
b-Quark tagging efficiency (eigenvector 3) [%]	∓0.33	-	±0.28	±0.28	∓0.20	-	±0.15	±0.30	-	-	±0.14	±0.16	∓0.12	∓0.27	-	-	∓0.32
c-Quark tagging efficiency (eigenvector 0) [%]	±0.42	±0.29	±0.19	±0.12	-	±0.33	±0.27	±0.19	±0.18	±0.34	±0.30	±0.18	±0.19	±0.44	±0.28	$^{+0.15}_{-0.14}$	±0.19
c-Quark tagging efficiency (eigenvector 1) [%]	-	∓0.12	∓0.24	$^{-0.33}_{+0.34}$	∓0.47	∓0.14	∓0.22	∓0.35	∓0.45	∓0.28	∓0.35	∓0.46	∓0.50	∓0.23	∓0.37	∓0.47	∓0.63
c-Quark tagging efficiency (eigenvector 2) [%]	±0.19	±0.12	-	-	∓0.20	±0.11	-	-	∓0.16	-	-	∓0.10	∓0.17	-	-	-	∓0.21
Light-jet tagging efficiency (eigenvector 0) [%]	$^{-0.52}_{+0.49}$	$^{-0.48}_{+0.49}$	∓0.39	∓0.36	$^{-0.54}_{+0.53}$	$^{-0.67}_{+0.69}$	$^{-0.62}_{+0.64}$	$^{-0.56}_{+0.57}$	$^{-0.62}_{+0.64}$	$^{-0.88}_{+0.90}$	$^{-0.86}_{+0.88}$	$^{-1.12}_{+1.24}$	$^{-1.02}_{+1.01}$	$^{-0.84}_{+0.86}$	$^{-0.76}_{+0.75}$	$^{-0.73}_{+0.75}$	∓1.02
Light-jet tagging efficiency (eigenvector 1) [%]	$^{+0.34}_{-0.33}$	±0.22	±0.11	-	-	±0.27	±0.20	-	-	$^{+0.28}_{-0.27}$	±0.20	-	±0.11	±0.24	$^{+0.10}_{-0.11}$	-	$^{+0.33}_{-0.34}$
Light-jet tagging efficiency (eigenvector 2) [%]	-	-	-	-	-	-	-	±0.10	-	-	-	$^{+0.26}_{-0.25}$	±0.13	-	±0.17	-	∓0.15
Light-jet tagging efficiency (eigenvector 3) [%]	$^{+0.10}_{-0.11}$	-	-	-	-	-	-	-	$^{-0.13}_{+0.14}$	-	-	$^{-0.30}_{+0.32}$	∓0.14	-	-	-	$^{-0.22}_{+0.21}$
Light-jet tagging efficiency (eigenvector 5) [%]	-	-	-	-	-	-	-	-	-	-	-	$^{-0.17}_{+0.18}$	-	-	-	-	-
b-Quark tagging extrapolation [%]	-	-	-	-	±0.58	-	-	-	±0.35	-	-	±0.16	±0.57	±0.68	±0.44	±0.41	$^{+1.09}_{-1.08}$
Electron energy resolution [%]	-	-	-	-	$^{-}_{-0.89}$	-	-	-	-	-	-	$^{-0.24}_{-}$	$^{-0.20}_{+0.10}$	$^{-0.50}_{+0.14}$	$^{+0.35}_{-}$	$^{-}_{-0.39}$	$^{-0.57}_{+0.25}$
Electron energy scale [%]	-	-	-	-	$^{-}_{-0.79}$	-	-	-	$^{+0.31}_{-}$	-	-	$^{-}_{-0.38}$	$^{-}_{-0.84}$	$^{-0.17}_{+0.81}$	-	$^{-}_{-0.57}$	$^{+0.37}_{-}$
Electron trigger efficiency [%]	±0.13	±0.12	±0.10	±0.10	±0.10	±0.12	±0.11	±0.11	±0.10	±0.11	±0.12	±0.12	±0.11	±0.10	±0.11	±0.11	±0.12
Electron reconstruction efficiency [%]	-	-	-	±0.10	±0.11	-	-	-	±0.10	-	-	-	-	±0.11	±0.10	-	-
Electron identification efficiency [%]	±0.33	±0.36	±0.43	±0.54	±0.67	±0.37	±0.39	±0.45	±0.57	±0.48	±0.43	±0.40	±0.50	±0.69	±0.57	±0.43	±0.39
Electron isolation efficiency [%]	-	-	±0.10	±0.27	±0.51	-	-	±0.15	±0.34	±0.15	±0.13	±0.11	±0.21	±0.48	±0.32	±0.14	-
Muon (ID) momentum resolution [%]	-	-	-	-	$^{-}_{-0.53}$	-	-	-	-	$^{+0.30}_{-}$	$^{-}_{-0.29}$	$^{+0.33}_{-}$	$^{-}_{-1.83}$	$^{+0.57}_{-}$	$^{-}_{-0.45}$	$^{-}_{-1.02}$	$^{-2.81}_{+0.28}$
Muon (MS) momentum resolution [%]	-	-	-	-	$^{-}_{-0.53}$	-	-	-	$^{+0.48}_{-}$	$^{+0.33}_{-}$	-	$^{+0.56}_{-}$	$^{-}_{-1.52}$	$^{+0.43}_{-}$	-	$^{-0.35}_{+0.44}$	$^{-3.24}_{+0.12}$
Muon (ID) sagitta o [%]	-	-	-	-	$^{-}_{-0.57}$	-	-	-	$^{+0.25}_{-}$	$^{-}_{+0.14}$	-	-	$^{+0.50}_{-}$	$^{+0.76}_{-}$	-	$^{-}_{-0.21}$	$^{-}_{-2.11}$
Muon energy scale [%]	-	-	-	-	$^{-}_{-0.70}$	-	-	-	$^{-}_{-0.47}$	$^{+0.30}_{-}$	$^{-0.18}_{-}$	$^{+0.56}_{-}$	$^{-}_{-1.60}$	$^{+0.42}_{-}$	$^{-}_{-0.93}$	$^{-0.21}_{+0.11}$	$^{+0.93}_{-0.54}$
Muon trigger efficiency stat [%]	±0.30	$^{+0.28}_{-0.29}$	$^{+0.26}_{-0.27}$	$^{+0.25}_{-0.26}$	±0.24	±0.29	±0.28	±0.27	$^{+0.25}_{-0.26}$	±0.28	$^{+0.28}_{-0.29}$	$^{+0.28}_{-0.29}$	±0.27	±0.28	±0.27	$^{+0.27}_{-0.28}$	$^{+0.32}_{-0.33}$
Muon trigger efficiency syst [%]	$^{+0.53}_{-0.52}$	$^{+0.50}_{-0.49}$	$^{+0.47}_{-0.46}$	$^{+0.44}_{-0.43}$	$^{+0.42}_{-0.41}$	$^{+0.51}_{-0.50}$	$^{+0.49}_{-0.48}$	$^{+0.48}_{-0.47}$	$^{+0.45}_{-0.44}$	$^{+0.49}_{-0.48}$	$^{+0.50}_{-0.49}$	$^{+0.51}_{-0.50}$	$^{+0.49}_{-0.48}$	$^{+0.48}_{-0.47}$	$^{+0.47}_{-0.46}$	$^{+0.49}_{-0.48}$	$^{+0.54}_{-0.53}$
Muon identification stat [%]	±0.10	-	-	-	-	-	-	-	-	-	-	-	-	-	-	-	±0.11
Muon identification syst [%]	±0.35	±0.34	±0.35	±0.41	±0.47	±0.35	±0.35	±0.37	$^{+0.43}_{-0.42}$	±0.38	±0.36	±0.36	±0.39	$^{+0.49}_{-0.48}$	±0.42	±0.37	±0.39
Muon isolation efficiency syst [%]	±0.11	±0.10	-	-	-	±0.10	±0.10	±0.10	-	±0.10	±0.10	±0.10	±0.10	±0.10	±0.10	±0.10	±0.11
E_{T}^{miss} Soft jet resolution para [%]	±0.18	±0.16	-	-	∓0.64	±0.14	±0.23	±0.36	±0.58	-	±0.23	±0.50	∓0.77	±0.21	∓0.44	-	±2.09
E_{T}^{miss} Soft jet resolution perp [%]	-	±0.12	±0.18	±0.23	∓0.89	±0.14	±0.34	-	∓0.16	-	±0.28	±0.33	∓0.12	∓0.67	∓0.41	-	±1.05
E_{T}^{miss} Soft jet scale [%]	$^{+0.21}_{-0.23}$	$^{+0.10}_{-0.23}$	$^{+0.21}_{-0.29}$	-	$^{-}_{-1.09}$	$^{+0.18}_{-}$	$^{+0.30}_{-}$	$^{+0.16}_{-0.12}$	$^{+0.21}_{-}$	$^{+0.27}_{-}$	-	$^{+0.44}_{-}$	$^{-}_{-2.94}$	$^{-0.36}_{+0.12}$	$^{-}_{-0.65}$	$^{+0.27}_{-0.88}$	$^{-}_{-0.49}$
Luminosity [%]	∓2.05	∓2.05	∓2.05	∓2.05	∓2.05	∓2.05	∓2.05	∓2.05	∓2.05	∓2.05	∓2.05	∓2.05	∓2.05	∓2.05	∓2.05	∓2.05	∓2.05
Z+jets cross-section [%]	±0.84	±0.40	±0.10	-	-	±0.49	±0.30	±0.17	±0.11	±0.48	±0.48	±0.79	±0.28	±0.35	±0.33	±0.40	±0.63
Monte Carlo sample statistics [%]	±0.28	±0.15	±0.21	±0.45	±1.47	±0.29	±0.22	±0.39	±1.30	±0.50	±0.50	±1.22	±2.87	±1.99	±1.52	±1.86	±4.78
ISR/FSR + scale [%]	$^{-0.11}_{+0.68}$	$^{+0.24}_{-}$	$^{+0.65}_{-}$	$^{-2.12}_{+0.75}$	$^{+5.39}_{-}$	$^{-}_{-0.48}$	$^{+0.38}_{-1.06}$	$^{+1.91}_{-}$	$^{+3.14}_{-}$	$^{+0.70}_{-}$	$^{-0.38}_{-}$	$^{-0.30}_{+0.69}$	$^{-}_{-6.00}$	$^{-3.81}_{+4.05}$	$^{-0.43}_{+1.51}$	$^{-}_{-3.38}$	$^{-}_{-13.5}$
Alternate hard-scattering model [%]	±12.5	±2.85	∓5.26	∓7.96	∓6.82	±10.0	±7.56	±4.20	±13.6	±9.32	±7.92	±1.51	±2.22	±11.0	±14.9	±4.19	∓1.24
Alternate parton-shower model [%]	±1.19	∓4.02	∓9.45	∓11.3	∓5.73	±15.5	±13.2	±6.88	±6.73	±14.4	±14.1	±9.46	±7.53	±6.03	±6.77	±12.2	±12.3
Inter PDF [%]	∓0.24	∓0.20	∓0.13	-	∓0.10	∓0.26	∓0.19	-	-	∓0.22	∓0.16	∓0.10	-	-	-	-	±0.13
Intra PDF [%]	±0.84	±0.86	±0.75	±0.52	±0.23	±0.59	±0.62	±0.56	±0.46	±0.35	±0.39	±0.43	±0.24	±0.41	±0.35	±0.53	±0.52
Fakes overall normalization, el [%]	±3.26	±0.86	±0.43	-	∓0.35	±2.17	±0.91	±0.44	∓0.16	±0.54	±0.20	-	∓0.18	$^{-0.23}_{+0.24}$	-	±1.38	-
Fakes overall normalization, mu [%]	±0.20	±0.10	-	∓0.12	∓0.19	±0.21	±0.16	±0.10	±0.14	±0.25	±0.19	±0.12	±0.98	±0.34	-	±0.18	∓0.12
Fakes alternative parametrization [%]	∓0.75	-	-	-	-	∓0.91	∓0.38	∓0.30	-	∓0.19	∓0.12	±0.70	±5.88	∓0.75	∓0.67	∓1.17	±2.41
W+jets heavy flavour component [%]	±1.41	±0.78	±0.37	±0.14	-	±0.88	±0.60	±0.30	±0.16	±0.83	±0.57	-	-	±0.15	-	-	-
W+jets Scales [%]	±1.26	±0.73	±0.37	±0.15	±0.30	±1.09	±0.92	±0.63	±0.63	±1.56	±1.58	±1.12	±1.10	±1.90	±1.31	±1.52	±2.07
Single Top DS/DR [%]	∓0.14	∓0.15	∓0.35	∓0.27	∓0.37	∓0.39	∓0.52	∓0.70	∓0.54	∓0.99	∓1.05	∓1.65	∓1.69	∓2.23	∓2.14	∓1.68	∓2.57
Single Top IFSR [%]	$^{-}_{-0.55}$	$^{-}_{-0.42}$	$^{-}_{-0.23}$	-	$^{-}_{-0.63}$	$^{-}_{-0.46}$	$^{-}_{-0.37}$	$^{-}_{-0.32}$	$^{+0.40}_{-0.11}$	$^{-}_{-0.38}$	$^{-}_{-0.46}$	$^{-}_{-1.41}$	$^{+0.40}_{-2.49}$	$^{-}_{-1.26}$	$^{+0.16}_{-0.81}$	$^{+0.71}_{-}$	$^{+0.17}_{-2.41}$

TABLE F.54: Table of systematics for the absolute differential cross-section at the parton level for the $p_{T}^{t,had}$ vs $p_{T}^{t\bar{t}}$ observable.

F.2.1.2 Boosted topology

Bins [GeV]	490–831.99	831.99–1007.69	1007.69–1192.80	1192.80–1406.15	1406.15–1657.15	1657.15–1948.94	1948.94–3000
$d\sigma$ / $dm^{t\bar{t}}[GeV]$: $m^{t\bar{t}}$ [pb/GeV]	$1.27 \cdot 10^{-2}$	$2.20 \cdot 10^{-2}$	$1.21 \cdot 10^{-2}$	$5.88 \cdot 10^{-3}$	$2.31 \cdot 10^{-3}$	$8.28 \cdot 10^{-4}$	$1.12 \cdot 10^{-4}$
Total Uncertainty [%]	+7.18 −6.71	+8.88 −8.89	+12.9 −12.6	+12.4 −10.5	+12.7 −13.8	+20.9 −19.7	+42.5 −38.9
Statistics [%]	±1.2	±1.1	±1.4	±1.9	±2.9	±5.2	±9.0
Systematics [%]	+7.03 −6.55	+8.78 −8.79	+12.8 −12.5	+12.2 −10.3	+12.2 −13.4	+20.0 −18.8	+41.3 −37.6
b-Tagged jet energy scale (JES) [%]	±0.16	+0.50 −0.56	+0.67 −0.69	+0.66 −0.79	+0.45 −0.35	+0.70 −0.50	+0.65 −0.56
Effective detector NP set 1 (JES) [%]	-	+0.14 −0.13	+0.20 −0.24	+0.24 −0.26	-	+0.26 −0.34	+0.57 −0.52
Effective detector NP set 2 (JES) [%]	+0.13 -	+0.11 −0.13	+0.21 −0.17	- −0.15	-	- −0.12	+0.28 −0.18
Effective mixed NP set 1 (JES) [%]	+0.50 −0.29	+0.79 −1.23	+1.63 −1.52	+2.25 −1.52	+1.43 −2.35	+3.45 −2.33	+3.93 −3.56
Effective mixed NP set 2 (JES) [%]	-	−0.11 +0.12	−0.14 +0.16	−0.23 +0.19	−0.10 +0.16	−0.15 +0.21	−0.33 +0.40
Effective mixed NP set 3 (JES) [%]	-	-	-	-	-	-	+0.30 −0.17
Effective modelling NP set 1 (JES) [%]	+1.61 −1.18	+1.29 −1.67	+1.74 −1.53	+1.84 −1.91	+1.52 −1.36	+1.01 −0.97	+2.50 −2.01
Effective modelling NP set 2 (JES) [%]	-	+0.32 −0.43	+0.76 −0.61	+0.82 −0.69	+0.62 −1.14	+1.90 −1.80	+2.86 −1.71
Effective modelling NP set 3 (JES) [%]	−0.13 +0.21	−0.50 +0.43	−0.60 +0.67	−0.72 +0.58	−0.38 +0.49	−0.28 +0.36	−0.49 +0.64
Effective modelling NP set 4 (JES) [%]	+0.11 −0.13	+0.14 −0.11	+0.17 −0.22	+0.19 −0.18	+0.15 −0.12	+0.33 −0.36	+0.65 −0.51
Effective statistical NP set 1 (JES) [%]	+0.16 -	+0.17 −0.15	+0.23 −0.25	+0.40 −0.39	+0.19 −0.76	+0.26 −0.50	+0.89 −0.87
Effective statistical NP set 2 (JES) [%]	−0.24 +0.21	-	-	-	+0.13 −0.19	+0.53 −0.68	+0.65 −0.59
Effective statistical NP set 3 (JES) [%]	-	−0.34	−0.58	−0.93	−0.82	−0.99	−0.84
Effective statistical NP set 4 (JES) [%]	+0.26 −0.20	+0.23 +0.37 −0.39	+0.74 +0.24 −0.27	+0.83 +0.14 −0.23	+0.55 -	+0.39 +0.21 -	+1.34 −0.36 +0.26
Effective statistical NP set 5 (JES) [%]	-	+0.30 −0.23	+0.19 −0.32	−0.19 -	-	−0.35 +0.13	−0.26 +0.18
Effective statistical NP set 6 (JES) [%]	-	-	±0.13	-	-	-	∓0.29
Effective statistical NP set 7 (JES) [%]	+0.13 −0.12	±0.16	±0.26	+0.34 −0.33	+0.20 −0.31	+0.27 −0.22	±0.44
η intercalibration model (JES) [%]	+0.85 −0.28	+0.47 −0.84	+1.07 −1.11	+1.57 −1.47	+1.32 −1.43	+1.76 −1.64	+3.18 −2.69
η intercalibration non closure (JES) [%]	-	−0.61	−0.68	−0.77	−0.90	−0.49	−0.57
η intercalibration total stat (JES) [%]	+0.39 +0.31	+0.47 +0.34	+0.53 ±0.43	+0.98 +0.42	+0.47 +0.38	+0.70 +0.34	+1.19 +0.57
Flavour composition (JES) [%]	−0.33 +1.89	−0.36 +1.53	+2.09	−0.49 +2.61	−0.26 +1.84	−0.46 +2.52	−0.93 +5.82
Flavour response (JES) [%]	−1.55 −0.93	−2.00 −1.12	−1.80 −1.03	−2.12 −1.15	−2.62 −0.88	−2.67 −0.83	−4.70 −0.69
Pile-up offset μ (JES) [%]	+0.98 -	+0.92 −0.16	+1.17 -	+1.15 -	+0.80 −0.27	+0.29 -	+1.43 -
Pile-up offset N_{PV} (JES) [%]	+0.11 +0.38	+0.15 +0.40	+0.63	+0.12 +0.61	+0.21 +0.17	+0.35 +0.43	−0.21 +0.58
Pile-up offset p_T (JES) [%]	−0.41 +0.63	−0.48 +0.76	−0.49 +1.45	−0.28 +1.62	−0.14 +0.66	−0.54 +2.00	−0.44 +2.23
Pile-up offset ρ topology (JES) [%]	−0.44 +2.46	−1.08 +2.14	−1.23 +2.55	−1.39 +2.93	−1.25 +1.62	−1.57 +1.08	−1.90 +3.41
Punch-through (JES) [%]	−2.01	−2.73	−2.14	−2.35	−1.97	−1.36	−3.46 +0.18
Jet vertex fraction [%]	-	-	-	-	-	-	−0.19
b-Quark tagging efficiency (eigenvector 0) [%]	+0.34 −0.38	+0.25 −0.28	+0.23 −0.27	+0.21 −0.26	+0.23 −0.28	+0.28 −0.33	+0.35 −0.41
b-Quark tagging efficiency (eigenvector 1) [%]	−1.73 +1.67	−1.47 +1.41	−1.55 +1.47	−1.67 +1.60	−1.72 +1.63	−1.83 +1.74	−2.56 +2.48
b-Quark tagging efficiency (eigenvector 2) [%]	−0.83 +0.81	−1.15 +1.12	−1.32 +1.27	−1.45 +1.40	−1.60 +1.55	−1.66 +1.60	−2.18 +2.13
b-Quark tagging efficiency (eigenvector 3) [%]	±0.23	-	∓0.14	∓0.22	∓0.27	∓0.26	∓0.43
b-Quark tagging efficiency (eigenvector 4) [%]	-	-	-	−0.12 +0.11	∓0.17	∓0.20	∓0.36
c-Quark tagging efficiency (eigenvector 0) [%]	-	-	-	-	-	-	∓0.11
c-Quark tagging efficiency (eigenvector 1) [%]	±0.10 −0.15	-	-	-	-	-	±0.15 −1.32
c-Quark tagging efficiency (eigenvector 2) [%]	+0.14 -	∓0.21 -	∓0.26 ∓0.10	∓0.39 ∓0.12	∓0.52 ∓0.20	∓0.65 ∓0.30	+1.33 ∓0.56
Light-jet tagging efficiency (eigenvector 0) [%]	∓0.41	−0.37 +0.38	∓0.48	−0.73 +0.74	−0.86 +0.85	−1.13 +1.12	−2.81 +2.80
Light-jet tagging efficiency (eigenvector 1) [%]	-	-	-	-	∓0.11	∓0.22	∓0.91
Light-jet tagging efficiency (eigenvector 2) [%]	-	-	-	±0.11	-	-	-
Light-jet tagging efficiency (eigenvector 3) [%]	-	-	∓0.14	∓0.20	∓0.27	∓0.30	∓0.70
Light-jet tagging efficiency (eigenvector 4) [%]	-	-	-	-	-	-	±0.10
Light-jet tagging efficiency (eigenvector 5) [%]	-	-	-	-	-	±0.22	±0.49
Light-jet tagging efficiency (eigenvector 6) [%]	-	-	-	-	-	∓0.18	−0.16 +0.17
Light-jet tagging efficiency (eigenvector 7) [%]	-	-	-	-	-	∓0.10	∓0.35
Light-jet tagging efficiency (eigenvector 9) [%]	-	-	-	-	-	-	∓0.11
b-Quark tagging extrapolation [%]	-	±0.14	±0.41	+0.61 −0.62	+0.98 −0.99	+1.26 −1.29	+2.50 −2.53
Electron energy resolution [%]	-	-	-	-	-	+0.25 -	-
Electron energy scale [%]	-	-	-	-	- −0.15	+0.70 -	+0.38 −0.80
Electron trigger efficiency [%]	±0.11	±0.11	±0.11	±0.12	±0.13	±0.15	±0.21
Electron reconstruction efficiency [%]	-	±0.10	±0.11	±0.12	±0.13	±0.14	±0.19
Electron identification efficiency [%]	±0.50	±0.60	±0.67	±0.72	±0.80	±0.93	±1.23
Electron isolation efficiency [%]	±0.20	±0.40	±0.52	±0.60	±0.71	±0.82	±1.05
Muon (ID) momentum resolution [%]	-	-	-	-	-	-	- −0.96
Muon (MS) momentum resolution [%]	-	-	-	-	- −0.11	-	-
Muon energy scale [%]	-	-	-	-	-	-	-
Muon trigger efficiency stat [%]	±0.28	±0.27	±0.28	±0.29	±0.30	±0.32	+0.35 −0.36
Muon trigger efficiency syst [%]	+0.49 −0.48	+0.47 −0.46	+0.49 −0.48	+0.52 −0.51	+0.55 −0.53	+0.56 −0.55	+0.66 −0.64
Muon identification stat [%]	-	-	-	-	±0.10	±0.11	±0.13
Muon identification syst [%]	+0.40 −0.39	+0.46 −0.45	±0.53	±0.59	+0.67 −0.66	+0.74 −0.73	±0.93
Muon isolation efficiency syst [%]	±0.10	-	±0.10	±0.11	±0.13	±0.15	±0.20
E_T^{miss} Soft jet resolution para [%]	±0.42	∓0.45	∓0.50	∓0.12	∓0.89	∓0.41	∓0.80
E_T^{miss} Soft jet resolution perp [%]	±0.54	∓0.26	∓0.61	∓0.35	∓0.47	∓0.49	∓1.28
E_T^{miss} Soft jet scale [%]	+0.37 −0.34	−0.23 -	−0.40 +0.42	−0.42 +0.64	−0.73 +0.38	−0.61 +0.55	−1.34 +0.75
Luminosity [%]	∓2.05	∓2.05	∓2.05	∓2.05	∓2.05	∓2.05	∓2.05
Z+jets cross-section [%]	±0.46	±0.26	±0.38	±0.60	±0.85	±1.28	±2.61
Diboson cross-section [%]	-	-	-	-	-	-	±0.10
$t\bar{t}V$ cross-section [%]	±0.13	±0.10	±0.11	±0.14	±0.16	±0.18	±0.25
Monte Carlo sample statistics [%]	±0.76	±0.66	±0.86	±1.18	±1.75	±2.83	±4.11
ISR/FSR + scale [%]	+1.70 -	+4.08 −2.79	+5.29 −4.92	+7.21 −4.09	+5.46 −6.71	+12.4 −10.5	+21.0 −12.1
Alternate hard-scattering model [%]	∓2.30	∓5.10	∓9.00	±0.39	∓3.06	∓4.38	±20.7
Alternate parton-shower model [%]	±0.97	∓1.80	∓1.90	∓3.01	∓2.45	±1.24	∓7.83
Fakes overall normalization, el [%]	±0.86	±0.55	±0.63	±0.65	±1.22	+2.92 −2.93	+5.31 −5.29
Fakes overall normalization, mu [%]	±0.36	±0.28	±0.23	±0.42	±0.30	±0.30	±0.42
Fakes alternative parametrization [%]	∓2.44	∓1.67	∓1.72	∓2.16	∓3.06	∓6.47	∓11.4
W+jets heavy flavour component [%]	±0.10	±0.13	-	-	-	±0.15	±0.21
W+jets Scales [%]	±2.50	±1.85	±2.92	±4.74	±6.40	±9.42	±19.3
W+jets α_S [%]	−0.14 +0.17	−0.12 +0.13	−0.19 +0.21	−0.29 +0.34	−0.40 +0.50	−0.53 +0.71	−1.12 +1.44
Single Top DS/DR [%]	∓0.86	∓1.26	∓1.99	∓3.20	∓4.71	∓5.69	∓9.20
Single Top IFSR [%]	+0.19 −0.29	- −0.50	- −0.53	+0.89 −0.93	- −0.97	+0.40 −1.08	+1.20 −3.61

TABLE F.55: Table of systematics for the absolute differential cross-section at the parton level for the $m_{t\bar{t}}$observable.

Bins [GeV]	350–410	410–475	475–545	545–630	630–845	845–2000
$d\sigma$ / $dp_T^{t,had}$ [pb/GeV]	$1.18 \cdot 10^{-1}$	$5.16 \cdot 10^{-2}$	$2.18 \cdot 10^{-2}$	$9.12 \cdot 10^{-3}$	$2.06 \cdot 10^{-3}$	$6.11 \cdot 10^{-5}$
Total Uncertainty [%]	+8.27 −8.14	+8.84 −8.79	+10.4 −9.75	+16.3 −15.9	+17.1 −14.7	+46.0 −44.1
Statistics [%]	±0.9	±1.2	±1.7	±2.6	±3.8	±13.
Systematics [%]	+8.20 −8.07	+8.72 −8.67	+10.1 −9.53	+16.0 −15.6	+16.6 −14.1	+43.6 −41.7
b-Tagged jet energy scale (JES) [%]	+0.41 −0.47	+0.43 −0.47	+0.64 −0.49	+0.62 −0.71	+0.60 −0.47	+0.48 −1.23
Effective detector NP set 1 (JES) [%]	-	-	+0.29 −0.22	-	+0.45 −0.26	+0.60 −0.75
Effective detector NP set 2 (JES) [%]	+0.10 −0.13	+0.13 -	+0.30 −0.17	+0.12 −0.10	-	+0.19 −0.42
Effective mixed NP set 1 (JES) [%]	+0.65 −0.84	+1.28 −0.96	+1.88 −1.71	+1.28 −2.04	+3.16 −2.33	+5.32 −6.35
Effective mixed NP set 2 (JES) [%]	-	-	−0.21	−0.22	−0.28	-
Effective mixed NP set 3 (JES) [%]	-	-	+0.31 -	-	+0.45 -	- −0.21
Effective modelling NP set 1 (JES) [%]	+1.46 −1.41	+1.53 −1.57	+1.98 −1.68	+1.34 −1.69	+1.64 −1.33	+2.07 −1.48
Effective modelling NP set 2 (JES) [%]	+0.14 −0.23	+0.42 −0.41	+0.86 −0.62	+0.78 −1.17	+1.48 −1.03	+5.40 −5.11
Effective modelling NP set 3 (JES) [%]	−0.34	−0.46	−0.58	−0.70	−0.46	+0.34
Effective modelling NP set 4 (JES) [%]	+0.31 −0.12	+0.44 −0.14	+0.86 −0.27	+0.38 -	+0.55 −0.54	−0.10 +0.77
Effective statistical NP set 1 (JES) [%]	−0.17 -	- +0.23	−0.17 ±0.41	+0.21	−0.34 +0.69	−0.97 +1.18
Effective statistical NP set 2 (JES) [%]	−0.13 −0.19	−0.10 −0.11	+0.26	−0.44	−0.40 −0.48	−1.37 −1.54
Effective statistical NP set 3 (JES) [%]	+0.16 -	+0.13 −0.45	−0.23 −0.82	−0.35 −1.26	−0.23 −0.90	−1.48 −0.33
Effective statistical NP set 4 (JES) [%]	+0.33 −0.39	+0.42 +0.35 −0.27	+1.02 +0.32 −0.13	+0.77 -	+1.34 −0.25 +0.33	+0.18 −0.30 +0.24
Effective statistical NP set 5 (JES) [%]	+0.14 −0.15	+0.35 −0.37	+0.43 −0.29	-	−0.46 +0.57	−0.71 +0.52
Effective statistical NP set 6 (JES) [%]	-	+0.16 −0.11	+0.50 −0.19	- −0.28	−0.16 +0.37	−0.64 +0.45
Effective statistical NP set 7 (JES) [%]	+0.10 −0.18	+0.20 −0.15	+0.47 −0.36	+0.13 −0.22	+0.47 −0.27	+0.46 −0.60
η intercalibration model (JES) [%]	+0.72 −0.77	+0.91 −0.83	+1.46 −0.94	+0.61 −1.33	+1.83 −1.44	+1.94 −2.63
η intercalibration non closure (JES) [%]	−0.44	−0.50	−0.53	−0.95	−0.38	−0.67
η intercalibration total stat (JES) [%]	+0.48 +0.32	+0.57 +0.36	+0.66 +0.57	+0.46 +0.16	+0.71 +0.59	+0.80 +0.81
Flavour composition (JES) [%]	−0.38 +1.73	−0.31 +1.92	−0.50 +2.41	−0.50 +1.94	−0.30 +2.76	−0.67 +5.24
Flavour response (JES) [%]	−1.81 +0.95	−1.83 −1.10 +1.08	−1.97 −1.22 +1.41	−2.44 −2.73 +0.49	−2.47 −0.48 +0.85	−5.40 +0.51 −0.26
Pile-up offset μ (JES) [%]	−0.19 +0.11	- +0.14	-	−0.26 -	-	+0.39 -
Pile-up offset N_{PV} (JES) [%]	±0.43	+0.43 −0.49	+0.63 −0.21	+0.15 −0.44	+0.80 −0.58	+1.48 −0.38
Pile-up offset p_T (JES) [%]	+0.70 −0.94	+1.20 −1.00	+1.46 −1.01	+0.65 −1.20	+1.87 −1.25	+1.32 −1.98
Pile-up offset ρ topology (JES) [%]	+2.44 −2.51	+2.38 −2.16	+2.72 −2.32	+1.71 −2.08	±1.77	+2.34 −1.99
Punch-through (JES) [%]	-	-	-	-	+0.12	+0.28
Jet vertex fraction [%]	+0.27 −0.31	+0.29 −0.33	+0.24 −0.28	+0.23 −0.27	+0.19 −0.24	+0.32 −0.37
b-Quark tagging efficiency (eigenvector 0) [%]	−1.52	−1.62	−1.64	−1.80	−1.96	−2.71
b-Quark tagging efficiency (eigenvector 1) [%]	+1.46 −1.12	+1.55 −1.18	+1.57 −1.22	+1.72 −1.33	+1.88 −1.40	+2.62 −1.79
b-Quark tagging efficiency (eigenvector 2) [%]	+1.09 -	+1.14 -	+1.18 -	+1.28 -	+1.36 ∓0.12	+1.74 ∓0.18
b-Quark tagging efficiency (eigenvector 3) [%]	-	-	-	∓0.10	∓0.17	−0.28 +0.27
b-Quark tagging efficiency (eigenvector 4) [%]	-	-	-	-	-	∓0.10
c-Quark tagging efficiency (eigenvector 0) [%]	-	-	-	-	±0.10	±0.12
c-Quark tagging efficiency (eigenvector 1) [%]	∓0.23	∓0.28	∓0.31	∓0.23	∓0.40	∓0.60
c-Quark tagging efficiency (eigenvector 2) [%]	-	-	∓0.10	-	∓0.14	−0.26 +0.27
Light-jet tagging efficiency (eigenvector 0) [%]	∓0.41	∓0.53	∓0.57	−0.61 +0.62	−1.09 +1.11	−2.57 +2.35
Light-jet tagging efficiency (eigenvector 1) [%]	-	-	-	-	-	−0.82 +0.81
Light-jet tagging efficiency (eigenvector 2) [%]	-	-	-	±0.10	-	−0.13 +0.16
Light-jet tagging efficiency (eigenvector 3) [%]	-	∓0.14	∓0.14	∓0.15	∓0.20	±0.13
Light-jet tagging efficiency (eigenvector 4) [%]	-	-	-	-	-	±0.27
Light-jet tagging efficiency (eigenvector 5) [%]	-	-	-	-	±0.15	±0.68
Light-jet tagging efficiency (eigenvector 6) [%]	-	-	-	-	-	∓0.24
Light-jet tagging efficiency (eigenvector 7) [%]	-	-	-	-	∓0.12	∓0.53
Light-jet tagging efficiency (eigenvector 8) [%]	-	-	-	-	-	±0.19
Light-jet tagging efficiency (eigenvector 9) [%]	-	-	-	-	-	∓0.20
b-Quark tagging extrapolation [%]	-	±0.34	+0.52 −0.53	+0.61 −0.62	+1.13 −1.15	+2.38 −2.48
Electron trigger efficiency [%]	±0.11	±0.11	±0.12	±0.11	±0.12	±0.15
Electron reconstruction efficiency [%]	±0.10	±0.11	±0.11	±0.11	±0.12	±0.16
Electron identification efficiency [%]	±0.57	±0.64	±0.68	±0.71	±0.77	±1.01
Electron isolation efficiency [%]	±0.33	±0.43	±0.52	±0.60	±0.74	±1.13
Muon trigger efficiency stat [%]	±0.28	+0.28 −0.29	±0.28	+0.27 −0.28	±0.30	±0.34
Muon trigger efficiency syst [%]	+0.49 −0.48	+0.49 −0.48	+0.49 −0.48	+0.50 −0.49	+0.51 −0.50	+0.57 −0.56
Muon identification stat [%]	-	-	-	-	-	±0.11
Muon identification syst [%]	±0.46	±0.50	+0.53 −0.52	±0.55	±0.58	±0.67
Muon isolation efficiency syst [%]	±0.10	±0.10	±0.10	±0.11	±0.13	±0.18
E_T^{miss} Soft jet resolution para [%]	∓0.25	∓0.24	-	∓0.29	-	∓0.16
E_T^{miss} Soft jet resolution perp [%]	∓0.23	∓0.12	-	∓0.27	±0.11	-
E_T^{miss} Soft jet scale [%]	−0.19 +0.11	−0.21 +0.19	- +0.14	-	-	+0.20 −0.11
Luminosity [%]	∓2.05	∓2.05	∓2.05	∓2.05	∓2.05	∓2.05
Z+jets cross-section [%]	±0.39	±0.46	±0.51	±0.53	±0.81	±1.59
Diboson cross-section [%]	-	-	-	-	-	±0.18
$t\bar{t}V$ cross-section [%]	±0.10	±0.12	±0.15	±0.17	±0.21	±0.36
Monte Carlo sample statistics [%]	±0.55	±0.74	±1.05	±1.51	±1.93	±5.40
ISR/FSR + scale [%]	+2.10 −0.59	- −0.99	+2.27 −1.25	+6.55 −4.04	+10.1 −6.26	+16.5 −7.36
Alternate hard-scattering model [%]	∓4.82	∓5.03	∓3.86	∓11.5	∓2.70	±31.6
Alternate parton-shower model [%]	±1.27	∓1.47	∓3.40	∓4.28	∓6.31	∓12.7
Fakes overall normalization, el [%]	±0.63	±0.72	±0.98	±1.13	±1.87	±2.79
Fakes overall normalization, mu [%]	±0.36	±0.38	±0.26	-	-	∓0.33
Fakes alternative parametrization [%]	∓2.01	∓2.21	∓2.48	∓2.44	∓3.59	∓4.93
W+jets heavy flavour component [%]	±0.16	-	-	-	-	±0.26
W+jets Scales [%]	±2.52	±3.22	±3.72	±4.31	±5.68	±12.4
W+jets α_S [%]	−0.16 +0.18	−0.20 +0.22	−0.23 +0.27	−0.24 +0.31	−0.34 +0.43	−0.67 +1.09
Single Top DS/DR [%]	∓1.23	∓1.67	∓2.55	∓3.35	∓4.55	∓10.7
Single Top IFSR [%]	- −0.42	- −0.60	+0.41 −0.91	- −0.66	+1.32 −0.52	+4.00 −2.16

TABLE F.56: Table of systematics for the absolute differential cross-section at the parton level for the p_T^{had} observable.

Bins [GeV] x [GeV]	490–900	900–1650	1650–3000	3000–3542	3542–5510
$d\sigma$ / $dm^{t\bar{t}}vsp_T^{had}$ [pb/GeV x GeV]	$1.40 \cdot 10^{-2}$	$7.34 \cdot 10^{-3}$	$1.61 \cdot 10^{-4}$	$6.30 \cdot 10^{-4}$	$4.42 \cdot 10^{-4}$
Total Uncertainty [%]	$^{+6.59}_{-6.38}$	$^{+10.2}_{-10.3}$	$^{+29.6}_{-26.7}$	$^{+15.6}_{-11.8}$	$^{+18.4}_{-17.3}$
Statistics [%]	±1.0	±0.9	±6.5	±4.6	±2.3
Systematics [%]	$^{+6.48}_{-6.27}$	±10.2	$^{+28.6}_{-25.6}$	$^{+14.7}_{-10.5}$	$^{+18.2}_{-17.1}$
b-Tagged jet energy scale (JES) [%]	$^{+0.23}_{-0.29}$	$^{+0.59}_{-0.68}$	$^{+0.67}_{-0.59}$	$^{+0.37}_{-0.15}$	$^{+0.79}_{-0.45}$
Effective detector NP set 1 (JES) [%]	-	$^{+0.16}_{-0.18}$	$^{+0.20}_{-0.56}$	$^{+0.18}_{-}$	$^{+0.27}_{-0.21}$
Effective detector NP set 2 (JES) [%]	-	±0.16	$^{+0.16}_{-0.32}$	-	$^{+0.11}_{-}$
Effective mixed NP set 1 (JES) [%]	$^{+0.54}_{-0.60}$	$^{+1.23}_{-1.39}$	$^{+2.73}_{-2.20}$	$^{+1.63}_{-1.25}$	$^{+3.05}_{-2.25}$
Effective mixed NP set 2 (JES) [%]	-	$^{+0.13}_{-0.14}$	$^{+0.17}_{-0.36}$	-	$^{+0.26}_{-0.21}$
Effective mixed NP set 3 (JES) [%]	-	-	$^{+0.12}_{-0.10}$	-	-
Effective modelling NP set 1 (JES) [%]	$^{+1.49}_{-1.28}$	$^{+1.49}_{-1.78}$	$^{+3.03}_{-1.84}$	$^{+1.36}_{-0.92}$	$^{+1.87}_{-1.21}$
Effective modelling NP set 2 (JES) [%]	$^{+0.17}_{-0.10}$	$^{+0.56}_{-0.61}$	$^{+1.70}_{-1.23}$	$^{+0.79}_{-}$	$^{+1.80}_{-1.22}$
Effective modelling NP set 3 (JES) [%]	$^{-0.26}_{+0.29}$	$^{-0.61}_{+0.51}$	$^{-1.06}_{+0.80}$	$^{-0.20}_{+0.55}$	$^{-0.24}_{+0.61}$
Effective modelling NP set 4 (JES) [%]	$^{+0.14}_{-0.12}$	$^{+0.14}_{-0.17}$	$^{+0.31}_{-0.62}$	-	$^{+0.29}_{-0.20}$
Effective statistical NP set 1 (JES) [%]	$^{+0.18}_{-}$	$^{+0.18}_{-0.24}$	$^{+0.19}_{-0.76}$	$^{+0.36}_{-0.15}$	$^{+0.51}_{-0.40}$
Effective statistical NP set 2 (JES) [%]	$^{-0.15}_{+0.20}$	-	$^{-}_{-0.39}$	$^{+0.15}_{-0.18}$	$^{+0.36}_{-0.30}$
Effective statistical NP set 3 (JES) [%]	-	$^{-0.62}_{+0.39}$	$^{-1.12}_{+1.27}$	$^{-0.55}_{+0.78}$	$^{-0.79}_{+1.25}$
Effective statistical NP set 4 (JES) [%]	$^{+0.32}_{-0.27}$	$^{+0.34}_{-0.35}$	$^{+0.30}_{-0.38}$	$^{-0.16}_{+0.14}$	$^{-0.10}_{+0.19}$
Effective statistical NP set 5 (JES) [%]	$^{+0.17}_{-0.18}$	$^{+0.31}_{-0.30}$	$^{-}_{-0.23}$	-	$^{-0.13}_{+0.25}$
Effective statistical NP set 6 (JES) [%]	-	-	-	-	-
Effective statistical NP set 7 (JES) [%]	$^{+0.12}_{-0.11}$	$^{+0.23}_{-0.26}$	$^{+0.33}_{-0.58}$	$^{+0.32}_{-}$	$^{+0.34}_{-0.24}$
η intercalibration model (JES) [%]	$^{+0.70}_{-0.41}$	$^{+0.90}_{-1.16}$	$^{+2.88}_{-3.32}$	$^{+0.85}_{-0.96}$	$^{+1.62}_{-1.04}$
η intercalibration non closure (JES) [%]	$^{-0.28}_{+0.51}$	$^{-0.69}_{+0.46}$	$^{-0.47}_{+0.69}$	$^{-0.19}_{+0.49}$	$^{-0.63}_{+0.92}$
η intercalibration total stat (JES) [%]	$^{+0.31}_{-0.30}$	$^{+0.40}_{-0.45}$	$^{+0.57}_{-0.88}$	$^{+0.25}_{-0.28}$	$^{+0.44}_{-0.36}$
Flavour composition (JES) [%]	$^{+1.71}_{-1.53}$	$^{+1.83}_{-2.14}$	$^{+4.24}_{-3.66}$	$^{+2.43}_{-1.80}$	$^{+2.97}_{-2.23}$
Flavour response (JES) [%]	$^{-0.94}_{+0.97}$	$^{-1.22}_{+1.02}$	$^{-1.83}_{+2.87}$	$^{-0.89}_{+0.71}$	$^{-0.31}_{+0.81}$
Pile-up offset μ (JES) [%]	$^{-0.11}_{+0.17}$	$^{-0.15}_{-}$	-	-	-
Pile-up offset N_{PV} (JES) [%]	$^{+0.41}_{-0.32}$	$^{+0.41}_{-0.52}$	$^{+1.63}_{-1.20}$	$^{+0.71}_{-0.18}$	$^{+0.65}_{-0.25}$
Pile-up offset p_T (JES) [%]	$^{+0.61}_{-0.60}$	$^{+1.15}_{-1.33}$	$^{+2.65}_{-1.72}$	$^{+1.01}_{-0.56}$	$^{+1.55}_{-1.00}$
Pile-up offset ρ topology (JES) [%]	$^{+2.41}_{-2.26}$	$^{+2.36}_{-2.53}$	$^{+3.80}_{-3.10}$	$^{+1.87}_{-1.56}$	$^{+2.09}_{-1.58}$
Punch-through (JES) [%]	-	-	-	-	-
Jet vertex fraction [%]	$^{+0.31}_{-0.35}$	$^{+0.24}_{-0.27}$	$^{+0.35}_{-0.41}$	$^{+0.35}_{-0.40}$	$^{+0.19}_{-0.24}$
b-Quark tagging efficiency (eigenvector 0) [%]	$^{-1.62}_{+1.56}$	$^{-1.52}_{+1.44}$	$^{-1.68}_{+1.59}$	$^{-1.95}_{+1.87}$	$^{-1.92}_{+1.85}$
b-Quark tagging efficiency (eigenvector 1) [%]	$^{-0.92}_{+0.89}$	$^{-1.33}_{+1.28}$	$^{-1.60}_{+1.55}$	$^{-0.74}_{+0.72}$	$^{-1.56}_{+1.51}$
b-Quark tagging efficiency (eigenvector 2) [%]	±0.16	∓0.14	∓0.28	$^{+0.36}_{-0.35}$	∓0.23
b-Quark tagging efficiency (eigenvector 3) [%]	-	-	∓0.16	-	∓0.21
c-Quark tagging efficiency (eigenvector 0) [%]	-	-	±0.11	±0.19	-
c-Quark tagging efficiency (eigenvector 1) [%]	∓0.15	∓0.32	∓1.03	-	∓0.39
c-Quark tagging efficiency (eigenvector 2) [%]	-	∓0.12	$^{-0.46}_{+0.45}$	-	∓0.14
Light-jet tagging efficiency (eigenvector 0) [%]	∓0.38	∓0.50	$^{-1.64}_{+1.62}$	$^{-0.88}_{+0.98}$	∓0.85
Light-jet tagging efficiency (eigenvector 1) [%]	-	-	∓0.23	$^{+0.11}_{-0.10}$	∓0.16
Light-jet tagging efficiency (eigenvector 2) [%]	-	-	±0.11	$^{+0.14}_{-0.15}$	-
Light-jet tagging efficiency (eigenvector 3) [%]	-	∓0.15	∓0.59	-	$^{-0.18}_{+0.17}$
Light-jet tagging efficiency (eigenvector 5) [%]	-	-	-	-	±0.14
Light-jet tagging efficiency (eigenvector 8) [%]	-	-	∓0.17	-	-
b-Quark tagging extrapolation [%]	-	$^{+0.37}_{-0.38}$	$^{+0.83}_{-0.84}$	-	$^{+1.18}_{-1.20}$
Electron energy resolution [%]	-	-	$^{-0.10}_{+0.11}$	-	-
Electron energy scale [%]	-	-	$^{+0.78}_{-0.44}$	-	-
Electron trigger efficiency [%]	±0.11	±0.11	±0.20	±0.12	±0.12
Electron reconstruction efficiency [%]	-	±0.11	±0.16	±0.10	±0.13
Electron identification efficiency [%]	±0.52	±0.67	±1.08	±0.55	±0.80
Electron isolation efficiency [%]	±0.25	±0.50	±0.68	±0.29	±0.79
Muon (ID) momentum resolution [%]	-	-	$^{-}_{-0.28}$	-	-
Muon (MS) momentum resolution [%]	-	-	$^{-}_{-0.31}$	-	-
Muon energy scale [%]	-	-	$^{-}_{-0.23}$	-	-
Muon trigger efficiency stat [%]	$^{+0.27}_{-0.28}$	±0.28	$^{+0.33}_{-0.34}$	$^{+0.29}_{-0.30}$	±0.29
Muon trigger efficiency syst [%]	$^{+0.48}_{-0.47}$	$^{+0.50}_{-0.49}$	$^{+0.63}_{-0.62}$	$^{+0.52}_{-0.51}$	$^{+0.50}_{-0.49}$
Muon identification stat [%]	-	-	±0.12	±0.10	-
Muon identification syst [%]	±0.40	±0.53	±0.87	±0.43	$^{+0.61}_{-0.60}$
Muon isolation efficiency syst [%]	±0.10	±0.10	±0.16	±0.11	±0.12
E_T^{miss} Soft jet resolution para [%]	±0.24	∓0.60	∓0.58	∓0.17	∓0.13
E_T^{miss} Soft jet resolution perp [%]	±0.47	∓0.65	∓0.99	-	∓0.13
E_T^{miss} Soft jet scale [%]	$^{+0.26}_{-0.30}$	$^{-0.50}_{+0.44}$	$^{-1.42}_{+2.00}$	$^{+0.32}_{-0.54}$	$^{-0.23}_{+0.15}$
Luminosity [%]	∓2.05	∓2.05	∓2.05	∓2.05	∓2.05
Z+jets cross-section [%]	±0.35	±0.42	$^{+2.32}_{-2.31}$	±0.66	±0.69
$t\bar{t}V$ cross-section [%]	±0.12	±0.11	±0.15	±0.22	±0.19
Monte Carlo sample statistics [%]	±0.62	±0.56	±3.88	±2.65	±1.28
ISR/FSR + scale [%]	$^{+1.03}_{-}$	$^{+4.36}_{-3.76}$	$^{+14.1}_{-7.20}$	$^{+10.0}_{-}$	$^{+11.3}_{-10.1}$
Alternate hard-scattering model [%]	∓2.72	∓5.82	±10.4	∓3.82	∓6.29
Alternate parton-shower model [%]	-	∓1.24	±6.17	∓3.25	∓7.13
Fakes overall normalization, el [%]	±0.70	±0.59	$^{+4.03}_{-4.02}$	±1.80	±1.44
Fakes overall normalization, mu [%]	±0.27	±0.42	±0.73	±0.56	∓0.25
Fakes alternative parametrization [%]	∓1.96	∓2.05	∓9.49	∓4.74	∓2.38
W+jets heavy flavour component [%]	±0.13	-	±0.29	-	-
W+jets Scales [%]	±1.96	±3.22	±15.5	±5.24	±5.22
W+jets α_S [%]	$^{-0.11}_{+0.13}$	$^{-0.21}_{+0.24}$	$^{-0.91}_{+1.09}$	$^{-0.28}_{+0.36}$	$^{-0.31}_{+0.40}$
Single Top DS/DR [%]	∓0.87	∓2.07	∓2.48	∓2.33	∓4.86
Single Top IFSR [%]	$^{-}_{-0.41}$	$^{-}_{-0.59}$	$^{+0.42}_{-1.76}$	$^{-}_{-0.54}$	$^{+0.77}_{-0.99}$

TABLE F.57: Table of systematics for the absolute differential cross-section at the parton level for the $m^{t\bar{t}}vsp_T^{had}$ observable.

F.2.2 Relative differential cross section

F.2.2.1 Resolved topology

Bins [GeV]	0–50	50–100	100–160	160–225	225–300	300–360	360–420	420–475	475–530	530–600	600–1000
$1/\sigma \cdot \mathrm{d}\sigma$ / $\mathrm{d}p_T^t$	$3.16 \cdot 10^{-3}$	$6.28 \cdot 10^{-3}$	$4.81 \cdot 10^{-3}$	$2.23 \cdot 10^{-3}$	$8.19 \cdot 10^{-4}$	$2.85 \cdot 10^{-4}$	$1.35 \cdot 10^{-4}$	$6.50 \cdot 10^{-5}$	$3.64 \cdot 10^{-5}$	$1.80 \cdot 10^{-5}$	$2.25 \cdot 10^{-6}$
Total Uncertainty [%]	+9.71 −9.83	+4.81 −4.73	+3.02 −3.08	+8.23 −8.25	+9.66 −9.58	±11.7	+8.91 −11.0	+9.52 −12.9	+30.2 −17.4	+35.1 −22.6	+48.3 −45.0
Statistics [%]	±0.3	±0.1	±0.2	±0.3	±0.5	±1.0	±2.0	±4.2	±7.5	±10.	±20.
Systematics [%]	+9.70 −9.82	+4.81 −4.73	+3.01 −3.07	+8.22 −8.24	+9.64 −9.56	+11.7 −11.6	+8.59 −10.8	+8.14 −11.9	+28.8 −15.0	+32.8 −18.8	+41.9 −38.1
Jet energy resolution [%]	∓0.39	-	-	-	±0.45	±0.54	±1.02	±1.84	±2.73	∓2.36	∓11.1
b-Tagged jet energy scale (JES) [%]	−0.83 +0.70	−0.22 +0.37	+0.33 −0.39	+0.45 −0.68	+0.45 −0.31	- +0.28	−1.30 +0.23	−0.46 +2.63	+5.44 -	+3.82 −1.39	- −3.58
Effective detector NP set 1 (JES) [%]	−0.16 -	-	-	-	-	- −0.20	- −0.89	- −0.74	+3.22 -	+1.78 -	- −6.74
Effective detector NP set 2 (JES) [%]	-	-	-	-	-	-	-	-	+3.10	−1.18	-
Effective mixed NP set 1 (JES) [%]	−0.45	−0.12	±0.13	+0.23	+0.10	+0.29	−0.76	−0.73	-	+3.31	−6.12
Effective mixed NP set 2 (JES) [%]	+0.28	+0.25		−0.30	−0.25	−0.22	−1.23	+0.32 −2.66	+6.46 -	+10.4 -	+3.46 −2.67
Effective mixed NP set 3 (JES) [%]	-	-	-	-	-	-	- −1.12	+0.67 +1.43	+3.50 +3.10	+1.07 +2.45	+0.75 −5.92
Effective modelling NP set 1 (JES) [%]	+0.16	+0.30	+0.19	−0.37	−0.96	−1.51	−1.16 −3.52	−2.30	+2.07	+6.77	- −2.89
Effective modelling NP set 2 (JES) [%]	-	−0.20	−0.25	+0.21 +0.23	+1.06 +0.23	+1.59 +0.40	+1.60	-	+4.12	+4.54	−3.52 +1.04
Effective modelling NP set 3 (JES) [%]	−0.41 +0.13	+0.26	-	−0.26	−0.37	−0.33	−0.74	+1.16 −1.23	-	-	−3.66
Effective modelling NP set 4 (JES) [%]	+0.26 −0.53	+0.24	-	−0.31 +0.27	−0.30 +0.38	−0.18 +0.20	- −0.90	−1.77 +0.21	+3.68 -	+4.29 -	−3.15 +3.08
Effective statistical NP set 1 (JES) [%]	-	-	-	-	-	-	- −1.23	- −1.87	+3.36 +0.94	+2.25 +3.67	- −2.29
Effective statistical NP set 2 (JES) [%]	-	-	-	-	−0.21 +0.15	−0.37 +0.36	- −0.58	- −1.54	-	-	+1.77 −4.95
Effective statistical NP set 3 (JES) [%]	−0.21 −0.16	-	-	-	+0.19 −0.11	+0.28 −0.29	- −1.20	- −1.19	+1.78 -	+2.97 −0.45	+0.90 −4.83
Effective statistical NP set 4 (JES) [%]	-	-	-	-	-	-	−0.80	- −2.26	+5.64 -	+6.47 -	-
Effective statistical NP set 5 (JES) [%]	−0.40	-	-	+0.31	+0.10	-	-	+0.60	+1.60	+1.98	−4.76 +1.89
Effective statistical NP set 6 (JES) [%]	+0.33	+0.25	−0.18	−0.29	−0.22	-	−0.68	−1.82	−0.95	−0.13	−1.70
Effective statistical NP set 7 (JES) [%]	-	-	-	−0.17	-	-	- −1.33	- −1.16	+3.70 -	+3.13 -	+1.90 -
Pile-up offset μ (JES) [%]	−0.17 -	-	-	-	-	-	-	+1.68	+3.11	+1.93	-
Pile-up offset N_{PV} (JES) [%]	-	-	-	-	+0.23	+0.48 +0.33	−1.40 -	−0.72 -	+3.67 -	+5.24 -	−8.41 +2.50
Pile-up offset p_T (JES) [%]	-	-	-	-	-	−0.36 −0.19	−1.48 -	−1.38 -	-	−1.99 +5.49	−1.92 −1.06
η intercalibration model (JES) [%]	−0.41 +0.22	-	+0.11 −0.17	+0.18 −0.27	-	+0.45 -	−0.99 -	−0.92 -	+2.94 -	-	+4.87 -
η intercalibration non closure (JES) [%]	-	-	-	-	-	- −0.42	- −1.02	- −1.10	+0.27 -	+2.72 −1.53	- −3.05
η intercalibration total stat (JES) [%]	−0.22	-	-	-	-	−0.34 +0.35	- −1.13	−1.22 +0.29	+2.17 −0.85	+0.58 −1.52	+2.56 −2.78
Flavour composition (JES) [%]	±0.39	+0.38	-	−0.59	−0.98	−1.76	−2.12	-	+1.94	+5.46	−0.61
Flavour response (JES) [%]	-	−0.35 -	−0.16 −0.11	+0.55 +0.11	+1.29 +0.37	+1.69 ±0.91	+1.13 +0.57	−1.21 -	+2.30 -	+3.89 -	+2.44 +1.65
Pile-up offset μ (JES) [%]	-	+0.20 -	+0.12 -	−0.23 -	−0.31 -	+0.26	−1.32 -	−1.18 -	+3.36	+2.24	-
Pile-up offset N_{PV} (JES) [%]	−0.24	-	-	-	-	−0.37	−0.83 -	−0.94 -	+3.53	+5.52	−3.87 +5.51
Pile-up offset p_T (JES) [%]	+0.19 −0.22	−0.32	+0.19	−0.20 +0.67	+0.56	+0.64 +0.43	−0.75 -	−0.80 -	+1.58	+3.04	+3.90
Pile-up offset ρ topology (JES) [%]	+0.68 −0.29	+0.37 +0.22	−0.21 +0.49	−0.69 -	−0.54 −1.12	−0.63 −2.33	−0.31 −3.12	−1.60 −3.56	−2.33 -	+7.92 -	−0.81 +2.49
Punch-through (JES) [%]	+0.31 -	−0.13 -	−0.56 -	- -	+1.15 -	+2.45 -	+2.61 -	+1.91 -	+3.65 +1.39	- -	- −3.01
Single particle high-p_T (JES) [%]	-	-	-	-	-	+0.16 -	−0.36 -	−0.28 -	+1.74	+1.26 +1.60	+2.53 +2.06
Jet vertex fraction [%]	±0.33	±0.17	-	−0.28 +0.29	−0.43 +0.44	−0.47 +0.48	−0.42 +0.43	−0.11 −0.34 +0.35	∓0.33	−0.22 +0.24	−0.39 +0.40
b-Quark tagging efficiency (eigenvector 0) [%]	−1.33	−0.63	+0.29	+1.14	+1.60	+1.60	+0.98	+0.38	−0.13	-	+0.82
b-Quark tagging efficiency (eigenvector 1) [%]	+1.24 +0.69	+0.58 +0.42	−0.27 -	−1.06 −0.62	−1.47 −1.16	−1.47 −1.57	−0.90 −1.61	−0.35 −1.70	+0.10 −2.09	−2.11	−0.76 −2.21
b-Quark tagging efficiency (eigenvector 2) [%]	+0.68 +0.39	+0.41 +0.24	-	+0.61 +0.32	+1.14 +0.68	+1.55 +1.00	+1.59 +1.19	+1.68 +1.41	−2.06 +1.70	+2.08 +1.78	+2.18 +1.62
b-Quark tagging efficiency (eigenvector 3) [%]	−0.38	−0.25	-	+0.33	+0.69	+1.01	+1.22	+1.44	+1.74	+1.81	+1.66
b-Quark tagging efficiency (eigenvector 4) [%]	∓0.31	∓0.15	-	±0.30	±0.33	±0.18	∓0.10	∓0.33	±0.45	∓0.52	∓0.35
b-Quark tagging efficiency (eigenvector 5) [%]	-	-	-	-	-	-	-	-	-	∓0.12	∓0.14
c-Quark tagging efficiency (eigenvector 0) [%]	+0.14 −0.13	-	-	-	∓0.14	±0.16	∓0.14	∓0.13	∓0.27	∓0.10	∓0.17
c-Quark tagging efficiency (eigenvector 1) [%]	±0.10	-	-	∓0.10	∓0.17	∓0.24	∓0.31	∓0.34	−0.32 +0.31	-	∓0.18
c-Quark tagging efficiency (eigenvector 2) [%]	-	-	-	-	∓0.15	∓0.20	∓0.27	∓0.27	∓0.28	∓0.10	∓0.15
Light-jet tagging efficiency (eigenvector 0) [%]	-	-	-	-	-	-	−0.10 +0.12	−0.47 +0.45	−0.74 +0.76	−0.74 +0.83	−0.21 +0.19
Light-jet tagging efficiency (eigenvector 1) [%]	±0.12	-	-	-	∓0.18	∓0.21	∓0.15	-	-	−1.22 +0.21	−1.35 +0.36
Light-jet tagging efficiency (eigenvector 2) [%]	-	-	-	-	-	-	-	∓0.15	-	+0.16 −0.18	+0.46 −0.45
Light-jet tagging efficiency (eigenvector 3) [%]	-	-	-	-	∓0.11	∓0.14	−0.14 +0.15	∓0.23	−0.31 +0.32	−0.28 +0.29	±0.13
Light-jet tagging efficiency (eigenvector 5) [%]	-	-	-	-	-	-	-	-	∓0.12	-	±0.15
Light-jet tagging efficiency (eigenvector 6) [%]	-	-	-	-	-	-	-	-	-	∓0.11	∓0.15
Light-jet tagging efficiency (eigenvector 7) [%]	-	-	-	-	-	-	-	-	-	±0.12	-
Light-jet tagging efficiency (eigenvector 11) [%]	-	-	-	-	-	-	-	-	-	-	±0.18
b-Quark tagging extrapolation [%]	-	-	-	-	-	±0.11	±0.46	±1.07	+1.69 −1.68	±2.23	+3.10 −3.06
Electron energy resolution [%]	-	-	-	-	-	-	- −0.70	- −0.54	+2.11 -	+1.26 −0.40	−3.82 +0.19
Electron energy scale [%]	-	-	-	-	-	-	−0.66	−0.84	+2.11 -	-	+0.12 −2.15
Electron identification efficiency [%]	-	-	-	-	-	±0.15	±0.18	+0.20 −0.21	±0.25	±0.19	±0.21
Electron isolation efficiency [%]	-	-	-	-	±0.10	±0.20	±0.27	±0.32	+0.43 −0.44	±0.41	±0.42
Muon (ID) momentum resolution [%]	- −0.20	-	-	-	-	-	- −0.63	- −0.35	+3.03 -	+1.30 -	- −3.88
Muon (MS) momentum resolution [%]	-	-	-	-	-	-	-	−0.80 +0.34	+4.36 -	+4.63 -	+0.85 −1.44
Muon (ID) sagitta ρ [%]	- −0.14	-	-	-	-	-	- −0.33	- −0.79	+1.24 +3.41	+1.38 +2.27	+2.41 -
Muon energy scale [%]	−0.20	-	-	-	-	-	−0.41	−0.95	-	-	−2.30
Muon identification syst [%]	-	-	-	-	-	-	-	±0.10	-	±0.14	±0.17
E_T^{miss} Soft jet resolution para [%]	-	-	-	-	-	±0.20	∓0.52	±0.25	±1.28	±3.28	±1.64
E_T^{miss} Soft jet resolution perp [%]	-	-	-	-	±0.10	-	∓0.96	∓1.01	±2.00	±0.37	∓2.72
E_T^{miss} Soft jet scale [%]	-	-	-	-	-	-	-	- −0.78	+2.80 -	+3.26 -	−1.84 +0.99
Z+jets cross-section [%]	±0.39	±0.16	∓0.12	∓0.29	∓0.31	∓0.37	−0.30 +0.31	∓0.23	∓0.12	-	-
Monte Carlo sample statistics [%]	±0.34	±0.12	±0.14	±0.21	±0.31	±0.58	±1.21	±2.58	±4.55	±6.41	±12.3
ISR/FSR + scale [%]	+0.30 -	+0.31 −0.33	- −0.39	−0.26 +0.41	−0.71 +0.66	−3.35 +3.28	−0.18 +1.95	- −5.09	+14.4 −4.37	+8.43 -	−9.04 +21.9
Alternate hard-scattering model [%]	±7.83	±4.07	∓2.26	∓6.90	∓7.57	∓9.41	∓3.89	∓2.76	∓4.81	∓14.2	∓25.8
Alternate parton-shower model [%]	±4.68	±1.98	∓1.52	∓3.78	∓4.55	∓3.83	±5.32	∓4.37	±11.0	±8.05	∓5.26
Inter PDF [%]	-	-	-	-	±0.13	±0.19	±0.19	±0.10	±0.19	∓0.41	-
Intra PDF [%]	-	-	-	-	∓0.16	∓0.32	∓0.51	∓0.51	±0.13	±0.40	-
Fakes overall normalization, el [%]	+2.33 −2.38	+0.64 −0.67	−0.83 +0.85	−1.21 +1.25	−1.65 +1.69	±0.17	−1.94 +2.01	−1.75 +1.80	−1.03 +1.06	−0.98 +1.01	−1.37 +1.41
Fakes overall normalization, mu [%]	±0.13	-	-	∓0.10	∓0.12	∓0.14	-	∓0.28	∓0.25	−0.41 +0.42	∓0.22
Fakes alternative parametrization [%]	∓0.48	∓0.28	±0.39	-	±0.55	∓0.37	±1.28	-	-	±1.09	±4.35
W+jets heavy flavour component [%]	±0.63	±0.23	∓0.14	∓0.40	∓0.62	∓0.71	∓0.72	∓0.81	∓0.83	∓0.79	∓0.62
W+jets Scales [%]	±0.41	±0.19	∓0.13	∓0.33	∓0.44	∓0.44	∓0.20	-	±0.72	±1.19	±0.36
Single Top DS/DR [%]	±0.14	±0.10	-	∓0.18	∓0.27	∓0.18	∓0.42	∓2.00	∓2.34	∓0.88	∓1.20
Single Top IFSR [%]	−0.20 -	-	-	-	+0.25 −0.11	+0.37 −0.17	+0.58 −0.21	+0.78 -	+0.76 −2.20	- −2.77	+0.64 −1.89

TABLE F.58: Table of systematics for the relative differential cross-section at the parton level for the $p_T^{t,had}$ observable.

Bins [Unit y^{t_h}]	-2.50—1.70	-1.70—1.20	-1.20—0.80	-0.80—0.40	-0.40–0	0–0.40	0.40–0.80	0.80–1.20	1.20–1.70	1.70–2.50
$1/\sigma \cdot \mathrm{d}\sigma \,/\, \mathrm{d}y^{t_h}$	$9.51 \cdot 10^{-2}$	$1.88 \cdot 10^{-1}$	$2.46 \cdot 10^{-1}$	$2.79 \cdot 10^{-1}$	$2.97 \cdot 10^{-1}$	$3.03 \cdot 10^{-1}$	$2.85 \cdot 10^{-1}$	$2.45 \cdot 10^{-1}$	$1.87 \cdot 10^{-1}$	$9.39 \cdot 10^{-2}$
Total Uncertainty [%]	+4.86 −4.71	+1.79 −1.71	+2.08 −2.11	+2.19 −2.07	+2.39 −2.29	+2.41 −2.68	+1.93 −1.68	+1.42 −1.28	+2.87 −3.18	+5.84 −5.97
Statistics [%]	±0.7	±0.4	±0.4	±0.3	±0.3	±0.3	±0.3	±0.4	±0.4	±0.7
Systematics [%]	+4.78 −4.63	+1.69 −1.61	+2.01 −2.05	+2.13 −2.01	+2.34 −2.25	+2.37 −2.64	+1.87 −1.61	+1.28 −1.12	+2.81 −3.13	+5.78 −5.90
Jet energy resolution [%]	∓0.41	∓0.32	±0.42	-	∓0.74	-	±0.32	±0.47	±0.46	∓0.21
b-Tagged jet energy scale (JES) [%]	-	-	-	-	-	−0.17	-	-	-	-
Effective detector NP set 1 (JES) [%]	-	-	-	-	-	-	-	-	-	-
Effective detector NP set 2 (JES) [%]	-	-	+0.23	-	-	-	-	-	-	-
Effective mixed NP set 1 (JES) [%]	-	-	-	+0.20	-	-	-	-	-	-
Effective mixed NP set 2 (JES) [%]	-	-	-	-	-	-	-	-	-	-
Effective mixed NP set 3 (JES) [%]	-	-	-	-	-	-	-	-	-	-
Effective modelling NP set 1 (JES) [%]	−0.92 +1.05	−0.38 +0.32	+0.12 −0.23	+0.54 −0.33	+0.42 −0.43	+0.30 −0.49	+0.37 −0.19	+0.22 -	−0.56 +0.16	−1.08 +1.01
Effective modelling NP set 2 (JES) [%]	-	-	-	-	-	−0.17	-	-	-	+0.23
Effective modelling NP set 3 (JES) [%]	-	-	-	+0.23 −0.15	-	-	+0.14 −0.10	-	-	−0.49 -
Effective modelling NP set 4 (JES) [%]	-	-	-	+0.24	-	-	-	-	-	-
Effective statistical NP set 1 (JES) [%]	−0.14 +0.22	-	-	-	+0.16 −0.11	-	-	-	-	-
Effective statistical NP set 2 (JES) [%]	+0.11 −0.13	-	-	-	-	-	-	-	−0.22 -	-
Effective statistical NP set 3 (JES) [%]	-	-	-	-	-	−0.21 -	-	-	−0.18 -	−0.21 −0.18
Effective statistical NP set 4 (JES) [%]	-	-	-	-	-	-	-	-	-	-
Effective statistical NP set 5 (JES) [%]	-	-	-	-	-	-	-	-	-	-
Effective statistical NP set 6 (JES) [%]	-	-	-	-	-	-	-	-	-	-
Effective statistical NP set 7 (JES) [%]	-	-	-	-	-	-	-	-	−0.20 -	-
η intercalibration model (JES) [%]	+0.29 −0.14	+0.50 −0.51	+0.22 −0.21	−0.12 +0.20	−0.31 +0.53	−0.50 +0.30	−0.29 +0.24	+0.30 -	+0.40 −0.53	−0.23 -
η intercalibration non closure (JES) [%]	+0.22 -	-	−0.23 +0.11	−0.37 +0.43	−0.12 +0.32	- −0.20	+0.36 −0.20	+0.38 −0.27	+0.13 −0.27	−0.20 -
η intercalibration total stat (JES) [%]	−0.12 +0.10	-	-	-	-	-	-	-	-	−0.20 -
Flavour composition (JES) [%]	−1.01 +1.13	−0.20 -	+0.17 −0.18	+0.50 −0.34	+0.27 −0.48	+0.27 −0.53	+0.33 −0.13	+0.26 −0.13	−0.37 +0.31	−1.16 +1.35
Flavour response (JES) [%]	+0.58 −0.52	-	−0.29 -	−0.14 +0.12	- +0.22	−0.26 -	-	- -	- −0.29	+0.32 −0.55
Pile-up offset μ (JES) [%]	-	-	-	-	-	-	-	+0.25 -	-	- −0.47
Pile-up offset N_{PV} (JES) [%]	-	-	+0.18 −0.15	-	+0.25 -	-	+0.25 -	-	- −0.37	−0.41 -
Pile-up offset p_T (JES) [%]	- −0.16	+0.19 -	-	-	- +0.16	-	-	-	-	- −0.24
Pile-up offset ρ topology (JES) [%]	−1.36 +1.45	−0.49 +0.45	+0.16 −0.34	+0.61 −0.67	+0.68 −0.45	+0.56 −0.70	+0.45 −0.22	-	−0.57 +0.46	−1.65 +1.34
Punch-through (JES) [%]	-	-	-	-	-	-	-	-	-	-
Single particle high-p_T (JES) [%]	-	-	-	-	-	-	-	-	-	-
Jet vertex fraction [%]	-	-	-	-	-	-	-	-	-	-
b-Quark tagging efficiency (eigenvector 0) [%]	+0.44 −0.41	±0.10	-	−0.14 +0.12	−0.14 +0.13	−0.18 +0.17	−0.14 +0.13	-	+0.15 −0.14	+0.40 −0.37
Light-jet tagging efficiency (eigenvector 0) [%]	−0.21 +0.23	-	-	+0.23 −0.32	-	-	-	+0.11 −0.16	-	−0.27 +0.31
Light-jet tagging efficiency (eigenvector 1) [%]	±0.10	-	-	−0.11 +0.10	-	-	-	-	-	-
Light-jet tagging efficiency (eigenvector 2) [%]	−0.13 +0.14	-	-	-	+0.16 −0.14	-	-	-	-	∓0.11 −0.20
Light-jet tagging efficiency (eigenvector 3) [%]	∓0.14	-	-	-	+0.13 −0.12	-	-	-	-	+0.21
Light-jet tagging efficiency (eigenvector 5) [%]	-	-	-	-	-	-	-	-	-	∓0.14
Light-jet tagging efficiency (eigenvector 7) [%]	-	-	-	-	-	-	-	-	-	∓0.10
Electron energy resolution [%]	-	-	-	-	-	-	-	-	-	-
Electron energy scale [%]	-	-	-	-	-	-	-	-	- −0.17	-
Muon (ID) momentum resolution [%]	+0.19 -	-	-	-	-	-	-	-	-	-
Muon (MS) momentum resolution [%]	-	-	-	-	-	-	-	-	-	-
Muon (ID) sagitta ρ [%]	-	-	-	-	-	-	-	-	-	-
Muon energy scale [%]	-	-	-	-	-	-	-	-	−0.24 −0.24	-
E_T^{miss} Soft jet resolution para [%]	-	-	-	-	-	-	±0.11	-	-	-
E_T^{miss} Soft jet resolution perp [%]	±0.15	-	∓0.11	-	-	∓0.11	-	-	∓0.12	±0.10
E_T^{miss} Soft jet scale [%]	-	-	-	-	−0.20 +0.17	-	-	-	-	-
Monte Carlo sample statistics [%]	±0.46	±0.30	±0.30	±0.32	±0.27	±0.24	±0.25	±0.42	±0.33	±0.51
ISR/FSR + scale [%]	- −0.14	+0.47 -	+0.44 -	+0.26 −0.37	−0.42 -	- +0.30	−0.18 +0.30	- −0.49	- −0.53	+0.65 −0.31
Alternate hard-scattering model [%]	∓3.03	∓0.49	∓1.70	±0.55	-	±1.50	±0.89	±0.16	∓1.69	±3.04
Alternate parton-shower model [%]	∓2.63	∓1.10	±0.20	±1.44	±1.47	±1.61	±1.09	±0.67	∓1.90	∓4.21
Inter PDF [%]	-	±0.10	-	-	-	-	-	-	±0.10	-
Intra PDF [%]	±0.24	-	-	-	-	-	-	-	-	±0.25
Fakes overall normalization, el [%]	−0.44 +0.45	−0.33 +0.34	−0.44 +0.46	+0.58 −0.60	+1.02 −1.04	±0.14	∓0.23	∓0.10	−0.57 +0.58	∓0.26
Fakes overall normalization, mu [%]	-	-	-	-	-	-	-	∓0.10	-	±0.17
Fakes alternative parametrization [%]	±0.47	∓0.18	∓0.37	∓0.11	∓0.23	-	±0.24	∓0.14	±0.44	±0.12
W+jets heavy flavour component [%]	∓0.16	-	-	-	-	±0.10	-	-	-	∓0.11
W+jets Scales [%]	-	-	-	-	-	-	-	-	∓0.13	-
Single Top DS/DR [%]	±0.12	-	-	∓0.11	-	-	-	-	-	-
Single Top IFSR [%]	-	−0.18 -	-	-	-	-	-	- −0.29	- −0.22	-

TABLE F.59: Table of systematics for the relative differential cross-section at the parton level for the $y^{t,had}$ observable.

Bins [GeV]	0–40	40–90	90–150	150–230	230–310	310–390	390–470	470–550	550–630	630–800
$1/\sigma \cdot \mathrm{d}\sigma \,/\, \mathrm{d}p_T^{t\bar{t}}$	$1.16 \cdot 10^{-2}$	$5.94 \cdot 10^{-3}$	$2.23 \cdot 10^{-3}$	$8.13 \cdot 10^{-4}$	$2.95 \cdot 10^{-4}$	$1.17 \cdot 10^{-4}$	$4.99 \cdot 10^{-5}$	$2.22 \cdot 10^{-5}$	$1.11 \cdot 10^{-5}$	$4.22 \cdot 10^{-6}$
Total Uncertainty [%]	±13.0	±11.2	±15.7	±13.6	+10.7 −10.4	+11.8 −11.7	+14.8 −15.9	+11.0 −14.6	+11.1 −15.1	+28.7 −21.8
Statistics [%]	±0.1	±0.1	±0.2	±0.4	±0.8	±1.6	±2.8	±4.6	±6.8	±11.
Systematics [%]	±13.0	±11.2	±15.7	±13.6	+10.6 −10.4	±11.6	+14.5 −15.5	+9.64 −13.6	+7.99 −13.0	+25.7 −17.7
Jet energy resolution [%]	∓1.91	±0.97	±2.84	±3.01	±1.74	±0.66	-	∓1.80	±2.96	±1.66
b-Tagged jet energy scale (JES) [%]	-	-	+0.36 −0.18	+0.40 -	-	−0.65 +0.43	−0.85 +0.12	+0.28 -	- −1.44	−0.33 +1.38
Effective detector NP set 1 (JES) [%]	-	-	-	-	+0.41 −0.27	- −0.35	+0.44 -	-	- −0.82	+1.48 -
Effective detector NP set 2 (JES) [%]	-	-	-	-	+0.32 -	- −0.29	-	+0.40	- −0.96	+3.43 -
Effective mixed NP set 1 (JES) [%]	-	-	-	+0.28 −0.22	+0.79 -	+0.57 −0.51	+0.16 −1.60	+0.12 −0.78	- −1.38	+3.98 −1.76
Effective mixed NP set 2 (JES) [%]	-	-	-	-	+0.38 -	-	+0.19 -	−0.72 -	-	+0.23 -
Effective mixed NP set 3 (JES) [%]	-	-	-	-	+0.26 -	- −0.22	+0.36 −0.92	+1.18 +0.25 −0.21	−0.83 - −1.79	−0.21 +3.77 -
Effective modelling NP set 1 (JES) [%]	−0.58 +0.55	+0.30 −0.34	+1.09 −0.92	+0.76 −0.86	+0.32 -	−1.22 +0.85	−1.79 +1.01	−0.29 +0.69	−0.93 +0.82	+3.54 -
Effective modelling NP set 2 (JES) [%]	-	-	-	-	-	-	-	+1.02	+1.44	+2.77
Effective modelling NP set 3 (JES) [%]	-	-	-	−0.14 -	−0.26 −0.45	−0.24 -	−0.40 −0.46	+0.36	−1.00 −2.31	−1.05 +1.92
Effective modelling NP set 4 (JES) [%]	-	-	+0.22 -	+0.20 -	+0.24 +0.34	−0.24 -	+0.10 -	−0.39 −1.06	+0.89 -	- +2.73
Effective statistical NP set 1 (JES) [%]	-	-	+0.14 -	−0.12 -	−0.14 +0.55	−0.22 -	−0.20 -	−0.33 -	−0.96 +0.40 -	+3.36 -
Effective statistical NP set 2 (JES) [%]	-	-	- +0.16	−0.14 -	+0.37 -	−0.40 -	+0.32 −0.57	+0.11 −0.58	−1.38 - −1.99	+4.14 -
Effective statistical NP set 3 (JES) [%]	-	-	-	-	-	−0.73 +0.34	−0.73 +1.32	+0.58 -	- −2.04	−0.92 +2.52
Effective statistical NP set 4 (JES) [%]	-	-	-	+0.15 −0.22	+0.50 -	-	+0.45 -	+0.47 −0.15	- −1.08	−0.35 +2.79
Effective statistical NP set 5 (JES) [%]	-	-	-	-	+0.29 -	+0.37 −0.24	+0.35 +0.79	+0.64 ∓0.48	+0.38 −2.39	−1.16 +3.81
Effective statistical NP set 6 (JES) [%]	-	-	-	−0.10 +0.13	+0.31 -	-	-	-	-	+0.38 -
Effective statistical NP set 7 (JES) [%]	-	-	-	-	±0.24	-	+0.41	+0.31	−1.80 −1.68	+1.22 -
η intercalibration model (JES) [%]	−0.22 +0.21	-	+0.44 −0.28	+0.43 −0.39	+0.38 -	−0.36 +0.23	−0.25 -	- −0.55	+0.57 +0.24 -	+1.85 −0.57
η intercalibration non closure (JES) [%]	-	-	−0.13 +0.29	−0.21 +0.20	+0.22 -	- +0.21	−0.79 -	+1.17	+1.40 -	−1.11 +0.20
η intercalibration total stat (JES) [%]	−0.10 +0.15	-	+0.29 −0.19	+0.27 −0.25	+0.62 -	- −0.52	−0.93 +0.73	−0.88 -	- −0.80	+1.86 -
Flavour composition (JES) [%]	−0.60 +0.62	+0.23 −0.29	+1.16 −1.13	+1.05 −1.07	+0.34 -	−1.23 +0.61	- −1.33	+0.77 -	+1.61 -	+0.54 -
Flavour response (JES) [%]	+0.36 −0.30	−0.18 +0.11	−0.66 +0.60	−0.64 +0.41	+0.34 -	-	- −0.56	+1.06 −1.16	+2.44 -	+2.89 -
Pile-up offset μ (JES) [%]	-	-	-	-	+0.37 -	-	-	−0.23	+0.32	+2.86 -
Pile-up offset N_{PV} (JES) [%]	−0.20 +0.16	-	+0.43 −0.28	+0.50 −0.32	−0.31 +0.35 -	−0.29 −0.65 +0.24	−0.29 - −0.76	+0.56 −0.83 +0.38	−0.38 -	+0.65 -
Pile-up offset p_T (JES) [%]	−0.14 +0.11	-	+0.34 −0.28	+0.48 −0.38	+0.17 −0.10	+0.10 −0.73	- −1.28	−0.21 -	- −0.98	+3.22 -
Pile-up offset ρ topology (JES) [%]	−0.92 +0.89	+0.46 −0.49	+1.75 −1.62	+1.56 −1.50	- +0.42	−1.60 +1.26	−2.02 +1.49	−2.10 +1.37	−1.14 +2.82	−0.44 +3.62
Punch-through (JES) [%]	-	-	-	-	+0.14	-	-	+0.37 −0.82	- −1.22	+1.58 -
Single particle high-p_T (JES) [%]	-	-	-	-	-	+0.30	-	- −0.21	+1.05 - −0.66	-
Jet vertex fraction [%]	-	-	-	-	-	−0.17 +0.16	−0.23 +0.27	∓0.30	∓0.30	∓0.32
b-Quark tagging efficiency (eigenvector 0) [%]	−0.37 +0.35	-	+0.66 −0.62	+0.86 −0.81	+0.58 −0.56	±0.38	+0.51 −0.50	+0.71 −0.66	+0.99 −0.92	+1.34 −1.24
b-Quark tagging efficiency (eigenvector 1) [%]	±0.15	-	∓0.18	−0.55 +0.54	−0.81 +0.80	−0.82 +0.80	−0.96 +0.94	−1.22 +1.20	−1.51 +1.49	−1.84 +1.81
b-Quark tagging efficiency (eigenvector 2) [%]	+0.11 −0.12	-	∓0.12	−0.39 +0.40	−0.61 +0.62	−0.69 +0.70	−0.76 +0.77	−0.84 +0.86	−1.02 +1.04	−1.20 +1.23
b-Quark tagging efficiency (eigenvector 3) [%]	-	-	±0.10	±0.17	-	-	-	-	-	-
c-Quark tagging efficiency (eigenvector 0) [%]	-	-	-	-	-	-	-	∓0.11	∓0.13	-
c-Quark tagging efficiency (eigenvector 1) [%]	-	-	-	∓0.14	∓0.21	∓0.24	∓0.22	∓0.13	∓0.13	−0.34 +0.33
c-Quark tagging efficiency (eigenvector 2) [%]	-	-	-	-	∓0.13	∓0.13	∓0.12	-	-	∓0.16
Light-jet tagging efficiency (eigenvector 0) [%]	-	-	-	−0.24 +0.25	−0.41 +0.43	−0.43 +0.45	−0.10 +0.11	±0.26	-	−0.75 +0.76
Light-jet tagging efficiency (eigenvector 1) [%]	-	-	-	-	-	-	∓0.16	−0.27 +0.26	-	+0.22 −0.23
Light-jet tagging efficiency (eigenvector 2) [%]	-	-	-	-	-	-	+0.16 −0.15	-	-	-
Light-jet tagging efficiency (eigenvector 3) [%]	-	-	-	∓0.10	∓0.10	-	-	-	-	-
Light-jet tagging efficiency (eigenvector 5) [%]	-	-	-	-	-	-	-	-	±0.14	±0.12
Light-jet tagging efficiency (eigenvector 6) [%]	-	-	-	-	-	-	-	-	∓0.10	−0.10 +0.11
b-Quark tagging extrapolation [%]	-	-	-	-	±0.13	±0.38	±0.52	±0.57	±0.68	±0.81
Electron energy resolution [%]	-	-	-	-	-	-	-	-	-	+1.22 -
Electron energy scale [%]	-	-	-	-	-	−0.35 -	-	-	−0.90 -	- +0.28
Electron identification efficiency [%]	-	-	-	-	-	−0.36 ±0.14	±0.16	−0.22 ±0.19	−0.50 ±0.21	+0.21 −0.22
Electron isolation efficiency [%]	-	-	-	-	-	±0.15	±0.23	±0.29	±0.33	±0.40
Muon (ID) momentum resolution [%]	-	-	-	-	+0.27 -	-	-	−0.32	+0.44	+2.32
Muon (MS) momentum resolution [%]	-	-	-	-	+0.45 -	−0.30 +0.24	−0.37 -	−0.50	−1.51 +0.48	+1.08 -
Muon (ID) sagitta ρ [%]	-	-	-	-	+0.26 -	−0.10 -	−0.22 −0.41	+1.00 -	-	+0.60 -
Muon energy scale [%]	-	-	-	-	+0.31 -	-	+0.14 -	−0.38 -	+0.34 -	+1.31 -
Muon identification syst [%]	-	-	-	-	-	-	−0.16 -	−0.55 -	−0.73 -	±0.14
E_T^{miss} Soft jet resolution para [%]	∓0.12	±0.14	±0.11	-	±0.31	±0.34	∓1.21	∓0.66	±1.93	∓0.72
E_T^{miss} Soft jet resolution perp [%]	∓0.18	±0.18	±0.18	-	±0.15	-	∓1.03	±0.37	∓0.33	±0.69
E_T^{miss} Soft jet scale [%]	-	-	-	−0.10 +0.19	−0.13 +0.44	- −0.26	−0.47 +0.14	+1.32 -	- −1.08	−1.46 +2.41
Z+jets cross-section [%]	-	-	-	-	-	-	∓0.10	∓0.23	∓0.27	∓0.20
Monte Carlo sample statistics [%]	±0.10	±0.11	±0.18	±0.30	±0.55	±1.00	±1.66	±2.64	±3.65	±6.03
ISR/FSR + scale [%]	−0.55 +0.59	+0.62 −0.32	+0.86 −1.21	- −1.30	+1.27 -	−0.87 +2.92	−4.21 +1.01	- −9.60	- −8.68	−3.46 +11.8
Alternate hard-scattering model [%]	∓7.13	±9.22	±4.18	-	±0.74	±4.56	∓1.58	∓5.73	∓1.15	±16.5
Alternate parton-shower model [%]	∓10.5	±6.26	±14.5	±12.9	±9.92	±9.69	±13.6	±5.46	±3.22	-
Inter PDF [%]	-	-	-	-	-	±0.16	±0.12	±0.17	±0.17	±0.39
Intra PDF [%]	±0.10	-	∓0.14	∓0.29	∓0.43	∓0.42	∓0.31	∓0.22	∓0.14	∓0.13
Fakes overall normalization, el [%]	-	+0.33 −0.34	-	−0.75 +0.77	−1.17 +1.21	−0.80 +0.82	−1.45 +1.48	−1.15 +1.18	−0.86 +0.88	−1.42 +1.46
Fakes overall normalization, mu [%]	-	-	±0.11	-	±0.10	±0.11	±0.13	∓0.30	-	-
Fakes alternative parametrization [%]	-	-	-	±0.21	±0.64	∓0.68	-	±0.89	±0.16	±0.41
W+jets heavy flavour component [%]	±0.10	-	∓0.12	∓0.13	∓0.40	∓0.75	∓0.85	∓0.74	∓0.67	∓0.70
W+jets Scales [%]	-	∓0.10	±0.12	±0.40	±0.73	±0.82	±0.62	-	±0.16	-
Single Top DS/DR [%]	±0.19	-	∓0.16	∓0.46	∓1.04	∓1.66	∓1.26	∓1.35	∓2.18	∓0.94
Single Top IFSR [%]	- +0.23	-	+0.11 −0.21	+0.20 −0.27	- −0.72	+0.41 −0.88	+0.64 −1.31	+0.95 -	+1.63 -	+1.89 −0.89

TABLE F.60: Table of systematics for the relative differential cross-section at the parton level for the $p_T^{t\bar{t}}$ observable.

Bins [GeV]	325–400	400–480	480–580	580–700	700–860	860–1020	1020–1250	1250–1500	1500–2000
$1/\sigma \cdot d\sigma$ / $dm^{t\bar{t}}$	$3.11 \cdot 10^{-3}$	$3.84 \cdot 10^{-3}$	$2.17 \cdot 10^{-3}$	$1.03 \cdot 10^{-3}$	$4.21 \cdot 10^{-4}$	$1.76 \cdot 10^{-4}$	$6.81 \cdot 10^{-5}$	$2.28 \cdot 10^{-5}$	$5.93 \cdot 10^{-6}$
Total Uncertainty [%]	±19.7	+1.36 −1.52	+7.52 −7.59	±11.6	+11.9 −11.8	+10.1 −9.47	+14.2 −14.1	+11.4 −9.64	+20.5 −21.4
Statistics [%]	±0.2	±0.1	±0.2	±0.3	±0.5	±0.8	±1.3	±2.5	±4.8
Systematics [%]	±19.7	+1.35 −1.51	+7.51 −7.58	±11.6	+11.9 −11.7	+10.0 −9.41	+14.1 −14.0	+11.0 −9.13	+19.6 −20.5
Jet energy resolution [%]	∓0.41	-	-	±0.22	±0.20	±1.08	±1.33	∓1.06	∓0.40
b-Tagged jet energy scale (JES) [%]	−0.80 +0.84	+0.10 −0.13	+0.40 −0.43	+0.33 −0.39	+0.13 −0.15	+0.44 -	-	+1.04 −2.55	-
Effective detector NP set 1 (JES) [%]	+0.22 -	-	-	+0.10 -	-	+0.30 -	-	+0.89 -	-
Effective detector NP set 2 (JES) [%]	-	-	-	−0.17 -	+0.16 −0.10	+0.48 -	−0.20 −0.27	+0.45 -	−1.64 -
Effective mixed NP set 1 (JES) [%]	−0.25 +0.50	-	-	+0.14 −0.25	+0.23 −0.24	+0.66 -	+0.39 −0.30	+1.41 -	−2.91 -
Effective mixed NP set 2 (JES) [%]	-	-	−0.25	-	-	+0.55 -	-	-	−2.95 -
Effective mixed NP set 3 (JES) [%]	-	-	-	-	-	-	+0.21 -	-	−1.64 -
Effective modelling NP set 1 (JES) [%]	-	+0.27 −0.29	- −0.20	−0.26 +0.23	−0.53 +0.76	−0.26 +1.26	−1.12 +0.52	+0.41 −0.13 −0.16 +0.58	−1.46 −1.33 +0.69
Effective modelling NP set 2 (JES) [%]	−0.18 +0.38	-	−0.21	+0.15 −0.21	+0.29 −0.19	+0.42 -	-	-	−0.69
Effective modelling NP set 3 (JES) [%]	+0.49 −0.29	-	−0.21 -	−0.19 +0.23	∓0.31	- +0.47	−0.14 +0.24	+1.11 -	−2.05
Effective modelling NP set 4 (JES) [%]	-	-	-	-	-	+0.43 -	-	+0.33 -	-
Effective statistical NP set 1 (JES) [%]	-	-	-	-	−0.17 +0.24	+0.46 -	+0.35 -	+0.80 -	−1.33 −1.48
Effective statistical NP set 2 (JES) [%]	-	-	-	-	-	+0.52 -	±0.13	+0.87 -	-
Effective statistical NP set 3 (JES) [%]	-	-	-	-	-	-	+0.51 -	+0.32 -	−2.44 -
Effective statistical NP set 4 (JES) [%]	−0.17 +0.44	-	- −0.30	+0.12 −0.22	+0.19 -	-	- −0.52	+1.66 -	−1.79 -
Effective statistical NP set 5 (JES) [%]	-	-	-	-	-	+0.27 -	-	+1.32 -	−1.79 -
Effective statistical NP set 6 (JES) [%]	-	-	-	-	-	+0.42 -	-	−0.12 -	−2.25 -
Effective statistical NP set 7 (JES) [%]	-	-	-	-	+0.21	+0.20	+0.23	+1.48 +1.18	−2.02 -
η intercalibration model (JES) [%]	−0.29 +0.49	-	- −0.27	+0.24 −0.26	+0.31 −0.13	+0.53 −0.16	+0.21 −0.44	+1.47 −0.35	−1.42 +1.78 −2.52
η intercalibration non closure (JES) [%]	-	-	-	-	-	+0.53 -	-	+0.43 -	-
η intercalibration total stat (JES) [%]	−0.10 +0.26	-	- −0.13	-	-	+0.29 -	−0.24 ±0.24	+0.53 -	−1.42 - −1.82
Flavour composition (JES) [%]	+0.36 −0.32	+0.21 −0.31	−0.20 +0.16	−0.53 +0.31	−0.40 +0.80	−0.19 +0.97	+0.50 -	−0.11 +1.77	- −1.65
Flavour response (JES) [%]	-	−0.14 -	-	+0.10 −0.13	+0.45 −0.15	+0.47 -	-	+0.40 -	- −1.23
Pile-up offset μ (JES) [%]	-	-	-	-	-	+0.42 -	+0.57 -	- +1.04	−1.37
Pile-up offset N_{PV} (JES) [%]	-	-	-	-	-	+0.41 -	- −0.29	+0.58 -	−1.66 -
Pile-up offset p_T (JES) [%]	+0.21 −0.63 +0.79	-	+0.26 −0.42	+0.32 −0.54	+0.56 −0.31	+0.71 -	+0.28 −0.92	+1.14 −0.11	−1.45
Pile-up offset ρ topology (JES) [%]	−0.34 +0.68	+0.44 −0.57	+0.19 −0.51	−0.29 -	−0.75 +1.00	−0.27 +1.42	−0.12 +0.73	+1.93 +0.29	−2.51 +0.57
Punch-through (JES) [%]	-	-	-	-	-	-	-	−0.10 -	−1.91 -
Single particle high-p_T (JES) [%]	-	-	-	-	-	-	-	-	−1.67
Jet vertex fraction [%]	±0.27	-	∓0.11	∓0.21	−0.25 +0.26	∓0.24	∓0.24	∓0.24	−0.20 +0.21
b-Quark tagging efficiency (eigenvector 0) [%]	−1.03 +0.96	−0.20 +0.18	+0.45 −0.42	+0.79 −0.73	+0.50 −0.84	+0.77 −0.71	+0.62 −0.58	+0.73 −0.68	+0.73 −0.69
b-Quark tagging efficiency (eigenvector 1) [%]	+0.62 −0.61	±0.22	−0.20 +0.19	−0.56 +0.55	−0.79 +0.78	−0.84 +0.82	−0.84 +0.83	−0.89 +0.87	−1.11 +1.10
b-Quark tagging efficiency (eigenvector 2) [%]	±0.30	±0.14	-	∓0.29	−0.46 +0.47	−0.52 +0.53	−0.54 +0.55	−0.59 +0.60	−0.70 +0.71
b-Quark tagging efficiency (eigenvector 3) [%]	∓0.23	-	±0.12	±0.19	±0.17	±0.12	±0.10	±0.10	±0.11
c-Quark tagging efficiency (eigenvector 1) [%]	-	-	-	-	∓0.11	∓0.12	∓0.16	∓0.16	∓0.29
c-Quark tagging efficiency (eigenvector 2) [%]	-	-	-	-	-	-	∓0.10	∓0.14	∓0.15
Light-jet tagging efficiency (eigenvector 0) [%]	-	-	-	-	-	−0.16 +0.19	−0.35 +0.40	−0.68 +0.67	−0.19 +0.17
Light-jet tagging efficiency (eigenvector 1) [%]	-	-	-	-	-	-	-	+0.11 −0.12	−0.22 +0.21
Light-jet tagging efficiency (eigenvector 2) [%]	-	-	-	-	-	-	-	-	-
Light-jet tagging efficiency (eigenvector 3) [%]	-	-	-	-	-	∓0.13	∓0.16	∓0.27	∓0.32
Light-jet tagging efficiency (eigenvector 5) [%]	-	-	-	-	-	-	-	∓0.12	∓0.14
b-Quark tagging extrapolation [%]	-	-	-	-	-	±0.10	±0.15	±0.18	+0.25 −0.24
Electron energy resolution [%]	-	-	-	-	-	+0.20 -	-	+0.21 −0.48	- −1.09
Electron energy scale [%]	-	-	-	-	-	-	+0.14 −0.13	- −0.61	- −1.90
Electron identification efficiency [%]	-	-	-	-	±0.10	±0.13	±0.16	±0.22	±0.28
Electron isolation efficiency [%]	-	-	-	-	±0.10	±0.13	±0.13	+0.14 −0.15	±0.16
Muon (ID) momentum resolution [%]	-	-	-	-	-	-	+0.28 -	+0.85 -	- −2.28
Muon (MS) momentum resolution [%]	-	-	-	-	-	-	-	+1.17 -	−0.69 -
Muon (ID) sagitta ρ [%]	-	-	-	-	-	-	-	-	-
Muon energy scale [%]	-	-	-	-	-	-	−0.20 -	+0.58 -	−0.65 -
Muon identification syst [%]	-	-	-	-	-	-	−0.32 ±0.12	±0.16	−2.19 ±0.17
E_T^{miss} Soft jet resolution para [%]	±0.12	-	-	-	-	±0.22	±0.13	±0.45	∓1.99
E_T^{miss} Soft jet resolution perp [%]	-	-	-	-	-	±0.26	±0.31	±0.17	∓3.62
E_T^{miss} Soft jet scale [%]	-	-	-	-	−0.11 +0.19	-	-	+0.64 -	- −1.84
Z+jets cross-section [%]	+0.21 −0.22	-	-	∓0.17	∓0.17	-	-	-	-
Monte Carlo sample statistics [%]	±0.21	±0.10	±0.19	±0.21	±0.31	±0.55	±0.93	±1.79	±3.51
ISR/FSR + scale [%]	- −0.61	+0.46 −0.58	+0.31 −0.27	−0.71 +0.58	−0.66 +1.54	+1.41 -	+1.16 -	+2.74 -	−1.47 +9.70
Alternate hard-scattering model [%]	±15.9	∓0.81	∓5.85	∓8.65	∓9.43	∓6.57	∓10.7	∓3.48	±7.38
Alternate parton-shower model [%]	±11.3	±0.66	∓4.59	∓7.50	∓6.79	∓6.28	∓8.33	∓7.35	∓13.7
Inter PDF [%]	-	-	-	-	-	-	-	±0.25	±0.62
Intra PDF [%]	∓0.10	-	-	-	±0.13	±0.32	±0.54	±0.66	±1.04
Fakes overall normalization, el [%]	+1.19 −1.22	-	−0.41 +0.42	−1.01 +1.04	-	−1.43 +1.47	−1.74 +1.79	−1.26 +1.29	−3.27 +3.37
Fakes overall normalization, mu [%]	-	-	-	-	-	-	-	±0.36	±0.45
Fakes alternative parametrization [%]	-	-	-	±0.25	-	∓0.10	-	±1.76	∓0.26
W+jets heavy flavour component [%]	±0.18	-	∓0.14	∓0.11	-	±0.20	±0.69	±1.04	±0.76
W+jets Scales [%]	±0.16	∓0.10	∓0.24	-	±0.11	±0.68	±1.36	±2.07	±2.66
Single Top DS/DR [%]	±0.13	-	-	∓0.19	∓0.10	±0.11	±0.16	±0.54	±0.21
Single Top IFSR [%]	- +0.16	-	-	-	-	- −0.21	+0.50 −0.11	+0.56 −0.52	- −0.31

TABLE F.61: Table of systematics for the relative differential cross-section at the parton level for the $m^{t\bar{t}}$ observable.

Bins [Unit $y^{t\bar{t}}$]	-2.50—1.80	-1.80—1.40	-1.40—1.10	-1.10—0.80	-0.80—0.50	-0.50—0.25	-0.25–0	0–0.25	0.25–0.50	0.50–0.80	0.80–1.10	1.10–1.40	1.40–1.80	1.80–2.50
$1/\sigma \cdot d\sigma$ / $dy^{t\bar{t}}$	$5.53 \cdot 10^{-2}$	$1.32 \cdot 10^{-1}$	$2.02 \cdot 10^{-1}$	$2.60 \cdot 10^{-1}$	$3.11 \cdot 10^{-1}$	$3.47 \cdot 10^{-1}$	$3.57 \cdot 10^{-1}$	$3.50 \cdot 10^{-1}$	$3.43 \cdot 10^{-1}$	$3.15 \cdot 10^{-1}$	$2.65 \cdot 10^{-1}$	$2.05 \cdot 10^{-1}$	$1.35 \cdot 10^{-1}$	$5.44 \cdot 10^{-2}$
Total Uncertainty [%]	+6.58 −6.23	+3.66 −3.76	+1.86 −1.37	+1.95 −1.83	+1.50 −1.33	+1.74 −1.58	+2.00 −2.31	+1.74 −2.20	+1.79 −1.55	+1.52 −1.50	+1.26 −1.53	+1.49 −1.78	+5.91 −5.94	+5.82 −5.94
Statistics [%]	±1.6	±0.7	±0.5	±0.4	±0.3	±0.3	±0.3	±0.3	±0.3	±0.3	±0.4	±0.5	±0.7	±1.6
Systematics [%]	+6.29 −5.92	+3.54 −3.65	+1.74 −1.20	+1.86 −1.73	+1.41 −1.23	+1.67 −1.51	+1.95 −2.27	+1.66 −2.14	+1.73 −1.48	+1.45 −1.43	+1.14 −1.44	+1.33 −1.66	+5.85 −5.87	+5.49 −5.62
Jet energy resolution [%]	∓0.30	∓0.52	-	±0.48	∓0.37	∓0.31	∓0.12	±0.20	-	-	∓0.16	±0.26	±0.84	±0.23
b-Tagged jet energy scale (JES) [%]	−0.48 +0.42	+0.17	-	−0.20	-	-	-	-	-	-	−0.20	-	−0.14 +0.21	+0.36 +0.23
Effective detector NP set 1 (JES) [%]	+0.54 -	-	-	-	-	-	-	-	-	-	- −0.25	- −0.20	+0.27 -	−0.31 +0.38
Effective detector NP set 2 (JES) [%]	-	-	+0.26	-	±0.10	-	-	-	-	-	-	-	+0.15	-
Effective mixed NP set 1 (JES) [%]	+0.25	−0.17	-	+0.26 +0.26	-	-	-	-	-	-	-	−0.15	−0.18 -	−0.41 -
Effective mixed NP set 2 (JES) [%]	+0.27	−0.28	-	-	-	-	-	-	-	-	-	-	- −0.26	-
Effective mixed NP set 3 (JES) [%]	+0.26	-	-	-	-	-	-	-	-	-	-	-	+0.21 -	-
Effective modelling NP set 1 (JES) [%]	−0.38 +0.62	−0.43 +0.34	−0.12 +0.23	+0.25 -	+0.24 −0.11	+0.14 −0.30	+0.22 −0.44	+0.24 −0.30	+0.24 −0.20	- −0.23	- -	−0.21 −0.12 +0.20	- −0.65 +0.66	+0.35 −1.24 +0.96
Effective modelling NP set 2 (JES) [%]	+0.51 -	-	-	-	-	-	-	-	-	-	- −0.20	- −0.29	-	-
Effective modelling NP set 3 (JES) [%]	−0.14 +0.54	-	-	-	-	-	-	-	-	-	-	-	-	-
Effective modelling NP set 4 (JES) [%]	+0.39 -	-	-	-	-	-	-	-	-	-	-	-	-	−0.21 +0.13
Effective statistical NP set 1 (JES) [%]	+0.55 -	+0.22 -	-	-	+0.11 -	+0.16 -	-	-	-	-	-	-	−0.14 +0.15	-
Effective statistical NP set 2 (JES) [%]	+0.20 -	- −0.27	+0.12 −0.16 +0.26	+0.20 -	-	-	-	-	-	-	-	-	+0.24 −0.17	- −0.35
Effective statistical NP set 3 (JES) [%]	−0.18 +0.35	-	-	-	-	-	-	-	-	-	-	-	-	−0.32 +0.17
Effective statistical NP set 4 (JES) [%]	+0.48 -	−0.16 +0.12	+0.10 −0.23	-	-	-	-	-	-	-	-	-	-	-
Effective statistical NP set 5 (JES) [%]	+0.31 -	- −0.23	- +0.25	-	-	-	-	-	-	-	-	-	-	+0.20 −0.50
Effective statistical NP set 6 (JES) [%]	+0.45 -	-	-	-	-	-	-	-	-	-	-	−0.25 -	-	-
Effective statistical NP set 7 (JES) [%]	+0.33 -	+0.14 -	+0.28 -	-	-	-	−0.23 +0.12	−0.26 +0.24	−0.11 +0.23	-	-	- −0.17	+0.23 −0.36	−0.39 -
η intercalibration model (JES) [%]	- -	−0.11 -	-	−0.22 +0.45	-	-	-	-	-	-	-	+0.27 −0.32	-	−0.40 +0.19
η intercalibration non closure (JES) [%]	-	−0.15	-	-	+0.26	+0.17	-	-	-	-	−0.34	-	-	-
η intercalibration total stat (JES) [%]	- +0.50	- +0.25	-	-	-	-	-	-	-	-	-	-	-	−0.42 +0.20
Flavour composition (JES) [%]	−0.44 +0.55	−0.57 +0.23	+0.20 -	+0.32 -	-	+0.22 −0.10	+0.21 −0.27	+0.21 −0.24	+0.29 −0.16	-	-	-	−0.33 +0.72	−1.34 -
Flavour response (JES) [%]	+0.45 -	-	-	-	-	-	−0.21 +0.15	-	-	- −0.21	-	-	+0.27 −0.41	+0.12 −0.44
Pile-up offset μ (JES) [%]	- −0.33	+0.10 −0.30	+0.20 -	+0.32 -	-	-	-	-	- +0.21	-	-	-	+0.24 -	- −0.25
Pile-up offset N_{PV} (JES) [%]	+0.11 −0.40	−0.32 -	+0.27 -	-	-	-	-	-	-	-	-	-	−0.21 -	- −0.41
Pile-up offset p_T (JES) [%]	+0.49 -	- −0.28	+0.31 −0.14	-	-	-	- −0.21	-	+0.10 −0.11	-	-	-	-	- −0.50
Pile-up offset ρ topology (JES) [%]	−1.40 +2.25	−0.97 +0.53	-	−0.13	+0.45 −0.21	+0.45 −0.38	+0.33 −0.56	+0.33 −0.71	+0.63 −0.36	+0.27 −0.26	-	−0.17 +0.43	−0.83 +0.96	−1.99 +1.15
Punch-through (JES) [%]	-	-	-	-	-	-	-	-	-	-	-	-	-	-
Single particle high-p_T (JES) [%]	- −0.22	-	-	-	-	-	-	-	-	-	-	-	-	+0.37 -
b-Quark tagging efficiency (eigenvector 0) [%]	-	+0.22 −0.20	+0.13 −0.12	-	-	-	−0.12 +0.11	−0.12 +0.11	-	-	-	-	+0.26 −0.24	+0.23 −0.21
Light-jet tagging efficiency (eigenvector 0) [%]	−0.28 +0.31	-	-	+0.27 −0.41	-	-	-	+0.15 −0.18	-	-	-	-	-	−0.34 +0.32
Light-jet tagging efficiency (eigenvector 1) [%]	±0.17	-	-	−0.12 +0.11	-	-	-	-	-	-	-	-	-	+0.22 −0.23
Light-jet tagging efficiency (eigenvector 2) [%]	∓0.16	-	-	−0.20 +0.15	-	-	-	-	-	-	-	-	-	±0.26
Light-jet tagging efficiency (eigenvector 3) [%]	∓0.12	-	-	−0.17 +0.14	-	-	-	-	-	-	-	-	-	−0.14 +0.15
Electron energy resolution [%]	+0.22 -	−0.36 -	+0.26 -	-	-	-	-	-	-	-	-	-	-	+0.12 −0.13
Electron energy scale [%]	-	-	-	-	-	-	-	-	-	-	-	-	-	+0.21 -
Electron identification efficiency [%]	±0.18	-	-	-	-	-	-	-	-	-	-	-	-	±0.19
Muon (ID) momentum resolution [%]	- −0.22	-	-	-	-	-	-	-	-	-	-	-	-	- +0.23
Muon (MS) momentum resolution [%]	-	-	-	-	-	- −0.20	-	-	-	-	-	-	-	+0.14 -
Muon (ID) sagitta ρ [%]	-	-	-	-	-	-	-	-	-	-	-	-	-	-
Muon energy scale [%]	−0.47 +0.27	-	-	-	-	-	-	-	-	-	-	-	−0.19 -	+0.26 -
Muon identification syst [%]	-	-	-	-	-	-	-	-	-	-	-	-	±0.10	±0.12
E_T^{miss} Soft jet resolution para [%]	±0.13	-	-	∓0.11	±0.12	-	-	-	±0.17	-	-	-	∓0.17	∓0.20
E_T^{miss} Soft jet resolution perp [%]	±0.57	±0.11	∓0.40	±0.12	∓0.10	±0.13	-	-	-	-	∓0.11	-	-	∓0.10
E_T^{miss} Soft jet scale [%]	+0.48 -	-	-	+0.16 -	−0.15 +0.13	-	-	-	-	-	-	-	-	-
Z+jets cross-section [%]	±0.15	-	-	-	-	-	-	-	-	-	-	-	-	-
Monte Carlo sample statistics [%]	±1.04	±0.52	±0.34	±0.39	±0.29	±0.28	±0.23	±0.33	±0.25	±0.25	±0.29	±0.36	±0.43	±1.05
ISR/FSR + scale [%]	−1.61 +0.74	+1.01	−0.34 +0.95	-	+0.34	+0.59	+0.56 −0.94	- −1.13	+0.32 −0.37	+0.61 -	-	−0.93 +0.35	- −1.06	−1.34 +2.54
Alternate hard-scattering model [%]	±0.88	∓0.40	∓0.53	∓0.59	∓0.39	-	∓1.45	±1.04	±0.96	-	∓0.11	∓0.32	±3.81	∓1.39
Alternate parton-shower model [%]	∓4.59	∓0.48	±0.21	±0.82	±0.88	±0.76	±0.70	±0.35	±0.80	±0.86	±0.74	∓0.56	∓3.74	∓2.69
Inter PDF [%]	±0.87	-	-	-	-	∓0.11	∓0.12	∓0.11	∓0.10	-	-	-	-	±0.88
Intra PDF [%]	±1.96	-	∓0.11	∓0.17	∓0.20	∓0.22	∓0.21	∓0.20	∓0.21	∓0.20	∓0.16	∓0.11	-	±1.92
Fakes overall normalization, el [%]	−0.90 +0.93	+2.03 −2.09	+0.37 −0.39	+0.63 −0.65	∓0.13	−0.66 +0.68	−0.28 +0.29	+0.93 −0.95	∓0.13	−0.76 +0.78	−0.49 +0.50	±0.17	+0.52 −0.54	−1.47 +1.52
Fakes overall normalization, mu [%]	±0.34	-	-	-	-	-	-	-	-	-	-	-	-	±0.13
Fakes alternative parametrization [%]	±0.98	∓2.36	∓0.59	∓0.84	±0.35	±0.83	±0.63	-	±0.14	±0.43	±0.55	∓0.75	∓1.24	±1.35
W+jets heavy flavour component [%]	-	-	-	-	-	-	-	-	-	-	-	-	-	±0.22
W+jets Scales [%]	±0.17	±0.17	-	-	-	-	-	-	±0.11	-	∓0.13	-	-	∓0.13
Single Top DS/DR [%]	-	-	-	-	-	-	∓0.11	-	-	-	∓0.12	-	±0.13	±0.20
Single Top IFSR [%]	- +0.28	-	- −0.20	-	-	-	-	- +0.19	-	-	-	-	+0.25 -	- −1.11

TABLE F.62: Table of systematics for the relative differential cross-section at the parton level for the $y^{t\bar{t}}$ observable.

Bins [GeV] x [GeV]	0–90	90–180	180–300	300–1000	1000–1080	1080–1170	1170–1280	1280–2000	2000–2080	2080–2170	2170–2270	2270–2370	2370–3000	3000–3090	3090–3180	3180–3280	3280–3370	3370–4000
$1/\sigma \cdot d\sigma \ / \ dm^{t\bar{t}} vs p_T^{t,had}$	$3.54 \cdot 10^{-3}$	$2.77 \cdot 10^{-3}$	$1.94 \cdot 10^{-4}$	$2.95 \cdot 10^{-6}$	$6.97 \cdot 10^{-4}$	$1.36 \cdot 10^{-3}$	$8.73 \cdot 10^{-4}$	$1.50 \cdot 10^{-5}$	$1.84 \cdot 10^{-4}$	$3.35 \cdot 10^{-4}$	$2.74 \cdot 10^{-4}$	$1.65 \cdot 10^{-4}$	$8.93 \cdot 10^{-6}$	$4.45 \cdot 10^{-5}$	$7.84 \cdot 10^{-5}$	$6.25 \cdot 10^{-5}$	$4.12 \cdot 10^{-5}$	$9.41 \cdot 10^{-6}$
Total Uncertainty [%]	+8.53 / −8.52	+3.38 / −3.43	+11.5 / −12.3	+10.8 / −10.2	+4.08 / −3.62	+10.3 / −10.4	+10.9 / −11.0	+10.9 / −12.2	+7.03 / −6.33	+7.32 / −6.61	+14.5 / −14.3	+18.4 / −18.2	+13.4 / −15.3	+20.8 / −18.1	+13.0 / −11.8	+14.5 / −13.8	+17.0 / −18.0	+17.5 / −7.59
Statistics [%]	±0.2	±0.2	±0.6	±4.5	±0.5	±0.3	±0.4	±1.2	±1.3	±0.8	±0.8	±0.9	±2.9	±3.3	±2.3	±2.0	±2.4	±3.9
Systematics [%]	±8.52	+3.36 / −3.42	+11.4 / −12.3	+9.45 / −8.83	+3.97 / −3.49	+10.3 / −10.4	+10.9 / −11.0	+10.8 / −12.1	+6.83 / −6.11	+7.24 / −6.52	+14.5 / −14.3	+18.4 / −18.2	+12.9 / −14.9	+20.4 / −17.5	+12.7 / −11.4	+14.2 / −13.6	+16.7 / −17.7	+16.9 / −5.96
Jet energy resolution [%]	∓0.70	±0.29	±0.74	-	±1.02	-	∓0.23	±1.47	±2.13	-	-	±0.26	±2.09	±0.52	±2.86	±1.29	∓0.74	±1.16
b-Tagged jet energy scale (JES) [%]	−0.56 / +0.62	+0.24 / −0.29	+0.34 / −0.75	+1.00 / -	- / +0.23	+0.32 / −0.46	+0.51 / −0.62	- / −0.18	−0.37 / +0.12	+0.32 / −0.36	+0.35 / −0.24	+0.21 / -	−0.50 / +0.48	+1.73 / -	+0.92 / -	+0.71 / -	- / −1.03	−1.43 / +1.65
Effective detector NP set 1 (JES) [%]	- / +0.11	-	- / −0.30	+1.21 / -	-	-	- / −0.16	- / −0.48	-	-	-	- / +0.22	- / −0.92	- / +1.76	- / +0.49	- / +0.44	- / −1.01	−0.63 / +0.62
Effective detector NP set 2 (JES) [%]	-	-	- / −0.26	+1.20 / -	-	-	-	- / −0.25	-	+0.22 / −0.24	- / +0.29	-	- / −0.86	- / +0.85	-	- / +0.51	- / −0.63	- / −0.66
Effective mixed NP set 1 (JES) [%]	−0.31 / +0.33	-	- / −0.25	+1.35 / −0.44	-	- / −0.27	+0.26 / −0.27	- / −0.63	+0.33 / -	+0.44 / −0.18	+0.24 / −0.41	+0.32 / −0.22	- / −1.13	- / +1.11	- / +0.89	- / +1.06	- / −0.60	+1.13 / −0.34
Effective mixed NP set 2 (JES) [%]	-	-	−0.39 / +0.11	+0.81 / -	-	-	-	-	-	-	-	-	- / −1.13	- / +0.93	- / +0.26	- / +0.83	- / −0.53	- / −0.76
Effective mixed NP set 3 (JES) [%]	-	-	- / −0.22	+0.35 / -	+0.23 / -	-	-	- / −0.36	+0.32 / −0.12	- / −0.25	- / +0.37	+0.15 / −0.16	- / −1.05	- / +0.66	- / +0.38	-	- / −0.46	- / −0.38
Effective modelling NP set 1 (JES) [%]	+0.21 / −0.13	+0.20 / −0.25	−0.68 / +0.11	−0.59 / +1.05	+0.65 / −0.51	+0.15 / −0.27	−0.73 / +0.53	−2.18 / +1.42	-	+0.30 / -	−0.32 / +0.75	−1.32 / +1.70	−2.84 / +2.36	- / +2.28	+0.47 / -	−0.25 / +0.95	- / −2.14	−1.11 / +2.01
Effective modelling NP set 2 (JES) [%]	−0.22 / +0.28	-	+0.13 / −0.21	+0.69 / −0.90	−0.11 / +0.28	-	+0.27 / −0.39	- / −0.37	±0.12	-	+0.37 / -	+0.44 / −0.23	- / −1.46	- / +0.72	- / +0.29	+0.95 / -	- / −0.89	+2.10 / -
Effective modelling NP set 3 (JES) [%]	+0.31 / −0.33	-	−0.28 / +0.24	- / −0.54	+0.24 / −0.16	- / −0.18	−0.33 / +0.38	- / −0.23	+0.30 / -	−0.32 / +0.29	−0.28 / +0.38	−0.30 / +0.46	- / −1.05	- / +1.89	- / +0.76	- / +0.88	- / −0.93	−0.28 / +0.65
Effective modelling NP set 4 (JES) [%]	-	-	- / −0.36	+1.78 / −0.77	-	-	-	- / −0.45	-	+0.42 / -	+0.32 / -	+0.33 / -	- / −2.27	- / +1.00	- / +0.64	- / +0.36	- / −0.77	−0.33 / +0.25
Effective statistical NP set 1 (JES) [%]	-	-	- / −0.29	- / −0.83	+0.19 / −0.13	-	−0.20 / +0.14	−0.66 / -	+0.27 / -	-	+0.44 / -	−0.28 / +0.44	- / −1.24	- / +2.12	- / +1.96	- / +0.68	- / −0.92	+0.12 / −0.25
Effective statistical NP set 2 (JES) [%]	-	-	-	+0.64 / -	+0.32 / -	-	+0.14 / −0.21	- / −0.98	+0.26 / -	-	-	+0.25 / -	- / −0.41	- / +0.43	- / −0.15	- / +0.57	- / −1.24	+1.21 / −0.33
Effective statistical NP set 3 (JES) [%]	-	-	- / −0.28	- / −0.85	-	-	-	- / −0.58	+0.30 / -	- / −0.16	-	-	−0.82 / +0.33	- / +1.46	+1.05 / +0.66	- / +0.64	-	−1.66 / +0.57
Effective statistical NP set 4 (JES) [%]	−0.21 / +0.35	-	+0.24 / −0.30	- / −0.31	-	- / −0.30	+0.28 / −0.31	- / −0.49	−0.23 / +0.36	+0.12 / -	+0.36 / −0.27	+0.22 / -	- / −0.89	- / −0.46	+0.21 / −0.30	- / +0.57	- / −1.71	+0.90 / -
Effective statistical NP set 5 (JES) [%]	-	-	- / −0.33	+1.00 / -	- / +0.26	-	−0.12 / -	- / −0.25	-	- / +0.39	-	-	- / −1.20	+1.07 / −0.25	+0.94 / -	- / +0.48	- / −0.72	- / +0.65
Effective statistical NP set 6 (JES) [%]	-	-	-	+1.42 / -	-	-	-	−0.35 / -	-	-	- / +0.20	- / +0.35	+0.38 / −0.84	+1.08 / +0.38	- / +0.70	−0.19 / +0.55	- / −0.99	- / −0.28
Effective statistical NP set 7 (JES) [%]	-	-	-	+0.69 / −0.27	-	-	+0.12 / -	- / −0.55	+0.37 / -	+0.30 / -	- / +0.25	- / +0.24	- / −1.57	- / +3.36	- / +0.43	+0.50 / −0.15	- / −0.29	- / +0.42
η intercalibration model (JES) [%]	−0.27 / +0.31	-	-	−0.89 / +0.50	+0.65 / −0.44	+0.15 / −0.41	-	−0.83 / +0.62	+0.84 / −0.85	+0.55 / −0.57	+0.65 / −0.12	−0.24 / +0.30	∓0.42	+1.78 / -	+1.24 / −0.62	+1.30 / −0.27	- / −1.47	-
η intercalibration non closure (JES) [%]	-	-	−0.31 / -	- / −0.80	-	-	-	- / −0.72	-	-	+0.24 / -	-	- / −1.24	−0.22 / +0.39	-	-	- / −0.67	+1.06 / +0.24
η intercalibration total stat (JES) [%]	- / +0.15	-	- / −0.20	- / −1.14	+0.24 / -	-	-	−0.48 / -	-	-	-	- / +0.52	−1.74 / +0.20	- / +0.71	- / +0.97	- / +0.50	- / −0.98	−0.57 / +0.30
Flavour composition (JES) [%]	±0.39	- / −0.20	−0.68 / +0.21	−2.34 / +2.04	±0.44	-	−1.01 / +0.85	−2.12 / +1.55	+0.84 / −0.34	-	−0.10 / +0.75	−1.21 / +1.99	−2.14 / +1.64	- / +5.33	- / +1.16	- / −0.11	- / −2.86	- / +1.62
Flavour response (JES) [%]	-	-	- / −0.49	+1.58 / -	−0.11 / +0.37	−0.13 / -	+0.27 / −0.33	+0.46 / −1.18	- / +0.20	-	+0.42 / -	+0.93 / −0.43	+1.66 / −1.83	- / +0.74	+0.12 / −0.38	+1.22 / +0.44	- / −1.60	- / +0.23
Pile-up offset μ (JES) [%]	-	-	-	- / −0.20	+0.24 / +0.21	-	-	- / −0.38	+0.19 / -	-	−0.18 / +0.14	+0.22 / -	- / −1.25	- / +1.24	+0.95 / -	- / +1.24	- / −0.81	- / +0.41
Pile-up offset N_{PV} (JES) [%]	-	-	−0.41 / +0.42	- / −0.53	-	-	-	−0.32 / +0.12	- / −0.27	-	-	−0.24 / +0.35	- / +0.39	−0.74 / +1.66	- / +0.18	- / +0.32	- / −1.29	- / −0.29
Pile-up offset p_T (JES) [%]	−0.57 / +0.59	-	- / −0.53	+0.71 / -	−0.15 / +0.16	+0.19 / −0.42	+0.65 / −0.74	- / −0.88	+0.44 / -	+0.35 / −0.41	+0.67 / −0.24	+0.88 / −0.39	+0.50 / -	−0.47 / +1.07	+0.20 / −0.44	- / +1.21	- / −2.50	+0.56 / +0.70
Pile-up offset ρ topology (JES) [%]	−0.13 / +0.14	+0.45 / −0.44	- / −0.40	−3.60 / +1.28	+0.49 / −0.61	+0.50 / −0.59	−0.72 / +0.35	−2.71 / +2.01	+0.33	+0.44 / -	−0.20 / +0.73	−2.06 / +2.59	−3.74 / +2.91	- / +4.36	+0.48 / -	−0.43 / +0.49	−2.25 / +0.73	−1.16 / +3.19
Punch-through (JES) [%]	-	-	- / −0.24	+0.49 / −0.19	-	-	-	- / −0.47	- / −0.19	-	+0.19 / -	-	−0.38 / +0.18	-	- / +0.31	-	-	−0.42 / +0.13
Single particle high-p_T (JES) [%]	-	-	-	+0.88 / -	-	-	-	-	- / −0.25	-	- / +0.26	-	- / −0.34	−0.19 / +0.53	- / −0.43	- / −0.48	- / −0.33	+0.34 / −0.74
Jet vertex fraction [%]	±0.25	-	∓0.25	−0.39 / +0.40	±0.22	-	−0.36 / +0.37	−0.45 / +0.46	+0.28 / −0.29	-	−0.35 / +0.36	−0.49 / +0.50	−0.40 / +0.41	±0.35	-	−0.35 / +0.36	−0.51 / +0.52	−0.43 / +0.44
b-Quark tagging efficiency (eigenvector 0) [%]	−0.98 / +0.91	+0.15 / −0.14	+1.24 / −1.15	+1.51 / −1.39	−0.84 / +0.77	+0.37 / −0.35	+1.36 / −1.25	+1.72 / −1.59	−0.97 / +0.88	±0.14	+1.39 / −1.28	+1.61 / −1.48	+0.73 / −0.67	−1.17 / +1.06	−0.12 / +0.10	+1.17 / −1.09	+1.56 / −1.44	+0.49 / −0.45
b-Quark tagging efficiency (eigenvector 1) [%]	+0.58 / −0.57	-	−0.63 / +0.61	−1.56 / +1.53	+0.42 / −0.41	∓0.15	−0.82 / +0.81	−1.34 / +1.33	+0.38 / −0.37	−0.12 / +0.11	−0.96 / +0.94	−1.59 / +1.57	−1.64 / +1.62	+0.33 / −0.32	−0.13 / +0.12	−0.94 / +0.92	−1.59 / +1.57	−1.91 / +1.89
b-Quark tagging efficiency (eigenvector 2) [%]	+0.30 / −0.31	-	−0.34 / +0.35	−1.01 / +1.03	±0.33	-	−0.45 / +0.46	−0.84 / +0.85	+0.37 / −0.38	-	−0.55 / +0.56	−1.00 / +1.01	−1.26 / +1.28	±0.33	-	−0.55 / +0.56	−1.07 / +1.09	−1.45 / +1.48
b-Quark tagging efficiency (eigenvector 3) [%]	∓0.23	-	±0.25	-	∓0.22	±0.12	±0.34	±0.27	∓0.23	±0.10	±0.31	±0.21	∓0.17	∓0.18	±0.11	±0.30	±0.15	∓0.32
c-Quark tagging efficiency (eigenvector 0) [%]	-	-	-	∓0.13	+0.11 / −0.10	-	∓0.11	±0.14	±0.13	-	∓0.11	∓0.19	∓0.15	±0.18	-	-	∓0.13	∓0.19
c-Quark tagging efficiency (eigenvector 1) [%]	-	-	∓0.14	∓0.44	-	-	∓0.12	−0.24 / +0.23	-	-	∓0.14	∓0.19	∓0.34	-	∓0.15	∓0.19	∓0.20	∓0.29
c-Quark tagging efficiency (eigenvector 2) [%]	-	-	-	∓0.24	-	-	∓0.10	∓0.19	-	-	∓0.10	∓0.20	∓0.29	-	-	∓0.12	∓0.19	∓0.27
Light-jet tagging efficiency (eigenvector 0) [%]	-	-	-	-	+0.17 / −0.23	-	-	-	−0.39 / +0.38	−0.21 / +0.23	-	∓0.14	-	−1.39 / +1.53	−1.16 / +1.37	−0.18 / +0.19	-	-
Light-jet tagging efficiency (eigenvector 1) [%]	-	-	−0.12 / +0.11	∓0.27	-	-	∓0.15	∓0.14	±0.28	±0.10	∓0.12	∓0.20	−0.16 / +0.15	±0.52	+0.54 / −0.51	-	∓0.31	∓0.20
Light-jet tagging efficiency (eigenvector 2) [%]	-	-	-	+0.19 / −0.18	-	-	-	-	−0.10 / +0.12	-	-	-	-	−0.11 / +0.12	−0.15 / +0.17	−0.13 / +0.14	-	∓0.13
Light-jet tagging efficiency (eigenvector 3) [%]	-	-	-	-	+0.12 / −0.13	-	-	∓0.12	-	-	-	∓0.10	−0.20 / +0.21	∓0.29	−0.20 / +0.21	−0.17 / +0.18	∓0.27	-
Light-jet tagging efficiency (eigenvector 5) [%]	-	-	-	-	-	-	-	-	-	-	-	-	-	∓0.31	∓0.22	-	-	-
Light-jet tagging efficiency (eigenvector 6) [%]	-	-	-	-	-	-	-	-	-	-	-	-	-	±0.15	±0.11	-	-	-
Light-jet tagging efficiency (eigenvector 7) [%]	-	-	-	-	-	-	-	-	-	-	-	-	-	∓0.17	∓0.13	-	-	-
b-Quark tagging extrapolation [%]	-	-	-	±0.37	-	-	-	-	-	-	-	-	±0.57	-	-	-	±0.18	±1.12
Electron energy resolution [%]	-	-	-	−0.12 / +0.45	-	-	-	- / −0.36	- / −0.46	-	+0.27 / -	+0.27 / -	- / −0.39	+0.11 / −0.35	-	- / −0.21	-	- / −0.81
Electron energy scale [%]	-	-	-	-	-	-	-	- / −0.60	-	-	-	-	−0.52 / +0.10	+0.71 / −0.40	-	−0.17 / +0.19	- / −0.78	- / −0.35
Electron identification efficiency [%]	-	-	-	-	-	-	-	-	-	-	±0.11	±0.17	±0.19	±0.18	±0.16	±0.17	+0.18 / −0.19	±0.28
Electron isolation efficiency [%]	-	-	-	-	-	-	-	-	-	-	±0.10	+0.23 / −0.24	±0.31	-	-	-	±0.23	±0.46
Muon (ID) momentum resolution [%]	-	-	- / −0.21	−0.42 / -	+0.23 / -	-	-	- / −0.44	−0.40 / -	−0.35 / +0.11	+0.26 / -	-	- / −0.94	+0.85 / -	−0.54 / +0.61	+0.82 / -	−0.30 / +0.26	- / −0.76
Muon (MS) momentum resolution [%]	-	-	- / −0.28	−0.93 / +0.97	+0.25 / -	-	-	−0.13 / +0.16	-	-	-	-	- / −0.61	+0.73 / -	- / −0.16	+0.83 / -	- / −0.68	+1.04 / -
Muon (ID) sagitta o [%]	-	-	-	-	+0.15 / -	-	-	-	-	-	-	-	+0.48 / −0.25	- / −0.51	- / −0.22	-	- / −0.17	- / −0.45
Muon energy scale [%]	-	-	-	+1.08 / -	-	-	-	-	-	-	+0.21 / -	-	- / −0.47	+1.24 / -	+0.39 / −0.27	- / −0.68	−0.54 / +0.30	±0.51
Muon identification syst [%]	-	-	-	-	-	-	-	-	±0.10	-	-	-	-	±0.16	±0.15	±0.12	±0.12	+0.15 / −0.14
E_T^{miss} Soft jet resolution para [%]	-	-	-	±0.95	-	∓0.20	-	±0.14	±0.14	∓0.26	±0.15	-	∓0.52	±1.06	∓0.86	-	-	±0.46
E_T^{miss} Soft jet resolution perp [%]	-	-	-	±0.11	±0.22	-	-	∓0.16	±0.24	-	±0.12	∓0.11	∓0.49	±0.74	-	±0.48	∓0.43	∓0.40
E_T^{miss} Soft jet scale [%]	-	-	+0.18 / −0.22	+1.34 / -	+0.20 / -	-	-	- / −0.35	-	−0.15 / +0.38	- / +0.19	- / +0.20	- / −1.06	+0.17 / −0.18	−0.42 / -	+0.39 / -	- / −0.49	−0.31 / +0.35
Z+jets cross-section [%]	±0.22	∓0.10	−0.20 / +0.21	-	±0.41	∓0.12	−0.33 / +0.34	−0.34 / +0.35	±0.76	-	∓0.35	∓0.42	∓0.32	±0.96	±0.49	−0.23 / +0.24	−0.36 / +0.37	∓0.27
Monte Carlo sample statistics [%]	±0.16	±0.15	±0.41	±2.72	±0.76	±0.22	±0.25	±0.75	±0.96	±0.55	±0.49	±0.55	±1.72	±2.66	±1.71	±1.37	±1.59	±2.50
ISR/FSR + scale [%]	- / −0.24	- / −0.53	−4.43 / +1.71	−4.78 / +4.86	+1.70 / −0.61	- / −0.42	+0.36 / -	−4.77 / +3.26	+2.92 / -	+3.07 / -	−0.29 / +0.73	−2.27 / +1.56	−2.31 / +0.77	- / −2.11	+3.65 / -	+0.44 / -	−2.60 / +4.64	+14.9 / -
Alternate hard-scattering model [%]	±6.92	±1.73	±3.11	±3.74	±0.35	∓6.92	∓8.59	∓4.14	∓2.83	∓4.69	∓10.3	∓14.5	∓7.22	∓15.3	∓8.63	∓6.83	∓6.72	∓1.28
Alternate parton-shower model [%]	±4.33	±2.57	±10.6	±0.16	∓1.95	∓7.62	∓6.04	±8.30	∓2.37	∓3.92	∓9.63	∓10.0	±8.84	∓1.56	∓3.79	∓11.2	∓14.1	∓2.39
Inter PDF [%]	-	-	±0.15	±0.21	∓0.13	-	±0.14	±0.31	∓0.35	∓0.30	-	±0.22	±0.22	∓0.25	∓0.15	-	±0.24	-
Intra PDF [%]	-	∓0.12	∓0.29	∓0.17	±0.44	±0.20	∓0.14	∓0.25	±0.68	±0.53	±0.19	∓0.28	∓0.55	±1.51	±1.17	∓0.87	±0.30	∓0.31
Fakes overall normalization, el [%]	+1.38 / −1.42	−0.76 / +0.78	−1.40 / +1.44	−1.88 / +1.94	+1.16 / −1.19	∓0.24	−1.62 / +1.67	−1.35 / +1.39	+1.44 / −1.47	+0.61 / −0.63	−1.31 / +1.35	-	−1.85 / +1.91	−0.91 / +0.94	−1.90 / +1.97	−2.12 / +2.19	−1.87 / +1.92	−1.80 / +1.85
Fakes overall normalization, mu [%]	-	-	∓0.14	∓0.37	∓0.22	-	∓0.12	-	±0.38	-	∓0.12	−0.16 / +0.17	∓0.22	∓0.30	±0.10	±0.29	∓0.33	-
Fakes alternative parametrization [%]	∓0.39	±0.55	±0.61	±0.90	∓0.95	∓0.25	±0.41	±0.92	-	∓0.11	-	∓0.33	-	∓0.54	±0.22	±0.77	∓0.46	±0.39
W+jets heavy flavour component [%]	±0.21	∓0.26	∓0.52	±0.96	±0.94	-	∓0.60	∓0.76	±2.23	±0.83	∓0.43	∓0.79	∓0.70	±4.48	±2.11	±0.32	∓0.63	∓0.81
W+jets Scales [%]	±0.11	∓0.32	∓0.24	±0.86	±0.62	-	∓0.59	∓0.40	±2.43	±1.37	∓0.35	∓0.67	∓0.29	±5.36	±4.24	±0.86	∓0.24	∓0.25
Single Top DS/DR [%]	±0.12	-	∓0.21	∓0.19	-	-	∓0.32	∓0.60	-	-	-	-	∓0.76	±0.60	±0.39	±0.23	±0.26	∓0.36
Single Top IFSR [%]	-	-	+0.15 / −0.13	+0.28 / -	- / −0.56	-	-	+0.23 / −0.50	- / −1.07	- / −0.30	- / +0.28	+0.34 / -	+0.49 / −0.50	- / −1.81	+0.61 / -	+0.12 / −0.59	+0.70 / -	+1.64 / -

TABLE F.63: Table of systematics for the relative differential cross-section at the parton level for the $p_T^{t,had}$ vs $m^{t\bar{t}}$ observable.

Bins [GeV] x [GeV]	0–60	60–150	150–280	280–410	410–800	800–880	880–980	980–1100	1100–1230	1230–1600	1600–1680	1680–1790	1790–1920	1920–2400	2400–2480	2480–2590	2590–3200
$1/\sigma \cdot d\sigma \;/\; dm^{t\bar{t}} vsp_T^{t\bar{t}}$	$6.41 \cdot 10^{-3}$	$1.75 \cdot 10^{-3}$	$3.32 \cdot 10^{-4}$	$6.18 \cdot 10^{-5}$	$6.65 \cdot 10^{-6}$	$2.49 \cdot 10^{-3}$	$6.19 \cdot 10^{-4}$	$1.40 \cdot 10^{-4}$	$3.23 \cdot 10^{-5}$	$4.43 \cdot 10^{-6}$	$7.60 \cdot 10^{-4}$	$2.06 \cdot 10^{-4}$	$5.27 \cdot 10^{-5}$	$5.43 \cdot 10^{-6}$	$1.99 \cdot 10^{-4}$	$6.48 \cdot 10^{-5}$	$6.67 \cdot 10^{-6}$
Total Uncertainty [%]	$^{+4.29}_{-4.64}$	±19.0	±18.6	$^{+15.9}_{-15.2}$	$^{+11.4}_{-11.3}$	±13.4	$^{+8.35}_{-8.26}$	$^{+9.88}_{-10.0}$	$^{+13.8}_{-15.3}$	$^{+14.0}_{-15.6}$	$^{+16.6}_{-16.5}$	$^{+6.26}_{-5.73}$	$^{+9.35}_{-9.95}$	$^{+13.4}_{-16.4}$	$^{+19.7}_{-19.6}$	$^{+8.26}_{-6.09}$	$^{+12.1}_{-9.78}$
Statistics [%]	±0.1	±0.2	±0.6	±1.7	±4.2	±0.2	±0.4	±0.9	±2.4	±5.4	±0.6	±0.8	±1.8	±4.5	±1.5	±1.9	±3.8
Systematics [%]	±4.58	±19.0	±18.6	$^{+15.8}_{-15.1}$	$^{+10.4}_{-10.2}$	±13.4	$^{+8.13}_{-8.22}$	$^{+9.82}_{-10.0}$	$^{+13.6}_{-15.1}$	$^{+12.5}_{-14.3}$	$^{+16.6}_{-16.5}$	$^{+6.19}_{-5.66}$	$^{+9.29}_{-9.71}$	$^{+12.7}_{-15.4}$	$^{+19.6}_{-19.3}$	±7.90	±11.3
Jet energy resolution [%]	∓1.37	±1.73	±2.96	±0.29	∓1.56	∓0.62	±2.59	±2.67	∓0.53	-	∓0.29	±1.95	±1.12	±4.00	∓0.35	±2.75	±5.15
b-Tagged jet energy scale (JES) [%]	$^{-0.31}_{+0.33}$	-	$^{+0.22}_{-}$	$^{-0.24}_{+0.31}$	$^{-1.03}_{+1.22}$	$^{+0.31}_{-0.38}$	$^{+0.54}_{-0.50}$	$^{+0.16}_{-}$	$^{-}_{-0.91}$	$^{-}_{-0.29}$	$^{-}_{-0.17}$	$^{+0.49}_{+0.30}$	$^{-}_{-0.34}$	$^{-0.13}_{-0.15}$	$^{+0.71}_{-}$	$^{-}_{+0.33}$	$^{+1.72}_{-0.14}$
Effective detector NP set 1 (JES) [%]	-	-	-	-	-	-	$^{-0.14}_{+0.46}$	$^{-0.27}_{-}$	$^{-1.15}_{-}$	$^{-1.32}_{-0.53}$	$^{-}_{+0.14}$	$^{-}_{+0.47}$	$^{-}_{-0.62}$	$^{+0.71}_{-0.90}$	$^{-}_{+0.37}$	$^{-}_{-0.24}$	$^{+0.52}_{-}$
Effective detector NP set 2 (JES) [%]	-	-	-	$^{+0.34}_{-0.23}$	-	-	-	-	$^{-}_{-1.59}$	$^{-}_{+1.10}$	-	-	$^{-}_{-0.62}$	$^{+0.49}_{+1.20}$	$^{-}_{+0.48}$	$^{-}_{+0.46}$	$^{-0.53}_{+2.60}$
Effective mixed NP set 1 (JES) [%]	$^{-0.28}_{+0.19}$	-	$^{+0.37}_{-0.37}$	$^{+0.26}_{-}$	$^{-}_{-2.17}$	$^{+0.14}_{-0.15}$	$^{+0.12}_{-0.29}$	$^{+0.29}_{-0.24}$	$^{+0.29}_{-0.89}$	$^{+1.18}_{-2.42}$	$^{+0.22}_{-0.20}$	$^{+0.39}_{-0.27}$	$^{-}_{-0.36}$	$^{+1.20}_{+1.63}$	$^{-}_{+0.38}$	$^{-}_{-}$	$^{-}_{-}$
Effective mixed NP set 2 (JES) [%]	-	-	-	$^{-0.13}_{+0.62}$	$^{-0.17}_{+1.02}$	-	-	$^{-0.24}_{+0.14}$	$^{-}_{-0.57}$	$^{-}_{-0.52}$	-	-	$^{-}_{-0.76}$	$^{-0.18}_{-0.31}$	$^{-}_{-}$	$^{-}_{-}$	$^{-0.53}_{+0.18}$
Effective mixed NP set 3 (JES) [%]	-	-	-	-	-	-	-	-	$^{-}_{-0.59}$	$^{-}_{-0.85}$	-	-	$^{-}_{-0.96}$	$^{-0.23}_{-0.47}$	-	-	-
Effective modelling NP set 1 (JES) [%]	$^{-0.26}_{+0.17}$	$^{+1.09}_{-0.91}$	$^{+0.97}_{-0.88}$	$^{-0.38}_{+0.96}$	$^{-1.06}_{+0.25}$	$^{-0.40}_{+0.31}$	$^{+0.76}_{-0.81}$	$^{+0.31}_{-0.33}$	$^{-1.74}_{+0.66}$	$^{-}_{-0.61}$	$^{-0.80}_{+0.99}$	$^{+0.48}_{+0.43}$	$^{-0.76}_{+0.13}$	$^{-1.11}_{+0.23}$	$^{-1.18}_{+1.91}$	$^{+0.40}_{+0.52}$	$^{+0.52}_{+1.94}$
Effective modelling NP set 2 (JES) [%]	-	$^{-0.15}_{+0.16}$	-	$^{+0.82}_{-}$	-	$^{+0.12}_{-}$	-	-	-	$^{+0.40}_{-0.78}$	$^{+0.34}_{-0.14}$	$^{-}_{-0.11}$	$^{-}_{-0.73}$	$^{+0.12}_{-0.45}$	$^{+0.39}_{-}$	$^{+0.63}_{-}$	$^{+1.38}_{-}$
Effective modelling NP set 3 (JES) [%]	-	$^{+0.23}_{-}$	$^{+0.23}_{-}$	-	-	-	$^{-0.20}_{+0.37}$	$^{-0.73}_{-}$	$^{-0.52}_{-}$	$^{-0.78}_{+0.71}$	$^{-0.14}_{+0.32}$	$^{-0.11}_{-}$	$^{-0.73}_{-}$	$^{-0.45}_{+1.19}$	$^{+0.59}_{-}$	$^{+0.51}_{-}$	$^{+0.63}_{-}$
Effective modelling NP set 4 (JES) [%]	$^{-0.18}_{-}$	$^{-0.14}_{-}$	$^{-}_{-}$	$^{-}_{+0.29}$	$^{-0.45}_{+0.42}$	$^{+0.15}_{-}$	$^{+0.20}_{-}$	$^{-0.55}_{-}$	$^{-0.71}_{-}$	$^{+1.20}_{-}$	$^{+0.26}_{+0.25}$	$^{+0.50}_{-}$	$^{-0.96}_{-}$	$^{-0.27}_{+0.46}$	$^{-}_{-}$	$^{-}_{-}$	$^{-}_{-}$
Effective statistical NP set 1 (JES) [%]	-	$^{+0.24}_{-0.16}$	-	-	$^{+0.66}_{-}$	-	-	$^{-0.26}_{+0.10}$	$^{-0.63}_{-}$	$^{-0.41}_{-}$	$^{-0.25}_{+0.18}$	$^{+0.44}_{-}$	$^{-0.98}_{-}$	$^{+0.51}_{-1.03}$	$^{-}_{+0.63}$	$^{-0.60}_{+0.50}$	$^{-0.40}_{+1.98}$
Effective statistical NP set 2 (JES) [%]	-	-	$^{+0.21}_{+0.30}$	$^{-0.12}_{+0.28}$	$^{+0.43}_{-}$	-	-	$^{-0.40}_{-}$	$^{-1.06}_{-}$	$^{-1.64}_{-}$	$^{+0.18}_{+0.20}$	$^{-}_{-}$	$^{-0.38}_{-0.50}$	$^{+1.12}_{+1.20}$	$^{+0.12}_{-}$	$^{+0.31}_{-}$	$^{+1.86}_{-}$
Effective statistical NP set 3 (JES) [%]	-	-	$^{+0.57}_{-}$	$^{-0.91}_{+1.58}$	$^{-}_{-}$	-	-	$^{-0.26}_{-0.36}$	$^{-1.33}_{-0.59}$	$^{-1.12}_{-0.64}$	$^{-}_{+0.18}$	$^{-}_{-}$	$^{-}_{-0.81}$	$^{-0.44}_{+0.33}$	$^{-0.36}_{+0.38}$	$^{-}_{-0.11}$	$^{+2.10}_{+0.48}$
Effective statistical NP set 4 (JES) [%]	$^{-0.12}_{+0.11}$	$^{-}_{+0.20}$	$^{+0.21}_{-}$	$^{+0.23}_{-}$	$^{-}_{-}$	$^{+0.29}_{-}$	$^{-0.28}_{-0.75}$	$^{-0.40}_{-0.68}$	$^{-}_{-1.04}$	$^{-}_{-0.65}$	$^{-}_{-}$	$^{+0.43}_{-}$	$^{-}_{-0.76}$	$^{+0.43}_{-}$	$^{+0.22}_{-}$	$^{+0.60}_{-}$	$^{+0.43}_{-}$
Effective statistical NP set 5 (JES) [%]	-	-	-	$^{+0.72}_{-0.16}$	$^{+0.90}_{+0.56}$	$^{-0.18}_{-}$	$^{-0.75}_{-}$	$^{-}_{-0.21}$	$^{-}_{-0.36}$	$^{-}_{-}$	$^{-}_{-}$	$^{+0.25}_{-}$	$^{-}_{-1.24}$	$^{+1.53}_{-}$	$^{-}_{-}$	$^{+1.29}_{-}$	$^{+0.84}_{-}$
Effective statistical NP set 6 (JES) [%]	-	-	-	$^{+0.31}_{-}$	$^{+0.68}_{-}$	-	-	-	$^{-}_{-}$	$^{+0.23}_{-}$	-	$^{+0.39}_{-}$	$^{-}_{-0.55}$	$^{+0.85}_{-}$	$^{-}_{+0.24}$	$^{-0.38}_{+0.56}$	$^{-0.60}_{+0.56}$
Effective statistical NP set 7 (JES) [%]	-	-	-	-	$^{-0.56}_{+0.44}$	-	$^{+0.12}_{-0.13}$	-	$^{-0.72}_{-}$	$^{-1.82}_{-1.24}$	-	$^{+0.48}_{-}$	$^{+0.98}_{-1.10}$	$^{+0.52}_{-0.10}$	-	-	$^{+0.84}_{-}$
η intercalibration model (JES) [%]	∓0.34	$^{+0.13}_{-0.17}$	$^{+0.45}_{-0.71}$	$^{+0.52}_{-}$	$^{+0.14}_{+0.81}$	$^{-0.14}_{-0.16}$	$^{-0.62}_{+0.52}$	$^{-0.71}_{-0.50}$	$^{-1.24}_{-1.91}$	$^{+0.39}_{-}$	$^{+0.36}_{-0.14}$	$^{+0.47}_{-0.13}$	$^{-}_{-0.77}$	$^{+0.53}_{-0.46}$	$^{+0.53}_{-0.50}$	$^{+1.21}_{-}$	$^{+2.55}_{-}$
η intercalibration non closure (JES) [%]	-	$^{-0.16}_{+0.23}$	$^{-0.38}_{+0.21}$	$^{-}_{+0.31}$	$^{+1.02}_{-}$	-	-	-	$^{-}_{-0.76}$	$^{+0.43}_{-}$	-	$^{+0.33}_{-}$	$^{-}_{-0.22}$	$^{-}_{-}$	$^{-}_{-}$	$^{-0.43}_{+0.20}$	$^{+0.62}_{-1.48}$
η intercalibration total stat (JES) [%]	∓0.14	$^{+0.23}_{-0.37}$	$^{+0.36}_{-0.31}$	$^{-}_{-0.34}$	$^{-0.80}_{+0.44}$	$^{-}_{-0.70}$	$^{\pm 0.26}_{+0.78}$	$^{+0.24}_{-0.27}$	$^{-}_{-0.62}$	$^{+0.60}_{-1.88}$	$^{-}_{+0.25}$	$^{+0.24}_{-0.47}$	$^{-0.64}_{-0.43}$	$^{-}_{-}$	$^{-}_{+1.44}$	$^{-0.22}_{+0.80}$	$^{+1.42}_{-0.49}$
Flavour composition (JES) [%]	$^{-0.19}_{+0.18}$	$^{-0.20}_{+1.20}$	$^{-}_{-1.32}$	$^{+0.65}_{+0.59}$	$^{+0.62}_{+0.24}$	$^{-0.68}_{+0.59}$	$^{-0.83}_{+0.40}$	$^{-0.83}_{+0.37}$	$^{-}_{-0.86}$	$^{+1.06}_{+1.32}$	$^{+1.05}_{-0.27}$	$^{+0.32}_{-}$	$^{-0.90}_{+0.21}$	$^{-0.93}_{+0.72}$	$^{-0.38}_{-0.46}$	$^{-0.52}_{-0.71}$	$^{-1.45}_{+0.84}$
Flavour response (JES) [%]	$^{-0.19}_{-}$	$^{+0.54}_{-0.21}$	$^{+0.39}_{-0.21}$	$^{-}_{+0.23}$	$^{-}_{-0.26}$	$^{-0.19}_{-}$	$^{+0.40}_{-}$	$^{-}_{-0.11}$	$^{-}_{-0.74}$	$^{+0.30}_{-0.44}$	$^{-}_{-}$	$^{-}_{-}$	$^{-}_{-0.80}$	$^{-1.54}_{+0.69}$	$^{-0.57}_{-}$	$^{+0.74}_{-0.40}$	$^{+2.29}_{-}$
Pile-up offset μ (JES) [%]	$^{-0.18}_{+0.10}$	$^{+0.17}_{-0.22}$	$^{+0.43}_{-0.39}$	$^{+0.64}_{-}$	$^{+0.58}_{-0.54}$	$^{-}_{-}$	$^{+0.11}_{-0.42}$	$^{-0.53}_{+0.60}$	$^{-}_{-1.37}$	$^{-}_{-0.60}$	$^{-0.29}_{+0.58}$	$^{+0.39}_{-}$	$^{-}_{-0.52}$	$^{-}_{-0.60}$	$^{-}_{+1.31}$	$^{-0.54}_{-0.76}$	$^{+1.69}_{-}$
Pile-up offset N_{PV} (JES) [%]	-	$^{-}_{-}$	$^{-0.36}_{+0.34}$	$^{+0.34}_{-}$	$^{+0.42}_{-0.67}$	$^{+0.29}_{-0.38}$	$^{-0.39}_{+0.42}$	$^{-0.33}_{+0.71}$	$^{-}_{-1.31}$	$^{-0.60}_{-2.24}$	$^{+0.58}_{-0.34}$	$^{+0.79}_{-0.23}$	$^{-}_{-0.34}$	$^{-}_{-1.26}$	$^{+0.37}_{-0.83}$	$^{-0.78}_{+0.44}$	$^{+0.47}_{-0.68}$
Pile-up offset ρ topology (JES) [%]	$^{-0.60}_{+0.50}$	$^{+1.51}_{-1.40}$	$^{+1.77}_{-1.43}$	$^{-1.03}_{+0.87}$	$^{-}_{+1.49}$	$^{-0.38}_{+0.29}$	$^{+1.45}_{-1.66}$	$^{+0.71}_{-0.65}$	$^{-1.31}_{+0.30}$	$^{-2.24}_{+2.42}$	$^{-0.34}_{+1.34}$	$^{+0.43}_{-}$	$^{-0.34}_{-}$	$^{-1.26}_{+1.53}$	$^{-0.83}_{+1.28}$	$^{+1.44}_{-1.14}$	$^{+1.00}_{-}$
Punch-through (JES) [%]	-	-	-	$^{+0.18}_{-}$	-	-	-	-	-	-	-	$^{+0.24}_{-}$	$^{-}_{-}$	$^{+1.53}_{-}$	-	-	$^{+1.00}_{-}$
Single particle high-p_T (JES) [%]	-	-	-	$^{+0.27}_{-}$	$^{-0.26}_{-}$	-	-	$^{-0.23}_{+0.10}$	$^{-}_{-0.32}$	$^{-0.46}_{+0.92}$	-	$^{+0.33}_{-}$	$^{+0.42}_{-}$	$^{-0.72}_{-}$	$^{+0.11}_{-}$	$^{-0.27}_{-}$	$^{-}_{-}$
Jet vertex fraction [%]	±0.12	±0.17	-	-	$^{-0.32}_{+0.23}$	∓0.17	-	$^{-0.14}_{+0.04}$	$^{-0.15}_{+0.15}$	∓0.34	$^{-0.28}_{+0.29}$	±0.20	∓0.19	∓0.27	$^{-0.77}_{+0.53}$	$^{-0.64}_{-0.25}$	$^{-0.50}_{+0.50}$
b-Quark tagging efficiency (eigenvector 0) [%]	$^{-0.80}_{+0.75}$	-	$^{+0.53}_{-0.51}$	±0.35	$^{+0.73}_{-0.68}$	$^{+0.47}_{-0.43}$	$^{+1.04}_{-0.95}$	$^{+0.68}_{-0.84}$	$^{+0.15}_{-0.44}$	$^{+0.71}_{-0.67}$	$^{+0.83}_{-0.86}$	$^{+1.23}_{-1.14}$	$^{+0.82}_{-0.75}$	$^{+0.19}_{-0.30}$	$^{+0.48}_{-0.44}$	$^{+1.10}_{-0.98}$	$^{+0.58}_{-1.38}$
b-Quark tagging efficiency (eigenvector 1) [%]	$^{-0.40}_{-0.48}$	±0.23	$^{-0.30}_{+0.28}$	$^{-0.57}_{+0.55}$	$^{-0.88}_{+0.96}$	$^{-0.36}_{+0.28}$	$^{-0.85}_{+0.44}$	$^{-0.84}_{+0.82}$	$^{-0.66}_{+0.84}$	$^{-1.54}_{+1.31}$	$^{-0.86}_{+0.78}$	$^{-0.84}_{+0.83}$	$^{-1.17}_{+1.13}$	$^{-1.58}_{+1.36}$	$^{-0.86}_{+0.77}$	$^{-0.95}_{+0.91}$	$^{-1.38}_{+1.34}$
b-Quark tagging efficiency (eigenvector 2) [%]	$^{-0.29}_{+0.28}$	$^{+0.12}_{-0.13}$	∓0.26	∓0.54	$^{-0.77}_{+0.72}$	∓0.11	±0.25	$^{-0.58}_{+0.59}$	$^{-0.79}_{+0.79}$	$^{-0.98}_{+1.00}$	$^{-0.42}_{+0.45}$	$^{+0.53}_{+0.53}$	$^{+0.82}_{-}$	$^{+1.00}_{+1.02}$	$^{-1.50}_{+0.51}$	$^{+0.59}_{-0.59}$	$^{+0.94}_{+0.96}$
b-Quark tagging efficiency (eigenvector 3) [%]	∓0.16	-	±0.10	-	-	∓0.14	±0.20	±0.15	-	-	∓0.17	±0.21	-	∓0.17	±0.10	±0.14	-
c-Quark tagging efficiency (eigenvector 0) [%]	-	-	-	-	-	-	-	-	-	∓0.13	∓0.10	-	-	∓0.14	-	-	-
c-Quark tagging efficiency (eigenvector 1) [%]	-	-	∓0.11	∓0.22	∓0.21	-	-	∓0.21	∓0.26	∓0.13	-	±0.15	±0.24	±0.35	±0.15	∓0.19	∓0.22
c-Quark tagging efficiency (eigenvector 2) [%]	-	-	-	∓0.13	-	-	-	∓0.13	-	∓0.15	-	-	±0.15	$^{-0.22}_{+0.23}$	-	∓0.11	∓0.15
Light-jet tagging efficiency (eigenvector 0) [%]	-	-	∓0.23	$^{-0.49}_{+0.51}$	-	$^{+0.14}_{-0.16}$	-	$^{-0.38}_{+0.43}$	∓0.49	-	-	$^{-0.14}_{+0.16}$	$^{-0.32}_{+0.33}$	$^{-0.52}_{+0.53}$	$^{-0.32}_{+0.37}$	$^{-0.67}_{+0.72}$	$^{-0.46}_{+0.45}$
Light-jet tagging efficiency (eigenvector 1) [%]	-	-	-	-	∓0.23	-	-	-	-	$^{-0.11}_{+0.10}$	-	-	-	-	-	$^{-0.55}_{-0.24}$	-
Light-jet tagging efficiency (eigenvector 2) [%]	-	-	-	$^{+0.14}_{-0.13}$	-	-	-	-	$^{+0.11}_{-0.10}$	-	-	-	-	±0.16	-	∓0.14	±0.10
Light-jet tagging efficiency (eigenvector 3) [%]	-	-	-	-	-	-	-	$^{-0.17}_{+0.18}$	-	-	-	-	$^{-0.13}_{+0.14}$	-	∓0.18	$^{-0.21}_{+0.23}$	±0.25
Light-jet tagging efficiency (eigenvector 5) [%]	-	-	-	-	-	-	-	-	-	±0.12	-	-	-	-	-	∓0.12	-
b-Quark tagging extrapolation [%]	-	-	-	±0.23	±0.37	-	-	-	±0.41	±0.77	-	-	±0.19	±0.85	±0.11	±0.16	±0.48
Electron energy resolution [%]	-	-	-	-	$^{+0.63}_{-}$	-	-	-	-	$^{+0.47}_{-0.49}$	-	-	-	$^{-0.84}_{-0.76}$	-	$^{+0.45}_{-0.40}$	$^{-0.59}_{+0.59}$
Electron energy scale [%]	-	-	-	-	$^{+0.22}_{-0.25}$	-	-	$^{-0.28}_{-}$	$^{-0.46}_{-}$	$^{+0.97}_{-}$	-	$^{+0.34}_{-}$	-	$^{-0.39}_{-}$	-	$^{-}_{-}$	$^{-}_{-}$
Electron identification efficiency [%]	-	-	-	-	±0.13	-	-	-	$^{-0.33}_{+0.16}$	$^{+0.20}_{-0.21}$	±0.10	±0.11	±0.17	$^{-0.44}_{\pm 0.24}$	$^{-1.27}_{\pm 0.17}$	$^{-0.50}_{\pm 0.18}$	$^{-}_{\pm 0.26}$
Electron isolation efficiency [%]	-	-	-	-	±0.19	-	-	-	$^{-0.17}_{\pm 0.20}$	±0.34	-	±0.11	±0.19	±0.38	±0.11	±0.14	±0.27
Muon (ID) momentum resolution [%]	-	-	-	$^{+0.37}_{-}$	$^{+0.28}_{-0.63}$	-	-	$^{+0.19}_{-0.16}$	-	$^{+0.76}_{-}$	-	-	$^{-0.37}_{-}$	$^{-0.71}_{+0.36}$	$^{+0.82}_{-}$	$^{-0.40}_{+0.10}$	$^{-}_{-0.49}$
Muon (MS) momentum resolution [%]	-	-	-	$^{+0.27}_{-}$	$^{-0.35}_{+0.16}$	-	-	$^{-0.20}_{+0.17}$	$^{-0.60}_{+0.16}$	$^{+0.95}_{-}$	-	-	$^{+0.15}_{-0.57}$	$^{-}_{-0.56}$	$^{+0.38}_{-}$	$^{-}_{-}$	$^{+0.65}_{-}$
Muon (ID) sagitta o [%]	-	-	-	$^{+0.53}_{-}$	$^{-}_{-}$	-	-	$^{-}_{-}$	$^{-}_{-}$	$^{+0.62}_{-}$	-	-	$^{-}_{-}$	$^{-}_{-1.03}$	$^{-}_{-0.30}$	$^{-}_{+0.74}$	$^{+0.96}_{-}$
Muon energy scale [%]	-	-	-	$^{+0.36}_{-}$	$^{-}_{-0.51}$	-	-	$^{-0.25}_{+0.84}$	$^{-}_{-0.30}$	$^{-0.21}_{-}$	-	$^{+0.42}_{-}$	$^{-}_{-0.38}$	$^{-0.14}_{-0.43}$	$^{-0.14}_{-}$	$^{+0.22}_{-0.35}$	$^{-0.19}_{+0.40}$
Muon identification syst [%]	-	-	-	-	-	-	-	-	-	-	-	-	-	±0.14	±0.13	±0.14	±0.17
E_T^{miss} Soft jet resolution para [%]	-	±0.13	-	±0.34	∓0.31	-	-	∓0.25	±0.25	∓0.27	-	±0.11	±0.11	±0.87	±0.33	±0.14	±1.89
E_T^{miss} Soft jet resolution perp [%]	-	±0.10	-	±0.10	∓0.75	-	-	-	±0.35	∓1.16	-	±0.11	±0.24	±0.93	±0.26	±0.41	±0.55
E_T^{miss} Soft jet scale [%]	-	-	±0.25	$^{+0.18}_{-0.12}$	$^{+1.08}_{-}$	-	-	$^{-0.41}_{+0.31}$	$^{-}_{-0.85}$	$^{-0.37}_{+1.31}$	$^{-0.19}_{+0.18}$	$^{-0.16}_{+0.29}$	$^{-0.24}_{+0.21}$	$^{-}_{-1.79}$	$^{-}_{-}$	$^{-0.39}_{+0.38}$	$^{+0.96}_{-}$
Z+jets cross-section [%]	±0.15	-	-	-	∓0.15	∓0.14	$^{-0.15}_{+0.16}$	-	-	±0.23	$^{-0.18}_{+0.19}$	±0.13	-	±0.13	-	±0.13	±0.33
Monte Carlo sample statistics [%]	±0.13	±0.21	±0.36	±1.02	±2.33	±0.23	±0.25	±0.66	±1.47	±3.22	±0.37	±0.50	±1.19	±2.93	±1.08	±1.36	±2.75
ISR/FSR + scale [%]	$^{-0.12}_{+0.18}$	$^{+0.38}_{-1.20}$	$^{-}_{-1.80}$	$^{-1.61}_{+4.15}$	$^{-3.51}_{+2.62}$	$^{-0.43}_{+0.43}$	$^{+0.71}_{-1.36}$	$^{+0.30}_{-0.28}$	$^{-}_{-0.83}$	$^{-6.71}_{+3.36}$	$^{-0.71}_{+1.42}$	$^{+1.13}_{-}$	$^{+3.01}_{-}$	$^{+0.57}_{-9.23}$	$^{+0.44}_{-}$	$^{+5.20}_{-}$	$^{-1.86}_{+1.43}$
Alternate hard-scattering model [%]	±2.93	±9.15	±3.88	±8.83	±6.57	∓8.29	∓1.19	∓2.39	±2.85	±5.11	∓11.2	∓3.93	±4.49	±1.50	∓12.9	±1.05	±2.57
Alternate parton-shower model [%]	∓2.84	±16.3	±17.7	±11.9	±5.18	∓10.4	±7.03	±8.45	±12.6	±9.09	∓11.9	±2.91	±6.57	±9.55	∓14.1	±1.74	±3.29
Inter PDF [%]	-	-	-	±0.18	±0.22	-	-	±0.10	±0.23	±0.36	-	-	-	-	-	±0.15	-
Intra PDF [%]	-	∓0.19	∓0.39	∓0.51	∓0.26	±0.16	-	∓0.28	∓0.34	∓0.25	±0.22	-	∓0.22	∓0.26	±0.75	±0.56	±0.24
Fakes overall normalization, el [%]	$^{+0.42}_{-0.43}$	$^{+0.50}_{-0.51}$	$^{-0.32}_{+0.33}$	$^{-0.72}_{+0.74}$	$^{-1.16}_{+1.19}$	$^{-0.39}_{+0.40}$	$^{-0.57}_{+0.59}$	$^{-1.73}_{+1.77}$	$^{-1.62}_{+1.67}$	$^{-1.57}_{+1.61}$	$^{-0.18}_{+0.19}$	±0.14	$^{-1.97}_{+2.03}$	$^{-1.53}_{+1.57}$	$^{-1.77}_{+1.85}$	$^{-1.93}_{+1.98}$	$^{-1.60}_{+1.65}$
Fakes overall normalization, mu [%]	-	-	-	∓0.19	-	-	-	±0.13	±0.54	-	-	-	-	±0.20	$^{-0.13}_{+0.14}$	±0.30	∓0.18
Fakes alternative parametrization [%]	±0.14	∓0.10	-	∓0.34	±0.53	-	∓0.45	±0.68	∓0.67	±0.99	±0.13	∓0.59	±0.21	±0.21	±0.17	∓0.47	±1.01
W+jets heavy flavour component [%]	±0.14	∓0.10	±0.20	∓0.73	∓0.85	-	∓0.20	∓0.28	∓0.81	∓0.89	-	-	∓0.13	±0.88	±0.85	±0.78	±0.21
W+jets Scales [%]	-	-	±0.24	±0.55	-	∓0.29	-	±0.54	±0.62	±0.25	-	±0.47	±1.38	±1.33	±1.31	±2.17	±2.28
Single Top DS/DR [%]	±0.16	-	∓0.26	∓0.78	∓0.92	-	∓0.32	∓1.38	∓2.58	∓0.69	±0.19	∓0.30	∓1.57	∓2.77	±0.71	∓0.15	∓1.04
Single Top IFSR [%]	$^{+0.23}_{-}$	-	$^{+0.36}_{-0.27}$	$^{+0.76}_{-}$	$^{+0.33}_{-0.55}$	-	$^{+0.11}_{-0.36}$	$^{-0.40}_{-}$	$^{-1.66}_{-}$	$^{+2.47}_{-}$	-	$^{+0.33}_{-}$	$^{-0.43}_{-}$	$^{-1.74}_{-}$	-	$^{+0.38}_{-0.16}$	$^{+2.57}_{-0.78}$

TABLE F.64: Table of systematics for the relative differential cross-section at the parton level for the $p_T^{t\bar{t}}$ vs $m^{t\bar{t}}$ observable.

Bins [GeV]x[GeV]	0–85	85–175	175–285	285–390	390–1000	1000–1085	1085–1175	1175–1285	1285–2000	2000–2085	2085–2175	2175–2300	2300–3000
$1/\sigma \cdot d\sigma$ / $d\|y^{t,had}\|vsp_T^{t,had}$	$1.85 \cdot 10^{-3}$	$2.09 \cdot 10^{-3}$	$6.61 \cdot 10^{-4}$	$1.40 \cdot 10^{-4}$	$1.05 \cdot 10^{-5}$	$1.52 \cdot 10^{-3}$	$1.63 \cdot 10^{-3}$	$4.82 \cdot 10^{-4}$	$1.97 \cdot 10^{-5}$	$1.04 \cdot 10^{-3}$	$1.04 \cdot 10^{-3}$	$2.44 \cdot 10^{-4}$	$6.44 \cdot 10^{-6}$
Total Uncertainty [%]	+13.3 −10.6	+2.20 −3.23	+8.05 −9.95	+12.7 −15.2	+11.4 −11.9	+7.18 −6.19	+2.96 −3.48	+8.79 −10.8	+11.1 −13.1	+4.76 −2.71	+4.15 −4.87	+9.61 −11.0	+11.5 −15.4
Statistics [%]	±0.3	±0.2	±0.4	±1.1	±3.9	±0.3	±0.3	±0.5	±1.3	±0.6	±0.5	±0.9	±2.6
Systematics [%]	+13.3 −10.6	+2.18 −3.22	+8.03 −9.93	+12.6 −15.1	+10.4 −11.0	+7.17 −6.17	+2.94 −3.46	+8.77 −10.8	+11.0 −13.0	+4.71 −2.62	+4.09 −4.83	+9.54 −10.9	+11.1 −15.0
Jet energy resolution [%]	±0.13	∓0.17	∓0.15	-	±2.68	±0.61	±0.43	∓0.23	±0.11	∓0.74	∓0.50	±0.24	±0.10
b-Tagged jet energy scale (JES) [%]	-	-	-	-	-	-	+0.22	-	-	−0.16	+0.14	-	−0.88
Effective detector NP set 1 (JES) [%]	+1.62 −1.09	−0.49 −0.14	−1.03	−0.50	+1.17 −1.47	+0.83 −0.28	−0.41	−1.05	−0.65	+0.37	−0.38	−0.66	-
Effective detector NP set 2 (JES) [%]	+0.88	-	−0.37	−0.61	+0.68	+0.42	−0.39	−0.77	−0.88	-	−0.42	−0.74	−1.64
Effective mixed NP set 1 (JES) [%]	+1.19	−0.32	−0.47	−0.48	-	-	-	−0.45	−0.86	-	−0.26	−0.50	−1.75
Effective mixed NP set 2 (JES) [%]	+0.81	−0.23	−0.83	−0.81	+0.33 −1.39 −0.30	+0.48 +0.30	−0.30	−0.74	−1.05	+0.28 +0.23	−0.23	−0.44	−0.79
Effective mixed NP set 3 (JES) [%]	+0.78	-	−0.59	−0.50	-	+0.36	-	−0.56	−0.58	-	−0.25	−0.35	−0.88
Effective modelling NP set 1 (JES) [%]	+1.40	−0.20 +0.45	−0.51	−0.62 −2.46	−0.80 +2.27	+0.49	-	−0.52 −1.12	−0.76 −2.36	−0.62	−0.20 −0.84	−0.43 −1.39	−0.90 −2.73
Effective modelling NP set 2 (JES) [%]	+1.03	−0.84	−0.89	+0.88	+0.24	-	−0.35	-	+0.45	+1.07	+0.42	+0.62	+1.11
Effective modelling NP set 3 (JES) [%]	+1.15	−0.20	−0.67	−0.83	−0.52	+0.65 +0.51	−0.27 −0.21	−0.77	−1.04	+0.37	−0.25 −0.22	−0.91	−1.51
Effective modelling NP set 4 (JES) [%]	+0.83	−0.29	−0.78	−0.74	−0.81	+0.37	-	−0.78	−1.08	-	-	−0.91	−0.88
Effective statistical NP set 1 (JES) [%]	+0.89	−0.24	−0.46	−0.70	−0.91 −0.39	+0.42	-	−0.54	−0.74	+0.31	-	−0.39	−0.83
Effective statistical NP set 2 (JES) [%]	+0.91	−0.25	−0.56	−1.03	+0.46 −0.65	+0.37	-	−0.74	−0.82	+0.41	−0.42	−0.56	−0.93
Effective statistical NP set 3 (JES) [%]	+0.78	−0.22	−0.54	−1.07	+0.49 −0.76	+0.36	−0.20	−0.67	−1.05	-	−0.32	−0.45	−1.53
Effective statistical NP set 4 (JES) [%]	+1.15	-	−0.46	−0.91	+0.29 +0.56	+0.45	-	−0.52	−0.70	+0.25	−0.26	−0.72	−0.77
Effective statistical NP set 5 (JES) [%]	+0.88	−0.28	−0.73	−0.67	−1.18 +0.66	+0.37	−0.24	−0.87	−1.01	+0.29	-	−0.57	−1.17
Effective statistical NP set 6 (JES) [%]	+0.77	−0.22	−0.67	−0.86	+1.35	+0.35	-	−0.56	−0.76	+0.23	−0.35	−0.42	−1.15
Effective statistical NP set 7 (JES) [%]	+0.81	−0.21	−0.57	−0.60	−0.18	+0.38	-	−0.62	−0.47	-	-	−0.81	−0.92
η intercalibration model (JES) [%]	+1.11	−0.34 −0.45	−0.51	−0.84 −1.44	+0.38	+0.38	+0.35	−0.47	−0.74	-	+0.12	−0.64 +0.29	−1.40
η intercalibration non closure (JES) [%]	+1.06	-	−0.79	+0.19	+0.87 +0.10	+0.43	−0.51	−0.94	−0.87	+0.49	−0.58	−1.00	−1.05
η intercalibration total stat (JES) [%]	+0.85	−0.29	−0.52	−0.94	−1.18 −0.42	+0.29	-	−0.60	−0.91	−0.25 +0.39	-	−0.59	−1.28
Flavour composition (JES) [%]	+1.61	−0.29 +0.21	−0.58 −1.03	−0.92 −2.28	+1.31 −0.12	+0.92	−0.27	−0.57 −1.18	−0.83 −2.11	−0.69	−1.04	−0.50 −1.36	−1.15 −2.91
Flavour response (JES) [%]	−0.20 +0.97	−0.73 −0.43	+0.21	+1.08 +0.23	+0.59	−0.20 +0.46	−0.29 −0.25	+0.15	+0.63	+1.25 +0.54	+0.61	+0.75	+1.62
Pile-up offset μ (JES) [%]	+0.81	-	−0.70	−1.22	−0.26	+0.34	-	−0.75	−1.38	−0.23 +0.25	±0.29	−0.90	−1.90
Pile-up offset N_{PV} (JES) [%]	+1.12	−0.35	−0.48	−0.78 −1.04	−0.58 +0.80	+0.28	-	−0.58	−0.61	-	-	−0.83	−1.03
Pile-up offset p_T (JES) [%]	+1.35	-	−0.43 −0.59	-	+1.39	−0.16	−0.41 +0.11	−0.86 +0.18	−0.86	−0.22	−0.29	−0.78 +0.18	−1.21
Pile-up offset ρ topology (JES) [%]	+1.30	−0.27 +0.95	−1.13	−1.04	−0.34 −1.97	+0.24 +0.29	−0.38 +0.38	−1.13	−0.98 −2.94	+0.62 −1.29	−0.30 −1.33	−0.77 −1.93	−2.48 −4.11
Punch-through (JES) [%]	+0.73	-	−0.59	−1.91	+1.73	+2.48	−0.58	−0.86	+1.11	+1.76	+0.66	+0.92	+2.12
Single particle high-p_T (JES) [%]	+0.71	-	−0.53	−0.53	−0.26 +0.40	+0.34	-	−0.61	−0.67	-	−0.23	−0.42	−0.72
Jet vertex fraction [%]	+0.98	-	−0.51	−0.63	−0.37 −0.35	+0.36	-	−0.52	−0.48 −0.85	-	-	−0.41	−0.92
b-Quark tagging efficiency (eigenvector 0) [%]	−0.55	-	−0.87 +0.76	−0.97 +1.01	+0.33 ±0.43	+0.51	-	−0.83 +0.78	+1.07	+0.48 +0.55	−0.26 +0.16	−0.81 +0.84	−1.07 +1.06
b-Quark tagging efficiency (eigenvector 1) [%]	+1.85 −1.33	−0.21	−1.72 −1.38	−1.90 −2.09	−1.76	−0.71 +1.16 +0.83	−0.31	−1.69 −1.37	−1.75 −1.66	−0.51 +0.76	−1.62 −1.58	−2.09 −2.51	−2.64 −3.61
b-Quark tagging efficiency (eigenvector 2) [%]	+0.99	-	+0.31	+1.05 +1.73	+1.77 +2.44	−0.38 +0.58	-	+0.35	+1.17 +1.11	+0.66	−0.21	+0.82 +0.92	+1.04 +1.62
b-Quark tagging efficiency (eigenvector 3) [%]	+0.94	-	−1.00	+0.50	+1.45 −0.35	+0.50	-	−0.97	+0.64	+0.53	-	-	+0.55
b-Quark tagging efficiency (eigenvector 4) [%]	+0.70	−0.21	−0.85	−0.69	+0.32	+0.26	−0.22	−0.82	−0.55	+0.35	−0.27	−0.75	−0.73
b-Quark tagging efficiency (eigenvector 5) [%]	+0.69	-	−0.56	−0.57	-	+0.26	-	−0.53	−0.46	+0.35	−0.21	−0.47	−0.64
c-Quark tagging efficiency (eigenvector 0) [%]	+0.79	-	−0.53	−0.50	-	+0.34	-	−0.51	−0.39	+0.42	-	−0.44	−0.57
c-Quark tagging efficiency (eigenvector 1) [%]	+0.79	-	−0.64	−0.66	−0.15 +0.12 −0.56	+0.35	-	−0.61	−0.57	+0.38	-	−0.54	−0.76
c-Quark tagging efficiency (eigenvector 2) [%]	+0.75	-	−0.66	−0.74	+0.53 −0.38	+0.33	-	−0.62	−0.57	+0.43	−0.21	−0.59	−0.91
Light-jet tagging efficiency (eigenvector 0) [%]	+0.70	-	−0.63	−0.71	+0.35	+0.25	-	−0.61	−0.57	+0.55	-	−0.53	−0.86
Light-jet tagging efficiency (eigenvector 1) [%]	+0.71	−0.22	−0.65	−0.66	- −0.19	+0.40	-	−0.57	−0.46	+0.51	−0.33	−0.65	−0.65
Light-jet tagging efficiency (eigenvector 2) [%]	+0.72	−0.20	−0.69	−0.75	+0.17	+0.29	-	−0.63	−0.55	+0.46	−0.26	−0.55	−0.72
Light-jet tagging efficiency (eigenvector 3) [%]	+0.77	−0.20	−0.63	−0.57	-	+0.37	-	−0.51	−0.40	+0.39	−0.32	−0.43	−0.61
Light-jet tagging efficiency (eigenvector 4) [%]	+0.69	-	−0.53	−0.59	-	+0.26	-	−0.59	−0.55	+0.34	−0.33	−0.68	−0.71
Light-jet tagging efficiency (eigenvector 5) [%]	+0.71	-	−0.53	−0.51	-	+0.31	-	−0.50	−0.39	+0.40	-	−0.44	−0.58
Light-jet tagging efficiency (eigenvector 6) [%]	+0.70	-	−0.55	−0.53	-	+0.28	-	−0.51	−0.39	+0.37	−0.27	−0.57	−0.58
Light-jet tagging efficiency (eigenvector 7) [%]	+0.70	-	−0.55	−0.54	-	+0.28	-	−0.50	−0.42	+0.39	−0.23	−0.50	−0.58
Light-jet tagging efficiency (eigenvector 8) [%]	+0.69	-	−0.56	−0.55	-	+0.26	-	−0.51	−0.43	+0.34	−0.25	−0.51	−0.58
Light-jet tagging efficiency (eigenvector 9) [%]	+0.69	-	−0.54	−0.52	-	+0.26	-	−0.50	−0.40	+0.35	-	−0.48	−0.66
Light-jet tagging efficiency (eigenvector 10) [%]	+0.68	-	−0.53	−0.51	-	+0.26	-	−0.50	−0.41	+0.35	−0.21	−0.45	−0.58
Light-jet tagging efficiency (eigenvector 11) [%]	+0.69	-	−0.52	−0.50	-	+0.26	-	−0.50	−0.40	+0.34	-	−0.45	−0.59
Light-jet tagging efficiency (eigenvector 12) [%]	+0.68	-	−0.53	−0.52	-	+0.25	-	−0.51	−0.41	+0.34	-	−0.44	−0.57
Light-jet tagging efficiency (eigenvector 13) [%]	+0.69	-	−0.52	−0.50	-	+0.25	-	−0.50	−0.39	+0.33	-	−0.44	−0.58
Light-jet tagging efficiency (eigenvector 14) [%]	+0.68	-	−0.53	−0.50	-	+0.25	-	−0.50	−0.39	+0.33	-	−0.43	−0.57
Light-jet tagging efficiency (eigenvector 15) [%]	+0.68	-	−0.52	−0.50	-	+0.25	-	−0.50	−0.39	+0.33	-	−0.43	−0.57
b-Quark tagging extrapolation [%]	+0.71	-	−0.52	−0.50	+1.10	+0.27	-	−0.50	−0.39	+0.35	-	−0.43	−0.57
b-Quark tagging extrapolation from c-Quark [%]	+0.70	-	−0.54	−0.64	−1.12	+0.27	-	−0.52	−0.55	+0.34	−0.20	−0.45	−0.78
Electron energy resolution [%]	+0.74	-	−0.54	−0.52	- −0.77	+0.29	-	−0.52	−0.40	+0.32	-	−0.44	−0.59
Electron energy scale [%]	+0.80	-	−0.52	−0.51	-	+0.31	-	−0.49	−0.57	+0.35	-	−0.43	−1.03
Electron trigger efficiency [%]	+0.69	-	−0.53	−0.68	−1.00	+0.26	-	−0.55	−0.56	+0.34	-	−0.47	−1.01
Electron reconstruction efficiency [%]	+0.69	-	−0.53	−0.51	-	+0.26	-	−0.51	−0.40	+0.34	-	−0.44	−0.58
Electron identification efficiency [%]	+0.73	-	−0.53	−0.52	-	+0.29	-	−0.51	−0.41	+0.37	-	−0.45	−0.60
Electron isolation efficiency [%]	+0.72	-	−0.59	−0.64	+0.21 −0.24	+0.29	-	−0.57	−0.55	+0.36	-	−0.51	−0.75
Muon (ID) momentum resolution [%]	+0.76	-	−0.58	−0.69	+0.33 −0.36	+0.36	-	−0.55	−0.60	+0.21	−0.20	−0.49	−0.81
Muon (MS) momentum resolution [%]	+0.79	-	−0.55	−0.57	−0.94 +0.12	+0.30	-	−0.54	−0.64	+0.29	−0.21	−0.53	−0.71
Muon (ID) sagitta ρ [%]	+0.77	−0.21	−0.43	−0.44	−0.61	+0.37	-	−0.65	−0.61	-	−0.22	−0.42	−0.80
Muon energy scale [%]	+0.78	-	−0.49	−0.42	−0.39	+0.27	-	−0.46	−0.37	+0.49	−0.20	−0.48	−1.04
Muon trigger efficiency stat [%]	+0.70	-	−0.43	−0.70	-	+0.27	-	−0.58	−0.46	+0.34	−0.21	−0.52	−1.00
Muon trigger efficiency syst [%]	+0.71	-	−0.54	−0.52	-	+0.28	-	−0.52	−0.41	+0.35	-	−0.45	−0.60
Muon identification stat [%]	+0.69	-	−0.55	−0.54	-	+0.26	-	−0.53	−0.43	+0.34	-	−0.46	−0.63
Muon identification syst [%]	+0.69	-	−0.53	−0.51	-	+0.26	-	−0.50	−0.40	+0.33	-	−0.43	−0.58
Muon isolation efficiency stat [%]	+0.69	-	−0.53	−0.55	-	+0.25	-	−0.51	−0.45	+0.33	-	−0.45	−0.65
Muon isolation efficiency syst [%]	+0.69	-	−0.52	−0.50	-	+0.26	-	−0.50	−0.39	+0.34	-	−0.43	−0.58
Muon TTVA efficiency stat [%]	+0.69	-	−0.53	−0.51	-	+0.26	-	−0.51	−0.40	+0.33	-	−0.44	−0.58
Muon TTVA efficiency syst [%]	+0.69	-	−0.53	−0.50	-	+0.25	-	−0.50	−0.39	+0.34	-	−0.43	−0.58
E_T^{miss} Soft jet resolution para [%]	±0.64	∓0.10	∓0.40	∓0.50	±0.32	±0.27	∓0.17	∓0.57	∓0.46	±0.25	∓0.22	∓0.30	∓0.83
E_T^{miss} Soft jet resolution perp [%]	±0.69	-	∓0.55	∓0.78	±0.36	±0.22	-	∓0.40	∓0.80	-	-	∓0.40	∓0.58
E_T^{miss} Soft jet scale [%]	+0.81	−0.28	−0.54	−0.58	−0.75	+0.28	-	−0.51	−0.67	+0.21	−0.23	−0.53	−0.41
Z+jets cross-section [%]	±0.32	-	−0.33 +0.34	∓0.38	∓0.18	±0.30	-	−0.31 +0.32	−0.34 +0.35	±0.13	-	∓0.17	∓0.38
Monte Carlo sample statistics [%]	±0.24	±0.17	±0.27	±0.65	±2.34	±0.24	±0.20	±0.34	±0.79	±0.38	±0.34	±0.66	±1.70
ISR/FSR + scale [%]	- −0.23	−0.38	+0.68	−4.30 +2.59	- −3.02	+0.39	- −1.78	-	−2.52 +3.59	+1.35 −0.30	+0.98 −0.44	+1.89	- −1.53
Alternate hard-scattering model [%]	±8.58	∓1.63	∓6.75	∓11.0	±3.33	±4.99	∓2.30	∓7.13	∓9.46	±1.04	±1.30	∓8.29	∓10.0
Alternate parton-shower model [%]	±5.33	±0.49	∓3.39	∓4.42	±7.07	±3.20	∓1.49	∓4.48	∓2.80	±1.29	∓3.47	∓3.45	±1.55
Inter PDF [%]	∓0.11	-	-	-	-	-	-	-	±0.11	∓0.10	-	±0.35	±0.36
Intra PDF [%]	-	-	∓0.18	∓0.20	-	∓0.11	-	-	-	±0.28	±0.38	±0.48	±0.38
Fakes overall normalization, el [%]	+2.27 −2.33	∓0.45	−1.69 +1.75	+0.69 −0.70	−1.91 +1.98	+0.68 −0.71	−0.57 +0.59	−1.56 +1.61	−1.62 +1.67	+0.41 −0.43	∓0.19	−1.25 +1.29	−1.63 +1.68
Fakes overall normalization, mu [%]	-	-	∓0.12	∓0.20	−0.20 +0.21	-	-	-	±0.23	±0.13	-	∓0.12	±0.19
Fakes alternative parametrization [%]	∓0.60	±0.47	±0.53	∓0.65	±0.67	∓0.62	∓0.14	±0.26	±0.60	∓0.12	±0.41	±0.51	±0.21
W+jets heavy flavour component [%]	±1.25	∓0.21	∓1.02	∓1.22	∓0.76	±0.64	∓0.25	∓0.97	∓1.08	±0.45	∓0.30	∓0.89	∓1.29
W+jets Scales [%]	±1.18	∓0.21	∓0.95	∓0.91	±0.18	±0.51	∓0.20	∓0.86	∓0.83	±0.28	∓0.30	∓0.66	∓0.91
Single Top DS/DR [%]	-	-	∓0.23	∓0.33	∓1.91	±0.13	-	∓0.32	∓0.15	±0.10	±0.18	∓0.24	±0.29
Single Top IFSR [%]	-	+0.24	+0.24	+0.42 −0.32	−1.08	-	-	−0.21	+0.41 −0.13	-	-	-	+1.26

TABLE F.65: Table of systematics for the relative differential cross-section at the parton level for the $p_T^{t,had}$ vs $|y|_T^{t,had}$ observable.

Bins [GeV] x [GeV]	0–80	80–150	150–250	250–350	350–1000	1000–1100	1100–1200	1200–1330	1330–2000	2000–2125	2125–2250	2250–2370	2370–3000	3000–3125	3125–3250	3250–3400	3400–4000
$1/\sigma \cdot d\sigma$ / $dp_T^{t\bar{t}} vs p_T^{t,had}$	$3.46 \cdot 10^{-3}$	$4.05 \cdot 10^{-3}$	$1.31 \cdot 10^{-3}$	$2.38 \cdot 10^{-4}$	$1.01 \cdot 10^{-5}$	$8.05 \cdot 10^{-4}$	$8.78 \cdot 10^{-4}$	$2.35 \cdot 10^{-4}$	$8.18 \cdot 10^{-6}$	$1.67 \cdot 10^{-4}$	$2.12 \cdot 10^{-4}$	$7.83 \cdot 10^{-5}$	$4.15 \cdot 10^{-6}$	$1.99 \cdot 10^{-5}$	$3.74 \cdot 10^{-5}$	$2.92 \cdot 10^{-5}$	$4.03 \cdot 10^{-6}$
Total Uncertainty [%]	$^{+7.63}_{-7.61}$	$^{+5.61}_{-5.62}$	±14.6	±18.3	$^{+15.8}_{-17.2}$	±15.5	±12.9	$^{+7.19}_{-6.85}$	$^{+12.1}_{-11.2}$	$^{+14.6}_{-14.4}$	$^{+13.6}_{-13.7}$	±10.8	$^{+12.1}_{-19.7}$	$^{+10.6}_{-10.4}$	$^{+11.8}_{-12.4}$	$^{+12.5}_{-14.0}$	$^{+20.3}_{-25.9}$
Statistics [%]	±0.2	±0.2	±0.3	±0.7	±2.5	±0.3	±0.3	±0.6	±2.1	±0.8	±0.8	±1.5	±4.7	±3.2	±2.5	±3.1	±7.6
Systematics [%]	$^{+7.62}_{-7.61}$	$^{+5.60}_{-5.61}$	±14.6	±18.3	$^{+15.5}_{-17.0}$	±15.5	$^{+12.9}_{-12.8}$	$^{+7.15}_{-6.81}$	$^{+11.9}_{-10.9}$	$^{+14.6}_{-14.3}$	$^{+13.6}_{-13.7}$	$^{+10.6}_{-10.7}$	$^{+10.8}_{-19.0}$	$^{+9.89}_{-9.77}$	$^{+11.4}_{-12.0}$	$^{+12.0}_{-13.5}$	$^{+18.1}_{-24.3}$
Jet energy resolution [%]	∓1.25	∓0.57	∓0.40	-	∓0.98	±2.33	±2.23	±1.75	±1.38	±2.64	±1.53	±3.13	±3.74	±0.51	∓0.45	∓0.27	∓0.61
b-Tagged jet energy scale (JES) [%]	$^{-0.74}_{+0.76}$	$^{+0.18}_{-0.16}$	$^{+0.58}_{-0.65}$	$^{+0.24}_{-}$	$^{-}_{-1.02}$	$^{+0.14}_{-}$	±0.59	$^{+0.43}_{-0.34}$	$^{-0.27}_{+0.93}$	$^{+0.29}_{-}$	$^{+0.15}_{-0.43}$	$^{+0.50}_{-}$	$^{-}_{-3.16}$	$^{-0.69}_{+0.83}$	$^{-}_{-0.84}$	$^{+0.44}_{-0.32}$	$^{-2.84}_{+2.70}$
Effective detector NP set 1 (JES) [%]	$^{-}_{+0.13}$	-	-	-	$^{-}_{-1.26}$	-	-	$^{-}_{-0.17}$	-	$^{+0.28}_{-}$	$^{+0.14}_{-0.19}$	-	$^{-}_{-2.03}$	$^{-}_{+0.63}$	$^{-}_{-0.35}$	$^{-}_{-0.29}$	$^{+0.14}_{-1.61}$
Effective detector NP set 2 (JES) [%]	-	-	-	-	$^{-}_{-1.03}$	-	$^{+0.11}_{-0.16}$	-	$^{+0.29}_{-0.13}$	-	-	-	$^{-}_{-1.89}$	$^{-}_{+0.48}$	-	$^{-0.38}_{+0.23}$	$^{-0.78}_{-}$
Effective mixed NP set 1 (JES) [%]	$^{-0.40}_{+0.42}$	-	$^{+0.22}_{-0.26}$	$^{+0.27}_{-0.17}$	$^{-}_{-1.11}$	-	$^{+0.24}_{-0.11}$	$^{+0.32}_{-0.42}$	$^{+0.36}_{-0.45}$	$^{+0.35}_{-0.16}$	$^{+0.35}_{-0.39}$	$^{-}_{+0.32}$	$^{-}_{-2.78}$	$^{+0.74}_{-1.41}$	$^{-}_{-1.12}$	$^{+0.46}_{-0.14}$	$^{+1.01}_{-2.05}$
Effective mixed NP set 2 (JES) [%]	-	-	-	-	$^{-}_{-1.11}$	-	-	-	$^{-}_{-0.40}$	$^{-}_{+0.30}$	$^{-0.19}_{+0.20}$	-	$^{-}_{-3.40}$	$^{-0.26}_{-}$	-	$^{-0.23}_{+0.71}$	$^{+0.19}_{-0.47}$
Effective mixed NP set 3 (JES) [%]	-	-	-	-	$^{-}_{-1.21}$	-	-	$^{+0.17}_{-0.11}$	-	-	-	$^{+0.25}_{-}$	$^{-}_{-2.33}$	$^{+0.42}_{-0.20}$	$^{-}_{-0.40}$	$^{-}_{-0.20}$	$^{+0.93}_{-}$
Effective modelling NP set 1 (JES) [%]	$^{-0.11}_{+0.19}$	-	$^{-0.59}_{+0.56}$	$^{-1.41}_{+1.82}$	$^{-3.68}_{+1.59}$	$^{+1.28}_{-1.09}$	$^{+1.10}_{-1.01}$	$^{-}_{+0.16}$	$^{-1.77}_{+1.90}$	$^{+1.31}_{-0.92}$	$^{+0.38}_{-0.37}$	$^{-1.22}_{+0.95}$	$^{-2.49}_{+0.24}$	-	$^{-1.32}_{+0.29}$	$^{-2.01}_{+0.86}$	$^{-3.92}_{+1.81}$
Effective modelling NP set 2 (JES) [%]	$^{-0.21}_{+0.32}$	-	$^{+0.27}_{-0.26}$	$^{+0.46}_{-0.18}$	$^{-}_{-0.91}$	$^{-0.10}_{+0.17}$	-	$^{+0.27}_{-0.22}$	$^{+0.37}_{-0.44}$	-	$^{+0.19}_{-0.25}$	$^{+0.10}_{-0.91}$	$^{-}_{-2.31}$	−0.56	$^{-}_{-0.53}$	$^{-}_{-0.36}$	$^{+3.44}_{-1.93}$
Effective modelling NP set 3 (JES) [%]	$^{+0.35}_{-0.34}$	-	$^{-0.25}_{+0.31}$	$^{-0.17}_{+0.42}$	$^{-}_{-0.73}$	$^{+0.18}_{-}$	$^{-0.15}_{+0.18}$	$^{-0.24}_{+0.52}$	$^{-}_{-0.54}$	$^{-}_{-0.11}$	$^{-0.31}_{-}$	$^{-}_{-0.28}$	$^{-}_{-4.05}$	+0.46	$^{-0.70}_{+0.39}$	$^{-0.56}_{+0.31}$	$^{+1.70}_{-}$
Effective modelling NP set 4 (JES) [%]	-	-	-	-	$^{-}_{-1.10}$	$^{-}_{+0.20}$	-	-	$^{-}_{-0.85}$	$^{+0.15}_{+0.29}$	$^{+0.28}_{-0.32}$	$^{+0.40}_{-0.37}$	$^{-}_{-2.46}$	$^{-}_{-0.43}$	$^{-}_{-0.43}$	$^{-}_{-1.05}$	$^{-}_{+0.59}$
Effective statistical NP set 1 (JES) [%]	-	-	$^{-0.16}_{-}$	$^{-0.18}_{+0.26}$	$^{-}_{-2.01}$	±0.21	$^{+0.18}_{-}$	∓0.29	$^{+0.75}_{-}$	$^{+0.25}_{-0.18}$	$^{+0.13}_{-0.24}$	$^{+0.21}_{-}$	$^{-}_{-2.28}$	$^{+0.42}_{-}$	$^{-}_{-0.99}$	$^{-}_{-0.62}$	$^{-}_{+1.39}$
Effective statistical NP set 2 (JES) [%]	-	-	±0.13	$^{+0.42}_{-0.13}$	$^{+0.28}_{-0.92}$	$^{-}_{+0.22}$	-	-	$^{-}_{-0.61}$	$^{-0.13}_{+0.27}$	$^{-0.16}_{+0.29}$	$^{-}_{-0.28}$	$^{-}_{-2.54}$	$^{+0.43}_{-0.47}$	$^{-}_{-0.49}$	$^{-}_{-0.21}$	$^{+3.35}_{-1.41}$
Effective statistical NP set 3 (JES) [%]	-	-	-	-	$^{-}_{-0.37}$	-	-	-	$^{-0.37}_{+0.38}$	$^{+0.61}_{-}$	-	$^{-}_{-0.83}$	$^{-}_{-1.54}$	$^{-0.43}_{+1.49}$	$^{-0.84}_{+0.72}$	$^{-}_{-0.81}$	$^{-}_{-0.42}$
Effective statistical NP set 4 (JES) [%]	$^{-0.24}_{+0.29}$	-	$^{+0.23}_{-0.27}$	$^{+0.10}_{-0.14}$	$^{-}_{-0.78}$	-	$^{+0.33}_{-0.15}$	$^{+0.37}_{-0.22}$	$^{-}_{-0.25}$	-	$^{+0.18}_{-0.32}$	$^{+0.31}_{-0.32}$	$^{-}_{-3.35}$	$^{-0.22}_{+1.39}$	$^{-}_{-0.40}$	$^{+0.16}_{-1.05}$	$^{-}_{-2.04}$
Effective statistical NP set 5 (JES) [%]	$^{+0.13}_{-}$	-	$^{-0.17}_{-}$	-	$^{-}_{-1.04}$	-	$^{-0.16}_{+0.22}$	$^{-}_{+0.21}$	$^{+0.50}_{-0.34}$	$^{+0.43}_{-}$	-	$^{+0.35}_{-0.20}$	$^{-}_{-2.19}$	$^{+0.35}_{-}$	$^{-}_{-0.89}$	$^{-}_{+0.27}$	$^{+1.49}_{-}$
Effective statistical NP set 6 (JES) [%]	-	-	$^{-0.11}_{+0.16}$	$^{+0.28}_{-}$	$^{-}_{-1.00}$	-	-	$^{+0.21}_{-}$	$^{+0.58}_{-}$	$^{-}_{+0.16}$	-	$^{-}_{-0.21}$	$^{-}_{-1.57}$	$^{+0.55}_{-0.50}$	$^{-}_{-0.27}$	$^{-0.13}_{+0.33}$	$^{+2.22}_{-3.79}$
Effective statistical NP set 7 (JES) [%]	-	-	-	-	$^{-}_{-0.58}$	-	-	$^{+0.17}_{-0.12}$	$^{-}_{-0.22}$	$^{+0.24}_{-}$	$^{-}_{-0.26}$	$^{-}_{-0.82}$	$^{-}_{-2.57}$	$^{-0.28}_{+0.24}$	$^{+0.30}_{-0.23}$	$^{-0.56}_{-}$	$^{+2.07}_{-3.07}$
η intercalibration model (JES) [%]	$^{-0.31}_{+0.34}$	-	$^{-}_{-0.12}$	$^{-}_{+0.30}$	$^{-}_{-2.13}$	$^{+0.40}_{-0.29}$	$^{+0.48}_{-0.42}$	$^{+0.26}_{-0.36}$	$^{+1.05}_{-}$	$^{+0.69}_{-0.38}$	$^{+0.42}_{-0.54}$	$^{+0.51}_{-0.12}$	$^{-0.49}_{+0.23}$	$^{+0.52}_{-}$	$^{-}_{-0.39}$	$^{-}_{-0.40}$	$^{-}_{-1.99}$
η intercalibration non closure (JES) [%]	-	-	-	-	$^{-}_{-1.62}$	$^{-0.20}_{+0.45}$	$^{-0.22}_{+0.30}$	-	$^{+0.40}_{-0.58}$	$^{-0.33}_{+0.28}$	$^{-0.21}_{-}$	$^{+0.15}_{+0.36}$	$^{-}_{-1.79}$	$^{-0.23}_{+0.53}$	$^{-}_{-0.32}$	$^{-}_{-1.14}$	$^{+2.70}_{-2.60}$
η intercalibration total stat (JES) [%]	$^{-0.13}_{+0.23}$	-	-	$^{-0.23}_{+0.42}$	$^{-1.38}_{-}$	$^{+0.30}_{-0.15}$	$^{+0.34}_{-0.25}$	$^{-}_{-0.32}$	$^{+0.37}_{-}$	$^{+0.41}_{-0.43}$	$^{+0.24}_{-0.37}$	-	$^{-}_{-2.68}$	-	$^{-0.33}_{+0.21}$	$^{-}_{-0.75}$	$^{+1.44}_{-}$
Flavour composition (JES) [%]	-	$^{-0.25}_{-}$	$^{-0.83}_{+1.07}$	$^{-1.78}_{+1.89}$	$^{-3.38}_{+1.85}$	$^{+1.46}_{-1.42}$	$^{+1.08}_{-1.07}$	$^{+0.22}_{-}$	$^{-1.05}_{+2.04}$	$^{+1.64}_{-1.36}$	$^{+0.52}_{-0.96}$	$^{-0.60}_{+0.80}$	$^{-}_{-2.73}$	$^{+0.66}_{-1.66}$	$^{-1.78}_{+0.57}$	$^{-2.30}_{+1.23}$	$^{-3.77}_{+1.47}$
Flavour response (JES) [%]	$^{+0.17}_{-}$	-	$^{+0.42}_{-0.29}$	$^{+1.04}_{-0.68}$	$^{+1.07}_{-2.48}$	$^{-0.72}_{+0.64}$	$^{-0.61}_{+0.68}$	-	$^{+0.94}_{-1.18}$	$^{-0.56}_{+0.82}$	$^{-0.67}_{+0.44}$	$^{-}_{-0.39}$	$^{-}_{-0.26}$	$^{-}_{-0.40}$	$^{+0.26}_{-0.47}$	$^{+0.28}_{-0.74}$	$^{+0.47}_{-}$
Pile-up offset μ (JES) [%]	-	-	-	-	$^{-}_{-1.25}$	-	-	$^{-}_{-0.20}$	$^{+0.20}_{-0.96}$	-	-	$^{+0.14}_{-0.42}$	$^{-}_{-2.00}$	$^{+0.53}_{-}$	$^{+0.37}_{-0.17}$	$^{-0.84}_{+0.16}$	$^{+2.30}_{-0.17}$
Pile-up offset N_{PV} (JES) [%]	$^{-0.18}_{+0.25}$	-	-	∓0.23	$^{-}_{-1.14}$	$^{+0.36}_{-0.24}$	$^{+0.35}_{-0.32}$	$^{+0.40}_{-0.42}$	$^{+0.57}_{-}$	$^{+0.83}_{-0.36}$	$^{+0.38}_{-0.42}$	$^{+0.34}_{-}$	$^{-}_{-1.02}$	$^{-1.08}_{+0.47}$	$^{-}_{-0.69}$	$^{-1.67}_{+0.71}$	$^{-1.20}_{+2.39}$
Pile-up offset p_T (JES) [%]	$^{-0.68}_{+0.69}$	-	$^{+0.66}_{-0.65}$	$^{+0.79}_{-0.48}$	$^{-}_{-0.88}$	-	$^{+0.46}_{-0.37}$	$^{+0.68}_{-0.52}$	$^{+0.45}_{-0.22}$	$^{+0.49}_{-0.46}$	$^{+0.41}_{-0.45}$	$^{+0.18}_{-0.33}$	$^{-}_{-1.25}$	$^{-0.60}_{-}$	$^{+0.30}_{-0.98}$	$^{-}_{-0.59}$	$^{+1.04}_{-4.05}$
Pile-up offset ρ topology (JES) [%]	$^{-0.61}_{+0.69}$	-	$^{-0.41}_{+0.49}$	$^{-2.19}_{+2.35}$	$^{-4.94}_{+3.83}$	$^{+1.81}_{-1.60}$	$^{+1.90}_{-1.83}$	$^{+0.21}_{-0.32}$	$^{-1.62}_{+3.31}$	$^{+1.81}_{-1.30}$	$^{+0.69}_{-0.99}$	$^{-0.76}_{+1.33}$	$^{-1.51}_{+0.52}$	$^{-}_{-0.77}$	$^{-1.34}_{+0.82}$	$^{-3.47}_{+2.18}$	$^{-5.45}_{+4.89}$
Punch-through (JES) [%]	-	-	-	-	$^{-}_{-0.58}$	-	-	-	$^{-0.52}_{+0.43}$	-	-	-	$^{-}_{-0.45}$	$^{+0.72}_{-}$	$^{+0.20}_{-0.18}$	$^{-}_{-0.63}$	$^{-}_{-1.08}$
Single particle high-p_T (JES) [%]	-	-	-	-	$^{-}_{-0.73}$	-	-	-	$^{+0.43}_{-}$	-	-	$^{+0.34}_{-}$	$^{-}_{-0.45}$	$^{+0.71}_{-}$	$^{+0.41}_{-}$	$^{-}_{-0.46}$	$^{+0.94}_{-1.25}$
Jet vertex fraction [%]	±0.26	-	$^{-0.32}_{+0.33}$	$^{-0.52}_{+0.54}$	$^{-0.48}_{+0.49}$	$^{+0.20}_{-0.21}$	-	∓0.31	$^{-0.40}_{+0.41}$	$^{+0.13}_{-0.15}$	$^{-0.11}_{+0.10}$	∓0.38	∓0.34	-	$^{-0.22}_{+0.21}$	∓0.42	$^{-0.31}_{+0.32}$
b-Quark tagging efficiency (eigenvector 0) [%]	$^{-1.30}_{+1.21}$	$^{-0.11}_{+0.10}$	$^{+1.06}_{-0.97}$	$^{+1.63}_{-1.50}$	$^{+0.92}_{-0.84}$	-	$^{+0.90}_{-0.85}$	$^{+1.73}_{-1.60}$	$^{+1.33}_{-1.23}$	$^{+0.10}_{-0.12}$	$^{+0.84}_{-0.80}$	$^{+1.56}_{-1.45}$	$^{+0.63}_{-0.58}$	$^{-0.59}_{+0.50}$	±0.43	$^{+1.33}_{-1.23}$	$^{+0.76}_{-0.73}$
b-Quark tagging efficiency (eigenvector 1) [%]	$^{+0.70}_{-0.68}$	±0.17	$^{-0.62}_{+0.61}$	$^{-1.50}_{+1.48}$	$^{-1.92}_{+1.91}$	±0.18	$^{-0.26}_{+0.25}$	$^{-0.95}_{+0.94}$	$^{-1.51}_{+1.49}$	$^{-0.33}_{+0.32}$	$^{-0.66}_{+0.64}$	$^{-1.27}_{+1.25}$	$^{-1.50}_{+1.48}$	$^{-0.68}_{+0.66}$	$^{-0.83}_{+0.81}$	$^{-1.18}_{+1.16}$	$^{-1.42}_{+1.38}$
b-Quark tagging efficiency (eigenvector 2) [%]	$^{+0.40}_{-0.41}$	$^{+0.12}_{-0.13}$	$^{-0.31}_{+0.32}$	$^{-0.90}_{+0.91}$	$^{-1.41}_{+1.44}$	-	∓0.13	$^{-0.56}_{+0.57}$	$^{-1.06}_{+1.09}$	∓0.33	$^{-0.47}_{+0.48}$	$^{-0.83}_{+0.85}$	$^{-1.16}_{+1.18}$	$^{-0.70}_{+0.71}$	$^{-0.65}_{+0.66}$	$^{-0.81}_{+0.82}$	$^{-1.21}_{+1.23}$
b-Quark tagging efficiency (eigenvector 3) [%]	∓0.30	-	±0.31	±0.30	∓0.17	-	±0.18	±0.32	-	-	±0.17	±0.18	-	∓0.25	-	-	∓0.29
c-Quark tagging efficiency (eigenvector 0) [%]	±0.12	-	∓0.11	∓0.17	∓0.24	-	-	∓0.10	∓0.12	-	-	∓0.12	∓0.10	±0.13	-	∓0.15	∓0.11
c-Quark tagging efficiency (eigenvector 1) [%]	±0.11	-	-	∓0.17	∓0.30	-	-	∓0.19	$^{-0.29}_{+0.28}$	∓0.12	∓0.19	∓0.29	∓0.33	-	∓0.20	∓0.31	∓0.46
c-Quark tagging efficiency (eigenvector 2) [%]	-	-	-	∓0.18	∓0.30	-	-	∓0.13	∓0.26	-	∓0.10	∓0.20	∓0.27	-	∓0.10	∓0.17	$^{-0.32}_{+0.31}$
Light-jet tagging efficiency (eigenvector 0) [%]	-	-	$^{+0.14}_{-0.13}$	±0.17	-	$^{-0.13}_{+0.15}$	-	-	-	$^{-0.34}_{+0.36}$	$^{-0.32}_{+0.33}$	$^{-0.59}_{+0.70}$	$^{-0.48}_{+0.47}$	$^{-0.30}_{+0.32}$	$^{-0.22}_{+0.21}$	$^{-0.19}_{+0.21}$	$^{-0.49}_{+0.48}$
Light-jet tagging efficiency (eigenvector 1) [%]	$^{+0.11}_{-0.10}$	-	∓0.11	∓0.20	∓0.13	-	-	∓0.15	∓0.16	-	-	∓0.26	∓0.11	-	∓0.11	∓0.14	$^{+0.10}_{-0.11}$
Light-jet tagging efficiency (eigenvector 2) [%]	-	-	-	-	-	-	-	-	-	-	-	$^{+0.23}_{-0.22}$	±0.10	-	±0.14	-	∓0.18
Light-jet tagging efficiency (eigenvector 3) [%]	-	-	-	-	∓0.12	-	-	∓0.10	$^{-0.16}_{+0.17}$	-	-	$^{-0.32}_{+0.35}$	$^{-0.16}_{+0.17}$	-	-	∓0.10	∓0.24
Light-jet tagging efficiency (eigenvector 5) [%]	-	-	-	-	-	-	-	-	-	-	-	$^{-0.14}_{+0.16}$	-	-	-	-	-
Light-jet tagging efficiency (eigenvector 9) [%]	-	-	-	-	-	-	-	-	-	-	-	-	-	-	-	-	±0.10
b-Quark tagging extrapolation [%]	-	-	-	-	±0.55	-	-	-	±0.33	-	-	±0.14	±0.55	±0.66	±0.41	±0.38	±1.06
Electron energy resolution [%]	-	-	-	-	$^{-}_{-0.89}$	-	-	-	-	-	-	$^{-0.22}_{-}$	$^{-0.18}_{+0.10}$	$^{-0.49}_{+0.15}$	$^{+0.36}_{-}$	$^{-}_{-0.39}$	$^{-0.55}_{+0.26}$
Electron energy scale [%]	-	-	-	-	$^{-}_{-0.81}$	-	-	-	$^{+0.33}_{-}$	-	-	$^{-}_{-0.36}$	$^{-}_{-0.85}$	$^{-0.18}_{+0.83}$	-	$^{-}_{-0.55}$	$^{+0.35}_{-}$
Electron identification efficiency [%]	-	-	-	±0.15	±0.28	-	-	-	±0.18	-	-	-	±0.11	±0.30	±0.18	-	-
Electron isolation efficiency [%]	-	-	-	±0.18	±0.43	-	-	-	±0.25	-	-	-	±0.13	±0.40	±0.23	-	-
Muon (ID) momentum resolution [%]	-	-	-	-	$^{-}_{-0.53}$	-	-	$^{+0.20}_{-}$	-	$^{+0.32}_{-}$	$^{-}_{-0.29}$	$^{+0.36}_{-}$	$^{-}_{-1.83}$	$^{+0.57}_{-}$	$^{-}_{-0.42}$	$^{-}_{-1.02}$	$^{-2.78}_{+0.28}$
Muon (MS) momentum resolution [%]	-	-	-	-	$^{-}_{-0.52}$	-	-	-	$^{-}_{+0.49}$	$^{-}_{+0.34}$	-	$^{-}_{+0.56}$	$^{-}_{-1.52}$	$^{-}_{+0.45}$	-	$^{-0.34}_{+0.44}$	$^{-3.23}_{+0.12}$
Muon (ID) sagitta o [%]	-	-	-	-	$^{-}_{-0.57}$	-	-	-	$^{+0.24}_{-}$	-	-	-	$^{+0.51}_{-}$	$^{+0.76}_{-}$	-	$^{-}_{-0.20}$	$^{-}_{-2.10}$
Muon energy scale [%]	-	-	-	-	$^{-}_{-0.68}$	-	-	-	$^{-}_{-0.48}$	$^{+0.15}_{+0.29}$	−0.15	+0.59	$^{-}_{-1.57}$	$^{+0.44}_{-}$	$^{-}_{-0.91}$	$^{-0.18}_{+0.11}$	$^{+0.96}_{-0.54}$
Muon identification syst [%]	-	-	-	-	±0.12	-	-	-	-	-	-	-	-	±0.13	-	-	-
E_T^{miss} Soft jet resolution para [%]	-	-	∓0.11	-	∓0.80	-	-	±0.20	±0.42	∓0.17	-	±0.34	∓0.93	-	∓0.60	∓0.16	±1.93
E_T^{miss} Soft jet resolution perp [%]	-	-	-	-	∓1.03	-	±0.20	∓0.10	∓0.30	-	±0.14	±0.19	∓0.26	∓0.80	∓0.55	∓0.13	±0.91
E_T^{miss} Soft jet scale [%]	-	-	-	-	$^{-}_{-0.90}$	-	-	-	$^{+0.41}_{-}$	$^{-}_{+0.48}$	-	$^{+0.35}_{-}$	$^{-}_{-2.75}$	$^{-0.53}_{+0.33}$	$^{-}_{-0.81}$	$^{+0.10}_{-0.68}$	$^{-}_{-0.66}$
Z+jets cross-section [%]	±0.38	-	∓0.36	$^{-0.45}_{+0.46}$	∓0.44	-	∓0.15	∓0.29	∓0.34	-	-	±0.32	∓0.18	∓0.10	∓0.12	-	±0.16
Monte Carlo sample statistics [%]	±0.23	±0.15	±0.22	±0.45	±1.46	±0.28	±0.22	±0.40	±1.30	±0.50	±0.50	±1.22	±2.87	±1.99	±1.51	±1.86	±4.77
ISR/FSR + scale [%]	$^{-0.23}_{+0.47}$	$^{+0.12}_{-0.14}$	$^{+0.53}_{-}$	$^{-2.24}_{+0.54}$	$^{+5.18}_{-}$	$^{-}_{-0.68}$	$^{+0.25}_{-1.26}$	$^{+1.78}_{-0.15}$	$^{+3.02}_{-}$	$^{+0.58}_{-0.28}$	$^{-}_{-0.50}$	$^{-0.42}_{+0.48}$	$^{-}_{-6.19}$	$^{-3.93}_{+3.84}$	$^{-0.55}_{+1.30}$	$^{-}_{-3.49}$	$^{-}_{-13.6}$
Alternate hard-scattering model [%]	±6.85	∓2.38	∓10.0	∓12.6	∓11.5	±4.42	±2.08	∓1.09	±7.87	±3.75	±2.43	∓3.64	∓2.97	±5.42	±9.14	∓1.10	∓6.27
Alternate parton-shower model [%]	±0.20	∓4.96	∓10.3	∓12.2	∓6.65	±14.3	±12.0	±5.84	±5.69	±13.2	±13.0	±8.40	±6.48	±5.00	±5.73	±11.1	±11.2
Inter PDF [%]	-	-	-	±0.17	-	-	-	-	±0.17	-	-	-	±0.14	±0.14	±0.15	±0.24	±0.33
Intra PDF [%]	±0.10	±0.11	-	∓0.21	∓0.50	∓0.15	∓0.11	∓0.17	∓0.27	∓0.38	∓0.35	∓0.31	∓0.49	∓0.32	∓0.38	∓0.20	∓0.21
Fakes overall normalization, el [%]	$^{+1.77}_{-1.81}$	$^{-0.59}_{+0.60}$	$^{-1.02}_{+1.05}$	$^{-1.42}_{+1.46}$	$^{-1.80}_{+1.85}$	$^{+0.69}_{-0.71}$	$^{-0.54}_{+0.56}$	$^{-1.00}_{+1.03}$	$^{-1.61}_{+1.66}$	$^{-0.91}_{+0.94}$	$^{-1.24}_{+1.28}$	$^{-1.40}_{+1.44}$	$^{-1.62}_{+1.67}$	$^{-1.68}_{+1.73}$	$^{-1.43}_{+1.47}$	-	$^{-1.42}_{+1.46}$
Fakes overall normalization, mu [%]	-	-	∓0.12	∓0.25	∓0.32	-	-	-	-	±0.12	-	-	∓0.85	±0.21	∓0.22	-	∓0.25
Fakes alternative parametrization [%]	∓0.45	±0.36	±0.25	±0.20	±0.38	∓0.61	-	-	±0.40	±0.10	±0.18	±1.01	±6.20	±0.45	±0.37	∓0.88	±2.72
W+jets heavy flavour component [%]	±0.58	-	∓0.44	∓0.67	∓0.74	-	∓0.21	∓0.52	∓0.66	-	∓0.24	∓0.74	∓0.90	∓0.66	∓0.83	∓0.88	∓0.90
W+jets Scales [%]	±0.35	∓0.16	∓0.52	∓0.73	∓0.59	∓0.19	-	∓0.26	∓0.26	±0.65	±0.67	±0.22	±0.19	±0.99	±0.40	±0.61	±1.16
Single Top DS/DR [%]	±0.19	±0.18	-	-	-	-	∓0.18	∓0.37	∓0.20	∓0.66	∓0.72	∓1.32	∓1.36	∓1.89	∓1.81	∓1.34	∓2.23
Single Top IFSR [%]	$^{-0.17}_{-}$	-	-	$^{+0.27}_{-}$	$^{+0.13}_{-0.41}$	$^{-}_{-0.24}$	$^{-}_{-0.14}$	$^{+0.21}_{-0.10}$	$^{+0.78}_{-}$	$^{-}_{-0.15}$	$^{-}_{-0.23}$	$^{-}_{-1.19}$	$^{+0.78}_{-2.27}$	$^{+0.35}_{-1.04}$	$^{+0.54}_{-0.58}$	$^{+1.09}_{-}$	$^{+0.55}_{-2.19}$

TABLE F.66: Table of systematics for the relative differential cross-section at the parton level for the $p_T^{t,had}$ vs $p_T^{t\bar{t}}$ observable.

F.2.2.2 Boosted topology

Bins [GeV]	490–831.99	831.99–1007.69	1007.69–1192.80	1192.80–1406.15	1406.15–1657.15	1657.15–1948.94	1948.94–3000
$1/\sigma \cdot \mathrm{d}\sigma \,/\, \mathrm{d}m^{t\bar{t}}[GeV] : m^{t\bar{t}}$	$1.01 \cdot 10^{-3}$	$1.74 \cdot 10^{-3}$	$9.58 \cdot 10^{-4}$	$4.64 \cdot 10^{-4}$	$1.82 \cdot 10^{-4}$	$6.54 \cdot 10^{-5}$	$8.82 \cdot 10^{-6}$
Total Uncertainty [%]	$^{+5.59}_{-4.59}$	$^{+2.53}_{-2.72}$	$^{+5.92}_{-6.32}$	$^{+6.87}_{+6.29}$	$^{+6.29}_{-7.85}$	$^{+14.0}_{-14.1}$	$^{+39.3}_{-37.2}$
Statistics [%]	±1.0	±1.0	±1.4	±1.9	±2.9	±5.1	±9.0
Systematics [%]	$^{+5.45}_{-4.43}$	$^{+2.24}_{-2.45}$	$^{+5.69}_{-6.10}$	$^{+6.50}_{-5.88}$	$^{+5.29}_{-7.07}$	$^{+12.7}_{-12.8}$	$^{+38.0}_{-35.9}$
b-Tagged jet energy scale (JES) [%]	$^{-0.27}_{+0.31}$	-	$^{+0.23}_{-0.22}$	$^{+0.21}_{-0.32}$	-	$^{+0.25}_{-}$	$^{+0.20}_{-}$
Effective detector NP set 1 (JES) [%]	-	-	-	$^{-}_{-0.13}$	-	$^{-}_{+0.11}$	$^{-}_{+0.42}$
Effective detector NP set 2 (JES) [%]	-	-	-	-	-	$^{-}_{-0.21}$	$^{-}_{-0.38}$
Effective mixed NP set 1 (JES) [%]	$^{-0.62}_{+0.83}$	$^{-}_{-0.32}$	$^{+0.50}_{-0.40}$	$^{+1.10}_{-0.40}$	$^{+0.29}_{-1.24}$	$^{+2.29}_{-1.22}$	$^{+0.14}_{+2.77}$
Effective mixed NP set 2 (JES) [%]	-	-	-	-	-	-	$^{-}_{-2.46}$
Effective mixed NP set 3 (JES) [%]	-	-	-	-	-	-	$^{-0.22}_{+0.27}$
Effective modelling NP set 1 (JES) [%]	$^{+0.30}_{-}$	$^{-}_{-0.25}$	$^{+0.18}_{-}$	$^{+0.28}_{-0.43}$	-	$^{-}_{\mp 0.52}$	$^{+0.26}_{+0.93}$
Effective modelling NP set 2 (JES) [%]	$^{-0.43}_{+0.41}$	-	$^{+0.33}_{-0.17}$	$^{+0.39}_{-0.25}$	$^{+0.19}_{-0.70}$	$^{+1.46}_{-1.36}$	$^{-0.53}_{+2.42}$
Effective modelling NP set 3 (JES) [%]	$^{+0.28}_{-0.21}$	-	$^{-0.19}_{+0.24}$	$^{-0.31}_{+0.16}$	-	-	$^{-1.28}_{-}$
Effective modelling NP set 4 (JES) [%]	-	-	-	-	-	$^{-}_{+0.17}$	$^{+0.21}_{+0.49}$
Effective statistical NP set 1 (JES) [%]	-	-	-	$^{-}_{\pm 0.19}$	-	$^{-}_{-0.20}$	$^{-0.35}_{+0.67}$
Effective statistical NP set 2 (JES) [%]	$^{-0.19}_{+0.17}$	-	-	$^{+0.20}_{-}$	$^{+0.18}_{-0.24}$	$^{-}_{+0.58}$	$^{-0.68}_{+0.70}$
Effective statistical NP set 3 (JES) [%]	$^{+0.33}_{-0.34}$	-	$^{-0.18}_{+0.38}$	$^{-0.53}_{+0.47}$	$^{-0.42}_{+0.20}$	$^{-0.73}_{+0.59}$	$^{-0.64}_{+0.44}$
Effective statistical NP set 4 (JES) [%]	-	$^{-}_{-0.14}$	-	-	$^{-0.14}_{+0.33}$	$^{+0.23}_{+0.26}$	$^{+0.98}_{-0.63}$
Effective statistical NP set 5 (JES) [%]	-	-	$^{+0.11}_{-0.14}$	-	$^{-0.13}_{+0.31}$	$^{-0.53}_{+0.32}$	$^{+0.52}_{-0.44}$
Effective statistical NP set 6 (JES) [%]	-	-	$^{+0.11}_{-0.10}$	-	-	$^{-0.12}_{+0.10}$	$^{+0.36}_{-0.30}$
Effective statistical NP set 7 (JES) [%]	-	-	-	$^{-}_{\pm 0.14}$	-	-	$^{+0.32}_{\pm 0.24}$
η intercalibration model (JES) [%]	-	−0.44	+0.15	+0.65	+0.40	+0.83	+2.24
η intercalibration non closure (JES) [%]	$^{+0.56}_{+0.41}$	-	$^{-0.27}_{-0.20}$	$^{-0.62}_{-0.29}$	−0.58	−0.80	−1.86
η intercalibration total stat (JES) [%]	−0.13	-	-	+0.46	−0.42	-	$^{-0.10}_{+0.66}$
Flavour composition (JES) [%]	-	-	-	-	-	-	$^{+0.21}_{-0.55}$
Flavour response (JES) [%]	$^{-}_{+0.36}$	$^{-}_{-0.41}$	-	$^{+0.64}_{-0.21}$	$^{-}_{-0.72}$	$^{+0.56}_{-0.77}$	$^{+3.80}_{-2.84}$
Pile-up offset μ (JES) [%]	-	-	-	$^{-0.11}_{+0.15}$	$^{+0.13}_{-0.19}$	$^{+0.18}_{-0.69}$	$^{+0.43}_{-}$
Pile-up offset N_{PV} (JES) [%]	-	-	$^{+0.18}_{-}$	-	$^{-0.15}_{-0.27}$	$^{+0.23}_{-}$	$^{-}_{-}$
Pile-up offset p_T (JES) [%]	−0.34	-	$^{+0.46}_{-0.27}$	+0.64	$^{+0.28}_{-}$	+1.01	+1.30
Pile-up offset ρ topology (JES) [%]	$^{+0.52}_{+0.29}$	−0.20	-	$^{-0.43}_{+0.55}$	−0.30	$^{-0.61}_{-1.25}$	$^{-0.95}_{+1.01}$
Punch-through (JES) [%]	-	−0.44	-	-	−0.73	+0.96	−1.18
Jet vertex fraction [%]	-	-	-	-	+0.33	-	$^{+0.17}_{-0.19}$
b-Quark tagging efficiency (eigenvector 0) [%]	−0.10	+0.15	-	-	-	−0.21	−0.95
b-Quark tagging efficiency (eigenvector 1) [%]	$^{+0.11}_{+0.32}$	−0.14	−0.16	−0.29	−0.45	$^{+0.18}_{-0.50}$	$^{+0.91}_{-1.03}$
b-Quark tagging efficiency (eigenvector 2) [%]	−0.30	-	+0.15	+0.28	+0.42	+0.48	+1.00
b-Quark tagging efficiency (eigenvector 3) [%]	±0.23	-	∓0.14	∓0.22	∓0.26	∓0.26	∓0.43
c-Quark tagging efficiency (eigenvector 1) [%]	-	-	-	∓0.10	∓0.15	∓0.19	∓0.34
c-Quark tagging efficiency (eigenvector 2) [%]	$^{+0.11}_{-0.10}$	-	-	∓0.13	∓0.26	∓0.39	∓1.06
Light-jet tagging efficiency (eigenvector 0) [%]	-	-	-	-	∓0.11	$^{-0.22}_{+0.21}$	∓0.48
Light-jet tagging efficiency (eigenvector 1) [%]	±0.10	$^{+0.14}_{-0.13}$	-	∓0.22	$^{-0.35}_{+0.33}$	$^{-0.62}_{+0.59}$	$^{-2.31}_{+2.27}$
Light-jet tagging efficiency (eigenvector 2) [%]	-	-	-	-	-	∓0.19	$^{-0.89}_{+0.88}$
Light-jet tagging efficiency (eigenvector 3) [%]	-	-	-	-	∓0.15	$^{-0.19}_{+0.18}$	∓0.58
Light-jet tagging efficiency (eigenvector 4) [%]	-	-	-	-	-	-	±0.10
Light-jet tagging efficiency (eigenvector 5) [%]	-	-	-	-	-	±0.20	±0.47
Light-jet tagging efficiency (eigenvector 6) [%]	-	-	-	-	-	∓0.14	∓0.13
Light-jet tagging efficiency (eigenvector 7) [%]	-	-	-	-	-	∓0.13	∓0.38
Light-jet tagging efficiency (eigenvector 9) [%]	-	-	-	-	-	-	∓0.13
b-Quark tagging extrapolation [%]	∓0.26	$^{-0.15}_{+0.16}$	±0.11	$^{+0.30}_{-0.31}$	$^{+0.67}_{-0.69}$	$^{+0.96}_{-0.98}$	$^{+2.19}_{-2.23}$
Electron energy resolution [%]	-	-	-	-	-	$^{+0.26}_{-}$	-
Electron energy scale [%]	-	-	-	-	$^{+0.10}_{-0.15}$	$^{+0.70}_{-}$	$^{+0.39}_{-0.80}$
Electron identification efficiency [%]	∓0.11	-	-	±0.10	±0.17	±0.31	$^{+0.60}_{-0.61}$
Electron isolation efficiency [%]	∓0.21	-	±0.11	±0.18	±0.29	$^{+0.40}_{-0.41}$	±0.63
Muon (ID) momentum resolution [%]	-	-	-	-	-	-	$^{-}_{-0.96}$
Muon (MS) momentum resolution [%]	-	-	-	-	-	-	$^{-}_{+0.12}$
Muon energy scale [%]	-	-	-	-	-	-	-
Muon trigger efficiency syst [%]	-	-	-	-	-	-	$^{+0.16}_{-0.15}$
Muon identification syst [%]	-	-	-	±0.10	±0.17	±0.24	±0.44
E_T^{miss} Soft jet resolution para [%]	±0.60	∓0.27	∓0.33	-	∓0.72	∓0.24	∓0.63
E_T^{miss} Soft jet resolution perp [%]	±0.65	∓0.16	∓0.50	∓0.25	∓0.36	∓0.38	∓1.17
E_T^{miss} Soft jet scale [%]	$^{+0.51}_{-0.43}$	-	$^{-0.26}_{+0.33}$	$^{-0.28}_{+0.55}$	$^{-0.60}_{+0.29}$	$^{-0.48}_{+0.46}$	$^{-1.21}_{+0.66}$
Z+jets cross-section [%]	-	∓0.20	-	±0.13	$^{+0.38}_{-0.39}$	±0.81	$^{+2.13}_{-2.15}$
$t\bar{t}V$ cross-section [%]	-	-	-	-	-	-	±0.12
Monte Carlo sample statistics [%]	±0.64	±0.60	±0.82	±1.14	±1.72	±2.80	±4.09
ISR/FSR + scale [%]	$^{-2.85}_{+4.15}$	$^{-}_{-0.45}$	$^{+1.09}_{-2.63}$	$^{+2.93}_{-1.78}$	$^{+1.25}_{-1.46}$	$^{+8.00}_{-8.39}$	$^{+16.1}_{-10.0}$
Alternate hard-scattering model [%]	±1.67	∓1.22	∓5.29	±4.48	±0.89	∓0.48	±25.6
Alternate parton-shower model [%]	±2.09	∓0.71	∓0.81	∓1.94	∓1.37	±2.36	∓6.80
Fakes overall normalization, el [%]	-	∓0.26	$^{-0.18}_{+0.19}$	∓0.17	$^{+0.39}_{-0.40}$	$^{+2.08}_{-2.12}$	$^{+4.45}_{-4.50}$
Fakes overall normalization, mu [%]	-	-	-	±0.11	-	-	±0.10
Fakes alternative parametrization [%]	∓0.16	±0.61	±0.56	±0.12	∓0.80	∓4.29	∓9.33
W+jets heavy flavour component [%]	-	-	-	-	-	-	±0.10
W+jets Scales [%]	∓0.63	∓1.27	∓0.22	±1.53	±3.14	±6.07	±15.7
W+jets α_S [%]	-	-	-	$^{-0.10}_{+0.11}$	$^{-0.20}_{+0.27}$	$^{-0.33}_{+0.48}$	$^{-0.92}_{+1.21}$
Single Top DS/DR [%]	±0.98	±0.57	∓0.17	∓1.40	∓2.93	∓3.93	∓7.51
Single Top IFSR [%]	$^{+0.26}_{-}$	$^{-0.40}_{-}$	-	$^{+0.84}_{-0.37}$	$^{-}_{-0.41}$	$^{+0.34}_{-0.52}$	$^{+1.15}_{-3.06}$

TABLE F.67: Table of systematics for the relative differential cross-section at the parton level for the $m_{t\bar{t}}$observable.

Bins [GeV]	350–410	410–475	475–545	545–630	630–845	845–2000
$1/\sigma \cdot \mathrm{d}\sigma$ / $\mathrm{d}p_T^{t,\mathrm{had}}$	$8.86 \cdot 10^{-3}$	$3.88 \cdot 10^{-3}$	$1.64 \cdot 10^{-3}$	$6.85 \cdot 10^{-4}$	$1.55 \cdot 10^{-4}$	$4.59 \cdot 10^{-6}$
Total Uncertainty [%]	$^{+2.53}_{-2.51}$	$^{+1.72}_{-3.18}$	$^{+4.13}_{-3.83}$	$^{+9.76}_{-9.40}$	$^{+12.1}_{-10.2}$	$^{+47.8}_{-46.6}$
Statistics [%]	±0.6	±1.1	±1.7	±2.5	±3.7	±13.
Systematics [%]	$^{+2.42}_{-2.40}$	$^{+1.05}_{-2.87}$	$^{+3.58}_{-3.24}$	$^{+9.29}_{-8.91}$	$^{+11.3}_{-9.32}$	$^{+45.6}_{-44.3}$
b-Tagged jet energy scale (JES) [%]	-	-	-	$^{+0.15}_{-0.21}$	-	-
Effective detector NP set 1 (JES) [%]	-	-	$^{+0.14}_{-}$	-	$^{+0.30}_{-0.12}$	$^{-0.73}_{+0.45}$
Effective detector NP set 2 (JES) [%]	-	-	$^{+0.17}_{-}$	-	-	$^{-0.60}_{-0.30}$
Effective mixed NP set 1 (JES) [%]	$^{-0.47}_{+0.31}$	-	$^{+0.74}_{-0.56}$	$^{+0.14}_{-0.89}$	$^{+2.00}_{-1.19}$	$^{+4.14}_{-5.26}$
Effective mixed NP set 2 (JES) [%]	-	-	$^{-0.10}_{+0.18}$	-	$^{-0.16}_{+0.32}$	-
Effective mixed NP set 3 (JES) [%]	-	-	-	-	-	-
Effective modelling NP set 1 (JES) [%]	-	-	$^{+0.43}_{-0.18}$	-	-	$^{+0.51}_{-}$
Effective modelling NP set 2 (JES) [%]	$^{-0.28}_{+0.22}$	-	$^{+0.42}_{-0.17}$	$^{+0.34}_{-0.72}$	$^{+1.04}_{-0.58}$	$^{+4.94}_{-4.68}$
Effective modelling NP set 3 (JES) [%]	-	-	$^{-0.15}_{+0.43}$	$^{-}_{-0.28}$	-	$^{+0.77}_{-0.52}$
Effective modelling NP set 4 (JES) [%]	-	-	-	$^{-0.19}_{-}$	$^{+0.38}_{-0.18}$	$^{+0.61}_{-0.80}$
Effective statistical NP set 1 (JES) [%]	-	-	$^{+0.20}_{-0.21}$	$^{+0.48}_{-0.24}$	$^{+0.48}_{-0.20}$	$^{+0.97}_{-1.18}$
Effective statistical NP set 2 (JES) [%]	$^{-0.13}_{+0.11}$	-	$^{+0.32}_{-0.28}$	$^{+0.13}_{-0.40}$	$^{+0.54}_{-0.28}$	$^{+1.60}_{-1.52}$
Effective statistical NP set 3 (JES) [%]	$^{+0.27}_{-0.32}$	-	$^{-0.44}_{+0.68}$	$^{-0.88}_{+0.43}$	$^{-0.52}_{+1.01}$	-
Effective statistical NP set 4 (JES) [%]	-	-	-	$^{-0.52}_{+0.20}$	$^{-0.53}_{+0.61}$	$^{-0.59}_{+0.52}$
Effective statistical NP set 5 (JES) [%]	-	$^{+0.16}_{-0.18}$	$^{+0.25}_{-0.10}$	$^{-0.22}_{+0.12}$	$^{-0.64}_{+0.76}$	$^{-0.90}_{+0.71}$
Effective statistical NP set 6 (JES) [%]	$^{-0.12}_{-}$	$^{+0.16}_{-}$	$^{+0.30}_{-0.17}$	$^{-}_{-0.26}$	$^{-0.15}_{+0.39}$	$^{-0.63}_{+0.47}$
Effective statistical NP set 7 (JES) [%]	-	-	$^{+0.27}_{-0.16}$	-	$^{+0.28}_{-}$	$^{+0.27}_{-0.40}$
η intercalibration model (JES) [%]	$^{-0.17}_{+0.11}$	-	$^{+0.55}_{-}$	$^{-}_{-0.45}$	$^{+0.91}_{-0.56}$	$^{+1.02}_{-1.76}$
η intercalibration non closure (JES) [%]	-	-	-	$^{-}_{-0.45}$	-	$^{-0.17}_{+0.26}$
η intercalibration total stat (JES) [%]	-	-	$^{+0.20}_{-0.11}$	$^{-}_{-0.20}$	$^{+0.22}_{-}$	$^{+0.44}_{-0.29}$
Flavour composition (JES) [%]	$^{-0.20}_{+0.12}$	-	$^{+0.46}_{-}$	$^{-}_{-}$	$^{+0.80}_{-0.55}$	$^{+3.23}_{-3.54}$
Flavour response (JES) [%]	-	-	$^{-}_{+0.41}$	$^{+0.28}_{-0.49}$	$^{+0.54}_{-0.14}$	$^{+1.55}_{-1.25}$
Pile-up offset μ (JES) [%]	-	-	-	-	$^{+0.20}_{-0.13}$	$^{+0.52}_{-}$
Pile-up offset N_{PV} (JES) [%]	-	-	$^{+0.21}_{-}$	$^{-}_{-0.31}$	$^{+0.33}_{-0.15}$	$^{+1.02}_{-}$
Pile-up offset p_T (JES) [%]	$^{-0.26}_{-}$	$^{+0.23}_{-}$	$^{+0.49}_{-}$	$^{-}_{-0.30}$	$^{+0.89}_{-0.25}$	$^{+0.35}_{-0.99}$
Pile-up offset ρ topology (JES) [%]	$^{-}_{-0.17}$	-	$^{+0.32}_{-}$	$^{-0.66}_{+0.26}$	$^{-0.60}_{+0.58}$	$^{-}_{+0.35}$
Punch-through (JES) [%]	-	-	-	-	$^{+0.11}_{-}$	$^{+0.27}_{-}$
b-Quark tagging efficiency (eigenvector 0) [%]	-	-	-	$^{-0.19}_{+0.18}$	$^{-0.35}_{+0.34}$	$^{-1.12}_{+1.07}$
b-Quark tagging efficiency (eigenvector 1) [%]	-	-	-	$^{+0.14}_{-0.15}$	$^{+0.21}_{-0.22}$	$^{+0.59}_{-0.62}$
b-Quark tagging efficiency (eigenvector 2) [%]	-	-	-	-	∓0.10	∓0.17
b-Quark tagging efficiency (eigenvector 3) [%]	-	-	-	-	$^{-0.16}_{+0.15}$	∓0.26
c-Quark tagging efficiency (eigenvector 1) [%]	-	-	-	-	$^{-0.13}_{+0.14}$	∓0.34
c-Quark tagging efficiency (eigenvector 2) [%]	-	-	-	-	-	∓0.18
Light-jet tagging efficiency (eigenvector 0) [%]	±0.10	-	-	-	$^{-0.57}_{+0.59}$	$^{-1.86}_{+1.82}$
Light-jet tagging efficiency (eigenvector 1) [%]	-	-	-	-	-	∓0.78
Light-jet tagging efficiency (eigenvector 2) [%]	-	-	-	-	-	∓0.23
Light-jet tagging efficiency (eigenvector 3) [%]	-	-	-	-	-	±0.25
Light-jet tagging efficiency (eigenvector 4) [%]	-	-	-	-	-	±0.27
Light-jet tagging efficiency (eigenvector 5) [%]	-	-	-	-	±0.13	±0.66
Light-jet tagging efficiency (eigenvector 6) [%]	-	-	-	-	-	∓0.20
Light-jet tagging efficiency (eigenvector 7) [%]	-	-	-	-	∓0.15	∓0.56
Light-jet tagging efficiency (eigenvector 8) [%]	-	-	-	-	-	±0.19
Light-jet tagging efficiency (eigenvector 9) [%]	-	-	-	-	-	∓0.22
Light-jet tagging efficiency (eigenvector 11) [%]	-	-	-	-	-	∓0.10
b-Quark tagging extrapolation [%]	∓0.20	-	$^{+0.22}_{-0.23}$	$^{+0.30}_{-0.32}$	$^{+0.83}_{-0.85}$	$^{+2.08}_{-2.18}$
Electron identification efficiency [%]	-	-	-	-	±0.15	±0.39
Electron isolation efficiency [%]	-	-	±0.10	±0.17	$^{+0.31}_{-0.32}$	$^{+0.70}_{-0.71}$
Muon identification syst [%]	-	-	-	-	-	±0.17
E_T^{miss} Soft jet resolution para [%]	-	-	±0.12	-	±0.27	-
E_T^{miss} Soft jet resolution perp [%]	-	-	±0.10	-	±0.28	±0.11
E_T^{miss} Soft jet scale [%]	-	-	-	-	-	$^{+0.38}_{-0.24}$
Z+jets cross-section [%]	-	-	-	-	±0.35	$^{+1.13}_{-1.14}$
Diboson cross-section [%]	-	-	-	-	-	±0.15
$t\bar{t}V$ cross-section [%]	-	-	-	-	-	±0.24
Monte Carlo sample statistics [%]	±0.39	±0.69	±1.03	±1.49	±1.91	±5.38
ISR/FSR + scale [%]	$^{-}_{+0.67}$	$^{-2.72}_{+0.27}$	-	$^{+4.31}_{-2.81}$	$^{+7.80}_{-5.06}$	$^{+14.1}_{-6.17}$
Alternate hard-scattering model [%]	-	∓0.25	±0.98	∓7.07	±2.19	±38.2
Alternate parton-shower model [%]	±2.01	∓0.75	∓2.69	∓3.58	∓5.62	∓12.0
Fakes overall normalization, el [%]	$^{-0.15}_{+0.16}$	-	±0.18	±0.33	$^{+1.06}_{-1.08}$	$^{+1.98}_{-2.01}$
Fakes overall normalization, mu [%]	-	-	-	∓0.23	∓0.39	$^{-0.64}_{+0.65}$
Fakes alternative parametrization [%]	±0.22	-	∓0.25	∓0.21	∓1.39	∓2.75
W+jets heavy flavour component [%]	-	-	-	-	-	±0.15
W+jets Scales [%]	∓0.61	-	±0.54	±1.12	±2.44	±9.05
W+jets α_S [%]	-	-	-	-	$^{-0.14}_{+0.19}$	$^{-0.48}_{+0.85}$
Single Top DS/DR [%]	±0.61	±0.16	∓0.72	∓1.54	∓2.76	∓9.09
Single Top IFSR [%]	$^{-0.17}_{+0.13}$	-	$^{+0.38}_{-0.35}$	-	$^{+1.30}_{-}$	$^{+3.97}_{-1.61}$

TABLE F.68: Table of systematics for the relative differential cross-section at the parton level for the p_T^{had} observable.

Bins [GeV] x [GeV]	490–900	900–1650	1650–3000	3000–3542	3542–5510
$1/\sigma \cdot \mathrm{d}\sigma$ / $\mathrm{d}m^{t\bar{t}}vsp_T^{had}$	$1.11 \cdot 10^{-3}$	$5.78 \cdot 10^{-4}$	$1.27 \cdot 10^{-5}$	$4.96 \cdot 10^{-5}$	$3.48 \cdot 10^{-5}$
Total Uncertainty [%]	+4.08 −3.91	+2.32 −2.92	+26.4 −24.8	+11.8 −7.06	+11.4 −11.7
Statistics [%]	±0.8	±0.8	±6.4	±4.5	±2.3
Systematics [%]	+3.97 −3.80	+2.10 −2.75	+25.3 −23.6	+10.6 −4.69	+11.1 −11.4
b-Tagged jet energy scale (JES) [%]	−0.21 +0.18	+0.14 −0.20	+0.23 −0.11	- +0.33	+0.34 -
Effective detector NP set 1 (JES) [%]	-	-	- −0.42	-	-
Effective detector NP set 2 (JES) [%]	-	-	- −0.20	-	-
Effective mixed NP set 1 (JES) [%]	−0.56 +0.53	+0.12 −0.26	+1.60 −1.08	+0.51 −0.12	+1.92 −1.23
Effective mixed NP set 2 (JES) [%]	-	-	−0.25 -	-	−0.10 +0.13
Effective mixed NP set 3 (JES) [%]	-	-	-	-	-
Effective modelling NP set 1 (JES) [%]	- +0.21	- −0.28	+1.46 −0.35	−0.18 +0.58	+0.31 -
Effective modelling NP set 2 (JES) [%]	−0.25 +0.32	- -	+1.27 −0.80	+0.52 -	+1.37 −0.79
Effective modelling NP set 3 (JES) [%]	+0.16 −0.13	−0.18 -	−0.63 +0.37	+0.23 -	-
Effective modelling NP set 4 (JES) [%]	-	-	+0.15 −0.47	-	-
Effective statistical NP set 1 (JES) [%]	-	-	- −0.56	-	+0.29 −0.20
Effective statistical NP set 2 (JES) [%]	- +0.15	- -	+0.13 −0.44	+0.20 −0.23	+0.41 −0.35
Effective statistical NP set 3 (JES) [%]	+0.33 −0.26	−0.22 -	−0.72 +0.92	−0.15 +0.43	−0.39 +0.89
Effective statistical NP set 4 (JES) [%]	-	-	-	−0.44 +0.41	−0.38 +0.45
Effective statistical NP set 5 (JES) [%]	-	+0.11 −0.10	- −0.36	−0.28 +0.30	−0.33 +0.44
Effective statistical NP set 7 (JES) [%]	-	-	+0.13 −0.39	-	-
η intercalibration model (JES) [%]	−0.19 +0.45	- −0.30	+1.96 −2.48	-	+0.71 −0.18
η intercalibration non closure (JES) [%]	+0.21 -	- −0.20	- -	+0.30 -	−0.14 +0.39
η intercalibration total stat (JES) [%]	-	-	+0.21 −0.50	−0.11 -	-
Flavour composition (JES) [%]	−0.20 +0.37	- −0.24	+2.27 −1.79	+0.49 -	+1.02 −0.33
Flavour response (JES) [%]	-	−0.19 -	−0.80 +1.85	+0.14 −0.28	+0.72 −0.19
Pile-up offset μ (JES) [%]	-	-	- −0.23	+0.23 −0.15	-
Pile-up offset N_{PV} (JES) [%]	-	-	+1.16 −0.78	+0.25 -	-
Pile-up offset p_T (JES) [%]	−0.35 +0.37	+0.17 −0.36	+1.66 −0.75	+0.41 -	+0.57 −0.27
Pile-up offset ρ topology (JES) [%]	-	- −0.21	+1.39 −0.79	−0.49 +0.78	+0.76
Punch-through (JES) [%]	-	-	-	-	-
b-Quark tagging efficiency (eigenvector 0) [%]	-	-	-	−0.34 +0.32	−0.32 +0.30
b-Quark tagging efficiency (eigenvector 1) [%]	+0.24 −0.22	−0.17 +0.16	−0.45 +0.42	+0.41 −0.39	−0.40 +0.38
b-Quark tagging efficiency (eigenvector 2) [%]	±0.17	∓0.13	∓0.27	±0.36	∓0.23
b-Quark tagging efficiency (eigenvector 3) [%]	-	-	∓0.14	-	∓0.19
c-Quark tagging efficiency (eigenvector 0) [%]	-	-	-	±0.13	-
c-Quark tagging efficiency (eigenvector 1) [%]	±0.10	-	−0.78 +0.77	±0.24	∓0.13
c-Quark tagging efficiency (eigenvector 2) [%]	-	-	∓0.37	±0.13	-
Light-jet tagging efficiency (eigenvector 0) [%]	±0.12	-	−1.14 +1.10	−0.37 +0.47	−0.35 +0.33
Light-jet tagging efficiency (eigenvector 1) [%]	-	-	∓0.21	±0.13	∓0.13
Light-jet tagging efficiency (eigenvector 3) [%]	-	-	∓0.47	-	-
Light-jet tagging efficiency (eigenvector 5) [%]	-	-	-	-	±0.13
Light-jet tagging efficiency (eigenvector 7) [%]	-	-	-	-	∓0.10
Light-jet tagging efficiency (eigenvector 8) [%]	-	-	∓0.17	-	-
b-Quark tagging extrapolation [%]	∓0.25	-	+0.54 −0.55	∓0.33	+0.89 −0.91
Electron energy resolution [%]	-	-	- +0.11	-	-
Electron energy scale [%]	-	-	+0.79 −0.44	-	-
Electron identification efficiency [%]	-	-	+0.45 −0.46	-	±0.18
Electron isolation efficiency [%]	∓0.16	-	+0.26 −0.27	∓0.12	±0.38
Muon (ID) momentum resolution [%]	-	-	- −0.29	-	-
Muon (MS) momentum resolution [%]	-	-	- −0.30	-	-
Muon energy scale [%]	-	-	−0.23 -	-	-
Muon trigger efficiency syst [%]	-	-	±0.13	-	-
Muon identification syst [%]	-	-	±0.38	-	±0.12
E_T^{miss} Soft jet resolution para [%]	±0.42	∓0.41	∓0.40	-	-
E_T^{miss} Soft jet resolution perp [%]	±0.58	∓0.54	∓0.88	-	-
E_T^{miss} Soft jet scale [%]	+0.41 −0.40	−0.36 +0.35	−1.28 +1.90	+0.46 −0.63	-
Z+jets cross-section [%]	∓0.10	-	+1.85 −1.87	±0.21	±0.24
$t\bar{t}V$ cross-section [%]	-	-	-	±0.10	-
Monte Carlo sample statistics [%]	±0.49	±0.49	±3.85	±2.63	±1.26
ISR/FSR + scale [%]	−2.64 +2.80	+0.56 −1.68	+10.0 −5.20	+9.53 -	+7.27 −8.25
Alternate hard-scattering model [%]	±1.51	∓1.72	±15.2	±0.35	∓2.21
Alternate parton-shower model [%]	±1.12	∓0.18	±7.31	∓2.21	∓6.13
Fakes overall normalization, el [%]	-	∓0.20	+3.20 −3.24	+0.99 −1.01	+0.63 −0.64
Fakes overall normalization, mu [%]	-	±0.11	+0.41 −0.42	+0.24 −0.25	∓0.57
Fakes alternative parametrization [%]	±0.28	±0.19	∓7.41	∓2.56	∓0.14
W+jets heavy flavour component [%]	-	-	±0.18	-	-
W+jets Scales [%]	∓1.10	±0.12	±12.1	±2.07	±2.06
W+jets α_S [%]	-	-	−0.71 +0.87	- +0.13	−0.11 +0.17
Single Top DS/DR [%]	±0.92	∓0.29	∓0.71	∓0.56	∓3.14
Single Top IFSR [%]	-	-	+0.38 −1.20	-	+0.74 −0.43

TABLE F.69: Table of systematics for the relative differential cross-section at the parton level for the $m^{t\bar{t}}vsp_T^{had}$ observable.

Bibliography

[1] Partial-symmetries of weak interactions. *Nuclear Physics*, 22(4):579 – 588, 1961. ISSN 0029-5582. doi:10.1016/0029-5582(61)90469-2.

[2] Steven Weinberg. A model of leptons. *Phys. Rev. Lett.*, 19:1264–1266, Nov 1967. doi:10.1103/PhysRevLett.19.1264.

[3] I.J.R. Aitchison, I.J.R. Aitchison, A.J.G. Hey, and A.J.G. Hey. *Gauge Theories in Particle Physics, Third Edition - 2 volume set*. Number v. 2 in Graduate Student Series in Physics. Taylor & Francis, 2004. ISBN 9780750309820. URL https://books.google.it/books?id=VQpHK06_3HgC.

[4] M. Tanabashi et al. Review of Particle Physics. *Phys. Rev.*, D98(3):030001, 2018. doi:10.1103/PhysRevD.98.030001.

[5] D. Hanneke, S. Fogwell Hoogerheide, and G. Gabrielse. Cavity control of a single-electron quantum cyclotron: Measuring the electron magnetic moment. *Phys. Rev. A*, 83:052122, May 2011. doi:10.1103/PhysRevA.83.052122. URL https://link.aps.org/doi/10.1103/PhysRevA.83.052122.

[6] T. D. Lee and C. N. Yang. Question of Parity Conservation in Weak Interactions. *Physical Review*, 104:254–258, October 1956. doi:10.1103/PhysRev.104.254.

[7] C. S. Wu, E. Ambler, R. W. Hayward, D. D. Hoppes, and R. P. Hudson. Experimental Test of Parity Conservation in Beta Decay. *Physical Review*, 105:1413–1415, February 1957. doi:10.1103/PhysRev.105.1413.

[8] J. Goldstone, A. Salam, and S. Weinberg. Broken Symmetries. *Physical Review*, 127: 965–970, August 1962. doi:10.1103/PhysRev.127.965.

[9] Georges Aad et al. Observation of a new particle in the search for the Standard Model Higgs boson with the ATLAS detector at the LHC. *Phys. Lett.*, B716:1–29, 2012. doi:10.1016/j.physletb.2012.08.020.

[10] Serguei Chatrchyan et al. Observation of a new boson at a mass of 125 GeV with the CMS experiment at the LHC. *Phys. Lett.*, B716:30–61, 2012. doi:10.1016/j.physletb.2012.08.021.

[11] Georges Aad et al. Combined Measurement of the Higgs Boson Mass in pp Collisions at $\sqrt{s}$ = 7 and 8 TeV with the ATLAS and CMS Experiments. *Phys. Rev. Lett.*, 114: 191803, 2015. doi:10.1103/PhysRevLett.114.191803.

[12] Peter W. Higgs. Broken Symmetries and the Masses of Gauge Bosons. *Phys. Rev. Lett.*, 13:508–509, 1964. doi:10.1103/PhysRevLett.13.508. [,160(1964)].

[13] F. Englert and R. Brout. Broken Symmetry and the Mass of Gauge Vector Mesons. *Phys. Rev. Lett.*, 13:321–323, 1964. doi:10.1103/PhysRevLett.13.321. [,157(1964)].

[14] Nicola Cabibbo. Unitary symmetry and leptonic decays. *Phys. Rev. Lett.*, 10:531–533, Jun 1963. doi:10.1103/PhysRevLett.10.531. URL `https://link.aps.org/doi/10.1103/PhysRevLett.10.531`.

[15] Makoto Kobayashi and Toshihide Maskawa. CP Violation in the Renormalizable Theory of Weak Interaction. *Prog. Theor. Phys.*, 49:652–657, 1973. doi:10.1143/PTP.49.652.

[16] H. David Politzer. Reliable Perturbative Results for Strong Interactions? *Phys. Rev. Lett.*, 30:1346–1349, 1973. doi:10.1103/PhysRevLett.30.1346. [,274(1973)].

[17] D. J. Gross and Frank Wilczek. ASYMPTOTICALLY FREE GAUGE THEORIES. 2. *Phys. Rev.*, D9:980–993, 1974. doi:10.1103/PhysRevD.9.980.

[18] John C. Collins, Davison E. Soper, and George F. Sterman. Factorization of Hard Processes in QCD. *Adv. Ser. Direct. High Energy Phys.*, 5:1–91, 1989. doi:10.1142/9789814503266_0001.

[19] Guido Altarelli and G. Parisi. Asymptotic Freedom in Parton Language. *Nucl. Phys.*, B126:298–318, 1977. doi:10.1016/0550-3213(77)90384-4.

[20] V. N. Gribov and L. N. Lipatov. Deep inelastic e p scattering in perturbation theory. *Sov. J. Nucl. Phys.*, 15:438–450, 1972. [Yad. Fiz.15,781(1972)].

[21] Yuri L. Dokshitzer. Calculation of the Structure Functions for Deep Inelastic Scattering and e+ e- Annihilation by Perturbation Theory in Quantum Chromodynamics. *Sov. Phys. JETP*, 46:641–653, 1977. [Zh. Eksp. Teor. Fiz.73,1216(1977)].

[22] L. A. Harland-Lang, A. D. Martin, P. Motylinski, and R. S. Thorne. Parton distributions in the LHC era: MMHT 2014 PDFs. *Eur. Phys. J.*, C75(5):204, 2015. doi:10.1140/epjc/s10052-015-3397-6.

[23] Sayipjamal Dulat, Tie-Jiun Hou, Jun Gao, Marco Guzzi, Joey Huston, Pavel Nadolsky, Jon Pumplin, Carl Schmidt, Daniel Stump, and C. P. Yuan. New parton distribution functions from a global analysis of quantum chromodynamics. *Phys. Rev.*, D93(3): 033006, 2016. doi:10.1103/PhysRevD.93.033006.

[24] Richard D. Ball et al. Parton distributions from high-precision collider data. *Eur. Phys. J.*, C77(10):663, 2017. doi:10.1140/epjc/s10052-017-5199-5.

[25] H. Abramowicz et al. Combination of measurements of inclusive deep inelastic $e^{\pm}p$ scattering cross sections and QCD analysis of HERA data. *Eur. Phys. J.*, C75(12):580, 2015. doi:10.1140/epjc/s10052-015-3710-4.

[26] R. Keith Ellis, W. James Stirling, and B. R. Webber. QCD and collider physics. *Camb. Monogr. Part. Phys. Nucl. Phys. Cosmol.*, 8:1–435, 1996.

[27] G. Dissertori, I. G. Knowles, and M. Schmelling. *High energy experiments and theory*. 2003.

[28] R.E. Marshak. *Conceptual Foundations of Modern Particle Physics*. World Scientific, 1993. ISBN 9789810211066. URL https://books.google.it/books?id=iYBZ1QRt9j4C.

[29] Martin L. Perl et al. Evidence for Anomalous Lepton Production in e+ - e- Annihilation. *Phys. Rev. Lett.*, 35:1489–1492, 1975. doi:10.1103/PhysRevLett.35.1489. [,193(1975)].

[30] S. W. Herb et al. Observation of a Dimuon Resonance at 9.5-GeV in 400-GeV Proton-Nucleus Collisions. *Phys. Rev. Lett.*, 39:252–255, 1977. doi:10.1103/PhysRevLett.39.252.

[31] F. Abe et al. Observation of top quark production in $\bar{p}p$ collisions. *Phys. Rev. Lett.*, 74: 2626–2631, 1995. doi:10.1103/PhysRevLett.74.2626.

[32] S. Abachi et al. Observation of the top quark. *Phys. Rev. Lett.*, 74:2632–2637, 1995. doi:10.1103/PhysRevLett.74.2632.

[33] R. Blair et al. The CDF-II detector: Technical design report. 1996.

[34] S. Aronson et al. Design Report. 1984.

[35] First combination of Tevatron and LHC measurements of the top-quark mass. 2014.

[36] Michał Czakon, Paul Fiedler, and Alexander Mitov. Total Top-Quark Pair-Production Cross Section at Hadron Colliders Through $O(\alpha\frac{4}{S})$. *Phys. Rev. Lett.*, 110:252004, 2013. doi:10.1103/PhysRevLett.110.252004.

[37] Michal Czakon and Alexander Mitov. Top++: A Program for the Calculation of the Top-Pair Cross-Section at Hadron Colliders. *Comput. Phys. Commun.*, 185:2930, 2014. doi:10.1016/j.cpc.2014.06.021.

[38] Michiel Botje et al. The PDF4LHC Working Group Interim Recommendations. 2011.

[39] A. D. Martin, W. J. Stirling, R. S. Thorne, and G. Watt. Uncertainties on alpha(S) in global PDF analyses and implications for predicted hadronic cross sections. *Eur. Phys. J.*, C64:653–680, 2009. doi:10.1140/epjc/s10052-009-1164-2.

[40] Jun Gao, Marco Guzzi, Joey Huston, Hung-Liang Lai, Zhao Li, Pavel Nadolsky, Jon Pumplin, Daniel Stump, and C. P. Yuan. CT10 next-to-next-to-leading order global analysis of QCD. *Phys. Rev.*, D89(3):033009, 2014. doi:10.1103/PhysRevD.89.033009.

[41] Richard D. Ball et al. Parton distributions with LHC data. *Nucl. Phys.*, B867:244–289, 2013. doi:10.1016/j.nuclphysb.2012.10.003.

[42] Michal Czakon, David Heymes, and Alexander Mitov. High-precision differential predictions for top-quark pairs at the LHC. *Phys. Rev. Lett.*, 116(8):082003, 2016. doi:10.1103/PhysRevLett.116.082003.

[43] Vardan Khachatryan et al. Measurement of the differential cross section for top quark pair production in pp collisions at $\sqrt{s}$ = 8 TeV. *Eur. Phys. J.*, C75(11):542, 2015. doi:10.1140/epjc/s10052-015-3709-x.

[44] Michal Czakon, David Heymes, Alexander Mitov, Davide Pagani, Ioannis Tsinikos, and Marco Zaro. Top-pair production at the LHC through NNLO QCD and NLO EW. *JHEP*, 10:186, 2017. doi:10.1007/JHEP10(2017)186.

[45] Michal Czakon, David Heymes, and Alexander Mitov. Dynamical scales for multi-TeV top-pair production at the LHC. *JHEP*, 04:071, 2017. doi:10.1007/JHEP04(2017)071.

[46] M. Aliev, H. Lacker, U. Langenfeld, S. Moch, P. Uwer, and M. Wiedermann. HATHOR: HAdronic Top and Heavy quarks crOss section calculatoR. *Comput. Phys. Commun.*, 182:1034–1046, 2011. doi:10.1016/j.cpc.2010.12.040.

[47] P. Kant, O. M. Kind, T. Kintscher, T. Lohse, T. Martini, S. Mölbitz, P. Rieck, and P. Uwer. HatHor for single top-quark production: Updated predictions and uncertainty estimates for single top-quark production in hadronic collisions. *Comput. Phys. Commun.*, 191:74–89, 2015. doi:10.1016/j.cpc.2015.02.001.

[48] A. D. Martin, W. J. Stirling, R. S. Thorne, and G. Watt. Parton distributions for the LHC. *Eur. Phys. J.*, C63:189–285, 2009. doi:10.1140/epjc/s10052-009-1072-5.

[49] Hung-Liang Lai, Marco Guzzi, Joey Huston, Zhao Li, Pavel M. Nadolsky, Jon Pumplin, and C. P. Yuan. New parton distributions for collider physics. *Phys. Rev.*, D82:074024, 2010. doi:10.1103/PhysRevD.82.074024.

[50] Stefano Frixione, Eric Laenen, Patrick Motylinski, Bryan R. Webber, and Chris D. White. Single-top hadroproduction in association with a W boson. *JHEP*, 07:029, 2008. doi:10.1088/1126-6708/2008/07/029.

[51] ATLAS Collaboration. Measurements of top-quark pair differential cross-sections in the lepton+jets channel in *pp* collisions at $\sqrt{s}$ = 13 TeV using the ATLAS detector. *JHEP*, 11:191, 2017. doi:10.1007/JHEP11(2017)191.

[52] ATLAS Collaboration. Measurements of top-quark pair differential cross-sections in the lepton+jets channel in pp collisions at $\sqrt{s}$ = 8 TeV using the ATLAS detector. *Eur. Phys. J. C*, 76:538, 2016. doi:10.1140/epjc/s10052-016-4366-4.

[53] Determination of the parton distribution functions of the proton from ATLAS measurements of differential W and Z/γ^* and $t\bar{t}$ cross sections. Technical Report ATL-PHYS-PUB-2018-017, CERN, Geneva, Aug 2018. URL http://cds.cern.ch/record/2633819.

[54] Albert M Sirunyan et al. Measurement of differential cross sections for the production of top quark pairs and of additional jets in lepton+jets events from pp collisions at $\sqrt{s}$ = 13 TeV. *Phys. Rev.*, D97(11):112003, 2018. doi:10.1103/PhysRevD.97.112003.

[55] Morad Aaboud et al. Measurements of differential cross sections of top quark pair production in association with jets in pp collisions at $\sqrt{s}$ = 13 TeV using the ATLAS detector. *JHEP*, 10:159, 2018. doi:10.1007/JHEP10(2018)159.

[56] Lyndon Evans and Philip Bryant. LHC Machine. *JINST*, 3:S08001, 2008. doi:10.1088/1748-0221/3/08/S08001.

[57] ATLAS Collaboration. The ATLAS Experiment at the CERN Large Hadron Collider. *JINST*, 3:S08003, 2008. doi:10.1088/1748-0221/3/08/S08003.

[58] S. Chatrchyan et al. The CMS Experiment at the CERN LHC. *JINST*, 3:S08004, 2008. doi:10.1088/1748-0221/3/08/S08004.

[59] A. Augusto Alves, Jr. et al. The LHCb Detector at the LHC. *JINST*, 3:S08005, 2008. doi:10.1088/1748-0221/3/08/S08005.

[60] K. Aamodt et al. The ALICE experiment at the CERN LHC. *JINST*, 3:S08002, 2008. doi:10.1088/1748-0221/3/08/S08002.

[61] G. Anelli et al. The TOTEM experiment at the CERN Large Hadron Collider. *JINST*, 3:S08007, 2008. doi:10.1088/1748-0221/3/08/S08007.

[62] O. Adriani et al. The LHCf detector at the CERN Large Hadron Collider. *JINST*, 3: S08006, 2008. doi:10.1088/1748-0221/3/08/S08006.

[63] J. L. Pinfold. The MoEDAL Experiment at the LHC - a New Light on the Terascale Frontier. *J. Phys. Conf. Ser.*, 631(1):012014, 2015. doi:10.1088/1742-6596/631/1/012014.

[64] A. Airapetian et al. ATLAS: Detector and physics performance technical design report. Volume 1. 1999.

[65] G. Aad et al. The ATLAS Inner Detector commissioning and calibration. *Eur. Phys. J.*, C70:787–821, 2010. doi:10.1140/epjc/s10052-010-1366-7.

[66] M. Capeans, G. Darbo, K. Einsweiler, M. Elsing, T. Flick, M. Garcia-Sciveres, C. Gemme, H. Pernegger, O. Rohne, and R. Vuillermet. ATLAS Insertable B-Layer Technical Design Report. 2010.

[67] ATLAS Insertable B-Layer Technical Design Report Addendum. 2012.

[68] G. Aad et al. ATLAS pixel detector electronics and sensors. *JINST*, 3:P07007, 2008. doi:10.1088/1748-0221/3/07/P07007.

[69] Georges Aad et al. Operation and performance of the ATLAS semiconductor tracker. *JINST*, 9:P08009, 2014. doi:10.1088/1748-0221/9/08/P08009.

[70] Adrian Vogel. ATLAS Transition Radiation Tracker (TRT): Straw tube gaseous detectors at high rates. *Nucl. Instrum. Meth.*, A732:277–280, 2013. doi:10.1016/j.nima.2013.07.020.

[71] ATLAS liquid argon calorimeter: Technical design report. 1996.

[72] ATLAS tile calorimeter: Technical design report. 1996.

[73] A. Artamonov et al. The ATLAS forward calorimeters. *JINST*, 3:P02010, 2008. doi:10.1088/1748-0221/3/02/P02010.

[74] ATLAS muon spectrometer: Technical design report. 1997. URL `http://cds.cern.ch/record/331068`.

[75] Georges Aad et al. Improved luminosity determination in pp collisions at sqrt(s) = 7 TeV using the ATLAS detector at the LHC. *Eur. Phys. J.*, C73(8):2518, 2013. doi:10.1140/epjc/s10052-013-2518-3.

[76] V. Cindro et al. The ATLAS beam conditions monitor. *JINST*, 3:P02004, 2008. doi:10.1088/1748-0221/3/02/P02004.

[77] I. Bird, K. Bos, N. Brook, D. Duellmann, C. Eck, I. Fisk, D. Foster, B. Gibbard, C. Grandi, F. Grey, et al. LHC computing Grid. Technical design report. 2005.

[78] G. Duckeck, D. Barberis, R. Hawkings, R. Jones, N. McCubbin, G. Poulard, D. Quarrie, T. Wenaus, and E. Obreshkov. ATLAS computing: Technical design report. 2005.

[79] ATLAS Collaboration. Athena Core Software. URL `http://atlas-computing.web.cern.ch/atlas-computing/packages/athenaCore/athenaCore.php`.

[80] Stefan Höche. Introduction to parton-shower event generators. In *Proceedings, Theoretical Advanced Study Institute in Elementary Particle Physics: Journeys Through the Precision Frontier: Amplitudes for Colliders (TASI 2014): Boulder, Colorado, June 2-27, 2014*, pages 235–295, 2015. doi:10.1142/9789814678766_0005.

[81] Torbjörn Sjöstrand. Status and developments of event generators. *PoS*, LHCP2016: 007, 2016. doi:10.22323/1.276.0007.

[82] ATLAS Collaboration. Measurement of the underlying event in jet events from 7 TeV proton–proton collisions with the ATLAS detector. *Eur. Phys. J. C*, 74:2965, 2014. doi:10.1140/epjc/s10052-014-2965-5.

[83] B. R. Webber. A QCD Model for Jet Fragmentation Including Soft Gluon Interference. *Nucl. Phys.*, B238:492–528, 1984. doi:10.1016/0550-3213(84)90333-X.

[84] G. Marchesini and B. R. Webber. Monte Carlo Simulation of General Hard Processes with Coherent QCD Radiation. *Nucl. Phys.*, B310:461–526, 1988. doi:10.1016/0550-3213(88)90089-2.

[85] Bo Andersson, G. Gustafson, G. Ingelman, and T. Sjostrand. Parton Fragmentation and String Dynamics. *Phys. Rept.*, 97:31–145, 1983. doi:10.1016/0370-1573(83)90080-7.

[86] Torbjorn Sjostrand. Jet Fragmentation of Nearby Partons. *Nucl. Phys.*, B248:469–502, 1984. doi:10.1016/0550-3213(84)90607-2.

[87] D. Amati and G. Veneziano. Preconfinement as a Property of Perturbative QCD. *Phys. Lett.*, 83B:87–92, 1979. doi:10.1016/0370-2693(79)90896-7.

[88] Simone Alioli, Paolo Nason, Carlo Oleari, and Emanuele Re. A general framework for implementing NLO calculations in shower Monte Carlo programs: the POWHEG BOX. *JHEP*, 06:043, 2010. doi:10.1007/JHEP06(2010)043.

[89] Paolo Nason. A New method for combining NLO QCD with shower Monte Carlo algorithms. *JHEP*, 11:040, 2004. doi:10.1088/1126-6708/2004/11/040.

[90] Stefano Frixione, Paolo Nason, and Carlo Oleari. Matching NLO QCD computations with Parton Shower simulations: the POWHEG method. *JHEP*, 11:070, 2007. doi:10.1088/1126-6708/2007/11/070.

[91] J. Alwall, R. Frederix, S. Frixione, V. Hirschi, F. Maltoni, O. Mattelaer, H. S. Shao, T. Stelzer, P. Torrielli, and M. Zaro. The automated computation of tree-level and next-to-leading order differential cross sections, and their matching to parton shower simulations. *JHEP*, 07:079, 2014. doi:10.1007/JHEP07(2014)079.

[92] Stefano Frixione and Bryan R. Webber. Matching NLO QCD computations and parton shower simulations. *JHEP*, 06:029, 2002. doi:10.1088/1126-6708/2002/06/029.

[93] Torbjorn Sjostrand, Stephen Mrenna, and Peter Z. Skands. A Brief Introduction to PYTHIA 8.1. *Comput. Phys. Commun.*, 178:852–867, 2008. doi:10.1016/j.cpc.2008.01.036.

[94] M. Bahr et al. Herwig++ Physics and Manual. *Eur. Phys. J.*, C58:639–707, 2008. doi:10.1140/epjc/s10052-008-0798-9.

[95] Johannes Bellm et al. Herwig 7.0/Herwig++ 3.0 release note. *Eur. Phys. J.*, C76(4):196, 2016. doi:10.1140/epjc/s10052-016-4018-8.

[96] T. Gleisberg, Stefan. Hoeche, F. Krauss, M. Schonherr, S. Schumann, F. Siegert, and J. Winter. Event generation with SHERPA 1.1. *JHEP*, 02:007, 2009. doi:10.1088/1126-6708/2009/02/007.

[97] ATLAS Collaboration. ATLAS Pythia 8 tunes to 7 TeV data. ATL-PHYS-PUB-2014-021, 2014. URL https://cds.cern.ch/record/1966419.

[98] John M. Campbell, R. Keith Ellis, Paolo Nason, and Emanuele Re. Top-Pair Production and Decay at NLO Matched with Parton Showers. *JHEP*, 04:114, 2015. doi:10.1007/JHEP04(2015)114.

[99] Richard D. Ball et al. Parton distributions for the LHC Run II. *JHEP*, 04:040, 2015. doi:10.1007/JHEP04(2015)040.

[100] Matteo Cacciari, Michal Czakon, Michelangelo Mangano, Alexander Mitov, and Paolo Nason. Top-pair production at hadron colliders with next-to-next-to-leading logarithmic soft-gluon resummation. *Phys. Lett.*, B710:612–622, 2012. doi:10.1016/j.physletb.2012.03.013.

[101] Michal Czakon and Alexander Mitov. NNLO corrections to top-pair production at hadron colliders: the all-fermionic scattering channels. *JHEP*, 12:054, 2012. doi:10.1007/JHEP12(2012)054.

[102] Michal Czakon and Alexander Mitov. NNLO corrections to top pair production at hadron colliders: the quark-gluon reaction. *JHEP*, 01:080, 2013. doi:10.1007/JHEP01(2013)080.

[103] Michael H. Seymour and Andrzej Siodmok. Constraining MPI models using σ_{eff} and recent Tevatron and LHC Underlying Event data. *JHEP*, 10:113, 2013. doi:10.1007/JHEP10(2013)113.

[104] Torbjorn Sjostrand, Stephen Mrenna, and Peter Z. Skands. PYTHIA 6.4 Physics and Manual. *JHEP*, 05:026, 2006. doi:10.1088/1126-6708/2006/05/026.

[105] J. Pumplin, D. R. Stump, J. Huston, H. L. Lai, Pavel M. Nadolsky, and W. K. Tung. New generation of parton distributions with uncertainties from global QCD analysis. *JHEP*, 07:012, 2002. doi:10.1088/1126-6708/2002/07/012.

[106] Peter Zeiler Skands. Tuning Monte Carlo Generators: The Perugia Tunes. *Phys. Rev.*, D82:074018, 2010. doi:10.1103/PhysRevD.82.074018.

[107] Nikolaos Kidonakis. Two-loop soft anomalous dimensions for single top quark associated production with a W- or H-. *Phys. Rev.*, D82:054018, 2010. doi:10.1103/PhysRevD.82.054018.

[108] Nikolaos Kidonakis. NNLL resummation for s-channel single top quark production. *Phys. Rev.*, D81:054028, 2010. doi:10.1103/PhysRevD.81.054028.

[109] Nikolaos Kidonakis. Next-to-next-to-leading-order collinear and soft gluon corrections for t-channel single top quark production. *Phys. Rev.*, D83:091503, 2011. doi:10.1103/PhysRevD.83.091503.

[110] S. Agostinelli et al. GEANT4: A Simulation toolkit. *Nucl. Instrum. Meth.*, A506:250–303, 2003. doi:10.1016/S0168-9002(03)01368-8.

[111] Andy Buckley, Jonathan Butterworth, Leif Lonnblad, David Grellscheid, Hendrik Hoeth, James Monk, Holger Schulz, and Frank Siegert. Rivet user manual. *Comput. Phys. Commun.*, 184:2803–2819, 2013. doi:10.1016/j.cpc.2013.05.021.

[112] Christian Gutschow and Francesco La Ruffa. ATLAS_2015_I1404878 Rivet routine. URL https://rivet.hepforge.org/analyses/ATLAS_2015_I1404878.html.

[113] Federica Fabbri, Christian Gutschow, Steffen Henkelmann, and Francesco La Ruffa. ATLAS_2017_I1614149 Rivet routine. URL https://rivet.hepforge.org/analyses/ATLAS_2017_I1614149.html.

[114] ATLAS Collaboration. Studies on top-quark Monte Carlo modelling for Top2016. ATL-PHYS-PUB-2016-020, 2016. URL https://cds.cern.ch/record/2216168.

[115] Improvements in $t\bar{t}$ modelling using NLO+PS Monte Carlo generators for Run2. Technical Report ATL-PHYS-PUB-2018-009, CERN, Geneva, Jul 2018. URL http://cds.cern.ch/record/2630327.

[116] T Cornelissen, M Elsing, S Fleischmann, W Liebig, E Moyse, and A Salzburger. Concepts, Design and Implementation of the ATLAS New Tracking (NEWT). Technical Report ATL-SOFT-PUB-2007-007. ATL-COM-SOFT-2007-002, CERN, Geneva, Mar 2007. URL https://cds.cern.ch/record/1020106.

[117] ATLAS Collaboration. The Optimization of ATLAS Track Reconstruction in Dense Environments. ATL-PHYS-PUB-2015-006, 2015. URL https://cds.cern.ch/record/2002609.

[118] Morad Aaboud et al. Reconstruction of primary vertices at the ATLAS experiment in Run 1 proton–proton collisions at the LHC. *Eur. Phys. J.*, C77(5):332, 2017. doi:10.1140/epjc/s10052-017-4887-5.

[119] ATLAS Collaboration. Performance of primary vertex reconstruction in proton–proton collisions at $\sqrt{s}$ = 7 TeV in the ATLAS experiment. ATLAS-CONF-2010-069, 2010. URL https://cds.cern.ch/record/1281344.

[120] ATLAS Collaboration. Electron reconstruction and identification efficiency measurements with the ATLAS detector using the 2011 LHC proton–proton collision data. *Eur. Phys. J. C*, 74:2941, 2014. doi:10.1140/epjc/s10052-014-2941-0.

[121] ATLAS Collaboration. Electron efficiency measurements with the ATLAS detector using the 2015 LHC proton–proton collision data. ATLAS-CONF-2016-024, 2016. URL https://cds.cern.ch/record/2157687.

[122] J. Illingworth and J. Kittler. A survey of the hough transform. *Computer Vision, Graphics, and Image Processing*, 44(1):87 – 116, 1988. ISSN 0734-189X. doi:https://doi.org/10.1016/S0734-189X(88)80033-1. URL http://www.sciencedirect.com/science/article/pii/S0734189X88800331.

[123] ATLAS Collaboration. Muon reconstruction performance of the ATLAS detector in proton–proton collision data at $\sqrt{s}$ = 13 TeV. *Eur. Phys. J. C*, 76:292, 2016. doi:10.1140/epjc/s10052-016-4120-y.

[124] ATLAS Collaboration. Topological cell clustering in the ATLAS calorimeters and its performance in LHC Run 1. *Eur. Phys. J. C*, 77:490, 2017. doi:10.1140/epjc/s10052-017-5004-5.

[125] John E. Huth et al. Toward a standardization of jet definitions. In *1990 DPF Summer Study on High-energy Physics: Research Directions for the Decade (Snowmass 90) Snowmass, Colorado, June 25-July 13, 1990*, pages 0134–136, 1990. URL http://lss.fnal.gov/cgi-bin/find_paper.pl?conf-90-249.

[126] Gavin P. Salam. Towards Jetography. *Eur. Phys. J.*, C67:637–686, 2010. doi:10.1140/epjc/s10052-010-1314-6.

[127] Matteo Cacciari, Gavin P. Salam, and Gregory Soyez. The anti-k_t jet clustering algorithm. *JHEP*, 04:063, 2008. doi:10.1088/1126-6708/2008/04/063.

[128] ATLAS Collaboration. Jet energy scale measurements and their systematic uncertainties in proton–proton collisions at $\sqrt{s}$ = 13 TeV with the ATLAS detector. *Phys. Rev. D*, 96:072002, 2017. doi:10.1103/PhysRevD.96.072002.

[129] Matteo Cacciari, Gavin P. Salam, and Gregory Soyez. The Catchment Area of Jets. *JHEP*, 04:005, 2008. doi:10.1088/1126-6708/2008/04/005.

[130] Matteo Cacciari and Gavin P. Salam. Pileup subtraction using jet areas. *Phys. Lett.*, B659:119–126, 2008. doi:10.1016/j.physletb.2007.09.077.

[131] ATLAS Collaboration. Tagging and suppression of pileup jets with the ATLAS detector. ATLAS-CONF-2014-018, 2014. URL https://cds.cern.ch/record/1700870.

[132] David Krohn, Jesse Thaler, and Lian-Tao Wang. Jet Trimming. *JHEP*, 02:084, 2010. doi:10.1007/JHEP02(2010)084.

[133] ATLAS Collaboration. Exclusive Jet Production with Forward Proton Tagging. Feasibility Studies for the AFP Project. ATL-PHYS-PUB-2015-003, 2015. URL https://cds.cern.ch/record/1993686.

[134] Jesse Thaler and Ken Van Tilburg. Identifying Boosted Objects with N-subjettiness. *JHEP*, 03:015, 2011. doi:10.1007/JHEP03(2011)015.

[135] Jesse Thaler and Ken Van Tilburg. Maximizing Boosted Top Identification by Minimizing N-subjettiness. *JHEP*, 02:093, 2012. doi:10.1007/JHEP02(2012)093.

[136] Benjamin Nachman, Pascal Nef, Ariel Schwartzman, Maximilian Swiatlowski, and Chaowaroj Wanotayaroj. Jets from Jets: Re-clustering as a tool for large radius jet reconstruction and grooming at the LHC. *JHEP*, 02:075, 2015. doi:10.1007/JHEP02(2015)075.

[137] ATLAS Collaboration. Jet reclustering and close-by effects in ATLAS Run 2. ATLAS-CONF-2017-062, 2017. URL https://cds.cern.ch/record/2275649.

[138] ATLAS Collaboration. Commissioning of the ATLAS high performance b-tagging algorithms in the 7 TeV collision data. ATLAS-CONF-2011-102, 2011. URL https://cds.cern.ch/record/1369219.

[139] ATLAS Collaboration. Optimisation of the ATLAS b-tagging performance for the 2016 LHC Run. ATL-PHYS-PUB-2016-012, 2016. URL https://cds.cern.ch/record/2160731.

[140] ATLAS Collaboration. Secondary vertex finding for jet flavour identification with the ATLAS detector. ATL-PHYS-PUB-2017-011, 2017. URL https://cds.cern.ch/record/2270366.

[141] ATLAS Collaboration. Topological b-hadron decay reconstruction and identification of b-jets with the JetFitter package in the ATLAS experiment at the LHC. Technical Report ATL-PHYS-PUB-2018-025, CERN, Geneva, Oct 2018. URL https://cds.cern.ch/record/2645405.

[142] ATLAS Collaboration. Expected performance of the ATLAS b-tagging algorithms in Run-2. ATL-PHYS-PUB-2015-022, 2015. URL https://cds.cern.ch/record/2037697.

[143] ATLAS Collaboration. Measurements of b-jet tagging efficiency with the ATLAS detector using $t\bar{t}$ events at $\sqrt{s} = 13\,\text{TeV}$. *JHEP*, 08:089, 2018. doi:10.1007/JHEP08(2018)089.

[144] ATLAS Collaboration. Measurement of b-tagging efficiency of c-jets in $t\bar{t}$ events using a likelihood approach with the ATLAS detector. ATLAS-CONF-2018-001, 2018. URL https://cds.cern.ch/record/2306649.

[145] ATLAS Collaboration. Calibration of light-flavour b-jet mistagging rates using ATLAS proton–proton collision data at $\sqrt{s}$ = 13 TeV. ATLAS-CONF-2018-006, 2018. URL https://cds.cern.ch/record/2314418.

[146] ATLAS Collaboration. Calibration of ATLAS b-tagging algorithms in dense jet environments. ATLAS-CONF-2016-001, 2015. URL https://cds.cern.ch/record/2127958.

[147] ATLAS Collaboration. Calibration of the ATLAS b-tagging algorithm in $t\bar{t}$ semi-leptonic events. Technical Report ATLAS-CONF-2018-045, CERN, Geneva, Sep 2018. URL http://cds.cern.ch/record/2638455.

[148] ATLAS Collaboration. Performance of missing transverse momentum reconstruction with the ATLAS detector using proton–proton collisions at $\sqrt{s}$ = 13 TeV. *Eur. Phys. J. C*, 78:903, 2018. doi:10.1140/epjc/s10052-018-6288-9.

[149] ATLAS Collaboration. ATLAS simulation of boson plus jets processes in Run 2. ATL-PHYS-PUB-2017-006, 2017. URL https://cds.cern.ch/record/2261937.

[150] ATLAS Collaboration. Estimation of non-prompt and fake lepton backgrounds in final states with top quarks produced in proton–proton collisions at $\sqrt{s}$ = 8 TeV with the ATLAS Detector. ATLAS-CONF-2014-058, 2014. URL https://cds.cern.ch/record/1951336.

[151] V. M. Abazov et al. Measurement of the $t\bar{t}$ production cross section in $p\bar{p}$ collisions at $\sqrt{s}$ = 1.96-TeV using kinematic characteristics of lepton + jets events. *Phys. Rev.*, D76: 092007, 2007. doi:10.1103/PhysRevD.76.092007.

[152] Johannes Erdmann, Stefan Guindon, Kevin Kroeninger, Boris Lemmer, Olaf Nackenhorst, Arnulf Quadt, and Philipp Stolte. A likelihood-based reconstruction algorithm for top-quark pairs and the KLFitter framework. *Nucl. Instrum. Meth.*, A748:18–25, 2014. doi:10.1016/j.nima.2014.02.029.

[153] ATLAS Collaboration. Measurements of top quark pair relative differential cross-sections with ATLAS in pp collisions at $\sqrt{s}$ = 7 TeV. *Eur. Phys. J. C*, 73:2261, 2013. doi:10.1140/epjc/s10052-012-2261-1.

[154] ATLAS Collaboration. Measurement of the charge asymmetry in top quark pair production in pp collisions at $\sqrt{s}$ = 7 TeV using the ATLAS detector. *Eur. Phys. J. C*, 72: 2039, 2012. doi:10.1140/epjc/s10052-012-2039-5.

[155] ATLAS Collaboration. Boosted hadronic top identification at ATLAS for early 13 TeV data. ATL-PHYS-PUB-2015-053, 2015. URL https://cds.cern.ch/record/2116351.

[156] Volker Blobel. An Unfolding method for high-energy physics experiments. In *Advanced Statistical Techniques in Particle Physics. Proceedings, Conference, Durham, UK,*

March 18-22, 2002, pages 258–267, 2002. URL http://www.ippp.dur.ac.uk/Workshops/02/statistics/proceedings//blobel2.pdf.

[157] Andreas Hocker and Vakhtang Kartvelishvili. SVD approach to data unfolding. *Nucl. Instrum. Meth.*, A372:469–481, 1996. doi:10.1016/0168-9002(95)01478-0.

[158] G. D'Agostini. Improved iterative Bayesian unfolding. In *Alliance Workshop on Unfolding and Data Correction Hamburg, Germany, May 27-28, 2010*, 2010.

[159] G. D'Agostini. A Multidimensional unfolding method based on Bayes' theorem. *Nucl. Instrum. Meth.*, A362:487–498, 1995. doi:10.1016/0168-9002(95)00274-X.

[160] Tim Adye. Unfolding algorithms and tests using RooUnfold, 2011.

[161] Matteo Cacciari, Gavin P. Salam, and Gregory Soyez. FastJet User Manual. *Eur. Phys. J. C*, 72:1896, 2012. doi:10.1140/epjc/s10052-012-1896-2.

[162] ATLAS Collaboration. Electron and photon energy calibration with the ATLAS detector using data collected in 2015 at $\sqrt{s}$ = 13 TeV. ATL-PHYS-PUB-2016-015, 2016. URL https://cds.cern.ch/record/2203514.

[163] ATLAS Collaboration. $E_{\mathrm{T}}^{\mathrm{miss}}$ performance in the ATLAS detector using 2015–2016 LHC pp collisions. ATLAS-CONF-2018-023, 2018. URL https://cds.cern.ch/record/2625233.

[164] ATLAS Collaboration. Luminosity determination in pp collisions at $\sqrt{s}$ = 8 TeV using the ATLAS detector at the LHC. *Eur. Phys. J. C*, 76:653, 2016. doi:10.1140/epjc/s10052-016-4466-1.

[165] ATLAS Collaboration. Simulation of top-quark production for the ATLAS experiment at $\sqrt{s}$ = 13 TeV. ATL-PHYS-PUB-2016-004, 2016. URL https://cds.cern.ch/record/2120417.

[166] Jon Butterworth et al. PDF4LHC recommendations for LHC Run II. *J. Phys. G*, 43: 023001, 2016. doi:10.1088/0954-3899/43/2/023001.

[167] A. Denner, S. Dittmaier, S. Kallweit, and S. Pozzorini. NLO QCD corrections to WWbb production at hadron colliders. *Phys. Rev. Lett.*, 106:052001, 2011. doi:10.1103/PhysRevLett.106.052001.

[168] Giuseppe Bevilacqua, Michal Czakon, Andreas van Hameren, Costas G. Papadopoulos, and Malgorzata Worek. Complete off-shell effects in top quark pair hadroproduction with leptonic decay at next-to-leading order. *JHEP*, 02:083, 2011. doi:10.1007/JHEP02(2011)083.

[169] L. Apanasevich et al. Evidence for parton k_T effects in high p_T particle production. *Phys. Rev. Lett.*, 81:2642–2645, 1998. doi:10.1103/PhysRevLett.81.2642.

[170] ATLAS Collaboration. Measurements of differential cross sections of top quark pair production in association with jets in pp collisions at $\sqrt{s}$ = 13 TeV using the ATLAS detector. *JHEP*, 10:159, 2018. doi:10.1007/JHEP10(2018)159.

[171] Richard D. Ball, Valerio Bertone, Stefano Carrazza, Luigi Del Debbio, Stefano Forte, Alberto Guffanti, Nathan P. Hartland, and Juan Rojo. Parton distributions with QED corrections. *Nucl. Phys.*, B877:290–320, 2013. doi:10.1016/j.nuclphysb.2013.10.010.

[172] Aneesh Manohar, Paolo Nason, Gavin P. Salam, and Giulia Zanderighi. How bright is the proton? A precise determination of the photon parton distribution function. *Phys. Rev. Lett.*, 117(24):242002, 2016. doi:10.1103/PhysRevLett.117.242002.

Acknowledgements

Questa tesi rappresenta anche la conclusione di un percorso molto importante per me, il Dottorato, in cui ho avuto la possibilità di crescere sia dal punto di vista professionale, che da quello personale. E' in occasioni come queste che è giusto cogliere il momento per ringraziare le persone importanti.

Un grazie va sicuramente alla mia famiglia per avermi supportato sempre, in ogni circostanza e da ogni punto di vista. Senza i miei genitori e mio fratello, non avrei mai potuto essere qui oggi.

Un grazie alla mia Giusi, per tutto l'amore e la pazienza che mi ha donato, soprattutto nel periodo di scrittura della tesi. So che non è stato facile starmi vicino, soprattutto nei periodi stressanti, ma non mi ha mai fatto mancare la sua dolcezza e la sua comprensione.

Un grazie a tutti gli amici, quelli di Cosenza, quelli di sempre, quelli di sempre che non sono più a Cosenza e quelli che a Cosenza non ci sono mai stati. A tutti gli amici in giro per il mondo che mi hanno regalato un sorriso, una chiacchiera davanti ad un caffè, che mi hanno arricchito e mi hanno donato un punto di vista diverso. Non faccio una lista, ma chi leggerà saprà di esserci.

Un grazie al Prof. Tassi, per l'infinita disponibilità, per l'altrettanto grande professionalità e per il supporto che non mi ha fatto mai mancare.

Infine, un grazie ai colleghi e a tutto il personale del Dipartimento di Fisica per aver condiviso con me questo percorso, e all'INFN e al CERN per avermi supportato in questi anni.